

**Food Engineering Series**

*Series Editor:* Gustavo V. Barbosa-Cánovas

Gustavo F. Gutiérrez-López

Liliana Alamilla-Beltrán

María del Pilar Buerá

Jorge Welti-Chanes

Efrén Parada-Arias

Gustavo V. Barbosa-Cánovas *Editors*

# Water Stress in Biological, Chemical, Pharmaceutical and Food Systems



Springer

# Food Engineering Series

## **Series Editor**

Gustavo V. Barbosa-Cánovas, Washington State University, USA

## **Advisory Board**

José Miguel Aguilera, Catholic University, Chile

Kezban Candog  n, Ankara University, Turkey

J. Peter Clark, Clark Consulting, USA

Richard W. Hartel, University of Wisconsin, USA

Albert Ibarz, University of Lleida, Spain

Jozef Kokini, Purdue University, USA

Michael McCarthy, University of California, USA

Keshavan Niranjan, University of Reading, United Kingdom

Micha Peleg, University of Massachusetts, USA

Shafiu Rahman, Sultan Qaboos University, Oman

M. Anandha Rao, Cornell University, USA

Yrj   Roos, University College Cork, Ireland

Jorge Welti-Chanes, Monterrey Institute of Technology, Mexico

More information about this series at <http://www.springer.com/series/5996>



Gustavo F. Gutiérrez-López

Liliana Alamilla-Beltrán • María del Pilar Buera

Jorge Welti-Chanes • Efrén Parada-Arias

Gustavo V. Barbosa-Cánovas

Editors

# Water Stress in Biological, Chemical, Pharmaceutical and Food Systems



Springer

*Editors*

Gustavo F. Gutiérrez-López  
Escuela Nacional de Ciencias Biológicas  
Instituto Politécnico Nacional  
México, Distrito Federal  
México

María del Pilar Buera  
Facultad de Ciencias Exactas y Naturales  
Universidad de Buenos Aires-CONICET  
Buenos Aires, Argentina

Efrén Parada-Arias  
Escuela Nacional de Ciencias Biológicas  
Instituto Politécnico Nacional  
México, Distrito Federal  
México

Liliana Alamilla-Beltrán  
Escuela Nacional de Ciencias Biológicas  
Instituto Politécnico Nacional  
México, Distrito Federal  
México

Jorge Welti-Chanes  
Departamento de Biotecnología e Ingeniería  
Tecnológico de Monterrey  
Monterrey, Nuevo León  
México

Gustavo V. Barbosa-Cánovas  
Food Engineering  
Washington State University  
Pullman, WA, USA

ISSN 1571-0297

Food Engineering Series

ISBN 978-1-4939-2577-3

DOI 10.1007/978-1-4939-2578-0

ISBN 978-1-4939-2578-0 (eBook)

Library of Congress Control Number: 2015939993

Springer New York Heidelberg Dordrecht London

© Springer Science+Business Media New York 2015

This work is subject to copyright. All rights are reserved by the Publisher, whether the whole or part of the material is concerned, specifically the rights of translation, reprinting, reuse of illustrations, recitation, broadcasting, reproduction on microfilms or in any other physical way, and transmission or information storage and retrieval, electronic adaptation, computer software, or by similar or dissimilar methodology now known or hereafter developed.

The use of general descriptive names, registered names, trademarks, service marks, etc. in this publication does not imply, even in the absence of a specific statement, that such names are exempt from the relevant protective laws and regulations and therefore free for general use.

The publisher, the authors and the editors are safe to assume that the advice and information in this book are believed to be true and accurate at the date of publication. Neither the publisher nor the authors or the editors give a warranty, express or implied, with respect to the material contained herein or for any errors or omissions that may have been made.

Printed on acid-free paper

Springer Science+Business Media LLC New York is part of Springer Science+Business Media ([www.springer.com](http://www.springer.com))

*To our families, institutions, fellow  
colleagues, and students.*



# Preface

This book is based on scientific presentations made at the 11th Symposium on the Properties of Water (ISOPOW 11) held in Querétaro, Mexico, September 5–9, 2010. This publication received decisive and integrated support from ISOPOW Central Committee and two Mexican academic institutions: *Instituto Politécnico Nacional* and *Tecnológico de Monterrey*.

A comprehensive review on novel aspects related to water stress in biological, chemical, food, and pharmaceutical systems is presented in this book. The chapters have been written by well-established authorities in their respective fields coming from research institutions and industry as well as by very promising young scientists making strides on these ever-evolving topics around the properties of water. One of the premises of this book is that a thorough update requires an in-depth knowledge of each subject under consideration where a number of disciplines are effectively integrated. This approach facilitates to appropriately formulate the latest on fundamental aspects; present the bases for innovative applications; and identify upcoming developments, as well as research and development needs. The understanding of water stresses in complex systems is a true challenge for scientists and practitioners. The mechanisms involved in the interaction of water with a number of compounds imply to follow a multi-interdisciplinary approach. The ISOPOW community is well acquainted with the challenges ahead and the approaches to be taken whenever dealing with water as part of complex systems. This implies, among others, to identify ongoing and upcoming efforts towards the use and inclusion of a diversity of intertwined disciplines, novel tools, and concepts to successfully integrate existing knowledge with potentially useful new developments.

ISOPOW is a nonprofit scientific organization which aims to advance the understanding of the properties of water in chemical, pharmaceutical, biological, and food systems and on the exploitation of findings on water properties in improved raw materials, intermediate and final products, as well as processes. One of the objectives of ISOPOW is to promote high level scientific symposia in different and targeted places around the world. Another objective is to generate a

publication from each Symposium containing the scientific highlights of this event, including invited speaker presentations and the results of investigations made by selected participants.

The first ISOPOW took place in Glasgow, Scotland, in 1974, following the pioneering initiative of the late Ron B. Duckworth and of Louis B. Rockland. Since then, all ISOPOWs are recognized for their quality and relevance to the field. Prior to the Symposium in Querétaro, ten ISOPOWs and two ISOPOW-PRACTICUMs were held in different parts of the world, marking the global dimension and impact of these meetings, as well as the interdisciplinary nature of the addressed subjects. It is worth mentioning that all the ISOPOWs were endorsed and partially sponsored, among others, by the International Union of Food Science and Technology (IUFoST). At ISOPOW 11, the latest insights on the scientific aspects of water properties in foods and other biological systems were presented, keeping the tradition of exploring and discussing the many roles of water from a multidisciplinary perspective. This is the complete list of ISOPOWs held before the one in Querétaro, Mexico.

- ISOPOW 1 Glasgow, U.K., 1974
- ISOPOW 2 Osaka, Japan, 1978
- ISOPOW 3 Beaune, France, 1983
- ISOPOW 4 Banff, Canada, 1987
- ISOPOW Practicum 1 Penang, Malaysia, 1987
- ISOPOW 5 Peñíscola, Spain, 1992
- ISOPOW Practicum 2, Puebla, Mexico, 1994
- ISOPOW 6 Santa Rosa, USA, 1996
- ISOPOW 7 Helsinki, Finland, 1998
- ISOPOW 8 Zichron Yaakov, Israel, 2000
- ISOPOW 9 Mar del Plata, Argentina, 2004
- ISOPOW 10 Bangkok, Thailand, 2007

A round table, chaired by David Reid, was held on the last day of ISOPOW 11 aimed to present the state of the art and to identify research needs on water stress in biological systems. David Reid, Brad Anderson, David Lechuga, Micha Peleg, Yrjö Roos, David Reid, Pilar Buera, and Gustavo Gutiérrez-López contributed a list of the topics which received the most attention during the entire scientific program. This promoted a vivid interaction from all the attendees facilitating the formulation of future endeavors in the topics under consideration. At the end of the meeting, Gustavo Barbosa-Cánovas presented “Future Research and Suggested Activities on the Properties of Water.” Some of the highlighted topics in need of attention were as follows: to the frequent misleading concepts on the concept of freezable and frozen water; modeling and predicting water behavior under a variety of stresses; dilution and dissolution in water matrices; plasticizing effect of water; crystallinity or amorphicity as evaluated by X-rays. A very interesting debate took place on the extrapolation of equations developed for a number of systems in conditions far from those at which they are frequently used in water science as well as on exploration and exploitation of the relationships among aw–water mobility–polymer science

approaches; adequate use of the water activity concept in predictive microbiology; risk assessment and its role, as a hurdle, in emerging food processing technologies; potential use of genomics to better understand the microbial responses to stresses such as water activity changes; applicability of sub-T<sub>g</sub> enthalpy relaxations for technological purposes; revisit the concept of “water mobility” in light of theories recently formulated; and analysis of the “Jamming” concept in relation to water mobility in biological systems. Another topic that received particular attention was the availability of instrumentation to complement and/or replace the water monolayer concept.

The ISOPOW 11 Scientific Committee carefully designed the Technical Program with the invaluable collaboration of all ISOPOW Central Committee members, which at the time of the Symposium were:

Pilar Buera, Universidad de Buenos Aires, Argentina, President

Louis B. Rockland, Foodtech Research and Development, USA, Honorary President

Yrjö H. Roos, University College Cork, Ireland, Secretary

Peter J. Lillford, University of York, UK

Gustavo Fidel Gutiérrez López, Instituto Politécnico Nacional, Mexico, Lead Organizer

David Lechuga, Nektar Therapeutics, USA

David S. Reid, University of California, USA

Denise Simatos, Université de Bourgogne, France

Imad Farhat, Firmenich, Switzerland

Brad Anderson, University of Kentucky, USA

Jim Leslie, Consultant, UK

Jorge Welti-Chanes, Tecnológico de Monterrey, Mexico

Miang Hoong Lim, University of Otago, New Zealand

Norio Murase, Tokyo Denki University, Japan

Patrick Gervais, Université de Bourgogne, France

Tanaboon Sajjaanantakul, Kasetsart University, Thailand

The meeting was developed within a friendly atmosphere and fulfilled all the traditional requirements of the ISOPOW philosophy: a good number of participants who were simultaneously involved in all the activities of the symposium shared breaks and meals which allowed ample time for intellectual interactions. Also, as recommended to organizers in the previous ISOPOW meeting, the participation of students was stimulated and enhanced by awarding bursaries. Young attendees willingly and enthusiastically participated in all the academic activities and scientific discussions.

This reference book will be particularly useful to professionals and students working on water science mainly dealing with food, chemical, biological, and pharmaceutical systems. It has a total of 61 chapters divided in four sections: (1) Advances in the assessment of water state in food, biological, and pharmaceutical systems; (2) Applied research on thermodynamics and physiochemical concepts on water in pharmaceutical and food products; (3) Water in enzymatic and

microbiological processes; and (4) Research on water in biological, chemical, food, and pharmaceutical products. The first seven chapters are based on invited lectures providing a very appropriate framework for the following 54 contributions which are addressing in depth a broad number of topics.

We hope this book will become a worthy addition to the body of knowledge on the science of water in biological and chemical materials and readers will find in it balanced, systematic, and harmonized information.

México, México

México, México

Buenos Aires, Argentina

Monterrey, México

México, México

Pullman, WA, USA

Gustavo F. Gutiérrez-López

Liliana Alamilla-Beltrán

María del Pilar Buera

Jorge Welti-Chanes

Efrén Parada-Arias

Gustavo V. Barbosa-Cánovas

# Acknowledgements

The editors wish to express their gratitude to the following institutions, companies, and individuals who contributed to making this book possible:

To the *Instituto Politécnico Nacional* (IPN), Mexico; the *Escuela Nacional de Ciencias Biológicas* (ENCB-IPN), Mexico; the *Tecnológico de Monterrey* (ITESEM), México; the *Universidad de Buenos Aires* (Argentina); Washington State University, Pullman, USA; and the International Union of Food Science and Technology (IUFoST)

To our sponsors: IPN, ENCB-IPN, ITESM, IUFoST, CICATA-IPN, UAQ-México, Kasetsart University (Thailand), Government of Querétero Anton Paar-Mexico, *Coca-Cola de Mexico* and *Asociación de Asociación de Embotelladoras Mexicanas de Coca-Cola*, Yakult (Mexico), and Decagon Devices (Mexico).

To The ISOPOW former Central Committee for trusting Mexico as a convenient venue for carrying out ISOPOW 11 and for their constant support and encouragement; to the ISOPOW 11 Organizing Committee team for their efficient and most intensive work and support towards the preparation of this book. Thanks to Melissa Danae Velarde for image editing and processing; Jeannie C. Bagby, Washington State University, Pullman, USA, for editing process; to Amor Monroy, Darío Téllez, Raquel González, and Leticia Peña for helping the editors prepare the final version of this book by revising references, formatting the manuscript, and incorporating in the text the editorial comments.



# Contents

<b>The State of Water and Its Impact on Pharmaceutical Systems: Lipid-Based Drug Delivery Systems and Amorphous Solids . . . . .</b>	<b>1</b>
B.D. Anderson	
<b>Food Preservation by Nanostructures-Water Interactions Control . . . . .</b>	<b>15</b>
E. Flores-Andrade, E. Azuara-Nieto, C.I. Beristain-Guevara, A. Monroy-Villagrana, D.I. Téllez-Medina, L.A. Pascual-Pineda L. Alamilla-Beltrán, and G.F. Gutiérrez-López	
<b>Water and Food Appearance . . . . .</b>	<b>27</b>
M.P. Buera, A.E. Farroni, and L.M. Agudelo-Laverde	
<b>Maillard Reaction in Limited Moisture and Low Water Activity Environment . . . . .</b>	<b>41</b>
C.W. Wong, H.B. Wijayanti, and B.R. Bhandari	
<b>Carbohydrates and Proteins as Nonequilibrium Components of Biological Materials . . . . .</b>	<b>65</b>
Y.H. Roos	
<b>Low-Temperature Mobility of Water in Sugar Glasses: Insights from Thermally Stimulated Current Study . . . . .</b>	<b>75</b>
S. Ewing, A. Hussain, G. Collins, C. Roberts, and E. Shalaev	
<b>Functional Behavior of Different Food Components as Affected by Water and Physical State . . . . .</b>	<b>89</b>
A. Marabi, L. Forny, and A. Gianfrancesco	
<b>Effect of Different Components of Edible/Biodegradable Composite Films on Water Relationships in the Polymer Matrix . . . . .</b>	<b>101</b>
A. Chiralt, P. Talens, F.M. Monedero, and M.J. Fabra	

<b>Glass Transition Observed with Cross-Linked Dextrans Containing a Small Amount of Water . . . . .</b>	115
N. Ijima and N. Murase	
<b>Sensorially and Instrumentally Detected Antiplastizicing Effect of Water in Cornflakes . . . . .</b>	125
A.E. Farroni, S. Guerrero, and M.P. Buera	
<b>Characterization of a Hydrate–Dehydrate System with Critical Transitions in the Typical Range of Processing and Storage Conditions . . . . .</b>	135
A.D. Otte and R. Pinal	
<b>Viscoelastic Sorption Behavior of Starch and Gluten . . . . .</b>	149
M.B.J. Meinders and L. Oliver	
<b>Molecular Weight Effects on Enthalpy Relaxation and Fragility of Amorphous Carbohydrates . . . . .</b>	161
R.M. Syamaladevi, G.V. Barbosa-Cánovas, S.J. Schmidt, and S.S. Sablani	
<b>Effect of Dehydration Conditions on the Bulk and Surface Properties of the Resulting Dehydrated Products . . . . .</b>	175
Y. Zhang and M.T. Carvajal	
<b>Moisture Sorption Isotherms of Foods: Experimental Methodology, Mathematical Analysis, and Practical Applications . . . . .</b>	187
C. Caballero-Cerón, J.A. Guerrero-Beltrán, H. Mújica-Paz, J.A. Torres, and J. Welti-Chanes	
<b>Understanding Cryopreservation of Oyster Oocytes from a Physical Chemistry Perspective . . . . .</b>	215
M.H. Lim, L.F. Siow, and L. Salinas-Flores	
<b>The Role of Water in the Cryopreservation of Seeds . . . . .</b>	231
N.E. Zaritzky	
<b>Water Activity and Microorganism Control: Past and Future . . . . .</b>	245
A. López-Malo and S.M. Alzamora	
<b>On Modeling the Effect of Water Activity on Microbial Growth and Mortality Kinetics . . . . .</b>	263
M. Peleg, M.G. Corradini, and M.D. Normand	
<b>Importance of Halophilic and Halotolerant Lactic Acid Bacteria in Cheeses . . . . .</b>	279
G. Melgar-Lalanne, F. Morales-Trejo, Y. Rivera-Espinoza, and H. Hernández-Sánchez	

<b>Influence of Water Activity and Molecular Mobility on Peroxidase Activity in Solution . . . . .</b>	289
G. Sacchetti, L. Neri, G. Bertolo, D. Torreggiani, and P. Pittia	
<b>Phase Transitions in Sugars and Protein Systems: Study of Stability of Lysozyme in Amorphous Sugar Matrices . . . . .</b>	299
L.M. Martínez, M. Videa, F. Mederos, Y. de Moral, M. Mora, and Cristina Pérez	
<b>An Exhaustive Study on Physicochemical and Structural Changes During Drying of Apple Discs . . . . .</b>	311
S.M. Casim, M.F. Mazzobre, and S.M. Alzamora	
<b>Defining High and Low Spray Drying Temperatures for <i>Aloe vera</i> Gel . . . . .</b>	319
I.N. García-Luna, J. Porras-Saavedra, F. Vergara-Balderas, J. Welti-Chanes, G.F. Gutiérrez-López, and L. Alamilla-Beltrán	
<b>Mexican Plum (<i>Spondias purpurea</i> L.) Moisture Sorption Properties . . . . .</b>	329
J.A. Guerrero-Beltrán, F. Ruiz-Hernández, and J. Welti-Chanes	
<b>Antioxidant Activity of Microencapsulated <i>Capsicum annuum</i> Oily Extract Obtained by Spray Drying . . . . .</b>	337
A.Y. Guadarrama-Lezama, L. Alamilla-Beltrán, E. Parada-Arias, M.E. Jaramillo-Flores, G.F. Gutiérrez-López, and L. Dorantes-Álvarez	
<b>Physical-Chemical Properties and Microstructure of Agave Powders Obtained by Spray Drying . . . . .</b>	345
M.F. Fabela-Morón, J. Porras-Saavedra, R. Martínez-Velarde, A. Jiménez-Aparicio, M.L. Arenas-Ocampo, and L. Alamilla-Beltrán	
<b>Stabilization and Controlled Release of Invertase Through the Addition of Trehalose in Wet and Dried Alginate-Chitosan Beads . . . . .</b>	353
P.R. Santagapita, M.F. Mazzobre, and M.P. Buera	
<b>Rheology and Stability of Citral/Sugar Microemulsions . . . . .</b>	361
N. Sosa, C. Schebor, and O.E. Pérez	
<b>Response Surface Methodology to Assay the Effect of the Addition of Proteins and Hydrocolloids on the Water Mobility of Gluten-Free Pasta Formulations . . . . .</b>	367
V.J. Larrosa, G. Lorenzo, N.E. Zaritzky, and A.N. Califano	
<b>Effects of <math>a_w</math> Reduction and Type of Sugar in Rheological Behavior, Water Mobility, and Structural Changes in Apples . . . . .</b>	375
S. Vicente, A. Nieto, and S.M. Alzamora	

<b>Effect of Water Content on Thermo-Physical Properties and Freezing Times of Foods . . . . .</b>	<b>383</b>
M.V. Santos, V. Vampa, A.N. Califano, and N.E. Zaritzky	
<b>Influence of Fluid Concentration on Freezing-Point Depression and Thermal Conductivity of Frozen Physalis Juice . . . . .</b>	<b>393</b>
J. Telis-Romero, G.I. Giraldo-Gómez, H.A. Villa-Vélez, D.M. Cano-Higuita, and V.R.N. Telis	
<b>Freezing Rate Effect on Thermal Transition of Blueberries . . . . .</b>	<b>405</b>
P. Díaz-Calderón, O. Henríquez, J. Enrione, and S. Matiacevich	
<b>Glass Transition Temperature of Some Thai Fruits Using Differential Scanning Calorimetry: Influence of Annealing and Sugar Composition . . . . .</b>	<b>413</b>
S. Charoenrein, N. Harnkarnsujarit, N. Lowithun, and K. Rengsutthi	
<b>Effect of Emulsifier on Complex Formation and In Vitro Digestibility of Gelatinized Potato Starch . . . . .</b>	<b>421</b>
K. Kawai, S. Takato, and K. Kajiwara	
<b>Influence of Alcohols and Polyols on the Behavior of Aqueous Solutions of <math>\beta</math>-Lactoglobulin at pH 5.5 . . . . .</b>	<b>427</b>
G.I. Giraldo and C.M. Romero	
<b>Effects of Protein Conformational Modifications, Enthalpy Relaxation, and Interaction with Water on the Solubility of Milk Protein Concentrate Powder . . . . .</b>	<b>437</b>
E. Haque and B.R. Bhandari	
<b>Active Edible Films Based on Modified Corn Starch for Food Applications . . . . .</b>	<b>451</b>
T. Arredondo-Ochoa, Y.M. Márquez-Hernández, B.E. García-Almendárez, and C. Regalado	
<b>Influence of Moisture Content and Temperature on the Stability of a Dehydrated Probiotic Dairy Product Containing <i>Bifidobacterium infantis</i> or <i>Lactobacillus acidophilus</i> . . . . .</b>	<b>461</b>
G. Trujillo-de Santiago and C. Rojas-de Gante	
<b>Effect of Relative Humidity on Shrinkage and Color Changes in Dehydrated Strawberry . . . . .</b>	<b>469</b>
L.M. Agudelo-Laverde, N. Acevedo, C. Schebor, and M.P. Buera	
<b>Effect of Blanching and/or Osmotic Dehydration on Texture and Rheological Properties of Apple Tissue . . . . .</b>	<b>477</b>
A.B. García Loredo, S. Guerrero, and S.M. Alzamora	

<b>Water Activity Depression of Tejocote Fruit (<i>Crataegus pubescens</i>) Using Osmotic Solutions and Pressure Gradients . . . . .</b>	<b>485</b>
A. Valdez-Fragoso, J. Welti-Chanes, and H. Mújica-Paz	
<b>Prediction Approach to the Glass Transition Temperature of Amorphous Carbohydrate Polymer . . . . .</b>	<b>493</b>
K. Kawai, K. Fukami, P. Thanatukson, C. Viriyarattanasak, and K. Kajiwara	
<b>Effect of Sugars on the Release of Aroma Compounds in Model Systems . . . . .</b>	<b>499</b>
P. Pittia, P. Piccone, and M. Martuscelli	
<b>Wetting Behavior of Chitosan Solutions on Blueberry Epicarp With or Without Epicuticular Waxes . . . . .</b>	<b>509</b>
O. Skurys, P. Velásquez, and F. Osorio	
<b>Influence of Brine Concentration on Moisture and NaCl Transport During Meat Salting . . . . .</b>	<b>519</b>
C. Ozuna, J.A. Cárcel, J.V. García-Pérez, R. Peña, and A. Mulet	
<b>Relationship Between Electrical Conductivity and Water Activity of Starch-Water Composites . . . . .</b>	<b>527</b>
E. Morales-Sánchez, M.L. Reyes-Vega, M. Gaytán-Martínez, J.D. Figueroa-Cárdenas, and G. Velázquez	
<b>Water Content, <math>\alpha_w</math>, and Enzyme Activity (Xaa-Prolyl-Dipeptidyl Aminopeptidase) During the Germination Process of Cocoa Beans (<i>Theobroma cacao</i> L.) . . . . .</b>	<b>533</b>
M.L. Sánchez-Mundo, M.X. Quintanilla-Carvajal, C. Bautista-Muñoz, G.F. Gutiérrez-López, and M.E. Jaramillo-Flores	
<b>Water Fraction Effect in the Rheological Behavior of Jalapeño Pepper Pulp . . . . .</b>	<b>541</b>
F. Santoyo, J. Viganó, and J. Telis-Romero	
<b>Study of Water Quality Through Hydro-Chemical Signature in León, Guanajuato, Mexico . . . . .</b>	<b>549</b>
S.A. Cortés, G.A. Lozano, and J. Pérez	
<b>Calorimetric and Thermogravimetric Analysis of <i>Agave tequilana</i> Weber Fibers . . . . .</b>	<b>557</b>
C. De Dios-Naranjo, R. Mora-Escobedo, G.F. Gutiérrez-López, J. Solorza-Feria, A. Flores-Morales, H. Yee-Madeira, and L. Alamilla-Beltrán	

<b>Study of Allspice Fluidized Bed Drying (<i>Pimenta dioica</i> L. Merrill) by Biochemical and Structural Analysis . . . . .</b>	<b>567</b>
A.E. Carpinteyro-Díaz, I. Anaya-Sosa, M.T. Cruz y Victoria, and T. Santiago-Pineda	
<b>Refined Hemisphaericin Stabilization by Microencapsulation with Arabic Gum and Spray Drying . . . . .</b>	<b>575</b>
L.A. Reyes, M.I. Cortés-Vázquez, M.C. Oliver-Salvador, J. Yáñez-Fernández, and R. Briones-Martínez	
<b>Salt Crystallization in Chitosan Films as Affected by Solvent pH and Moisture Content . . . . .</b>	<b>585</b>
M. Vargas, C. González-Martínez, and A. Chiralt	
<b>Water Antiplasticization Effect in Biscuits as Affected by Glucose and Sucrose Addition . . . . .</b>	<b>593</b>
P. Pittia, G. Di Teodoro, and G. Sacchetti	
<b>Physicochemical Characterization of Regional Breads Produced in the Northern Mountains of Puebla State, Mexico . . . . .</b>	<b>605</b>
N. Güemes-Vera, S. Soto-Simental, M.I. Reyes-Santamaría, and J.F. Hernández-Chávez	
<b>Structural Relaxation of Salmon Gelatin Films in the Glassy State . . . . .</b>	<b>611</b>
J. Enrione, C. Sáez, D. López, O. Skurlys, and C. Acevedo	
<b>Relationship Between Raw Material Characteristics and Dehydration Parameters of Vegetables Dried Using a New Kind of Solar Dryer . . . . .</b>	<b>621</b>
G. Bertolo, A. Maestrelli, and M. Della Campa	
<b>Caking Process and Microstructural Changes of Wall Materials Used in Spray-Drying Process . . . . .</b>	<b>629</b>
J. Porras-Saavedra, E. Palacios-González, J. Yáñez-Fernández, M.F. Mazzobre, M.P. Buera, and L. Alamilla-Beltrán	
<b>Food Matrix Structure Quality Preservation: Water Removal Operation Conditions Control During Convective Drying . . . . .</b>	<b>637</b>
H. Necoechea-Mondragón, D.Y. Morales-Delgado, E. Parada-Arias, M. Cornejo-Mazón, and D.I. Téllez-Medina	
<b>Editors' Biographies . . . . .</b>	<b>647</b>
<b>Index . . . . .</b>	<b>649</b>

# Contributors

**C. Acevedo** Centro de Biotecnología, Universidad Técnica Federico Santa María, Valparaíso, Chile

**N. Acevedo** Departamento de Industrias, Facultad de Ciencias Exactas y Naturales, Universidad de Buenos Aires, Buenos Aires, Argentina

**L.M. Agudelo-Laverde** Departamento de Industrias y de Química Orgánica, Facultad de Ciencias Exactas y Naturales, Universidad de Buenos Aires, Buenos Aires, Argentina

**L. Alamilla-Beltrán** Escuela Nacional de Ciencias, Instituto Politécnico Nacional, México, D.F., México

**S.M. Alzamora** Departamento de Industrias, Facultad de Ciencias Exactas y Naturales, Universidad de Buenos Aires, Ciudad Universitaria, Buenos Aires, Argentina

**I. Anaya-Sosa** Departamento de Graduados e Investigación en Alimentos, Escuela Nacional de Ciencias Biológicas (IPN), México, D.F., Mexico

**B.D. Anderson** Department of Pharmaceutical Sciences, College of Pharmacy, University of Kentucky, Lexington, KY, USA

**M.L. Arenas-Ocampo** Centro de Desarrollo de Productos Bióticos, Instituto Politécnico Nacional, Yautepec, Morelos, Mexico

**T. Arredondo-Ochoa** DIPA, PROPAC, Facultad de Química, Universidad Autónoma de Querétaro, Querétaro, Qro, Mexico

**E. Azuara-Nieto** Instituto de Ciencias Básicas, Universidad Veracruzana, Xalapa, Veracruz, México

**G.V. Barbosa-Cánoyas** Biological Systems Engineering Department, Washington State University, Pullman, WA, USA

**C. Bautista-Muñoz** Laboratorio de Fisiología Vegetal y Biotecnología, Colegio de Posgraduados, Cárdenas, Mexico

**C.I. Beristain-Guevara** Instituto de Ciencias Básicas, Universidad Veracruzana, Xalapa, Veracruz, Mexico

**G. Bertolo** ACU, Associazione Consumatori Utenti, Milan, Italy

**B.R. Bhandari** School of Agriculture and Food Sciences, The University of Queensland, Brisbane, QLD, Australia

**R. Briones-Martínez** Laboratorio de Enzimas Vegetales, Centro de Desarrollo de Productos Bióticos del IPN, Yautepec, Morelos, Mexico

**M.P. Buera** Departamentos de Industrias, Facultad de Ciencias Exactas y Naturales, University of Buenos Aires, Argentina

National Council of Scientific and Technical Research (CONICET), Buenos Aires, Argentina

**C. Caballero-Cerón** Centro de Biotecnología FEMSA, Escuela de Biotecnología y Alimentos, Tecnológico de Monterrey, Monterrey, Nuevo León, Mexico

**A.N. Califano** Centro de Investigación y Desarrollo en Criotecnología de Alimentos (CIDCA), Facultad de Ciencias Exactas, UNLP-CONICET, La Plata, Argentina

**D.M. Cano-Higuita** Departamento de Engenharia e Tecnologia de Alimentos, Universidade Estadual Paulista, São José do Rio Preto, São Paulo, Brazil

**J.A. Cárcel** Grupo de Análisis y Simulación de Procesos Agroalimentarios, Departamento de Tecnología de Alimentos, Universitat Politècnica de València, Valencia, Spain

**A.E. Carpintero-Díaz** Departamento de Graduados e Investigación en Alimentos, Escuela Nacional de Ciencias Biológicas (IPN), México, D.F., Mexico

**M.T. Carvajal** Industrial and Physical Pharmacy and Agricultural and Biological Engineering, Purdue University, West Lafayette, IN, USA

**S.M. Casim** Departamento de Industrias, Facultad de Ciencias Exactas y Naturales, Universidad de Buenos Aires, Buenos Aires, Argentina

**S. Charoenrein** Department of food science and technology, Faculty of Agro-Industry, Kasetsart University, Bangkok, Thailand

**A. Chiralt** Institute of Food Engineering for Development, Department of Food Technology, Universitat Politecnica de Valencia, Camino de Vera, Valencia, Spain

**G. Collins** New Jersey Institute of Technology, Newark, NJ, USA

**M. Cornejo-Mazón** Departamento de Biofísica, Escuela Nacional de Ciencias Biológicas, Instituto Politécnico Nacional, Mexico, D.F., Mexico

**M.G. Corradini** Instituto de Tecnología, Facultad de Ingeniería y Ciencias Exactas, Universidad Argentina de la Empresa, Buenos Aires, Argentina

**S.A. Cortés** Instituto de Geofísica, Universidad Nacional Autónoma de México (UNAM), México, D.F., Mexico

**M.I. Cortés-Vázquez** Laboratorio de Enzimas Vegetales, Centro de Desarrollo de Productos Bióticos del IPN, Yautepec, Morelos, Mexico

**M.T. Cruz y Victoria** Departamento de Graduados e Investigación en Alimentos, Escuela Nacional de Ciencias Biológicas (IPN), México, D.F., Mexico

**M. Della Campa** Consiglio per la Ricerca e la Sperimentazione in Agricoltura, Unità di Ricerca per i Processi dell'Industria Agroalimentare C.R.A.-I.A.A, Milan, Italy

**P. Díaz** Departamento de Ciencias y Tecnología de Alimentos, Facultad Tecnológica, Universidad de Santiago de Chile, Santiago, Chile

**C. De Dios-Naranjo** Departamento de Graduados e Investigación en Alimentos, Escuela Nacional de Ciencias Biológicas, Instituto Politécnico Nacional, México, D.F., Mexico

**L. Dorantes-Álvarez** Departamento de Graduados e Investigación en Alimentos, Escuela Nacional de Ciencias Biológicas, Instituto Politécnico Nacional, México, D.F., Mexico

**J. Enrione** Escuela de Nutricion y Dietética, Facultad de Medicina, Universidad de los Andes, Av., Monseñor Álvaro del Portillo 12.455, Las Condes, Santiago, Chile

**S. Ewing** Pfizer Inc, Groton, CT, USA

**M.F. Fabela-Morón** Departamento de Graduados e Investigación en Alimentos, Escuela Nacional de Ciencias Biológicas, Instituto Politécnico Nacional, México, D.F., Mexico

Centro de Desarrollo de Productos Bióticos, Instituto Politécnico Nacional, Carretera Yautepec-Jojutla, Apartado Postal 24, Yautepec, Morelos, Mexico

**M.J. Fabra** Institute of Food Engineering for Development, Department of Food Technology, Universitat Politecnica de Valencia, Valencia, Spain

**A.E. Farroni** Departamentos de Industrias y de Química Orgánica, Facultad de Ciencias Exactas y Naturales, University of Buenos Aires (FCEyN-UBA), Buenos Aires, Argentina

Laboratorio de Calidad de Alimentos, Suelos y Agua, EEA, Pergamino, Instituto Nacional de Tecnología Agropecuaria, Pergamino, Buenos Aires, Argentina

**J.D. Figueroa-Cárdenas** CINVESTAV del IPN Unidad Querétaro, Querétaro, Mexico

**E. Flores-Andrade** Facultad de Ciencias Químicas, Universidad Veracruzana, Orizaba, Veracruz, Mexico

**A. Flores-Morales** Instituto Tecnológico del Altiplano de Tlaxcala, Tlaxcala, Mexico

**L. Forny** Nestlé Research Center, Lausanne, Switzerland

**K. Fukami** San-ei Sucrochemical Co., Ltd., Chita, Aichi, Japan

**B.E. García-Almendárez** DIPA, PROPAC, Facultad de Química, Universidad Autónoma de Querétaro, Querétaro, Qro, Mexico

**A.B. García Loredo** Departamento de Industrias, Facultad de Ciencias Exactas y Naturales, Universidad de Buenos Aires, Ciudad Universitaria, Buenos Aires, Argentina

**I.N. García-Luna** Escuela Nacional de Ciencias Biológicas-IPN, México, D.F., Mexico

**J.V. García-Pérez** Grupo de Análisis y Simulación de Procesos Agroalimentarios, Departamento de Tecnología de Alimentos, Universitat Politècnica de València, Valencia, Spain

**M. Gaytán-Martínez** CINVESTAV del IPN Unidad Querétaro, Querétaro, Mexico

**A. Gianfrancesco** Nestlé Research Center, Lausanne, Switzerland

**G.I. Giraldo-Gómez** Departamento de Física y Química, Universidad Nacional de Colombia, Manizales, Colombia

**C. González-Martínez** Departamento de Tecnología de Alimentos-Instituto Universitario de Ingeniería de Alimentos para el Desarrollo, Universidad Politécnica de Valencia, Valencia, Spain

**A.Y. Guadarrama-Lezama** Departamento de Graduados e Investigación en Alimentos, Escuela Nacional de Ciencias Biológicas, Instituto Politécnico Nacional, México, D.F., Mexico

**N. Güemes-Vera** Instituto de Ciencias Agropecuarias, Universidad Autónoma del Estado de Hidalgo, Tulancingo, Hidalgo, Mexico

**S. Guerrero** Departamento de Industrias, Facultad de Ciencias Exactas y Naturales, Universidad de Buenos Aires, Ciudad Universitaria, Buenos Aires, Argentina

Member of Consejo Nacional de Investigaciones, Científicas y Técnicas, República, Argentina

**J.A. Guerrero-Beltrán** Departamento de Ingeniería Química, Alimentos y Ambiental, Universidad de las Américas Puebla, Cholula, Puebla, Mexico

**G.F. Gutiérrez-López** Escuela Nacional de Ciencias, Biológicas, Instituto Politécnico Nacional, México, D.F., México

**N. Harnkarnsujarit** Department of food science and technology, Faculty of Agro-Industry, Kasetsart University, Bangkok, Thailand

**E. Haque** School of Applied Sciences, RMIT University, Melbourne, VIC, Australia

**O. Henríquez** Departamento de Ciencias y Tecnología de Alimentos, Facultad Tecnológica, Universidad de Santiago de Chile, Santiago, Chile

**J.F. Hernández-Chávez** Departamento de Ciencias Veterinarias y Agronómicas del, Instituto Tecnológico de Sonora, Ciudad Obregón, Sonora, Mexico

**H. Hernández-Sánchez** Departamento de Graduados e Investigación en Alimentos, Escuela Nacional de Ciencias Biológicas, Instituto Politécnico Nacional, México, D.F., Mexico

**A. Hussain** Pfizer Inc, Groton, CT, USA

New Jersey Institute of Technology, Newark, NJ, USA

**N. Ijima** Life Science and Engineering, Graduate School of Science and Engineering, Tokyo Denki University, Hatoyama-cho, Hiki-gun, Saitama, Japan

**M.E. Jaramillo-Flores** Departamento de Graduados e Investigación en Alimentos, Escuela Nacional de Ciencias Biológicas, Instituto Politécnico Nacional, México, D.F., Mexico

**A. Jiménez-Aparicio** Centro de Desarrollo de Productos Bióticos, Instituto Politécnico Nacional, Yautepec, Morelos, Mexico

**K. Kajiwara** Department of Bioscience and biotechnology, Tokyo University of Technology, Hachioji, Tokyo, Japan

**K. Kawai** Department of Biofunctional Science and Technology, Graduate School of Biosphere Science, Hiroshima University, Higashi-Hiroshima, Hiroshima, Japan

**V.J. Larrosa** Centro de Investigación y Desarrollo en Criotecnología de Alimentos (CIDCA), Facultad de Ciencias Exactas, UNLP-CONICET, La Plata, Argentina

**M.H. Lim** Department of Food Science, University of Otago, Dunedin, New Zealand

**D. López** Departamento de Ciencia y Tecnología de los Alimentos, Universidad de Santiago de Chile, Santiago, Chile

**A. López-Malo** Departamento de Ingeniería Química, Alimentos y Ambiental, Escuela de Ingeniería, Universidad de las Américas Puebla, Cholula, Puebla, Mexico

**G. Lorenzo** Centro de Investigación y Desarrollo en Criotecnología de Alimentos (CIDCA), Facultad de Ciencias Exactas, UNLP-CONICET, La Plata, Argentina

Departamento de Ingeniería Química, Facultad de Ingeniería, UNLP, La Plata, Argentina

**N. Lowithun** Department of Food Science and Technology, Faculty of Agro-Industry, Kasetsart University, Bangkok, Thailand

Institute of Food Research and Product Development, Kasetsart University, Bangkok, Thailand

**G.A. Lozano** Centro de Investigación en Ciencia Aplicada y Tecnología Avanzada (CICATA, Unidad Querétaro), Instituto Politécnico Nacional (IPN), Santiago de Querétaro, Querétaro, Mexico

**A. Maestrelli** Consiglio per la Ricerca e la Sperimentazione in Agricoltura, Unità di Ricerca per i Processi dell'Industria Agroalimentare C.R.A.-I.A.A, Milan, Italy

**A. Marabi** Nestlé Research Center, Lausanne, Switzerland

**Y.M. Márquez-Hernández** DIPA, PROPAC, Facultad de Química, Universidad Autónoma de Querétaro, Querétaro, Qro, Mexico

**L.M. Martínez** Department of Chemistry, Instituto Tecnológico y de Estudios Superiores de Monterrey, Monterrey, Nuevo León, Mexico

**R. Martínez-Velarde** Centro de Desarrollo de Productos Bióticos, Instituto Politécnico Nacional, Yautepec, Morelos, Mexico

**M. Martuscelli** Faculty of Bioscience and Technology for Food, Agriculture and Environment, University of Teramo, Mosciano S. Angelo, Teramo, Italy

**S. Matiacevich** Departamento de Ciencias y Tecnología de Alimentos, Facultad Tecnológica, Universidad de Santiago de Chile, Santiago, Chile

**M.F. Mazzobre** Departamentos de Industrias y de Química Orgánica, Facultad de Ciencias Exactas y Naturales, University of Buenos Aires (FCEyN-UBA). Consejo Nacional de Investigaciones científicas y Técnicas de la República Argentina. Ciudad Universitaria, (1428) C.A.B.A., Buenos Aires, Argentina

**F. Mederos** Department of Chemistry, Instituto Tecnológico y de Estudios Superiores de Monterrey, Monterrey, Nuevo León, Mexico

**M.B.J. Meinders** Top Institute Food & Nutrition, Wageningen, The Netherlands  
Wageningen University and Research Centre, Wageningen, The Netherlands

**G. Melgar-Lalanne** Departamento de Graduados e Investigación en Alimentos, Escuela Nacional de Ciencias Biológicas, Instituto Politécnico Nacional, México, D.F., Mexico

**F.M. Monedero** Institute of Food Engineering for Development, Department of Food Technology, Universitat Politecnica de Valencia, Valencia, Spain

**A. Monroy-Villagrana** Escuela Nacional de Ciencias Biológicas, Instituto Politécnico Nacional, México, D.F., Mexico

**M. Mora** Department of Chemistry, Instituto Tecnológico y de Estudios Superiores de Monterrey, Monterrey, Nuevo León, Mexico

**R. Mora-Escobedo** Departamento de Graduados e Investigación en Alimentos, Escuela Nacional de Ciencias Biológicas, Instituto Politécnico Nacional, México, D.F., Mexico

**Y. de Moral** Department of Chemistry, Instituto Tecnológico y de Estudios Superiores de Monterrey, Monterrey, Nuevo León, Mexico

**D.Y. Morales-Delgado** Departamento de Graduados e Investigación en Alimentos, Escuela Nacional de Ciencias Biológicas, Instituto Politécnico Nacional, Mexico, D.F., Mexico

**E. Morales-Sánchez** CICATA-IPN Querétaro, Querétaro, Mexico

**F. Morales-Trejo** Departamento de Graduados e Investigación en Alimentos, Escuela Nacional de Ciencias Biológicas, Instituto Politécnico Nacional, México, D.F., Mexico

**H. Mújica-Paz** Escuela de Ingeniería y Ciencias, Tecnológico de Monterrey, Monterrey, Nuevo León, Mexico

**A. Mulet** Grupo de Análisis y Simulación de Procesos Agroalimentarios, Departamento de Tecnología de Alimentos, Universitat Politècnica de València, Valencia, Spain

**N. Murase** Life Science and Engineering, Graduate School of Science and Engineering, Tokyo Denki University, Hatoyama-cho, Hiki-gun, Saitama, Japan

**H. Necoechea-Mondragón** Dirección de Investigación, Secretaría de Investigación y Posgrado, Instituto Politécnico Nacional, México, D.F., Mexico

**L. Neri** Department of Food Science, University of Teramo, Teramo, Italy

**A. Nieto** Departamento de Industrias, Facultad de Ciencias Exactas y Naturales, Universidad de Buenos Aires, Buenos Aires, Argentina

CONICET, Ciudad Universitaria, Ciudad Autonoma de Buenos Aires, Argentina

**M.D. Normand** Department of Food Science, University of Massachusetts, Amherst, MA, USA

**L. Oliver** Top Institute Food & Nutrition, Wageningen, The Netherlands

Instituto Universitario de Ingenieria de Alimentos para el Desarrollo, Universidad Politécnica de Valencia, Valencia, Spain

**M.C. Oliver-Salvador** Laboratorio de Biotecnología Alimentaria, Unidad Profesional Interdisciplinaria de Biotecnología del IPN, México, D.F., Mexico

**F. Osorio** Department of Food Science and Technology, Universidad de Santiago de Chile, Avenida Ecuador 3769, Santiago, Chile

**A.D. Otte** Department of Industrial and Physical Pharmacy, Purdue University, West Lafayette, IN, USA

**C. Ozuna** Grupo de Análisis y Simulación de Procesos Agroalimentarios, Departamento de Tecnología de Alimentos, Universitat Politècnica de València, Valencia, Spain

**E. Palacios-González** Laboratorio de Microscopía Electrónica de Ultra Alta Resolución (LAMEUAR), Instituto Mexicano del Petróleo, México, D.F., Mexico

**E. Parada-Arias** Departamento de Graduados e Investigación en Alimentos, Escuela Nacional de Ciencias Biológicas, Instituto Politécnico Nacional, México, D.F., México

**M. Peleg** Department of Food Science, University of Massachusetts, Amherst, MA, USA

**R. Peña** Grupo de Análisis y Simulación de Procesos Agroalimentarios, Departamento de Tecnología de Alimentos, Universitat Politècnica de València, Valencia, Spain

**O.E. Pérez** Departamento de Industrias, Facultad de Ciencias Exactas y Naturales, Universidad de Buenos Aires, Ciudad de Buenos Aires, Argentina

Consejo Nacional de Investigaciones Científicas y Técnicas de la República Argentina, CONICET, Ciudad de Buenos Aires, Argentina

**J. Pérez** Centro de Geociencias, Universidad Nacional Autónoma de México (UNAM), Querétaro, Mexico

**P. Piccone** Faculty of Bioscience and TEchnology for Food, Agriculture and Environment, University of Teramo, Teramo, Italy

**R. Pinal** Department of Industrial and Physical Pharmacy, Purdue University, West Lafayette, IN, USA

**P. Pittia** Faculty of Bioscience and TEchnology for Food, Agriculture and Environment, University of Teramo, Teramo, Italy

**J. Porras-Saavedra** Departamento de Graduados e Investigación en Alimentos, Escuela Nacional de Ciencias Biológicas, Instituto Politécnico Nacional, México, D.F., Mexico

**M.X. Quintanilla-Carvajal** Departamento de Graduados e Investigación en Alimentos, Escuela Nacional de Ciencias Biológicas, Instituto Politécnico Nacional, México, D.F., Mexico

**C. Regalado** DIPA, PROPAC, Facultad de Química, Universidad Autónoma de Querétaro, Querétaro, Qro, Mexico

**L.A. Reyes** Laboratorio de Biotecnología Alimentaria, Unidad Profesional Interdisciplinaria de Biotecnología del IPN, México, D.F., Mexico

**M.I. Reyes-Santamaria** Instituto de Ciencias Agropecuarias, Universidad Autónoma del Estado de Hidalgo, Tulancingo, Hidalgo, Mexico

**M.L. Reyes-Vega** CICATA-IPN Querétaro, Querétaro, Mexico

UAC, Posgrado en Alimentos, Saltillo, Mexico

**K. Rengsutthi** Department of food science and technology, Faculty of Agro-Industry, Kasetsart University, Bangkok, Thailand

**Y. Rivera-Espinoza** Departamento de Graduados e Investigación en Alimentos, Escuela Nacional de Ciencias Biológicas, Instituto Politécnico Nacional, México, D.F., Mexico

**C. Roberts** Department of Chemical Engineering, University of Delaware, Newark, DE, USA

**C. Rojas-de Gante** Instituto Tecnológico y de Estudios Superiores de Monterrey, Monterrey, Nuevo León, Mexico

**C.M. Romero** Departamento de Química, Universidad Nacional de Colombia, Bogotá, Colombia

**Y.H. Roos** Food Technology, School of Food and Nutritional Sciences, University College Cork, Cork, Ireland

**F. Ruiz-Hernández** Departamento de Ingeniería Química, Alimentos y Ambiental, Universidad de las Américas Puebla, Cholula, Puebla, Mexico

**S.S. Sablani** Biological Systems Engineering Department, Washington State University, Pullman, WA, USA

**G. Sacchetti** Department of Food Science, University of Teramo, Teramo, Italy

**C. Sáez** Escuela de Nutrición y Dietética, Facultad de Medicina, Universidad de los Andes, Av. Monseñor Álvaro del Portillo 12.455, Las Condes, Santiago, Chile

**L. Salinas-Flores** Department of Food Science, University of Otago, Dunedin, New Zealand

**M.L. Sánchez-Mundo** Departamento de Graduados e Investigación en Alimentos, Escuela Nacional de Ciencias Biológicas-Instituto Politécnico Nacional, México, D.F., Mexico

**P.R. Santagapita** Departamentos de Industrias y de Química Orgánica, Facultad de Ciencias Exactas y Naturales, University of Buenos Aires (FCEyN-UBA).

National Council of Scientific and Technical Research (CONICET), Buenos Aires, Argentina

National Council of Scientific and Technical Research (CONICET), Buenos Aires, Argentina

**T. Santiago-Pineda** Facultad de Ciencias Químicas, Universidad Veracruzana, Orizaba, Veracruz, Mexico

**M.V. Santos** Centro de Investigación y Desarrollo en Criotecnología de Alimentos (CIDCA), Facultad de Ciencias Exactas, UNLP-CONICET La Plata, La Plata, Argentina

Departamento de Ingeniería Química, Facultad de Ingeniería, UNLP, La Plata, Argentina

**F. Santoyo** Departamento de Ciencias Exactas, Tecnologías y Metodologías, CUSur, Universidad de Guadalajara, Ciudad Guzmán, Jalisco, Mexico

**C. Schebor** Departamento de Industrias, Universidad de Buenos Aires, Ciudad Universitaria, Ciudad de Buenos Aires, Argentina

Departamento de Química Orgánica, Facultad de Ciencias Exactas y Naturales, Universidad de Buenos Aires, Ciudad Universitaria, Ciudad de Buenos Aires, Argentina

Consejo Nacional de Investigaciones Científicas y Técnicas de la República Argentina, CONICET, Ciudad de Buenos Aires, Argentina

**S.J. Schmidt** Food Science and Human Nutrition, University of Illinois at Urbana Champaign, Urbana, IL, USA

**E. Shalaev** Pfizer Inc, Groton, CT, USA

Allergan Inc, Irvine, CA, USA

**L.F. Siew** School of Science, Monash University, Kuala Lumpur, Malaysia

**O. Skurlys** Department of Mechanical Engineering, Universidad Técnica Federico Santa María, Santiago, Chile

**J. Solorza-Feria** Centro de Desarrollo de Productos Bióticos, Instituto Politécnico Nacional, Yautepec, Morelos, Mexico

**N. Sosa** Departamento de Industrias, Universidad de Buenos Aires, Ciudad de Buenos Aires, Argentina

Departamento de Química Orgánica, Facultad de Ciencias Exactas y Naturales, Universidad de Buenos Aires, Ciudad de Buenos Aires, Argentina

Departamentos de Industrias y de Química Orgánica, Facultad de Ciencias Exactas y Naturales, University of Buenos Aires (FCEyN-UBA), National Council of Scientific and Technical Research (CONICET), Buenos Aires, Argentina

**S. Soto-Simental** Instituto de Ciencias Agropecuarias, Universidad Autónoma del Estado de Hidalgo, Tulancingo, Hidalgo, Mexico

**R.M. Syamaladevi** Biological Systems Engineering Department, Washington State University, Pullman, WA, USA

**S. Takato** Department of Bioscience and biotechnology, Tokyo University of Technology, Hachioji, Tokyo, Japan

**P. Talens** Institute of Food Engineering for Development, Department of Food Technology, Universitat Politècnica de Valencia, Valencia, Spain

**V.R.N. Telis** Departamento de Engenharia e Tecnologia de Alimentos, Universidade Estadual Paulista, São José do Rio Preto, São Paulo, Brazil

**J. Telis-Romero** Departamento de Engenharia e Tecnología de Alimentos, Universidade Estadual Paulista, São José do Rio Preto, São Paulo, Brazil

**D.I. Téllez-Medina** Departamento de Graduados e Investigacion en Alimentos, Escuela Nacional de Ciencias Biologicas, Instituto Politécnico Nacional, Carpio y Plan de Ayala s/n, Mexico City, Mexico

**G. Di Teodoro** Department of Food Science, University of Teramo, Teramo, Italy

**P. Thanatuksorn** School of Bioscience and Biotechnology, Tokyo University of Technology, Hachioji, Tokyo, Japan

**D. Torreggiani** CRA, Milan, Italy

**J.A. Torres** Food Process Engineering Group, Department of Food Science and Technology, Oregon State University, Corvallis, OR, USA

**G. Trujillo-de Santiago** Instituto Tecnológico y de Estudios Superiores de Monterrey, Monterrey, Nuevo León, Mexico

**A. Valdez-Fragoso** Escuela de Ingeniería y Ciencias, Tecnológico de Monterrey, Monterrey, Nuevo León, Mexico

**V. Vampa** Departamento de Ciencias Básicas, Facultad de Ingeniería, UNLP, La Plata, Argentina

**M. Vargas** Departamento de Tecnología de Alimentos-Instituto Universitario de Ingeniería de Alimentos para el Desarrollo, Universidad Politécnica de Valencia, Valencia, Spain

**P. Velásquez** Departamento de Ingeniería Química y Bioprocessos, Pontificia Universidad Católica de Chile (PUC), Santiago, Chile

**G. Velázquez** CICATA-IPN Querétaro, Querétaro, Mexico

**F. Vergara-Balderas** Universidad de las Américas (UDLA), Cholula, Puebla, Mexico

**S. Vicente** ANPCyT, Universidad de Buenos Aires, Buenos Aires, Argentina

Departamento de Industrias, Facultad de Ciencias Exactas y Naturales, Universidad de Buenos Aires, Buenos Aires, Argentina

**M. Videu** Department of Chemistry, Instituto Tecnológico y de Estudios Superiores de Monterrey, Monterrey, Nuevo León, Mexico

**J. Viganó** Departamento de Engenharia e Tecnologia de Alimentos, Universidade Estadual Paulista, São José do Rio Preto, São Paulo, Brazil

**H.A. Villa-Vélez** Departamento de Engenharia e Tecnologia de Alimentos, Universidade Estadual Paulista, São José do Rio Preto, São Paulo, Brazil

**C. Viriyattanasak** School of Bioscience and Biotechnology, Tokyo University of Technology, Hachioji, Tokyo, Japan

**J. Welti-Chanes** Escuela de Ingeniería y Ciencias, Tecnológico de Monterrey, Av. Eugenio Garza Sada 2501 Sur, Col. Tecnológico, Monterrey, México

**H.B. Wijayanti** School of Agriculture and Food Sciences, The University of Queensland, Brisbane, QLD, Australia

**C.W. Wong** School of Agriculture and Food Sciences, The University of Queensland, Brisbane, QLD, Australia

**J. Yáñez-Fernández** Departamento de Bioingeniería de la Unidad Profesional Interdisciplinaria de Biotecnología, Instituto Politécnico Nacional. Av. Acueducto s/n, Barrio la Laguna Ticomán, Mexico City, Mexico

**H. Yee-Madeira** Escuela Superior de Física y Matemáticas-Instituto Politécnico Nacional. Ave. Instituto Politécnico Nacional S/N, San Pedro Zacatenco, C.P. 07738, México, D.F., México

**N.E. Zaritzky** Centro de Investigación y Desarrollo en Criotecnología de Alimentos (CIDCA), Facultad de Ciencias Exactas, UNLP-CONICET, La Plata, Argentina

Departamento de Ingeniería Química, Facultad de Ingeniería, UNLP, La Plata, Argentina

**Y. Zhang** Industrial and Physical Pharmacy and Agricultural and Biological Engineering, Purdue University, West Lafayette, IN, USA

# The State of Water and Its Impact on Pharmaceutical Systems: Lipid-Based Drug Delivery Systems and Amorphous Solids

B.D. Anderson

## Abbreviations

DOPC	1,2-Dioleoyl- <i>sn</i> -glycero-3-phosphocholine
IMC	Indomethacin
MD	Molecular dynamics
PVAc	Polyvinylacetate
PVP	Polyvinylpyrrolidone
RH	Relative humidity

## 1 Introduction

Physicochemical properties relevant to aqueous pharmaceutical formulations such as drug solubility and stability have clearly been a focal point of research for many decades. As a result, pharmaceutical scientists have access to a large body of knowledge that provides a framework for understanding the properties of drugs in aqueous solution, such as the kinetics and mechanisms of their degradation, solubility as influenced by ionizable substituents and various solution equilibria, etc. However, most drug products are manufactured, stored, and most frequently administered as solid formulations (e.g., tablets, capsules, suppositories, polymer implants, transdermal patches) rather than as aqueous solutions or suspensions. For these nonaqueous systems, the state of current understanding of the equilibria and kinetics that govern performance is less advanced. Recently, interest in various nonaqueous delivery systems has been increasing because, as drug potency has

---

B.D. Anderson (✉)

Department of Pharmaceutical Sciences, College of Pharmacy, University of Kentucky,  
Lexington, KY 40506, USA  
e-mail: [bande2@email.uky.edu](mailto:bande2@email.uky.edu)

received greater emphasis during the selection of new drug candidates, the lead compounds emerging from these selection processes tend to be more lipophilic and less water soluble. Consequently, a variety of amorphous or lipid-based delivery systems such as self-emulsifying or self-microemulsifying lipid dispersions often administered in soft gelatin capsule form for oral delivery are now being considered for commercialization. Similarly, various types of colloidal or nanoparticle formulations (e.g., nanosuspensions, solid-lipid nanoparticles, liposomes, micelles, polymeric micelles) in which the drug is suspended as a nano-sized particle or incorporated into a lipid particle have become increasingly attractive as possible vehicles for enhancing the bioavailability of orally administered drugs having poor water solubility, controlling drug release, enabling intravenous injection of nearly insoluble compounds, reducing side effects after intravenous administration, and in some cases providing enhanced permeability and retention in tumor tissue for the treatment of cancer.

In all of the aforementioned solid formulations, lipid dispersions, and nanoparticle or colloidal systems, the drug molecules may reside largely in a nonaqueous environment. Nevertheless, water is ever present in such environments and may have an impact on the formulation properties that is disproportionate in terms of the wt% of water present. Removing all water from a product and preventing atmospheric moisture from diffusing into a product are virtually impossible. The small size of a water molecule enhances its diffusivity through packaging materials and the drug formulation matrix, while the low molecular weight of water means that even trace quantities of water may represent a significant molar percentage in relation to the active pharmaceutical ingredient.

After administration of one of the above solid or lipid-based drug delivery systems to a patient, the uptake of water into the formulation matrix and its interactions with various components of the formulation remain of interest but for quite different reasons. In such cases, water is no longer a contaminant to be avoided. Rather, it becomes essential in facilitating dispersion of the delivery system and ultimately governs the kinetics of drug release and overall bioavailability. Many lipid dispersions and amorphous solid dispersions have recently been designed with the intent of producing supersaturated aqueous solutions of the drug after their administration in order to promote oral bioavailability. For these systems, understanding how to optimize performance extends beyond knowledge of their equilibrium properties and will ultimately require a deeper understanding of the dynamics of water uptake and the effect of water on other processes that influence delivery system performance.

Our laboratory has been employing both experiments and molecular dynamics (MD) computer simulations to address a number of questions relating to the state of water and its impact on the performance of lipid-based delivery systems and amorphous solid matrices useful for pharmaceutical formulations (Anderson and Marra 1999; Cao et al. 2004; Xiang and Anderson 2004, 2005, 2013; Rane and Anderson 2008a, b; Anderson et al. 2010). Some of these questions relate to the state of water in lipid-based formulations and amorphous solids. For example: (1) What factors govern the extent and rate of H<sub>2</sub>O uptake?; (2) Where are water molecules

located and how is the water organized?; (3) Do sorbed water molecules alter the local structure of the matrix?; and (4) Does the presence of water alter the solvent characteristics of the amorphous or lipid matrix, possibly leading to either enhanced solubility or perhaps unwanted phase transformations?

For a number of years, we have also had interest in various properties of lipid bilayer membranes, such as the influence of lipid composition and permeant structure on permeant binding to bilayer membranes (Xiang and Anderson 1994a, 1999; Xiang et al. 2006; Tejwani et al. 2010, 2011) and membrane transport (Xiang et al. 1992; Xiang and Anderson 1993, 1994b, c, 1995a, b, 1997, 1998a, b, 2002, 2006; Mayer 2001; Mayer and Anderson 2002; Mayer et al. 2003) and the design of liposomal drug delivery systems with optimal loading and release characteristics (Joguparthi and Anderson 2008a, b; Joguparthi et al. 2008a, b; Modi et al. 2012). Particularly relevant to the present discussion are these questions: (1) Where does water reside in lipid bilayers?; (2) How does the presence of water in the lipid bilayer influence drug binding and permeability? These questions will be addressed in this review through a combination of experiments and molecular dynamics computer simulations, which can shed light on the molecular phenomena underlying the experimental observations.

## 2 Molecular Dynamics Simulations

Molecular dynamics simulations as performed in this laboratory involve the construction of an ensemble of the molecules of interest within a supercomputer. The complete atomic detail of the molecules comprising the system of interest is represented. Typically, the ensemble includes molecules of a polymer excipient, lipid, or membrane matrix along with a small number of solute (drug) molecules and perhaps several water molecules. For each atom in the ensemble, Newton's equations of motion are integrated over time to obtain information on position, velocity, and acceleration of each atom subject to certain constraints reflecting the forces acting on each atom as obtained from a potential function ( $U$ ), as shown below:

$$U = \sum_{\text{bonds}} \frac{k_{ij}^b}{2} \left( r_{ij} - r_{ij}^{\text{eq}} \right)^2 + \sum_{\text{angles}} \frac{k_{ijk}^\theta}{2} \left( \theta_{ijk} - \theta_{ijk}^{\text{eq}} \right)^2 + \sum_{\text{dihedrals}} k^d [1 + \cos(n(\phi - \phi^{\text{eq}}))] + \sum_{i < j} \left[ \frac{A_{ij}}{r_{ij}^{12}} - \frac{B_{ij}}{r_{ij}^6} + \frac{q_i q_j}{4\pi\epsilon_0 r_{ij}} \right]$$

The terms in the above equation refer to contributions due to covalent bond energies, bond angles, dihedrals, and intermolecular van der Waals and electrostatic interactions. Numerous references available can provide further details on the potential function or molecular dynamics simulations in general (see, for example, Allen 2004 and Tieleman et al. 1997).

### 3 Water Uptake, Distribution, and Effects on Drug Solubility in Lipid Vehicles Composed of Triglycerides and Monoglycerides

In several recent publications, we have addressed drug solubility, water uptake, and the state of water in various mono-, di-, or triglycerides or their mixtures that have been popular formulation components for use in lipid-based drug delivery systems (Anderson and Marra 1999; Cao et al. 2004; Rane et al. 2008; Rane and Anderson 2008a, b; Anderson et al. 2010). Typical lipid-based delivery vehicles contain triglycerides of varying chain length combined with surfactants/emulsifiers such as long-chain carboxylic acids, mono- and diglycerides, phospholipids, or pegylated versions of these compounds. Water-soluble organic solvents such as polyethylene glycol or glycerol may also be included. Shown in Fig. 1 are the structures of a medium-chain triglyceride (tricaprylin) and two medium-chain monoglycerides (monocaprylin and monocaprin) often used in lipid-based formulations. These lipids were employed in experimental studies in our laboratory, aimed at understanding the specific intermolecular interactions that govern water uptake into these lipid solvents. As shown by the phase diagram in Fig. 1, Friberg and Mandell (1970) demonstrated that mixtures containing monocaprylin and tricaprylin form microemulsions upon dilution with water. Similar behavior would be expected in the stomach after administration of a pre-concentrate to

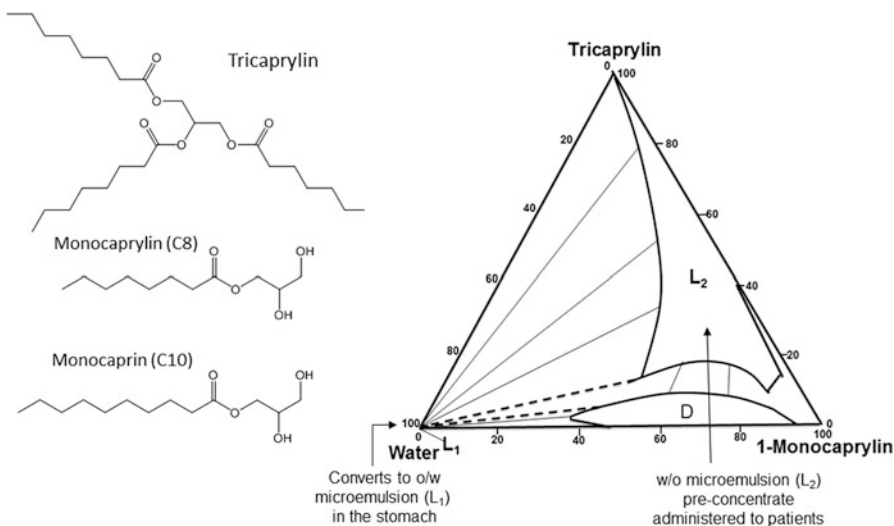


**Fig. 1** Molecular structures of tricaprylin, monocaprylin, and monocaprin used as model lipids for studies of water uptake and solubility. The phase diagram for systems containing varying percentages of tricaprylin, monocaprylin, and water from Friberg and Mandell (1970) illustrates the microemulsion formation that occurs when mixtures of tricaprylin and monocaprylin contain small percentages of water. *Right panel* reprinted with kind permission from Springer Science + Business Media: J Am Oil Chem Soc, Phase equilibria and their influence on the properties of emulsions, 47 (5), 1970, 149–152, Friberg S, Mandell L, figure number 2

patients. Thus, the dynamics of water uptake into these solvent mixtures leading to the formation of stable microemulsion particles and the thermodynamics associated with their stability and solvent characteristics are important features underlying their use in enhancing oral drug bioavailability.

Given the diversity and complexity of such lipid mixtures, simple quantitative principles that govern water uptake, its organization, its effects on organization of the lipids, and its effects on the solubility of drugs in lipid formulations would be desirable to elucidate. We have been interested, in particular, in the important role of hydrogen bonding, both in determining water uptake and its organization in lipid mixtures. Figure 2 (left panel) illustrates the water uptake as a function of monoglyceride concentration in triglyceride/monoglyceride mixtures at 37 °C and 100 % relative humidity, either in the presence of an added solute (benzamide) at its saturation solubility or in the absence of solute. Triglycerides consisting of tricaprylin and monoglycerides consisting of either monocaprylin (C8) or monocaprin (C10) were employed. Water content increased approximately linearly with the relative humidity (Rane et al. 2008) and, as evidenced by the profiles, was similar at the same molar concentration of either monoglyceride, indicating that the most important variable is the molar concentration of hydroxyl groups in the lipid mixture. The effects of monoglyceride concentration and water uptake on the solubility of benzamide are shown in the right panel of Fig. 2. An increase in the concentration of monoglyceride in the lipid mixture resulted in corresponding increases in benzamide solubility. As benzamide is an amide-containing solute, this enhanced solubility is likely due to the formation of hydrogen bonds between the amide carbonyl and hydroxyl groups in the lipid mixtures. As shown by the

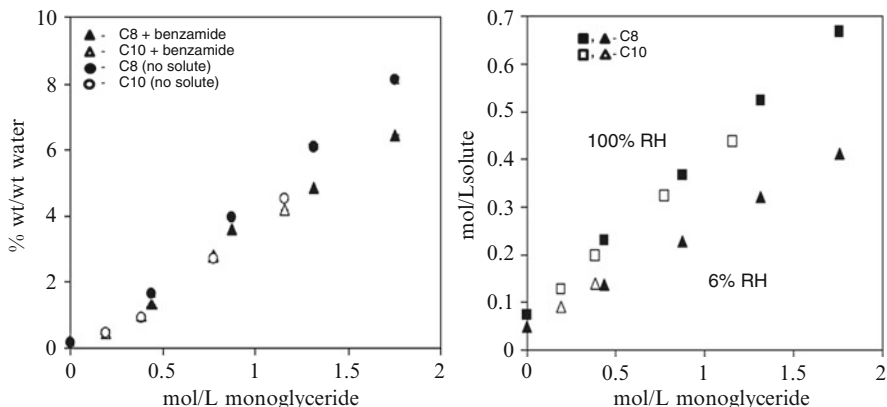


**Fig. 2** Left panel: Water uptake as a function of monoglyceride concentration at 37 °C in monocaprylin (C8)/tricaprylin or monocaprin (C10)/tricaprylin mixtures in the absence of solute or saturated with benzamide. Right panel: Benzamide solubility as a function of monoglyceride concentration in monocaprylin (C8)/tricaprylin or monocaprin (C10)/tricaprylin mixtures at 100 % or 6 % relative humidity. Reprinted with kind permission from Springer Science + Business Media: Pharm Res, Quantitative Solubility Relationships and the Effect of Water Uptake in Triglyceride/Monoglyceride Microemulsions, 25 (5), 2007, 1158–1174, Rane SS, Cao Y, Anderson BD, figure numbers 1B (left panel) and slight modification of figure 2A (right panel)

higher benzamide solubility in these lipid mixtures at a high relative humidity (RH) of 100 % compared to relatively dry conditions (6 % RH), water uptake also enhances the solubility of benzamide. Surprisingly, however, the presence of benzamide at saturation concentrations did not appear to influence water uptake. As shown by the left panel in Fig. 2, water uptake was either the same or perhaps slightly lower in lipid mixtures saturated with benzamide.

Molecular dynamics computer simulations may provide valuable insights into molecular interactions in lipid mixtures. We conducted MD simulations in a lipid mixture containing 60 % tricaprylin and 40 % monopalmitin that was saturated with water, a system that coincides with one of the compositions examined in experimental studies. These simulations employed 111 molecules of monopalmitin, 77 molecules of tricaprylin, and 219 molecules of TIP3P water with a single molecule of benzamide solute (Rane and Anderson 2008b).

A snapshot of the distribution of water molecules taken from one of these simulations is shown in Fig. 3. Most striking is the fact that the water molecules are not uniformly distributed in the lipid mixture. Rather, most of the water molecules reside in interconnecting clusters wherein they are hydrogen bonded to each other. Individual water molecules within each cluster were tracked over time, which revealed that individual water molecules within each cluster were highly mobile, but excursions of individual molecules between clusters were much less frequent.

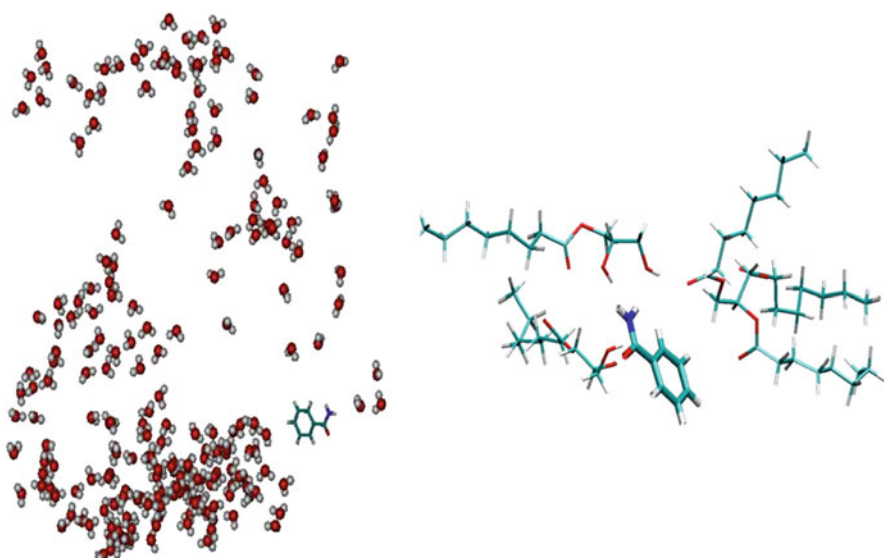


**Fig. 3** *Left panel:* Snapshot from a molecular dynamics simulation showing the distribution of water molecules in a water saturated 60 % tricaprylin/40 % monopalmitin lipid mixture at 37 °C. Water molecules are rarely found to be hydrogen bonded to the single molecule of benzamide. *Right panel:* Monopalmitin chains hydrogen bonded to benzamide

Gradually, individual water clusters would shrink or expand as others contracted. Radial distribution functions indicated that the lipid environment surrounding individual water clusters was enriched in hydroxyl and carbonyl groups and somewhat depleted in alkyl chain atoms, indicative of hydrogen bonding between polar functional groups in the lipid chains and water molecules within the cluster.

The significant influence of water content on the solubility of benzamide (Fig. 2) suggests that it may be important to carefully control the water content in lipid formulations to ensure the desired drug solubility. For benzamide, the solubility enhancement that was found experimentally at high relative humidity would be consistent with the expectation that water molecules would enhance benzamide's solubility through hydrogen bonding, but the MD simulation snapshot shown in Fig. 3 indicated that benzamide was generally far removed from any water clusters. During the entire dynamic simulation (30 ns) monomers of water would only occasionally localize in the vicinity of the benzamide molecule, forming a hydrogen bond with the benzamide carbonyl. The amide nitrogen typically formed hydrogen bonds with adjacent lipid oxygen atoms. There was at most one water molecule interacting with benzamide at any given time. Thus, the enhancement in the solubility of benzamide with increasing water content may not simply reflect an increase in benzamide-water hydrogen bonding.

#### 4 Water Uptake and Its Implications in an Amorphous Glass (PVP)

Unlike moisture uptake in crystals, where stepwise changes in water content occur with increasing relative humidity due to formation of stoichiometric hydrates, water uptake in amorphous solids increases in a continuous fashion with relative humidity, though the increases are not typically linear. Studies of moisture uptake in polyvinylpyrrolidone (PVP), polyvinylacetate (PVAc), and their copolymers (Taylor et al. 2001) demonstrated an important role of the functional group composition of the polymer in determining water affinity. PVP exhibits substantially greater water affinity than PVAc, presumably due to the greater hydrogen-bond accepting ability of the amide carbonyl in PVP. The water uptake obtained in PVP/PVAc copolymers was close to that predicted assuming additivity of the functional group contributions from the individual PVP and PVAc chains, as expected if hydrogen bond formation were the dominant factor governing water uptake.

Molecular interactions such as hydrogen bonding may be significantly affected, however, by the degree of metastability of a given amorphous glass. Dawson et al. (2009) recently found substantial differences in the water uptake profiles for an ordinary indomethacin (IMC) glass prepared by cooling, an annealed glass, and a more stable glass prepared by vapor deposition, with the more stable glass exhibiting a fivefold lower moisture uptake than an ordinary glass. Dramatic differences in the rates of water uptake were also noted. The authors speculated

that water sorption into indomethacin is driven by hydrogen bonding and that in stable IMC glasses, more hydrogen bonds are formed between IMC molecules themselves, leaving fewer hydrogen-bonding sites available for water molecules. This competition would account for the reduced water uptake in more stable IMC glasses. Physical aging of trehalose for 120 h at 373 K resulted in a decrease in equilibrium moisture uptake from 1.4 to 0.8 % at 10 % relative humidity (Surana et al. 2004), again suggesting that water uptake in amorphous solids depends not only on the functional groups present in the amorphous material but also on their availability for interaction with water.

We have recently conducted an MD simulation of an amorphous indomethacin glass to investigate various structural and dynamic properties, including the interactions of water with IMC. The assembly consisted of 105 indomethacin molecules and 12 water molecules, corresponding to a water content of 0.6 % w/w (Xiang and Anderson 2012). At this relatively low water content, >90 % of the water molecules at any given time formed 1–3 hydrogen bonds with indomethacin with probabilities of  $0.36 \pm 0.13$ ,  $0.28 \pm 0.07$ , and  $0.29 \pm 0.10$ , respectively. Figure 4 (left panel) is a snapshot of the distribution of water molecules in IMC indicating that, even at 0.6 % w/w water content, some water dimers co-exist with monomers. The right panel in Fig. 4 shows the probability distribution for either the IMC carboxylic acid group or water to donate a hydrogen to various atoms. Water molecules acting as hydrogen donors have a similar tendency to form hydrogen bonds with the IMC benzoyl C=O ( $39 \pm 8$  %) and the carboxylic acid C=O ( $37 \pm 12$  %) with a smaller percentage forming hydrogen bonds at the OCH<sub>3</sub> group ( $12 \pm 6$  %) or with other water molecules ( $12 \pm 9$  %).

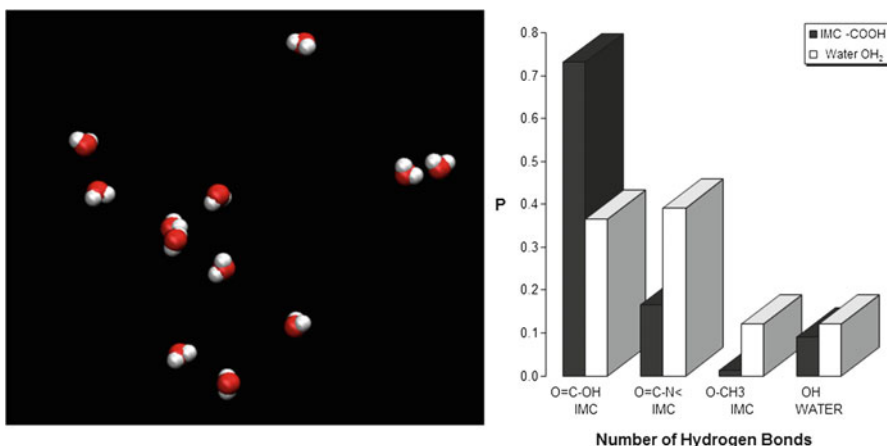


**Fig. 4** *Left panel:* A representative snapshot showing the water distribution in an amorphous IMC glass at 298 K. *Right panel:* Probability distributions for different HB acceptor sites to form hydrogen bonds with either the IMC –COOH (black) or the water H–O groups (white) in the simulated IMC glass at 298 K

Several investigators have examined the state of water in amorphous PVP, with the following general conclusions. Lebedeva et al. (1999) determined from FTIR spectra of sorbed water in PVP at lower water contents that water molecules were predominantly hydrogen bonded to PVP carbonyl oxygen atoms. At higher water concentrations, experimental data suggest that water self-associates in PVP. For example, Taylor et al. concluded from peak shifts in the Raman spectra for the PVP carbonyl and water at various relative humidities that some water molecules were hydrogen bonded directly to the polymer, while additional water molecules were hydrogen bonded to each other (Taylor et al. 2001).

Our group has also conducted molecular dynamics simulations to explore the distribution and plasticization effects of water, along with other phenomena in PVP polymer assemblies containing six PVP chains (each having 40 monomers) with 8–167 water molecules, corresponding to approximately 0.5 % and 10 % w/w water, respectively (Xiang and Anderson 2004, 2005). Consistent with the experimental evidence, we found that at higher water content, water self-associates to form hydrogen-bonded strands or clusters, similar to the pattern previously observed in lipid mixtures. As shown in Fig. 5, this tendency for water to

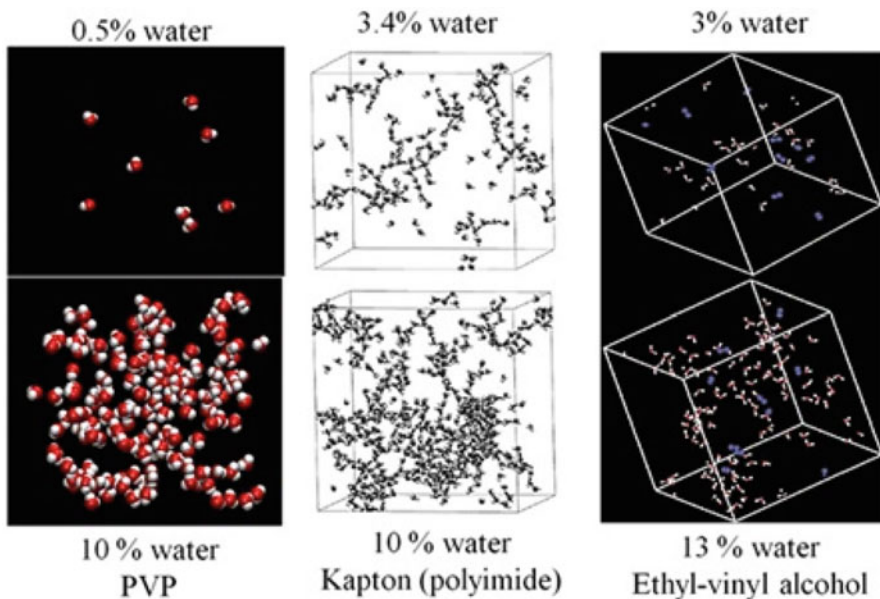


**Fig. 5** Water clustering with increasing water content as demonstrated in molecular dynamics simulations in various polymers. *Left panel* reprinted with kind permission from Springer Science + Business Media: Pharm Res, Distribution and Effect of Water Content on Molecular Mobility in Poly(vinylpyrrolidone) Glasses: A Molecular Dynamics Simulation, 22 (8), 2005, 1205–1214, Xiang T-X, Anderson BD, figure number 4. *Middle panel* reprinted with kind permission from American Chemical Society: Macromolecules, Molecular Dynamics Simulation Study of Water in Amorphous Kapton, 41 (9), 2008, 3349–3362, Marque G, Neyertz S, Verdu J, Prunier V and Brown D, figure number 16. *Right panel* reprinted with kind permission from Elsevier: Polymer, Effect of absorbed water on oxygen transport in EVOH matrices: A molecular dynamics study, 45 (10), 2004, 3555–3564, Kucukpinar E, Doruker P, figure number 5

self-associate at higher concentrations in amorphous polymers has been reported in several simulation studies (Xiang and Anderson 2005; Marque et al. 2008; Kucukpinar and Doruker 2004). The implications of these observations and their effects on water affinity, rates of water uptake, and the solubility of active pharmaceutical ingredients in amorphous solids are under investigation, but not fully understood.

## 5 Water Distribution, Mobility, and Effects on Transbilayer Diffusion of Permeants in Lipid Bilayers

Numerous experimental (Xiang et al. 1992; Xiang and Anderson 1993, 1994b, c, 1995a, b, 1997, 1998a, b; Mayer 2001; Mayer and Anderson 2002; Mayer et al. 2003) and computational (Xiang and Anderson 2002, 2006) studies in our laboratories and others have established that the barrier domain for small drug-like molecular permeability across lipid bilayer membranes is the hydrocarbon-like acyl chain interior. This region is nearly devoid of water, as illustrated by the results of a recent MD simulation in 1,2-dioleoyl-*sn*-glycero-3-phosphocholine (DOPC) bilayers, where the center of the bilayer is indicated at 0.0 Å (Fig. 6, left panel). Given that most drug molecules have one or more polar functional groups, the dislocation

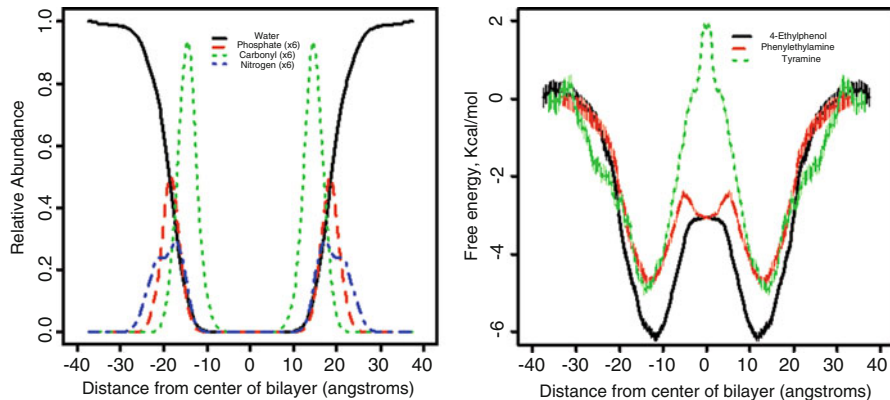


**Fig. 6** *Left panel:* Position-dependent distributions of various atoms, molecules, or functional groups in a DOPC bilayer as determined in MD simulations. The distribution for water molecules was reduced by sixfold in relation to other atoms and functional groups shown. *Right panel:* Free energies of transfer of various solutes from water to various locations within the DOPC bilayer. Reprinted with kind permission from American Chemical Society: Mol Pharmaceutics, An Atomic and Molecular View of the Depth Dependence of the Free Energies of Solute Transfer from Water into Lipid Bilayers, 8 (6), 2011, 2204–2215, Tejwani RW, Davis ME, Anderson BD, and Stouch TR, figure 2

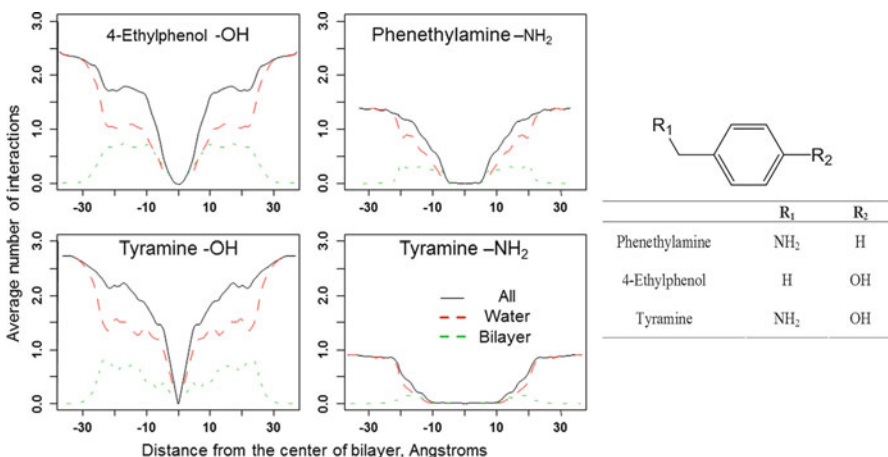


**Fig. 7** Average number of hydrogen bond interactions formed by phenethylamine, 4-ethylphenol, and tyramine versus their location in a DOPC lipid bilayer. The location indicated is that of the phenyl carbon attached to the ethyl chain (the actual location of the hydrogen bond may within 2–5 Å of this position). *Left panel* reprinted with kind permission from American Chemical Society: Mol Pharmaceutics, An Atomic and Molecular View of the Depth Dependence of the Free Energies of Solute Transfer from Water into Lipid Bilayers, 8 (6), 2011, 2204–2215, Tejwani RW, Davis ME, Anderson BD, and Stouch TR, modified from figure 4 (*upper panels*)

of drug molecules from the interfacial region of the bilayer where the polar groups are hydrogen bonded to water or phospholipid head groups into the hydrocarbon interior is energetically highly unfavorable.

We recently explored the membrane partitioning and permeabilities of a set of structurally related permeants, as shown in Fig. 7 (i.e., phenethylamine, 4-ethylphenol, and tyramine), in an effort to couple experimental results to results from MD simulations (Tejwani et al. 2010, 2011). In particular, the effects of the hydroxyl and amine substituents, either alone or when both were present on the same molecule (as in tyramine) on the free energy profiles within DOPC bilayers, were examined, as shown in the right panel of Fig. 6. Two prominent features were noted in the free energy profiles. The water/bilayer interface was the preferred binding region for all solutes, while the highest free energy region (least favorable for partitioning) was the center of the bilayer. The barrier domain region in the hydrocarbon chain interior was found to be highly selective to the number of polar residues on the permeant, while the preferred binding region at the interface was relatively insensitive to such differences in chemical structure.

These differences in chemical selectivity between the interfacial region and the hydrocarbon interior reflect the abilities of permeants to adopt orientations that favor hydrogen bonding with water or polar head groups in the interfacial region, while in the hydrocarbon chain interior all hydrogen bonds are lost, unless the molecule is sufficiently large to span a significant fraction of the bilayer thickness. This is shown by the number of hydrogen bond interactions that each of the three

solutes formed at various locations within the bilayer, as illustrated in Fig. 7. As the permeants move away from the bilayer interface, a substantial fraction of the hydrogen bonds are formed with water molecules that have partially penetrated the bilayer.

In some snapshots from the MD simulations, we were able to observe that removal of a solute from the interface was facilitated by hydrogen bonding to water molecules, which were in turn linked to either another water molecule closer to the interface or one of the polar atoms in the phospholipid head group. Water wires involving multiple hydrogen-bonded water molecule chains accompanied by head-group migration appear to be particularly important in facilitating anion and cation transport across bilayers (Xiang and Anderson 2006; Tepper and Voth 2006; MacCallum et al. 2008), since the free energy penalty for removing water of solvation from a charged residue is extremely large.

## 6 Conclusions

Because of its small size, enhanced mobility, and hydrogen-bonding capacity, water may have profound effects on local molecular organization in both lipid vehicles and amorphous solids frequently utilized as pharmaceutical formulations. The presence of moisture may determine both the physical stability and chemical stability of these systems by altering either the system thermodynamics, molecular dynamics, or both. Water-induced reorganization of local structure in lipid bilayer membranes may be essential for the transport of highly polar permeants such as anions and cations. Molecular dynamics simulations coupled with experiments on similar systems are providing valuable molecular insights into these important phenomena.

**Acknowledgements** The author would like to acknowledge the contributions of several colleagues or former colleagues who were largely responsible for the results in the publications from our laboratory cited in this chapter, including Drs. Tian-xiang Xiang, Michelle Marra, Yichen Cao, Sagar Rane, Peter Mayer, Riku Niemi, Ravi Tejwani, Vijay Joguparthi, and Sweta Modi.

## References

- Allen MP (2004) Introduction to molecular dynamics simulation. In: Attig N, Binder K, Grubmuller H, Kremer K (eds) Computational soft matter: from synthetic polymers to proteins, Lecture notes. John von Neumann Institute for Computing, Juelich, Germany, pp 1–28
- Anderson BD, Marra MT (1999) Chemical and related factors controlling lipid solubility. Bulletin Technique Gatefosse 11–19
- Anderson BD, Rane SS, Xiang T-X (2010) Understanding the role of water in non-aqueous pharmaceutical systems. In: Reid DS, Sajjaanantakul T, Lillford PJ, Charoenrein S (eds) Water properties in food, health, pharmaceutical and biological systems: ISOPOW 10. Wiley-Blackwell, Ames, IA, p 616

- Cao Y, Marra M, Anderson BD (2004) Predictive relationships for the effects of triglyceride ester concentration and water uptake on solubility and partitioning of small molecules into lipid vehicles. *J Pharm Sci* 93:2768–2779
- Dawson KJ, Kearns KL, Ediger MD, Sacchetti MJ, Zografi GD (2009) Highly stable indomethacin glasses resist uptake of water vapor. *J Phys Chem B* 113:2422–2427
- Friberg S, Mandell L (1970) Phase equilibria and their influence on the properties of emulsions. *J Am Oil Chem Soc* 47:149–152
- Joguparthi V, Anderson BD (2008a) Effect of cyclodextrin complexation on the liposome permeability of a model hydrophobic weak acid. *Pharm Res* 25:2505–2515
- Joguparthi V, Anderson BD (2008b) Liposomal delivery of hydrophobic weak acids: enhancement of drug retention using a high intraliposomal pH. *J Pharm Sci* 97:433–454
- Joguparthi V, Feng S, Anderson BD (2008a) Determination of intraliposomal pH and its effect on membrane partitioning and passive loading of a hydrophobic camptothecin, DB-67. *Int J Pharm* 352:17–28
- Joguparthi V, Xiang T-X, Anderson BD (2008b) Liposome transport of hydrophobic drugs: gel phase lipid bilayer permeability and partitioning of the lactone form of a hydrophobic camptothecin, DB-67. *J Pharm Sci* 97:400–420
- Kucukpinar E, Doruker P (2004) Effect of absorbed water on oxygen transport in EVOH matrices. A molecular dynamics study. *Polymer* 45:3555–3564
- Lebedeva TL, Feldstein M, Kuptsov SA, Plate NA (1999) The products of water H-bonding to poly(N-vinyl pyrrolidone) in solid state. In: Spectroscopy of biological molecules: new directions. 8th European conference on the spectroscopy of biological molecules, Enschede, Netherlands, pp 581–582
- MacCallum JL, Bennett WF, Tieleman DP (2008) Distribution of amino acids in a lipid bilayer from computer simulations. *Biophys J* 94:3393–3404
- Marque G, Neyertz S, Verdu J, Prunier V, Brown D (2008) Molecular dynamics simulation study of water in amorphous kapton. *Macromolecules* 41:3349–3362
- Mayer PT (2001) Functional group contributions to peptide permeability in lipid bilayer membranes: the role of peptide conformation and length. University of Utah, Salt Lake City, p 227
- Mayer PT, Anderson BD (2002) Transport across 1,9-decadiene precisely mimics the chemical selectivity of the barrier domain in egg lecithin bilayers. *J Pharm Sci* 91:640–646
- Mayer PT, Xiang T-X, Niemi R, Anderson BD (2003) A hydrophobicity scale for the lipid bilayer barrier domain from peptide permeabilities: nonadditivities in residue contributions. *Biochemistry* 42:1624–1636
- Modi S, Xiang T-X, Anderson BD (2012) Enhanced active liposomal loading of a poorly soluble ionizable drug using supersaturated drug solutions. *J Control Release* 162:330–339
- Rane SS, Anderson BD (2008a) Molecular dynamics simulations of functional group effects on solvation thermodynamics of model solutes in decane and tricaprylin. *Mol Pharm* 5 (6):1023–1036
- Rane SS, Anderson BD (2008b) What determines drug solubility in lipid vehicles: is it predictable? *Adv Drug Deliv Rev* 60:638–656
- Rane S, Cao Y, Anderson BD (2008) Quantitative solubility relationships and the effect of water uptake in triglyceride/monoglyceride microemulsions. *Pharm Res* 25:1158–1174
- Surana R, Pyne A, Suryanarayanan R (2004) Effect of preparation method on physical properties of amorphous trehalose. *Pharm Res* 21:1167–1176
- Taylor LS, Langkilde FW, Zografi G (2001) Fourier transform Raman spectroscopic study of the interaction of water vapor with amorphous polymers. *J Pharm Sci* 90:888–901
- Tejwani RW, Davis ME, Anderson BD, Stouch TR (2010) Functional group dependence of solute partitioning to various locations in a DOPC bilayer: I. A comparison of molecular dynamics simulations with experiment. *J Pharm Sci* 100:2636–2646
- Tejwani RW, Davis ME, Anderson BD, Stouch TR (2011) An atomic and molecular view of the depth dependence of the free energies of solute transfer from water into lipid bilayers. *Mol Pharm* 8:2204–2215

- Tepper HL, Voth GA (2006) Mechanisms of passive ion permeation through lipid bilayers: insights from simulations. *J Phys Chem B* 110:21327–21337
- Tieleman DP, Marrink SJ, Berendsen HJ (1997) A computer perspective of membranes: molecular dynamics studies of lipid bilayer systems. *Biochim Biophys Acta* 1331(3):235–270
- Xiang T-X, Anderson BD (1993) Diffusion of ionizable solutes across planar lipid bilayer membranes: boundary layer pH gradients and the effects of buffers. *Pharm Res* 10:1654–1661
- Xiang T-X, Anderson BD (1994a) Molecular distributions in interphases: a statistical mechanical theory combined with molecular dynamics simulation. *Biophys J* 66:561–573
- Xiang T-X, Anderson BD (1994b) Substituent contributions to the transport of substituted p-toluidic acids in lipid bilayer membranes. *J Pharm Sci* 83:1511–1518
- Xiang T-X, Anderson BD (1994c) The relationship between permeant size and permeability in lipid bilayer membranes. *J Membr Biol* 140:111–121
- Xiang T-X, Anderson BD (1995a) Development of a combined paramagnetic ion-induced line broadening/dynamic light scattering method for permeability measurements across lipid bilayer membranes. *J Pharm Sci* 84:1308–1315
- Xiang T-X, Anderson BD (1995b) Phospholipid surface density determines the partitioning and permeability behavior of acetic acid in DMPC:cholesterol bilayers. *J Membr Biol* 148:157–167
- Xiang T-X, Anderson BD (1997) Permeability of acetic acid across gel and liquid-crystalline lipid bilayers conforms to free-surface-area theory. *Biophys J* 72:223–237
- Xiang T-X, Anderson BD (1998a) Influence of chain ordering on the selectivity of dipalmitoylphosphatidylcholine bilayer membranes for permeant size and shape. *Biophys J* 75:2658–2671
- Xiang T-X, Anderson BD (1998b) Phase structures of binary lipid bilayers as revealed by permeability of small molecules. *Biochim Biophys Acta* 1370:64–76
- Xiang T-X, Anderson BD (1999) Molecular dissolution processes in lipid bilayers: a molecular dynamics simulation. *J Chem Phys* 110:1807–1818
- Xiang T-X, Anderson BD (2002) A computer simulation of functional group contributions to free energy in water and a DPPC lipid bilayer. *Biophys J* 82:2052–2066
- Xiang T-X, Anderson BD (2004) A molecular dynamics simulation of reactant mobility in an amorphous formulation of a peptide in poly(vinylpyrrolidone). *J Pharm Sci* 93:855–876
- Xiang T-X, Anderson BD (2005) Distribution and effect of water content on molecular mobility in poly(vinylpyrrolidone) glasses: a molecular dynamics simulation. *Pharm Res* 22:1205–1214
- Xiang T-X, Anderson BD (2006) Liposomal drug transport: a molecular perspective from molecular dynamics simulations in lipid bilayers. *Adv Drug Deliv Rev* 58:1357–1378
- Xiang TX, Anderson BD (2013) Molecular dynamics simulation of amorphous indomethacin. *Mol Pharm* 10(1):102–14
- Xiang T-X, Chen X, Anderson BD (1992) Transport methods for probing the barrier domain of lipid bilayer membranes. *Biophys J* 63:78–88
- Xiang T-X, Jiang Z-Q, Anderson BD (2006) Molecular dynamics simulations and experimental studies of binding and mobility of 7-t-butylidimethylsilyl-10-hydroxycamptothecin (DB-67) and its 20(S)-4-aminobutyrate ester in DMPC membranes. *Mol Pharm* 3:589–600

# Food Preservation by Nanostructures-Water Interactions Control

E. Flores-Andrade, E. Azuara-Nieto, C.I. Beristain-Guevara,  
A. Monroy-Villagrana, D.I. Téllez-Medina, L.A. Pascual-Pineda,  
L. Alamilla-Beltrán, and G.F. Gutiérrez-López

## Abbreviations

$a_w$	Water activity
FD	Fractal dimension
$K$	Boltzmann's constant
$N$	Entire system
$n$	Cooperative rearrangement
$N-n$	Regions whose state does not allow such a transition
RH	Relative humidity
$S_c$	Configurational entropy of the system
$s_c$	Configurational entropy of the subsystem with $z$ molecules
$T$	Absolute temperature
$T_1$	Spin-lattice relaxation time
$T_{2s}$	Spin-spin relaxation time

---

E. Flores-Andrade • L.A. Pascual-Pineda  
Facultad de Ciencias Químicas, Universidad Veracruzana, Prolongación Oriente 6, 94340  
Orizaba, Veracruz, Mexico

E. Azuara-Nieto • C.I. Beristain-Guevara  
Instituto de Ciencias Básicas, Universidad Veracruzana, Av. Dr. Rafael Sánchez Altamirano  
s/n, Col. Industrial-Animas, Apdo. Postal 575, 91000 Xalapa, Veracruz, Mexico

A. Monroy-Villagrana • L. Alamilla-Beltrán • G.F. Gutiérrez-López (✉)  
Escuela Nacional de Ciencias Biológicas, Instituto Politécnico Nacional, Prolongación Carpio  
y Plan de Ayala, Delegación Miguel Hidalgo, 11340 México D. F., México  
e-mail: [gusfgl@gmail.com](mailto:gusfgl@gmail.com)

D.I. Téllez-Medina  
Departamento de Graduados e Investigación en Alimentos, Escuela Nacional de Ciencias  
Biológicas, Instituto Politécnico Nacional, Carpio y Plan de Ayala s/n, Mexico City,  
DF CP 11340, Mexico

$T_g$	Glass transition temperature
$W_{c1}/N$	Average number of configurations depending on the size of $z$
$z$	Energetic barrier

## 1 Introduction

Initially, the water content was used as a control parameter for predicting the stability of food. However, it was insufficient to determine the chemical and microbiological stability since they do not depend only on the water content, but on how the water is bound to the food components (Rahman 2010). Under the same conditions of environmental relative humidity (RH %), different foods may have different equilibrium moisture content, while at the same moisture content, these foods may differ completely in their physicochemical and microbiological stability (Vermeulen et al. 2014; Kalichevsky-Dong 2000).

Typically, to define the conditions under which food must be preserved, especially dehydrated foods, the water activity ( $a_w$ ) and glass transition temperature ( $T_g$ ) are employed (Mrad et al. 2013; Roos 1993). This is a combination of the use of water-matrix energetic interactions ( $a_w$ ) and low molecular mobility ( $T < T_g$ ) in order to allow for the product quality to be maintained longer. However, many real storage conditions do not match the values predicted by these parameters.

In recent years, the effect of microstructure on the chemical and microbiological stability of foods has been widely recognized (Kong and Singh 2011; Creed 2010; Azuara-Nieto and Beristain-Guevara 2007); Azuara and Beristain 2006; Hills et al. 2001) and the control of the food structure has been performed by manipulating the operation conditions in different processes such as convective drying, freeze drying and freezing, among others, so allowing to evaluate the properties of the final product at macroscopic level (Anwar and Kunz 2011; Khraisheh et al. 2004). Nonetheless, there is scarce research on the microstructural changes in the food solid matrix due to processing and its relation to the behavior of water at nanometric scale.

Nanoscience deals with the study of phenomena on a scale of 0.1–100 nm and the manipulation of materials at the atomic, molecular, and macromolecular scales, whose properties may differ completely from those at the macroscopic level. Nanotechnology, on the other hand, deals with the design, characterization, production, and application of structures such as devices, systems, and materials by controlling the shape and size at the nanoscale (Chellaram et al. 2014; Knowles et al. 2006; Salerno et al. 2008).

Studying the behavior of fluids on surfaces and microstructures has been important in some areas of science and engineering, including food science, since the properties of nanoconfined fluids markedly differ from those non-nanoconfined (Ortony et al. 2014; Biggin and Sansom 2001). The aim of this chapter is to examine how nanostructuration can modify food energy barriers and steric interactions between water and food matrix and how this can be helpful to modify in a controlled fashion the conditions to preserve products.

## 2 Parameters of Stability

### 2.1 Water Activity ( $a_w$ )

The chemical and microbiological stability of foods is qualitatively represented by a map of stability (Labuza et al. 1972). The most frequently used equations for predicting the most suitable conditions for preservation of dried foods are the BET (Brunauer, Emmett, and Teller) and GAB (Guggenheim, Anderson, and De Boer) models. These equations allow calculating the monolayer value, which has been considered the point of maximum stability. Although the term  $a_w$  has been useful as stability parameter, it only applies to systems with a true thermodynamic equilibrium, which is rare in foods with low and intermediate moisture contents. In this type of foods, the equilibrium between  $a_w$  regions may be so slow that it is not reached during the product's shelf life; it is considered, then, that they are in a state of thermodynamic metastability (Kalichevsky-Dong 2000).

### 2.2 Glass Transition Temperature ( $T_g$ )

The glass transition temperature ( $T_g$ ) is defined as the temperature where the amorphous polymers undergo a transition between glassy and rubbery states. The amorphous and partially crystalline structures are formed during some food processing operations, such as extrusion, baking, concentration, and drying (Roos et al. 1996). The properties of amorphous polymers can be related to their glass transition temperature which is important to the physical stability of foods. The  $T_g$  of a material depends on the moisture content, degree of crystallinity of the sample, and the rate of temperature change (Kayacier and Singh 2002). It has been proposed that the glass transition affects those chemical and enzymatic reactions which are controlled by diffusion, since changes in the molecular mobility occur as the temperature decreases to the vicinity of the  $T_g$  (Slade and Levine 1991). These reactions in foods are associated with changes in moisture content,  $a_w$ , temperature, pH, reactant concentration, and structure (Bell and Touma 1996). In the glassy state ( $T < T_g$ ), the mobility of the reactive molecules is reduced due to inter- and intramolecular arrangements of the food matrix, which increases the viscosity of the medium and reduces the deterioration rate of the diffusion limited processes. In contrast, at temperatures above the glass transition temperature ( $T > T_g$ ), the material is in a rubbery state due to a decrease in viscosity and an increase in molecular mobility and the probability of deteriorating reactions (Roos 1993; Kalichevsky-Dong 2000; Ludescher et al. 2001). Regarding microbial stability, Slade and Levine (1991) proposed to replace the use of  $a_w$  with the relationship  $T_g$ :water content. Also, Gould and Christian (1998) indicated that the very viscous states (glassy state) of foods can interfere with microbial growth due to restriction of the diffusion of nutrients. However, Chirife and Buera (1994) demonstrated that microbial

growth in the foods can occur in both, glassy ( $T < T_g$ ) and rubbery, states ( $T > T_g$ ) and indicated that the microbial stability primarily depends on the  $a_w$ .

### 3 Thermodynamic Parameters

Beristain and Azuara (1990) developed a method which allows recommending the most appropriate storage conditions for dry products if the moisture level at which the minimum integral entropy of water molecules occurs is known. This point is considered as the one with the maximum order of water molecules adsorbed on the food microstructure and sometimes does not match neither the monolayer value nor the predicted  $T_g$  for preserving foodstuffs (Beristain et al. 2002). Furthermore, it has been proven that the relationship between the thermodynamic parameters of enthalpy and entropy allows determining the mechanism that controls the interaction of water molecules with food. The enthalpic control relates with the energy aspects characteristic of the chemical composition of food, whereas the entropic control refers to microstructural factors whose interaction with water molecules is independent of ionic or polar affinity between the adsorbate and adsorbent molecules (Beristain et al. 1996; Azuara and Beristain 2006).

### 4 Water Confined in Nanostructures

Carbon nanotubes have been used as ideal models for studying the behavior of fluids in channels of biological materials (cells, membranes, surface proteins, microcapillaries, and aquaporins) and micro- and mesoporous solid matrices (Huang et al. 2005; Liu et al. 2013; Peponi et al. 2014). The behavior of water confined in nanometric spaces differs from that of the water at the macroscopic level.

Several studies with multiwalled carbon nanotubes whose diameters are about 5 nm have shown that the behavior of water is not the same as the one in nanotubes with larger diameters (Sealy 2004). Moreover, in single-walled nanotubes with diameter lower than 1.5 nm, it occurs spontaneous and continuous filling of water molecules arranged in a linear fashion (in the middle of the nanotube) and tetrahedral order (water molecules in contact with the wall of the nanotube). This property allows for exploitation of nanotubes as channels for water and protons. Although the modification of the hydrophilic and hydrophobic properties of the nanotube wall does not affect the structure of water molecules, this has an effect on the transport through the nanotubes. Another characteristic of water molecules in nanometric spaces is that they orderly occupy spaces when are near to the walls of the nanotubes, preferably orienting their dipole moment perpendicularly to such walls (Hummer et al. 2001; Marañón and Marañón 2003).

By using techniques such as thermoporometry and solid state NMR, it is possible to identify two types of water molecules in the porous matrix of the material: (1) water molecules that directly interact with the pore walls and whose properties differ from those of the (2) molecules in the center of the pore. The relaxation rate of the spin of protons near to the surface is extremely fast due to the restriction caused by the pore wall. As a consequence, the relaxation rates have two contributions, one for water molecules near the surface of the pore and the other for molecules in the pore center (Chui et al. 1995). Furthermore, through thermoporometry, it has been determined that in the pore surface a thin layer of unfreezable water may exist unlike that frozen in the pore center (Yamamoto et al. 2005). The effect of physical barriers on the behavior of water, especially at the nanoscale, is clear. In this case an entropic mechanism could be considered for the interaction of water molecules with carbon nanotubes.

The interactions between the water molecules and the solid matrix of the food can be explained from enthalpic and entropic mechanisms and by means of micropore-water interactions. Azuara and Beristain (2006) used the Dubinin-Radushkevich model to calculate the volume of micropores, with the theory of compensation and minimum integral entropy in order to determine the mechanism that controls the water sorption in dehydrated products. These authors assessed the water adsorption in several yogurt products subjected to different drying processes and found that the value of minimum entropy shifted to higher moisture contents as the micropore volume increased (Azuara and Beristain 2006). In addition, the amount of water confined in the food nanometric spaces (micropores with less than 2 nm size) calculated by the Dubinin-Radushkevich method was similar to the moisture content indicated by the minimum integral entropy. Also, Flores-Andrade et al. (2009) studied enthalpy-entropy compensation in osmotically dehydrated agar gel and also found that nanopores controlled the water mobility phenomena.

Hummer et al. (2001) pointed out that hydrogen bonds in the carbon nanotube are protected against environmental fluctuations, so that the bonds' half-life is extended up to 5.6 ps compared with 1 ps for water at macroscopic level. Probably, water at the minimum integral entropy is less available to participate in chemical and enzymatic reactions because it would be energetically inconvenient.

## 5 Minimum Entropy and Cooperatively Rearrangement Regions

Adam and Gibbs (1965) developed a theory that relates the structure relaxation time (kinetic parameter) with the configurational entropy (thermodynamic parameter) of the system. This theory is based on the molecular mobility of fluids at temperatures approaching the  $T_g$  in terms of molecular cooperatively rearranging regions. According to this theory, the molecular movement occurs in regions of critical size  $z^*$  (atoms, molecules, etc.), and the probability of configurational modifications

changes according to  $\exp(-z^*KT)$ , which is the energetic barrier to obtain the cooperatively rearranging region by monomers with  $z^*$ ,  $K$  is the Boltzmann's constant and  $T$  is absolute temperature (Perez 1994; Johari 2000; Corezzi et al. 2002).

The cooperatively rearranging region  $z$  is defined as the smallest region that can undergo a transition to a new configuration without any simultaneous configurational change outside of its limits. In other words, it is a subsystem of the system with enough energy fluctuations to rearrange itself into a configuration independent of its environment; the probability of a cooperatively rearranging region is a function of the number of molecules that form the region  $z$  (Adam and Gibbs 1965). The subsystem of  $z$  molecules interacts with the macroscopic system and, since there is a thermal and mechanical contact between subsystems or regions, the entire system  $N$  is considered as the set of subsystems within which two kinds of regions exist: those that reside in a state that allows a cooperative rearrangement ( $n$ ) and regions whose state does not allow such a transition ( $N-n$ ).

The configurational entropy of the system is expressed as  $S_c = N s_c$  where  $s_c$  is the configurational entropy of the subsystem with  $z$  molecules and is defined as  $z = s_c K \ln(W_{c1}/N)$ , where  $W_{c1}/N$  is the average number of configurations depending on the size of  $z$ .

In the zone of minimum entropy, water molecules are arranged so that there are strong interactions between the water molecules and the adsorbent (Nunes and Rotstein 1991). At this point, it is likely that the set of water molecules into a micropore acts as a region  $z$ , which is in a state of cooperative rearrangement with minimum configurational entropy and low transition probability.

The mobility of the molecules of a substance can be evaluated by means of solid state NMR. Ruan et al. (1999) assumed that the short component of the spin-spin relaxation ( $T_{2s}$ ) provides information on the molecular structure. These researchers found that a L- or U-shaped graph is obtained by plotting  $T_{2s}$  and  $T_1$  relaxation times as a function of temperature in maltodextrin samples at certain moisture content. The  $T_g$  of the maltodextrin samples was derived from the point where a slope shift occurs. In general, changes in the  $T_{2s}$  with temperature are associated to changes in molecular mobility;  $T_{2s}$  increases when the molecule mobility increases in the system ( $T > T_g$ , rubbery state) and decreases when the system is in glassy state ( $T < T_g$ ). Since the theory of Adams and Gibbs was conceived to explain the glass transition in terms of molecular mobility and given this can be characterized by means of NMR, the mobility of adsorbed molecules can be expressed in terms of cooperatively rearranging regions.

Zimmerman et al. (1956) showed that the relaxation time of the adsorbed molecules tends to a minimum as the moisture content of the sample decreases. The kinetic parameter considered by the theory of Adams and Gibbs is the dielectric relaxation time; however, Zimmerman et al. (1956) compared the nuclear relaxation times with dielectric relaxation times obtained by Kurosaki (1954) for water molecules adsorbed on silica gel and found consistent behavior between measurements. In general, both measurements tend to decrease when water molecules interact strongly with the microstructure of the adsorbent.

Therefore, the behavior of water molecules confined in nanometric spaces could be described in terms of the molecular kinetics theory proposed by Adam and Gibbs.

## 6 Potential Application of Nanostructuration to Foods

The application of nanotechnology in areas such as materials science, chemistry, biology, medicine, among others suggests the possibility of applying its principles in the food area, with potential applications in the production of nanostructured food materials in order to allow for controlled interaction between water molecules and the food nanostructure (Chellaram et al. 2014; Salerno et al. 2008; Knowles et al. 2006).

There are several methods for nanostructuring materials, which are based primarily on a self-assembling of nanocavities at molecular level. However, the mould in which the nanostructuring has been made is not easy to produce and is destroyed at the end of the process (Ying 1999).

The breath figures method allows creating well-defined structures with a porous hexagonal arrangement (honeycomb), flexible, monodisperse pore distribution, and pore sizes ranging from 50 nm to 20 µm for various applications (Bunz 2006). In this case, there is a nanostructure of defined, geometrically ordered cavities.

A method for obtaining a microporous sugar-salt complex was proposed by Zeller and Saleeb (1996). They defined a micropore size range between 1 and 7.5 nm. Although no geometric arrangement was observed in the microstructure, as in the firstly mentioned method, this procedure produced nanostructured, defined cavities. These nanostructures do not have a Euclidean geometry, but they probably possess a fractal arrangement.

Nanostructured systems exhibit unusual properties that depend on their size and that can be exploited in some fields of science and technology (Wang 2014). Consequently, considerable efforts have been made to understand and develop these kind of materials. Nanostructured systems are classified as nanocrystalline and nanoporous ones. Among the former are the nanoparticles, which can be used in food processing. Nanoporous systems can be produced from a self-assembling of cavities or nanometric-size spaces (Jani et al. 2013; Ying 1999). The microporous structure with well-defined pore diameters may be used as molecular sieves or matrices which act as receptors for highly reactive chemical or biological molecules (Li et al. 2014).

Nanostructuration of food materials can not only allow a better control of its stability but also promote better nutrition. Aguilera (2005) mentions an example of considerations about nanostructure when refers to starch digestibility in the small intestine, where the enzymatic activity is limited by the porosity and permeability of the micropores in the matrix of the processed starch. This can help people with diabetes to maintain low levels of blood glucose.

Regarding microbial stability, it has been demonstrated that, at the same  $a_w$ , microorganism survival depends on microstructural aspects of the support medium used for microbial growth (Hills et al. 2001). Probably due to entropic and energy mechanisms already considered, the water contained in the micropores is practically inaccessible to the microorganism, which makes difficult its growth. Therefore, the distribution of water in a solid matrix microstructure depends on its nature and the nature of the microorganism, so that food nanostructuration may allow for a better control against microbial growth.

The term “undefined nanostructuration” could be applied to the non-ordered microstructure produced by some kind of processing which allows obtaining nanometric spaces, such as micropores (with  $<20 \text{ \AA}$  pore diameter), in the final product and influences the setting of stability conditions.

## 7 Description of Food Morphology

Fractal geometry is a branch of mathematics that is based upon the use of algorithms and fractional dimensions to describe the morphology of objects which are not adequately described by Euclidean geometry (García-Armenta et al. 2014; Mandelbrot and Riedi 1997). A fractal is a geometric figure composed of fragments in an infinite variety of sizes, so that each of them is a reduced copy of the whole. The latter property of fractals is called self-similarity, i.e., fractals are scale independent and generally characterized by the presence of infinite detail, infinite length, and the lack of smoothness or differentiability.

A natural fractal is a figure that shows self-similarity from a statistical point of view, within a range of magnification at which the profile is analyzed (Barletta and Barbosa-Cánovas 1993). One way to assess the heterogeneity of a solid (a food, for instance) is in terms of the fractal dimension (FD), which may be obtained by various methods such as sorption isotherms (Fripiat et al. 1986; Wang and Li 1997; Calzetta-Resio et al. 1999) and image analysis. In the latter, FD is calculated from the boundary (Alamilla-Beltrán et al. 2005) or the surface (Chanona et al. 2003) of the material.

The modifications in the food morphology during processing can be described in terms of the fractal dimension. Chanona et al. (2003) studied the change in the heterogeneity of the surface of a model food system during convective drying and concluded that the FD may be a quantitative index of the heterogeneity of the material. Thereby, the use of fractal theory may help to characterize nanostructured cavities in foods.

## 8 Conclusions

While it is difficult to produce geometrically arranged nanocavities in foods, it is possible to generate nanocavities whose pore size and interaction with water molecules are similar to those of carbon nanotubes.

The water molecules capable to be adsorbed in a nanostructured food might orderly arrange within these nanocavities, which would limit their entropy for participating in chemical reactions and microbiological degradation. Therefore, the nanostructuration of foods may allow for a control of water mobility and therefore for a better management of the storage conditions without adding chemical preservatives, thus better maintaining their organoleptic and nutritional attributes.

## References

- Adam G, Gibbs JH (1965) Temperature dependence of cooperative relaxation properties in glass-forming liquids. *J Chem Phys* 43(1):139–147
- Aguilera JM (2005) Why food microstructure? *J Food Eng* 67(1–2):3–11
- Alamilla-Beltrán L, Chanona-Pérez JJ, Jiménez-Aparicio AR, Gutiérrez-López GF (2005) Description of morphological changes of particles along spray drying. *J Food Eng* 67 (1–2):179–184
- Azuara E, Beristain CI (2006) Enthalpic and entropic mechanisms related to water sorption of yogurt. *Drying Technol* 24:1501–1507
- Azuara-Nieto E, Beristain-Guevara CI (2007) Estudio termodinámico y cinético de la adsorción de agua en proteína de suero de leche. *Rev Mex Ing Quím* 6(3):359–365
- Barletta BJ, Barbosa-Cánovas GV (1993) An attrition index to assess fines formation and particle size reduction in tapped agglomerated food powders. *Powder Technol* 77(1):89–93
- Bell LN, Touma DE (1996) Glass transition temperatures determined using a temperature-cycling differential scanning calorimeter. *J Food Sci* 61(4):807–810
- Beristain CI, Azuara E (1990) Maximal stability of dried products. *Ciencia (México)* 41 (3):229–236
- Beristain CI, García HS, Azuara E (1996) Enthalpy-entropy compensation in food vapor adsorption. *J Food Eng* 30:405–415
- Beristain CI, Azuara E, Vernon-Carter EJ (2002) Effect of water activity on the stability to oxidation of spray-dried encapsulated orange peel oil using mesquite gum (*Prosopis juliflora*) as wall material. *J Food Sci* 67:206–211
- Biggin PC, Sansom MSP (2001) Channel gating: Twist to open. *Curr Biol* 11(9):R364–R366
- Bunz UHF (2006) Breath figures as a dynamic templating method for polymers and nanomaterials. *Adv Mater* 18(8):973–989
- Calzetta-Resio A, Aguerre RJ, Suárez C (1999) Analysis of the sorptional characteristics of amaranth starch. *J Food Eng* 42(1):51–57
- Chanona JJ, Alamilla L, Farrera RR, Quevedo R, Aguilera JM, Gutiérrez GF (2003) Description of the convective air-drying of a food model by means of the fractal theory. *Food Sci Technol Int* 9:3207–3213
- Chellaram C, Murugaboopathi G, John AA, Sivakumar R, Ganesan S, Krithika S, Priya G (2014) Significance of nanotechnology in food industry. *APCBEE Proc* 8:109–113
- Chirife J, Buera MP (1994) Water activity, glass transition and microbial stability in concentrated/semitmoist food systems. *J Food Sci* 59(5):921–927

- Chui MM, Phillips RJ, McCarthy MJ (1995) Measurement of the porous microstructure of hydrogels by nuclear magnetic resonance. *J Colloid Interface Sci* 174(2):336–344
- Corezzi S, Fioretto D, Casalini R, Rolla PA (2002) Glass transition of an epoxy resin induced by temperature, pressure and chemical conversion: a rationale based on configurational entropy. *J Non-Cryst Solids* 307–310:281–287
- Creed PG (2010) Chemical deterioration and physical instability in ready-to-eat meals and catered foods. In: Skibsted LH, Risbo J, Andersen ML (eds) *Chemical deterioration and physical instability of food and beverages*. Woodhead Publishing, Cambridge, pp 608–662
- Djendoubi Mrad N, Bonazzi C, Courtois F, Kechaou N, Mihoubi NB (2013) Moisture desorption isotherms and glass transition temperatures of osmo-dehydrated apple and pear. *Food Bioproducts Processing* 91(2):121–128
- Flores-Andrade E, Beristain CI, Vernon-Carter EJ, Gutiérrez-López GF, Azuara E (2009) Enthalpy-entropy compensation and water transfer mechanism in osmotically dehydrated agar gel. *Drying Technol* 27(6):999–1009
- Fripiat JJ, Gatineau L, Van Damme H (1986) Multilayer physical adsorption on fractal surfaces. *Langmuir* 2(5):562–567
- García-Armenta E, Téllez-Medina DI, Alamilla-Beltrán L, Arana-Errasquín R, Hernández-Sánchez H, Gutiérrez-López GF (2014) Multifractal breakage patterns of thick maltodextrin agglomerates. *Powder Technol* 266:440–446
- Gould GW, Christian JHB (1998) Characterization of the state of water in foods - biological aspects. In: Seow C (ed) *Food preservation by moisture control*. Elsevier Applied Science, London, pp 43–56
- Hills BP, Arnould L, Bossu C, Ridge YP (2001) Microstructural factors controlling the survival of food-borne pathogens in porous media. *Int J Food Microbiol* 66(3):163–173
- Huang H, Liu CH, Wu Y, Fan S (2005) Aligned carbon nanotube composite films for thermal management. *Adv Mater* 17(13):1652–1656
- Hummer G, Rasaiah JC, Noworyta JP (2001) Water conduction through the hydrophobic channel of a carbon nanotube. *Nature* 414:188–190
- Jani AMMD, Losic D, Voelcker NH (2013) Nanoporous anodic aluminium oxide: advances in surface engineering and emerging applications. *Prog Mater Sci* 58(5):636–704
- Johari GP (2000) On the origin of the heat capacity feature of annealed ices and ice clathrates, and interpreting water's diffusivity in terms of the entropy. *Chem Phys* 258(2–3):277–290
- Kalichevsky-Dong MT (2000) The glass transition and microbial stability. In: Kilcast D, Subramaniam P (eds) *The stability and shelf-life of food*. Woodhead Publishing, Cambridge, pp 25–54
- Kayacier A, Singh RK (2002) Glass transition studies of baked tortilla chips using dynamic mechanical thermal analysis. *LWT Food Sci Technol* 35(1):34–37
- Khraisheh MAM, McMinn WAM, Magee TRA (2004) Quality and structural changes in starchy foods during microwave and convective drying. *Food Res Int* 37(5):497–503
- Knowles MRH, Rutherford G, Karnakis D, Dobrev T, Petkov P, Dimov S (2006) *Laser micro-milling of ceramics, dielectrics and metals using nanosecond and picosecond lasers*. Second international conference on multi-material micro manufacture, pp 131–134
- Kong F, Singh RP (2011) Chemical deterioration and physical instability of foods and beverages. In: Kilcast D, Subramaniam P (eds) *Food and beverage stability and shelf life*. Woodhead Publishing, Cambridge, pp 29–62
- Kurosaki S (1954) The dielectric behavior of sorbed water on silica gel. *J Phys Chem* 58 (4):320–324
- Labuza TP, McNally L, Gallagher D, Hawkes J, Hurtado F (1972) Stability of intermediate moisture foods. 1. Lipid Oxidation. *J Food Sci* 37(1):154–159
- Li XY, Zhao QL, Xu TT, Huang J, Wei LH, Ma Z (2014) Highly ordered microporous polystyrene-b-poly(acrylic acid) films: study on the influencing factors in their fabrication via a static breath-figure method. *Eur Polym J* 50:135–141

- Liu CX, Lang WZ, Shi BB, Guo YJ (2013) Fabrication of ordered honeycomb porous polyvinyl chloride (PVC) films by breath figures method. *Mater Lett* 107:53–55
- Ludescher RD, Shah NK, McCaul CP, Simon KV (2001) Beyond Tg: optical luminescence measurements of molecular mobility in amorphous solid foods. *Food Hydrocoll* 15 (4–6):331–339
- Mandelbrot BB, Riedi RH (1997) Inverse measures, the inversion formula, and discontinuous multifractals. *Adv Appl Math* 18(1):50–58
- Marañón J, Marañón J (2003) Confined water in nanotube. *J Mol Struct (THEOCHEM)* 623 (1–3):159–166
- Nunes RV, Rotstein E (1991) Thermodynamics of the water-foodstuff equilibrium. *Drying Technology: An International Journal* 9(1):113–137
- Ortony JH, Choi SH, Spruell JM, Hunt JN, Lynd NA, Krogstad DV, Urban VS, Hawker CJ, Kramer EJ, Han S (2014) Fluidity and water in nanoscale domains define coacervate hydrogels. *Chem Sci* 5:58–67
- Peponi L, Puglia D, Torre L, Valentini L, Kenny JM (2014) Processing of nanostructured polymers and advanced polymeric based nanocomposites. *Materials Science and Engineering: R: Reports* 85:1–46
- Perez J (1994) Theories of liquid-glass transition. *J Food Eng* 22(1–4):89–114
- Rahman MS (2010) Food stability determination by macro–micro region concept in the state diagram and by defining a critical temperature. *J Food Eng* 99(4):402–416
- Roos Y (1993) Melting and glass transitions of low molecular weight carbohydrates. *Carbohydr Res* 238:39–48
- Roos YH, Karel M, Kokini JL (1996) Glass transitions in low moisture and frozen foods: effects on shelf life and quality. *Food Technol* 50(11):95–108
- Ruan R, Long Z, Chen P, Huang V, Almaer S, Taub I (1999) Pulse NMR study of glass transition in maltodextrin. *J Food Sci* 64(1):6–9
- Salerno M, Landoni P, Verganti R (2008) Designing foresight studies for Nanoscience and Nanotechnology (NST) future developments. *Technol Forecast Soc Chang* 75(8):1202–1223
- Sealy C (2004) Water on the nanoscale: carbon nanotubes. *Materials Today* 7(12):12
- Slade L, Levine H (1991) Beyond water activity: recent advances based on an alternative approach to the assessment of food quality and safety. *Crit Rev Food Sci Nutr* 30(2–3):115–360
- Sri Haryani Anwar SH, Kunz B (2011) The influence of drying methods on the stabilization of fish oil microcapsules: comparison of spray granulation, spray drying, and freeze drying. *J Food Eng* 105(2):367–378
- Vermeulen A, Marvig CL, Daelman J, Xhaferi R, Nielsen DS, Devlieghere F (2014) Strategies to increase the stability of intermediate moisture foods towards *Zygosaccharomyces rouxii*: the effect of temperature, ethanol, pH and water activity, with or without the influence of organic acids. *Food Microbiol* 45:119–125
- Wang Y (2014) Nanoge geochemistry: nanostructures, emergent properties and their control on geochemical reactions and mass transfers. *Chem Geol* 378–379:1–23
- Wang F, Li S (1997) Determination of the surface fractal dimension for porous media by capillary condensation. *Ind Eng Chem Res* 36(5):1598–1602
- Yamamoto T, Endo A, Inagi Y, Ohmori T, Nakaiwa M (2005) Evaluation of thermoporometry for characterization of mesoporous materials. *J Colloid Interface Sci* 284(2):614–620
- Zeller BL, Saleeb FZ (1996) Production of microporous sugars for adsorption of volatile flavors. *J Food Sci* 61(4):749–752
- Ying JY, Mehnert CP, Wong MS (1999) Synthesis and applications of supramolecular-templated mesoporous materials. *Angew Chem Int Ed* 38(1):56–77
- Zimmerman JR, Holmes BG, Lasater JA (1956) A study of adsorbed water on silica gel by nuclear resonance techniques. *J Phys Chem* 60(9):1157–1161

# Water and Food Appearance

M.P. Buera, A.E. Farroni, and L.M. Agudelo-Laverde

## Abbreviations

CVS	Computer vision system
ESEM	Electron microscope by environmental mode
$K$	Attenuation coefficient
$N$	Refraction indexes
$R_\infty$	Reflectance of an infinitely thick layer of the material
RH	Relative humidity
$S$	Dispersion coefficient
SEM	Scanning electron microscopy
$T_g$	Glass transition temperature

---

M.P. Buera (✉)

Departamentos de Industrias y de Química Orgánica, Facultad de Ciencias, Exactas y Naturales, University of Buenos Aires (FCEyN-UBA), Buenos Aires, Argentina

National Council of Scientific and Technical Research (CONICET), Buenos Aires, Argentina  
e-mail: [pilar@di.fcen.uba.ar](mailto:pilar@di.fcen.uba.ar)

A.E. Farroni

Departamento de Industrias, Facultad de Ciencias Exactas y Naturales, Universidad de Buenos Aires, Buenos Aires, Argentina

Laboratorio de Calidad de Alimentos, Suelos y Agua, EEA Pergamino, Instituto Nacional de Tecnología Agropecuaria, Av. Frondizi Km 4.5, 2700 Pergamino, Buenos Aires, Argentina  
e-mail: [farroni.abel@inta.gob.ar](mailto:farroni.abel@inta.gob.ar)

L.M. Agudelo-Laverde

Departamentos de Industrias y de Química Orgánica, Facultad de Ciencias, Exactas y Naturales, University of Buenos Aires (FCEyN-UBA), Buenos Aires, Argentina

## 1 Introduction

Food appearance depends not only on its chromatic characteristics (hue, saturation) and luminosity but also on the spatial distribution of light inside the food material, which determines appearance aspects such as transparency and gloss.

The perception of food color is based on visual sensations, which depend on the spectral distribution of light. This aspect has been widely analyzed in food science.

The modes of appearance produced by different spatial distributions of light were denoted as “cesia” by the architect Cesar Janello in 1965. An atlas of *cesia* was later developed, which found application mainly in relation to paintings, architecture, and ambient illumination materials (Caivano 1991, 1994, 1996; Caivano et al. 2004).

Because chromatic properties define the color of a given material by means of three variables (hue, saturation and luminosity), the three variables proposed for *cesia* are perceived permeability (or its opposite, opacity), darkness (or its opposite, lightness or luminosity, which is shared with the color properties), and diffusivity (or its opposite, regularity), related to the distinctness of image and referring to the sharpness of images produced by reflection and by transmission (Caivano et al. 2004).

Permeability ranges from opaque samples to transparent samples, passing through samples with different degrees of perceived transparency. The variation of darkness can be perceived by reflectance or transmittance, while the variation of diffusivity involves perceptions from matte or translucent to glossy. Both reflection and transmission may occur regularly (specularly) or diffusely, and any intermediate combination may also appear.

In foods, the defined *cesia* characteristics represent important physical aspects of food quality which are perceived by human vision. Nevertheless, these characteristics have received little attention by food researchers in comparison with chromatic attributes, possibly because of the difficulty of easily and adequately measuring and specifying the stimuli that generate those phenomena.

During processing or storage of foods, many structural changes occur, which can induce changes in color, gloss, transparency, and luminosity. While stimuli for color can be produced by primary sources (objects that emit light) or by secondary sources (objects that reflect or transmit the light coming from another source), the variations of *cesia* only occur in secondary sources, that is to say, in objects that produce changes in the spatial distribution of the light they receive. These changes are mainly due to microtextural variations on the surface or in the volume of the object. If these textural variations are of a rather small size, then visual texture changes are not perceived, while the effect produced on light is noticed (Caivano et al. 2004).

Translucent materials are those that both transmit and scatter light. The degree to which an object is translucent depends on the extent to which the light entering a sample is reflected, scattered, or absorbed. As a phenomenon, translucency occurs between the extremes of transparency and opaqueness (Hutchings 1999).

The aim of the present work is to analyze the effect of water on changes in the distribution of light inside food materials and their impact on the perception of the chromatic properties.

## 2 Potential Causes of Transparency/Opacity Changes

### 2.1 Dehydration or Rehydration

While slices of fresh vegetables look translucent, the same samples behave like opaque materials after freeze-drying (Agudelo-Laverde et al. 2012, 2013). Also, as illustrated in Fig. 1a for fresh and dehydrated beetroot, color perception is different when comparing fresh and dehydrated vegetables; luminosity values are higher and the values of chromatic variables are lower in the dried vegetables. This effect has been studied in food matrices such as tomato, kiwi, and strawberries in which these became of dull appearance after drying (Talens et al. 2002; Lana et al. 2006; Agudelo-Laverde et al. 2013).

It is interesting to note that the fresh vegetables contain a mass fraction of water higher than 85 %, and this amount decreases to less than 2 % due to the drying process, causing a concentration of all the food components, including pigments. Thus, it would be expected that the dried material would have more intense chromatic attributes than the fresh material. However, during freeze-drying, the water present in the inter- and intracellular spaces of the fresh material is replaced by air, and the samples become opaque due to the presence of air cavities created in

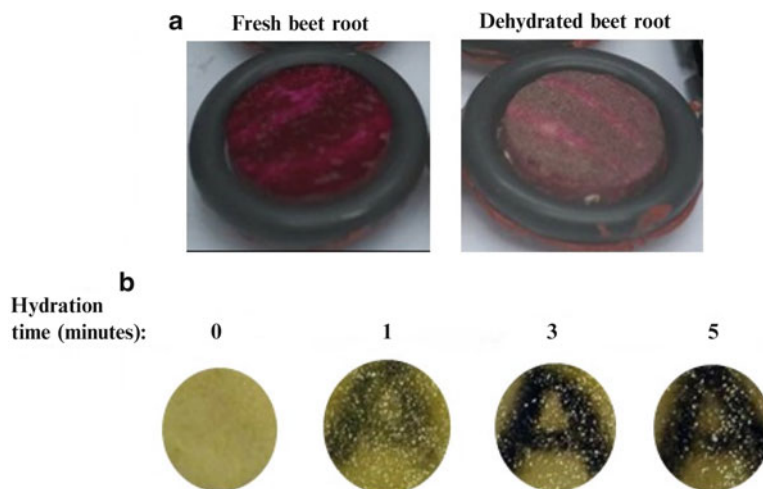


**Fig. 1** Effects of water on food appearance: color enlightening on beetroot due to dehydration (a) and translucence increase due to rehydration of apple discs (b)

the dried material. Their reflectance measurements and visual appearance do not reflect the actual pigment concentration. This phenomenon has been widely studied in the paper industry and is attributed to the diffusion of light inside a material at interphases of different refraction indexes (Saarela et al. 2008).

Upon rehydration by imbibition, water (of refractive index much closer to that of the solids than air) occupies part of the pores generated in freeze-drying process (Lana et al. 2006; Talens et al. 2002), and the samples recover transparency, as shown in Fig. 1b for the imbibition of freeze-dried apple slices at different times.

## 2.2 Appearance/Disappearance of Particles (Crystals/Bubbles Formation or Solids Dissolution)

Light scattering due to the presence of microscale particles causes a lightening effect when the wavelength of light approaches the particles' radius. Figure 2a shows that increasing the concentration of scattering particles (in this case nondairy cream) at a constant Maillard pigment concentration promotes a whitening appearance.

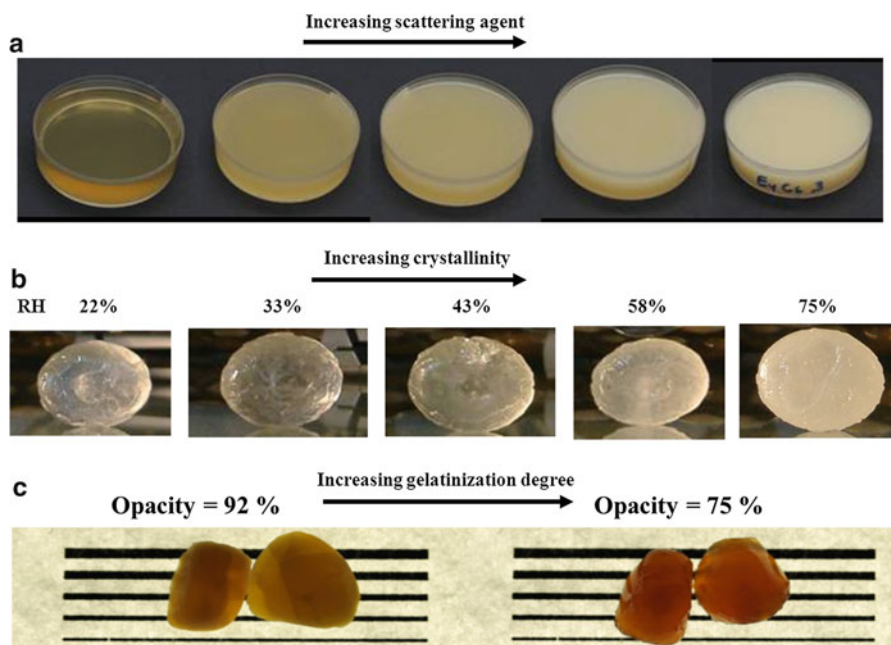


**Fig. 2** Color enlightening due to increasing concentration of light scattering particles: at constant pigment concentration (a); effect of sugar crystallization in amorphous hard candies promoted by increased mobility with increasing relative humidity (b); and opacity changes due to gelatinization degree (c)

In the same way, hard candies stored above the glass transition temperature become “whiter” as relative humidity (RH) increases, due to the higher amount of sugar crystals, which increases with temperature-glass transition temperature ( $T-T_g$ ) thus causing increased light scattering (Fig. 2b).

Starch is a highly structured polymer; it has crystalline as well as amorphous regions structured in layers inside starch granules. This structure produces the effect of opacity in corn grits (Fig. 2c, left), which show opacity values close to 1 (calculation formula is detailed in Sect. 3.3). Samples in Fig. 2c were placed over a scale of lines with increasing thickness and retro-illuminated. In this way, transparency could be compared semiquantitatively by observing which lines remained visible through the sample. Upon gelatinization in the excess of water during cooking of grits in cornflakes production, the water interacts with glucose units in the starch molecules, replacing glucose-glucose interchain interactions. Crystalline structure of starch is lost, the material matrix becomes more homogeneous after cooking, and therefore opacity decreases (transparency increases), as shown in Fig. 2c, right for the cooked grits. It is to be noted that simple measurements such as transparency/opacity, appropriately standardized, may be used to obtain relevant information and control the cooking process.

### 3 Materials and Methodology for the Study of Appearance Properties

#### 3.1 Materials

Changes in translucency due to different hydration degrees were evaluated in powders obtained from freeze-dried fruits. Powdered melon and pear were then rehydrated at several RH values, in the range of 11–84 %.

In order to evaluate structural changes promoted by starch gelatinization, compression, and high-temperature treatments, corn grits from different stages of cornflakes production were analyzed. The cornflakes production is comprised of several stages: firstly, corn kernels are milled to remove germ and bran and grits are obtained. Then, corn grits are mixed with water, sugar, and malt extract and steam-batch cooked. The flaking process is performed by compressing cooked grits (after tempering), between two steel rolls to obtain the flaked product. The final toasting step is carried out under hot air current at approximately 200 °C. Along this process the samples undergo important chemical and physical changes.

### 3.2 Chromatic Attributes

The chromatic properties and luminosity of samples presented in this work were obtained by a computer vision system (CVS) composed of a high resolution (10.1 megapixel) digital camera (EOS 40D, Canon Inc., Japan) with an EF-S 60 mm f2.8 macro lens (Canon Inc., Japan) operated through software. The samples were placed in a standardized diffuse-illumination cabinet painted with Munsell 7 gray color, using a D65 standard light source. The angle between the camera lens axis and the lighting source axis was 45°, at which the diffuse reflection responsible for the color occurs. CIELAB color coordinates (luminosity,  $L^*$ , red/green  $a^*$ , and yellow/blue,  $b^*$ ) were calculated from the images using Adobe Photoshop software (Yam and Papadakis 2004).

For browning degree determination at the different process stages of cornflakes, the absorbance at 420 nm was measured in the protease hydrolyzed extracts and the color CIE tristimulus values  $X$ ,  $Y$ , and  $Z$  (D65 light source and 2° observer angle) were calculated from a transmittance spectrum in a Shimadzu 1620 UV-VIS spectrophotometer, from which the hue angle ( $h'_{ab}$ ) and the browning index (BI) were obtained as previously described (Buera and Resnik 1990):

$$\text{BI} = \frac{x - 0.31}{0.172} \quad (1)$$

where  $x$  is the CIE 1931 chromatic coordinate obtained for illuminant  $C$  at 2° observer.

### 3.3 Opacity

Opacity degree of samples was calculated as the ratio of  $L^*$  values when the samples are measured with black ( $L^*_{\text{b}}$ ) and white ( $L^*_{\text{w}}$ ) backgrounds (Eq. (2)), at a given sample thickness. An opacity value of 1 corresponds to an opaque sample, while lower values correspond to different degrees of translucency. As sample thickness increases, opacity increases. At a certain thickness, at which the measured reflectance is independent on the background, the material behaves as opaque.

$$\text{Opacity} = \frac{L^*_{\text{blackbackground}}}{L^*_{\text{whitebackground}}} \quad (2)$$

### 3.4 Translucence

The Kubelka–Munk analysis was originally derived in 1931; this analysis found extensive use in the industry of paints and inks (Džimbeg-Malčić et al. 2011). The Kubelka–Munk analysis was also applied to food materials in which the color is

affected by the background, such as in the case of translucent samples (Law and Norris 1973; Budiastra et al. 1998; MacDougall 2002; Talens et al. 2002; Rozycki et al. 2010).

Reflectance measurements are used to calculate the variables of Kubelka–Munk theory, as described by Judd and Wyszecki (1975), through the following equations:

$$a = \frac{1}{2} \left[ R + \left( \frac{R_0 - R + R_g}{R_0 \times R_g} \right) \right] \quad (3)$$

$$b = (a^2 - 1)^{1/2} \quad (4)$$

$$R_\infty = a - b \quad (5)$$

$$K/S = \frac{(1 - R_\infty)^2}{2 \times R_\infty} \quad (6)$$

$$S = \frac{1}{b} \operatorname{arctgh} \left[ \frac{(1 - a \times R_0)}{b \times R_0} \right] \quad (7)$$

$$K = S(a - 1) \quad (8)$$

In these equations,  $S$  is the dispersion coefficient, which is related to the scattering particles in the media;  $K$  is the attenuation coefficient, which is related to the pigment concentration; and  $R_\infty$  is the reflectance of an infinitely thick layer of the material, determined through Eqs. (3) and (4) in terms of the reflectance  $R$  of the sample layer backed by a white background with a known reflectance  $R_g$  and the reflectance  $R_0$  of the sample with an ideal black background. The ratio between the absorption coefficient ( $K$ ) and the scattering coefficient ( $S$ ),  $K/S$ , was observed to correlate with browning development in several translucent food systems (Rozycki et al. 2010).

## 4 Translucence Changes

### 4.1 Fruit Products

The  $K$  and  $S$  values were calculated for powdered melon and pear systems at several RH at which the samples were stored. Figure 3 shows that the scattering coefficient,  $S$ , in both materials decreased drastically at about 30 % RH and above. Since  $S$  represents the amount of scattering particles in the samples, it can be concluded that the scattering points inside the fruit powders decrease due to hydration, and transparency consequently increased when water started to fill the pores of the dried material.

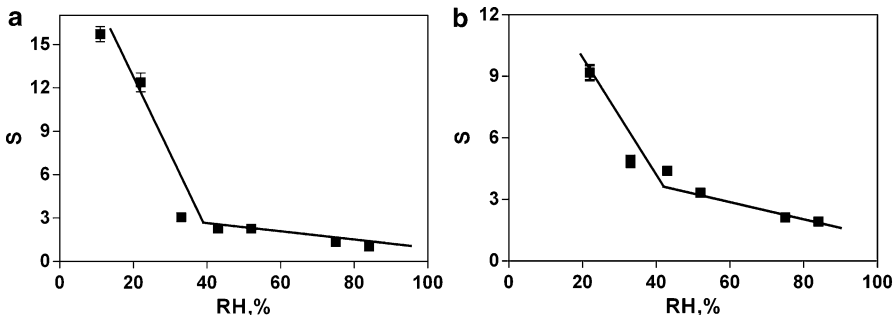


**Fig. 3** Scattering coefficient ( $S$ ) as a function of relative humidity for melon (a) and pear (b) powders

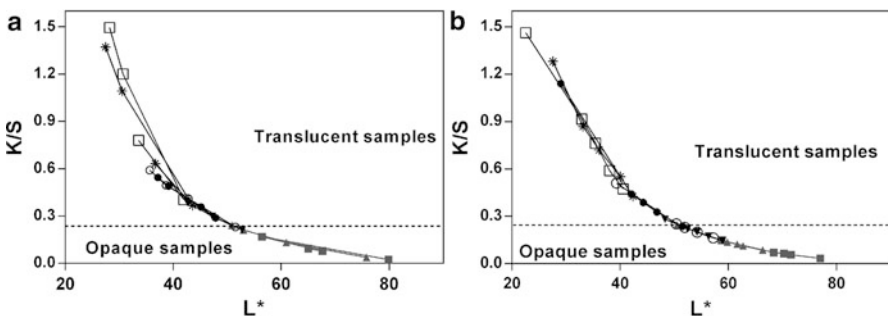


**Fig. 4**  $K/S$  as a function of luminosity ( $L^*$ ) from dehydrated powders of melon (a) and pear (b), after humidification at relative humidities of 11 (filled square), 22 (filled triangle), 33 (filled inverted triangle), 43 (open circle), 52 (filled circle), 75 (star), and 84 % (open square). The dotted line indicates the limit between opaque and translucent samples

Besides the opacity changes, the samples also became darker. Figure 4 shows the relationship between  $K/S$  and  $L^*$  values for powdered samples of melon (a) and pear (b) rehumidified at several RH. Both variables were related to the degree of darkening promoted by nonenzymatic reactions. At low RH values (11–22 % RH), the systems behave as opaque materials (according to the previous discussion in relation to Fig. 3), and the variation of  $K/S$  values is smaller than that for the  $L^*$  values. However, with increasing RH the systems are more translucent, and  $K/S$  becomes more sensitive to detect sample darkening than  $L^*$  values. In this way, the selected variable to detect color changes sensitively is also dependent on the hydration degree. The simple measurement of  $L^*$  is adequately sensitive when the materials behave as opaque. However, when translucence increases, the  $K/S$  variable from the Kubelka–Munk theory is a better alternative and requires measurements under black and white backgrounds.

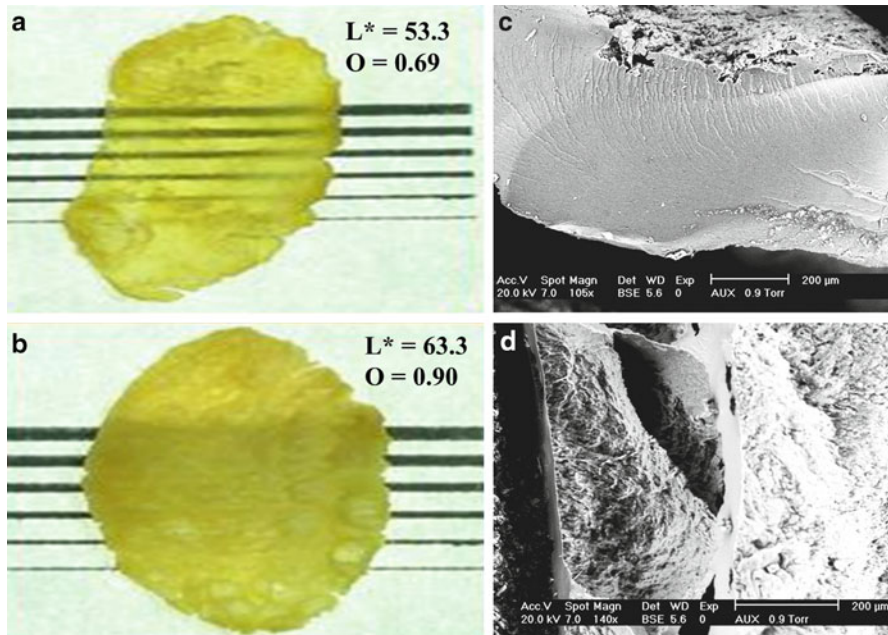


**Fig. 5** Retro-illuminated images of flaked grits (**a**) and toasted cornflakes (**b**). The *black lines* in the back are no longer seen in the toasted cornflakes due to the bubbles formation during toasting. Luminosity ( $L^*$ ) and Opacity ( $O$ ) values for each samples are also indicated. Images (**c**) and (**d**) correspond to SEM micrographs of flaked and toasted samples, respectively

## 4.2 Cereal Products

Figure 5 shows flaked and toasted corn grits obtained from intermediate stages of cornflake processing. As described previously, transparency can be compared semiquantitatively by observing which lines remain visible through samples when they are placed over a scale of lines with increasing thickness and retro-illuminated. As can be clearly observed, coincident to the measured opacity (also indicated in Fig. 5), the flaked grits are quite transparent, but opacity increased after the toasting step. The observation of sample microstructure (through a Philips XL 30 electron microscope by environmental mode (ESEM) without previous sample treatment) showed that the toasting process created a porous structure due to sudden water evaporation, as shown in the scanning electron microscopy (SEM) micrographs in the left side of Fig. 5. This change in structure had a major effect on appearance and increased opacity.

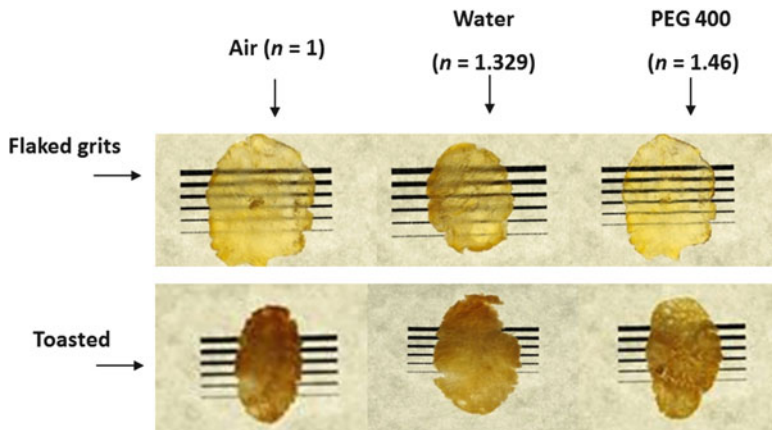


**Fig. 6** Transparentization of flaked grits and toasted cornflakes through  $n$  matching, by imbibition in air, water, and polyethyleneglycol (PEG) 400

#### 4.2.1 Transparentization by Refractive Index Matching

Inhomogeneities present in the internal structure of samples explain the changes in appearance shown in previous figures. When light passes through a transparent media and encounters different phases with different refraction indexes ( $n$ ), the path of light beams changes on every interface due to refraction. In the example of toasted cornflakes samples, the pores are filled with air and the refractive index mismatch between the air and the matrix is significant. Thus, many scattering events occurred within the cornflake, the paths of separate photons rapidly became chaotic, and the opacity of the final material increased as compared to the flaked samples.

When the pores are filled with air, the refractive index mismatch between the air and the matrix is significant. By imbibiting the sample with fluids of which the refraction index is closer to that of the matrix, the  $n$  could be homogenized. This effect is shown in Fig. 6, where flaked grits imbibed with polyethylene glycol (PEG) 400 ( $n = 1.46$ ) look more transparent than flaked grits imbibed in water ( $n = 1.33$ ) or air ( $n = 1$ ).

#### 4.2.2 Correlation Between Reflectance and Chemical Markers of the Maillard Reaction

Table 1 shows the correlation coefficients between the analyzed variables for the complete process of cornflake production, including all stages. It is to be noted that those variables derived from surface (reflectance) measurements ( $h'_{ab}$ ,  $L^*$ , and  $K/S$ ) correlated between them (shaded region in the upper part of Table 1). On the other

**Table 1** Correlation coefficients ( $r^2$ ) for the variables taken from reflectance measurements:  $L^*$ , hue ( $h'_{ab}$ ), and the ratio between the absorption and scattering Kubelka–Munk coefficients ( $K/S$ ); and from aqueous extracts after enzymatic treatment: absorbance at 420 nm ( $A_{420}$ ) and browning index (BI), for the entire cornflake production process

	$L^*$	$h'_{ab}$	$K/S$	$A_{420}$	BI
$L^*$	1	0.91	-0.97*	-0.18	0.01
$h'_{ab}$		1	-0.97*	0.17	0.04
$K/S$			1	0.09	0.01
$A_{420}$				1	0.98
BI					1

\*Indicates statistically significant correlation  $p < 0.05$

**Table 2** Correlation coefficients ( $r^2$ ) for the variables taken from reflectance measurements:  $L^*$ , hue ( $h'_{ab}$ ), the ratio between the absorption and scattering Kubelka–Munk coefficients ( $K/S$ ); and from aqueous extracts after enzymatic treatment: absorbance at 420 nm ( $A_{420}$ ) and browning index (BI), for cooking process only

	$L^*$	$h'_{ab}$	$K/S$	$A_{420}$	BI
$L^*$	1	0.94*	-0.97*	-0.82*	-0.81*
$h'_{ab}$		1	-0.94*	-0.75*	-0.68*
$K/S$			1	0.77*	0.76*
$A_{420}$				1	0.97*
BI					1

\*Indicates statistically significant correlation  $p < 0.05$

hand, the chemical markers for the Maillard reaction in the aqueous extracts ( $A_{420}$  and BI) were highly correlated (shaded region in the underside of Table 1). However, due to shape and transparency changes, surface variables did not correlate with the values obtained from solubilized extracts.

Experiments with model systems are shown in Table 2. This model only included the cooking step of corn grits, avoiding the dramatic shape and structural changes produced by flaking and toasting. During cooking of corn grits, slight changes in shape and surface rugosity take place, and reflectance variables correlated better with those chemical markers obtained after pigment solubilization in aqueous extracts.

## 5 Conclusions

The chromatic perception of foods is affected not only by pigment development but also by changes in optical properties that are caused by supramolecular transitions (crystallization, gelatinization), formation of bubbles, and other structural changes affecting sample microstructure, which depend on the degree of hydration.

Many changes produced during food processing involve the destruction or generation of interfaces and affect the way in which light interacts with the sample matrix. The extension of most of those changes is defined by water content. An integral approach that takes into account color, pigment concentration, as well as the effect of water on the microstructure and the effect of water on the physical changes is important in order to understand visual color perception of foods.

## 6 Future Work

The mathematical development of *cesia* solids, such as those available for the chromatic aspects of appearance, will allow better analysis and prediction of the integrated aspects affecting sample visual characteristics. Such development will provide tools for innovative product development and for process control and will necessarily require multidisciplinary interactions, involving concepts from physics, mathematics, chemistry, engineering, photography, imaging, and architecture.

## References

- Agudelo-Laverde LM, Schebor C, Buera MP (2012) Color determination in dehydrated fruits: image analysis and photolorimetry. In: Caivano JL, Buera MP (eds) Color in food: technological and psychophysical aspects. CRC, Boca Raton, pp 155–162
- Agudelo-Laverde LM, Schebor C, Buera MP (2013) Water content effect on the chromatic attributes of dehydrated strawberries during storage, as evaluated by image analysis. *LWT Food Sci Technol* 52:157–162
- Budiastra IW, Ikeda Y, Nishizu T (1998) Optical methods for quality evaluation of fruits, 1: optical properties of selected fruits using the Kubelka-Munk theory and their relationships with fruit maturity and sugar content. *J Jpn Soc Agric Mach* 60:117–128
- Buera M, Resnik S (1990) Colorimetric measurements in a turbid medium: hydrolyzed concentrated cheese whey. *Die Farbe* 35:268–272
- Caivano JL (1991) Cesia: a system of visual signs complementing color. *Color Res Appl* 16:258–268
- Caivano JL (1994) Appearance (*cesia*): construction of scales by means of spinning disks. *Color Res Appl* 19:351–362
- Caivano JL (1996) Cesia: its relation to color in terms of the trichromatic theory. *Die Farbe* 4 (1/3):51–63
- Caivano JL, Menghi I, Iadisernia N (2004) Cesia and paints: an atlas of cesia with painted samples. AIC 2004 Color and Paints, Interim Meeting of the International Color Association, Proceedings
- Hutchings JB (1999) Food color and appearance, 2nd edn. Kluwer Academic/Plenum Publishers, London, pp 61–90
- Džimbeg-Malčić V, Barbarić-Mikočević Ž, Itrić K (2011) Kubelka-Munk theory in describing optical properties of paper (I). *Tech Gaz* 18(1):117–124
- Judd DB, Wyszecki G (1975) Color in business, science and industry, 3rd edn. Wiley, New York, pp 395–442
- Lana MM, Hogenkamp M, Koehorst RBM (2006) Application of Kubelka-Munk analysis to the study of translucency in fresh – cut tomato. *Innov Food Sci Emerg Technol* 7:302–308

- Law SE, Norris KH (1973) Kubelka-Munk light-scattering coefficients of model particulate systems. *Trans ASAE* 16(5):914
- MacDougall DB (2002) Color measurement of food: principles and practice. In: MacDougall DB (ed) *Color in food-improving quality, Food science and technology*. Woodhead Publishing, Cambridge, pp 33–63
- Rozycki SD, Buera MP, Piagentini AM, Costa SC, Pauleti MS (2010) Advances in the study of the kinetics of color and fluorescence development in concentrated milk systems. *J Food Eng* 101:59–66
- Saarela J, Heikkilä S, Fabritius T, Haapala A, Myllyla R (2008) Refractive index matching improves optical object detection in paper. *Meas Sci Technol* 19:1–8
- Talens P, Martínez Navarrete N, Fito P, Chiralt A (2002) Changes in optical and mechanical properties during osmodehydrofreezing of kiwi fruit. *Innova Food Sci Emerg Technol* 3:191–199
- Yam K, Papadakis S (2004) A simple digital imaging method for measuring and analyzing color of food surfaces. *J Food Eng* 61:137–141

# **Maillard Reaction in Limited Moisture and Low Water Activity Environment**

**C.W. Wong, H.B. Wijayanti, and B.R. Bhandari**

## **Abbreviations**

$a_w$	Water activity
IMF	Intermediate moisture food
$\Delta E^*$	Color difference
$k$	Reaction rate constants
$r^2$	Coefficients of determination
$C$	Values of index (color)
$t$	Time
$K$	Relation between the zero-order kinetic constant for the color formation
$k_0$	Zero-order kinetic constant for the color formation
$k_1$	First-order kinetic constant for the color disappearance
$t_0$	Induction time
ANOVA	Analysis of variance
MRPs	Maillard reaction products

## **1 Introduction**

Maillard reaction is a nonenzymatic browning reaction that involves the reaction of carbonyl groups, primarily reducing sugars with free amino groups which cause the changes of chemical and physiological properties of proteins (Labuza and Saltmarsh 1981). It results in the development of complex mixtures of colored

---

C.W. Wong • H.B. Wijayanti • B.R. Bhandari (✉)

School of Agriculture and Food Sciences, The University of Queensland,  
Brisbane, QLD 4072, Australia  
e-mail: [b.bhandari@uq.edu.au](mailto:b.bhandari@uq.edu.au)

and colorless reaction products which range from flavor volatiles (low molecular weight compounds) to melanoidins, a series of brown pigments with high molecular weights (Carabasa-Giribet and Ibarz-Ribas 2000; Martins and Van-Boekel 2005); these effects could be either desirable or undesirable. Browning and the formation of aroma are desired in baking, roasting, or frying, while it is undesirable in the foods which have a typical weak or other color of their own such as browning in the products of condensed milk, white dried soups, tomato soup, etc. and generation of off-flavors in food during storage. Besides, Maillard reaction can also have negative effects on nutritional values such as the losses of essential amino acids, as well as the formation of mutagenic compounds (Belitz et al. 2004).

The rate of Maillard reaction and the nature of the colored products are controlled by its immediate chemical environment including temperature, heating time, pH, and the composition of the system (nature, concentration, and proportion of the reactants), as well as water activity ( $a_w$ ). The regulation of all these factors is one of the ways to control the Maillard reaction progress and hence the browning compounds formed in the system (Ames 1990; Laroque et al. 2008).

Water activity is believed to be one of the important factors in controlling the Maillard reaction. The chemical reaction is controlled by the effect of moisture content or  $a_w$  on reactant dissolution, mobility, and concentration. An increase in  $a_w$  to a certain level can increase reactant solubility and mobility and thus the rate of chemical reaction. However, the reaction rate will decrease when  $a_w$  increases further. This is because the moisture content tends to dilute the concentration of reactants; thus, it limits the availability of mobile water lowering the mobility of the system and thereby decreases the reaction rate. The maximum browning rate generally had been observed in most foods at  $a_w$  0.65–0.75, and reaction will cease at  $a_w$  below 0.3 (Warmbier et al. 1976).

Glycerol is a liquid humectant which contains residual water of less than 0.5 %. It is naturally present in many foods and is used as food additive, as well as a conditioner, moisturizer, and solvent for flavor extracts (Cerny and Guntz-Dubini 2006). It also helps to lower the  $a_w$  in the food; therefore, it increases the microbial stability of the food and provides longer shelf life to the product especially in intermediate moisture food (IMF). The glass transition temperature of the pure glycerol is  $>-80^\circ\text{C}$  (He et al. 2006). Therefore, glycerol has a sufficient molecular mobility at higher temperatures than  $-80^\circ\text{C}$  to allow the chemical reactions to occur.

Maillard reaction has been proved to occur even at low  $a_w$  due to the presence of glycerol. This was thought to be an effect of reduced  $a_w$  and the different physiochemical environments (Cerny and Guntz-Dubini 2006). This effect was studied few decades ago (Warmbier et al. 1976; Eichner and Karel 1972; Labuza and Saltmarch 1981; Mustapha et al. 1998; Sherwin and Labuza 2003). Eichner and Karel (1972) studied the extent of Maillard browning in a liquid model system of glycine-glucose in glycerol and found that browning rate increased with decreasing water activity. Besides, Mustapha et al. (1998) noted high browning in xylose/lysine in glycerol model system if no water was added, even though the reactants were not fully solubilized. These authors added that the maximum browning

occurred if moisture content increased up to 30–40 %. Similarly, Sherwin and Labuza (2003) reported that high browning rates were observed over the  $a_w$  of 0.11–0.75 in the glycerol model system in their study. They proved that  $a_w$  cannot be used alone as an indicator to predict the nonenzymatic browning reaction rate because solubility and interference reactant mobility within the total phase are the main key for reactions to proceed. Their result showed that the addition of liquid phase humectants (glycerol) in a model system of D-glucose-caseinate-sodium benzoate had a higher reaction rate compared to control at low to intermediate  $a_w$ . However, acceleration of the Maillard reaction caused by added humectants has not been previously reported. Further understanding of the Maillard reactions in limited water but mobile system would be helpful to explain the stability issues of many dried and intermediate food products. Therefore, the objective of this research is to investigate the Maillard reaction in non-water semipolar model liquid systems. Glycerol has been found solubilizing all the common sugars (fructose, glucose, lactose, maltose, and sucrose) at various degrees (Bhandari 2010). The hypothesis of this research was that if glycerol can dissolve solutes (reactant molecules), then it will promote various chemical reactions in foods in the similar way that water does, by increasing the molecular mobility of the system.

## 2 Materials and Methods

### 2.1 Preparation of Model System

Chemicals used in this study included hexoses (D-glucose, D-fructose) and a disaccharide (lactose), amino acid (glycine), and glycerol (99.5 % v/v). All the chemicals used were of the analytical grade supplied by Ajax Finechem (Sydney, Australia).

The model systems used in the experiment consisted of 13.5 mg of reducing sugar and 6.68 mg of glycine in 3.5 mL of glycerol at three added moisture levels: 0, 5, and 10 % (v/v). The calculated  $a_w$  for the three moisture levels was as follows: ~0 ( $a_w = 0.025$ ), 5 ( $a_w = 0.21$ ), and 10 % ( $a_w = 0.36$ ). These  $a_w$  values were predicted based on *Couchman-Karasz* model as illustrated by Katkov and Levine (2004). All sugars and glycine were dried in vacuum oven at 65 °C for 1–2 h in order to obtain anhydrous condition in the system. The samples were considered to be close to “zero” % moisture content (actual moisture contents were determined to be 0.5 %, since pure glycerol contained 0.5 % (v/v) moisture). The residual moisture in the dried sugars and amino acid can be considered negligible since the amount of sugars and amino acid used in the experiment was very low. 0.1567 mL and 0.3308 mL of Milli-Q water was added to adjust the moisture level to 5 and 10 % (v/v) in 3.5 mL glycerol. The samples were prepared in a Pyrex glass test tube and heated for 1, 2, 3, 4, 10, 17, and 24 h at 100 °C. The test tubes containing samples with ~0 % moisture were uncapped to ensure minimum residual moisture capture in the product, whereas the samples with 5 and 10 % moisture

were capped to avoid moisture evaporation. Each sample was mixed with a vortex mixer for 30 s, before and after heating. At different lengths of heating time up to 24 h, the samples were removed from the oven and cooled immediately to room temperature before color measurement analyses.

As for control, a series of sample consisting only glycine and glycerol without reducing sugars were prepared with the same concentration and treated at the same heating conditions. Systems consisting of each reducing sugar only in glycerol were also prepared and treated at the same heating temperature and time conditions to ensure that there is no caramelization of sugars. This can otherwise interfere the results. This step should not be overlooked. All treatments were performed in duplicate as per the experimental design described in Sect. 2.4 below.

## 2.2 Color Parameters and Absorbance Measurements

Absorbance values to determine the extent of browning in the Maillard reaction were analyzed by spectrophotometry. Spectrophotometric measurements were performed in a UV/VIS spectrophotometer (Shimadzu UV-1700 PharmaSpec series, Tokyo, Japan) using 1 cm quartz cell. The absorption spectra were determined over the wavelength range of 200–500 nm. Before analysis, 0.5 mL of samples (reaction products) from each test tube was taken and diluted to 10 mL by using Milli-Q water (5:100 v/v) in a 10 mL volumetric flask. The absorbance was recorded at 280 and 420 nm.

The CIE  $L^*$ ,  $a^*$ , and  $b^*$  values were measured by chromameter (CR-400, Minolta, Crystal Lake, III., USA). Tristimulus values give a three-dimensional value for color in which equal distances approximate to equal perceived color differences. The  $L^*$ ,  $a^*$ , and  $b^*$  values are the three dimensions of the measured color which gives specific color value of the material.  $L^*$  values represent light-dark spectrum;  $a^*$  value represents the green-red spectrum, while  $b^*$  value represents blue-yellow spectrum. This method has been used to measure the intensity of the browning in the Maillard product by various researchers (Ozdemir and Devres 2000). Color difference ( $\Delta E^*$ ) was expressed as  $((\Delta a^*)^2 + (\Delta b^*)^2 + (\Delta L^*)^2)^{1/2}$ . Three measurements were obtained from each sample and these values were averaged. Calibration was performed against a standard white tile (calibration plate CR-400) each time when the instrument was used.

## 2.3 Kinetic Studies

The data were subjected to regression analysis to determine the reaction order of the browning reaction. Reaction rate constants ( $k$ ) and their coefficients of determination ( $r^2$ ) were calculated. General reaction rate equation was used to evaluate the kinetic reaction rate order, when:

$$n = 0 \text{ (zero-order), } C = C_0 - kt, \quad (1)$$

$$n = 1 \text{ (first-order), } C = C_0 \exp(-kt) \quad (2)$$

The rate of browning reaction is expressed as:

$$\frac{dC}{dt} = kC^n, \quad (3)$$

where  $C$  is the values of index (color),  $n$  is the reaction order,  $k$  is the reaction rate constant, and  $t$  is time. In some cases, the following combined equation (4) (a pseudo-first-order kinetics) was tested according to Carabasa-Giribet and Ibarz-Ribas (2000):

$$C = K(1 - \exp(-(k_1)(t - t_0))) \quad (4)$$

where  $K$  is the relation between the zero-order kinetic constant for the color formation ( $k_0$ ) and the first-order kinetic constant for the color disappearance ( $k_1$ ) and  $t_0$  is the induction time.

## 2.4 Experimental Design and Statistical Analysis

The objective of this experiment was to study the effects of different independent variables, namely, heating time and moisture content on the nonenzymatic browning reaction, prepared from various sugar-amino acid-glycerol model systems. The dependent variables (experimental response) that were investigated in this study were the extent of browning (absorbance) and the intensity of browning (CIE  $L^*$ ,  $a^*$ , and  $b^*$  values). All data was collected from a completely randomized experiment, and all samples were independent and freshly prepared. Experiments were performed at least twice.

All experimental data were analyzed using the analysis of variance (ANOVA) and linear regression data analysis tools in Minitab version 15 and Microsoft Excel 2003, respectively. Whereas the nonlinear regression was done by SigmaPlot 10.0, ANOVA was performed to find out the effect of moisture and heating time on the development of browning color in the model systems. The level of statistical significance for the process variables was defined at  $p < 0.05$ . Results reported were the average of the data.

### 3 Results and Discussion

#### 3.1 Preliminary Results

##### 3.1.1 Color Development in Control

Preliminary experiments were conducted to investigate whether each reducing sugar-glycerol system and glycine-glycerol system, which was the control used in this experiment, could develop brown color under the experimental conditions. Results showed that there was no color development in each tested reducing sugar-glycerol system even though the reducing sugars were fully dissolved in glycerol either in the presence of moisture or in the absence of moisture when heated up to 24 h. No color development was noted when glycerol was heated alone under the experimental condition. This is because Maillard reaction will only occur if there is a condensation or interaction between carbonyl group from sugar and a free amine group from an amino acid (Labuza and Saltmarch 1981). However, brown color development was noted when glycine-glycerol systems heated in the absence of sugars, which also was observed in the studies from Obanu et al. (1977) and Seow and Cheah (1985). It should be noted that glycerol, a sugar alcohol, belongs to the polyol group; therefore, browning reaction did not occur between glycerol and reducing sugars, but had some effect on glycine-glycerol systems (Fig. 1a). However, the development of color was low in glycine-glycerol system as compared to each reducing sugar-glycine-glycerol model system as shown in Fig. 1b.

##### 3.1.2 Determination of Spectrum Peak

With the aim of finding the peak of absorbance vs. wavelength, the absorbance spectra between 200 and 500 nm were recorded. Simple structure compounds, produced during the early stages of Maillard reaction, are related to absorbance in the UV region (Zegota and Bachman 1987). The analysis of the spectra of browning at different moisture conditions and temperatures used allowed the detection of changes related to subsequent stages of Maillard reaction. The first stages of the browning reaction in the systems used are characterized by the appearance of absorption around 280 nm that can be related to heterocyclic derivatives. This absorbing material becomes progressively reduced due to the appearance of more complex compounds absorbing at 350 nm as the reaction proceeds (Cuzzoni et al. 1998). Wijewickreme et al. (1997) reported that the appearance of absorbance at 320 nm is due to the formation of soluble pre-melanoidins, while the absorbance at 420 nm has been used as the end-point measurement for quantifying the yield of high molecular weight melanoidins (Fogliano et al. 1999).

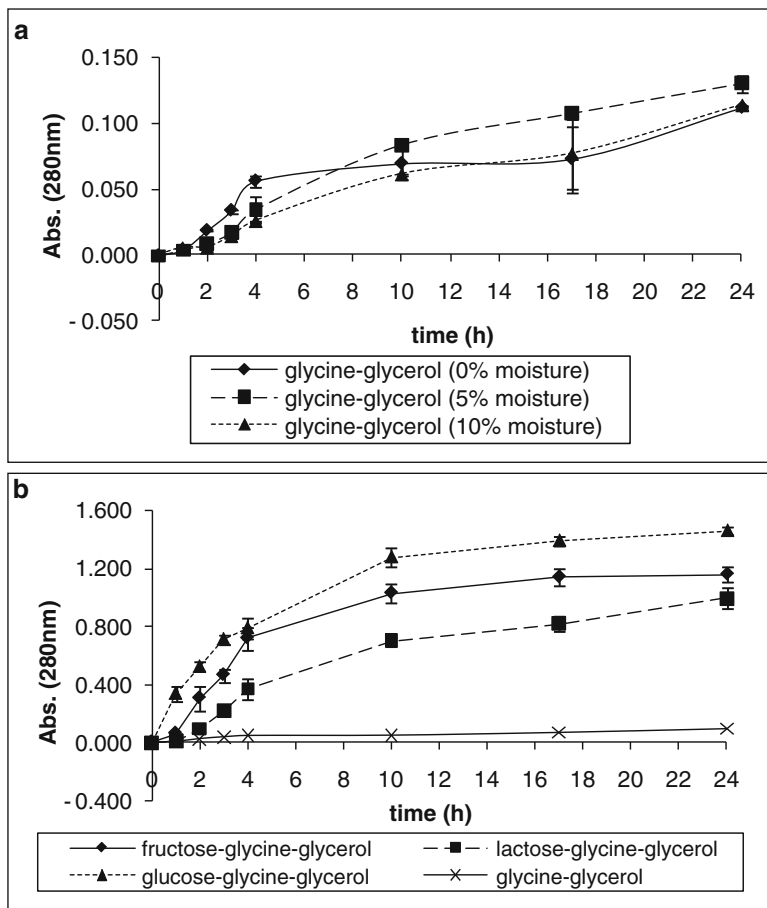


**Fig. 1** (a) Absorbance of control (glycine-glycerol) at three moisture levels monitored at 280 nm. (b) Comparison of absorbance (280 nm) between sugar-glycine-glycerol model systems with control (glycine-glycerol) at moisture level 0 %

In this experiment, the absorbance peak was observed along the wavelength between 282 and 293 nm for glucose and lactose and 278–293 nm for fructose. Absorbance peaks also occurred between 335 and 344 nm for glucose. In any case, this range of wavelength has been associated with an early stage of the reaction and low molecular weight of Maillard reaction product such as furans, pyrroles, and pyrazines (Lu et al. 2005a). Pyrazine compounds were present abundantly in the glycerol model system (Lu et al. 2005b). Figure 2a illustrated the trend of absorbance spectra of three sugars at 0 % moisture level when heated for 24 h. Obviously, the absorbance peak of these three sugars was not occurring at the exactly same wavelength. Absorbance peaks were shifted to a slightly higher wavelength if moisture was present which is shown in Fig. 2b. This indicated that the brown pigments produced in each reducing sugar-amino acid-glycerol model system

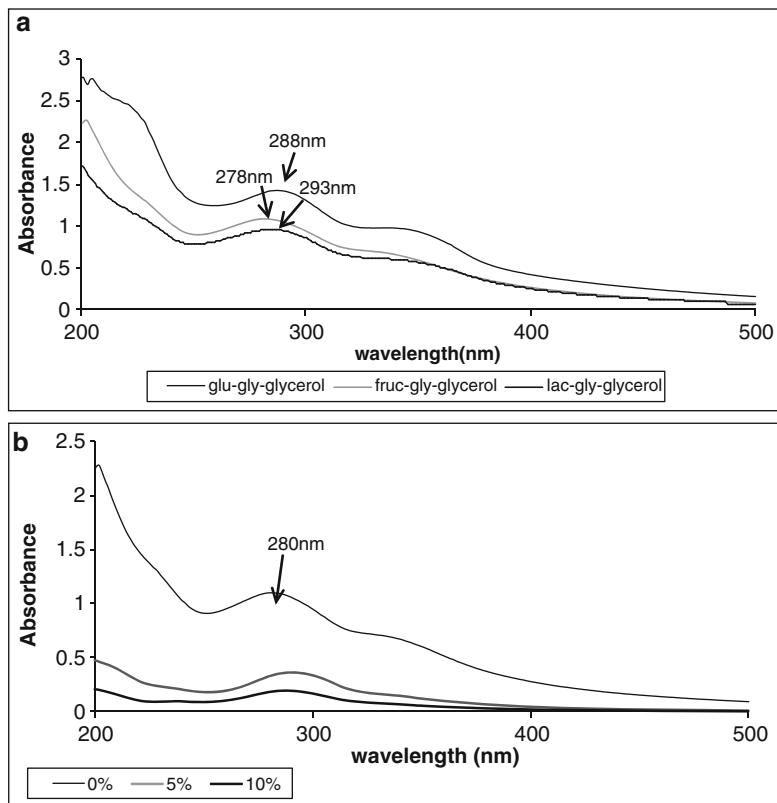


**Fig. 2** (a) Absorbance spectra of glucose-, fructose-, and lactose-glycine-glycerol model system at 0 % moisture level and heated for 24 h. (b) Absorbance spectra of fructose-glycine-glycerol model system at three moisture levels and heated for 24 h. All values refer to diluted samples (5:100 v/v)

heated under different experimental conditions are more likely to consist of a variety of several low molecular weight chromophores. Besides, no obvious absorbance peak was observed at wavelength 420 nm, which is associated with the presence of high molecular weight browning compounds, as melanoidins, even though high browning was visually observed especially when the samples with 0 % moisture were heated. It is believed that the presence of high molecular weight color material is mainly due to the colored low molecular weight molecules that were physically entrapped in the high molecular weight polymers that formed in the system, which has been reported by Fogliano et al. (1999) in gluten-glucose system under wet and dry conditions. Before this study, Hofmann (1998) also deemed that low molecular weight compounds were the main responsible factor for color formation in foods rather than high molecular weight compounds.

**Fig. 3** Picture of browning color in glucose-glycine-glycerol system at 0, 5, and 10 % moisture content (*from left to right*) after heated for 24 h



### 3.1.3 Effect of Moisture Content in the Color Development

All sugars in the glycine-glycerol systems showed the highest browning at moisture content 0 % (w/w), followed by 5 % (w/w), and 10 % (w/w) showed the least browning (Fig. 3). The intensity of the browning increased over heating time.

This observation indicated that the role of water, which used to increase the solubility of the reactant and mobility of the system, thus the rate of the chemical reaction, could be replaced by using glycerol. This finding once again proved that glycerol was able to shift the water activity downward (Warmbier et al. 1976; Eichner and Karel 1972; Mustapha et al. 1998) and hence the water activity for the maximum browning to occur either due to the hygroscopic nature (Mustapha et al. 1998) or the plasticizing effect of the glycerol itself (Eichner and Karel 1972). In any case, glycerol was proved to enhance the molecular mobility of the system and brought the maximum browning to the system at lower water activity. Water activity, in this case, was not the major factor for browning.

In this study, solubilization of the reactants (sugars and glycine) was visually observed whether there was sediment at the bottom of the test tubes. High browning was observed when no water was added to the sugar-glycine-glycerol model system (0 % moisture level), even though the reactants especially for fructose- and lactose-glycine were not completely soluble in glycerol during the first few hours heating time. This finding was in line with the study from Mustapha et al. (1998) who also observed the same phenomenon in lysine and xylose in the glycerol model system than in an aqueous matrix. However, all these three sugars were confirmed to be solubilized completely in the glycerol at 0 % moisture level after a few hours of heating time. Glucose was solubilized in the glycerol at the first hour heating time at 100 °C.

The rate of the Maillard reaction is dependent on the temperature, moisture, and heating time (Ames 1990; Misharina et al. 1992). The increasing of the browning reaction was being observed along the increasing of heating time. The browning reaction decreased as the moisture content in the glycerol model system increased.

Water, which acts as a strong polar solvent, decreased the browning rates for at least two reasons: first, a more structured liquid would be formed due to the presence of water in the solution impeding the collision of reactants by hydrogen bonding and dipole interaction between water molecules and the reactants or intermediates that developed in the solution; second, the activation step may be involved in liquidating electrical charge in the reactive molecules, and this can cause the browning rate to decrease if the content of the more polar molecule water increased.

### 3.1.4 Color Parameters

The tristimulus coordinates ( $L^*$ ,  $a^*$ , and  $b^*$  values) for each samples in the model system were measured. ANOVA was performed to determine the significant effect of the factors such as heating time and moisture content on the color changes in each sugar-glycine in glycerol model system. The measurement of glucose-, lactose-, and fructose-glycine in glycerol model systems showed that moisture content and heating time significantly affected  $L^*$ ,  $a^*$ , and  $b^*$  of the color development in the system ( $p < 0.05$ ) during heating.

A detailed analysis with one-way ANOVA was performed to determine the effect of each moisture content and heating time on the color changes in the model system. For lactose-glycine in glycerol model system, there was no significant difference over the range of moisture content studied in this experiment in  $L^*$  and  $a^*$  values ( $p > 0.05$ ), only at the first heating hour, while  $b^*$  value was significantly affected. Other than that, the effect of heating time on  $L^*$ ,  $a^*$ , and  $b^*$  values for all reducing sugar-glycine in glycerol model system was significant ( $p < 0.05$ ).

Here,  $L^*$  represents the “lightness,” while  $a^*$  and  $b^*$  are the color intensity coordinates where  $+a^*$  is the red direction,  $-a^*$  is the green direction,  $+b^*$  is the yellow direction, and  $-b^*$  is the blue direction (Gu et al. 2006; Ozdemir and Devres 2000). Redness ( $a^*$ ) and yellowness ( $b^*$ ) color parameters for glucose-, fructose-, and lactose-glycine in glycerol model system were measured and plotted in Fig. 4 at three moisture levels (a) 0 %, (b) 5 %, and (c) 10 %.

As can be seen in Fig. 4a, at moisture level 0 %, the redness ( $a^*$ ) and yellowness ( $b^*$ ) values for the three sugar-glycines in glycerol model system were unexpectedly decreased over time, even though the intensity of the color getting darker (observed visually) or the  $L^*$  values (not shown in data) were decreased over time. The trend of the  $L^*$  values was in the same direction as  $a^*$  and  $b^*$  values’ trend; as  $a^*$  and  $b^*$  values decreased,  $L^*$  values decreased at the same time. The  $a^*$  and  $b^*$  values in lactose-glycine in glycerol model system increased at the beginning, but the yellowness ( $b^*$ ) decreased when it reached the maximum point at 2 h heating time and shifted to  $+a^*$  value at 3 h heating. Both  $a^*$  and  $b^*$  values decreased over time after that. For fructose-glycine in glycerol model system,  $b^*$  value reached the maximum point at 1 h heating time, but started to decrease at 2 h heating time. The band was shifted to  $+a^*$  or the redness was increased at 2 h heating time, and both  $a^*$  and  $b^*$  values decreased over time after 2 h heating. Glucose-glycine in glycerol model system decreased over time after both  $a^*$  and  $b^*$  values reached the maximum point at the first

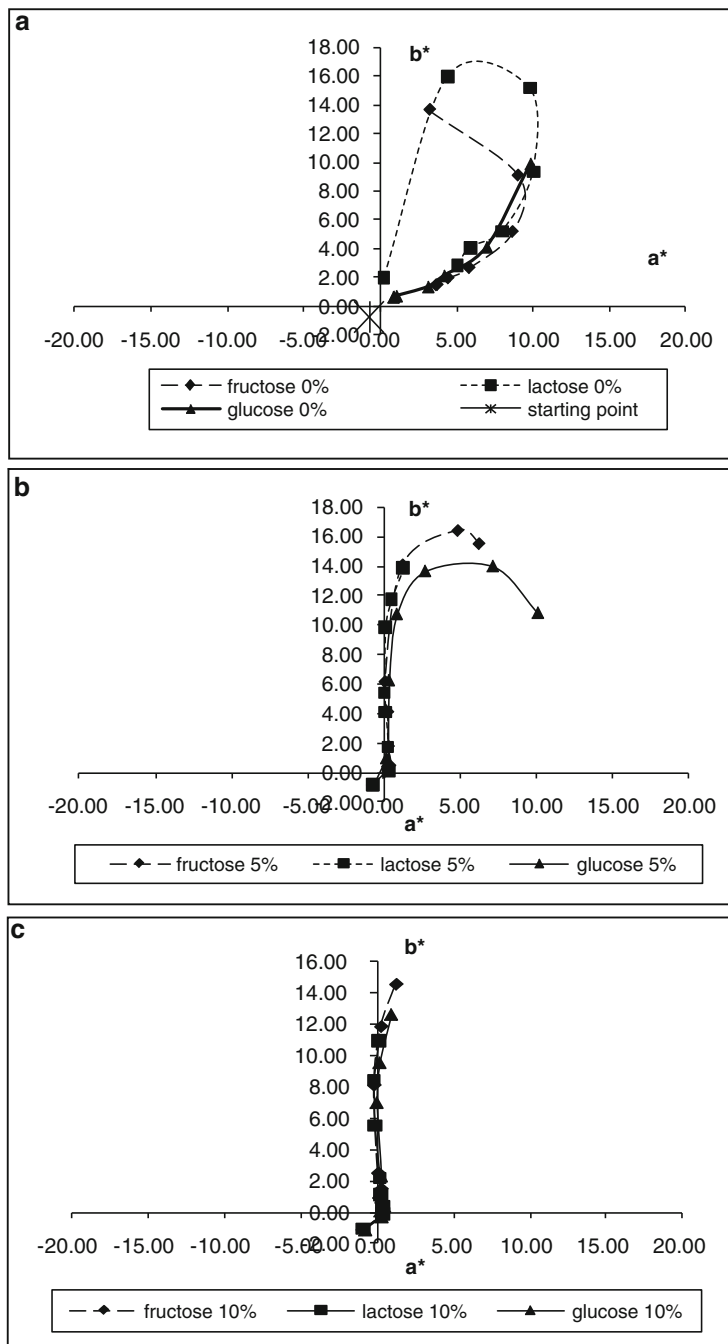


**Fig. 4**  $a^*$  vs.  $b^*$  plot with the heating time (from 0 to 24 h) at 100 °C for fructose-, lactose-, and glucose-glycine-glycerol system at moisture content (a) 0 %, (b) 5 %, and (c) 10 %

hour heating time. Generally, the behavior for all these three sugar-glycines in glycerol model system in  $a^*$  and  $b^*$  plot was similar at 0 % moisture content as  $a^*$  and  $b^*$  values decreased over time after they reached the maximum point, respectively, even though marked browning was visually observed.

In contrast, for the system at 5 and 10 % moisture levels, as illustrated in Fig. 4b, c, yellowness ( $b^*$ ) increased over time, but there were slight inconsistent changes in  $a^*$  values, especially for 10 % moisture level model system. It should be noted that the trend for glucose and fructose model system in  $b^*$  values was similar to the model system at 0 % moisture level during the end of the process, when the color of the samples began getting darker (visually observed) or  $L^*$  values decreased as heating time increased. The trends for both sugar model systems shifted to  $+a^*$  at the end of few hours heating time, and yellowness ( $b^*$ ) was decreased significantly for glucose model system and slightly decreased for fructose model system. The similar trend was expected for lactose model system if longer heating time was tested, since the drawn band was shifted slightly to  $+a^*$ , and it was postulated that the trend of  $a^*$  and  $b^*$  values will decrease after they reach the maximum point, as the other two sugars behaved.

The decrease of yellowness and redness over time was observed in 0 % moisture and also in some samples in 5 % moisture model system, especially in glucose model system, even though strong browning was visually observed. However, it could be explained as below:

- The decrease of lightness ( $L^*$ ) over time was attributed to the less amount of light scattering. Reactants had reacted in the glycerol and browning formed over time; hence, it is reasonable to find that browning color of the solution became stronger as the heating time increased.
- The decrease of  $a^*$  and  $b^*$  values might be due to the brown color being too dark to be detected. Referring to Fig. 5 and the picture illustrated in Fig. 6, the

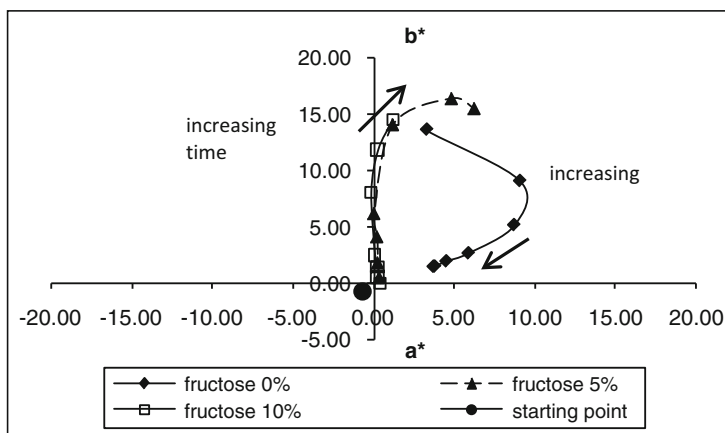


**Fig. 5**  $a^*$  vs.  $b^*$  plot with the heating time (from 0 to 24 h) at 100 °C for fructose-glycine-glycerol model system at moisture content 0, 5, and 10 %. Note: 2 points were overlapping at 17 and 24 h at moisture level 0 %

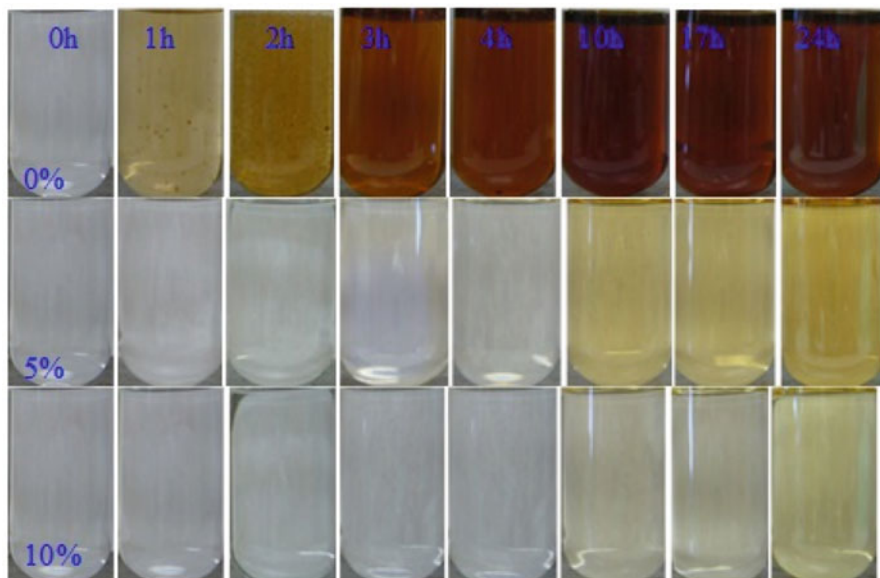


**Fig. 6** Color development in fructose-glycine in glycerol model system at moisture level of 0, 5, and 10 % (*top to bottom*)

- $b^*$  value reached the maximum point when the sample turned from the optically transparent color into light yellow brown at heating time 1 h (Fig. 6 1 h moisture 0 %,). The trend was then shifted to  $+a^*$  (redness) while going down to  $-b^*$  direction at the 2 h heating time. Both  $a^*$  and  $b^*$  values tended to decrease from heating time at 3 h. This indicated that the colorimeter could only be able to detect the formation of yellowish color up to 1 h in fructose-glycine in glycerol model system at 0 % moisture content (Fig. 6 1 h moisture 0 %), while formation of redness until 2 h (Fig. 6 2 h moisture 0 %).
- (c) For 5 % moisture level, the  $b^*$  values (yellowness) increased over time up to 17 h. The trend tended to shift to the  $+a^*$  (redness) after 10 h heating time. The  $b^*$  value (yellowness) decreased after 17 h heating time (Fig. 5). The colorimeter could only detect the formation of yellowish color up to 17 h as shown in Fig. 6 (17 h, moisture 5 %).
  - (d) Therefore, it can be concluded that the tolerance of the colorimeter in detecting yellowish pigment was only up to the color intensity as illustrated in Fig. 6 (17 h, moisture 5 %; 1 h, moisture 0 %) or lighter. Therefore, it seems that it is not a problem for the model system consisting of 10 % moisture content, due to the lightness of the brown color formed in this system.

Sherwin and Labuza (2003) reported that the change of  $b$  value showed a consistent increase over time and correlates well to brown pigment production; therefore, it was thought to be a most reliable measurement than absorbance method; however, it is not the case for this experiment. Authors also deemed that

$L$  and  $a^*$  values were not useful indicators for brown pigment production, due to the variability of these parameters which was greater than any consistent increase or decrease (Sherwin and Labuza 2003). This is true for  $a^*$  values in this experiment but not  $L^*$  values.  $L^*$  values were showing consistent decrease (data not shown) as the darkness of the samples increased.

The color difference ( $\Delta E^*$ ) of three sugar model systems was plotted in Fig. 7a–c at three moisture levels. Clearly, the formation of color in these three sugar model systems was very high at 0 % moisture level. For glucose-glycine model system (Fig. 7a), the color changed significantly during the first induction time, but after all, it remained unchanged over the heating time. A similar trend was also observed in fructose and lactose model systems that increased significantly at the first few hours of heating time and remained constant after reaching the maximum point at a certain heating time. At 5 and 10 % moisture levels, the color changes ( $\Delta E^*$ ), for glucose and fructose model system increased steadily over time, but less significant color change was observed for lactose model system.

### 3.1.5 Reaction Rate and Kinetic Order

Absorbance was measured at 280 and 420 nm, and the results showed that color development was significantly affected by moisture content and heating time ( $p < 0.05$ ). The rate of nonenzymatic browning reaction at three different moisture levels of the model systems increased with the heating time. As expected, the browning rate was the highest in 0 % moisture content model system, since the strong browning was visually observed as illustrated in Fig. 8, followed by 5 % and then 10 % moisture content model system which gave the least browning rate. Comparing both absorbances at 280 and 420 nm, the rate obtained at 280 nm was higher than the one at 420 nm, and this has been reported by many other researchers (Warmbier et al. 1976; Carabasa-Giribet and Ibarz-Ribas 2000; Miao and Roos 2004) (Fig. 8). This trend was typical for food models with low and intermediate water contents (Warmbier et al. 1976).

Generally, the nonenzymatic browning reaction in foods follows either first order (see Eq. (2)) or zero order (see Eq. (1)) (Warmbier et al. 1976; Kamman and Labuza 1985; Laroque et al. 2008; Miao and Roos 2004). When the change in intermediate Maillard reaction products (MRPs) yields a linear plot versus reaction time, it is regarded as zero-order reaction; when the production of MRPs increases in the course of the Maillard reaction and finally reaches a plateau phase, the reaction is called first order with respect to intermediate MRPs (Laroque et al. 2008). However, it is not always possible to apply kinetics as simple as zero or first order to describe the color changes in Maillard reaction (Ibarz et al. 1999). Two stage mechanisms in the nonenzymatic browning reaction were proposed by Ibarz et al. (1999) on the basis of the color deterioration produced in thermal treatments. The first stage consists of browned polymeric compound formation which is regarded as a zero-order kinetics, while the second stage is the decomposition of these brown pigments to give colorless compounds (or color destruction)

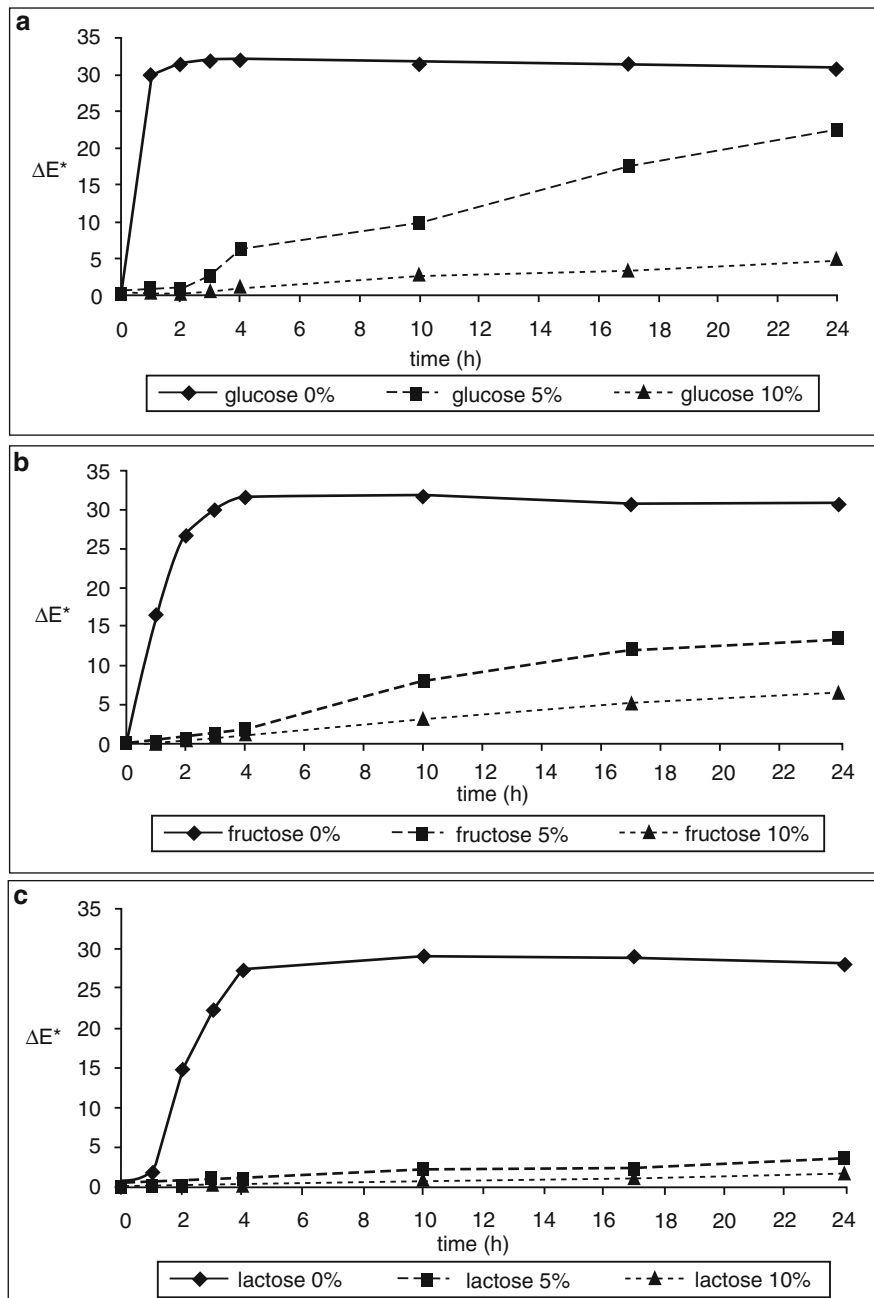


**Fig. 7** The color difference ( $\Delta E^*$ ) of three sugar-glycines in glycerol model system, namely, (a) glucose, (b) fructose, and (c) lactose, at 0, 5, and 10 % moisture content

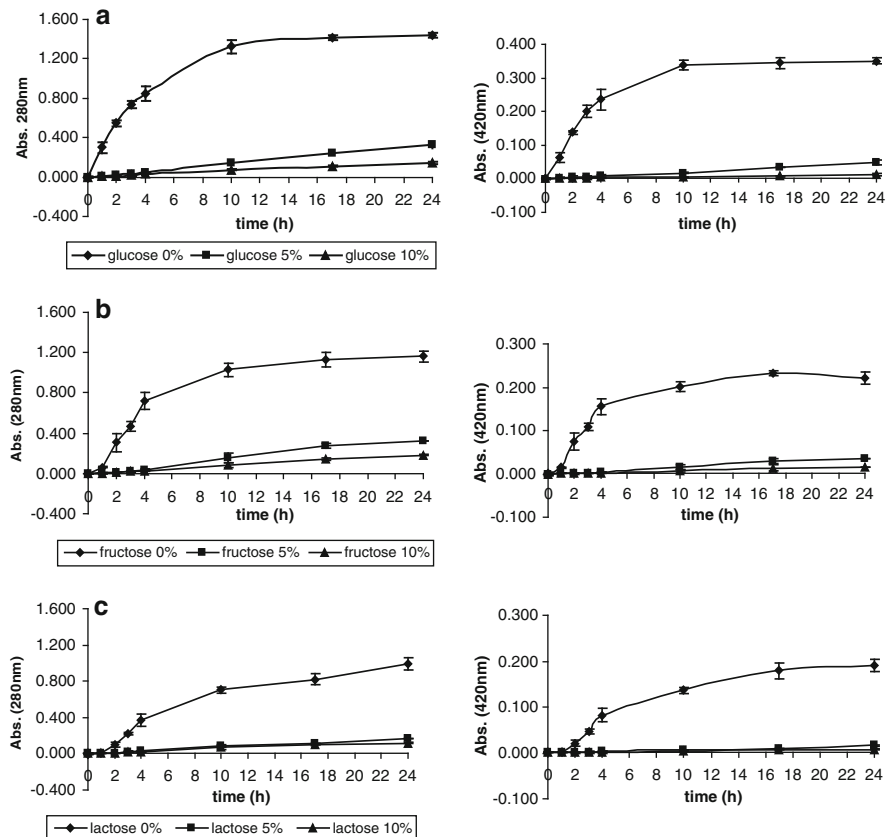


**Fig. 8** Plot of absorbance at 280 nm (a) and 420 nm (b) vs. heating time for glucose-glycine in glycerol model system at 0, 5, and 10 % moisture level. Data were fitted to the kinetic model of Eq. (1) (a and b) and Eq. (4) (c). The kinetic prediction data is also shown on each graph

which is regarded as a first-order kinetics (Ibarz et al. 1999; Carabasa-Giribet and Ibarz-Ribas 2000). Color destruction generally occurs when the reaction took place at high temperature with excessive heating time.

Plots of absorbance at either 280 or 420 nm in 0 % moisture content in glycerol model system for glucose and fructose showed a linear increase in absorbance during initial induction period, but the trend remained unchanged or reached plateau phase at the final stage. However, the curve did not fit well to either zero-order or first-order kinetic models, and it was noted that the plot actually followed pseudo-first-order kinetics as described by Carabasa-Giribet and Ibarz-Ribas (2000) (results not shown). In this case, it was considered that two stages occurred in the nonenzymatic browning reaction. The first one was the color formation (zero-order kinetics), while the second stage was the formation of colorless compounds which followed first-order kinetics. The kinetics of the Maillard reaction is very complex due to the many reaction paths and the effect of experimental condition. The

formation color and colorless compounds in the reaction can usually be described as zero-order kinetics at short heating times, but become complex at longer heating time and higher temperatures.

In contrast, lactose in 0 % moisture glycerol model system showed a linear increase over heating time and fitted well to zero-order kinetic model. Plots of absorbance for the reducing sugar-glycine in glycerol at 5 and 10 % moisture level model system were also fitted to linear regression and showed that both systems followed zero-order kinetic reaction. All of these fitted well to zero-order kinetics probably due to the low initial color formation in the system and also slow browning rate.

### 3.1.6 Reactivity of Reducing Sugars in Maillard Reaction

Browning rate is significantly influenced by the type of reducing sugar involved in the reaction (Schwartzberg and Hartel 1992; Naranjo et al. 1998). The tendency of the relative reactivity of different sugars in the Maillard reaction that follows in the descending order pentoses > hexoses > disaccharides and aldoses > ketoses is well recognized (Laroque et al. 2008; Mauron 1990).

In this experiment, three reducing sugars that included aldohexoses (glucose), ketohexoses (fructose), and disaccharide (lactose) were selected, and their absorbencies were recorded. The plot for sugar-glycine in glycerol 0, 5, and 10 % moisture model systems, monitored at absorbance 280 nm, is shown in Fig. 9. The rate of browning was used to determine the reactivity of reducing sugars.

Clearly, the rate of browning is highest in glucose-glycine in 0 % moisture content glycerol model system, followed by fructose and finally lactose; hence, the reactivity of these reducing sugars toward glycine was glucose > fructose > lactose; this trend was also observed in the absorbance plot at 420 nm. The result is consistent with previous findings (Oliver et al. 2006; Buera et al. 1987) in moderately high moisture level model systems. It should be noted that most studies were conducted in a liquid model system, which mainly used water as a solvent. In this case, it should be said that water activity did not influence the reactivity of sugars, since the reactivity of glucose was confirmed in 0 % moisture system in the present study and also observed in other studies at moderately high moisture levels. Against all expectations, the absorbance values of fructose were higher than glucose at 5 % moisture level during 10 and 17 h heating time. Both absorbance values for glucose and fructose overlapped at the same point when it came to 24 h heating time, while browning rate for fructose was higher than glucose when moisture level reached 10 % over all the heating time. Therefore, reactivity of sugar at 5 and 10 % moisture levels was fructose > glucose > lactose. However, glucose was still the most reactive sugar if compared to fructose in the formation of high molecular weight compounds at 420 nm (Fig. 10). It should be noted that the absorbance values for both sugars were very close especially at 10 and 17 h heating time. Glucose showed a linear increase during all the induction period. On the other hand, fructose was noted more reactive than glucose when the moisture level increased to 10 %, which

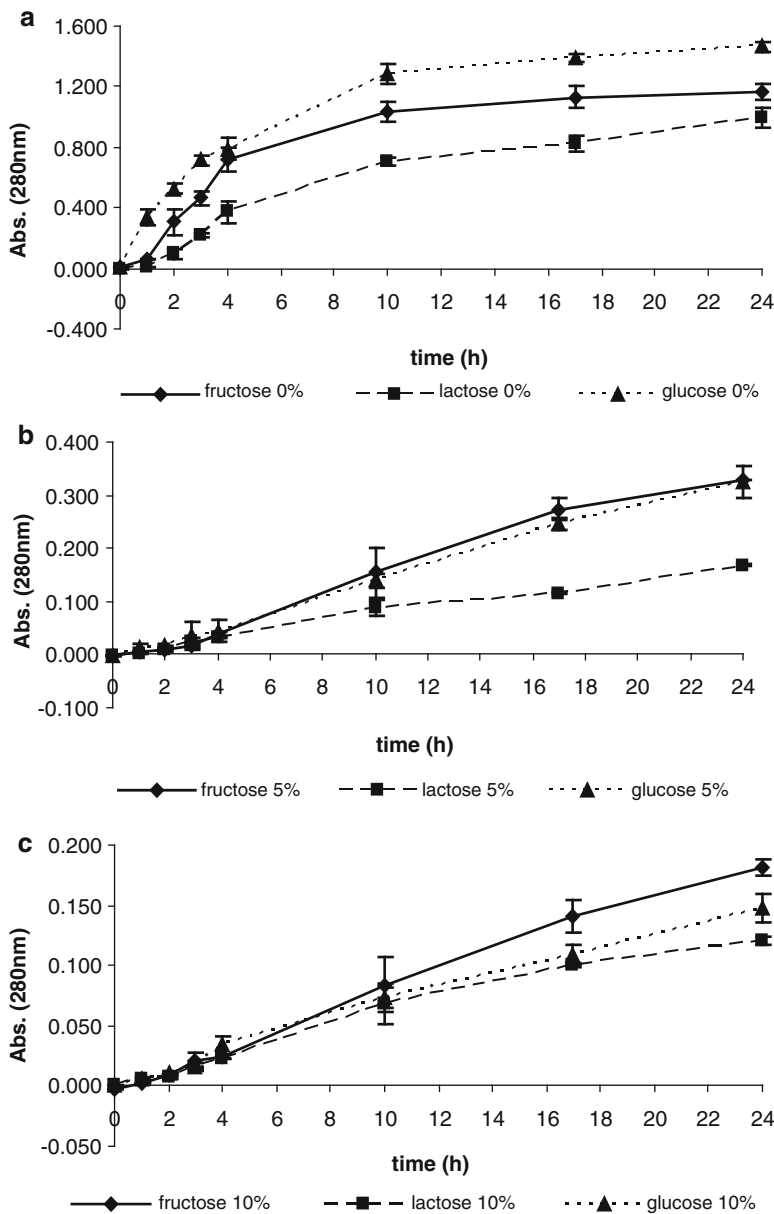


**Fig. 9** Time course of the absorbance (280 nm) of fructose-, glucose-, lactose-glycine in glycerol model system at (a) 0 %, (b) 5 %, and (c) 10 % moisture level after heated at 100 °C with assumed pH 7

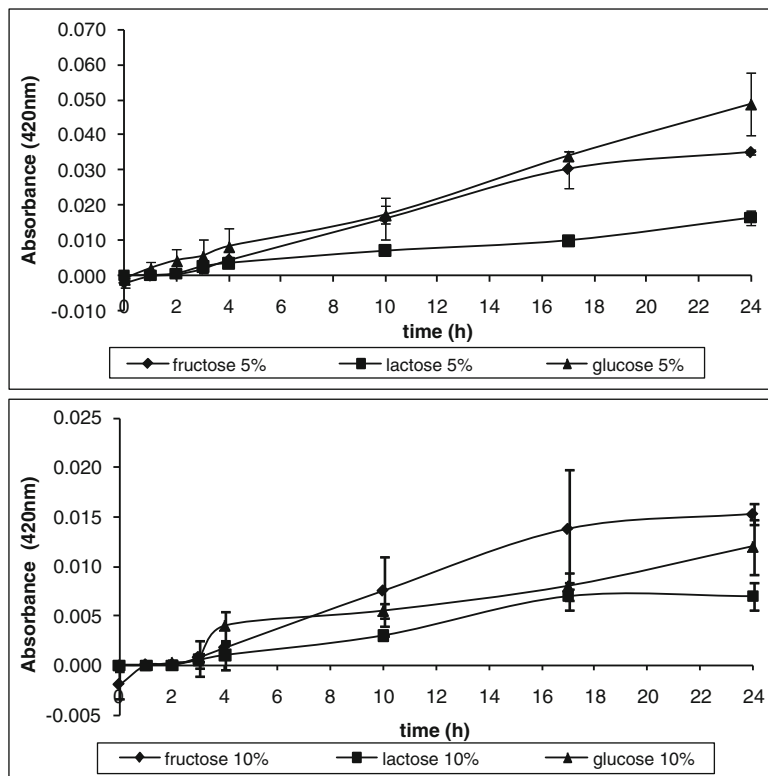


**Fig. 10** Comparison of absorbance plot of sugar-glycine in glycerol model system with different moisture levels at 420 nm

is similar to the plot at 280 nm (Fig. 9c). Lactose still remained the least reactive sugar, which showed a lower browning rate than the others.

The descending order of the reactivity of reducing sugars, glucose > fructose > lactose, in the browning development is widely recognized and supported by many studies. However, there are still major conflicts on the reactivity of sugars on the degree of browning, as some authors noted fructose is more reactive than glucose (Benjakul et al. 2005; Brands and van-Boekel 2002) which was also noted in our study in 5 and 10 % moisture glycerol model systems. These discrepancies were sometimes explained as higher participation of ketoses to browning via caramelization compared to aldoses (Jing and Kitts 2004; Ajandouz et al. 2001). However, this was not the case in the present study. When sugars were heated alone in glycerol with moisture or without moisture, the solutions were visually clear, and no color changes were noted, either by assessing the values of  $L^*$ ,  $a^*$ , and  $b^*$  or absorbance, even though the samples were heated at temperature 100 °C for 24 h (assumed pH ≈ 7). This finding is on the contrary to the study from Ajandouz et al. (2001) who noted caramelization occurred in aqueous solutions of

fructose after heating to 100 °C at pH 7. The discrepancy of the results from Ajandouz et al. (2001) and our present study might be caused by the protective effect of glycerol to the sugars.

In the case for 5 and 10 % moisture model system at absorbance 280 nm, the reactivity of fructose was higher than glucose could be attributed to the glycerol (solvent), which is used in this study to create different moisture environments, as different types of reducing sugar used will produce different synthesized products in the chemical composition (Wijewickreme and Kitts 1997), depending on the condition and environment that the reaction takes place. Moreover, Suarez et al. (1988) noted that Heyns products resulting from glycation with ketoses were highly reactive and facilitate faster conversion to fluorophores compared to ketonic groups present in Amadori products; therefore, ketose sugars are more reactive in nonenzymatic glycation reactions (Wijewickreme and Kitts 1997). The similar explanation was also given by Ajandouz et al. (2001), who claimed that this observation might be due to the formation of some rate-limiting intermediates during the nonenzymatic browning reaction of glucose, but not in fructose. Besides, the difference of the reactivity of glucose and fructose could be also attributed to the different mechanisms of the reaction that take place for fructose and glucose (Ajandouz et al. 2001) at different moisture levels in glycerol model system.

Moderate browning was observed for fructose- and glucose-glycine in glycerol model system over the range of tested moisture levels. However, the color development in lactose-glycine system was not as strong as the other two sugars, over the range of moisture level and testing time. Oliver et al. (2006) who tested the reactivity of reducing sugars against caseinate explained that the slight yellow developing in caseinate-lactose system can be attributed to the galactopyranoside group in the Amadori rearrangement compound formed from protein-lactose interaction, and this acted to protect the C-4 hydroxyl group of glucose (in lactose) and hence delay browning, which could be used to explain the reactivity of lactose in the present study.

## 4 Conclusion and Recommendations for Future Research

Maillard reaction has proved to occur at low moisture environment, even as low as 0 % moisture content, in all reducing sugar-glycine-glycerol model systems. The browning rate was found maximum at 0 % moisture model system, followed by 5 %, and then 10 %. Once again, it has been proved that water activity was not one of the important parameters for Maillard reaction to take place.

In the present study, the browning rate for glucose- and fructose-glycine in glycerol at 0 % moisture model system obeyed the pseudo-first-order kinetics, a combined equation of zero-order and first-order reaction which has been reported previously, while others besides fructose and glucose in 0 % moisture model system followed to zero-order reaction.

In the case of the reactivity reducing sugars in the early stage of the reaction (absorbance 280 nm) in the present study, glucose was noted more reactive than fructose in 0 % moisture model system, but fructose became more reactive than glucose when the moisture content in the model system increased to 5 and 10 %. Lactose remained the least reactive reducing sugars. The phenomena have been discussed widely in the past; however, the reaction pathway that these aldo- and ketohexoses took place in either aqueous or glycerol model system is unclear. This needs further investigation.

Maillard reaction is very complex since the rate of nonenzymatic browning was not only influenced by water activity, but also temperature, heating time, solvent used in the system, type of reducing sugars, and amino acids. Other parameters include pH and the presence of transition metal ions which were not included in the present study. All these parameters will influence the browning rate that needs to be studied further.

Simple reaction pathway of the Maillard reaction has been established, but the complex reaction pathway remains unclear. The study of the reaction pathway due to the discovery of the Maillard reaction occurring in glycerol model system in a limited moisture environment will pose another big challenge ahead in Maillard chemistry field.

Since Maillard reaction has proved to occur at low moisture content, with the high browning rate, it is recommended that the next research studies the profile of the browning compounds that generated from such a low moisture system. Few studies had been carried out in the past to investigate the aroma and flavor profile or mutagenic compounds in sugar-amino acid-glycerol model system at different water activities and relatively high temperatures. However, more effort should be put to indentify more volatile and nonvolatile compound, potential antioxidant, as well as carcinogenic compounds (if any) of the resulting MRPs, by testing different types of sugars and amino acids at different moisture levels and heating temperatures. By obtaining all these knowledge, Maillard reaction is therefore able to be controlled, in order to obtain desired color, flavors and aromas, potential antioxidant, and low carcinogenic compounds.

Besides, it is also suggested that the experiments can be conducted in a real food system by applying the knowledge from the model system. Since Maillard reaction proved to occur at low moisture content, the success of this research will help to enhance the shelf life of the intermediate moisture food (IMF) products, and hence, great contribution could be made in the food industry.

## References

- Ajandouz EH, Tchiakpe LS, Ore FD, Benajiba A, Puigserver A (2001) Effects of pH on caramelization and Maillard reaction kinetics in fructose-lysine model systems. *J Food Sci* 66(7):926–931
- Ames JM (1990) Control of the reaction in food systems. *Trends Food Sci Technol* 1:150–154

- Belitz H D, Grosch W, Schieberle P (2004) Food chemistry, 3rd revised edn. Springer, Berlin
- Benjakul S, Lerttittikul W, Baurer F (2005) Antioxidant activity of Maillard reaction products from a porcine plasma protein-sugar model system. *Food Chem* 93:189–196
- Bhandari BR (2010) Beyond water: waterlike functions of other biological compounds in a waterless system. In: Reid DS, Sajjaanantakul T, Lillford PJ, Charoenrein S (eds) Water properties in food, health, pharmaceutical and biological systems: ISOPOW 10. Wiley-Blackwell, Ames, IA, pp 157–164
- Brands CMJ, van Boekel MAJS (2002) Kinetic modeling of reactions in heated monosaccharide-casein systems. *J Agric Food Chem* 50:6725–6739
- Buera MDP, Chirife J, Resnik SL, Wetzler G (1987) Nonenzymatic browning in liquid model systems of high water activity: kinetics of color changes due to Maillard's reaction between different single sugars and glycine and comparison with caramelization browning. *J Food Sci* 52(4):1063–1067
- Carabasa-Giribet M, Ibarz-Ribas A (2000) Kinetics of colour development in aqueous glucose systems at high temperatures. *J Food Eng* 44:181–189
- Cerny C, Guntz-Dubini R (2006) Glycerol, another pyrazine precursor in the Maillard reaction. *Recent Advances and Trends, Flavor Science*, pp 351–354
- Cuzzoni MT, Stoppini G, Gazzani G (1998) Influence of water activity and reaction temperature of ribose-lysine and glucose-lysine Maillard systems on mutagenicity, absorbance and content of furfurals. *Food Chem Toxicol* 26(10):815–822
- Eichner K, Karel M (1972) The influence of water content and water activity on the sugar-amino browning reaction in model systems under various conditions. *J Agric Food Chem* 20 (2):218–223
- Fogliano V, Monti SM, Musella T, Randazzo G, Ritieni A (1999) Formation of coloured Maillard reaction products in a gluten-glucose model system. *Food Chem* 66:293–299
- Gu YS, Corradini MG, McClemlnts DJ, DesRochers J (2006) Properties of low moisture composite materials consisting of oil droplets dispersed in a protein-carbohydrate-glycerol matrix: effect of continuous phase composition. *J Agric Food Chem* 54:417–424
- He X, Fowler A, Toner M (2006) Water activity and mobility in solutions of glycerol and small molecular weight sugars: Implication for cryo- and lyopreservation. *J Appl Phys* 100 (074702):1–11
- Hofmann T (1998) Characterization of the chemical structure of novel colored Maillard reaction products from furan-2-carboxaldehyde and amino acids. *J Agric Food Chem* 46:932–940
- Ibarz A, Pagan J, Garza S (1999) Kinetic models for color changes in pear puree during heating at relatively high temperatures. *J Food Eng* 39:415–422
- Jing H, Kitts DD (2004) Antioxidant activity of sugar-lysine Maillard reaction products in cell free and cell culture systems. *Arch Biochem Biophys* 429:154–163
- Kamman JF, Labuza TP (1985) A comparison of the effect of oil versus plasticized vegetable shortening on rates of glucose utilization in nonenzymatic browning. *J Food Process Preserv* 9:217–222
- Katkov II, Levine F (2004) Prediction of the glass transition temperature of water solutions: comparison of different models. *Cryobiology* 49:62–82
- Labuza TP, Saltmarch M (1981) The nonenzymatic browning reaction as affected by water in foods. In: Rockland LB, Stewart GF (eds) Water activity: influences on food quality. Academic Press, Inc., New York, pp 605–650
- Laroque D, Inisan C, Berger C, Vouland E, Dufosse L (2008) Kinetic study on the Maillard reaction. Consideration of sugar reactivity. *Food Chem* 111:1032–1042
- Lu CY, Hao Z, Payne R, Ho CT (2005a) Effects of water content on volatile generation and peptide degradation in the Maillard reaction of glycine, diglycine, and triglycine. *J Agric Food Chem* 53:6443–6447
- Lu CY, Payne R, Ho CT (2005b) The effect of water content on volatile formation from the Maillard reaction of peptides and glucose. *Ann N Y Acad Sci* 1043:894

- Martins SIFS, Van-Boekel MAJS (2005) A kinetic model for glucose/glycine Maillard reaction pathways. *Food Chem* 90:257–269
- Mauron J (1990) Influence of processing on protein quality. *J Nutr Sci Vitaminol* 36:557–569
- Miao S, Roos H (2004) Nonenzymatic browning kinetics of a carbohydrate-based low-moisture food system at temperatures applicable to spray drying. *J Agric Food Chem* 52(16):5250–5257
- Misharina TA, Golovnya RV, Yakovleva VN (1992) Effect of time and temperature on the preparation of pyrazines in model reactions of the synthesis of aroma-forming substances. *Russ Chem Bull* 41(7):1258–1263
- Mustapha WAW, Hill SE, Blanshard JMV, Derbyshire W (1998) Maillard reactions: do the properties of liquid matrices matter? *Food Chem* 62(4):441–449
- Naranjo GB, Malec LS, Vigo MS (1998) Reducing sugars effect on available lysine loss of casein by moderate heat treatment. *Food Chem* 62(3):309–313
- Obanu ZA, Ledward DA, Lawrie RA (1977) Reactivity of glycerol in intermediate moisture meats. *Meat Sci* 1:177–183
- Oliver CM, Melton LD, Stanley RA (2006) Glycation of caseinate by Fructose and fructooligosaccharides during controlled heat treatment in the ‘dry’ state. *J Sci Food Agric* 86:722–731
- Ozdemir M, Devres O (2000) Kinetics of color changes of hazelnuts during roasting. *J Food Eng* 44:31–38
- Schwartzberg HG, Hartel RW (1992) Physical chemistry of foods. Marcel Dekker, New York
- Seow CC, Cheah PB (1985) Reactivity of sorbic acid and glycerol in non-enzymatic browning in liquid intermediate moisture model systems. *Food Chem* 18:71–80
- Sherwin CP, Labuza TP (2003) Role of moisture in Maillard browning reaction rate in intermediate moisture foods: comparing solvent phase and matrix properties. *J Food Sci* 68:588–594
- Suarez G, Rajaram R, Bhuyan KC, Oronsky AL, Goidl JA (1988) Administration of an aldose reductase inhibitor induces a decrease of collagen fluorescence in diabetic rats. *J Clin Investig* 82:624–627
- Warmbier HC, Schnickels RA, Labuza TP (1976) Effect of glycerol on non-enzymatic browning in a solid intermediate moisture model food system. *J Food Sci* 41(3):528–531
- Wijewickreme AN, Kitts DD (1997) Influence of reaction conditions on the oxidative behavior of model Maillard reaction products. *J Agric Food Chem* 45:4571–4576
- Wijewickreme AN, Kitts DD, Durance TD (1997) Reaction conditions influence the elementary composition and metal chelating affinity of nondialyzable model Maillard reaction products. *J Agric Food Chem* 45:4577–4583
- Zegota A, Bachman S (1987) Nonenzymatic browning induced by gamma-irradiation in model system. *Z Lebensmittelunters Forsch* 184:3–7

# Carbohydrates and Proteins as Nonequilibrium Components of Biological Materials

Y.H. Roos

## Abbreviations

$a_w$	Water activity
$C_1$	Universal coefficient
$C_2$	Universal coefficient
$T$	Temperature
$t_{cr}$	Crystallization time
$T_g$	Glass transition temperature
WLF	Williams-Landel-Ferry relationship

## 1 Introduction

Carbohydrates and proteins form the main hydrophilic phases in biological materials. Water solubility and formation of glass-like structures at high solids contents are well-known properties of carbohydrates, particularly of low molecular weight sugars (White and Cakebread 1966). Natural biological materials, including foods, often contain carbohydrates mixed with proteins and other hydrophilic substances in their aqueous phase.

Food materials can be preserved by using dehydration or freezing processes that reduce water content or the effective concentration of water (water activity,  $a_w$ ) for the support of biological functions, as microbial growth. Such processes remove water from hydrophilic solids and produce concentrated solids systems that

---

Y.H. Roos (✉)

Food Technology, School of Food and Nutritional Sciences,  
University College Cork, Cork, Ireland  
e-mail: [yrjo.roos@ucc.ie](mailto:yrjo.roos@ucc.ie)

typically exist in nonequilibrium states. These nonequilibrium states result from supercooling and supersaturation of food components, establishing driving forces toward equilibrium states. Consequently, various time-dependent changes in physicochemical properties of the materials contribute to their stability and the reduced shelf life of foods. These time-dependent phenomena in food materials include changes in microstructure, variations in rates of biochemical processes and rates of chemical and enzymatic reactions, as well as various crystallization and recrystallization phenomena (Le Meste et al. 2002).

Food solids properties are dependent on molecular arrangements, which are highly dependent on thermal and water content history. Temperature and water plasticization also relate to the physical state of food solids. The physical state of nonequilibrium, noncrystalline solids is related to their glass transition and glass transition temperature ( $T_g$ ).  $T_g$ s have previously been reported for carbohydrates (Roos 1993), proteins (Toufeili et al. 2002), and complex food solids (e.g., Sablani et al. 2007). Although glass transitions of complex foods can be measured, results primarily show the glass transition of the main carbohydrate or miscible solids components (Silalai and Roos 2011; Potes et al. 2012).  $T_g$  is often measured using differential scanning calorimetry, but dielectric and mechanical relaxations and relaxation times can be derived from dynamic and isothermal dielectric and mechanical measurements (Le Meste et al. 2002; Silalai and Roos 2011; Potes et al. 2012). Glass transition as such does not provide information on rates of physicochemical changes, which need to be measured or derived from relaxation times data. Data on molecular mobility may also be obtained from electron spin resonance measurements and nuclear magnetic resonance spectroscopic studies (Le Meste et al. 2002; Roudaut et al. 2009).

Food processing and shelf life control require data on changes and kinetics around and above the glass transition. Our studies have investigated dielectric and mechanical relaxation properties and relaxation times and their correlation with stickiness, caking, and crystallization phenomena of food solids. These properties and their effects on kinetics and stability of nonequilibrium food systems with data on food solids miscibility and phase separation will be presented.

## 2 Dielectric and Mechanical Relaxation Times

Dielectric relaxation times derived from the  $\alpha$ -relaxation have been reported for several carbohydrates (Noel et al. 1996; Shinyashiki et al. 2008). The comprehensive data of Shinyashiki et al. (2008) for noncrystalline fructose at various water contents were particularly interesting. Our analysis of their data showed that the structural relaxation times decreased in line with the Williams-Landel-Ferry (WLF) relationship (Williams et al. 1955) with increasing temperature above  $T_g$ . Structural relaxation times at constant water content decreased, showing typical water plasticization of hydrophilic food solids. This finding was also apparent in an “Angell” plot showing relaxation times against  $T_g/T$  (Angell et al. 1994; Angell 2002). Water

content dependence of fragility defined as a deviation from Arrhenius kinetics above the  $T_g$  was apparent. However, the WLF relationship showed that apparent differences in fragilities resulted from the  $T_g/T$  scaling, but not from true differences in the relaxation behavior of noncrystalline fructose above its  $T_g$ . Dielectric loss,  $\epsilon''$ , for fructose and glucose in Fig. 1 at various frequencies and temperatures was shown. The frequencies ( $f$ ), corresponding to the peak values of  $\epsilon''$  at various temperatures, were used to derive structural relaxation times,  $\tau$ , as  $\tau = 1/2\pi f$ . These data agreed with WLF temperature dependence, although differences in fragilities were apparent in the Angell plot (Fig. 2). More importantly, it can be shown that structural relaxations follow an enormous  $T_g$  dependence from  $T_g$  to approximately  $T_g + 30^\circ\text{C}$  (Fig. 2). Consequently, there is a high importance to characterize food

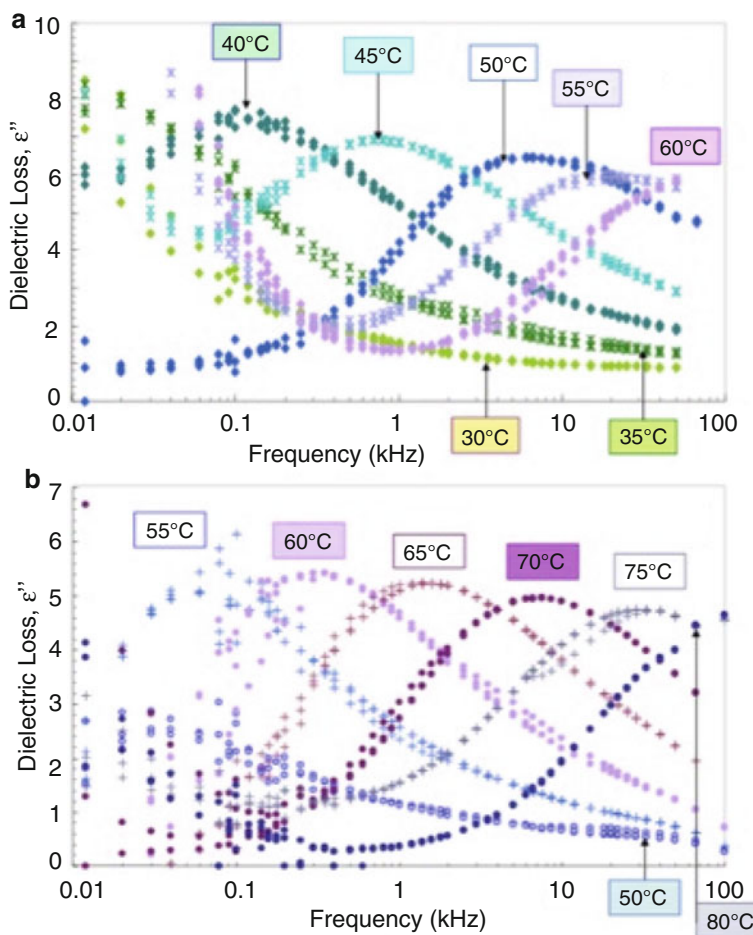


**Fig. 1** Dielectric loss,  $\epsilon''$ , for amorphous fructose (a) and glucose (b) at various temperatures and frequencies

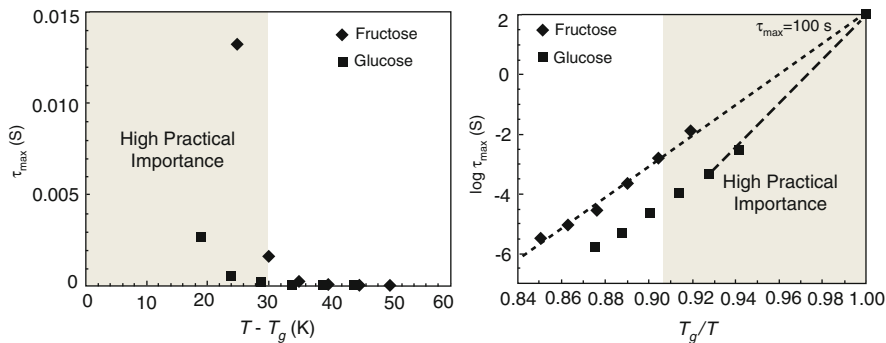


**Fig. 2** Temperature dependence of dielectric relaxation times of amorphous fructose and glucose above glass transition as a function of  $T - T_g$  and  $T_g/T$  (Angell plot). The difference in  $T_g/T$  plotting is due to the differences in glass transition temperatures (fructose  $T_g = 282$  K; glucose  $T_g = 304$  K)

systems for their analogous dielectric and mechanical relaxation properties over the range from  $T_g$  to  $T_g + 30$  °C at minimum. It should be noted that the WLF relationship shows differences in relaxation times as a function of temperature above the calorimetric onset  $T_g$  (i.e.,  $T - T_g$ ), while the  $T_g/T$  scaling of Angell plots cannot be used to compare materials with different  $T_g$  values. Consequently, a comparison of relaxation times of the same material with different water plasticization levels using an Angell plot is not appropriate and may give highly misleading information on the effects of plasticization on fragility and relaxation behavior. Accordingly, fragility values, as defined by Angell (e.g., Angell 2002), cannot be used to assess relaxation properties of glass formers above their  $T_g$ .

Numerous studies have shown that the mechanical and dielectric behavior of simple low molecular weight sugars is typical of nonequilibrium liquids (Noel et al. 1996; Silalai and Roos 2011; Potes et al. 2012). Such sugars show dramatic changes in modulus and dielectric behavior around the glass transition. When carbohydrates and sugars are dissolved in water with suspended proteins, such as dairy solids or soy proteins, the glass transition behavior of the systems seems to follow that of the carbohydrate components (Zhou and Roos 2011). For a phase-separated system, the  $T_g$  when plotted against  $\alpha_w$  is composition independent, and the data overlap that of the component suffering the glass transition. When the carbohydrate composition is modified by alteration of the low and high molecular weight carbohydrate fractions, it may be noted that glass transition occurs at a higher temperature with increasing average molecular weight (Silalai and Roos 2011; Potes et al. 2012). Water plasticization studies of such systems need to consider whether multiple glass formers are plasticized as a mixture of miscible components (e.g., high DE maltodextrins with sugars) or do components, such as proteins and sugars, exhibit phase separation. Phase separation of food components may also result in significant differences in dielectric and mechanical relaxation properties. Dielectric properties may be dominated by relaxation properties of small molecular weight carbohydrates and their water plasticization. Conversely,

mechanical relaxation times may show a significant difference caused by phase-separated macromolecules, for example, proteins (Silalai and Roos 2011).

### 3 Fluidness Characteristics

A normal thermodynamic melting process of pure crystalline solids produces a liquid from a solid at one single temperature. The structural relaxation times of the liquid and solid states differ over multiple logarithmic decades. In supercooled liquids, changes in relaxation times occur at and above the glass transition. Dielectric and dynamical mechanical properties, along with measured viscosities of glass-forming materials at various levels of water, show the  $T - T_g$ -dependent decrease in structural relaxation times, as originally described by Williams et al. (1955) and further emphasized by Slade and Levine (1991).

An increase in temperature or water plasticization above the  $T_g$  causes an exponential decrease in structural relaxation times, as shown in Fig. 3. For a typical glass former in food systems, such as glucose, the decrease in relaxation time over the calorimetric glass transition temperature range of 10 °C (Roos 1993) is three logarithmic decades (Fig. 3). Such a dramatic change in structural relaxation times over a relatively narrow temperature range has significant effects on the physico-chemical properties of food solids. The definition of fragility by Angell (2002) aimed to explain the non-Arrhenius behavior of glass formers. The definition of fragility is valid only at the  $T_g$ , and it is necessary to emphasize the importance of the use of the WLF relationship in the modeling of temperature dependence of structural

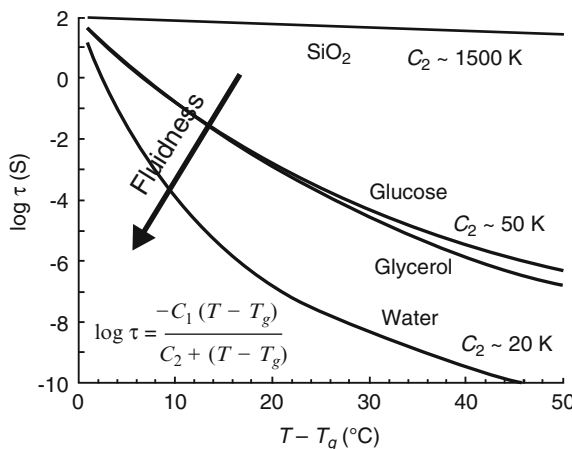


**Fig. 3** Fluidness of common glass formers in foods shown by a plot of the structural relaxation time ( $\log \tau$ ) against temperature above the glass transition onset temperature ( $T - T_g$ ). The  $C_2$  value of the WLF relationship shown is a measure of fluidness, i.e., fluidness decreases with increasing  $C_2$  value

relaxation times above the  $T_g$ . It should be noted, however, that significant differences in measured relaxation times of complex food systems may result from the phase separation of components and differences in their molecular weight (Silalai and Roos 2011; Zhou and Roos 2011; Potes et al. 2012). The WLF constant  $C_2$  describes the steepness of the logarithmic decrease in structural relaxation times with increasing  $T - T_g$  (Fig. 3). The  $C_2$  value provides a measure of “fluidness” of food components. Differences in fluidness indicate variations in molecular mobility of different glass formers above the glass transition and give a clear measure for comparison of effects of glass transition on mobility-related properties.

## 4 Fluidness in Food Processing and Storage

### 4.1 Effects on Microstructure

Structural relaxation times and their variations during food processing are significantly dependent on dynamic changes in water content. Typical food processes where structural relaxation times control solids mobility and concomitant formation of microstructure include food freezing, dehydration processes, baking, extrusion, and manufacturing of confectionary products. The resultant materials are typically noncrystalline solids showing glass transitions for at least some of the components or mixtures of miscible components.

Formation of food microstructure relates to fluidness of solids through the rate at which food solids can relax during dehydration to respond to the loss of volume resulting from evaporation of water (Karel et al. 1994). In natural foods, several factors, including the characteristics of cell wall polymers, further contribute to the overall shrinkage of complex food solids. Freeze-drying is a typical process where microstructural changes during sublimation are minimal. Volume retention in freeze-drying benefits from glass formation of solids as a result of freeze concentration during the freezing process and concomitant formation of a separate ice phase (Harnkarnsujarit et al. 2012). A successful freeze-drying process retains the highly freeze-concentrated solids network that can support its own weight during sublimation of ice. A glassy state or high enough viscosity of solids is required to resist the gravitational stress appearing as sublimation increases void volume (porosity). The freeze-concentrated solids remain as a membrane network, hosting pores left by the ice crystals. In other dehydration processes, some water plasticization of solids enhances viscous flow, i.e., the microstructure of the dehydrated solids is formed during evaporation of water. It may be assumed that the fluidness characteristics of food solids and their level of water plasticization during formation of microstructures in food processing are significant factors affecting the final properties of the materials, particularly shrinkage in dehydration and formation of expanded solids in extrusion or puffing.

## 4.2 Stickiness and Relaxation Times

Stickiness and caking properties of food solids are of fundamental importance in spray drying, in agglomeration and granulation processes, and in storage and distribution of food powders. Stickiness and caking are typical of materials containing amorphous sugars because of their sensitivity to water and temperature and the formation of interparticle liquid bridges due to viscous flow above the glass transition. Roos and Karel (1991) showed that sticky points determined for sucrose-fructose (7:1) syrup were at approximately 10–20 °C above the  $T_g$ . Determination of structural relaxation times by using dielectric and mechanical measurements provides information on rates of changes in glass-forming materials. The structural relaxation times can also be correlated with particle contact times and viscosity values for liquid flow in contact of particles. Such studies allow comparison of food solids and possible manipulation of solids compositions to enhance dehydration properties and to achieve improved stability of food powders.

Downton et al. (1982) studied the stickiness and viscosity of sucrose-fructose (7:1) solids at various water contents. Their results showed that stickiness occurred at critical viscosities of  $10^6$ – $10^8$  Pa s and contact times of 1–10 s. It was also shown that the viscosity of the noncrystallizing sucrose-fructose solids above the glass transition followed the WLF temperature dependence (Soesanto and Williams 1981). Figure 4 shows the relationships of structural relaxation times, viscosity, contact time, and temperature above the glass transition. These hypothetical data were derived using the WLF relationship with its “universal” coefficients,  $C_1 = -17.44$  and  $C_2 = 51.6$ , and the data for critical viscosities and contact times

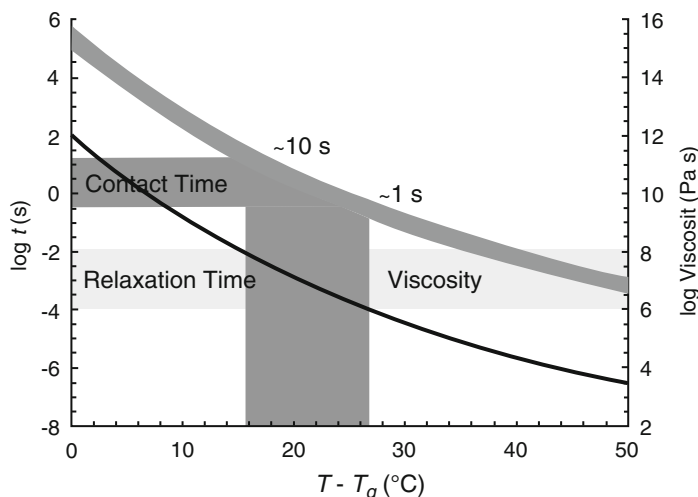


**Fig. 4** Relationships of structural relaxation time, particle contact time, and viscosity according to data of Downton et al. (1982) and the WLF relationship using the universal constants  $C_1 = -17.44$  and  $C_2 = 51.6$  K

from Downton et al. (1982). The relationships established in Fig. 4 showed that the contact times of 1–10 s corresponded to structural relaxation times of  $10^{-4}$  s to  $10^{-2}$  s at 16–27 °C above the  $T_g$ . It is important to note that the  $T_g$  values used are onset temperatures of the calorimetric glass transitions at which the structural relaxation times are approximately 100 s (Angell 2002).

### 4.3 Component Crystallization

Crystallization of amorphous sugars may result in rapid deterioration of low water food powders during storage and distribution. Crystallization and recrystallization phenomena also dominate quality losses in frozen foods, confectionary, and baked foods. Roos and Karel (1990, 1991) investigated crystallization of amorphous lactose, sucrose, and mixtures of sucrose and starch. Their data indicated an instant crystallization of the sugars at approximately 50 °C above the  $T_g$ . Polymeric components, such as starch, delayed crystallization of sugars (Roos and Karel 1991).

Roos and Karel (1992) investigated time dependence of crystallization of amorphous sugars and time to crystallization ( $\tau_{cr}$ ) of amorphous lactose at various water contents and  $T - T_g$ . They found that the time to crystallization followed the WLF relationship when plotted against  $T - T_g$  using the “universal” constants  $C_1 = -17.44$  and  $C_2 = 51.6$ . Figure 5 shows structural relaxation times against  $T - T_g$  according to the WLF relationship using the universal constants as well as data for amorphous lactose plasticized at 0.33  $a_w$ . The data show that time to

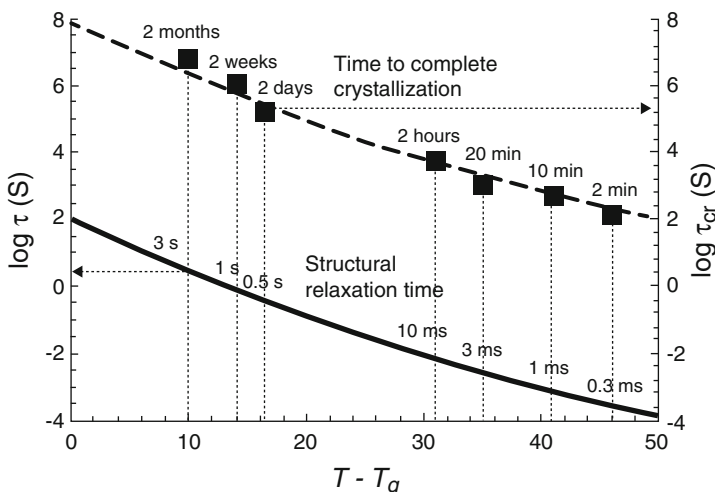


**Fig. 5** Time to crystallization,  $\tau$ , of amorphous lactose at water plasticization level corresponding to 0.33  $a_w$  at room temperature. The data shown are from Roos and Karel (1990, 1991, 1992), with WLF relationship fit to the relaxation time and time-to-crystallization data

crystallization is strongly dependent on the  $T - T_g$ , and time to complete crystallization is approximately 6 logarithmic decades longer than the structural relaxation time. As the structural relaxation time at the calorimetric glass transition approaches 100 s, the corresponding time to crystallization approaches  $10^8$  s, i.e., about 3 years, while time to complete crystallization occurs in 10 s during a dynamic heating at about 60 °C above the  $T_g$ . These time-to-crystallization data agree well with dynamic and isothermal crystallization studies, as shown by the experimental data in Fig. 5.

Our studies have shown that proteins and sugars exist largely as phase-separated components in amorphous food solids, such as spray-dried skim milk (Silalai and Roos 2011). The carbohydrate components exhibit their individual water sorption and glass transition properties (Silalai and Roos 2011; Zhou and Roos 2011; Potes et al. 2012). The predominant glass transition measured for such food systems is that of the carbohydrate component. Our earlier studies showed that as a result of mixing with proteins, lactose crystallization was significantly delayed, and the effect of delaying crystallization was dependent on the protein (Haque and Ross 2004). The instant crystallization of amorphous lactose occurred at 45 °C above the  $T_g$  in a dynamic differential scanning calorimeter (DSC) measurement with a corresponding structural relaxation time of  $10^{-3.5}$  s, while instant crystallization in the presence of proteins (25 % of solids) occurred at 70–80 °C above the  $T_g$  corresponding to a relaxation time of  $10^{-6}$  to  $10^{-5}$  s. Studies on skim milk powder (Silalai and Roos 2011) and other lactose-protein systems (Zhou and Roos 2011) show that relaxation times of lactose molecules are not affected by phase-separated proteins, but higher mobility is required to compensate for hindered diffusion, nucleation, and crystal growth of the crystallizing species in a complex food matrix. In miscible carbohydrate systems, crystallization is inhibited by the component carbohydrates. Studies of lactose-maltodextrin systems showed that small molecular weight components are more efficient inhibitors of sugar crystallization than larger molecules (Potes et al. 2012).

## 5 Conclusions

Carbohydrates and proteins form noncrystalline structures in food systems. These materials may exist as noncrystalline solids and they become plasticized by water. At increasing water contents, glass transitions may take place and result in rapidly decreasing structural relaxation times. The structural relaxation times correlate with microstructural changes in food processing and storage, particle stickiness in dehydration, and crystallization times of amorphous sugars. Food composition and phase separation of components may alter water plasticization characteristics and diffusion of components in complex food materials.

## References

- Angell CA (2002) Liquid fragility and the glass transition in water and aqueous solutions. *Chem Rev* 102:2627–2650
- Angell CA, Bressel RD, Green JL, Kanno H, Oguni M, Sare EJ (1994) Liquid fragility and the glass transition in water and aqueous solutions. *J Food Eng* 22:115–142
- Downton GE, Flores-Luna JL, King CJ (1982) Mechanism of stickiness in hygroscopic, amorphous powders. *Ind Eng Chem Fundam* 21:447–451
- Haque MK, Ross YH (2004) Water plasticization and crystallization of lactose in spray-dried lactose/protein mixtures. *J Food Sci* 69(1):FEP23–FEP29
- Harnkarnsujarit N, Charoenrein S, Roos YH (2012) Microstructure formation of maltodextrin and sugar matrices in freeze-dried systems. *Carbohydr Polym* 88:734–742
- Karel M, Anglea S, Buera P, Karmas R, Levi G, Roos Y (1994) Stability-related transitions of amorphous foods. *Thermochim Acta* 246:249–269
- Le Meste M, Champion D, Roudaut G, Blond G, Simatos D (2002) Glass transition and food technology: a critical appraisal. *J Food Sci* 67:2444–2458
- Noel TR, Parker R, Ring SG (1996) A comparative study of the dielectric relaxation behaviour of glucose, maltose, and their mixtures with water in the liquid and glassy states. *Carbohydr Res* 282:193–206
- Potes N, Kerry JP, Roos YH (2012) Additivity of water sorption, alpha-relaxations and crystallization inhibition in lactose-maltodextrin systems. *Carbohydr Polym* 89(4):1050–1059
- Roos Y (1993) Melting and glass transitions of low molecular weight carbohydrates. *Carbohydr Res* 238:39–48
- Roos Y, Karel M (1990) Differential scanning calorimetry study of phase transitions affecting the quality of dehydrated materials. *Biotechnol Prog* 6:159–163
- Roos Y, Karel M (1991) Plasticizing effect of water on thermal behavior and crystallization of amorphous food models. *J Food Sci* 56:38–43
- Roos Y, Karel M (1992) Crystallization of amorphous lactose. *J Food Sci* 57:775–777
- Roudaut G, Farhat I, Poirier-Brulez F, Champion D (2009) Influence of water, temperature and sucrose on dynamics in glassy starch-based products studied by low field  $^1\text{H}$  NMR. *Carbohydr Polym* 77:489–495
- Sablani SS, Kasapis S, Rahman MS (2007) Evaluating water activity and glass transition concepts for food stability. *J Food Eng* 78:266–271
- Shinyashiki N, Shinohara M, Iwata Y, Goto T, Oyama M, Suzuki S, Yamamoto W, Yagihara S, Inoue T, Oyaizu S, Yamamoto S, Ngai KL, Capaccioli S (2008) The glass transition and dielectric secondary relaxation of fructose-water mixtures. *J Phys Chem B* 112:15470–15477
- Silalai N, Roos YH (2011) Mechanical relaxation times as indicators of stickiness in skim milk-maltodextrin solids systems. *J Food Eng* 106:306–317
- Slade L, Levine H (1991) Beyond water activity: recent advances based on an alternative approach to the assessment of food quality and safety. *Crit Rev Food Sci Nutr* 30:115–360
- Soesanto T, Williams MC (1981) Volumetric interpretation of viscosity for concentrated and dilute sugar solutions. *J Phys Chem* 85:3338–3341
- Toufeili I, Lambert IA, Kokini JL (2002) Effect of glass transition and cross-linking on rheological properties of gluten: development of a preliminary state diagram. *Cereal Chem* 79:138–142
- White GW, Cakebread SH (1966) The glassy state in certain sugar-containing food products. *J Food Technol* 1:73–82
- Williams ML, Landel RF, Ferry JD (1955) The temperature dependence of relaxation mechanisms in amorphous polymers and other glass-forming liquids. *J Am Chem Soc* 77:3701–3707
- Zhou Y, Roos YH (2011) Characterization of carbohydrate-protein matrices for nutrient delivery. *J Food Sci* 76:E368–E376

# Low-Temperature Mobility of Water in Sugar Glasses: Insights from Thermally Stimulated Current Study

S. Ewing, A. Hussain, G. Collins, C. Roberts, and E. Shalaev

## Abbreviations

D <sub>2</sub> O	Water
DSC	Differential scanning calorimetry
HB	Hydrogen bonding
LDA	Low-density amorphous solid water
NMR	Nuclear magnetic resonance
P1	Calorimetric peak
Px	Calorimetric peak
RH	Relative humidity
T <sub>1</sub>	Spin-lattice relaxation times
T <sub>g</sub>	Glass transition temperature
T <sub>gw</sub>	Glass transition of water in sugar matrix

---

S. Ewing  
Pfizer Inc, Groton, CT, USA

A. Hussain  
Pfizer Inc, Groton, CT, USA  
New Jersey Institute of Technology, Newark, NJ, USA

G. Collins  
New Jersey Institute of Technology, Newark, NJ, USA

C. Roberts  
Department of Chemical Engineering, University of Delaware, Newark, DE 19716, USA

E. Shalaev (✉)  
Pfizer Inc, Groton, CT, USA  
Allergan Inc, Irvine, CA, USA  
e-mail: [shalaev\\_evgenyi@allergan.com](mailto:shalaev_evgenyi@allergan.com)

T <sub>p</sub>	Polarizing temperature
TSC	Thermally stimulated current
TSdC	Thermally stimulated depolarization current
TSpC	Thermally stimulated polarization current

## 1 Introduction

Aqueous solutions of carbohydrates form a noncrystalline solid (glassy) state upon freezing and dehydration (Franks 1997). This glass-forming ability of sugars is essential for protection of proteins, liposomes, and biological membranes, and other biological systems against stresses imposed by freezing and desiccation, and during long-term storage (Koster 1991). Physical and chemical transformations in the glassy state are usually much slower than those in solution. However, degradative processes in glasses proceed with a measurable rate in many cases. Water represents a main destabilizing factor common in all amorphous systems. Water is a ubiquitous plasticizer, which lowers the glass transition temperature of a system. Water content in such systems varies from a few percent, as in freeze-dried pharmaceuticals and biopharmaceuticals, to ~30 %, as in maximally freeze-concentrated solutions of sugars and proteins.

Arguably, the most basic, but global, measure of molecular mobility is the calorimetric glass transition temperature ( $T_g$ ), which can be conveniently measured by DSC in the majority of cases. However, it has been recognized that not all molecular mobility (and degradative processes associated with it) is fully arrested around  $T_g$ . For example, translational mobility of water molecules proceeds with measurable rates even well below the  $T_g$  (Aldous et al. 1997). Furthermore, it has been shown by nuclear magnetic resonance (NMR) that mobility of water molecules in concentrated sugar-water systems can be decoupled from sugar molecules (Girlich and Lüdemann 1994). In that study, temperature dependence of spin-lattice relaxation times ( $T_1$ ) for water ( $D_2O$ ) and sucrose was studied as a function of sucrose concentration. At high concentrations of sucrose (>60 wt%),  $T_1$  for water molecules became uncoupled from that for sucrose, when the temperature was near or slightly higher than  $T_g$ , whereas at lower sucrose concentrations (<50 wt%), those of sucrose and water were coupled. For example, in 80 % sucrose solution, the decoupling temperature was approximately 295 K. Moreover, the  $T_1$  values for water in the concentrated solutions were similar to that for pure  $D_2O$ . Based on those observations, it was suggested by Girlich and Lüdemann (1994) that sucrose molecules form a gel-like network, whereas water molecules retain at least their rotational mobility. Note that in the same study it was reported that the ideal glass transition temperature for water in sugar glasses is very low, i.e., approximately 115 K. However, this estimation was apparently based on extrapolation from higher temperature measurements. Therefore, a direct low-temperature study of mobility of water in such systems is warranted.

In this study, we used the thermally stimulated current (TSC) method to explore if the decoupling in mobility between sucrose and water molecules, which was reported by Girlich and Lüdemann (1994), persists in the wide temperature range, in particular below the calorimetric glass transition temperature. In addition, we probed whether similar behavior can be expected in other polyhydroxy compounds by using sorbitol, a sugar alcohol. TSC is a thermal analytical technique that has been used to study dipole relaxation in different types of materials, including synthetic polymers, small molecular-weight glass-formers, and proteins (Teyssedre et al. 1995; Fagegaltier et al. 1997; Correia et al. 2000; Galop and Collins 2001; Shmeis et al. 2004; Reddy et al. 2009). In addition, TSC has been used to study low-temperature molecular mobility in aqueous sugar solutions (Pissis et al. 1983) and hexagonal ice (Johari and Jones 1975; Apekis et al. 1983). A brief description of the TSC method is provided in Sect. 2. In the present study, we investigated highly concentrated sucrose-water and sorbitol-water solutions and freeze-dried amorphous sucrose, i.e., systems in which no ice is formed upon cooling. Ice formation would result in two-phase systems, with water molecules distributed between crystalline ice (usually, hexagonal) phase and an amorphous phase consisting of the solute and remaining water. With such a two-phase system, the experimental TSC signal would have contributions from both water molecules in ice and water in the amorphous phase, which could complicate interpretation of the results.

## 2 Materials and Methods

### 2.1 Materials

Sucrose and D-Sorbitol (Sigma-Aldrich) were used as received. Deionized water was used to prepare solutions. Solutions with 65–90 % w/w sorbitol and 70–76.3 % w/w sucrose were prepared by heating the weighted amount of a powder (sorbitol or sucrose) and water using a hot plate or a water bath in a closed glass container and stirring the solutions until they turned clear. Before loading the solution into the TSC sample holder, solutions were visually evaluated for evidence of solute crystallization. If crystallization was observed, those samples were discarded.

Amorphous sorbitol was prepared by melting crystalline sorbitol, followed by quenching. Amorphous sucrose was prepared by freeze-drying from 5 % aqueous sucrose solution in glass vials using an FTS LyoStar I freeze dryer. The product temperature was maintained below the collapse temperature of  $-33\text{ }^{\circ}\text{C}$ , and secondary drying temperature was  $40\text{ }^{\circ}\text{C}$ . To prepare amorphous samples of sucrose with elevated water content, freeze-dried sucrose powder in aluminum DSC and TSC sample holders was equilibrated in desiccators containing either saturated lithium chloride solution (11 % relative humidity, RH) or saturated potassium

acetate solution (23 % RH). Vacuum was pulled to evacuate the desiccators, and the freeze-dried samples were allowed to equilibrate for at least 4 days. To estimate water content in these samples, the Tg was measured by DSC, and the Tg vs. water content curve from Girlich and Lüdemann (1994), reproduced in Fig. 4, was used to determine corresponding water content. Water contents were determined to be 1.6 % w/w (range of 0.5–2.8 % w/w), 3.9 % w/w (range of 3.3–4.4 % w/w), and 6.8 % w/w for the freeze-dried sample and after equilibration at 11 % and 23 % RH, respectively, based on the Tg values (midpoint) of  $61.5 \pm 9$  °C,  $44.5 \pm 4$  °C, and 22.5 °C, respectively.

## 2.2 Thermally Stimulated Current

Thermally stimulated current detects the mobility of dipoles and other permanent or induced electric charges. There are two basic TSC techniques, namely thermally stimulated polarization current (TSpC) and thermally stimulated depolarization current (TSdC) (Vanderschueren and Gasiot 1979). In the depolarization experiments (TSdC), a sample is polarized by a permanent electric field at a relatively high temperature where there is significant molecular mobility to allow the attainment of equilibrium. The polarization is frozen in by quenching the sample to a low temperature, and then the electric field is removed. Depolarization is measured during heating of such a sample without an electric field. When the dipoles become mobile, an electric current is induced by the spontaneous depolarization, and this current is measured by an electrometer. In the polarization method (TSpC), an electric field is applied at low temperature, where dipoles are immobile and polarization of dipoles by the electric field is detected during heating of the sample. A potential advantage of the TSpC method is that the sample is not exposed to higher temperature prior to the measurements (as with TSdC experiments), thus allowing characterization of the sample with “as is” thermal history and minimizing the potential for both chemical degradation and physical changes (e.g., crystallization) of temperature-sensitive materials. In addition, TSpC experiments are often performed prior to TSdC measurements on an unknown sample, in order to choose polarization temperature.

Thermally stimulated current experiments were performed with a TSC/RMA instrument (Thermold, CT) equipped with stainless steel electrodes. The TSC instrument was calibrated using melting of indium at the heating rate 7 °C/min. Two different sample preparation methods were used. In the first method, a sample holder consisting of a differential scanning calorimeter (DSC) aluminum pan, a Teflon sheet, a Teflon ring that serves as a spacer, and a Teflon lid was used. Powder samples and solutions were loaded into the small cavity formed by a Teflon ring on top of a Teflon sheet that was fitted into an aluminum Perkin-Elmer DSC pan. The samples were compacted into the cavity and then covered with a Teflon lid that was crimped onto the pan containing the sample. The Teflon lid was used to insulate the electrode from charge injection at the sample surface and to minimize contributions

from the ionic conductivity of the sample to the TSC signal. This approach is known as a blocking electrode. In the second method, a solution was sandwiched between two Teflon sheets in the cavity of the Teflon ring placed. Both methods gave comparable results.

In TSpC experiments, the sample was cooled to approximately  $-170\text{ }^{\circ}\text{C}$ , and then a polarizing static field of 100 V was applied during heating at  $7\text{ }^{\circ}\text{C}/\text{min}$ . In several experiments, higher voltages of 200 and 300 V were used. Polarization current was measured while heating in the presence of the applied field. TSdC experiments were performed by first heating the sample to a polarizing temperature ( $T_p$ ), and then holding at  $T_p$  isothermally in the presence of a polarizing field for 2 min. Polarization temperature of  $-50\text{ }^{\circ}\text{C}$  was used for 70 and 80 % sorbitol, and  $-20\text{ }^{\circ}\text{C}$  for 90 % sorbitol. Typically, a polarization voltage of 100 V was used; several experiments were performed at a higher voltage of 200 and 300 V. The sample was then cooled using liquid nitrogen in the presence of the applied field to sub-zero temperature and held for 1 min. The polarizing field was then removed, and the depolarization current was measured while heating the sample at  $7\text{ }^{\circ}\text{C}/\text{min}$ . For the sorbitol system, both polarization (TSpC) and depolarization (TSdC) experiments were performed, while the sucrose system was investigated using TSpC mode. Temperature of the TSC events was measured manually from a position of a peak on a TSC curve.

### 2.3 Differential Scanning Calorimetry (DSC)

DSC analysis was performed with a TA Instruments Modulated DSC Q1000 equipped with a refrigerated cooling system. Nitrogen was used as a purge gas with a flow rate at 50 ml/min. Calibration was performed using indium as the standard. Samples were sealed in aluminum hermetic pans, cooled to  $-90\text{ }^{\circ}\text{C}$ , and heated at a rate of  $10\text{ }^{\circ}\text{C}/\text{min}$ .

## 3 Results

Representative TSpC heating curves of 73.1 % w/w sucrose solution are shown in Fig. 1. The experiments were performed at 100 V, 200 V, and 300 V, respectively, using both positive and negative voltage. Three broad signals, marked as P1, P2, and P3, were observed. At lower temperatures below approximately  $-60\text{ }^{\circ}\text{C}$ , the negative and positive curves represent nominally mirror images, whereas above  $-60\text{ }^{\circ}\text{C}$  significant difference between negative and positive curves was observed. In addition, the lower-temperature portions of the curves scaled with the field. This observation, i.e., proportionality with the field and mirror image of P1 and P2 events, is indicative of dipole relaxation process. On the other hand, the nature of higher temperature events is less certain and probably involves additional

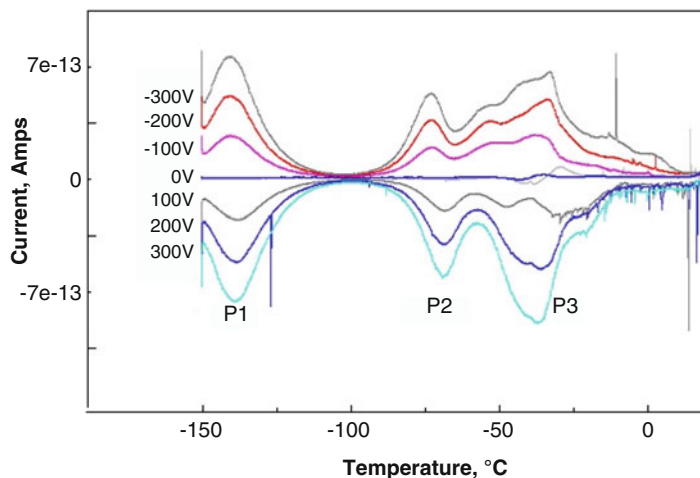


**Fig. 1** TSpC heating curves for 73.12 % sucrose solution in water obtained at variable polarization voltages (100, 200, 300, and 0 V, as shown in the graph) and with two different directions of the polarizing field

mechanisms such as charge space polarization, as such mechanisms demonstrate more complex behavior with changes in the field direction and strength. In addition, in TSpC runs performed at 0 V (no field), signals were detected above  $-50^{\circ}\text{C}$ , whereas no signal was observed at lower temperatures (Fig. 1). Signals at 0 V are indicative of spontaneous non-dipole relaxation events. Results for the 0 V runs are consistent with the dipole relaxation nature of the P1 event. Similar results were observed for solutions with sucrose content of 70 and 76.3 % w/w (curves not shown). Note that these solutions are expected to remain in the amorphous state during experiments, as reflected in a number of publications about this system.

Representative TSpC curves for freeze-dried sucrose are shown in Fig. 2. Similar to results for solutions with water content of 30–23.7 % w/w (sucrose content 70–76.3 % w/w), several events were observed at higher temperatures, around the calorimetric Tg. In addition, two weak (but reproducible) peaks, marked as P1 and Px, were observed in the low-temperature region, as illustrated in Fig. 2 (insert). As shown in Fig. 2 (insert), the strength of the event marked as P1 increases proportionally to the polarizing field voltage. Proportionality of the P1 signal to the polarizing field is consistent with dipole relaxation. The nature of the Px event is unclear. Note that the Px event was observed in freeze-dried samples only, and that freeze-dried samples usually have relatively high surface area, commonly around  $1\text{ m}^2/\text{g}$ ; therefore the Px signal is probably related to charges located on the solid/air interface.

The signal strength for P1 event for samples with higher water content (23.7–30 % w/w) was much higher than that for low water content samples (5–1 % w/w water). Indeed, average signal strength (normalized to the voltage of polarized field) was approximately an order of magnitude higher in samples with 23–30 % of water as compared with low water content samples,  $-(2.6 \pm 1.0) \times 10^{-15}$  vs.  $-(0.11 \pm 0.05) \times 10^{-15}\text{ A/V}$ . This observation that the P1 signal is much weaker in low water samples indicates that this event is most likely related to water molecules.

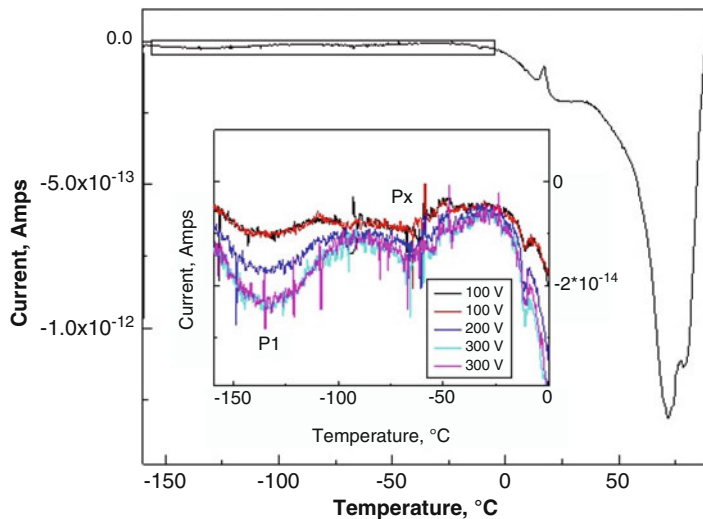


**Fig. 2** Representative TSpC heating curves of freeze-dried sucrose. *Inset:* magnified part of TSpC curves showing the low-temperature P1 event at different voltages of the polarizing field. Area of magnification is shown on the main curve as a *rectangle*

Representative DSC heating curves for sorbitol samples with variable concentration of water are presented in Fig. 3a. In all samples, glass transition was detected, whereas no evidence of water crystallization was observed. In solutions with the lowest concentration of sorbitol (65 % w/w), during heating scan to higher temperatures, i.e., above the  $T_g$ , it was observed the exotherm of water crystallization and ice melting endotherm. This finding is consistent with low-temperature X-ray diffraction studies of concentrated solutions of sorbitol where neither water nor sorbitol crystallization was observed on the timescale of the experiment (data not shown). Therefore, these samples are expected to remain completely amorphous during TSC experiments. Typical TSpC heating curves for sorbitol glasses with water content from 35 to 0 % w/w are shown in Fig. 3b. The low-temperature relaxation event, P1, was observed in all sorbitol-water samples, whereas it was not detected in amorphous sorbitol without water. Note that a relatively weak and broad low-temperature event attributed to beta-relaxation (Johari-Goldstein relaxation) was observed in pure sorbitol using the TSDC method (Correia et al. 2001; Ramos et al. 2007). The apparent discrepancy between the literature, where a low-temperature event was detected in pure sorbitol, and the present study, with a lack of such events in pure sorbitol, might be attributed to different sample configurations used. Indeed, the sample was in direct contact with an electrode in the study of Ramos et al. (2007), whereas in the present study, the sample was isolated from the electrode by Teflon. Isolating the sample from the electrode could have an impact on the signal strength, and therefore on the detection of such low strength signals as beta-relaxation. The P1 event was observed in both TSpC and TSdC experiments for sorbitol-water samples, and its strength was directly

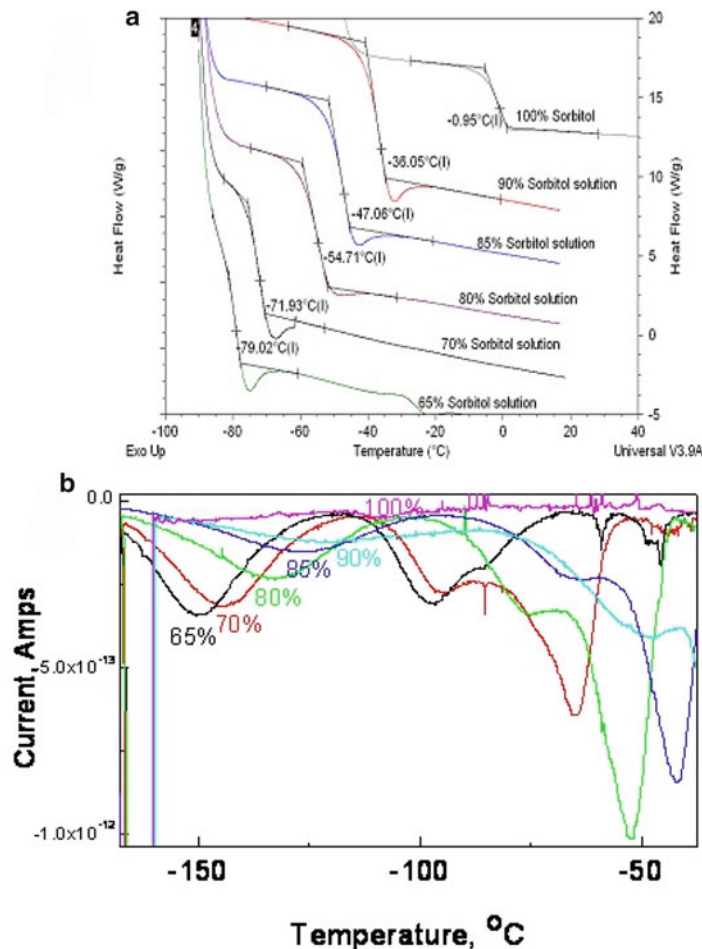


**Fig. 3** Representative DSC (a) and TSpC (b) curves of sorbitol-water samples with different concentration. Concentrations are shown in % w/w

proportional to the voltage of the polarizing field (curves not shown). These observations, i.e., the direct proportionality between the voltage and the signal, and the mirror images produced with TSpC and TSdC are usually considered to be the “signature” of a dipole relaxation. Several higher temperature TSC events were also observed in the sorbitol-water system; investigation of these transitions is outside the scope of the present study and is not considered here. Temperatures of the P1 event increased with the increase in sorbitol concentration, as can be seen in Fig. 4. P1 values are plotted in Fig. 4, along with the calorimetric  $T_g$ ; also,  $T_g$  data from the literature are shown for comparison.

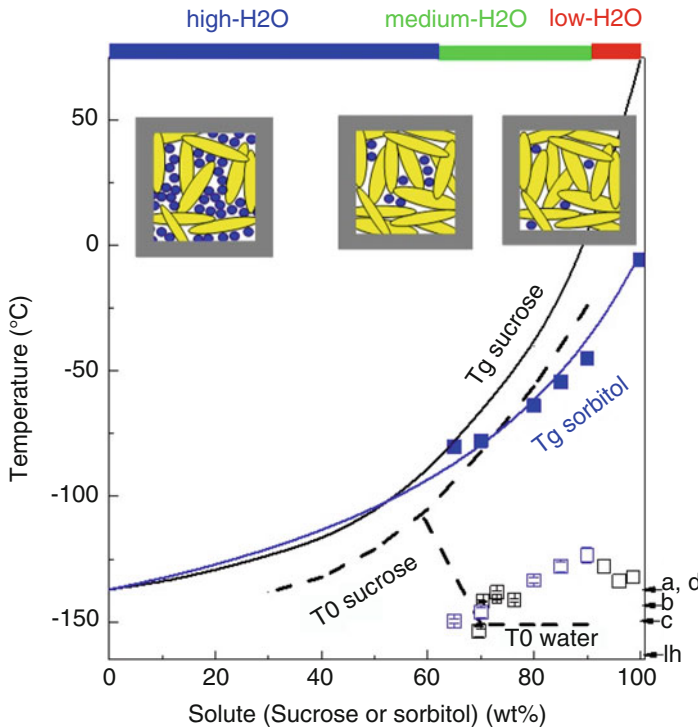


**Fig. 4** Calorimetric Tg and TSC events in sucrose-water: Solid black line represents the T<sub>g</sub> curve of sucrose-water (Girlich and Lüdemann 1994). Blue line and blue symbols represent the sorbitol-water systems. Dotted line is the T<sub>0</sub> values for water-sucrose system according to Girlich and Lüdemann (1994). The Tg line for sorbitol was constructed by fitting the DSC Tg (onset) data from Talja and Roos (2001) (symbols not shown) and the present study (blue filled squares) to the Gordon-Taylor equation (Gordon and Taylor 1952) with  $K$  as a fitting parameter  $Tg = (w_1Tg_1 + Kw_2Tg_2)/(w_1 + Kw_2)$ , where  $Tg_1$  and  $Tg_2 = 136$  K are the glass transition temperatures and  $w_1$  and  $w_2$  are the weight fractions of sorbitol and water, respectively, and  $K$  is a constant.  $K$  was determined to be  $3.1 \pm 0.2$ . The arrows indicate temperature of the Tg for pure water ( $-137$  °C for hyperquenched glassy water (Johari et al. 1987),  $-144$  °C for the produced LDA (Mayer 1991),  $-149$  °C for LDA (Handa and Klug 1988),  $-138$  °C for vapor-condensate (Sugisaki et al. 1968)) and for the rotational mobility of water in hexagonal ice (Johari and Jones 1975). Schematic representation of the microscopic structure of a sorbitol-water system is presented at the top, with three regions of different water concentration. Water and sorbitol molecules are shown as blue and yellow objects, respectively. The Figure was published previously in Authelin et al. (2014)

## 4 Discussion

A low-temperature TSC event, P1, was detected in both sucrose-water and sorbitol-water glasses at approximately  $-153$  to  $-128$  °C (sucrose-water) and  $-150$  to  $-125$  °C (sorbitol-water). While there are several potential types of physical processes which could cause a TSC signal (such as space charge polarization),

the P1 event indicates all of the main signatures of dipole relaxation, i.e., linear response of the strength with voltage, and mirror image of signals obtained with  $+/-$  directions of the polarizing field (sucrose) and TSpC/TSdC (sorbitol). In addition, the fact that the P1 event was not detected in pure sorbitol (i.e., at 0 % water), and that the intensity of the signal was much lower in low water samples as compared with higher water samples in both sucrose-water and sorbitol-water systems, allows us to conclude that the origin of a P1 event is due to dielectric relaxation of water dipoles, probably because of the rotational mobility of water molecules, and that the temperature of the P1 event corresponds to the onset of dipole relaxation of water in sorbitol and sucrose glasses.

The concentration-related changes in P1 temperature were similar in both sucrose-water and sorbitol-water systems; this observation can be attributed to either similarity in water-sucrose and water-sorbitol interaction, or negligible water-solute interaction as related to that of water-water contacts. The first explanation (similar water-sucrose and water-sorbitol interactions) seems more likely, as the P1 temperature changed with the water content, whereas a lack of concentration dependence could be expected under the second scenario (i.e., predominantly water-water interactions).

It is interesting to compare the P1 temperature in sucrose and sorbitol glasses with the glass transition temperature reported for pure amorphous water. Indeed, from a general perspective, the glass transition event corresponds to the onset of rotational and translational cooperative movements (during heating), and therefore the P1 event may resemble the glass transition behavior. To highlight this resemblance, we attribute the P1 event to the glass transition of water in sugar matrix ( $T_{gw}$ ). In low-density amorphous solid water (LDA), the glass transition temperature is reported to lie in the range of  $-150$  to  $-135$  °C, depending on the sample preparation and measurement technique (Sugisaki et al. 1968; Johari et al. 1987; Handa and Klug 1988; Mayer 1991). Interestingly, using  $-150$  °C as a lower boundary indicates that  $T_{gw}$  decreases with increasing water content and has reached the  $-150$  °C boundary by the point of 40 % w/w water (see Fig. 4). A plausible interpretation of these observations is that  $T_{gw}$  measured by TSC for lower water contents reflects the average orientational mobility of water molecules within an effectively rigid matrix of sugar molecules that form a percolating sugar-hydrogen bonding (HB) network. Above this threshold (i.e., at lower sugar concentration), the glass constitutes a percolating HB network of water molecules, with a competing or complementary network of sugar-sugar and sugar-water HBs. If this network is similar to that of pure water in terms of activation barriers for rotational motion that liberate water-water and water-sugar HBs, it can be expected that the  $T_{gw}$  would be similar to  $T_g$  for pure water at these lower sugar concentrations.

On the lower water concentration side of the threshold level near 40 % w/w water, it seems reasonable that  $T_{gw}$  first increases with decreasing water content, if more and more water molecules are forced to balance between HBs with other water molecules that are more rotationally mobile, and sugars that are locked into a percolating sugar HB matrix that is well below its  $T_g$ . Eventually, at low enough water levels, most water molecules become isolated from other water molecules

and effectively observe the same local environment, independently of further reduction in bulk water content. Based on the data in Fig. 4 for sucrose-water, this last transition appears to occur in the vicinity of 10 % w/w water. Interestingly, earlier results from NMR suggested a qualitatively similar decoupling of water dynamics from a dependence on bulk composition, although the T<sub>0</sub> values obtained from the (Girlich and Lüdemann 1994) NMR study were different from the T<sub>gw</sub> observed in this study. It should be noted that the T<sub>0</sub> values (shown in Fig. 4) were extrapolated from higher temperature (Girlich and Lüdemann 1994). As such, it is possible that the seeming disagreement between the T<sub>0</sub> results and the directly measured P<sub>1</sub> transition temperatures here is simply a result of statistical uncertainties inherent in any extrapolated quantity. It should be also clarified that the T<sub>0</sub> values at higher water concentrations are a combination of both sugar and water mobility, as it is not possible to separately extrapolate T<sub>0</sub> for sugar and water under conditions where both are mobile and strongly coupled to the T<sub>g</sub> of the system (Girlich and Lüdemann 1994).

Finally, it would be worthwhile to compare low-temperature TSC events in low water sugar systems with the behavior of pure water, i.e., hexagonal ice. In a systematic investigation of ice by TSdC by Johari and Jones (1975), a low-temperature thermal depolarization current event was detected for hexagonal ice at approximately 110 K ( $-163^{\circ}\text{C}$ ) at the heating rate of 0.0023 K/s. This event was assigned to the relaxation of frozen-in orientation polarization of water molecules in ice (Johari and Jones 1975). In the present study, we also observed dipole relaxation in pure ice samples, albeit at somewhat higher temperature,  $-140^{\circ}\text{C}$  (130 K). The  $20^{\circ}\text{C}$  difference between Johari and Jones (1975) and the present work may be due to the higher scanning rate used in the present study; indeed, it was noted in Johari and Jones (1975) that the temperature of the TSdC event increased with increase in the heating rate.

Overall, the similarity in the temperatures of the dipole relaxation events in low water content sugar samples and in pure ice may reflect similar fundamental mechanisms of water mobility in sugar glasses and in ice, although in sugar glasses, sugar-water interactions probably have noticeable impact, as reflected in the concentration dependence of the T<sub>gw</sub> (Fig. 4). Also, this concentration dependence implies that decoupling between water and sugar is probably partial at best and may be affected by the differences between the percolation threshold for a primarily mixed-HB percolating matrix of sugar molecules and that for a matrix in which water molecules are primarily isolated from one another.

## 5 Conclusions

Investigation of concentrated sugar-water solutions and glasses by thermally stimulated current method reveals that there is a characteristic temperature (T<sub>gw</sub>) associated with the onset of mobility of water. The temperature range of the T<sub>gw</sub> event observed in this study was  $-125$  to  $-155^{\circ}\text{C}$ , which is similar to the T<sub>g</sub>

observed in LDA, i.e.,  $-135$  to  $-150$  °C. This observation is consistent with a recent neutron diffraction study, according to which the structure of water clusters in 70 % sorbitol solution was very similar to that of LDA, but different from the bulk water (Chou et al. 2012). Tgw is apparently independent of sugar type, as both sucrose and sorbitol samples showed similar Tgw value at comparable water content. From the concentration dependence of Tgw, two regions can be identified, i.e., intermediate water region (35–10 % water) and low water region (10–0 % water). Schematic drawings of the structure of amorphous sorbitol-water system are given in Fig. 4, showing three water regions. In the intermediate water region, water mobility decreased (Tgw increased), with a decrease in water content; Tgw changes were parallel with Tg changes in a semiquantitative manner. In the low water content region, however, water mobility did not change or increase (Tgw decreased) with decrease in water content. In future studies, it would be important to study the transition from intermediate to low water behavior in a variety of systems in order to improve understanding of cryo- and lyo-protection of biological systems by sugars.

**Acknowledgements** The study was supported in part by a Pfizer Global Research and Development summer internship provided to Ali Hussain.

## References

- Aldous BJ, Franks F, Greer AL (1997) Diffusion of water within an amorphous carbohydrate. *J Mater Sci* 32:301–308
- Apakis L, Pissis P, Boudoros G (1983) Depolarization thermocurrents in ice Ih at low temperature depending on the electrode material. Polarization mechanism. *Nuovo Cimento* 2D:932–946
- Authelin J-R, MacKenzie AP, Rasmussen DH, Shalaev EY (2014) Water clusters in amorphous pharmaceuticals. *J Pharm Sci* 103:2663–2672
- Chou SG, Soper AK, Khodadadi S, Curtis JE, Krueger S, Cicerone MT, Fitch A, Shalaev EY (2012) Pronounced micro-heterogeneity in a sorbitol-water mixture observed through variable temperature neutron scattering. *J Phys Chem B* 116:4439–4447
- Correia NT, Alvarez C, Moura Ramos JJ, Descamps M (2000) Molecular motions in molecular glasses as studied by thermally stimulated depolarisation currents. *Chem Phys* 252:151–163
- Correia NT, Alvarez C, Rames JJM, Descamps M (2001) The  $\beta - \alpha$  branching in D-sorbitol as studied by thermally stimulated depolarization currents (TSDC). *J Phys Chem B* 105:5663–5669
- Fagegaltier N, Lamure A, Lacabanne C, Caron A, Misfud H, Bauer A (1997) Thermal analysis of amorphous phase in a pharmaceutical drug. *J Therm Anal* 48:459–464
- Franks F (1997) Phase changes and chemical reactions in solid aqueous solutions: science and technology. *Pure Appl Chem* 69:915–920
- Galop M, Collins GL (2001) Thermally stimulated current observed in pharmaceutical products. *Thermochim Acta* 37:367–368
- Girlich D, Lüdemann H-D (1994) Molecular mobility of the water molecules in aqueous sucrose solutions, studied by  $^2\text{H}$ -NMR relaxation. *Z Naturforsch C J Biosci* 49c:250–257
- Gordon M, Taylor JS (1952) Ideal copolymers and the second-order transitions of synthetic rubbers. I. Non-crystalline copolymers. *J Appl Chem* 2(9):493–500

- Handa YP, Klug DD (1988) Heat capacity and glass transition behavior of amorphous ice. *J Phys Chem* 92:3323–3325
- Johari GP, Jones SJ (1975) Study of the low-temperature “transition” in ice Ih by thermally stimulated depolarization measurements. *J Chem Phys* 62:4213–4223
- Johari GP, Hallbrucker A, Mayer E (1987) The glass–liquid transition of hyperquenched water. *Nature* 330:552–553
- Koster KL (1991) Glass formation and desiccation tolerance in seeds. *Plant Physiol* 96:302–304
- Mayer E (1991) Calorimetric glass transition in the amorphous forms of water: a comparison. *J Mol Struct* 250:403–411
- Pissis P, Diamanti D, Boudouris G (1983) Depolarisation thermocurrents in frozen aqueous solutions of glucose. *J Phys D Appl Phys* 16:1311–1322
- Ramos JJM, Diogo HP, Pinto SS (2007) Effect of physical aging on the Johari-Goldstein and  $\alpha$  relaxations of D-sorbitol: a study by thermally stimulated depolarization currents. *J Chem Phys* 126:144506
- Reddy R, Chang L, Luthra S, Collins G, Lopez C, Shamblin SL, Pikal MJ, Gatlin LA, Shalaev EY (2009) The glass transition and sub-t-g-relaxation in pharmaceutical powders and dried proteins by thermally stimulated current. *J Pharm Sci* 98:81–93
- Shmeis RA, Wang Z, Krill SL (2004) A mechanistic investigation of an amorphous pharmaceutical and its solid dispersions. Part I. A comparative analysis by thermally stimulated depolarization current and differential scanning calorimetry. *Pharm Res* 21:2025–2030
- Sugisaki M, Suga H, Seki S (1968) Calorimetric study of glassy state. V. Heat capacities of glassy water and cubic ice. *Bull Chem Soc Jpn* 41:2591–2599
- Talja RA, Roos YH (2001) Phase and state transition effects on dielectric, mechanical, and thermal properties of polyols. *Thermochim Acta* 380:109–121
- Teyssedre G, Bernes A, Lacabanne C (1995) Investigation of dielectric relaxations associated with the glass transition of vinylidene fluoride and trifluoroethylene copolymers by thermally stimulated current. *J Polym Sci B Polym Phys* 33:2419–2428
- Vanderschueren J, Gasiot J (1979) Field-induced thermally stimulated currents. In: Bräunlich P (ed) Thermally stimulated relaxation in solids. Springer, Berlin, pp 135–223

# Functional Behavior of Different Food Components as Affected by Water and Physical State

A. Marabi, L. Forny, and A. Gianfrancesco

## Abbreviations

$a_w$	Water activity
DE	Dextrose equivalent
FD	Freeze-dried
MW	Molecular weight
PEGs	Polyethylene glycols
SMP	Skim milk powder

## 1 Introduction

The presence of water in foods, and the vast number of roles that water plays, is an old and well-researched topic. There are countless interactions in which water impacts the food chain, starting from irrigation of crops, harvested raw materials, storing and processing, and finished goods properties such as shelf life, microbiological quality and safety, functional properties, palatability and profitability, to name a few.

In order to better understand and control the processing steps used to manufacture different food products, it is essential to understand, control, and exploit the unique properties of water and how it affects and transforms the ingredients utilized.

In this chapter, we will focus on how different food components, namely carbohydrates, proteins, and fat, are affected by the presence of water. We put

---

A. Marabi (✉) • L. Forny • A. Gianfrancesco  
Nestlé Research Center, Lausanne, Switzerland  
e-mail: [Alejandro.Marabi@IL.nestle.com](mailto:Alejandro.Marabi@IL.nestle.com)

special emphasis on powdered foods, as this category represents a significant portion of what is popularly known as convenience foods. Moreover, during the past 10 years, a significant increase in the number of food and beverage products launched in the form of powder was observed. From fewer than 300 new products launched in 2000, this category soared to more than 2,400 products that were introduced to the market worldwide in 2010.

The success attained by this category can be related to a number of important advantages inherent to food powders, including:

- Consumer convenience (anytime, anywhere)
- Separate production from consumption sites
- Reduced transportation cost
- Bacteriological and shelf stability

In addition to these advantages, food powders also present a number of physical, chemical, and sensory attributes that need to be attained in order to successfully address consumer needs, including:

- Free flowing, for ease of production, filling, dosing, and consumption
- Easily wettable, in order to avoid lumps
- Quick to disperse, resulting in a homogeneous liquid
- Rapidly soluble, so all ingredients attain desired functionality
- Similar to the original product after reconstitution, leading to increased acceptance and sensorial preference

Powders that reconstitute in hot and cold water with minimal stirring and without formation of lumps or undissolved sediments are referred to as instant powders. At the consumer level, rapid and complete reconstitution of dehydrated products is a key quality indicator. Reconstitution time is defined as the time needed to transform a powder into a homogeneous solution. In general, the aim is to shorten reconstitution time through optimized microstructure, supramolecular structure, or composition. Consequently, there is a crucial need to identify and understand fundamental factors and rate-limiting steps affecting the reconstitution process.

In this process, we have investigated how the presence of water, and consequently the physical state of different food components including carbohydrates, proteins, and fat, would impact the reconstitution process of food powders. Our main challenge is how to design food powders with the desired dissolution properties. It is worth noting that, even if counterintuitive, the faster dissolution kinetics will not always lead to the best reconstituted products.

A summary of the steps and factors included in the reconstitution process is presented in Fig. 1. The four well-established steps of wetting, sinking, dispersing, and dissolving the powder (Schubert 1987) should be evaluated and quantified, not only as a function of the physicochemical properties of the powder and the conditions of the liquid (e.g., temperature, mixing energy), as is often the case, but also as a function of the thermodynamics process. This approach is widely used in the pharmaceutical industry (Gao and Rytting 2006; Dilworth et al. 2004), but has seldom been used in food sciences (Marabi et al. 2007).

**Fig. 1** The four steps required to achieve good reconstitution of food powders and the main intrinsic and extrinsic factors affecting the process

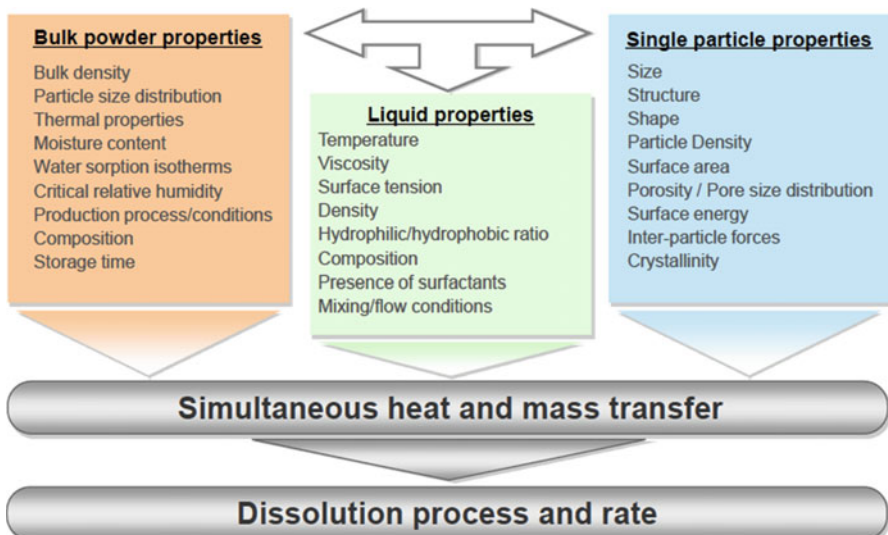
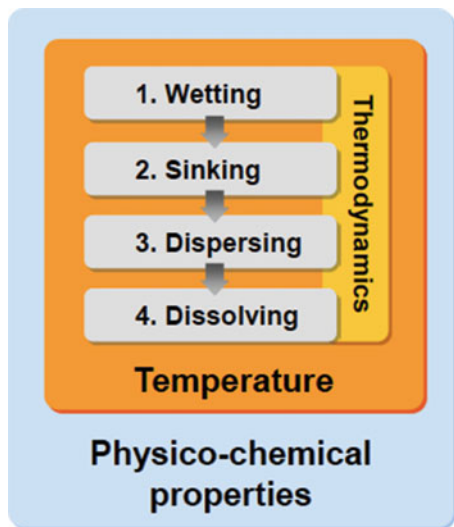


**Fig. 2** Integrated approach to elucidate the complex interactions taking place from the moment the consumer fills a spoon with a powder until it is possible to enjoy a chocolate drink

It was previously demonstrated (Marabi et al. 2007, 2008a, b) that an integrated approach (as shown in Fig. 2), including the key properties of the bulk powder, the single particles to be dissolved, and the liquid, is paramount in order to elucidate the complex interactions taking place from the moment the consumer fills a spoon with a powder until it is possible to enjoy a chocolate drink. The solid and liquid

properties, as well as the physical processes taking place, including both heat and mass transfer, should be considered in order to gain a deeper understanding of the complex interactions taking place during the reconstitution process.

## 2 The Impact of Water, Physical State, and Molecular Weight on the Dissolution of Carbohydrates

In order to exemplify the important role of material state on the dissolution process, a simple example is presented in Fig. 3. The data was measured in a Setaram C80 Calvet-type calorimeter. The curves show the endo- or exothermic effect observed as a result of the state of sucrose during the dissolution process. When completely amorphous sucrose is dissolved, a fast and exothermic response (10 J/g) is observed. In contrast, when crystalline sucrose is dissolved, a highly endothermic curve results (18 J/g). When a partially recrystallized sample is dissolved, a mixed reaction is obtained. It is worth noting that, in this case, and for many other samples in which amorphous and crystalline materials are present simultaneously, the exothermic peak is always observed first.

The fact that different physical states show opposite thermodynamic behavior highlights that the kinetics of the process might be related to the thermal response observed. This is exemplified by a simple example in which crystalline sucrose spheres were dissolved in different liquid mixtures (water and polyethylene glycols, PEGs) at 30 °C. As shown in Fig. 4, a linear correlation was observed

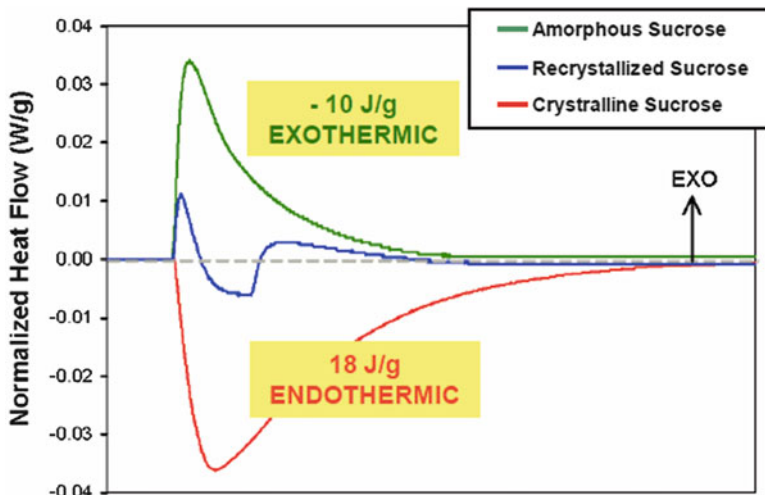


**Fig. 3** Thermal response upon dissolution of sucrose in amorphous and crystalline states; a partially recrystallized sample is also shown

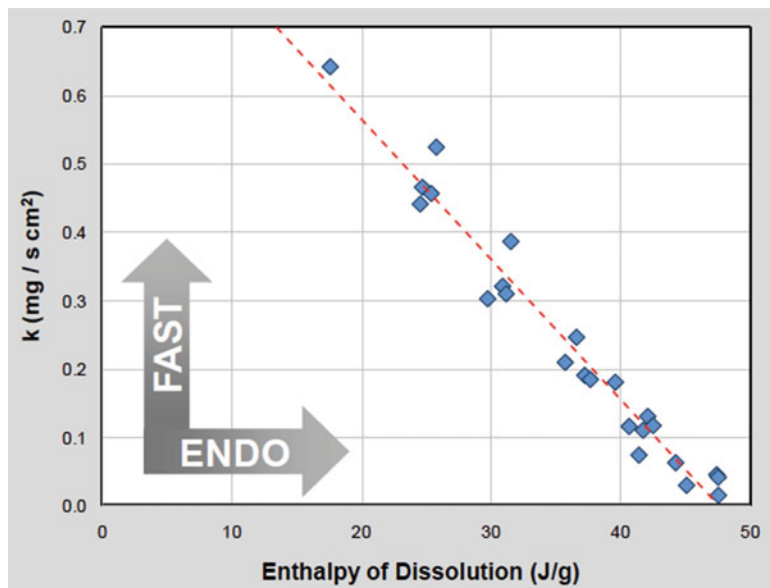


**Fig. 4** Correlation between enthalpy of dissolution and dissolution rate constant ( $k$ ) for sucrose spheres dissolved in different solutions (adapted from Marabi et al. 2008a)

between the dissolution rate constant and the enthalpy of dissolution. In this case, more endothermic thermal responses were related to slower dissolution rates. This example highlights the importance of the interaction between the solid and the liquid in which it is dissolved, and also the fact that the thermodynamics of the process can be effectively used to predict or even “tune” the dissolution rate. This has further practical applications, as it is well known that the fastest dissolution rates are not always desired, since particles that dissolve too quickly might lead to the generation of lumps, in which the outer layers are dissolved and generate a highly viscous boundary enclosing and avoiding the dissolution of the dry powder inside.

The impact of the water content of maltodextrin (dextrose equivalent, DE, 21) and the physical state of skim milk powder (SMP) samples was also studied in terms of its thermodynamic response upon dissolution (Figs. 5 and 6). The samples were characterized by their enthalpy of dissolution at three different conditions: freeze-dried (FD); after equilibration at 54.4 % RVP; and after FD of the equilibrated samples. The dissolution was found to be exothermic for all tested samples, and the curves showed similar shapes. A clear decrease in the exothermic response is observed when FD and equilibrated samples are compared. Lower exothermic response is linked to higher moisture content of the samples. However, there is a significant difference between the two samples. In the case of maltodextrin, exothermic heat of dissolution is fully recovered after the equilibrated sample is dried. In contrast, when the equilibrated SMP sample is dried, only ca. 50 % of the heat of

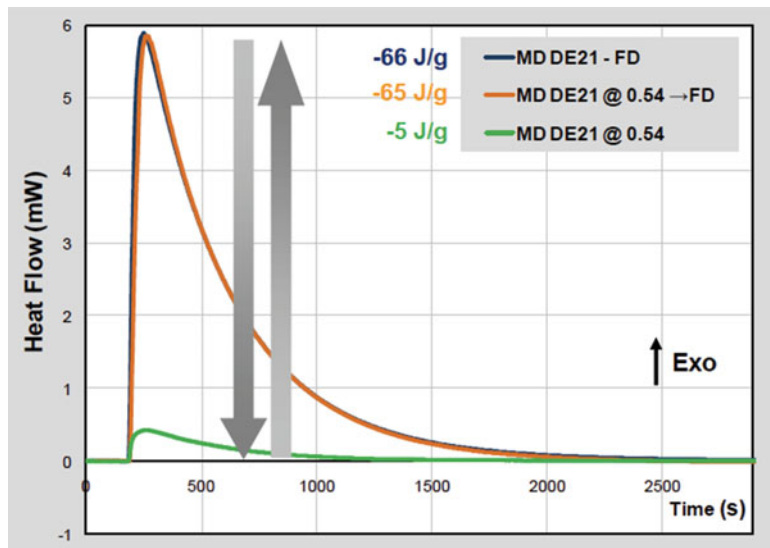


**Fig. 5** Typical dissolution calorimetry curves of tested maltodextrin powders. All samples showed an exothermic response; however, increased moisture content led to a less exothermic dissolution process (adapted from Marabi et al. 2007)

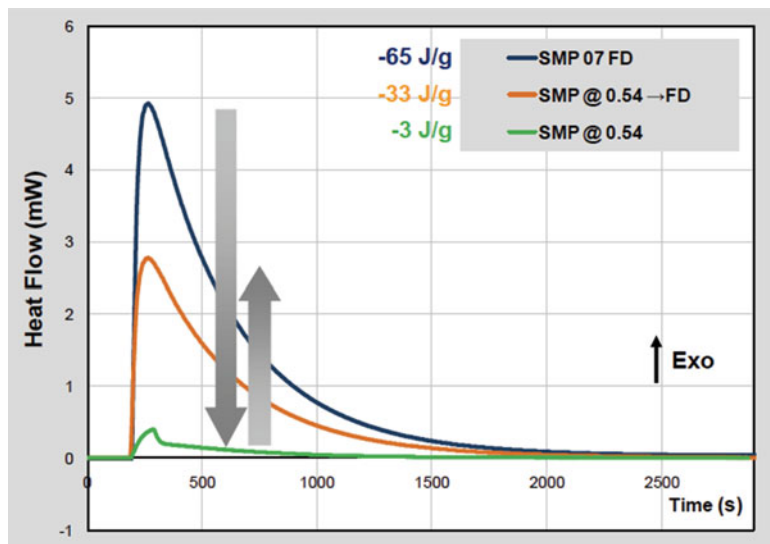


**Fig. 6** Typical dissolution calorimetry curves of tested skim milk powders. All samples showed an exothermic response; however, increased moisture content and recrystallized lactose led to a less exothermic dissolution process (adapted from Marabi et al. 2007)

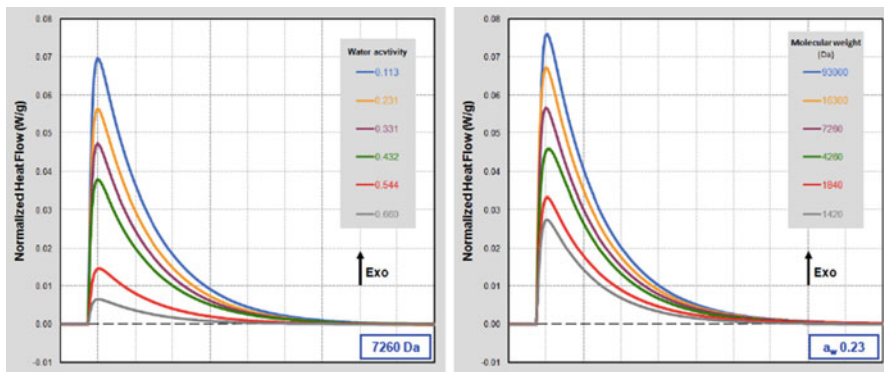


**Fig. 7** Dissolution calorimetry curves of maltodextrins having different molecular weights at a fixed water activity and single molecular weight equilibrated at various water activities

dissolution is recovered. This is due to the recrystallized lactose in the samples, which has an endothermic response, and therefore total heat liberated is diminished accordingly by the fraction of crystalline material. The impact of these findings on the kinetics of dissolution is shown in a video recording, which can be seen in the published work (Marabi et al. 2007).

In order to further understand the different factors affecting the enthalpy of dissolution and the kinetics of the process, further measurements were conducted on different materials. One typical example is shown in Fig. 7. In this case, dissolution enthalpy of maltodextrin DE21 equilibrated at different water activities, as well as different DE values equilibrated at a water activity of 0.23, is shown. Clearly, increasing the water activity of the sample leads to fewer exothermic responses. These results can be explained in terms of the new bonds formed during the dissolution process, indicating that drier material forms more new bonds with water molecules, releasing more energy than when such bonds already exist, and therefore less energy is dissipated during the dissolution process (Haque and Roos 2006). Molecular weight (MW) also showed a significant impact on the heat of dissolution measured. In this case, higher MWs resulted in more exothermic responses. This effect has not previously been reported and is currently under investigation. However, there are practical implications in designing complex formulations of food powders. By characterizing the thermal behavior of single ingredients, it is possible to predict the response of various products. In this case, by using the right amount of exothermic materials at the correct water activity, the dissolution kinetics of commercial products were significantly improved.

### 3 The Impact of Water and Structure on Dissolution of Proteins

Apart from carbohydrates, proteins are another important category of key constituents of food powders. Dissolution behavior of proteins can thus affect the overall rehydration of several food products, such as infant formulae, and be a limiting step for effective reconstitution.

For instance, Fig. 8 shows the overall reconstitution behavior of micellar casein and Na-caseinate in water. The evolution of concentration across time is measured by an electric conductivity probe.

It can be observed that, compared to carbohydrates, the timescale for complete dissolution of proteins is much longer (minutes vs. seconds), and it is strongly dependent on the protein structure. Na-caseinate dissolves much more slowly than micellar casein, due to its open structure, in which hydrophobic sites are exposed. A similar effect can be noticed when proteins are denatured; for instance, denatured  $\beta$ -lactoglobulin is almost insoluble, while its native form can easily be rehydrated.

It can also be noticed that the initial water activity (and thus water content) of the powder plays an important role. For Na-caseinate, higher water activity leads to statistically significant faster initial dissolution. However, for other proteins opposite behavior has been observed.

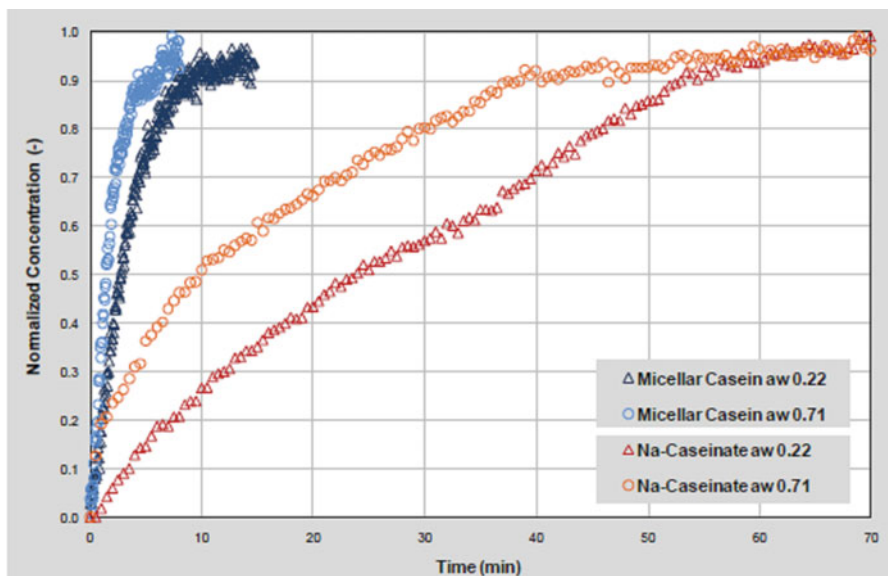


**Fig. 8** Overall reconstitution behavior of micellar casein and Na-caseinate powders equilibrated at  $a_w = 0.22$  and 0.71 (dissolution in water, 2 % w/v, 750 rpm stirring)

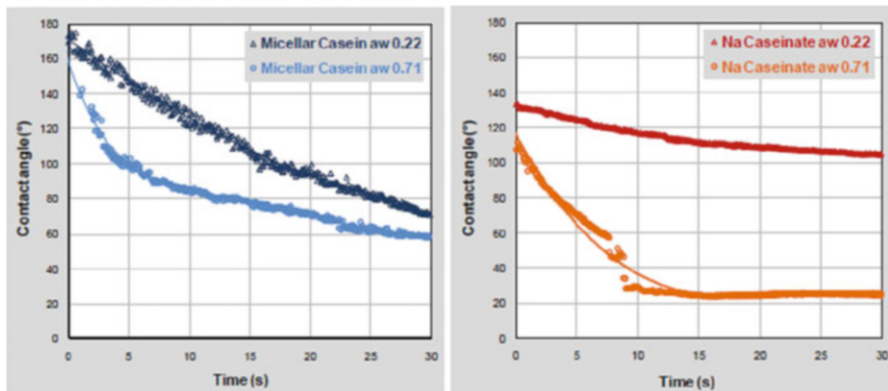


**Fig. 9** Evolution of effective contact angle between a water drop and a layer of powder along time (left: micellar casein layer; right: Na-caseinate layer). In both cases, powders were equilibrated at  $a_w$  of 0.22 and 0.71

In previous works, Gaiani et al. (2006, 2007) attempted to distinguish the relative importance of the different reconstitution steps (Fig. 1) during dissolution of phosphocaseinate.

In our study, we were able to demonstrate that the determining step for protein rehydration was the wetting of the powder. Figure 9 shows the evolution of the effective angle of contact between a drop of water and a layer of powder.

A large value of the angle suggests the hydrophobicity of the powder, as the water drop remains spherical, without spreading on the powder layer. It can be observed that different proteins exhibit behavior similar to that shown by conductivity experiments (Fig. 8). Powders that are more easily rehydrated have a lower angle of contact and, importantly, show a fast decrease of the angle's value in the first seconds. This means that the powder is easily wetted by the water drop. On the other hand, the less soluble powder (Na-caseinate at water activity,  $a_w$ , 0.22) shows only a slight decrease of the contact angle after 30 s. These results suggest that the initial powder's water content has a tremendous effect on wettability, although the reasons for this are still unclear. Further investigations are necessary to clarify whether structural modifications are induced by difference in initial water activity, and why the effect is different depending on the considered protein.

Finally, thermal analysis of protein powders showed that the enthalpy of dissolution can be directly related to their overall rehydration behavior (Fig. 10). A highly exothermic enthalpy of dissolution corresponded to the easiest rehydration. As already discussed for carbohydrates, calorimetry can thus be a valuable tool to characterize the behavior of single ingredients and design powders possessing the desired dissolution behavior.

Attention should, however, be paid to the fact that this technique has not been adapted to analyze powders which are very slow to be dissolved, as undissolved lumps can remain in the calorimeter cell, giving misleading results.

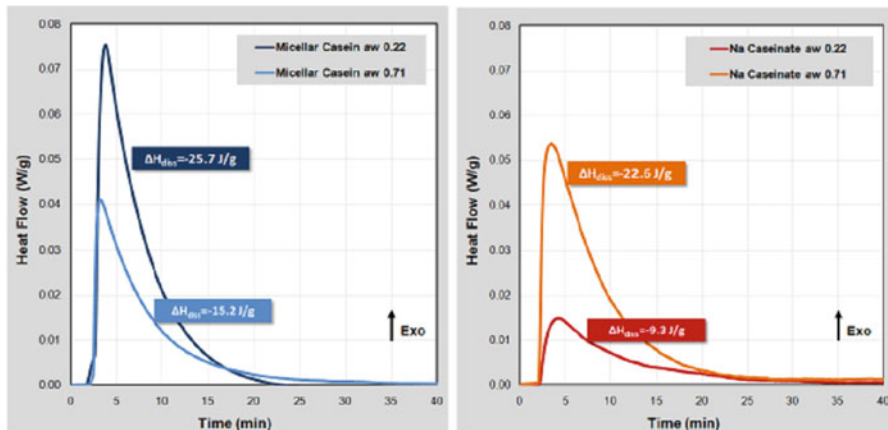


**Fig. 10** Dissolution calorimetry curves with calculated enthalpy of dissolution of micellar casein and Na-caseinate powders, equilibrated at different water activities

## 4 Conclusions

- Food powders are an important food product category, and they account for a significant portion of new products launched every year.
- Key properties of ingredients and finished products should be studied and understood in order to optimize their functionality.
- The physical state and water content of food powders will impact their ultimate behavior, and should therefore be controlled in order to optimize performance and ensure consumer satisfaction.
- Measuring and understanding the thermodynamics of the dissolution process provided additional insight, which, coupled with dissolution kinetics, will result in products adapted to consumer needs.
- Incorporation of new ingredients in existing products presents a challenge, and therefore there is a need to carefully design and present all aspects of newly developed products.

## References

- Dilworth SE, Buckton G, Gaisford S, Ramos R (2004) Approaches to determine the enthalpy of crystallisation, and amorphous content, of lactose from isothermal calorimetric data. *Int J Pharm* 284:83–94
- Gaiani C, Scher J, Schuck P, Hardy J, Desobry S, Banon S (2006) The dissolution behaviour of native phosphocaseinate as a function of concentration and temperature using a rheological approach. *Int Dairy J* 16:1427–1434
- Gaiani C, Schuck P, Scher J, Desobry S, Banon S (2007) Dairy powder rehydration: influence of protein state, incorporation mode, and agglomeration. *J Dairy Sci* 90:570–581

- Gao D, Rytting JH (2006) Use of solution calorimetry to determine the extent of crystallinity of drugs and excipients. *Int J Pharm* 151:183–192
- Haque MK, Roos YH (2006) Differences in the physical state and thermal behavior of spray-dried and freeze-dried lactose and lactose/protein mixtures. *Innovat Food Sci Emerg Technol* 7:62–73
- Marabi A, Mayor G, Raemy A, Bauwens I, Claude J, Burbidge AS, Wallach R, Saguy IS (2007) Solution calorimetry: a novel perspective into the dissolution process of food powders. *Food Res Int* 40:1286–1298
- Marabi A, Mayor G, Raemy A, Burbidge AS, Wallach R, Saguy IS (2008a) Assessing dissolution kinetics of powders by a single particle approach. *Chem Eng J* 139:118–127
- Marabi A, Raemy A, Bauwens I, Burbidge AS, Wallach R, Saguy IS (2008b) Effect of fat content on the dissolution enthalpy and kinetics of a model food powder. *J Food Eng* 85:518–527
- Schubert H (1987) Food particle technology. I. Properties of particles and particulate food systems. *J Food Eng* 6:1–32

# **Effect of Different Components of Edible/ Biodegradable Composite Films on Water Relationships in the Polymer Matrix**

**A. Chiralt, P. Talens, F.M. Monedero, and M.J. Fabra**

## **Abbreviations**

AFM	Atomic force microscopy
$a_w$	Water activity
BW	Beeswax
$E$	Elongation at break
EEP	Ethanol extract of propolis
EM	Elastic module
HPMC	Hydroxypropyl methylcellulose
NaCas	Sodium caseinate
OA	Oleic acid
SPI	Soy protein isolate
Tg	Glass transition temperature
Tr1	Solid-solid transition
Tr2	Solid-liquid transition
TS	Tensile at break
WSC	Water sorption capacity
WVP	Water vapor permeability

---

A. Chiralt (✉) • P. Talens • F.M. Monedero • M.J. Fabra

Institute of Food Engineering for Development, Department of Food Technology,  
Universitat Politècnica de Valencia, Camino de Vera, s/n., 46022 Valencia, Spain  
e-mail: [dchiralt@tal.upv.es](mailto:dchiralt@tal.upv.es)

## 1 Introduction

Films and coatings based on edible/biodegradable hydrocolloids have received special attention in the last few years as an alternative to preserve foods with several possibilities: to maintain sensory and nutritional properties or microbial stability, to reduce moisture losses or mechanical damage, to improve food appearance (especially gloss), to add different food ingredients such as color or aroma compounds, to incorporate bioactive compounds such as antimicrobials or antioxidants, and to reduce the use of plastic packaging. Films or coatings must be transparent, flavorless, and odorless and they must have adequate water vapor permeability and selective permeability to gases and volatiles. They must not represent a health risk and be low cost (Krochta and de Mulder-Johnston 1997; Tharanathan 2003).

The usual components of films and coatings are hydrocolloids, i.e., polysaccharides or proteins, which show good mechanical properties and good barrier properties to gases ( $O_2$  y  $CO_2$ ) or aroma compounds, but poor water vapor barrier properties due to their hydrophilic nature. Plasticizers, such as glycerol or sorbitol (these are the most frequently used), are usually incorporated at a determined ratio, which gives adequate flexibility to the film, decreasing brittleness, but enhancing the poor water vapor barrier properties of hydrocolloids, also due to their hydrophilic nature. The incorporation of hydrophobic compounds, such as lipids, in the film forming formulations allows us to significantly reduce water uptake capacity and water vapor permeability of the films or coatings (Morillon et al. 2002; Srinivasa et al. 2007). In general, lipids show good water vapor barrier properties, but poor ability to form films and, in some cases, they give rise to undesirable properties, such as rancidity development. In some cases, lipid compounds provide the film with additional functional properties, such as antimicrobial or antioxidant capacity, as occurs with some essential oils (Gómez-Estaca et al. 2010; Sánchez-González et al. 2010, 2011).

Surfactants, fatty acids, or different nonpolar, organic compounds have been incorporated to film formulations giving rise to heterogeneous dispersions due to the lack of miscibility with the hydrophilic macromolecules (Fabra et al. 2009a; Jiménez et al. 2010). Thus, composite films were obtained where it is possible to optimize the film properties since they have better water vapor barrier properties (Debeaufort et al. 2000; Elsabee et al. 2008), selective permeability to  $O_2$  and  $CO_2$  (Alves et al. 2010) or other volatiles (Fabra et al. 2009b; Hambleton et al. 2011), durability, and structural cohesion.

The heterogeneous structure of the composite film forming dispersions also occurs in the dried film which shows a continuous matrix of hydrocolloid and miscible compounds, such as plasticizer, and dispersed particles of different sizes and shapes, depending on the structural properties of the initial dispersion and the film drying conditions (Villalobos et al. 2005). Figure 1 shows the microstructure of some films obtained with sodium caseinate and glycerol where lipids, oleic acid (OA), beeswax (BW), and their mixture, in a ratio of 70:30, were incorporated.

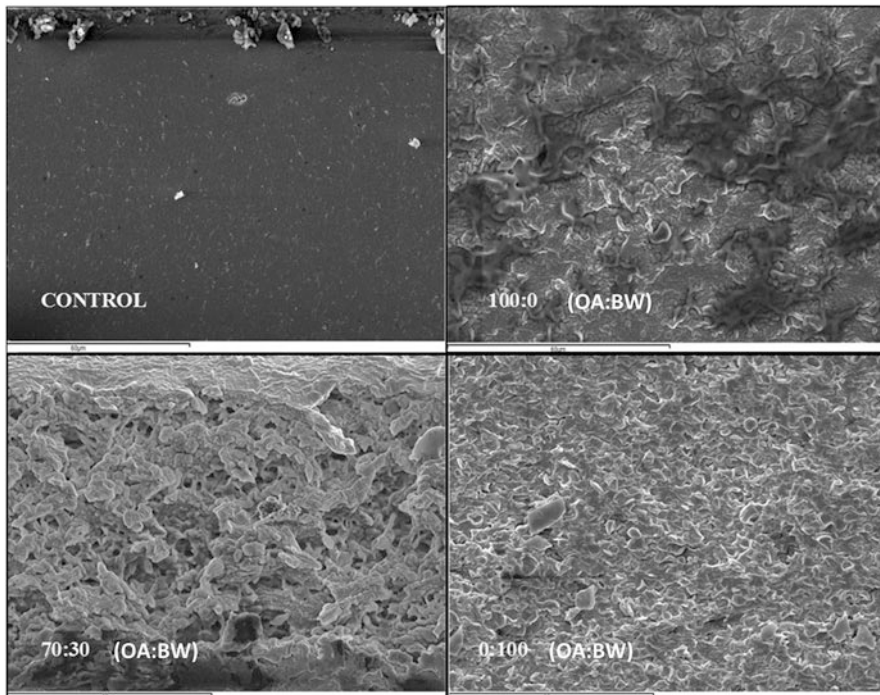


**Fig. 1** SEM micrographs of the cross section of sodium caseinate-glycerol (1:0.30) films without (control) and with lipids (oleic acid beeswax mixtures in the ratios 1:0, 0.3:0.7 and 0:1)

The protein-lipid ratio was 1:0.5 in all cases. The lipid dispersed phase can be appreciated, showing clear differences depending on the lipid composition. The heterogeneity of the structure is also reflected in the film surface, as has been observed by the atomic force microscopy (AFM) (Fabra et al. 2009a, c). The different surface topography is the result of the initial lipid particle size in the film forming dispersion and the destabilization phenomenon, which occur during film drying and which imply flocculation, coalescence, and creaming of lipid particles. The more unstable dispersions lead to a greater surface roughness of the films due to the faster progression of destabilization phenomena and, as a result, the lipid migration to the film surface is more intense. Surface roughness has a high impact on the film gloss; the greater the surface roughness, the lower the gloss (Villalobos et al. 2005; Fabra et al. 2009a).

In polar lipids, such as fatty acids, the lipid self-association phenomenon plays an important role in the film microstructure. This phenomenon is determined by molecular interactions in the film forming dispersion and their changes in line with the water evaporation during the film formation. Several authors observed a multilayered structure for saturated fatty acids (lauric, palmitic, and stearic) in sodium caseinate (Fabra et al. 2009c) and hydroxypropyl methylcellulose (Jiménez et al. 2010) films. This was associated with the growth of the molecular

aggregations in the bilayer self-association of the lipid molecules during film drying and the final crystallization of fatty acids in the polymer matrix. The length of lipid layers in the matrix was greater for lauric acid and decreased as the fatty acid chain length increased. This indicates that the growth of the molecule aggregates during film drying was more effective when the fatty acid chain was shorter, probably due to its greater molecular mobility. These successive lipid layers in the film matrix greatly contribute to reduce water vapor permeability, thus improving the water barrier properties; the longer the lipid layers, the lower the water vapor permeability (WVP) values. Films containing stearic acid, of a more hydrophobic nature, showed the poorest water barrier properties, which can be explained by these structural effects. These considerations underline the importance of relating the properties of the film forming dispersions with the relevant characteristics of the films. The properties related with the stability of the film forming dispersion such as rheology, particle size distribution, zeta-potential, or contact angle on a determined surface affect the properties related to the film functionality to a great extent.

Optical properties of the films such as gloss and transparency are important, since they have an impact on product appearance and are greatly affected by the degree of the film's structural heterogeneity (Villalobos et al. 2005; Ozdemir and Floros 2008; Fabra et al. 2009a). Nevertheless, one of the most relevant properties of the films/coatings is the water affinity and water sorption behavior, since equilibrium water content of the film impacts directly on its mass transport properties (water vapor and gas permeability) and mechanical resistance, which are decisive for the film's practical applications.

Components of the hydrocolloid matrix can interact to a different degree with the polymer chain/groups, giving rise to systems where water relationships can change considerably, as compared with pure hydrocolloid. Some examples of how the compounds incorporated into the polymer matrix can affect water sorption capacity, phase transitions, or molecular mobility are commented on for some protein or polysaccharide matrices.

## 2 Effect of Film Plasticizers on Film Water Sorption Behavior

Plasticizers, such as glycerol, or sorbitol, are usual components of films they have a great impact on the sorption behavior and water sorption capacity (WSC) of the hydrocolloid films due to their hydrophilic nature. Figure 2a shows the sorption isotherms, at 5 and 20 °C, of films based on soy protein isolate (SPI), both pure and combined with glycerol in a ratio 1:0.3, where the promotion of the WSC of the matrix due to the glycerol addition can be observed at both temperatures. This promotion is particularly intense at high water activity levels, when the solvent effects of water are exhibited for films containing low molecular weight polar solutes, such as glycerol.

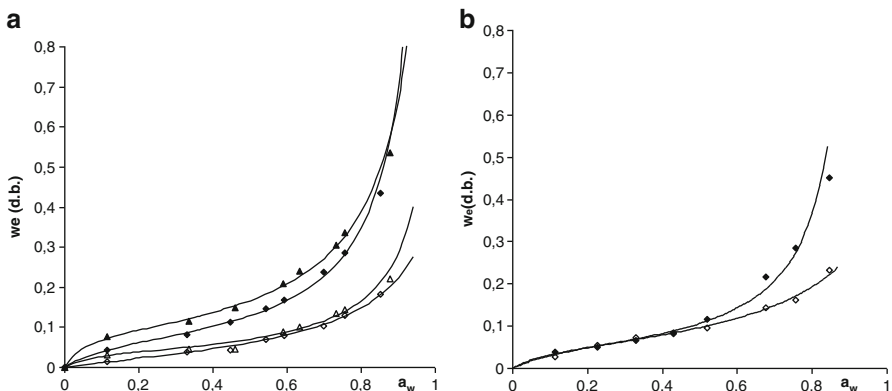


**Fig. 2** Effect of plasticizer (glycerol) on water sorption isotherms of biopolymer films based on soy protein isolate (a), at 5 °C (triangles) and 20 °C (rhombus), and sodium caseinate (b), at 25 °C. *Closed symbols: samples without glycerol, open symbols: samples with glycerol*

Similar behavior can be observed for WSC of sodium caseinate (NaCas) at 25 °C when glycerol is incorporated at the same ratio (Fig. 2b). In all cases, the incorporation of glycerol to hydrocolloid implied the promotion of the hygroscopic nature of the film mainly from water activity ( $a_w$ ) of 0.4 onwards and, as commented above, this can be attributed to the promotion of solvent effects from a determined  $a_w$  value, when low molecular weight polar solutes are present. This solvent effect allows the system to incorporate a great amount of bonded water without a notable increase of  $a_w$ . Thus, the high water uptake in sodium caseinate or SPI films containing glycerol from  $a_w = 0.6$  did not appear in pure hydrocolloids due to the absence of this kind of polar solutes. The effect on water sorption behavior was observed by Kristo and Biliaderis (2006) to be similar for sodium caseinate and pullulan matrices when these contained sorbitol.

### 3 Effect of Lipids on Water Sorption Behavior of Hydrocolloid Films

Lipids are also usually added to the film formulation in order to improve water barrier properties. The incorporation of these compounds also changes the WSC of the film. The effect of lipids can be very different, depending on the hydrocolloid-lipid interactions in the matrix. The incorporation of lipids usually reduces water sorption due to the fact that lipids correspond to a fraction of solids with small water uptake capacity, especially for the more hydrophobic compounds. This has been observed for films of sodium caseinate (with 0.3 g of glycerol/g protein) containing oleic acid (OA) and beeswax (BW) mixtures (Fabra et al. 2010). In this case, the amount of water uptake was estimated from the values obtained for the lipid-free film and the mass fraction of the nonlipid solids (caseinate plus glycerol) and

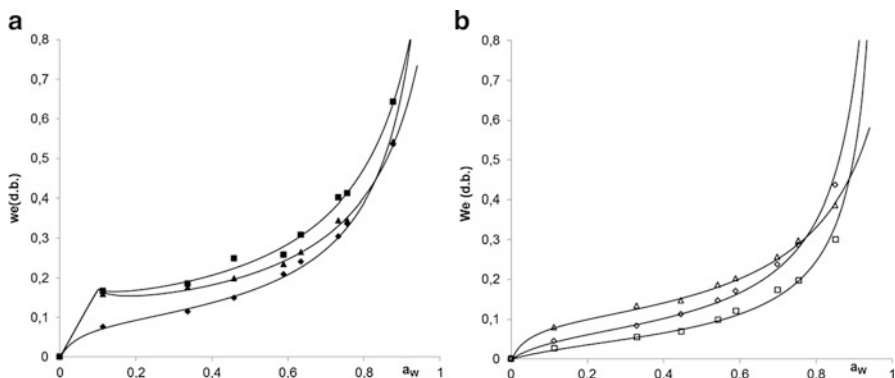


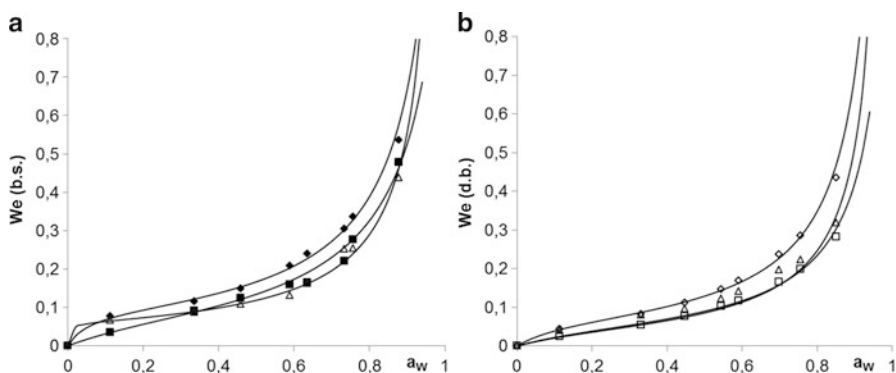
**Fig. 3** Effect of oleic acid on water sorption isotherms of soy protein isolate films containing glycerol (1:0.3) in different lipid-protein ratios (0.5 (triangles) and 0.25 (squares)) at 5 °C (a) and 20 °C (b)

predicted values were compared with the experimental ones. The comparison showed that the values agreed quite closely. Nevertheless, for films containing oleic acid experimental values are slightly greater than predicted, which means that a certain amount of water uptake in this case is retained by the lipid. Nevertheless, the opposite behavior was observed for films containing pure BW, where predicted values are lower than the experimental ones, thus indicating that BW seems to inhibit the water sorption capacity of the protein matrix, probably due to the promotion of hydrophobic interactions in the lipid-protein matrix which reduce the active points for water adsorption.

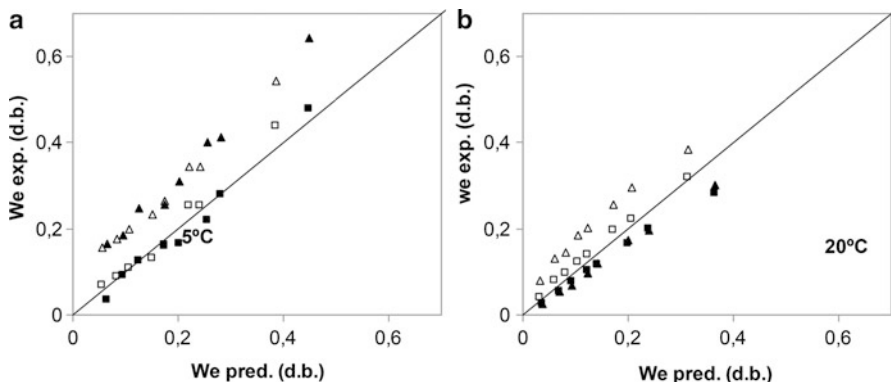
Figure 3 shows the effect of the incorporation of OA to SPI matrices containing glycerol (0.3 g/g protein) on water sorption behavior at 5 and 20 °C. A different effect of lipid can be observed at each temperature for different lipid-protein ratios (0.25 and 0.5 g/g protein). For the highest ratio, OA promotes water adsorption at both 5 and 20 °C, which indicates that a greater amount of water sorption active groups are exhibited in the matrix when OA interacts with the SPI chains. Nevertheless, when the OA-protein ratio decreased to 0.25 g lipid/g protein, a clear decrease in the water sorption capacity was observed when film was equilibrated at 20 °C. This seems to indicate that changes in molecular interactions are induced by the temperature increase, which affects the number of water sorption active points.

Figure 4 shows the sorption behavior of SPI-glycerol films, at 5 and 20 °C, when BW was incorporated at two different ratios, 0.25 and 0.5 g lipid/g protein. Very similar behavior can be observed in both cases where WSC of the matrix decreased because of the addition of BW.

By only considering the contribution of the nonlipid fraction, the predicted moisture content values of lipid-containing SPI films were compared with the experimental values (as shown in Fig. 5). For OA at 5 °C, points were observed to deviate greatly from the diagonal, as expected from the previously mentioned promotion of WSC, clearly showing the increase in the number of active points in



**Fig. 4** Effect of beeswax on water sorption isotherms of soy protein isolate films containing glycerol (1:0.3) in different lipid-protein ratios (0.5 (triangles) and 0.25 (squares)) at 5 °C (a) and 20 °C (b)



**Fig. 5** Comparison of experimental and predicted values of equilibrium water content of SPI films containing glycerol (1:0.3 protein-glycerol ratio) and lipids: OA (triangles) and BW (squares) in a ratio protein-lipid of 1:0.25 (full symbols) and 1:0.50 (empty symbols), at 5 °C (a) and 20 °C (b)

the matrix due to the OA-SPI interactions. At this temperature, no different behavior was observed between the films containing a different ratio of OA. Nevertheless, at 20 °C, only the films with the greatest OA ratio showed a greater WSC than SPI-Gly films, whereas a slightly negative deviation was observed for films with the lowest OA ratio, similar to that provoked by BW. This suggests that only a part of the OA molecules contributes to the enhancement of the hygroscopic character of the polymer network, depending on the temperature. This interactive OA amount was exceeded by the lowest lipid ratio at 5 °C, but this ratio was not high enough at 20 °C. It seems that there are not enough lipids to provoke a similar effect to that observed at 5 °C in the protein network when the lipid-protein ratio decreases and hydrophobic interactions are promoted in line with the temperature increase. No notable deviations from the

diagonal were observed for films containing BW at either temperature, thus indicating that this component is in a separate phase, hardly interacting with the polymer network.

The effect of the incorporation of other organic compounds, such as ethanol extract of propolis (EEP), on the WSC of hydroxypropyl methylcellulose (HPMC) films has been described for films equilibrated at 5 and 25 °C and 55 or 75 % relative humidity (RH) (Pastor et al. 2010). A decrease in the equilibrium water content of the film when the content of EEP in the film increased was observed for all of the equilibration conditions. Nevertheless, it is remarkable that when moisture content was referred to the HPMC basis (g water/g HPMC), no significant change in water content was detected until there was nearly 10 % of EEP in the film. However, a significant and similar decrease was obtained for the two greatest EEP ratios (0.167 and 0.231 g/g dried film) in the films. This reduction was greater for samples equilibrated at low RH conditions (about 80 and 60 % reduction at 5 and 25 °C, respectively) than for those equilibrated at high RH (about 10 % at both temperatures). These results seem to indicate that whereas at low propolis contents the interactions with the EEP compounds seem not to affect the sorption behavior notably, at the highest propolis contents, these compounds notably modify the water-film relationships, thus reducing the ability of the polymer chains to bond water molecules. This fact coincides with notable differences observed in the behavior of the most highly EEP concentrated (1.0 and 1.5 %, wt) film forming dispersions which points to the bonding of HPMC chains to the EEP components, thus limiting their capacity for water interactions. The degree of the polymer bonding was greater at low moisture contents in the films and seems to reduce in line with the water gain in the matrix. In this sense, it is remarkable that the temperature effect on water sorption, which is related to the sorption enthalpy, was very similar for all samples containing different ratios of EEP at high water contents (when samples were equilibrated at about 75 % RH). Nevertheless, it is greatly reduced at low water contents (when samples were equilibrated at 56 % RH) for the highest ratios of propolis in the films. This indicates a great decrease of the water sorption enthalpy in these samples, which points to the promotion of the hydrophobicity of the matrix, associated with the above-mentioned bonding of HPMC to the propolis compounds, which blocks the HPMC active points.

#### 4 Effect of Film Components on Phase Transitions

Component interactions in the hydrocolloid films may affect phase transitions, particularly glass transition temperature ( $T_g$ ) of the polymer, which can induce changes in the barrier and mechanical properties at a determined temperature. The difference between the product temperature and  $T_g$  determines the rate at which diffusion-dependent processes, such as mass transport, occur in the system (Roos 1995) and so it has a great incidence on film barrier properties. Phase transition analysis by DSC in NaCas films containing lipids (OA and BW) was carried out in

**Table 1** Values of the glass transition temperature ( $T_g$ ) of sodium caseinate films (NaCas) containing 0.3 g glycerol/g protein (NaCas-Gly) and 0.5 g oleic acid/g protein (NaCas-Gly-OA) as a function of the equilibrium water activity of the films

$a_w$	$T_g$ (°C)		
	NaCas	NaCas-Gly	NaCas-Gly-OA
0	112 (2.8)	59.7 (0.3)	62.1 (0.7)
0.113	104 (1.8)	58 (4)	58.8 (0.6)
0.225	96.7 (1.9)	57.2 (0.7)	58.2 (0.1)
0.33	85 (0.4)	55.7 (0.6)	57.7 (0.2)
0.43	79 (1)	55.4 (0.5)	53.6 (0.6)
0.52	71 (0.8)	55.1 (1.5)	51.6 (0.2)
0.675	59.2 (0.5)	52.2 (1.1)	41.8 (0.2)
0.755	56.3 (0.2)	51.1 (0.6)	34.5 (0.4)
0.845	52.1 (0.3)	49 (1.7)	28.1 (03.1)

order to know how the protein-lipid interactions affect the film properties (Fabra et al. 2010). In this sense, glass transition of the hydrocolloid matrices and lipid melting endotherm were characterized as a function of the sample water activity ( $a_w$ ). Table 1 shows the values of  $T_g$  (midpoint) obtained for pure sodium caseinate, sodium caseinate-glycerol film (1:0.3 ratio), and sodium caseinate-glycerol-OA film (1:0.3:0.5 ratios) as a function of the sample  $a_w$ . For samples containing BW,  $T_g$  was not obtained because of the fact that the melting endotherm of BW extends over a wide temperature range, overlapping the glass transition of the amorphous matrix. The expected decrease of  $T_g$  when sample  $a_w$  decreases can be observed for all samples, as corresponds to the plasticizing effect of water, which implies a reduction in the mean molecular weight in the system and the corresponding increase in the molecular mobility of the amorphous solid.

It is remarkable that the presence of glycerol implies a marked decrease in the  $T_g$  values with respect to the values obtained for caseinate at the same  $a_w$ , mainly at low  $a_w$  values. This is coherent with the plasticizing role of glycerol, decreasing the mean molecular weight in the system and affecting molecular mobility and mechanical behavior of the material. The plasticizing effect of water in this case is very mild, since the  $T_g$  decrease with  $a_w$  is very small. This indicates that the glycerol interactions in the matrix inhibit the effect of water and no subsequent, significant plasticization effect was induced. In the completely dried film, 0.3 g of glycerol/g of protein allows the  $T_g$  to reach a value in the order of that obtained in the pure caseinate film at  $a_w = 0.675$ .

The observed behavior indicates that water plasticization effect is more effective in caseinate than in the caseinate-glycerol system, which has also been observed for caseinate and pullulan matrices containing sorbitol as plasticizer (Kristo and Biliaderis 2006) and for gluten matrices when fructose, glucose, and sucrose are incorporated (Kalichevsky et al. 1992). The main factor responsible for this behavior could be the great water bonding capacity of glycerol and other polyol plasticizers that limits the water interactions with the polymer chains and determines the final distribution of water in the system.

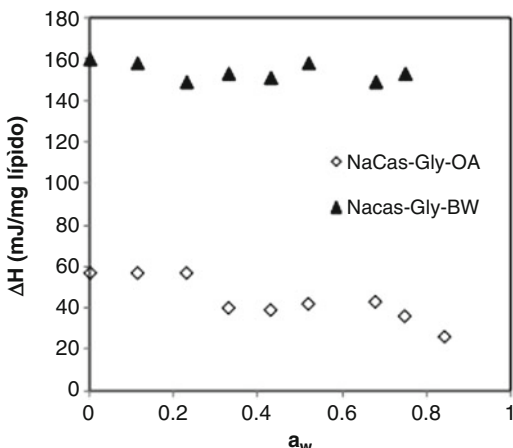
In the samples containing OA, no significant effect of this component on  $T_g$  values was observed below  $a_w = 0.43$ , which seems to indicate that OA is in a

separate phase and no notable interactions with the caseinate matrix take place. However, a different tendency was observed from this  $a_w$  value onwards, where Tg in the samples containing OA showed a more decreasing tendency with  $a_w$ . This behavior indicates that the plasticizing effect of water on the caseinate-glycerol system was promoted in the presence of OA from intermediate  $a_w$  values onwards, where the molecular mobility has reached a critical level. Interactions of OA in the caseinate matrix could limit the protein chain aggregations to some extent, provoking this effect.

When the Gordon and Taylor equation was fitted to the Tg-water content relationship for the different samples, the above-mentioned glycerol and OA effects on Tg were reflected in significant changes in both  $T_{g_{as}}$  and  $k$  parameters (Fabra et al. 2010). The  $k$  value is a measure of the water plasticization effect, which is very small in samples containing glycerol ( $k = 0.12$ ), as compared with pure caseinate ( $k = 1.56$ ), and slightly increases when OA is incorporated in the matrix ( $k = 0.68$ ), in agreement with the promotion of the water plasticization effect caused by OA. The Tg values of the anhydrous solids ( $T_{gs}$ ) were 109, 58, and 63 °C, respectively, for caseinate, caseinate-glycerol, and caseinate-glycerol-OA films.

The protein-lipid interactions may also affect lipid phase transitions, melting temperature range, and enthalpy. Fabra et al. (2010) analyzed lipid phase transition in the sodium caseinate films containing OA and BW, equilibrated at different  $a_w$  values, in order to obtain complementary information about their interactions in the film matrix. No significant differences were observed between pure BW melting characteristics (initial melting temperature: 31.3 ( $\pm 2.4$ ) °C, final melting temperature: 88.3 ( $\pm 2.8$ ) °C, peak temperature: 69.4 ( $\pm 1.2$ ) °C, and melting enthalpy 159 ( $\pm 9$ ) J/g) and those obtained for BW in films equilibrated at different  $a_w$ . The initial and final temperatures of the endotherm were 29 and 84 °C respectively, peak temperature was 66.4 ( $\pm 0.5$ ) °C, and melting enthalpy was 155 ( $\pm 6$ ) J/g BW, without significant differences associated with the equilibrium  $a_w$  (Fig. 6). This seems to indicate that no notable interactions were developed between protein and wax, which behave as if they were in separate phases. Nevertheless, significant differences were observed among OA melting endotherms of the pure compound and OA films equilibrated at different  $a_w$  values. Pure OA behaves in a similar way to that described by other authors (Cedeño et al. 2001), with a solid-solid transition (Tr1) at about -50 °C ( $\Delta H = 5.0$  J/g) and a solid-liquid transition (Tr2) at about 5 °C ( $\Delta H = 75.5$  J/g), showing a broad melting endotherm. The obtained values for the melting enthalpy (Tr2) appear in Fig. 6, as a function of the equilibrium  $a_w$  value, where a significant reduction was observed in line with the  $a_w$  increase. So, in film samples, OA crystallization was inhibited to quite an extent, as deduced from the melting enthalpy reduction, and this inhibition increases in line with the increase in sample  $a_w$ , despite the fact that the associated increase in molecular mobility usually promotes crystallization rates. These results are in agreement with that previously commented on with respect to the OA interactions in the caseinate matrix, which seem to be promoted when  $a_w$  increases. These interactions lead to the bonding of OA molecules which then are not able to crystallize. So, a part of OA seems to be linked to the caseinate molecules and when the water content increases

**Fig. 6** Melting enthalpy of oleic acid and beeswax embedded in sodium caseinate films as a function of the equilibrium water activity of the film



in the sample, these bonds weaken the polymeric cross-linking in the matrix, making it softer (lower  $T_g$  values). This has a great impact on the film's mechanical and barrier properties due to the influence of molecular mobility on both rheological properties and diffusional processes. In fact, films containing OA showed a marked decrease in both elastic module (EM) and tensile at break (TS) and a sharp increase in elongation at break ( $E$ ), enhanced by the increase in  $a_w$ , as compared with the lipid-free caseinate films (Fabra et al. 2010). It is remarkable that the film with OA did not break under the mechanical test conditions when  $a_w$  is 0.75. However, when BW was the lipid present, the film was more fragile and broke at much lower deformation levels, showing the effect of the matrix discontinuities and the fact that the solid dispersed phase was less deformable (Fabra et al. 2010).

## 5 Final Remarks

The results commented on reflect the impact of water and lipid-protein interactions on film functionality. Lipids are usually incorporated to modify film barrier properties which are essential to define their application. In this sense, in the composite films obtained through emulsification of components, the development of compound interactions, such as in the case of the OA-caseinate or OA-SPI systems, gives rise to particular functional properties of the film that are not expected in films formed with the lipid dispersed in a separate phase. These aspects are very important in the developing of emulsified polymer films, since two kinds of fillers can be found: inactive or active. Whereas the former only gives rise to discontinuities in the polymer continuous matrix, the latter greatly modifies the properties of this matrix, by changing the cross-linking behavior of the polymer chains, which leads to more marked differences in the film behavior. Physical properties of heterogeneous systems are much more affected by the characteristics of the continuous

phase than those of the dispersed phase. So, when active fillers are incorporated in the matrix, the product can behave very differently than when the matrix is not filled. Phase transition analysis as a function of water activity is a good approach to identify the degree of polymer-filler interactions, which in turn are usually affected by water content, and so to predict the final effect of the filler on the film equilibrated at different relative humidities.

**Acknowledgment** The authors acknowledge the financial support from Spanish Ministerio de Educación y Ciencia throughout the project AGL2007-01009 and AGL2010-20694.

## References

- Alves VD, Costa N, Colehoso IM (2010) Barrier properties of biodegradable composite films based on kappa-carrageenan/pectin blends and mica flakes. *Carbohydr Polym* 79:269–276
- Cedenó FO, Prieto MM, Espina A, García JR (2001) Measurements of temperature and melting heat of some pure fatty acids and their binary and ternary mixtures by differential scanning calorimetry. *Thermochim Acta* 369:39–50
- Debeaufort F, Quezada-Gallo JA, Delporte B, Voilley A (2000) Lipid hydrophobicity and physical state effects on the properties of bilayer edible films. *J Membr Sci* 180:47–55
- Elsabee MZ, Abdou ES, Nagy KSA, Eweis M (2008) Surface modification of polypropylene films by chitosan and chitosan/pectin multilayer. *Carbohydr Polym* 71:187–195
- Fabra MJ, Talens P, Chiralt A (2009a) Microstructure and optical properties of sodium caseinate films containing oleic acid–beeswax mixtures. *Food Hydrocoll* 23:676–683
- Fabra MJ, Hambleton A, Talens P, Debeaufort F, Chiralt A, Voilley A (2009b) Influence of interactions on water and aroma permeabilities of  $\text{t}$ -carrageenan–oleic acid–beeswax films used for flavour encapsulation. *Carbohydr Polym* 76:325–332
- Fabra MJ, Jiménez A, Atarés L, Talens P, Chiralt A (2009c) Effect of fatty acids and beeswax addition on properties of sodium caseinate dispersions and films. *Biomacromolecules* 10:1500–1507
- Fabra MJ, Talens P, Chiralt A (2010) Water sorption isotherms and phase transitions of sodium caseinate–lipid films as affected by lipid interactions. *Food Hydrocoll* 24:384–391
- Gómez-Estaca J, López de Lacey A, López-Caballero ME, Gómez-Guillén MC, Montero P (2010) Biodegradable gelatin–chitosan films incorporated with essential oils as antimicrobial agents for fish preservation. *Food Microbiol* 27:889–896
- Hambleton A, Voilley A, Debeaufort F (2011) Transport parameters for aroma compounds through  $\text{t}$ -carrageenan and sodium alginate-based edible films. *Food Hydrocoll* 25:1128–1133
- Jiménez A, Fabra MJ, Talens P, Chiralt A (2010) Effect of lipid self-association on the microstructure and physical properties of hydroxypropyl-methylcellulose edible films containing fatty acids. *Carbohydr Polym* 82:585–593
- Kalichevsky MT, Jaroskiewicz EM, Blanshard JMV (1992) Glass transition of gluten. 1. Gluten and gluten–sugar mixtures. *Int J Biol Macromol* 14:257–266
- Kristo E, Biliaderis CG (2006) Water sorption and thermo-mechanical properties of water/sorbitol-plasticized composite biopolymer films: caseinate-pullulan bilayers and blends. *Food Hydrocoll* 20:1057–1071
- Krochta JM, de Mulder-Johnston C (1997) Edible and biodegradable polymer films: challenges and opportunities. *Food Technol* 51:61–74
- Morillon V, Debeaufort F, Blond G, Capelle M, Voilley A (2002) Factors affecting the moisture permeability of lipid-based edible films: a review. *Crit Rev Food Sci Nutr* 42:67–89

- Ozdemir M, Floros JD (2008) Optimization of edible whey protein films containing preservatives for mechanical and optical properties. *J Food Eng* 84:116–123
- Pastor C, Sánchez-González L, Cháfer M, Chiralt A, González-Martínez C (2010) Physical and antifungal properties of hydroxypropyl-methylcellulose based films containing propolis as affected by moisture content. *Carbohydr Polym* 82:1174–1183
- Roos YH (1995) Phase transitions in food. Academic, San Diego, CA, 360 p
- Sánchez-González L, González-Martínez C, Chiralt A, Cháfer M (2010) Physical and antimicrobial properties of chitosan-tea tree essential oil composite films. *J Food Eng* 98:443–452
- Sánchez-González L, Cháfer M, Hernández M, Chiralt A, González-Martínez C (2011) Antimicrobial activity of polysaccharide films containing essential oils. *Food Control* 22:1302–1310
- Srinivasa PC, Ramesh MN, Tharanathan RN (2007) Effect of plasticizers and fatty acids on mechanical and permeability characteristics of chitosan films. *Food Hydrocoll* 21:1113–1122
- Tharanathan RN (2003) Biodegradable films and composite coatings: past, present and future. *Trends Food Sci Technol* 14:71–78
- Villalobos R, Chanona J, Hernández P, Gutiérrez G, Chiralt A (2005) Gloss and transparency of hydroxypropyl-methylcellulose films containing surfactants as affected by their microstructure. *Food Hydrocoll* 19:53–61

# Glass Transition Observed with Cross-Linked Dextrans Containing a Small Amount of Water

N. Ijima and N. Murase

## Abbreviations

DSC	Differential scanning calorimetry
ESR	Electron spin resonance spectrometer
G25, G200, G15	Sephadex gels
NMR	Nuclear magnetic resonance
$T_g$	Glass transition temperature
XRD	X-ray diffractometry

## 1 Introduction

Many biological systems and foods take on a gelling state in their ordinary condition. Gels consisting of various polymers are also used in the pharmaceutical and medical industries. Thus, it is of practical importance to characterize the polymer network in gels in order to understand their physical properties. Moreover, it is necessary to rationalize freezing and/or freeze-drying processes of the gels on the basis of scientific fundamentals for the preparation of frozen and freeze-dried products (Franks 1986). For differential scanning calorimetry (DSC) studies conducted from this standpoint, it was found by one of the present authors that water in polymer gels sometimes remains partially unfrozen during cooling below  $-50\text{ }^{\circ}\text{C}$  and freezes during subsequent heating (rewarming) (Murase et al. 1982, 1986). The occurrence of ice crystallization during rewarming, especially that

---

N. Ijima • N. Murase (✉)

Life Science and Engineering, Graduate School of Science and Engineering,  
Tokyo Denki University, Hatoyama-cho, Hiki-gun, Saitama 350-0394, Japan  
e-mail: [nmurase@mail.dendai.ac.jp](mailto:nmurase@mail.dendai.ac.jp)

observed with a cross-linked dextran, depends on the density of cross-links, as well as on water content and cooling rate. The density of cross-links is presumably related with the flexibility of polymer chains and water diffusivity through the polymer network in gels (Murase and Watanabe 1989; Ruike et al. 1999).

Although unfrozen water in the polymer gels has been indicated to be in a vitreous state, mechanisms of vitrification (glass transition) and ice crystallization during rewarming of the polymer gels still remain unclear after intensive studies using various physical techniques such as DSC, electron spin resonance spectrometer (ESR) (Murase et al. 1986), nuclear magnetic resonance (NMR) (Murase and Watanabe 1989), X-ray diffractometry (XRD)-DSC simultaneous measurements (Murase et al. 2002), Raman scattering (Murase et al. 2002), and synchrotron radiation XRD (Murase et al. 2004).

As glass transition temperature ( $T_g$ ) for pure water is reported to be around  $-137^\circ\text{C}$  (136 K) (Johari et al. 1987), unfrozen water in polymer gels might turn into a glassy state by further cooling below  $-50^\circ\text{C}$ . There is another possibility, however, that it is vitrified together with polymer matrices at higher subzero temperatures when freezing occurs, as liquid water was not observed below  $-50^\circ\text{C}$  by the ESR spin probe method (Murase et al. 1986).

Cross-linked dextran–water systems previously discussed were gels containing a large amount of water, where water forms a phase separated from hydrated polymers. In the case of polymer–water systems forming a single phase with a small amount of water, ice crystallization does not occur during cooling. Instead, water in the system functions as a plasticizer, decreasing  $T_g$  due to polymers, and the glass transition was actually detected with cross-linked dextran–water systems (Cojazzi and Pizzoli 1999; Murase et al. 2007). Vitrification of water in gels with a large amount of water might be relevant to glass transition due to hydrated polymers. Thus, is it possible to extrapolate from the  $T_g$  of hydrated polymers to that of water forming a separated phase. Although connection between the two glass transitions is of importance not only from the standpoint of water science but also from the practical standpoint, this connection is unclear and has not yet been studied.

In this study, glass transition of cross-linked dextrans containing a small amount of water was precisely investigated by differential scanning calorimetry with a focus on the flexibility of polymer chains.

## 2 Materials and Methods

### 2.1 Materials

The materials used in this study were cross-linked dextrans (Sephadex, GE Healthcare UK, Giles, England) and used without further purification. Sephadex takes a bead form with a diameter of ca. 100  $\mu\text{m}$ . Among various Sephadexes different in density of cross-links, Sephadex G25 and G200 were mainly used in

this study, but G15 was also used in some cases. The density of cross-links was highest for G15, with the smallest G number among the three Sephadexes.

## 2.2 Sample Preparation

Samples were first dried in a drying oven for 3 h. The temperature of drying was kept at 80 °C to prevent the occurrence of dehydration reaction between and/or within dextran molecules when heated above that temperature. Dried samples were placed in a desiccator containing P<sub>4</sub>O<sub>10</sub> for 1 week and kept at 30 °C to assure complete drying. Samples containing a large amount of water were prepared directly in aluminum pans by adding deionized water to dried samples. In the case of preparation of hydrated polymers containing a small amount of water, dried samples were transferred to desiccators where relative humidity was controlled with aqueous solutions saturated with inorganic salts, and kept for another 1 week at 30 °C. Water content in the samples was determined by measuring the weight increase.

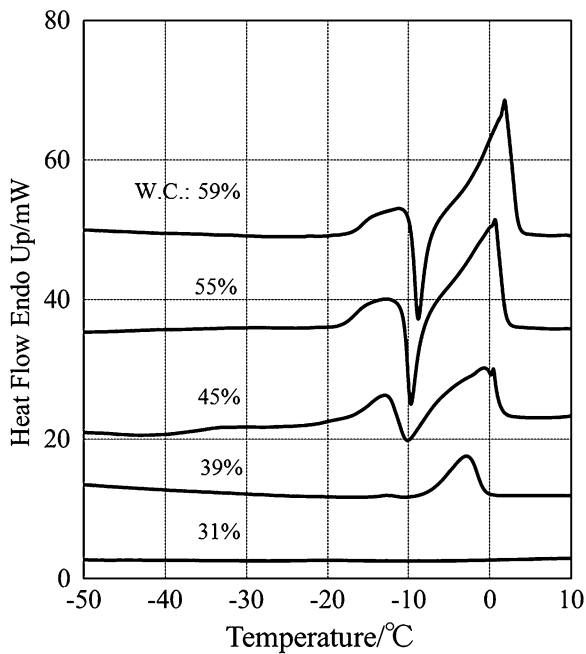
## 2.3 DSC Measurement

For the investigation of freezing behavior of gels with a large amount of water, about 10 mg of the sample was placed in an aluminum pan, and it was hermetically sealed. Cooling was conducted from 30 to –50 °C, followed by heating to 30 °C. Cooling and heating rates were 5 °C/min. For the investigation of glass transition behavior without freezing, 15–20 mg of the polymer sample containing 0–30 wt% water was placed in an aluminum pan. Samples, once heated to 60 °C, were cooled to –20 °C, kept at that temperature for 2 min, followed by heating to 80 °C. For the measurement of enthalpy relaxation, samples held at predetermined temperatures below  $T_g$  for different times were cooled to –20 °C, followed by heating to 80 °C. Cooling and heating scans using the same samples were successively repeated to investigate the effect of thermal history. Rates of cooling and heating were 20 °C/min. No weight loss of samples was confirmed after each experiment. DSC measurements were carried out by the use of a Pyris 1 (Perkin Elmer Inc, MA, USA) equipped with a cooling unit.

## 3 Results

DSC rewarming traces obtained with G25 (Sephadex) gels containing different amounts of water are shown in Fig. 1. For the gel containing more than 31 wt% water, ice melting endotherm was observed, indicating the appearance of water

**Fig. 1** DSC rewarming traces obtained with Sephadex G25 gels dependent on water content. Cooling and heating rates: 5 °C/min. Water content (W.C.) is indicated by wet basis (Murase et al. 2007)



phase separated from the hydrated cross-linked dextran. Neither ice melting endotherm during rewarming nor ice crystallization exotherm during precedent cooling was observed with gel containing water less than 30 wt%; therefore, the polymer–water system forms a single phase. An exotherm due to ice crystallization during rewarming appeared with the gel containing more than 39 wt% water, which became more noticeable with the increase in water content. An endothermic trend prior to the exotherm started at ca. -18 °C (Murase et al. 1986, 2007). Change in heat capacity due to glass transition, however, was not identified, since it might overlap with the endothermic trend, probably due to melting of small ice crystals (Fig. 1).

DSC rewarming traces obtained with G25 and G200 (Sephadex) containing a small amount of water below 30 wt% are shown in Fig. 2. Within the range of water content, dextran–water systems form a single phase. Change in heat capacity due to glass transition was clearly indicated with the systems.  $T_g$ s decreased with increasing water. Moreover, enthalpy relaxation was observed in the first rewarming trace with gel samples containing water less than 14.2 wt% for G25 and less than 15.7 wt% for G200 (Fig. 2a, c). Enthalpy relaxation disappeared, however, in the second rewarming traces after the cooling following the first rewarming heated to 80 °C (Fig. 2b, d). For samples containing 30 wt% water for G25 and 29.7 wt% for G200,  $T_g$ s were observed at ca. -16 °C and -17 °C, respectively. For samples containing water less than 9.0 wt% for G25 and 10.9 wt% for G200, DSC rewarming traces behaved complicatedly around the glass transition.

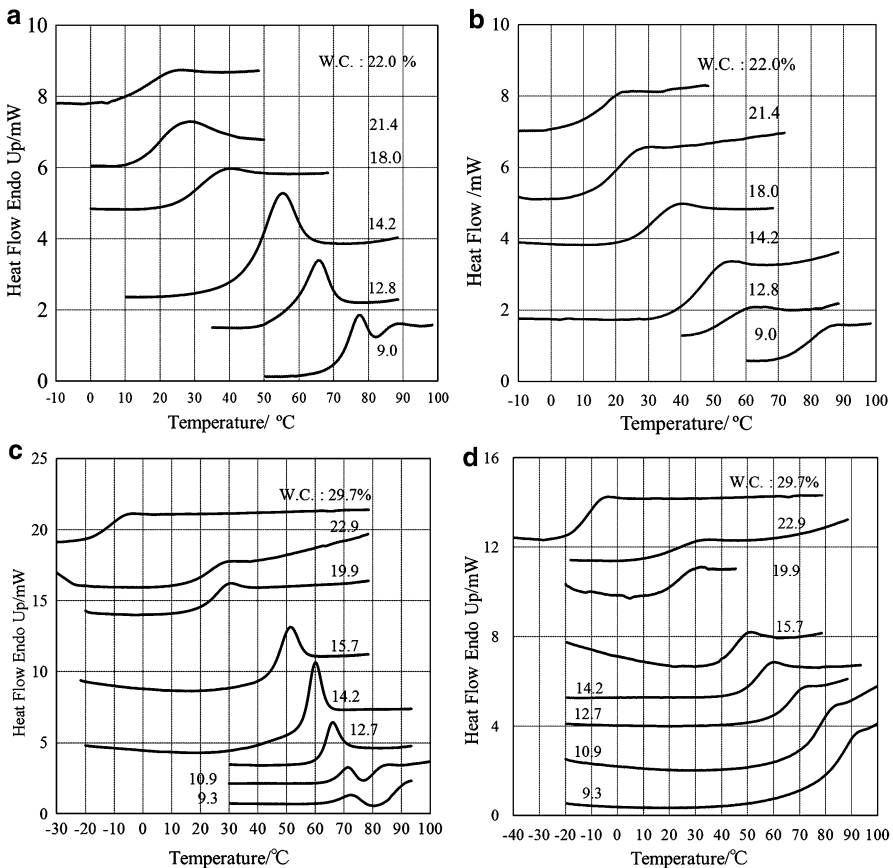


**Fig. 2** DSC first rewarming and second warming traces obtained with Sephadex G25 and G200 containing a small amount of water. Second rewarming was conducted after cooling to  $-20\text{ }^{\circ}\text{C}$  following first rewarming to  $80\text{ }^{\circ}\text{C}$ . **(a)** First rewarming for G25; **(b)** second rewarming for G25; **(c)** first rewarming for G200; **(d)** second rewarming for G200

$T_g$ s were plotted against water content, and  $T_g$ -composition curves obtained by the use of regression analysis are shown in Fig. 3. In the present study, onset temperatures using second rewarming traces were adopted as  $T_g$  values. It was found that a  $T_g$ -composition curve obtained for G200 was not so different from the curve obtained for G25, but was slightly higher in temperature than that of G25.

For the comparison of glass transition behavior observed with hydrated dextrans of different cross-link density, first rewarming traces obtained with G15, G25 and G200 were overlaid in Fig. 4a. It can be noticed that not only is enthalpy relaxation remarkable but also the temperature range of glass transition is narrowest with G200 among the three Sephadexes. With the G15 sample, glass transition was scarcely observed. Moreover, the increment of heat capacity at the glass transition is larger with the G200 sample than at G25. In Fig. 4b, second rewarming traces are

**Fig. 3**  $T_g$ -composition curves obtained with Sephadex containing a small amount of water lower than 30 wt% (Murase et al. 2007)

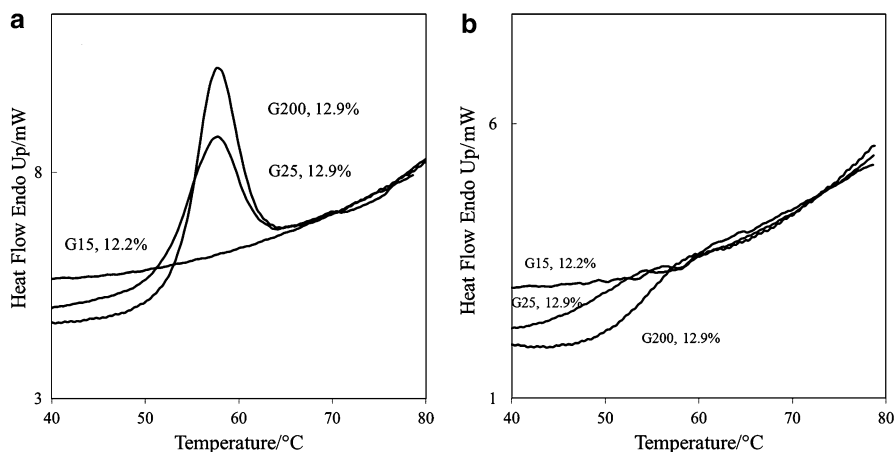
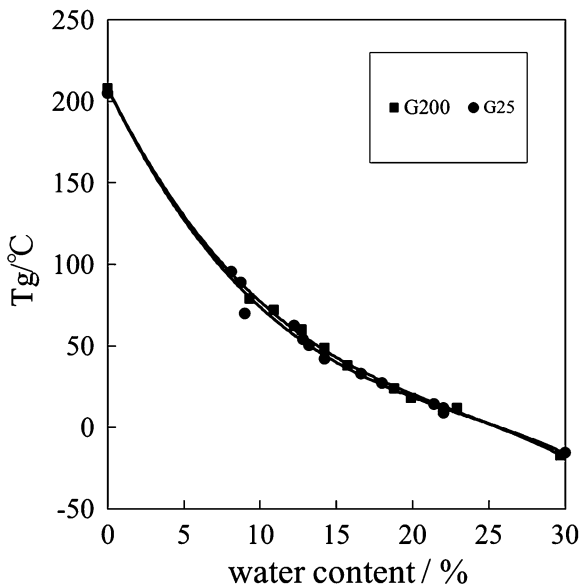


**Fig. 4** Glass transition and enthalpy relaxation behavior dependent on density of cross-links. Samples for DSC first rewarming (a) were held at 35 °C for 10 days (G25 and G200) or 7 days (G15) before measurement. Second rewarming (b) was carried out successively after first rewarming, followed by cooling

overlaid. These results were obtained after heat treatment to eliminate the thermal history. Except for the disappearance of enthalpy relaxation, glass transition behavior dependent on the cross-link density was similar to that observed in first rewarming traces. The increment of heat capacity at the glass transition obtained with second rewarming traces was 0.2–0.3 J/g°C for G25 and 0.35–0.45 J/g°C for G200, respectively.

## 4 Discussion

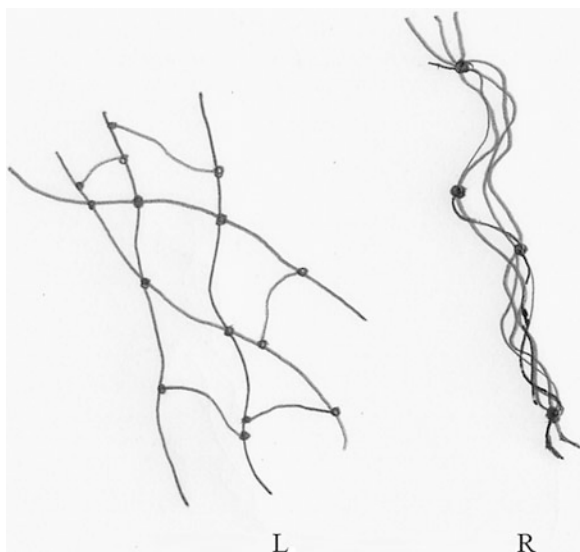
In cross-linked dextran–water systems containing a small amount of water, water plays the role of plasticizer as the glass transition temperature decreased with the water content. Experimental data are often analyzed by the use of the Gordon–Taylor equation (Gordon and Taylor 1952) for the preparation of  $T_g$ -composition curves. Such analysis, however, was difficult in this case, as the  $T_g$  for dried cross-linked dextrans, expected to be above 200 °C, was not accurately obtained because of the progress of dehydration reaction between hydroxyl groups in the molecules. In fact, the color of the samples turned yellow when heated above 80 °C. In this study,  $T_g$ -composition curves were obtained by the use of regression analysis.  $T_{gs}$  obtained for dried G25 and G200 were 205 °C and 208 °C, respectively, which are in good agreement with the temperature in the literature (Cojazzi and Pizzoli 1999).

Glass transition behavior was dependent upon the density of cross-links. Although  $T_g$ -composition curves were not so different from each other, the curve for G200 lies slightly higher in temperature than that for G25. The increment of heat capacity at glass transition was larger, and the temperature range of the transition was narrower with dextrans of lower cross-link density than those of the higher one. Moreover, remarkable enthalpy relaxation was observed with G25 and G200. With G15, however, glass transition was scarcely observed. These results presumably reflect the flexibility of dextran chains determined by density of cross-links. Since dextran chains in G15 are severely restricted in motion and interaction between dextran chains because of a higher density of cross-links than G25 and G200, they are not easy to turn into a glassy state.

Enthalpy relaxation was remarkably observed in the first rewarming trace, with both G25 and G200 samples containing water less than 14.2 wt% for G25 and 15.7 wt% for G200. Since the samples were held for 7–10 days at 30–33 °C, which is lower than  $T_g$  of the samples containing 16 wt% water, ca. 35 °C, cross-linked dextrans might have relaxed in enthalpy during storage. As a result, an endotherm due to enthalpy relaxation appeared in the first rewarming trace at glass transition. For samples containing water at more than 18 wt%, storage temperature becomes higher than  $T_g$ . Thus, dextran molecules turn into a rubbery state. Second rewarming was conducted soon after the first rewarming, heated to 80 °C, followed by cooling below  $T_g$ ; dextran molecules were considered to have little time to relax in enthalpy, leading to the disappearance of enthalpy relaxation in the second rewarming traces. With samples containing water less than 9.0 wt% for G25 and 10.9 wt% for G200, DSC first rewarming traces behaved complicatedly around the glass transition. The reason for this might be incomplete elimination of thermal history by the previous heating to 60 °C before the first rewarming, in addition to heterogeneous moisture distribution in the sample.

There are various theories for the glass transition of polymer systems. The free volume theory can explain molecular weight dependency by considering the molecular end effect (Fox and Flory 1950). On the other hand, glass transition behavior dependent on the density of cross-links is rationally explained by the

**Fig. 5** Schematic representation of cross-linked polymer chains. *L* (*left*): cross-link density is high, and polymer chains are hard to interact each other; *R* (*right*): cross-link density is low, and polymer chains are ready to interact and associate with each other. Therefore, the number of CRR increases with decreasing temperature



Adam–Gibbs theory (Adam and Gibbs 1965). With decrease in temperature, the number of CRR (cooperatively rearranging regions) increases in the case of dextrans of lower cross-link density, as the dextran chains are flexible and easily associate with each other. On the other hand, the number hardly increases with decrease in temperature in the case of dextrans of higher cross-link density, as they are restricted in motion and interaction between dextran chains prevented by the cross-links. A schematic representation is shown in Fig. 5.

The lowest  $T_g$  obtained with hydrated G25 of maximum water content to form a single phase was ca.  $-16\text{ }^\circ\text{C}$ . With G25 gel containing 55–59 wt% water, the initiation temperature of the endothermic trend prior to the exotherm during rewarming was ca.  $-18\text{ }^\circ\text{C}$ . The coincidence of two temperatures indicates that some water in the G25 gel forming a separated phase is vitrified together with hydration water around dextrans at the time of freezing, as the temperature is below  $T_g$  of hydration water.

## 5 Conclusions

Glass transition behavior of cross-linked dextrans containing a small amount of water, studied by DSC, was found to depend on the density of cross-links.  $T_g$ -composition curves of different cross-link density were not very different, but the increment of heat capacity at glass transition was larger, and the temperature range of the transition was narrower with the polymers of lower cross-link density than those of higher densities. Remarkable enthalpy relaxation was also observed in polymers of lower cross-link density. The dependency of glass transition can be

explained by the higher flexibility of polymer chains of lower cross-link density. Moreover, the lowest  $T_g$  of hydrated Sephadex G25, a kind of crosslinked dextran, to form a single phase, was assumed to correspond with  $T_g$  of the frozen Sephadex G25 gel, which indicates ice crystallization exotherm during rewarming.

## References

- Adam G, Gibbs JH (1965) On the temperature dependence of cooperative relaxation properties in glass-forming liquids. *J Chem Phys* 43:139–145
- Cojazzi G, Pizzoli M (1999) Thermal behavior of water in crosslinked dextran. *Macromol Chem Phys* 200:2356–2364
- Fox TG, Flory PI (1950) Second-order transition temperatures and related properties of polystyrene. I. Influence of molecular weight. *J Appl Phys* 21:581–591
- Franks F (1986) Biophysics and biochemistry at low temperature. Cambridge University Press, Cambridge, UK
- Gordon M, Taylor JS (1952) Ideal copolymers and the second-order transitions of synthetic rubbers. I. Non-crystalline copolymers. *J Appl Chem* 2:493–500
- Johari GP, Hallbrucker A, Mayer E, Hofer K (1987) The glass-liquid transition of hyperquenched water. *Nature* 330:552–553
- Murase N, Watanabe T (1989) Nuclear magnetic relaxation studies of the compartmentalized water in cross-linked polymer gels. *Magn Reson Med* 9:1–7
- Murase N, Shiraishi M, Koga S, Gonda K (1982) Low-temperature calorimetric studies of compartmentalized water in hydrogel systems (I). *CryoLetters* 3:251–254
- Murase N, Gonda K, Watanabe T (1986) Unfrozen compartmentalized water in gels and its anomalous crystallization during warming. *J Phys Chem* 90:5420–5426
- Murase N, Ruike M, Yoshioka S, Katagiri C, Takahashi H (2002) Glass transition and ice crystallisation of water in polymer gels, studied by oscillation DSC, XRD-DSC simultaneous measurements, and Raman spectroscopy. In: Levine H (ed) Amorphous food and pharmaceutical systems. Royal Society of Chemistry, Cambridge, pp 339–346
- Murase N, Abe S, Takahashi H, Katagiri C, Kikegawa T (2004) Two-dimensional diffraction study of ice crystallization in polymer gels. *CryoLetters* 25:227–234
- Murase N, Yamada S, Iijima N (2007) Ice crystallization in gels and foods manipulated by the polymer network. In: Reid DS, Sajaanantakul T, Lillford PJ, Charoenrein S (eds) Water properties in food, health, pharmaceutical and biological systems. Wiley-Blackwell, Ames, IA, pp 373–83
- Ruike M, Takada S, Murase N, Watanabe T (1999) Changes in the bead structure of crosslinked polymer gels during drying and freezing. *CryoLetters* 20:61–68

# Sensorially and Instrumentally Detected Antiplastizicing Effect of Water in Cornflakes

A.E. Farroni, S. Guerrero, and M.P. Buera

## Abbreviations

$A_0$	Area under compression curve
CPMG	Carr-Purcell-Meiboom-Gill sequence
DSC	Differential scanning calorimetry
$F_{(t)}$	Force as function of time
$H_{(t)}$	Sample height as a function of time
$H_0$	Sample initial height
H-TR-NMR	Time-resolved proton nuclear magnetic resonance
RVP	Relative vapor pressures
$T_2$	Spin-spin transverse relaxation times

---

S. Guerrero is member of Consejo Nacional de Investigaciones Científicas y Técnicas de la República Argentina.

A.E. Farroni (✉)  
Departamento de Industrias, Facultad de Ciencias Exactas y Naturales, Universidad de Buenos Aires, Buenos Aires, Argentina

Laboratorio de Calidad de Alimentos, Suelos y Agua, EEA Pergamino, Instituto Nacional de Tecnología Agropecuaria, Av. Frondizi Km 4.5, 2700 Pergamino, Buenos Aires, Argentina  
e-mail: [farroni.abel@inta.gob.ar](mailto:farroni.abel@inta.gob.ar)

S. Guerrero  
Departamento de Industrias, Facultad de Ciencias Exactas y Naturales, Universidad de Buenos Aires, Ciudad Universitaria, Buenos Aires, Argentina

M.P. Buera  
Departamentos de Industrias y de Química Orgánica, Facultad de Ciencias Exactas y Naturales, University of Buenos Aires (FCEyN-UBA)

National Council of Scientific and Technical Research (CONICET), Buenos Aires, Argentina  
e-mail: [pilar@di.fcen.uba.ar](mailto:pilar@di.fcen.uba.ar)

$T_{2\text{LHahn}}$	Spin-spin transverse relaxation times for second proton population
$T_{2\text{SHahn}}$	Spin-spin transverse relaxation times for one proton population
$T_g$	Glass transition temperature
Wc	Water content
$\varepsilon_E$	Engineering strain
$\sigma_E$	Engineering stress
T	Interpulse time value

## 1 Introduction

Textural properties are key drivers for food acceptability (Chauvin et al. 2008). In low-moisture cereal foods, quality depends mainly on textural attributes like crispness (Fontanet et al. 1997). Water is one of the most important factors affecting texture of low-moisture foods, and its effect has been extensively studied (Labuza et al. 1970; Roos et al. 1996; Peleg 1998; Jacoby and King 2001; Lewicki 2004; Castro-Prada et al. 2009). It is also known that water affects glass transition temperature (Chen et al. 1997), which is widely used in assessing stability (Roos 2010). In order to measure water mobility in complex and heterogeneous systems, nuclear magnetic resonance spectroscopy has been widely used (Chinachoti et al. 2006). On the other hand, in low-moisture starchy food, other processes that take place at glassy state, such as physical aging and toughening, could affect textural properties (Suwonsichon and Peleg 1998; Chang et al. 2000; Chung and Lim 2004).

The shelf life stability and textural properties of cornflakes are closely related to their mechanical and thermal properties. Results of a previous work indicated that while compression force showed a maximum as a function of water content (wc), glass transition temperature ( $T_g$ ) decreased progressively as wc and water mobility increased (Farroni et al. 2010). The aim of this study was to analyze the effect of water and molecular mobility on textural properties of cornflakes.

## 2 Materials and Methods

### 2.1 Samples

Cornflakes produced from corn grits by the classical gelatinization-flaking were provided by a local manufacturer. Samples were equilibrated over saturated salt solutions at relative vapor pressures (RVP) in the range between 11 and 80 % (LiCl: 0.11, MgCl<sub>2</sub>: 0.33, K<sub>2</sub>CO<sub>3</sub>: 0.44, NaCl: 0.75, KCl: 0.84) (Greenspan 1977). For higher water content, samples were sprayed with water and allowed to equilibrate overnight in sealed vessels. Water content was determined according to AACC-approved method 44-16 (AACC 1995) and expressed on a dry basis (%db). None of the analyzed samples presented any evidence of fungal growth during storage upon examination by ocular stereoscope (Unitron MS, N.Y.).

## 2.2 Glass Transition Measurement

Glass transition was measured by differential scanning calorimetry as the onset temperature of discontinuities in heat flow vs. temperature curves (indicating a change in specific heat). Approximately 15 mg of ground samples was weighed with a precision of 0.01 mg, sealed into aluminum pans (40  $\mu$ l capacity), and loaded into a model 822 differential scanning calorimetry (DSC) (Mettler Toledo, Schwerzenbach, Switzerland). The DSC thermograms were obtained from -50 to 150 °C at a heating rate of 10 °C/min.

## 2.3 Molecular Mobility

Molecular mobility was assessed by time-resolved proton nuclear magnetic resonance ( $^1\text{H}$ -TR-NMR) measuring the spin-spin transverse relaxation times ( $T_2$ ). A pulsed  $^1\text{H}$  NMR spectrometer Bruker Minispec model mq 20 (Bruker Biospin GmbH, Rheinstetten, Germany), with a 0.47 T magnetic field operating at resonance frequency of 20 MHz, was used for the measurements. Hahn spin echo sequence (90°–180°) with an interpulse range of 0.001–4 ms was used to measure relaxation times up to 1.5 ms. For higher  $T_2$ , Carr-Purcell-Meiboom-Gill (CPMG) sequence was used (Ruan and Chen 1998). This sequence consists of a single 90° pulse, followed by a series of 180° pulses at times  $\tau$ ,  $3\tau$ ,  $5\tau$ , etc., which produced spin echoes at times  $2\tau$ ,  $4\tau$ ,  $6\tau$ , etc. The decay envelopes were fitted to monoexponential or biexponential decay equations.

## 2.4 Mechanical Properties

Mechanical properties were measured by a compression test employing a model 1011 universal testing machine (Instron, Canton, Massachusetts, USA) equipped with a 35 mm in diameter piston. A 30 mm thick bed of cornflakes (weight between 10 and 12 g) was compressed in a 50 mm diameter cylinder up to a fixed 30 % deformation (Suwonsichon and Peleg 1998; Peleg 1998), using the piston at 50 mm/min velocity. Force vs. distance data were transformed into engineering stress ( $\sigma_E$ ) vs. engineering strain ( $\varepsilon_E$ ) using Eqs. (1) and (2) (Fiszman and Durán 1997):

$$\sigma_E = \frac{F_{(t)}}{A_0} \quad (1)$$

$$\varepsilon_E = \frac{H_{(t)}}{H_0} \quad (2)$$

where  $F_{(t)}$  is force as function of time,  $H_0$  is sample initial height,  $H_{(t)}$  is sample height as a function of time, and  $A_0$  is the area under compression curve.

Deformability modulus was calculated as the slope of  $\sigma_E$  vs.  $\varepsilon_E$  curves in the lineal region (Eq. 3) (Mohsenin and Mittal 1977; Hicsasmaz and Rizvi 2005):

$$E_d = \frac{\sigma_{E(t)}}{\varepsilon_{E(t)}} \quad (3)$$

The Lorentzian equation (Peng and Lu 2005; Yang et al. 2010) was fitted to deformability modulus vs. water content data (Eq. 4):

$$y = \frac{A}{1 + \left(\frac{(x-x_o)}{\gamma}\right)^2} + b \quad (4)$$

where  $y$  is the value of the dependent variable (in this case  $E_d$ );  $x$  is the independent variable (water content);  $A$  is the amplitude when  $y$  reaches maximum value;  $x_o$  is the  $x$  value when  $y=A$ ;  $\gamma$  is the width of the curve when  $y=A/2$ ; and  $b$  is the asymptotic value of  $y$ .

## 2.5 Oral Texture Profile

A sensory panel was trained with the texture profile method following the procedures described by Civille and Szczesniak (1973) during 35–40 h (2 h per week) to recognize texture attributes of hardness and crispness. The panel was composed of nine panelists (three males, six females), all between the ages of 27–42. Standard rating scales described by Hough et al. (1994) were used. The scale of crispness was developed for this work using local food standards. The panel worked with the definition of crispness and the measurement technique based on the work of Chauvin et al. (2008). Standard samples were selected from available local food products using the crispness scale described by Meilgaard et al. (1999) as a guide.

The samples were presented to the panelists in white plastic cups identified by three digits chosen at random. Evaluations were performed in individual booths under white light. The panelists were also provided with mineral water and unsalted crackers to clean their palate between samples.

The variation of crispness with water content was modeled using the Fermi equation, as described by Harris and Peleg (1996), and for hardness; after testing various models, the best fit was found using the Lorentzian equation:

$$y = \frac{y_0 + kx}{1 + e^{\frac{x-x_c}{b}}} \quad (5)$$

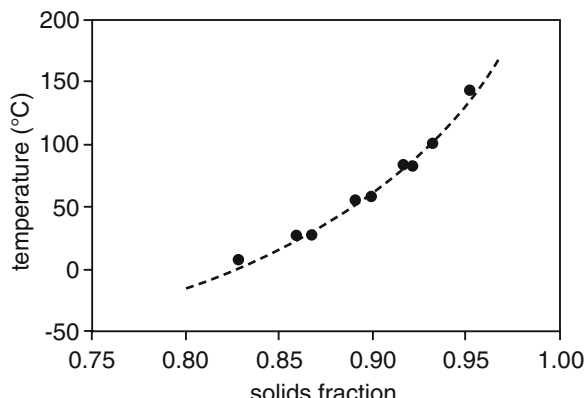
where  $x$  is the water content on a dry basis;  $y$  is the crispness value;  $y_0$  is the crispness value at zero water content;  $k$  is the slope of the initial part of the curve; and  $x_c$  is the water content, where  $y = \frac{y_0+kx_c}{2}$  and  $b$  is related to the step shape at water content near to  $x_c$ .

### 3 Results and Discussion

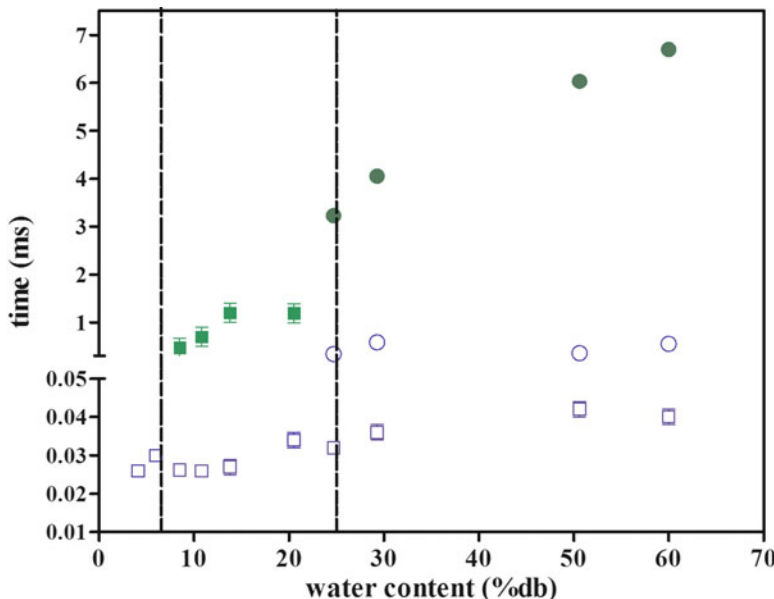
#### 3.1 Glass Transition and Molecular Mobility

Figure 1 shows the glass transition temperature ( $T_g$ ), as function of solids content.  $T_g$  decreased as water content increased, as expected for such systems. The water content that corresponded to glass transition at 25 °C was about 16 %db.

Figure 2 shows the  $T_2$  relaxation measured by  $^1\text{H}$ -TR-NMR. At water contents below 6.5 (%db), only one proton population was found (indicated as  $T_{2\text{SHahn}}$ ), which was related to solids and water closely interacting with them. At higher water contents, a second proton population ( $T_{2\text{LHahn}}$ ) related to water molecules with higher mobility, and therefore showing less interaction with solids, was found (Chen et al. 1997; Choi and Kerr 2003).  $T_{2\text{LHahn}}$  value increased as water content increased, reflecting the increase in molecular mobility, and reached a plateau at water content of approximately 14 %db. At water content of 25 %db, a third population of protons was found. The Hahn spin echo sequence is limited in measuring relaxation times due to the effect of diffusion. The CPMG sequence is able to detect proton populations with higher mobility compared to the Hahn sequence, but can only measure populations with relaxation times higher than the first interpulse time value ( $\tau$ ) (Ruan and Chen 1998). Accordingly, the Hahn



**Fig. 1** Glass transition temperature of cornflakes as a function of solids fraction



**Fig. 2** NMR relaxation times for different proton populations as a function of water content. (□)  $T_{2\text{SHahn}}$ , (■)  $T_{2\text{LHahn}}$ , (○)  $T_{2\text{SCPMG}}$ , (●)  $T_{2\text{LCPMG}}$

sequence was used to measure the  $T_2$  of protons related to solids and water interacting with them, and CPMG was used to measure the higher mobility populations in the range of 25–60 %db water content. At water contents higher than 25 %db, three proton populations were present.  $T_{2\text{SHahn}}$ , as already described;  $T_{2\text{SCPMG}}$ , which corresponds to the same population indicated as  $T_{2\text{LHahn}}$ ; and the third population ( $T_{2\text{LCPMG}}$ ), which corresponds to more mobile protons. It should be noted that at water contents lower than 25 %db, only one population was found using the CPMG sequence (data not shown).  $T_{2\text{SCPMG}}$  values remained almost constant in the water content range 25–60 %db, while  $T_{2\text{LCPMG}}$  value showed a sharp increase, indicating the increment in mobility of the free water population. It is important to note that the occurrence of freezeable water found by DSC was located at water content of 29 %db.

### 3.2 Mechanical Properties

Figure 3 shows a graph of deformability modulus ( $E_d$ ) vs. water content.  $E_d$  showed a maximum at 13 %db, indicating the antiplasticizing effect of water. At low water content, low force was required to deform cornflake samples. As water content increased beyond 13 %db,  $E_d$  showed an important decrease, evidencing the plasticizing effect of water.

**Fig. 3**  $E_d$  vs. water content (%db) for cornflakes. (Filled circle) Experimental measurements; (solid line) theoretical curve according to Lorentzian function; (vertical line) standard deviation. Best fit parameters are indicated in the graph

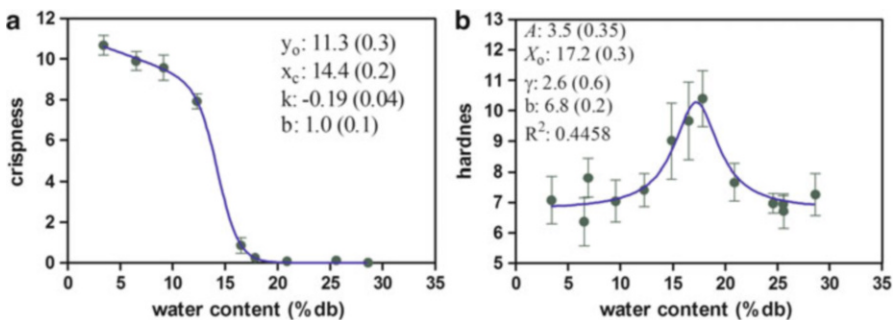
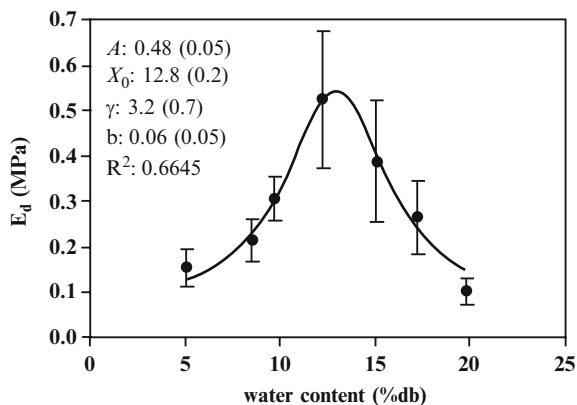


**Fig. 4** Sensory properties of cornflakes as a function of water content. (a) crispness; (b) hardness; (filled circle) experimental measurements; (solid line) theoretical curves; (vertical line) standard deviation. Best fit parameters are indicated in the graph

### 3.3 Oral Texture Measurements

Figure 4a, b shows the results of oral textural measurements. Crispness value showed a sharp decrease when water content reached a critical value ( $14.0 \pm 0.3$  %db) and at higher water contents decreased to zero. Hardness value was low in low water content samples. Sensory hardness value increased as water content increased and showed a maximum at a water content value of 17 % db, indicating that antiplasticizing effect of water was evidenced in sensory properties. At water contents higher than 17 %, sensory hardness decreased.

### 3.4 Integrated Results

Mathematical models for mechanical and sensory properties of cornflakes are shown in Fig. 5, together with glass transition curve. An integrated analysis of

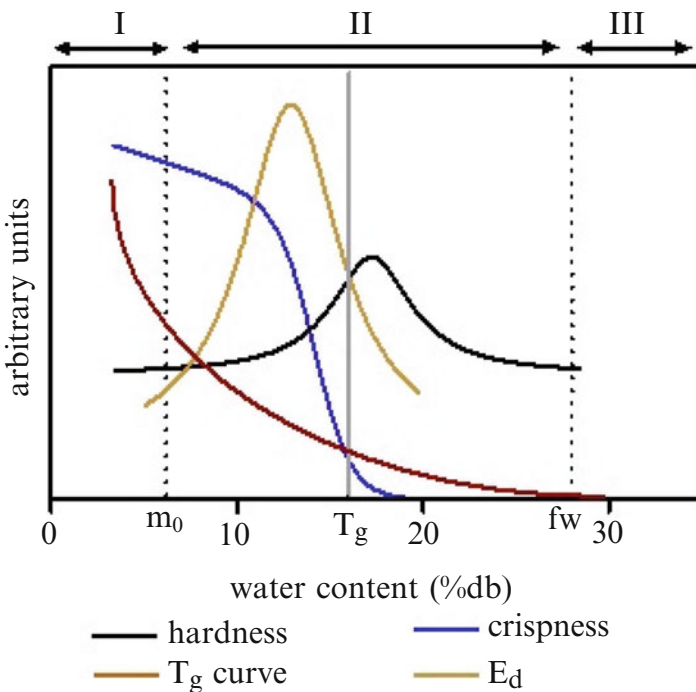


**Fig. 5** Scheme of variation of sensory and mechanical properties of cornflakes along water content scale. The three zones of water sorption isotherm are indicated with roman numerals.  $m_0$  = hydration limit;  $T_g$  = water content corresponding to glass transition at 25 °C; fw = frozen water

water sorption data, calorimetric measurements, and molecular mobility allowed three levels of hydration for amorphous materials to be demonstrated (Reid and Fennema 2008). In level I, only one proton population was present ( $T_{2\text{SHahn}}$ ). This region is limited by the occurrence of two proton populations measured by RMN, and the corresponding water content corresponds to the hydration limit ( $m_0$  in the graph) and is coincident with the GAB monolayer value (6 %db) determined in a previous work (Farroni et al. 2008). In level I, cornflakes had optimum sensory characteristics, i.e., maximum crispness and low hardness, which correspond to the brittle behavior desired in this type of food. Level II corresponds to the occurrence of two proton populations ( $T_{2\text{SHahn}}$  and  $T_{2\text{LHahn}}$ ). In this region the main changes that occurred were that cornflakes had loose crispness and were perceived as harder. It is to be noted that these changes, including the antiplasticizing effect of water, occurred while the sample was in the glassy state. Water content corresponding to a glass transition at the experimental temperature (25 °C) was indicated in the graph with a gray line and labeled as  $T_g$ . When the sample was in the rubbery state, crispness was not detectable, and plasticizing effect was evidenced in sensory and mechanical properties by softening of the sample. The upper limit of level II was

related to the occurrence of frozen water by DSC (fw in the graph). As indicated previously, at a water content value of 25 (%db), a third proton population was evidenced by RMN, and at a wc value near 29 (%db), this water had mobility enough to freeze. In region III water can act as a solvent and crystallize during cooling to  $-50^{\circ}\text{C}$ .

Maximum of sensory hardness was shifted to higher water content compared to  $E_d$  maximum. Deformation speed in sensory and mechanical tests was not coincident, and this difference could affect the correlation between those parameters and the critical water content at which transitions occurred (Castro-Prada et al. 2009). A possible explanation for the antiplasticization effect could be that at very low water content below  $T_g$ , vibrational movements cause an increase in energy dissipation during deformation, fracture speed propagation decreases, and therefore, total energy required for deformation increases; thus, an increase in required stress is observed.

## 4 Conclusions

For the first time, the antiplasticizing effect at water content below 16 (%db) was not only instrumentally but also sensorially detected and should be taken into account when assessing organoleptic changes of low-moisture brittle food. The maximum hardness detected by the trained panel occurred in the glass transition region at water contents at which neither frozen water nor the  $^1\text{H}$  NMR long relaxation time  $T_2$  was observed. In this way, the characterization of water effects on several properties was useful to predict changes detected by consumers in stored low water cereal-based products.

## References

- AACC (1995) Approved methods of the American Association of Cereal Chemists. 44-16. The Association, St. Paul, MN
- Castro-Prada EM, Primo-Martín C, Meinders MBJ, Hamer RJ, Van Vliet T (2009) Relationship between water activity, deformation speed, and crispness characterization. *J Texture Stud* 40 (2):127–156
- Chang YP, Cheah PB, Ceow CC (2000) Plasticizing-antiplasticizing effects of water on physical properties of tapioca starch films in the glassy state. *J Food Sci* 65(3):445–451
- Chauvin MA, Younce F, Ross C, Swanson B (2008) Standard scales for crispness, crackliness and crunchiness in dry and wet foods: relationship with acoustical determinations. *J Texture Stud* 39:345–368
- Chen PL, Long Z, Ruan RR, Labuza TP (1997) Nuclear magnetic resonance studies of water mobility in bread during storage. *Lebensm-Wiss Technol* 30(2):178–183
- Chinachoti P, Vittadini E, Chatakanonda P, Vodovotz Y (2006) Characterization of molecular mobility in carbohydrate food systems by NMR. In: Webb Graham A (ed) Modern magnetic resonance. Springer, Dordrecht, Netherlands, pp 1703–1712

- Choi SG, Kerr WL (2003)  $^1\text{H}$ -NMR studies of molecular mobility in wheat starch. *Food Res Int* 36:341–348
- Chung HJ, Lim ST (2004) Physical aging of glassy normal and waxy rice starches: thermal and mechanical characterization. *Carbohydrate Polym* 57(1):15–21
- Civille GV, Szczesniak AS (1973) Guidelines to training a texture profile panel. *J Texture Stud* 4:204–223
- Farroni AE, Matiacevich SB, Guerrero S, Alzamora S, Buera MP (2008) Multi-level approach for the analysis of water effects in corn flakes. *J Agric Food Chem* 56(15):6447–6453
- Farroni AE, Matiacevich SB, Buera MP (2010) Thermal transitions and molecular mobility in corn flakes as affected by water content. In: Reid DS, Sajjaanantakul T, Lillford PJ, Charoenrein S (eds) *Water properties in food, health, pharmaceutical and biological systems: ISOPOW 10*. Wiley-Blackwell, Ames, IA, pp 583–590
- Fiszman S, Durán L (1997) *Reología de Sólidos y Textura*. In: Aguilera JM (ed) *Temas en Tecnología de Alimentos*. Instituto Politécnico Nacional, Dirección de Publicaciones y Material Educativo, México DF, p 229
- Fontanet I, Davidou S, Dacremont C, Le Meste M (1997) Effect of water on the mechanical behaviour of extruded flat bread. *J Cereal Sci* 25:303–311
- Greenspan L (1977) Humidity fixed points of binary saturated aqueous solutions. *J Res Natl Bur Stand* 81:89–96
- Harris M, Peleg M (1996) Patterns of textural changes in brittle cellular cereal foods caused by moisture sorption. *Cereal Chem* 73:225–231
- Hicsasmaz Z, Rizvi SSH (2005) Effect of size and shape on modulus of deformability. *LWT Food Sci Technol* 38(4):431–435
- Hough G, Contarini A, Muñoz A (1994) Training a texture profile panel and constructing standard rating scales in Argentina. *J Texture Stud* 25:45–57
- Jacoby D, King C (2001) Sensory evaluation in snack foods development and production. In: Lucas EW, Rooney LW (eds) *Snack foods processing*. CRC Press, London
- Labuza T, Tannenbaum S, Karel M (1970) Water content and stability of low-moisture and intermediate moisture foods. *Food Technol* 24:543–550
- Lewicki PP (2004) Water as the determinant of food engineering properties. A review. *J Food Eng* 61(4):483–495
- Meilgaard MC, Strauss S, Carr BT, Civille GV (1999) *Sensory evaluation techniques*. CRC Press LLC., Boca Raton, FL
- Mohsenin NN, Mittal JP (1977) Use of rheological terms and correlation of compatible measurements in food texture research. *J Texture Stud* 8(4):395–408
- Peleg M (1998) Mechanical properties of dry brittle cereal products. In: Reid E (ed) *The properties of water in foods*. CRC Press, London, pp 233–253
- Peng Y, Lu R (2005) Modeling multispectral scattering profiles for prediction of apple fruit firmness. *Trans ASAE* 48:235–242
- Reid DS, Fennema OR (2008) Water and ice. In: Damodaran S, Parkin KL, Fennema OR (eds) *Food chemistry*. CRC Press, Boca Ratón, FL, pp 18–77
- Roos YH (2010) Glass transition temperature and its relevance in food processing. *Annu Rev Food Sci Technol* 1(1):469–496
- Roos YH, Karel M, Kokini JL (1996) Glass transitions in low moisture and frozen foods: effects on shelf life and quality. *Food Technol* 50(11):95–108
- Ruan RR, Chen PL (1998) Nuclear magnetic resonance techniques. In: Ruan RR, Chen PL (eds) *Water in foods and biological materials: a nuclear magnetic resonance approach*. Technomic, Lancaster, pp 17–24
- Suwonsichon T, Peleg M (1998) Instrumental and sensory detection of simultaneous brittleness loss and moisture toughening in three puffed cereals. *J Texture Stud* 29:255–274
- Yang J, Huang M, Peng J, Shi J (2010) Rapid determination of the moisture content of milk powder by microwave sensor. *Measurement*. doi:[10.1016/j.measurement.2010.08.007](https://doi.org/10.1016/j.measurement.2010.08.007)

# Characterization of a Hydrate–Dehydrate System with Critical Transitions in the Typical Range of Processing and Storage Conditions

A.D. Otte and R. Pinal

## Abbreviations

A	Hydrate species
A	Isolated site hydrates
B	Channel hydrates
DSC	Differential scanning calorimetry
K	Constant
$K_{sp}$	Constant
RH	Relative humidity
TGA	Thermogravimetric analysis
W	Water species

## 1 Introduction

Hydrates are solid adducts where the parent compound (in this case a drug molecule) and water come together to form a crystalline lattice (Khankari and Grant 1995). The incorporation of water molecule(s) into the crystalline structure produces a new and distinct unit cell, i.e., with its own mechanical and thermodynamic properties, which are often significantly different from those of the anhydrous crystal form of the drug. Figure 1 depicts the transformation of the anhydrous crystal into the hydrate by the presence of water. Figure 1b shows the formation of the hydrate as observed in the corresponding water uptake isotherm. Hydrate formation involves an equilibrium analogous to that of the activity of the hydrogen

---

A.D. Otte • R. Pinal (✉)

Department of Industrial and Physical Pharmacy, Purdue University, West Lafayette, IN, USA  
e-mail: [rpinal@purdue.edu](mailto:rpinal@purdue.edu)

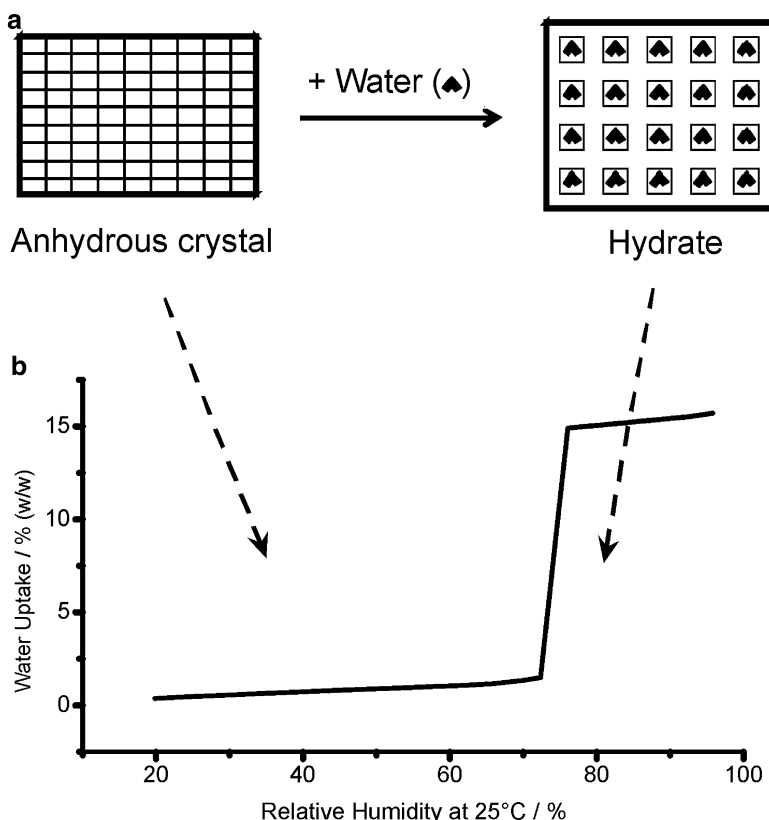


**Fig. 1** Formation of a hydrate. (a) Pictorial description of the transformation from crystalline anhydrous to crystalline hydrate. (b) Theoretical diagram of hydrate formation as a function of water activity

ion on the protonation/deprotonation of acids and bases. In the case of the hydrate, the water activity (estimated by means of the relative humidity, RH), results in two regions. There is a critical RH value below which the anhydrous form is the stable solid. The hydrate is the stable form when the water activity is above the critical RH value. The formation of hydrates is a subject of considerable interest in the pharmaceutical industry. Water is often the solvent of choice for some industrial processes such as wet granulation and aqueous based film coating. The small size of the water molecule, and its ability to act as both a hydrogen donor and acceptor, are factors that promote incorporation into crystalline lattices. Solid-state transitions from hydration or dehydration are possible during processing steps such as drying, mixing, granulation, or tabletting (Jorgensen et al. 2002).

The changes produced upon dehydration can affect further processing and functionality. For example, the greater number of intermolecular hydrogen bonds in theophylline monohydrate, in relation to the anhydrous solid form, results in a

material with a higher mechanical strength relative to its anhydrous counterpart (Agbada and York 1994). Most notably, solubility between the hydrate and anhydrate form can vary significantly. A hydrate is, as a rule, less soluble *in water*, than the anhydrous form of the same drug. This fact can be readily recognized from the equilibrium of hydrate formation:



$$K = \frac{[A_L][W_L]}{AW_s} \quad (2)$$

$$K_{sp} = [A_L][W_L] \quad (3)$$

Where  $AW_s$ ,  $A$ , and  $W$  denote the hydrate, and the drug and water species, respectively, and the subscripts S and L denote solid and liquid (solution) state, respectively. Since the concentration (activity) of water is a factor in the solubility product (Eq. 3), by Le Chatelier's principle, the result is that by increasing the activity of water in the solvent (up to the end point where pure water is the solvent), the concentration of the drug in solution is "pushed down." If a situation where the hydrate is more soluble than the anhydrous form is encountered, the explanation is likely to be found in the particle properties of the materials involved, such as quality of the crystals involved. The vast majority of organic drug molecules exist in different crystal forms, including anhydrous polymorphs and hydrates, each with different solubility (Pudipeddi and Serajuddin 2005). The differences in solubility of crystal forms affect their dissolution rate and potentially their bioavailability. Ampicillin trihydrate for example, exhibits lower solubility and lower plasma concentration values than its anhydrous counterpart (Poole and Bahal 1968). It is important to emphasize that while the potential effect of solubility on bioavailability applies to all different (anhydrous and hydrated) crystal forms, hydrates tend to produce more consistent and significant reductions on observed blood levels during product development. From a bioavailability standpoint, all crystal forms of the drug are important, hydrates are especially so. In pharmaceutical development, the anhydrous form of a drug, with its higher aqueous solubility relative to the hydrate, is often desired. However, since water is ubiquitous in the atmosphere, hydrate formation is a constant potential issue, the relevance of which extends beyond solid form selection for pharmaceutical processing; it can affect handling, storage, and stability of pharmaceuticals.

Hydrates are typically classified according to two general criteria. One classification is based on whether the number of water molecules in the crystal maintains a fixed ratio in relation to the drug molecules. Accordingly, hydrates can be stoichiometric or non-stoichiometric. Stoichiometric hydrates are composed of a fixed number of water molecules per host molecule, at a given temperature, pressure and relative humidity. In non-stoichiometric hydrates water composition varies with water activity, without significant alteration of crystal structure, relative to increasing or decreasing water content (anisotropic expansion and contraction is commonly observed). These water molecules are usually not firmly bound. Instead, they fill interstitial spaces in the unit cell without forming strong hydrogen bonds.

$\beta$ -Cyclodextrin is an example of a non-stoichiometric hydrate, where clusters of water molecules are found in the cyclodextrin cavities, while additional water molecules act as space-fillers between neighboring cyclodextrin molecules (Steiner and Koellner 1994). Another classification criterion (Morris 1999) separates hydrates into three main types: isolated site, channel, and ion associated. This classification is based on the way the water molecules are entrapped into the crystal lattice. Ion coordinated hydrates form coordination bonds between the water molecule and ions present in the host molecule. Knowledge of the structure and dehydration behavior of the hydrate is important, as the type and physicochemical properties of the products of dehydration vary. An interesting example is calteridol calcium (Morris 1999), a hydrate in which 14 water molecules exist in what can be considered three different levels of binding energy, including ion association of water. The case study presented here does not involve an ion associated hydrate, so this type of material is not covered in detail. Isolated site and channel hydrates are further discussed below.

While one of the classification criteria is based on composition and the other on structure, it can be said that the two criteria examine the same attributes of hydrates, i.e., different types of behavior encountered during pharmaceutical processing and stability, but from different perspective. Specifically, in terms of energetics or ease of dehydration as a function of environmental conditions. The following is only a “rule of thumb,” but it is useful from a practical point of view. Isolated site hydrates tend to be stoichiometric, whereas non-stoichiometric hydrates are, more often than not, of the channel type. From a handling and processing point of view, stoichiometry, or lack thereof, tends to reflect the type of hydrate (isolated site or channel), with direct implications on the ability of the material to maintain its integrity, in terms of water content, under different handling and storage conditions. Figure 2 shows the energetics of dehydration of two types of hydrates: isolated site (a) and channel (b). The figure indicates the overlay plots of differential scanning calorimetry (DSC) and thermogravimetric analysis (TGA) of two hydrates. The hydrate in Fig. 2a is of the isolated site type, where the water molecules are caged in by the drug molecules in well-defined and isolated crystallographic sites. The caged water

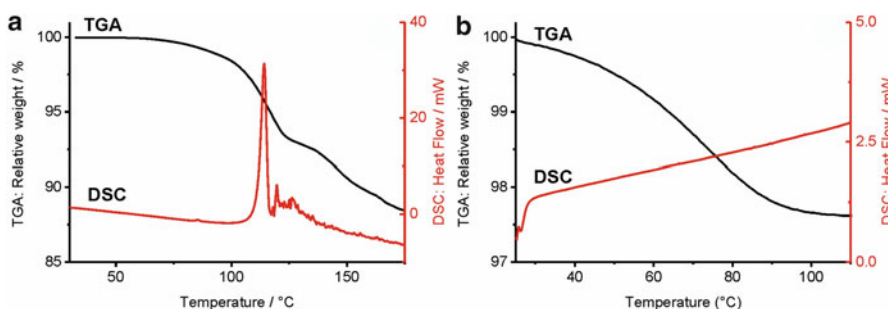


**Fig. 2** Energetics of hydration. (a) High energy of hydration observed in hydrates of the isolated site class. (b) Low energy hydration observed in channel hydrates

molecules interact only with the major component (drug), and are isolated from direct contact with other water molecules. The hydrate on Fig. 2b, on the other hand, corresponds to a channel hydrate, where the water molecules are loosely held inside tunnel-like structures created by the drug molecules. The two types of hydrate exhibit substantially different behavior. The isolated site hydrate (Fig. 2a) maintains its integrity as temperature increases. This hydrate does not begin to lose its water until the temperature approaches 100 °C, the boiling point of water. Notice that the dehydration endotherm is observed at a temperature greater than 100 °C. The caged-in nature of the water entrapment in this type of hydrate results in strong energy of hydration, requiring temperatures on the order of the boiling point of water (or even higher) for dehydration. In contrast, it is clear that the water in the hydrate of Fig. 2b is loosely bound. Notice that dehydration begins to take place at temperatures slightly above room temperature. Furthermore, dehydration in this case gradually increases with temperature such that it is complete at a temperature below the boiling point of water. One very significant difference between Fig. 2a and b is the absence of a dehydration endotherm in the latter. In channel hydrates, water can be so loosely bound that it does not exhibit a clearly identifiable calorimetric dehydration event. In this case, the energy of dehydration is contained in the upward drift of the DSC baseline throughout the thermogram.

Figure 2 also reveals information regarding the stoichiometry of the two hydrates. The isolated site hydrate (a) can be considered stoichiometric, since its water content is fixed and maintained upon heating until forced dehydration takes place at a sufficiently high temperature. The channel hydrate (b), on the other hand, readily loses water with temperature, such that there is no fixed stoichiometry between water and drug molecules. It should be pointed out that temperature is not the only factor affecting the level of hydration (or stoichiometry) in channel hydrates. The relative humidity has a similar effect. Specifically, for a channel (non-stoichiometric) hydrate, the corresponding vertical step illustrated in Fig. 1a would not be as sharp and often presents significant hysteresis between sorption and desorption.

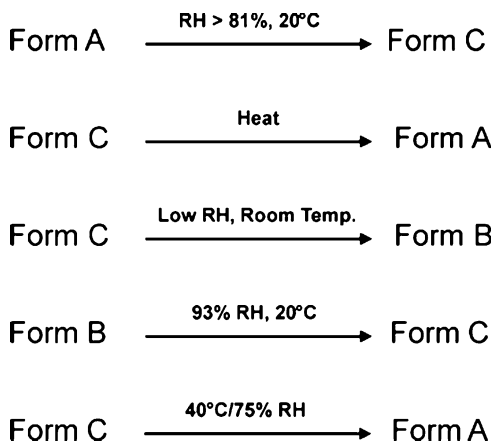
Dehydration of a crystalline hydrate is a complex process, possibly resulting in a number of intermediaries and final states. Dehydration can result in an anhydrate form either via direct transformation or through an intermediate amorphous phase (Allen et al. 1978). Water loss can result in a melt, an amorphous form or a crystalline form of lower hydration. Dehydration is also a dynamic process, which can trigger and be accompanied by liquid-solid and solid-solid transformations. An illustrative example is a pentahydrate converting to anything from a tetrahydrate to monohydrate (Saleki-Gerhardt et al. 1995; Zhu and Grant 2001; Lester et al. 2006). Desolvation can also result in a “dehydrated hydrate,” an isomorphic desolvate where the crystal lattice is retained even with the absence of water molecules (Stephenson et al. 1998). Hydrates can also exhibit

polymorphism or can transform to a different polymorphic form upon dehydration (McMahon et al. 1996). For successful formulation development, not only is knowledge of the structure and hydration/dehydration process important, but also how the compound of interest interacts with other excipients. Below, we present a hydrate system in which the processing conditions have a strong effect on the solid form obtained.

## 2 Materials and Methods

The hydrate system of a drug candidate is used as an illustrative example of a situation where critical transitions are located in the typical range of processing and storage conditions. The assessment was primarily conducted using X-ray powder diffraction and hygroscopicity measurements. The drug exists in three solid forms: A, B, and C. Figure 3 shows the X-ray diffraction patterns of the three crystal forms.

The temperature and humidity conditions for interconversion among the three solid forms is shown in the table below. At high humidity, form A produces form C. Drying form C with heat restores form A. However, drying form C at room temperature produces form B.



The diagram above shows that transformations among the solid phases occur under temperature conditions typical of normal handling and storage. A system like this can be considered to present high risk for transformations during processing or shelf life. Therefore, this system represents an example where establishing the relationship among the different solid phases is a critical task of development. The results of this type of investigation are discussed below.

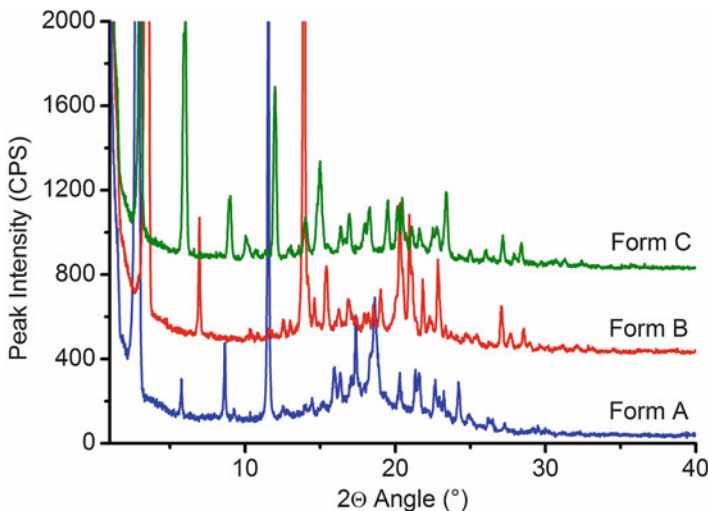


**Fig. 3** X-ray powder diffraction of the three crystalline forms obtained with the drug of the study

### 3 Results and Discussion

Initial characterization data indicates that any of the three solid phases involved can transform into either of the other two forms through a rather finely balanced interaction between temperature and relative humidity. These observations in turn suggest that the approach to establishing the relationship among different crystal forms should be a study that exploits the differences in the energetics of hydration. Accordingly, the hygroscopicity of the solid forms was carried out as a function of temperature. Figure 4 shows the water uptake isotherms of form A at different temperatures. The isotherms show the formation of the hydrate form and hysteresis with a degree that is temperature dependent. It is noteworthy that at 10 and 15 °C, high RH results in an additional hydration step that is not observed at higher (near room temperature conditions) temperatures. Figure 5 shows the water sorption isotherms of form A at 30 and 40 °C. At these temperatures, there is no hydrate formation, and the solid exhibits low (less than 1 % uptake) hygroscopicity. The results in Figs. 4 and 5 indicate that hydration of form A is highly sensitive to temperature. The hydrate is readily formed at 25 °C, as seen in Fig. 4. However, 30 °C is too high for hydrate formation to occur, as shown in Fig. 5. The water uptake isotherms of form B at 25 °C are shown in Fig. 6.

Hydration of form B is also highly sensitive to temperature. The hydrated form is readily produced at 25 °C. However, initial characterization results (see diagram above) show that at 40 °C and 75 % RH, form B converts to anhydrous form A.

To enable use of the results presented in the isotherms shown in Figs. 4, 5, and 6 so the information could be used as a guide for product development, the information was synthesized in the form of a phase diagram. Figure 7 presents a phase

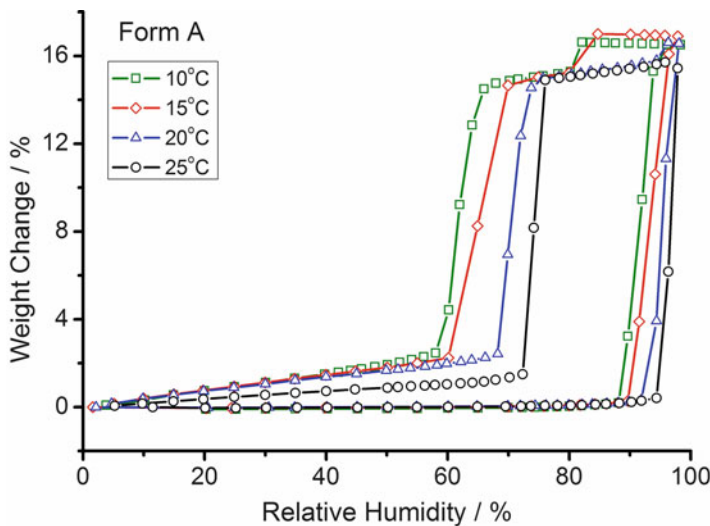


Fig. 4 Water uptake isotherms of Form A at different temperatures

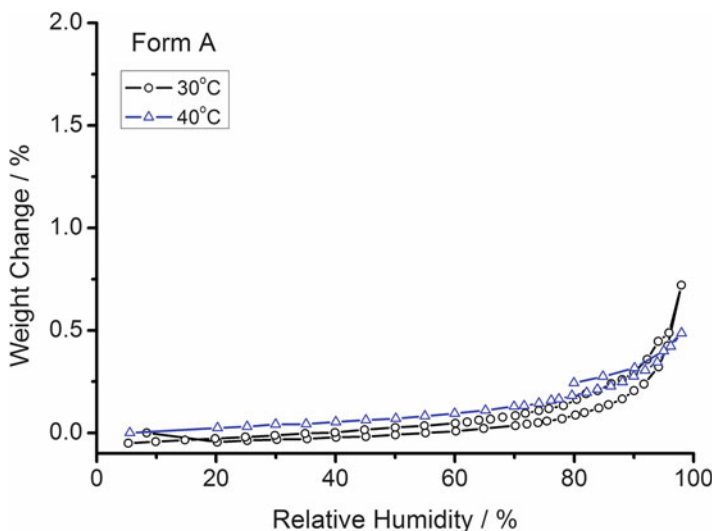


Fig. 5 Water uptake isotherms of Form A at the relatively high temperatures of 30 and 40 °C

diagram delineating the stability regions of different forms of the drug, as a function of temperature and relative humidity. Dots on the figure correspond to experimental observations, whereas solid and dashed boundaries are interpolations and extrapolations, respectively.

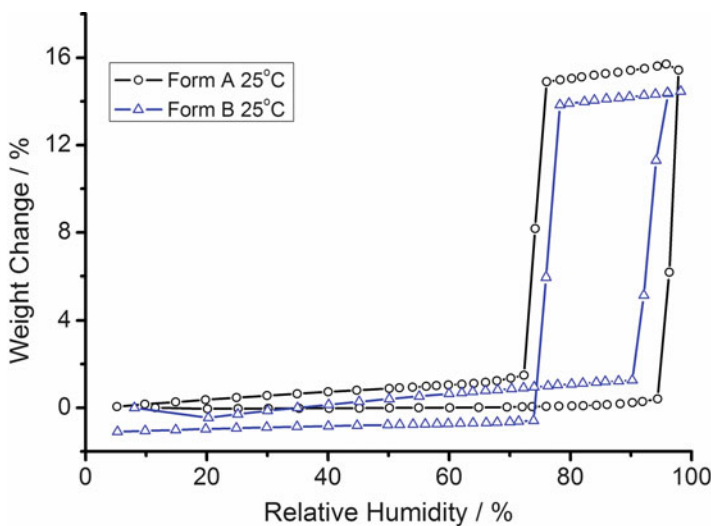


Fig. 6 Comparison of the water uptake isotherms of forms A and B at 25 °C

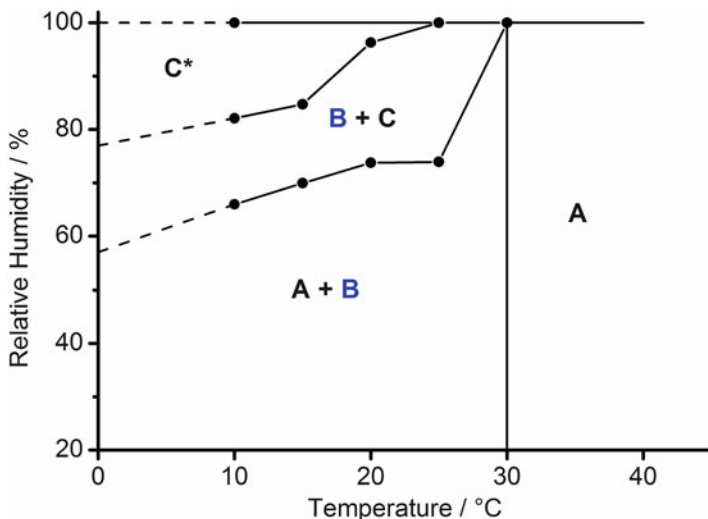
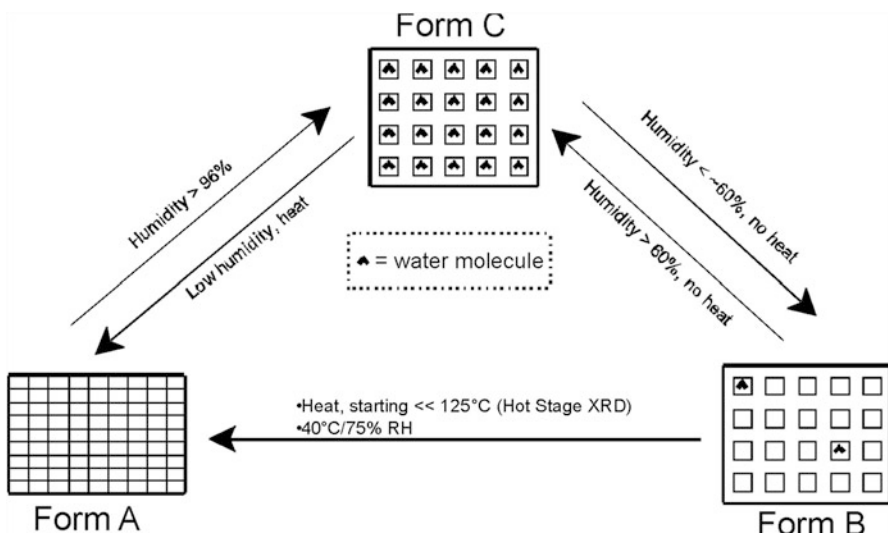


Fig. 7 Phase diagram of the three isolated crystalline forms of the drug of the study

The different forms of the drug can be described as follows: Form A is anhydrous, and Form C is a hydrate with seven moles of water. Both forms are thermodynamically stable but under different conditions of temperature and relative humidity. Form C\* is a newly found stable hydrate with approximately a half mole more water than Form C. Form C\* was only observed at temperatures below 25 °C and RH > 80 %. Form B is a dehydrated hydrate and can be described



**Fig. 8** Pictorial representation of the relationship among the different solid forms represented in the phase diagram of Fig. 7

as thermodynamically unstable, but kinetically very stable. It represents the intermediate of dehydration of Form C to yield Form A. Form B, although crystalline, is not a true thermodynamic phase; its presence reflects the formation of Form C at some stage in the sample's history. The phase diagram in Fig. 7 captures both thermodynamic and kinetic information relevant to the development of the drug. The results obtained suggest that Form A is the only suitable crystal form for product development as a solid dosage form.

Some characteristics of the interconversion among forms, including the non-equilibrium transformations associated with Form B, are:

1. From the region labeled “A + B”: by increasing relative humidity, Form A will yield Form B and/or Form C, depending on experimental conditions.
2. From the region labeled “A + B”: by increasing relative humidity, Form B will yield only Form C.
3. From the region labeled “A + B”: heating Forms A or B above 30 °C will result in Form A.
4. From the region labeled “B + C”: decreasing the relative humidity will result in Form B.
5. The region labeled C\* corresponds to a hydrate with half a molecule more of water than Form C. This region may correspond to a new hydrate form, or simply to a higher crystal quality of Form C.

The relationship between different crystal forms of the drug for which distinctive X-ray patterns were obtained is depicted in Fig. 8, which is a pictorial representation of the conversion scheme shown in Fig. 7. Form A is shown as the anhydrous

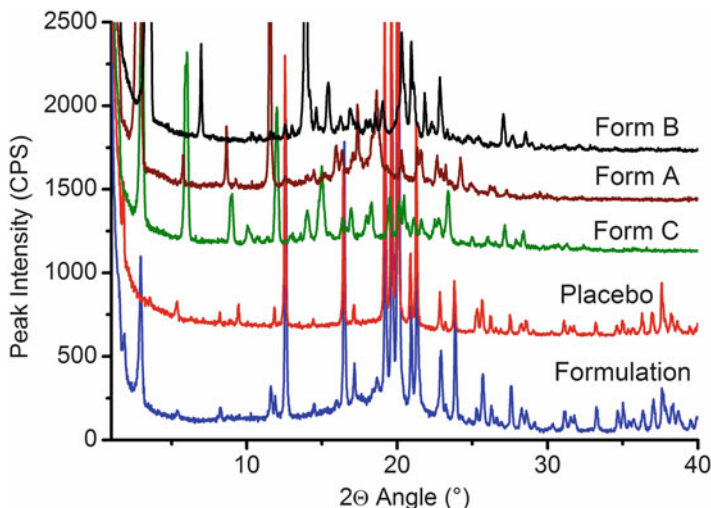


**Fig. 9** X-ray powder diffraction patterns of the final formulation of the drug in the study and the placebo. Diffractograms for pure forms A and C are shown for comparison

crystal, Form C as the hydrate, and Form B is shown as corresponding to dehydrated hydrate, with empty cavities left upon the removal of the water molecules from Form C.

The information captured in Figs. 7 and 8 is very useful for understanding the transformations taking place under different temperature and humidity conditions of pharmaceutical processing. However, it is critical to ascertain the form actually present in the formulation used to manufacture the final dosage form. Wet granulation is one of the most common unit operations employed in the manufacture of solid dosage forms. The process involves exposure of the drug to water, followed by drying. For a compound with properties like those of the drug in this case study, it can be a challenging task to establish the crystal form actually present in the final formulation. Figure 9 shows the X-ray patterns of the final formulation, as well as the placebo. Diffractograms of forms A and C are also shown for reference.

In principle, the range below the  $10^\circ$   $2\Theta$  angle reflects the crystal form contained in the formulation. However, the excipients (inactive components) of the formulation have a confounding effect on the assessment. It is not a straightforward task to unambiguously identify the crystalline form of the drug present in the formulation in a case like this. Figure 9 shows that at the  $2\Theta$  angle of  $3^\circ$ , there is a peak present in the formulation but absent in the placebo. A complicating factor is that both Forms A and C show a peak in the same region. It was investigated whether the peak at  $3^\circ$   $2\Theta$  in the formulation reflects the presence of Form A or the presence of Form C. Under the hypothesis that the drug exists as Form A in the formulation, the approach consisted of inducing the formation of Form C in the formulation. A sample of the formulation was exposed to 100 % RH at low temperature ( $10^\circ\text{C}$ ) for a period of 9 days. The exposed formulation sample was then subjected

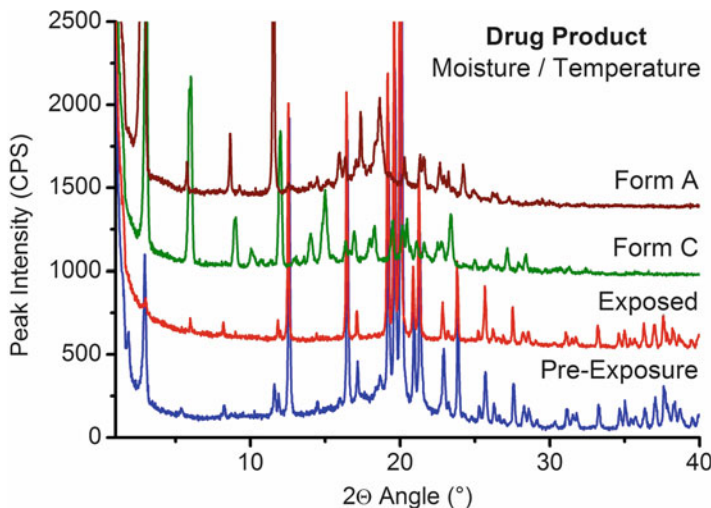


**Fig. 10** Change in X-ray pattern observed upon exposing the final formulation to high humidity and low temperature ( $10^{\circ}\text{C}$ ) in order to induce the formation of Form C in the product

**Table 1** Different crystal form dispositions in a hypothetical wet granulation, along with the feasible events the different dispositions reflect

Granulation containing	Reflects
Form A + Form B	A non-homogeneous wetting of the particles or A non-homogeneous drying of the granules
Form I + Form X	Water content very nonuniform in the granulation
Form II + Form X	High and nonuniform water content in the granulation
Form I + Form II + Form X	Non-intimate wetting of the particles, nonuniform drying of the granules, highly nonuniform final water content

to X-ray diffraction analysis. The results are shown in Fig. 10. Exposing the sample to high humidity and low temperature, which induces the formation of the hydrate (Form C) resulted in the virtual disappearance of the peak at  $3^{\circ}$  in the formulation. This result indicates that the crystal form in the formulation is the anhydrous Form A.

One feature of systems in which it is possible to isolate a kinetically stable intermediary solid such as Form B, is that the properties of the material are dependent on the sample history. This feature therefore has potential use as a process monitoring/diagnostic tool. Table 1 presents different crystal form dispositions in a hypothetical wet granulation, along with the feasible events the different dispositions reflect.

## 4 Conclusions

Hydrates are frequently encountered in pharmaceutical development. They often represent the solid state form with the greatest potentially detrimental effect on the bioavailability of the drug. Therefore, the characterization of hydration–dehydration properties, as well as the different crystal forms involved, is particularly important. The hysteresis of hydration–dehydration encountered in practice results in a wide range of variation in terms of the temperature and humidity conditions favorable for the formation (or not) of the different solid forms. It is important to not misinterpret mechanical stability as thermodynamic stability and vice versa, as exemplified by Form B in this case. The case study discussed here presents an illustrative example in the sense that less than optimal instrument signal/data is part of the pharmaceutical reality when conducting characterization studies on hydrates, particularly in final formulations or dosage forms. Indirect observation of solid state phenomena is sometimes necessary, and often unavoidable. However, despite all of the seemingly confounding effects, polymorph characterization proves to be a very objective fact finding exercise.

## References

- Agbada CO, York P (1994) Dehydration of theophylline monohydrate powder: effects of particle-size and sample weight. *Int J Pharm* 106:33–40
- Allen PV, Rahn PD, Sarapu AC, Vanderwielen AJ (1978) Physical characterization of erythromycin: anhydrate, monohydrate, and dihydrate crystalline solids. *J Pharm Sci* 67:1087–1093
- Jorgensen A, Rantanen J, Karjalainen M, Khriachtchev L, Rasanen E, Yliruusi J (2002) Hydrate formation during wet granulation studied by spectroscopic methods and multivariate analysis. *Pharm Res* 19:1285–1291
- Khankari RK, Grant DJW (1995) Pharmaceutical hydrates. *Thermochim Acta* 248:61–79
- Lester C, Lubey G, Dicks M, Andol G, Vaughn D, Cambron RT, Poiesz K, Redman-Furey N (2006) Dehydration of risedronate hemi-pentahydrate: analytical and physical characterization. *J Pharm Sci* 95:2631–2644
- McMahon LE, Timmins P, Williams AC, York P (1996) Characterization of dihydrates prepared from carbamazepine polymorphs. *J Pharm Sci* 85:1064–1069
- Morris KR (1999) Structural aspects of hydrates and solvates. In: Brittain HG (ed) Polymorphism in pharmaceutical solids. Marcel Dekker, New York, NY, pp 126–179
- Poole JW, Bahal CK (1968) Dissolution behavior and solubility of anhydrous and trihydrate forms of ampicillin. *J Pharm Sci* 57:1945–1948
- Pudipeddi M, Serajuddin ATM (2005) Trends in solubility of polymorphs. *J Pharm Sci* 94:929–938
- Saleki-Gerhardt A, Stowell JG, Byrn SR, Zografi G (1995) Hydration and dehydration of crystalline and amorphous forms of raffinose. *J Pharm Sci* 84:318–323
- Steiner T, Koellner G (1994) Crystalline  $\beta$ -cyclodextrin hydrate at various humidities: fast, continuous, and reversible dehydration studied by X-ray diffraction. *J Am Chem Soc* 116:5122–5128
- Stephenson GA, Groleau EG, Kleemann RL, Xu W, Rigsbee DR (1998) Formation of isomorphic desolvates: creating a molecular vacuum. *J Pharm Sci* 87:536–542
- Zhu HJ, Grant DJW (2001) Dehydration behavior of nedocromil magnesium pentahydrate. *Int J Pharm* 215:251–262

# Viscoelastic Sorption Behavior of Starch and Gluten

M.B.J. Meinders and L. Oliver

## Abbreviations

$a_{w,o}$	Water activity
$B_c$	Material constant
$D$	Diffusion coefficient
$De$	Deborah number
FH	Flory-Huggins theory
$K_b$	Bulk osmotic modulus
$l$	Size of the sample
MDSC	Modulated differential scanning calorimetry
PDE	Partial differential equation
$P_{w,o}$	Water partial pressure
$R_g$	Universal gas constant
RH	Relative humidity
SLS	Standard Linear Solid
$T$	Temperature
$T_g$	Glass transition temperature

---

M.B.J. Meinders (✉)

Top Institute Food & Nutrition, P.O Box 557, 6700 AN Wageningen, The Netherlands

Food and Biobased Research, Wageningen University and Research Centre,  
P.O. Box 17, 3700 AA Wageningen, The Netherlands

e-mail: [marcel.meinders@wur.nl](mailto:marcel.meinders@wur.nl)

L. Oliver (✉)

Top Institute Food & Nutrition, P.O Box 557, 6700 AN Wageningen, The Netherlands

Instituto Universitario de Ingeniería de Alimentos para el Desarrollo, Universidad Politécnica  
de Valencia, Valencia, Spain

e-mail: [laura.oliverhernandez@wur.nl](mailto:laura.oliverhernandez@wur.nl)

$\hat{V}_w$	Specific volume of water
$X$	Spatial Lagrangian coordinate
$x$	Eulerian coordinate
$y_w$	Water mass fractions
$\mu_w$	Chemical potential of the water
$\mu_{w,FH}$	Chemical potential due to the mixing of the polymer and the water
$\mu_{w,o}$	Chemical potential of the outside environment
$\sigma$	Stress in the system or osmotic pressure
$\tau_D$	Ratio of the diffusion time
$\phi_p$	Polymer volume fraction
$\phi_w$	Water volume fraction
$\phi_{wg}$	Water volume fraction at glass-rubber transition
$\chi$	Flory-Huggins interaction parameter

## 1 Introduction

The migration of gasses and liquids through (bio) polymers plays an important role in numerous applications and processes like, e.g., drying and (re)wetting of foods and food ingredients, packaging, and controlled release. A good understanding of the transport mechanisms is therefore of great importance to control these processes. The transport of solvents through (bio) polymers is a complex process and involves diffusion due to water concentration gradients, swelling, shrinkage, and relaxation of the polymeric matrix. Often also transitions between the glassy, rubbery, and/or viscous states of the polymer system are involved.

Here we report on a theoretical and experimental study of water transport in biopolymer films of starch and gluten. Relaxation effects of the polymer matrix seem important for the migration of water in biopolymer systems like starch and gluten (Oliver and Meinders 2011). This seems the case for a broad water activity range, but especially when the system is in the neighborhood of the glass transition. There are various models published that take into account the viscoelastic relaxation effects of the polymeric matrix (Wu and Peppas 1993; Vrentas and Vrentas 2001; Pawan et al. 2004).

These models are solved using as boundary condition a step change of the water volume fraction at the sample boundary. Results indicate three regimes, depending on the ratio of the diffusion time  $\tau_D = l^2/D$  (with  $l$  the size of the sample and  $D$  the diffusion coefficient) and matrix relaxation time  $\tau_1$ . This ratio is often called the diffusion or sorption Deborah number and is defined as  $De = \tau_1/\tau_D$ . When  $De \approx \infty$  ( $\tau_1 \gg \tau_D$ ), the system behaves as an elastic solid, there is negligible time variation of the polymer structure during the diffusion process, and water migration can be described by Fickian diffusion (elastic diffusion). Similarly, when  $De \approx 0$  ( $\tau_1 \ll \tau_D$ ), the system behaves as a viscous fluid and water migration can also be described by Fickian diffusion (viscous diffusion). When  $De \approx 1$  ( $\tau_1 \approx \tau_D$ ), the rearrangement of polymer chains and the movement of solvent occur in comparable

time scales, so the observed behavior is not consistent with the classical diffusion theory (viscoelastic or anomalous diffusion).

We observed, however, that sorption curves of amorphous starch and gluten showed non-Fickian features with characteristic relaxation times that are significantly different than the characteristic diffusion time. This seems not in line with the published results mentioned above. To understand and describe this behavior, we extended the viscoelastic diffusion model and allowed variation of the water volume fraction and stress of the sample boundary. The model attempts to describe both the dynamical sorption behavior and the equilibrium values (isotherm) in a single set of physical parameters of the polymer-water system: the Flory-Huggins interaction parameter, the diffusion constant, and a concise set of rheological parameters to describe the viscoelastic behavior of the polymer.

## 2 Materials and Experimental Methods

Starch and gluten films were prepared by casting. Starch/water or gluten/ethanol/water mixtures were poured in a polypropylene dish of 97 mm diameter and water was allowed to evaporate in a climate chamber. Film thickness was varied by varying the amount of biopolymer solution. Step-change dynamic water vapor sorption experiments were performed at ambient temperature ( $T = 25\text{ }^{\circ}\text{C}$ ) using an automatic multisample moisture sorption analyzer SPSx-11 (Projekt Messtechnik, Ulm, Germany). Modulated differential scanning calorimetry (MDSC) was used to measure the glass transition temperature ( $T_g$ ) of the biopolymer films at different water mass fractions ( $y_w$ ). For a detailed description of the preparation of the biopolymer films as well as the gravimetric sorption and MDSC measurements, we refer to Oliver and Meinders (2011).

## 3 Model

### 3.1 Viscoelastic Diffusion

Various models have been published that take into account the viscoelastic relaxation effects of the polymeric matrix (Wu and Peppas 1993; Vrentas and Vrentas 2001; Pawan et al. 2004); the models are all based on the assumption that the free energy (and chemical potential) can be described as the sum of a solvent-polymer mixing term and a stress term. Here we will discuss shortly the model of Singh et al. (Pawan et al. 2004) that will be used as a starting point to describe the water migration in biopolymers. Their model was derived using multiscale thermodynamical theory for the swelling of biopolymers by modeling the solid phase as

viscoelastic and the fluid phase as viscous. For a one-dimensional sheet the water transport equation can be expressed as

$$\frac{\partial \phi_w}{\partial t} = (1 - \phi_w)^2 \frac{\partial}{\partial X} \left[ D(1 - \phi_w) \frac{\partial \phi_w}{\partial X} - B_c(1 - \phi_w) \frac{\partial \sigma}{\partial X} \right] \quad (1)$$

where  $\phi_w$  is the water volume fraction,  $\partial/\partial t$  is the partial time derivative,  $D$  is the water diffusion coefficient,  $B_c$  is a material constant,  $\sigma = \sigma(\phi_{w,t})$  is the stress in the system or osmotic pressure. The model is expressed in terms of the spatial Lagrangian coordinate  $X$  in order to account for the swelling and shrinkage of the polymeric material upon water adsorption and desorption, respectively. The Lagrangian coordinate system is chosen to be that of the dry polymer material. If we assume incompressibility, then the relation between the Eulerian and Lagrangian coordinates  $x$  and  $X$ , respectively, can be approximated for a 1D sheet by

$$\partial X = (1 - \phi_w) \partial x \quad (2)$$

The first term in Eq. (1) corresponds to Fickian diffusion while the second term describes the matrix relaxation effects.

### 3.2 Boundary Conditions and Isotherm

Here we want to describe dynamical sorption curves of step-like gravimetric sorption experiments of biopolymer films of starch and gluten. In a step-change sorption experiment, the mass of the sample is measured as a function of time at a certain set environmental relative humidity or water activity ( $a_{w,0}$ ). At a certain time, usually when the sample is believed to have reached a steady state,  $a_{w,0}$  is changed to a new value. We assume that the sample is in equilibrium at the beginning of a step change. We also assume a constant temperature ( $T$ ). Furthermore we assume that at the boundary of the sample the chemical potential of the water ( $\mu_w$ ) is equal to that of the outside environment  $\mu_{w,0}$ ,

$$\mu_{w,0} = R_g T \ln \alpha_{w,0} = R_g T \ln \frac{P_{w,0}}{P} \quad (3)$$

where  $\alpha_{w,0}$  and  $P_{w,0}/P$  are the water activity and the water partial pressure or relative humidity (RH) of the environment, and  $R_g$  is the universal gas constant.

To describe the water chemical potential of the water-polymer system, which is directly related to the isotherm, the approach of Leibler and Sekimoto (Leibler and Sekimoto 1993) is followed. They considered the mixing of a solvent and polymer. It is assumed that the chemical potential can be written as the sum of the chemical potential due to the mixing,  $\mu_{w,FH}$  and due to the stress in the system  $\mu_{w,\sigma}$

$$\mu_w = \mu_{w,FH} + \mu_{w,\sigma} \quad (4)$$

The chemical potential due to the mixing of the polymer and the water ( $\mu_{w,FH}$ ) is assessed by the Flory-Huggins (FH) theory for large polymers (like starch and gluten)

$$\frac{\mu_{w,FH}}{R_g T} = \ln \phi_w + (1 - \phi_w) + \chi(1 - \phi_w)^2 \quad (5)$$

where  $\chi$  is the Flory-Huggins interaction parameter describing the enthalpic interaction between the polymer and water molecules. The FH Eq. (5) assumes a mobile water-polymer mixture. For the immobile glassy state, an extra term  $\mu_{w,\sigma}$  is added to the chemical potential that resembles the stress in the system that is built up when water is removed from the stiffened polymer matrix. Due to the immobilization of the polymer matrix in the glassy state, extra energy is needed to shrink the system further when the external relative solvent pressure is decreased.

In general, the stress  $\sigma$  for incompressible system is related to the chemical potential of the water c.q. solvent by

$$\mu_{w,\sigma} = -\hat{V}_w \quad (6)$$

where  $\hat{V}_w$  is the specific volume of water.

Leibler and Sekimoto assumed a fully elastic glassy state with its mechanical/rheological properties described by a constant bulk osmotic modulus ( $K_b$ ) that was assumed to be zero in the rubbery state (i.e., when  $\phi_w > \phi_{w,g}$ , where  $\phi_{w,g}$  is the critical water volume fraction at the glass-rubber transition at temperature  $T$ ).

However, we observed in the dynamical sorption experiments of starch and gluten (Oliver and Meinders 2011) that the water-polymer system behaves viscoelastic in the glassy state with finite relaxation times. Therefore, the boundary condition (“isotherm”) cannot be considered to be constant during an experiment. The stress and the water volume fraction at the boundary of the system depend on time and must be calculated using an appropriate rheological viscoelastic model (see below). We assumed that the water chemical potential of the environment (Eq. 3) is equal to that of the system (Eq. 4). Differentiation gives

$$\frac{d\mu_w}{dt} = \frac{d\mu_{w,FH}}{dt} - \hat{V}_w \frac{d\sigma}{dt} \quad (7)$$

Together with the appropriate rheological model that gives an expression for  $d\sigma/dt$  and

$$\frac{d\mu_{w,FH}}{dt} = R_g T \left( \frac{1}{\phi_p - 1} + \left( 1 - \frac{1}{N} \right) + 2\chi\phi_p \right) \frac{d\phi_p}{dt} \quad (8)$$

which is derived from differentiating the Flory-Huggins equation with respect to the polymer volume fraction  $\phi_p$ ; the boundary values of the state variables can be solved as a function time  $t$  and the forcing  $a_{w,o}$  and change therein  $da_{w,o}/dt$ . This is then used as the boundary condition to calculate the sorption dynamics.

### 3.3 Rheological Model

Many systems do not relax with a single relaxation time. For example, different polymer segments of a polymer of different sizes and properties can contribute to the relaxation process. The system cannot well be described by a single relaxation time but a distribution of various relaxation times is needed. For polymer-water mixtures often the stretched exponential is used to characterize the relaxation function (Ediger et al. 1996; Le Meste et al. 2002). To describe the sorption behavior of starch and gluten, we observed that more than one relaxation mode is needed. We approximate their relaxation behavior by the so-called Wiechert model with at most two Maxwell elements placed in parallel with a Hookean spring. The constitutive relations are then given by

$$\frac{\partial \sigma}{\partial t} = (k_e + k_1 + k_2) \frac{\partial \varepsilon}{\partial t} - \left( \frac{1}{\tau_1} - \frac{1}{\tau_2} \right) \sigma_1 \frac{\sigma}{\tau_2} + \frac{k_e \varepsilon}{\tau_2} \quad (9)$$

$$\frac{\partial \sigma_1}{\partial t} = k_1 \frac{\partial \varepsilon}{\partial t} - \frac{\sigma_1}{\tau_1} \quad (10)$$

where  $k_e$ ,  $k_1$ , and  $k_2$  are the spring constants;  $\tau_i = k_i/\eta_i$  and  $\eta_i$  are the relaxation times and viscosity of the two Maxwell elements; and  $\varepsilon$  is the strain. The latter can be defined in various ways; here we used  $\varepsilon = (\phi_w - \phi_{w,g})\phi_w$ . The Wiechert model reduces for  $k_2 = 0$  to a Standard Linear Solid (SLS),  $k_e = k_2 = 0$  to a Maxwell, and for  $k_1 = k_2 = 0$  to a fully elastic system.

This set of ODEs can be solved giving the appropriate initial values for the state variable  $\sigma$ ,  $\sigma_1$ , and  $\varepsilon$ .

The coupled set of partial differential equation (PDE), Eqs. (1) and (9), and applying appropriate initial and boundary conditions can be solved using standard PDE solvers. The model calculations and fitting with experimental data have been performed using Matlab (Mathworks).

## 4 Results and Discussion

### 4.1 Isotherms

Figure 1 shows the measured isotherms of gluten and starch films for different thicknesses and duplicates. Also shown are fits of the Flory-Huggins model including an extra stress term for the chemical potential in the glassy state (Eq. 4). Model parameters are shown in Table 1 and Fig. 3. An elastic model is used to describe the stress in the glassy state as a function of the volume fraction. It is seen that the model seems to describe the measured isotherms of starch and gluten well with reasonable parameters that are similar as found in literature (Oliver and Meinders 2011; Nicholls et al. 1995). The obtained values for the elastic modulus (about  $5 \times 10^8 \text{ N/m}^2$ ) seem lower as those found in literature (about between 1 and  $2 \times 10^9 \text{ N/m}^2$  (Nicholls et al. 1995; Chang et al. 2000)). The isotherm measurements of the same material but differing in film thickness show a large variation. We think that an important reason for this is that the samples have different histories, like, e.g., different drying and cooling rates. When the water-polymer system is going from the supercooled liquid to the glassy state, the molecular motion of the polymer will be frozen. This also involves that stress will be built up in the glassy system upon further cooling and/or drying. Below the glass transition short-range molecular motions, involving water, side chains, and even main chains, are still occurring (see, e.g., Ediger et al. 1996; Le Meste et al. 2002). The precise process of immobilization of the polymer matrix occurs over a broad temperature and/or water content range and depends on the history. This makes that a number of properties of the glass like  $T_g$ ,  $a_{w,g}$ , isotherm, and relaxation phenomena depend on the history of the sample.

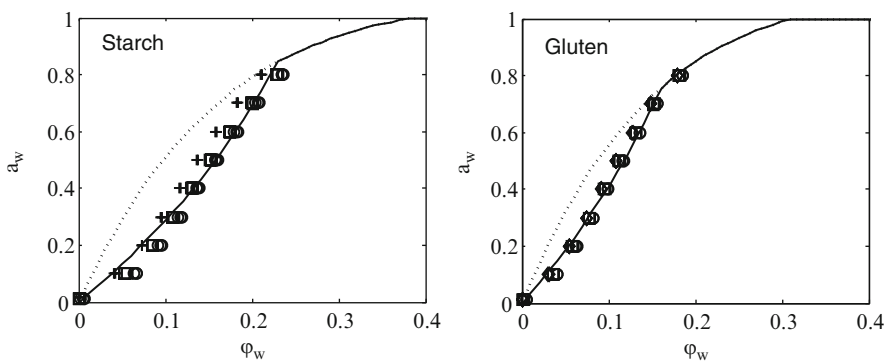


**Fig. 1** Experimental isotherm of starch (left panel) and gluten films (right panel). Different symbols indicate different film thicknesses. Also shown are the simulated isotherms (Eq. 4). The dotted line corresponds to the FH isotherm (Eq. 5), while the continuous line is obtained by adding the stress term (Eq. 6) for an elastic glassy state. Model parameters are shown in Table 1

**Table 1** Parameters used to describe the sorption behavior of starch and gluten

	Starch	Gluten	
$\phi_{w,g}$	0.23	0.16	Glass transition water volume fraction
$\chi$	0.9	1	Flory-Huggins interaction parameter
$k_e$	$5 \times 10^8$	$6 \times 10^8 \text{ N/m}^3$	Spring constant
$\rho_w$	1,000	$\text{kg/m}^3$	Density of the water
$\rho_p$	1,450	$\text{kg/m}^3$	Density of the polymer
$M_w$	$18 \times 10^{-3}$	kg/mol	Molecular mass water
$M_p$	$1 \times 10^{10}$	kg/mol	Molecular mass polymer
$T$	298	K	Temperature
$R_g$	8.31	J/K/mol	Universal gas constant

## 4.2 Dynamical Sorption

Figure 2 shows typical examples of experimental and modeled dynamical sorption curves of starch and gluten films for different RH steps (as indicated). Parameter values are shown in Table 1 and Fig. 3. It is seen that already at low  $a_w$  the sorption curves can not well be described by Fickian diffusion. However, the observed sorption behavior can perfectly be described by the viscoelastic diffusion model. This turns out to be so for all films and RH steps. For gluten and the  $a_w$  region of 0.2–0.3, the stress in the system was modeled using the SLS. We assumed that just before the step change in  $a_w$  the Maxwell element was relaxed. The evolution of the water volume fraction at the boundary is shown in the inset of the figure. In this case the relaxation time is of the same order than the characteristic diffusion time. For the  $a_w$  region 0.3–0.4, the experimental  $\phi_w$  does not really reach an equilibrium after about 50 h. Furthermore it is seen that also the Fickian curve can also not describe the experimental sorption behavior at short times. Both observations suggest that more than one relaxation time play a role. Therefore we modeled the stress in the system with a Wiechert model. Just before the step change in  $a_w$ , it is assumed that one Maxwell element (indicated with index 1) was relaxed, while the other (Ediger et al. 1996) is under tension. When the water activity exceeds the initial value, it is assumed that the second Maxwell element is allowed to relax. This corresponds to the situation that an increase of water volume fraction induces mobility in the polymeric matrix. The evolution of the water volume fraction at the boundary is shown in the inset of the figure.

For the starch films, similar as is the case for gluten, more than two relaxation modes are needed in order to correctly describe the sorption curves. For starch both Maxwell elements are relaxed just before the step change in  $a_w$ .

Although further investigation of the parameters is needed and ongoing, the obtained parameter values seem reasonable. However, at this moment it seems not possible to describe all dynamical sorption curves of one material with only one single value for the glass transition and rheological constants. We believe that this is due to the fact that the glass transition occurs over a broad range of water

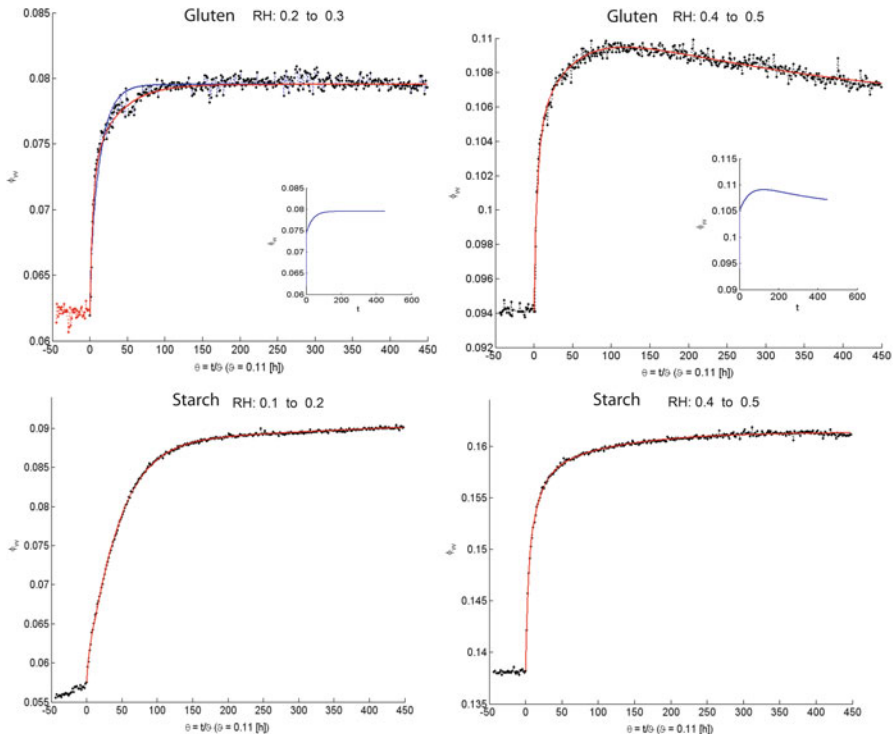


**Fig. 2** Typical examples of dynamical sorption curves of gluten (top panels) and starch (bottom panels) films. Gluten and starch films are 75  $\mu\text{m}$  and 104  $\mu\text{m}$  thick, respectively. RH steps are indicated. The figures show the water volume fraction  $\varphi_w$ , as a function of dimensionless time  $\theta = t/0.11 \text{ h}^{-1}$ . The dots are experimental data and the red lines correspond to the best fit of the viscoelastic diffusion model. The blue line (only top left panel) corresponds to a best fit of the Fickian diffusion model. The insets (top panels) show the evolution of the water volume fraction at the boundary

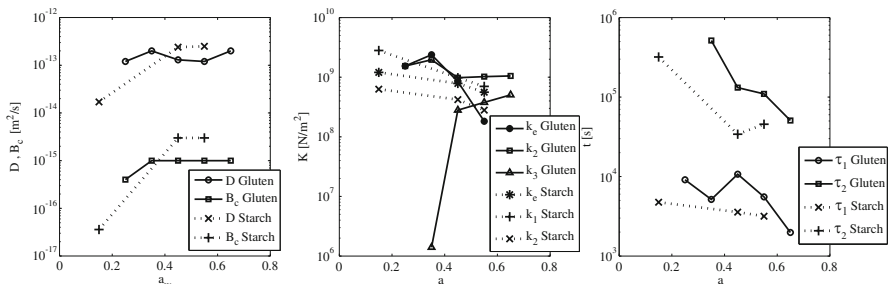


**Fig. 3** Values of the model parameters describing the sorption behavior of gluten. Other parameters are shown in Table 1

activities. Moreover, the glass transition is associated with motions of the polymer backbone (especially measured with DSC), but also other molecular motions may occur that affect water sorption.

Furthermore, this viscoelastic diffusion model can also describe the hysteresis as always observed between adsorption and desorption (Meinders and van Vliet 2009). Different histories of the samples will cause that different stresses are present in the sample so that a different isotherm and dynamical sorption behavior is observed. For a desorption curve, which is measured shortly after the adsorption isotherm, there is ample time for the system to relax the stresses that are built up when going through the glass transition. This causes that at the same  $a_w$  and in the glassy state the water volume fraction of the desorption isotherm will be larger than that of the adsorption isotherm.

## 5 Conclusions

A study to the dynamical and equilibrium sorption behavior of starch and gluten films has been performed. A viscoelastic diffusion model is proposed to describe the sorption behavior of these biopolymer films for the whole range of water activities. Dynamical sorption curves of starch and gluten measured at different water activities (ranging from 0.1 to 0.8) show that matrix relaxations play an important role in the water sorption process, also far below the glass transition. The model attempts to describe both the dynamical sorption behavior and the equilibrium values (isotherm) in a single set of physical parameters of the polymer, the Flory-Huggins interaction parameter, the diffusion constant, and a concise set of rheological parameters to describe the viscoelastic behavior of the polymer. It turns out that the isotherms and all dynamical sorption curves can be very well described by the model. However, the sorption behavior for all water activities could not be described by only one single consistent concise set of parameters. This is believed to be due to the fact that only one single  $a_{w,g}$  is assumed for a compound. In practice however, the glass transition seems to occur over a broad range of water activities (at the same temperature). When the water-polymer system is going from the supercooled liquid to the glassy state, the molecular motion of the polymer will be frozen. This also involves that stress will be built up in the glassy system upon further cooling and/or drying. Below the glass transition polymer relaxation continues. The precise process of immobilization and relaxation of the polymer occurs over a broad temperature and/or water content range. Furthermore it will depend on the history, like cooling and/or drying rate. This makes that a number of properties of the glass like  $T_g$ ,  $a_{w,g}$ , isotherm, and relaxation phenomena depend on the history of the sample. This viscoelastic diffusion model can therefore also explain and describe the hysteresis that is often observed between adsorption and desorption.

## References

- Chang YP, Cheah PB, Seow CC (2000) Plasticizing-antiplasticizing effects of water on physical properties of tapioca starch films in the glassy state. *J Food Sci* 65(3):445–451
- Ediger MD, Angell CA, Nagel SR (1996) Supercooled liquids and glasses. *J Phys Chem* 100(31):13200–13212
- Le Meste M, Champion D, Roudaut G, Simakatos D (2002) Glass transition and food technology: a critical appraisal. *J Food Sci* 67(7):2444–2458
- Leibler L, Sekimoto K (1993) On the sorption of gases and liquids in glassy polymers. *Macromolecules* 26(25):6937–6939
- Meinders MBJ, van Vliet T (2009) Modeling water sorption dynamics of cellular solid food systems using free volume theory. *Food Hydrocoll* 23:2234–2242
- Nicholls RJ, Appelqvist IAM, Davies AP, Ingman SJ, Lillford PJ (1995) Glass transitions and the fracture behaviour of gluten and starches within the glassy state. *J Cereal Sci* 21(1):25–36
- Oliver L, Meinders MBJ (2011) Dynamic water vapour sorption in gluten and starch films. *J Cereal Sci* 54:409
- Pawan PS, Maier DE, Cushman JH, Haghghi K, Corvalan C (2004) Effect of viscoelastic relaxation on moisture transport in foods. Part I: solution of general transport equation. *J Math Biol* 49(1):1–19
- Vrentas JS, Vrentas CM (2001) Viscoelastic diffusion. *J Polym Sci B* 39:1529–1547
- Wu JC, Peppas NA (1993) Modeling of penetrant diffusion in glassy polymers with an integral sorption Deborah number. *J Polym Sci B* 31(11):1503–1518

# Molecular Weight Effects on Enthalpy Relaxation and Fragility of Amorphous Carbohydrates

R.M. Syamaladevi, G.V. Barbosa-Cánovas, S.J. Schmidt,  
and S.S. Sablani

## Abbreviations

$C_p(\text{glass})$	Heat capacity of a material system in the glassy state
$C_p(\text{liquid})$	Heat capacity of a material system in the rubbery state
DSC	Differential scanning calorimetry
KWW	Kohlrausch-Williams-Watts equation
LSD	Least square difference
$m$	Fragility index
MDSC	Modulated differential scanning calorimeter
$R$	Gas constant
$t$	Aging time
$T_g$	Glass transition temperature
$T_{ge}$	End point glass transition temperatures
$T_{gi}$	Glass transition width approach by identifying the onset
$T_{gm}$	Mid temperature between $T_{gi}$ and $T_{ge}$
$\beta$	Relaxation distribution parameter
$\Delta C_p$	Heat capacity change at the glass transition temperature
$\Delta E$	Activation energy for structural relaxations at $T_g$
$\Delta H_\infty$	Total enthalpy available for relaxation during the aging time

---

R.M. Syamaladevi • G.V. Barbosa-Cánovas • S.S. Sablani (✉)  
Biological Systems Engineering Department, Washington State University,  
Pullman, WA 99164-6120, USA  
e-mail: [ssablani@wsu.edu](mailto:ssablani@wsu.edu)

S.J. Schmidt  
Food Science and Human Nutrition, University of Illinois at Urbana Champaign, 367 Bevier Hall, 905 South Goodwin Ave., Urbana, IL 61801, USA

$\Delta H_{\text{relax}}$	Enthalpy relaxation during the aging time
$\tau$ (days)	Mean molecular relaxation time of the entire amorphous system
$\varphi(t)$	Relaxation function

## 1 Introduction

Many food processing techniques such as dehydration, concentration, extrusion, and freezing produce amorphous foods that can be stored below their glass transition temperature (Wungtanagorn and Schmidt 2001). Below glass transition temperature ( $T_g$ ), amorphous food constituents exist in a thermodynamically unstable nonequilibrium and disordered state. Isothermal storage/aging of glassy amorphous food components results in structural relaxations that achieve a more stable equilibrium state over extended time periods (Struik 1978). Since the equilibrium state is a low energy state, some of the energy is lost/relaxed in the nonequilibrium glassy amorphous state during isothermal storage of food components. This energy can be recovered in the form of enthalpy during the reheating of the glassy system by using a differential scanning calorimeter, since physical aging is a reversible process. The enthalpy recovered during reheating of the aged material system is a measure of the system's molecular mobility at the selected aging temperature (Gupta et al. 2004). Structural relaxation in the glassy state of amorphous food components during isothermal storage/aging is also known as enthalpy relaxation/physical aging. Many macroscopic properties of glassy materials, such as volume, enthalpy, refractive index, electrical conductivity, and viscosity, change during physical aging (Struik 1978). The changes in macroscopic properties may adversely affect the physicochemical stability during the isothermal storage of low water amorphous foods and food constituents (Farahnaky et al. 2008).

Nonexponential expressions, such as the Kohlrausch-Williams-Watts (KWW) equation, are used extensively to describe the kinetics of enthalpy relaxation in glassy materials during aging (Hancock et al. 1995). The KWW equation is expressed as:

$$\varphi_t = \exp \left( \frac{-t}{\tau} \right)^\beta \quad (1)$$

$$\phi_t = 1 - \frac{\Delta H_{\text{relax}}}{\Delta H_\infty} = \exp \left( \frac{-t}{\tau} \right)^\beta \quad (2)$$

$$\Delta H_\infty = \Delta C_p (T_g - T_a) \quad (3)$$

where  $\varphi(t)$  is the relaxation function, indicating the kinetics of nonequilibrium to equilibrium transformation of the system;  $\varphi(t)$  provides an estimation of unreleased enthalpy or the extent of enthalpy relaxation at the specific annealing temperature. The  $\tau$  (days) obtained from the KWW equation is the mean molecular relaxation time of the entire amorphous system, and  $\beta$  is the relaxation distribution parameter.  $\Delta H_\infty$  and  $\Delta H_{\text{relax}}$  are the total enthalpy available for relaxation and the enthalpy

**Table 1** Difference between strong and fragile polymer systems

Strong	Fragile
Broad glass transitions ( $T_{gi} - T_{ge}$ values in the range of 10–30 °C)	Narrow glass transitions ( $T_{gi} - T_{ge}$ values in the range of 5–10 °C)
Less than 60 % change in heat capacity difference ( $\Delta C_p$ ) between glassy and rubbery states	60–80 % change in heat capacity difference ( $\Delta C_p$ ) between glassy and rubbery states
$C_{p(\text{liquid})}/C_{p(\text{glass})}$ of fragile systems is less than 1.1	$C_{p(\text{liquid})}/C_{p(\text{glass})}$ of fragile systems is greater than 1.1
Fragility index ( $m$ ) value between 16 and 100	Fragility index ( $m$ ) value between 100 and 200

relaxation during the aging time ( $t$ ), respectively;  $\Delta C_p$  is a heat capacity change at the glass transition temperature ( $T_g$ ) and aging temperature ( $T_a$ ).

The fragility concept was introduced by Angell (1985), which has practical implications in predicting the physical and chemical stability of foods. The fragility concept differentiates the amorphous systems as being either strong or fragile, based on the temperature dependency of dynamic properties, structural changes, and relaxation behavior near or above  $T_g$ . Differences between fragile and strong systems are presented in Table 1. A fragility index ( $m$ ) was introduced to better quantify the fragility concept (Angell 1985). The fragility index is defined as:

$$m = \frac{\Delta E}{2.303RT_g} \quad (4)$$

where  $\Delta E$  is the activation energy for structural relaxations at  $T_g$ , and  $R$  is the gas constant.

The objective of this study was to investigate the effects of molecular weight on enthalpy relaxation and the fragility of amorphous carbohydrates. Anhydrous glucose, maltose, and maltotriose were chosen to characterize amorphous carbohydrates with increasing molecular weight.

## 2 Materials and Methods

Anhydrous glucose, maltose, and maltotriose were purchased from Fisher Scientific (Pittsburg, PA). Glucose, maltose, and maltotriose solutions were prepared by dissolving them in distilled water (10 g carbohydrates/100 g water). The carbohydrate solutions were dried in a laboratory freeze dryer (VirTis Freeze Mobile 24 with Unitop 600L, Virtis SP Industries Co., New York). Initially the carbohydrate solutions were frozen to –35 °C. The frozen carbohydrate solutions were transferred to a freeze dryer shelf maintained at –25 °C. The shelf temperature was increased to 20 °C with a vacuum of 20 Pa and condenser temperature at –60 °C. After 48 h of freeze drying, glucose, maltose, and maltotriose were kept in a

desiccator with  $P_2O_5$  at room temperature (298 K) for 2 days. The moisture content of dry amorphous carbohydrates was analyzed using the vacuum oven method ( $\sim 0.005$  kg H<sub>2</sub>O/kg sample).

## 2.1 Differential Scanning Calorimetry (DSC)

Enthalpy relaxation experiments were conducted using a modulated differential scanning calorimeter (MDSC) (Q2000, TA Instruments, New Castle, DE) using nitrogen as the purge gas at a rate of 50 mL/min. The selected modulation amplitude and modulation period were  $\pm 0.5$  °C and 45 s, respectively (Lammert et al. 1999). In  $T_g$  identification experiments, small amounts (10–20 mg) of freeze-dried glucose, maltose, and maltotriose were first scanned between  $T_{gi} - 50$  and  $T_{gi} + 100$  (above their melting temperatures). The carbohydrates were cooled back to  $T_{gi} - 50$  to make carbohydrate glasses. Further, in the second scan, the carbohydrates were heated above the respective melting points of the selected carbohydrates ( $\sim T_{gi} + 100$ ) and then cooled back to 25 °C.  $T_{gi}$  was identified as the temperature equivalent to the intersection of the regression line before the step change in the reversible heat flow curve and inflection tangent of MDSC thermogram during the second scan (Fig. 2). Similarly,  $T_{ge}$  was identified as the intersection of the tangent after the step change in the reversible heat flow curve and inflection tangent of MDSC thermogram.  $T_{gm}$  was assigned as the mid temperature between  $T_{gi}$  and  $T_{ge}$ , corresponding to 50 % transition (Fig. 2). The temperature selected for aging of glucose, maltose, and maltotriose was 5 °C below their respective  $T_{gi}$ , since maximum enthalpy relaxation is found near  $T_g$  (Fig. 1). For aging experiments, the carbohydrates were aged/annealed isothermally at ( $T_{gi} - 5$ ) for selected periods of time (0.5–48 h) during the second scan. After aging, the carbohydrates were cooled back to  $T_{gi} - 50$  and further heated to  $T_{gi} + 100$  and then cooled back to 25 °C. The enthalpy recovered during reheating was determined by drawing a linear baseline to the enthalpy endotherm in the nonreversible heat flow curve of MDSC thermogram during the third scan (Fig. 2). In the nonreversible heat flow thermogram of an unaged sample, an endotherm attributable to the frequency effect appears (Wang and Pikal 2010). To determine the enthalpy corresponding to the frequency effect, the unaged carbohydrates were heated to  $T_{gi} + 100$  (above their melting temperatures) and then cooled back to  $T_{gi} - 50$ . Furthermore, in the second scan, the carbohydrates were heated to  $T_{gi} + 100$  and then cooled back to 25 °C. The enthalpy corresponding to the frequency effect was determined by drawing a linear baseline to the enthalpy endotherm in the nonreversible heat flow curve of MDSC thermogram similar to the aged carbohydrates. The actual enthalpy recovered during the aging process is obtained by subtracting the frequency effect from the enthalpy in the nonreversible heat flow thermogram of aged sample (Wang and Pikal 2010). Enthalpy relaxation data were fitted with the KWW equation using Statistica® version 5 to obtain the values of characteristic  $\tau$  and  $\beta$ . Fragility indices ( $m$ ) of glucose, maltose, and maltotriose were determined by the glass transition

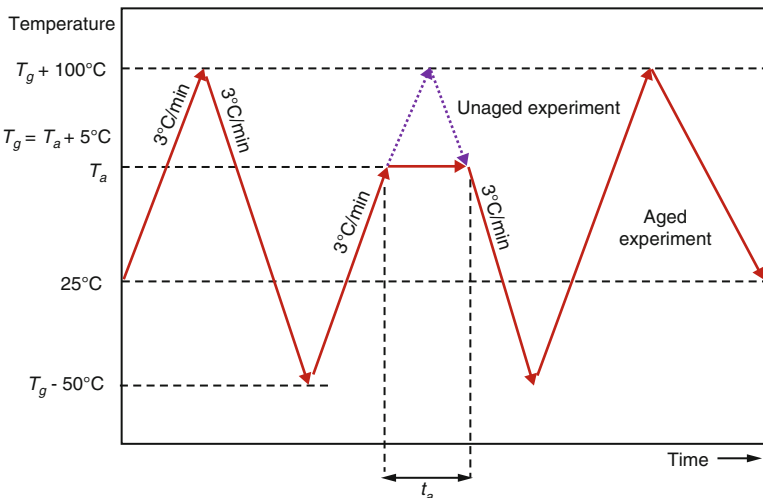


**Fig. 1** Enthalpy relaxation experimental protocol for amorphous carbohydrates. *Aged experiment*: Glucose, maltose, and maltotriose were scanned above the respective melting points of the selected carbohydrates ( $\sim T_g + 100^\circ\text{C}$ ) to remove their thermal history after equilibration at  $25^\circ\text{C}$  for 5 min. Then the carbohydrates were scanned to ( $T_{gi} - 50$ ) at  $3^\circ\text{C}/\text{min}$  to make a carbohydrate glass. The carbohydrates were scanned to ( $T_{gi} - 5$ ) and annealed isothermally at ( $T_{gi} - 5$ ) for selected periods of time (0.5–48 h). After aging, samples were cooled to ( $T_{gi} - 50$ ). After equilibrating the carbohydrates for 1 min, they were reheated to ( $T_{gi} + 50$ ) at a rate of  $3^\circ\text{C}/\text{min}$ . *Unaged experiment*: Glucose, maltose, and maltotriose were scanned above the respective melting points of the selected carbohydrates ( $T_g + 100^\circ\text{C}$ ) to remove their thermal history after equilibration at  $25^\circ\text{C}$  for 5 min. Then the carbohydrates were scanned to ( $T_{gi} - 50$ ) at  $3^\circ\text{C}/\text{min}$  to make a carbohydrate glass. Then the samples were reheated to ( $T_{gi} + 50$ ) at a rate of  $3^\circ\text{C}/\text{min}$

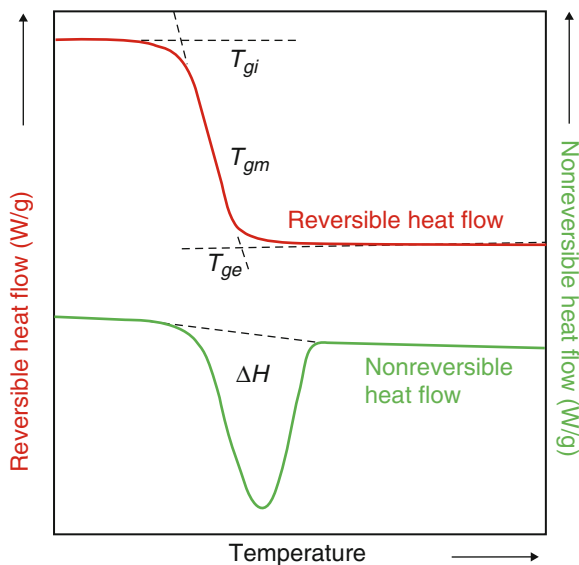
width approach by identifying the onset ( $T_{gi}$ ), end point glass transition temperatures ( $T_{ge}$ ), and  $\Delta C_p$ .

The fragility of amorphous carbohydrates was determined by calculating the activation enthalpy of structural relaxation (Moynihan 1993). Activation enthalpy and glass transition width are related by:

$$\left(\frac{\Delta E}{R}\right)\left(\frac{1}{T_{gi}} - \frac{1}{T_{ge}}\right) = \text{Constant} \quad (5)$$

where  $\Delta E$  is the activation energy for structural relaxations at the glass transition temperature and  $T_{gi}$  and  $T_{ge}$  are the onset and end point glass transition temperatures. By studying several material systems, the constant in the Eq. (5) was identified as  $5 \pm 0.5$ . In the current study, the value of the constant was selected as 5. The activation enthalpy and fragility index ( $m$ ) are related in Eq. (5) (Crowley and Zografi 2001).

**Fig. 2** Identification of onset and end point glass transition temperatures ( $T_{gi}$ , and  $T_{ge}$  respectively) and enthalpy recovered ( $\Delta H$ ) using an MDSC thermogram



Statistical significance of the results was analyzed using SAS 9.1 (SAS Institute, Inc., Cary, NC, USA). A value of  $P \leq 0.05$  was selected as statistically significant using the least square difference (LSD) method.

### 3 Results and Discussion

#### 3.1 Glass Transition Temperature vs. Aging Conditions

Molecular weights of glucose, maltose, and maltotriose were 180 g/mol, 342 g/mol, and 504 g/mol, respectively. The obtained  $T_{gi}$  of unaged glucose, maltose, and maltotriose was  $34.5 \pm 0.20$  °C,  $78.5 \pm 1.75$  °C, and  $128.8 \pm 4.13$  °C, respectively. Generally, no significant difference was observed between the  $T_{gi}$  of unaged and aged carbohydrates, with the exception of maltotriose (Table 2). Wungtanagorn and Schmidt (2001) mentioned that the increase or decrease of  $T_g$  with aging time is dependent on the method used in the assignment of  $T_g$ . No statistically significant difference in  $T_{gi}$  was observed for glucose aged for selected aging periods (0–48 h). Significant difference in  $T_{gi}$  was observed between maltose aged for 12 and 48 h (Table 2). The  $T_{gi}$  of maltotriose aged for 48 h was significantly different from maltotriose aged for 0.5–12 h (Table 2). During the determination of  $T_{gi}$ , carbohydrates were heated above their melting points using MDSC, which could result in thermal decomposition, thus influencing  $T_{gi}$  values (Lee et al. 2011a, b). Glass transition temperature width ( $T_{ge} - T_{gi}$ ) of glucose did not change significantly during isothermal aging at  $(T_{gi} - 5)$  for 0.5–48 h (Table 2). The  $(T_{ge} - T_{gi})$  of

**Table 2** Onset ( $T_{gi}$ ) glass transition temperatures of glucose, maltose, and maltotriose aged at ( $T_{gi} - 5$ ) for selected times

Time $t$ , (h)	Glucose		Maltose		Maltotriose	
	$T_{gi}$ (°C)	$(T_{ge} - T_{gi})$ (°C)	$T_{gi}$ (°C)	$(T_{ge} - T_{gi})$ (°C)	$T_{gi}$ (°C)	$(T_{ge} - T_{gi})$ (°C)
0	34.5 <sup>e</sup> (0.20)*	6.3 <sup>h,i</sup> (0.29)	78.5 <sup>c,d</sup> (1.75)	10.2 <sup>g,h</sup> (1.18)	128.8 <sup>a</sup> (4.13)	11.4 <sup>f,g,h</sup> (3.09)
0.5	36.5 <sup>e</sup> (0.50)	5.0 <sup>i</sup> (0.14)	76.8 <sup>c,d</sup> (4.90)	9.2 <sup>g,h,i</sup> (0.59)	131.7 <sup>a</sup> (0.14)	7.7 <sup>h,i</sup> (0.71)
1	36.2 <sup>e</sup> (0.35)	4.6 <sup>i</sup> (0.23)	76.3 <sup>c,d</sup> (3.70)	10.2 <sup>g,h</sup> (2.52)	131.6 <sup>a</sup> (4.51)	7.8 <sup>h,i</sup> (1.13)
2	36.3 <sup>e</sup> (0.07)	5.0 <sup>i</sup> (0.06)	79.1 <sup>c,d</sup> (1.90)	8.1 <sup>h,i</sup> (0.13)	133.4 <sup>a</sup> (1.47)	6.3 <sup>h,i</sup> (0.35)
6	36.4 <sup>e</sup> (0.07)	4.9 <sup>i</sup> (0.05)	76.0 <sup>c,d</sup> (2.60)	11.0 <sup>f,g,h</sup> (0.25)	132.4 <sup>a</sup> (4.20)	7.9 <sup>h,i</sup> (0)
12	36.6 <sup>e</sup> (0)	5.1 <sup>i</sup> (0)	81.6 <sup>c</sup> (0)	9.8 <sup>g,h,i</sup> (0.42)	132.7 <sup>a</sup> (3.79)	8.1 <sup>h,i</sup> (0)
48	36.1 <sup>e</sup> (0)	5.2 <sup>i</sup> (0)	72.7 <sup>d</sup> (0)	13.8 <sup>f,g</sup> (0)	113.7 <sup>b</sup> (0)	15.4 <sup>f</sup> (0)

Same superscripts within a column indicate there is no significant difference ( $P \geq 0.05$ ) in values

\*Values in parentheses represent the standard deviation of at least two replicates

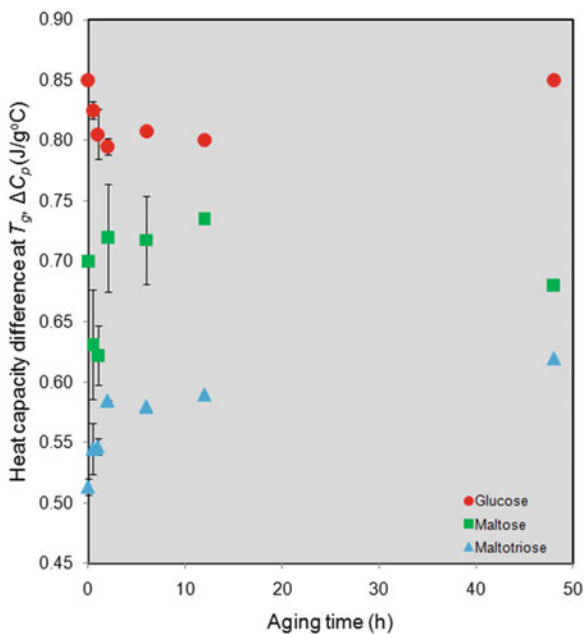
unaged glucose was significantly different from aged glucose (0.5–48 h). The ( $T_{ge} - T_{gi}$ ) of 2 h aged maltose was significantly different from maltotriose and glucose (Table 2). The ( $T_{ge} - T_{gi}$ ) of maltotriose aged for 48 h was significantly different from maltose and glucose of aged maltotriose (Table 2).

The heat capacity change ( $\Delta C_p$ ) at  $T_g$  of glucose, maltose, and maltotriose was measured as the difference in  $C_p$  values between glassy and rubbery states in the MDSC thermogram. The heat capacity change ( $\Delta C_p$ ) at  $T_g$  of maltotriose was less than that of other selected carbohydrates, which can be attributed to its higher chain rigidity and molecular weight (McGonigle et al. 2005) (Fig. 3). A slight increase in  $\Delta C_p$  at  $T_g$  with aging time was observed for maltose and maltotriose, while a fluctuating trend in  $\Delta C_p$  was observed for glucose (Fig. 3). Since the equilibrium state has a smaller heat capacity and free energy compared to glassy and rubbery states, an increase in  $\Delta C_p$  is expected after aging (Chung and Lim 2003). In the current study, the difference in the trends in  $\Delta C_p$  with aging time could be due to thermal decomposition resulting from heating the carbohydrates above their melting points using the MDSC (Lee et al. 2011a, b).

### 3.2 Molecular Weight Dependence of Enthalpy Relaxation Time

Total enthalpy decreased, while relaxed enthalpy increased with increasing aging time for glucose, maltose, and maltotriose (Fig. 4). The rate of enthalpy relaxation

**Fig. 3** Variation in specific heat at glass transition temperature ( $\Delta C_p$ ) for selected aging times during aging of glucose, maltose, and maltotriose at ( $T_g - 5$ )

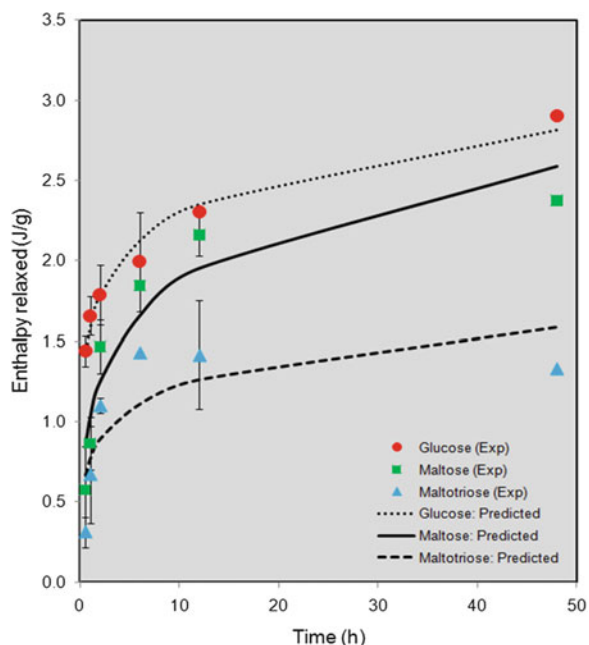


of selected carbohydrates decreased gradually during aging due to the decrease in total enthalpy during aging (Fig. 4). The relaxed enthalpy was greater for glucose than maltose and maltotriose during aging (Fig. 4), which can be attributed to its smaller molecular weight and higher specific volume and resulting smaller chain rigidity (McGonigle et al. 2005). The relaxation enthalpies of maltotriose were much smaller than the relaxation enthalpies of glucose and maltose. Hence, maltotriose may be preferably used in food formulations to reduce structural relaxation during storage.

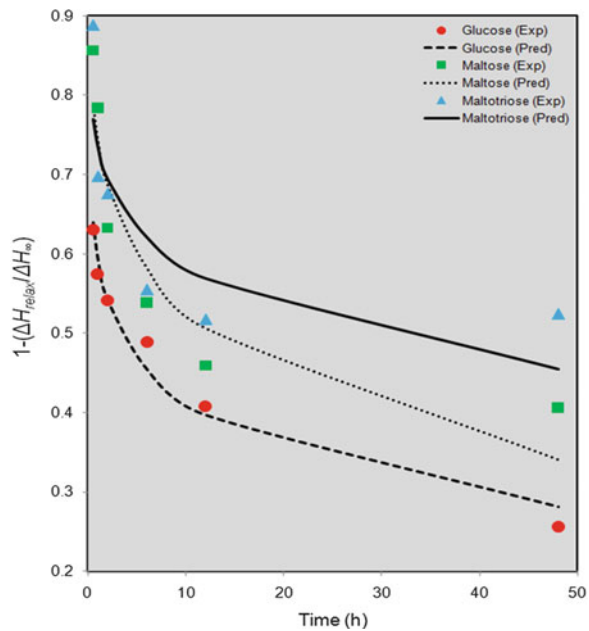
The KWW equation was used to fit the enthalpy relaxation kinetics of the selected amorphous carbohydrates; KWW adjustable parameters are presented in Fig. 5 and Table 3. An exponential relationship between  $\tau$  values and molecular weight of the selected amorphous carbohydrates was obtained (Fig. 6). The larger  $\tau$  value for maltotriose could be attributed to its smaller specific volume, resulting in more restriction of its relaxing elements during aging. The molecular mobility of glassy maltotriose might be smaller than the molecular mobility of glucose and maltose at a specific aging temperature. Based on the  $\tau$  value, maltotriose could be preferable in food formulations in comparison with glucose and maltose. By studying the enthalpy relaxation behavior of different molecular weight carbohydrates, a database of enthalpy relaxation in relation to molecular weight can be developed.

The parameter  $\beta$  characterizes the deviation of the relaxation from exponential behavior. The value of  $\beta$  varies between 0 and 1 (Christensen et al. 2002). When

**Fig. 4** Amount of relaxation enthalpy after aging of glucose, maltose, and maltotriose at ( $T_g - 5$ ) for selected aging times

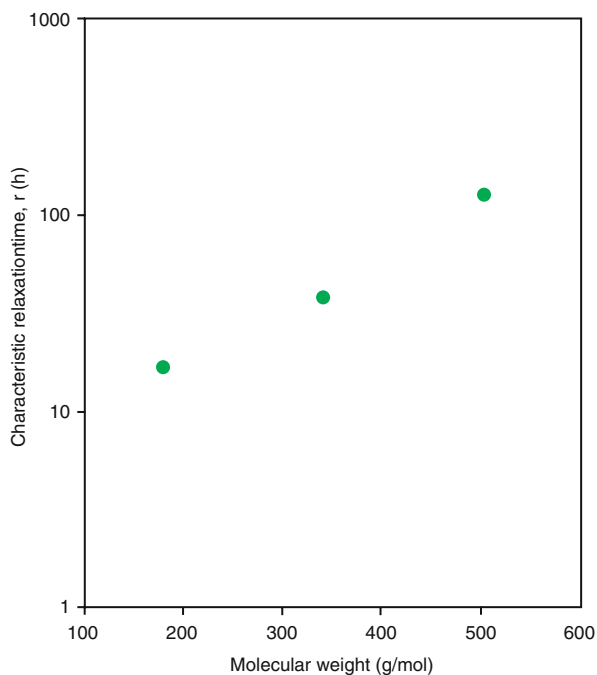


**Fig. 5** Variation of  $(1 - \Delta H_{\text{relax}}/\Delta H_\infty)$  for selected aging times during aging of glucose, maltose, and maltotriose at ( $T_{gi} - 5$ )



**Table 3** Experimental values of  $\Delta H_\infty$ ,  $\tau$ ,  $\beta$ ,  $\tau_{\varphi(t)=50\%}$ , and  $\tau_{\varphi(t)=1\%}$  calculated for glucose, maltose, and maltotriose

Amorphous system	KWW equation				
	Total enthalpy available for relaxation, $\Delta H_\infty$ (J/g)	Characteristic relaxation time, $\tau$ (h)	Relaxation distribution parameter, $\beta$	Relaxation time corresponding to 50 % of the maximum enthalpy, $\tau_{\varphi(t)=50\%}$ (h)	Relaxation time corresponding to 99 % of the maximum enthalpy, $\tau_{\varphi(t)=1\%}$ (h)
Glucose	3.94	16.9	0.23	50.9	338.4
Maltose	3.23	38.4	0.33	80.7	535.9
Maltotriose	2.54	128.6	0.24	371.4	2,467.6

**Fig. 6** Characteristic relaxation time ( $\tau$ ) dependence on molecular weight of glucose, maltose, and maltotriose during isothermal aging at ( $T_{gi} - 5$ )

$\beta = 1$ , the KWW equation is equivalent to an exponential expression. In the current study,  $\beta$  values obtained for glucose, maltose, and maltotriose were 0.23, 0.33, and 0.24, respectively. A  $\beta$  value much smaller than 1 shows the nonexponentiality and broad distribution of the enthalpy relaxations (Liu et al. 2006). The relaxation times present an abrupt change at the glass transition, when the  $\beta$  value is close to 1 (Liu et al. 2006). The  $\beta$  value obtained for glucose is smaller than that of raspberry powder. Smaller values of  $\beta$  represent hydrogen bonding and coupling between relaxing elements of the studied carbohydrates (Arrighi et al. 2005). The value of

$\Delta H_\infty$  decreased with molecular weight for the selected carbohydrates (Table 3). The greater  $\Delta H_\infty$  of glucose is attributed to its higher  $\Delta C_p$  at  $T_g$ . Relaxation time corresponding to 50 % of the maximum enthalpy ( $\tau_{\varphi(t)=50\%}$ ) and 99 % of the maximum enthalpy ( $\tau_{\varphi(t)=99\%}$ ) during the aging process is determined at ( $T_{gi} - 5$ ) from  $\tau$  and  $\beta$  values (Liu et al. 2007). The  $\tau_{\varphi(t)=50\%}$  values were 50.9 h, 80.7 h, and 371.4 h, while  $\tau_{\varphi(t)=99\%}$  values were 338.4 h, 535.9 h, and 2,467.6 h for glucose, maltose, and maltotriose, respectively.

### 3.3 Fragility of Amorphous Carbohydrates

Fragility of an amorphous system shows variations in specific properties at  $T_{gi}$ . Using Eq. (5), the activation enthalpy of structural relaxations ( $\Delta E$ ) of glucose, maltose, and maltotriose at the glass transition temperature was 692.8 kJ/mol, 593.2 kJ/mol, and 750.9 kJ/mol, respectively. Fragility indices ( $m$ ) of glucose, maltose, and maltotriose determined using the glass transition width approaches were 105, 88.1, and 97.6, respectively (Table 4). The  $m$  values of the selected amorphous carbohydrates indicate the fragile behavior of glucose, while maltose and maltotriose are comparatively stronger in nature. No linear relationship between  $m$  values and molecular weights of the amorphous carbohydrates was observed. Maltose and maltotriose exhibited similar, but higher, glass transition widths ( $T_{ge} - T_{gi}$ ) than glucose. Further, the  $\Delta E$  of maltose was smaller than the  $\Delta E$  of maltotriose calculated using Eq. (5). Hence, the  $m$  of maltose was smaller than the  $m$  of maltotriose and glucose.

The ratio of the heat capacity of a material system in the rubbery state to the heat capacity of the material system in the glassy state ( $C_{p(\text{liquid})}/C_{p(\text{glass})}$ ) of glucose, maltose, and maltotriose, 2.21, 1.65, and 1.24 (Table 4), respectively indicates the fragile behavior of selected amorphous carbohydrates. The fragility of the selected carbohydrates increased as molecular weight increased with regard to the  $C_{p(\text{liquid})}/$

**Table 4** Fragility prediction for selected amorphous carbohydrates by selected methods

Amorphous system	Fragility parameter ( $m$ ) using activation enthalpy at glass transition temperature	Fragility prediction based on $m$ value	* $C_{p(\text{liquid})}/C_{p(\text{glass})}$	Fragility prediction based on $C_{p(\text{liquid})}/C_{p(\text{glass})}$ value
Unaged Glucose	105	Fragile <sup>a</sup>	2.21	Fragile <sup>b</sup>
Unaged Maltose	88.1	Strong <sup>a</sup>	1.65	Fragile <sup>b</sup>
Unaged Maltotriose	97.6	Strong <sup>a</sup>	1.24	Fragile <sup>b</sup>

<sup>a</sup>Strong systems:  $16 < m < 100$ ; Fragile systems:  $100 < m < 200$

<sup>b</sup>Strong systems:  $C_{p(\text{liquid})}/C_{p(\text{glass})} < 1.1$ ; Fragile systems:  $C_{p(\text{liquid})}/C_{p(\text{glass})} > 1.1$

\*Ratio of heat capacity of material system in the rubbery state to heat capacity of the material system in the glassy state

$C_{p(\text{glass})}$  ratio (Table 4). Glucose, maltose, and maltotriose exhibited a small  $\Delta C_p$  at  $T_g$  and are categorized as fragile. A greater  $\Delta C_p$  at  $T_g$  for maltotriose demonstrates its stronger nature in comparison to glucose and fructose. One possible explanation for this discrepancy in the fragility of glucose, maltose, and maltotriose could be the thermal decomposition of carbohydrates to smaller components resulting by heating them above their melting points, which may have influenced the fragility determination (Lee et al. 2011a, b). Previous literature presents inconsistencies in fragility predictions by different methods for various systems. No clear explanation is available for the difference in fragility predictions by different methods (Wungtanagorn and Schmidt 2001). Thus, more research is required for clarification of this discrepancy.

The physical, chemical, and structural stability of amorphous food systems is related to their fragility, as this will provide information on the variation in dynamic properties and relaxation times of amorphous systems near or above  $T_g$  (Hancock et al. 1995). Above  $T_g$ , strong systems exhibit greater relaxation times, while below  $T_g$  a reversal of dynamic properties and relaxation times occurs (Mao et al. 2010). Many physicochemical degradation reactions can be controlled by molecular mobility/relaxations in food systems where relaxation times provide useful information on the rates of these reactions. By relating fragility to the relaxation times, the temperature dependence of relaxations and thereby the rates of degradation reactions in amorphous systems can be predicted (Hatley 1997). For instance, the rate of molecular mobility of fragile systems is changed by approximately one order of magnitude for every 10 °C difference in temperature, whereas in strong systems, the rate of molecular mobility changes approximately every 25 °C (Hancock et al. 1995). Hatley (1997) reported that fragile systems may be preferable in their glassy state, since dynamic properties such as viscosity increase rapidly with small decreases in storage temperature, which could increase the stability of glassy systems.

The enthalpy relaxation data of the current study can be used to predict the enthalpy relaxation behavior of selected amorphous carbohydrates with molecular weight between glucose and maltotriose. Also, the estimated relaxation times can be used to predict the physicochemical stability of amorphous carbohydrates, which could also reduce the cost and time of complex experiments. However, a relationship between relaxation times and rates of physicochemical degradation reactions should be established for such a comparison (Miller and Lechuga-Ballesteros 2006). Thus, enthalpy relaxation time and fragility information obtained may be used to predict various physicochemical changes in selected carbohydrates during their long-term glassy state storage.

## 4 Conclusions

Maltotriose exhibited greater glass transition temperature and characteristic enthalpy relaxation time than glucose and maltose. As molecular weight increased, relaxation enthalpy decreased, while characteristic relaxation time increased for

glucose, maltose, and maltotriose. The enthalpy relaxation data of glucose, maltose, and maltotriose might be used to predict the enthalpy relaxation behavior of specific molecular weight materials. The fragility indices ( $m$ ) determined using the glass transition width approach presented fragile behavior for glucose, while maltose and maltotriose were comparatively stronger in nature. A discrepancy in the prediction of fragility of selected amorphous carbohydrates was observed in the research and requires further study.

## References

- Angell CA (1985) Spectroscopy simulation and scattering, and the medium range order problem in glass. *J Non Cryst Solids* 73:1–17
- Arrighi V, Cowie JMG, Ferguson R, McEwen IJ, McGonigle EA, Pethrick RA, Princi E (2005) Physical aging in poly(4-hydroxy styrene)/poly(vinyl methyl ether) blends. *Polym Int* 55:749–756
- Christensen KL, Pedersen GP, Kristensen HG (2002) Physical stability of redispersible dry emulsions containing amorphous sucrose. *Eur J Pharm Biopharm* 53(2):147–153
- Chung HJ, Lim ST (2003) Physical aging of glassy normal and waxy rice starches: effect of aging time on glass transition and enthalpy relaxation. *Food Hydrocoll* 17(6):855–861
- Crowley KJ, Zografi G (2001) The use of thermal methods for predicting glass former fragility. *Thermochim Acta* 380(2):79–93
- Farahnaky A, Guerrero A, Hill SE, Mitchell JR (2008) Physical aging of cray fish flour at low moisture contents. *J Therm Anal Calorim* 93(2):595–598
- Gupta P, Kakumanu VK, Bansal AK (2004) Stability and solubility of Celecoxib-PVP amorphous dispersions: a molecular perspective. *Pharm Res* 21(10):1762–1969
- Hancock BC, Shamblin SL, Zografi G (1995) Molecular mobility of amorphous pharmaceutical solids below their glass transition temperatures. *Pharm Res* 12(6):799–806
- Hatley RHM (1997) Glass fragility and stability of pharmaceutical preparations-Excipient selection. *Pharm Dev Tech* 2(3):257–264
- Lammert AM, Lammert RM, Schmidt SJ (1999) Physical aging of maltose glasses as measured by standard and modulated differential scanning calorimetry. *J Therm Anal Calorim* 55:949–975
- Lee JW, Thomas LC, Jerrell J, Feng H, Cadwallader KR, Schmidt SJ (2011a) Investigation of thermal decomposition as the kinetic process that causes the loss of crystalline structure in sucrose using a chemical analysis approach (Part II). *J Agric Food Chem* 59:702–712
- Lee JW, Thomas LC, Schmidt SJ (2011b) Investigation of the heating rate dependency associated with the loss of crystalline structure in sucrose, glucose and fructose using a thermal analysis approach (Part I). *J Agric Food Chem* 59:684–701
- Liu YT, Bhandari B, Zhou WB (2006) Glass transition and enthalpy relaxation of amorphous food saccharides: a review. *J Agric Food Chem* 54(16):5701–5717
- Liu Y, Bhandari B, Zhou W (2007) Study of glass transition and enthalpy relaxation of mixtures of amorphous sucrose and amorphous tapioca starch syrup solid by differential scanning calorimetry (DSC). *J Food Eng* 81:599–610
- Mao C, Chamarth SP, Byrn SR, Pinal R (2010) Theoretical and experimental considerations on the enthalpic relaxation of organic glasses using differential scanning calorimetry. *J Phys Chem* 114:268–279
- McGonigle EA, Cowie JMG, Arrighi V, Pethrick RA (2005) Enthalpy relaxation and free volume changes in aged styrene copolymers containing hydrogen bonding co-monomer. *J Mater Sci* 40:1869–1881

- Miller DP, Lechuga-Ballesteros D (2006) Rapid assessment of the structural relaxation behavior of amorphous pharmaceutical solids: effect of residual water on molecular mobility. *Pharm Res* 23(10):2291–2305
- Moynihan CT (1993) Correlation between the width of glass transition region and the temperature dependence of the viscosity of high-T<sub>g</sub> glasses. *J Am Ceram Soc* 76(5):1081–1087
- Struik LCE (1978) Physical aging in amorphous polymers and other materials. Elsevier Scientific Pub, Co., Amsterdam
- Wang B, Pikal M (2010) The impact of thermal treatment on the stability of freeze-dried amorphous pharmaceuticals: I. Dimer formation in sodium ethacrycate. *J Pharm Sci* 99 (2):663–682
- Wungtanagorn R, Schmidt SJ (2001) Phenomenological study of enthalpy relaxation of amorphous glucose, fructose, and their mixture. *Thermochim Acta* 369:95–116

# **Effect of Dehydration Conditions on the Bulk and Surface Properties of the Resulting Dehydrated Products**

**Y. Zhang and M.T. Carvajal**

## **Abbreviations**

DSC	Differential scanning calorimetry
ETD	Everhart-Thornley detector
SEM	Scanning electronic microscopy
TLD	Through-the-lens detectors
TSPC	Thermally stimulated polarized current
XRPD	X-ray powder diffraction

## **1 Introduction**

The ability to control the transformation of hydrate/anhydrate of materials, whether a drug compound or food ingredient, during processing is a very important phenomenon in the pharmaceutical and food industries, since this transformation could change both the physical and chemical properties of materials, such as dissolution rate, dispersibility, bioavailability, density, and chemical stability, to mention a few (Khankari and Grant 1995; Makoto et al. 2001; Suzanne et al. 1998). In addition, the hydrated-dehydrated material is affected by the microenvironment of the various unit operations during manufacturing, where water is involved and may be absorbed or released into the system (Mirza et al. 2007), depending on the integrity of the material.

---

Y. Zhang • M.T. Carvajal (✉)

Industrial and Physical Pharmacy and Agricultural and Biological Engineering,  
Purdue University, West Lafayette, IN 47907, USA  
e-mail: [tcarvaja@purdue.edu](mailto:tcarvaja@purdue.edu)

Hydrate is usually a thermodynamic unstable state which experiences dehydration during the manufacturing process, as well as in storage. Studies on the effect of environmental conditions on the process of dehydration, as well as the physical/chemical properties of the resulting anhydrous material, have been reported. It is known that dehydration is usually accompanied by the loss of crystal structure in the material, followed by recrystallization to the anhydrate (Galwey 2000; Murphy et al. 2002). Han and Suryanarayanan (1998) studied the effect of temperature and water vapor pressure on the kinetics and mechanism of dehydration. Kishi et al. (2002) investigated the effect of humidity on dehydration products and found that storage at different humidity may result in a hydrate with different crystal forms. Yamauchi et al. (2011) were among the first to report an insight into the bulk and surface properties of anhydrated and dehydrated hydrate forms. Since surface properties of the resulting dehydrated particles are important in controlling stability, understanding the relationship between the dehydration condition and the surface (morphology and surface energy) is the focus of the work presented herein. Thymine, theophylline, and cytosine (hydrated and dehydrated) were used in this study.

## 2 Materials and Methods

### 2.1 Materials

Crystalline thymine, theophylline, and cytosine were purchased from Sigma (St. Louis, MO). The crystallinity of these materials was assumed to be 100 %.

### 2.2 Preparation of the Hydrate, Dehydrated, and Anhydrous Forms

About 1 g anhydrous compound was dissolved in 20 ml water at 60 °C to prepare a saturated solution. The saturated solution was cooled to 0 °C to facilitate recrystallization. The resulting crystals were harvested and filtered with filter paper (Waterman, No. 4). The filtrate was moved to a 20 ml glass vial covered with aluminum foil with three holes about 1 mm in diameter. The vial was left undisturbed in a fume hood in order to facilitate the evaporation of water residue.

#### Dehydration:

Two dehydrated forms were prepared by heating the hydrate form to 60 °C and 140 °C for 24 h and 1 h, respectively.

### ***2.3 Preparation of Anhydrous Form***

About 1.5 g anhydrous compound was dissolved in 20 ml water at 40 °C to prepare the saturated solution. The saturated solution was cooled to 0 °C and recrystallization occurred. The resulting crystals were harvested and filtered with filter paper (Waterman, No. 4). The filtrate was moved to another 20 ml glass vial covered with aluminum foil with three holes of about 1 mm in diameter. The vial was left undisturbed in a fume hood in order to facilitate the evaporation of solvent residue.

### ***2.4 X-ray Powder Diffraction (XRPD)***

X-ray powder diffraction (XRPD) patterns were carried out on a Bruker D5000 diffractometer (Bruker AXS Inc., Madison, WI) using copper radiation. The tube voltage and amperage were set to 40 kV and 40 mA, respectively. The divergence and scattering slits were set at 1 mm, and the receiving slit was set at 0.6 mm. Diffracted radiation was detected by a Kevex PSI detector. A theta-two theta continuous scan at 2.4°/min (1 s/0.04° step) from 3.0 to 40° 2θ was used. An alumina standard was analyzed to check the instrument alignment. Data were collected and analyzed using Bruker axis software Version 7.0. Samples were prepared by placing them in a quartz holder.

### ***2.5 Differential Scanning Calorimetry (DSC)***

TA Q1000 DSC (TA instruments, New Castle, DE) was used for thermal studies up to the melting point. Approximately 5 mg of sample was placed in the pan and covered with a lid, and then a hole manually was punctured in the center. The samples were analyzed from 0 to 50 °C above the melting point of the sample at a rate of 10 °C/min. The experiments took place under nitrogen at a flow rate of 20 mL/min.

### ***2.6 Scanning Electronic Microscopy (SEM)***

Samples were sprinkled onto sample holders covered with double-coated transparent adhesive tape. Excess was blown off and the samples were coated with Pt (60 s) prior to imaging.

Samples were imaged with FEI Nova nanoSEM field emission SEM (FEI Company, Hillsboro, OR) using Everhart-Thornley (ETD) or high-resolution through-the-lens (TLD) detectors. Parameters were 5 kV accelerating voltage,

~4.5 mm working distance, spot 3, and 30  $\mu\text{m}$  aperture. Magnifications were 1–40 K and are accurate as indicated when the images were displayed in a 30  $\times$  26 cm format. The micron bar was accurate at any display size.

### 3 Results and Discussion

The hydrates of theophylline and cytosine were heated at 60 °C and 140 °C, respectively, and the dehydrated products were tested for any changes in the structure.

Figures 1 and 2 show the XRPD patterns of the anhydrate products of theophylline and cytosine, respectively. The XRPD results revealed that for each compound, the samples prepared under different heating temperatures had very similar patterns, indicating mostly identical crystal structures.

The melting point of the dehydrated forms of cytosine, theophylline, and thymine prepared under 60 and 140 °C was determined by DSC (Fig. 3). The onset and peak temperatures of the melt were measured and are summarized in Tables 1, 2, and 3. It can be seen that by dehydrating at different temperatures, there was a shift in the melting temperature. Specifically, the high dehydration temperature on cytosine showed higher impact on the melting of the resulting sample. Similarly, for theophylline, the sample dehydrated at 140 °C had higher melting than that processed under 60 °C, although this trend was not obvious using the onset point of melting peak. On the other hand, the dehydration temperature on the thymine samples showed an opposite effect on melting. This melting temperature slightly decreased with increased dehydration temperature, in contrast to the trend observed in cytosine and theophylline.

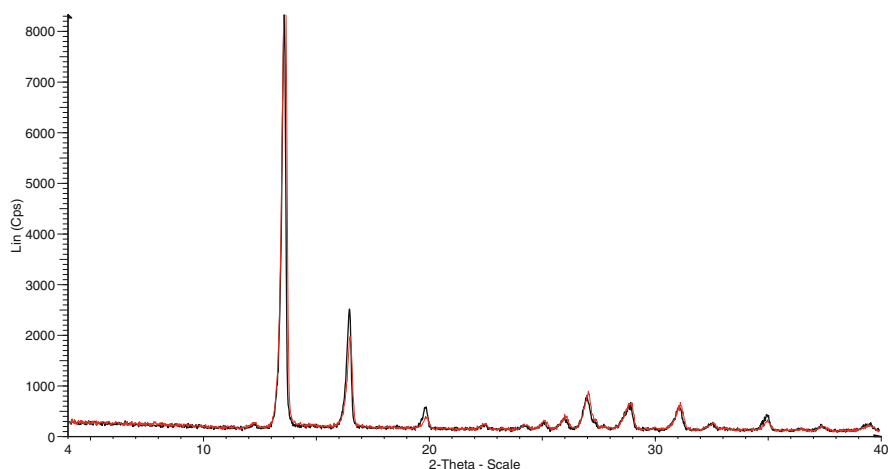


**Fig. 1** Anhydrate cytosine forms prepared under 60 °C (black line) and 140 °C (red line)

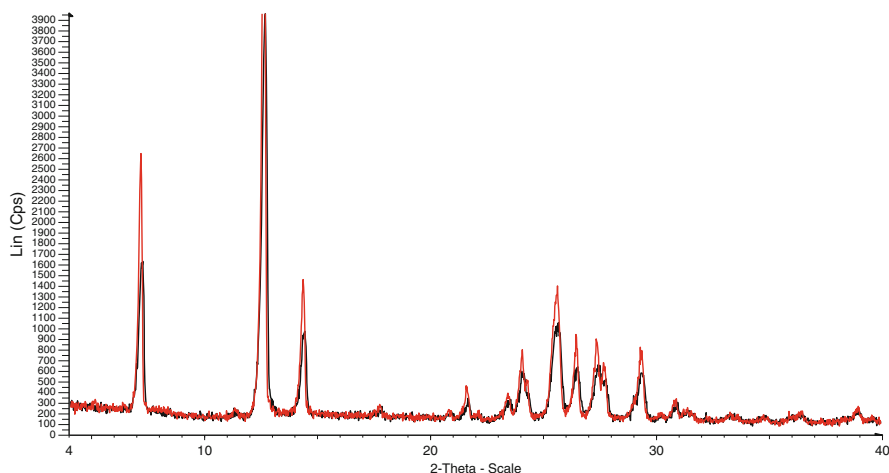


**Fig. 2** Anhydrate theophylline forms prepared under 60 °C (black line) and 140 °C (red line)

The morphology of dehydrated forms were also observed using SEM. Figure 4 shows the surface and cross section of the cytosine crystals of the resulting dehydrated forms from the two temperatures. It can be seen that the surface of crystals made under 140 °C is slightly rougher than those made under 60 °C. The morphologies of the cross section from both are very similar.

Figure 5 shows the surface and cross section of the theophylline crystals for the two dehydrated forms. The SEM pictures show that dehydration at a 140 °C produced smaller crystals along an axial of the crystal lattice from the original hydrate crystals. This phenomenon could be explained that since the theophylline hydrate is a tunnel hydrate, therefore, when water molecules leave the crystal, voids are left in the tunnel. These voids could collapse by further heating; the original large needle crystals then become smaller needle crystals along the tunnel. Also, it can be observed that the surface of the dehydrated form of 140 °C is rougher or more corrugated than that at 60 °C.

Figure 6 shows the surface and cross section of the thymine crystals in two dehydrated forms. It is known that thymine shows a tunnel hydrate, and the outcome of this compound is similar to that of theophylline. However, the tunnel within the crystal is more noticeable than that in the theophylline crystal. The crystals show obvious surface morphology changes: smooth, corrugated, and lamella. Variability of the surfaces after processing will have an impact on the functionality and performance of powders upon flow, compaction, and stability (Galwey 2000).

An additional technique was used in an attempt to gain fundamental insight to potentially further explain the resulting morphology and behavior of the two dehydrated forms. A thermally stimulated polarized current (TSPC) experiment was carried out for theophylline for the 60 and 140 °C samples from –100 to 100 °C

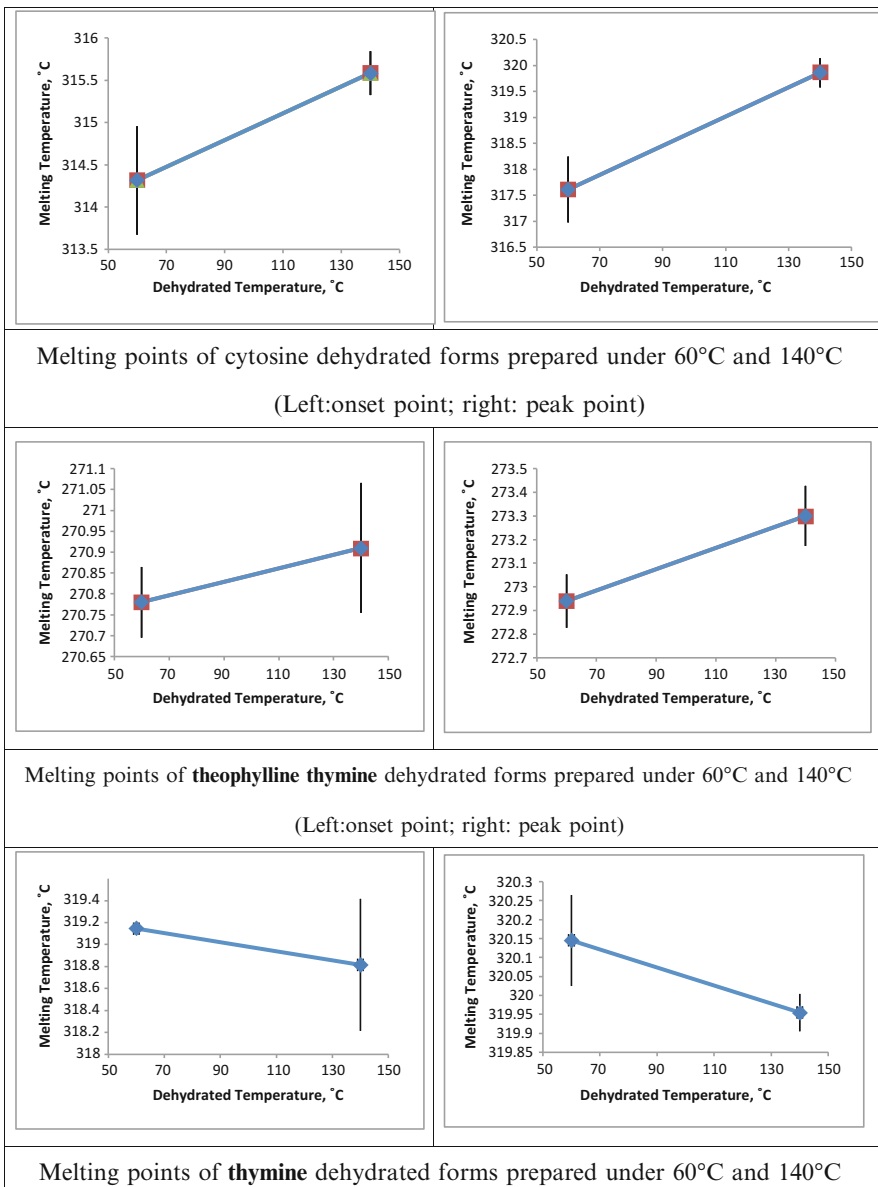


**Fig. 3** Melting points of thymine dehydrated forms prepared under 60 and 140 °C

**Table 1** Melting point of cytosine dehydrated forms prepared under 60 and 140 °C

	60 °C		140 °C	
	Onset	Peak	Onset	Peak
Repeat 1	313.86	318.06	315.40	319.66
Repeat 2	314.77	317.16	315.77	320.06

**Table 2** Melting point of theophylline dehydrated forms prepared under 60 and 140 °C

	60 °C		140 °C	
	Onset	Peak	Onset	Peak
Repeat 1	270.84	273.02	271.02	273.39
Repeat 2	270.72	272.86	270.80	273.21

**Table 3** Melting point of thymine dehydrated forms prepared under 60 and 140 °C

	60 °C		140 °C	
	Onset	Peak	Onset	Peak
Repeat 1	319.14	320.06	318.39	319.92
Repeat 2	319.14	320.23	319.24	319.99

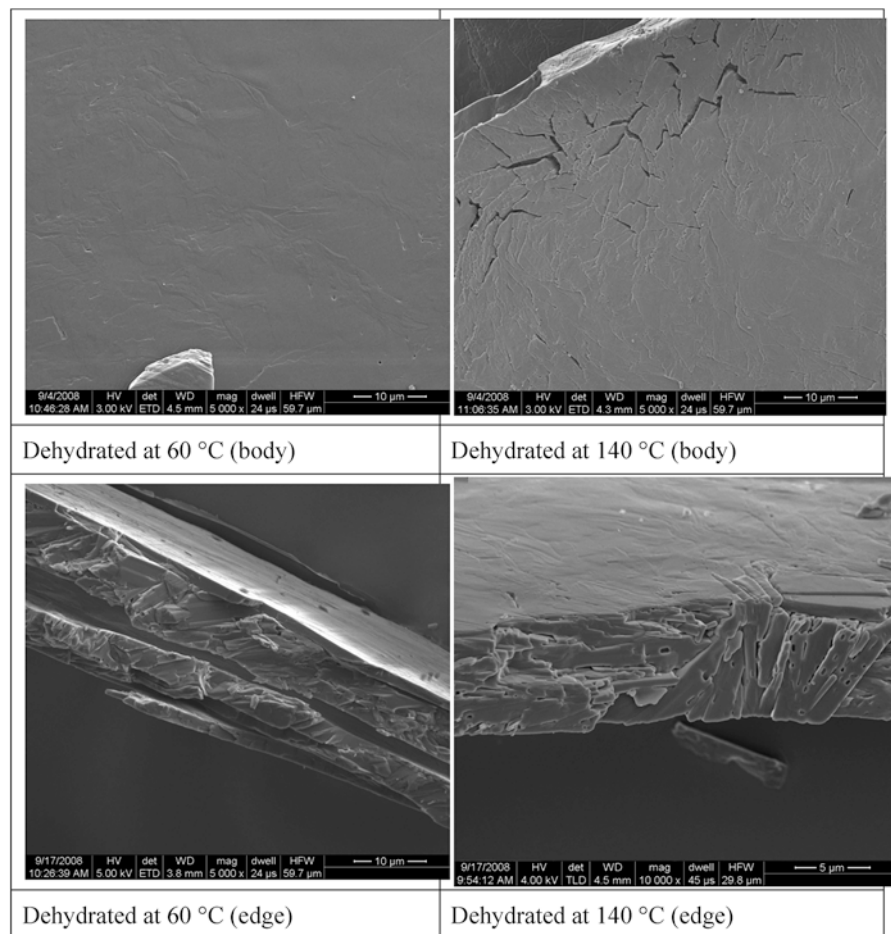


**Fig. 4** SEM images of cytosine (*Left*: sample dehydrated at 60 °C; *Right*: sample dehydrated at 140 °C)

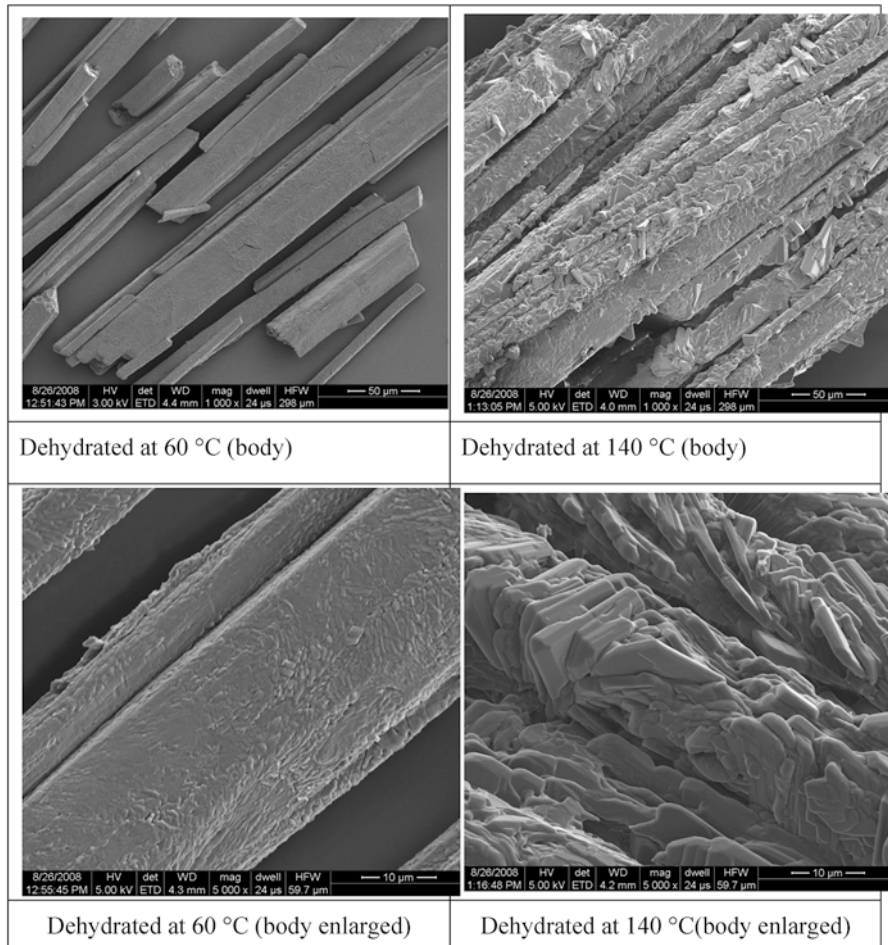


**Fig. 5** SEM images of theophylline (*Left*: sample dehydrated at 60 °C; *Right*: sample dehydrated at 140 °C)

(Fig. 7). Slight differences were observed in this case in the range below 100 °C; however, at higher temperature up to 200 °C, there was a clear depolarization event and differences between the two samples dehydrated at 140 and 60 °C. This may suggest that there is some mobility of molecules below 200 °C.

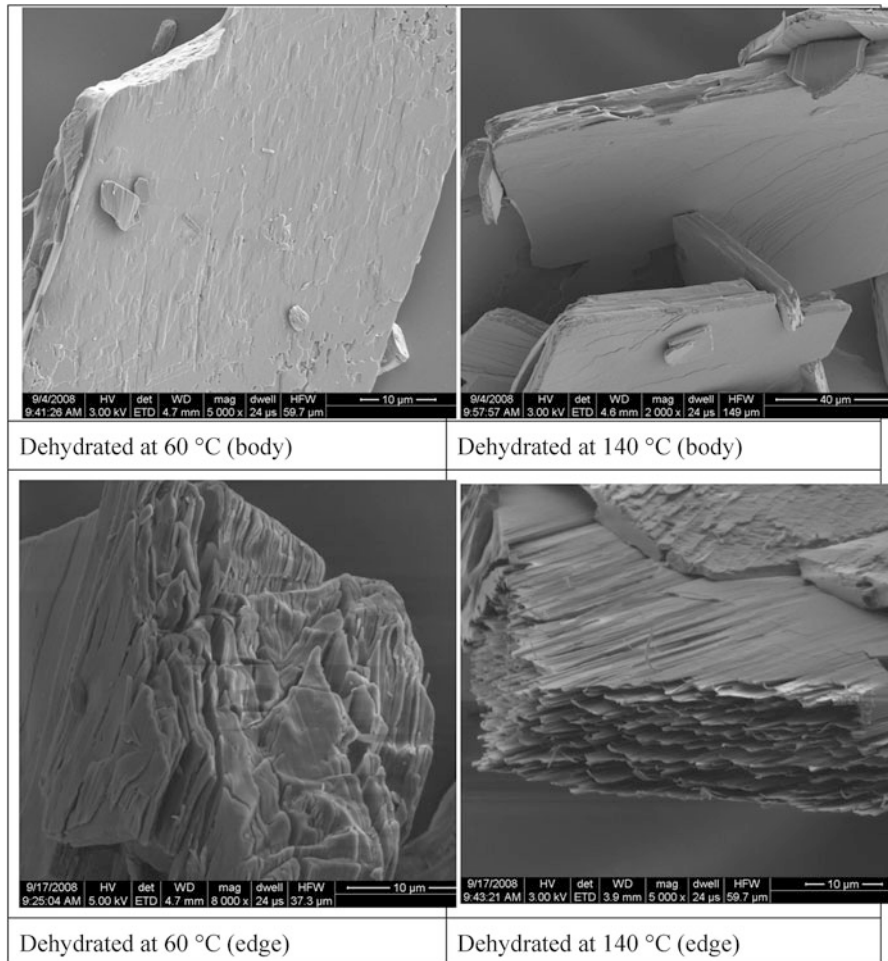


**Fig. 6** SEM images of thymine (*Left*: sample dehydrated at 60 °C; *Right*: sample dehydrated at 140 °C)

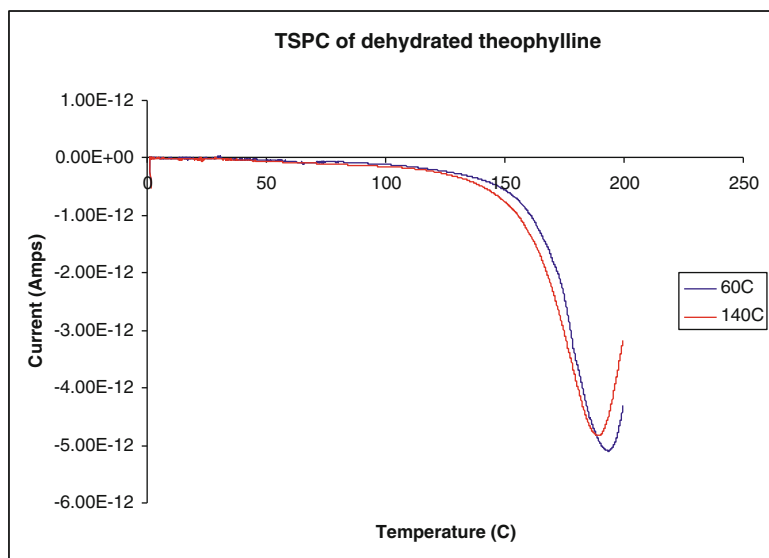


**Fig. 7** TSPC profile for the 60 and 140 °C theophylline samples (Yamauchi et al. 2011)

## 4 Conclusions

The effect of dehydration temperature on the melting temperature and surface morphology of the resulting dehydrated forms for three drug compounds was investigated. It was found that the higher the dehydration temperature the higher the melting point for samples of cytosine and theophylline, and that the melting of thymine was lowered. In addition, higher dehydration temperature resulted in a much rougher surface morphology of samples than lower dehydration temperature.

**Acknowledgments** We are grateful to the Dane O. Kildsig Center for Pharmaceutical Processing Research (CPPR) for funding. Also, we thank Dr. Yinyan Zhao for conducting the TSPC analysis.

## References

- Chamarthy SP, Pinal R, Carvajal TM (2009) Elucidating raw material variability-importance of surface properties and functionality in pharmaceutical powders. *AAPS PharmSci Tech* 10 (3):780–788
- Galwey AK (2000) Structure and order in thermal dehydrations of crystalline solids. *Thermochim Acta* 355:181–238
- Han J, Suryanarayanan R (1998) Influence of environmental conditions on the kinetics and mechanism of dehydration of carbamazepine hydrate. *Pharm Dev Tech* 3(4):587–596
- Khankari R, Grant DJW (1995) Pharmaceutical hydrates. *Thermochim Acta* 248(2):61–79

- Kishi A, Otsuka M, Matsuda Y (2002) The effect of humidity on dehydration behavior of nitrofurantoin monohydrate studied by humidity controlled simultaneous instrument for x-ray diffractometry and differential scanning calorimetry (XRD-DSC). *Coll Surf B* 25 (4):81–291
- Leung SS, Padden BE, Munson EJ, Grant DJW (1998) Hydration and dehydration behavior of aspartame hemihydrate. *J Pharm Sci* 87(4):508–513
- Mirza S, Miroshnyk I, Rantanen J, Altonen J, Harjula P, Kiljunen E, Heinamaki J, Yliruusi J (2007) Solid-state properties and relationship between anhydrate and monohydrate of baclofen. *J Pharm Sci* 96(9):399–2408
- Murphy D, Rodriguez-Cintron F, Langevin B, Kelly RC, Rodriguez-Hornedo N (2002) Solution-mediated phase transformation of anhydrous to dihydrate carbamazepine and the effect of lattice disorder. *Int J Pharm* 246:121–134
- Ono M, Tozuka Y, Oguchi T, Yamamoto K (2001) Effects of dehydration temperatures on moisture absorption and dissolution behavior of theophylline. *Chem Pharm Bull* 49 (12):1526–1530
- Trasi N, Teresa Carvajal M (2009) Final report to the Dane Kildsig, Center for Pharmaceutical Processing (CPPR). Purdue University, West Lafayette, IN
- Yamauchi M, Lee EH, Otte A, Byrn SR, Carvajal MT (2011) Contrasting the surface and bulk properties of anhydrate and dehydrated hydrate materials. *Cryst Growth Des* 11(3):692–698

# **Moisture Sorption Isotherms of Foods: Experimental Methodology, Mathematical Analysis, and Practical Applications**

**C. Caballero-Cerón, J.A. Guerrero-Beltrán, H. Mújica-Paz,  
J.A. Torres, and J. Welti-Chanes**

## **Abbreviations**

$\Delta G$	Gibb's free energy value
$\Delta H$	Enthalpy
$\Delta S$	Entropy
$A$	Constant of Halsey equation
ASE	Average standard error
$a_w$	Water activity
$a_{w,calc.}$	Water activity values estimated with the model
$a_{w,exp}$	Experimental water activity values
$B$	Constant of Halsey equation
BET	Brunauer-Emmett-Teller equation
$C$	Adsorbent constant, interaction energy constant

---

C. Caballero-Cerón

Centro de Biotecnología FEMSA, Escuela de Biotecnología y Alimentos,  
Tecnológico de Monterrey, Av. Eugenio Garza Sada 2501 Sur, Col. Tecnológico,  
Monterrey, N.L. 64849, Mexico

J.A. Guerrero-Beltrán (✉)

Departamento de Ingeniería Química, Alimentos y Ambiental, Universidad de las  
Américas-Puebla, Sta. Catarina Mártir, Cholula, Puebla 72820, Mexico  
e-mail: [joseangel150@hotmail.com](mailto:joseangel150@hotmail.com)

H. Mújica-Paz • J. Welti-Chanes (✉)

Escuela de Ingeniería y Ciencias, Tecnológico de Monterrey, Av. Eugenio Garza Sada 2501  
Sur, Col. Tecnológico, Monterrey, Nuevo León 64849, México  
e-mail: [h.mujica@itesm.mx](mailto:h.mujica@itesm.mx); [jwelti@itesm.mx](mailto:jwelti@itesm.mx)

J.A. Torres

Food Process Engineering Group, Department of Food Science and Technology,  
Oregon State University, 100 Wiegand Hall, Corvallis, OR 97331, USA

DDI	Dynamic dew point isotherm method
Ds	Dried solids
DSC	Differential scanning calorimetry
DVS	Dynamic vapor sorption method
$F, G$ , and $H$	Constants of Lewicki equation
GAB	Guggenheim, Anderson, and De Boer equation
$H_1$	Condensation heat of pure water (J mol <sup>-1</sup> )
$H_m$	Total sorption heat of the monolayer (J mol <sup>-1</sup> )
$H_q$	Total sorption heat of subsequent water layers (J mol <sup>-1</sup> )
$K$	Interaction energy constant
$k$ and $n$	Constants of Henderson equation
$M$	Linearized portion slope of the sorption isotherm in the range of interest
MRD	Measurements of deviation between predicted data
$Q$	Isosteric heat of sorption
$-Q/R$	Slope in the lineal relationship of $\ln a_w$ against the inverse absolute temperature
$q_{st}$	Isosteric heat of sorption
$R$	Ideal gas constant
$R$	Ideal gas constant
$R^2$	Coefficient of determination
RH	Relative humidity
RMSE	Measurements of deviation between experimental data
$T$	Absolute temperature
$T_B$	Isokinetic temperature
$T_g$	Glass transition temperature
$T_{hm}$	Harmonic temperature
$X$	Moisture content
$X_i$	Average moisture content values
$X_{i, \text{ calc.}}$	Calculated moisture content values
$X_{i, \text{ exp}}$	Experimental moisture content values
$X_m$	Monolayer moisture values

## 1 Introduction

Knowing the moisture content of a product is insufficient to predict its stability, making it necessary to also know its water activity ( $a_w$ ), a thermodynamic property describing the interactions between water molecules and the food matrix. Moisture sorption isotherms, i.e., the relationship between moisture content and  $a_w$  at constant pressure and temperature describing the sorption process of water molecules into a specific material, are useful when identifying optimal food dehydration and storage conditions. Moisture sorption properties affect physicochemical and biological phenomena such as enzymatic degradation, microbial activity, food

microstructure, sensory quality deterioration, nutrient losses, and other changes limiting the shelf life of food products. Some of these phenomena are associated with water mobility, which is also related with the phase transitions from a “glass” or amorphous to a “rubbery” state. Glass transition is a second order phase transition associated with time, temperature, and moisture content. When fresh foods are dried, water removal leaves behind an amorphous material. A desirable final product moisture level is one that corresponds to a glass transition temperature ( $T_g$ ) higher than the product storage temperature. Therefore, knowing  $T_g$  helps in setting the food storage and/or process conditions required to retain textural properties and to predict the shelf life of low and intermediate moisture content foods.

The aim of this work is to present information on food moisture sorption isotherms and their relationship with product composition and temperature. Advantages and disadvantages of experimental methods available to obtain sorption isotherms are reviewed, equations describing experimental data are then discussed, and finally, practical applications to shelf life estimations due to moisture gain or loss are presented.

## 2 Moisture Sorption Isotherms

Moisture sorption isotherms are a graphical representation of the thermodynamic equilibrium between moisture content and the water activity at a given temperature and pressure (Iglesias and Chirife 1982). The shape of the moisture sorption isotherms changes with temperature, composition, pressure, physical state of the components, and the process of dehydration/humidification used; every product isotherm is unique (Goula et al. 2008; Vega-Gálvez et al. 2009). Moisture sorption isotherms describe how water molecules are adsorbed by a specific material, and are used to predict the shelf life of food and pharmaceutical products due to moisture gain (adsorption) or loss (desorption), and also to define storage, transport, and process conditions, or to estimate the energy requirements of a dehydration process (Arlabosse et al. 2003; Iglesias and Chirife 1982; Lewicki 2000). The adsorption/desorption process is not fully reversible (Fig. 1), i.e., at the same  $a_w$  a larger moisture content is observed during the desorption process, a phenomenon called hysteresis (Basu et al. 2006; Al-Muhtaseb et al. 2002).

Five isotherm types have been reported (Fig. 2). Type I or Langmuir isotherms are observed when water molecules are absorbed by materials mostly as a single monolayer; Type II, shown by soluble materials, are sigmoidal isotherms with an asymptotic tendency when  $a_w$  approaches 1.0; Type III corresponds to high sugar concentration products; Type IV describes hydrophilic solids; and Type V represents adsorption of water molecules as multilayers (Basu et al. 2006; Al-Muhtaseb et al. 2002). Most food products exhibit Type II or III.

**Fig. 1** Schematic representation of moisture sorption isotherms for food products showing hysteresis phenomenon

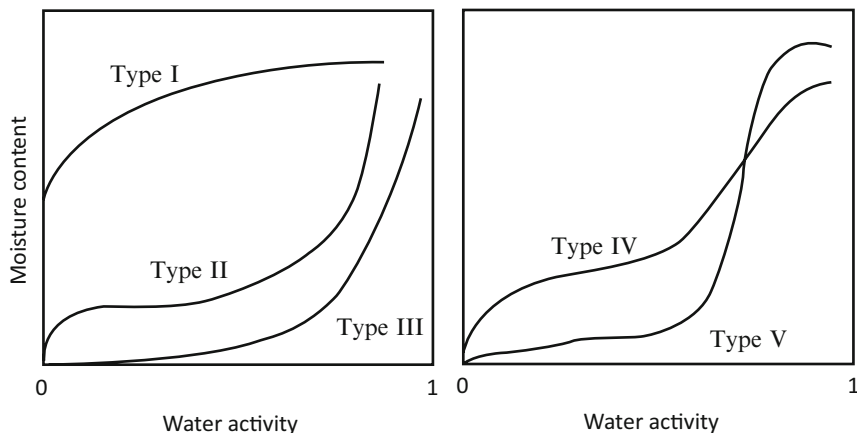
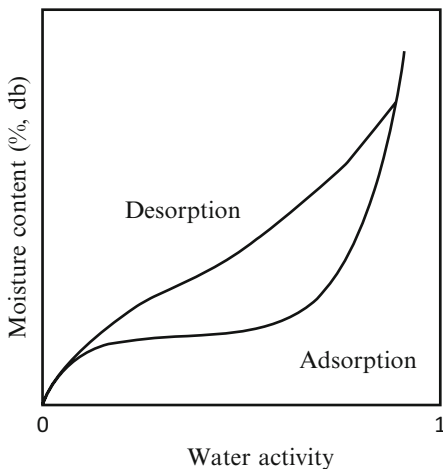


**Fig. 2** Five types of sorption isotherms

## 2.1 Monolayer Moisture Content

The monolayer moisture content is defined as the water necessary to cover by absorption to hydrophilic and polar groups the entire food surface, including pores and capillaries (Rahman 2009; Furmaniak et al. 2009). This moisture level is used as a stability parameter for dried products, since this bound water can be assumed as being unavailable to participate in reactions requiring water as a solvent or to exert a plasticizing role (Bell and Labuza 2000; Basu et al. 2006). Water absorbed in excess of the monolayer value is arranged into multilayers bound by hydrogen bonds, and can interact with other chemical compounds of the food matrix or participate in the transport of soluble compounds (Rahman 1995; Furmaniak

et al. 2009). From a practical point of view, the monolayer value is a reference parameter defining for dried products a moisture content value for maximal product stability.

## 2.2 *Temperature and Composition Effects on Moisture Sorption Properties*

Many factors affect the sorption isotherm, but the most important ones are food composition and temperature (Goula et al. 2008; Vega-Gálvez et al. 2009).

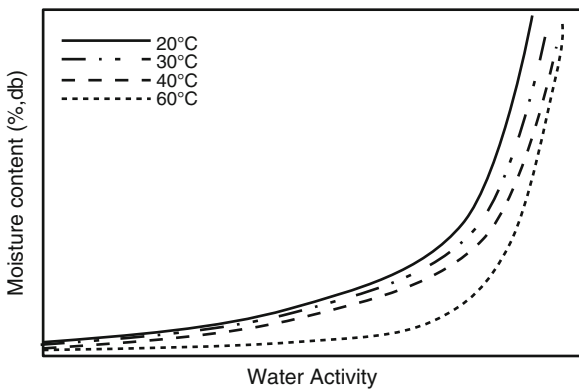
### 2.2.1 **Chemical Composition and Moisture Sorption Properties**

Food systems are complex matrices constituted by a continuous aqueous phase and a small fraction of dispersed solids. Soluble compounds in the aqueous phase consist of sugars, salts, and others, while the solid phase is constituted by insoluble polymers such as starch, proteins, and insoluble fiber (Moreira et al. 2009). The relationship of moisture and water activity depends on the food composition and how water molecules interact with food compounds, i.e., how many polar sites are available for the binding of water molecules (Iglesias and Chirife 1982; Kingsly and Ileleji 2009; Moreira et al. 2009; Myhara et al. 1998). While water soluble molecules such as sugars, salts, or soluble fibers bind water molecules contributing to vapor pressure reduction, insoluble solids with no binding sites do not, thus higher values of  $a_w$  are reached at the same equilibrium moisture content (Goula et al. 2008; Moreira et al. 2009).

### 2.2.2 **Effect of Temperature on Sorption Isotherms**

Temperature influences the water molecular mobility in a food system, as well as the dynamic exchange between the vapor and the absorbed phases. In addition, the binding energy between molecules decreases when temperature increases, so a reduction in the adsorption capacity of water molecules is observed, leading to changes in the sorption isotherm (Quirijns et al. 2005; McMinn et al. 2003). As shown in Fig. 3, temperature increases  $a_w$  at the same equilibrium moisture content, reflecting a reduction in the total number of active sites for water adsorption as a result of physical and/or chemical changes due to the temperature increase (Goula et al. 2008; Quirijns et al. 2005).

**Fig. 3** Effect of temperature on moisture sorption isotherms



### 3 Experimental Methods for the Determination of Moisture Sorption Isotherms

Experimental methods are divided into those with the air relative humidity and/or temperature continuously changing, and those known as dynamic methods, in contrast with static methods where air properties are kept constant during  $a_w$  determination.

#### 3.1 Static Methods

In static methods, samples in hermetic and closed vessels are kept in contact with air at constant relative humidity (RH) and temperature until equilibrium between the sample and air is reached. These methods can be classified as hygrometric, manometric, and gravimetric (Iglesias and Chirife 1982). In hygrometric methods, the surrounding food atmosphere vapor pressure is measured using dew point and electrical sensors (Spiess and Wolf 1987). In manometric methods, air vapor pressure in equilibrium with the food sample is measured (Goula et al. 2008; Spiess and Wolf 1987). In gravimetric methods, equilibrium is evaluated by following weight changes (Iglesias and Chirife 1982) in samples (2 g approx.) with known moisture content in contact with air at constant RH and temperature. Weight loss (desorption) or gain (adsorption) is evaluated until equilibrium is reached, i.e., when the difference between two consecutive measurements is approximately  $\pm 0.0010$  g. The measuring system consists of a series of hermetic containers (glass jars or desiccators), a glass or plastic base (usually a petri dish), and weighing bottles where samples are placed (Iglesias and Chirife 1982; Bell and Labuza 2000; Spiess and Wolf 1987). Hermetic flasks (or desiccators) are placed in a constant room temperature or in an incubator. Saturated salt solutions, sulfuric acid, or glycerol solutions are used to control the RH. Saturated salt solutions are

**Table 1** Water activity generated by oversaturated salt solutions at different temperatures (adapted from López-Malo et al. 1994)

Salt	Water activity		
	Temperature (°C)		
	25	30	35
Lithium chloride, LiCl	0.111	0.112	0.113
Potassium acetate, CH <sub>3</sub> COOK	0.252	0.244	0.237
Magnesium chloride, MgCl <sub>2</sub>	0.325	0.322	0.319
Potassium carbonate, K <sub>2</sub> CO <sub>3</sub>	0.434	0.432	0.431
Magnesium nitrate, Mg(NO <sub>3</sub> ) <sub>2</sub>	0.524	0.511	0.499
Sodium bromide, NaBr	0.573	0.559	0.545
Potassium iodide, KI	0.686	0.676	0.669
Strontium chloride, SrCl <sub>2</sub>	0.707	0.691	0.676
Sodium chloride, NaCl	0.755	0.753	0.752
Ammonium chloride, NH <sub>4</sub> Cl	0.777	0.763	0.754
Ammonium sulfate (NH <sub>4</sub> ) <sub>2</sub> SO <sub>4</sub>	0.807	0.801	0.798
Potassium chloride, KCl	0.843	0.836	0.830
Barium chloride, BaCl <sub>2</sub>	0.904	0.901	0.898
Potassium nitrite, KNO <sub>2</sub>	0.931	0.917	0.906
Potassium sulfate, K <sub>2</sub> SO <sub>4</sub>	0.976	0.974	0.972

preferred, as they are thermally stable and show small RH variation with temperature changes, as well as being stable to changes in sample moisture content (Greenspan 1977; Rockland 1960; Spiess and Wolf 1987). Table 1 shows the most common salts employed in the 0.11–0.976  $a_w$  interval (López-Malo et al. 1994).

Static methods are simple to operate and allow multiple samples to be analyzed simultaneously, but determination times are long, samples must be removed from the system for weighing which may modify their equilibrium moisture, requiring large sample quantities for a complete isotherm, and determination points are discrete (Yu et al. 2008a, b; Lewicki 2000). Long determination times are required to ensure that thermodynamic equilibrium between samples and air is reached (Spackman and Schmidt 2010). However, these long times may result in mold growth in samples with RH greater than 75 %, causing the loss of experimental data (Bell and Labuza 2000; Yu et al. 2008a, b; Baucour and Daudin 2000). Automatic and dynamic methods have been developed to avoid these experimental limitations.

### 3.2 Dynamic Methods

Samples are placed on a microbalance and an air stream with known RH and constant temperature passes continuously over them. Constant exposure to air flow and the small sample weight reduce the determination time from days to hours, making it possible to measure points at high  $a_w$  levels without the risk of microbial growth or physicochemical changes in the sample (Rahman and

Al-Belushi 2006; Arlabosse et al. 2003; Spackman and Schmidt 2010; Yu et al. 2008c). Only one sample is needed for the complete sorption isotherm, weight is automatically recorded, and sample handling is reduced (Rahman and Al-Belushi 2006; Yu et al. 2008b). The automated equipment most frequently used is based on the gravimetric method and uses dew point sensors (Carter and Fontana 2008; Spackman and Schmidt 2010).

### 3.2.1 Dynamic Vapor Sorption Method (DVS)

In this method, sample weight is continuously recorded at a constant RH and temperature. RH is controlled by using a continuous gas flow mix of dry nitrogen and water vapor. RH changes are programmed as fixed steps controlled by time or RH values, while weight is continuously measured until equilibrium is reached for each RH evaluated (Rahman and Al-Belushi 2006; Li and Schmidt 2011). Equipment consists of two symmetric chambers kept at the same RH and temperature, one for the sample and the other as an empty cell used for reference (Rahman and Al-Belushi 2006; Roman-Gutierrez et al. 2002). The sample size is small (mg), reducing the equilibrium time from days to hours for each point in the sorption isotherm (Arlabosse et al. 2003; Spackman and Schmidt 2010; Rahman and Al-Belushi 2006). Other DVS method applications include determination of drying microkinetics and evaluation of time-depending phase changes such as glass transitions, deliquescence points, crystallizations, and others physicochemical changes (Yu et al. 2008b; Rahman and Al-Belushi 2006; Spackman and Schmidt 2010). In some cases, thermodynamic equilibrium is not reached due to the fast exposure of the sample to the gas flow leading to sorption isotherm differences with those obtained by other methods (Roman-Gutierrez et al. 2002).

### 3.2.2 Dynamic Dew Point Isotherm Method (DDI)

Water activity and sample weight changes due to continuous flow of a saturated vapor stream (adsorption) or dried air (desorption) over the sample are measured directly (Schmidt and Lee 2012; Carter and Fontana 2008). Air flow stops after  $a_w$  changes of 0.015 units approximately, and weight and water activity are measured for each point. Thermodynamic equilibrium may not be reached during measurement, and thus results may differ from those obtained by other methods, particularly for samples with a slow rate of water diffusion (Schmidt and Lee 2012; Carter and Fontana 2008). This method has been used to evaluate time-depending phase changes (Yao et al. 2011; Yuan et al. 2011). The sample chamber in the isotherms generator consists of a precision balance, a standard mirror dew point sensor, inflow ports for dry air and water saturated air, and an infrared temperature sensor. Dry air is obtained by air circulation through a packed desiccant column, while the water

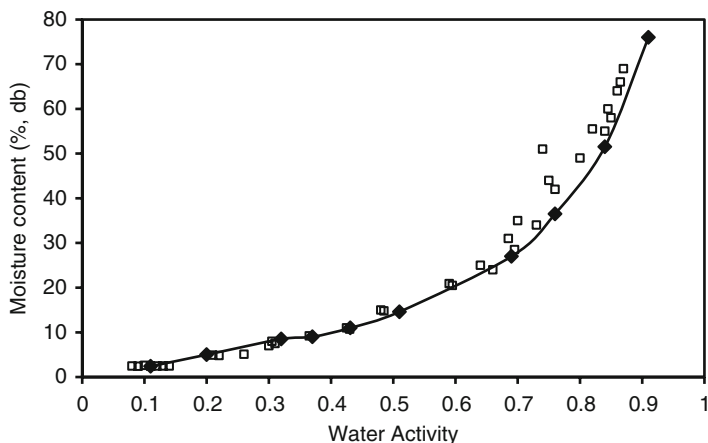


**Fig. 4** Sorption isotherm at 32 °C of apple obtained by DDI method (open square) and gravimetric static method (filled diamond) (unpublished data)

saturated air is obtained by air circulation through a water reservoir (Schmidt and Lee 2012; Carter and Fontana 2008). The DDI method is designed to obtain a complete sorption isotherm (adsorption and desorption) with one sample in a short time period of approximately 24 h, obtaining a high resolution isotherm (>50 points for isotherm). As more data become available, isotherms can be used to obtain additional information on the adsorption of water molecules, as well as phase changes due to moisture content changes. Apple moisture isotherms at 32 °C obtained by conventional static and DDI methods show the same behavior, but the resolution is higher for the latter (Fig. 4). Studies on phase changes such as crystallization, glass transition, and deliquescence points have been reported (Carter and Fontana 2008; Schmidt and Lee 2012; Yao et al. 2011; Yuan et al. 2011; Spackman and Schmidt 2010; Carter and Schmidt 2012). Yuan et al. (Yuan et al. 2011) evaluated the polydextrose glass transition, obtaining  $T_g$  values similar to those determined by differential scanning calorimetry (DSC). Yao et al. (2011) measured the deliquescence point for crystalline sucrose at 15, 25, and 35 °C. Although  $T_g$  values obtained by the DDI method are restricted to the 15–40 °C equipment operation limits, these are the most common temperature storage conditions; thus, results will be useful when setting food storage and shipping conditions. Schmidt and Lee (2012) observed that sorption isotherms for corn starch, isolated soy protein, microcrystalline cellulose, and crystalline sucrose obtained by DDI and static gravimetric methods were similar. However, those for lactose and corn flakes differed, which was assumed to be associated with phase transitions or slow water diffusion rate, respectively (Carter and Fontana 2008). Diffusion rate can be increased by decreasing the particle size or reducing air flow, yielding DDI results in agreement with those obtained by other methods (Schmidt and Lee 2012).

## 4 Modeling Sorption Isotherms

Mathematical models proposed to describe experimental sorption isotherms for food products can be classified according to the number of parameters used, or on whether they are based on theoretical or empirical assumptions (Basu et al. 2006; Bhandari and Adhikari 2008). Most models used 2–3 parameters, and the one selected should describe the experimental data well, have less mathematical complexity, and provide mechanistic information on the food hygroscopic properties (Basu et al. 2006). Foods are complex systems, and thus a single model cannot describe all products (Al-Muhtaseb et al. 2002; Bhandari and Adhikari 2008). In the mathematical models presented next,  $X$  and  $X_m$  are the moisture content and monolayer moisture values ( $\text{gH}_2\text{O}/100 \text{ g dried solids}$ ), respectively.

### 4.1 Brunauer-Emmett-Teller (BET) Equation (Brunauer et al. 1938)

The BET equation, a semiempirical 2-parameter model, describes the  $a_w < 0.5$  region (Al-Muhtaseb et al. 2002; Bhandari and Adhikari 2008) as follows:

$$X = \frac{X_m C a_w}{(1 - a_w)[1 + (C - 1)a_w]} \quad (1)$$

where  $C$  is an adsorbent constant. This model assumes that the sorption heat in the monolayer is constant and equal to the water vaporization heat plus a constant related to the interaction site, the sorption heat for water molecules above the monolayer value is equal to that for pure water, water sorption occurs only on specific food structure sites, and the sorption surface is homogeneous. The monolayer moisture content defines the moisture content for the maximum stability of dehydrated products.

### 4.2 Guggenheim, Anderson, and De Boer (GAB) Equation (van den Berg and Bruins 1981)

The GAB model, a semi-theoretical 3-parameter equation, describes water adsorption as a multilayer phenomenon (van den Berg and Bruins 1981; Jouppila and Roos 1997) as follows:

$$X = \frac{X_m C K a_w}{(1 - K a_w)[1 + (C - 1)K a_w]} \quad (2)$$

where  $C$  and  $K$  are interaction energy constants for the monolayer and the other water molecules are adsorbed on individual sites, respectively. Equations (3) and (4) are the temperature functions used to evaluate the constants  $C$  and  $K$ :

$$C = C_0 \exp\left(\frac{H_1 - H_m}{RT}\right) \quad (3)$$

$$K = K_0 \exp\left(\frac{H_1 - H_q}{RT}\right) \quad (4)$$

where  $H_1$ ,  $H_m$ , and  $H_q$  are, respectively, the condensation heat of pure water (J/mol), total sorption heat of the monolayer (J/mol), and total sorption heat of subsequent water layers (J/mol),  $T$  is the absolute temperature (K) and  $R$  is the ideal gas constant (8.314 J/mol/K) (Talla et al. 2005).  $X_m$  is considered temperature independent, but in some cases it has been shown to decrease when temperature increases (Goula et al. 2008; Quirijns et al. 2005). This monolayer moisture content decrease may be due to a reduction of the active binding water sites as a result of physical or chemical changes induced by temperature. The temperature function for  $X_m$  can be expressed as:

$$X_m = X_{m,0} \exp\left(\frac{\Delta H_X}{RT}\right) \quad (5)$$

where  $X_{m,0}$  and  $\Delta H_X$  (J/mol) are constants. The GAB model assumes that water adsorption is a multilayer phenomenon without lateral interactions of water molecules. The monolayer covers the complete sorbent surface with water molecules bound very tightly in the monolayer, whereas the subsequent 2–9 multilayers have less interaction with the sorbent (Quirijns et al. 2005). Timmermann et al. (2001) observed that the GAB parameters are more representative than the corresponding BET parameters for food products, whereas Singh and Singh (1996) showed that it can describe different food isotherm types. The temperature, moisture content, and  $a_w$  intervals tested in this latter work were 4–140 °C, 2–77 %, and 0.059–0.99, respectively.

#### 4.3 Halsey Equation (Halsey 1948)

This model overcomes BET limitations (Rahman 1995) by assuming that the potential energy of water molecules varies with the inverse of their distance from the food surface and can describe a wide variety of food isotherms in the 0.1–0.8  $a_w$  interval and is expressed as follows:

$$X = \left[ \frac{-A}{RT \ln a_w} \right]^{1/c} \quad (6)$$

where  $A$  and  $C$  are constants, and  $T$  is the absolute temperature (K). As the term  $RT$  does not eliminate the temperature dependence of constants  $A$  or  $B$ , this expression is simplified as follows (Iglesias and Chirife 1976; Basu et al. 2006):

$$X = \left[ \frac{-A'}{\ln a_w} \right]^{1/B} \quad (7)$$

where  $A'$  is a new constant and may be related to temperature as an exponential function:

$$X = \left[ \frac{-\exp(A + BT)}{\ln a_w} \right]^{1/C} \quad (8)$$

where  $A$ ,  $B$ , and  $C$  are constants for each isotherm.

#### 4.4 Henderson Equation (Henderson 1952)

The Henderson model, an empirical relationship between adsorbed moisture and  $a_w$  used to describe moisture sorption isotherms of food products, but with rather limited applicability as compared with other models, is expressed as (Rahman 1995):

$$1 - a_w = \exp(-kTX^n) \quad (9)$$

where  $k$  and  $n$  are constants and  $T$  is the temperature (°C). The following expression is a modification of the original Henderson equation considering  $k$  as temperature function:

$$1 - a_w = \exp[-A(T + B)X^n] \quad (10)$$

where  $A$ ,  $B$ , and  $C$  are model constants.

#### 4.5 Kühn Equation (Kühn 1964)

This theoretical model, based on a capillary condensation concept and applied most frequently to vegetable and animal products (Akanbi et al. 2006; Escobedo-Avellaneda et al. 2011a, b), is expressed as follows:

$$X = -\frac{k}{\ln a_w} + B' \quad (11)$$

where  $k$  and  $B'$  are constants.

#### 4.6 Oswin Equation (Oswin 1946)

The Oswin equation, an empirical model to describe sigmoidal moisture isotherms, can be represented as follows:

$$X = A \left[ \frac{a_w}{1 - a_w} \right]^B \quad (12)$$

where  $A$  and  $B$  are constants. Applications of this equation include high starch content products and also different vegetable products (Al-Muhtaseb et al. 2002).

#### 4.7 Lewicki Equation (Lewicki 1998, 2000)

Assuming that food moisture can be described as pure and hydration water, Lewicki (2000) proposed the following 2-parameter model related to Raoult's law:

$$X = A \left[ \frac{1}{a_w} - 1 \right]^{b-1} \quad (13)$$

where  $A$  and  $b$  are constants. This equation can yield better results than the GAB model, especially when  $a_w$  is close to 1.0. Although this equation is similar to the Oswin model (Eq. 12), some differences between these two equations can be noted. In contrast with the 2-parameter Lewicki expression (Eq. 13), the Oswin equation is an empirical model, and thus its constants have no physical meaning. In addition, the point  $a_w = 1$  is excluded (Lewicki 2000; McMinn et al. 2004). Lewicki (1998) proposed the following 3-parameter model based on a 2-function expression to describe processes occurring in parallel, the first one predominating at high  $a_w$ , with the second being more important at low  $a_w$ :

$$X = \frac{F}{(1 - a_w)^G} + \frac{F}{1 + a_w^H} \quad (14)$$

where  $F$ ,  $G$ , and  $H$  are constants. This equation was tested using 31 sorption isotherms reported for various food products yielding better results than those obtained for the GAB, but not as good as those for the Peleg model (Eq. 16).

McMinn et al. (2004) showed that while the 2- and 3-parameter Lewicki equations well describe experimental data for high starch products, the 3-parameter equation gives better results for food products with Type II isotherms within the 30–60 °C temperature range, and the 2-parameter equation was superior to the GAB equation. However, sorption isotherms of potato, high amylose, and high amylopectin starch powders cannot be described using the Lewicki equations.

#### **4.8 Smith Equation (Smith 1947)**

The Smith model, an empirical equation describing the high  $a_w$  portion of sorption isotherms for products containing high molecular weight solutes (Rahman 1995), can be represented as follows:

$$X = A + B \log(1 - a_w) \quad (15)$$

where  $A$  and  $B$  are constants,  $A$  is the moisture fraction absorbed on the first fraction, and  $B$  is the water in the multilayer fraction. This model, limited to the 0.5–0.95  $a_w$  interval (Al-Muhtaseb et al. 2004; Rahman 1995), assumes that there are two fractions of water molecules adsorbed on the food surface. The first fraction with a condensation heat higher than the one for pure water follows the Langmuir model, while the second fraction consisting of a multilayer of condensed water molecules formed only after the first is absorbed, preventing any evaporation from the first fraction. The Smith model describes only the behavior of the second fraction (Al-Muhtaseb et al. 2002).

#### **4.9 Peleg Equation (Peleg 1993)**

The Peleg model is a semiempirical 4-parameter equation describing sigmoidal and non-sigmoidal isotherms as follows:

$$X = K_1 a_w^{n_1} + K_2 a_w^{n_2} \quad (16)$$

where  $K_1$ ,  $K_2$ ,  $n_1$ , and  $n_2$  are constants and  $n_1 < 1$  and  $n_2 > 1$ . When  $a_w \rightarrow 1$ ,  $X \rightarrow K_1 + K_1$ ; however, the adsorbed moisture content values do not reach these values at  $a_w$  values close to 1.0. Therefore, this equation is used for  $a_w < 0.95$  (Lewicki 1998).

## 5 Analysis of Applicability for Modeling of Food Sorption Isotherms

Models selected to describe experimental sorption data must be evaluated using statistical indices such as the coefficient of determination ( $R^2$ , Eq. 17), root mean squared error (RMSE, Eq. 18), mean relative deviation (MRD, Eq. 19), and average standard error (ASE, Eq. 17):

$$R^2 = 1 - \frac{\sum_{i=1}^n (X_{i,\text{calc}} - X_{i,\text{exp}})^2}{\sum_{i=1}^n (X_{i,\text{exp}} - \bar{X}_{i,\text{exp}})^2} \quad (17)$$

$$\text{RMSE} = \sqrt{\sum_{i=1}^n (X_{i,\text{calc}} - X_{i,\text{exp}})^2} \quad (18)$$

$$\text{MRD} = \frac{1}{n} \sum_{i=1}^n \left| \frac{X_{i,\text{calc}} - X_{i,\text{exp}}}{X_{i,\text{exp}}} \right| \quad (19)$$

$$\text{ASE} = \frac{100}{n} \sum_{i=1}^n \text{abs} \left[ \frac{a_{w,\text{calc}} - a_{w,\text{exp}}}{1 - a_{w,\text{exp}}} \right] \quad (20)$$

where  $a_{w,\text{calc}}$  and  $a_{w,\text{exp}}$  are the  $a_w$  values estimated with the model and experimental value, respectively, while  $X_{i,\text{exp}}$ ,  $X_{i,\text{calc}}$ ,  $\bar{X}_i$  are the experimental, calculated, and average moisture content values, respectively, and  $n$  is the number of experimental data points.  $R^2$  quantifies the portion of the total variation explained by regression, so when  $R^2$  is closer to 1, the model better fits the experimental data. RMSE and MRD values are measurements of deviation between experimental and predicted data, and low values of RMSE and MRD are expected for equations best describing the experimental data. When  $\text{MRD} < 10\%$ , the equation can be used to describe experimental data (Ruiz-López and Herman-Lara 2009; Basu et al. 2006). Plotting the residuals ( $X - X_{\text{calc}}$ ) against the independent variable is also a measure of error distribution, i.e., when the model suitably describes the experimental data, the residuals should be randomly independent errors with a zero mean, constant variance and arranged in a normal distribution. If residual plots have a clear pattern, the model should be rejected (Basu et al. 2006).

## 6 Models Used to Describe Food Moisture Sorption Isotherms

Examples of mathematical models describing sorption isotherms for fruit products, as summarized in Table 2, show the GAB equation as the most widely used, since this theoretical 3-parameter equation provides estimates of monolayer moisture values and is able to take temperature effects into consideration. Reported MRD values for fruit sorption data under 10 % indicate a good fitness to experimental data. On the other hand, the BET equation describing only the low  $a_w$  isotherm portion is used by most authors to estimate moisture monolayer values, which are

**Table 2** Mathematical equations used to describe fruit moisture sorption isotherms

Equation	Samples
GAB	Grapes (Kaymak-Ertekin and Sultanoğlu 2001), apricots (Kaymak-Ertekin and Sultanoğlu 2001), apple (Duarte Goneli et al. 2010; Kaymak-Ertekin and Sultanoğlu 2001; Spiess and Wolf 1987), mango (Rockland 1960; Timmermann et al. 2001; Hossain et al. 2001), banana (Ferro-Fontan et al. 1982; Jouppila and Roos 1997; Kaya and Kahyaoglu 2007; Moreira et al. 2009; Timmermann et al. 2001; Yan et al. 2008a, b), pineapple (Iglesias and Chirife 1976; Timmermann et al. 2001), gnetum (Eim et al. 2011), strawberries (Moraga et al. 2006), kiwi (Moraga et al. 2011), blue berries (Liu et al. 2010; Vega-Gálvez et al. 2009), dates (Belarbi et al. 2000), persimmon (Benedetti et al. 2011), papaya (Lewicki 1998)
BET	Grapes (Kaymak-Ertekin and Sultanoğlu 2001), apricots (Kaymak-Ertekin and Sultanoğlu 2001), apple (Kaymak-Ertekin and Sultanoğlu 2001), mango (Rockland 1960; Timmermann et al. 2001), banana (Ferro-Fontan et al. 1982; Jouppila and Roos 1997; Moreira et al. 2009; Timmermann et al. 2001; Yan et al. 2008a), pineapple (Timmermann et al. 2001), strawberries (Moraga et al. 2006), kiwi (Moraga et al. 2011), blue berries (Vega-Gálvez et al. 2009), dates (Belarbi et al. 2000)
Halsey	Grapes (Kaymak-Ertekin and Sultanoğlu 2001), apricots (Kaymak-Ertekin and Sultanoğlu 2001), apple (Kaymak-Ertekin and Sultanoğlu 2001), mango (Rockland 1960), banana (Ferro-Fontan et al. 1982; Jouppila and Roos 1997; Yan et al. 2008a), blue berries (Vega-Gálvez et al. 2009)
Henderson	Grapes (Kaymak-Ertekin and Sultanoğlu 2001), apricots (Kaymak-Ertekin and Sultanoğlu 2001), apple (Kaymak-Ertekin and Sultanoğlu 2001), mango (Quirijns et al. 2005; Rockland 1960), banana (Ferro-Fontan et al. 1982; Jouppila and Roos 1997; Yan et al. 2008b), pineapple (Iglesias and Chirife 1976), blue berries (Vega-Gálvez et al. 2009), persimmon (Benedetti et al. 2011)
Kühn	
Lewicki	Persimmon (Benedetti et al. 2011)
Oswin	Grapes (Kaymak-Ertekin and Sultanoğlu 2001), apricot (Kaymak-Ertekin and Sultanoğlu 2001), apple (Kaymak-Ertekin and Sultanoğlu 2001), mango (Rockland 1960), banana (Ferro-Fontan et al. 1982; Yan et al. 2008b), blue berries (Vega-Gálvez et al. 2009), persimmon (Benedetti et al. 2011)
Peleg	Persimmon (Benedetti et al. 2011)
Smith	Mango (Rockland 1960), banana (Ferro-Fontan et al. 1982), pineapple (Iglesias and Chirife 1976), blue berries (Vega-Gálvez et al. 2009)

**Table 3** Mathematical equations used to describe vegetables moisture sorption isotherms

Equation	Samples
GAB	Tomato pulp (Greenspan 1977), potato (Kaymak-Ertekin and Sultanoğlu 2001; McMinn and Magee 2003; Medeiros et al. 2006), mushrooms (Sharma et al. 2009), onion (Talla et al. 2005; Viswanathan et al. 2003), red pepper (Kim et al. 1991; Kingsly and Ileleji 2009), raw bamboo (Corey et al. 2011), gluten potato (Viollaz and Rovedo 1999), green pepper (Kingsly and Ileleji 2009), tomato slices (Akanbi et al. 2006), carrot (Escobedo-Avellaneda et al. 2011a), Mexican red sauce (Escobedo-Avellaneda et al. 2011b)
BET	Tomato pulp (Greenspan 1977), mushrooms (Baucour and Daudin 2000), potato (Kaymak-Ertekin and Sultanoğlu 2001; Medeiros et al. 2006), onion (Viswanathan et al. 2003), red pepper (Kingsly and Ileleji 2009), raw bamboo (Corey et al. 2011), green pepper (Kingsly and Ileleji 2009), tomato slices (Iglesias and Chirife 1982), Mexican red sauce (Escobedo-Avellaneda et al. 2011b)
Halsey	Mushrooms (Sharma et al. 2009), potato (Kaymak-Ertekin and Sultanoğlu 2001; McMinn and Magee 2003; Medeiros et al. 2006), onion (Viswanathan et al. 2003), green pepper (Greenspan 1977), tomato slices (Akanbi et al. 2006), carrot (Escobedo-Avellaneda et al. 2011a), Mexican red sauce (Escobedo-Avellaneda et al. 2011b)
Henderson	Potato (Kaymak-Ertekin and Sultanoğlu 2001), mushrooms (Sharma et al. 2009), onion (Viswanathan et al. 2003), carrot (Escobedo-Avellaneda et al. 2011a), Mexican red sauce (Escobedo-Avellaneda et al. 2011b)
Kühn	Tomato slices (Akanbi et al. 2006), mushrooms (Sharma et al. 2009), Mexican red sauce (Escobedo-Avellaneda et al. 2011b)
Lewicki	
Oswin	Tomato pulp (Greenspan 1977), potato (Kaymak-Ertekin and Sultanoğlu 2001; Medeiros et al. 2006), mushrooms (Sharma et al. 2009), tomato slices (Akanbi et al. 2006), carrots (Escobedo-Avellaneda et al. 2011a)
Peleg	Tomato pulp (Greenspan 1977), turnip top leaves and stems (Moreira et al. 2005), carrots (Escobedo-Avellaneda et al. 2011a), Mexican red sauce (Escobedo-Avellaneda et al. 2011b)
Smith	Tomato pulp (Greenspan 1977), mushrooms (Sharma et al. 2009), carrot (Escobedo-Avellaneda et al. 2011a)

then compared to those obtained with the GAB model. The reported values of MRD above 15 % for the Halsey, Henderson, and Oswin equations show that these equations are not suitable for high sugar content products such as fruits.

The mathematical description of sorption isotherms for vegetable products, particularly spray dried tomato pulp (Table 3), shows that in the 20–60 °C temperature range the GAB model best describes the experimental data (MRE < 4 %) followed by the Peleg equation (MRE < 11 %). The Halsey, Henderson, and Oswin equations were not successful in showing MRE values reaching 86 % for the Halsey equation. In contrast, for green pepper, red pepper, and samples with high starch content such as potato, the Halsey and Oswin equations showed better results with MRE values in the 3.7–10.0 % range, while for mushrooms and carrots, the Henderson model was the most suitable with MRE of 0.42 % and 4.7 %, respectively. Table 4 summarizes equations describing the moisture isotherm for other

**Table 4** Mathematical equation used to describe diverse food products moisture sorption isotherm

Equation	Samples
GAB	Cocoa beans (Menkov 2000; Sá and Sereno 1994), millet flour (Jamali et al. 2006), Basundi ready to use (Schmidt and Lee 2012), <i>Chenopodium ambrosioides</i> (pazote) (Johnson and Brennan 2000), cowpea and its protein insolated (Ayrancı and Duman 2005), bitter orange leaves (Moraga et al. 2004), curd powder (Varghese et al. 2008), rice crackers (Singh and Singh 1996), maltodextrin (Lim et al. 1995), safflower petals and tarragon (Kaymak-Ertekin and Gedik 2003), fish flour (Lemus-Mondaca et al. 2009), cornmeal (Gabas et al. 1999), freeze-dried milk products (Katekawa and Silva 2007), starch gels (McMinn et al. 2004), potato starch (Al-Muhtaseb et al. 2002), bean flour (Mohamed et al. 2005), amaranth grains (Peleg 1993), macaroni (Arslan and Toğrul 2005), rice (Tonon et al. 2009), lentil seeds (Menkov et al. 2004), corn starch (Pott et al. 2005)
BET	Cocoa beans (Menkov 2000; Sá and Sereno 1994), millet flour (Jamali et al. 2006), Basundi ready to use (Schmidt and Lee 2012), cowpea and its protein insolated (Ayrancı and Duman 2005), walnut flour (Menkov et al. 2005), curd powder (Varghese et al. 2008), safflower petals and tarragon (Kaymak-Ertekin and Gedik 2003), fish flour (Lemus-Mondaca et al. 2009), cornmeal (Gabas et al. 1999), freeze-dried milk products (Katekawa and Silva 2007), bean flour (Mohamed et al. 2005), macaroni (Arslan and Toğrul 2005), rice (Tonon et al. 2009), lentil seeds (Menkov et al. 2004), corn starch (Pott et al. 2005)
Halsey	Cocoa beans (Sá and Sereno 1994), cowpea and its protein insolated (Ayrancı and Duman 2005), curd powder (Varghese et al. 2008), safflower petals and tarragon (Kaymak-Ertekin and Gedik 2003), freeze-dried milk products (Jamali et al. 2006), starch gels (McMinn et al. 2004), potato starch (Al-Muhtaseb et al. 2002), corn starch (Pott et al. 2005)
Henderson	Curd powder (Varghese et al. 2008), cocoa beans (Sá and Sereno 1994), cowpea and its protein insolated (Ayrancı and Duman 2005), freeze-dried milk products (Katekawa and Silva 2007), starch gels (McMinn et al. 2004), macaroni (Arslan and Toğrul 2005), rice (Tonon et al. 2009), potato starch (Al-Muhtaseb et al. 2002), corn starch (Pott et al. 2005)
Kühn	Cocoa beans (Sá and Sereno 1994), cowpea and its protein insolated (Ayrancı and Duman 2005), freeze-dried milk products (Katekawa and Silva 2007)
Lewicki	Corn starch (Pott et al. 2005)
Oswin	Cowpea and its protein insolated (Ayrancı and Duman 2005), curd powder (Varghese et al. 2008), safflower petals and tarragon (Kaymak-Ertekin and Gedik 2003), freeze-dried milk products (Katekawa and Silva 2007), macaroni (Arslan and Toğrul 2005), rice (Tonon et al. 2009)
Peleg	Starch gels (McMinn et al. 2004), macaroni (Arslan and Toğrul 2005), rice (Tonon et al. 2009), potato starch (Al-Muhtaseb et al. 2002)
Smith	Cocoa beans (Sá and Sereno 1994), cowpea and its protein insolated (Ayrancı and Duman 2005), curd powder (Varghese et al. 2008), starch gels (McMinn et al. 2004), potato starch (Al-Muhtaseb et al. 2002), macaroni (Arslan and Toğrul 2005), rice (Tonon et al. 2009), corn starch (Pott et al. 2005)

food products. For amaranth grains and bean flour, the Henderson, Halsey, and Oswin models had  $MRD < 10\%$ , confirming that these equations can be used to describe high starch products. In conclusion, the models best describing moisture isotherms vary with the product type and composition.

## 7 Thermodynamic Properties: Sorption Heat, Enthalpy ( $\Delta H$ ), and Entropy ( $\Delta S$ )

The determination of thermodynamic sorption properties can lead to an understanding of the molecular interactions between water molecules and the sorbent (Aguerre et al. 1986; Beristain et al. 1996). Enthalpy changes ( $\Delta H$ ) measure energy changes due to the molecular interaction between water molecules and sorbent during sorption processes, while entropy changes ( $\Delta S$ ) can be associated with binding or repulsive forces in the system. Finally, Gibb's free energy ( $\Delta G$ ) is associated with water affinity and provides a criterion to assess whether water sorption occurs as a spontaneous process (Beristain et al. 1996; Apostolopoulos and Gilbert 1990).

Thermodynamic sorption properties can be obtained when moisture isotherms are available at two or more temperature values. Food moisture sorption capacity may decrease with temperature, indicating that the hygroscopic characteristics of the sorbent decreases as well, which can be explained thermodynamically by using the Clausius-Clapeyron relationship (Aguerre et al. 1986; Gabas et al. 1999):

$$\ln a_w = -\frac{Q}{R} \frac{1}{T} \quad (21)$$

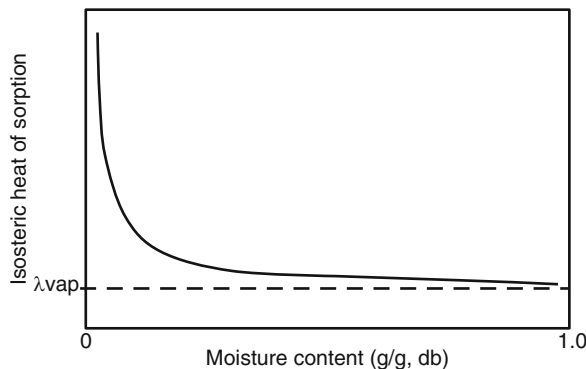
where  $a_w$  is water activity,  $-Q/R$  is the slope in the lineal relationship of  $\ln a_w$  against the inverse absolute temperature ( $T$ ),  $Q$  is isosteric heat of sorption, and  $R$  is the ideal gas constant. The net isosteric heat of adsorption is used to calculate the binding energy between water molecules as follows:

$$\ln a_w = \frac{\Delta H}{RT} - \frac{\Delta S}{R} \quad (22)$$

A linear relationship between the enthalpy and entropy of the moisture sorption forces has been shown for several products where the slope represents the isokinetic temperature ( $T_B$ ) and the intercept is the Gibb's free energy value ( $\Delta G_B$ ) (Aguerre et al. 1986; Beristain et al. 1996; Ferro-Fontan et al. 1982). This relationship (Eq. 23) is known as the enthalpy-entropy compensation or isokinetic theory. This relationship determines if sorption phenomena are controlled by enthalpic or entropic processes.  $T_B$ , defined as the temperature at which all reactions in the series proceed at the same rate, can be compared to the harmonic temperature ( $T_{hm}$ , Eq. 24) to confirm the existence of enthalpy-entropy compensation. When  $T_B > T_{hm}$ , the sorption process is enthalpy controlled, while  $T_{hm} > T_B$  indicates that the process is entropy controlled (Aguerre et al. 1986; Gabas et al. 2000).

$$\Delta H = T_B \Delta S + \Delta G_B \quad (23)$$

**Fig. 5** Schematic representation of isosteric heat of sorption against moisture content in food products



$$T_{\text{hm}} = \frac{n}{\sum_{i=1}^n (1/T)} \quad (24)$$

Beristain et al. (1996) observed the existence of two different mechanisms of moisture adsorption in potato and macadamia nuts. At low  $a_w$ , the process was enthalpy controlled, while subsequent moisture gain is entropy controlled. In contrast, in dried fruits (raisins, currants, figs, prunes, and apricots) the process was enthalpy controlled for the entire moisture content range. Enthalpy-controlled processes were also observed for plum pulp and skin (Gabas et al. 1999), spray dried tomato pulp (Goula et al. 2008), loquat and quince (Moreira et al. 2008), and other high sugar content products.

Isosteric heat of sorption ( $q_{\text{st}}$ ) dependency on food moisture content (Fig. 5) shows that as moisture content increases and  $a_w$  approaches 1.0, it comes close to the vaporization heat of pure water. Values are higher at low moisture values (<20 %) because water molecules in this zone bind directly to the food components. In high sugar content products,  $q_{\text{st}}$  values are higher than in high insoluble fiber content products because in the former, water molecules form hydrogen bonds with sugar molecules and more energy will be required to break them. The isosteric heat of sorption should be considered when evaluating energy requirements in food drying processes (Gabas et al. 1999).

## 8 Applications of Moisture Sorption Isotherms

Sorption isotherms are used to predict the stability of foods sensitive to moisture changes during storage (Bell and Labuza 2000), including microbial activity prediction, evaluation of chemical changes due to moisture gain or loss, enzymatic

reactions, lipid oxidation, and nonenzymatic browning (Iglesias and Chirife 1982). Physical changes may take place during the adsorption process, including stickiness, caking, crystallization, and other alterations caused by  $a_w$  changes. Knowledge of moisture content or  $a_w$  value leading to undesirable changes in product quality, defined as the critical moisture sorption point (MSP), could improve food transport and storage to prevent undesirable product changes.

Product quality losses have also been related to the glass transition point of dehydrated products. An amorphous state is reached in foods with high sugar content when they have been dehydrated; however, when phase changes to a rubbery state, quality loss can occur within days and even hours. The viscosity of amorphous material is around  $10^{12}$  Pa s, and the mobility of water molecules will be low enough to prevent microbial and enzymatic degradation reactions (Xie et al. 2010; Rahman et al. 2003; Liu et al. 2010). This phase change from a glassy state to a rubbery state is known as glass transition, which is a temperature, moisture content, and time dependent process.

Phase transitions can be accelerated by increasing temperature or adding a plasticizer. In high sugar products, water can serve as the plasticizer; thus, the increase in moisture content may decrease the glass transition temperature to the storage temperature (Yuan et al. 2011). The moisture content at which a glass transition takes place at a given storage temperature is a critical moisture content value. Estimations of the critical moisture content and  $a_w$  at the glass transition point are presented in Fig. 6 for structural or texture changes in the final product due to the gain of water (Tonon et al. 2009).

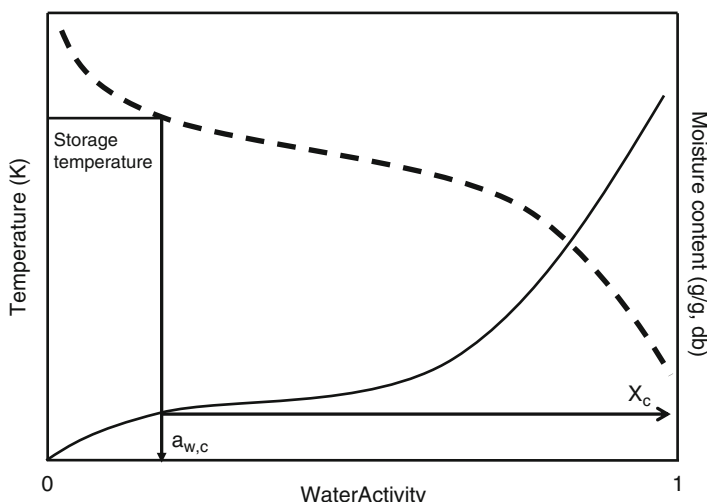


**Fig. 6** Graphical representation of glass transition (dashed line) and moisture sorption isotherms (solid line) used to predict critical moisture content by dried products in order to prevent changes on structural or texture properties

## 9 Sorption Isotherms and Shelf Life Predictions Considering Parameter Variability

Moisture isotherms can be used to select the most appropriate packaging material to achieve a desired shelf life (Welti-Chanes et al. 2008; Escobedo-Avellaneda et al. 2011a). Since the adsorption and desorption processes are not the same due to the hysteresis phenomenon, it is important to use adsorption isotherms when analyzing moisture gain and desorption isotherms. An adequate predictive model is crucial to accurately predict the shelf life of products, such as the one proposed by Labuza and Altunakar (2007):

$$\ln\left(\frac{X_e - X_i}{X_e - X_c}\right) = \frac{k A \cdot p_v^0}{x ds \cdot m} \theta \quad (25)$$

where  $X$  is moisture content (g H<sub>2</sub>O/g dried solids) with the subindices i and c corresponding to the initial and critical values, respectively, while e describes the equilibrium with the storage RH;  $k/x$  (g/m<sup>2</sup> dia mmHg) is the permeance of the packaging film,  $A$  (m<sup>2</sup>) is the packaging area,  $ds$  (g solids) are the dried solids of the food,  $p_v^0$  (mm Hg) is the water vapor pressure at the sorption isotherm temperature,  $m$  is the linearized portion slope of the sorption isotherm in the range of interest (Fig. 7), and  $\theta$  (days) is the estimated shelf life (Bourlieu et al. 2009). Equation (24) allows estimations of shelf life time by considering initial moisture content, moisture content at which the product becomes unacceptable to the consumer, temperature and RH of storage, and packaging material. This equation can be used in a deterministic mode, i.e., when parameter variability is not considered in the calculation and therefore the predicted value does not include a shelf life confidence

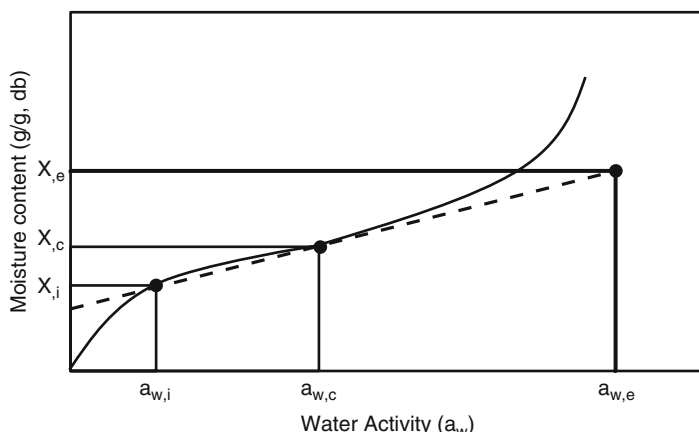


**Fig. 7** Sorption isotherm (*solid line*) used to calculate parameters in shelf life equation for dried foods, where  $X_c$ ,  $X_i$ , and  $X_e$  are the critical, initial, and equilibrium moisture content, respectively

assessment. On the other hand, a Monte Carlo procedure was recently used to consider the variability of the moisture isotherm to estimate frequency distributions for the shelf life of dehydrated tomato slices, chopped onions, and green beans slices (Escobedo-Avellaneda et al. 2011b). A Monte Carlo procedure is a statistical method that allows the generation of frequency distributions describing all possible values for a given outcome (Chotyakul et al. 2011, 2012). This procedure takes into account the statistical variability of all parameters used. Escobedo-Avellaneda et al. (2011b) showed a shelf life of 175.5, 62, and 57 days for tomato, onion, and green beans of intermediate and low moisture content when the variability of GAB parameters and  $a_w$  values was not taken into account. On the other hand, when the standard deviation of GAB parameters and  $a_w$  values was considered, shelf life frequency distributions of about 130–270 days, 55–69 days, and 51–65 days for tomato, onion, and green beans were obtained, respectively. If the accepted probability that the shelf life would fail before the time specified were 5 %, the recommended shelf life for tomato, onion, and green beans would be 150 days, 58 days, and 53 days, respectively. On the other hand, if the average values for the prediction model parameters were used to estimate shelf life, the probability of product failure before this value would be equal to or higher than 50 %. Therefore, the Monte Carlo method proposed by these authors is an effective tool to determine the shelf life of food products with an acceptable risk of product failure before the shelf life declared by the producer on its label.

## 10 Final Remarks

Sorption isotherms play a critical role in the description of the properties of hygroscopic materials and are used to establish proper handling and storage conditions to extend the shelf life of low and intermediate moisture content products. The described experimental methods for determination of sorption isotherms are critical for estimation of the hygroscopic properties of foods. Automatic equipment has been developed to facilitate obtaining sorption isotherms, reducing experimental times and even increasing the resolution of the experimental data obtained. However, studies with these units should be expanded to include more complex systems and improve their design and the procedures to follow when using them. Methods to determine which equations can best describe experimental moisture sorption data allow more accurate prediction of conditions of stability, and necessary processes in the study data have shown that no equation can describe all products and the entire  $a_w$  range. Adequate descriptions of the moisture data for various products in the 0.03–0.95  $a_w$  range have been reported for the GAB, Peleg, and Lewicki 3-parameter equations. Thermodynamic properties from sorption isotherms can be used in drying process design, or in shelf life prediction for intermediate and low moisture content products, or in setting storage condition and selection of the properties of the packaging materials. Finally, nondeterministic

calculation procedures such as the Monte Carlo method represent a new opportunity to improve shelf life estimations.

**Acknowledgments** The authors acknowledge the financial support from Tecnológico de Monterrey (Research Chair Funds CAT-00200 and Nutrigenómica), and author Claudia Caballero-Cerón thanks for the financial support for her graduate studies to CONACYT and Tecnológico de Monterrey.

## References

- Aguerre RJ, Suárez C, Viollaz PE (1986) Enthalpy-entropy compensation in sorption phenomena: application to the prediction of the effect of temperature on food isotherms. *J Food Sci* 51:1547–1549
- Akanbi CT, Adeyemi RS, Ojo A (2006) Drying characteristics and sorption isotherm of tomato slices. *J Food Eng* 73:157–163
- Al-Muhtaseb AH, McMinn WAM, Magee TRA (2002) Moisture sorption isotherm characteristics of food products: a review. *Trans IChemE* 80:118–128
- Al-Muhtaseb AH, McMinn WAM, Magee TRA (2004) Water sorption isotherms of starch powders. Part 1: Mathematical description of experimental data. *J Food Eng* 61:297–307
- Apostolopoulos D, Gilbert SG (1990) Water sorption of coffee solubles by frontal inverse gas chromatography: thermodynamic considerations. *J Food Sci* 55:475–477
- Arlabosse P, Rodier E, Ferrasse JH, Chavez S, Lecomte D (2003) Comparison between static and dynamic methods for sorption isotherm measurements. *Dry Tech* 21:479–497
- Arslan N, Toğrul H (2005) Modeling of water sorption isotherms of macaroni stored in a chamber under controlled humidity and thermodynamic approach. *J Food Eng* 69:133–145
- Ayrancı E, Duman O (2005) Moisture sorption isotherms of cowpea (*Vigna unguiculata* L. Walp) and its protein isolate at 10, 20 and 30 °C. *J Food Eng* 70:83–91
- Basu S, Shivhare US, Mujumdar AS (2006) Models for sorption isotherms for foods: a review. *Dry Tech* 24:917–930
- Baucour P, Daudin J (2000) Development of a new method for fast measurement of water sorption isotherms in the high humidity range validation on gelatin gel. *J Food Eng* 44:97–107
- Belarbi A, Aymard C, Meot JM, Themelin A, Reynes M (2000) Water desorption isotherms for eleven varieties of dates. *J Food Eng* 43:103–107
- Bell LN, Labuza TP (2000) Moisture sorption: practical aspects of isotherm measurement and use, 2nd edn. American Association of Cereal Chemists, St. Paul, MN
- Benedetti PDCD, Pedro MAM, Telis-Romero J, Telis VRN (2011) Influence of encapsulating materials on water sorption isotherms of vacuum-dried persimmon pulp powder. *J Food Process Preserv* 35:423–431
- Beristain CI, Garcia HS, Azuara E (1996) Enthalpy-entropy compensation in food vapor adsorption. *J Food Eng* 30:3–4
- Bhandari BR, Adhikari B (2008) Water activity in food processing and preservation. In: Chen XD, Arun SM (eds) *Drying technologies in food processing*. Blackwell Publishing Ltd., West Sussex, pp 55–89
- Bourlieu C, Guillard V, Vallès-Pamiès B, Guilbert S, Gontard N (2009) Edible moisture barriers: how to assess of their potential and limits in food products shelf-life extension? *Crit Rev Food Sci Nutr* 49:474–499
- Brunauer S, Emmett PH, Teller E (1938) Adsorption of gases in multimolecular layers. *J Am Chem Soc* 60:309–319
- Carter B, Fontana A (2008) Dynamic dewpoint isotherm versus other moisture sorption isotherm methods. Application note. Decagon Devices, Pullman, WA

- Carter BP, Schmidt SJ (2012) Developments in glass transition determination in foods using moisture sorption isotherms. *Food Chem* 132:1693. doi:[10.1016/j.foodchem.2011.06.022](https://doi.org/10.1016/j.foodchem.2011.06.022)
- Chotyakul N, Velazquez G, Torres JA (2011) Assessment of the uncertainty in thermal food processing decisions based on microbial safety objectives. *J Food Eng* 102:247–256
- Chotyakul N, Pérez Lamela C, Torres JA (2012) Effect of model parameter variability on the uncertainty of refrigerated microbial shelf-life estimates. *J Food Process Eng* 35:829. doi:[10.1111/j.1745-4530.2010.00631.x](https://doi.org/10.1111/j.1745-4530.2010.00631.x)
- Corey ME, Kerr WL, Mulligan JH, Lavelli V (2011) Phytochemical stability in dried apple and green tea functional products as related to moisture properties. *LWT Food Sci Technol* 44:67–74
- Duarte Goneli AL, Corrêa PC, Horta De Oliveira GH, Ferreira Gomes C, Mendes Botelho F (2010) Water sorption isotherms and thermodynamic properties of pearl millet grain. *Int J Food Sci Technol* 45:828–838
- Eim VS, Rosselló C, Femenia A, Simal S (2011) Moisture sorption isotherms and thermodynamic properties of carrot. *Int J Food Eng* 7(3):1. doi:[10.2202/1556-3758.1804](https://doi.org/10.2202/1556-3758.1804)
- Escobedo-Avellaneda Z, Pérez-Pérez MC, Bárcenas-Pozos ME, Welti-Chanes J (2011a) Moisture adsorption isotherms of freeze-dried and air-dried Mexican red sauce. *J Food Process Eng* 34:1931–1945
- Escobedo-Avellaneda Z, Velazquez G, Torres JA, Welti-Chanes J (2011b) Inclusion of the variability of model parameters on shelf-life estimations for low and intermediate moisture vegetables. *LWT Food Sci Technol* 47:364–370
- Ferro-Fontan C, Chirife J, Sancho E, Iglesias HA (1982) Analysis of a model for water sorption phenomena in foods. *J Food Sci* 47:1590–1594
- Furmaniak S, Terzyk AP, Golembiewski R, Gauden PA, Czepirski L (2009) Searching the most optimal model of water sorption on foodstuffs in the whole range of relative humidity. *Food Res Int* 42:1203–1214
- Gabas AL, Telis-Romero J, Menegalli FC (1999) Thermodynamic models for water sorption by grape skin and pulp. *Dry Tech* 17:962–974
- Gabas AL, Menegalli FC, Telis-Romero J (2000) Water sorption enthalpy-entropy compensation based on isotherms of plum skin and pulp. *J Food Sci* 65:680–684
- Goula AM, Karapantsios TD, Achilias DS, Adamopoulos KG (2008) Water sorption isotherms and glass transition temperature of spray dried tomato pulp. *J Food Eng* 85:73–83
- Greenspan L (1977) Humidity fixed points of binary saturated aqueous solutions. *J Res Natl Bur Stand* 81a:89–112
- Halsey G (1948) Physical adsorption in non-uniform surfaces. *J Chem Phys* 16:931
- Henderson SM (1952) A basic concept of equilibrium moisture. *Agric Eng* 33:29–35
- Hossain MD, Bala BK, Hossain MA, Mondol MRA (2001) Sorption isotherms and heat of sorption of pineapple. *J Food Eng* 48:103–107
- Iglesias HA, Chirife J (1976) Equilibrium moisture contents of air dried beef. Dependence on drying temperature. *Int J Food Sci Technol* 11:565–573
- Iglesias HA, Chirife J (1982) Handbook of food isotherms. Academic, New York, NY
- Jamali A, Kouhila M, Mohamed LA, Jaouhari JT, Idimam AI, Abdenouri N (2006) Sorption isotherms of Chenopodium ambrosioides leaves at three temperatures. *J Food Eng* 72:77–84
- Johnson P-NT, Brennan JG (2000) Moisture sorption isotherm characteristics of plantain (*Musa*, AAB). *J Food Eng* 44:79–84
- Jouppila K, Roos YH (1997) Water sorption isotherms of freeze-dried milk products: applicability of linear and non-linear regression analysis in modeling. *Int J Food Sci Technol* 32:459–471
- Katekawa ME, Silva MA (2007) On the influence of glass transition on shrinkage in convective drying of fruits: a case study of banana drying. *Dry Tech* 25:1659–1666
- Kaya S, Kahyaoglu T (2007) Moisture sorption and thermodynamic properties of safflower petals and tarragon. *J Food Eng* 78:413–421
- Kaymak-Ertekin F, Gedik A (2003) Sorption isotherms and isosteric heat of sorption for grapes, apricots, apples and potatoes. *LWT Food Sci Technol* 37:429–438

- Kaymak-Ertekin F, Sultanoğlu M (2001) Moisture sorption isotherm characteristics of peppers. *J Food Eng* 47:225–231
- Kim HK, Song Y, Yam KL (1991) Water sorption characteristics of dried red peppers (*Capsicum annuum* L.). *Int J Food Sci Technol* 29:339–345
- Kingsly ARP, Ileleji KE (2009) Sorption isotherm of corn distillers dried grains with solubles (DDGS) and its prediction using chemical composition. *Food Chem* 116:939–946
- Kühn I (1964) A new theoretical analysis of adsorption phenomena. Introductory part: the characteristic expression of the main regular types of adsorption isotherms by single simple equation. *J Coll Sci* 19:685–698
- Labuza TP, Altunakar B (2007) Water activity prediction and moisture sorption isotherms. In: Barbosa-Cánovas GV, Fontana AJ, Schmidt SJ, Labuza TP (eds) *Water activity in foods: Fundamentals and applications*. IFT/Blackwell, Ames, IA, pp 109–154
- Lemus-Mondaca R, Betoret N, Vega-Galváz A, Lara-Aravena E (2009) Dehydration characteristics of papaya (*Carica pubescens*): determination of equilibrium moisture content and diffusion coefficient. *J Food Process Eng* 32:645–663
- Lewicki PP (1998) A three parameter equation for food moisture sorption isotherms. *J Food Process Eng* 21:127–144
- Lewicki PP (2000) Raoult's law based food water sorption isotherm. *J Food Eng* 43:31–40
- Li QE, Schmidt SJ (2011) Use of ramping and equilibrium water vapor sorption methods to determine the critical relative humidity at which the glassy to rubbery transition occurs in polydextrose. *J Food Sci* 76:149–157
- Lim LT, Tang J, He J (1995) Moisture sorption characteristics of freeze dried blueberries. *J Food Sci* 60:810–814
- Liu P, Yu L, Wang X, Li D, Chen L, Li X (2010) Glass transition temperature of starches with different amylose/amyolectin ratios. *J Cereal Sci* 51:388–391
- López-Malo A, Palou E, Argaiz A (1994) Measurement of water activity of saturated salt solutions at various temperatures. In: Argaiz A, López-Malo A, Palou E, Corte P (eds) *Proceeding of the session, ISOPOW Practicum II*. Universidad de las Américas Puebla, Puebla, pp 113–116
- McMinn WAM, Magee TRA (2003) Thermodynamic properties of moisture sorption of potato. *J Food Eng* 60:157–165
- McMinn WAM, Al-Muhtaseb AH, Magee TRA (2003) Moisture sorption characteristics of starch gels. Part 1: Mathematical description of experimental data. *J Food Process Eng* 26:323–338
- McMinn WAM, Al-Muhtaseb AH, Magee TRA (2004) Assessment of two- and three-parameter Lewicki models for description of sorption phenomena of starch materials. *J Sci Food Agric* 84:1695–1700
- Medeiros ML, Ayrosa AMIB, Pitombo RNM, Lannes SCS (2006) Sorption isotherms of cocoa and cupuassu products. *J Food Eng* 73:402–406
- Menkov ND (2000) Moisture sorption isotherms of lentil seeds at several temperatures. *J Food Eng* 44:205–211
- Menkov ND, Durakova AG, Krasteva A (2004) Moisture sorption isotherms of walnut flour at several temperatures. *Biotechnol Biotechnol Equip* 18:201–206
- Menkov ND, Durakova AG, Krasteva A (2005) Moisture sorption isotherms of common bean flour at several temperatures. *Electron J Environ Agric Food Chem* 4:892–898
- Mohamed LA, Kouhila M, Jamali A, Lahsasni S, Mahrouz M (2005) Moisture sorption isotherms and heat of sorption of bitter orange leaves (*Citrus aurantium*). *J Food Eng* 67:491–498
- Moraga G, Martínez-Navarrete N, Chiralt A (2004) Water sorption isotherms and glass transition in strawberries: influence of pretreatment. *J Food Eng* 62:315–321
- Moraga G, Martínez-Navarrete N, Chiralt A (2006) Water sorption isotherms and phase transitions in kiwifruit. *J Food Eng* 72:147–156
- Moraga G, Talens P, Moraga MJ, Martínez-Navarrete N (2011) Implication of water activity and glass transition on the mechanical and optical properties of freeze-dried apple and banana slices. *J Food Eng* 106:212–219

- Moreira R, Chenlo F, Vázquez MJ, Cameán P (2005) Sorption isotherms of turnip top leaves and stems in the temperature range from 298 to 328 K. *J Food Eng* 71:193–199
- Moreira R, Chenlo F, Torres MD, Vallejo N (2008) Thermodynamic analysis of experimental sorption isotherms of loquat and quince fruits. *J Food Eng* 88:514–521
- Moreira R, Chenlo F, Torres MD (2009) Simplified algorithm for the prediction of water sorption isotherms of fruits, vegetables and legumes based upon chemical composition. *J Food Eng* 94 (3–4):334–343
- Myhara RM, Taylor MS, Slominski BA, Al-Bulushi I (1998) Moisture sorption isotherms and chemical composition of Omani dates. *J Food Eng* 37:471–479
- Oswin CR (1946) The kinetics of package life. III. The isotherm. *J Soc Chem Ind* 65(12):419–421
- Peleg M (1993) Assessment of a semi-empirical four parameter general model for sigmoid moisture sorption isotherms. *J Food Process Eng* 16:21–37
- Pott I, Neidhart S, Mühlbauer W, Carle R (2005) Quality improvement of non-sulphited mango slices by drying at high temperatures. *Innov Food Sci Emerg Technol* 6:412–419
- Quirijns EJ, van Boxtel AJB, van Loon WKP, van Straten G (2005) Sorption isotherms, GAB parameters and isosteric heat of sorption. *J Sci Food Agric* 85:1805–1814
- Rahman MS (1995) Food properties handbook. CRC, Boca Raton, FL
- Rahman MS (2009) Food stability beyond water activity and glass transition: macro-micro region concept in the state diagram. *Int J Food Prop* 12:726–740
- Rahman MS, Al-Belushi RH (2006) Dynamic isopiestic method (DIM): measuring moisture sorption isotherm of freeze-dried garlic powder and other potential uses of DIM. *Int J Food Prop* 9:421–437
- Rahman MS, Kasapis S, Guizani N, Al-Amri OS (2003) State diagram of tuna meat: freezing curve and glass transition. *J Food Eng* 57:321–326
- Rockland LR (1960) Saturated salt solutions for static control of relative humidity between 5° and 40°C. *Anal Chem* 32:1375–1376
- Roman-Gutierrez AD, Guilbert S, Cuq B (2002) Distribution of water between wheat flour components: a dynamic water vapor adsorption study. *J Cereal Sci* 36:347–355
- Ruiz-López II, Herman-Lara E (2009) Statistical indices for the selection of food sorption isotherm models statistical indices for the selection of food sorption isotherm models. *Dry Tech* 27:726–738
- Sá MM, Sereno AM (1994) Glass transition and state diagrams for typical natural fruits and vegetables. *Thermochim Acta* 246:285–297
- Schmidt SJ, Lee JW (2012) Comparison between water vapor sorption isotherms obtained using the new dynamic dewpoint isotherm method and those obtained using the standard saturated salt slurry method. *Int J Food Prop* 15:236–248
- Sharma P, Singh RRB, Singh AK, Patel AA, Patil GR (2009) Sorption isotherms and thermodynamics of water sorption of ready-to-use Basundi mix. *LWT Food Sci Technol* 4:441–445
- Singh PC, Singh RK (1996) Application of GAB model for water sorption isotherms of food products. *J Food Process Preserv* 20:203–220
- Smith SE (1947) The sorption of water vapor by high polymers. *J Am Chem Soc* 69:646–651
- Spackman CCW, Schmidt SJ (2010) Characterizing the physical state and textural stability of sugar gum pastes. *Food Chem* 119:490–499
- Spiess WEL, Wolf W (1987) Critical evaluation of methods to determine moisture sorption isotherms. In: Rockland LR, Beuchat LR (eds) Water activity: theory and applications to food. Institute of Food Technologists, Chicago, IL, pp 215–233
- Talla A, Jannot Y, Elambo Nkeg G, Puiggall J-R (2005) Experimental determination and modeling of sorption isotherms of tropical fruits: banana, mango, and pineapple experimental determination and modeling of sorption isotherms of tropical. *Dry Tech* 23:1477–1498
- Timmermann EO, Chirife J, Iglesias HA (2001) Water sorption isotherms of foods and foodstuffs: BET or GAB parameters? *J Food Eng* 48:19–31

- Tonon RV, Baroni AF, Brabet C, Gibert O, Pallet D, Hubinger MD (2009) Water sorption and glass transition temperature of spray dried açai (*Euterpe oleracea* Mart.) juice. *J Food Eng* 94:215–221
- van den Berg C, Bruins S (1981) Water activity and its estimation in food systems: theoretical aspects. In: Rockland LR, Stewart GF (eds) *Water activity: influence on food quality*. Academic Press, Inc., New York, NY, pp 1–61
- Varghese KS, Ramachandranair SV, Mishra HN (2008) Moisture sorption characteristics of curd (Indian yogurt) powder. *Int J Dairy Technol* 62:85–92
- Vega-Gálvez A, López J, Miranda M, DiScala K, Yagnam F, Uribe E (2009) Mathematical modeling of moisture sorption isotherms and determination of isosteric heat of blueberry variety O'Neil. *Int J Food Sci Technol* 44:2033–2041
- Viollaz PE, Rovedo CO (1999) Equilibrium sorption isotherms and thermodynamic properties of starch and gluten. *J Food Eng* 40:287–292
- Viswanathan R, Jayas DS, Hulasare RB (2003) Sorption isotherms of tomato slices and onion shreds. *Biosyst Eng* 86:465–472
- Welti-Chanes J, Pérez E, Guerrero-Beltrán JA, Alzamora SM, Vergara-Balderas F (2008) Applications of water activity management in the food industry. In: Barbosa-Canovas GV, Fontana AJ, Schmidt AR, Labuza TP (eds) *Water: activity in foods*. Blackwell Publishing Ltd., Oxford, UK, pp 341–357
- Xie F, Liu W-C, Liu P, Wang J, Halley PJ, Yu L (2010) Starch thermal transitions comparatively studied by DSC and MTDSC. *Starch* 62:350–357
- Yan Z, Sousa-Gallagher J, Oliveira FAR (2008a) Sorption isotherms and moisture sorption hysteresis of intermediate moisture content banana. *J Food Eng* 86:342–348
- Yan Z, Sousa-Gallagher MJ, Oliveira FAR (2008b) Effect of temperature and initial moisture content on sorption isotherms of banana dried by tunnel drier. *Int J Food Sci Technol* 43:1430–1436
- Yao W, Yu X, Lee JW, Yuan X, Schmidt SJ (2011) Measuring the deliquescence point of crystalline sucrose as a function of temperature using a new automatic isotherm generator. *Int J Food Prop* 14:882–893
- Yu X, Kappes SM, Bello-Pérez LA, Schmidt SJ (2008a) Investigating the moisture sorption behavior of amorphous sucrose using a dynamic humidity generating instrument. *J Food Sci* 73(1):25–35
- Yu X, Martin SE, Schmidt SJ (2008b) Exploring the problem of mold growth and the efficacy of various mold inhibitor methods during moisture sorption isotherm measurements. *J Food Sci* 73:69–81
- Yu X, Schmidt AR, Bello-Pérez LA, Schmidt SJ (2008c) Determination of the bulk moisture diffusion coefficient for corn starch using an automated water sorption instrument. *J Agric Food Chem* 56:50–58
- Yuan X, Carter BP, Schmidt SJ (2011) Determining the critical relative humidity at which the glassy to rubbery transition occurs in polydextrose using an automatic water vapor sorption instrument. *J Food Sci* 76(1):78–89

# **Understanding Cryopreservation of Oyster Oocytes from a Physical Chemistry Perspective**

**M.H. Lim, L.F. Siow, and L. Salinas-Flores**

## **Abbreviations**

CF	Carboxyfluorescein
CPA	Cryoprotection agents
DPPC	Dipalmitoylphosphocholine
EPC	Egg yolk phosphatidylcholine
IIF	Intracellular ice formation
LUV	Large unilaminar vesicles
TEM	Transmission electron microscopy

## **1 Introduction**

Cryopreservation applies to the freezing, storage (usually long-term) at a very low temperature, thawing, and successful recovery of living cells. There are seven basic steps in cryopreservation protocols: sample collection, maintenance of collected material in extender solutions, quality assessment, refrigerated storage, freezing, thawing, and viability assessment (Tiersch 2000). Cell viability can be affected at any of these steps, although most damage occurs due to exposure of cells to high

---

M.H. Lim (✉)

Nutrition and Bioproduct Research Theme, Crops for the Future,  
University of Nottingham Malaysia Campus, Semenyih, Selangor, Malaysia  
e-mail: [mianglim@cffresearch.org](mailto:mianglim@cffresearch.org)

L.F. Siow

School of Science, Monash University, Sunway Campus, Selangor, Malaysia

L. Salinas-Flores

Department of Food Science, University of Otago, Dunedin, New Zealand

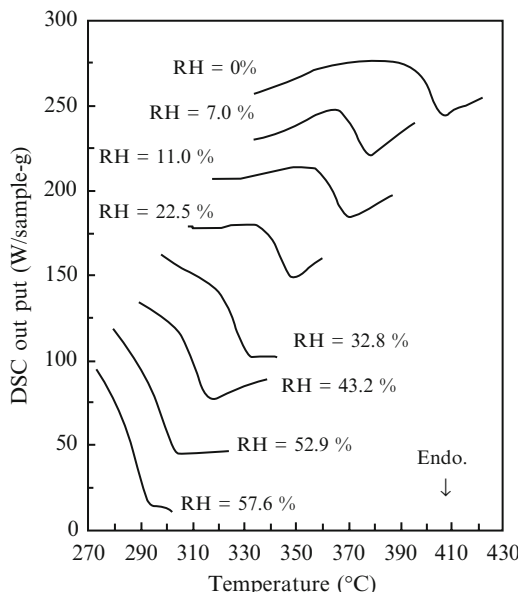


**Fig. 1** Schematic representation of a cell undergoing a freezing process. Water and solute content of the cell and its extracellular medium are at equilibrium before freezing. As temperature goes below the freezing point of the medium, ice is usually formed extracellularly, initially. As a result, solutes are extracellularly being frozen in concentrated form. An osmotic gradient created in this way causes the intracellular water to diffuse out of the cell. Intracellular ice may be formed if there is remaining water in the cell when the temperature goes below its freezing point. *s* = solutes, *w* = water, blue triangles = ice crystals

concentrations of intra- and extracellular solutes or due to intracellular ice formation (IIF) during cooling and/or thawing. It has been suggested that the growth and propagation of intracellular ice crystals cause cell death through disruption of the cell membrane. Extracellular ice has also been shown to cause mechanical damage of cells (Sterling 1968; Rubinsky et al. 1990). The formation of extracellular ice also increases solute concentration in the remaining unfrozen matrix (Mazur et al. 1972; Pegg 2002), which leads to additional stress such as solute toxicity (Mazur et al. 1972) and causes cells to shrink osmotically (Lovelock 1953; Steponkus et al. 1983). The consequences of the freezing process on a cell are represented schematically in Fig. 1.

## 2 Effect of Rate of Cooling

The rate of cooling of the cellular materials affects the rate of ice formation, which usually occurs spontaneously in the extracellular matrix. The rate of extracellular freezing, in turn, affects the rate of cell dehydration, concentration of intra- and

extracellular solutes and formation of intracellular ice. Membrane permeability of cells is an additional factor that affects the rate of water diffusion out of the cells. In studies of cells of the same biological sources, cell membrane permeability is presumed to be constant; therefore, only the effect of cooling rates are discussed in this paper.

In slow cooling rates, formation of extracellular ice (spontaneous or manually seeded) creates an osmotic gradient between the concentrated solutes in the extracellular unfrozen matrix and the less concentrated intracellular matrix, and thus water diffuses out of the cells. The slow decrease in temperature gradually dehydrates and shrinks the cells through the gradual increase of solute concentration in the unfrozen matrix. As a result, the most common cryo-injury is caused by high solute concentration (Fahy et al. 1990) and excessive cell shrinkage (Steponkus et al. 1981). However, in other studies, it has been shown that freeze-concentration of cells is more detrimental than solute concentration effects (Mazur 1984; Mazur and Cole 1985). In slow freezing, if the cells are allowed to undergo enough dehydration, then no intracellular ice will be formed.

In fast cooling rates, the formation of ice in the extracellular matrix is so fast that there is insufficient time for cells to exosmose most of the intracellular water, and thus intracellular freezing is likely to happen (Acker and McGann 2003). Intracellular ice formation is the most common cryo-injury when fast cooling rates are used in cryopreservation. Rapid thawing is especially required of these cells, as intracellular ice crystals tend to recrystallize during warming and damage the cells (Mazur 1970; Gao and Critser 2002). Nonetheless, fast cooling rates have proven to be effective in some cases (Hagedorn et al. 2004), probably because the cells are exposed to less concentrated solutes for a shorter period of time.

An ideal cooling rate could be such that it is slow enough to allow cell dehydration and reduction of IIF without excessive shrinkage, but fast enough to avoid the effect of a concentrated solute environment. Cryopreservation protocols are specific to each cell types (Mazur 1984). Therefore, the complexity of cellular freezing calls for a better understanding of the freezing process during cryopreservation. This paper discusses two approaches taken to evaluate the consequences of the freezing process. The first approach is through a systematic analysis of the freezing steps with the live cells (oyster oocytes); the second approach uses liposomes as a model cell membrane system undergoing a similar process.

## 2.1 *Cryopreservation of Oyster Oocytes*

A detailed study on the viability of oyster oocytes cryopreserved using a previously published protocol (Tervit et al. 2005), hereafter referred to as the standard protocol, was tested at each of the steps of the protocol in an effort to understand which of the steps caused damage to the oocytes. Cryomicroscopy and transmission electron microscopy were used to assess the presence of intracellular ice in the cells. Details of methods and results in this section can be referred to in Salinas-Flores et al. (2008).

Oyster oocytes were collected from Pacific oysters (*Crassostrea gigas*) from marine farms throughout New Zealand. Oocyte viability (% fertilized) was assessed at each of the following steps of the cryopreservation process, where a subsequent step is an additional step to the previous ones: (a) after loading with cryoprotection agents (CPA) and equilibration for 10 min at 20 °C, (b) after cooling to 10 °C at 1 °C min<sup>-1</sup> and before seeding, (c) after a 5 min hold at 10 °C and seeding, (d) after cooling to 35 °C at 0.3 °C min<sup>-1</sup>, and (e) after plunging into liquid nitrogen. A control treatment was included by fertilizing fresh oocytes.

The results of the ability of oocytes to fertilize after each of the steps in the standard protocol show that the highest fertilization rate was recorded for the control with fresh oocytes (84.0 ± 2.3 %); steps a, b, and c were not significantly different from the control ( $P > 0.05$ ). Lowest fertilization was recorded for step e, where oocytes were plunged into liquid nitrogen (36.1 ± 5.0 %), and step d was not significantly from step e. Steps d and e were both significantly different from the control.

### 2.1.1 Assessment of IIF by Cryomicroscopy

Cryomicroscopy was used to determine whether IIF had occurred in oocytes. A programmable cold stage (HCS302 Instec, Boulder, CO) was used to observe the events that occur during cooling and warming of oyster oocytes. The effect of three cooling rates on the temperature of intracellular ice formation was assessed by recording the temperature at which oyster oocytes darkened. The cumulative frequency of darkened oocytes as a function of temperature is presented in Fig. 2.

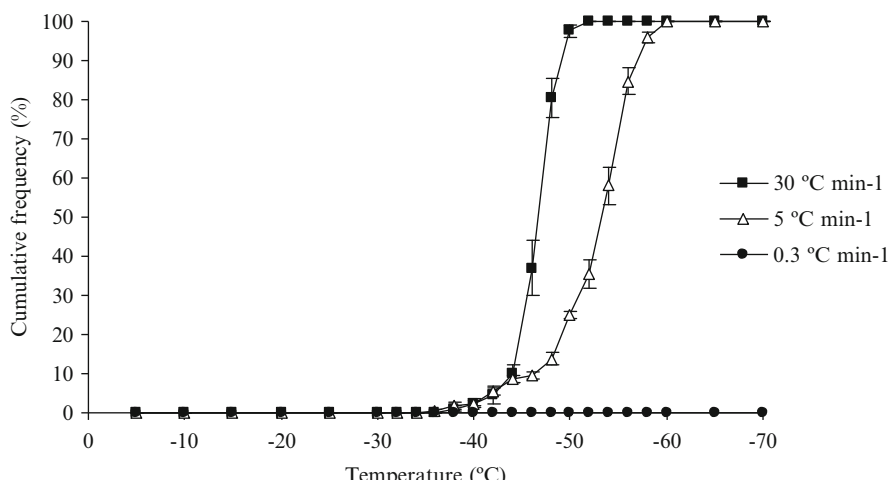


**Fig. 2** Effect of cooling rate on the temperature of intracellular ice formation in oyster oocytes. Oocytes were loaded with 10 % ethylene glycol in deionized water and cooled to -10 °C, then cooled to -70 °C at 30, 5 or 0.3 °C min<sup>-1</sup> (data represent a mean of ±SEM;  $n = 3$ )

For oocytes cooled at  $30\text{ }^{\circ}\text{C min}^{-1}$ , cell darkening was observed between  $-38.0$  and  $-52.0\text{ }^{\circ}\text{C}$ , with a median value of  $-46.6 \pm 0.2\text{ }^{\circ}\text{C}$ . For oocytes cooled at  $5\text{ }^{\circ}\text{C min}^{-1}$ , darkening occurred between  $-36.4$  and  $-60.3\text{ }^{\circ}\text{C}$ , with a median value of  $-53.9 \pm 0.1\text{ }^{\circ}\text{C}$ . No cell darkening was observed when oocytes were cooled at  $0.3\text{ }^{\circ}\text{C min}^{-1}$ . These results indicated that the oocytes did not form intracellular ice when they were cooled at the very slow rate of  $0.3\text{ }^{\circ}\text{C min}^{-1}$ .

### 2.1.2 Assessment of IIF by Transmission Electron Microscopy (TEM)

Verification of the absence of IIF in oocytes cooled at  $0.3\text{ }^{\circ}\text{C min}^{-1}$  was carried out in the TEM (Salinas et al. 2008). Under the TEM, ice crystals were observed as white, round or oval structures homogeneously spread throughout the cell (Fig. 3a, b) and were distinct from the abundant lipid droplets, which appeared as black and dark gray, round structures. Although it was found that all oocytes contained ice crystals in the cytoplasm, only some of them contained ice in the nucleus. This observation led to the development of the cooling programs (Table 1) to target IIF reduction.

### 2.1.3 The Effect of Cooling Rates, Holding Times, and Plunging Temperatures on IIF and Post-Thaw Fertilization

As a result of the above studies, the cooling rate to the plunging temperature (step d) and the plunging temperatures (step e) were further investigated. Variables such as a slower post-extracellular ice formation-cooling rate ( $0.1\text{ }^{\circ}\text{C min}^{-1}$  versus  $0.3\text{ }^{\circ}\text{C min}^{-1}$ ); longer holding time at the plunge temperature (30 min versus 0 min) and lower plunge temperature ( $-60\text{ }^{\circ}\text{C}$  versus  $-35\text{ }^{\circ}\text{C}$ ) were assessed as outlined in Table 1. Samples corresponding to Programs A and H were analyzed in detail on the TEM.

The average post-thaw fertilization rates are given in Table 2. These rates were plotted against the total time of exposure to extracellular ice formation (Fig. 4). Table 2 shows that programs A, B E, and F, which are oocytes with plunging temperature at  $-35\text{ }^{\circ}\text{C}$  have significantly higher post-thaw fertilization rates than those plunged at  $-60\text{ }^{\circ}\text{C}$  (programs C, D, G, and H). This result can be better illustrated in Fig. 4, where the overall post-thaw fertilization rate of oocytes plunged at  $-35\text{ }^{\circ}\text{C}$  (data clustered in ovals) is higher than that of oocytes plunged at  $-60\text{ }^{\circ}\text{C}$  (data clustered in rectangles), indicating it was critical that the plunging temperature of the samples into liquid nitrogen cannot be too low. Groups that were plunged at  $-60\text{ }^{\circ}\text{C}$  (programs G and H) yielded the lowest post-thaw fertilization rates. The figure also shows a definitive lower fertilization rate of the samples plunged at  $-60\text{ }^{\circ}\text{C}$  and cooled at  $0.1\text{ }^{\circ}\text{C min}^{-1}$  as opposed to the rest of the treatments, which could be an indication of the oocytes being in a freeze concentrated condition for a much longer period than the other treatments. On the other hand, the holding time for 30 min at the plunging temperature was not significant in affecting the fertilization rate.

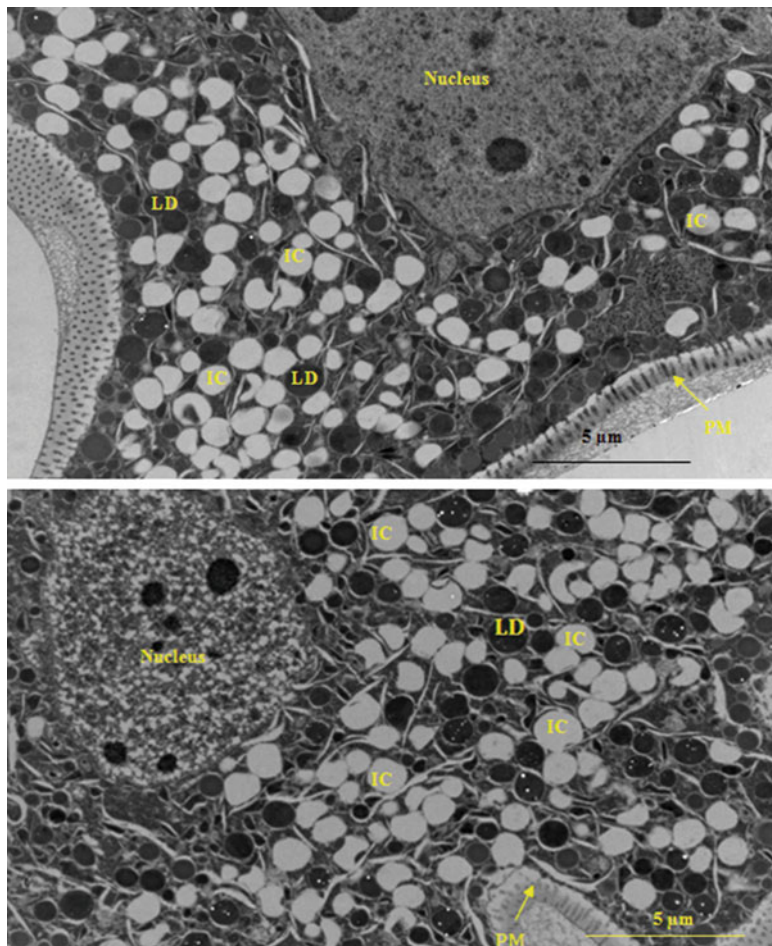


**Fig. 3** Transmission electron micrographs of oyster oocytes after freeze substitution. Oocytes were frozen using the protocol of Tervit et al. (2005). Instead of thawing the samples, sections of the straws were cut under liquid nitrogen, freeze substituted, and prepared for electron microscopy. For visual simplicity, only the relevant structures are labeled in (a) (*IC* ice crystals, *N* nucleus, *LD* lipid droplets, *PM* plasma membrane). Scale bar on the *bottom right* measures 5  $\mu\text{m}$

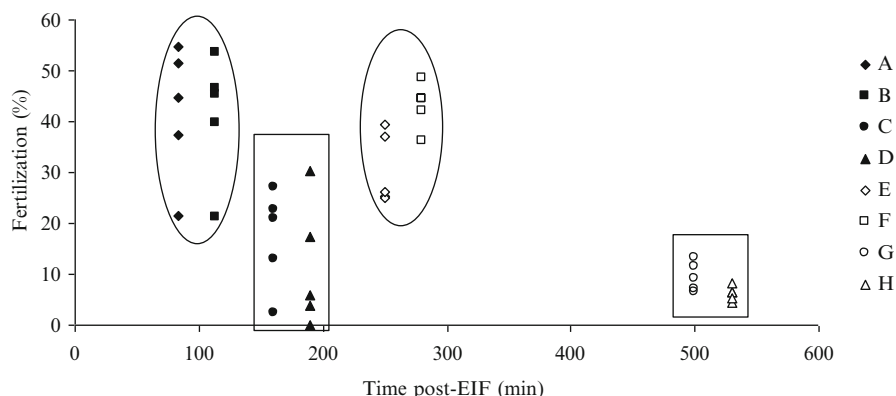
A further detailed TEM analysis of oocytes from programs A and H shows that despite the fertilization rate in program A being significantly higher than H, the mean diameter of the ice crystals in the cytoplasm was found not to differ significantly between the two programs ( $P > 0.05$ ). More interestingly, the amount of ice in the cytoplasm and the proportion of oocytes with ice crystals in the nucleus were significantly higher in the A program than in the H program ( $P < 0.05$ ). Therefore, it was evident that IIF in oyster oocytes was not detrimental for their survival during cryopreservation.

**Table 1** Cooling programs used to reduce intracellular ice formation in oyster oocytes

Program	Cooling rate (°C min <sup>-1</sup> )	Holding time (min)	Plunge temperature (°C)
A <sup>a</sup>	0.3	0	-35
B		30	
C	0.3	0	-60
D		30	
E	0.1	0	-35
F		30	
G		0	-60
H		30	

<sup>a</sup>Standard protocol**Table 2** Post-thaw fertilization rate of oyster oocytes cooled with different programs aimed to reduce intracellular ice formation (data represent mean ± SEM; n = 5; superscripts next to the values indicate significant differences ( $P < 0.05$ ))

Program	Fertilization (%)
A	42.0 (±5.9) <sup>a</sup>
B	41.2 (±5.5) <sup>a</sup>
C	17.3 (±4.3) <sup>b,c</sup>
D	11.5 (±5.5) <sup>c</sup>
E	30.6 (±3.1) <sup>a,b</sup>
F	43.2 (±2.0) <sup>a</sup>
G	9.4 (±1.3) <sup>c</sup>
H	6.2 (±0.6) <sup>c</sup>

**Fig. 4** Effect of time of exposure post-extracellular ice formation (EIF) on the post-thaw fertilization rate of oyster oocytes cooled with different programs (solid figures indicate a cooling rate of 0.3 °C min<sup>-1</sup>; clear figures indicate 0.1 °C min<sup>-1</sup>; same shape of figures indicate same holding time; data clustered in ovals indicate a -35 °C plunge into liquid nitrogen, data clustered in rectangles indicate a -60 °C plunge)

In summary, despite Pacific oocytes being cooled with the standard protocol undergoing IIF, they still maintain a high post-thaw fertilization rate. This indicates that IIF was not detrimental to the viability of the Pacific oyster oocytes. These results support previous reports that state that intracellular ice is not necessarily a main cause of cell death (Muldrew et al. 2004). The current study also shows that reducing the concentration of solutes in the intracellular and extracellular unfrozen matrix by cooling at a slower cooling rate, and to lower plunging temperatures, decreased the fertilization most significantly. This could probably be because of the prolonged detrimental effect of the highly concentrated unfrozen matrix on the oocytes, suggesting that Pacific oyster oocytes could survive IIF more than solute effects and cell shrinkage.

## ***2.2 Liposomes as a Membrane Model System for Freezing Studies***

Liposomes were used as a simplified membrane model system for studying freeze injury at the plasma membrane level. As phosphatidylcholine is the major component in cell membranes, large unilaminar vesicles (LUV) made from egg yolk phosphatidylcholine (EPC) and dipalmitoylphosphocholine (DPPC) were used in this study. EPC consisted of a mixture of acyl chain lengths, which resemble the composition of biological membranes. DPPC was also used, as a comparison, since intraliposomal water was retained in the DPPC LUV and froze around  $-40\text{ }^{\circ}\text{C}$  (Kristiansen and Westh 1991; Kristiansen 1992), which mimicked intracellular freezing at fast cooling rates. Carboxyfluorescein (CF) was encapsulated as a marker for monitoring LUV stability. Details of methods and results in this section can be found in Siow et al. (2007).

### **2.2.1 Effect of Freezing Temperatures and Cooling Rates on the Stability of EPC LUV**

The study showed that there is an abrupt increase in leakage of EPC LUV between  $-5$  and  $-10\text{ }^{\circ}\text{C}$  (Fig. 5), which was demonstrated to coincide with the temperatures of extraliposomal ice formation, as observed at around  $-7\text{ }^{\circ}\text{C}$  from a DSC scan (results not shown).

In addition to the detrimental effect that could arise from the extra-liposomal ice formation (Sterling 1968; Rubinsky et al. 1990), numerous previous studies have shown that leakage increases at the gel–liquid-crystal phase transition temperature of the phospholipid bilayer (Siminovitch and Chapman 1971; Higgins et al. 1986). In the current study, the abrupt increase between  $-5$  and  $-10\text{ }^{\circ}\text{C}$  coincided with the EPC undergoing phase transition at  $-8\text{ }^{\circ}\text{C}$  during cooling from room temperature to  $-60\text{ }^{\circ}\text{C}$  and at  $-15\text{ }^{\circ}\text{C}$  during heating from  $-60$  to  $20\text{ }^{\circ}\text{C}$ , as determined by DSC

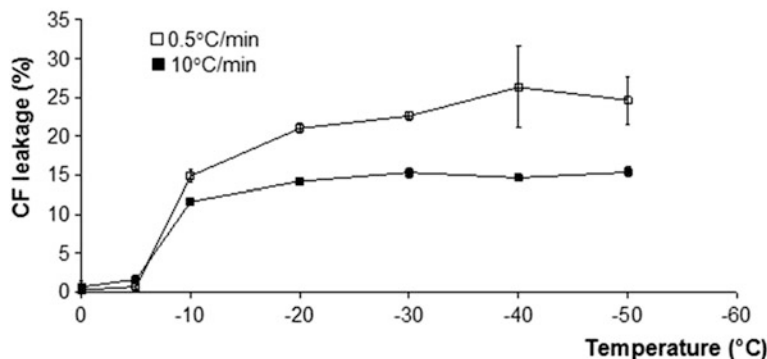


**Fig. 5** Effect of cooling rates on the CF leakage of EPC LUV. Approximately 20 mg of the EPC LUV was cooled from 20 °C to the respective temperatures at 0.5 and at 10 °C min<sup>-1</sup>. Samples were held for 1 min at the final temperature before they were heated to 20 °C at 10 °C min<sup>-1</sup>.  $n=3$

(results not shown). This result was in accordance with previous studies (Ladbrook and Chapman 1969; Chapman 1975).

As water forms ice, the phase volume of the unfrozen matrix decreases. The reduction of the phase volume of the unfrozen matrix freeze-concentrate the EPC LUV, eventually leading to the aggregation of vesicles (Fig. 6b). The effect of freeze-concentration of the EPC LUV, however, did not seem to lead to a higher leakage of the EPC LUV as temperatures decreased to lower temperatures at 10 °C min<sup>-1</sup> (Fig. 5). At a slower cooling rate of 0.5 °C min<sup>-1</sup>, the leakage pattern was the same as for 10 °C min<sup>-1</sup>. However, the osmotic pressure difference across the bilayers caused an additional stress to the LUV, and therefore higher leakage was observed.

### 2.2.2 EPC at Various Holding Temperatures

The increase in leakage of EPC LUV with increased holding time at -15 °C (Fig. 7) was probably due to the fluid and deformable nature of the bilayer of EPC LUV. EPC consists of phospholipids with a mixture of hydrocarbons of different chain lengths, resulting in a broad phase transition temperature (Ladbrook and Chapman 1969; Chapman 1975). As mentioned above, the phase transition of the EPC dispersion was observed at -8 °C when the sample was cooled from room temperature to -60 °C, and at -15 °C during heating from -60 to 20 °C (results not shown). We suggest that the CF leaked out from the fluid and deformable vesicles at -15 °C, and that its bilayer was in dynamic and fluctuating gel-fluid phases that coexist close to the phase transition. This observation was also made by Leidy et al. (2001). The fluid and deformable nature of the EPC LUV at -15 °C can be noted in Fig. 6a, in which some of the EPC LUV were flattened instead of retaining their spherical shape. At lower temperatures, the EPC LUV were likely to become

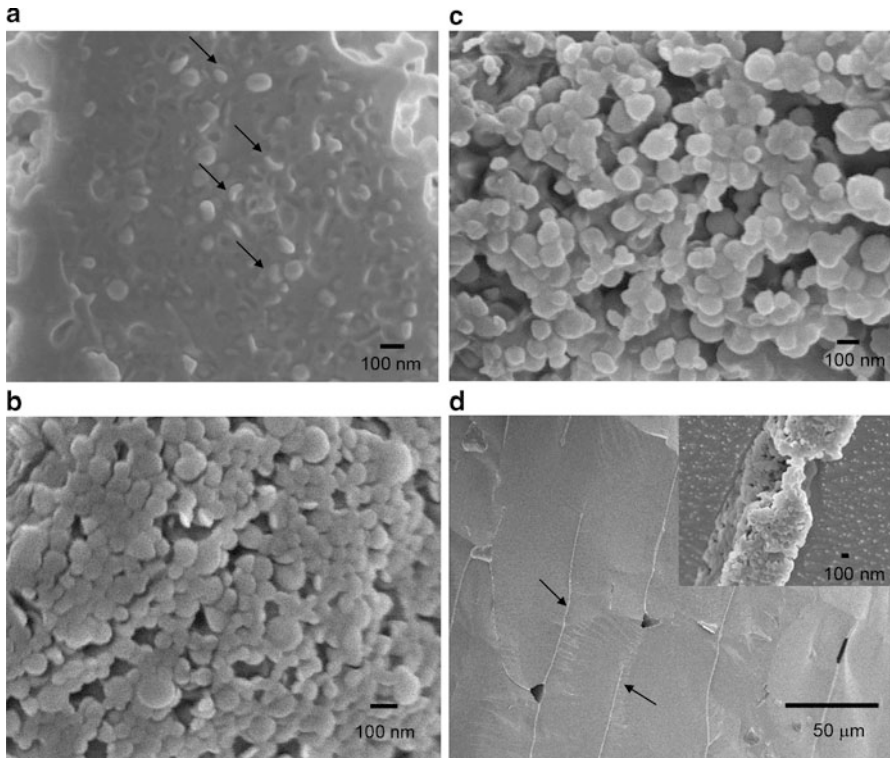


**Fig. 6** Scanning electron micrographs of EPC LUV and DPPC LUV that were cooled to  $-15$ ,  $-40$ , and  $-55$  °C at  $10$  °C min $^{-1}$ . (a) EPC LUV at  $-15$  °C; arrows show the squashed and flattened EPC LUV, (b) EPC LUV at  $-55$  °C, (c) DPPC LUV at  $-15$  °C, (d) DPPC LUV at  $-40$  °C; arrows show the freeze-concentrated DPPC LUV at the unfrozen channels. The *inset* in the micrographs shows a magnified unfrozen channel

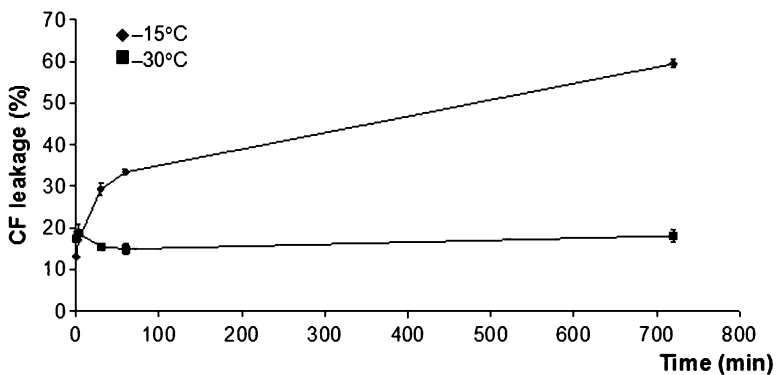


**Fig. 7** Effect of holding time on the CF leakage of EPC LUV. EPC LUV (approximately 20 mg) were cooled from 20 °C to  $-15$  °C or  $-30$  °C at  $10$  °C min $^{-1}$ . Samples were held at the defined temperatures ( $-15$  or  $-30$  °C) for the respective holding time before they were heated to 20 °C at  $10$  °C min $^{-1}$ .  $n=3$

more solid, hence preventing more leakage at temperatures below  $-30\text{ }^{\circ}\text{C}$ . This inference is obtained from the electron micrographs, where the vesicles appeared to be less deformable at  $-30\text{ }^{\circ}\text{C}$  than at  $-15\text{ }^{\circ}\text{C}$  (Fig. 6a and b, respectively).

### 2.2.3 Effect of Freezing Temperatures and Cooling Rates on the Stability of DPPC LUV

As for the DPPC LUV, leakage that started at  $-10\text{ }^{\circ}\text{C}$ , followed by the subsequent rapid increase in leakage between  $-10$  and  $-25\text{ }^{\circ}\text{C}$  (Fig. 8), was also near the temperature of extraliposomal ice formation that occurred at around  $-9\text{ }^{\circ}\text{C}$  (from DSC scans, not shown). A similar observation has been reported in a previous study in which a significant leakage of the hydrogenated soybean phosphatidylcholine liposomes was detected at the extraliposomal ice formation temperature of between  $-6$  and  $-8\text{ }^{\circ}\text{C}$  (Fransen et al. 1986). Since nucleation is a stochastic event, a broad temperature range of the extraliposomal ice formation was observed in the current study.

In contrast to EPC, DPPC undergoes the phase transition at  $41\text{ }^{\circ}\text{C}$  (Chapman et al. 1967; Mason and Huang 1981; Crowe et al. 1989). Therefore, extraliposomal ice formation was believed to be solely responsible for the leakage of DPPC LUV that started at  $-10\text{ }^{\circ}\text{C}$  and the subsequent rapid increase of leakage between  $-10$  and  $-25\text{ }^{\circ}\text{C}$  (Fig. 8). The detrimental effect of the extracellular ice has been previously reported (Sterling 1968; Rubinsky et al. 1990). Such deleterious effects of the extraliposomal ice was apparent for the DPPC LUV, but not for the EPC LUV.

The freeze-concentrated, compressed, and aggregated DPPC LUV in the unfrozen matrix (Fig. 6c, d) contributed to the gradual increase in leakage of DPPC LUV as the increase in ice phase volume as temperatures were lowered to  $-40\text{ }^{\circ}\text{C}$  at  $10\text{ }^{\circ}\text{C min}^{-1}$  (Fig. 8). It should be noted that the reduction of the phase volume of

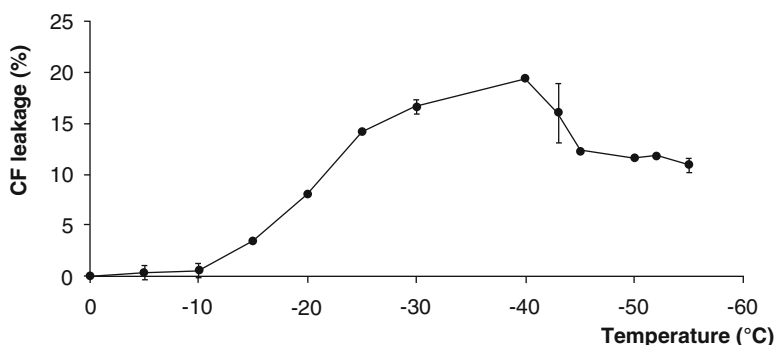


**Fig. 8** Effect of subzero temperatures on the CF leakage of the dispersion of DPPC LUV. Approximately 20 mg of the EPC LUV was cooled from  $20\text{ }^{\circ}\text{C}$  to the respective temperatures at  $10\text{ }^{\circ}\text{C min}^{-1}$ . Samples were held for 1 min at the final temperature before they were heated to  $20\text{ }^{\circ}\text{C}$  at  $10\text{ }^{\circ}\text{C min}^{-1}$ .  $n=3$

the unfrozen matrix also caused an increase of salt concentration in the unfrozen matrix (Meryman 1974; Mazur 1984). The increase of salt concentration and the subsequent increase in osmotic pressure in the unfrozen matrix had been ascribed to the promotion of cellular dehydration, which accounted for the slow freeze-injury involving freezing rates of below 1°/min (Meryman 1974).

In the current study, extraliposomal ice formation of the DPPC LUV was observed at -9 °C, and intraliposomal freezing was observed at -43 °C when cooled at a relatively fast cooling rate of 10 °C/min (Fig. 8). Consequently, the DPPC LUV could have been exposed to osmotic stress across the bilayer upon extraliposomal ice formation and before intraliposomal ice formation. Exposure of DPPC LUV to osmotic stress, however, was short, since the cooling rate was relatively fast. In Fig. 6c, d, the DPPC LUV appeared to be solid spherical at -15 and -40 °C. Thus, lesion and leakage of the DPPC LUV was mainly caused by the freeze-concentration and compression effects, which were a result of the phase volume reduction of the unfrozen matrix. The decrease and leveling off in leakage of DPPC LUV at temperatures below -40 °C coincided with the temperature of intraliposomal freezing (from DSC scans, not shown). This result suggested that intraliposomal freezing prevented CF diffusion, as the DPPC LUV were thawed from subfreezing temperatures. The decrease of leakage, in particular, was due to the DPPC LUV being both intra- and extraliposomally frozen, thus preventing the diffusion of CF before both the intra- and extraliposomal ice were melted. In comparison, DPPC LUV that were only frozen in the extraliposomal space at temperatures above -43 °C allowed CF diffusion from the intraliposomal to the extra-liposomal space before the melting of the extraliposomal ice.

#### 2.2.4 DPPC LUV at Various Holding Temperatures

There was relatively low leakage for DPPC LUV held at -15 °C compared to the other subzero temperatures (Fig. 9). The leakage was also lower than for the EPC LUV that were held at the same temperature. DPPC are phospholipids with 16 carbons in their acyl chain. Therefore, DPPC is at the gel phase at room temperature and changes into the liquid-crystal phase at a much higher temperature (41 °C). At -15 °C, DPPC LUV were in the gel phase and were likely to be more solid than the EPC LUV. This was supported by the electron micrographs in which the DPPC LUV appeared to be spherical and less deformable than the EPC LUV at -15 °C (Fig. 6a, c). Thus, CF could remain trapped and, as a result, low leakage was observed.

The percentage of CF leakage of DPPC LUV that was held at -50 °C was lower compared to those held at -40 °C (Fig. 9). Intraliposomal freezing of the DPPC LUV found at -43 °C (Fig. 8) may prevent further CF diffusion at -50 °C. Supporting the results found in the current study, Kristiansen (1992) found that below -40 °C, leakage of DPPC multilamellar vesicles leveled off because the matrix solidification was complete. Similar observations were also made for both egg lecithin liposomes (Higgins et al. 1986) and multilamellar liposomes consisting

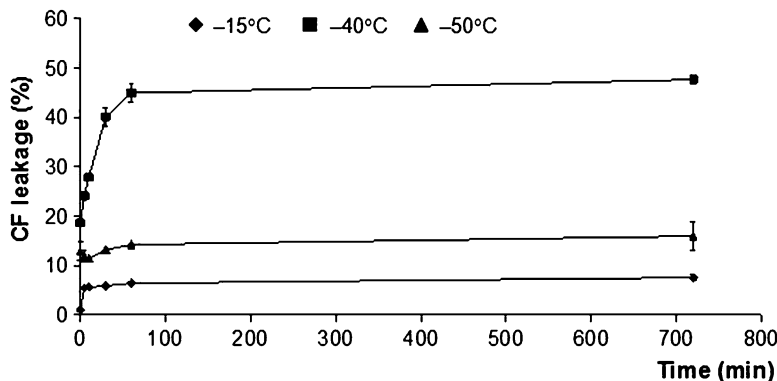


**Fig. 9** Effect of holding time on the CF leakage of DPPC LUV. DPPC LUV (approximately 20 mg) were cooled from 20 °C to -15 °C or -40 °C or -50 °C at 10 °C min<sup>-1</sup>. Samples were held at the defined temperatures (-15 or -30 °C) for the respective holding time before they were heated to 20 °C at 10 °C min<sup>-1</sup>.  $n = 3$

of hydrogenated soybean lecithin and dicetyl phosphate (DCP), respectively (Fransen et al. 1986).

In summary, the freezing behaviors of EPC and DPPC LUV were characterized both quantitatively and qualitatively and substantially resembled cellular freezing behaviors. Extraliposomal ice formation and the simultaneous reduction of phase volume of the unfrozen matrix led to increased CF leakage. This effect varies among the phospholipids. The freeze-concentrated DPPC LUV have a higher leakage compared to EPC LUV with decreasing temperature because their phase transition temperature is higher and therefore causes more mechanical damage at low temperatures.

### 3 Overall Summary

The use of large unilamellar, EPC and DPPC LUV offers suitable membrane model systems for the study and improvement of cryopreservation procedures. For example, when a slower rate of freezing was used, a higher leakage was observed and this relates to the cellular dehydration induced by the osmotic stress at slow cooling rate, which was conducive to prevent intracellular freezing if cells could withstand the resultant osmotic shrinkage. Conversely, since we learned from the Pacific oyster oocytes study that they could survive IIF more than solute effects and cell shrinkage, an appropriate freezing rate could be investigated to produce an optimal rate using the model system.

The variations in the phase transition of both the EPC and DPPC LUV illustrated that mechanical damage at low subfreezing temperatures due to the extracellular ice could be avoided by having a more fluid membrane. On the other hand, if the cells

have a more fluid membrane structure, they are more permeable or “leaky” at higher subfreezing temperatures. Therefore, this study suggests that manipulating the cell membrane fluidity/solidity of oocytes by changing the diet of oysters could be one way to control the rate of water diffusion in and out of the cells under a controlled freezing condition.

To have a closer representation of a biological membrane, liposomal model systems need to show increased complexity by including other cell membrane components, such as more heterogeneous phospholipids, proteins, and sugars. Such increased complexity would allow a better understanding of the dynamics and prediction of the kinetics of cell freezing. In this study, both the cellular and liposomal studies showed that high phase volume of ice could cause cell distortion and compression with the ice channels in the concentrated unfrozen matrix. Therefore, a careful study of the ice dynamics could be a future focus to improve the cryopreservation procedures.

## References

- Acker JP, McGann LE (2003) Protective effect of intracellular ice during freezing. *Cryobiology* 46:197–202
- Chapman D (1975) Phase transitions and fluidity characteristics of lipids and cell membranes. *Q Rev Biophys* 8:185–235
- Chapman D, Williams RM, Ladbrooke BD (1967) Physical studies of phospholipids. VI. Thermotropic and lyotropic mesomorphism of some 1,2-diacyl-phosphatidylcholines (lecithins). *Chem Phys Lipids* 1:445–475
- Crowe JH, McKersie BD, Crowe LM (1989) Effects of free fatty acids and transition temperature on the stability of dry liposomes. *Biochim Biophys Acta* 979:7–10
- Fahy GM, Lilley TH, Linsdell H, John Douglas MS, Meryman HT (1990) Cryoprotectant toxicity and cryoprotectant toxicity reduction: in search of molecular mechanisms. *Cryobiology* 27:247–268
- Fransen GJ, Salemink PJM, Crommelin DJA (1986) Critical parameters in freezing of liposomes. *Int J Pharm* 33:27–35
- Gao D, Critser JK (2002) Mechanisms of cryoinjury in cells. *ILAR J* 41:187–196
- Hagedorn M, Peterson A, Mazur P, Kleinhans FW (2004) High ice nucleation temperature of zebra fish embryos: slow-freezing is not an option. *Cryobiology* 49:181–189
- Higgins J, Hodges NA, Olliff CJ, Phillips AJ (1986) Factors influencing cryoprotective activity and drug leakage from liposomes after freezing. *J Pharm Pharmacol* 38:259–263
- Kristiansen J (1992) Leakage of a trapped fluorescent marker from liposomes: effects of eutectic crystallization of NaCl and internal freezing. *Cryobiology* 29:575–584
- Kristiansen J, Westh P (1991) Freezing behavior of multilamellar vesicles in 0.9 percent sodium chloride. *Cryo-Lett* 12:167–176
- Ladbrook BD, Chapman D (1969) Thermal analysis of lipids, proteins and biological membranes. A review and summary of some recent studies. *Chem Phys Lipids* 3:304–367
- Leidy G, Wolkers WF, Jorgensen K, Mouritsen OG, Crowe JH (2001) Lateral organization and domain formation in a two component lipid membrane system. *Biophys J* 80:1819–1828
- Lovelock JE (1953) The haemolysis of human red blood cells by freezing and thawing. *Biochim Biophys Acta* 10:414–426
- Mason JT, Huang CH (1981) Chain-length dependent thermodynamics of saturated symmetric chain phosphatidylcholine bilayers. *Lipids* 16:604–608

- Mazur P (1970) Cryobiology: the freezing of biological systems. *Science* 168:939–949
- Mazur P (1984) Freezing of living cells—mechanisms and implications. *Am J Physiol* 247: C125–C142
- Mazur P, Cole KW (1985) Influence of cell concentration on the contribution of unfrozen fraction and salt concentration to the survival of slowly frozen human erythrocytes. *Cryobiology* 22:509–536
- Mazur P, Leibo SP, Chu EHY (1972) 2-factor hypothesis of freezing injury—evidence from Chinese-hamster tissue-culture cells. *Exp Cell Res* 71:345–355
- Meryman HT (1974) Freezing injury and its prevention in living cells. *Annu Rev Biophys Bioeng* 3:341–363
- Muldrew K, Acker JP, Elliot JAW, McGann LE (2004) The water to ice transition: Implications for living cells. In: Fuller BJ, Lane N, Benson EE (eds) *Life in the frozen state*. CRC, Boca Raton, FL, pp 67–108
- Pegg DE (2002) The history and principles of cryopreservation. *Semin Reprod Med* 20:5–13
- Rubinsky B, Lee CY, Bastacky J, Onik G (1990) The process of freezing and the mechanism of damage during hepatic cryosurgery. *Cryobiology* 27:85–97
- Salinas-Flores L, Adams SL, Wharton DA, Downes MF, Lim MH (2008) Survival of Pacific oyster, *Crassostrea gigas*, oocytes in relation to intracellular ice formation. *Cryobiology* 56:28–35
- Siminovitch D, Chapman D (1971) Liposome bilayer model systems of freezing living cells. *FEBS Lett* 16:207–212
- Siow LF, Rades T, Lim MH (2007) Characterizing the freezing behavior of liposomes as a tool to understand the cryopreservation procedures. *Cryobiology* 55:210–221
- Steponkus PL, Wolfe J, Dowgert MF (1981) Stressess induced by contraction and expansion during a freeze thaw cycle: A membrane perspective. In: Morris GJ, Clarke A (eds) *Effects of low temperatures on biological membranes*. Academic, Toronto, pp 307–322
- Steponkus PL, Dowgert MF, Gordonkamm, WJ (1983) Destabilization of the plasma membrane of isolated plant protoplasts during a freeze thaw cycle - the influence of cold acclimation. *Cryobiology* 20:448–465
- Sterling C (1968) Effect of low temperature on structure and firmness of apple tissue. *J Food Sci* 33:577–580
- Tervit HR, Adams SL, Roberts RD, McGowan LT, Pugh PA, Smith JF, Janke AR (2005) Successful cryopreservation of Pacific oyster (*Crassostrea gigas*) oocytes. *Cryobiology* 51:142–151
- Tiersch TR (2000) Introduction. In: Tiersch TR, Mazik PM (eds) *Cryopreservation in aquatic species*. World Aquaculture Society, Baton Rouge, LA, pp XIX–XV

# The Role of Water in the Cryopreservation of Seeds

N.E. Zaritzky

## Abbreviations

$\Delta H_L$	Lipid melting enthalpy
$\Delta H_T$	Total enthalpy
db	Dry basis
DSC	Differential scanning calorimetry
ERH%	Equilibrium relative humidity
GAB	Guggenheim-Anderson-de Boer <i>equation</i>
l	Latent heat of ice melting
LN	Liquid nitrogen
RH	Relative humidity
wb	Wet mass basis
WC	Water content of the seeds
WC <sub>50</sub>	Seed desiccation sensitivity
WC <sub>u</sub>	Unfrozen water content

## 1 Introduction

Plant genetic resources are vitally important for human beings and the sustainability of the planet. Biodiversity conservation is the practice of protecting and preserving the abundance and variety of all species (Lambardi et al. 2004; Walters 2006).

---

N.E. Zaritzky (✉)

Centro de Investigación y Desarrollo en Criotecnología de Alimentos (CIDCA), Facultad de Ciencias Exactas, UNLP-CONICET, 47 y 116, La Plata 1900, Argentina

Departamento de Ingeniería Química, Facultad de Ingeniería, UNLP, La Plata, Argentina  
e-mail: [zaritzky@ing.unlp.edu.ar](mailto:zaritzky@ing.unlp.edu.ar)

Neotropical ecosystems are submitted to constant pressure by human activity; in these ecosystems the number of plants at risk of genetic depletion or extinction and the loss of important genetic resources is continuously increasing. Preservation of plant biodiversity avoids the risk that species and plant varieties may become extinct, producing a definitive loss of their genetic variability. Preservation of plants only in field collections is risky, as valuable germplasm can be lost (genetic erosion) because of pests, diseases, and adverse weather conditions.

Seed storage is the most effective and efficient method for the ex situ preservation of plant genetic resources; cryopreservation can provide an important contribution to long-term conservation of valuable germplasm. Cryobiology (the study of life at low temperature) and anhydrobiology (the study of life at low water content) have some features in common, because, in environmental freezing, one of the major causes of damage is freezing-induced dehydration.

A seed is a small embryonic plant enclosed in a covering called the seed coat, usually with some stored food. The seed is the site of partial development of the embryo and the linkage between successive generations, and a critical intermediate stage in the life cycle of angiosperms and gymnosperms, which guarantees the propagation and survival of the species. The formation of the seed completes the process of reproduction in seed plants; the biological function of seeds ensures propagation of the species.

Seeds are fundamentally a means of reproduction; most seeds are the product of sexual reproduction, which produces a remixing of genetic material and phenotype variability. Other important functions of the seeds include nourishment of the embryo, dispersal to a new location, and dormancy during unfavorable conditions. Seed storage longevity depends on intrinsic properties of the species and on external factors during storage, such as temperature, relative humidity (RH) and, to a lesser extent, composition of the gaseous atmosphere.

Five levels of hydration in seed tissues were identified by Vertucci (1990). At these levels, water exhibits different physical properties, and seeds show different metabolic status. Level V corresponds to a high water content ( $>0.75 \text{ gH}_2\text{O g}^{-1} \text{ wb}$ , wet basis) and the water properties in the tissue are similar to those of a dilute solution; the metabolism is normal and seeds germinate. As the water content decreases (Level IV,  $0.75\text{--}0.45 \text{ gH}_2\text{O g}^{-1} \text{ wb}$ ), properties of water are similar to a concentrated solution where the interaction between water and solutes becomes stronger, and the system deviates from “ideal” behavior; water content is inadequate for cell growth and germination, but respiration occurs and synthesis of protein and nucleic acid is produced. On removal of more water (Level III,  $0.45\text{--}0.25 \text{ gH}_2\text{O g}^{-1} \text{ wb}$ ), synthesis of protein and nucleic acid is not significant, but some respiration occurs. In level II ( $0.25\text{--}0.08 \text{ gH}_2\text{O g}^{-1} \text{ wb}$ ) only low-level catabolic events are slowly produced. In levels III and II the solution becomes concentrated and viscous, having the properties of a glass. At very low water content (Level I,  $<0.08 \text{ gH}_2\text{O g}^{-1} \text{ wb}$ ), there is no metabolic activity; water is tightly associated with macromolecular surfaces and its mobility is reduced (“bound water”) (Vertucci 1989b; Vertucci and Farrant 1995; Pammeter and Berjak 2000).

## 2 Relationships Between Seed Structure and Storage Behavior

Sensitivity to desiccation and low temperatures limits the storage potential of seeds and their genetic conservation. Research on over 9,000 plant species has demonstrated that seeds can be grouped according to their storage behavior in both orthodox seeds and nonorthodox seeds. A great number of tropical species are nonorthodox seeds, including recalcitrant (Roberts 1973) and intermediate seeds (Ellis et al. 1990, 1991). The main characteristics of these seeds, according to Bonner (2008) include the following:

- True orthodox seeds can be stored for long periods at seed moisture contents of 5–10 % and subfreezing temperatures.
- Sub-orthodox seeds can be stored under the same conditions, but for shorter periods due to high lipid content or thin seed coats.
- Temperate recalcitrant seeds cannot be dried at all, but can be stored for 3–5 years at near-freezing temperatures.
- Tropical recalcitrant seeds cannot be dried, and they do not survive at temperatures below 10–15 °C.

Orthodox seeds acquire desiccation tolerance during development, can be dried to low water contents and retain viability in the dry state for predictable periods (Vertucci and Roos 1990). Examples of orthodox seeds include bean (*Phaseolus vulgaris* L.), pea (*Pisum sativum*), mungbean (*Vigna radiata*), sunflower (*Helianthus annuus*), and soybean (*Glycine max*). Most agricultural crops produce orthodox seeds, since they undergo a drying phase as they mature on the plant and usually contain around 20–30 % water when mature and are ready to harvest. After collection, orthodox seeds survive further drying to at least 5 % water content. Mature orthodox seeds can be dehydrated without damage to very low levels of moisture. The stability of orthodox seeds in the dry state has been a crucial factor in the development of agriculture and human civilization. Low water content is known to slow deteriorative chemical reactions in dry seeds. Studies of seed storage over two centuries have confirmed this observation and thus the preservation of seeds at low or ultra-low water content has been advocated.

Intracellular glasses have been detected in a number of seeds. High levels of sugars and other biopolymers in seeds result in a rapid increase in cytoplasmic viscosity during drying, which prevents the cellular biological system from reaching physical and chemical equilibrium in a measurable time frame. As a result, cytoplasmic components become vitrified, and intracellular glasses form during drying. It has been suggested that the formation of intracellular glasses may be a strategy for seeds to survive desiccation (Burke 1986; Williams and Leopold 1989; Sun 1997). Cytoplasmic vitrification minimizes major changes in molecular organization and cellular structures during dehydration, thus leading to the preservation of biological structures. The high viscosity of the glassy state immobilizes cellular constituents, thus inhibiting diffusion and slowing deleterious reactions or

changes in structures and chemical composition. In orthodox seeds, all water is bounded unfrozen water (structural water), which seems to be a crucial factor to tolerate desiccation; in storage, the longevity of seeds increases with a reduction of the water content (Vertucci and Leopold 1987; Vertucci 1989a, c, 1990; Sun and Leopold 1993). Low water content enables orthodox seeds to be stored at freezing temperatures without harm, as there is insufficient water for lethal ice-crystals to form. Most orthodox seeds remain viable for many years, even under less than ideal storage conditions. The lower limit of moisture content varies substantially between crop species, i.e., about 6 % moisture content for pea (*Pisum sativum*) and mung bean (*Vigna radiata*), and about 2 % for sunflower (*Helianthus annuus*). These moisture contents coincide with 10–12 % equilibrium relative humidity at 20 °C ( $aw = 0.1\text{--}0.12$ ). Orthodox seeds are able to withstand dehydration to water contents below 5 % wet basis (equivalent to 0.053 gH<sub>2</sub>O g<sup>-1</sup> dry basis). Successful storage of orthodox seeds was achieved under 3–7 % moisture content and –18 °C (Walters 2006). Long-term storage of orthodox seeds has also been achieved by cryopreservation (or cryostorage) at ultra-low temperatures from –80 to –196 °C with liquid nitrogen (LN). An essential first step in seed cryopreservation is the determination of optimum (safe) moisture contents for each orthodox species, particularly those with oily seeds. Long-term storage stability of orthodox seeds was correlated with the presence of a glassy state.

Figure 1 shows a schematic diagram of glass transition temperatures as a function of water content in seeds (dry basis). The graph (adapted from Sun 1997), is based on information from three seed species, *Glycine max*, *Phaseolus vulgaris*, and *Pisum sativum*, as reported by Bruni and Leopold (1991, 1992);

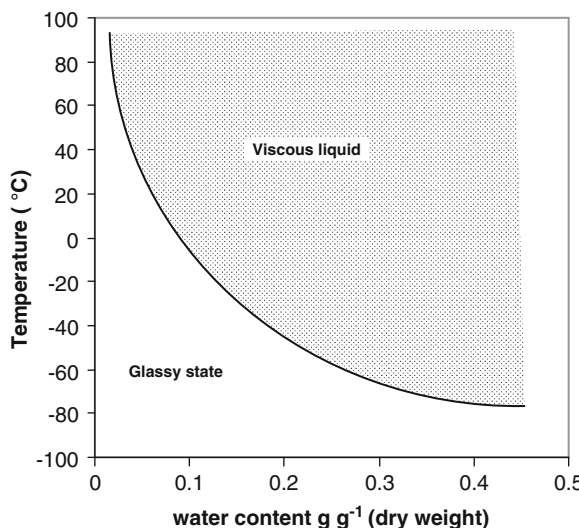


**Fig. 1** Schematic representation of glass transition curve for different citrus seeds, based on data of three seed species: *Glycine max*, *Phaseolus vulgaris*, and *Pisum sativum*, as reported by Bruni and Leopold (1991, 1992), Sun and Leopold (1994), Sun et al. (1994), Leprince and Walters-Vertucci (1995), Williams and Leopold (1995), and Sun (1997)

Sun and Leopold (1994); Sun et al. (1994); Leprince and Walters-Vertucci (1995); and Williams and Leopold (1995). The effect of water content on storage stability appeared to be largely related to the plasticization effect of water on intracellular glasses in orthodox seeds.

In contrast, recalcitrant seeds do not undergo maturation drying maintaining a high water content; that is, they do not experience a reduced cellular metabolism and are sensitive to desiccation and to low temperatures (Pammeter et al. 1991; Pammeter and Berjak 2000). Recalcitrant seeds cannot be dried and cannot be stored at subzero temperatures because they are damaged by freezing injury resulting from ice formation. Examples of recalcitrant seeds included avocado (*Persea Americana*), mango (*Mangifera indica* L.), cacao (*Theobroma cacao*), and tea (*Camellia sinensis*). Due to the active metabolism in the hydrated state, viable recalcitrant seeds cannot be stored for long-term periods. The longevity of recalcitrant seeds is short, from a few weeks to a few months for species adapted to tropical environments, and up to about 3 years for several species adapted to temperate environments. Recalcitrant seeds neither tolerate nor survive desiccation. The dehydration of recalcitrant tissues produces membrane deterioration (plasmalemma and mitochondria), protein denaturation, reduction of respiratory rate, and reduction in ATP level. When freshly harvested recalcitrant seeds are dried, viability is reduced considerably at certain moisture content ("critical moisture content" or "lowest safe moisture content"). If drying continues further, viability is eventually reduced to zero. The sensitivity of recalcitrant seeds to low temperatures is due to their high water content. Critical moisture contents for loss of viability on desiccation vary greatly among recalcitrant species, as well as among cultivars and seed lots, depending on the stage of seed maturity at time of collection. Recalcitrant seeds are present in at least 70% of tropical trees. Oxidative processes and free radical reactions seem to be involved in cellular and molecular deterioration; seeds show a strong resistance to rehydration, and loss of cellular integrity leads to a loss of viability. The water content at which recalcitrant seeds start to lose viability is relatively high; it is far above that at which a glassy state can exist at room temperature and nonfreezable water is lost.

Recalcitrant seeds are characterized by high water content at maturity 0.43–4.0 gH<sub>2</sub>O g<sup>-1</sup> (dry basis, db), which is 30–80 % on a wet mass basis (wb); they cannot survive drying below around 20–30 % water content (wb). For example, *Avicennia marina* seeds are unable to survive water content lower than 0.5 gH<sub>2</sub>O g<sup>-1</sup> (db) (33 % wb); cacao (*Theobroma cacao*) seeds rapidly lose germination when they are dried to 0.26 gH<sub>2</sub>O g<sup>-1</sup> db. Highly recalcitrant seeds are unable to survive water content lower than 0.5 gH<sub>2</sub>O g<sup>-1</sup> db (33 % wb). Recalcitrant seeds are unable to survive below 0.42–0.25 gH<sub>2</sub>O g<sup>-1</sup> (30–20 % wb).

Recalcitrant and orthodox seeds differ greatly in their ecology and morphology. Recalcitrant seeds primarily come from perennial trees in the moist tropics. In some cases, they also come from temperate tree or aquatic species. Most orthodox seeds come from annual species grown in open fields. With respect to morphology, recalcitrant seeds differ from orthodox seeds not only in size, but also complexity and viability. Generally, recalcitrant seeds are covered with fleshy or juicy layers and impermeable testa. These structures maintain the seeds in a high-moisture

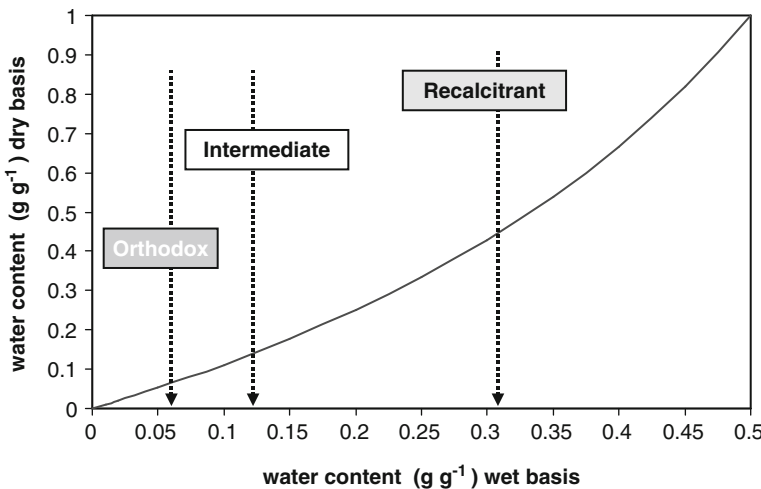


**Fig. 2** Schematic diagram showing approximate values of safe moisture levels (minimum water content) for recalcitrant, intermediate, and orthodox seeds, expressed on a dry or a wet basis

environment. High moisture content of recalcitrant seeds makes them sensitive to desiccation and chilling injury. The large seed and impermeable seed coat benefit recalcitrant seeds, since they are less likely to be affected by minor fluctuations in relative humidity that might occur prior to germination.

Intermediate seeds have properties somewhat in between those of orthodox and recalcitrant seeds. Some intermediate seeds may be stored at subzero temperatures, but many are injured by freezing temperatures, while others (usually those of tropical origin) do not store well below 10 °C. Intermediate seeds are exemplified by many tropical and subtropical species, such as neem (*Azadirachta indica*), a tropical evergreen tree with medicinal properties, palm oil (*Elaeis guinensis*), coffee (*Coffea arabica*), and *Citrus* species (Dussert et al. 2001; Hamilton et al. 2008, 2009; Hor et al. 2005; Makeen et al. 2007; Sacandé et al. 2000). Intermediate seeds survive dehydration to minimum water content in the range of 0.114–0.176 g g<sup>-1</sup> (10–15 % wb), but suffer desiccation injury if dried further.

Figure 2 schematically shows the approximate values of safe moisture levels (minimum water content) for recalcitrant, intermediate, and orthodox seeds, expressed on a dry and a wet basis.

### 3 Mechanisms Implicated in Desiccation Tolerance of Seeds

Pammerter and Berjak (2000) compared subcellular organization and metabolic activity during development of seeds of three species that attain different levels of desiccation tolerance: *Avicennia marina*, which is very sensitive to desiccation; *Aesculus hippocastanum*, which shows an increase in tolerance with development,

but at shedding was still sensitive; and *Phaseolus vulgaris*, an orthodox seed that increased in tolerance with development, and during maturation drying became even more tolerant.

Moisture level below  $0.5 \text{ g g}^{-1} \text{ db}$  (33 % wb) was lethal for the highly recalcitrant tropical species *Avicennia marina*, a tropical wetland species commonly known as gray mangrove or white mangrove, a species of mangrove tree that develops in the zones of estuarine areas. The moderately recalcitrant *Aesculus hippocastanum* is a temperate terrestrial species that can tolerate dehydration between 0.42 and  $0.25 \text{ g g}^{-1} \text{ db}$  (30–20 % wb). The orthodox seed *Phaseolus vulgaris* tolerates water contents as low as  $0.08 \text{ g g}^{-1} \text{ db}$  (9 % wb) without viability loss.

Study of these seeds was conducted at three developmental stages: stage 1, immediately post histo-differentiation; stage 2, in the middle of the reserve accumulation phase; and stage 3, at the end of reserve accumulation. Different processes or mechanisms are proposed to confer protection against desiccation in seeds; their deficiency or absence could contribute to relative degrees of desiccation sensitivity.

The most important intracellular physical characteristics of dehydration resistance in seeds were determined according to Pammerer and Berjak (2000):

- Reduction of the degree of vacuolation that increases the mechanical resilience of cells to dehydration. *Avicennia marina* is a highly recalcitrant seed and one of the species most sensitive to desiccation. It is highly vacuolated, and this condition does not change with development, supporting the concept that drying of highly vacuolated material leads to mechanical damage. In contrast, the more tolerant species showed a decline in vacuolation with development.
- Integrity of the cytoskeleton, which is formed by microtubules and microfilaments; it is an integrated intracellular support system, and contributes to the organization of the cytoplasm and the nucleus.
- Conformation of DNA, chromatin, and nuclear architecture: maintenance of the integrity of genetic DNA material in the desiccated condition in orthodox seeds, and/or its rapid repair when seeds are dehydrated, is considered to be a fundamental requirement for desiccation tolerance.
- Intracellular de-differentiation is a characteristic of maturing desiccation-tolerant seeds. Intracellular structures are simplified and minimized (minimization of surface areas of membranes and mitochondria) in maturing desiccation-tolerant seeds. Mitochondria of the root meristem cells of recalcitrant seeds were highly differentiated and had the appearance of active mitochondria, while those in orthodox seeds were de-differentiated and appeared inactive. In orthodox seeds, there was a decline in the contribution of mitochondria to cell volume with development, and by the end of reserve accumulation, the degree of differentiation of mitochondria was very low.
- “Switching off” of metabolism: Decrease in respiratory rate is an essential event enabling an orthodox seed to withstand rapid loss of water. Recalcitrant seeds are, in contrast, metabolically active. Measured respiration rates were high in the

recalcitrant seeds *Avicennia marina* and *Aesculus hippocastanum* throughout development, while the respiration rates of the orthodox seeds of *Phaseolus vulgaris* were low, even though the seeds had not gone through maturation drying and were still hydrated.

- Presence and efficient operation of antioxidant systems (free-radical scavenging systems) should be maximally effective during maturation drying of orthodox seeds and when seeds take up water upon imbibition. In contrast, uncontrolled free-radical generation occurs during dehydration of recalcitrant seeds, thus producing damage.
- Accumulation of protective molecules, including late embryogenic accumulating/abundant proteins (LEA), (or dehydrin-like proteins).
- Accumulation of nonreducing sugars, sucrose and certain oligosaccharides, or galactosyl cyclitols; these protect macromolecules against denaturation and also minimize liquid crystalline gel phase transformations of the lipid bilayer of membranes. Membrane phase behavior during dehydration and rehydration is important to the survival of seeds and other anhydrobiotic tissues.
- Deployment of endogenous amphipathic molecules into membranes upon water loss may be a prerequisite for desiccation tolerance; these molecules serve to maintain the integrity of membranes in the dry state in desiccation-tolerant organisms by lowering the water content at which the phase change of membrane lipids occurs. The essential property for desiccation tolerance is that they must be reversible, reestablishing the membranes in a functional condition upon rehydration.

Other mechanisms implicated in desiccation tolerance of seeds are (Pammerter and Berjak 2000):

- The presence of an effective peripheral oleosin layer around lipid bodies: All plant seeds that store triglycerides, such as sunflower, canola, and cottonseed, sequester these oils in specialized organelles called oleosomes, which are spherical in shape, 1–3 µm in diameter. Oleosomes are surrounded by a phospholipid layer, which is encapsulated by proteins called oleosins. Oleosins have a central, hydrophobic domain that interacts with the periphery of the lipid, and an amphipathic N-terminal domain that, with the C-terminal domain, facilitates interaction with the aqueous cytomatrix. The oleosin boundary of lipid bodies allows these hydrophobic masses to be accommodated as discrete entities in the aqueous cytomatrix under hydrated conditions, and their role during dehydration is to prevent the bodies from coalescing in desiccation-tolerant seeds.
- The presence and operation of repair mechanisms during rehydration (replacement of damaged rRNA, repair of DNA lesions, and protein-synthesizing systems).
- Amount and nature of insoluble reserves accumulated: Recalcitrant seeds stored reserves as soluble sugars, while the more tolerant species accumulated insoluble reserves during development.

## 4 Subzero Storage Temperatures of Seeds

Ex situ conservation practices are becoming a priority procedure in safeguarding genetic resources, especially through germplasm repositories, e.g., in field gene banks or in conventional germplasm gene banks at  $-20^{\circ}\text{C}$ . However, such methods may not represent ideal conditions for maintaining germplasm securely in the long term. In field gene banks, germplasm integrity is subjected to unexpected changes of environmental biotic and abiotic components.

Recommendations for conventional seed bank storage are 3–7 % seed moisture content (wb) and  $-18^{\circ}\text{C}$  in hermetically sealed containers. Seeds having intermediate or recalcitrant storage behavior are cold-sensitive; consequently, they cannot be stored in standard seed gene banks at  $-20^{\circ}\text{C}$  (Roberts 1973; Ellis et al. 1990). Although living organisms may suffer severe stress due to the freezing process, it has been postulated that biological activities are greatly minimized under cryogenic conditions.

Cryopreservation is proposed as the most favorable and safest technique for preserving germplasm and preventing its deterioration. Further studies are required to determine the feasibility of using cryogenic storage conditions, especially for nonorthodox seeds. Cryostorage techniques have an important application for preserving species, allowing seeds to be stored at ultra-low temperatures that reduce metabolic rates and deterioration. Long-term storage of orthodox seeds has been achieved by cryopreservation at ultra-low temperatures from  $-80$  to  $-196^{\circ}\text{C}$  with liquid nitrogen (LN). In contrast, recalcitrant seeds do not survive drying and freezing during ex-situ conservation, i.e., they cannot resist the effects of drying or temperatures less than  $10^{\circ}\text{C}$  and cannot be stored for long periods like orthodox seeds because they can lose their viability.

Intermediate seeds can withstand partial dehydration, but they cannot be stored under conventional gene bank conditions because they are cold-sensitive and desiccation does not increase their longevity (Ellis et al. 1990). Intermediate seeds cannot be stored in LN without a previous partial dehydration process. The water content of seeds at the moment of immersion in LN must be regarded as the most critical factor in cryopreservation. One important factor is the cooling rate. If a liquid is cooled sufficiently quickly, freezing and vitrification can be avoided, thus forming an amorphous glass phase.

## 5 Cryopreservation of Citrus Seeds: A Case Study

Species that are freezing or desiccation tolerant have been observed to accumulate solutes, especially sucrose and trehalose. For nonorthodox seed species, cryopreservation is the only technique available for long-term germplasm conservation. In the case of intermediate seed-propagated species, seeds are partially desiccation tolerant and, therefore, the whole seed cryopreservation is the first option to be tested.

Seed moisture content and germination conditions need to be optimized to maximize freezing tolerance and recovery following the cryopreservation process (Dussert et al. 2001; Hor et al. 2005).

Graiver et al. (2011), analyzed the optimal moisture content hydration status for cryopreservation of different *Citrus* seeds: *Citrus sinensis* (sweet orange), *Citrus paradise* (grapefruit), *Citrus reticulata* var. Criolla and *Citrus reticulata* var. Dancy (mandarin).

The tolerance (viability) of these seeds to desiccation at different relative humidities was compared to the viability of the seeds that were desiccated prior to the LN treatment.

Seeds were extracted manually from freshly harvested mature fruits of the different *Citrus* species. After extraction, seed were surface-sterilized by immersion in ethanol aqueous solution, followed by treatment in sodium hypochlorite aqueous solution. Seeds were then rinsed twice in tap water and in distilled water and immediately surface dried. To analyze tolerance to desiccation, seeds without testa (endocarp) were placed under desiccation conditions by equilibration at 20 °C over seven saturated salt solutions (LiCl, MgCl<sub>2</sub>, K<sub>2</sub>CO<sub>3</sub>, NaNO<sub>2</sub>, NaCl, KCl, KNO<sub>3</sub>) with constant equilibrium relative humidity (ERH%) of 11, 32, 43, 64, 75, 85, and 95 %, respectively. Water content of the seeds (WC) was determined gravimetrically after oven-drying the seeds at 103 °C until constant weight and expressed on dry basis (g H<sub>2</sub>O g<sup>-1</sup> db). A desiccation period of 35 days was applied for the different assayed ERH, in order to achieve equilibrium conditions (constant weight). Water sorption isotherms were obtained from the data of WC and the corresponding ERH of the saturated salt solutions; the curves were modeled using Guggenheim-Anderson-de Boer (GAB) equation and the simplified D'arcy and Watt model proposed by Dussert et al. (2001).

Seed viability was analyzed using germination experiments. Seeds were sown in hermetic controlled germination conditions (humid sand in covered plastic box and kept in a growth chamber at 25 °C in the dark). The percentage of normal seedlings was evaluated 4–6 weeks after sowing.

Figure 3 shows the effect of the desiccation ERH on the viability of one of the tested citrus seeds (grapefruit, *Citrus paradise*). Similar results were reported by Graiver et al. (2011) for the other tested seeds. As can be observed, as the ERH% of the desiccation stage increased, the number of germinated seeds was higher. A decline in the germination percentage was observed for all of the tested *Citrus* seeds when desiccation was conducted at ERH < 75 %. Seed desiccation sensitivity (WC<sub>50</sub>) was quantified by the quantal response model of Dussert et al. (1999).

In order to analyze the feasibility of cryopreservation of citrus seeds, the viability of seeds (germinability) submitted to different levels of desiccation, followed by LN treatment was measured. To study the tolerance to LN exposure, seeds were previously desiccated by equilibration at 20 °C over the seven saturated salt solutions, wrapped in aluminum foil and then immersed in LN 1 h. After the cooling period, seeds were immersed for 5 min in a water-bath at 37 °C and directly placed under germination conditions. Figure 3 shows the germinability percentages of seeds previously desiccated at different ERH, and then submitted to LN; as can be observed, viability was significantly lower than in the case of seeds that were only desiccated. A similar pattern of sensitivity to LN exposure after desiccation was observed for all of the tested citrus seeds. No survival was achieved at the

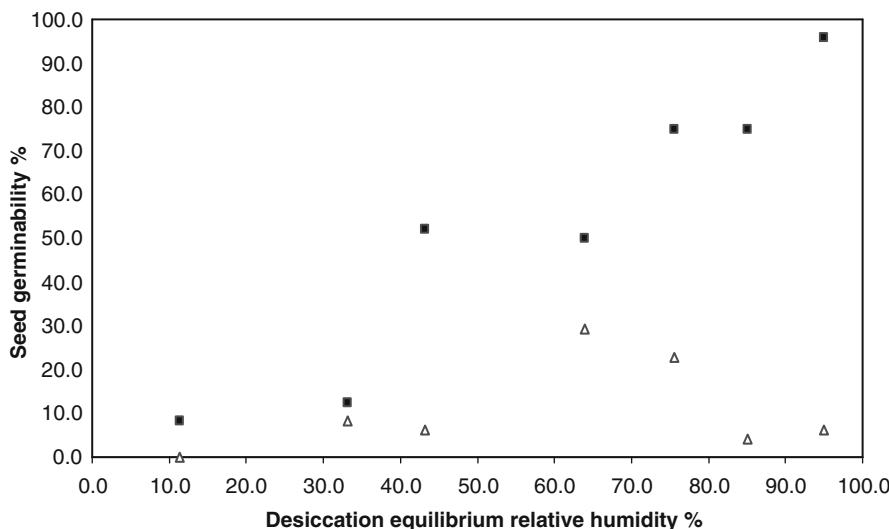


**Fig. 3** Viability of *Citrus paradisi* seeds determined by % of germinability (normal seedling percentage) after desiccation at different ERH% (filled square) or desiccation at different ERH%, followed by liquid nitrogen treatment (open triangle). (Adapted from Graiver et al. 2011)

lowest assayed ERH; a maximum survival was observed between 64 and 85 % desiccation ERH, depending on the species, and a decline in seed viability percentage was found at higher ERH values. The optimal ERH ranges to achieve maximum germinability in cryopreserved seeds were 75–85 % for *C. sinensis* and 64–75 % for *C. paradisi* (Graiver et al. 2011).

In order to relate the obtained results of viability with the amount of frozen water in the seeds, differential scanning calorimetry (DSC) was used to determine thermal transitions of water and lipid melting phenomena during warming of cotyledon tissue. *Citrus* seeds, previously equilibrated at different ERH ranging between 11 and 95 % (Graiver et al. 2011) were cooled in the DSC to  $-120^{\circ}\text{C}$  at a rate of  $20\text{ }^{\circ}\text{C min}^{-1}$ ; after 2 min at this temperature, the samples were heated from  $-120$  to  $100\text{ }^{\circ}\text{C}$  at a warming rate of  $10\text{ }^{\circ}\text{C min}^{-1}$ . Enthalpies of water melting transition were determined for each previous desiccation condition, and the corresponding frozen water contents were calculated. After DSC analysis, pans were punctured and the sample dry weight was determined. Final water content of dried seeds ranged between 35 and  $52\text{ g H}_2\text{O kg}^{-1}$  db for the tested species. Seed oil was extracted from the samples after 10 days drying over silica gel; dry seeds were ground and oil was extracted using the Soxhlet method (petroleum ether). Extracted oils were measured gravimetrically; the lipid content of the tested *Citrus* seeds ranged between  $336$  and  $435\text{ g kg}^{-1}$  db. Seeds that were desiccated on silica gel were also analyzed by DSC to identify the melting transition of the seed lipids.

Figure 4 (inset) shows DSC thermal transitions of three samples: (a) untreated seed (seed that was not submitted to dehydration), with a large peak of water melting; (b) seed dehydrated in silica gel; and (c) extracted seed lipid phase. It

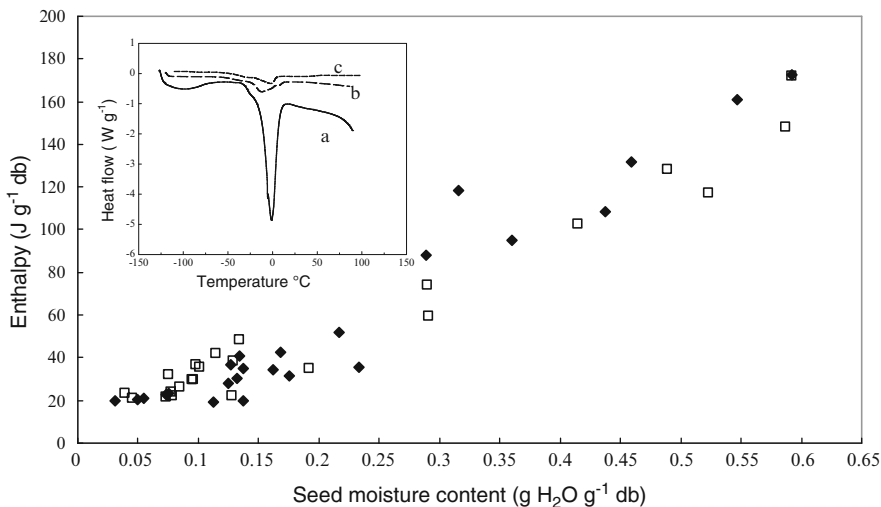


**Fig. 4** Total enthalpy measured by DSC as a function of moisture content of seed samples for *C. paradisi* (filled diamond) and *C. sinensis* (open square). Inset: DSC heating thermograms of Citrus seed samples: (a) untreated seed, (b) seed desiccated on silica gel, (c) seed lipid extract. (Adapted from Graiver et al. 2011)

can be noted that the endotherm of the silica gel dehydrated seed was similar to that of the lipid extract. In addition, lipid and ice melting events are overlapping; therefore, to calculate the unfrozen water fraction, the lipid enthalpy must be subtracted from the total enthalpy values. Additionally, in Fig. 4 the peak areas of the DSC thermograms (total enthalpy) for *C. paradisi* and *C. sinensis* seeds that were dehydrated at different ERH previous to DSC cooling and warming programs were plotted as a function of the moisture content of the seed samples. It can be observed that at low moisture contents in the tissue, asymptotic values of enthalpy ( $20 \text{ J g}^{-1}$  dry basis) can be attributed to the presence of lipids in the seeds were reached. Unfrozen water content ( $WC_u$ ) was calculated as follows:

$$WC_u = WC - \left( \frac{\Delta H_T - \Delta H_L}{\lambda} \right) (1 + WC)$$

where:  $WC$  = total water content (dry basis);  $\Delta H_T$  = total enthalpy measured by DSC ( $\text{J g}^{-1}$  dry basis);  $\lambda$  = latent heat of ice melting;  $\Delta H_L$  = lipid melting enthalpy ( $\text{J g}^{-1}$  dry basis). The obtained average values of unfrozen water content ( $WC_u$ ) expressed as  $\text{g H}_2\text{O g}^{-1}$  db were 0.14 and 0.13 for *C. sinensis* and *C. paradise*, respectively. The values of  $WC_u$  in *Citrus* sp. were found to be negatively correlated to seed lipid content (Hor et al. 2005; Graiver et al. 2011). Finally, it is important to relate the unfrozen water content in the seeds with LN tolerance.

Using the water sorption isotherms of each citrus seed, the equilibrium relative humidity (ERH%) of the desiccation atmosphere leading to the  $WC_u$  determined by DSC was obtained. For the measured values of  $WC_u$  ( $0.14 \text{ g H}_2\text{O g}^{-1}$  db for

*C. sinensis* and  $0.13 \text{ g H}_2\text{O g}^{-1} \text{ db}$  for *C. paradisi*) the obtained ERH% were 81 % for *C. sinensis* and 67 % for *C. paradisi*. These ERH% are included in the optimum ranges for seed cryopreservation determined by the germinability tests, resulting in 75–85 % for *C. sinensis* and 64–75 % for *C. paradisi*. Therefore, seed survival was maximized when dehydration previous to LN treatment was performed at the highest ERH%, leading to the absence of frozen water in the tissue.

## 6 Conclusions

The controlled dehydration process before liquid nitrogen exposure constitutes a satisfactory method by which nonorthodox oily seeds withstand cryopreservation processes. In cryopreservation, the usual goal is to achieve intracellular vitrification while avoiding intracellular ice formation and membrane damage. The limit of dehydration previous to LN treatment in intermediate *Citrus* species corresponds to the unfrozen water content in the seed. The current results offer additional evidence that lipid-rich seeds do not withstand the presence of frozen water in their tissues during the cooling/thawing process. These results agree with the findings of Vertucci (1990) and Hor et al. (2005). The *Citrus* species studied by Graiver et al. (2011) shared an important common feature for the response of the seeds to LN exposure, which is that the optimal desiccation ERH ranged between 64 and 85 %, corresponding to the higher values of *C. sinensis* and *C. reticulata* var. Criolla and var. Dancy and the lowest to *C. paradisi*.

## References

- Bonner FT (2008) Storage of seeds. Chapter 4. In: The woody plant seed manual. USDA Agricultural Handbook 727, USA, pp 85–96
- Bruni F, Leopold AC (1991) Glass transitions in soybean seeds: relevance to anhydrous biology. *Plant Physiol* 96:660–663
- Bruni F, Leopold AC (1992) Pools of water in anhydrobiotic organisms: a thermally stimulated depolarization current study. *Biophys J* 63:663–672
- Burke MJ (1986) The glass state and survival of anhydrous biological systems. In: Leopold AC (ed) Membranes, metabolism and dry organism. Cornell University Press, New York, pp 358–364
- Dussert S, Chabriange N, Engelmann F, Hamon S (1999) Quantitative estimation of seed desiccation sensitivity using a quantal response model: application to nine species of the genus *Coffea* L. *Seed Sci Res* 9:135–144
- Dussert S, Chabriange N, Rocquelain G, Engelmann F, Lopez M, Hamon S (2001) Tolerance of coffee (*Coffea* spp.) seeds to ultra-low temperature exposure in relation to calorimetric properties of tissue water, lipid composition, and cooling procedure. *Plant Physiol* 129:495–504
- Ellis RH, Hong TD, Roberts EH (1990) An intermediate category of seed storage behaviour? I. Coffee. *J Exp Bot* 41:1167–1174
- Ellis RH, Hong TD, Roberts EH (1991) An intermediate category of seed storage behaviour? II. Effects of provenance immaturity, and imbibition on desiccation-tolerance in coffee. *J Exp Bot* 42:653–657

- Graiver N, Califano A, Zaritzky N (2011) Partial dehydration and cryopreservation of citrus seeds. *J Sci Food Agric* 91(14):2544–2550
- Hamilton KN, Ashmore SE, Drew RA (2008) Desiccation and cryopreservation tolerance of near mature seeds of *Citrus garrawayae*. *Seed Sci Technol* 36:157–161
- Hamilton KN, Ashmore SE, Pritchard HW (2009) Thermal analysis and cryopreservation of seeds of australian wild Citrus species (Rutaceae): *Citrus australasica*, *C inodora* and *C garrawayi*. *CryoLetters* 30:268–279
- Hor YL, Kim YJ, Ugap A, Chabrilange N, Sinniah UR, Engelmann F, Dussert S (2005) Optimal hydration status for cryopreservation of intermediate oily seeds: citrus as a case study. *Ann Bot* 95:1153–1161
- Lambardi M, De Carlo A, Biricolti S, Puglia AM, Lombardo G, Siragusa M, De Pasquale F (2004) Zygotic and nucellar embryo survival following dehydration/cryopreservation of Citrus intact seeds. *CryoLetters* 25:81–90
- Leprince O, Walters-Vertucci C (1995) A calorimetric study of the glass transition behaviours in axes of bean seeds with relevance to storage stability. *Plant Physiol* 109:1471–1481
- Makeen MA, Normah MN, Dussert S, Clyde MM (2007) The influence of desiccation and rehydration on the survival of polyembryonic seed of *Citrus suhuiensis* cv. Limau madu. *Sci Hortic* 112:376–381
- Pammeter NW, Berjak P (2000) Aspects of recalcitrant seed physiology. *R Bras Fisiol Veg* 12:56–69
- Pammeter NW, Vertucci CW, Berjak P (1991) Homeohydrous (recalcitrant) seeds: dehydration, the state of water and viability characteristics in *Landoiphia kirkii*. *Plant Physiol* 96:1093–1098
- Roberts EH (1973) Predicting the storage life of seeds. *Seed Sci Technol* 1:499–514
- Sacandé M, Buitink J, Hoekstra FA (2000) A study of water relations in neem (*Azadirachta indica*) seed that is characterized by complex storage behaviour. *J Exp Bot* 51:635–643
- Sun WQ (1997) Glassy state and seed storage stability: the WLF kinetics of seed viability loss at  $T > T_g$  and the plasticization effect of water on storage stability. *Ann Bot* 79:291–297
- Sun WQ, Irving TC, Leopold AC (1994) The role of sugar, vitrification and membrane phase transition in seed desiccation tolerance. *Physiol Plant* 90:621–628
- Sun WQ, Leopold AC (1993) Acquisition of desiccation tolerance in soybean. *Physiol Plant* 87:403–409
- Sun WQ, Leopold AC (1994) Glassy state and seed storage stability: a viability equation analysis. *Ann Bot* 74:601–604
- Vertucci CW (1989a) Effects of cooling rates on seeds exposed to liquid nitrogen temperature. *Plant Physiol* 90:1478–1485
- Vertucci CW (1989b) The effects of low water contents on physiological activities of seeds. *Physiol Plant* 77:172–176
- Vertucci CW (1989c) Relationship between thermal transitions and freezing injury in pea and soybean seeds. *Plant Physiol* 90:1121–1128
- Vertucci CW (1990) Calorimetric studies of the state of water in seed tissues. *Biophys J* 58:1463–1471
- Vertucci CW, Farrant JM (1995) Acquisition and loss of desiccation tolerance. In: Galili G, Kigel J (eds) *Seed development and germination*. Marcel Dekker, Inc., New York
- Vertucci CW, Leopold AC (1987) Water binding in legume seeds. *Plant Physiol* 85:224–231
- Vertucci CW, Roos EE (1990) Theoretical basis of protocols for seed storage. *Plant Physiol* 94:1019–1023
- Walters C (2006) Water properties and cell longevity. In: Buera M, Welti Chanes J, Lillford P, Corti H (eds) *Water properties of food, pharmaceutical and biological materials*. PUSA, CRC, Boca Raton
- Williams RJ, Leopold AC (1989) The glassy state in corn embryos. *Plant Physiol* 89:977–981
- Williams RJ, Leopold AC (1995) Changes in glass transition temperatures in germinating pea seeds. *Seed Sci Res* 5:117–120

# Water Activity and Microorganism Control: Past and Future

A. López-Malo and S.M. Alzamora

## Abbreviations

ABR	Antibiotic resistance
$a_w$	Water activity
BHI	<i>Brain-heart infusion</i>
DT	Dehydration tolerance
HM	High moisture-available
IM	Intermediate moisture-available
LPT	Long-term persistence
TT	Thermal treatments
TUT	Thermo-ultrasonic

## 1 Introduction

The influence of water or moisture content of foods on shelf-life has been recognized since early ages; most primitive cultures found a convenient way to reduce moisture content in foods to a level that prevents or delays microbial

---

S.M. Alzamora is member of Consejo Nacional de Investigaciones Científicas y Técnicas de la República Argentina.

A. López-Malo (✉)  
Departamento de Ingeniería Química, Alimentos y Ambiental, Escuela de Ingeniería,  
Universidad de las Américas Puebla, Puebla, Mexico  
e-mail: [aurelio.lopezm@udlap.mx](mailto:aurelio.lopezm@udlap.mx)

S.M. Alzamora  
Departamento de Industrias, Facultad de Ciencias Exactas y Naturales,  
Universidad de Buenos Aires, Ciudad Universitaria, Buenos Aires, Argentina

spoilage, such as drying, salting, and adding sugars. In some cases, the spoilage of products subjected to these procedures has also been referred to in the following ways: halophilic bacteria can grow in salted products; osmophilic yeasts may ferment sugar in preserved foods; and some dried foods can be spoiled by xerophilic molds (Mossel 1975). Substantial interest in the influence of water activity ( $a_w$ ) on food product quality and stability, promoted by empirical observations between total moisture content and product stability, began during the middle of the last century. Scott (1957) introduced the concept of  $a_w$  as a quantitative approach to define the influence of moisture content on microbial response in foods. Microbiologists recognized that  $a_w$ , rather than moisture content, controlled microbial response, as well as sporulation and/or toxin production (Jay et al. 2005). The relationship between  $a_w$  and food-borne microorganisms has been the topic of study by food researchers over the past several decades (Christian 2000; Chirife 1995; Lenovich 1987). Microbiologists have investigated how microorganisms respond under different conditions of temperature, pH, additives, atmosphere composition, and  $a_w$  (Hocking and Pitt 1987; Beuchat 1996). The influence of  $a_w$  in microbial death, survival, sporulation, and toxin production in food has been extensively studied by food microbiologists (Lenovich 1987; Beuchat 1983, 1987; Hocking and Christian 1996; Gutierrez et al. 1995). The  $a_w$  principle has been included in various government regulations, with the recognition that control of  $a_w$  as an important critical control point for risk analysis, as defined by the HACCP concept, sets up  $a_w$  limits on food products.

However, trends in food consumption and safety during the last few decades have significantly impacted the way in which the  $a_w$  concept is primarily used in food preservation design. Consumers increasingly demand fresh-like food products that are less heavily preserved/processed (e.g. with high  $a_w$  and lower added preservatives), and more convenient and nutritious. To correspond these trends without compromising safety, a number of combinations of several stress factors, such as reduced  $a_w$ , in a multifactorial food preservation approach ("hurdle" technology), have been developed in the past 20 years. Targeted application of the hurdle concept has aimed to improving the quality and safety of foods (Alzamora et al. 2000a, b; Leistner and Gould 2002; Raso and Barbosa-Cánovas 2003; Ross et al. 2003; Allende et al. 2006; Tapia and Welti-Chanes 2012).

## 2 Microbial Growth and $a_w$

When a microorganism is transferred to a new environment, there are three possible outcomes: growth, survival, or death. Microbial survival, growth or death is based on the ability of the microorganism to adapt in the new environment. Besides the presence of nutrients, the most important factors for growth and toxin production are temperature,  $a_w$ , pH, and oxygen. The basis for survival and death of microorganisms as influenced by  $a_w$  is complex. Several intrinsic and extrinsic factors may affect this relation, but these factors differ within food types and processes. Temperature, pH, atmosphere composition, chemical, and other physical treatments

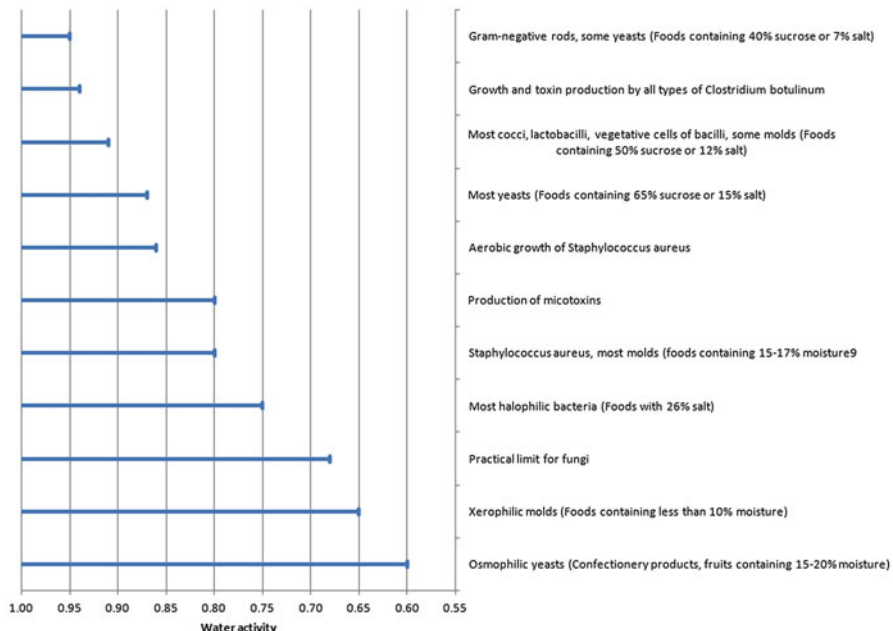


**Fig. 1** Water activity and food microbial spoilage

are some extrinsic factors that influence food microbial spoilage and therefore influence the  $a_w$ -microbial response. The use of combinations of extrinsic and intrinsic factors together with lowered  $a_w$  levels is common in the food industry (Alzamora et al. 2003). Generally, as the food  $a_w$  moves toward the microbial minimal  $a_w$  for growth, changes in other environmental factors will have a greater impact on death or survival.

Taking into account  $a_w$  values related to possible microbial responses, minimum  $a_w$  values that allow microbial growth for different types of microorganisms are essential for product design and stability. Figure 1 displays  $a_w$  range and its influence on some microbial responses; similar tables can be consulted elsewhere (Corry 1973; Beuchat 1983, 1987; Gould 1989a) and can be used to classify osmosensitive and osmotolerant microorganisms, as well as to find minimum  $a_w$  values for growth or toxin production of several pathogenic and spoilage microorganisms. Table 1 shows minimal  $a_w$  for growth of selected food-borne pathogens when pH and temperature are optimum for growth (i.e.,  $a_w$  is employed as the only preservation factor to inhibit microbial growth). At  $a_w < 0.90$ – $0.92$ , bacteria are usually inhibited, including pathogenic bacteria, with the exception of *Staphylococcus aureus*, which can grow at  $a_w$  0.86. Bacteria rarely spoil foods with  $a_w$  values below 0.85, the exceptions being brines and salted foods that may be spoiled by moderate and extreme halophilic bacteria (Hocking and Christian 1996). Yeast and molds are more tolerant to reduced  $a_w$ , but usually no growth exists below  $a_w$  of 0.62 (Scott 1957; Hocking and Pitt 1987).

**Table 1** Minimal  $a_w$  for growth (optimum pH and temperature) of selected foodborne pathogens (adapted from various sources)

<i>Aeromonas hydrophila</i>	0.97
<i>Bacillus cereus</i>	0.93
<i>Campylobacter jejuni</i>	0.99
<i>Clostridium botulinum E</i>	0.96
<i>Clostridium botulinum A &amp; B</i>	0.94
<i>Clostridium botulinum G</i>	0.96
<i>Clostridium perfringens</i>	0.94
<i>Escherichia coli</i>	0.93
<i>Listeria monocytogenes</i>	0.92
<i>Salmonella</i> spp.	0.94
<i>Shigella</i> spp.	0.96
<i>Staphylococcus aureus</i> (aerobic)	0.86
<i>Staphylococcus aureus</i> (anaerobic)	0.91
<i>Vibrio parahaemolyticus</i>	0.93
<i>Yersinia enterocolitica</i>	0.96

Ecological factors and their interactions determine the possible microbial response in foods. Interaction between  $a_w$  and pH is extremely important in determining the prevailing microflora of a specific food.  $a_w$  and pH, alone or in combination, are frequently the main factors that establish bacterial or fungal growth (IFT 2003), while other possible factors (temperature, gas composition atmosphere, redox potential, physical state, antimicrobial substances, etc.) often determine the type of bacteria and/or fungi that may survive and grow (Hocking and Christian 1996). Major spoilage organisms in high water activity foods (0.98–0.99) are different types of bacteria; at such high  $a_w$  values, pH will be also a critical factor in determining the type of microorganism that causes spoilage. Bacteria generally predominate at pHs values above 4.0, while fungal growth are more evident below pH 4.0. The majority of yeasts and molds that cause spoilage are nonxerophilic, growing well at high  $a_w$ , particularly in sugar-rich environments. At  $a_w$  values below 0.95, even if common spoilage bacteria are still present, may not be capable of growing in the food.

When  $a_w$  and pH are used to control microbial spoilage, microbial response is influenced by the acid and solute types used to adjust pH and  $a_w$ . For instance, *Debaryomyces hansenii* is a yeast that is frequently implicated in the spoilage of high acid and/or low water activity (high salt or sugar) foods. Its growth response must be determined in order to establish product shelf-life of foods where stability relies either on acidity,  $a_w$  reduction or their combination. Palou and López-Malo (2001) evaluated *Debaryomyces hansenii* response in laboratory media formulated at  $a_w$  0.95 or 0.90, pH 4.5 or 3.5, when using sodium chloride, sucrose or glucose to adjust  $a_w$ , in combination with acetic, citric, phosphoric, or tartaric acid to reduce pH. The number of viable cells was evaluated and compared with the initial population, determining if growth, inhibition (growth delay), or yeast death occurred. In 10 combinations of the 48 tested, yeast death was observed (Table 2), while only 4 combinations caused inhibition. At pH 3.5, acetic acid promoted

**Table 2** *Debaryomyces hansenii* response at selected  $a_w$  and pH values adjusted with different solutes and acids

	Acid	pH	Solute		
			NaCl	Glucose	Sucrose
$a_w$ 0.95	Acetic	3.5	D	D	D
		4.5	G	G	G
	Citric	3.5	G	G	G
		4.5	G	G	G
	Phosphoric	3.5	G	G	G
		4.5	G	G	G
	Tartaric	3.5	D	G	G
		4.5	G	G	G
	Acetic	3.5	D	D	D
		4.5	G	G	G
$a_w$ 0.90	Citric	3.5	D	G	G
		4.5	D	G	G
	Phosphoric	3.5	D	G	G
		4.5	D	G	G
	Tartaric	3.5	D	D	G
		4.5	D	G	G

G-growth

D-death

*D. hansenii* death at  $a_w$  0.95 or 0.90 independently of solute type. The use of sodium chloride to adjust  $a_w$  caused yeast inhibition or death in more cases than the use of glucose or sucrose. Citric and phosphoric acids allowed yeast growth at  $a_w$  0.95 (sodium chloride, glucose, or sucrose) or  $a_w$  0.90 (glucose or sucrose). Acid and solute type exhibited an important effect on *D. hansenii* growth response, demonstrating the importance of their selection when used to adjust pH and  $a_w$  in foods.

As an example of water activity effects on bacterial growth and the effect of different solutes used to adjust  $a_w$ , Fig. 2 displays the growth curves of *Enterobacter sakazakii* (ATCC 51329) at selected water activity values when using sodium chloride or glycerol as  $a_w$  depressing solutes (Delgado-Portales et al. 2007). Growth curves were affected by  $a_w$  and by the solute used to adjust  $a_w$ . By using the Gompertz equation, parameters of the sigmoideal growth curves were obtained (Table 3). The resulting values presented the same tendency as the two solutes tested. A decrease in the growth rate and higher lag times were observed as  $a_w$  of the system decreased. A slight reduction in food  $a_w$  indicates that microorganisms surviving processing in such foods, or contaminating the food after processing, will be osmoregulating at some level. Since homeostatic responses often require the expenditure of energy by the stressed cells, restriction of availability would be expected to result in lower growth rates. Regarding the effect of solute type, Brewer (1999) indicated that, in general, sodium chloride is more inhibitory than glycerol and sucrose for bacteria that are considered halo-sensible (most spore-formers, Enterobacteriaceae, *Pseudomonas fluorescens*) and less inhibitory than glycerol to halotolerant bacteria (Micrococcaceae, *Vibrio*). At  $a_w$  0.96,

**Fig. 2** *Enterobacter sakazakii* (ATCC 51329) growth curves of selected water activity values when using sodium chloride or glycerol as  $a_w$  depressing solutes. (Adapted from Delgado-Portales et al. 2007)

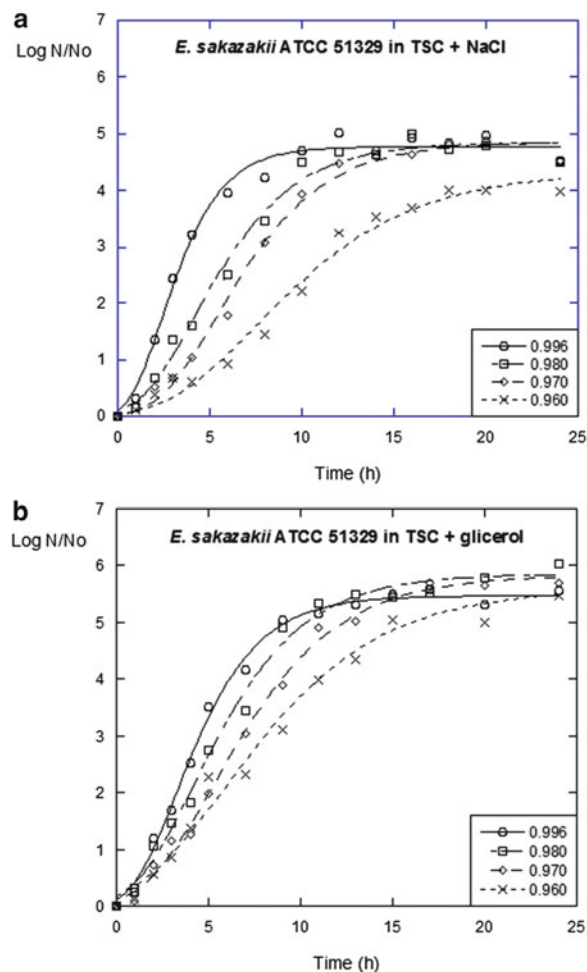


**Table 3** Gompertz parameters for *Enterobacter sakazakii* (ATCC 51329) growth at selected water activity values when using sodium chloride or glycerol as  $a_w$  depressing solutes

	Lag time $\lambda$ (h)	Growth rate ( $\mu\text{m}$ ) Log (N/No)/h	Maximum population density Log (N/No)
Control ( $a_w$ 0.996)	$0.64 \pm 0.11$	$2.64 \pm 0.12$	$4.7 \pm 0.1$
<i>TSB + NaCl</i>			
$a_w$ 0.98	$1.22 \pm 0.13$	$1.61 \pm 0.11$	$4.8 \pm 0.1$
$a_w$ 0.97	$2.20 \pm 0.21$	$1.51 \pm 0.09$	$4.8 \pm 0.1$
$a_w$ 0.96	$2.69 \pm 0.20$	$0.90 \pm 0.06$	$4.4 \pm 0.1$
<i>TSB + glycerol</i>			
$a_w$ 0.98	$0.93 \pm 0.11$	$1.77 \pm 0.08$	$5.8 \pm 0.1$
$a_w$ 0.97	$1.52 \pm 0.13$	$1.55 \pm 0.07$	$5.8 \pm 0.1$
$a_w$ 0.96	$1.11 \pm 0.10$	$1.18 \pm 0.10$	$5.6 \pm 0.1$

a decrease in growth rate and an increase in lag time was observed when media were adjusted with NaCl. It can be seen that evaluated  $a_w$  values allow growth and that minimum  $a_w$  for growth of this strain is lower than 0.96. Breeuwer et al. (2003) evaluated the behavior of different strains of *E. sakazakii* in brain–heart infusion (BHI) broth adjusted to  $a_w$  0.934 with sorbitol and found that minimum  $a_w$  for growth was between 0.93 and 0.96, although it should be noted that profound differences may exist between strains of this organism (Breeuwer et al. 2003; Buchanan 2003; Edelson-Mammel et al. 2006). Gould (1989a) recognized that in some instances solute effects may depend on the ability of the solute to permeate the cell membrane, as in the case of glycerol, which readily permeates the membrane of many bacteria, and therefore has a lower inhibitory water activity. Chirife (1994) discussed in detail the “specific solute effect” for *S. aureus*. He concluded that the inhibitory effects of solutes most often present in low  $a_w$ —preserved foods, such as NaCl and sucrose, are primarily related to their  $a_w$  lowering capacity. But for other solutes such as ethanol, propylene glycol, butylene glycol, and various polyethylene glycols, antibacterial effects (attributed mainly to the effects of these molecules on membrane enzymes responsible for peptidoglycan synthesis) are important.

The sequence of hurdles has been shown to be crucial for the survival of pathogens. Tiganitas et al. (2009) studied the effect of lethal and sublethal pH (adjusted with lactic acid to 4.0 and 4.5) and  $a_w$  (adjusted with NaCl, 15 and 20 % NaCl) stresses on the inactivation or growth of *Listeria monocytogenes* and *Salmonella* Typhimurium, simulating various processing conditions (e.g. ripening of cheese, fermentation of meat). Sequential exposure to the stresses resulted in faster reductions than exposure to double stresses applied simultaneously. The pH then NaCl sequence was more detrimental to pathogens than the reverse sequence. Acid tolerance of *L. monocytogenes* was higher than osmotic tolerance, while the opposite was observed for *Salmonella*. These results suggest that during food processing, the sequence and severity of the stresses applied significantly affect inactivation of *L. monocytogenes* and *Salmonella*. These findings are not in agreement with previous reports in which adaptation to acid was shown to confer cross-tolerance to other stresses, such as heat and salt (Leyer and Johnson 1993). Rather, such protection was linked to HCl and acetic acid adaptation, instead of adaptation to lactic acid. These results evidence the necessity of further research in situations in which pathogens undergo exposure to multiple hurdles.

Better knowledge of the relation of water in foods has led to the rediscovery and optimization of older preservation techniques and to a renewed interest in foods that are shelf-stable due to control of water activity (Alzamora et al. 2003), including dried, intermediate and high moisture foods with inherent empiric preservation factors, and also to novel products (especially food products with high water activity), for which the hurdles are intentionally selected and applied. In the search for foods with superior quality, the importance of considering the combined action of reduced  $a_w$  with other preservation factors as a system to develop new food products is a current trend in food processing. Minimally processed foods represent a new variety of products that has responded to these demands. Therefore, the control of  $a_w$  for food design is being used in many ways (Alzamora et al. 2003),

i.e., at various stages of the food distribution chain, during storage, processing, and/or packaging as a “back-up” hurdle in existing minimally processed products with short shelf-life to diminish microbial pathogenic risk and/or increase their shelf-life; to obtain products with long shelf-life (fully dehydrated and intermediate moisture products); and as a preservative factor (together with other emerging and/or traditional preservative factors) to obtain high moisture novel foods by hurdle techniques.

There are two main categories of foods with reduced  $a_w$  whose stability is based on a combination of factors, i.e. intermediate moisture-available (IM) and high moisture-available (HM) foods. IM foods generally range from 0.60 to 0.90  $a_w$  and 10–50 % moisture content (Alzamora et al. 1995). Additional preservation factors provide a margin of safety against resistance to  $a_w$  spoilage microorganisms (mainly molds and yeasts, and some bacterial species). Lowering  $a_w$  is often combined with chemical preservatives (i.e., sorbates, sulphites, benzoates, and antimicrobials of natural origin), a reduction of pH, and sometimes with competitive microorganisms. Other IM products receive thermal treatment during manufacturing process that inactivates heat-sensitive microorganisms, while the subsequent hot filling in sealed containers further improves microbial stability (Leistner and Gould 2002). Most IM foods are designed in such way that they can be stored at ambient temperature for several months (Karel 1973, 1976). Many IM products, due to the addition of very high amounts of solutes (such as sugar or salt) to reduce  $a_w$  to the desired level, are too sweet or too salty, becoming undesirable from a nutritional and sensory point of view. Therefore, this category of products has been subjected in the last decade to continuous revision and discussion.

High-moisture foods have  $a_w$  values above 0.90; in this category, the reduction of  $a_w$  is a microbial stress factor of less relative importance because most microorganisms are able to proliferate (Leistner and Gould 2002). Stability at ambient temperature can be reached by applying a designed hurdle technology approach. HM fresh-like fruits and cooked meat products, preserved by the interaction of  $a_w$ —mild heat treatment—pH—preservatives, and that can be stored without refrigeration, represent a rational application of the combined approach (Alzamora et al. 1995, 2000a, b; Leistner and Gould 2002). Most shelf-stable foods do not rely solely on  $a_w$  for microbial control, but on other preservation factors. The combination of  $a_w$  and pH acts as a relevant factor in many of these products by preventing proliferation of pathogenic microorganisms, while other approaches (antimicrobials, thermal treatment, etc.) play a secondary role, mainly against spoilage flora (Tapia et al. 1994). Different approaches have been explored for obtaining shelf-stability and fresh-like quality in fruit products. Commercial, minimally processed fruits are fresh (with high moisture), and are prepared for convenient consumption and distribution to the consumer in a fresh-like state. Minimum processing includes minimum preparation procedures such as washing, peeling and/or cutting, and packing, after which the fruit product is usually placed in refrigerated storage where its stability varies depending on the type of product, processing, and storage conditions. If fresh-like fruit is the goal, dehydration should

not be used in processing. Reduction of  $a_w$  by addition of humectants should be employed at a minimal level to maintain the product in a high moisture state. To compensate for the high moisture left in the product, a controlled blanching can be applied without affecting sensory and nutritional properties; pH reductions can be made that will not impair flavor; and preservatives can be added to alleviate the risk of potential spoilage microflora. In conjunction with the above-mentioned factors, slight thermal treatment, pH reduction, slight  $a_w$  reduction, and the addition of antimicrobials (sorbic or benzoic acid, sulfite), all used in conjunction with hurdle technology principles applied to fruits, make up an interesting alternative to IM preservation of fruits, as well as to commercial minimally processed refrigerated fruits (Alzamora et al. 1989, 1993, 1995; Guerrero et al. 1994; Cerrutti et al. 1997).

### 3 Microbial Survival/Inactivation and Impact of $a_w$

It is important to note that low  $a_w$  inhibits growth, but does not kill bacteria (or does so very slowly). On the contrary, nonsporing bacteria that may contaminate food before or after processing steps seem to be protected by the low  $a_w$  and survive with little or no reduction in the amount of cfu for long periods of time (Lund et al. 2000). Thus,  $a_w$  reduction is a very effective method to eliminate the risk of toxigenic bacteria (i.e., bacteria that grow in food and produce toxins) such as *Staphylococcus aureus*, *Clostridium botulinum*, and *Bacillus cereus*, but it does not eliminate the risk posed by infectious bacteria, i.e. *Salmonella* and some *E. coli* strains.

The effects of temperature on survival of microorganisms have been widely documented, with the heat resistance of vegetative cells and spores as influenced by  $a_w$  being probably the most broadly studied area in terms of microbial inactivation (Gould 2000; Leistner 2000). In general, vegetative cells and spores of fungi are more resistant as  $a_w$  of the heating menstrum is reduced. The type of solute used to adjust  $a_w$  to the same value may result in significant differences in the heat resistance of a given microorganism. Small molecular weight compounds such as sodium chloride and glycerol were shown to decrease the resistance of heat resistant strains of *Salmonella*, whereas the heat resistance of heat-sensitive strains was increased. Larger molecular weight solutes, such as sucrose, exerted a more protective effect against heat inactivation.

Commercial and legal requirements regarding the safety of food products have focused attention on the development and improvement of decontamination methods. Due to the presence of a specific microflora adapted to low water content, the decontamination of dried powders, such as milk powder, flour, herbs and spices, egg products, algal powders, and carrageenans, is difficult. The heat resistance of dried vegetative cells is many times higher than the resistance of the same microorganisms in an aqueous solution, but much more research is needed to understand the relation  $a_w$ -microorganism thermotolerance. Fine and Gervais (2005) developed a process for heat treatment of seeds and food powders based on very short

heat stresses at very high temperatures, followed by instantaneous cooling with a cold gas. They found that heat resistance of *Bacillus subtilis* spores and *Saccharomyces cerevisiae* cells was strongly improved for initial  $a_w$  values in the range of 0.3–0.5, but viability of cells and spores was lowest for treatments at initial values of  $a_w$  in the range of 0.1–0.2 and at  $a_w$  values greater than 0.6. In the case of vegetative cells, the complex influence of hydration on cell thermostability has been attributed to opposing effects. Without hydrogen bond-forming compounds, such as water, the conformational flexibility of proteins is reduced and the thermal denaturation of those proteins requires greater energy. But structures such as membranes suffer from extreme dehydration and require minimal water to adopt their functional properties. Gruzdev et al. (2012) analyzed the persistence of *Salmonella Typhimurium* during dehydration and subsequent cold storage and found that dehydration tolerance (DT) and long-term persistence (LPT) were influenced by various growth conditions (phase of growth, growth medium, temperature, and NaCl concentration). Both DT and LPT were enhanced when dehydration was combined with a basic pH and the presence of exogenous trehalose and sucrose. A long dehydration rate enhanced bacterial survival, apparently through de novo synthesis of critical metabolites required for adaptation to the desiccation stress. Moreover, during cold storage many dehydrated cells were found to be in the “viable but non cultivable” state, which may hamper detection on dry food items.

At present, physical, nonthermal processes (high hydrostatic pressure, manothermo-sonication, oscillating magnetic fields, pulsed electric fields, light pulses, etc.), are receiving considerable attention, since in combination with other conventional hurdles, these processes offer potential use for the microbial stabilization of fresh-like food products with little degradation of nutritional and sensory properties. With these novel processes, not a sterile product, but only a reduction of the microbial load is intended, and growth of the residual microorganisms is inhibited by additional, conventional hurdles, such as lowered  $a_w$ . Interesting results have been reported for obtaining minimally processed avocado sauce, avocado purée, and banana purée (Palou et al. 2000, 2002). These fruit products were preserved by the interaction of blanching-high pressure-pH- $a_w$ -preservatives, and the combination of heat treatment and high pressure significant decreased browning reactions (Alzamora et al. 2000a, b). Another group of hurdles presently of special interest are “natural preservatives” (spices and their extracts, lysozyme, chitosan, etc.) (Leistner 2000). As an example, high moisture strawberry can be preserved for at least 3 months by combining mild heat treatment, 3,000 ppm vanillin (instead of synthetic antimicrobials), 500 ppm ascorbic acid, and adjustment of  $a_w$  to 0.95 and pH to 3.0 (Cerrutti et al. 1997).

Low frequency ultrasound can be included in the formulation of combined methods of food preservation to diminish the intensity of traditional factors. An efficient selection of factors depends on microbial inactivation kinetics. The combined effect of simultaneous application of heat (45, 50, or 55 °C) and low frequency ultrasound (20 kHz) at 90 µm amplitude on *Zygosaccharomyces bailii* viability suspended in laboratory media formulated at different  $a_w$  (0.99, 0.97, or 0.95) were evaluated by López-Malo et al. (2001). Survival curves followed first

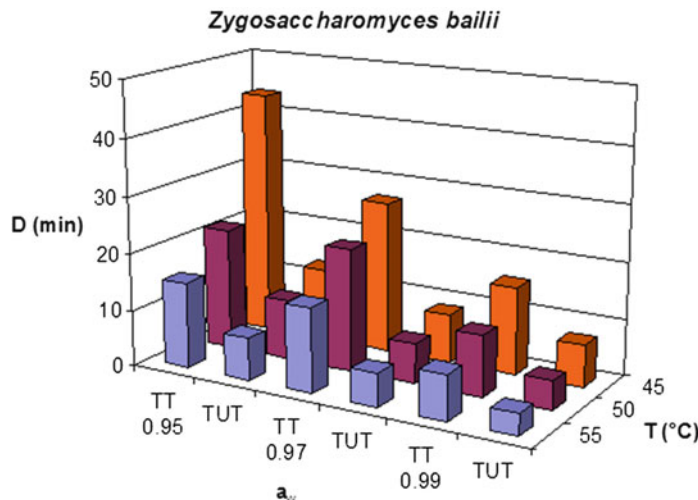


**Fig. 3** Decimal reduction times ( $D$ ) for *Zygosaccharomyces bailii* inactivation when subjected to thermal (TT) or thermo-ultrasonic (TUT) treatments at selected  $a_w$  values

order inactivation kinetics, and  $D$  values were calculated.  $D$  values were lower for  $a_w$  0.99 than for 0.97 or 0.95, being significantly ( $p < 0.05$ ) lower for thermo-ultrasonic (TUT) than for thermal treatments (TT). *Z. bailii*  $D$  values at 45 °C were reduced from 15.4 (TT) to 7.4 (TUT) min ( $a_w$  0.99), from 26.8 (TT) to 8.6 (TUT) min ( $a_w$  0.97), and from 43.5 (TT) to 12.9 (TUT) min ( $a_w$  0.95). TUT significantly ( $p < 0.05$ ) reduced the heat-protective effect of reduced  $a_w$ , demonstrating that a combination of heat and ultrasound can be applied to inactivate yeast cells, reducing heat treatment intensity, especially in  $a_w$  reduced media (Fig. 3).

Palou et al. (1998) evaluated the effect of  $a_w$  of the suspension media (0.98 or 0.95) on the survival of *Zygosaccharomyces bailii* subjected to high hydrostatic pressure treatments (Fig. 4). Their findings demonstrate that  $a_w$  has an important influence on yeast survival after high pressure treatments, becoming more resistant as  $a_w$  decreases.

#### 4 Mechanism of Action of Osmotic Stress

From a microbiological point of view, food preservation involves microbial exposure to a hostile situation to prevent or delay their growth, shorten their survival or cause their death (Gould 2000). When stress is sensed by a microorganism, signals that induce mechanisms to cope with the stressor are developed. These mechanisms involve modifications in gene expression and protein activities (Capozzi et al. 2009). However, microorganisms have developed different mechanisms of resistance to the effects of these stress factors. Internal media stability (composition

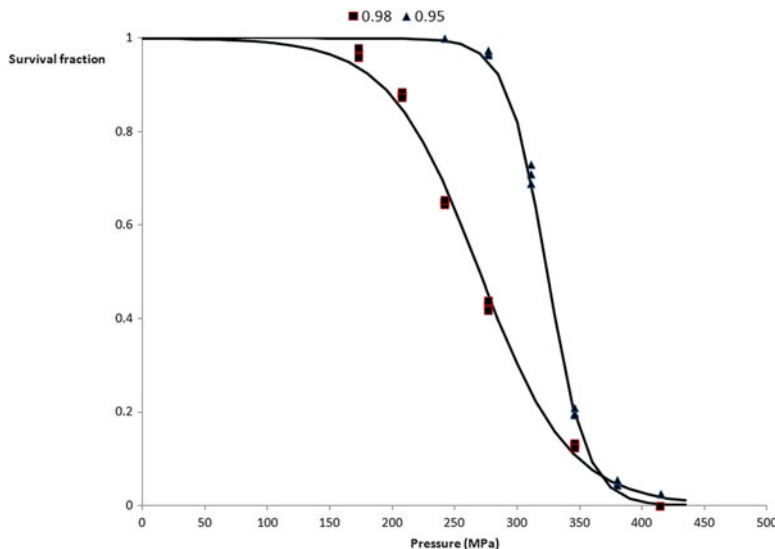


**Fig. 4** Survival curves of *Zygosaccharomyces bailii* suspended in media formulated with selected  $a_w$  values and exposed to high-pressure treatments. (Adapted from Palou et al. 1998)

and volume of fluids) is vital for survival and growth. Cell homeostasis is maintained through reaction mechanisms that act in response to relative minor changes in physiological variables, leading to a series of events that will in turn restore the altered variable to its original value (Gould 1996). These homeostatic mechanisms act to ensure that microbial cell physiological activities remain relatively unchanged, even when the environment around the cell is different and greatly perturbed (Leistner and Gould 2002). In the case of vegetative microorganisms, the homeostatic mechanisms are energy-dependent because the cell must expend energy to resist the stress factors, e.g., to repair damaged components and to synthesize new cell components. In the case of spores, the homeostatic mechanisms is not energy-consuming but they are built in prior to being exposed to an environmental stress (Leistner and Gould 2002). Preservation factors must overcome microbial homeostatic resistance in order to be effective.

Regarding  $a_w$  status, all microorganisms must deal with changes in water availability in their surroundings, since the concentration of solutes within the cell is higher than that in the environment (Kempf and Bremer 1998). Supporting this difference on opposite sides of the semipermeable cytoplasmic membrane is essential, since positive turgor is considered as the driving force for cell expansion. As a result of changes in the osmolality of the medium (decreasing  $a_w$ ), passive flow of water across microbial cell membranes occurs, resulting in a loss of turgor. Microorganisms do not possess active transport mechanisms for water; hence, turgor is adjusted by controlling osmotically active solutes in the cytoplasm

(Kempf and Bremer 1998). The general mechanism managed by microbial cells that are able to overcome the initial loss following a hyperosmotic shock is the accumulation of cytoplasmatic solute(s) so as to increase the internal osmotic pressure, which can restore turgor (Gould 1989a; Gutierrez et al. 1995). Osmotic regulation involves the expression of a number of genes to optimize growth under the stress condition, allowing cells to modulate the rate of acquisition of compatible solutes. A great variety of solutes can be accumulated by various microorganisms (i.e. cations, amino and imino acids, polyols, and sugars). These solutes allow continued activity of cytoplasmic enzymes at lower  $a_w$  values; are soluble to high concentrations; and the cell membrane exhibits controlled permeability to them. Compatible solutes may be transported from the medium or synthesized de novo in the cytoplasm. The accumulation process is energy dependent and causes an increase in maintaining metabolism, with consequent reduction in the microbial growth rate. Control of microbial survival or growth in foods by modification of  $a_w$  is attained when the target microorganism is unable to carry out these effects; in other words, the mechanisms exceed the osmoregulatory capacity of the cell. In terms of microbial control, different strategies can be employed: using  $a_w$  as the only microbial stress factor and, therefore,  $a_w$  must be reduced to very low levels; or using other stress factors in combination with lowering of  $a_w$  ("hurdle concept" or combined methods), thus reducing the amount of energy available for osmoregulation.

Osmotic induction of general stress systems results in the consequent development of multitolerances towards other environmental stresses when subjected to hypertonic environments (Pichereau et al. 2000; O'Byrne and Booth 2002).

New food preservation strategies can be developed on a sound scientific base if combination of hurdles is considered, taking into account their different modes of action over microbial cells and the mechanisms mediating microbial adaptive responses (Ross et al. 2003; Gould 1996). Our knowledge of these subjects is, however, far for complete. Nowadays, the advent of new methodic developments may provide a significant conceptual advance in the understanding of responses in microorganisms to a variety of environmental stresses (Brul et al. 2006). Many advances in recent years have been made to understand the behavior of stressed microorganisms and food preservation. McMahon et al. (2007) found that sublethal stresses (high/low temperature, osmotic and pH stress) which food pathogens encounter in modern food preservation systems increase the inter- and intra-specific horizontal transmission of selected antibiotic resistance (ABR) plasmids. So, increased use of bacteriostatic (sublethal) rather than bactericidal (lethal) food preservation systems may contribute to the dissemination of ABR among important food pathogens.

Other important concept of enormous importance for the food industry has to do with heterogeneity within bacterial populations (Booth 2002). In traditional analysis, the homogeneity of the population of cells in terms of their biochemistry and responsiveness has been assumed. But homogeneity is neither required nor desirable for survival; moreover, heterogeneity is an intrinsic factor in organisms which assures that, when a stress is imposed, some cells will survive and become the new

colonists of the newly encountered environment. In this sense, recent studies have pointed out the variability in the growth limits of individual microbial cells as  $a_w$  is reduced. Assuming that each colony was derived from a single cell, and considering the number of cells of *Salmonella enteritidis* inoculated, Koutsoumanis (2008) determined that as NaCl concentration increased and pH decreased, the number of cells able to grow decreased. As the inoculum size increased, NaCl growth limits of *S. enteritidis* increased and became less variable. The author noted the need for stochastic approaches in quantitative microbiology, especially at environments close to the boundary of growth. As contamination of foods with pathogens occurs at very low levels, it is clear that the behavior of single cells should be taken into account through stochastic models.

A new scientific approach to study the survival strategies of microorganisms of concern in various foods by using “genomics” technology (genomics, transcriptomics, proteomics, and metabolomics) is being explored by various groups (Brul et al. 2006, 2008). Integration of molecular biology and classical physiology (the so-called “functional genomics”) could lead to a molecular mechanistic basis of the survival strategies of pathogens of concern. In this way, preservation factors could be optimally combined to obtain synergistic or additive effects on the inhibition of unwanted microorganisms.

## 5 Water Activity Control: Future

Even though there exist restrictions and sensory problems that may cause the reduction of  $a_w$  in some food products, the employment of this preservation factor continues to be useful in process design, food formulation, food quality, and in the selection of storage conditions. Microbiological relation to water activity has an important impact and practical implications in the food industry. It is clear that  $a_w$  plays a significant role in the survival and death of microorganisms in foods and, in combination with other traditional preservation factors,  $a_w$  is being used nowadays as the basis for chemical and microbial stability in a wide range of products.

Food safety and stability have been controlled by the food processing industry using a number of methods. Vegetative microbial cells and spores are destroyed or restricted by the individual or combined use of the following traditional preservation methods: heat sterilization, pasteurization, refrigeration, freezing, water activity control, cooking, acidification, fermentation, vacuum packaging, and/or adding antimicrobial agents. The extensive use of these procedures has maintained the low-risk status of the food supply. However, the new generation of minimally processed, fresher, antimicrobial, and additive-free food products has less resistance to spoilage and allows greater risks of food-borne illness if any abuse occurs. Traditional preservation procedures generally base their intensity on microbial control, so after destroying, eliminating, or substantially reducing initial microbial counts, measures to prevent recontamination should be taken, which often results in a safe and stable product (Baird-Parker 1995). If microbial hazard or spoilage cannot be totally eliminated from

the food, microbial growth and toxin production must be inhibited. Microbial growth can be inhibited by combining intrinsic food characteristics with extrinsic product storage and packaging conditions. If confident judgment about food quality, stability, and safety is to be made, it is essential to rely on a better understanding of survival to  $a_w$  stressor, accurate quantitative data and mechanistic predictive models about combined factors affecting growth or survival of unwanted microorganisms are needed (Gould 1989b; Buchanan 1992; Alzamora and López-Malo 2002).

## References

- Allende A, Tomás-Barberán FA, Gil MI (2006) Minimal processing for healthy traditional foods. *Trends Food Sci Technol* 17:513–519
- Alzamora SM, Cerruti P, Guerrero S, López Malo A (1995) Minimally processed fruits by combined methods. In: Welti Chanes J, Barbosa Cánovas GV (eds) *Food preservation by moisture control fundamentals and applications*. Technomic Pub Co, Lancaster, pp 463–492
- Alzamora SM, Fito P, López-Malo A, Tapia MS, Parada-Arias E (2000a) Minimally processed fruit using vacuum impregnation, natural antimicrobial addition and/or high hydrostatic pressure techniques. In: Alzamora SM, Tapia MS, López Malo A (eds) *Minimally processed fruits and vegetables Fundamental aspects and applications*. Aspen Publishers, Inc., Gaithersburg, pp 293–315
- Alzamora SM, Gerschenson LN, Cerruti P, Rojas AM (1989) Shelf stable pineapple for long term non refrigerated storage. *Lebensm Wiss Technol* 22:233–236
- Alzamora SM, López-Malo A (2002) Microbial behavior modeling as a tool in the design and control of processed foods. In: Welti-Chanes J, Barbosa-Canovas GV, Aguilera JM (eds) *Engineering and food for the 21st century*. CRC, Boca Raton, pp 631–650
- Alzamora SM, López-Malo A, Tapia MS (2000b) *Minimally processed fruits and vegetables: fundamentals and applications*. Aspen Publishers, Inc., Gaithersburg
- Alzamora SM, Tapia MS, Argaiz A, Welti J (1993) Application of combined methods technology in minimally processed fruits. *Food Res Int* 26(125):130
- Alzamora SM, Tapia MS, López-Malo A, Welti-Chanes J (2003) The control of water activity. In: Zeuthen P, Bogh-Sorensen L (eds) *Food preservation techniques*. CRC, Cambridge, England, pp 126–143
- Baird-Parker AC (1995) Development of industrial procedures to ensure the microbiological safety of food. *Food Control* 6:29–36
- Beuchat LR (1983) Influence of water activity on growth, metabolic activities and survival of yeasts and molds. *J Food Prot* 46:135–140
- Beuchat LR (1987) Influence of water activity on sporulation, germination, outgrowth, and toxin production. In: Rockland LB, Beuchat LR (eds) *Water activity: theory and applications to food*. Marcel Dekker, Inc., New York
- Beuchat LR (1996) Detection and enumeration of microorganisms in hurdle technology foods, with particular consideration of foods with reduced water activity. In: Barbosa-Cánovas GV, Welti-Chanes J (eds) *Food preservation by moisture control. Fundamentals and applications*. Technomic Publishing Company, Lancaster
- Booth IR (2002) Stress and single cell: Intrapopulation diversity is a mechanism to ensure survival upon exposure to stress. *Int J Food Microbiol* 78:19–30
- Breeuwer P, Lardeau A, Peterz M, Joosten HM (2003) Desiccation and heat tolerance of *Enterobacter sakazakii*. *J Appl Microbiol* 95:967–973
- Brewer MS (1999) Traditional preservatives. Sodium chloride. In: Robinson RK, Batt C, Patel P (eds) *Encyclopedia of food microbiology-2*. Academic, London, pp 1723–1728

- Brul S, Menzonides FIC, Hellingwerf KJ, Teixeira de Matos MJ (2008) Microbial system biology: new frontiers open to predictive microbiology. *Int J Food Microbiol* 128:16–21
- Brul S, Schuren F, Montijn R, Keijser BJF, van der Spek H, Oomes SJCM (2006) The impact of functional genomics on microbiological food quality and safety. *Int J Food Microbiol* 112:195–199
- Buchanan RL (1992) Predictive microbiology: mathematical modeling of microbial growth in foods. In: Finley JW, Robinson SF, Armstrong DJ (eds) *Food safety assessment*, ACS series. American Chemical Society, Washington, DC, pp 250–260
- Buchanan RL (2003) Resistance-thermal and other DHHS. Food and Drug Administration. Center for Food Safety and Applied Nutrition. [www.fda.gov/ohrms/dockets/ac/03/slides/3939s1\\_buchanan\\_](http://www.fda.gov/ohrms/dockets/ac/03/slides/3939s1_buchanan_)
- Capozzi V, Fiocco D, Amodio ML, Gallone A, Spano G (2009) Bacterial stressors in minimally processed food. *Int J Mol Sci* 10:3076–3105
- Cerrutti P, Alzamora SM, Vidales SL (1997) Vanillin as antimicrobial for producing shelf stable strawberry purée. *J Food Sci* 62:608–610
- Chirife J (1994) Specific solute effects with special reference to *Staphylococcus aureus*. In: Fito P, Mulet A, McKenna B (eds) *Water in foods. Fundamental aspects and their significance in relation to processing of foods*. Elsevier Applied Science, Great Britain, pp 409–419
- Chirife J (1995) An update on water activity measurements and prediction in intermediate and high moisture foods: the role of some non-equilibrium situations. In: Barbosa-Cánovas G, Welti-Chanes J (eds) *Food preservation by moisture control. Fundamentals and Applications*. Technomic Publishing Company, Lancaster, pp 169–189
- Christian JHB (2000) Drying and reduction of water activity. In: Lund BM, Baird-Parker TC, Gould GW (eds) *The microbiological safety and quality of foods*. Aspen Pub., Maryland, pp 146–174
- Corry JEL (1973) The water relations and heat resistance of microorganisms. *Prog Ind Microbiol* 12:73–80
- Delgado-Portales RE, Palou E, López-Malo A (2007) Probabilistic modeling of *Enterobacter sakazakii* survival to desiccation after growth at selected water activities. International association for food protection annual meeting
- Edelson-Mammel S, Porteous MK, Buchanan RL (2006) Acid resistance of twelve strains of *Enterobacter sakazakii*, and the impact of habituating the cells to an acidic environment. *J Food Sci* 71:201–207
- Fine F, Gervais P (2005) A new high temperature short time process for microbial decontamination of seeds and food powers. *Powder Technol* 157:108–113
- Gould GW (1989a) Drying, raised osmotic pressure and low water activity. In: Gould GW (ed) *Mechanisms of action of food preservation procedures*. Elsevier Applied Science, New York
- Gould GW (1989b) Predictive mathematical modelling of microbial growth and survival in foods. *Food Sci Technol Today* 3(2):89–92
- Gould GW (1996) Methods for preservation and extension of shelf life. *Int Food Microbiol* 33:51–64
- Gould GW (2000) Induced tolerance of microorganisms to stress factors. In: Alzamora SM, Tapia MS, Lopez-Malo A (eds) *Minimally processed fruits and vegetables. Fundamental aspects and applications*. Aspen Publishers Inc, Gaithersburg, pp 29–37
- Gruzdev N, Pinto R, Sela Saldinger S (2012) Persistence of *Salmonella enterica* during dehydration and subsequent cold storage. *Food Microbiol* 32:415–422
- Guerrero S, Alzamora SM, Gerschenson LN (1994) Development of a shelf stable banana purée by combined factors: microbial stability. *J Food Prot* 57:902–907
- Gutierrez C, Abey T, Booth IR (1995) Physiology of the osmotic stress response in microorganisms. *Int J Food Microbiol* 28:233
- Hocking AD, Christian JHB (1996) Microbial ecology interactions in the processing of foods. In: Barbosa-Cánovas G, Welti-Chanes J (eds) *Food preservation by moisture control. Fundamentals and applications*. Technomic Publishing Company, Lancaster

- Hocking AD, Pitt JI (1987) Media and methods for enumeration of microorganisms with consideration of water activity. In: Rockland LB, Beuchat LR (eds) Water activity: theory and applications to food. Marcel Dekker, Inc., New York
- IFT (2003) Analysis of microbial hazards related to time/temperature control of foods for safety. *Compr Rev Food Sci Food Safety* 2:33–41
- Jay JM, Loessner MJ, Golden DA (2005) Modern food microbiology. Springer Science + Business Media, Inc., New York
- Karel M (1973) Recent research and development in the field of low moisture and intermediate moisture foods. *CRC Crit Rev Food Technol* 3:329–373
- Karel M (1976) Technology and application of new intermediate moisture foods. In: Davies R, Birch GG, Parker KJ (eds) Intermediate moisture foods. Applied Science Publishers Ltd, London, pp 4–31
- Kempf B, Bremer E (1998) Uptake and synthesis of compatible solutes as microbial stress responses to high-osmolality environments. *Arch Microbiol* 170:319–330
- Koutsoumanis K (2008) A study on the variability in the growth limits of individual cells and its effect on the behavior of microbial populations. *Int J Food Microbiol* 128:116–121
- Leistner L (2000) Hurdle technology in the design of minimally processed foods. In: Alzamora SM, Tapia MS, Lopez-Malo A (eds) Minimally processed fruits and vegetables. Fundamental Aspects and Applications. Aspen Publishers Inc., Gaithersbug, pp 13–27
- Leistner L, Gould GW (2002) Hurdle technologies. Combination treatments for food stability, safety and quality. Kluwer Academic, New York
- Lenovitch LM (1987) Survival and death of microorganisms as influenced by water activity. In: Rockland LB, Beuchat L (eds) Water activity: theory and applications to food. Marcel Dekker, Inc., New York, pp 119–136
- Leyer GJ, Johnson EA (1993) Acid adaptation induces cross-protection against environmental stresses in *Salmonella typhimurium*. *Appl Environ Microbiol* 59:1842–1847
- López-Malo A, Palou E, Franco-Corzo A (2001) Yeast inactivation kinetics during thermo-ultrasonication treatments at selected water activities and pHs. International association for food protection annual meeting
- Lund BM, Baird-Parker TC, Gould GW (2000) The microbial safety and quality of food. Aspen Publishers, Inc., Gaithersburg, pp 387–388
- McMahon MAS, Blair IS, Moore JE, Mc Dowell DA (2007) The rate of horizontal transmission of antibiotic resistance plasmids is increased in food preservation-stressed bacteria. *J Appl Microbiol* 103:1883–1888
- Mossel DAA (1975) Water and microorganisms in foods—a synthesis. In: Duckworth RB (ed) Water relations in foods. Academic, New York
- O'Byrne C, Booth IR (2002) Osmoregulation and its importance to food—borne microorganisms. *Int J Food Microbiol* 74:203–216
- Palou E, López-Malo A (2001) Solute type effects on Debaryomyces hansenii growth response in selected water activity and pH media. Institute of Food Technologists (IFT) annual meeting
- Palou E, Lopez-Malo A, Barbosa-Canovas GV, Welti-Chanes J (2000) High hydrostatic pressure and minimal processing. In: Alzamora SM, Tapia MS, López-Malo A (eds) Minimally processed fruits and vegetables. Fundamental aspects. Aspen Publishers, Gaithersburg, pp 205–222
- Palou E, Lopez-Malo A, Barbosa-Canovas GV, Welti-Chanes J, Davidson PM, Swanson BG (1998) High hydrostatic pressure come-up time and yeast viability. *J Food Prot* 61:1657–1660
- Palou E, Lopez-Malo A, Welti-Chanes J (2002) Innovative fruit preservation methods using high pressure. In: Welti-Chanes J, Barbosa-Canovas GV, Aguilera JM (eds) Engineering and food for the 21st century. CRC, Boca Raton, pp 715–725
- Pichereau V, Hartke A, Auffray I (2000) Starvation and osmotic stress induced multiresistances influence of extracellular compounds. *Int J Food Microbiol* 55:19–25
- Raso J, Barbosa-Cánovas GV (2003) Nonthermal preservation of foods using combined processing technique. *Crit Rev Food Sci Nutr* 43:265–285

- Ross AIV, Griffiths MW, Mittal GS, Deeth HC (2003) Combining nonthermal technologies to control foodborne microorganisms. *Int J Food Microbiol* 89:125–138
- Scott WJ (1957) Water relations of food spoilage microorganisms. *Adv Food Res* 6:549–556
- Tapia MS, Aguilera JM, Chirife J, Parada E, Welti J (1994) Identification of microbial stability factors in traditional foods from Iberoamerica. *Rev Esp Cienc Tecnol Alim* 34:145–163
- Tapia MS, Welti-Chanes J (2012) Hurdle technology principles applied in decontamination of whole and fresh-cut produce. In: Gómez López VM (ed) *Decontamination of fresh and minimally processed produce*, 1st edn. Wiley, New York, pp 417–449
- Tiganitas A, Zeaki N, Gounadaki AS, Drosinos EH, Skandamis PN (2009) Study of the effect of lethal and sublethal pH and aw stresses on the inactivation or growth of *Listeria monocytogenes* and *Salmonella Typhimurium*. *Int J Food Microbiol* 134:104–112

# On Modeling the Effect of Water Activity on Microbial Growth and Mortality Kinetics

M. Peleg, M.G. Corradini, and M.D. Normand

## Abbreviations

$a_w$	Water activity
$k$	Growth rate parameter
$\lambda$	Lag time
ODE	Ordinary differential equation
$P$	Probability
$P_d$	Momentary probability rate of cell division
$P_m$	Momentary probability rate of cell mortality
$t$	Time
$t_c$	Location of the inflection point
$Y(t)$	Linear or logarithmic growth ratio
$Y_{\text{asym}}$	Asymptotic linear or logarithmic growth ratio
$\mu_{\max}$	Maximum specific growth rate - the slope of the growth curve at $t_c$

---

M. Peleg (✉) • M.D. Normand

Department of Food Science, University of Massachusetts, Amherst, MA 01003, USA  
e-mail: [micha.peleg@foodsci.umass.edu](mailto:micha.peleg@foodsci.umass.edu)

M.G. Corradini

Department of Food Science, Rutgers University, New Brunswick, NJ 08901, USA

## 1 Introduction

The effect of moisture on the growth of different kinds of bacteria, yeasts, and molds in or on foods has traditionally been depicted in the form of a rate vs. water activity ( $a_w$ ) plot such as that shown in Fig. 1. The rate curve of each organism type begins (or ends) at a point along the  $a_w$ -axis. At lower  $a_w$  levels, presumably, the particular type of organism does not grow, i.e., its growth rate is zero. While such plots can and have been successfully used to identify safe water activities for food storage, for example, they do not always tell the whole story. One reason is that the borderline between growth and no-growth is rarely sharp. Another reason is that a plot of this kind does not fully reveal what happens above the marked water activity threshold. Moreover, in many foods, water activity control is accompanied by a drying process, in which case the temperature history may affect the type or number of organisms remaining in the food, and/or the introduction of a complementary agent such as salt or chemical preservative. To deal with these aspects of microbial growth inhibition, it is necessary to develop a kinetic model of growth whose parameters account for the role of all pertinent factors that affect a food's biological stability and that of their interactions. The same can be said about chemical and physical changes that inevitably occur during food preservation, especially when heat or drying is involved. Such changes can consist of two kinds: degradation, notably the loss of freshness and nutrients, or synthesis, notably the accumulation of Maillard reaction products, but also other compounds that impart off flavor. Water activity, and factors such as pH and salt concentration, affect the heat resistance not only of microorganisms, including bacterial spores, but also of enzymes. The subject has been amply studied and there is a large body of literature covering its various aspects.

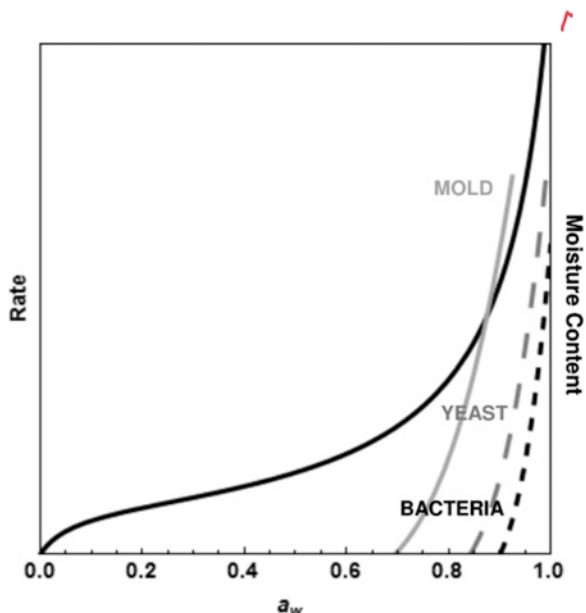


**Fig. 1** Classic moisture sorption isotherm and how it affects microbial growth

The objective of this chapter is not to summarize the results of the numerous studies; this task is better left to professional microbiologists who have much better insight into the biology and biochemistry of microbial growth; they also possess the tools to evaluate what has been published in the literature and to assess their practical implications in food preservation. The main goal here is to discuss ways to introduce the role of water activity into existing kinetic rate models of microbial growth and inactivation, and to present a new class of probabilistic models that can account for simultaneous growth and mortality that sometimes ensue.

## 2 Microbial Growth Curves

A typical microbial growth curve has four regions representing the lag phase, exponential growth phase, stationary phase, and mortality phase, shown schematically in Fig. 2. Most of the studies of microbial growth kinetics have focused on the sigmoid part of the curve, i.e., the first three phases. This is a reasonable approach because most foods become inedible or unsafe to eat long before the mortality phase sets in. The Gompertz model and several variants of the logistic (Verhulst) equation are the most commonly used growth models in food microbiology (McMeekin et al. 1993; McKellar and Lu 2004; van Boekel 2009). All of these models deal with net growth and therefore do not account for cell mortality, which at least theoretically can occur not only during the stationary phases but also during the lag and exponential phases. A notable exception is the quasi-chemical model developed at the US Army Natick R&D laboratory, which takes into account the

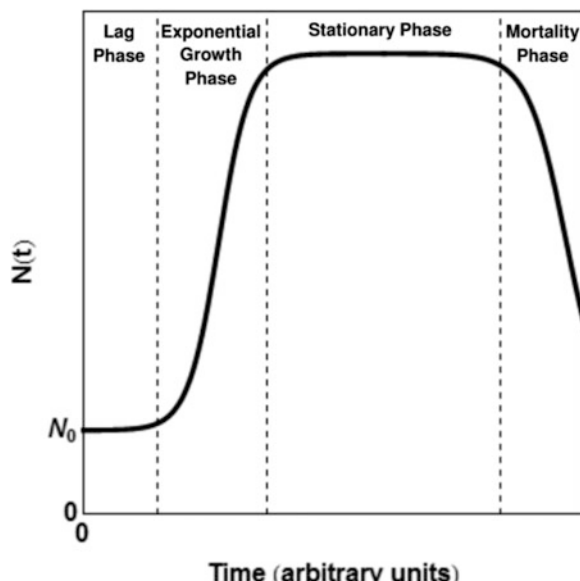


**Fig. 2** Schematic view of the four phases of microbial growth in a closed habitat

release of polluting metabolites by the cells, and hence for simultaneous division and mortality at any phase (Taub et al. 2003). Since the conventional growth models do not account for mortality, none of them can be considered as being fundamental in the strict sense of the term, and any mechanistic proposed interpretation of their parameters must be based on *independent experimental evidence*. In other words, the shape of the growth curve alone does not contain enough information to account for the continuously changing roles of cell physical growth, division, and mortality during a microbial population's growth cycle.

The sigmoid part of a more or less symmetric isothermal growth curve should be characterized by no less than three parameters, as demonstrated in Fig. 3, in order to separately account for the asymptotic growth level, the location of the inflection point of the growth curve, and the slope of the curve at this point. At least in principle, these three characteristics need not vary in a predetermined manner as a result of changes in food temperature, water activity, pH, salt concentration, oxygen tension, etc. Much of the published research on microbial growth has focused on the effect of temperature, water activity and pH on the maximum specific growth rate ( $\mu_{\max}$ ), i.e., the growth curve's slope at its inflection point. However, to extrapolate accelerated storage data to ambient conditions, it is necessary to determine the effect of these factors not only on the rate (Fig. 4) but also on all three parameters as shown schematically in Figs. 5, 6, and 7, in order to produce the whole growth curve, as described below. Moreover, in order to predict a dynamic growth pattern,

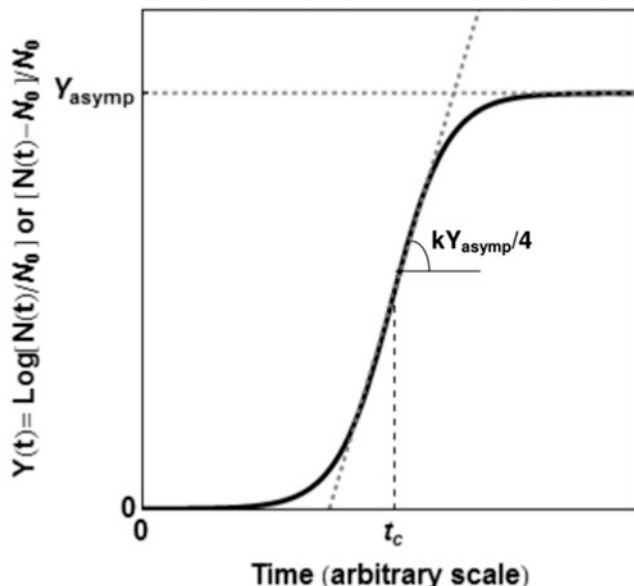


**Fig. 3** Schematic view of a growth curve described by the shifted logistic model (Eq. 1) and its parameters

**Fig. 4** Schematic view of the traditional way to extrapolate accelerated storage data. Notice that it is only applicable when the kinetics of the process can be characterized by a single rate parameter

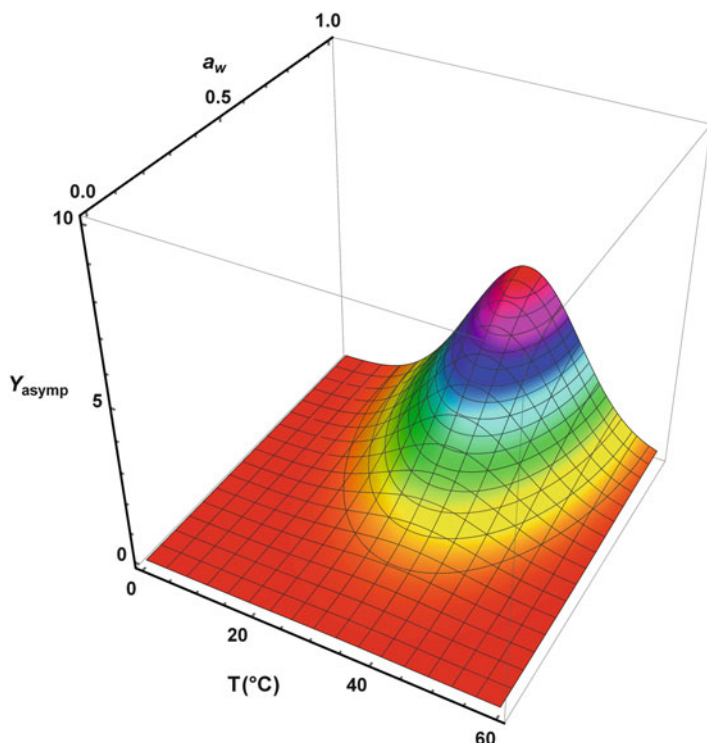
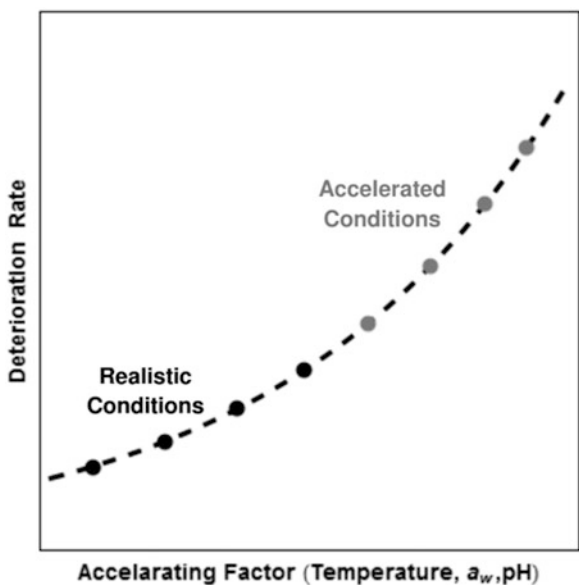


**Fig. 5** Schematic view of the effect of temperature and water activity combinations on asymptotic growth level ( $Y_{\text{asymp}}$ )

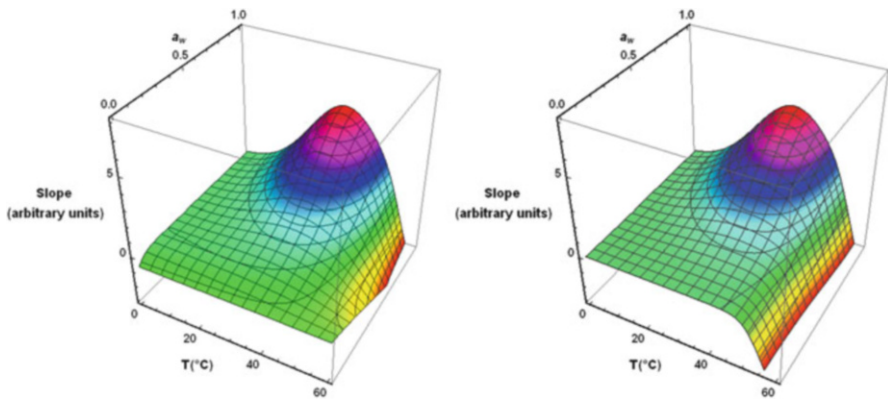


**Fig. 6** Schematic view of the effect of temperature and water activity combinations on maximum growth rate ( $\mu_{max}$  or  $kY_{asym}/4$  in terms of the shifted logistic model). *Left*—when water activity does not affect the organism's heat resistance; *right*—when dryness increases heat resistance

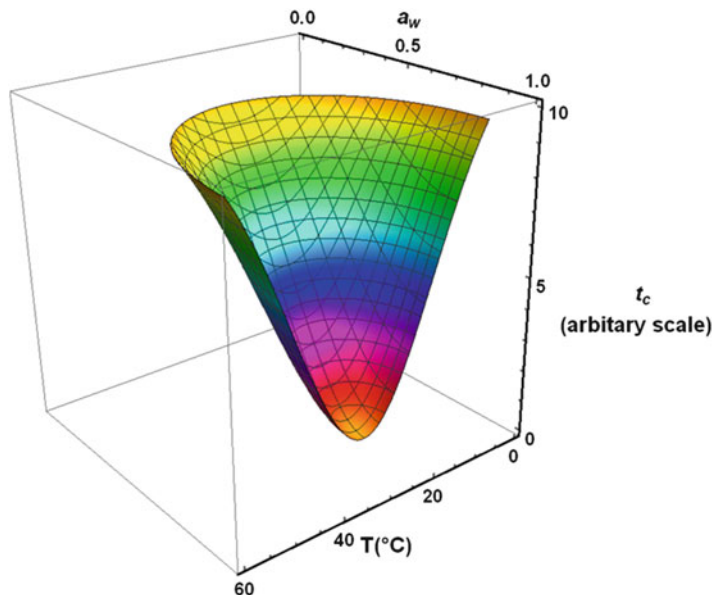


**Fig. 7** Schematic view of the effect of temperature and water activity combinations on inflection point location ( $t_c$ ). Similar relationship will emerge for the “lag time” ( $\lambda$ )

i.e., when some or all of the factors that affect the growth vary simultaneously, each of the three parameters' dependency on the pertinent factors should be determined experimentally. The hypothetical temperature and  $a_w$  dependencies of the three growth parameters shown in Figs. 5, 6, and 7 give a clue as to how the three

relationships of a microorganism might appear. Figure 5 shows how different temperature–water activity combinations affect overall growth level, which is represented by  $Y_{\text{asymp}}$  (Fig. 3). Peak growth will be observed at the optimal temperature and high  $a_w$ . From this point,  $Y_{\text{asymp}}$  will diminish and eventually drop to zero when it is too cold, too hot, or too dry for the organism to grow. At low and moderate temperatures, heat usually accelerates the growth, which will be manifested in a higher  $\mu_{\max}$  (or  $kY_{\text{asymp}}/4$  in terms of the shifted logistic model), as described below and as shown in Fig. 6. However, excessive heat can become a cause of mortality, as is also shown in the figure. Mathematically, this result will be manifested by the rate parameter (or the slope of the curve) changing sign, becoming negative as thermal inactivation ensues (Fig. 6—left). In general, lowering the water activity impedes microbial growth and hence the preservation by drying. However, by lowering their water activity, the heat resistance of many bacterial spores and cells may actually increase. This will alter the growth rate–temperature– $a_w$  relationship in a manner shown schematically in Fig. 6—right. The lag time ( $\lambda$ ), or the time at which the growth rate is maximal ( $t_c$ , in terms of the shifted logistic model, as shown in Fig. 4), is expected to be the shortest at the optimal temperature. It will become progressively longer as the temperature rises or drops beyond this point. It will also become longer when the water activity drops, shown schematically in Fig. 7. Obviously, where growth ceases altogether, both the lag time,  $\lambda$ , and the time to reach  $t_c$  will tend to infinity. Theoretically, once the temperature and water activity dependencies of all three parameters have been determined, they can be incorporated into the growth rate equation coefficients and used to generate and predict dynamic growth or growth/inactivation curves. These, however, would be reliable only if the temperature and water activity vary within the range of conditions in which the model coefficients have been determined experimentally (Peleg 2006). Equation (1) is an example of a model for variable temperature–water activity conditions, based on the shifted logistic equation model (Peleg 2006; van Boekel 2009):

$$Y(t) = \frac{Y_{\text{asymp}}}{1 + \exp\{k[T(a_w(t))]\{t_c[T(a_w(t))] - t\}\}} - \frac{Y_{\text{asymp}}}{1 + \exp\{k[T(a_w(t))]\}t_c[T(a_w(t))]} \quad (1)$$

This equation describes the relationship between the linear or logarithmic growth ratio  $Y(t)$ ,  $Y(t) = [N(t) - N_0]/N_0$  or  $\log[N(t)/N_0]$  vs. time, and contains the already mentioned three parameters— $Y_{\text{asymp}}$ , the asymptotic linear or logarithmic growth ratio,  $t_c$ , the growth curve inflection point location, and  $k$ , a representative of the growth rate—which are all functions of the particular temperature–water activity conditions under which the growth curve has been determined. The maximum specific growth rate ( $\mu_{\max}$ ) according to this model is  $kY_{\text{asymp}}/4$ .

In principle, and in the case of temperature alone in practice (Corradini and Peleg 2006a), this model could be used to extrapolate isothermal accelerated

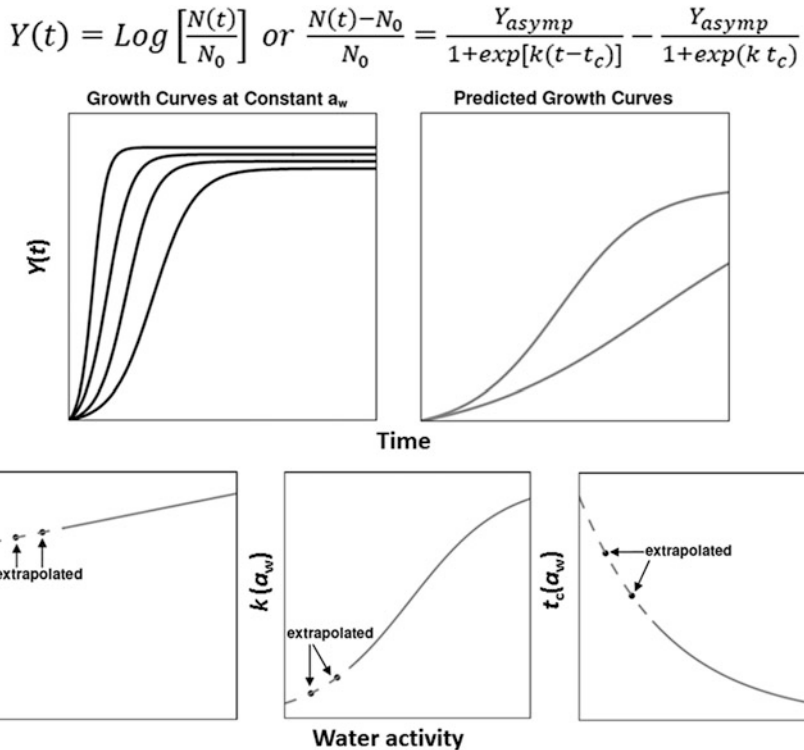


**Fig. 8** Schematic view of the extrapolation of accelerated storage data of microbial growth using the shifted logistic equation as a model

storage data as shown schematically in Fig. 8. The figure demonstrates that by extrapolating all three parameters, the entire growth curve can be generated at ambient conditions, which would be impossible on the basis of  $\mu_{\max}$  alone.

Like all of the rate models that have been derived from the logistic (Verhulst) model, this model too is based on the notion that the momentary growth (or inactivation) rate,  $dY(t)/dt$ , is the isothermal rate at the momentary temperature–water activity conditions, at the time,  $t^*$ , which corresponds to the momentary population size, i.e.,

$$\frac{dY(t)}{dt} = \frac{k[T(a_w(t))] Y_{asym}[T(a_w(t))] \exp(k[T(a_w(t))] \{t_c[T(a_w(t))] - t^*(t)\})}{1 + \exp\{k[T(a_w(t))] \{t_c[T(a_w(t))] - t^*(t)\}\}^2} \quad (2)$$

where

$$t^*(t) = \frac{1}{k(T(a_w(t)))} \log_e \left[ \frac{\exp[k(T(a_w(t)))t_c(T(a_w(t)))](Y_{asym}(T(a_w(t))) + Y(t)\{1 + \exp[k(T(a_w(t)))t_c(T(a_w(t))]\}\})}{Y_{asym}(T(a_w(t)))\exp[k(T(a_w(t)))t_c(T(a_w(t)))] - Y(t)\{1 + \exp[k(T(a_w(t)))t_c(T(a_w(t))]\}\}} \right] \quad (3)$$

Despite its cumbersome appearance, Eq. (2) is an ordinary differential equation (ODE) which can be solved easily by modern mathematical software to produce the sought dynamic growth or growth/inactivation curve. The difficulty, therefore, is not in the differential equation solution, but in the effort to generate the experimental database from which the terms  $Y_{asym}[T(a_w(t))]$ ,  $t_c[T(a_w(t))]$ , and  $k[T(a_w(t))]$  can be derived. The shift factor in Eq. (1),  $1/[1 + \exp(kt_c)]$ , is necessary in order to guarantee that  $Y[0] = 0$  so that it can serve as a boundary condition in the differential equation solution.

In the traditional modeling approach,  $\mu_{max}$  alone is expressed as a function of the temperature–water activity combination. The structure of this function is based on an a priori assumption of how the temperature and water activity act together, the Gamma Hypothesis being a notable example (Ross and Dalgaard 2004). However, since the interactions between growth promoting and inhibitory factors are completely determined by the specific organism and the actual habitat characteristics, it is unlikely that they are governed by a set of universal rules. Therefore, until such rules are discovered or their existence proven, microbial growth will need to be described by ad hoc empirical models. However, its empirical character notwithstanding, the three-parameter approach allows for the distinction between growth suppression or promotion ( $Y_{asym}$ ), growth delay or advance ( $t_c$ ), and its acceleration or deceleration ( $k$  or  $kY_{asym}/4$ ). This approach also does not require that the three must always rise or fall in unison following predetermined rules.

### 3 Chemical Changes and Microbial Inactivation

When a chemical reaction or microbial inactivation follows first or other fixed order kinetics, determining the exponential rate constant, or other characteristic rate constant, as a function of temperature,  $a_w$  and/or other factor(s) will be theoretically sufficient to construct the progress curve of the process under dynamic conditions. This has been the basis of the conventional method for estimating changes in processed, stored, or shipped foods, by extrapolating accelerated storage data (Fig. 4) and constructing time–temperature integrators for in situ measurements. In all these applications, it has been assumed, almost universally, that the temperature dependence of the characteristic rate constant of the process follows the Arrhenius equation, and in some cases the log-linear model, and its hallmark, the  $z$  value. This traditional approach has serious limitations when it comes to nonlinear biological processes and chemical and biochemical reactions, especially when they

occur in a continuously changing physical and chemical environment, such as food being processed or even stored. The validity of the assumption that there is a temperature or moisture independent energy of activation in such systems is highly questionable (Peleg 2006). There is also doubt as to whether complex interactive biological or chemical processes can have the same mechanism when the temperature–water activity conditions vary, and it is even unclear whether all of the reactants are the same. Most of these problems can be avoided by accounting for the nonlinear kinetics of the process in the rate equation construction. An example is the Weibullian model based on that under stationary conditions:

$$\log Y(t) = -b[T(a_w(t))]t^{n[T(a_w(t))]} \quad (4)$$

where  $Y(t)$  here can be the survival ratio of an organism, i.e.,  $N(t)/N_0$ , or of a chemical component like a vitamin, i.e.,  $C(t)/C_0$  (Corradini and Peleg 2004a), and  $b[T(a_w(t))]$  and  $n[T(a_w(t))]$  are temperature and water activity-dependent coefficients. Notice that first-order kinetics is just a special case of the Weibullian model (Eq. 4) where  $n[T(a_w(t))]=1$ .

In principle, the Weibullian model can be used to extrapolate accelerated storage data and generate entire survival or degradation curves for stationary ambient temperature–water activity conditions. This requires the extrapolation of the model's two parameters, as shown schematically in Fig. 9. The same applies to alternative models of nonlinear decay or synthesis kinetics. They may have two or more parameters, all of which need to be extrapolated in order to produce the entire curve. The potential of this approach has been demonstrated with vitamin C degradation during frozen storage, albeit with the temperature alone being the accelerating factor (Corradini and Peleg 2006b).

If the momentary logarithmic inactivation or degradation rate is indeed the logarithmic rate at the momentary temperature–water activity conditions at the time that corresponds to the system's momentary state,  $Y(t)$ , the Weibullian model can be converted into the dynamic rate equation:

$$\frac{d\log Y(t)}{dt} = -b[T(a_w(t))]n[T(a_w(t))]\left(\frac{-\log Y(t)}{b[T(a_w(t))]}\right)^{\frac{n[T(a_w(t))]-1}{n[T(a_w(t))]}} \quad (5)$$

The rate model (Eq. 5) is an ODE and can be easily solved numerically by modern mathematical software for almost any conceivable temperature–water activity history. But here, too, the main hurdle in the model implementation is not the mathematical solution, but the amount of experimental work needed to determine the temperature–water activity of the coefficients and/or the effect of other factors' dependence. Like the growth model described in the previous section, the predictive ability of Eq. (5) has been demonstrated with experimental data, albeit with only temperature variability (e.g., Corradini and Peleg 2004b; Pardey et al. 2005).

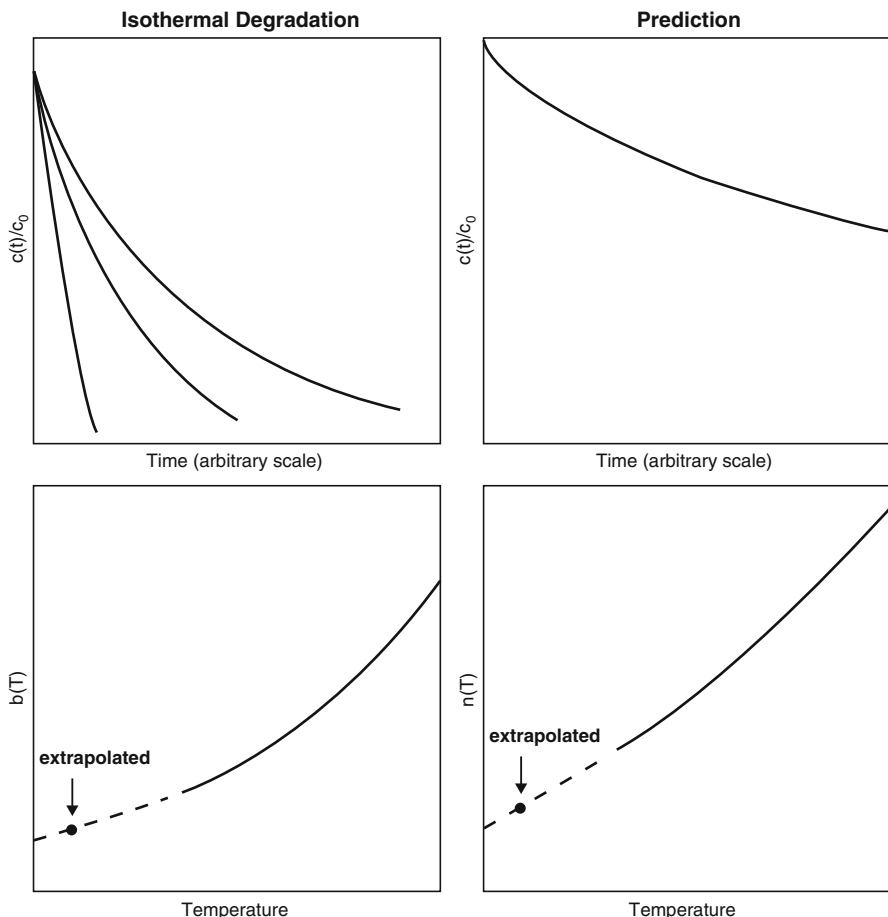


**Fig. 9** Schematic view of the extrapolation of accelerated storage data of microbial inactivation or chemical degradation using the Weibullian model

#### 4 Probabilistic Models

All kinetic models used to describe microbial growth or mortality are continuous and deterministic, as they should be, and therefore only apply to large populations of cell or spores. Yet, especially when it comes to pathogens, the number of cells that affect the safety of a food item can sometimes be small, and hence the frequently sporadic and haphazard incidence of food poisoning episodes. Similar patterns can also be observed in microbial spoilage of food products. There are cases where some, but not all, units of the same shipment spoil early in a pattern that cannot be attributed to faulty packaging, different storage conditions, or recontamination. Scenarios involving only a few microbial cells can be produced

by probabilistic models of the kind recently described by Horowitz et al. (2010). These models are based on the notion that after a time lapse  $\Delta t$ , an initially viable cell can be found divided with a probability  $P_{d1}\Delta t$ , dead with a probability  $P_{m1}\Delta t_1$ , or alive but undivided with a probability  $1 - (P_{d1} + P_{m1})\Delta t_1$  where  $P_{d1}$  and  $P_{m1}$  are the *momentary probability rates* of the cell's division and mortality, respectively (Fig. 10). After another time interval,  $\Delta t_2$ , each surviving living cell, again, will be found divided, dead or alive, but undivided with new probabilities  $P_{d2}\Delta t_2$ ,  $P_{m2}\Delta t_2$ , or  $1 - (P_{d2} + P_{m2})\Delta t_2$ , respectively, and so on for  $\Delta t_3$ ,  $\Delta t_4$ , etc., until the end of the experiment. When there is more than one cell, the same applies to each and its progenies as shown schematically in Fig. 10. The sum of the numbers of surviving cells, calculated after each iteration, will then be the population size and its plot

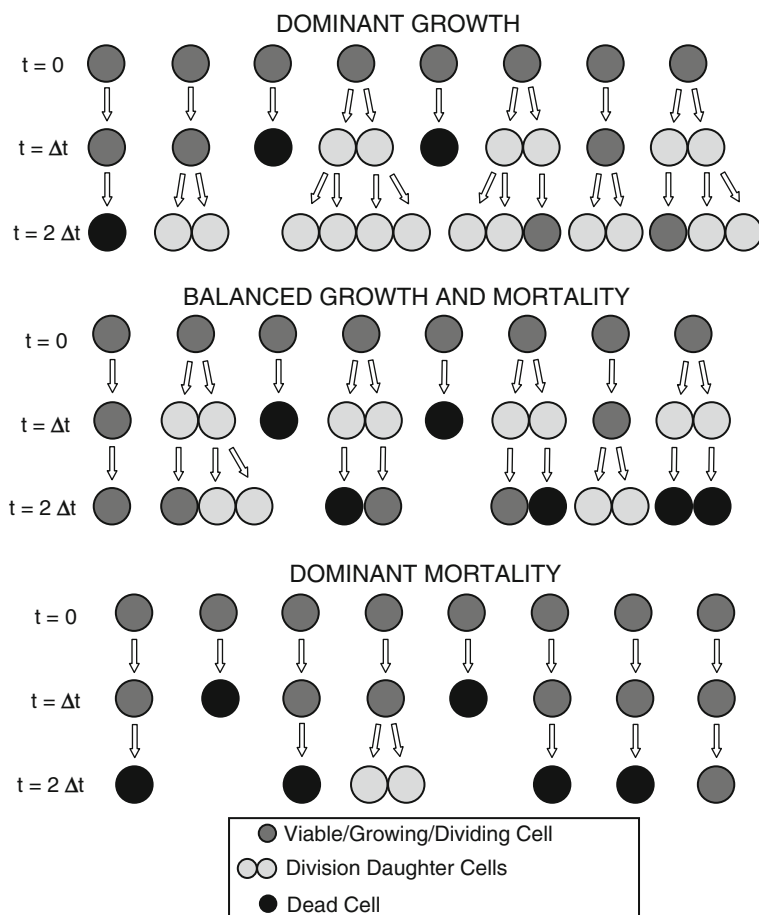


**Fig. 10** Schematic view of the probabilistic model of cell division and mortality (first two iterations). Notice that the probabilities of division and mortality change with time. For mathematical formulation of the model, see Horowitz et al. (2010)

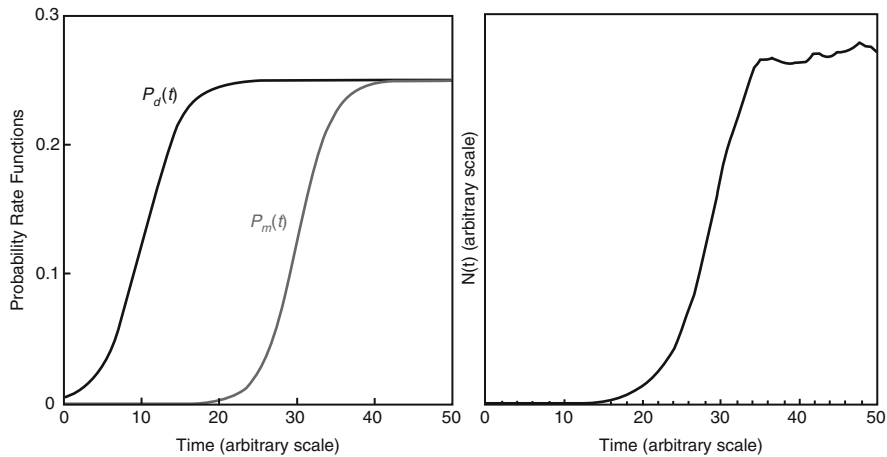


**Fig. 11** Generation of a sigmoid growth curve with the discrete version of the probabilistic model. *Left*—division and mortality probability rate functions; *right*—total number of cells

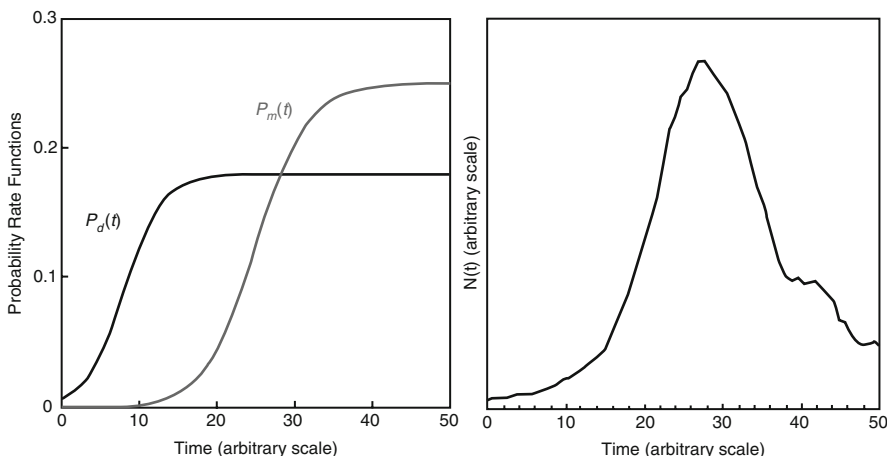


**Fig. 12** Generation of growth followed by mortality curve with the discrete version of the probabilistic model. *Left*—division and mortality probability rate functions; *right*—total number of cells

against time the growth curve,  $N(t)$  vs.  $t$ . It can be shown that as the initial number of followed cells increases, the growth curve becomes smoother and more deterministic (Horowitz et al. 2010). According to this model, a sigmoid growth curve is produced when the probability rate functions,  $P_d(t)$  and  $P_m(t)$ , converge (Fig. 11). When  $P_d(t)$  is surpassed by  $P_m(t)$  (Fig. 12), the result is growth followed by mortality. Or, conversely, if  $P_d(t)$  surpasses  $P_m(t)$  (Fig. 13), the result is inactivation followed by renewed growth. According to this model, pure inactivation occurs when  $P_d(t) = 0$  and pure growth when  $P_m(t) = 0$ . In other words, almost all of the commonly

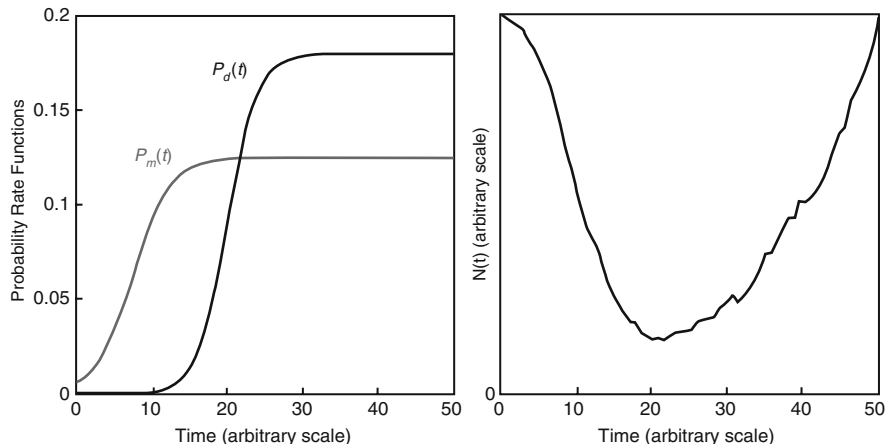


**Fig. 13** Generation of inactivation and resumed growth curve with the discrete version of the probabilistic model. *Left*—division and mortality probability rate functions; *right*—total number of cells

observed microbial growth, growth/mortality, mortality/growth, and mortality patterns can be described within the framework of a single probabilistic model. This model enables simulation of the fate of an individual cell or a small group of cells, as shown in Figs. 11, 12, and 13. The same mathematical form is applicable for static and dynamic temperature and temperature–water activity histories, or any other combination of varying factors that promote and suppress growth.

When  $\Delta t \rightarrow 0$  and the number of steps  $\rightarrow \infty$ , the model becomes continuous and fully deterministic. With the proper selection of probability rate functions,  $P_d(t)$  and  $P_m(t)$ , the growth or mortality curve,  $N(t)$  vs.  $t$  relationship, can be written in the form of an algebraic expression (Horowitz et al. 2010). The coefficients of this expression can be determined from experimental data obtained with large microbial populations by standard nonlinear regression procedures. At least in principle, once the growth/mortality parameters have been determined in this way, the model can be used to estimate the fate of small groups of cells, to predict spoilage patterns in actual foods, and to assess the risk of surviving pathogens. Again, the difficulty is not in the construction and application of the mathematical model but in obtaining sufficient experimental data under sufficient combinations of temperature, water activity, and other pertinent factors to determine the model's coefficients.

## 5 Concluding Remarks and Future Challenges

Water activity variations during processing, shipping, and storage of food, or of pharmaceutical products for that matter, are almost always accompanied by temperature fluctuations or changes as well as other factors that play a role in microbial

growth and mortality. Microbial growth and mortality rarely follow first order or any other fixed order kinetics. Therefore, most, if not all, traditional models, which are based on a single rate constant and its temperature and water activity dependence, are ill-suited for extrapolation of accelerated storage data and predicting dynamic patterns. A more promising approach would be to determine the temperature–water activity dependence of all pertinent kinetic parameters and incorporate it in the growth or inactivation rate equation coefficients. Doing so may require considerable experimental work, and it will be a challenge to future research to minimize the effort and cost.

Regardless of whether the growth/mortality model is derived from kinetic or probabilistic considerations, inclusion of parameters that account for the combined role of several factors in its mathematical structure will inevitably render it cumbersome. Nevertheless, the model, if kinetic, will most likely be an ODE that can be easily solved numerically by modern mathematical software. The growth/mortality model itself need not be unique. This has been demonstrated with existing models. Therefore, a new model's form could be chosen in light of simplicity and convenience considerations only. Although not generally recognized by users, all current microbial growth and inactivation models are empirical (or phenomenological), claims to the contrary concerning some of them notwithstanding. Thus, the only requirements for any new class of models are mathematical consistency and demonstrated predictive ability; prediction here refers to the ability of a model to estimate survival and growth data not used in the model's parameters determination. In other words, good fit and successful interpolation are not considered prediction in the strict scientific sense of the term.

One reason that none of the traditional models of microbial growth can be considered fundamental is that they only deal with the net change in the microbial population size and hence overlook mortality, which can occur at any growth phase. While this might not be a handicap when large populations are concerned, it can become a serious flaw when only a few cells are involved. At least in principle, a fully probabilistic model based on varying division and mortality probability rates can remedy this shortcoming of the current kinetic models. Fully probabilistic models might be particularly suitable to the analysis, and perhaps prediction, of the fate of individual or small groups of cells, such as those of very virulent but not widely spread pathogens. A stochastic and discrete model can be converted into a deterministic and continuous one. In this form it will apply to large populations, which will make it much easier to determine its parameters and their temperature–water activity dependence experimentally, using standard laboratory and data analysis procedures. Once determined, the parameters can be incorporated in the stochastic version and be used to simulate and perhaps predict spoilage and food poisoning patterns. Full development of the concept and its applications are still in the future. Yet, it already suggests ways to resolve outstanding issues in predictive microbiology. A great challenge to future researchers will be to combine the rate and stochastic models with heat and mass transfer theories in order to account for spatial as well as temporal changes in microbial populations in foods. Another challenge will be to develop predictive models for growth and inactivation on food

surfaces. These models will most probably be very different from those developed for organisms evenly dispersed in the bulk, because they will need to account for biofilms formation and its kinetics, as well as for local variations in moisture and chemical composition along the food's surface during the microbial growth.

**Acknowledgments** Contribution of the Massachusetts Agricultural Experiment Station at Amherst

## References

- Corradini MG, Peleg M (2004a) A model of non-isothermal degradation of nutrients, pigments and enzymes. *J Sci Food Agric* 84:217–226
- Corradini MG, Peleg M (2004b) Demonstration of the Weibull-Log logistic survival model's applicability to non isothermal inactivation of *E. coli* K12 MG1655. *J Food Prot* 67:2617–2621
- Corradini MG, Peleg M (2006a) Shelf-life estimation from accelerated storage data. *Trends Food Sci Technol* 18:37–47
- Corradini MG, Peleg M (2006b) Prediction of vitamin loss during non isothermal heat processes & storage with non linear kinetics models. *Trends Food Sci Technol* 17:24–34
- Horowitz J, Normand MD, Corradini MG, Peleg M (2010) A probabilistic model of growth, division, and mortality of microbial cells. *Appl Environ Microbiol* 76:230–242
- McKellar RC, Lu X (2004) Primary models. In: McKellar RC, Lu X (eds) Modeling microbial responses on foods. Boca Raton, CRC
- McMeekin TA, Olley JN, Ross T, Ratkowsky DA (1993) Predictive microbiology: theory and application. Wiley, New York
- Pardey KK, Schuchmann HP, Schubert H (2005) Modelling the thermal inactivation of vegetative microorganisms. *Chem Ing Tech* 77:841–852
- Peleg M (2006) Advanced quantitative microbiology for food and biosystems: models for predicting growth and inactivation. CRC, Boca Raton
- Ross T, Dalgaard P (2004) Secondary models in modeling microbial responses. In: Lu X, McKellar RC (eds) Food. CRC, Boca Raton, pp 63–150
- Taub IA, Feeherry FE, Ross EW, Kustin K, Doona CJ (2003) A quasi-chemical kinetics model for the growth and death of *Staphylococcus aureus* in intermediate moisture bread. *J Food Sci* 68:2530–2537
- van Boekel MAJS (2009) Kinetic modeling of reactions in foods. CRC, Boca Raton

# Importance of Halophilic and Halotolerant Lactic Acid Bacteria in Cheeses

G. Melgar-Lalanne, F. Morales-Trejo, Y. Rivera-Espinoza,  
and H. Hernández-Sánchez

## Abbreviations

$a_w$	Water activity
HALAB	Halophilic and alkaliphilic lactic acid bacteria
NSLAB	Nonstarter lactic acid bacteria

## 1 Introduction

### 1.1 Water Activity and Chemical Composition of Cheeses

Water plays a significant role in cheese texture and in bacterial metabolism and consequently is very important for the events that occur during cheese ripening. The influence of water content and water activity ( $a_w$ ) on cheese quality is very complex, due to changes in chemical composition during the continuous ripening of the product. Salt, along with pH, water activity, and redox potential, helps to minimize spoilage and prevents the growth of pathogens and spoilage organisms in cheese. This dairy product contains different low molecular weight compounds which are partly produced during ripening or, as in the case of salt, are added during manufacturing. These low molecular soluble compounds are mainly responsible for the water activity in cheeses.

Milk enzymes and lactic acid bacteria starter cultures progressively hydrolyze milk compounds and lower water activity. Such changes are relatively small in

---

G. Melgar-Lalanne • F. Morales-Trejo • Y. Rivera-Espinoza • H. Hernández-Sánchez (✉)  
Departamento de Graduados e Investigación en Alimentos, Escuela Nacional de Ciencias  
Biológicas, Instituto Politécnico Nacional, México, DF, México  
e-mail: [hhernan1955@yahoo.com](mailto:hhernan1955@yahoo.com)

fresh cheeses, but very unique in semihard and hard cheeses. The addition of NaCl and loss of water during storage provide a supplementary effect to lower the water activity of the product. For most cheese varieties, the salt to moisture ratio is the most significant factor to manipulate the water activity.

Moisture content in cheese ranges from 32 % in Parmesan cheese to 79 % in cottage cheese. Salt content is in the range of 1.45 % in Emmental cheese to 11.41 % in some Roquefort cheeses; and  $a_w$  varies from 0.995 for fresh unripened cheeses to 0.91 for Parmesan cheese (Marcos et al. 1981). In most cheese varieties with a moisture content above 40 %, the  $a_w$  values depend mostly on the moisture and NaCl contents. Many techniques for calculating the water activity of cheeses from their chemical composition have been published. A nomograph for calculation of  $a_w$  of soft cheeses from percentages of moisture (% H<sub>2</sub>O) and salt (% NaCl) was developed by Esteban and Marcos (1982). The additional  $a_w$  drop in ripened cheeses is caused to a great extent by the aqueous concentration of other solutes such as nonprotein nitrogen (NPN) compounds of low molecular weight released by proteolysis. Linear regression analysis has been used to predict the water activity values of brie and Camembert cheeses from ash, NaCl, and nonprotein nitrogen content and of Bleu de Bresse, Cabrales, Danablu, Edelpilzkäse, Gorgonzola, and Roquefort from ash and soluble nitrogen data (Fernández-Salguero et al. 1986).

## 1.2 Models Involving Salt Concentration in Cheeses

Work in the field of modeling the effect of salt concentration on the growth of different microorganisms or on the distribution and final concentration of NaCl in cheeses with time is abundant. The effect of pH (4–6), NaCl (1.5–3 %) corresponding to values of  $a_w$  (0.987–0.910), and temperature (10–30 °C) on the growth of *Mucor racemosus* isolated from Camembert cheese can be predicted by means of primary and secondary modeling (Bekada et al. 2008). This indicates that predictive modeling of the effect of many growth-limiting factors can be performed by the use of statistical tools such as response surface methodology, Taguchi orthogonal designs, and others. Other phenomena such as salt diffusion can be modeled. Multicomponent approaches to salt and water diffusion in cheese have been used to build theoretically based models. One such model was developed using the Maxwell–Stefan equation to predict NaCl increase and moisture decrease in cheese during brine salting. This type of model is used to calculate changes in the NaCl and moisture profile, as well as dimensions of the cheese. The best solutions are obtained when the diffusivities are represented as functions of curd porosity and salt concentration (Payne and Morrison 1999). The shape of the cheese is also very important for the evaluation of solute diffusion phenomena in cheeses. Salt will diffuse differently in a brick kind of cheese compared to a cylindrical cheese (like Gruyere). Simple expressions to determine diffusion coefficients of solutes have been obtained by use of the generalized Fick law form as a constitutive equation for

the diffusive molar flux of solutes; the shape of the cheese is very important to solve this equation. With these expressions, the corresponding effective diffusion coefficients of NaCl and KCl in cheese were obtained (Zorrilla and Rubiolo 1994). A list of effective diffusion coefficients for several cheeses has also been published (Vélez-Ruiz 2011) which is very useful to evaluate salting times.

### **1.3 General Roles of Salt in Cheese**

NaCl has many roles in cheese making. Some of these roles include preservation against spoilage and pathogenic microorganisms, influence on the final flavor and texture of the product, and as a complementary source of sodium. During cheese ripening, the presence of salt involves many other key roles, such as the control of microbial growth and activity and the control of various enzyme activities in the cheese. It also has a strong influence on the physical changes in cheese proteins, which in turn influence cheese texture, protein solubility, and protein conformation. Salt, along with pH and calcium level, has a great effect on the extent of *para*- $\kappa$ -casein aggregation, which then affects the water-binding capacity of the protein matrix, its tendency for syneresis, its rheological characteristics, and its cooking properties (Guinee 2004).

### **1.4 Halophilic and Halotolerant Microorganisms**

Halophiles are extremophile microorganisms that thrive in environments with very high salt levels. The property of halophilism is prevalent within the bacterial realm. Halophilic bacteria and archaea are abundant in environments such as salt lakes, saline soils, and salted foods. Most species retain their intracellular ionic concentrations at low levels while synthesizing or accumulating organic solutes to provide osmotic pressure equilibrium of the cytoplasm with the surrounding medium. Complex mechanisms of adjustment of the intracellular environments and the properties of the cytoplasmic membrane and cell wall enable rapid adaptation to changes in the NaCl concentration of the environment. Approaches to the study of genetics of this adaptation have recently been developed for several moderate halophiles, opening the way toward comprehension of haloadaptation at the molecular level (Ventosa et al. 1998). Based on optimal saline environments, halophilic organisms can be grouped into three categories: extreme halophiles, moderate halophiles, and slightly halophilic or halotolerant organisms. Extreme halophiles need 15–35 % salt to grow adequately. These concentrations are considered extreme compared to seawater, which is only 3 % NaCl. Living in high salinity poses a serious stress that halophiles have overcome through special processes or adaptations. The stress lies in the ability of the microorganisms to keep an internal osmotic potential that equals their external environment. Osmosis is the process in

which water moves from an area of high concentration to an area of low concentration. In order for cells to retain water, they must have an osmotic potential equal to their external environment. As salinity increases in the surroundings, its osmotic potential decreases. If a non-halophilic microorganism is placed in a solution with a high amount of dissolved salts, the cellular water will enter the solution causing the cell to plasmolyze. Halophiles have adapted to life at high salinity in many different ways. One of these ways is through the modification of their external cell walls. They tend to have negatively charged proteins on the outer side of their cell walls which stabilize it by binding to positively charged sodium ions in their external environments. If salt concentration decreases, the cell walls usually become unstable and break down. There are two strategies that halophilic microorganisms have evolved to deal with high-salt environments. In the “compatible solute” strategy, cells maintain low concentrations of salt in their cytoplasm by balancing osmotic potential with organic, compatible solutes. Cells accomplish this by the synthesis or uptake of the so-called compatible solutes. Compatible solutes include polyols such as glycerol, sugars and their derivatives, amino acids and their derivatives, and quaternary amines such as glycine betaine. Energetically, this is an expensive process. Autotrophs utilize between 30 and 90 molecules of ATP to synthesize one molecule of the compatible solutes. Heterotrophs use between 23 and 79 ATP. The relative proportions of the compatible solutes vary with salt concentration, temperature, and carbon source (Wohlfart et al. 1990). Energy is also expended in pumping out salts that dissolve into the cell. The uptake of available compatible solutes in the environment is an adaptation that has evolved to diminish the energy cost of living in high salt concentrations. A different strategy to adapt to high-salt environment is called the “salt-in” strategy, which was first discovered in *Halobacteria*. Microorganisms following this strategy adapt their interior protein chemistry to high salt concentration. The thermodynamic adjustment of the cell is achieved by raising the salt concentration in the cytoplasm. Cells can have internal concentrations that are osmotically equivalent to their external environment. This “salt-in” strategy is primarily used by aerobic, extremely halophilic archaea and anaerobic bacteria. They maintain osmotically equivalent internal concentrations by accumulating high concentrations of potassium chloride (Oren et al. 1997). Potassium ions enter the cell passively via a uniport transport system (facilitated diffusion). Sodium ions are pumped out. Chloride ions enter the cell against the membrane potential via cotransport with sodium ions. For every three molecules of KCl accumulated, two ATP are hydrolyzed, making this strategy more energy efficient than the “compatible solute” strategy. To use this strategy, all enzymes and structural cell components must be adapted to high salt concentrations to ensure proper cell function. The effect of the accumulation of potassium and/or sodium in the cytoplasm is that it is exposed to an increasing ionic strength. To adapt their enzymes to an ionic cytoplasm, proteins of halophilic anaerobic bacteria and halophilic archaea contain a predominance of acidic amino acids over basic amino acids. The final result is the predominance of charged amino acids on the surface of enzymes and ribosomes, which is thought to even out the hydration covering of the molecule in a high ionic environment. In low-saline media, the

excess of negatively charged ions will destabilize the structure of the molecule, due to repulsion when the shielding cations are removed (Eisenberg and Wachtel 1987).

## 1.5 *Halophilic Lactic Acid Bacteria in Cheeses*

Until recently, the possible presence of halophilic or halotolerant lactic acid bacteria had been given little attention. However, Ishikawa et al. (2006) isolated and characterized LAB in cheeses using saline and alkaline media (7 % NaCl glucose–yeast extract–peptone–fish extract broth and pH 9.5 agar media for pour-plating and enrichment culture). This practice revealed the presence of halophilic and alkaliophilic lactic acid bacteria (HALAB) of possible marine origin in various European cheeses to provide a basis from which to envision their possible roles in the ripening process. They are believed to have come from marine environments via sea salt added to the cheeses.

Some of these HALAB were partially characterized. *Marinilactibacillus psychrotolerans* is a marine-inhabiting HALAB with optimal growth of 2.0–3.75 % NaCl and pH 8.5–9.0. This pH of optimal growth indicates that this organism is also alkaliophilic. *M. psychrotolerans* has been reported to be present in the rind of German and French red-smear soft cheeses as a minor proportion of the ripening microbial consortia (Maoz et al. 2003; Feurer et al. 2004) and in contaminated Italian dry-cured hams as part of the dominant spoiling microbiota (Rastelli et al. 2005). The genus *Alkalibacterium* was first reported as *A. olivoapovliticus*, which was isolated from the basic wash waters of edible olive and is halophilic and alkaliophilic (Ntougias and Russell 2001). *Alkalibacterium* metabolizes carbohydrate by lactic acid fermentation. It is commonly part of the microbiota present during green olive fermentation. The processing method includes treatment with dilute NaOH solution to debitter the olives, followed by one to three rinses to remove the excess alkali. Finally, the olives are placed into a brine in which lactic acid fermentation takes place (Brenes et al. 1995). Other HALAB that have been isolated from fermented foods include *Alkalibacterium psychrotolerans*, *Alkalibacterium iburiense*, *Carnobacterium mobile*, and some strains of *Streptococcus thermophilus*.

One key step in the cheese-making process is the addition of starter cultures. *Lactococcus lactis* is a very important constituent of the so-called mesophilic cultures. This microorganism can grow well in environments with up to 4 % NaCl, indicating that its growth would stop in cheeses, such as blue, Parmesan, or some cheddars, with final content of salt above 5 %. However, there are reports of halotolerant *L. lactis* subsp. *lactis* strains, isolated from marine environments (from the intestinal tract of coastal fish), which can grow in media with up to 6 % salt (Itoi et al. 2008). These strains could have interesting applications in cheese technology. This is also true for the entire LAB of marine origin (Kathiresan and Thirunee-lakandan 2008).

## 2 Halotolerant Lactic Acid Bacteria in Mexican Cheeses

Our group has begun some research on the microbiota of certain Mexican regional cheeses. Many cheeses in Mexico are prepared from raw milk, and the nonstarter lactic acid bacteria (NSLAB) play a key role in the final characteristics of the products. The first cheese to be analyzed was doble-crema (double-cream) cheese. This cheese is traditionally prepared in the state of Chiapas, and the samples we purchased had 48.2 % moisture, 5.34 % salt,  $a_w$  of 0.972, and a pH of 4.03. The halotolerant strains isolated from this cheese were *Lactobacillus acidipiscis*, *Enterococcus faecium*, *L. plantarum*, *L. farciminis*, *L. rhamnosus*, and *L. pentosus*. The second cheese, Cotija, is prepared in the state of Michoacán. This product had 39.5 % moisture, 6.36 % salt,  $a_w$  of 0.862, and a pH of 6.29. The halotolerant lactic acid bacteria isolated included *Lactobacillus acidipiscis*, *Tetragenococcus halophilus*, *Weissella thailandensis*, and *L. pentosus* (Morales et al. 2011). These microorganisms will be studied to evaluate their role in cheese ripening and their possible probiotic potential.

## 3 Modeling of Halotolerance

Halophiles can be defined as those organisms that can grow in the presence of salt and which actually require high concentrations of NaCl. Microorganisms that can withstand, but not require, high concentrations of salt to grow are known as halotolerants. In the case of LAB, halophiles will only be able to grow in a salt-added MRS medium. Our group was interested in evaluating these characteristics for the halotolerant LAB isolated from the Mexican cheeses, so experiments were performed and the results are presented here. The halotolerance of three strains of LAB isolated from Chiapas double-cream cheese (*Lactobacillus acidipiscis*, *L. plantarum*, and *L. pentosus*) was compared with that of two commercial probiotic LAB strains (*L. casei* Shirota and *L. plantarum* 299v) by measuring the absorbance at 560 nm after 24 h of incubation at 32 °C in MRS broth added with salt concentrations in the range of 0–16 %. Curves of inhibition at each concentration were fitted by Mystat v12.02 software (Systat Software, Inc., Chicago, IL, USA) using nonlinear least-squares regression in a sigmoidal dose–response model with variable slope, also known as the four-parameter logistic equation (1):

$$y = C + \frac{D - C}{1 + \left(\frac{X}{I_{50}}\right)^b} \quad (1)$$

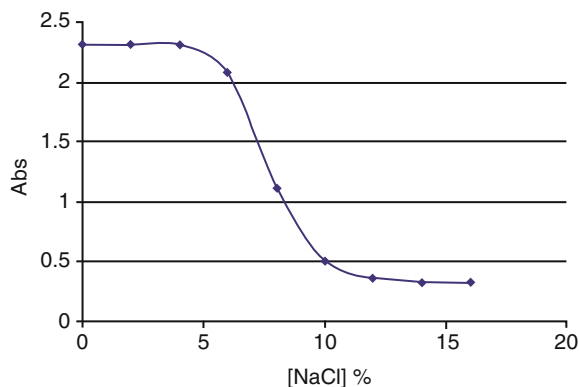
In this equation,  $C$  is the absorbance at extreme conditions (16 % salt),  $D$  is the absorbance at 0 % salt,  $X$  is salt concentration (%),  $I_{50}$  is the concentration of salt necessary to reach an absorbance of  $D/2$ , and  $b$  is a constant of the experiment.

**Table 1** Parameters of the logistic dose–response model for halotolerance and determination coefficient ( $R^2$ ) for five lactic acid bacteria

LAB strain	$C$	$D - C$	$I_{50}$	$b$	$R^2$
<i>L. acidipiscis</i>	0.323	2	7.622	8.377	0.997
<i>L. casei</i> Shirota	0.365	1.825	7.895	7.225	0.995
<i>L. plantarum</i> 299v	0.390	2.021	7.573	6.458	0.989
<i>L. plantarum</i>	0.405	1.854	7.984	8.498	0.996
<i>L. pentosus</i>	0.289	1.989	8.606	4.685	0.975

*L. casei* Shirota was isolated from Yakult™ (Yakult Mexico, Mexico City, Mexico) and *L. plantarum* 299v was isolated from Protransitus LP (Laboratorios Salvat, S.A., Barcelona, Spain)

**Fig. 1** Absorbance at 560 nm of *Lactobacillus acidipiscis* after 24 h of growth in MRS broth with different salt concentrations at 32 °C



The results are shown in Table 1. All of the curves were similar, and the curve obtained for *L. acidipiscis* is shown as an example in Fig. 1. It can be observed that all of the data could be fitted with high determination coefficients to a four-parameter logistic dose–response equation. It can also be observed that the two strains of *L. plantarum* have the highest halotolerance (i.e., they had the highest  $C$  values) of all of the LAB tested. This is the first time that halotolerance has been modeled using a dose–response curve.

## 4 Conclusions

Halophilic organisms are widespread and found in all three domains of cellular life (archaea, bacteria, and eukaryote).

The “salt-in” strategy uses less energy, but requires intracellular adaptations. Only a few prokaryotes use it.

All other halophiles use the “compatible solute” strategy, which is energy expensive, but does not require special adaptations.

In the case of cheeses, halophiles and halotolerants can contribute to some characteristics of the final products; thus, their lipolytic and proteolytic activities must also be studied.

The presence of halotolerant lactic acid bacteria has also been reported in Mexican cheeses with high salt content, such as Chiapas double-cream and Cotija cheeses.

The degree of halotolerance of lactic acid bacteria can be adequately modeled by logistic dose-response equations.

## References

- Bekada AMA, Benakriche B, Hamadi K, Bensoltane A (2008) Modelling of effects of water activity, pH and temperature on the growth rate of *Mucor racemosus* isolated from soft Camembert cheese. *World J Agric Sci* 4(6):790–794
- Brenes M, Rejano L, García P, Sánchez AH, Garrido A (1995) Biochemical changes in phenolic compounds during Spanish-style green olive processing. *J Agric Food Chem* 43:2702–2706
- Eisenberg H, Wachtel EJ (1987) Structural studies of halophilic proteins, ribosomes, and organelles of bacteria adapted to extreme salt concentrations. *Annu Rev Biophys Biophys Chem* 16:69–92
- Esteban MA, Marcos A (1982) Nomograph for predicting water activity of soft cheese. *J Dairy Sci* 65:1795–1797
- Esteban MA, Marcos A, Alcalá M, Gómez R (1991) Calculation of water activity in surface mould-ripened soft cheeses from their chemical composition. *Food Chem* 40:147–157
- Fernández-Salguero J, Alcalá M, Marcos A, Esteban MA (1986) Measurement and calculation of water activity in Blue cheese. *J Dairy Res* 53:639–644
- Feurer C, Irmlinger F, Spinnler HE, Glaser P, Vallaeyns T (2004) Assessment of the rind microbial diversity in a farmhouse-produced vs a pasteurized industrially produced soft red-smear cheese using both cultivation and rDNA-based methods. *J Appl Microbiol* 97:546–556
- Guinée TP (2004) Salting and the role of salt in cheese. *Int Dairy J* 57:99–109
- Ishikawa M, Kodama K, Yasuda H, Okamoto-Kainuma A, Koizumi K, Yamasato K (2006) Presence of halophilic and alkaliphilic lactic acid bacteria in various cheeses. *Lett Appl Microbiol* 44:308–313
- Itoi S, Abe T, Washio S, Ikuno E, Kanomata Y, Sugita H (2008) Isolation of halotolerant *Lactococcus lactis* subsp. *lactis* from intestinal tract of coastal fish. *Int J Food Microbiol* 121:116–121
- Kathiresan K, Thiruneelakandan G (2008) Prospects of lactic acid bacteria of marine origin. *Indian J Biotechnol* 7:170–177
- Maoz A, Mayr R, Scherer S (2003) Temporal stability of two complex antilisterial cheese-ripening microbial consortia. *Appl Environ Microbiol* 69:4012–4018
- Marcos A, Alcalá M, Fernández-Salguero J, Esteban MA (1981) Water activity and chemical composition of cheese. *J Dairy Sci* 62:622–626
- Morales F, Morales JI, Hernández CH, Hernández-Sánchez H (2011) Isolation and partial characterization of halotolerant lactic acid bacteria from two Mexican cheeses. *Appl Biochem Biotechnol* 164:889–905
- Ntougias S, Russell NJ (2001) *Alkalibacterium olivoapovliticus* gen. nov., sp. nov., a new obligately alkaliphilic bacterium isolated from edible-olive wash-waters. *Int J Syst Evol Microbiol* 51:1161–1170
- Oren A, Heldal M, Norland S (1997) X-ray microanalysis of intracellular ions in the anaerobic halophilic eubacterium *Haloanaerobium praevalens*. *Can J Microbiol* 43(6):588–592

- Payne MR, Morrison KR (1999) A multi-component approach to salt and water diffusion in cheese. *Int Dairy J* 9(12):887–894
- Rastelli E, Giraffa G, Carminati D, Parolari G, Barbuti S (2005) Identification and characterization of halotolerant bacteria in spoiled dry-cured hams. *Meat Sci* 70:241–246
- Vélez-Ruiz JF (2011) Mass transfer in cheese. In: El-Amin M (Ed). Advanced topics in mass transfer. Intech Open Access ebook
- Ventosa A, Nieto JJ, Oren A (1998) Biology of moderately halophilic aerobic bacteria. *Microbiol Mol Biol Rev* 62(2):504–544
- Wohlfart A, Severin J, Galinski EA (1990) The spectrum of compatible solutes in heterotrophic halophilic eubacteria of the family Halomonadaceae. *J Gen Microbiol* 136:705–712
- Zorrilla SE, Rubiolo AC (1994) A model for using the diffusion cell in the determination of multicomponent diffusion coefficients in gels or foods. *Chem Eng Sci* 49(13):2123–2128

# Influence of Water Activity and Molecular Mobility on Peroxidase Activity in Solution

G. Sacchetti, L. Neri, G. Bertolo, D. Torreggiani, and P. Pittia

## Abbreviations

$a_w$	Water activity
Tg	Glass transition temperature
D	Translational diffusion
WLF equation	Williams–Landel–Ferry equation
HRP	Horseradish peroxidase

## 1 Introduction

Water is one of the most critical components in foods and biological systems because it affects several physicochemical properties of these systems with effects on their chemical and enzymatic stability (Bell 2007).

Water availability in foods has historically been described by the concept of water activity ( $a_w$ ), whereby water freedom in a system is expressed in terms of

---

G. Sacchetti (✉) • L. Neri

Department of Food Science, University of Teramo, Via C.R. Lerici 1, Mosciano S. Angelo, 64023 Teramo, Italy  
e-mail: [gsacchetti@unite.it](mailto:gsacchetti@unite.it)

G. Bertolo  
ACU, Associazione Consumatori Utenti, Milan, Italy

D. Torreggiani  
CRA, Via Giacomo Venezian 26, 20133 Milan, Italy

P. Pittia  
Faculty of Bioscience and Technology for Food, Agriculture and Environment,  
University of Teramo, Via C.R. Lerici 1, Mosciano S. Angelo, 64023 Teramo, Italy

relative water vapor pressure (Reid 2007). The relationship between water activity and chemical and enzymatic reactions has been described by Labuza et al. (1970) in their food stability map. In this map, the enzymatic activity is retained to be positively affected by water activity.

Several authors have investigated the dependence of enzyme catalysis on  $a_w$  (Acker 1963, 1969; Tome et al. 1978; Schwimmer 1980; Lee and Kim 1995); in dry solid foods, the  $a_w$  increase upon water sorption resulted in the enhancement of enzymatic activity, while in liquid models the  $a_w$  decrease with solute addition did not always depleted the enzymatic activity (Acker 1969). This happens because the lowering of water activity by solute addition affects not only the  $a_w$  of the system but also its water content and molecular mobility.

Several authors (Farwell and Ackerman 1963; Silver and Karel 1981; Lim and Reid 1991; Kerr et al. 1993; Kouassi and Roos 2000) discussed the inhibition of enzymatic activity that occurs in concentrated food systems in terms of molecular mobility, since in such systems the rates of chemical reactions may become diffusion limited; in this case, the ability for reacting molecules to diffuse toward each other, rather than the activation energy of the activated complex, is the rate limiting factor.

Enzymatic reactions are mainly controlled by diffusion in highly viscous aqueous systems, and the concentration of co-solutes was proven to influence the catalysis via change in the physical properties of the system (Farwell and Ackerman 1963; Cicerone and Soles 2004). On the basis of this result, it is evident that water activity is not the only factor that influences the enzymatic activity in concentrated systems, and other physical parameters that describe the molecular mobility within a system, such as viscosity and glass transition temperature ( $T_g$ ), should be taken into account (Kouassi and Roos 2000; Bell 2007).

Viscosity is referred to as an index of the mobility of a system since it is related to the translational diffusion ( $D$ ) by the Stokes relationship. Kramers' theory (Kramers 1940) predicts that the rate for protein dynamics should have an inverse relationship with viscosity. Large amplitude (global) protein motions (particularly those involving exterior portions of the protein) appear to follow Kramers' relation at viscosities above  $\approx 1$  cP (Ansari et al. 1992; Hagen et al. 1995), while diffusive motions involving smaller portions of the protein are less likely to follow Kramers' relation, especially at high viscosities. Deviations from Kramers' relation for exterior protein motions have been attributed to solvent composition and differences between bulk macroviscosity and local microviscosity in the immediate vicinity of the protein. Moreover, by increasing the viscosity of the system, the solvent motions may not be assumed infinitely fast compared to those of the solute (Cicerone and Soles 2004).

At very high viscosities, protein dynamics are often discussed in terms of  $T_g$  (Lim and Reid 1991; Kerr et al. 1993; Manzocco et al. 1999; Buitnik et al. 2000; Cicerone and Soles 2004; Bell 2007), which corresponds to the temperature at which a supercooled liquid loses its translational mobility and its molecules may exhibit only rotational motions. Below glass transition temperature, chemical and biological reactions are retained to be impeded, while, above  $T_g$ , molecules become mobile and diffusion-limited reactions could occur (Slade and Levine 1991; Roos 2007).

A complete inhibition of enzymatic activity below Tg was not always achieved, but enzymatic reaction seems to be diffusion limited above Tg (Chen et al. 1999a; Kouassi and Roos 2000). The Williams–Landel–Ferry (WLF) equation (Williams et al. 1955), which accurately describes the viscosity changes due to temperature shift between Tg and Tg + 100 °C, has been used to describe the enzymatic activity above Tg for a system at constant composition.

Other authors have observed that in frozen or partially frozen systems conditioned at temperature above Tg (the glass transition temperature of the maximally concentrated solution), the enzymatic activity followed a WLF-type relation with T–Tg (Manzocco et al. 1999; Terefe et al. 2004) or T–Tg (Lim and Reid 1991; Kerr et al. 1993; Terefe et al. 2004).

Many authors (Nelson and Labuza 1994; Bell 2007) have suggested that reactant mobility and diffusion within a matrix could be related to both solvent characteristics, described by  $a_w$ , and system mobility, which could be described in terms of Tg and viscosity. However, the individual effect of water activity and molecular mobility on enzyme activity in complex food systems has not been fully disclosed. This is because the effect of system mobility on enzymatic activity has been studied either in supercooled systems with an equilibrium ice phase (Lim and Reid 1991; Kerr et al. 1993; Manzocco et al. 1999) where  $a_w$  is solely determined by the storage temperature or in highly concentrated systems above Tg where the water content has been varied together with  $a_w$  and Tg (Chen et al. 1999a, b; Kouassi and Roos 2000, 2001, 2002).

The aim of this paper is to summarize and critically discuss the results obtained in previous studies by our research group (Neri 2010; Neri et al. 2010, 2011) which investigated the individual and combined effect of water activity, bulk viscosity, and T'g on the activity of horseradish peroxidase (HRP) in buffered concentrated solutions. Peroxidase was chosen as the target enzyme since it occurs naturally in nearly all plants and animals and, due to its nonspecific action, shows a detrimental effect on many biological systems and foods, where it is among the main causes for the formation of off-color and off-flavor formation (Burnette 1977; Tijskens et al. 1997).

## 2 Enzymatic Activity in Concentrated Solutions

### 2.1 *Physical Properties of Concentrated Ligand, Polymer, and Ligand–Polymer Solutions*

In order to study the influence of  $a_w$ , bulk viscosity and glass transition temperature on enzymatic activity, the latter was plotted as a function of the inverse of bulk viscosity and the individual effect of  $a_w$  lowering, and Tg shift due to cosolvent addition was analyzed (Neri 2010). The T'g parameter was taken into consideration instead of Tg because the latter is correlated to the water content, which in turn

affects both the  $a_w$  and viscosity of the solution, while the T'g value is exclusively related to the chemical characteristics (mostly the molecular weight) of the solute (Roos and Karel 1991; Slade and Levine 1991). The T'g parameter could thus enable the investigation of the specific solute effect in systems with different viscosities.

The lowering of water activity by the addition of ligands (sodium chloride, glucose, and sorbitol) determined a reduction of enzymatic activity (Table 1).

Sodium chloride, when added in small amounts, depleted the  $a_w$  of the solutions without or little affecting their T'g and viscosity, while glucose, being a larger solute and a weaker osmotic agent, depleted the  $a_w$  of the solutions only when present at high concentrations, thus also determining an increase of the system viscosity and T'g (Table 1). The addition of maltodextrin with DE 8.7 increased the viscosity and T'g of the solutions by only slightly affecting their water activity (Table 1). With the addition of ligands to polymer solutions, it was possible to obtain solutions with the same water activity and different viscosities and T'g values.

## 2.2 HRP Activity in Ligands and Polymer Binary Solutions

The addition of both ligands and maltodextrin limited HRP activity; salt affected water activity by minimally affecting bulk viscosity and Tg, while maltodextrin increased viscosity by minimally affecting  $a_w$ . The rate of enzymatic reaction was not linearly correlated to  $\eta^{-1}$ , as predicted by Kramers' theory, but a power-law relationship  $k \propto \eta^{-\nu}$  between viscosity and protein dynamics was observed (Fig. 1). This indicates that in the high viscosity range, the rate of enzymatic reactions is much more hindered by a viscosity increase than in low viscosity ranges.

At high water activity ( $a_w = 0.98$ ), sodium chloride addition inhibited enzymatic activity more than the other co-solutes due to both its ionic nature, which could affect the rate of enzymatic reaction at low viscosities by electrostatic effects (Farwell and Ackerman 1963), and to a specific interaction with HRP (Laurenti et al. 2000). On the contrary, at water activity value of 0.87, glucose was more effective than sodium chloride in limiting enzymatic activity due to its viscosity-improving effect (Table 1).

Glucose inhibited enzyme activity by affecting the  $a_w$ , viscosity, and T'g of the system. When viscosity was equal, maltodextrin limited HRP activity more than glucose even though negligible water activity changes occurred (Fig. 1). This result, which is due to the higher T'g of maltodextrin, seems to confirm the hypothesis of Kouassi and Roos (2001), which suggested that molecular mobility is an important factor for the regulation of enzyme activity even at high water activities.

The effect of T'g on enzymatic activity was further studied using maltodextrins of different molecular weights. In diluted solutions with low viscosity values, an increase of maltodextrin size from DE 33 to DE 8.7 did not limit HRP activity, likely due to the increase of  $a_w$ , but a further increase of molecular size to DE 2.5 determined a decrease of enzymatic activity (Neri et al. 2011). In highly

**Table 1** Composition and physical properties of binary and ternary solutions and HRP activity in the solutions

Solutes (S)	Solute $w_{S/W_W}$ (g 100 g <sup>-1</sup> )	Maltodextrin $w_M/w_W$ (g 100 g <sup>-1</sup> )	Water activity	Kinematic viscosity (10 <sup>-6</sup> m <sup>2</sup> s <sup>-1</sup> )	T <sub>g</sub> (°C)	HRP activity (%)
Phosphate buffer	0	0	0.999 ± 0.003	1.09 ± 0.00	n.d.	100.00 ± 0.25
Maltodextrin DE8.7	0	15.00	0.997 ± 0.003	3.49 ± 0.01	-10.5 ± 0.07	71.17 ± 5.22
	0	30.00	0.995 ± 0.003	20.1 ± 0.03	-10.1 ± 0.28	37.28 ± 4.27
Sodium chloride	3.52	0	0.981 ± 0.003	1.09 ± 0.03	n.d.	93.69 ± 1.48
	18.00	0	0.866 ± 0.003	1.27 ± 0.00	n.d.	80.39 ± 1.61
	3.52	15.00	0.978 ± 0.003	2.96 ± 0.05	-10.7 ± 0.3	59.62 ± 1.38
	3.52	30.00	0.976 ± 0.003	8.92 ± 0.07	-10.7 ± 0.8	41.09 ± 0.91
Sorbitol	18.56	0	0.978 ± 0.003	1.61 ± 0.01	-44.8 ± 0.3	99.94 ± 1.51
	18.56	15.00	0.975 ± 0.003	4.33 ± 0.02	-38.7 ± 0.1	76.02 ± 1.47
	18.56	30.00	0.973 ± 0.003	11.3 ± 0.32	-35.5 ± 0.1	59.88 ± 2.40
Glucose	16.33	0	0.980 ± 0.003	1.49 ± 0.01	-44.2 ± 0.4	97.15 ± 2.93
	50.00	0	0.873 ± 0.003	9.28 ± 0.14	-43.5 ± 0.4	68.63 ± 5.87
	16.33	15.00	0.977 ± 0.003	4.14 ± 0.24	-35.7 ± 0.1	66.17 ± 2.20
	16.33	30.00	0.975 ± 0.003	11.3 ± 0.14	-30.3 ± 0.2	40.99 ± 1.94
Maltodextrin DE 33	0	10.00	0.997 ± 0.003	1.39 ± 0.00	-21.8 ± 0.1	87.47 ± 1.94
	0	20.00	0.998 ± 0.003	2.14 ± 0.00	-21.5 ± 0.3	74.88 ± 1.54
	0	30.00	0.993 ± 0.003	3.92 ± 0.00	-21.3 ± 0.3	62.62 ± 0.78
	0	51.6	0.977 ± 0.003	32.7 ± 0.43	-21.3 ± 0.3	22.29 ± 0.42

n.d. non-detectable

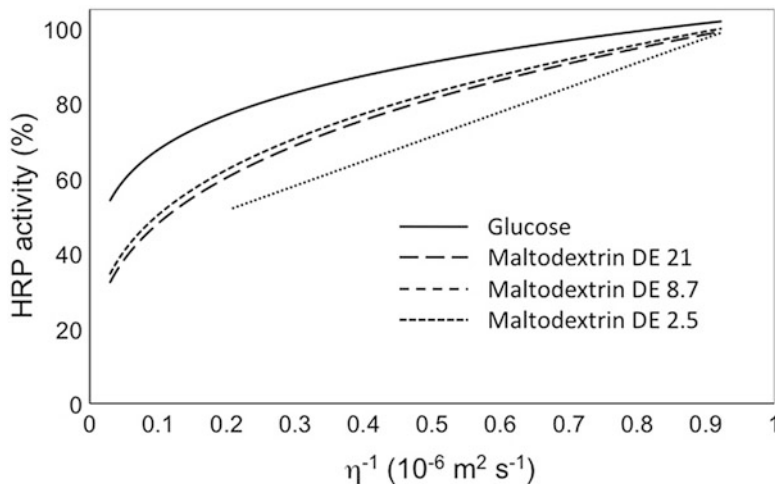


**Fig. 1** Horseradish peroxidase activity in glucose and maltodextrin systems as a function of the inverse of kinematic viscosity (modified from Neri et al. 2011)

concentrated solutions ( $h \approx 40 \text{ mPa s}$ ), HRP activity decreased at the increase of maltodextrin size by following a WLF-type dependence on T'g (Neri et al. 2011).

### 2.3 HRP Activity in Ternary Ligand–Polymer Solutions

In order to better understand the role of water activity and viscosity on enzyme activity, ternary systems characterized by different water activities and viscosities were obtained by the combination of salt, glucose, sorbitol, and maltodextrin with DE 8.7 (Table 1).

In ternary solutions with the same viscosity, the  $a_w$  reduction, upon salt addition, determined a peroxidase inhibition (Fig. 2). Sodium chloride inhibited HRP activity exclusively by depleting  $a_w$  since it did not affect T'g (Neri et al. 2011).

The inhibition of HRP by water activity reduction was more effective at low viscosity than at high viscosity, thus suggesting that in high viscosity systems enzyme inhibition is mainly due to the hindrance of molecular mobility. On the other hand, the hindrance of enzyme activity by a viscosity increase was more effective at the lowest water activity than at the highest, and this result seems to be in contrast with that suggested by Kouassi and Roos (2002).

In sorbitol–maltodextrin ternary solutions, peroxidase activity was always inhibited by a viscosity increase (Fig. 3). On the other hand, water activity reduction from 0.99 to 0.98 determined an increase of HRP activity. By taking into account the T'g changes, it is possible to affirm that, viscosity being equal,  $a_w$  depletion increased the HRP activity because sorbitol addition to the maltodextrin solution

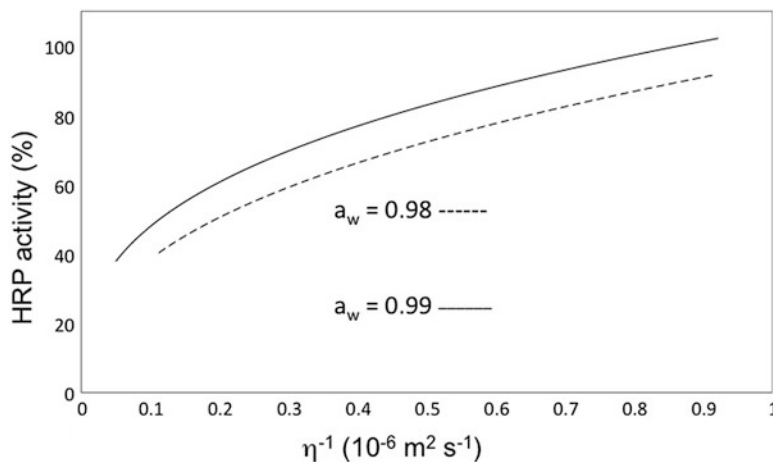


**Fig. 2** Horseradish peroxidase activity in ternary sodium chloride–maltodextrin systems with different  $a_w$  values as a function of the inverse of kinematic viscosity (modified from Neri et al. 2010)

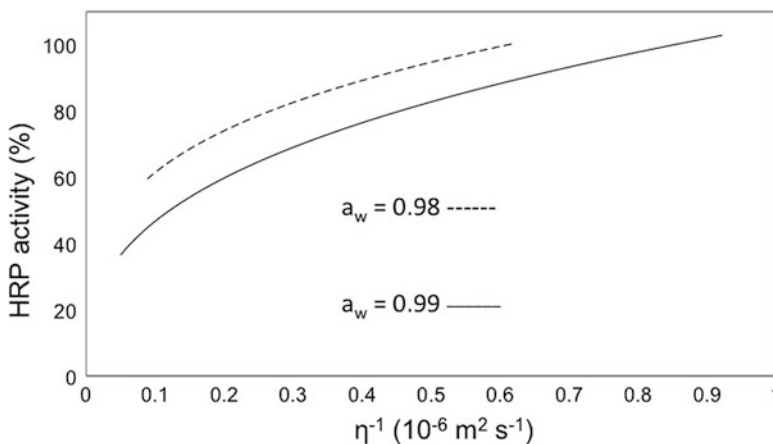


**Fig. 3** Horseradish peroxidase activity in ternary sorbitol–maltodextrin systems with different  $a_w$  values as a function of the inverse of kinematic viscosity (modified from Neri et al. 2010)

determined a dramatic decrease of the T'g (Neri et al. 2010). On the basis of the overall data trend (Fig. 2),  $a_w$  and T'g seemed to play a minor role in HRP inhibition in highly viscous solutions, where the enzymatic activity is mainly dependent on viscosity.

In glucose–maltodextrin ternary solutions, peroxidase activity was always inhibited by a viscosity increase (Fig. 4) as well, and this effect was more evident at lower  $a_w$  values than at higher  $a_w$  values. In maltodextrin systems, lowering of water

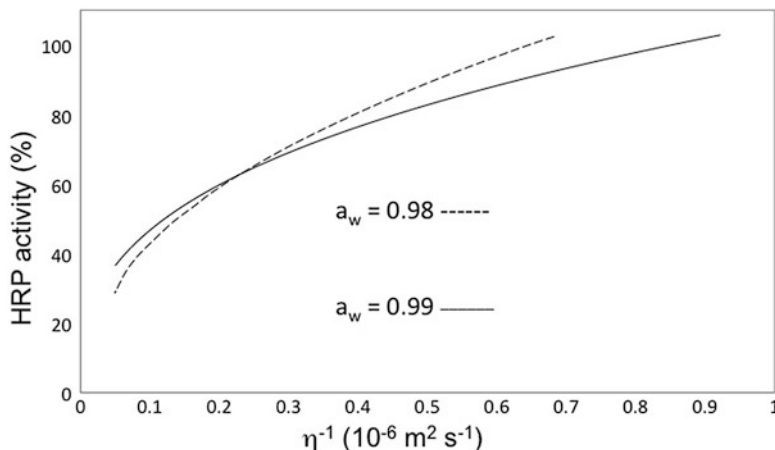


**Fig. 4** Horseradish peroxidase activity in ternary glucose–maltodextrin systems with different  $a_w$  values as a function of the inverse of kinematic viscosity (modified from Neri 2010)

activity by glucose addition determined an HRP activity increase in the low viscosity region and an HRP activity decrease in the high viscosity region. In the latter region, water activity being equal ( $\approx 0.98$ ), glucose and ternary glucose–maltodextrin solutions showed a higher T'g than sorbitol and ternary sorbitol–maltodextrin solutions (Table 1), permitting direct observation of a negative effect of water activity lowering on HRP activity.

By taking into account the T'g changes, it is possible to affirm that, viscosity being equal, an  $a_w$  depletion from 0.99 to 0.98 could differently affect HRP activity depending on the effect of the co-solute on the T'g of the system (Neri 2010; Neri et al. 2010, 2011). On the other hand,  $a_w$  and T'g seem to play a minor role in HRP inhibition in highly viscous solutions, where the enzymatic activity is mainly dependent on the viscosity-dictated molecular mobility.

On the basis of this data, it is possible to affirm that, although viscosity is the main factor regulating HRP activity in concentrated solutions, T'g and  $a_w$  changes should not be overlooked in order to describe or predict the enzymatic activity in a system.

### 3 Conclusions

The effectiveness of a solute in the inhibition of enzymatic activity in concentrated solutions depends on the thermodynamical properties of the solution, as described by  $a_w$ , and on the mobility of the system, as described by  $\eta^{-\nu}$  and T'g.

In viscous binary solutions, the mobility of the system as described by viscosity and T'g is the most important factor in the inhibition of enzymatic activity, while water activity has different effects depending on the chemical nature of the solute.

In complex ternary systems characterized by the same viscosity value,  $a_w$  lowering does not always result in a decrease of enzymatic activity, especially when it is achieved by the addition of a ligand which acts as a plasticizer by depleting the T'g of the system.

Chemical and physical stability factors were proven to play a key role on the regulation of enzymatic activity in solutions; thus, a deeper understanding of their importance is needed to better investigate the enzyme activity and stability of biological systems. Moreover, investigations on the effect of co-solutes, which could be used by the industry to achieve enzymatic stability, could find practical application in the shelf-life testing of foods and pharmaceutical formulation.

## References

- Acker L (1963) Enzyme activity at low water contents. In: Leitch JM, Rhodes DN (eds) Recent advances in food science, 3rd edn. Butterworths, London, pp 239–347
- Acker L (1969) Water activity and enzyme activity. *Food Technol* 23:1257–1270
- Ansari AC, Jones CM, Henry ER, Hofrichter J, Eaton WA (1992) The role of protein viscosity in the dynamics of protein conformational changes. *Science* 256:1796–1798
- Bell LN (2007) Moisture effects on food's chemical stability. In: Barbosa-Cánovas GV et al (eds) Water activity in foods. Fundamentals and applications. Blackwell Publishing, Oxford, pp 173–198
- Buitnik J, van den Dries IJ, Hoekstra FA, Alberda M, Hemminga M (2000) High critical temperature above Tg may contribute to the stability of biological systems. *Biophys J* 79:1119–1128
- Burnette FS (1977) Peroxidase and its relationship to food flavor and quality: a review. *J Food Sci* 42:1–6
- Chen YH, Aull JL, Bell LN (1999a) Invertase storage stability and sucrose hydrolysis in solids as affected by water activity and glass transition. *J Agric Food Chem* 47:504–509
- Chen YH, Aull JL, Bell LN (1999b) Solid state tyrosinase stability as affected by water activity and glass transition. *Food Res Int* 32:467–472
- Cicerone MT, Soles CL (2004) Fast dynamics and stabilization of proteins: ternary glasses of trehalose and glycerol. *Biophys J* 86:3836–3845
- Farwell RW, Ackerman E (1963) Effect of physical factors on reactions of horse-radish peroxidase complexes with reduced cytochrome c. *Biophys J* 86:479–491
- Hagen SJ, Hofrichter J, Eaton WA (1995) Protein reaction kinetics in a room temperature glass. *Science* 269:959–962
- Kerr WL, Lim MH, Reid DS, Chen H (1993) Chemical reaction kinetics in relation to glass transition temperatures in frozen food polymer solutions. *J Sci Food Agric* 61:51–56
- Kouassi K, Roos YH (2000) Glass transition and water effects on sucrose inversion by invertase in a lactose-sucrose system. *J Agric Food Chem* 48:2461–2466
- Kouassi K, Roos YH (2001) Glass transition and water effects on sucrose inversion in noncrystalline carbohydrate food systems. *Food Res Int* 34:895–901
- Kouassi K, Roos YH (2002) Glass transition, water, and glycerol effects on sucrose inversion in pullulan-sucrose systems. *J Food Sci* 67:3402–3407
- Kramers HA (1940) Brownian motion in a field of force and the diffusion model of chemical reaction. *Physica* 7:284–304
- Labuza TP, Tannenbaum SR, Karel M (1970) Water content and stability of low moisture and intermediate moisture foods. *Food Technol* 24:543–550

- Laurenti E, Suriano G, Ghibaudo EM, Ferrari RP (2000) Ionic strength and pH effect on the Fe(III)-imidazolate bond in the heme pocket of horseradish peroxidase: an EPR and UV-visible combined approach. *J Inorg Biochem* 81:259–266
- Lee SB, Kim KJ (1995) Effect of water activity on enzyme hydration and enzyme reaction rate in organic solvent. *J Ferment Bioeng* 79:473–478
- Lim MH, Reid DS (1991) Studies of reaction kinetics in relation to the  $T_g$  of polymers in frozen model systems. In: Slade L, Levine H (eds) *Water relationships in food*. Plenum, New York, pp 102–122
- Manzocco L, Nicoli MC, Anese M, Pitotti A, Maltini E (1999) Polyphenoloxidase and peroxidase activity in partially frozen systems with different physical properties. *Food Res Int* 31:363–370
- Nelson KA, Labuza TP (1994) Water activity and food polymer science: Implications of state on Arrhenius and WLF models in predicting shelf life. *J Food Eng* 22:271–289
- Neri L (2010) Enzymatic inactivation and quality of semi-finished plant foods intended for freezing. PhD dissertation. University of Teramo, Italy
- Neri L, Pittia P, Bertolo G, Torreggiani D, Sacchetti G (2011) Influence of water activity and molecular mobility on peroxidase activity in glucose and maltodextrin solution. *Food Biophys* 6:281–287
- Neri L, Pittia P, Bertolo G, Torreggiani D, Sacchetti G (2010) Influence of water activity and molecular mobility on peroxidase activity in salt and sorbitol-maltodextrin systems. *J Food Eng* 101:289–295
- Reid DS (2007) Water activity: fundamentals and relationships. In: Barbosa-Cánovas GV et al (eds) *Water activity in foods. Fundamentals and applications*. Blackwell Publishing, Oxford, pp 15–28
- Roos Y (2007) Water activity and glass transition. In: Barbosa-Cánovas GV (ed) *Water activity in foods: fundamentals and applications*. Blackwell Publishing, Oxford, pp 29–45
- Roos Y, Karel M (1991) Phase transitions of mixtures of amorphous polysaccharides and sugars. *Biotechnol Progr* 7:49–53
- Schwimmer S (1980) Influence of water activity on enzyme reactivity and stability. *Food Technol* 34(5):64–74, 82, 83
- Silver M, Karel M (1981) The behavior of invertase in model systems at low moisture contents. *J Food Biochem* 5:283–311
- Slade L, Levine H (1991) Beyond water activity: recent advances based on an alternative approach to the assessment of food quality and safety. *Crit Rev Food Sci Nutr* 30:115–360
- Terefe NS, Van Loey A, Hendrickx M (2004) Modelling the kinetics of enzyme-catalysed reactions in frozen systems: the alkaline phosphatase catalysed hydrolysis of di-sodium-p-nitrophenyl phosphate. *Innov Food Sci Emerg* 5:335–344
- Tijssens LMM, Rodis PS, Hertog MLATM, Waldron KW, Ingham L, Proxenia N, van Dijk C (1997) Activity of peroxidase during blanching of peaches, carrots and potatoes. *J Food Eng* 34:355–370
- Tome D, Nicolas J, Drapron R (1978) Influence of water activity on the reaction catalyzed by polyphenoloxidase (E.C.1.14.18.1.) from mushrooms in organic liquid media. *Lebensm-Wiss Technol* 11:38–41
- Williams ML, Landel RF, Ferry JD (1955) Temperature dependence of relaxation mechanisms in amorphous polymer and other glass-forming liquids. *J Am Chem Soc* 77:3701–3707

# Phase Transitions in Sugars and Protein Systems: Study of Stability of Lysozyme in Amorphous Sugar Matrices

L.M. Martínez, M. Videá, F. Mederos, Y. de Moral, M. Mora,  
and Cristina Pérez

## Abbreviations

DSC	Differential scanning calorimetry
DTA	Differential thermal analysis
$T_g$	Glass transition temperatures
$T_m$	Thermal stability

## 1 Introduction

In the last decades, development of products resulting from the application of molecular biology and biotechnology has demonstrated accelerated progress; as a result, the use of biological products such as proteins and enzymes has increased considerably in the food and pharmaceutical industry (Wanh 2000; Richards et al. 2002). Since most of these biomolecules, particularly enzymes, are extremely sensible to changes in temperature, pH, ionic force, and water concentration, scientists in these fields are in constant search of new methodologies and techniques to improve their stability. In industrial processes, biomolecules are obtained in aqueous solutions; however, in this medium their shelf life is relatively short. A remarkable improvement in the stability of protein based drugs has been obtained when these biomolecules are taken to a dry state; unfortunately, the freeze drying or spray-drying processes (which are the most common used techniques to obtain dry protein) expose these molecules to extreme conditions that cause a considerable

---

L.M. Martínez (✉) • M. Videá • F. Mederos • Y. de Moral • M. Mora • C. Pérez  
Department of Chemistry, Tecnológico de Monterrey, Campus Monterrey, Monterrey, Mexico  
e-mail: [luzvidea@itesm.mx](mailto:luzvidea@itesm.mx)

decrease in their activity (Passot et al. 2005; Liao et al. 2004; Hinrichs et al. 2001; Heller et al. 1999).

In the last decade the pharmaceutical and biochemical industry has turned to vitreous materials of sugars and analogous compounds as preserving agents in the drying processes and storage of thermolabile molecules (Nicholls 2004; Ohtake and Wang 2011). The idea of using amorphous sugars for preservation purposes comes from mimicking the natural phenomenon of anhydrobiosis observed in some species of spores, fungi, plants, and other organisms, which have the capacity to survive complete dehydration and extreme conditions of temperature (Buitink and Leprince 2008; Buitnik and Leprince 2004). This resistance to drought has been associated to the biosynthesis of nonreducing sugars like trehalose and sucrose.

The mechanism that explains the specific participation of these sugars in the biopreservation phenomenon is a controversial subject; some scientists (Crowe et al. 1984; Carpenter and Crowe 1989) suggest that trehalose and other reducing sugars can form hydrogen bonds that can replace the essential water molecules responsible for maintenance of the tertiary structure of proteins. In numerous studies it has been demonstrated that biological membranes conserve their structure and functionality when they are dehydrated in the presence of trehalose or other saccharides (Higl et al. 2007; Patist and Zoerb 2005; Oliver et al. 2001); nevertheless, it is not clear why not all substances that can form hydrogen bonds confer preservation with the same efficiency as nonreducing sugars like trehalose or sucrose. In one study conducted by Crowe et al. (1984), it was found that the degree of efficiency in the preservation of dehydrated membranes in the presence of polyols studied was: glycerol < sucrose < maltose < trehalose. Analyzing these results, Green and Angell (1989) showed that this order coincides with the increasing order of their glass transition temperatures ( $T_g$ ). This finding opened the vitrification theory, which proposes that in order to observe the preservation phenomenon it is essential that the saccharides are in their glassy state, at which the viscosity reaches values as great as  $10^{12}$  Pa s, where the movement of molecules and diffusion phenomena are extremely slow.

At the glassy state most chemical reactions, such as the decomposition process, are temporarily suspended. Several studies have shown that when nonreducing sugars are present, the thermal stability of biomolecules is increased, and their structure is preserved during the drying processes due to the *in situ* formation of a vitreous matrix. Therefore, proteins are immobilized in the glass matrix and thus protected from the degenerative effects of the processes of crystallization of water or solutes present in the formulation during water loss or drying (Buitink and Leprince 2004). This process allows storage at room temperature and eliminates the need for refrigeration (Nicholls 2004; Worrall et al. 2001; Fox 1995). Although it is clear that sugar vitrification has much to do with the preservation (Higl et al. 2007; Duncan et al. 1999) of biomolecules, there is evidence that other parameters, including the presence of the proteins, play an important role in the glass formation system and, therefore, on the preservation phenomenon (Buitink et al. 2000). These theories only partially explain the mechanism of stabilization, since not all compounds with hydroxyl groups are similar to trehalose, nor are all

glass-forming compounds effective in the preservation of biomolecules. To date, no successful theory has been proposed to explain the mechanism in its entirety (Grigera and Bolzicco 2008).

Because the biopreservation mechanism has not been fully established, the use of glassy sugars cannot easily be generalized to all kind of biomolecules; thus, industries are working by trial and error to find systems that can stabilize specific biomolecules as efficiently as the process occurs in nature.

In order to optimize the preservation of labile molecules, it is important to study the properties of biomolecules and preservation agents (nonreducing sugars) as a function of temperature. We present the results of a study of phase transitions of pure carbohydrates and proteins on aqueous solution and proteins stabilized with nonreducing sugars taking as a biomolecule model the enzyme lysozyme. The basic concepts of thermal properties on vitreous materials and proteins are presented. It is important to mention that the terms sugar, saccharide, and carbohydrate as the terms amorphous and vitreous will be used interchangeably.

## ***1.1 Basic Concepts of Amorphous Carbohydrate and Thermal Stability of Proteins***

To understand the role of the amorphous matrix on preservation, it is necessary to be familiar with properties of the glass state, which are described below.

### **1.1.1 Amorphous State and Glass Transition Temperature ( $T_g$ )**

A glass can be considered as a liquid that has lost its ability to flow or as an amorphous solid with structural features typical of a liquid that presents glass transition temperature, which is the temperature at which a glassy material loses thermomechanical stability and changes from an amorphous solid highly viscous ( $10^{12}$  Pa s) into a liquid. The transformation of a liquid into a glass can be observed by monitoring changes in the material's properties as the enthalpy is a function of temperature. Experimental measurement of the glass transition temperature can be done by measuring the heat capacity of a material as a function of temperature. The  $T_g$  determines the temperature at which thermomechanical stability and viscoelastic properties of an amorphous solid start to change to be transformed into a supercooled liquid (Angell 1995). Figure 1 shows the three ways in which a  $T_g$  can be reported based on the position of the “transition.” To achieve an efficient system for the purpose of preservation, a transition temperature above room temperature is preferred.

**Fig. 1** Thermogram showing three different temperatures at which the glass transition temperature ( $T_g$ ) can be reported. This measurement corresponds to a nonreducing sugar sample, measured with a differential scanning calorimeter (DSC) at heating rate of 10 °C/min

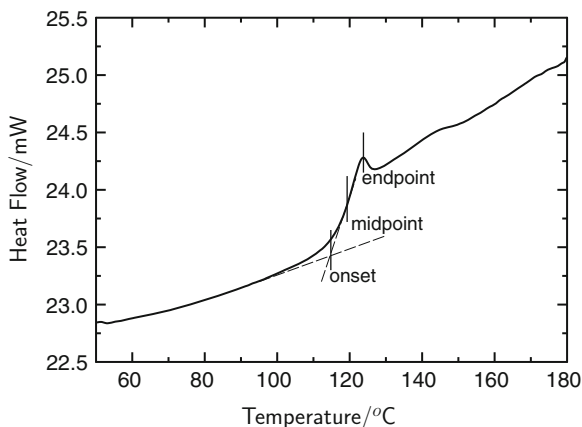


**Table 1** Glass transition temperature  $T_g$  of three nonreducing sugars reported in the literature

Method of preparation of the amorphous solid (water content)	Sucrose $T_g$ (°C)	Trehalose $T_g$ (°C)	Raffinose $T_g$ (°C)	Reference
<i>Freeze drying</i> (Karl Fischer < 0.2 %)	74	115	102	Zografi and Saleki-Gerhardt (1994)
<i>Freeze drying</i> (Karl Fischer < 0.3 %)	70 (onset)	114 (onset)	NR	Sheri et al. (1999)
	78 (endpoint)	123 (endpoint)		
<i>Heating</i> (0.1–0.5 g) above melting temperature (water content not measured; dehydration assumed due to melting temperature)	62	100	NR	Roos (1993)
<i>Quick drying</i> of 10 µl of water-solution [20 mg/ml of sugar] (no water assumed due to absence of band at 1650 cm <sup>-1</sup> )	57	108	108	Wolkers et al. (2004)

### 1.1.2 Glass Transition Temperature ( $T_g$ ) of Nonreducing Sugars

A comparison of the thermal stability of several preservation agents using values of  $T_g$  reported in the literature is very complicated, since the experimental conditions under which these temperatures were measured can be very different depending on the position at which the temperature is measured (onset, midpoint, or end point; see Fig. 1) and also due to the thermal history of the sample, content of water, and heating rate of the measurement. Unfortunately, these parameters are not always reported. Table 1 summarizes the information reported in the literature for three sugars commonly used as preservation agents.

### 1.1.3 Thermal Stability of Proteins ( $T_m$ )

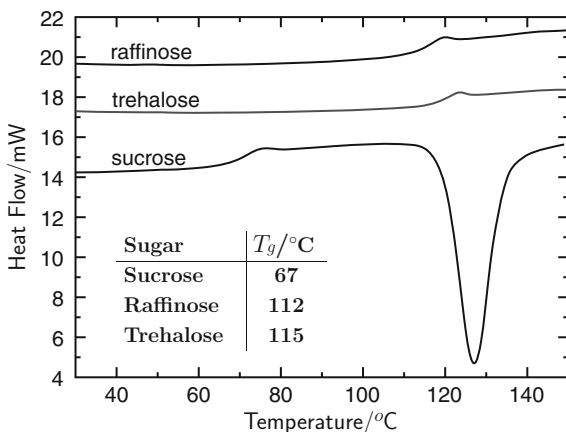
The evaluation of thermal stability ( $T_m$ ) and changes in the conformation of biomolecules such as enzymes and proteins as a function of temperature is also very important in order to understand its preservation. Thermal analysis can be used to determine the maximum temperature at which proteins are stable (denaturation temperature,  $T_m$ ) and the enthalpy associated with this process. To describe this process, it can be considered that a protein is a molecule composed of a large number of amino acids, linked together by peptide bonds (primary structure). In addition, the side chains of these amino acids, can establish interactions of the type called "hydrogen bonds," which causes the protein to acquire a characteristic shape and suitable for the performance of their intended functions (secondary structure). The process of distortion, then, according to the Lumry and Eyring model (Lumry and Eyring 1954), consists of two stages: the first is the cleavage of the protein and may be reversible, and the second involves a breakdown of the molecule and is an irreversible process. Either of these steps involves a certain amount of energy being released or absorbed, so it is expected to be possible to detect the denaturation process using thermal analysis.

In a study by Nath et al. (1998) thermal stability of the enzyme alcohol dehydrogenase in aqueous solution was investigated by measuring the biological activity of the enzyme at different temperatures and measuring the denaturation process using differential scanning calorimetry (DSC). Although these two measurements are based on different principles (kinetic in the case of measurement of biological activity and thermodynamics using DSC), both measurements lead to equivalent results for the thermal stability of protein, in which denaturation of the enzyme occurred at 63 and 70 °C in the absence and presence of sucrose (44 % w/w), respectively. Although there are other publications (Cueto et al. 2003; Sun et al. 1998; Sochava 1997) demonstrating that techniques based on thermal analysis can be very useful for evaluating protein stability, most of these studies have been carried out either in solution or at the dry state (freeze-dried or spray-dried proteins–sugar systems) (Lu et al. 2007; Liao et al. 2002a, b; Bell et al. 1995), but no systematic study has been carried out using the same model biomolecule to correlate the preservation effect of the same preservation agents, in solution and at the dry state.

## 2 Experimental Results of Phase Transitions of Sugars and Proteins Using as a Model Lysozyme

The experimental work of the present study of phase transitions of sugars and lysozyme was carried out in the following steps: (1) thermal characterization of pure amorphous sugars; (2) evaluation of the thermal stability of enzymes in solution, studying the effect of concentration of sugar and concentration of preservation agent; and (3) evaluation of the thermal stability of enzyme–carbohydrate systems after drying in the presence of different sugars.

**Fig. 2** Thermograms showing glass transition temperatures of the disaccharides sucrose and trehalose and a trisaccharide: raffinose. Values reported correspond to the onset temperature. Heating rate of measurement 10 °C/min



## 2.1 Methods and Materials

The amorphous matrices were prepared using the following carbohydrates: D-(+)-Trehalose dihydrate (Sigma T5251), Sucrose 99 % (Sigma S5016), and D-(+)-Raffinose pentahydrate 98 % (Sigma R0250). The model enzyme used was lysozyme (Sigma Aldrich, Lot 094K1454); glass transition temperature of the sugar glasses and thermal analysis of the enzyme–carbohydrate systems were determined on a Pyris 1 DSC instrument and with a homemade differential thermal analysis (DTA) instrument (Martínez et al. 2007, 2013). Glass transition temperatures are reported using onset of the  $T_g$  in all cases.

## 2.2 Phase Transitions of Amorphous Sugars: Sucrose, Trehalose, and Raffinose

Thermal stability of pure amorphous carbohydrate matrices prepared by drying aqueous solution by microwave heating were characterized by determining their glass transition temperature by DSC at a heating rate of 10 °C/min (Martínez et al. 2011). Figure 2 shows the thermograms obtained for each of the matrices. As can be observed, sucrose tends to crystallize when it is heated above 120 °C. Raffinose and trehalose did not show any crystallization, even though they were heated up to 220 °C.

## 2.3 Thermal Denaturation of Lysozyme in Solution

In order to study thermal stability and phase transition of proteins with and without preservation agents in solution, denaturation temperature ( $T_m$ ) of the enzyme was evaluated in aqueous solution, first at different concentration of the enzyme, then

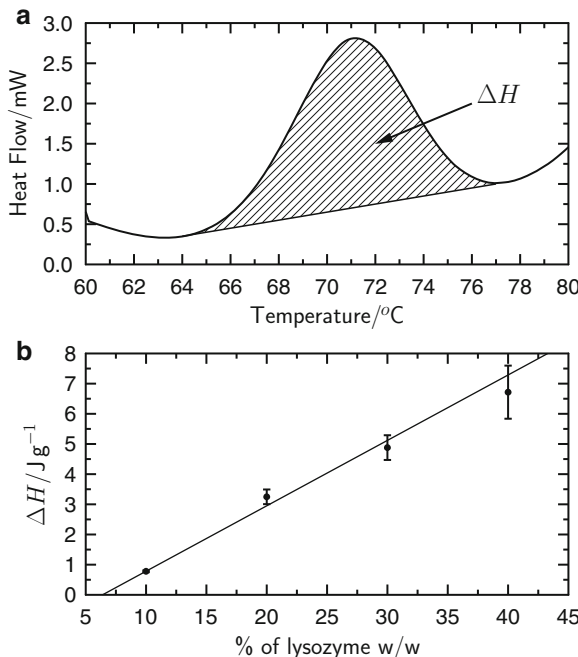


**Fig. 3** Thermal denaturation of lysozyme in aqueous solutions. Denaturation enthalpy as a function of the concentration of enzyme. (a) Thermogram showing the area underneath the endothermic peak that corresponds to the enthalpy of denaturation for the enzyme. (b) Linear dependency of the denaturation enthalpy with the concentration of lysozyme in aqueous solution (10, 20, 30, and 40 % w/w)

with different concentrations of preservation agents, and finally with different types of preservation agents.

#### (a) Effect of concentration of enzyme

Aqueous solutions of lysozyme were prepared containing 10, 20, 30, and 40 % (w/w) of the enzyme, respectively. The temperature and enthalpy of denaturation were measured by differential scanning calorimeter (DSC) using a heating rate of 10 °C/min. Figure 3a shows an example of the thermograms obtained; the denaturation temperature of lysozyme in solution occurred between 71 and 72 °C. The denaturation enthalpy, corresponding to the area beneath the curve, was calculated for each solution. Good linear correlation of the denaturation enthalpy with the enzyme concentration is shown in Fig. 3b. It is important to mention that as the concentration of the enzyme increases, the standard deviation of the measurements increases. It is probable that the saturation of the solution interferes with this measurement.

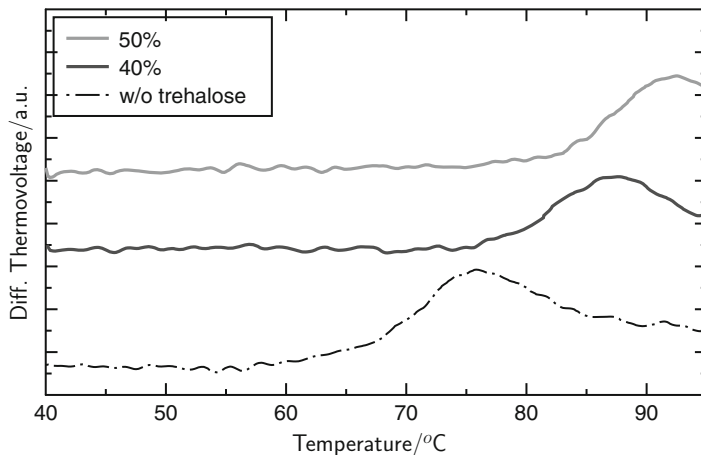


**Fig. 4** Thermograms showing  $T_m$  of lysozyme in aqueous solution and in the presence of different amounts of trehalose. Measurements are done at a heating rate of 10 °C/min

#### (b) Effect of concentration of preservation agent

To study the effect of concentration of the preservation agent (in this case, trehalose) on denaturation temperature of the enzyme on solution, different amounts of trehalose (40 and 50 % w/w) were added to an aqueous solution containing 20 % w/w of the enzyme. These measurements were conducted with a homemade DTA instrument (Martínez et al. 2007, 2013) at a heating rate of 10 °C/min. As shown in Fig. 4, the larger the content of sugar, the higher the thermal stability ( $T_m$  of the enzyme). When comparing denaturation temperatures of the enzyme on aqueous solution with no preservation agent measured by the commercial DSC and the homemade DTA the results ( $T_m$ ) are the same, independent of the instrument used.

#### 2.4 Thermal Denaturation of Lysozyme in Solution and Dried State: Effect of Type of Sugar

For the purpose of studying the effect of type of sugar on thermal stability of the enzyme in solution, three types of sugars were added to aqueous solutions of 20 % w/w lysozyme. It is important to mention that the effect of type of sugar on solution can only be analyzed in highly concentrated solutions (above 45 % w/w). To compare these results in the dried state, aqueous solutions of lysozyme were freeze-dried in the presence of the same sugars. Figure 5a shows thermograms obtained on solution and Fig. 5b shows results of freeze-dried samples.

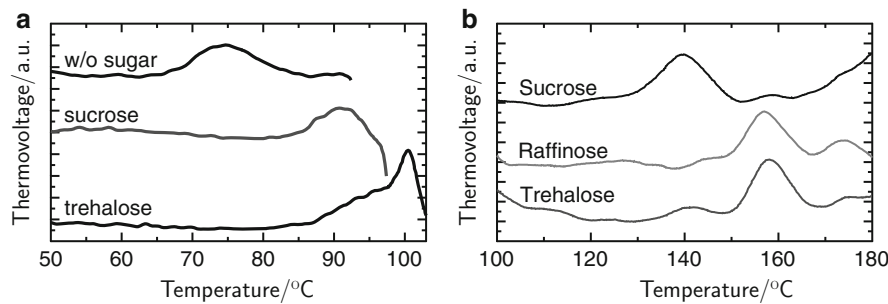


**Fig. 5** Thermograms showing thermal denaturation of lysozyme containing different types of sugars. Results compare the denaturation temperatures of (a) aqueous solutions and (b) freeze-dried samples. Measurements were done with DTA at heating rate of 10 °C/min

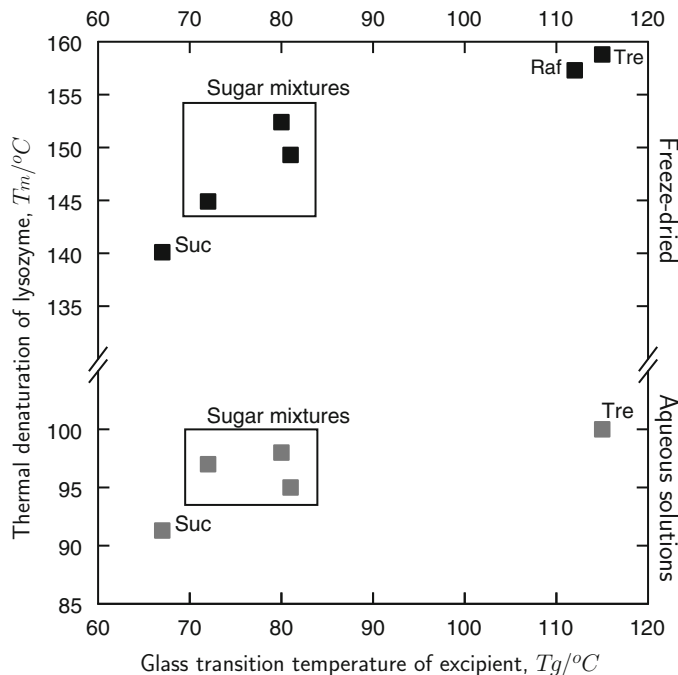


**Fig. 6** Comparison of  $T_m$  and  $T_g$  of enzyme in solution and freeze-dried. The tendency of thermal stability observed in aqueous solutions is similar for freeze-dried samples

In order to study the synergic effects of several sugars on the same system, formulations based on mixtures of sugars were also analyzed. From the results obtained, it was observed that the higher the glass transition temperature of the excipient (pure sugar or the mixture), the higher the  $T_m$  of the enzyme, independent of whether the enzyme is in a dried state or in an aqueous concentrated solution. See Fig. 6.

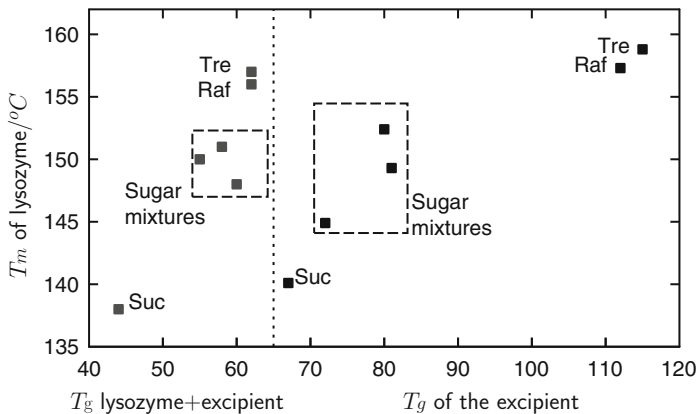
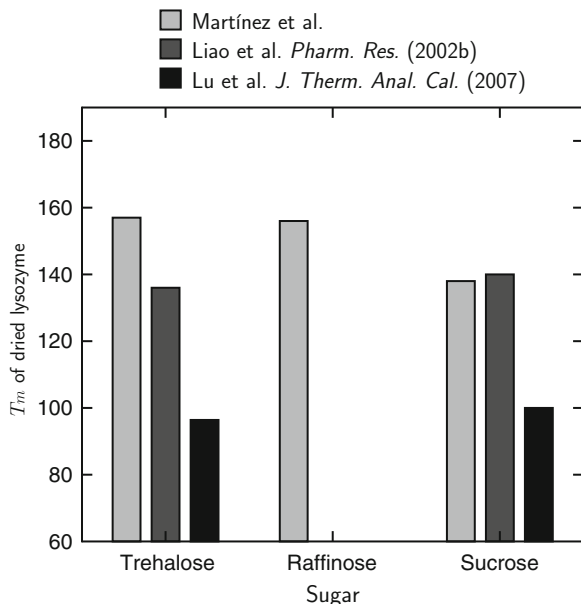


**Fig. 7** Denaturation temperatures of lysozyme and glass transition temperature of the freeze-dried enzyme–sugar systems

**Fig. 8** Comparison of thermal stability ( $T_m$ ) of lysozyme preserved in different sugars. The results of this work are compared with those of (Liao et al. 2002b) and (Lu et al. 2007)



In another series of experiments, enzyme–carbohydrate systems obtained by freeze drying were evaluated to determine the  $T_g$  of lysozyme–sugar matrices and  $T_m$  of the enzyme incorporated into the carbohydrate glassy matrices, with both using one sugar or mixtures of several sugars as the excipient. These measurements were determined by DSC at a heating rate of 10 °C/min; the results are shown in Fig. 7.

### 3 Conclusions

The degree of thermal stability conferred to the enzyme by sugar glasses depends on concentration of the excipient, type of excipient, and drying process, among other parameters. The selection of an efficient preservation agent for freeze-dried biomolecules can be a time-consuming task if the set of experimental parameters considered in order to determine its optimal performance is incomplete. Therefore, it is relevant for development of the appropriate preservation agent to validate experimental test procedures of thermal stability of biomolecules directly in concentrated solution, which allows a much faster and useful tool to make predictions on efficiency of thermal stability, since these results can be extrapolated to the performance of the preservation agents in dried systems. The results of this work, summarized in Fig. 8, show how by using information from concentrated aqueous solutions we have been able to improve thermal stability of the same enzyme when compared with other results from the literature.

### References

- Angell A (1995) Formation of glasses from liquids and biopolymers. *Science* 267:1924–1935
- Bell LN, Hageman MJ, Muraoka LM (1995) Thermally induced denaturation of lyophilized bovine somatotropin and lysozyme as impacted by moisture and excipients. *J Pharm Sci* 84:707–712
- Buitink J, Van den Dries IJ, Hoekstra FA, Alberda M, Hemminga MA (2000) High critical temperature above  $T_g$  may contribute to the stability of biological systems. *Biophys J* 79 (2):1119–1128
- Buitink J, Leprince O (2004) Glass formation in plant anhydrobiotes: survival in the dry state. *Cryobiology* 48:215–228
- Buitink J, Leprince O (2008) Intracellular glasses and seed survival in the dry state. *C R Biol* 331 (10):788–795
- Carpenter JF, Crowe JH (1989) An infrared spectroscopic study of the interactions of carbohydrates with dried proteins. *Biochemistry* 28:3916–3922
- Crowe LM (1984) Lessons from nature: the role of sugars in anhydrobiosis. *Comp Biochem Physiol A* 131:505–513
- Crowe JH, Crowe LM, Womersley C, Mouradian R (1984) Preservation of functional integrity during long term storage of a biological membrane. *Biochim Biophys Acta* 778(3):615–617
- Cueto M, Dorta MJ, Munguía O, Llabrés M (2003) New approach to stability assessment of protein solution formulations by differential scanning calorimetry. *Int J Pharm* 252:159–166
- Duncan QM, Royal PG, Kett VL, Hopton ML (1999) The relevance of the amorphous state to pharmaceutical dosage forms: glassy drugs and freeze dried systems. *Int J Pharm* 179:179–207
- Fox KC (1995) Putting proteins under glass. *Science* 267:1922–1923
- Green JL, Angell CA (1989) Phase relations and vitrification in saccharide-water solutions and the trehalose anomaly. *J Phys Chem* 93:2880–2882
- Grigera JR, Bolzicco V (2008) Molecular mobility and ageing of sugar glasses. *Food Chem* 106 (4):1314–1317
- Heller M, Carpenter J, Randolph T (1999) Protein formulation and lyophilization cycle design: prevention of damage due to freeze-concentration induced phase separation. *Biotechnol Bioeng* 63(2):166–174

- Higl B, Kurtmann L, Carlsen CU, Ratjen J, Först P, Skibsted LH, Ulrich K, Risbo J (2007) Impact of water activity, temperature, and physical state on the storage stability of *Lactobacillus paracasei* ssp. *Paracasei* freeze-dried in a lactose matrix. *Biotechnol Prog* 23:794–800
- Hinrichs WLJ, Prinsen MG, Frijlink HW (2001) Inulin glasses for the stabilization of therapeutic proteins. *Int J Pharm* 215:163–174
- Liao Y-H, Brown MB, Martin GP (2004) Investigation of the stabilisation of freeze-dried lysozyme and the physical properties of the formulations. *Eur J Pharm Biopharm* 58:15–24
- Liao Y-H, Brown M, Quader A, Martin GP (2002a) Protective mechanism of stabilizing excipients against dehydration in the freeze-drying of proteins. *Pharm Res* 19(12):1854–1861
- Liao Y-H, Brown MB, Nazir T, Quader A, Martin GP (2002b) Effects of sucrose and trehalose on the preservation of the native structure of spray-dried lysozyme. *Pharm Res* 19(12):1847–1853
- Lumry R, Eyring H (1954) Conformation changes of proteins. *J Phys Chem* 58:110–120
- Lu J, Wang X-J, Liu Y-X, Ching C (2007) Thermal and FTIR investigation of freeze-dried protein-excipient mixtures. *J Therm Anal Calorim* 89(3):913–919
- Martínez LM, Videá M, Mederos F, Mesquita J (2007) Constructing a high-sensitivity, computer-interfaced, differential thermal analysis device for teaching and research. *J Chem Educ* 84 (7):1222–1223
- Martínez LM, Videá M, Mesquita, J (2013) Design, construction and calibration of a portable multi sample DTA setup. *Thermochim. Acta* 560:89–94
- Martínez LM, Videá M, Mederos F, de Moral Y (2011) Preservation effect of vitreous non reducing carbohydrates on the enzymatic activity, denaturation temperature and retention of native structure of Lysozyme. *J Mex Chem Soc* 55(3):185–189
- Nath S, Satpathy GR, Mantri R, Deep S, Ahluwalia J (1998) Thermal stability of alcohol dehydrogenase enzyme determined by activity assay and calorimetry. *Thermochim Acta* 309:193–196
- Nicholls H (2004) Cash injection for thermostable vaccines. *Drug Discov Today* 9(22):945
- Ohtake S, Wang J (2011) Trehalose: current use and future applications. *J Pharm Sci* 100 (6):2020–2053
- Oliver AE, Leprince O, Wolkers WF, Hincha DK, Heyer AG, Crowe JH (2001) Non-disaccharide-based mechanisms of protection during drying. *Criobiology* 43(2):151–167
- Passot S, Fonseca F, Alarcon-Lorca M, Rolland D, Marin M (2005) Physical characterisation of formulations for the development of two stable freeze-dried proteins during both dried and liquid storage. *Eur J Pharm Biopharm* 60(3):335–348
- Patist A, Zoerb H (2005) Preservation mechanisms of trehalose in food and biosystems. *Colloids Surf A* 40(2):107–113
- Richards AB, Krakowka S, Dexter LB, Schmid H, Wolterbeek APM, Waalkens-Berendsen DH, Shigoyuki A, Kurimoto M (2002) Trehalose: a review of properties, history of use and human tolerance, and results of multiple safety studies. *Food Chem Toxicol* 40(7):871–898
- Roos Y (1993) Melting and glass transitions of low molecular weight carbohydrates. *Carbohydr Res* 238:39–48
- Sheri LS, Tang X, Chang L, Hancock BC, Pikal MJ (1999) Characterization of the time scales of molecular motion in pharmaceutically important glasses. *J Phys Chem B* 103(20):4113–4121
- Sochava IV (1997) Heat capacity and thermodynamic characteristics of denaturation and glass transition of hydrated and anhydrous proteins. *Biophys Chem* 69:31–41
- Sun WQ, Davison P, Chan HSO (1998) Protein stability in the amorphous carbohydrate matrix: relevance to anyhydrobiosis. *Biochim Biophys Acta* 1425:245–254
- Wanh W (2000) Lyophilization and development of solid protein pharmaceuticals. *Int J Pharm* 203:1–60
- Wolkers WF, Oliver A, Tablin F, Crowe JH (2004) Fourier-transform infrared spectroscopy study of sugar glasses. *Carbohydr Res* 339(6):1077–1085
- Worrall EE, Litamoi JK, Seck BM, Ayelet G (2001) Xerovac: an ultra rapid method for the dehydration and preservation of live attenuated Rinderpest and Peste des Petits ruminants vaccines. *Vaccine* 19:834–839
- Zografi G, Saleki-Gerhardt A (1994) Non-isothermal crystallization of sucrose from amorphous state. *Pharm Res* 11(8):1166–1173

# An Exhaustive Study on Physicochemical and Structural Changes During Drying of Apple Discs

S.M. Casim, M.F. Mazzobre, and S.M. Alzamora

## Abbreviations

<sup>1</sup> H-NMR	Proton nuclear magnetic resonance
A	Area under curve
$A_i$	Signal amplitude
ANOVA	Analysis of variance
BI	Browning index
CPMG	Carr–Purcell–Meiboom–Gill pulse sequence
D	Deformation at the rupture point
ESEM	Environmental scanning electronic microscopy
FID	Flame ionization detector
$F_{\max}$	Maximum rupture force
I	Signal intensity of the water strongly associated with the matrix
LM	Light microscopy

---

S.M. Alzamora is member of Consejo Nacional de Investigaciones Científicas y Técnicas de la República Argentina.

S.M. Casim (✉)

Departamento de Industrias, Facultad de Ciencias Exactas y Naturales,  
Universidad de Buenos Aires, Ciudad Universitaria, (1428) C.A.B.A., Buenos Aires, Argentina  
e-mail: [smcasim@hotmail.com.ar](mailto:smcasim@hotmail.com.ar)

M.F. Mazzobre

Departamentos de Industrias y de Química Orgánica, Facultad de Ciencias Exactas y Naturales, University of Buenos Aires (FCEyN-UBA), Consejo Nacional de Investigaciones científicas y Técnicas de la República Argentina, Ciudad Universitaria, (1428) C.A.B.A.  
Buenos Aires, Argentina

S.M. Alzamora

Departamento de Industrias, Facultad de Ciencias Exactas y Naturales, Universidad de Buenos Aires, Ciudad Universitari, Buenos Aires, Argentina

MANOVA	Multivariate analysis of variance
PCA	Principal component analysis
RVP	Relative vapor pressure values
$S$	Slope in the initial linear portion of the force–deformation curve
$t$	Time
$T_2$	Spin–spin relaxation time
$T_{2\text{CPMG}}$	Spin–spin relaxation time using Carr–Purcell–Meiboom–Gill pulse sequence
$T_{2\text{FID}}$	Spin–spin relaxation time free induction decay
$T_{2i}$	Spin–spin relaxation time of the $i$ population
$T_{2L}$	Proton relaxation time of the water strongly associated with the matrix
$T_{2S}$	Relaxation time of the protons of polymeric chains

## 1 Introduction

Dehydration is one of the most employed techniques in the preservation and development of foods. Water is a vital component in the structural preservation and functional integrity of vegetable tissues. As a consequence of its removal during convective air drying, great physicochemical changes in biopolymer composition and spatial conformation are presented, inducing disarrangements and/or destruction of the natural structure, shrinkage, changes in water and biopolymer mobility and distribution, changes in thermal transitions, color changes, and modification in mechanical properties, among others. These characteristics have been identified as the most important properties associated with modifications in quality properties of fruits (Chapman 1994; Krokida et al. 1998, 2000; Ruan and Chen 1998).

The objectives of this study were: (1) to analyze, during air drying of apple tissue, the changes in water mobility, thermal transitions, mechanical behavior, color changes, and shrinkage, and (2) to relate those changes with the structure modifications determined by microscopy.

## 2 Materials and Methods

Apple (*Malus pumila*, Granny Smith cv) discs, 3 cm in diameter and 0.6 cm in thickness, were air-dried (60 °C, 3 m/s) during different times to obtain products with different moisture contents and relative vapor pressure values (RVP: 0.98, 0.96, 0.94, 0.91, 0.87, 0.82, 0.75, 0.60, 0.47, 0.40, 0.30) (D'Ambrogio de Argüeso 1986). Water content was determined gravimetrically in a vacuum oven (60 °C). RVP was measured with a hygrometer Aqua Lab (CX-2, Decagon Devices Inc., USA). Water mobility was studied by measuring the spin–spin relaxation times  $T_2$  using a low field nuclear magnetic resonance spectrometer Bruker Minispec mq20 (Bruker Biospin GmbH, Germany). Flame ionization detector (FID) method was applied to determine

the  $T_2$  corresponding to protons with fast relaxation as related to the solid matrix and water interacting strongly with them (Eq. 1). Carr–Purcell–Meiboom–Gill (CPMG) sequence was applied to study the protons with high mobility as related to free water and water with low interaction with solids. Experimental curves from CPMG sequence were fitted by nonlinear regression according to Eq. (2):

$$I = A_s \times e^{-\left(\frac{t}{T_{2s}}\right)^2} + A_L \times e^{-\left(\frac{t}{T_{2L}}\right)} \quad (1)$$

$$I = \sum A_i \times e^{-\left(\frac{t}{T_{2i}}\right)} \quad (2)$$

where  $I$  is the signal intensity at time  $t$ ,  $A_i$  is the signal amplitude, and  $T_{2i}$  is the spin–spin relaxation time,  $T_{2s}$  is the relaxation time of the protons of polymeric chains, and  $T_{2L}$  is the proton relaxation time of the water strongly associated with the matrix. Thermal transitions were studied by differential scanning calorimetry (DSC 822e, Mettler Toledo, Switzerland). Mechanical properties (maximum rupture force,  $F_{max}$ ; deformation at the rupture point,  $D$ ; slope in the initial linear portion of the force–deformation curve,  $S$ ; and area under curve,  $A$ ) were determined by puncture test with an Instron Testing Machine (model 1101, USA). Browning degree was evaluated with a spectrophotometer (Minolta CM-508-d). Shrinkage was studied by volume displacement method using *n*-heptane as solvent. Structure changes were evaluated by light microscopy (LM) (Carl Zeiss Axioscope BI2, Germany) and environmental scanning electronic microscopy (ESEM) (Phillips, XL30, Holland) (Snaar and Van As 1992; Rao 2003). The results were statistically analyzed using Infostat program (v. 2009, Cordoba National University, Argentina). Multivariate analysis of variance (MANOVA) and principal component analysis (PCA) were used to analyze rheological properties, water mobility, and color data. Analysis of variance (ANOVA) was applied to analyze shrinkage data.

### 3 Results and Discussion

Maximum rupture force  $F_{max}$  increased as drying time increased, while the slope of the initial linear portion  $S$  decreased up to RVP 0.96. Then remained approximately constant until RVP  $\approx 0.47$  and abruptly increased for lower RVP values, showing that at low RVP values apple tissue turned more resistant to rupture and to deformation (more rigid) due to water removal and solid concentration (Fig. 1a). An important change in the pattern of mechanical parameters was observed when moisture content was nearly the monolayer water content (0.10 g water/g d.b.). An increment in  $A$  was also observed, indicating an increase in the work needed for rupture. On the other hand,  $D$  showed an opposite behavior to  $S$ ; it increased as the product turned from high moisture to intermediate moisture contents (i.e., the tissue became more deformable), and then, at lower moisture contents, the resistance to deformation increased (Fig. 1b). The volume of apple discs decreased until

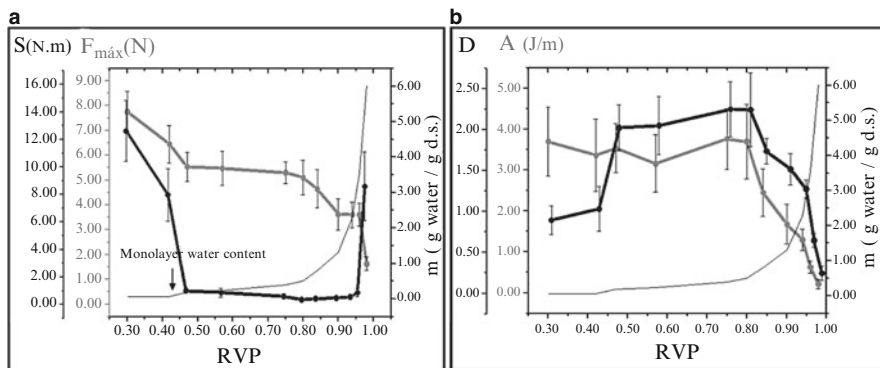


**Fig. 1** Evolution of mechanical properties as a function of RVP during convective air drying of apple tissue (left axis). Moisture content (dry basis) corresponding to the RVP (right axis). **(a)**  $F_{\text{máx}}$  and  $S$ ; **(b)**  $D$  and  $A$ . Error bar indicates the standard deviation

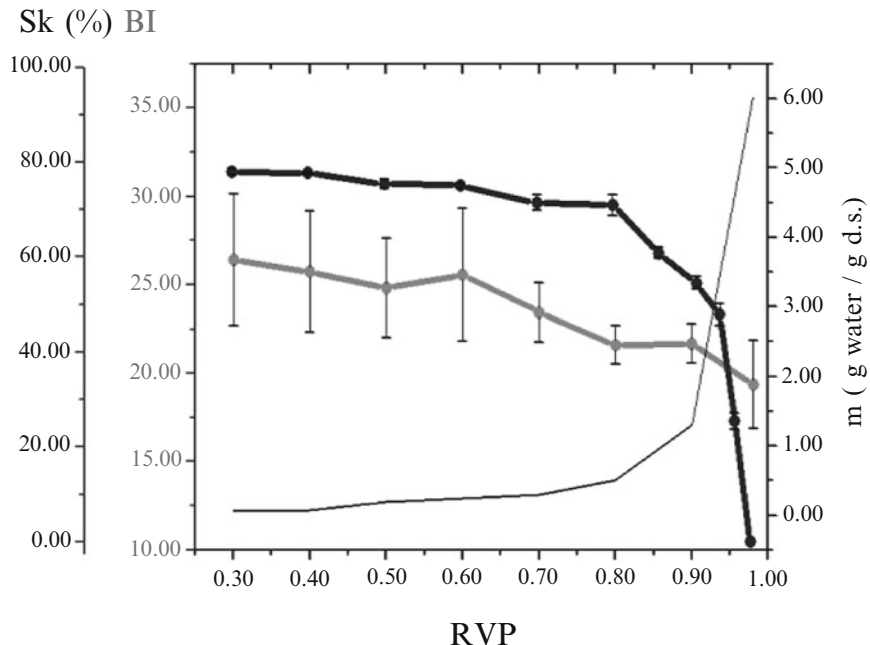


**Fig. 2** Evolution of shrinkage (Sk) and browning index (BI) as a function of RVP during convective air drying of apple tissue (left axis). Moisture content (dry basis) corresponding to the RVP (right axis). Error bar indicates the standard deviation

reaching  $\text{RPV} \approx 0.47$  and then remained approximately constant (Fig. 2). Browning index (BI) slightly, but significantly, increased along the process (Fig. 2).

Proton nuclear magnetic resonance ( $^1\text{H-NMR}$ ) studies indicated different water populations with different distribution and mobility along the drying process. From

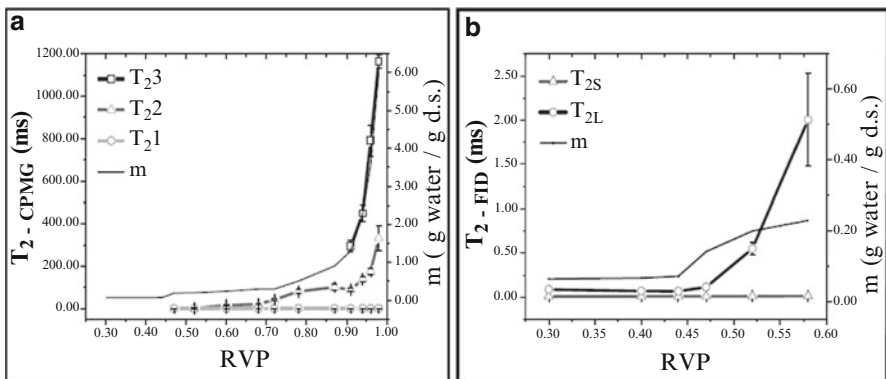


**Fig. 3** Evolution of relaxation times  $T_2$  as a function of RVP during convective air drying of apple tissue (left axis). Moisture content ( $m$ ) (dry basis) corresponding to the RVP (right axis). (a) CPMG sequence; (b) FID method. Error bar indicates the standard deviation

**Table 1** MANOVA of mechanical properties. Hotelling (Bonferroni) test

RVP	0.98	0.96	0.94	0.91	0.87	0.78	0.74	0.58	0.47	0.40	0.30
MANOVA <sup>a</sup>	A	B	C	C	D	E	E	F	EF	G	H

<sup>a</sup>Different letters indicate significant differences ( $p \leq 0.05$ )

**Table 2** MANOVA of  $T_2$  from CPMG sequence. Hotelling (Bonferroni) test

RVP	0.98	0.96	0.94	0.91	0.87	0.78	0.74	0.58	0.47	0.40	0.30
MANOVA <sup>a</sup>	A	B	C	D	E	E	F	FG	G	H	I

<sup>a</sup>Different letters indicate significant differences ( $p \leq 0.05$ )

CPMG sequence, three populations at high moisture contents were detected; meanwhile, at intermediate moisture values, only two populations were noticed, and at low moisture contents, only one population was observed until moisture contents closer to the monolayer value (Fig. 3a). Each  $T_{2i}$  gradually diminished, indicating a reduction in water mobility, although this decrease was more pronounced in  $T_{23}$  values, as related to free water (Fig. 3a). The MANOVA of CPMG parameters indicated significant differences between all samples (Tables 1 and 2). On the other hand, the FID method showed no significant changes in  $T_{2S}$  value, but an important decrease in  $T_{2L}$  was observed as water was removed until the monolayer water content was reached; then,  $T_{2L}$  remained the same with no significant changes (Fig. 3b). Nevertheless, at this water content, the relative proportion of the protons that contributed to the solid signal was larger than the amount of protons contributing to the liquid signal, meaning that around the monolayer water content the solid components of the tissue were those with dominant influence over the physicochemical properties of the studied system (results not shown).

For  $RVP \leq 0.96$ , an inverse correlation could be seen in  $F_{max}$ ,  $S$ , and  $T_{2CPMG}$  behavior. In low moisture samples ( $RVP \leq 0.47$ ), because of the disappearance of CPMG signal and the reduction in mobility of the water that interacts with the cell wall polymers, the water would be less available to act as a structure plasticizer, increasing both mechanical parameters.

As expected, thermal transition analysis indicated that glass transition temperature increased as moisture content decreased. The final product at  $RVP \approx 0.30$  still stayed in rubbery state (results not shown).

The fresh tissue showed turgid cells with parietal cytoplasm and important intercellular spaces (Fig. 4a, d). At  $RVP \approx 0.91$ , the cells seemed shrunken and deformed, with less contact, some interrupted membranes and undulated cell walls (Fig. 4b, e). At  $RVP \approx 0.30$ , a much collapsed cellular arrangement was presented, with high shrinkage and notable porosity. Some cell walls appeared disrupted with low density (Fig. 4c, f).

Among the causes of the changes observed during drying, the following could can be mentioned: (1) the concentration of solids due to water removal and the increase on tissue viscosity; (2) the disorganization and loss of membrane integrity and functionality and the subsequent change in the protein interaction with neighboring water molecules and the diffusive interchange between compartments; (3) the compactness and alteration of cell wall and, accordingly, the modification of water interaction with cell wall macromolecules and mechanical properties, and (4) the loss of turgor that decreased rigidity at high and intermediate moisture ranges (Slade and Levine 1991; Ruan and Chen 1998; Lewicki and Lukaszuk 2000; Lewicki and Pawlak 2003).

## 4 Conclusions

Mechanical properties of apple tissue were strongly influenced by moisture content and water mobility. Fresh tissue and high/intermediate moisture content samples showed viscoelastic behavior; however, as drying proceeded, the fruit matrix became more and more viscous, with a decrease in the molecular mobility, evolving to a plastic behavior, and finally becoming fragile and brittle at very low moisture content. The material became rigid and acquired a considerable mechanical resistance to rupture.

A clear change in the behavior pattern was noted in many physicochemical parameters ( $F_{max}$ ,  $S$ ,  $T_{2CPMG}$ ,  $T_{2FID}$ ) near the monolayer water value, despite the permanence of apple samples in a rubbery state.

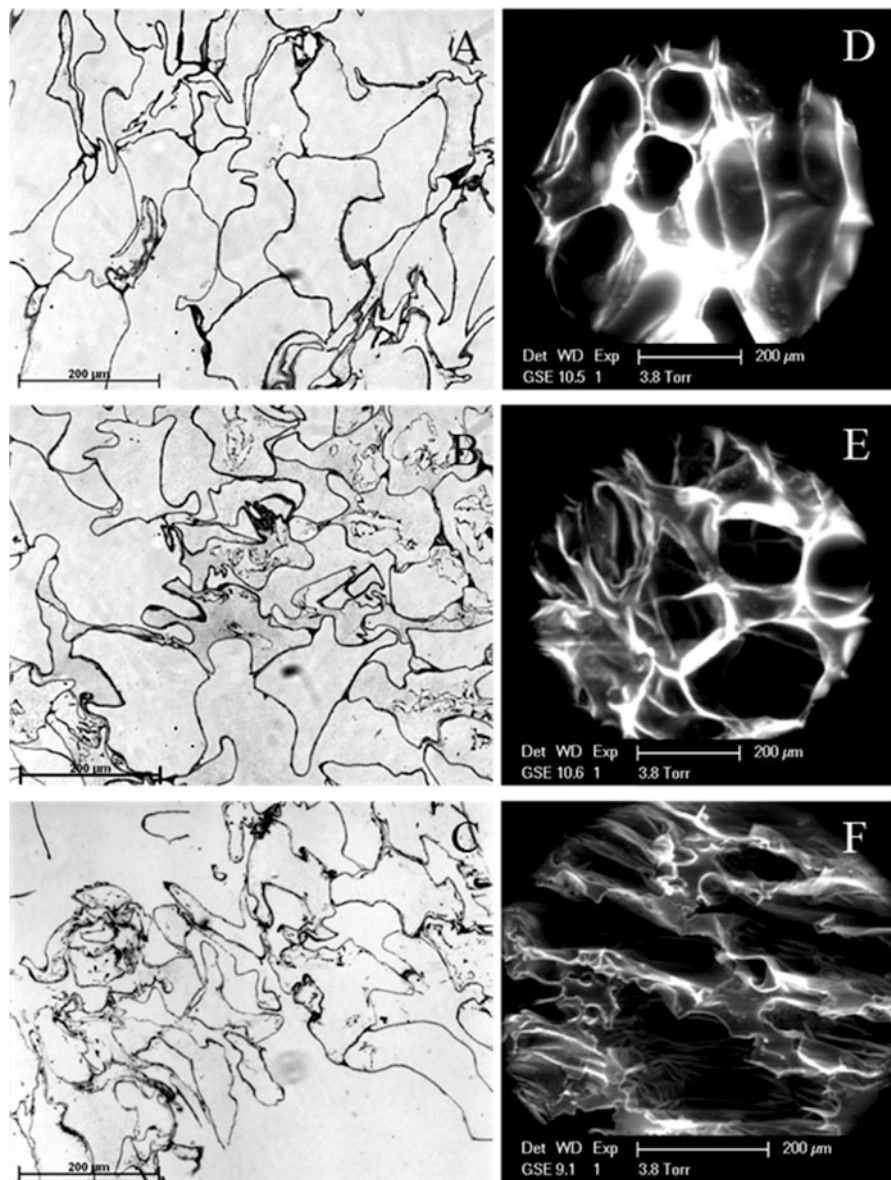


**Fig. 4** Microscopic observations of apple tissue. (a–c) LM; (d–f) ESEM. (a) and (d) fresh tissue; (b) and (e) dried apple at RVP 0.91; (c) and (f) dried apple at RVP 0.30

## References

- Chapman D (1994) The role of water in biomembrane structure. *J Food Eng* 22:376–380
- D'Ambrogio de Argüeso A (1986) Manual de Técnicas en Histología Vegetal. Hemisferio Sur S. A, Buenos Aires, Argentine
- Krokida MK, Karathanos V, Maroulis Z (2000) Compression analysis of dehydrated agricultural product. *Drying Technol* 18:395–408
- Krokida MK, Maroulis Z, Marinou-Kouris D (1998) Viscoelastic behavior of dehydrated carrot and potato. *Drying Technol* 16:687–703
- Lewicki P, Pawlak G (2003) Effect of drying on microstructure of plant tissue. *Drying Technol* 21:657–683
- Lewicki PP, Lukaszuk A (2000) Changes of rheological properties of apple tissue undergoing convective drying. *Drying Technol* 18:707–722
- Rao MA (2003) Phase transitions, food texture and structure. In: Brian M. McKenna (Ed). *Texture in food vol. 1: semi-solid foods*. Woodhead Publishing Ltd., Cambridge, UK, pp 36–62
- Ruan RR, Chen PL (1998) Water in foods and biological material: a nuclear magnetic resonance approach. Technomic Publishing Company, Inc., Lancaster
- Slade L, Levine HA (1991) A food polymers science approach to structure, property relations in food systems. In: Slade L, Levine H (eds) *Water transitions in Foods*. Plenum, New York, pp 29–101
- Snaar JEM, Van As H (1992) Probing water compartments and membrane permeability in plant cells by <sup>1</sup>H-NMR relaxation measurements. *Biophys J* 63:1654–1658

# Defining High and Low Spray Drying Temperatures for *Aloe vera* Gel

I.N. García-Luna, J. Porras-Saavedra, F. Vergara-Balderas,  
J. Welti-Chanes, G.F. Gutiérrez-López, and L. Alamilla-Beltrán

## Abbreviations

ANOVA	Analysis of variance
$a_w$	Water activity
$C_G$	Energy constant relating to the temperature
GAB	Guggenheim-Anderson-De Boer equation
$K_G$	Energy constant relating to the temperature
$\mu$	Media of the analyzed continuous variable
$M$	Moisture content of the powder
$M_o$	Theoretical water content of the monolayer
$T_1$	Input temperatures
$T_2$	Output temperatures
$T_g$	Glass transition temperature
$T_{gm}$	Mix glass transition temperature
$T_{gs}$	Solids glass transition temperature
$T_{gw}$	Water glass transition temperature

---

I.N. García-Luna • J. Porras-Saavedra • G.F. Gutiérrez-López • L. Alamilla-Beltrán (✉)  
Escuela Nacional de Ciencias Biológicas-IPN, Carpio y Plan de Ayala s/n, Col.  
Santo Tomás. Deleg. Miguel Hidalgo. C.P. 11340, México, D.F., Mexico  
e-mail: [liliana.alamilla@gmail.com](mailto:liliana.alamilla@gmail.com)

F. Vergara-Balderas  
Universidad de las Américas (UDLA), Sta. Catarina MÁrtir. Cholula. C.P. 72810,  
Puebla, Puebla, Mexico

J. Welti-Chanes  
Escuela de Ingeniería y Ciencias, Tecnológico de Monterrey, Av. Eugenio  
Garza Sada 2501 Sur, Col. Tecnológico, Monterrey, Nuevo León 64849, México  
e-mail: [jwelti@itesm.mx](mailto:jwelti@itesm.mx)

$X_m$	Water weight fraction
$X_s$	Solids weight fraction
$\sigma$	Standard deviation of the analyzed continuous variable

## 1 Introduction

Spray drying is widely used in the food industry to obtain products in the form of powder (Masters 1991; Filková and Mujumdar 1999; Nijdam and Langrish 2005; Roustapour et al. 2006; León et al. 2010). Three types of modes of contact between drying air and the food product can be found: parallel (co-current), counter-current, or mixed (fountain). The latter is a combination of parallel and counter current flow patterns, which implies that the already dry material comes into contact with drops being sprayed, favoring the formation of agglomerates. In turn, the formation of agglomerates raises the rehydration capacity of the final product (Masters 1991; Vega et al. 2001; Peighambardoust et al. 2011). Although spray drying is a common method used for drying thermolabile materials, there are few reports about the dehydrating conditions used for *Aloe vera* industrial processing. This plant is widely used in the pharmaceutical, cosmetological, and food areas because of the beneficial effects it provides as a functional ingredient in food and cosmetic products (Simal et al. 2000). However, it has been reported that when gel obtained from the *Aloe vera* leaf is subjected to thermal processing, changes in its components and functional properties, such as wettability, water retention, and oil adsorption capacity, among others, can occur (Eshun and He 2004; García et al. 2010). Aloe gel contains 98.5 % water, and the remaining solid material consists of polysaccharides, fat, and water-soluble vitamins, minerals, enzymes, phenolic compounds, and organic acids (Bozzi et al. 2007; Eshun and He 2004; Hamman 2008). Several studies have focused on assessing the physical, chemical and functional changes caused by *Aloe vera* gel processing conditions, especially during dehydration through convective drying (Simal et al. 2000; Femenia et al. 2003; Miranda et al. 2009; García et al. 2010; Gulia et al. 2010). However, to date there is limited data regarding the effect that spray drying temperature has on the physical, calorimetric, and functional characteristics of *Aloe vera*. Therefore, the objective of this study was to evaluate the effect of spray drying temperatures on obtaining *Aloe vera* gel in powder form.

## 2 Materials and Methods

### 2.1 Obtaining *Aloe vera* Powder

*Aloe vera* gel was obtained from the “Flor de *Aloe*” Company (Puebla, México), which was filtered for processing in a Mobile Minor 2000 spray dryer (Gea-Niro, Dinamarca) equipped with a dual fluid nozzle in a source-type arrangement and without any addition of drying aid. The inlet ( $T_1$ ) and outlet ( $T_2$ ) drying-air

temperatures used were 220, 225, and 250 °C and 70, 80, and 90 °C, respectively. The feed stream varied between 1.12 and 1.85 L/h, depending on the desired outlet air temperature when the pressure of the air spray was 1.53 kg cm<sup>-2</sup>. Powder samples were gathered at the cyclone base and stored in sealed containers for further analysis, which was performed three times in every case.

## 2.2 Powder Analysis

The moisture content of *Aloe vera* gel without processing was determined using a thermo gravimetric method, by means of a thermo balance MB 300 (Brainweigh, USA). Moisture content of the powder ( $M$ ) was determined using the vacuum drying oven method according to 920.151 (AOAC 1997).

Water activity ( $a_w$ ) was determined using Aqualab 4TE equipment (Decagon Devices, USA) from 1 g (0.035 oz) of the powder while maintaining a temperature of 24.5 ± 0.1 °C (Fang and Bhandari 2011).

## 2.3 Guggenheim–Anderson–De Boer Equation (GAB)

In order to understand the adsorption process of water by the amorphous powders, the GAB model (van den Berg and Bruins 1981) was applied to the experimental data using the linearized form expressed by Eq. (1):

$$\frac{a_w}{M} = \frac{1}{M_o C_G K_G} + \frac{C_G^{-2}}{M_o C_G} a_w + \frac{K_G(1 - C_G)}{M_o C_G} a_{w^2} \quad (1)$$

where  $M$  is the moisture content (g of water/100 g of dry solid),  $a_w$  is the water activity,  $M_o$  is the theoretical water content of the monolayer, and  $C_G$  and  $K_G$  are energy constants relating to the temperature.

## 2.4 Glass Transition Temperature ( $T_g$ )

Glass transition temperature of the powders was determined by a differential scanning calorimeter (Diamond, Perkin Elmer, USA) using 15 mg of sample powder in 20 µL sealed aluminum capsules and applying a temperature sweep from –20 to 120 °C and a heating rate of 20 °C/min (Ozmen and Langrish 2002). In order to understand the relationship between the glass transition temperature with different solid and moisture content ( $M$ ), the Gordon and Taylor equation was applied (Gordon and Taylor 1952), as expressed by Eq. (2):

$$T_{gm} = \frac{X_s T_{gs} + k X_w T_{gw}}{X_s + k X_w} \quad (2)$$

where  $T_{gm}$ ,  $T_{gs}$ , and  $T_{gw}$  are the mix, solids, and water glass transition temperatures, respectively, expressed in ( $^{\circ}\text{C}$ );  $X_s$  and  $X_m$  are the solids and water weight fractions, respectively; and  $k$  is the Gordon and Taylor constant, which is related to the level of interaction between the system components. The model parameters ( $k$  and  $T_{gs}$ ) of Eq. (2) were estimated using a nonlinear regression analysis where  $T_{gw}$  was  $-135\text{ }^{\circ}\text{C}$  (Sablani et al. 2007; Welti-Chanes et al. 1999).

## 2.5 Statistical Analysis

The statistical significance of data was evaluated using the analysis of variance (ANOVA) analysis with  $\alpha = 0.05$ . The statistical analysis was performed using the statistical program MINITAB, version 15 (Minitab, Inc, USA).

To verify the existence of two or more groups and mathematically differentiating between them, the normal distribution density function was used. Normal distribution is defined as a continuous variable distribution that is specified by two parameters: mean and standard deviation (Eq. 3):

$$f(x) = \frac{1}{\sigma \sqrt{2\pi}} e^{-\frac{1}{2}(\frac{x-\mu}{\sigma})^2} \quad (3)$$

where  $\mu$  is the mean and  $\sigma$  is the standard deviation of the analyzed continuous variable. Densities were obtained for each of the relationships discussed: moisture content, water activity, and glass transition-moisture content.

## 3 Results and Discussion

### 3.1 Moisture Content (M) and Water Activity ( $a_w$ )

$M$  (kg of water/kg of dry solid) of gel powder showed values between 0.01 and 0.03 (kg of water/kg dry solids), with no significant difference found at a level of  $\alpha = 0.05$  for any of the obtained products under the different drying-air temperatures. These values are similar to those previously obtained for various powder products at different drying conditions (mucilage nopal, nopal juice, and acai pulp) (Tono et al. 2008; León et al. 2010).  $a_w$  ranged from 0.18 to 0.30, without a clear relationship between inlet/outlet drying-air temperature effect and  $a_w$ . Similar values of  $a_w$  have been reported for other powder products, such as watermelon (0.20–0.29) (Quck et al. 2007), milk (0.2–0.6) (Laroche et al. 2005), and bayberry

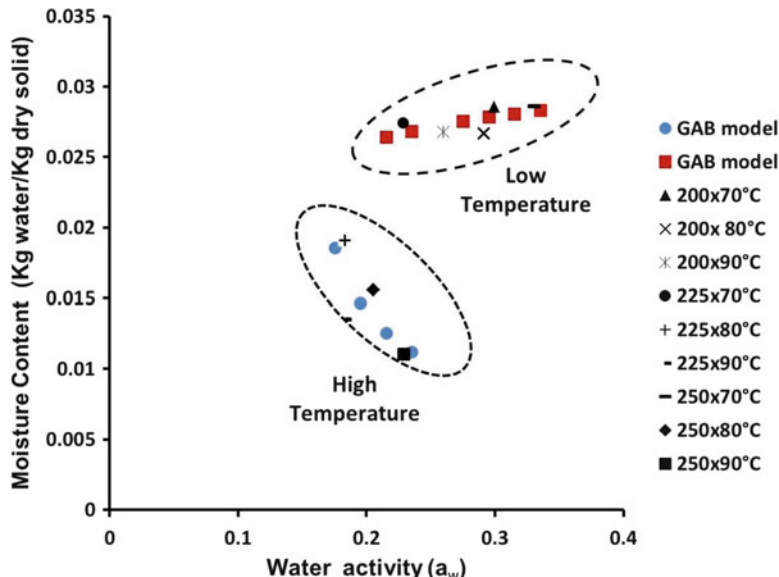


**Fig. 1** Moisture content ( $M$ ) and water activity ( $a_w$ ) in relation to samples obtained at different inlet air temperatures, and moisture adsorption behavior (GAB model) of *Aloe* powders obtained by spray drying

(0.1–0.3) (Fang and Bhandari 2011). For all *Aloe vera* gel powder samples, the existing relation between  $M$  and  $a_w$  is observed in Fig. 1, and the existence of two different data groups is also identified in this figure. In the first group, which was called the low temperature group, samples were assessed using inlet/outlet temperatures of 200/70, 200/80, 200/90, 225/70, and 250/70 °C. These conditions correspond to all cases in which the lower inlet and three outlet temperatures were used, and also to the 225 and 250 °C temperature conditions, in which the lower outlet temperature was used. The second group, denoted as the high temperature group, had the samples with the lowest values of  $M$  and  $a_w$ , and corresponded to the highest inlet/outlet drying-air temperatures (225/80, 225/90, 250/80, and 250/90 °C). When inlet temperatures of 200 °C and any outlet temperature were used, the  $M$  and  $a_w$  values of the products were higher; at 225 and 250 °C inlet temperatures and 70 °C outlet temperature, materials were located within the low temperature drying groups. All conditions were grouped as high temperature.

### 3.2 Analysis of the GAB Equation Adjustment

Applying the GAB model to  $M$  and  $a_w$ , the results showed that they can also be grouped into the low and the high temperature groups (Fig. 1). In the first case, it is possible that drying temperatures causes minor heat damage to the material;

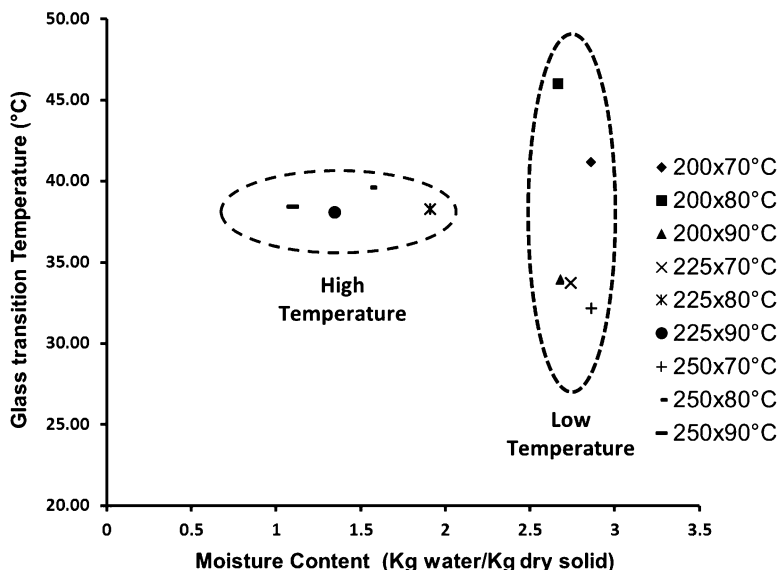


**Fig. 2** Relationship between glass transition temperature ( $T_g$ ) and moisture content ( $M$ ) for *Aloe* gel powders obtained from different drying conditions

therefore, they could belong to the same isotherm, which may indicate that under these drying conditions, the original chemical composition of the material does not change significantly. The opposite could occur in the high temperature group, where the material may present different characteristics from those obtained at low temperatures. Therefore, they would be associated with different hygroscopic properties.

### 3.3 Glass Transition Temperature ( $T_g$ )

Thermograms of product obtained under different drying conditions showed that  $T_g$  ranged from 33 to 45 °C. These values match those reported for other similar material, such as maltodextrins (10–20 DE), where  $T_g$  was reported to be in the range of 45.4–54.7 °C (Cai and Corke 2000). In addition, whole and pulp strawberry had a  $T_g$  of 30 °C and a moisture content of 1.4 % (Moraga et al. 2004). Foster et al. (2006) reported that for lactose–glucose and lactose–fructose mixtures (both with  $a_w = 0.23$ ) a  $T_g$  of 25 °C and 30 °C, respectively, and León et al. (2010) reported that spray dried nopal mucilage powder had a  $T_g$  of 45 °C with 7.2 % moisture. In the literature, there are reports of different glass transition temperatures for different carbohydrates, such as mannose (31 °C), glucose (31 °C), galactose (32 °C), and sucrose (62 °C) (Bhandari and Howes 1999). Figure 2 shows the

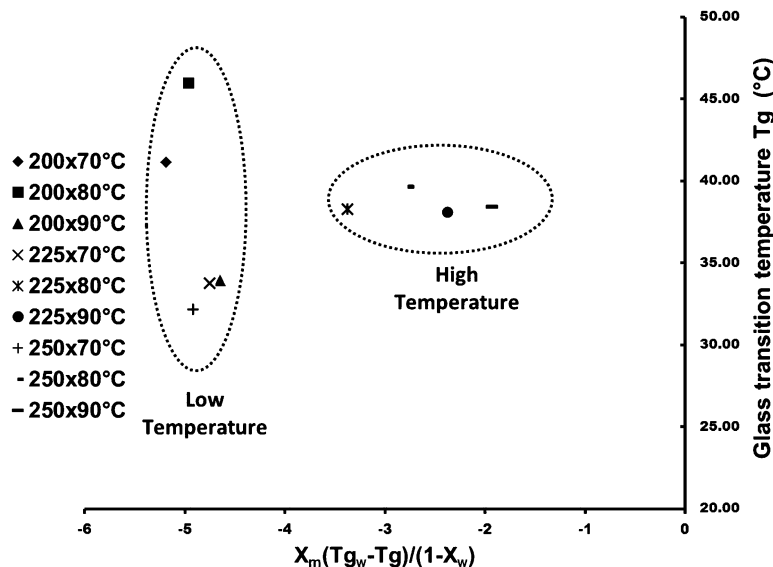


**Fig. 3** Glass transition temperature ( $T_g$ ) variation of *Aloe* gel powder obtained by spray drying according to Gordon and Taylor model

relationship of  $T_g$  and M for the different powders obtained; even though a direct relationship between these properties could not be observed, it was possible to classify all obtained powders into groups identified. It has been suggested that *Aloe* gel powder remains in a vitreous state at room temperature, regardless of the drying-air temperature. Moreover, at higher temperatures and moisture levels, the plasticization effect can increase the loss of powder quality. The results experimentally obtained ( $M$ ,  $a_w$ , and  $T_g$ ) were analyzed using the Gordon and Taylor model (Eq. 2) to determine if exists any correlation between experimental values of water activity and glass transition. The results for all powders obtained at the different drying-air temperatures showed relatively low values of  $a_w$  (0.18–0.33). The interval of water activity at which the samples are located is a narrow section of the values of water activity (0.1–0.9) which should cover the samples, as indicated in the analysis of the model of Gordon and Taylor. In this case, separation of the samples in the high and low temperature groups was also verified (Fig. 3).

## 4 Conclusions

In this study, the *Aloe vera* gel (without drying adjuvant) can be spray dried using an inlet drying-air temperature greater than or equal to 200 °C and the outlet drying-air temperatures from 70 to 90 °C, in a fountain type arrangement. The drying-air

temperatures can be classified into high or low drying temperature groups according to changes in the values of  $M$ ,  $a_w$ , and  $T_g$  properties of the powders obtained, and assessed through the normal distribution density function. The GAB equation and the Gordon–Taylor model are useful tools to identify the effects of the drying-air temperature on the physical properties of dehydrated material, as well as to categorize if a spray drying temperature is low or high.

However, it is important evaluate the prime thermolabile components of the gel, as well as the chemical changes observed, to achieve a better understanding of the relationship of these changes with the hygroscopic properties and transition phases of the powder product.

**Acknowledgements** The authors acknowledge the financial support of research projects: SIP 2011745, 20121173, 20111167, 20121754 and CONACyT 84287, as well as the PIFI-program, COFAA-IPN, Tecnológico de Monterrey and CONACyT for study grants.

## References

- AOAC (1997) Official methods of analysis of AOAC International. Gaithersburg, Maryland
- Bhandari BR, Howes T (1999) Implication of glass transition for the drying and stability of dried foods. *J Food Eng* 40:71–79
- Bozzi A, Perrin C, Austin S, Arce-Vera F (2007) Quality and authenticity of commercial *Aloe vera* powders. *Food Chem* 103:22–30
- Cai YZ, Corke H (2000) Production and properties of spray dried Amaranthus betacyanin pigments. *J Food Sci* 65:1248–1252
- Eshun K, He Q (2004) *Aloe vera*: A valuable ingredient for the food, pharmaceutical and cosmetic industries—a review. *Crit Rev Food Sci Nutr* 44:91–96
- Fang Z, Bhandari B (2011) Effect of spray drying and storage on the stability of bayberry polyphenols. *Food Chem* 129:1139–1147
- Femenia A, García-Pascual P, Simal S, Roselló C (2003) Effects of heat treatment and dehydration on bioactive polysaccharide acemannan and cell wall polymers from *Aloe barbadensis* Miller. *Carbohydr Polym* 51:397–405
- Filková I, Mujumdar AS (1999) Industrial spray drying systems. In: Mujumdar AS (ed) *Handbook of industrial drying*, 3rd edn. CRC, New York
- Foster KD, Bronlund JE, Paterson AHJ (2006) Glass transition related cohesion of amorphous sugar powders. *J Food Eng* 77:997–1006
- García SP, Mognetti C, Bello A, Martínez MJ (2010) Osmotic dehydration of *Aloe vera* (*Aloe barbadensis* Miller). *J Food Eng* 97:154–160
- Gordon M, Taylor JS (1952) Ideal copolymers and the second order transitions of synthetic rubbers. I Noncrystalline copolymers. *J Appl Chem* 2:493–500
- Julia A, Sharma HK, Sarkar BC, Upadhyay A, Shitandi A (2010) Changes in physicochemical and functional properties during convective drying of *Aloe vera* (*Aloe barbadensis*) leaves. *Food Bioprod Process* 88:161–164
- Hamman J (2008) Composition and Applications of *Aloe vera* leaf gel. *Molecules* 13:1599–1616
- Laroche C, Fine F, Gervais P (2005) Water activity affects heat resistance of microorganisms in food powders. *Int J Food Microbiol* 97:307–315
- León MFM, Méndez LLL, Rodríguez RJ (2010) Spray drying of mucilage (*Opuntia ficus-indica*): effects on powder properties and characterization. *Carbohydr Polym* 81:864–870
- Masters K (1991) *Spray drying handbook*. Longman Scientific & Technical, New York

- Miranda M, Maureira H, Rodríguez K, Vega-Gálvez A (2009) Influence of temperature on the drying kinetics, physicochemical properties, and antioxidant capacity of *Aloe vera* (*Aloe barbadensis* Miller) gel. *J Food Eng* 91:297–304
- Moraga G, Martínez-Navarrete N, Chiralt A (2004) Water sorption isotherms and glass transition in strawberries: influence of pretreatment. *J Food Eng* 62:315–321
- Nijdam JJ, Langrish TAG (2005) An investigation of milk powders produced by a laboratory-scale spray dryer. *Dry Technol* 23:1043–1056
- Ozmen L, Langrish TAG (2002) Comparison of glass transition temperature and sticky point temperature for skim milk powder. *Dry Technol* 20:1177–1192
- Peighambardoust SH, Golshan TA, Hesari J (2011) Application of spray drying for preservation of lactic acid starter cultures: a review. *Trends Food Sci Technol* 22:215–224
- Quek Y, King N, Swedlund P (2007) The physicochemical properties of spray-dried watermelon powders. *Chem Eng Process Process Intensif* 46:386–392
- Roustaour QR, Hosseinalipour M, Ghobadian L (2006) An experimental investigation of lime juice drying in a pilot plant spray dryer. *Dry Technol* 24:181–188
- Sablani SS, Kasapis S, Rahman MS (2007) Evaluating water activity and glass transition concepts for food stability. *J Food Eng* 78:266–271
- Simal S, Femenia A, Llull P, Roselló C (2000) Dehydration of *Aloe vera*: Simulation of drying curves and evaluation of functional properties. *J Food Eng* 43:109–114
- Tono RV, Brabet C, Hubinger MD (2008) Influence of process conditions on the physicochemical properties of açai (*Euterpe oleracea* Mart.) powder produced by spray drying. *J Food Eng* 88:411–418
- van den Berg C, Bruins S (1981) Water activity and its estimation in food systems: theoretical aspects. In: Rockland LR, Stewart GF (eds) *Water activity: influence on food quality*. Academic, New York, pp 1–61
- Vega MH, Góngora NMM, Barbosa CGV (2001) Advances in dehydration of foods. *J Food Eng* 49:271–289
- Welti-Chanes J, Guerrero JA, Barcenas ME, Aguilera JM, Vergara F, Barbosa-Canovas GV (1999) Glass transition temperature ( $T_g$ ) and water activity ( $a_w$ ) of dehydrated apple products. *J Food Process Eng* 22:91–101

# Mexican Plum (*Spondias purpurea* L.) Moisture Sorption Properties

J.A. Guerrero-Beltrán, F. Ruiz-Hernández, and J. Welti-Chanes

## Abbreviations

ASE	Average standard error
$a_w$	Water activity
$a_{wexp}$	Experimental water activities
$a_{wpred}$	Predicted water activities
BET	Brunauer-Emmett-Teller
C	Constant of Guggenheim
GAB	Guggenheim-Anderson-De Boer
K	Factor for the multilayer prosperities
MMC	Monolayer moisture contents
Oswin	Oswin equation
TSS	Total soluble solids
W	Moisture content
$W_m$	Monolayer moisture content
$\alpha$	Constant of Guggenheim-Anderson-De Boer equation in polynomial form
$\beta$	Constant of Guggenheim-Anderson-De Boer equation in polynomial form
$\gamma$	Constant of Guggenheim-Anderson-De Boer equation in polynomial form

---

J.A. Guerrero-Beltrán (✉) • F. Ruiz-Hernández

Departamento de Ingeniería Química, Alimentos y Ambiental, Universidad de las Américas  
Puebla, Ex Hacienda Sta. Catarina Mártir, Cholula, Puebla 72820, Mexico

e-mail: [joseangel150@hotmail.com](mailto:joseangel150@hotmail.com)

J. Welti-Chanes

Escuela de Ingeniería y Ciencias, Tecnológico de Monterrey, Av. Eugenio  
Garza Sada 2501 Sur, Col. Tecnológico, Monterrey, Nuevo León 64849, México  
e-mail: [jwelti@itesm.mx](mailto:jwelti@itesm.mx)

## 1 Introduction

Fresh fruits, no matter where they come from, are perishable products due to their high moisture content. Some fruits are protected with an external thick peel or film that allows them to remain fresh for a long time if they are appropriately handled. However, other fruits, even though they have a thick peel, have very short growing periods. This is the case of prickly pear, mamey, litchi, pitaya or pitahaya, black and yellow sapote, and Mexican plum, just to mention a few. Pitaya or pitahaya and Mexican plum possess a delicate peel that may allow the fruit to remain fresh for a very short time, after which the peel can become dry or be broken due to dryness or overripening. All of these fruits grow in Mexico because of the microclimates that exist throughout the country. Therefore, to take advantage of these fruits that last for a short time or because of overproduction, it is necessary to apply or use conventional and/or new processing technologies to deliver new or processed fruit products to domestic and overseas consumers.

One way to increase fruit stability is to remove water by using spray or freeze-drying processes to obtain fruit powders. Fruit powders can be used to prepare blends with other food powders or to prepare other high-moisture-content processed fruit products such as jellies, jams, juices, or nectars. Transportation of fruit powders may reduce cost since water is no longer transported, while approaches such as refrigeration or freezing of fruit products can result in greater expense for transportation. Therefore, obtaining powders may be the best alternative for having fresh fruit products available anytime and anywhere. However, powders may undergo physical and chemical changes if they are not handled appropriately. Fruit powders can show caking due to moisture sorption or crystallize due to modification of the fruit component. Consequently, powders' physical properties may change and affect their functional properties, which in turn may affect the preparation of other fruit products.

Various mathematical methods describe the relationship of moisture content and water activity of dehydrated foods. The moisture sorption data of fruit powders can be analyzed during a number of mathematical models to determine the critical moisture sorption properties. These moisture sorption properties are useful for predicting moisture content at different relative humidities. Also, the critical moisture sorption properties can provide an idea regarding storage conditions at different temperatures and moisture conditions when storing foods in chambers, large packages, or small containers, as well as the packaging materials required for each type of food powder. The Guggenheim-Anderson-De Boer (GAB) (van den Berg and Bruin 1981), Brunauer-Emmett-Teller (BET) (Brunauer et al. 1938), and Oswin (Oswin 1946), among other equations, are mathematical models frequently used for fitting of moisture content vs. water activity experimental data or to obtain the critical moisture sorption properties of foods. The objective of this research was to obtain moisture sorption isotherms and model the experimental data of Mexican plum powder.

## 2 Materials and Methods

### 2.1 Fruit Pulp

Unripe Mexican plums (*Spondias purpurea* L.) were purchased at the Cholula, Puebla, marketplace in January (Fig. 1). Plums were stored at room temperature until achieving edible characteristics; then a purée was obtained using a pulper machine. Purée was analyzed for pH, total soluble solids (TSS), titratable acidity, and moisture content.

### 2.2 Freeze-Drying

Plum purée was poured into Petri dishes and then placed on freeze-dryer (Labconco) chamber trays to be frozen at  $-18^{\circ}\text{C}$  during the night. The frozen pulp was then freeze-dried at  $25^{\circ}\text{C}$  and  $10\text{ }\mu\text{mHg}$  for 24–48 h.

### 2.3 Moisture Sorption Isotherms

The gravimetric static method, with discontinuous registration of weight changes, was used for measuring the change in weight of powder. Plum powder was placed



**Fig. 1** Mexican plum (*Spondias purpurea* L.) fruit

in a vacuum desiccator containing  $P_2O_5$  as the desiccant material. Powder was allowed to stand at room temperature, until it was completely dry. An amount of powder of about 100–150 mg was weighed into weighing bottles and placed in chambers containing oversaturated salts of lithium chloride, potassium acetate, magnesium chloride, potassium carbonate, magnesium nitrate, sodium bromide, strontium chloride, sodium chloride, potassium chloride, barium chloride, and potassium sulfate to create water activity environments of 0.111, 0.252, 0.325, 0.434, 0.524, 0.559, 0.691, 0.753, 0.836, 0.901, and 0.974, respectively (López-Malo et al. 1994). Chambers were sealed and placed in ovens at temperatures of 21, 32, and  $40 \pm 2$  °C until powder reached equilibrium in moisture content. The final equilibrium in moisture absorption was obtained when the difference in weight of powders was approximately  $\pm 0.0010$  g.

## 2.4 Modeling

The moisture sorption data were fitted using the GAB, BET, and Oswin models to determine the critical moisture sorption properties of the fruit powder.

Brunauer-Emmett-Teller (BET) model (Brunauer et al. 1938) equation is useful within the range 0.11–0.45 of water activity. A straight line is obtained from the relationship shown below:

$$\frac{a_w}{(1 - a_w)W} = \left( \frac{C - 1}{W_m C} \right) a_w + \frac{1}{W_m C}$$

where  $a_w$  is water activity,  $W$  is moisture content (gH<sub>2</sub>O/100 g d.s.),  $W_m$  is the monolayer moisture content (gH<sub>2</sub>O/100 g d.s.), and  $C$  is a constant related with the net sorption heat.

Guggenheim-Anderson-De Boer (GAB) model (van den Berg and Bruin 1981) is useful within the 0–0.95 water activity range:

$$m = \frac{m_o C K a_w}{(1 - K a_w)(1 - K a_w + C K a_w)}$$

where  $a_w$  is water activity,  $m$  is moisture content (gH<sub>2</sub>O/100 g d.s.),  $m_o$  is the monolayer moisture content (gH<sub>2</sub>O/100 g d.s.),  $C$  is the constant of Guggenheim, and  $K$  is a factor for the multilayer prosperities. In polynomial form,

$$\frac{a_w}{m} = \alpha(a_w)^2 + \beta(a_w) + \gamma$$

where  $\alpha$ ,  $\beta$ , and  $\gamma$  are constants (100 g d.s./gH<sub>2</sub>O).

Oswin model (Oswin 1946) can be useful for the entire water activity range:

$$W = a \left[ \frac{a_w}{(1 - a_w)} \right]^n$$

where  $a_w$  is water activity,  $W$  is moisture content (gH<sub>2</sub>O/100 g d.s.), and  $a$ ,  $n$  are constants.

Average standard error (ASE) can be used to see the fitting goodness of a specific model:

$$\text{ASE} = \frac{1}{n} \sum_{i=1}^n \text{abs} \left[ \frac{a_{w\text{pred}} - a_{w\text{exp}}}{1 - a_{w\text{exp}}} \right] \times 100$$

where  $a_{w\text{pred}}$  and  $a_{w\text{exp}}$  are the predicted and experimental water activities, respectively.

### 3 Results and Discussion

#### 3.1 Plum Physicochemical Characteristics

The ripe Mexican plums had an orange-/yellow-colored peel. This type of fruit has a large stone, weighing as much as  $25 \pm 2$  % of the whole fruit. The amounts of purée and peel were  $60.6 \pm 3$  and  $14.0 \pm 1$  %, respectively. This type of plum is a nonacid fruit (pH 4.03; acidity of  $0.36 \pm 0.01$  % citric acid), with very high content of total soluble solids ( $21.13 \pm 0.12$  %) and moisture content of  $77.93 \pm 0.43$  %.

#### 3.2 Moisture Sorption Isotherms

Sorption isotherms of type II (BET classification) were obtained for the Mexican plum powder at the three selected temperatures (Fig. 2). This type of behavior is common in fruits with high sugar content. In general, the sugar content in plum consists of fructose, glucose, and sucrose. These soluble solids are the main chemical products that contribute to suppress the water activity of the plum powder.

#### 3.3 Moisture Sorption Modeling

BET Model (0–0.45  $a_w$ ). Table 1 shows the BET moisture sorption characteristics of Mexican plum powder. The monolayer moisture content decreases as temperature increases; this value was not higher than 5.39 g H<sub>2</sub>O/100 g d.s. presented at 21 °C. Low monolayer moistures are due to the high content of sugars (96 %) in powders.

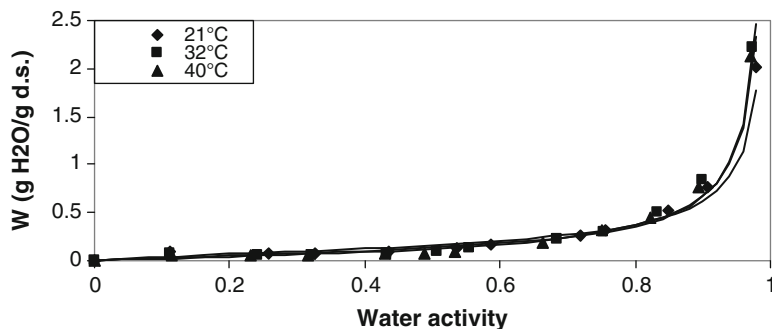


**Fig. 2** Oswin modeling of the sorption properties of *Spondias purpurea* L. powder

**Table 1** Moisture sorption characteristics of *Spondias purpurea* powder using the BET<sup>a</sup> model

Temp. (°C)	<i>m</i> (g H <sub>2</sub> O/g d.s.)	<i>b</i> (g d.s./g H <sub>2</sub> O)	<i>R</i> <sup>2</sup>	<i>C</i>	<i>W<sub>m</sub></i> (g H <sub>2</sub> O/100 g d.s.)	<i>a<sub>wm</sub></i>
21	18.84	-0.301	0.993	-61.7	5.39	-
32	24.09	-0.024	0.962	-1019.7	4.15	-
40	23.72	0.233	0.964	102.8	4.17	0.0897

<sup>a</sup>*a<sub>w</sub>* 0.11–0.45; *m*, slope; *b*, intercept; *R*<sup>2</sup>, correlation coefficient; *C* is a constant related with the net sorption heat; *W<sub>m</sub>* is the monolayer moisture content; *a<sub>wm</sub>* is the monolayer water activity

**Table 2** Coefficients of the second-order representation of the GAB model for moisture sorption characteristics of *Spondias purpurea* powder

Temp. (°C)	$\alpha$	$\beta$	$\gamma$	$R^2$
21	-16.430	16.027	0.0727	0.945
32	-21.225	19.643	0.4621	0.866
40	-23.968	22.089	0.4630	0.884

$\alpha$ ,  $\beta$ , and  $\gamma$  are constants;  $R^2$  is the correlation coefficient

**GAB Model.** Table 2 shows the second-order polynomial coefficients of the GAB model used to determine moisture sorption properties of *Spondias purpurea*. GAB monolayer moisture contents (MMC) were calculated; those values decreased as temperature increased. MMC are similar to those obtained using the BET model (Table 1). Average standard errors are presented in Table 3; the lower standard error (7.87 %) was obtained from the moisture sorption data obtained at 40 °C. However, the GAB model fit experimental data in a better way in the water activity range of 0–0.7.

**Oswin Model.** Table 4 depicts the Oswin parameters for the moisture sorption properties of Mexican plum powder (Fig. 2). The correlation coefficients obtained with this model were higher than those obtained with the GAB model (Table 3). Consequently, the average standard errors (ASE) were smaller than that of the GAB

**Table 3** Moisture sorption characteristics of *Spondias purpurea* powder using the GAB<sup>a</sup> model

Temp. (°C)	K	$m_o$ (g H <sub>2</sub> O/100 g d.s.)	C	$R^2$	ASE <sup>b</sup> (%)
21	1.02	6.18	218.04	0.945	33.76
32	1.054	4.85	42.31	0.866	38.21
40	1.061	4.33	46.94	0.884	7.87

<sup>a</sup> $a_w$  up to 0.97; K, factor of correction for multilayer properties;  $m_o$ , monolayer moisture content; C, constant of Guggenheim;  $R^2$ , correlation coefficient; <sup>b</sup> $a_w$  up to 0.90

**Table 4** Moisture sorption characteristics of Mexican plum powder using the Oswin<sup>a</sup> model

Temp. (°C)	n	ln a	a	$R^2$	ASE <sup>a</sup> (%)
21	0.62	-1.837	0.1592	0.931	13.67
32	0.734	-2.014	0.1334	0.923	12.94
40	0.774	-2.11	0.1213	0.939	12.81

<sup>a</sup> $a_w$  up to 0.977; n, slope; ln a = intercept; a, constant;  $R^2$ , correlation coefficient

model. These ASE values are still large to adequately fit the experimental sorption moisture data. However, this fitting is better than that obtained with the GAB model, since it was obtained from the whole water activity range (0–0.970).

## 4 Conclusions

Type II isotherms were obtained using the gravimetric static method with discontinuous registration of weight changes for Mexican plum powders. The monolayer moisture content, obtained using the BET or GAB model, was in the range 6.18–4.17 g H<sub>2</sub>O/100 g d.s. The average standard error, obtained using the GAB or Oswin fitting, was in the range 7.87–33.76. However, the Oswin model better fit the moisture sorption experimental data of Mexican plum powders.

## References

- Brunauer S, Emmett PH, Teller E (1938) Adsorption of gases in multimolecular layers. J Am Chem Soc 60:309–319
- López-Malo A, Palou E, Argaiz A (1994) Measurement of water activity of saturated salt solutions at various temperatures. In: Argaiz, A. López-Malo, E. Palou, and P. Corte (Eds). Proceedings of the poster session, ISOPOW Practicum II. A. Depto. Ingeniería Química y Alimentos. Universidad de las Américas-Puebla, Cholula, Puebla, México, pp 113–116
- Oswin CR (1946) The kinetics of package life. III. The isotherm. J Soc Chem Ind 65:419–421
- van den Berg C, Bruin S (1981) Water activity and its estimation in food systems: theoretical aspects. In: Rockland LB, Stewart GF (eds) Water activity: influences on food quality. Academic, New York, pp 1–61

# **Antioxidant Activity of Microencapsulated *Capsicum annuum* Oily Extract Obtained by Spray Drying**

**A.Y. Guadarrama-Lezama, L. Alamilla-Beltrán, E. Parada-Arias,  
M.E. Jaramillo-Flores, G.F. Gutiérrez-López, and L. Dorantes-Álvarez**

## **Abbreviations**

ABTS	2,2-Azinobis-(3-ethylbenzothiazoline-6-sulfonic acid)
Ast <sub>0</sub>	Absorbance of sample at initial time
Ast <sub>f</sub>	Absorbance of sample at final time
GA	Gum arabic
MDX	Maltodextrin
O/W	Oil-in-water emulsion was prepared
OEC	Oily extract of chile
SD	Standard deviation
SEM	Scanning electron microscopy
Trolox	6-Hydroxy-2,5,7,8-tetramethylchroman-2-carboxylic acid

## **1 Introduction**

There is great interest today in development of food additives obtained from vegetables and fruits, due to the presence of phytochemicals and the potential use of these substances as functional ingredients. Chiles are used in the manufacture of condiments and food formulations because of their pigmentation and flavor. In addition to its provitamin and antimicrobial properties (Acero-Ortega et al. 2005), Capsicum has shown antioxidant activity because of its content of polyphenolic

---

A.Y. Guadarrama-Lezama • L. Alamilla-Beltrán • E. Parada-Arias • M.E. Jaramillo-Flores  
G.F. Gutiérrez-López • L. Dorantes-Álvarez (✉)  
Departamento de Graduados e Investigación en Alimentos, Escuela Nacional de Ciencias  
Biológicas, Instituto Politécnico Nacional, Carpio y Plan de Ayala,  
s/n CP, 11340 México D.F., Mexico  
e-mail: [lidiadorantesa@gmail.com](mailto:lidiadorantesa@gmail.com)

compounds and carotenoids. Carotenoid consumption has been associated with a lower risk of developing chronic degenerative diseases (Matsuji et al. 1998; Dutta et al. 2005). In some studies, certain carotenoids were identified in the fruits of dry chile (*Capsicum annuum* L. grosum Sendt), such as  $\beta$ -carotene,  $\alpha$ -carotene,  $\beta$ -cryptoxanthin, zeaxanthin, lutein, capsanthin, capsorubin, and criptocapsina (Collera-Zúñiga et al. 2005). Carotenoids can be extracted from chile's natural matrix in order to use their properties as phytochemicals; however, due to the unsaturated nature of chile's molecular structure, once carotenoids are extracted, they can be modified by isomerization and subsequent oxidative degradation, resulting in the loss of antioxidant activity with formation of fractions carotenoids called apocarotenoids (Maoka et al. 2001).

One possible way to delay degradation reactions of carotenoids contained in *Capsicum* extracts is through microencapsulation by spray drying. The encapsulation process has been reported as an effective technique that allows the protection of food ingredients against chemical degradation by environmental factors (McNamee et al. 1998). In the spray-drying process, microcapsules are obtained in powder form or agglomerated with enhanced shelf life due to reduction of water activity. Biopolymer membranes that form the walls of the microcapsules are semipermeable, determining both the release behavior of the material and the morphology of the microcapsules (Shahidi and Han 1993). Morphological changes and size of particles during the encapsulation process are related with moisture content and drying temperature, as described by Alamilla-Beltrán et al. (2005). Most spray-dried particles have roughness that can be corroborated by scanning electron microscopy (SEM). In order to monitor changes in terms of shrinkage, shape, surface, and volume of these particles, the morphology of the microcapsules can be correlated with the functional properties of the encapsulated bioactive compounds contained in an oily extract. The aim of this study was to obtain an oily extract of *Capsicum* and evaluate its antioxidant activity retention when microencapsulated by spray drying.

## 2 Materials and Methods

### 2.1 Materials

Dried chile (*Capsicum annuum* L. grossum Sendt) was used for this work. Edible vegetable corn oil was purchased from a local market in Mexico City, Mexico. The wall materials used for microencapsulation were gum arabic, food grade E414 (Distribuidora Química LEFE S.A. de C.V., Mexico City, Mexico), and maltodextrin 20 DE (CPI Ingredientes S.A. de C.V., State of Mexico, Mexico). Potassium persulfate ( $K_2S_2O_8$ ) and 2,2-azinobis-(3-ethylbenzothiazoline-6-sulfonic acid) (ABTS) radical were purchased from Sigma Chemical Company, St. Louis, MO, USA. The water used in the experiments was doubly distilled.

## 2.2 Extract Preparation

Dried chiles were manually cleaned by removing all foreign matter and then cut into small squares. Next, 50 g of chile was mixed with 250 mL of corn oil heated to 70 °C at 5,500 rpm and extracted in a Thermomix (TM31, Vorwerk, España) until a homogeneous mixture was obtained. The extract of chile was filtered in order to separate solids and to obtain an oily extract of chile (OEC).

## 2.3 Determination of Antioxidant Activity by the Method of Radical ABTS<sup>+</sup> in Oily Extract

The antioxidant activity of *Capsicum* extract was evaluated by studying its ability to bleach the 2,2-azinobis-(3-ethylbenzothiazoline-6-sulfonic acid) radical (ABTS<sup>+</sup>). The ABTS<sup>+</sup> was prepared by the reaction of ABTS solution ( $3.84 \times 10^{-2}$  g) with  $6.6 \times 10^{-3}$  g potassium persulfate (K<sub>2</sub>S<sub>2</sub>O<sub>8</sub>) (both solutions were prepared in 10 mL of bi-distilled water). The solution was stored for 12–16 h in the dark and at 10 °C (solution A). 0.5 mL of solution A was put in anhydrous ethanol solution, until it completed 50 mL, and it was adjusted to 0.7 ± 0.02 absorbance in a spectrophotometer (Genesys 10UV Scanning Thermo Spectronic) at 734 nm to determine antioxidant activity of the extracts. 200 µL oily extract was diluted with 800 µL acetone (Fermont, México) from this extract; 10 µL was taken to react with 990 µL of ABTS<sup>+</sup> radical. The absorbance at 734 nm was taken at 20 °C, exactly 1 min after initial mixing. The percent of inhibition was calculated as follows:

$$\% \text{Inhibition} = \frac{(A_{st_0} - A_{st_f})}{(A_{st_0}) - \left[ \frac{A_{dt_0} - A_{dt_f}}{A_{dt_0}} \right]} \times 100 \quad (1)$$

where

A<sub>st<sub>0</sub></sub> and A<sub>st<sub>f</sub></sub>: Absorbance of sample at initial and final times

A<sub>dt<sub>0</sub></sub> and A<sub>dt<sub>f</sub></sub>: Absorbance of dissolvent at initial and final times

A standard curve was constructed using different concentrations of Trolox (6-hydroxy-2,5,7,8-tetramethylchroman-2-carboxylic acid; Sigma Chemical Company, St. Louis, MO, USA). All measurements were performed in triplicate, and the average ± standard deviation (SD) was reported. In all cases, the effect of acetone and initial values of antioxidant activity of oil were determined.

## 2.4 Preparation of the Oil-in-Water Emulsions and Spray Drying

Oil-in-water emulsion was prepared (O/W) using, as wall materials, gum arabic (GA) and maltodextrin (MDX) 20 DE (dextrose equivalent) in a 1:1 ratio. The biopolymers were dissolved in warm water (35 °C) with manual stirring to facilitate the process of dissolution. The solution was stored for 24 h in order to achieve complete rehydration of polymers. Oily extract of *Capsicum* (2 %) was added drop by drop to the water polymeric solution, while homogenization in a Polytron (Kinematica PT200D Type Luzern-Switzerland) was carried out by 3 min. In the preparation of emulsions, an ice bath was used to maintain the temperature below 30 °C (Koberstein-Hadja and Dickinson 1996) and avoid instability in the system. Subsequently, the emulsion was fed by a peristaltic pump (Watson-Marlow 520S) with a feed flow of 16 mL/min to a spray dryer (Mobile Minor™ 2000, Niro, Denmark). A two-fluid pneumatic nozzle atomizer was used in fountain flow. The inlet and outlet drying air temperatures used for the microencapsulation were  $200 \pm 2$  °C and  $90 \pm 2$  °C, respectively.

## 2.5 Antioxidant Activity of Oily Extract Nonencapsulated in Microcapsules

To determine the antioxidant activity of nonencapsulated extract, 2 g of microcapsules was placed in a flask and 40 mL of hexane was added, and the mixture was stirred with a magnetic bar for 20 min. After the extraction time required, the powder and dissolvent were separated by filtration with Whatman No.1; the solution containing the oily extract of chile was transferred to a round bottom flask of 50 mL, and then the oily extract was separated from the dissolvent by evaporation in a rotary evaporator (Buchi Rotavapor® RVacuum-210/R-215) at 69 °C (boiling point of hexane). The amount of chile oily extract was calculated gravimetrically by weight difference between the initial weight of the clean flask and the weight of the flask with the extract residue. The antioxidant activity of oily extract was determined.

To determine antioxidant activity of the encapsulated extract, the biopolymer was first separated by dissolution with water (2 mL), adding 10 mL of acetone and centrifuging at 3,700 rpm for 15 min. The supernatant containing the oily extract with acetone was evaporated and gravimetrically quantified, and antioxidant activity was determined as 2.3.

## 2.6 Evaluation of Water Activity and Moisture Content of Microencapsulated OEC

The water activity of the microcapsules was determined using an AquaLab (Decagon Devices, Model 4 TE, USA) at 25 °C. Moisture content of the microcapsules was determined gravimetrically using official AOAC method (AOAC 1995).

## 2.7 Morphology of Microcapsules by Scanning Electron Microscopy (SEM)

The morphology and appearance of surface microcapsules was examined by SEM (Jeol, Model JSM-5800LV, Japan). Microcapsules were put in a metal die, which had a two-sided adhesive carbon tape attached to it (Ted Pella, Redding, CA, USA). The samples were then coated with gold ions (Rosenberg and Young 1993) using a sputter coater (Denton Vacuum Model Desk II). Microcapsules were observed at an accelerating voltage of 15 kV.

## 3 Results and Discussion

### 3.1 Antioxidant Activity in Oily Extract and Encapsulated

Antioxidant activity in oily extract was  $32.30 \pm 2.0$  µmol Trolox/mL. For this work, nonencapsulated extract is defined as that portion of lipid material that remains on the surface of microcapsules. The antioxidant activity of nonencapsulated chile oily extract was less than 10 µmol Trolox/mL, while the antioxidant activity of oily extract contained in 2 g of microcapsules was  $29.45 \pm 2.1$  µmol Trolox/mL. In all cases, the content of oily extract encapsulated was higher than the extract nonencapsulated, giving a percent of encapsulated oil of 60 %, which may be improved by optimizing the homogenization process as well as modifying the drying conditions during the microencapsulation process.

The results showed that the microencapsulation process by spray drying does not degrade the carotenoids present in the oily extract. The antioxidant activity was preserved in 91.17 % of the oily extract, probably because the evaporation of water is so fast that the sprayed droplet is kept cold until reaching the state of drying due to absorption of heat in the vaporization of the liquid (Gharsallaoui et al. 2007). So the extract encapsulated in biopolymers has no direct contact with the drying air and the contact is very short; therefore, the temperature that would be reached by the emulsion droplet corresponds to the wet bulb temperature (~40 °C). The presence of nonencapsulated oil in the microcapsules may be attributed to the use of inlet and outlet temperatures above 210/90 °C during the spray-drying process; in both

conditions, the formation of pores or fractures in surface microcapsules have been reported (Bhandari et al. 1992). Also, the homogenization process may have an influence on the presence of nonencapsulated oil, although the antioxidant activity of the extracts was not affected.

### **3.2 Water Activity and Moisture Content of Encapsulates**

Both water activity and moisture content are considered as quality parameters that characterize the powdered food. These parameters are important to help prevent spoilage reactions. The effect of water activity in foods and their interaction with components have been studied. Some authors have considered the value of the monolayer (0.2–0.3 water activity) as the range of maximum stability of dehydrated products, and this effect is related to the reduced mobility of water in the monolayer, in which water is tightly bound and cannot act as a reaction medium. It is considered that at these values of water activity, food powders are stable. The microcapsules containing oily extract showed a 0.22 water activity and 5 % of moisture content; therefore, at this value, degradation reactions are not present, favoring the preservation of carotenoids contained in capsicum extract.

The moisture content on physical changes of the biopolymer matrix used to encapsulate the oily extract may affect the distribution of oil, allowing the accessibility of oxygen to the oil phase, accelerating the degradation process. It is therefore important to keep the moisture content at a low level as well as the water activity of the microencapsulated oil to avoid any degradation process.

### **3.3 Morphology of Microcapsules by Scanning Electron Microscopy (SEM)**

By using scanning electron microscopy, it was possible to see that the capsules showed an irregular geometry, typical of spray-dried materials; large and deep dents can be seen (Fig. 1a), while other dents are small and relatively shallow (Fig. 1b), small particles that can occupy spaces between large particles are also present (Fig. 1c), which may affect rehydration or flow properties. Presence of fractures in the capsule was not observed, and this fact is important for preserving the antioxidant activity of the capsicum extract.

Capsules formed have an elastic and enveloping external film, which is due to the presence of protein contained in the structure of gum arabic (Yadav et al. 2007), helping to avoid the presence of superficial fractures. The oxidative process also is avoided using maltodextrin as wall material (Buffo and Reineccius 2000). Non-homogeneity in the surface of the particles may be undesirable in terms of retention of microencapsulated extract; however, it is noteworthy that the wetting and rehydration times are closely related to the external topography of the

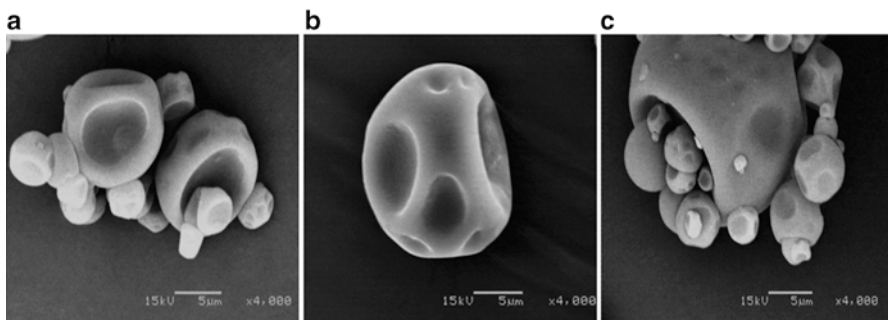


**Fig. 1** Scanning electron microscopy (SEM) micrographs of the microcapsules obtained. Particles with large and deep dents can be seen (a), while others dents are small and relatively shallow (b). Small particles that can occupy spaces between large particles were also present (c)

microcapsules. Water penetration is better in areas that have defects, which facilitates its adsorption at specific sites (Pérez-Alonso et al. 2009).

Any change in the physical state of a product has the potential to affect the characteristics of the ingredients of the product. Therefore, morphology is an important feature to be considered in microencapsulation processes, as it is related to the moisture content, temperature, and water activity in which they are stored and with preservation of the antioxidant activity of the *Capsicum* extract.

The above result indicates that the carotenoids from Capsicum could be an alternative source for use as natural antioxidants and can be used in the formulation of functional food products.

## 4 Conclusions

Chile oily extract with antioxidant activity was encapsulated, maintaining its antioxidant capacity. The value of water activity (0.20) of the encapsulated extract is considered to be in a high stability range for dehydrated products. Chile can be encapsulated as a natural source of antioxidants and may be incorporated in functional foods.

**Acknowledgements** The authors thank the financial support for this research from the National Polytechnic Institute through SIP project 20121026 and 20121754 and the PIFI program as well as from the Institute of Science and Technology of Mexico City's Government (ICYTDF), through the project PICS08-15.

## References

- Acero-Ortega C, Dorantes L, Hernández-Sánchez H, Tapia MS, Gutiérrez-López G, Alzamora S, López-Malo A (2005) Response surface analysis of the effects of *Capsicum* extract, temperature and pH on the growth and inactivation of *Listeria monocytogenes*. J Food Eng 67:247–252

- Alamilla-Beltrán L, Chanona-Pérez JJ, Jiménez-Aparicio AR, Gutiérrez-López GF (2005) Description of morphological changes of particles along spray drying. *J Food Eng* 67:179–184
- AOAC (1995) Association of Official Analytical Chemists International. AOAC, Arlington, VA
- Bhandari BR, Dumoulin ED, Richard HMJ, Noleau RI, Lebert AM (1992) Flavor encapsulation by spray-drying: application to citral and linalyl acetate. *J Food Sci* 57(1):217–221
- Buffo R, Reineccius GA (2000) Optimization of gum acacia/modified starches/maltodextrin blends for the spray drying of flavours. *\*\*Perfumer Flavorist* 25:37–49
- Collera-Zúñiga O, García FJ, Meléndez RG (2005) Comparative study of carotenoid composition in three Mexican varieties of *Capsicum annuum* L. *Food Chem* 90:109–114
- Dutta D, Chaudhuri UR, Chakraborty R (2005) Structure, health benefits, antioxidant property and processing and storage of carotenoids. *Afr J Biotechnol* 4(13):1510–1520
- Gharsallaoui A, Roudaut G, Chambón O, Voilley A, Saurel R (2007) Applications of spray-drying in microencapsulation of food ingredients: an overview. *Food Res Int* 40:1107–1121
- Koberstein-Hadja A, Dickinson E (1996) Stability of water in oil in water emulsions containing faba bean proteins. *Food Hydrocoll* 10:251–254
- Maoka T, Fujiwara Y, Hashimoto K, Akimoto N (2001) Isolation of a series of apocarotenoids from the fruits of the red paprika *Capsicum annuum* L. *J Agric Food Chem* 49:1601–1606
- Matsufuji H, Nakamuro H, Chino M, Mitsuhashi T (1998) Antioxidant activity of capsanthin and the fatty acids esters in paprika (*Capsicum annuum*). *J Agric Food Chem* 46:3462–3472
- McNamee BF, O'Riordan ED, O'Sullivan M (1998) Emulsification and microencapsulation properties of gum Arabic. *J Agric Food Chem* 46:4551–4555
- Pérez-Alonso C, Fabela-Morón MF, Guadarrama-Lezama AY, Barrera-Pichardo JF, Alamilla-Beltrán L, Rodríguez-Huezo ME (2009) Interrelationship between the structural features and rehydration properties of spray dried manzano chilli sauce microcapsules. *Rev Mex Ing Quím* 8(2):187–196
- Rosenberg M, Young SL (1993) Whey protein as microencapsulating agents: microencapsulation of anhydrous milk fat-structure evaluation. *Food Struct* 12:31–41
- Shahidi F, Han X (1993) Encapsulation of food ingredients. *Crit Rev Food Sci Nutr* 33(6):501–507
- Yadav MP, Igartuburu JM, Yan Y, Nothnagel EA (2007) Chemical investigation of the structural basis of the emulsifying activity of gum arabic. *Food Hydrocoll* 21(2):297–308

# **Physical–Chemical Properties and Microstructure of Agave Powders Obtained by Spray Drying**

**M.F. Fabela-Morón, J. Porras-Saavedra, R. Martínez-Velarde,  
A. Jiménez-Aparicio, M.L. Arenas-Ocampo, and L. Alamilla-Beltrán**

## **Abbreviations**

ANOVA	Analysis of variance
Df	Fractal dimension
FDc	Fractal dimension of contour
FDt	Fractal dimension of texture
FOS	Fructooligosacharides
SDBC	Shifting differential box-counting method
SEM	Scanning electron microscopy
$T_{\text{inlet}}/T_{\text{outlet}}$	Inlet and outlet temperature

---

M.F. Fabela-Morón

Departamento de Graduados e Investigación en Alimentos, Escuela Nacional de Ciencias Biológicas, Instituto Politécnico Nacional, Carpio y Plan de Ayala s/n. Col. Santo Tomás. Deleg Miguel Hidalgo, 11340 México D.F., Mexico

Centro de Desarrollo de Productos Bióticos, Instituto Politécnico Nacional, Carretera Yautepec-Joxtla, Km. 6, calle CEPROBI No. 8, Col. San Isidro, Apartado Postal 24, 62731 Yautepec, Morelos, Mexico

J. Porras-Saavedra • L. Alamilla-Beltrán (✉)

Departamento de Graduados e Investigación en Alimentos, Escuela Nacional de Ciencias Biológicas, Instituto Politécnico Nacional, Carpio y Plan de Ayala s/n. Col. Santo Tomás. Deleg Miguel Hidalgo, 11340 México D.F., Mexico

e-mail: [liliana.alamilla@gmail.com](mailto:liliana.alamilla@gmail.com)

R. Martínez-Velarde • A. Jiménez-Aparicio • M.L. Arenas-Ocampo

Centro de Desarrollo de Productos Bióticos, Instituto Politécnico Nacional, Carretera Yautepec-Joxtla, Km. 6, calle CEPROBI No. 8, Col. San Isidro, Apartado Postal 24, 62731 Yautepec, Morelos, Mexico

## 1 Introduction

In Mexico, the *Agave* plant is an important economic and cultural resource, representing great native biodiversity due to the taxonomic diversity of the species within its territory, such as the *Agave angustifolia* Haw. Agave plants contain sugars and fructooligosacharides (FOS) as reserve polymers with special characteristics that allow diversification of its use in foods (García-Mendoza 2002; Madrigal and Sangronis 2007).

Dehydration by spray drying is an efficient method of conservation that allows the obtaining of stable products with low moisture content. Spray drying is a widely used process for the manufacture of powders, which satisfy a vast array of societal demands in the areas of foods, nutrition, health, and medicine. This technique offers short contact of the fed product with the drying air, with minimal damage on original properties of the processed material (Rodríguez-Hernández et al. 2005; Chen et al. 2011).

Food powders are classified into different categories according to their properties during processing. The characteristics of food powders depend on different aspects such as physicochemical and thermodynamically properties, chemical composition of materials, obtaining conditions, moisture content, water activity, and morphology and microstructure of particles. All of these aspects have an effect on the final quality of food, since they are important in determining the handling, processing, storage conditions, and functionality of food products. However, scientific and technical descriptions of food powder properties remain incomplete. Traditionally, the properties of food powders have been described by using parameters of the bulk powders, since it is important to consider other parameters as microstructure and its relation with processing conditions to describe and characterize the powders (Jha et al. 2002; Alamilla-Beltrán et al. 2005; Barbosa-Cánovas et al. 2005; León-Martínez et al. 2010).

In this sense, irregular surfaces and textures of food powders have successfully been characterized through fractal analysis. Quantification of the irregularity of the contours and surfaces of food materials can be determined by evaluation of their fractal dimension ( $D_f$ ) by extracting structural and microstructural features from images, which can aid in the evaluation of descriptors in a numerical form (Quintanilla-Carvajal et al. 2011). The aim of this work was to study the effect of operation conditions on physical-chemical properties and microstructure of agave powders obtained by spray drying.

## 2 Materials and Methods

### 2.1 Material Preparation

The raw material, agave extract (*Agave angustifolia* Haw) was obtained from Morelos State, Mexico. The extract was dehydrated by spray drying to obtain agave powders. Powder was prepared using a two-fluid nozzle as atomizer, and a

laboratory spray dryer (Mobile Minor, Niro, Denmark). Two inlet/outlet drying air temperatures of 160/70 °C (Sample C1) and 180/80 °C (Sample C2) were tested (Lingyun et al. 2007; Gharsallaoui et al. 2007; León-Martínez et al. 2010).

## 2.2 Powder Characterization

Moisture content was determined by thermogravimetric method (AOAC 32.1.03); water activity was measured through Aqualab water activity meter with temperature compensation (Aqualab 4T, Decagon Devices, Inc., Pullman, EUA); true and bulk densities (g/mL) were measured according to Jumah et al. (2000) and Jha et al. (2002) methodology; rehydration, wettability times and dispersability properties of powders were measured according to Barbosa-Cánovas et al. (2005)

Morphology of powders was performed by Scanning Electron Microscopy (SEM) (Jeol, JSM-5800LV, Japan). The images of the powders were acquired through Scanning Electron Microscopy (SEM) and processed using the software Image J 1.43® through plugin FracLac 2.5, the Box Counting method to evaluate the Fractal Dimension of Contour (FDc), and the shifting differential box-counting method (SDBC) to evaluate Fractal Dimension of Texture (FDt) (Chen et al. 2011).

Statistical analysis by one-way analysis of variance (ANOVA) and the Tukey's test with a confidence level of 95 % was employed to set all pairwise comparisons between samples and was performed with the Minitab V.16 statistical package.

## 3 Results and Discussion

To obtain agave powders by spray drying process, two phases were identified. In the first phase, hot air transfers latent heat to evaporate the surface water of the product, with an interchange of heat and humidity between the sprayed droplets and drying air. This phase is a function of extreme conditions of temperature, air humidity, feed concentration, and pressure. In the second phase, spray drying is denominated as restrictive drying, because the shift of water depends on the physical and chemical nature of the solid, temperature, and moisture content (Vehring et al. 2007; Goula and Adamopoulos 2010).

For processing of agave powders, a relationship was observed between inlet and outlet temperature ( $T_{\text{inlet}}/T_{\text{outlet}}$ ) temperatures regarding moisture content of the powders obtained. In the case of increasing  $T_{\text{inlet}}/T_{\text{outlet}}$  temperatures, moisture content decreases as well as water activity (Table 1). In this sense, is important to consider the importance of drying conditions for the appropriate dehydration of agave extract to obtain powder, avoiding the presence of solids encrusted on the wall drying chamber; therefore, inlet and outlet air temperatures are usually the main variables controlling water content, bulk properties, and morphology of the powder (Masters 1985; Thankkitsunthorn et al. 2009).

**Table 1** Moisture content and water activity of *Agave angustifolia* Haw powders obtained at different air-drying temperatures

Samples	$T_{in/out}$ (°C)	Moisture content (% wb)	Water activity ( $A_w$ )
C1	160/70	$5.5 \pm 0.14^a$	$0.32 \pm 0.21^a$
C2	180/80	$4.8 \pm 0.06^a$	$0.22 \pm 0.03^a$

<sup>a</sup>Different lower case letters in the same column for each analysis indicate significant differences among treatments ( $P < 0.05$ ).

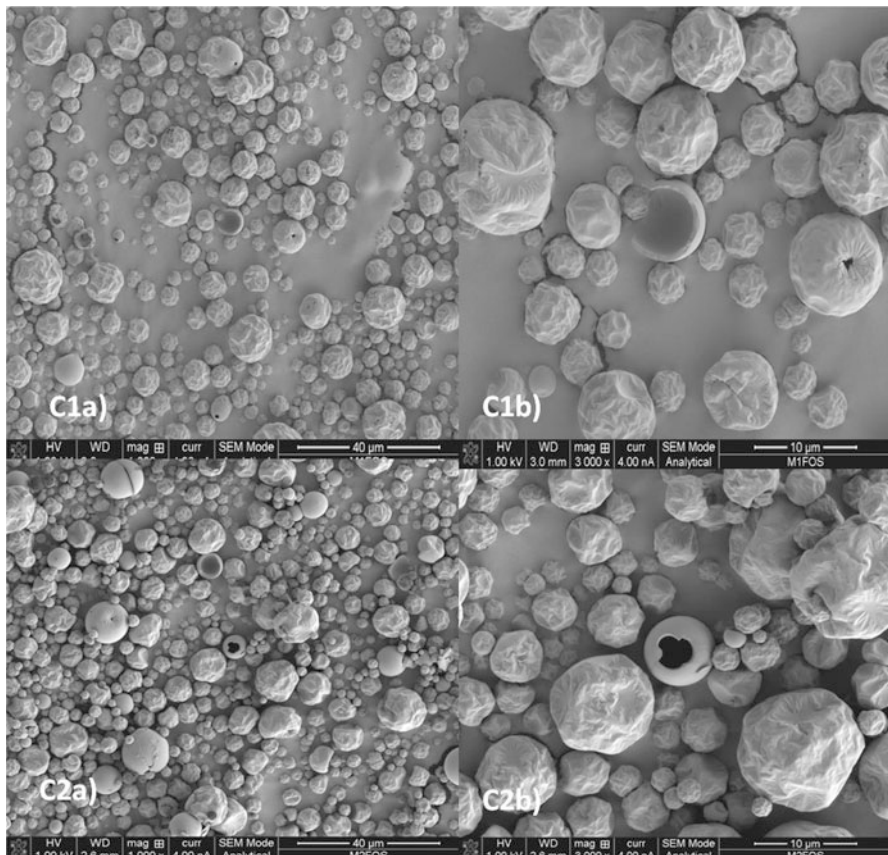


**Fig. 1** Images acquired by SEM of *Agave angustifolia* Haw powders: (1a) Sample C1, observed at 1,000×; (2a) Sample C1, observed at 3,000×; (1b) Sample C2, observed at 1,000×; (2b) Sample C2, observed at 3,000×

It is important to emphasize that during the spray drying process, conversion of liquid extract of agave to a powder product is accompanied by a loss of weight and volume of droplets, resulting in the development of particles. At the temperatures of process used, morphology of particles, evaluated by SEM, is described in Fig. 1. In

both cases, particles were structured by a film or crust on the surface and evident shrinkage. Theoretically, during crust formation, the temperature of the product usually remains below the boiling point of water (Masters 1985; Alamilla-Beltrán et al. 2005; Barbosa-Cánovas et al. 2005; Vehring et al. 2007; Goula and Adamopoulos 2010).

Bulk density and true density vary in function of moisture content and the  $T_{\text{inlet}}/T_{\text{outlet}}$ . At air-drying temperature of 180/80 °C, bulk density is lower than the agave powder obtained at the condition of 160/70 °C; the same relation was observed for water activity where powder tended to be cohesive at moisture content of 5.5 % (wb). Density determinations of food powders are fundamental for the establishment of storage, processing, and distribution conditions, so this merits particular consideration. In this case, the bulk density decreases while increasing air-drying temperature, maybe because this characteristic is related to the particle structure developed during the drying process, while true density and water activity increased when  $T_{\text{inlet}}/T_{\text{outlet}}$  increased, due to the space between particles and the moisture content and water activity associated with increase of cohesiveness by interactions between links of particle (Gallo et al. 2010; Goula and Adamopoulos 2010). Results show that all of the operating parameters significantly affect the physical properties of powder.

With increasing inlet/outlet air temperatures, the wettability of powder is reduced and its rehydration time is augmented; dispersibility was the same value at 97 % in both cases, and water activity values were 0.18 and 0.22. Agave powder presents excellent behavior as an instant and rehydratable powder due to low rehydration time (less than 60 min) and its dispersibility, comparable with milk powder, sugars, fruit juice powders, etc. (Barbosa-Cánovas et al. 2005; Thankitsunthorn et al. 2009).

High values of wettability and rehydration of agave powders (Table 2) are related to the presence of components such as FOS and sugar in the powder, which cause shorter wetting times on powders. The rehydration process involves interactions between the powder and water, which is mainly delineated by the adsorption mechanisms of the compounds present on the powder and its affinity with water. In addition, changes in osmotic pressure because of the presence of solids content due to penetration of dissolvent can cause swelling and relaxation of material, which affects interaction between particle to particle and particle to dissolvent; where water provokes the ordering of polymeric chains by steric effect, water adsorption continues, and at the same time there is a dissolution process (Barbosa-Cánovas et al. 2005; Gaiani et al. 2009).

Particles of agave powder obtained for both temperatures presented morphology with rough surfaces and some smooth surfaces with a few dents. This topography is a common shape developed during the spray drying process, making it possible to modify the particle morphology depending on the spray drying conditions.

In agave powder, the shape and texture of particles had an effect on bulk density, with a tendency to compaction. Particles obtained presented shrinkage and a rough surface, because during the drying process phenomena such as expansion and shrinking of particles may exist. Fractal dimension determination is a useful tool

**Table 2** Properties of *Agave angustifolia* Haw powders

Properties	C1	C2
Density (g/mL)	1.0522 ± 0.016 <sup>a</sup>	1.0742 ± 0.003 <sup>a</sup>
Tapped density (g/mL)	0.6239 ± 0.02 <sup>a</sup>	0.5871 ± 0.02 <sup>a</sup>
Rehydration time (s)	459.2 <sup>a</sup> ± 23.5 <sup>a</sup>	570.8 ± 5.57 <sup>a</sup>
Wettability time (s)	47.5 ± 3.53 <sup>a</sup>	40.75 ± 1.06 <sup>a</sup>
Dispersibility (%)	97.07 ± 0.00 <sup>a</sup>	97.07 ± 0.00 <sup>a</sup>
Fractal dimension of contour	1.79 ± 0.027 <sup>a</sup>	1.82 ± 0.023 <sup>a</sup>
Fractal dimension of texture	2.67 ± 0.33 <sup>a</sup>	2.62 ± 0.28 <sup>a</sup>

<sup>a</sup>Different lower case letters in the same row for each analysis indicate significant differences among treatments ( $P < 0.05$ ).

that helps to characterize the irregularities of texture and contour of particles associated with powder microstructure by the presence of dents. Agave powders showed fractal dimension of contour (DFc) values of 1.79 and 1.82 and fractal dimension of texture (DFt) values of 2.67 and 2.62, in both cases, are morphometric parameters that quantify topological dimensions of powders, considering Euclidean geometry and self-similarity as essential property in a fractal object, values between 0 and 1 represent a smooth surface; values near to 2–3 represent a rough surface; therefore, values obtained on agave powders describe particles with rounded contour related to a near spherical shape, and texture roughness can be related to drying air temperatures. When Tinlet/outlet increases, DFc increases proportionally, and the DFt decreases, as shown in Fig. 1 and Table 2. The advantage of a texture with rough surfaces is that this texture favors rehydration properties on powders (Oakley 1997; Walton 2000; Alamilla-Beltrán et al. 2005; Li et al. 2009), due to the presence of irregular surface, which may facilitate interaction between particle and water, thus improving the absorption of water, rehydration, and wettability of agave powder.

## 4 Conclusions

Operation conditions in spray drying, with respect to inlet/outlet temperatures of drying air, influence physicochemical properties and microstructure of agave powders. Moisture content, water activity, and bulk properties have an interesting relationship with rehydration behavior and microstructure of the powders, showing short wettability and rehydration times with excellent dispersability in water.

**Acknowledgments** The authors wish to thank the financial support of Instituto Politécnico Nacional through SIP project 20121754 as well as program PIFI-IPN and COFAA-I.P.N, CONACyT, projects 80576, 84287; and scholarships for the PhD studies of Miriam Fabiola Fabela and Josefina Porras Saavedra. We also acknowledge the experimental support of CNMN-IPN in conducting this work.

## References

- Alamilla-Beltrán L, Chanona-Pérez JJ, Jiménez-Aparicio AR, Gutiérrez-López GF (2005) Description of morphological changes of particles along spray drying. *J Food Eng* 67:179–184
- Barbosa-Cánovas GV, Ortega-Rivas E, Juliano P, Yan H (2005) *Food powders. Physical properties, processing, and functionality*. Kluwer, New York
- Chen XD, Sidhu HS, Nelson MI (2011) Theoretical probing of the phenomenon of the formation of the outermost surface layer of a multi-component particle, and the surface chemical composition after the rapid removal of water in spray drying. *Chem Eng Sci* 66(24):6375–6384
- Gaiani CJ, Scher P, Schuc S, Desobry S, Banon C (2009) Use of a turbidity sensor to determine dairy powder rehydration properties. *Powder Technol* 190:2–5, <http://www.sciencedirect.com/science/article/pii/S0032591008002258>
- Gallo L, Llabot JM, Alemandi D, Bucalá V, Piña J (2010) Influence of spray-drying operating conditions on *Rhamnus purshiana* (*Cáscara sagrada*) extract powder physical properties. *Powder Technol* 208:205–214
- García-Mendoza A (2002) Distribution of Agave (Agavaceae) en Mexico. *Cact Succ J* 74(4):177–187
- Gharsallaoui A, Roudaut G, Chambón O, Voilley A, Saurel R (2007) Applications of spray-drying in microencapsulation of food ingredients: an overview. *Food Res Int* 40:1107–1121
- Goula AM, Adamopoulos KG (2010) A new technique for spray drying orange juice concentrate. *Innov Food Sci Emerg Technol* 11:342–351
- Jha A, Ambalal-Patel A, Bijoy-Singh RR (2002) Physico-chemical properties of instant *Kheer* mix. *Lait* 82:501–513
- Jumah RY, Tashtoush B, Shaker RR, Zraiy AF (2000) Manufacturing parameters and quality characteristics of spray dried jameed. *Drying Technol* 18:967–984
- León-Martínez FM, Méndez-Lagunas LL, Rodríguez-Ramírez J (2010) Spray drying of nopal mucilage (*Opuntia ficus-indica*): effects on powder properties and characterization. *Carbohydr Polym* 81(4):864–870
- Li J, Du Q, Sun C (2009) An improved box-counting method for image fractal dimension estimation. *Pattern Recogn* 42:2460–2469
- Lingyun W, Jianhua W, Xiaodong Z, Da T, Yalin Y, Chenggang C, Tianhua F, Fan Z (2007) Studies on the extracting technical conditions of inulin from Jerusalem artichoke tubers. *J Food Eng* 79:1087–1093
- Madrigal L, Sangronis E (2007) Inulin and derivates as key ingredients in functional foods. *Arch Latinoam Nutr* 57(4):387–396
- Masters K (1985) *Spray Drying Handbook*, 4th edn. Halsted, New York
- Oakley DE (1997) Produce uniform particles by spray drying. *Chem Eng Prog* 12:48–54
- Quintanilla-Carvajal MX, Meraz-Torres LS, Alamilla-Beltrán L, Chanona-Pérez JJ, Terres-Rojas E, Hernández-Sánchez H, Jiménez-Aparicio AR, Gutiérrez-López GF (2011) Morphometric characterization of spray-dried microcapsules before and after alpha-tocopherol extraction. *Rev Mex Ing Quím* 10(2):301–312
- Rodríguez-Hernández GR, González GR, Grajales-Lagunes A, Ruiz-Cabrera MA, Abud-Archila M (2005) Spray drying of cactus pear juice (*Opuntia streptacantha*): effect on the physico-chemical properties of powder and reconstituted product. *Drying Technol* 23:955–973
- Thankitsunthorn S, Thawornphiphatdit C, Laohaprasit N, Srzednicki G (2009) Effects of drying temperature on quality of dried Indian Gooseberry powder. *Int Food Res J* 16:355–361
- Vehring R, Foss WR, Lechuga-Ballesteros D (2007) Particle formation in spray drying. *J Aerosol Sci* 38:728–746
- Walton DE (2000) The morphology of spray dried particles a qualitative view. *Drying Technol* 18(9):1943–1986

# **Stabilization and Controlled Release of Invertase Through the Addition of Trehalose in Wet and Dried Alginate-Chitosan Beads**

**P.R. Santagapita, M.F. Mazzobre, and M.P. Buera**

## **Abbreviations**

A	Alginate
$A_{\text{Y}}$	Maximum invertase activity corresponding to the active invertase present in the beads
$A_t$	Invertase activity at time t
A-TCh	Alginate-trehalose-chitosan beads
Ch	Chitosan
FD	Freeze-drying
$k$	Constant related to geometric and structural characteristics to the macromolecular network
$n$	Release mechanism type
SEM	Scanning electron microscopy
T	$\alpha$ - $\alpha$ -Trehalose dehydrate
$t$	Time
VD	Vacuum drying

---

P.R. Santagapita • M.F. Mazzobre • M.P. Buera (✉)

Departamentos de Industrias y de Química Orgánica, Facultad de Ciencias Exactas y Naturales, University of Buenos Aires (FCEyN-UBA), National Council of Scientific and Technical Research (CONICET), Buenos Aires, Argentina  
e-mail: [pilar@di.fcen.uba.ar](mailto:pilar@di.fcen.uba.ar)

## 1 Introduction

The stability and controlled release of certain active substances (such as flavors, drugs, enzymes, essential oils, etc.) can be achieved through encapsulation. Ionically cross-linked hydrogels such as alginate- or alginate-chitosan-CaCl<sub>2</sub> beads were proposed as suitable materials for encapsulation systems (Deladino et al. 2008; Han et al. 2008). Alginate beads coated with chitosan were used for encapsulation and release of different proteins (Coppi and Iannuccelli 2009; Zhou et al. 2010). Direct interaction between them forms beads with improved mechanical properties associated with reinforcement of bead structure due to chitosan binding to free alginate sites by cooperative ionic bounds (Deladino et al. 2008).

Dehydration and freezing were generally performed to enhance stability of labile proteins. These processes were usually carried out in the presence of additives such as saccharides; trehalose is one of the most used among those additives. Even though several enzymes have been stabilized through immobilization in glassy sugar matrices (Lee et al. 2006; Santagapita et al. 2008), they failed to provide a controlled release.

Trehalose was fundamental in achieving adequate invertase protection during freezing, drying (freeze-, vacuum-, or air-drying) and mild thermal treatment (at 50 °C, between 6 and 22 °C above their  $T_g$ ), but was not effective in preventing enzyme functionality damage during bead generation (Santagapita et al. 2011, 2012). On the other hand, inclusion of chitosan in the bead walls prevented enzyme activity losses during bead generation, without showing detrimental effects on its conservation during drying or thermal treatment.

Our goal was to study the effect of trehalose and chitosan addition on the release mechanism of invertase encapsulated in wet alginate-calcium beads and the effect of drying method.

## 2 Materials and Methods

### 2.1 Materials

Sodium alginate (A) (from *Laminaria hyperborean*,  $M_w$  of  $1.97 \times 10^5$  Da, mannuronate/guluronate ratio = 0.6) was obtained from BDH (UK). Chitosan (Ch) (86 % of amination degrees and  $M_w$  of  $1.8 \times 10^5$  Da) was obtained from Cicarelli S.A., Argentina. Invertase enzyme from *Saccharomyces cerevisiae* (E.C. 3.2.1.26, 1,840 U/mg,  $M_w$  of 270 kDa) was obtained from Fluka (Switzerland).  $\alpha$ - $\alpha$ -Trehalose dihydrate (T) was obtained from Hayashibara Co. Ltd. (Japan).

## 2.2 *Gel Bead Preparation*

Beads were prepared according to the drop method described elsewhere (Santagapita et al. 2011). All solutions were prepared in 50 mM acetate buffer pH 3.8. A peristaltic pump was used to drop 10 mL of the 1 % w/v alginate-enzyme mixture (117 U/mL) into 100 mL of 2.5 % w/v CaCl<sub>2</sub>, which was prepared with or without 20 % T or 0.5 % Ch. Bead generation was performed in a cold bath under constant stirring, with a needle size of 0.25 × 6 mm, a 6 cm needle-solution distance, and a pump speed of 9.0 rpm. The beads were then hardened for 15 min in the CaCl<sub>2</sub> solution and washed five times with cold water.

## 2.3 *Physical Treatment of the Beads: Dehydration*

Bead dehydration was performed by two different methods: vacuum-drying (VD) and freeze-drying (FD). VD was performed in an oven operating at a chamber pressure of 113 mbar during 4 h at 25 °C. FD of beads (frozen 24 h at –18 °C and exposed to liquid nitrogen) was performed during 12 h in a Heto-Holten A/S, cooling trap model CT 110 freeze-dryer (Heto Lab Equipment, Denmark) operating at a condenser plate temperature of –110 °C. After dehydration, the beads were maintained in vacuum desiccators until determination of their corresponding treatments or property.

## 2.4 *Digital Image Analysis*

Bead size and shape evaluation was carried out by analyzing digital images captured by a digital camera installed on a microscope (magnification at 7×). Pictures were analyzed using Image J software. Feret's diameter (longest distance between any two points along bead boundary) and circularity (how closely particle shape resembles a circle) were analyzed for at least 50 (wet systems) or 40 beads (dried systems).

## 2.5 *Enzyme Release*

Enzymatic activity determination was chosen to follow the delivery of the enzyme due to low enzyme concentration (0.5–0.4 µg protein/bead) to quantify protein content. Eight beads were placed in microcentrifuge tubes (in duplicate) with 120 µL of cold (4 °C) sodium acetate buffer 50 mM pH 4.5 and were gently shaken. Then, after appropriate times, enzymatic activity was determined in the beads

(Subheading 2.6). The release curves were modeled by Peppas equation (Peppas 1985) using GraphPad Prism v5 software.

## 2.6 Invertase Activity

Invertase activity was determined by spectrophotometry in four beads by adding 400  $\mu\text{L}$  of sucrose solution (200 mM in sodium acetate buffer 50 mM pH 4.6) and then incubating for 10 min at 37 °C in a water bath. The samples were introduced for 10 min in a water bath heated at 100 °C to stop the enzyme reaction. The reducing sugars were determined at 546 nm using the 3,5-dinitrosalicylic acid method (Bernfeld 1955).

## 3 Results and Discussion

### 3.1 Bead Characterization

Wet alginate beads were dried by freeze-drying (FD) and by vacuum-drying (VD). A digital image processing technique was used to obtain bead size (determined as Feret's diameter) and circularity after optical microscopy analysis. The relative changes of these parameters after dehydration, in relation to those of the wet beads, are shown in Fig. 1. Wet beads had a diameter between 1.3 and 1.6 mm, and circularity was around  $0.84 \pm 0.04$  for the three employed formulations. After drying, the bead size was considerably reduced, mainly during VD (Fig. 1). Trehalose greatly reduced the loss in size for the FD samples. Upon drying, the beads lost circularity, particularly during FD. The presence of trehalose seemed to preserve circularity, especially during VD. There were no further differences in both size and circularity due to chitosan addition in alginate-trehalose-chitosan beads (A-TCh) with respect to trehalose inclusion (alginate-trehalose beads (A-T)). Drying method affected the size and shape of the beads more than the composition change.

As previously observed (Santagapita et al. 2012), scanning electron microscopy (SEM) images obtained for dried beads indicated that bead surface characteristics depended both on the type of drying and on composition (presence of trehalose and/or chitosan). The surface of FD alginate beads was smoother than that of VD beads, and average pore sizes were 30 nm and 100 nm, respectively. A smoother surface was observed in trehalose presence (A-T and A-TCh beads). The alginate beads with chitosan (A-TCh) showed a rougher surface than alginate (A) or A-T beads, as a consequence of alginate-chitosan interaction (Deladino et al. 2008).

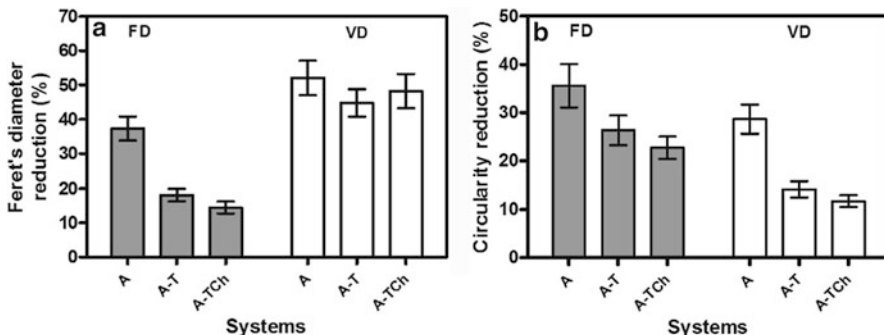


**Fig. 1** Percentage reduction of Feret's diameter (a) and circularity (b) of freeze-dried (FD) and vacuum-dried (VD) alginate beads in relation to corresponding wet beads. Standard deviation values are included. A alginate; T trehalose; Ch chitosan

### 3.2 Enzyme Release and Transport Mechanism Modeling

To define potential applications of an encapsulated system, it is critical to know the release behavior of an encapsulated biomolecule, especially when large molecules are considered. The diffusion of proteins from the alginate network is dependent on several factors, such as molecular weight and overall net charge of the protein (Martinsen et al. 1989), as well as alginate concentration and mannuronic/guluronic acid ratio (Wee and Gombotz 1998; Smidsrød and Skjak-Braek 1990). Also, electrostatic interactions between alginate and enzymes could define the release mechanism. Alginate  $pK_a$  values are 3.38 and 3.65 (Smidsrød and Skjak-Braek 1990). The isoelectric point of chitosan is 6.3 (Mi et al. 1997), while that for invertase is 4–4.5 (Schülke and Schmid 1988). Thus, at the pH of the release experiment (4.5), alginate was negatively charged, chitosan was protonated, and the enzyme global charge was neutral; thus, a low effect of electrostatic interactions was expected on enzyme release.

Enzyme release was evaluated by the  $A_t/A_\infty$  relation as a function of time, where  $A_t$  is the invertase activity at time  $t$  and  $A_\infty$  is maximum invertase activity corresponding to the active invertase present in the beads. Figure 2a shows the invertase release from wet beads as a function of time. A mathematical modeling (Peppas model) was applied in order to analyze enzyme release, which relates the fractional release of a drug with time:

$$A_t/A_\infty = kt^n, \quad (1)$$

as previously discussed (Santagapita et al. 2011).  $k$  (in  $s^{-n}$ ) is a constant related to geometric and structural characteristics to the macromolecular network and to the released agent;  $t$  is the time (s), and  $n$  is indicative of release mechanism type (dimensionless). The release of several substances from dry and wet beads was previously analyzed (Coppi and Iannuccelli 2009; Deladino et al. 2008;

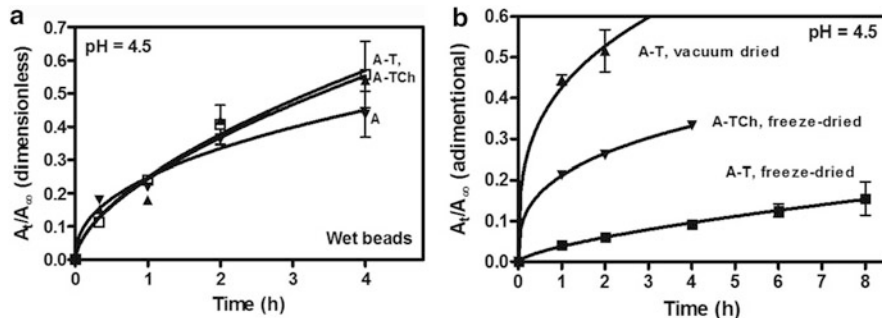


**Fig. 2** Enzyme release from wet (a) and dried beads (b) as a function of incubation time in acetate buffer pH 4.5 at 5 °C. Full lines show the fitting obtained by using Peppas equation (Eq. (1)); symbols represent experimental values. A alginic acid; T trehalose; Ch chitosan

**Table 1** Release exponent obtained by Peppas equation (Eq. (1)), transport mechanism, and relative rates between diffusion and polymer chains relaxation from swellable and non-swellable spherical systems

Release exponent ( $n$ )	Transport mechanism	Diffusion rate vs. polymer chains relaxation rate
0.43	Fickian diffusion	Diff. rate < relax. rate
$0.43 < n < 0.85^a$	Anomalous	Diff. rate ≈ relax. rate
$0.43 < n < 1^b$	Anomalous	Diff. rate ≈ relax. rate
0.85 <sup>a</sup>	Transport case II	Diff. rate > relax. rate
1 <sup>b</sup>	Transport case II (zero-order kinetic)	Diff. rate > relax. rate

<sup>a</sup>Polymers that swell when rehydrated

<sup>b</sup>Polymers that do not swell when rehydrated

Shu et al. 2010). Table 1 indicates the limits of  $n$  and the transport mechanism (according to Alfrey et al. 1966) for spherical systems (Pothakamury and Barbosa-Cánovas 1995). The  $n$  higher limit always corresponds to a transport limited by the rate of the polymer chains relaxation, independent of whether the polymers swell or do not swell. The  $n$  and  $k$  parameters obtained by applying (1) to the data shown in Fig. 2a are shown in Table 2, with  $R^2$  higher than 0.96. The enzyme release from A beads showed an  $n$  value of 0.43. Therefore, the main transport mechanism was Fickian and limited by diffusion. The presence of trehalose and chitosan slightly influenced the release mechanism by changing the  $n$  value, which was still close to the 0.43 limit for Fickian diffusion, but indicated a certain influence of the polymer chains relaxation in the transport mechanism. It is not indicated that a comparison of  $k$  values when  $n$  values were different (A vs. A-T or A-TCh) should be performed. However, both bead systems containing trehalose showed similar  $n$  and  $k$  values, which reveals that there were no structural differences between them.

**Table 2**  $n$  and  $k$  parameters obtained from Peppas equation and transport type for invertase release from wet and dried beads in acetate buffer (50 mM) at pH 4.5

pH 4.5	$n$	$k \times 10^3$ (s <sup>-n</sup> )	Type of transport
A, wet beads	0.43 ± 0.05	7.6 ± 0.5	<i>Fickian</i> diffusion
A-T, wet beads	0.50 ± 0.05	5.0 ± 0.3	Anomalous
A-TCh, wet beads	0.49 ± 0.05	5.0 ± 0.7	Anomalous
A-T, vacuum-dried	0.31 ± 0.02	34.0 ± 0.8	<i>Fickian</i> diffusion
A-T, freeze-dried	0.30 ± 0.06	9.0 ± 0.5	<i>Fickian</i> diffusion
A-TCh, freeze-dried	0.33 ± 0.01	14.5 ± 0.1	<i>Fickian</i> diffusion

A alginate; T trehalose; Ch chitosan

Invertase release was much faster in VD beads than in those in FD, as shown in Fig. 2b. This result is in agreement with porous size calculated by analyzing SEM images. Table 2 shows the parameters obtained by fitting the experimental values with (1), with  $R^2$  higher than 0.997.  $n$  values were  $<0.43$  for both types of A-T dried beads. Even though this situation ( $n < 0.43$ ) was not contemplated in Table 1, according to Peppas (1985), the use of (1) to analyze systems that have pores leads to  $n$  values  $<0.43$ , but could still be treated as *Fickian* diffusion. A combined mechanism of diffusion partially through a swollen matrix and partially through water-filled pores shifts the release exponent  $n$  toward smaller values. Other authors have also related this behavior to *Fickian* diffusion of a drug from alginate-chitosan particles (Coppi and Iannuccelli 2009). A great difference was found in the  $k$  parameter (Table 2) for both dried A-T beads. Since both types of dried beads were spherical (i.e., having the same geometry), the  $k$  parameter shows a great difference in the structure between them, according to SEM images. The inclusion of chitosan in the FD A-T beads increased enzyme release rate with respect to A-T beads, but the type of release mechanism was still the same, thus maintaining the same profile for the release curve. The  $k$  value was higher in relation to A-T beads, indicating that the difference in release rate was related to structural factors.

## 4 Conclusions

- Dried bead microstructure depended on both drying method and composition, leading to lower enzyme release rates from alginate-trehalose freeze-dried beads, which showed smooth surface with no porous structure.
- The use of a semiempirical equation allowed the establishment of certain characteristics of the enzyme release mechanism. Trehalose and chitosan inclusion, hydration degree, and drying method greatly influence the transport mechanism of enzyme release in alginate beads.

- The combination of encapsulation in alginate-chitosan beads with drying immobilization in an amorphous trehalose matrix, which remained in a glassy state at ambient temperature, was an efficient strategy to achieve enzyme stability and its controlled release.

**Acknowledgments** The authors acknowledge the financial support of ANPCYT (PICT 0928), CONICET (PIP 100846), and UBA (Project UBACyT 20020100100397).

## References

- Alfrey E, Gurnee EF, Lloyd WG (1966) Diffusion in glassy polymers. *J Polym Sci C* 12:249–261
- Bernfeld P (1955) Amylases,  $\alpha$  and  $\beta$ . *Methods Enzymol* 1:149–158
- Coppi G, Iannuccelli V (2009) Alginate/chitosan microparticles for tamoxifen delivery to the lymphatic system. *Int J Pharm* 367:127–132
- Deladino L, Anbinder PS, Navarro AS, Martino MN (2008) Encapsulation of natural antioxidants extracted from *Ilex paraguariensis*. *Carbohydr Polym* 71:126–134
- Wee SF, Gombotz WR (1998) Protein release from alginate matrices. *Adv Drug Deliv Rev* 31:267–285
- Han J, Guenier A-S, Salmieri S, Lacroix M (2008) Alginate and chitosan functionalization for micronutrient encapsulation. *J Agric Food Chem* 56:2528–2535
- Lee SL, Hafeman AE, Debenedetti PG, Pethica BA, Moore DJ (2006) Solid-state stabilization of  $\alpha$ -chymotrypsin and catalase with carbohydrates. *Ind Eng Chem Res* 45:5134–5147
- Martinsen A, Skjak-Braek G, Smidsrød O (1989) Alginate as immobilization material: I. Correlation between chemical and physical properties of alginate gel beads. *Biotechnol Bioeng* 33:79–89
- Mi F-L, Her N-L, Kuan C-Y, Wong T-B, Shyu S-S (1997) Chitosan tablets for controlled-release of theophylline—effect of polymer-drug wet or dry blending and anionic-cationic interpolymer complex. *J Appl Polym Sci* 66:2495–2505
- Peppas NA (1985) Analysis of Fickian and non-Fickian drug release from polymers. *Pharm Acta Helv* 60:110–111
- Pothakamury UR, Barbosa-Cánovas GV (1995) Fundamental aspects of controlled release in foods. *Trends Food Sci Technol* 6:397–406
- Santagapita PR, Gómez Brizuela L, Mazzobre MF, Ramirez H, Corti HR, Villalonga Santana R, Buera MP (2008) Structure/function relationships of several biopolymers as related to invertase stability in dehydrated systems. *Biomacromolecules* 9:741–747
- Santagapita PR, Mazzobre MF, Buera MP (2011) Formulation and drying of alginate beads for controlled release and stabilization of invertase. *Biomacromolecules* 12:3147–3155
- Santagapita PR, Mazzobre MF, Buera MP (2012) Invertase stability in alginate beads: effect of trehalose and chitosan inclusion and of drying methods. *Food Res Int* 47:321–330
- Schülke N, Schmid FX (1988) Effect of glycosylation on the mechanism of renaturation of invertase from yeast. *J Biol Chem* 263:8832–8837
- Shu S, Sun C, Zhang X, Wu Z, Wang Z, Li C (2010) Hallow and degradable polyelectrolyte nanocapsules for protein drug delivery. *Acta Biomater* 6:210–217
- Smidsrød O, Skjak-Braek G (1990) Alginate as immobilization matrix for cells. *Trends Biotechnol* 8:71–78
- Zhou Z-d, Li G-y, Li Y-j (2010) Immobilization of *Saccharomyces cerevisiae* alcohol dehydrogenase on hybrid alginate-chitosan beads. *Int J Biol Macromol* 47:21–26

# Rheology and Stability of Citral/Sugar Microemulsions

N. Sosa, C. Schebor, and O.E. Pérez

## Abbreviations

$T_2$	Relaxation times
$^1\text{H}$ NMR	Proton nuclear magnetic resonance
T	Trehalose
T-MD	Trehalose-maltodextrin
S	Sucrose
S-MD	Sucrose-maltodextrin
T	Shear stress
$\Gamma$	Shear rate
$D_{3,2}$	Volume-surface mean diameter
SDS	Sodium dodecyl sulfate
$D_{4,3}$	Equivalent volume-mean diameter

---

N. Sosa • C. Schebor

Departamento de Industrias, Universidad de Buenos Aires, Ciudad Universitaria,  
1428 Ciudad de Buenos Aires, Argentina

Departamento de Química Orgánica, Facultad de Ciencias Exactas y Naturales,  
Universidad de Buenos Aires, Ciudad Universitaria, 1428 Ciudad de Buenos Aires, Argentina

Consejo Nacional de Investigaciones Científicas y Técnicas de la República Argentina,  
CONICET, Ciudad de Buenos Aires, Argentina

O.E. Pérez (✉)

Departamento de Industrias, Universidad de Buenos Aires, Ciudad Universitaria,  
1428 Ciudad de Buenos Aires, Argentina

Consejo Nacional de Investigaciones Científicas y Técnicas de la República Argentina,  
CONICET, Ciudad de Buenos Aires, Argentina  
e-mail: [operez@di.fcen.uba.ar](mailto:operez@di.fcen.uba.ar)

CPMG	Carr-Purcell-Meiboom-Gill sequence
$T_{2-1}$	Relaxation times of protons in the less mobile water fractions
$T_{2-2}$	Relaxation times of protons in the more mobile water fractions

## 1 Introduction

Microencapsulation of hydrophobic flavors is of great importance in the flavoring and food industries, since solid or liquid microencapsulated food flavors exhibit good chemical stability and a controlled release. Spray drying is generally used to produce flavor powders in a short time (Gharsallaoui et al. 2010). As an initial step for drying, oil flavors must be emulsified. It is possible to form emulsions that are kinetically stable for a reasonable period of time by including substances known as emulsifiers and/or thickening agents prior to homogenization (McClements 1999). The choice of a wall material for microencapsulation by spray drying is very important for encapsulation efficiency and microcapsule stability. The carrier material should dissolve easily and be water soluble, bland, and inexpensive, have good oil-emulsifying and droplet-stabilizing properties, exhibit low solution viscosities at high solids levels, and have excellent film-forming properties and form amorphous powders upon drying. Carrier systems are usually formulated by combining a number of water-soluble components (carbohydrates, gums, and proteins) (Gharsallaoui et al. 2010). It is well known that, among other factors, the type of carrier governs flavor retention during the spray-drying process (Thijssen 1971); for this reason, disaccharides are sometimes included in commercial formulations to improve retention characteristics.

The objective of this work was to characterize and determine the stability of emulsions formed by citral and several matrices. Focus was centered on the interactions between water and matrix solutes and their impact on viscosity and emulsion stability.

## 2 Materials and Methods

### 2.1 Preparation of Samples

Pre-emulsions were prepared by mixing (2 min at 750 rpm) water, starch and either sucrose or trehalose, maltodextrin, and citral oil. The exact mass of each ingredient in the systems is detailed in Table 1. Emulsion formation was completed by high-speed blending the pre-emulsions (10 min at 16,000) into an ice bath to avoid thermal effects.

**Table 1** Constituents (expressed as g/100 g) of emulsions formed by citral oil and an aqueous phase containing trehalose (T), sucrose (S), trehalose-maltodextrin (TM-D), sucrose-maltodextrin (SM-D)

Emulsions	Citral	Water	Modified starch	Trehalose	Sucrose	Maltodextrin
T	5.0	60.0	3.0	32.0	—	—
S	5.0	60.0	3.0	—	32.0	—
T-MD	5.0	60.0	3.0	32.0	—	16.0
S-MD	5.0	60.0	3.0	—	32.0	16.0

## 2.2 Measurements

- (a) Apparent viscosity of emulsions was measured with a Brookfield viscometer at 25 °C.
- (b) The droplet size of emulsions was measured by light scattering.
- (c) The stability of emulsions was analyzed using a vertical scan analyzer at 25 °C.

Molecular mobility was estimated by measuring the  $T_2$  relaxation times using a time-resolved proton nuclear magnetic resonance ( $^1\text{H}$  NMR). Significant differences between sample properties were determined by analysis of variance using the general linear model procedure. An alpha level of 0.05 ( $P < 0.05$ ) was used to determine significance.

## 3 Results and Discussion

Figure 1 shows the flux curves for trehalose (T), trehalose-maltodextrin (T-MD), sucrose (S), and sucrose-maltodextrin (S-MD) emulsions. For all emulsions, shear stress ( $\tau$ ) increased linearly as shear rate ( $\gamma$ ) increased. Viscosity,  $\partial\tau/\partial\gamma$ , remained constant upon shear stress variation, corroborating the Newtonian character of the emulsions. Emulsions containing maltodextrin resulted in a more viscous product, as polysaccharides are known to increase the viscosity of the continuous phase. All emulsions presented similar droplet size distribution, with a multimodal pattern as in the volume vs. droplets size plots (not shown). The number size distribution indicated only one population, with droplet sizes lower than 0.3 μm. The volume-surface mean diameter ( $D_{3,2}$ ) and the equivalent volume-mean diameter ( $D_{4,3}$ ), both derived from droplet size distribution, were used to characterize droplet diameters (Table 2).  $D_{3,2}$  provides a measure of the mean diameter where most of the particles fall. Emulsions containing MD presented much smaller  $D_{3,2}$  diameter.  $D_{4,3}$  is a very sensitive parameter in relation to changes in particle size involving destabilization processes (flocculation, coalescence). All samples presented high  $D_{4,3}$  values. In order to identify the type of instability occurring in the emulsions, emulsions were treated with sodium dodecyl sulfate (SDS), which acts in dissociating any existing

**Fig. 1** Flow curves of emulsions trehalose (T), sucrose (S), trehalose-maltodextrin (TMD), and sucrose-maltodextrin (SMD). Measurements were made at 25 °C and natural pH. Each point corresponds to the mean of  $n = 2 \pm \text{SD}$  determinations

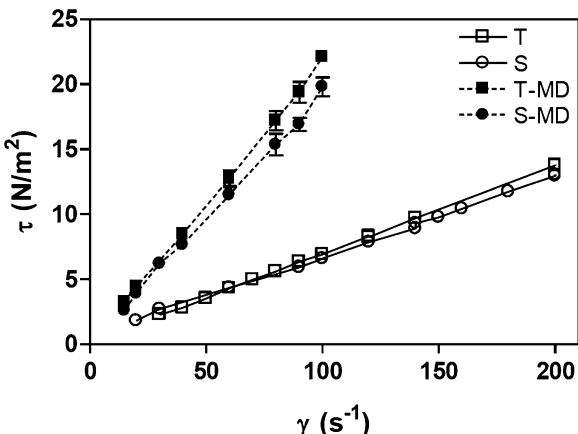


**Table 2** Volume-surface mean diameter ( $D_{3,2}$ ) and equivalent volume-mean diameter ( $D_{4,3}$ ) characterizing trehalose (T), sucrose (S), trehalose-maltodextrin (TM-D), and sucrose-maltodextrin (SM-D) emulsions

Emulsions	$D_{3,2}$	$D_{4,3}$	$D_{4,3-SDS}$
T	$16.60 \pm 4.09^{\text{a}}$	$332.27 \pm 4.56^{\text{a}}$	$15.09 \pm 1.23^{\text{a}}$
S	$24.66 \pm 4.37^{\text{b}}$	$315.99 \pm 4.12^{\text{b}}$	$1.240 \pm 0.07^{\text{b}}$
T-MD	$3.930 \pm 0.56^{\text{c}}$	$281.20 \pm 6.65^{\text{c}}$	$0.250 \pm 0.01^{\text{c}}$
S-MD	$0.730 \pm 0.04^{\text{c}}$	$216.41 \pm 9.86^{\text{d}}$	$0.670 \pm 0.02^{\text{d}}$

Average for  $n = 2 \pm \text{SD}$  independently prepared emulsions. Different superscripts indicate significant differences ( $p < 0.05$ )

flocs (Anton et al. 2002). A persistent droplet association indicated by the highest  $D_{4,3-SDS}$  values was observed for T emulsions, which indicated a certain degree of coalescence. This phenomenon was also seen for the S emulsions, but to a lesser extent. The MD-containing samples showed very low  $D_{4,3-SDS}$  values, which means that no coalescence had developed, but only reversible aggregation was present.

To study the global stability of the emulsions, backscattering (BS) profiles were analyzed every 30 min for a total storage time of 3 h (Fig. 2). At each analyzed time, the distribution of particles was homogeneous along the entire tube, since a regular backscattering profile was obtained for these emulsions. A uniform decrease in the backscattering profiles all along the entire tube length was observed after 30 min, which was indicative of an increment of the mean droplet diameter, i.e., flocculation (Álvarez Cerimedo et al. 2010). A minor decrease in BS % was observed after 30 min.

To elucidate the influence of different formulation components on the molecular mobility of the systems, transverse relaxation times  $T_2$  associated with slow relaxing protons (related to populations of water molecules displaying little

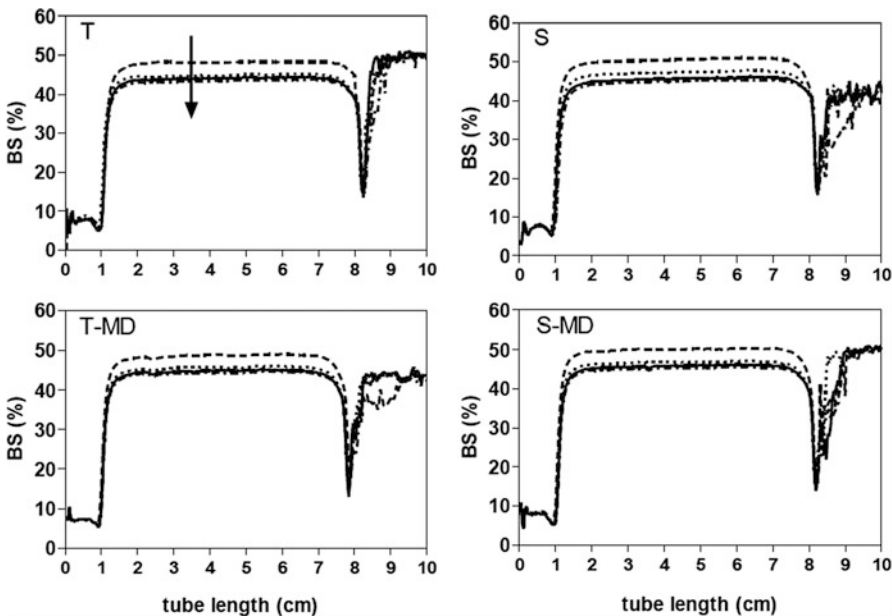
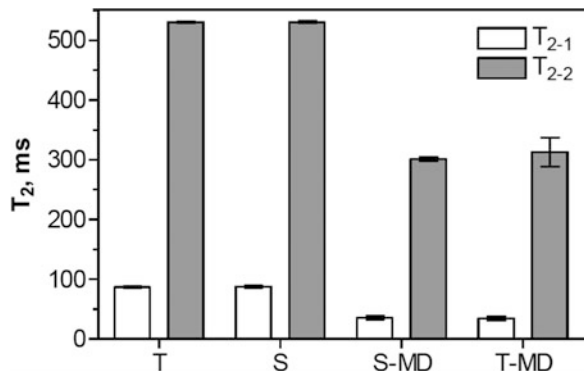


**Fig. 2** Variation of backscattering (BS) profiles as a function of tube length, also shown with emulsion storage time (samples were stored for 180 min; arrow denotes time). Measurements were made at 25 °C and natural pH. Each curve represents the mean value of two independently prepared samples

**Fig. 3**  $^1\text{H}$  NMR  $T_2$  relaxation times obtained after the application of CPMG pulse sequence at 25 °C



interaction with solids) were measured using the CPMG sequence (Fig. 3). Relaxation times  $T_{2-1}$  and  $T_{2-2}$  correspond to protons in the less and more mobile water fractions, respectively. The presence of MD caused an important reduction in water molecular mobility.

## 4 Conclusions

Carrier systems are usually formulated by combining several components. In the case of citral emulsions that will be spray dried, a combination of ingredients is necessary to contribute to emulsion formation, aroma retention, and improve stability. Emulsion stability was strongly influenced by continuous phase viscosity, affecting both droplet diameter and destabilization processes. In this sense, MD was a key ingredient to provide more stable emulsions. The disaccharides alone promoted more instability; however, their inclusion must be considered in order to achieve better flavor retention upon spray drying.

## References

- Álvarez Cerimedo MS, Iriart CH, Candal RJ, Herrera ML (2010) Stability of emulsions formulated with high concentrations of sodium caseinate and trehalose. *Food Res Int* 43(5):1482–1493
- Anton M, Beaumal V, Brossard C, Llamas G, le Denmat M (2002) Droplet flocculation and physical stability of oil-in-water emulsions prepared with hen egg yolk. In: Anton M (ed) *Food emulsions and dispersions*. Research Signpost, Kerala, pp 15–28
- Gharsallaoui A, Saurel R, Chambin O, Cases E, Voilley A, Cayot P (2010) Utilisation of pectin coating to enhance spray-dry stability of pea protein-stabilised oil-in-water emulsions. *Food Chem* 122:447–454
- McClements DJ (1999) Emulsion formation. In: McClements DJ (ed) *Food emulsions: principles, practice and techniques*. CRC Press, Boca Raton, FL, pp 161–183
- Thijssen HAC (1971) Flavour retention in drying preconcentrated food liquids. *J Appl Chem Biotechnol* 21:372–377

# **Response Surface Methodology to Assay the Effect of the Addition of Proteins and Hydrocolloids on the Water Mobility of Gluten-Free Pasta Formulations**

**V.J. Larrosa, G. Lorenzo, N.E. Zaritzky, and A.N. Califano**

## **Abbreviations**

DSC	Differential scanning calorimetry
MDSC	Modulated differential scanning calorimetry
Peak <i>G</i>	Swelling of the starch amorphous region and a cooperative mediated melting of starch crystallites
Peak <i>M1</i>	Melting of the most stable crystallites
Peak <i>M2</i>	Melting of the amylose–lipid complexes
RSM	Response surface methodology
$T_c$	Conclusion temperature
$T_g$	Glass transition temperature
T <sub>mw</sub>	Ice peak melting temperature
$T_o$	Onset temperature
$T_p$	Peak temperature
$X_i$	Coded process variables ( <i>G</i> , <i>P</i> , <i>W</i> )
<i>Y</i>	Corresponding response variable
$\beta$	Regression coefficients
$\Delta H_m$	Latent heat of ice melting

---

V.J. Larrosa • A.N. Califano

Centro de Investigación y Desarrollo en Criotecnología de Alimentos (CIDCA), Facultad de Ciencias Exactas, UNLP-CONICET, 47 y 116, La Plata 1900, Argentina

G. Lorenzo (✉) • N.E. Zaritzky

Centro de Investigación y Desarrollo en Criotecnología de Alimentos (CIDCA), Facultad de Ciencias Exactas, UNLP-CONICET, 47 y 116, La Plata 1900, Argentina

Departamento de Ingeniería Química, Facultad de Ingeniería, UNLP, La Plata, Argentina  
e-mail: [lorenzogabriel@gmail.com](mailto:lorenzogabriel@gmail.com)

## 1 Introduction

In gluten-free pasta formulation (suitable for those suffering from celiac disease), the influence of each constituent has a major importance on the final product quality, especially water and hydrocolloid contents used to replace the gluten matrix. Gluten-free doughs are mixed dispersed systems; the dispersion medium contains several types of dispersed particles, with two main construction materials—polysaccharides and proteins. Four levels of structural hierarchy in dispersed food systems can be distinguished: submolecular, molecular, supermolecular, and macroscopic. Structural functions of a biopolymer depend upon its place in the structural hierarchy of the product (Tolstoguzov 2000).

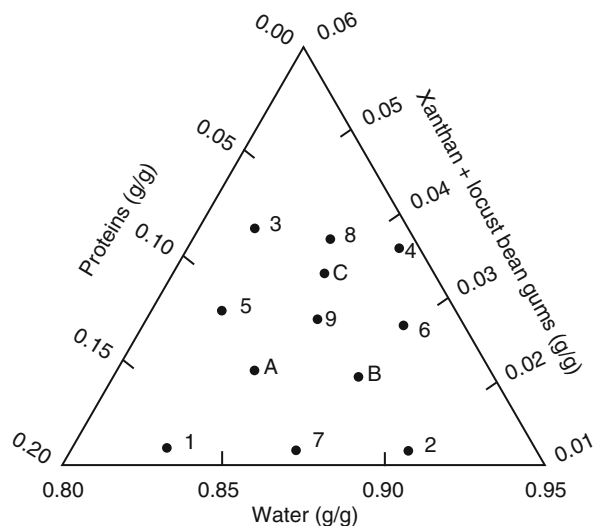
The presence of hydrocolloids and proteins in dough may modify the mobility of water to interact with starch in the gelatinization process (Blanshard 1987). The amount of water content and the presence of different components such as sugars, gums, and proteins affect the extent to which the amorphous regions are plasticized during gelatinization, modifying the corresponding enthalpy and the peak temperature in a differential scanning calorimetry (DSC) thermogram.

The extent of hindered mobility of water molecules is related to the amount of the unfrozen water content of the systems and their glass transition temperature ( $T_g$ ) and influences the conditions for starch gelatinization. The aim of this chapter is to use response surface methodology (RSM) to analyze the effect of the addition of proteins and hydrocolloids on water–starch interaction during gelatinization in gluten-free doughs using a triangular mixture design through the analysis of thermograms obtained by modulated differential scanning calorimetry (MDSC). The amount of unfrozen water, water melting temperature, and glass transition temperature for each formulation are also studied, and their relationship with dough composition is determined.

## 2 Mixture Design for Surface Response Analysis

Mixture designs are a special category of response surface designs that are particularly useful when the actual amounts of a component (factor) do not matter, but instead the proportion of the whole made up by each component is taken into account along with the interdependence of factors, by assuming that the factors must have a sum equal to a constant value (Cornell 2002). In the present work, a simplex-centroid augmented design with constraints was chosen to study the effect of adding gums (0.51–2.52 %), protein (0.68–6.70 %), and water (35.5–39.5 %) to a dough formulation containing fixed mass fractions of corn starch and corn flour (4:1 ratio, 53.5 %), NaCl (1.1 %), and sunflower oil (2.7 %). The design consisted of 12 runs: four points at the extreme vertices of the feasible quadrangular region (1,2,3,4), four points at the edge centroids (5,6,7,8), one point at the overall centroid (9), and three added points (A,B,C) to evenly cover the experimental region (Fig. 1).

**Fig. 1** Simplex-centroid augmented design; mass fractions are expressed as coded variables



Surface response analysis was used to determine the relationship of the unfrozen water of this composite system:

$$Y = \sum_{i=1}^3 \beta_i X_i + \sum_{i=1}^2 \sum_{j=i+1}^3 \beta_{ij} X_i X_j + \beta_{123} \prod_{i=1}^3 X_i \quad (1)$$

where  $Y$  is the corresponding response variable,  $X_i$  are the coded process variables ( $G$ ,  $P$ ,  $W$ ), and  $\beta$  are the regression coefficients. The same methodology was followed with the peak temperature of water melting.

### 3 Effect of Dough Composition on Water Mobility

Thermograms were performed from  $-50$  °C to  $140$  °C, at a heating rate of  $5$  °C/min, with a modulation of  $\pm 1$  °C and a  $60$  s period, using a modulated DSC (model Q100, TA Instruments). For each endotherm, onset ( $T_o$ ), peak ( $T_p$ ), and conclusion ( $T_c$ ) temperatures of the gelatinization phenomena, as well as the ice peak melting temperature ( $T_{mw}$ ) and the  $T_g$  of each sample were also determined. For all formulations assayed in this work, thermograms show that the characteristic  $T_{mw}$  between  $-5$  and  $-8$  °C and above  $65$  °C starch gelatinization transition was noticeable (Fig. 2). The latent heat of ice melting ( $\Delta H_m$ ) was obtained by integrating the melting peak of thermograms; this value was later used to estimate the frozen water fraction in the food material (Roos 1986).

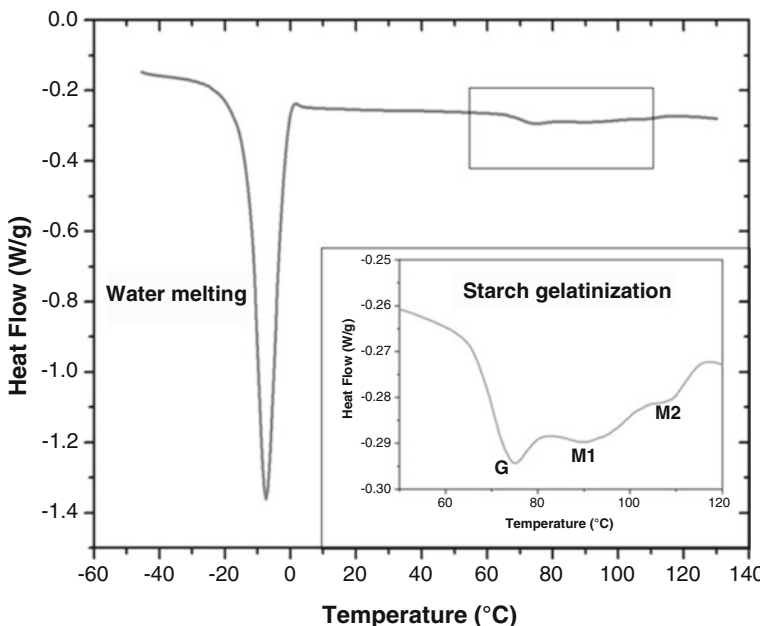


**Fig. 2** Complete DSC thermogram corresponding to sample 9. The *inset* shows the gelatinization transitions (*G*) and (*M1*) and the melting of the amylose–lipid complexes (*M2*)

Response surface methodology (RSM) was successfully applied to a complex system such as gluten-free dough to analyze the effect of each component on the thermal behavior of the dough and to reveal interactions between those components. The behavior of the unfrozen water of the composite systems was modeled using Eq. (1) resulting in a “saddle”-type surface. This process involves several interactions between components (Fig. 3a), where the largest influence corresponded to gums and the interaction between gums and water. Mixture of solutes and water results in altered properties of both constituents. Hydrophilic groups cause changes in the structure and mobility of adjacent water, and water causes changes in reactivity and sometimes in the structure of hydrophilic groups (Fennema 1996). Ions and ionic groups of organic molecules hinder mobility of water molecules to a greater degree than other types of solutes. From a conceptual standpoint, it is useful to think of unfrozen water as water that exists in the vicinity of solutes and other nonaqueous constituents and which exhibits properties that are significantly altered from those of bulk water in the same system (Fennema 1996).

The water melting peak temperature ranged from  $-5\text{ }^{\circ}\text{C}$  to  $-8\text{ }^{\circ}\text{C}$  for all gluten-free doughs assayed; dependence on water, proteins, and hydrocolloids content was modeled. A saddlelike effect, as can be observed in Fig. 3b, was also shown, and regression coefficients for  $T_{mw}$  exhibited the same trend as in unfrozen water content; the negative value of the interaction coefficient suggests the presence of an antagonistic effect between hydrocolloid concentration and water content.

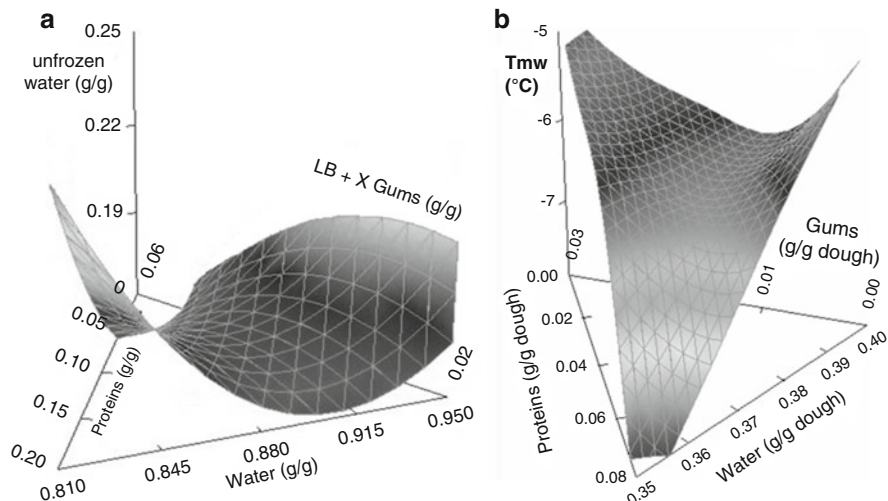


**Fig. 3** Surface response of (a) unfrozen water content (g/g total water) and (b) peak melting temperature ( $T_{mw}$ ) as a function of dough composition (expressed as coded variables)

The glass transition denotes a change from brittle to rubbery behavior at a temperature " $T_g$ ."  $T_g$  depends on molecular characteristics, composition, and compatibility of the components in the amorphous matrix (Kalichevsky and Blanshard 1992; Roos and Karel 1991) and is related to the water mobility.  $T_g$  was determined from the first derivative of the thermogram at the inflection point for each sample. Glass transition temperatures were around  $-26\text{ }^{\circ}\text{C}$  (from  $-24$  to  $-29\text{ }^{\circ}\text{C}$ ) for all tested formulations, and it was similar to those reported wheat flour doughs (Räsänen et al. 1998; Laaksonen and Roos 2000). This temperature was influenced by the quantities of water added in the formulations. Clearly, it can be observed that increasing the amount of water available to freeze in the dough produced a decrease in  $T_g$  (Fig. 4a). This result occurs because the average molecular weight of the mixture decreases.

#### 4 Influence of Dough Composition on Starch Gelatinization Temperatures

Gelatinization is a key physicochemical transformation that starch granules undergo when subjected to heat treatment in the presence of water. Gelatinization induces a number of changes in starch granules such as loss of order, swelling, exudation of amylose, improved digestibility, granule disruption, enhanced solubility, and increased viscosity. From DSC studies, gelatinization is resultantly an endothermic process, although it could involve the following two stages (Stevens and Elton 1971): (1) cleavage of existing hydrogen bonds (endothermic) due to

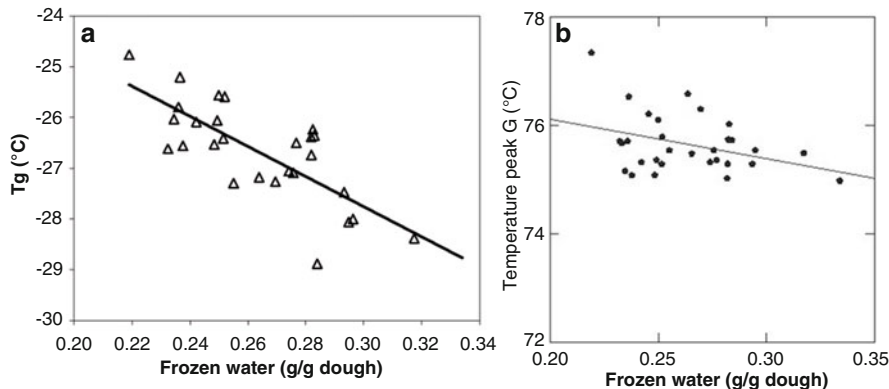


**Fig. 4** Relationship between the amount of frozen water content in the gluten-free doughs (g water/g dough) on (a) the glass transition temperature,  $T_g$  (°C), and (b) temperature of gelatinization peak  $G$  determined by DSC

hydration and swelling of amorphous regions which facilitates molecular mobility and then provokes an irreversible molecular transition and (2) formation of new bonds (involving water) to give a less ordered structure (exothermic) and dissociation of double helices and expansion of granules as the polymers hydrate.

When dough was heated in the DSC, a characteristic biphasic endotherm appeared: Peak  $G$  which has been assigned to the swelling of the starch amorphous region and a cooperative mediated melting of starch crystallites, Peak  $M1$  which corresponds to the melting of the most stable crystallites, and Peak  $M2$  which is assigned to the melting of the amylose–lipid complexes. The appearance of peaks  $G$  and  $M1$  demonstrates that there was not enough water available in the system for the gelatinization process (Fig. 2).

For the starch/water system, it was found that onset temperature ( $T_o$ ) reflected the initiation of this process. Onset temperature was followed by a peak ( $T_p$ ) and concluded at  $T_c$ . After  $T_c$ , all amylopectin double helices were dissociated, although swollen granule structures were retained until more extensive temperature was been applied (Tester and Debon 2000). Specifically, for the studied cornstarch/water mixtures, values of 60.6, 66.9, and 74.0 °C were obtained for  $T_o$ ,  $T_p$ , and  $T_c$ , respectively. The temperature range  $T_c - T_o = 13.4$  °C represents the so-called gelatinization period. Sandhu et al. (2004) found that the  $T_o$ ,  $T_p$ , and  $T_c$  of corn starches–water mixture ranged from 60 to 69.3 °C, 71.5 to 73.1 °C, and 76.5 to 78.0 °C, respectively. For starches of five open pollinated corn populations, White et al. (1990) found the gelatinization period between 8.7 and 16.4 °C. For the formulations of gluten-free doughs assayed in this work,  $T_o$  ranged from 67.1 to 69.2 °C,  $T_p$  from 75.1 to 78.2 °C, and  $T_c$  from 81.9 to 88.1 °C, and the gelatinization period varied between 14.0 and 18.9 °C.

Peak  $G$  temperature increased when the amount of water decreased, maintaining constant gum concentration, that is, less water was available to penetrate the granule and mediate in the gelatinization process. Once all available water that

was external to the granule was exhausted, the cooperative plasticization process was arrested, and further gelatinization depended upon increased levels of molecular mobility and granular swelling that were initiated and enhanced by heat. These conditions demanded heating to higher temperatures. The obtained results also showed that for a given water content, the addition of hydrocolloids caused a significant increase ( $p < 0.05$ ) of peak  $G$ ; this was probably the result of the starch–hydrocolloid interaction, which produced a more stable structure, and less water mobility due to gums–water interactions, requiring a higher temperature for disorganization.

Moreover, when the frozen water content of the dough was progressively reduced (0.334–0.219 g water/g dough), endotherms shifted to higher temperatures (peak  $G$  from 74.98 to 77.34 °C) as less water was available (Fig. 4b). As the amount of frozen water decreased, water mobility diminished and the water-diffusion-mediated step of the transition (peak  $G$ ) required more energy. With respect to the gelatinization enthalpies, no significant differences ( $P > 0.05$ ) were observed among the samples studied.

These results support the hypothesis that a reduced level of solvent plasticization, resulting from the addition of nonaqueous solutes to a pure water system, produces elevation of the gelatinization temperature. The reduced level of solvent plasticization of the amorphous growth ring regions requires input of a greater amount of thermal energy before the starch granule swells and begins to gelatinize.

## 5 Conclusions

The effect of protein and hydrocolloid content on water availability in gluten-free pasta formulation was studied using differential scanning calorimetry. Predictive regression models were used to plot mixture response surfaces of unfrozen water content and melting temperature of water as a function of composition. The response surface methodology led to a “saddle”-type relationship between the unfrozen water and the dough composition, showing the complex interactions between single components. Increasing the amount of water in the dough available to freeze produced a decrease in glass transition temperatures of the systems, reflecting the higher mobility of macromolecules present.

A biphasic endotherm was observed in the gelatinization transition for all formulations, and a significant displacement to higher temperatures of the endotherms was observed when hydrocolloid content was increased or water content decreased as water mobility decreased and the water-diffusion-mediated step of the transition (peak  $G$ ) needed more energy to occur.

## References

- Blanshard JMV (1987) Starch granule structure and function: a physicochemical approach. In: Galliard T (ed) *Starch: properties and potential*. Wiley, New York, pp 17–18
- Cornell JA (2002) Experiments with mixtures: designs, models, and the analysis of mixture. Wiley, New York, pp. 22–95 and 132–220
- Fennema OR (1996) Water and ice. In: Fennema OR (ed) *Food chemistry*. Marcel Dekker, New York, pp 17–94
- Kalichevsky MT, Blanshard JMV (1992) A study of the effect of water on the glass transition of 1:1 mixtures of amylopectin, casein and gluten using DSC and DMTA. *Carbohydr Polym* 19:271–278
- Laaksonen T, Roos YH (2000) Thermal, dynamic-mechanical, and dielectric analysis of phase and state transitions of frozen wheat doughs. *J Cereal Sci* 32:281–292
- Räsänen J, Blanshard JMV, Mitchell JR, Derbyshire W, Autio K (1998) Properties of frozen wheat doughs at subzero temperatures. *J Cereal Sci* 28:1–14
- Roos YH (1986) Phase transitions and unfreezable water content of carrots, reindeer meat and white bread studied using differential scanning calorimetry. *J Food Sci* 51:684–686
- Roos YH, Karel M (1991) Water and molecular weight effects on glass transition in amorphous carbohydrates and carbohydrate solutions. *J Food Sci* 56:1676–1681
- Sandhu KS, Singh N, Kaur M (2004) Characteristics of the different types and their grain fractions: physicochemical, thermal, morphological, and rheological properties of starches. *J Food Eng* 64:119–127
- Stevens DJ, Elton GAH (1971) Thermal properties of the starch–water system. Part I. Measurement of heat of gelatinisation by differential scanning calorimetry. *Starch-Starke* 23:8–11
- Tester RF, Debon SJ (2000) Annealing of starch. A review. *Int J Biol Macromol* 27:1–12
- Tolstoguzov VB (2000) Foods as dispersed systems. Thermodynamic aspects of composition–property relationships in formulated food. *J Therm Anal Calorim* 61:397–409
- White PJ, Abbas IR, Pollak L, Johnson LJ (1990) Intra and interpopulation variability of thermal properties in maize starch. *Cereal Chem* 67:70–73

# Effects of $a_w$ Reduction and Type of Sugar in Rheological Behavior, Water Mobility, and Structural Changes in Apples

S. Vicente, A. Nieto, and S.M. Alzamora

## Abbreviations

$^1\text{H}$ NMR	Pulsed nuclear magnetic resonance spectrometer
C1	Constant
C2	Constant
C3	Constant
CPMG	Carr-Purcell-Meiboom-Gill sequence
$E_d$	Deformability modulus
$\gamma$	Strain
$G'$	Storage moduli
$G''$	Loss moduli
$h_0$	Coefficient of viscosity associated with Newtonian flow
$h_i$	Coefficients of viscosity associated with the Kelvin-Voigt elements

---

S.M. Alzamora is member of Consejo Nacional de Investigaciones Científicas y Técnicas de la República Argentina.

S. Vicente  
ANPCyT, Universidad de Buenos Aires, Buenos Aires, Argentina

Departamento de Industrias, Facultad de Ciencias Exactas y Naturales,  
Universidad de Buenos Aires, Buenos Aires, Argentina

A. Nieto (✉)  
Departamento de Industrias, Facultad de Ciencias Exactas y Naturales,  
Universidad de Buenos Aires, Buenos Aires, Argentina

CONICET, Ciudad Universitaria, Ciudad Autonoma de Buenos Aires 1428, Argentina  
e-mail: [andrea@di.fcen.uba.ar](mailto:andrea@di.fcen.uba.ar)

S.M. Alzamora  
Departamento de Industrias, Facultad de Ciencias Exactas y Naturales, Universidad de Buenos Aires, Ciudad Universitaria, Buenos Aires, Argentina

$J(t)$	Creep compliance
$J_0$	Instantaneous compliance
$J_i$	Retarded compliances
$\lambda_i$	Retardation times
LM	Optical microscopy
LM	Light microscopy
MANOVA	Multivariate analysis of variance
$\sigma_R$	True stress
$(\sigma_R^R)$	True rupture stress
$\tau$	Constant stress applied
$t$	Time
$T_2$	Transverse relaxation times
TEM	Transmission electron microscopy
TEM	Transmission electron microscopy
$W$	Work at rupture or toughness
$w$	Frequency
$\varepsilon_R$	Hencky strain
$\varepsilon_R^R$	True rupture strain at $\sigma_R^R$

## 1 Introduction

Osmotic dehydration is an operation that is commonly used to obtain minimally processed high-moisture fruits with characteristics close to those of fresh fruits. Many mechanisms are involved in mass transfer of solutes inside the product with an opposite flux of water, but also physical, micro-, and macrostructural modifications occur that influence interactions between water, structure, chemical compounds, and the mechanical behavior of fruits (Alzamora et al. 2000).

The aim of this study was to evaluate the effect of two humectants, glucose and trehalose, at two different water activities ( $a_w$ ), 0.94 or 0.97, on the rheological behavior of osmotically dehydrated parenchymatous apple tissues at large deformations (compression test) and small deformations (dynamic oscillatory shear and creep/recovery test), water mobility (spin-spin relaxation times), and micro- and ultrastructure studies (light microscopy (LM) and transmission electron microscopy (TEM)).

## 2 Materials and Methods

Fresh apples (*Malus pumila*, Granny Smith var.; 13 °Brix;  $a_w = 0.98$ ) were cut to obtain outer parenchyma cylinders (15 mm in diameter, 15 mm in thickness) for compression test, water mobility analysis and structural observations, and discs (30 mm diameter, 6 mm in length) for dynamic tests.

Osmotic dehydration was performed by immersing apple pieces into 22.0 % w/w and 38.7 % w/w glucose or 34.4 % w/w and 48.0 % w/w trehalose aqueous solutions with forced convection at atmospheric pressure to reach  $a_w$  0.97 or  $a_w$  0.94, respectively.

Mechanical behavior at large deformations was determined by uniaxial compression with an Instron 1011 machine (USA) (20 mm/min head rate, 500 N load range, 30 replicates). True stress ( $\sigma_R$ ), Hencky strain ( $\epsilon_R$ ), true rupture stress ( $\sigma_R^R$ ), true rupture strain at  $\sigma_R^R$  ( $\epsilon_R^R$ ), deformability modulus ( $E_d$ ) up to 10 % of compression, and work at rupture or toughness ( $W$ ) were obtained (Peleg 1978).

Viscoelastic properties were characterized in a Paar Physica MCR 300 rheometer (Austria) (controlled strain mode 3 cm diameter parallel plate geometry, 12 replicates). Storage ( $G'$ ) and loss ( $G''$ ) moduli were measured in the linear viscoelastic range (using a strain amplitude value of 0.01 % and frequency ( $\omega$ ) 0.1–100 s<sup>-1</sup>). Creep/recovery test was conducted by applying a constant shear stress of 35 Pa until 100 s (recovery: 200 s). A mechanical model consisting of a spring in series with two Voigt elements and a dashpot element was used to fit the compliance response (Eq. (1)):

$$J(t, \tau) = (J_0) + \sum_{i=1}^2 (J_i) \left( 1 - e^{-t/\lambda_i} \right) + (t/\eta_0) \quad (1)$$

where  $J$  ( $t, \tau$ ) is the creep compliance ( $=\gamma(t)/\tau$ ) with  $\gamma(t)$  being the strain at time  $t$  and  $\tau$  the constant stress applied;  $J_0$  is the instantaneous compliance at  $t = 0$ ;  $J_i$  are the retarded compliances;  $\lambda_i$  ( $=\eta_i \times J_i$ ) are the retardation times and  $\eta_i$  are the coefficients of viscosity associated with the Kelvin-Voigt elements; and  $\eta_0$  is the coefficient of viscosity associated with Newtonian flow and its inverse, the steady-state fluidity of the material.

Transverse relaxation times ( $T_2$ ) were determined in a Bruker Minispec mq/20 pulsed nuclear magnetic resonance spectrometer (<sup>1</sup>H NMR) (0.47 T; 20 MHz) using the Carr-Purcell-Meiboom-Gill sequence (CPMG) (2 ms pulse spacing; 8 scans; recycled delay 4 s) (6 replicates). The  $T_2$  relaxation experimental curves were fitted by a three-exponential equation, and  $A_i$  values were normalized (Peleg 1978, 1984):

$$Y = (y_0) + \sum_{i=1}^n (A_i) \left( e^{-t/T_{2i}} \right) \quad (2)$$

Changes in the microstructure and ultrastructure of apple tissue were assessed using optical microscopy (LM) (Carl Zeiss Axioskop 2) and transmission electron microscopy (TEM) (JEOL JEM 1200 EX II).

Fresh apple samples were used in each case as controls (called control 0.94 and control 0.97 for experiments at  $a_w$  0.94 and 0.97, respectively).

Statgraphics Plus (USA) and the InfoStat (Argentina) software were used for nonlinear regression and for one-factor multivariate analysis of variance (MANOVA), respectively. In the multivariate analysis, Hotelling test was applied to determine significance level with Bonferroni-corrected level of  $\alpha = 0.05$ .

### 3 Results and Discussion

Compression curves for fresh apple showed a linear force-strain relationship, followed by a nonlinear region where force also increased with strain up to the failure point and then started to decrease. Overall, treated apples were less firm and more deformable than fresh apples (Fig. 1). The values of mechanical parameters were significantly different between fresh and treated apples. There were significant differences between apples osmotically dehydrated with glucose or trehalose at both levels of  $a_w$ . True rupture stress values were higher at  $a_w$  0.94 than at  $a_w$  0.97 (Table 1).

Storage modulus  $G'$  greatly exceeded loss modulus  $G''$  for raw and treated tissues, showing a solid behavior dominating the viscoelastic response over the entire frequency range. There was a significant decrease in  $G'$  and  $G''$  values due to all osmotic treatments (Fig. 2), indicating decreased elasticity and viscosity of apple sample, probably associated with damage to the integrity of tissue structure. In general, initial and decay compliances and steady-state fluidity significantly increased by the treatments (Fig. 3, Table 2). The increase in deformability was greater for apples treated with trehalose than for apples treated with glucose as humectants at both levels of  $a_w$ . Retarding times were not significantly affected by the different treatments.

The analysis of magnetization decay curves of fresh apple showed the presence of three components. Average values of relaxation times and relative amplitudes for control 0.97 (86.3 % w/w moisture content) were  $T_{23} = 950 \pm 60$  ms;

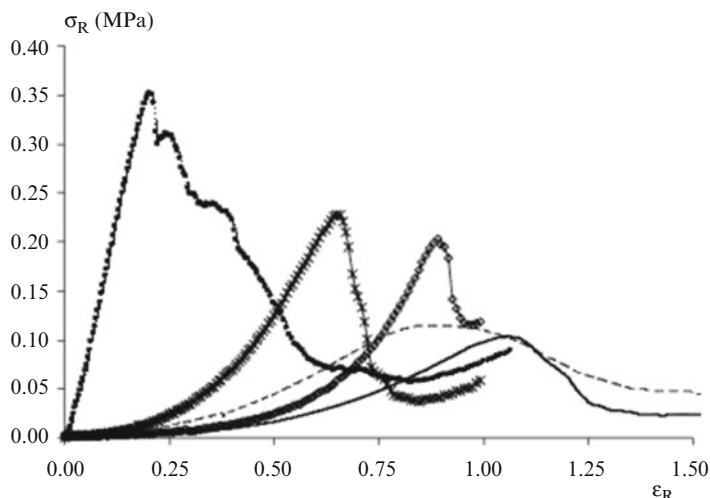


**Fig. 1** Typical compression curves of true stress vs. true strain for fresh apple (control) and apples osmotically dehydrated in aqueous solutions of glucose or trehalose at  $a_w = 0.97$  or  $a_w = 0.94$ . Control (filled circle); glucose,  $a_w$  0.94 (cross); glucose,  $a_w$  0.97 (single solid line); trehalose,  $a_w$  0.94 (diamond); trehalose,  $a_w$  0.97 (spaced solid line)

**Table 1** Mean values of compression parameters for apples osmotically dehydrated in aqueous solutions of glucose and trehalose with  $\alpha_w = 0.97$  or  $\alpha_w = 0.94$

Treatment	$\sigma_R^R$ (MPa) ± SD	$\varepsilon_R^R$ ± SD	$E_d$ (MPa) ± SD	$W$ (MJ/m <sup>3</sup> ) ± SD	
Control 0.97	0.33 ± 0.04	0.26 ± 0.02	1.7 ± 0.2	44 ± 8	A
Control 0.94	0.34 ± 0.03	0.19 ± 0.02	2.1 ± 0.3	37 ± 7	B
Immersed in 22.0 % w/w glucose solution	0.11 ± 0.02	0.79 ± 0.06	0.04 ± 0.01	37 ± 6	C
Immersed in 34.4 % w/w trehalose solution	0.12 ± 0.02	1.02 ± 0.07	0.02 ± 0.01	36 ± 5	D
Immersed in 38.7 % w/w glucose solution	0.23 ± 0.04	0.64 ± 0.08	0.05 ± 0.02	41 ± 7	E
Immersed in 48.0 % w/w trehalose solution	0.22 ± 0.07	0.81 ± 0.07	0.03 ± 0.01	42 ± 6	F

MANOVA of treatments was highly significant for viscoelastic measurements ( $F_{20, 652} = 33.16$ ;  $P < 0.0001$ ). Post hoc multiple comparisons used Hotelling tests based on Bonferroni correction  $\alpha = 0.05$ . Different letters indicate significant differences at  $P \leq 0.05$ . Control 0.97 and Control 0.94: controls (fresh apple) for the fruit batch used for tests at  $\alpha_w$  0.97 and 0.94, respectively. SD standard deviation

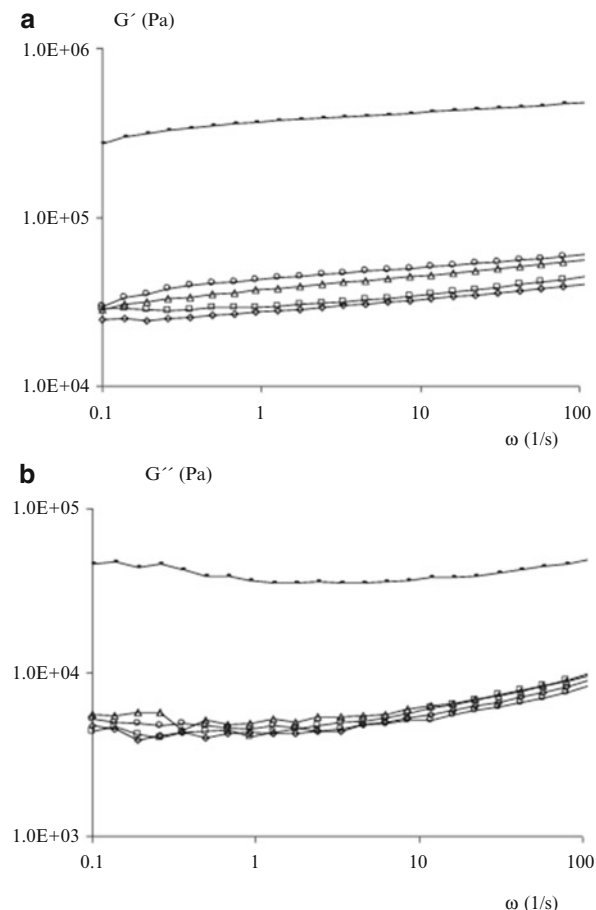


**Fig. 2** Mechanical spectrum for fresh apple (control) and apples osmotically dehydrated in aqueous solutions of glucose or trehalose at  $\alpha_w = 0.97$  or  $\alpha_w = 0.94$ . (a) Storage modulus  $G'$ ; (b) loss modulus  $G''$ . Control (single solid line); glucose,  $\alpha_w$  0.97 (open circle); glucose,  $\alpha_w$  0.94 (diamond); trehalose,  $\alpha_w$  0.97 (triangle); trehalose,  $\alpha_w$  0.94 (square)

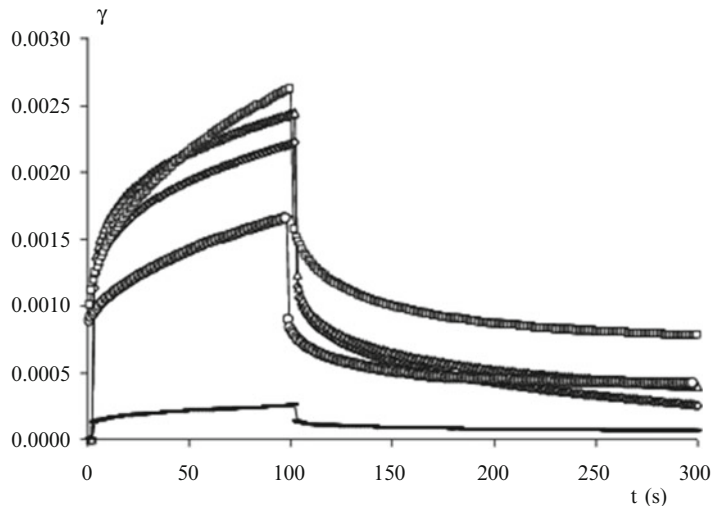


**Fig. 3** Typical experimental creep/recovery curves (deformation  $\gamma$  vs. time  $t$ ) for fresh apple (control) and apples osmotically dehydrated in aqueous solutions of glucose or trehalose at  $a_w = 0.97$  or  $a_w = 0.94$ . Control (single solid line); glucose,  $a_w$  0.97 (open circle); glucose,  $a_w$  0.94 (diamond); trehalose,  $a_w$  0.97 (triangle); trehalose,  $a_w$  0.94 (square)

**Table 2** Means of viscoelastic parameters derived by fitting Eq. (2) to compliance curves from creep phase for apples osmotically dehydrated in aqueous solutions of glucose and trehalose with  $a_w = 0.97$  or  $a_w = 0.94$

Treatment	$J_0 \times 10^6$ (1/Pa) ± SD	$J_1 \times 10^6$ (1/Pa) ± SD	$J_2 \times 10^6$ (1/Pa) ± SD	$\lambda_1$ (s) ± SD	$\lambda_2$ (s) ± SD	$\eta_0 \times 10^{-7}$ (Pa s) ± SD	
Control 0.94	$3 \pm 1$	$2 \pm 1$	$0.9 \pm 0.3$	$31 \pm 15$	$2 \pm 1$	$9 \pm 2$	A
Control 0.97	$4 \pm 1$	$2.3 \pm 0.3$	$0.9 \pm 0.3$	$30 \pm 12$	$3 \pm 2$	$5 \pm 2$	B
Immersed in 22.0 % w/w glu- cose solution	$21 \pm 2$	$9 \pm 2$	$5 \pm 1$	$27 \pm 7$	$2.8 \pm 0.4$	$1.05 \pm 0.06$	C
Immersed in 34.4 % w/w treha- lose solution	$27 \pm 3$	$18 \pm 3$	$9 \pm 3$	$30 \pm 7$	$2.7 \pm 0.4$	$0.6 \pm 0.1$	D
Immersed in 38.7 % w/w glu- cose solution	$28 \pm 2$	$12 \pm 2$	$7.3 \pm 0.8$	$22 \pm 2$	$2.2 \pm 0.2$	$0.9 \pm 0.2$	D
Immersed in 48.0 % w/w treha- lose solution	$32 \pm 5$	$15 \pm 3$	$9 \pm 2$	$21 \pm 3$	$2.3 \pm 0.3$	$0.8 \pm 0.2$	D

MANOVA of treatments was highly significant for viscoelastic measurements ( $F_{30, 265} = 5.83$ ;  $P < 0.0001$ ). Post hoc multiple comparisons used Hotelling tests based on Bonferroni correction  $\alpha = 0.05$ . Different letters indicate significant differences at  $P \leq 0.05$ . SD standard deviation. Control 0.97 and Control 0.94: controls (fresh apple) for the fruit lot used for tests at  $a_w$  0.97 and 0.94, respectively

**Table 3** Mean proton transverse relaxation times and signal percentages of the two components for apples osmotically dehydrated in aqueous solutions of glucose and trehalose with  $a_w = 0.97$  or  $a_w = 0.94$

Treatment	$C_1$ (%) ± SD	$C_2$ (%) ± SD	$T_{21}$ (ms) ± SD	$T_{22}$ (ms) ± SD	
Immersed in 22.0 % w/w glucose solution	24 ± 9	76 ± 9	72 ± 25	290 ± 38	A
Immersed in 34.4 % w/w trehalose solution	40 ± 8	60 ± 9	63 ± 12	201 ± 20	B
Immersed in 38.7 % w/w glucose solution	27 ± 1	73 ± 1	56 ± 5	337 ± 12	C
Immersed in 48.0 % w/w trehalose solution	39 ± 3	61 ± 3	31 ± 4	215 ± 20	D

MANOVA of treatments was highly significant for viscoelastic measurements ( $F_{9, 126} = 23.32$ ;  $P < 0.0001$ ). Post hoc multiple comparisons used Hotelling tests based on Bonferroni correction  $\alpha = 0.05$ . Different letters indicate significant differences at  $P \leq 0.05$ . SD standard deviation

$T_{22} = 205 \pm 45$  ms;  $T_{21} = 50 \pm 11$  ms;  $C_3 = 67 \pm 2$  %;  $C_2 = 18 \pm 4$  %; and  $C_1 = 15 \pm 3$  %. For control 0.94 (88.0 % w/w moisture content), the mean values were  $T_{23} = 1,207 \pm 100$  ms;  $T_{22} = 325 \pm 20$  ms;  $T_{21} = 57 \pm 8$  ms;  $C_3 = 72 \pm 3$  %;  $C_2 = 21 \pm 2$  %; and  $C_1 = 17 \pm 1$  %. As can be observed,  $T_{22}$  and  $T_{23}$  values depended on the water content of the fresh fruit. The relaxation time  $T_{21}$  is attributed to the protons in the less mobile water fraction. The relaxation time  $T_{22}$  is attributed to water fraction with low mobility. The relaxation time  $T_{23}$  is attributed to the protons in the most mobile water fraction.  $T_{2i}$  values of the three groups were significantly reduced by osmosis, and this reduction was in general greater in apples treated with trehalose. Relaxation rates in treated apples were much faster than in fresh tissue. The transverse relaxation of water protons in osmotically dehydrated tissues was better described by two exponentials, denoting only two populations of water (Table 3).

Microscopic observations showed different structural features mainly at cell wall and membrane integrity or plasmolysis between apples impregnated with glucose or trehalose. Overall, osmosis provoked plasmolysis (for tissues treated with trehalose) or rupture of membranes (for tissues treated with glucose), reducing turgor pressure. Plasmolysis or rupture and contraction of tissues were greater at the lowest  $a_w$ . Trehalose-treated tissues showed middle lamella areas of intense electron density and much more undulated cell walls, compared with those treated with glucose (Ferrando and Spiess 2001).

## 4 Conclusions

The loss of turgor could explain the lower elasticity and stiffness (lower  $E_d$ ,  $G'$  and higher  $J_0$ ) and lower compression strength (less  $\sigma_R^R$ ) in apples subjected to osmosis. The plasticization of the wall structure made by sugars as well as the compactness

of the walls due to the removal of water and the lack of turgor could be responsible for the greater deformation of osmotic dehydrated tissues (higher  $\epsilon_R^R$  and higher capacitances  $J_i$ ) (Martinez et al. 2007).

These results can improve preservation technology design for minimally processed apples where  $a_w$  reduction is one of the hurdles to obtain fruit stability.

**Acknowledgements** The authors want to thank the financial support from Universidad de Buenos Aires, CONICET, and ANPCyT of Argentina and from BID. They also thank Cargill Inc., Argentina, and EXPOFRUT S.A. for supplying the trehalose and the apples.

## References

- Alzamora SM, Castro MA, Vidales SL, Nieto AB, Salvatori DM (2000) The role of tissue microstructure in the textural characteristics of minimally processed fruits. In: Alzamora SM, Tapia MS, López MA (eds) Minimally processed fruits and vegetables: fundamental aspects and applications. Aspen Publishers Inc, Gaithersburg, MD
- Ferrando M, Spiess WEL (2001) Cellular response of plant tissue during the osmotic treatment with sucrose, maltose and trehalose solutions. *J Food Eng* 49:115–127
- Martinez VY, Nieto AB, Salvatori DM, Castro MA, Viollaz PE, Alzamora SM (2007) Viscoelastic characteristics of Granny Smith apple during glucose osmotic dehydration. *J Food Eng* 83:394–403
- Peleg M (1978) An empirical method for estimation of the yield stress from relaxation data. *Mater Sci Eng* 33:289–293
- Peleg M (1984) A note on the various strain measures at large compressive deformations. *J Texture Stud* 15:317–326

# **Effect of Water Content on Thermo-Physical Properties and Freezing Times of Foods**

**M.V. Santos, V. Vampa, A.N. Califano, and N.E. Zaritzky**

## **Abbreviations**

DSC	Differential scanning calorimetry
$E$	Kirchhoff function
FEM	Finite element method
$H$	Enthalpy
$h$	Surface heat transfer coefficient
$k$	Global conductivity
$k_i$	Thermal conductivity of the component $i$
$m$	Global force vector
$T_f$	Freezing temperature
$T_m$	Onset temperature of melting
$T_p$	Peak temperature
$x_b$	Unfreezeable water
$x_h$	Mass fraction of ice
$x_i$	Mass fraction of each component
$x_i^v$	Volumetric fraction of each component

---

M.V. Santos • N.E. Zaritzky (✉)

Centro de Investigación y Desarrollo en Criotecnología de Alimentos (CIDCA), Facultad de Ciencias Exactas, UNLP-CONICET La Plata, 47 y 116, La Plata, 1900, Argentina

Departamento de Ingeniería Química, Facultad de Ingeniería, UNLP, La Plata, Argentina  
e-mail: [mvsantosd@yahoo.com.ar](mailto:mvsantosd@yahoo.com.ar); [zaritzky@ing.unlp.edu.ar](mailto:zaritzky@ing.unlp.edu.ar)

V. Vampa

Departamento de Ciencias Básicas, Facultad de Ingeniería, UNLP, La Plata, Argentina

A.N. Califano

Centro de Investigación y Desarrollo en Criotecnología de Alimentos (CIDCA), Facultad de Ciencias Exactas, UNLP-CONICET La Plata, 47 y 116, La Plata, 1900, Argentina

$x_{w0}$	Total mass fraction of water in the foodstuff
$\Delta H_m$	Latent heat of melting of each substance
$\rho(T)$	Global density
$\rho_i$	Density of the component $i$

## 1 Introduction

For the prediction of temperature change in different foodstuffs during freezing and thawing processes, accurate estimation of the thermo-physical properties of the product is necessary, such as specific heat, density, freezable water content, enthalpy, and initial freezing temperature. These data allow the adequate design and optimization of equipment and processes. Water is a main component in all foods and greatly influences the behavior of these properties, depending on its concentration. During the freezing process, which involves the phase change of water into ice, the specific heat, thermal conductivity, and density undergo abrupt changes due to the latent heat release. This complex process does not have an analytical solution and it can be described as a highly nonlinear mathematical problem. Many difficulties arise when trying to numerically simulate the freezing process, especially when using the finite element method (FEM), which is especially useful when dealing with irregular-shaped foodstuffs. Several techniques have been applied to consider the large latent heat release when using FEM. One traditional method is the use of the apparent specific heat, where the sensible heat is merged with the latent heat to produce a specific heat curve with a large peak around the freezing point, which can be considered a quasi-delta-Dirac function with temperature (depending on the amount of water in the food product) (Pham 2008). However, this method usually destabilizes the numerical solution. Implementation of the enthalpy method, which can be obtained through the integration of the specific heat with temperature (Fikiin 1996; Comini et al. 1990; Pham 2008; Santos et al. 2010), and the Kirchhoff function, which is the integral of the thermal conductivity, allows the reformulation of the heat transfer differential equation into a transformed partial differential system with two mutually related dependent variables  $H$  (enthalpy) and  $E$  (Kirchhoff function) (Scheerlinck et al. 2001). These functions,  $H$  and  $E$  versus temperature, are smoother mathematical functions compared to the specific heat, thermal conductivity, and density versus temperature, avoiding inaccuracies and/or divergence of the numerical method. Even though it brings great advantage to the resolution of the problem, with the simultaneous enhancement of the computational speed of the program, this transformation of variables is not widely used in the literature. Unleavened dough and cooked minced meat were selected due to their significant difference in water content in order to explore the performance of the computational code written using the enthalpy-Kirchhoff formulation. Another important reason is because cooked minced meat and dough are both present in several ready-to-eat meals, therefore contributing valuable information to food processors interested in optimizing cooling and freezing operating conditions of semi- or fully processed goods.

The objectives of this work are (1) to experimentally determine by differential scanning calorimetry (DSC) the thermo-physical properties of dough and cooked minced meat in the freezing range: specific heat as a function of temperature, bound water, heat of melting, initial freezing temperature, etc.; (2) to develop and validate a finite element algorithm to simulate the freezing process in regular and irregularly shaped foodstuffs; and (3) to introduce appropriate equations of the thermo-physical properties in the numerical program to assess the effect of total water content, bound water, and surface heat transfer coefficient on freezing times in an irregular food system.

## 2 Materials and Methods

Two different food materials, unleavened dough and cooked minced meat, which have significant difference in moisture content, were selected. Thermal properties of these products were determined using experimental measurements and predictive equations.

### 2.1 Experimental Measurements

A differential scanning calorimeter (DSC), TA Instruments, New Castle, Delaware, USA, model Q100 controlled by a TA 5000 module with a quench cooling system under a nitrogen atmosphere at 20 mL/min was used. Samples of cooked minced lean beef and the dough were enclosed in sealed aluminum pans, and an empty pan was used as a reference sample. Pans were heated at 2 °C/min from –50 to 100 °C. The specific heat was calculated following ASTM E1269 instructions. Figure 1 shows the apparent Cp values as a function of temperature for dough and cooked minced meat, respectively, as obtained through DSC runs. The latent heat of melting of each substance ( $\Delta H_m$ ), the onset temperature of melting ( $T_m$ ), and the peak temperature ( $T_p$ ) were determined. The  $\Delta H_m$  was calculated by integrating the peaks in the melting curves; this value was used to estimate the unfreezable water fraction in the food material. Unfreezable water ( $x_b$ ), at –40 °C, was considered as the difference between total water content and the amount of frozen water in the deep frozen material. The fraction of frozen water was obtained from the ratio between the latent heat of melting determined for the material and the heat of melting of pure water, 333.2 J/g. The moisture contents (%) of the products were determined by drying triplicate samples in an oven at 80 °C until reaching constant weight. The initial freezing temperature ( $T_f$ ) was experimentally determined from the cooling curves where  $T_f$  was measured by using thermocouples inserted in the samples and applying the tangent method. Table 1 shows the obtained data using DSC measurements  $T_p$ ,  $T_m$ ,  $\Delta H_m$ ,  $x_b$ ,  $x_{w0}$ , and the total water content of the samples ( $x_{w0}(\%)$ ).

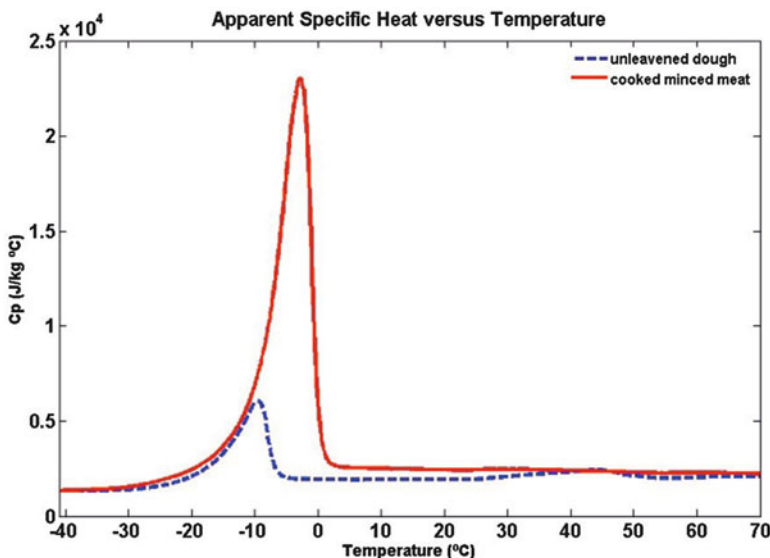


**Fig. 1** Apparent specific heat versus temperature of dough and meat obtained through DSC measurements

**Table 1** Experimental data obtained through DSC measurements. SEM values are in parentheses

	$T_p$ (°C)	$T_m$ (°C)	$\Delta H_m$ (J/g)	$x_b$ (%)	$x_{w0}$ (%)
Cooked minced meat	-3.17 (0.24)	-8.86 (0.79)	172.05 (14.25)	14.66 (2.31)	66.29 (1.96)
Unleavened dough	-9.45 (0.74)	-18.29 (1.38)	33.27 (5.82)	19.26 (1.155)	29.25 (0.59)

## 2.2 Thermal Conductivity of Dough and Meat

Thermal conductivity of dough and cooked meat was calculated using predictive equations. In the case of frozen dough, the Choi and Okos (1986) equation was used for the thermal conductivity and density:

$$k(T) = \sum x_i^v \cdot k_i(T) \quad (1)$$

where  $k$  is the global conductivity,  $k_i$  is the thermal conductivity of the component  $i$  (where  $i$  corresponds to the different components: water, ice (if the temperature is lower than the initial freezing temperature  $T_f$ ), carbohydrate, fat, etc.), and  $x_i^v$  corresponds to the volumetric fraction of each component. The density was

$$\rho(T) = \frac{1}{\sum \frac{x_i}{\rho_i}} \quad (2)$$

where  $\rho(T)$  is the global density and  $\rho_i$  is the density of the component  $i$  (water, carbohydrates, ice, ash, etc.). The fractions “ $x_i$ ” correspond to the mass fraction of each component. Ice content as a function temperature (at  $T < T_f$ ) was estimated using the equation proposed by Miles et al. (1983):

$$x_h = (x_{w0} - x_b) \left( 1 - \frac{T_f}{T} \right) \quad (3)$$

where  $x_h$  is the mass fraction of ice, and  $x_{w0}$  is the total mass fraction of water in the foodstuff. At a temperature range above  $T_f$ , the formula proposed by Sorenfors (1973) for minced meat was applied to calculate the thermal conductivity as a function of the water content in the meat product:

$$k(x_{w0}) = 0.096 + 0.34 \cdot x_{w0} \quad (4)$$

At temperatures below freezing state the following was used (Miles et al. 1983):

$$k(T) = 1.745 \cdot \left( 1 - \frac{T_f}{T} \right) + 0.233 \quad (5)$$

Figure 2a, b shows the thermal conductivity as a function of temperature, which was used in the numerical simulations for dough and meat, respectively. The dough composition given by the producer was 47 % carbohydrates, 30 % water, 15 % fat, 6 % protein, and 2 % fiber; these values were used in Eqs. 1 and 2 to estimate the thermal properties versus temperature.

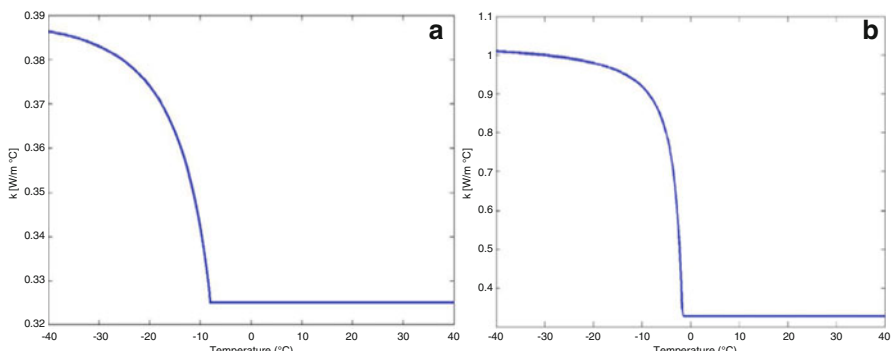


**Fig. 2** Thermal conductivity versus temperature for (a) dough, and (b) cooked minced lean meat

## 2.3 Numerical Model

The original heat transfer equation in cylindrical coordinates is

$$C_p(T) \frac{\partial T}{\partial t} r = \frac{\partial}{\partial r} \left( k(T) r \frac{\partial T}{\partial r} \right) + \frac{\partial}{\partial z} \left( k(T) r \frac{\partial T}{\partial z} \right) = \nabla \cdot (k(T) r \nabla T) \quad \text{in } \Omega \quad (6)$$

The equation is valid in the domain  $\Omega$ , where  $T$  is the temperature, and  $r$  and  $z$  the radial and axial coordinates, respectively. The boundary and initial conditions are

$$\left( \frac{\partial T}{\partial z} \cdot nz + \frac{\partial T}{\partial r} \cdot nr \right) k = h(T_{\text{ext}} - T) \quad t \geq 0 \text{ in } \partial\Omega_1 \quad (7)$$

$$\left( \frac{\partial T}{\partial z} \cdot nz + \frac{\partial T}{\partial r} \cdot nr \right) k = 0 \quad t \geq 0 \text{ in } \partial\Omega_2 \quad (8)$$

$$T = T_0 \quad t = 0 \text{ in } \Omega \quad (9)$$

where  $\partial\Omega_1$  is the domain of the convective interface which corresponds to the surface in contact with the cooling air,  $nz$  and  $nr$  are the normal outward unit vector components,  $\partial\Omega_2$  is the domain with axial symmetry (flux zero condition),  $T_{\text{ext}}$  is the external air temperature,  $T_0$  is the initial temperature, and  $h$  is the surface heat transfer coefficient. By performing the following change of variables:

$$H = \int_{T^*}^T \rho(T) C_p(T) dT$$

$$E = \int_{T^*}^T k(T) dT$$

where  $H$  is defined as the volumetric specific enthalpy,  $E$  is the Kirchhoff function that represents the thermal conductivity integral (Comini et al. 1990; Fikiin 1996), and  $T^*$  is a reference temperature that corresponds to a zero value of  $H$  and  $E$ . By inserting  $H$  and  $E$  in Eqs. (6–9) the following equations were obtained:

$$\frac{\partial H}{\partial t} = \nabla^2 E \quad \text{in } \delta\Omega \quad t \geq 0 \quad (10)$$

$$-(\nabla E) \cdot n = h(T - T_{\text{ext}}) \quad \text{in } \delta\Omega \quad t \geq 0 \quad (11)$$

$$H = H_0 \quad t = 0 \quad (12)$$

In order to solve the new governing heat transfer equation, a numerical finite element algorithm was developed. The enthalpy distribution at any point in the domain was approximated by using interpolating functions and the node enthalpies

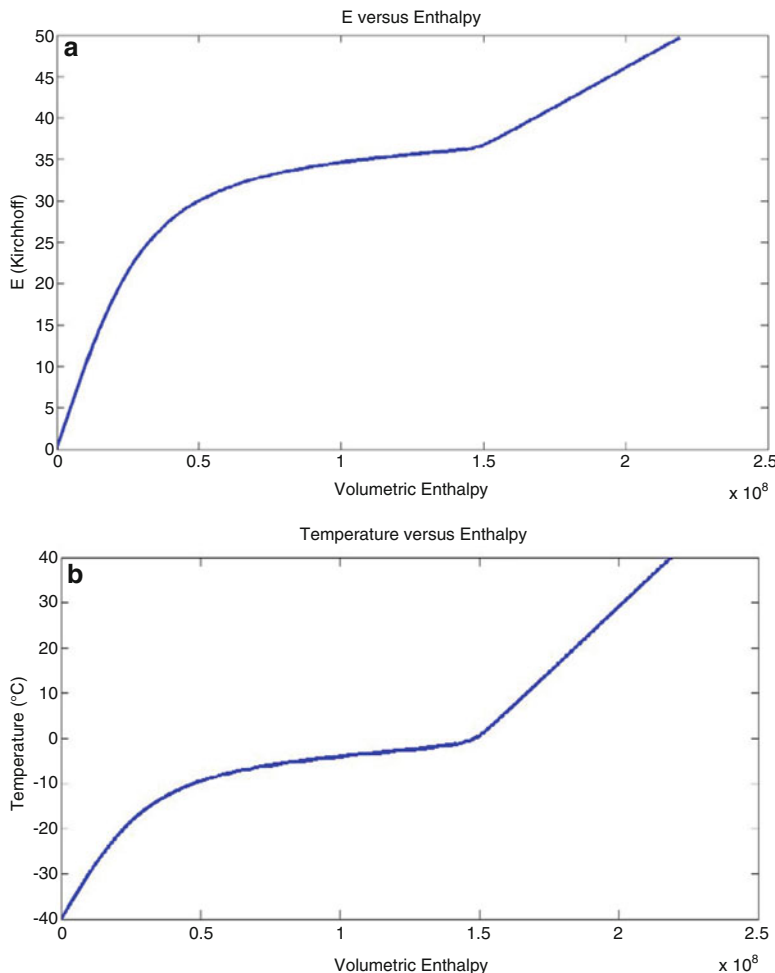


**Fig. 3** (a) Kirchhoff versus enthalpy, and (b) temperature versus enthalpy for cooked minced meat

in the given element. The resulting equation after applying the weight residual formulation and Galerkin method in the FEM was (Bathe 1996)

$$CG \frac{dH}{dt} + FG \cdot T(H) + KG \cdot E(H) = m \quad (13)$$

which represents a system of ordinary differential equations, where CG is the global capacitance matrix, KG is the global conductance matrix, FG is the global convection matrix, and  $m$  is the global force vector. The input functions  $T(H)$  and  $E(H)$  are shown in Fig. 3a, b. A constant value of density equal to  $604 \text{ kg/m}^3$  was used for the

meat product in the calculation of the volumetric enthalpy. Since there is no analytical solution for the simulation of a phase change problem, the numerical code was compared with experimental freezing curves found in the literature for irregular minced meat objects containing 75 % water (Cleland et al. 1987; Califano and Zaritzky 1997). The numerical predictions resulted in agreement with the experimental data, even though the material exhibited a sharp phase change. Furthermore, the numerical simulations were contrasted with experimental time-temperature freezing curves of two finite cylinders (dough and cooked minced meat). Several samples were placed in a tunnel freezer with circulating air in order to obtain similar industrial operating conditions. The temperature curves of the samples at several points inside the product were recorded using a temperature acquisition device (Testo 175, Testo AG, Germany); the surface heat transfer coefficient of the system was  $h = 11 \text{ W/m}^2 \text{ }^\circ\text{C}$ . The maximum difference between the predicted and experimental temperatures for all experiments undertaken was less than  $3.2 \text{ }^\circ\text{C}$ . As a result, the code was checked against experiments developed in the present work as well as with data found in the literature, which demonstrates that the numerical solutions correspond with accurate temperature predictions.

### 3 Simulation of the Freezing Process of an Irregular Bi-dimensional Object with Different Water Contents

The numerical code was used to calculate freezing times of an irregular shape commonly found in industrial processing of dough. The dimensions of the irregular domain were fixed according to the industrial process, and it could not be assimilated as a regular object. It has a symmetry axis, and therefore it was considered a solid of revolution. Figure 4a shows the mesh used for the finite element simulation, considering that there was a symmetry condition at border 1. The code used as input two established the thermal properties corresponding to unfermented dough and minced meat, which had a significant difference in their amount of water, in order to visualize their effect on the thermo-physical properties and freezing times. Moreover, the effect of the heat transfer coefficients was also analyzed. Freezing time values were calculated considering an initial uniform temperature of  $5 \text{ }^\circ\text{C}$ , an external fluid temperature of  $-30 \text{ }^\circ\text{C}$ , and a final temperature of  $-15 \text{ }^\circ\text{C}$  at the warmest point inside the foodstuff. The finite element code developed in this work was very stable and required minimum computational efforts (CPU times  $< 5 \text{ min}$ ); this code also solves highly nonlinear problems such as freezing, which has an apparent specific heat with a very high peak around the freezing region. This is an important aspect, because most common commercial software are not able to solve this type of phase change problems. In the case of dough, freezing times of samples with the same dry matter formulation but different total water contents of 29 and 40 % wb are compared in Table 2; the corresponding values of bound water were considered in each case. Freezing times for minced meat with different moisture

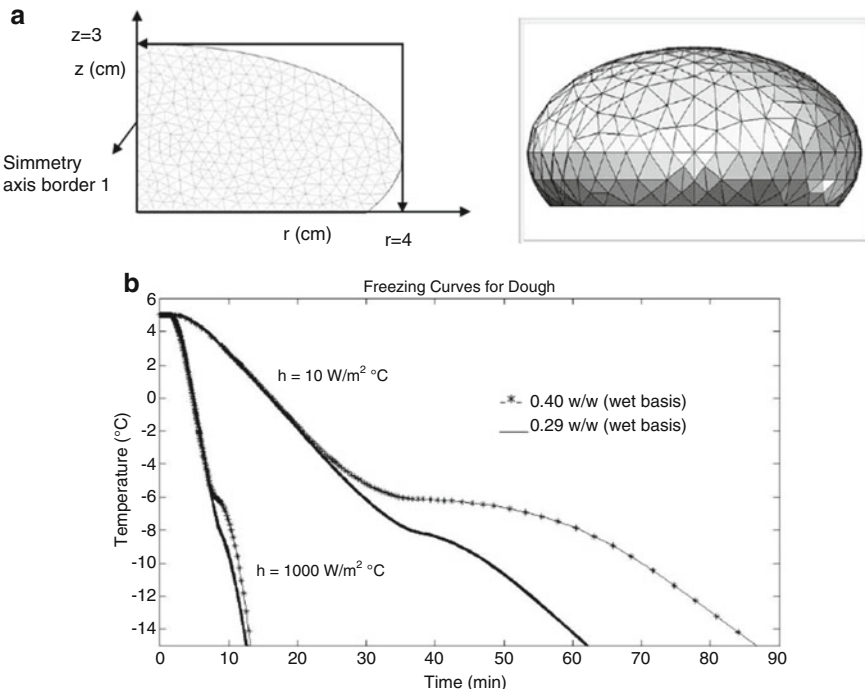


**Fig. 4** (a) Geometry and mesh of bi-dimensional object used in simulations, and (b) freezing curves for dough with different water contents considering initial uniform temperature of 5 °C, and external fluid temperature of −30 °C

**Table 2** Freezing times applied to dough with different moisture contents  $T_{\text{ext}} = -30 \text{ °C}$

Surface heat transfer coefficient $h (\text{W/m}^2 \text{ °C})$	Dough		Minced meat	
	$x_{w0} = 0.29$	$x_{w0} = 0.40$	$x_{w0} = 0.66$	$x_{w0} = 0.72$
	$x_b = 0.192$	$x_b = 0.166$	$x_b = 0.146$	$x_b = 0.125$
	Freezing times (min) $T_{\text{ext}} = -30 \text{ °C}$			
5	108.83	161.32	243.95	261.61
20	40.18	52.31	68.93	72.94
100	18.79	22.19	22.84	23.57
1,000	12.74	13.32	11.00	11.00

\*water mass fraction (w/w wet basis)

contents but the same dry matter composition is also shown in Table 2. As an example, Fig. 4b shows the time–temperature curves for dough formulations with different free water contents. The extension of the plateau zone depends on the  $h$  value, being shorter as  $h$  increases. Similar behavior was observed for minced meat. When freezing is conducted with low heat transfer coefficients (stagnant air chambers)  $h \leq 20 \text{ W/m}^2 \text{ °C}$ , products with the same geometry but different free water contents ( $x_{\text{free}} = x_{w0} - x_b$ ) such as dough (29 and 40 % water wet basis) and

meat (66 and 72 % wet basis) show an increase of the freezing times as the amount of freezable water increases due to a larger amount of latent heat of ice crystallization that has to be removed from the sample. In contrast, for higher  $h$  values, freezing times become almost independent of the food water content. The Biot number ( $Bi = h*L/k$ ) has an important effect on these results since there is an internal heat transfer control and the thermal conductivity ( $k$ ) of the solid governs the freezing rate. Then, as  $k$  increases with the ice content, foods containing more ice will be frozen at higher rates. This analysis explains the shorter freezing times of meat with respect to dough at high  $h$  values. It is commonly assumed that foodstuffs with large amounts of water will need more time to reach a certain final freezing temperature. This study shows that this statement is not always true and that freezing times are greatly dependent on the bound water present and the surface heat transfer coefficient ( $h$ ), as well as the total moisture content. This code, combined with accurate thermo-physical data, allows the adequate design and optimization of equipment and processes used in the freezing industry in a fast and accurate manner.

## References

- Bathe KJ (1996) Finite element procedures. Prentice Hall, NJ, p 1037
- Califano A, Zaritzky N (1997) Simulation of freezing or thawing heat conduction in irregular two dimensional domains by a boundary fitted grid method. *LWT Food Sci Technol* 30:70–76
- Choi Y, Okos MR (1986) Effects of temperature and composition on the thermal properties of foods. In: Le Maguer M, Jelen P (eds) Food engineering and process application. Transport phenomena, vol 1. Elsevier, New York, pp 93–103
- Cleland DJ, Cleland AC, Earle RL, Byrne SJ (1987) Prediction of freezing and thawing times for multi-dimensional shapes by numerical methods. *Int J Refrig* 10:32–39
- Comini G, Nonino C, Saro O (1990) Performance of enthalpy-based algorithms for isothermal phase change. In: Wrobel LC, Brebbia CA, Nowak AJ (eds) Advanced computational methods in heat transfer, vol 3: phase change and combustion simulation. Proceedings of the first international conference. Springer, Berlin, pp 3–13
- Fikiin KA (1996) Generalized numerical modeling of unsteady heat transfer during cooling and freezing using an improved enthalpy method and quasi-one-dimensional formulation. *Int J Refrig* 19(2):132–140
- Miles CA, van Beek G, Veerkamp CH (1983) Calculation of thermophysical properties of foods. In: Jowitt R et al (eds) Physical properties of foods. Applied Science Publishers, London, pp 269–312
- Pham QT (2008) Modelling of freezing processes. In: Evans J (ed) Frozen food science and technology. Blackwell, Oxford, pp 51–80
- Santos MV, Vampa V, Califano A, Zaritzky N (2010) Numerical simulations of chilling and freezing processes applied to bakery products in irregularly 3D geometries. *J Food Eng* 100:32–42
- Scheerlinck N, Verboven P, Fikiin KA, de Baerdemaeker J, Nicolaï BM (2001) Finite element computation of unsteady phase change heat transfer during freezing or thawing of food using a combined enthalpy and Kirchhoff transform method. *Trans ASAE* 44(2):429–438
- Sorenfors P (1973) Determination of the thermal conductivity of minced meat. *Food Sci Technol* 7 (7):236–243

# Influence of Fluid Concentration on Freezing-Point Depression and Thermal Conductivity of Frozen Physalis Juice

J. Telis-Romero, G.I. Giraldo-Gómez, H.A. Villa-Vélez,  
D.M. Cano-Higuita, and V.R.N. Telis

## Abbreviations

FPD	Freezing-point depression
$q$	Heat flux
$r$	Radius
$R_1$	External radius of the cylinder (m)
$R_2$	Internal radius of the cylinder (m)
$S$	Surface area of a cylinder of radius r
$T$	Temperature
$T_1$	Steady-state temperature in the internal cylinder
$T_2$	Steady-state temperature in the thermostatic bath where the cell was immersed
$T_f$	Initial freezing temperature (°C)
$W$	Thermal resistance
$X_{\text{ice}}$	Frozen water fraction
$X_w$	Water fraction ( $\text{kg kg}^{-1}$ )
$\lambda$	Thermal conductivity of the sample at the average temperature

---

J. Telis-Romero (✉) • H.A. Villa-Vélez • D.M. Cano-Higuita • V.R.N. Telis  
Departamento de Engenharia e Tecnologia de Alimentos, Universidade Estadual Paulista,  
São José do Rio Preto, São Paulo 15054-000, Brazil  
e-mail: [javier@ibilce.unesp.br](mailto:javier@ibilce.unesp.br); [harvey@ibilce.unesp.br](mailto:harvey@ibilce.unesp.br); [dianacano@higuita@gmail.com](mailto:dianacano@higuita@gmail.com);  
[vanianic@ibilce.unesp.br](mailto:vanianic@ibilce.unesp.br)

G.I. Giraldo-Gómez  
Departamento de Física y Química, Universidad Nacional de Colombia, Manizales, Colombia  
e-mail: [gigiralogo@unal.edu.co](mailto:gigiralogo@unal.edu.co)

## 1 Introduction

The physalis (*Physalis peruviana* L.), member of the family *Solanaceae* and the genus *Physalis* spp., consists of more than 80 varieties; their main characteristic is that their fruits are locked inside a sepal in bucket form. This fruit, originally from the South American Andes, is the best known species of this genus. It is also characterized by its high sugar content and significant amount of vitamins A, B, and C, as well as iron and phosphorus, which could be considered as medicinal properties (Puente et al. 2010). Colombia is the main producer of physalis, followed by South Africa. Colombian physalis is characterized as having a more pronounced color and higher sugar content, making it more appealing in the market. At present, various processed products from the physalis are available, including jams, jellies, raisins, and candies covered in chocolate, juices, nectars, and pulps. According to the National Research Council, the juice of overripe physalis has a high pectinase content, making it an excellent raw material to prepare jams and derivative products, with low production costs (Ministerio de Agricultura y Desarrollo Rural 2009).

Most unit operations for fruit juice processing utilize heat transfer. Modelling and optimization of these operations are difficult, since juice and physical properties change considerably with concentration and temperature. Physical and thermal properties of foods determined at temperatures above freezing are of limited use at freezing conditions. Many food properties show a unique dependence on the state of the water in a food material. During the freezing process, water changes gradually from the liquid phase to solid ice. Since the properties of ice are different from those of liquid water, properties of food determined at temperatures above freezing are often not valid for subfreezing conditions (Singh and Sarkar 2005).

To determine the thermal properties of juices and derivatives, it is essential to calculate parameters such as temperature distribution during freezing, frozen storage, and estimation of freezing time. In food engineering processes, the study of freezing time is important, because it is a tool to estimate refrigeration requirements for freezing systems, as well as for designing and dimensioning the equipment necessary for industry (Delgado and Sun 2001).

In this chapter, results of investigations in thermophysical properties of physalis frozen juice are presented. Freezing-point depression (FPD) and thermal conductivity at several temperatures and concentrations were calculated (Gabas et al. 2003; Giraldo et al. 2010). This investigation provides important values for the freezing storage process, improving preservation and facilitating the marketing of physalis juice for both export and internal consumption.

## 2 Freezing-Point Depression of Frozen Physalis Juice

The freezing-point temperature relative to 0 °C, also called “freezing-point depression,” which increases along with increasing solute concentration, is an important thermophysical property in freezing processes. In general, a food consists of product solids and water. As sensible heat is removed, the temperature of the mixture containing solids and water decreases. Just below the initial freezing point, the water begins to turn into ice. As more heat is removed, more of the water converts into ice, and the remaining solution becomes more concentrated in terms of product solids. Because of the higher solid concentration, the temperature at which freezing will occur is depressed (Singh 1995).

When considering the heat to be removed during freezing of a food product, a change in phase is involved, and the latent heat of fusion must be considered. Water in a food does not completely change all of the food into ice at the freezing point. Some unfrozen water exists below the freezing point, and therefore Siebel's equations for specific heat below the freezing point are very inaccurate (Singh and Sarkar 2005). The best method for determining the amount of heat that must be removed during freezing, or the heat input for thawing, is by calculating the enthalpy change. One method for calculating enthalpy change below the freezing point (reliable only for moisture contents between 73 and 94 %) is the procedure of Chang and Tao (1981).

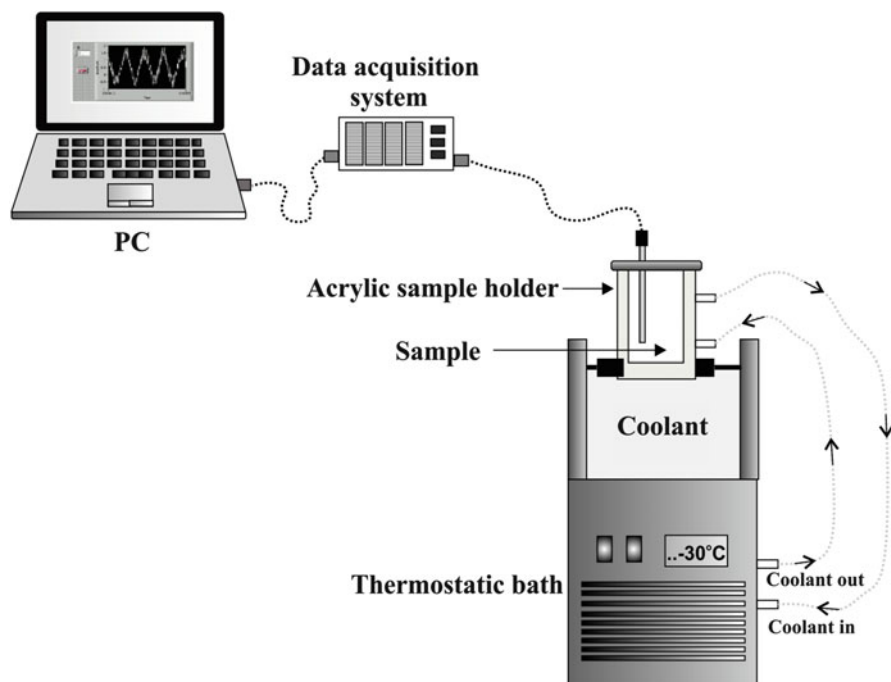


**Fig. 1** Schematic diagram of the apparatus used for measuring freezing-point depression

Experimentally, the FPD is calculated by equipment built on a laboratory scale, as described in Fig. 1. This equipment consists of a sample holder cylinder constructed of acrylic (inner diameter 2.7 cm, height 12.5 cm, and a wall thickness of 1 mm), connected by a thermostatic bath cooling (Cole Palmer, USA). Ethylene glycol-water mixture (50:50) is used as coolant, allowing temperatures to reach a cooling temperature of  $-50^{\circ}\text{C}$ . The equipment temperature was maintained at  $-30^{\circ}\text{C}$  for all experiments. For this experiment, physalis juice was prepared using fruit with homogeneous color and size from the same batch ( $\text{pH} = 3$ ,  $^{\circ}\text{Brix} = 14$ , acidity = 1.96 g citric acid/100 ml). The juice was extracted (in a juice extractor), filtered, and concentrated (under vacuum about  $1.07 \times 10^4$  Pa, abs. into a rotary evaporator), to obtain juices with soluble solid contents in the range of 15–50°Brix (measured at  $25^{\circ}\text{C}$  with a refractometer). Each sample of physalis juice was placed inside the sample holder cylinder, which was cooled by a thermostatic bath. The temperature of the sample contained in the cylinder was measured by a thermocouple (calibrated with ethylene-glycol) fixed in a lab stand. The thermocouple was placed to a distance of 9 cm in the cylinder (from the surface to the base) which transmits data in time intervals of 1 min through a data acquisition system (model TT302, SMAR, Sertãozinho, SP, Brazil) (model TT302, SMAR, Sertãozinho, SP, Brazil) (Chen et al. 1996; Telis et al. 2007).

Table 1 shows the experimental results of FPD for different concentrations of physalis juice.

It can be observed that the initial freezing point of physalis juice increased as the concentration of soluble solids increased, obtaining values of FPD between  $-5.4$  and  $-16.3^{\circ}\text{C}$  for concentrations of soluble solids between 15.0 and 50.0, respectively. Also, a decrease of 314.7 % of FPD was observed when the concentration of physalis juice increased to 20–50°Brix. These results show a similar tendency to the results reported by Chen and Chen (1996) for solutions of NaCl, in which a decrease of 60 % of FPD when the concentration of solution increased from 5.93 to 13.86 % was observed (Chen and Chen 1996).

Telis et al. (2007) determined the FPD for mango and papaya pulp in the range of  $-26$  to  $74^{\circ}\text{C}$ . In this investigation, it was found that FPD was not affected by variables such as sample size, supercooling, or location of measuring (Telis et al. 2007). Freezing point data are also available for other aqueous solutions (Lerici et al. 1983), milk (Chen et al. 1996), and coffee extract (Barnett 1973).

**Table 1** Freezing-point depression at different physalis juice concentrations

Fraction water (w/w)	$^{\circ}\text{Brix}$	Freezing-point depression ( $^{\circ}\text{C}$ )
0.50	50.0	-16.3
0.57	43.0	-13.4
0.64	36.0	-11.1
0.71	29.0	-9.2
0.78	22.0	-6.1
0.85	15.0	-5.4

In order to establish the relationship between FPD and soluble solids, the mathematical model of Miles et al. (1983) was used. The following Eq. (1) was adjusted with a determination coefficient ( $R^2$ ) of 0.983 for all experimental data:

$$T_f = \frac{29.683(1 - X_w)}{0.149(1 - X_w) - 1} \quad (1)$$

where  $T_f$  is the initial freezing temperature ( $^{\circ}\text{C}$ ), and  $X_w$  is the water fraction ( $\text{kg kg}^{-1}$ ).

Although the measurement of freezing point is difficult for many products, we can easily estimate the freezing point from the soluble solids, according to the mathematical model showed above.

### 3 Thermal Conductivity

Many models to predict thermal conductivity of foods have been published, but they almost always have been adjusted with experimental data, due to the effect of solid structure and ice formation on thermal conductivity (Delgado et al. 1997). These models, based on heat conduction through perpendicular layers, provide a better fit in a defined range, taking into account the rapid increase of ice thermal conductivity when temperature decreases in values under  $0\text{ }^{\circ}\text{C}$ . The parameters of these equations determined the ability to predict thermal conductivity correctly at different temperatures in the range of application (Singh and Sarkar 2005).

Measurement of thermal conductivity has involved the use of both steady-state and non-steady-state methods. A steady-state method used a guarded plate to measure the thermal conductivity of frozen foods, and a non-steady-state method used a probe to measure the thermal conductivity of food materials (Singh and Sarkar 2005).

For the steady state, conduction inside the cell is described by the Fourier equation in cylindrical coordinates, with boundary conditions corresponding to heat transfer between two concentric cylindrical surfaces at constant temperature, as given by Eqs. (2)–(4):

$$\frac{\partial \dot{q}}{\partial S} = -\lambda(T) \frac{\partial T}{\partial r} \quad (2)$$

$$T(r = R_1) = T_1 \quad (3)$$

$$T(r = R_2) = T_2 \quad (4)$$

where  $\dot{q}$  is the heat flux in the thermal resistance (W),  $r$  the radius (m),  $R_1$  and  $R_2$  the external and internal radius of the cylinder (m), respectively,  $S$  the surface area of a cylinder of radius  $r$  ( $\text{m}^2$ ),  $T$  the temperature ( $^{\circ}\text{C}$ ),  $T_1$  the steady-state temperature in

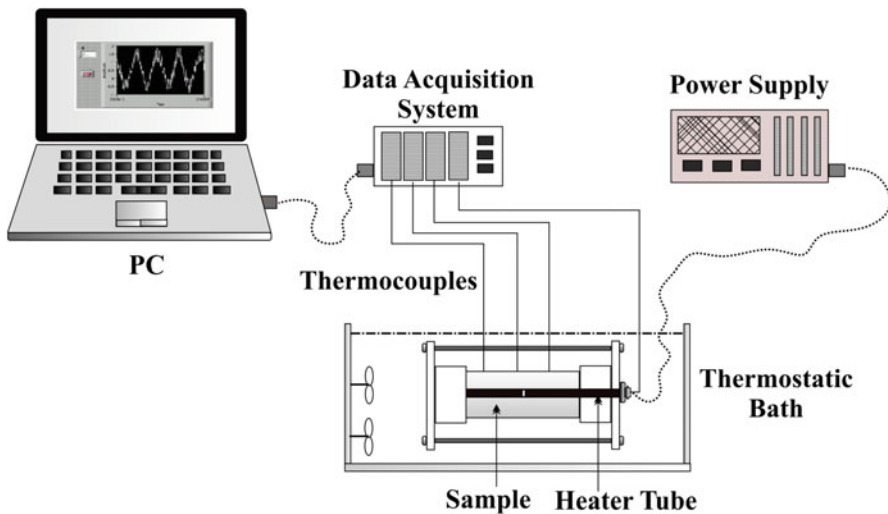


**Fig. 2** Schematic diagram of the apparatus used for measuring effective thermal conductivity

the internal cylinder ( $^{\circ}\text{C}$ ),  $T_2$  the steady-state temperature in the thermostatic bath where the cell was immersed ( $^{\circ}\text{C}$ ), and  $\lambda$  the thermal conductivity of the sample at the average temperature  $(T_1+T_2)/2$  ( $\text{W m}^{-1}\text{°C}^{-1}$ ) (Chen et al. 1996).

Equation (2) can be integrated to find the thermal conductivity in samples,  $\lambda$ , from experimental measurements of  $T_1$  and  $T_2$  under controlled conditions (Delgado et al. 1997; Gabas et al. 2003; Telis et al. 2007):

$$\lambda = \dot{q} \frac{\log\left(\frac{R_2}{R_1}\right)}{2\pi(T_1 - T_2)} \quad (5)$$

Experimentally, the thermal conductivity is calculated by a coaxial dual-cylinder apparatus, shown in Fig. 2.

The heater is a uniformly distributed electric resistance inserted along the axis of the inner cylinder (220 mm long and 20 mm in diameter) to provide a radial heat flux. Samples of physalis juice at different concentrations were loaded into the annular space between the inner and outer cylinders (inner diameter of 42 mm and length of 220 mm), with both ends being fitted with nylon stoppers to prevent axial heat transfer. Before being loaded, samples were degassed under vacuum for 20 min to remove air bubbles. Only 95 % of the available volume was filled with sample in order to allow expansion during freezing. The apparatus was then immersed into a thermostatic bath (model MA-184, Marconi, São Paulo, Brazil) containing ethyl alcohol mixture (50:50). The power input to the heater resistance was made by means of a laboratory DC power supply (model MPS-3006D, Minipa, São Paulo, Brazil), which permitted adjustment of the current with a stability of 0.05 %. Temperatures were monitored with an accuracy of 0.6  $^{\circ}\text{C}$  by an HP data

logger model 75.000-B, an interface HP-IB, and an HP PC running a data acquisition program written in IBASIC. In order to measure temperature, one and three copper-constantan thermocouples were embedded at the surfaces of the inner and outer cylinders, respectively (Telis et al. 2007).

Table 2 shows results of thermal conductivity of physalis juice at different temperatures (25 to  $-24^{\circ}\text{C}$ ) and sample concentrations (15–50°Brix).

In Table 2, it can be observed that heat flux increased as temperature difference increased, independent of the bath temperature. In this experiment, at temperatures between 0.8 and  $3.2^{\circ}\text{C}$ , no significant effect on conductivity was observed in the range of heat flux. Also, it can be observed that above the freezing point, thermal conductivity decreased slightly when concentration increased, independent of temperature. The concentration effect may be due to the lower intrinsic thermal conductivity of the solute compared with that of water.

In order to allow for analysis of the quantitative effect of frozen water fraction ( $X_{\text{ice}}$ ) on thermal conductivity below the initial freezing point, the van Beek equation (Eq. (6)), presented by Miles et al. (1983), was used to estimate the corresponding values, which are included in Table 2 (Delgado et al. 1997):

$$X_{\text{ice}} = X_w \left( 1 - \frac{T_f}{T} \right) \quad (6)$$

where  $T$  and  $T_f$  are the sample temperature ( $^{\circ}\text{C}$ ) and the initial freezing temperature ( $^{\circ}\text{C}$ ), respectively.

The above equation was used to determine the frozen water of food at any temperature. This method is simple, and the procedure involves the following steps: assuming that the initial freezing temperature and the water fraction are known; that their values are substituted in Eq. (6); and that the term representing the frozen soluble solids is calculated.

For all concentrations of physalis juice, in the frozen state, thermal conductivity was strongly affected by both juice concentration and temperature. Thermal conductivity increased with decreasing concentration and temperature. This behavior is a consequence of the higher fraction of ice present in the more diluted samples exposed to temperatures well below their initial freezing point. Schwartzberg (1981) presented a mathematical study of the food-freezing process and reported that the thermal conductivity of ice is roughly 3.7 times greater than that of water, which explains the marked increase in thermal conductivity of foods during freezing (Schwartzberg 1981).

In order to find real value for thermal conductivity values above the freezing point and below the freezing point (Fig. 3), Eqs. (7) and (8) are proposed.

Equation (7), which was obtained from water fraction ( $X_w$ ) and temperature, was adjusted from experimental data above the freezing point ( $R^2 = 0.988$ ). This equation describes the concentration effect when the intrinsic thermal conductivity of solute is lower compared to the water:

**Table 2** Thermal conductivity and frozen water fraction of different physalis juices above (shadow) and below (white) freezing point

Temperature (°C)		-24	-21	-18	-15	-8	0	5	15	25
Fraction water (w/w)	°Brix	Thermal conductivity ( $\text{W m}^{-1} \text{K}^{-1}$ )								
0.50	50.0	0.613	0.544	0.409	0.388	0.398	0.398	0.401	0.389	0.388
0.57	43.0	0.833	0.686	0.590	0.434	0.436	0.417	0.435	0.430	0.429
0.64	36.0	0.921	0.930	0.773	0.647	0.440	0.492	0.482	0.467	0.485
0.71	29.0	1.178	1.019	0.946	0.821	0.433	0.503	0.535	0.524	0.533
0.78	22.0	1.434	1.426	1.309	1.245	0.648	0.562	0.567	0.578	0.566
0.85	15.0	1.526	1.456	1.502	1.276	0.881	0.604	0.598	0.609	0.596
Frozen water fraction <sup>a</sup>										
0.50	50.0	0.160	0.112	0.047	0	0	0	0	0	0
0.57	43.0	0.252	0.206	0.146	0.061	0	0	0	0	0
0.64	36.0	0.344	0.302	0.245	0.166	0	0	0	0	0
0.71	29.0	0.438	0.399	0.347	0.275	0	0	0	0	0
0.78	22.0	0.582	0.553	0.516	0.463	0.185	0	0	0	0
0.85	15.0	0.659	0.631	0.595	0.544	0.276	0	0	0	0

<sup>a</sup>Estimated by Eq. (6)

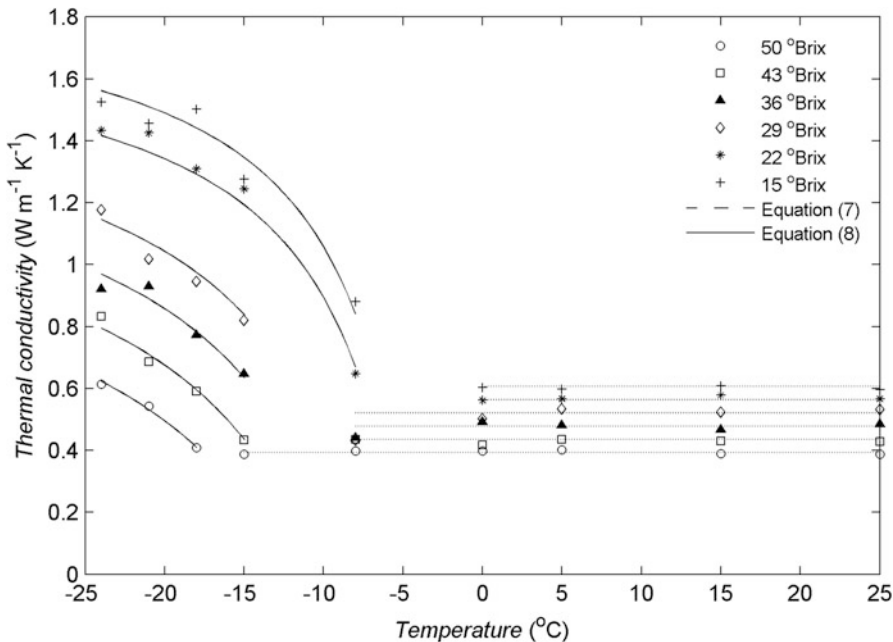


**Fig. 3** Thermal conductivity for physalis juice at different temperatures and concentrations

$$\lambda = 0.0876 + 0.611(X_w) - 2.6 \times 10^{-7}(T) \quad (7)$$

Experimental results of thermal conductivity below the freezing point can be described by the Fikiin equation (Eq. (8)), which was fitted to the experimental data by a multiple regression procedure, resulting in  $R^2 = 0.989$  (Schwartzberg 1981):

$$\lambda = 1.884X_w \left( 1 - \frac{T_f}{T} \right) + 0.321 \quad (8)$$

Comparing Eqs. (7) and (8), it is revealed, except for the constants that exhibit the same dependence of temperature and water fraction, we can conclude that the frozen water fraction is the main factor affecting thermal conductivity in the frozen domain.

## 4 Conclusions

The average value of FPD varied between  $-3.4$  and  $-14.1$  °C for physalis juice concentrations in the range of 20–50°Brix. As expected, the initial freezing point decreased with an increase in physalis juice concentration. The coaxial

dual-cylinder method was applied with good accuracy for measuring the effective thermal conductivity of frozen physalis juice at different concentrations. In the frozen state, the thermal conductivity decreased with increasing concentration and temperature. The mass fraction of ice in physalis juice increased during freezing, causing an increase in the thermal conductivity of the aqueous mixture due to the higher thermal conductivity of ice compared to that of pure water.

Predictive methods generally require input values for initial freezing temperature, product moisture content, and thermal properties of unfrozen product. Any errors associated with these values can lead to erroneous predictions. Fortunately, food properties under unfrozen conditions can be measured quite accurately by using well-established procedures.

**Acknowledgements** The authors would like to acknowledge and thank CNPq and FAPESP (process 2009/13033-9, 2009/03840-4) for their financial support.

## References

- Barnett S (1973) Freezing of coffee extract to produce a dark coloured freeze-dried product. *AICHE Symp Ser* 132(69):26–32
- Chang HD, Tao LC (1981) Correlations of enthalpies of food systems. *J Food Sci* 46 (5):1493–1497
- Chen P, Chen XD, Free KW (1996) Measurement and data interpretation of the freezing point depression of milks. *J Food Eng* 30(1–2):239–253
- Chen XD, Chen P (1996) Freezing of aqueous solution in a simple apparatus designed for measuring freezing point. *Food Res Int* 29(8):723–729
- Delgado AE, Gallo A, de Piante D, Rubiolo A (1997) Thermal conductivity and frozen strawberry and spinach. *J Food Eng* 31(2):137–146
- Delgado AE, Sun DW (2001) Heat and mass transfer models for predicting freezing processes: a review. *J Food Eng* 47(3):157–174
- Gabas AL, Telis-Romero J, Telis VRN (2003) Influence of fluid concentration on freezing point depression and thermal conductivity of frozen orange juice. *Int J Food Prop* 6:543–556
- Giraldo GI, Gabas AL, Telis VRN, Telis-Romero J (2010) Propiedades termofísicas del jugo concentrado de lulo a temperaturas por encima del punto de congelación. *Cienc Tecnol Aliment* 30(1):90–95
- Lericci CR, Piva M, Dallarosa M (1983) Water activity and freezing point depression of aqueous solutions and liquid foods. *J Food Sci* 48:1667–1669
- Miles CA, van Beek G, Veerkamp CH (1983) Calculation of thermophysical properties of foods I. In: Jowitt R et al (eds) *Physical properties of foods*. Applied Science Publishers Ltd, Barking, Essex, pp 269–312
- Ministerio de Agricultura y Desarrollo Rural (2009) La uchuva colombiana líder en el mundo, Boletín Informativo del Ministerio de Agricultura y Desarrollo Rural, Bogotá, Colombia, 1–3
- Puente LA, Pinto-Muñoz CA, Castro ES, Cortés M (2010) Physalis peruviana Linnaeus, the multiple properties of a highly functional fruit: a review. *Food Res Int* 44(7):1733–1740
- Schwartzberg HG (1981) Mathematical analysis of the freezing and thawing of foods. *AICHE Summer National Meeting*, Detroit, USA, pp 1–33

- Singh RP (1995) Thermal properties of frozen foods. In: Rao RS (ed) *Engineering properties of foods*. Marcel Dekker, New York, pp 139–167
- Singh RP, Sarkar A (2005) Thermal properties of frozen foods. In: Rao MA, Rizvi SSH, Datta AK (eds) *Engineering properties of foods*. Taylor & Francis, Boca Raton, FL, pp 175–201
- Telis VRN, Telis-Romero J, Sobral PJA, Gabas AL (2007) Freezing point and thermal conductivity of tropical fruit pulps: mango and papaya. *Int J Food Prop* 10(1):73–84

# Freezing Rate Effect on Thermal Transition of Blueberries

P. Díaz-Calderón, O. Henríquez, J. Enrione, and S. Matiacevich

## Abbreviations

ANOVA	Analysis of variance
DSC	Differential Scanning Calorimeter
IQF	Individual quick freezing
T <sub>g</sub>	Glass transition
ΔC <sub>p</sub>	Change in the specific heat across the glass transition
ΔH	Change in enthalpy

## 1 Introduction

World blueberry consumption has risen mainly due to of its health benefits (Nicoletta et al. 2008), such as low calories and the presence of anticancer and antioxidant compounds that prevent various diseases, which allow to explain blueberries have become an important component of a healthy diet (Yrjo

---

P. Díaz-Calderón

Biopolymer Research and Engineering Lab, School of Nutrition and Dietetics,  
Universidad de los Andes, Monseñor Alvaro del Portillo 12455, Las Condes, Santiago, Chile

O. Henríquez • S. Matiacevich (✉)

Departamento de Ciencias y Tecnología de Alimentos, Facultad Tecnológica,  
Universidad de Santiago de Chile, Av. Libertador Bernardo O'Higgins No 3363,  
Estación Central, Santiago, Chile  
e-mail: [silvia.matiacevich@usach.cl](mailto:silvia.matiacevich@usach.cl)

J. Enrione

Escuela de Nutrición y Dietética, Facultad de Medicina, Universidad de los Andes, Av.  
Monseñor Alvaro del Portillo 12.455, Las Condes, Santiago, Chile  
e-mail: [jenrione@uandes.cl](mailto:jenrione@uandes.cl)

et al. 1996). Chile is the biggest producer of blueberries in South America and the largest exporter to northern markets (Federación de Productores de Fruta de Chile 2009; Frederick 2009). Blueberries are small blue fruits from the genus *Vaccinium*, with high nutritional value and potential anti-disease effects, but with a short shelf life of about 20 days under refrigeration conditions at a temperature close to 0 °C (Yommi and Godoy 2010). Due to its short shelf life, conservation methods such as freezing are required. The effect of freezing rates on fruit quality and their optimal conditions are strongly dependent on the type of food.

In order to improve the freezing process and to increase the shelf life of this frozen fruit, the objective of this work was to analyze the effect of freezing rate on their thermal transition, as part of a comprehensive study of blueberry conservation.

## 2 Materials and Methods

Two cultivars of blueberries (*Brigitte* and *Duke*) from the Highbush variety, hand-harvested in mid-January and mid-February of 2010, respectively, packaged in plastic boxes and stored under refrigerated conditions were obtained from crop fields of Hortifrut S.A (Curacaví, Chile) and generously donated by the Blueberry Committee of Chile.

Prior to the experimental work, fruits were selected manually, discarding those that were damaged, those without peduncle and flower residues and any red (unripe) fruit, in order to determine fruit quality parameters (i.e., moisture and solids soluble content). Moisture content of fresh blueberries was determined gravimetrically (AOAC 1995) and was expressed on a % wet basis (g water/100 g wet sample). Twelve blueberries were dried in an oven (Wiseven, Korea) at 105 °C for 24 h until constant weight was reached. Total soluble solids concentration was determined by placing 1 mL of blueberry juice obtained from the pulp of five berries, on a portable refractometer (0–32°Brix, RHB-32ATC). Each analysis was performed in triplicate.

The glass transition temperature ( $T_g$ ), water crystallization and melting temperatures from pulp and cuticle were determined by calorimetry using Differential Scanning Calorimeter (DSC) (Diamond DSC, Perkin Elmer, USA). All scans were performed in triplicate following the same protocol. Five blueberries were selected, the cuticle was removed from each berry using a scalpel, and the pulp was ground and homogenized. ~20 mg of pulp, cuticle and extracted epicuticular wax were weighed separately and hermetically sealed in aluminum pans (40 µL). The performed thermal profile consisted of cooling from 30 °C to -70 °C at 40 °C/min (intermediate cooling rate) or at 5 °C/min (slow cooling rate), isothermal holding at -70 °C for 15 min and heating to 95 °C at 10 °C/min of scanning rate. The glass transition temperature was considered as the midpoint in the change of heat capacity. Crystallization and melting water crystals temperature was defined as the onset of the endothermic peak. The change in the specific heat through the glass transition,  $\Delta C_p$  (J/g °C) and the energy ( $\Delta H$  (J/g)) associated with crystallization/melting transitions were also calculated.

In order to achieve the water content of samples after DSC analysis, the pans were punctured and dried in an oven at 100 °C for 7 days. Therefore, enthalpy values were expressed in dry basis (J/g dry sample).

Statistical significance between data were analyzed by analysis of variance (ANOVA) and *t*-test using Prism GraphPad, v4 software. Width of melting water peak obtained by DSC was obtained by fitting the data with Lorentz equation ( $R^2 > 0.95$ ) using Origin v8 software.

### 3 Results and Discussion

Evaluation of the fruit quality parameters showed that no significant differences ( $p > 0.05$ ) were obtained in moisture content between cultivars ( $84 \pm 2\% \text{ w.b.}$ ). However, marked differences ( $p < 0.05$ ) were observed in total soluble solids concentration ( $15.2 \pm 0.8\text{ }^\circ\text{Brix}$  and  $10.7 \pm 0.7\text{ }^\circ\text{Brix}$  for *Brigitte* and *Duke*, respectively).

Thermal behavior of a complex system such as blueberries was successfully analyzed by DSC. Thermal transitions observed for both the pulp and cuticle from both cultivars showed similar thermal profiles, where  $T_g$  and exothermic and endothermic transitions associated with water crystallization and ice melting, respectively, can be obtained. Thermo grams obtained from blueberries were similar to those reported previously in literature for other freeze-dried fruits equilibrated to equivalent range of relative humidity (Sá and Sereno 1994; Moraga et al. 2006; Roopesh et al. 2010).

The onset of glass transition temperature ( $T_g$ ) was determined at  $-44 \pm 2\text{ }^\circ\text{C}$  (Fig. 1), and no significant differences ( $p > 0.05$ ) were observed between cultivars, which is in accordance with the high water content of both fresh cultivars ( $84 \pm 2\% \text{ wb}$ ). These results for fresh blueberries of cultivars *Duke* and *Brigitte* were in

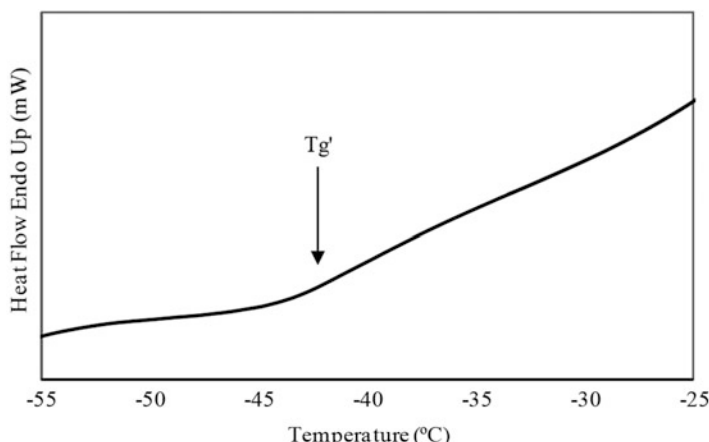


**Fig. 1** Glass transition temperature ( $T_g'$ ) obtained by DSC of thermal transitions for fresh blueberries (cultivars *Duke* and *Brigitte*)

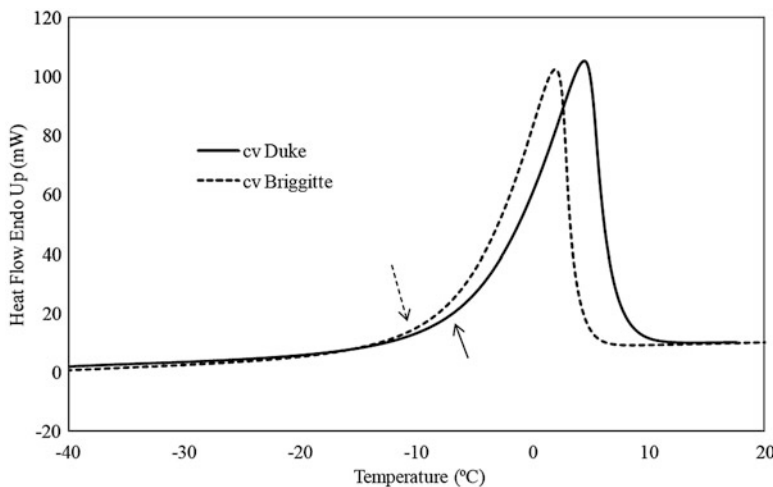


**Fig. 2** Crystal water melting temperatures obtained by DSC in both cultivars analyzed (*Duke* and *Brigitte*). Arrows indicate the onset of temperature transition

accordance with values reported previously for blueberry juice ( $-43.9\text{ }^{\circ}\text{C}$ ) made from a pool of cultivars of *Vaccinium corymbosum L* (Koster 1991) and for wild blueberry juice (onset at  $-45.7\text{ }^{\circ}\text{C}$ ) (Wojtas et al. 1999). The literature has attributed the  $T_g$  value of this fruit to the presence of sugar, specifically glucose and fructose in a 1:1 ratio (Rizzolo et al. 2003; Roopesh et al. 2010), but this was not confirmed in the present study.

The onset of exothermic transitions, considered as water crystallization temperature, was  $-14.0 \pm 0.9\text{ }^{\circ}\text{C}$  and  $-16.7 \pm 0.7\text{ }^{\circ}\text{C}$  for cultivars *Duke* and *Brigitte*, respectively. Meanwhile, the onset of endothermic transitions associated with the melting temperature of water crystals, were  $-4.7 \pm 1\text{ }^{\circ}\text{C}$  and  $-7.0 \pm 1.0\text{ }^{\circ}\text{C}$  for cultivars *Duke* and *Brigitte*, respectively (Fig. 2). The significant differences ( $p < 0.05$ ) in the onset temperatures between both cultivars (Fig. 2), which was lower in cv. *Brigitte* than cv. *Duke* could be explained by the higher soluble solids concentration ( $^{\circ}\text{Brix}$ ) observed in cv. *Brigitte*. The presence of unfrozen water indicates that deteriorative reactions are not restricted.

Interestingly, as observed in Fig. 3, the temperatures attributed to crystallization and melting of water crystals were not significantly different ( $p > 0.05$ ) between freezing rates (slow and intermediate) and between cuticle (78 %, w.b.) and pulp (68 %, w.b.) for the same cultivar. These results can be explained by the dependency of the temperatures of crystallization and melting of water crystal on the concentration of soluble solids measured (by colligative properties) rather than their water content (Nunes et al. 2004).

The width of the peak associated with the melting transition of water crystal was slightly higher at slow ( $7.5 \pm 1.5\text{ }^{\circ}\text{C}$ ) than intermediate freezing rate ( $5.1 \pm 1.3\text{ }^{\circ}\text{C}$ ) in both cultivars (Fig. 3). This behavior was related with a larger distribution in ice crystal size, since at slower rate of freezing less nucleation will be induced, which

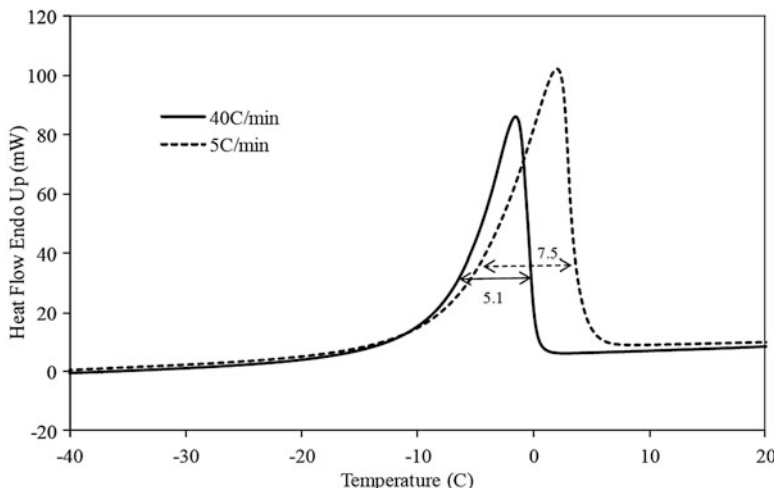


**Fig. 3** Crystal water endotherms obtained by DSC in cv. *Duke* at different cooling rates. Numbers indicate the width of endotherm. Similar behavior was observed in cv. *Brigitte*

**Table 1** Normalized enthalpy values (AH) obtained from both cultivars of fresh blueberries frozen at two different cooling rates and for blueberries stored at 5 °C during 22 days

Fruit	Freezing rate (°C/min)	CV. Duke		CV. Briggitta	
		ΔH (J/g dry sample)	Lower energy released (%)	ΔH (J/g dry sample)	Lower energy released (%)
Pulp	5	2,722	43	940	48.3
Pulp	40	1,556		486	
Cuticle	5	2,118	77	1,604	80.7
Cuticle	40	489		310	

Coefficient of Variation (CV) was lower than 10 % in all cases

will produce larger ice crystals and more dislocation (migration) of water molecules in comparison with faster cooling rates, which would allow producing higher nucleation and smaller ice crystals.

Table 1 summarizes the values of normalized enthalpy for water crystal melting obtained at 5 °C/min (slow rate) and 40 °C/min (intermediate rate or individual quick freezing (IQF) rate), for pulp and cuticle from both cultivars. By comparing the ice melting enthalpy, smaller endotherms were observed at higher freezing rate in both cultivars, showing a significant decrease of 43 % and 48.3 % for pulp and 77 % and 80.7 % for the cuticle for cv. *Duke* and cv. *Brigitte*, respectively. It is important to consider that a higher enthalpy implies higher content of frozen water, which might affect the internal structure of fruit, especially when the fruit is thawed. Thus, the cuticle would be less affected by ice formation and by different freezing rates, which is important when considering the potential protective role of cuticle on fruit integrity. Wojtas et al. (1999) reported that the formation of large ice

crystals in the area just below the skin, where the pigment is located, could cause sufficient structural damage to compromise the compartmentalization of the anthocyanin in the cell and cause its subsequent “bleeding.” Hence, it is possible that differences in freezing rate may affect the textural properties of the fruit, where a fruit slowly frozen may show lower firmness or hardness and higher drip than a fruit frozen by IQF. Further studies are necessary to confirm this hypothesis.

## 4 Conclusions

Thermal transitions of complex fruit systems such as blueberries were successfully analyzed by DSC. Thermal behavior between blueberry cultivars was similar in both frozen processes. Differences in the onset of water crystallization were observed between cultivars due to differences in soluble solids content ( $^{\circ}$ Brix). Temperatures related with crystallization and melting of ice crystals were not significantly different ( $p > 0.05$ ) between freezing rates (slow and intermediate) and between cuticle (78 %, w.b.) and pulp (68 %, w.b.) for the same cultivar. Lower enthalpies ( $\Delta H$ ) related to ice crystal melting were observed at higher freezing rates in pulp and cuticle in both cultivars; however, it is necessary to link this variation with possible differences in textural and structural properties of fruits.

Although larger differences between pulp and cuticle, between *Duke* and *Brigitte* cultivars and between low and intermediate freezing rate were not observed, the results obtained in this study may have important industrial implications. Our results suggest that possible blueberry quality after a freezing process is not affected by factors related with freezing rate, cultivars, or fruit components (pulp or cuticle).

**Acknowledgements** The authors acknowledge the financial support of Innova Chile-Corfo CT11 PUT-20, CONICYT Project PBCT-PSD-62 and DICYT 339 from VRIDEI-Universidad de Santiago de Chile.

## References

- AOAC (1995) Official methods of analysis of AOAC International. CRC Press, Washington, DC
- Federación de Productores de Fruta de Chile (2009) Breve resumen temporada 2008-2009 en los principales mercados de destino. Rev Fedefruta 125:30–39
- Frederick B (2009) En volumen, Arándanos de Chile más fuerte que nunca. Revista del Campo, El Mercurio. [http://berriesofchilenoticias.blogspot.mx/2009/01/en-volumen-arndanos-de-chile-ms-fuerte\\_15.html](http://berriesofchilenoticias.blogspot.mx/2009/01/en-volumen-arndanos-de-chile-ms-fuerte_15.html). Accessed 15 March 2013
- Koster KL (1991) Glass formation and desiccation tolerance in seeds. Plant Physiol 96:302–304
- Moraga G, Martínez-Navarrete N, Chiralt A (2006) Water sorption isotherms and phase transitions in kiwifruit. J Food Eng 72:147–156
- Nicoletta S, Spinardi A, Di Egidio V, Mignani I, Casiraghi E (2008) Evaluation of quality and nutraceutical content of blueberries (*Vaccinium corymbosum* L.) by near and mid-infrared spectroscopy. Postharvest Biol Tech 50:31–36

- Nunes MCN, Emond JP, Brecht JK (2004) Quality curves for highbush blueberries as a function of the storage temperature. *Small Fruits Rev* 3:423–440
- Rizzolo A, Nani RC, Viscardi D, Bertolo G, Torreggiani D (2003) Modification of glass transition temperature through carbohydrates addition and anthocyanin and soluble phenol stability of frozen blueberry juices. *J Food Eng* 56:229–231
- Roopesh SM, Sablani SS, Tang J, Powers J, Swanson BG (2010) Water sorption and glass transition temperatures in red raspberry (*Rubus idaeus*). *Thermochim Acta* 503–504:90–96
- Sá MM, Sereno AM (1994) Glass transitions and state diagrams for typical natural fruits and vegetables. *Thermochim Acta* 246:285–297
- Wojtas A, Douglas Goff P, Stark R, Carbyn S (1999) The effect of freezing method and frozen storage conditions on the microstructure of wild blueberries as observed by cold-stage scanning electron microscopy. *Scanning* 21:334–347
- Yommi A, Godoy C (2010) Arándanos, Fisiología y tecnologías de postcosecha. <http://www.inta.gov.ar/balcarce/info/documentos/agric/posco/fruyhort/arandano.htm>. Accessed 23 March 2010
- Yrjo R, Kokini JL, Karel M (1996) Glass transitions in low moisture and frozen foods effects on shelf life and quality. *Food Tech* 50:95–108

# Glass Transition Temperature of Some Thai Fruits Using Differential Scanning Calorimetry: Influence of Annealing and Sugar Composition

S. Charoenrein, N. Harnkarnsujarit, N. Lowithun, and K. Rengsutthi

## Abbreviations

ANOVA	Analysis of variance
$C_p$	Heat capacity
DSC	Differential scanning calorimetry
HPLC	High performance liquid chromatography
RID	Refractive index detector
$T_g$	Glass transition temperature
$T_{g'1}$	Lower glass transition temperature
$T_{g'2}$	Higher glass transition temperature

## 1 Introduction

Glass transition is a nature of second-order time-temperature-water dependent transition, which is generally characterized by a discontinuity in physical, mechanical, electrical, thermal, and other properties of a material. In the case of complex multicomponent mixtures, such as foods, the discontinuity occurs in a range of

---

S. Charoenrein (✉) • N. Harnkarnsujarit • K. Rengsutthi  
Department of Food Science and Technology, Faculty of Agro-Industry,  
Kasetsart University, Bangkok 10900, Thailand  
e-mail: [fagisscr@ku.ac.th](mailto:fagisscr@ku.ac.th)

N. Lowithun  
Department of Food Science and Technology, Faculty of Agro-Industry,  
Kasetsart University, Bangkok 10900, Thailand

Institute of Food Research and Product Development, Kasetsart University,  
Bangkok 10900, Thailand

temperatures. The most common method used to determine glass transition temperature ( $T_g$ ) is differential scanning calorimetry (DSC), which detects the change in heat capacity ( $C_p$ ) that occurs over the transition temperature range (Roos 1995; Rahman 2004).

In a system containing freezable water, the  $T_g$  of maximally freeze-concentrated unfrozen matrix is denoted  $T_g'$ . The maximal-freeze-concentration condition can be achieved using slow cooling and/or annealing of the samples during DSC measurement. Annealing has a potential to allow for the complete (i.e., maximum) formation of ice (Rahman 2004).

The glass transition behavior of foods plays a key role in the quality and storage stability of frozen products because the rates of deteriorative changes in frozen food are closely related to the  $T_g'$  (Roos 1995). It also assists in identifying food stability during storage as well as selecting suitable conditions of temperature and moisture content for processing (Rahman 2004). Consequently, knowledge about the  $T_g'$  is important to food industry. However, procedures for  $T_g'$  measurement using DSC is reported to differ in regard to sample size, cooling rates, warming rates, holding times and temperatures, and annealing conditions (Roos and Karel 1991). It has been found that annealing affects the  $T_g'$  of foods and solutions (Rahman 2004).

Optimum annealing conditions are required for accurate  $T_g'$  measurement of the maximal-freeze-concentration condition (Rahman 2004). Roos (1993) proposed the optimum annealing condition to determine  $T_g'$  by DSC to anneal samples at  $T_m' - 1$  for 15 min. In this study the annealing at midpoint of the temperature range between the endpoint of lower transition and the onset of higher transition is proposed. To verify this method, sugar solutions including sucrose, trehalose, and maltitol were used to determine for their  $T_g'$  using a DSC.

There is a scarcity of information on the  $T_g'$  of real food systems, partly due to their complexity. The objectives of this study were to investigate the  $T_g'$  of rambutan, mango, and longan and to determine the effect of annealing temperatures on the  $T_g'$  values of these fruits.

## 2 Materials and Methods

### 2.1 Materials

Longan (*Dimocarpus longan*), mango (*Mangifera indica*), and rambutan (*Nephelium lappaceum*) were purchased from a local market in Bangkok, Thailand. Fruits were selected for their homogeneity in size, color, maturity, and lack of blemishes. They were washed in tap water and peeled. Each fruit pulp (500 g) was blended (commercial blender, Waring, USA) and centrifuged (CN-1050, Hsiangtai, Taiwan) at 1,700 g for 15 min. The supernatant was taken as fruit juice and used for the analysis.

Sucrose (Mitr Phol Sugar Corp., Suphanburi, Thailand), trehalose (Treha<sup>TM</sup>; Hayashibara Co., Okayama, Japan), and maltitol (MALTISOL MS 65; Siam Sorbitol Co., Bangkok, Thailand) were used for verification of the DSC determination.

## 2.2 Methods

### 2.2.1 DSC Determination of $T_g'$ and the Annealing Study

Glass transitions of 20 % sugar (sucrose, trehalose, and maltitol) solutions and the fruit juices extracted were investigated using a DSC. The DSC used was a PerkinElmer Pyris 1 DSC equipped with an Intracooler subambient accessory. Nitrogen gas was used as the purge gas at a flow rate of 20 mL/min during calibration and measurements. The instrument was calibrated using indium and cyclohexane. Samples (10–13 mg) were weighed in volatile aluminum pans and hermetically sealed. An empty aluminum pan was used as a reference sample.

Sugar solutions and fruit samples were determined for  $T_g'$  by the method of Lowithun and Charoenrein (2009). To determine the  $T_g'$  of the samples in a non-annealing state, the samples were cooled from 25 to –60 °C at a rate of 25 °C/min, held for 15 min, and subsequently heated to 10 °C at a rate of 5 °C/min. For isothermal annealing measurements, the samples were cooled to –60 °C and held for 15 min, heated to annealing temperature and held for 30 min; cooled back to –60 °C at a rate of 10 °C/min, held for 15 min, and subsequently reheated to 10 °C at a rate of 5 °C/min. In this experiment, annealing temperature was selected as the midpoint of the temperature range between the endpoint of lower transition and the onset of higher transition at non-annealed conditions. DSC measurements were carried out in duplicate. PerkinElmer software was used in obtaining the  $T_g'$ , which was determined as the inflection point of the heat capacity change at transition temperature.

### 2.2.2 Sugar Analysis Using a High Performance Liquid Chromatography (HPLC)

Extracted fruit juices were determined for sugar composition using an HPLC (Agilent Model 1100 Series, Agilent Technologies, USA) according to AOAC Official Method 977.20 (Horwitz 2000). Juice samples were subjected to a Zorbax Carbohydrate column (5 µm, 4.6 × 150 mm) (Agilent Technologies, USA) combined with a refractive index detector (RID). The mobile phase consisted of acetonitrile and water (75:25) with a flow rate of 1 mL/min. The amount of sugar was calculated from the external standard. The sugar analysis was performed in duplicate.

### 2.2.3 Statistical Analysis

The difference among mean values ( $p \leq 0.05$ ) was determined by analysis of variance (ANOVA) and Duncan's multiple range tests using SPSS software.

## 3 Results and Discussion

### 3.1 Verification of the DSC Method Using Sugar Solutions

DSC thermograms of sugar solutions and fruit juices typically show two endothermic transitions prior to an ice melting endothermic peak (Fig. 1). This phenomenon has been reported in carbohydrate solutions and foods that contain freezable water (Goff and Sahagian 1996; Goff et al. 2003; Rahman 2004; Ohkuma et al. 2008; Fabra et al. 2009; Sacha and Steven 2009). Goff et al. (2003) proposed that the lower transition ( $T_g'_{1}$ ) represents the glass transition of the bulk phase ( $T_g'$ ), whereas the higher transition ( $T_g'_{2}$ ) is related to the presence of solute inclusions within ice crystals. Therefore, the  $T_g'_{1}$  has been assumed to be the  $T_g'$  of the samples in this study.

The annealing process was achieved at the midpoint of the temperature range between the endpoint of lower transition and the onset of higher transition at non-annealed conditions for 30 min. The results of DSC measurement show that the  $T_g'$  values of sugar solutions in annealed conditions are  $-40.2\text{ }^{\circ}\text{C}$ ,  $-36.7\text{ }^{\circ}\text{C}$ , and  $-41.3\text{ }^{\circ}\text{C}$  for sucrose, trehalose, and maltitol, respectively (Table 1). These values are close to the ranges previously reported by Roos (1995) who showed that the  $T_g'$  values of frozen sucrose, trehalose, and maltitol solutions at midpoint are  $-41$ ,  $-35$ , and  $-42\text{ }^{\circ}\text{C}$ , respectively. This demonstrates that the annealing method in this study can be used to determine the  $T_g'$  values of the samples.

### 3.2 Influence of Annealing on Glass Transition Temperature

The DSC measurements of both sugar solutions and fruit juices revealed that the annealing resulted in an increase in the  $T_g'_{1}$  values, whereas the  $T_g'_{2}$  was unaffected (Tables 1 and 2). This is in agreement with Pyne et al. (2003) and Sahagian and Goff (1994). The annealing process has a potential to allow for the crystallization of ice in the system; subsequently, the system becomes maximally freeze-concentrated. The crystallization of the ice decreases the amount of unfrozen water and also the effect of water plasticization in freeze-concentrated matrix (Pyne et al. 2003). The results indicate that the annealing process influences the  $T_g'_{1}$ , which refers to the  $T_g'$  of the bulk system, whereas no effect of annealing was observed on the  $T_g'_{2}$  of both sugar and fruit samples. The  $T_g'_{2}$  overlaps with the

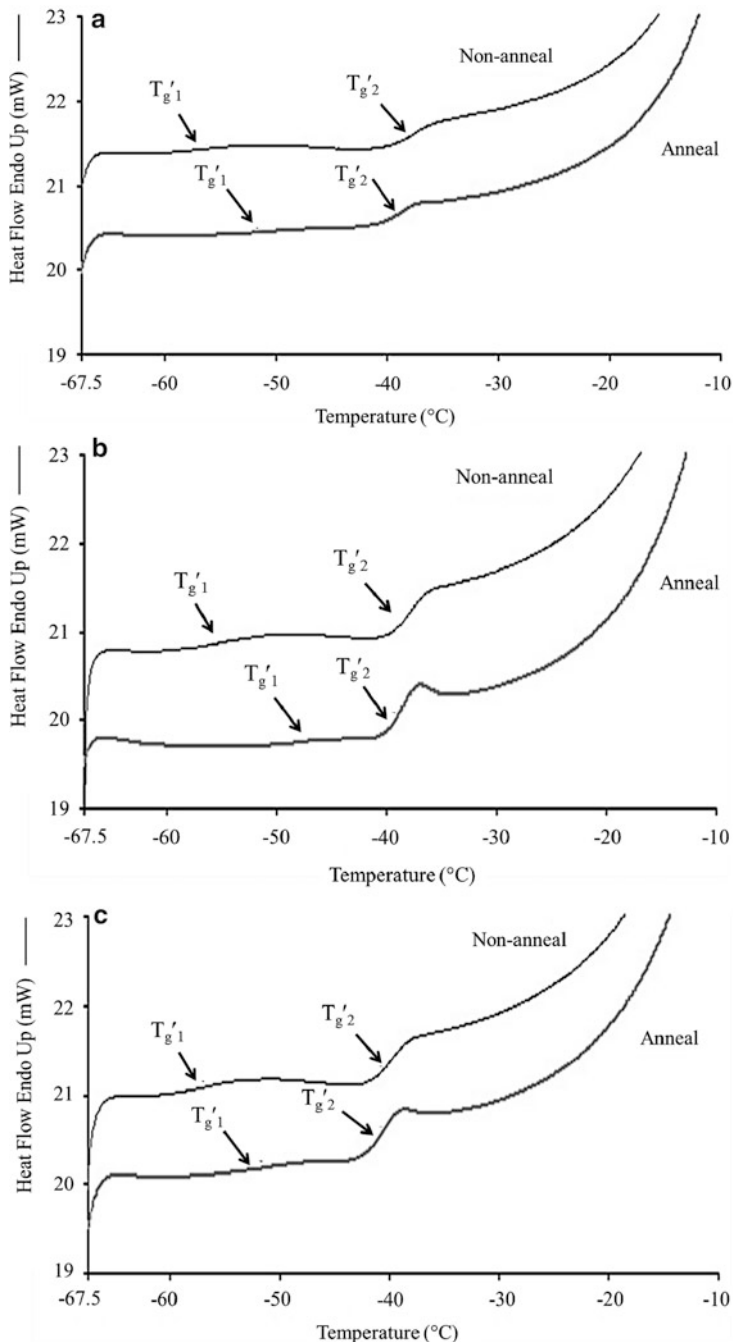


**Fig. 1** DSC thermograms of rambutan (a), mango (b), and longan (c) juice samples with annealed and non-annealed condition

**Table 1**  $T_g'$ <sub>1</sub> and  $T_g'$ <sub>2</sub> of 20 % sucrose, trehalose, and maltitol solution non annealed and annealed<sup>a</sup> condition

Transition temperature (°C)	Condition	Sugar solution (20 % w/w)		
		Sucrose	Trehalose	Maltitol
$T_g'$ <sub>1</sub>	Non-anneal	$-44.6 \pm 0.3$	$-40.5 \pm 0.2$	$-47.7 \pm 0.0$
	Anneal	$-40.2 \pm 0.5$	$-36.7 \pm 0.5$	$-41.3 \pm 0.0$
$T_g'$ <sub>2</sub>	Non-anneal	$-31.5 \pm 0.2$	$-28.3 \pm 0.0$	$-32.6 \pm 0.8$
	Anneal	$-31.7 \pm 0.3$	$-28.1 \pm 0.5$	$-33.8 \pm 0.3$

<sup>a</sup>Annealed temperatures for sucrose, trehalose, and maltitol were  $-38$ ,  $-33$ , and  $-39$  °C, respectively

**Table 2**  $T_g'$ <sub>1</sub> and  $T_g'$ <sub>2</sub> values of rambutan, mango, and longan in non annealed and annealed<sup>a</sup> condition

Transition temperature (°C)	Condition	Rambutan	Mango	Longan
$T_g'$ <sub>1</sub>	Non-anneal	$-51.7 \pm 0.4$	$-56.1 \pm 0.0$	$-56.1 \pm 0.0$
	Anneal	$-48.6 \pm 0.3$	$-51.7 \pm 0.0$	$-53.6 \pm 0.4$
$T_g'$ <sub>2</sub>	Non-anneal	$-36.2 \pm 0.0$	$-36.8 \pm 0.4$	$-39.4 \pm 0.2$
	Anneal	$-36.7 \pm 0.5$	$-38.1 \pm 0.1$	$-39.5 \pm 0.1$

<sup>a</sup>Annealed temperatures for rambutan, mango, and longan were  $-43$ ,  $-46$ , and  $-47.8$  °C, respectively

onset of ice melting and is related to the presence of solute inclusions within ice crystals (Goff et al. 2003; Pyne et al. 2003). However, in a perspective of freeze drying,  $T_g'$ <sub>2</sub> is probably a more relevant temperature, since structural collapse is observed a few degrees above  $T_g'$ <sub>2</sub> (Pyne et al. 2003; Sacha and Steven 2009).

### 3.3 $T_g'$ and Sugar Composition of Longan, Mango, and Rambutan

The HPLC sugar analysis revealed that sucrose, fructose, and glucose are the major sugar components in longan, mango, and rambutan. Table 3 shows the amount of sugar found in sample juices. In all fruit samples, sucrose is the main sugar, whereas the amount of glucose and fructose are similar in each fruit.

$T_g'$ <sub>1</sub> and  $T_g'$ <sub>2</sub> values of rambutan, mango, and longan juice in non-annealed and annealed conditions are shown in Table 2. Although small molecular weight compounds such as sugar are known as plasticizers that decrease  $T_g'$  of the system (Roos 1995), the results showed that  $T_g'$  of fruits and total amount of sugars (Table 3) are not well correlated. This reflects that the  $T_g'$  is independent of the amount of total sugar.

The  $T_g'$  of fruits is mainly due to its sugar component (Aguilera et al. 1998; Telis and Sobral 2001). Aguilera et al. (1998) showed that  $T_g'$  of apple tissues coincides

**Table 3** Sugar composition of rambutan, mango, and longan

Sugar composition	Rambutan	Mango	Longan
Total sugars (g/100 g)	19.06 ± 0.13 <sup>b</sup>	20.35 ± 0.62 <sup>a</sup>	17.25 ± 0.07 <sup>c</sup>
Sucrose (g/100 g)	13.06 ± 0.08 <sup>b</sup>	14.09 ± 0.42 <sup>a</sup>	10.33 ± 0.26 <sup>c</sup>
Fructose (g/100 g)	2.93 ± 0.33 <sup>a</sup>	3.25 ± 0.38 <sup>a</sup>	3.54 ± 0.01 <sup>a</sup>
Glucose (g/100 g)	3.07 ± 0.38 <sup>a</sup>	3.01 ± 0.58 <sup>a</sup>	3.39 ± 0.33 <sup>a</sup>
Monosaccharides–sucrose ratio	0.46:1.00	0.44:1.00	0.67:1.00

Values with different superscripts within the same row are significantly different ( $p \leq 0.05$ )

with the sugar mixture in juice.  $T_g'$  of neither cell wall nor apple pectin was observed. Many researchers have revealed that  $T_g'$  of anhydrous dehydrated fruits correspond to the  $T_g'$  of the main sugar component, such as fructose in grape and apples (Sa and Sereno 1994; Welti-Chanes et al. 1999). Roos (1995) reported that the  $T_g'$  values of glucose, fructose, and sucrose are –53, –53, and –41 °C, respectively. The  $T_g'$  of longan (–53.6 °C), mango (–51.7 °C), and rambutan (–48.6 °C) are in the range of these sugars, which are the fruit compositions. Although sucrose is the main sugar component in the three fruit samples, their  $T_g'$  values are different. This reflects that  $T_g'$  values of fruits are not affected by only one predominant sugar composition. The difference among  $T_g'$  values of fruit samples might be due to the variation of sugar compositions.

The ratio of monosaccharides (glucose and fructose) and sucrose was calculated. Rambutan had the highest monosaccharides–sucrose ratio, whereas mango and rambutan have similar ratios. Although longan contains the lowest amount of total sugars, it has the highest monosaccharides–sucrose ratio, which is coincident with the lowest  $T_g'1$  and  $T_g'2$  values. The high ratio of monosaccharides–sucrose in the samples resulted in the lowest  $T_g'$  of longan. The results suggest that  $T_g'$  values of fruits is greater influenced by the monosaccharides–sucrose ratio than by the amount of total sugars.

## 4 Conclusion

The annealing process has a potential to allow time for the maximum formation of ice. The  $T_g'$  values increased in all annealed sugar solutions (sucrose, trehalose, and maltitol) and fruit samples (longan, mango, and rambutan). The annealing at a temperature between the endpoint of lower transition and the onset of higher transition at non-annealed conditions for 30 min resulted in a higher  $T_g'$ . Moreover, monosaccharides–sucrose ratio played an important role in  $T_g'$ .

**Acknowledgements** The authors acknowledge the financial support of Kasetsart University Research and Development Institute (KURDI), under the SRU-FPF project.

## References

- Aguilera JM, Cuadros TR, Del Valle JM (1998) Differential scanning calorimetry of low-moisture apple products. *Carbohyd Polym* 37:79–86
- Fabra MJ, Talens P, Moraga G, Martínez-Navarrete N (2009) Sorption isotherm and state diagram of grapefruit as a tool to improve product processing and stability. *J Food Eng* 93:52–58
- Goff HD, Sahagian ME (1996) Glass transitions in aqueous carbohydrate solutions and their relevance to frozen food stability. *Thermochim Acta* 280(281):449–464
- Goff HD, Verespej E, Jermann D (2003) Glass transitions in frozen sucrose solutions are influenced by solute inclusions within ice crystals. *Thermochim Acta* 399:43–55
- Horwitz W (ed) (2000) Official methods of analysis of AOAC International, 17th edn. AOAC International, Gaithersburg
- Lowithun N, Charoenrein S (2009) Influence of osmodehydrofreezing with different sugars on the quality of frozen rambutan. *Int J Food Sci Tech* 44:2183–2188
- Ohkuma C, Kawai K, Viriyarattnasak C, Mahawanich T, Tantratian S, Takai R, Suzuki T (2008) Glass transition properties of frozen and freeze-dried surimi products: effects of sugar and moisture on the glass transition temperature. *Food Hydrocolloid* 22:255–262
- Pyne A, Surana R, Suryanarayanan R (2003) Enthalpic relaxation in frozen aqueous trehalose solutions. *Thermochim Acta* 405:225–234
- Rahman MS (2004) State diagram of date flesh using differential scanning calorimetry (DSC). *Int J Food Prop* 7:407–428
- Roos YH (1993) Water activity and physical state effects on amorphous food stability. *J Food Process Pres* 16:433–447
- Roos YH (1995) Phase transition in foods. Academic, New York
- Roos Y, Karel M (1991) Amorphous state and delayed Ice formation in sucrose solutions. *Int J Food Sci Tech* 26:553–566
- Sa MM, Sereno AM (1994) Glass transitions and state diagrams for typical natural fruits and vegetables. *Thermochim Acta* 246:285–297
- Sacha GA, Steven LN (2009) Thermal analysis of frozen solutions: multiple glass transitions in amorphous systems. *J Pharm Sci-US* 98:3397–3405
- Sahagian ME, Goff HD (1994) Effect of freezing rate on the thermal, mechanical and physical aging properties of the glassy state in frozen sucrose solutions. *Thermochim Acta* 246:271–283
- Telis VRN, Sobral PJA (2001) Glass transitions and state diagram for freeze-dried pineapple. *LWT-Food Sci Technol* 34:199–205
- Welti-Chanes J, Guerrero JA, Barcenas ME, Aguilera JM, Vergara F, Barbosa-Canovas GV (1999) Glass transition temperature ( $T_g$ ) and water activity ( $a_w$ ) of dehydrated apple products. *J Food Process Eng* 22:91–101

# **Effect of Emulsifier on Complex Formation and In Vitro Digestibility of Gelatinized Potato Starch**

**K. Kawai, S. Takato, and K. Kajiwara**

## **Abbreviations**

CI	Complex index
DG-Pam	Decaglycerol palmitic acid ester
GOPOD	Glucose oxidase–peroxidase method
OD	Optical density
Pam	Palmitic acid
$T_m$	Melting temperature

## **1 Introduction**

It is known that amylose and lipid compounds form a helical inclusion complex in gelatinized starch. The complex formation has attracted much attention because of impact on retrogradation (Tufvesson et al. 2001), *in vivo* (Holm et al. 1983) and *in vitro* (Guraya et al. 1997; Crowe et al. 2000) digestibility, and rheological properties (Kaur and Singh 2000; Gelders et al. 2006) of gelatinized starch.

In our previous study (Kawai et al. 2012), effects of the type and amount of fatty acid (0–2.0 mmol/g-starch of lauric, myristic, palmitic, stearic, oleic, and linoleic acids) on the complex formation, thermal properties, and *in vitro* digestibility of

---

K. Kawai (✉)

Department of Biofunctional Science and Technology, Graduate School of Biosphere Science, Hiroshima University, 1-4-4 Kagamiyama, Higashi-Hiroshima, Hiroshima 739-8528, Japan  
e-mail: [kawai@hiroshima-u.ac.jp](mailto:kawai@hiroshima-u.ac.jp)

S. Takato • K. Kajiwara

Department of Bioscience and biotechnology, Tokyo University of Technology, 1404-1 Katakura-cho, Hachioji, Tokyo 192-0982, Japan

gelatinized potato starch–fatty acid mixtures were investigated. From the results, it was found that the extent of complex formation tended to increase with decrease in the number of carbons and increase in the number of double bonds in the fatty acid used. In addition, it was demonstrated that a certain amount of fatty acid reduced the starch content hydrolyzed at a given condition. This result was related to the extent of complex formation and its helical order characterized by melting temperature ( $T_m$ ) of the complex. On the other hand, it was demonstrated that many types of emulsifier showed a higher degree of complex formation than that of the fatty acids (Guraya et al. 1997). In addition, a kind of emulsifiers (e.g., decaglycerol monostearate and decaglycerol monooleate) reduced greatly the hydrolysis of starch. This will be because the hydrophilic emulsifiers have greater dispersivity in the gelatinized starch than the fatty acids. However, the data are not yet sufficient to permit a complete understanding of the characteristics of complex formation, because the complex formation and its chemical and physical properties are affected by many factors.

In order to obtain some insight into the subject, decaglycerol palmitic acid ester (DG-Pam) was employed as a hydrophilic emulsifier, and effect of DG-Pam on complex formation and in vitro digestibility of gelatinized potato starch was investigated. In addition, the results were compared with those of palmitic acid (Pam) reported in our previous study (Kawai et al. 2012).

## 2 Materials and Methods

### 2.1 Sample Preparation

Potato starch was purchased from Kanto Chemical Co., Inc., Japan. DG-Pam (HLB = 15) was provided by Mitsubishi-Kagaku Foods Co., Tokyo, Japan.

A potato starch suspension (2 %, w/w) was prepared in a glass vial, and the starch suspension was stirred for 20 min at approximately 95 °C using a magnetic stirrer. The gelatinized starch (5 g) and DG-Pam (0–30 mg) were hermetically put into a glass vial, and the mixture was mixed intermittently using a vortex.

### 2.2 Complex Index

The sample (5 g) was mixed with 25 ml of deionized water for 2 min by vortex, and centrifuged at approximately 1,500 g. The supernatant (0.4 ml) was mixed with 8.6 ml of deionized water and 1 ml of iodine solution (2.0 % (w/w) KI and 1.3 % (w/w) I<sub>2</sub> aqueous mixture). The optical density (OD) values of the sample and a reference (gelatinized potato starch alone) were measured at 690 nm, and complex index (CI) was evaluated as follow:

$$\text{CI} (\%) = 100 \times (\text{OD of reference} - \text{OD of sample}) / \text{OD of reference}$$

All testes were performed in triplicate and the results averaged.

### 2.3 Melting Temperature

$T_m$  of the complex was investigated using a DSC822 (Mettler Toledo International, Inc., Tokyo, Japan). The 150 mg/g-starch mixture was quickly frozen by liquid nitrogen and freeze-dried for 72 h, and the obtained solid was ground. The sample (2–4 mg) was put into an aluminum DSC pan, and then water was added in order to adjust the water content to more than 70 %. The DSC pan was hermetically sealed, and then heating scan was performed at 5 °C/min at a temperature range of 25 °C to 120 °C. All tests were performed in triplicate and the results averaged.

### 2.4 In Vitro Digestibility

Pancreatic  $\alpha$ -amylase (30 U/ml) and amyloglucosidase (3 U/ml) in 0.1 M sodium maleate buffer (pH 6.0) was prepared, and the enzyme mixture (4 ml) and sample (5 g) were enclosed in a 15-ml tube. The tube was laid on a seesaw shaker and shaken continuously at 30 strokes/min at 37 °C for 20 min. After the treatment, 4 ml of ethanol was added into the tube and the mixture is centrifuged at approximately 1,500 g for 10 min. The supernatant was removed, and then the precipitate was stirred with 2 ml of 2 M KOH for 20 min. Furthermore, 8 ml of 1.2 M sodium acetate buffer (pH 3.8) and 0.1 ml of amyloglucosidase in 50 % glycerol aqueous solution (3,300 U/ml) were added, and the mixture was stirred at 50 °C for 30 min. The mixture was centrifuged at approximately 1,500 g for 10 min, and the amount of glucose in the supernatant was analyzed quantitatively according to the glucose oxidase-peroxidase method (GOPOD). All tests were performed in triplicate and the results averaged.

## 3 Results and Discussion

Effects of DG-Pam and Pam on CI of the samples are shown in Fig. 1. The CI values increased with the amount of the additives. The CI value of the DG-Pam samples was much higher than that of the Pam samples. Since DG-Pam is more hydrophilic than Pam, there will be many opportunities for contact and complex formation with amylose in the gelatinized potato starch.

DSC thermogram for the DG-Pam sample showed an endothermic peak due to the melting of complex (data not shown). From the onset point of the peak,  $T_m$  of the DG-Pam complex was evaluated to be  $84.5 \pm 1.5$  °C. This value was lower than that of Pam complex ( $91.3 \pm 1.5$  °C) (Kawai et al. 2012). The fact that the complex has a higher  $T_m$  reflects that helical length of the complex is longer. This means that the physical strength of the DG-Pam complex is lower than that of Pam.

**Fig. 1** Effects of decaglycerol palmitic acid ester and palmitic acid on the CI value. The values are expressed as mean  $\pm$  SD ( $n = 3$ )

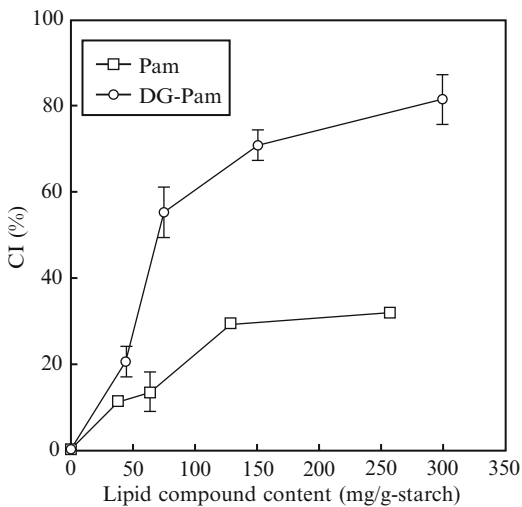
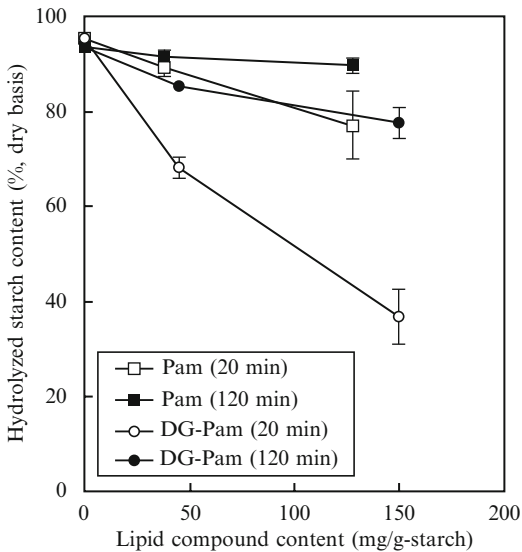


**Fig. 2** Effects of decaglycerol palmitic acid ester and palmitic acid on the starch content hydrolyzed within 20 and 120 min. The values are expressed as mean  $\pm$  SD ( $n = 3$ )



Effects of PG-Pam and Pam on starch contents hydrolyzed within 20 min and 120 min for the samples are shown in Fig. 2. The starch contents hydrolyzed within 20 min decreased with increase in the amount of the additives. The hydrolyzed starch content for the DG-Pam sample was always lower than that of the Pam sample. There was a minor effect of Pam on the hydrolyzed starch content within 120 min. The hydrolyzed starch content for DG-Pam sample, on the other hand, slightly decreased with increase in the amount of DG-Pam.

In our previous study (Kawai et al. 2012), it was suggested that the decrease in the hydrolyzed starch content was affected by the quantity and quality of the complex; they were characterized by CI and by  $T_m$ , respectively. The DG-Pam sample showed much higher CI but lower  $T_m$  of complex than those of the Pam sample. Thus, the low hydrolyzed starch content for DG-Pam sample will be attributed to the large amount of complex. In addition, DG-Pam may form complex during the hydrolysis treatment (Tufvesson et al. 2003). Non-complexed Pam will crystallize in the system, because the  $T_m$  of Pam (63 °C) is much higher than the hydrolysis treatment temperature (37 °C). On the other hand, DG-Pam exists as liquid molecules in the gelatinized potato starch, and thus non-complexed DG-Pam has potentially complex forming ability during hydrolysis treatment. The hydrolysis of amylopectin and amylose cause a decrease in the viscosity of system, and then the complex formation between partially hydrolyzed amylose and DG-Pam will be promoted temporarily as suggested in a previous study (Heinemann et al. 2005). In addition, partial hydrolyzed amylopectin may form a complex with DG-Pam. The short chain branches of amylopectin are not long enough to form a complex with lipids. Furthermore, steric hindrance between the branches of amylopectin also prevents the complex formation. However, the chain length of amylopectin of potato starch is much longer than other botanical types of starch (Hizukuri 1986; Hoover 1995). In addition, the steric hindrance between the branches of amylopectin will loosen during the hydrolysis treatment. In order to understand the relationship between the molecular structure of complex and the in vitro digestibility of starch, further studies are required.

## References

- Crowe TC, Seligman SA, Copeland L (2000) Inhibition of enzymic digestion of amylose by free fatty acids in vitro contributes to resistant starch formation. *J Nutr* 130:2006
- Gelders GG, Goesaert H, Delcour JA (2006) Amylose-lipid complexes as controlled lipid release agents during starch gelatinization and pasting. *J Agric Food Chem* 54:1493
- Guraya HS, Kadan RS, Champagne ET (1997) Effect of rice starch-lipid complexes on in vitro digestibility, complexing index, and viscosity. *Cereal Chem* 74:561
- Heinemann C, Zinsli M, Renggli A, Escher F, Conde-Petit B (2005) Influence of amylose-flavor complexation on build-up and breakdown of starch structures in aqueous food model systems. *LWT-Food Sci Technol* 38:885
- Hizukuri S (1986) Polymodal distribution of the chain lengths of amylopectins, and its significance. *Carbohydr Polym* 147:342
- Holm J, Björck I, Ostrowska S, Eliasson AC, Asp NG, Larsson K, Lundquist I (1983) Digestibility of amylose-lipid complexes in-vitro and in-vivo. *Starch-Starke* 35:294
- Hoover R (1995) Starch retrogradation. *Food Rev Int* 11:331
- Kaur K, Singh N (2000) Amylose-lipid complex formation during cooking of rice flour. *Food Chem* 71:511
- Kawai K, Takato S, Sasaki T, Kajiwara K (2012) Complex formation, thermal properties, and in vitro digestibility of gelatinized starch-fatty acid mixtures. *Food Hydrocoll* 27:228
- Tufvesson F, Skrabanja V, Björck I, Elmståhl HL, Eliasson AC (2001) Digestibility of starch systems containing amylose-glycerol monopalmitin complexes. *LWT-Food Sci Technol* 34:131
- Tufvesson F, Wahlgren M, Eliasson AC (2003) Formation of amylase-lipid complexes and effects of temperature treatment. Part 2. Fatty acids. *Starch/Stärke* 55:138

# Influence of Alcohols and Polyols on the Behavior of Aqueous Solutions of $\beta$ -Lactoglobulin at pH 5.5

G.I. Giraldo and C.M. Romero

## Abbreviations

$C_0$	Protein concentration in the bulk
D	Diffusion coefficient of the protein in the solvent
k	Boltzmann constant
T	Absolute temperature
t	Drop lifetime
$T_m$	Denaturation temperature
$X_{OH}$	Alcohol concentration expressed in mole fraction
$\beta A-\beta H$	$\beta$ barrel with eight antiparallel $\beta$ strands
$\beta I$	Additional $\beta$ strand
$\gamma$	Surface tension of the protein solution
$\gamma_0$	Surface tension of the aqueous solvent
$\Pi$	Surface pressures

## 1 Introduction

Protein native conformation is controlled by molecular interactions among protein and solvent molecules and intramolecular interactions between protein functional groups. Several factors affect these interactions, such as changes in temperature,

---

G.I. Giraldo (✉)

Departamento de Física y Química, Universidad Nacional de Colombia, Manizales, Colombia  
e-mail: [gigiraldogo@unal.edu.co](mailto:gigiraldogo@unal.edu.co)

C.M. Romero

Departamento de Química, Universidad Nacional de Colombia, Bogotá, Colombia

pressure, pH, ligand concentration, or solvent modifications caused by the presence of different substances.

Protein stability has been intensively studied; however, the role of solvents remains controversial. It is known that alcohols induce denaturation of proteins while polyols protect the native conformation of proteins against denaturation, but the mechanism has not been elucidated. Many proposals to explain the effect of cosolutes on protein stability can be found in the literature. Some authors suggest that osmolyte–water interactions and the induced modification of water structure are responsible for the observed changes, while other authors consider that the folding/unfolding process is a consequence of direct cosolute–protein interactions.

The major protein in bovine whey is  $\beta$ -lactoglobulin, which represents approximately 10 % of milk proteins and 58 % of whey protein. It has nutritional and unique properties that are used for industrial applications as food additive, emulsion stabilizer and as a foaming and texturizing agent.

Several results show that thermal denaturation of lactoglobulin is highly dependent on the protein environment. We seek to understand the effect of small cosolutes on protein stability, and for this purpose our group has studied the thermal behavior of aqueous solutions of  $\beta$ -lactoglobulin in the presence of alcohols and polyols with four carbon atoms. These cosolutes were selected to examine the effect of the gradual increase in the number of OH groups in the medium on  $\beta$ -lactoglobulin stability and to obtain information about the main interactions involved in the folding/unfolding process.

In this work, we focus on the most relevant results we have obtained on  $\beta$ -lactoglobulin stability in aqueous solutions of alcohols and polyols from thermal stability, viscosity, and surface tension measurements. The experimental conditions seek to minimize protein–protein interactions and to ensure laminar flow. Reversibility studies showed that for a protein concentration of  $0.1 \text{ mg ml}^{-1}$  at pH 5.5, the unfolding/refolding process is reversible up to denaturation temperature. Alcohol concentration expressed in mole fraction ( $X_{\text{OH}}$ ) is in the range between 0.00 and 0.02, with the exception of butanol due to its low solubility in water. To determine thermal stability, spectroscopic measurements were made in acetate buffer  $10 \text{ mM}$  pH 5.5.

## 2 Aqueous Solutions of $\beta$ -Lactoglobulin

$\beta$ -lactoglobulin is a small globular protein that contains 162 amino acid residues and has a molecular weight of  $18,362 \text{ g mol}^{-1}$ . The secondary structure of  $\beta$ -lactoglobulin comprises a  $\beta$  barrel with eight antiparallel  $\beta$  strands ( $\beta\text{A}$ – $\beta\text{H}$ ), an additional  $\beta$  strand ( $\beta\text{I}$ ) involved in dimer formation, a short  $\alpha$ -helix segment, and three helicoidal turns (Qin et al. 1998; Oliveira et al. 2001). Structure patterns for  $\beta$ -lactoglobulin solution in acetate buffer pH 5.5 obtained by circular dichroism analysis give 36 % of  $\beta$ -strand profile, 19 % of  $\alpha$ -helix elements, 19 % of helicoidal turns, and 23 % of non-structured regions (Giraldo et al. 2010).

According to the literature, in aqueous solution at low temperatures and neutral or near neutral pH, a mixture of monomeric and dimeric forms has been reported (Joyce et al. 1996): between pH 5.2 and 7.5 the dimeric form is dominant, while below pH 3.0 and above pH 8.0,  $\beta$ -lactoglobulin exists as a monomer (Apenten et al. 2002).

### 3 Thermal Denaturation

Many studies have been developed taking  $\beta$ -lactoglobulin as a model protein; however, results about the temperature effect are not conclusive. While most authors assume that thermal denaturation of lactoglobulin can be represented by a two state reversible transition between native and unfolded states as is usual for small globular proteins (Boye et al. 1996; Romero et al. 2007), other authors say that the unfolding process follows a three state model with the formation of a stable monomer as intermediate state (D'Alfonso et al. 2002) suggesting that the number of states involved in this process is very sensitive to the protein environment (Griko et al. 1994). There is a general agreement that above 90 °C, irreversible aggregation takes place.

Thermal denaturation of the protein was followed by fluorescence spectroscopy. The thermal denaturation curves show that at the conditions of the study, the denaturation temperature ( $T_m$ ) for  $\beta$ -lactoglobulin in acetate buffer is 359.1 K, in good agreement with the data reported in the literature. The unfolding process of  $\beta$ -lactoglobulin in buffer and in the presence of alcohols and polyols is well described by a two-state reversible transition between native and unfolded states, and no intermediate state is observed (Romero et al. 2007).

The effect of alcohols and polyols on denaturation temperature, as shown in Table 1, depends clearly on the number of OH groups, as well as on concentration. Change in  $T_m$  was determined from results previously reported (Romero et al. 2007).

1-butanol and 1,2, butenediol produce a continuous decrease in  $T_m$  with the effect being more pronounced with butanol; 1,2,4-butanetriol has a very small effect and

**Table 1** Change in denaturation temperature ( $\Delta T_m$ ) of  $\beta$ -lactoglobulin in aqueous solutions of alcohols and polyols of four carbon atoms with respect to the behavior of protein in buffer<sup>a</sup>

Cosolute	$\Delta T_m$					
	X <sub>OH</sub>	0.000	0.005	0.010	0.0150	0.020
1-butanol	0.0	−7.3	−26.2	−31.4		
1,2-butanediol	0.0	−3.8	−4.6	−6.1	−7.9	
1,2,4-butanetriol	0.0	−3.0	−4.1	−3.5	−6.8	
1,2,3,4-butanetetrol	0.0	−8.4	−6.8	−3.9	−1.2	

<sup>a</sup>Modified from Romero et al. (2007)

1,2,3,4-butanetetrol shows a complex behavior: after an initial decrease in temperature, this polyol produces an increase in temperature as concentration increases.

According to the obtained results, the denaturing effect of the alcohols decreases in the following order:

1-butanol > 1,2,4-butanetriol > 1,2,3,4-butanetetrol.

## 4 Adsorption Behavior of $\beta$ -Lactoglobulin

Protein adsorption is a complex dynamic process that depends on protein structure, intermolecular forces between the adsorbed molecules and the solvent, solute–solute and solvent–solvent interactions, and the addition of cosolutes.

Two general models have been used to describe protein adsorption at the air–water interface. The first is a three step model in which the first step is controlled by diffusion and is represented by Eq. (1) (Rao and Damodaran 2000; Gómez et al. 2008):

$$\pi = 2kC_0T \left( \frac{Dt}{3.14} \right)^{1/2} = At^{1/2} \quad (1)$$

where  $k$  is the Boltzmann constant,  $C_0$  is the protein concentration in the bulk,  $D$  is the diffusion coefficient of the protein in the solvent,  $T$  is the absolute temperature, and  $t$  is the drop lifetime at which the surface pressure is measured. The second step is the adsorption of the protein at the interface, and the last step is the protein rearrangement at the fluid interface in a slow process accompanied by partial unfolding. The adsorption and rearrangement of adsorbed molecules in one or two steps is represented by semiempirical first-order rate equations in which  $\pi_f$ ,  $\pi_0$ , and  $\pi$  are the surface pressures at the final adsorption time of each step,  $t_0$  is the initial time of the step,  $t$  is the measured time for drop formation, and  $k_i$  is a first-order rate constant (Madgassi 1996; Ruíz-Henestrosa et al. 2007).

$$\pi = \pi_f - \pi_0 e^{-k_i(t-t_0)} \quad (2)$$

In the two step models, the protein moves from the bulk phase to the fluid interface in a rapid way, controlled by diffusion, and in the next step the protein is adsorbed and reorientation and conformational changes of the protein take place (Baeza et al. 2005; Alahverdjieva et al. 2008). For small globular proteins at low concentration, it is usually considered that adsorption at the air–water interface occurs in two main steps: diffusion and rearrangement.

Some authors have proposed that the stabilizing effect of sugars and polyols is a consequence of the increase in the surface tension of water caused by the addition of these compounds (Lin and Timasheff 1996; Chanasattru et al. 2008). However, glycerol and other polyols decrease the surface tension of water while increasing

**Table 2** Surface tension of solutions of 1-butanol, 1,2-butanediol, and 1,2,3,4-butanetetrol in water and in the presence of  $\beta$ -lactoglobulin (BLG) at 298.15 K

Cosolute ( $X_{OH}$ )	Surface tension (mN/m)					
	1-butanol		1,2-butanediol		1,2,3,4-butanetetrol	
		+ BLG		+ BLG		+BLG
0.000	71.99	61.4	71.99	61.4	71.99	61.40
0.005	44.11	34.92	59.56	49.56	71.02	56.60
0.010	35.81	26.99	56.14	46.35	71.58	57.17
0.015	29.15	20.46	53.89	44.59	72.14	57.01
0.020			50.28	40.68	72.70	56.38

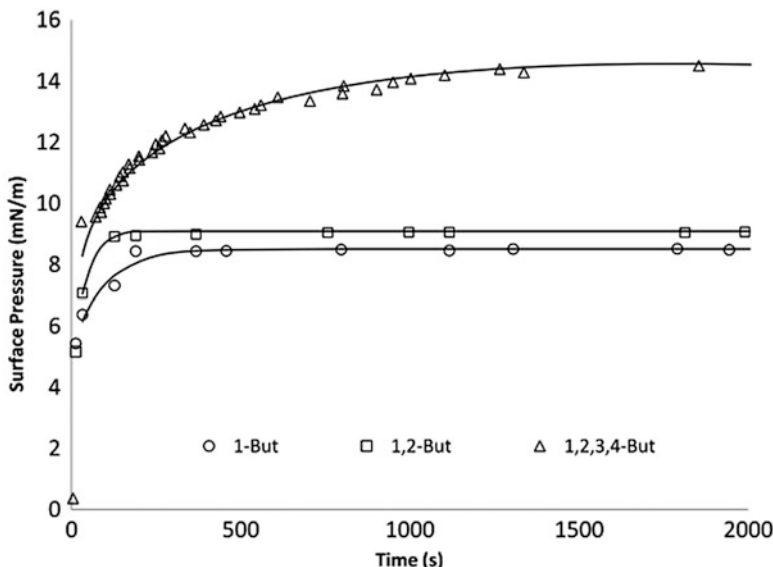
protein stability. Other results with lactalbumin in the presence of polyols and glucose show that even though the denaturation temperature increases as the solvent's surface tension becomes higher, there is no general correlation between the surface tension of the solvent and the change in the denaturation temperature (Romero and Albis 2010).

Table 2 shows the results for the surface tension of solutions of 1-butanol, 1,2-butanediol, and 1,2,3,4-butanetetrol in water and in the presence of  $\beta$ -lactoglobulin at 298.15 K. 1-butanol and 1,2-butanediol induce an important decrease in the surface tension of water, while 1,2,3,4-butanetetrol, which is the most hydrophilic of the cosolutes employed, increases the surface tension of water. For aqueous solutions of  $\beta$ -lactoglobulin, the addition of polyols decreases the surface tension, with the change being higher as the number of hydroxyl groups increase.

The evolution of the adsorption process with time was followed at 298.15 K in terms of the surface pressure ( $\pi$ ) defined as the difference between the surface tension of the protein solution ( $\gamma$ ) and the surface tension of the aqueous solvent ( $\gamma_0$ ). Figure 1 shows the behavior of surface pressure of  $\beta$ -lactoglobulin in aqueous solutions of 1-butanol, 1,2-butanediol, and 1,2,3,4-butanetetrol at 298.15 K. The addition of polyols increases the surface pressure, with the change being higher as the number of hydroxyl groups increase (Mendieta 2010).

Experimental data, adjusted by nonlinear regression, show that the adsorption behavior of lactoglobulin at the air–water interface can be represented as a three-step process: a very rapid step due to diffusion and two additional steps that follow a logarithmic behavior. Time lag is not observed.

The most relevant result is that in general a correlation between the change in surface tension of the aqueous solvent and the denaturation temperature of  $\beta$ -lactoglobulin is not observed, as some authors have suggested for other proteins. However, for each of the cosolutes considered, the change in denaturation temperature increases as the solvent surface tension becomes higher.



**Fig. 1** Effect of 1-butanol, 1,2-butanediol, and 1,2,3,4-butanetetrol on the adsorption profiles of  $\beta$ -lactoglobulin at 298.15 K

## 5 Viscosity of Aqueous Solutions of $\beta$ -Lactoglobulin

The viscosity of protein solutions depends on concentration, shape, size, flexibility, and charge of the macromolecule and is affected by external factors such as temperature, pH, ionic strength, and the solvent. Several industrial applications of proteins are very sensitive to flow behavior and are specially affected by the behavior of viscosity with temperature. In this regard, information about physical and flow properties of proteins is important.

Figure 2 shows the experimental behavior of the viscosity of solutions of  $\beta$ -lactoglobulin in water and in aqueous solutions of 1-butanol, 1,2-butanediol, 1,2,3-butanetriol, and 1,2,3,4-butanetetrol studied between 5 and 80 °C at the highest alcohol concentration employed (mole fraction 0.015 for 1-butanol and 0.02 for the other cosolutes).

At all temperatures, protein viscosity increases with alcohol concentration. This effect is larger for 1-butanol and diminishes with the number of hydroxyl groups. For all the cosolutes, the solvent viscosity increases when the protein is added, except for 1,2,3,4-butanetetrol (Romero et al. 2007). This behavior has been reported by other authors.

The energy of activation for viscous flow was calculated from the dependence of viscosity on temperature, adjusting the experimental data to an Arrhenius-type expression.

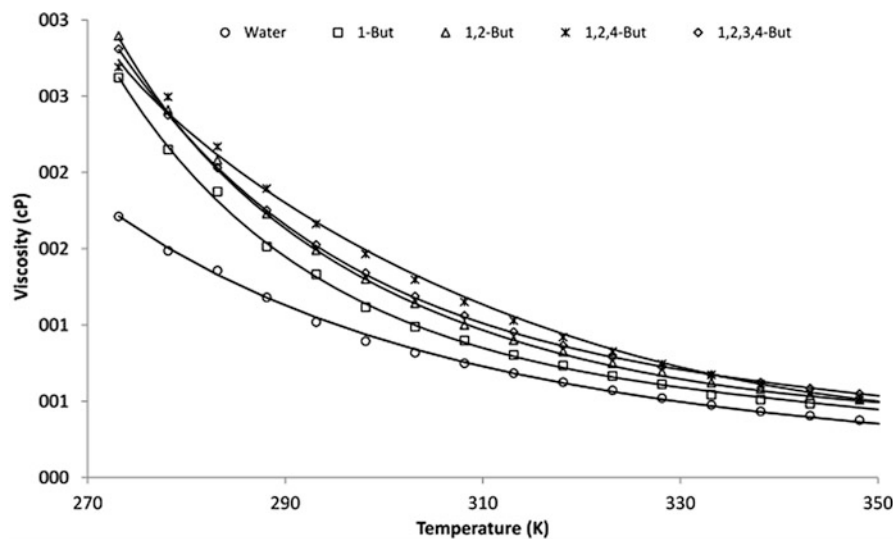


**Fig. 2** Effect of temperature on the viscosity of aqueous solutions of  $\beta$ -lactoglobulin in the presence of alcohols and polyols of four carbon atoms

**Table 3** Activation energies of  $\beta$ -lactoglobulin in aqueous solutions of alcohols and polyols of four carbon atoms

Cosolute	$E_a \text{ kJ mol}^{-1}$					
	$X_{\text{OH}}$	0.000	0.005	0.010	0.015	0.020
1-butanol		16.33	17.58	18.42	19.12	
1,2-butanediol		16.33	17.29	18.02	18.55	18.95
1,4-butanediol		16.33	17.34	17.67	18.18	18.59
1,2,4-butanetriol		16.33	17.24	17.41	17.64	18.34
1,2,3,4-butanetetrol		16.33	17.29	17.44	17.43	17.49

Table 3 summarizes the values of activation energy obtained for the solutions of  $\beta$ -lactoglobulin in water and in the aqueous alcohol solutions.

The results show an increase in the activation energy with respect to its value in water suggesting a smaller mobility of the protein in the presence of the selected cosolutes. The activation energy increases with concentration being the largest increment due to butanol. The increase of activation energy follows the order: 1-butanol > 1,2-butanediol > 1,2,3-butanetriol  $\cong$  1,2,3,4-butanetetrol. The observed change in the case of butanetetrol is almost negligible and the energy value remains nearly constant as concentration increases (Romero et al. 2008).

## 6 Conclusions

The above is a very brief survey of what we have found studying the thermodynamic behavior of  $\beta$ -lactoglobulin in the attempt to comprehend protein stability.

The denaturing effect induced by alcohols and polyols depends clearly on the number of OH groups, as well on concentration. The behavior of thermal denaturation of aqueous solutions of  $\beta$ -lactoglobulin in alcohols and polyols of four carbon atoms shows that 1-butanol produces the largest decrease in  $T_m$  as alcohol concentration increases. The effect diminishes as the number of hydroxyl groups increase and for 1,2,3,4-butanetetrol, which is a typical hydrophilic solute, an increase in temperature is observed as concentration increases. In the case of butanediols, the decrease in  $T_m$  is greater for 1,2-butanediol, which has a larger hydrophobic domain due to the vicinal position of the OH groups, and with 1,2,4-butanetriol a negligible effect is observed.

The number and position of OH groups is also clearly reflected on the surface and viscometric behavior of  $\beta$ -lactoglobulin in aqueous solution. The decrease of surface tension with alcohol mole fraction becomes less pronounced as the number of OH groups increases, while for 1,2,3,4-butanetetrol the behavior changes and the solution surface tension becomes larger than the corresponding value for water. The largest increase in activation energy is due to butanol, and diminishes as the number of OH groups increase.

Experimental results reveal that thermal stability, surface tension and viscometric properties of aqueous solutions of  $\beta$ -lactoglobulin are clearly influenced by the presence of alcohols and polyols. The observed behavior follows a similar trend to that observed for the properties of these alcohols in water, suggesting that their effect on  $\beta$ -lactoglobulin stability is a consequence of the alcohol–water interaction and the induced modification in solvent structure, rather than alcohol–protein interactions.

**Acknowledgments** The authors would like to acknowledge the support given by Universidad Nacional de Colombia, campus Manizales and Bogotá and to ISOPOW which accepted this work to be published as part of the book. We also want to express our gratitude to those colleagues and students who, directly or indirectly, contributed to this work.

## References

- Alahverdjieva VS, Grigoriev DO, Ferri JK, Fainerman VB, Aksenenko EV (2008) Adsorption behaviour of hen egg-white lysozyme at the air/water interface. *Colloids Surf A: Physicochem Eng Aspects* 323:167–174
- Aperten RKO, Khokhar S, Galani D (2002) Stability parameters for  $\beta$ -lactoglobulin thermal dissociation and unfolding in phosphate buffer at pH 7.0. *Food Hydrocoll* 16:95–103
- Baeza R, Sanchez CC, Pilosof AM, Patino JM (2005) Interactions of polysaccharides with  $\beta$ -lactoglobulin adsorbed films at the air–water interface. *Food Hydrocoll* 19:239–248

- Boye JI, Ismail AA, Alli I (1996) Effects of physicochemical factors on the secondary structure of beta-lactoglobulin. *J Dairy Res* 63:97–109
- Chanasatru W, Decker EA, McClements J (2008) Impact of cosolvents (polyols) on globular protein functionality: Ultrasonic velocity, density, surface tension and solubility study. *Food Hydrocoll* 22:1475–1484
- D'Alfonso L, Collini M, Baldini G (2002) Does  $\beta$ -lactoglobulin denaturation occur via an intermediate state? *Biochemistry* 41:326–333
- Giraldo GI, Lozano JM, Romero CM (2010) Efecto de alcoholes y polioles sobre la estabilidad estructural de la B-lactoglobulina en solución acuosa. *Rev Colomb Quim* 39:7–18
- Gómez JM, Henestrosa VP, Sánchez C (2008) Patino J M. *Food Hydrocoll* 22:1105–1116
- Griko YV, Freire E, Privalov PL (1994) Energetics of the alpha-lactalbumin states: a calorimetric and statistical thermodynamic study. *Biochemistry* 33:1889–1899
- Joyce IB, Ashraf AI, Intezar A (1996) Effect of physicochemical factors on the secondary structure of  $\beta$ -Lactoglobulin. *J Dairy Res* 63:97–109
- Lin TY, Timasheff S (1996) On the role of surface tension in the stabilization of globular proteins. *Protein Sci* 5:372–381
- Madgassi S (1996) Surface activity of proteins: chemical and physicochemical modifications. Marcel Dekker, Inc., New York
- Mendieta N (2010) Influencia del 1-butanol, 1,2-butanodiol y eritritol sobre la estabilidad térmica de la  $\beta$ -lactoglobulina. Chemistry Final Work, Universidad Nacional de Colombia, Bogota
- Oliveira KM, Valente-Mesquita VL, Botelho MM, Sawyer L, Ferreira ST, Polikarpov I (2001) Crystal structures of bovine beta-lactoglobulin in the orthorhombic space group C222(1). Structural differences between genetic variants A and B and features of the Tanford transition. *Eur J Biochem* 268:477–483
- Qin BY, Bewley MC, Creamer K, Baker HM, Baker EN, Jameson GB (1998) Structural basis of the Tanford transition of bovine beta-lactoglobulin. *Biochemistry* 37:14014–14023
- Rao CS, Damodaran S (2000) Is surface pressure a measure of interfacial water activity? Evidence from protein adsorption behavior at interfaces. *Langmuir* 16:9468–77
- Romero CM, Albis A (2010) Influence of polyols and glucose on the surface tension of bovine  $\alpha$ -lactalbumin in aqueous solution. *J Solution Chem* 39:1865–1876
- Romero CM, Lozano JM, Giraldo GI, Sancho J (2007) Thermal stability of  $\beta$ -lactoglobulin in the presence of aqueous solution of alcohols and polyols. *Int J Biol Macromol* 40:423–428
- Romero CM, Lozano JM, Giraldo GI (2008) Effect of temperature on partial molar volumes and viscosities of dilute aqueous solutions of 1-butanol, 1,2-butanediol, 1,4-butanediol, 1,2,4-butanetriol, and butanetetrol. *Phys Chem Liq* 46:78–85
- Ruiz-Henestrosa VP, Sánchez CC, Escobar MM, Jiménez JP, Rodríguez FM, Patino MR (2007) Interfacial and foaming characteristics of soy globulins as a function of pH and ionic strength. *Colloids Surf A: Physicochem Eng Aspects* 309:202–215

# Effects of Protein Conformational Modifications, Enthalpy Relaxation, and Interaction with Water on the Solubility of Milk Protein Concentrate Powder

E. Haque and B.R. Bhandari

## Abbreviations

$a_w$	Water activity
CP	Cross polarization
CPMAS	Cross polarization magic angle spinning
CSA	Chemical shift anisotropy
DP	Direct polarization
MAS	Magic angle spinning
MPC	Milk protein concentrate
NMR	Nuclear magnetic resonance

## 1 Introduction

Dairy powder is one of the most widely used dry food ingredients because of its high nutritional value and taste. Being in the dry state it is easy to handle and requires less transportation and storage cost. Despite many years of development and research, a gradual loss of milk proteins solubility and functional properties on storage is still

---

Part of this content comes from the thesis (E. Haque 2011).

E. Haque (✉)

School of Applied Sciences, RMIT University, City Campus, 459-469 Swanston St. Building 39, Level 4, Room 8, Melbourne, VIC 3000, Australia

e-mail: [enamul.haque@rmit.edu.au](mailto:enamul.haque@rmit.edu.au)

B.R. Bhandari

School of Agriculture and Food Sciences, The University of Queensland, Brisbane, QLD 4072, Australia

e-mail: [b.bhandari@uq.edu.au](mailto:b.bhandari@uq.edu.au)

remains a big issue for the dairy powder producing industries. There is a lack of fundamental understanding of changes in protein structure at a molecular level during the processing of milk to produce milk powder and also during storage due to moisture uptake and equilibration. Protein stability is usually associated with an ability to maintain primary and secondary structures. Transformation of proteins native (folded) structure to denatured (unfolded) structure alters its functionality (Fasman 1989). Besides protein denaturation there are many other factors that may cause physicochemical changes in high protein powder which lead to decrease in solubility and other functional properties (Thomas et al. 2004). This review will highlight the underlying mechanisms of the gradual loss of functional properties, especially solubility, of high protein dairy powders and to discover a chemical and/or technological means to improve this loss of solubility upon storage.

## 2 Dairy Proteins: Structure and Physicochemical Properties

### 2.1 Milk Proteins

Milk proteins are one of the most widely consumed food proteins. Normal bovine milk contains roughly 30–35 g protein/L consisting of two main categories of protein, i.e., caseins and whey proteins (Fox 1982). The caseins, which account for 76–86 % of the total protein, can be represented by four gene products:  $\alpha_1$ -caseins,  $\alpha_2$ -caseins,  $\beta$ -caseins, and  $\kappa$ -caseins (Risso et al. 2007). The major whey proteins representative gene products are  $\beta$ -lactoglobulins,  $\alpha$ -lactalbumins, immunoglobulins, and serum albumin, in order of decreasing amounts.

### 2.2 Casein

Casein is the major protein fraction in bovine milk, occurring in the aqueous phase of milk as stable colloidal aggregates known as casein micelles. All the caseins are relatively small molecules ~20–24,000 Da, and are insoluble at their isoelectric points, pH = 4.5–4.9 which has a major influence on their functional properties (Fox 1988). All caseins are phosphorylated to a variable extent and usually the phosphate is esterified to the polypeptides as monoesters of serine.  $\alpha_1$ -caseins usually contain 8 mol P/mol protein, whereas  $\alpha_2$ -caseins consist of four proteins with a common polypeptide but 10–13 mol P/mol protein.  $\beta$ -casein usually contains 5 mol P/mol protein though some genetic variants contain only four phosphate residues. Most molecules of  $\kappa$ -casein contain only one mole P per mole protein but studies suggest that some minor  $\kappa$ -casein may contain 2–3 phosphate groups (Vreeman et al. 1986).

The caseins are strongly hydrophobic in order  $\beta > \kappa > \alpha s_1 > \alpha s_2$ . However, the hydrophobic and polar or charged residues are not uniformly distributed throughout the sequences.

Studies using circular dichroism and optical rotary dispersion suggest that the caseins have little secondary structure. However, theoretical considerations suggest that  $\alpha s_1$ -casein probably possesses some  $\beta$ -sheet structure and  $\beta$ -turns. Up to 10 % of the  $\beta$ -casein molecule may exist as  $\alpha$ -helices (sequence 97–103 and 138–146), 13 % as  $\beta$ -sheet (sequence 52–60, 77–87, 187–195), and 77 % as unordered structures (Creamer et al. 1981).  $\kappa$  appears to be the most highly structured of the caseins with 23 % of the sequence as  $\alpha$ -helices, 31 % as  $\beta$ -sheet, and 24 % as  $\beta$ -turns (Fox 1988).

Due to the high content of phosphoseryl residues,  $\alpha s_1$ ,  $\alpha s_2$ , and  $\beta$ -caseins strongly bind polyvalent cations mainly  $\text{Ca}^{2+}$  but also  $\text{Zn}^{2+}$  which are nutritionally important, leading to charge neutralization, aggregation, and eventually precipitation. Many of the technologically important properties of milk, such as heat stability, rennet coagulation, and the syneresis properties of rennet gels, are strongly influenced by  $\text{Ca}^{2+}$  in the manufacture of certain dairy products (Fox 1988).

All the caseins contain high numbers of proline residues which are fairly uniformly distributed throughout the sequences. Prolyl residues interrupt  $\alpha$ -helical and  $\beta$ -sheet structures but give the casein a type of stable poly-L-proline helical structure. The caseins are therefore, relatively small, amphipathic, randomly coiled, unstructured, open molecules. These features of caseins markedly influence their functional properties.

### 2.2.1 Casein Micelles

In normal milk most (~95 %) of the casein exists as coarse colloidal particles called micelles with a molecular weight of  $\sim 10^8$ . Casein micelles are roughly spherical, fairly swollen particles with a diameter ranging from 80 to 680 nm (Risso et al. 2007). The micelles consist of (dry basis) ~6 % of small ions, principally calcium, phosphate, magnesium, and citrate, referred to collectively as colloidal calcium phosphate (CCP). In milk, the micelles are highly hydrated, typically  $\sim 2$  g  $\text{H}_2\text{O}/\text{g}$  protein (Fox 1988). The technological properties of milk are very strongly influenced by the stability of casein micelles, the structure of which has been the subject of considerable research. According to classical theory (Horne 2006; Slattery and Evard 1973) it is believed that the micelles are composed of spherical submicelles, 10–15 nm in diameter, and have a porous structure.  $\kappa$  which is the principal micelle-stabilizing factor is located predominantly at the surface although other caseins can also be present at the surface. An assumption is that the presence of  $\kappa$ -casein in casein micelle outer layer limits their growth and determines the size. In the last 20 years or more it has been suggested by different authors based on different technical approaches that higher proportion of  $\kappa$ -casein corresponds to the formation of smaller and more solvated micelles (Anema and Creamer 1993; GutierrezAdan et al. 1996). The submicelles are linked together by colloidal

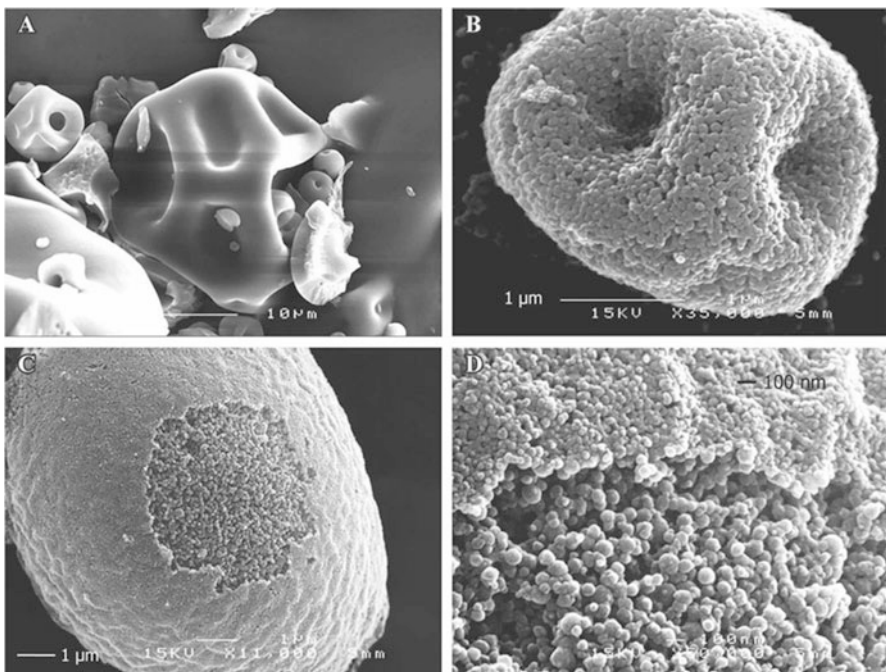


**Fig. 1** Field emission scanning electron micrographs of aged milk protein concentrate powder particles after 2-month storage at 20 °C and water activity of 0.23. (a) spray-dried powder particle; (b, c) hydrated powder particle after rehydration for 10 min; (d) details of the surface of the rehydrated powder particle ( $\times 50,000$ ) observed in panel (c). Adapted from Mimouni et al. 2010a

calcium phosphate (CCP) and hydrophobic association, with contributions from other secondary forces. Removal of CCP by acidification, EDTA etc causes dissociation of the micelles to particles of molecular weight  $\sim 10^6$  but it is not known whether these represents the original submicelles (Fox 1988). There are about 25,000 organic phosphate residues per micelle,  $\sim 40\%$  of which can be linked in pairs via  $\text{Ca}_3(\text{PO}_4)_2$ , calcium acting as counter-ion for most of the remainder.

The denaturation of the whey protein and the formation of covalent complexes with casein can modify the micellar surface, increasing the steric stabilization and producing a diminution in the number of hydrophobic sites that could be able to give interparticle hydrophobic interaction (Risso et al. 2007).

Recent research using scanning electron microscopy (SEM) suggests that interactions between casein micelles during storage have detrimental effect on the decline of solubility of MPC. Interaction between casein micelles resulted in a porous gel-like structure that restrain the dispersion of individual micelles into the surrounding phase without preventing water penetration and solubilization of nonmicellar components. Upon ageing of the MPC powder, increased interactions occurred between and within micelles, leading to compaction of micelles and formation of a monolayer skin of casein micelles packed close together as shown in Fig. 1, which is the main cause of the slow dissolution of stored MPC powder (Mimouni et al. 2010a).

## 2.3 Whey Proteins

Whey Proteins represent ~20 % of nitrogen in bovine milk. The whey protein can be fractionated into two principal groups, an insoluble lactoglobulin fraction and a soluble lactalbumin fraction. The lactalbumin fraction contains  $\beta$ -lactoglobulin,  $\alpha$ -lactalbumin, bovine serum albumin (BSA), and several minor proteins, the most significant of which are lactotransferrin, serotransferrin, and  $\beta_2$ -microglobulin (Fox 1988).

## 3 Milk Powder Ageing Effect

During storage of milk powders, many physicochemical changes occurred including lactose glass transitions (Schuck et al. 2005; Thomas et al. 2004). Storage time and conditions such as temperature, relative humidity (water activity) cause changes in milk powder. They can have important consequences on physical (flowability) and functional properties such as emulsifying and foaming properties (Anema et al. 2006; Stapelfeldt et al. 1997). The mechanical stress may enhance protein unfolding which is detrimental to powder solubility. Besides, this molecular mobility is favored upon ageing and both chemical (Maillard reactions and) and enzymatic reactions occur (Thomas et al. 2004).

High protein dairy powder undergo gradual loss of solubility and functional properties on storage which still remains an issue for the dairy powder producing industries (Anema et al. 2006; Havea 2006; Haque et al. 2011). There is a lack of understanding of underlying molecular mechanisms associated with protein denaturation that induce change in functionality specially solubility of MPC. It is generally believed that protein conformational modifications and water–protein interactions are two major factors that induce instability of protein and eventually affect solubility. Structural/enthalpy relaxation of protein molecules may also have some effect on solubility of amorphous high protein powders. Recent studies on MPC solubility show that storage-induced loss of MPC powder solubility was due to change in rehydration kinetics and not related to formation of insoluble materials in the course of storage. Also the release of casein micelles from powder particles was the rate-limiting step of the MPC rehydration process and was inhibited upon storage (Mimouni et al. 2010b).

### 3.1 Lactose Crystallization

Lactose crystallization is characterized by two steps. First primary nucleation occurs; small crystals are formed, which are locally concentrated within the amorphous glass. Secondary nucleation is promoted from these small crystals. Secondly,

crystal growth occurs, which is governed by diffusion phenomena and counterbalanced by crystal solubilization (Thomas et al. 2004). Lactose crystallization occurs between its glass transitions ( $T_g$ ) and melting ( $T_m$ ) temperature. Nucleation favored when the storage temperature is close to  $T_g$  (Thomas et al. 2004).

Amorphous lactose is very hygroscopic and an increase in water content is observed in milk powder during storage at high relative humidity (>50 % RH) leading to lactose crystallization (Jouppila et al. 1997). If amorphous lactose absorbs sufficient water during storage it acquires molecular mobility and becomes crystalline into one or more of polymorphic forms (Jouppila et al. 1997). Lactose crystallization is characterized by water release, since  $\alpha$ - and  $\beta$ -lactose crystalline forms are less hygroscopic. This phenomena is observed in the sorption isotherm of lactose and milk powders where lactose crystallization corresponds to a break in sorption curve between 40 and 50 % RH (Thomas et al. 2004). As water acts as a plasticizer, sorbed water during storage and water of crystallization lowers  $T_g$  and promotes crystallization (Bhandari and Howes 1999). Lactose crystallization may depend on the lactose protein ratio in milk powder. Crystallization is easily induced in skim milk powder (SMP), whereas it is delayed or even inhibited in whole milk powder (WMP) (Morgan et al. 2005). Thomas et al. reported that interactions between  $\beta$ -lactoglobulin and lactose resulted in stabilization of  $\beta$ -lg-lactose (90:10) powder against lactose crystallization and the lactose crystallization was delayed (Thomas et al. 2005). The presence of sugar may also alter lactose crystallization. Thomsen et al. reported the effect of addition of sucrose to amorphous lactose and to whole milk powder. Sucrose addition lowered  $T_g$  slightly and increased the induction time for crystallization. In the case of WMP,  $T_g$  was not changed but induction time increased significantly (Thomsen et al. 2006).

Lactose crystallization can lead to modification of protein structure. During spray drying lactose replaces water molecules bound to hydrated milk protein via hydrogen bonding with polar groups on the protein. Milk proteins keep their native structure and are therefore soluble even in whole milk powder (Arakawa et al. 2001). The transition of amorphous lactose to the crystalline form destabilizes the matrix and can result in protein denaturation. This structure modification of milk proteins may enhance protein aggregation and cause loss of solubility of milk powder (Thomas et al. 2004). The water release during crystallization may modify non-covalent interaction, such as electrostatic interaction and hydrogen bonding (Thomas et al. 2004).

### 3.2 Maillard Reaction

The Maillard or nonenzymatic browning reaction occurs between a carbohydrate with a free (or potentially free) aldehyde group and the free amino acid group of an amino acid or protein (Nasirpour et al. 2006). The nonenzymatic reaction can occur progressively during storage. The nature and extent of the Maillard reaction depend

on numerous factors, including water activity, pH, temperature, and physicochemical state of the component (Morgan et al. 2005). In milk products, the Maillard reaction begins by lactose condensation on some amino acid residues (lactosylation) and involves a wide range of subsequent reactions (Thomas et al. 2004). Lactosylation leads to the formation of stable Amadori product such as  $\epsilon$ -N-deoxylactulosyl D-lysine also named lactusil-lysin (De Block et al. 1998). The effect of Maillard reactions is to decrease powder quality due to the modification of proteins, and nutritional quality is also damaged. In a recent study it was suggested that protein cross-linking, a possible cause of loss of solubility of MPC powder, may occur via advanced Maillard reaction products (e.g., methylglyoxal) or dehydroalanine (Le et al. 2013).

### **3.3 Protein Conformational Modifications**

Change in protein secondary structural components ( $\alpha$ -helix,  $\beta$ -sheet, and  $\beta$ -turn) could affect the functional properties such as solubility upon storage of milk powder specially high protein dairy powder like MPC (Kher et al. 2007). Proteins are stable in their low-energy, native (folded) state; unfolding or denaturation exposes hydrophobic regions of proteins with greater adoption of  $\beta$ -sheet structures, which promote aggregation via protein–protein interactions, leading to destabilization (Arrondo and Goni 1999).

The role of protein conformational modification on the change in solubility of MPC upon ageing is explored in our recent study. Samples were examined periodically to determine change in solubility and protein conformation by Fourier transform infrared (FTIR) spectroscopy and principal component analysis (PCA). The solubility of MPC decreased significantly with ageing and this process was enhanced by increasing water activity ( $a_w$ ) and storage temperature. Minor changes in protein secondary structural components ( $\alpha$ -helix,  $\beta$ -sheet, and  $\beta$ -turn) upon storage were observed with FTIR which indicated some degree of unfolding of protein molecules (Fig. 2). PCA of the FTIR data was able to discriminate samples according to moisture content, storage period. Partial least squares (PLS) analysis shows some correlation between FTIR spectral feature and solubility (Haque et al. 2010).

### **3.4 Enthalpy Relaxation**

Many milk powder including MPC produced via spray drying remain in amorphous glassy and thermodynamically nonequilibrium state (Bhandari and Hartel 2005) Below glass transition temperature ( $T_g$ ) amorphous glassy system like MPC would approach a thermodynamically more stable state upon ageing with a reduction in molecular mobility. This kind of change is known as enthalpy relaxation or

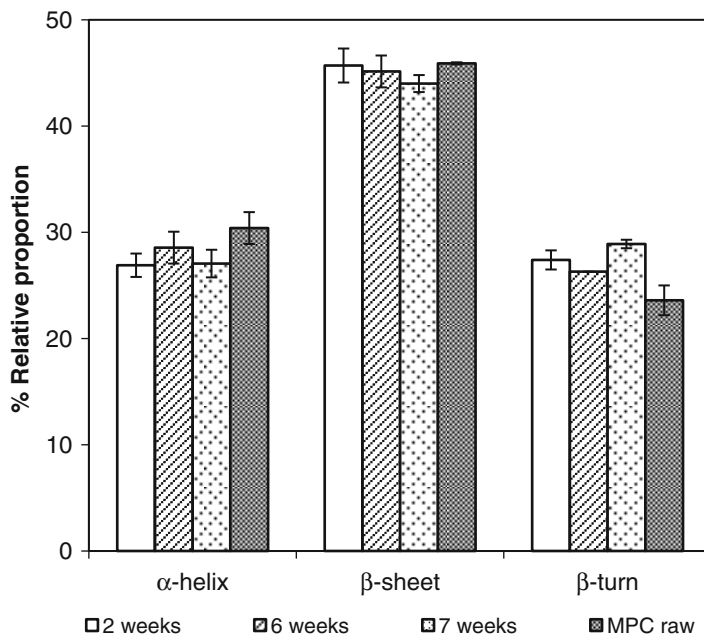
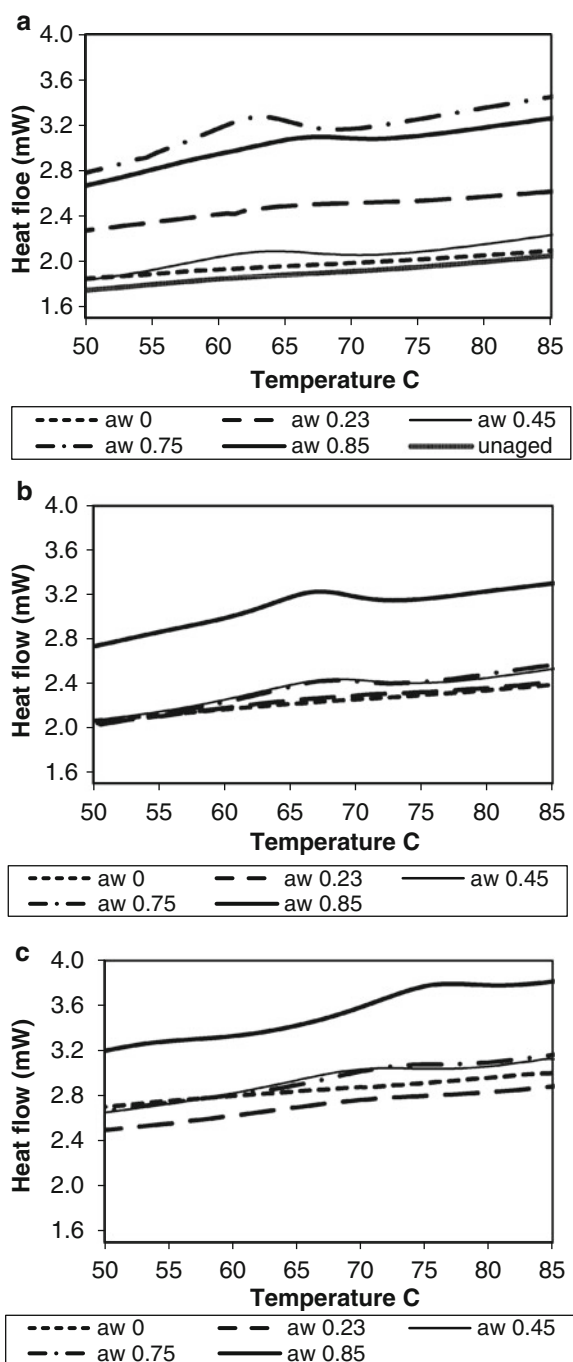


**Fig. 2** Relative fractions of different secondary structural components after high-temperature ( $45^{\circ}\text{C}$ ) storage at  $a_w$  0.0. Adapted from Haque et al. 2010

structural relaxation or  $\beta$ -relaxation (Liu et al. 2006; Correia et al. 2009; Zhou and Labuza 2007). In a glass, translational and rotational mobility of large molecules are restricted and only rotation and vibration of small groups of atoms still exists. These motion do not involve surrounding atoms/molecules and mainly local (Liu et al. 2006). Thus,  $\beta$ -relaxation is caused by the specific chemical groups such as side groups branched on a polymer chain. It could affect the physical properties of amorphous food materials such as MPC powder during storage. A number of factors can affect the enthalpy relaxation such as previous thermal history, ageing period and water activity etc (Haque et al. 2006; Descamps et al. 2009).

In our recent study, kinetics of enthalpy relaxation of milk protein concentrate (MPC) powder upon short- and long-term (up to 48 days) storage at  $25^{\circ}\text{C}$  and a range of  $a_w$  values (0–0.85) were studied by differential scanning calorimetry (DSC). Long-term storage showed that enthalpy relaxation depends on both storage period and water activity. The enthalpy value was much less for lower moisture content (mc) ( $a_w \leq 0.23$ , mc  $\leq 5.5\%$ ) than for higher mc ( $a_w \geq 0.45$ , mc  $\geq 8\%$ ) samples for a particular storage period (Fig. 3). Also for storage under defined relative humidity conditions, the enthalpic region moved to higher temperature and the overshoot value increased slowly with increasing storage period at least up to 48 days as shown in Fig. 3. The results suggest that the presence of more water molecules in close proximity to the protein surface facilitates kinetic unfreezing and subsequent motion of molecular segments of protein molecules towards thermodynamic equilibrium (Haque et al. 2012).

**Fig. 3** Representative DSC thermograms (first scan) of MPC powder stored at 25 °C and at different  $a_w$  for (a) 14, (b) 33, and (c) 48 days. Adapted from Haque et al. 2012

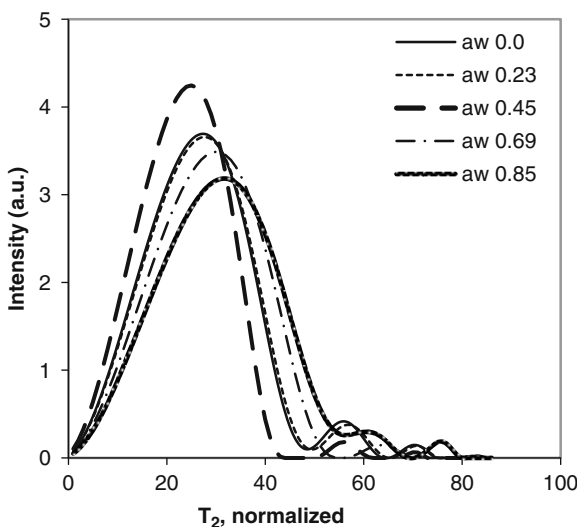


### 3.5 Water–Protein Interactions

Water plays an important role with respect to the properties of food systems. The water in food influences the physical or textural characteristics of the product as well as its chemical stability (Bell and Labuza 2000). The quality of preserved foods can depend on the moisture content, moisture migration, or moisture uptake during storage. The extent of sorption or desorption from food products depends on the vapor pressure of water present in the food system and in the surroundings (Basu et al. 2006). The water in food has been classified as “bound” water (or non-freezing water) and “retention” water (free water and capillary water). Bound water is claimed to correspond to structural water while water retain in a protein matrix like casein micelles or casein gels can be designated as “retention” water (Hardy et al. 2002). However, these static descriptions as “bound” or “retained” can be misleading, as water molecules can be exchange between different sites rapidly even in a matrix that is below its glass transition temperature. Measurement of water properties using advanced instrumental techniques such as NMR relaxometry can reflect these exchange processes. Several types of interaction between water and food solids may occur at the molecular level. These include Columbic interactions between charged groups, London-van der Waals forces, steric effects, solution effects, capillary condensation, plasticizing of macromolecular structure, and multiple effect between various components (Van der Berg and Bruin 1981). Liquid water is composed of transient H-bonded clusters of disturbed ice-like structures at 0 °C where there is 10 % free (non-bonded) hydroxyl (OH) groups, and this increases to 35–40 % at 100 °C (Kinsella and Fox 1986). There is strong cooperative H bonding among water molecules in bulk water with assemblies of for example six-membered hexagonal rings in rapid exchange with free water molecules (Luck 1981). The charged groups on proteins alter the normal structure of the water in their vicinity, and water become oriented in layers around these groups (Kinsella and Fox 1986). Polar groups (hydroxyl, carboxyl, and amide) attract water via H bonding. Apolar groups and hydrophobic regions induce local clathrate or crystalline hydrate structures in their immediate vicinity. The innermost molecules are polarized and immobilized with an intermediate region of less structured molecules and an outer shell of normally tetrahedrally oriented water molecules (Kinsella and Fox 1986).

A generalized sequence is found for the progressing interaction of water with protein with increasing equilibrium relative humidity (ERH) or water activity ( $a_w$ ). As the water activity increases additional water molecules progressively associated with protein in less structured layers and as capillary-held water. These water molecules show a gradual continuum in physical properties from highly structured initial layers to normal bulk liquid water (Kinsella and Fox 1986). At low  $a_w$  (0.2), water molecules bind to specific sites on the protein, and at the BET monolayer, where there is an average of one molecule of water per polar group. As vapor pressure is increased ( $a_w$  0.2–0.7), the nonionic groups and the

**Fig. 4** T<sub>2</sub> distribution profile of MPC samples stored at room temperature ( $24 \pm 1^\circ\text{C}$ ) for 3 weeks period. X-axis is in logarithmic scale. Adapted from Haque et al. 2010



accessible peptide bonds are progressively saturated. These peptide bonds may account over 50 % of the water bound at  $a_w$  0.6–0.8 (Kinsella and Fox 1986). Above  $a_w$  0.7, multilayer water with negligible restricted mobility is H bonded to the previous layer, and eventually bulk water becomes entrapped in voids and crevices.

In our recent study water status (interaction of water with the protein molecule/surface) of MPC powder stored at varying  $a_w$  for up to 12 weeks was determined by measuring the transverse relaxation time ( $T_2$ ) with proton nuclear magnetic resonance (<sup>1</sup>H NMR). The NMR- $T_2$  results indicated the presence of three distinct populations of water molecules (differing in their interaction with and distance from protein surfaces) and that the proton signal intensity and  $T_2$  values of proton fractions varied with storage condition (humidity, temperature) and ageing (Fig. 4) (Haque et al. 2010). As shown in Fig. 4, with increasing  $a_w$ ,  $T_2$  value for water population close to the protein surface decrease up to  $a_w$  0.45 (mc 8.2 %) and then increase for higher  $a_w$  samples, indicating higher interaction with protein surface for lower  $a_w$  samples. This study also show that with longer storage period water population close to the protein surface (short  $T_2$  fraction) increased with time, indicating enhanced water–protein interactions (Haque et al. 2010).

In another study using solid state <sup>13</sup>C NMR, we probed the changes in molecular structure and dynamics of proteins in MPC with varying moisture content (5.5–16.5 % w/w) over a storage period. The results indicate a slight higher rigidity of molecular domains of protein molecules of non-aged MPC compared to that of the long aged (14 weeks at 25 °C) MPC (Fig. 5). It could be suggested from this observation that long-term storage at high relative humidity (RH) may reduce rigidity of the molecular domains due to interaction with water rather than short-term storage at high RH (Haque et al. 2015).

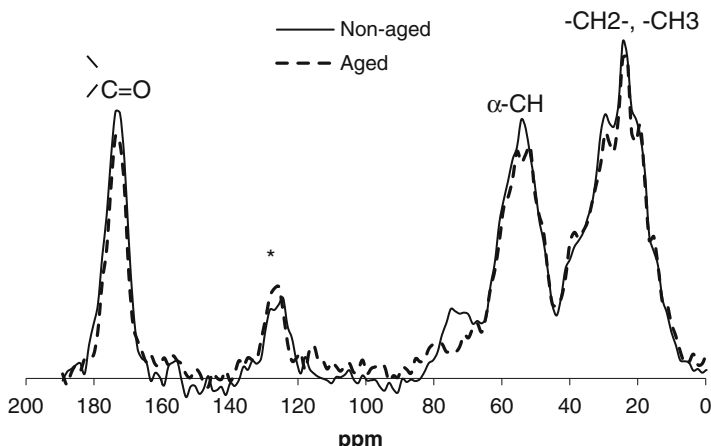


**Fig. 5** CPMAS spectra of MPC (non-aged and stored at  $a_w$  0.85 for 14 weeks at 25 °C temperature) for a 500  $\mu$ s contact time. \*spinning side band. Adapted from Haque et al. 2015

## 4 Conclusion

In this review the underlying molecular mechanism associated with protein denaturation and loss of solubility in high protein dairy powder system is presented. Protein conformational modifications, kinetics of water–protein interactions, enthalpy or structural relaxation, change in structural and dynamic feature of protein molecules are the major areas of investigations reviewed. This review provides a collective knowledge in this area of research and help to discover a chemical and/or technological means to improve the loss of solubility of high protein dairy powder upon storage.

**Acknowledgement** This research was supported by Dairy Innovation Australia Limited and the Australian Research Council (ARC) through ARC Linkage Grant No LP0669191 and ARC Linkage Infrastructure Grants No LE0775684 and LE0668517.

## References

- Anema SG, Creamer LK (1993) Effect of the a and B variants of both alpha(Si)- and kappa-casein on bovine casein micelle solvation and kappa-casein content. *J Dairy Res* 60(4):505–516
- Anema SG, Pinder DN, Hunter RJ, Hemar Y (2006) Effects of storage temperature on the solubility of milk protein concentrate (MPC85). *Food Hydrocoll* 20(2–3):386–393
- Arakawa T, Prestrelski SJ, Kenney WC, Carpenter JF (2001) Factors affecting short-term and long-term stabilities of proteins. *Adv Drug Deliv Rev* 46(1–3):307–326
- Arrondo JLR, Goni FM (1999) Structure and dynamics of membrane proteins as studied by infrared spectroscopy. *Progress Biophys Mol Biol* 72(4):367–405

- Basu S, Shivhare US, Mujumdar AS (2006) Models for sorption isotherms for foods: a review (vol 24, pg 917, 2006). *Dry Technol* 24(12):1705–1705
- Bell LN, Labuza TP (2000) Moisture sorption: practical aspects of isotherm measurement and use, 2nd edn. American Association of Cereal Chemists, St. Paul, MN
- Bhandari BR, Hartel RW (2005) Phase transitions during food powder production and powder stability. In: Encapsulated and powdered foods, vol 146. Crc Press-Taylor & Francis Group, Boca Raton, pp 261–292
- Bhandari BR, Howes T (1999) Implication of glass transition for the drying and stability of dried foods. *J Food Eng* 40(1–2):71–79
- Correia NT, Diogo HP, Ramos JMM (2009) Slow molecular mobility in the amorphous solid state of fructose: fragility and aging. *J Food Sci* 74(9):E526–E533
- Creamer LK, Richardson T, Parry DAD (1981) Secondary structure of bovine alpha s1- and beta-casein in solution. *Arch Biochem Biophys* 211(2):689–696
- De Block J, Merchiers M, Van Renterghem R (1998) Capillary electrophoresis of the whey protein fraction of milk powders: a possible method for monitoring storage conditions. *Int Dairy J* 8 (9):787–792
- Descamps N, Palzer S, Zuercher U (2009) The amorphous state of spray-dried maltodextrin: sub-sub-T<sub>g</sub> enthalpy relaxation and impact of temperature and water annealing. *Carbohydr Res* 344 (1):85–90
- Fasman GD (1989) Prediction of protein structure and the principles of protein conformation. Plenum Press, New York
- Fox PF (1982) Developments in dairy chemistry. Elsevier Applied Science Publishers, London
- Fox PF (1988) The milk protein system. In: Fox PF (ed) Developments in dairy chemistry-4-functional milk proteins. Elsevier Applied Science, London, pp 1–53
- GutierrezAdan A, Maga EA, Meade H, Shoemaker CF, Medrano JF, Anderson GB, Murray JD (1996) Alterations of the physical characteristics of milk from transgenic mice producing bovine kappa-casein. *J Dairy Sci* 79(5):791–799
- Haque E (2011) Ageing induced solubility loss of milk protein concentrate powder: effect of protein conformational modifications, enthalpy relaxation and interaction with water (doctoral dissertation). The University of Queensland, Brisbane
- Haque MK, Kawai K, Suzuki T (2006) Glass transition and enthalpy relaxation of amorphous lactose glass. *Carbohydr Res* 341(11):1884–1889
- Haque E, Bhandari BR, Gidley MJ, Deeth HC, Moller SM, Whittaker AK (2010) Protein conformational modifications and kinetics of water-protein interactions in milk protein concentrate powder upon ageing: effect on solubility. *J Agric Food Chem* 58(13):7748–7755
- Haque E, Bhandari BR, Gidley MJ, Deeth HC, Whittaker AK (2011) Ageing-induced solubility loss in milk protein concentrate powder: effect of protein conformational modifications and interactions with water. *J Sci Food Agric* 91(14):2576–2581
- Haque E, Whittaker AK, Gidley MJ, Deeth HC, Fibrianto K, Bhandari BR (2012) Kinetics of enthalpy relaxation of milk protein concentrate powder upon ageing and its effect on solubility. *Food Chem* 134(3):1368–1373. doi:[10.1016/j.foodchem.2012.03.034](https://doi.org/10.1016/j.foodchem.2012.03.034)
- Haque E, Bhandari BR, Gidley MJ, Deeth HC, Whittaker AK (2015) Change in molecular structure and dynamics of protein in milk protein concentrate powder upon ageing by solid-state carbon NMR. *Food Hydrocoll* 44:66–70
- Hardy J, Scher J, Banon S (2002) Water activity and hydration of dairy powders. *Lait* 82 (4):441–452
- Havea P (2006) Protein interactions in milk protein concentrate powders. *Int Dairy J* 16 (5):415–422
- Horne D (2006) Casein micelle structure: models and muddles. *Curr Opin Colloid Interface Sci* 11:148–153
- Jouppila K, Kansikas J, Roos YH (1997) Glass transition, water plasticization, and lactose crystallization in skim milk powder. *J Dairy Sci* 80(12):3152–3160

- Kher A, Udabage P, McKinnon I, McNaughton D, Augustin MA (2007) FTIR investigation of spray-dried milk protein concentrate powders. *Vib Spectrosc* 44(2):375–381
- Kinsella JE, Fox PF (1986) Water sorption by proteins—milk and whey proteins. *Crc Critical Reviews Food Sci Nutr* 24(2):91–139
- Le TT, Holland JW, Bhesh B, Alewood PF, Deeth HC (2013) Direct evidence for the role of Maillard reaction products in protein cross-linking in milk powder during storage. *Int Dairy J* 31(2):83–91
- Liu YT, Bhandari B, Zhou WB (2006) Glass transition and enthalpy relaxation of amorphous food saccharides: a review. *J Agric Food Chem* 54(16):5701–5717
- Luck WA (1981) In: Rockland LB, Stewart GF (eds) *Water activity: influences on food quality: a treatise on the influence of bound and free water on the quality and stability of foods and other natural products*. Academic, New York, NY, p 407
- Mimouni A, Deeth HC, Whittaker AK, Gidley MJ, Bhandari BR (2010a) Investigation of the microstructure of milk protein concentrate powders during rehydration: alterations during storage. *J Dairy Sci* 93(2):463–472
- Mimouni A, Deeth HC, Whittaker AK, Gidley MJ, Bhandari BR (2010b) Rehydration of high-protein-containing dairy powder: slow- and fast-dissolving components and storage effects. *Dairy Sci Technol* 90(2–3):335–344
- Morgan F, Nouzille CA, Baechler R, Vuataz G, Raemy A (2005) Lactose crystallisation and early Maillard reaction in skim milk powder and whey protein concentrates. *Lait* 85(4–5):315–323
- Nasirpour A, Scher J, Desobry S (2006) Baby foods: formulations and interactions—a review. *Crit Rev Food Sci Nutr* 46(8):665–681
- Risso PH, Relling VM, Armesto MS, Pires MS, Gatti CA (2007) Effect of size, proteic composition, and heat treatment on the colloidal stability of proteolyzed bovine casein micelles. *Colloid Polym Sci* 285(7):809–817
- Schuck P, Blanchard E, Dolivet A, Mejean S, Onillon E, Jeantet R (2005) Water activity and glass transition in dairy ingredients. *Lait* 85(4–5):295–304
- Slattery CW, Evard R (1973) Model for formation and structure of casein micelles from subunits of variable composition. *Biochimica Et Biophysica Acta* 317(2):529–538
- Stapelfeldt H, Nielsen BR, Skibsted LH (1997) Effect of heat treatment, water activity and storage temperature on the oxidative stability of whole milk powder. *Int Dairy J* 7(5):331–339
- Thomas MEC, Scher J, Desobry-Banon S, Desobry S (2004) Milk powders ageing: effect on physical and functional properties. *Crit Rev Food Sci Nutr* 44(5):297–322
- Thomas M, Scher J, Desobry S (2005) Study of lactose/beta-lactoglobulin interactions during storage. *Lait* 85(4–5):325–333
- Thomsen MK, Reimer S, Risbo J, Skibsted LH (2006) Lactose crystallization in whole milk powder. Effect of added sucrose. *Milchwissenschaft-Milk Sci Int* 61(4):430–433
- Van der Berg C, Bruin X (1981) In: Rockland LB, Stewart GF (eds) *Water activity: influences on food quality: a treatise on the influence of bound and free water on the quality and stability of foods and other natural products*. New York Academic Press, New York, p 1
- Vreeman HJ, Visser S, Slangen CJ, Vanriiel JAM (1986) Characterization of bovine kappa-casein fractions and the kinetics of chymosin-induced macropeptide release from carbohydrate-free and carbohydrate-containing fractions determined by high-performance Gel-permeation chromatography. *Biochem J* 240(1):87–97
- Zhou P, Labuza TP (2007) Effect of water content on glass transition and protein aggregation of whey protein powders during short-term storage. *Food Biophy* 2(2–3):108–116

# Active Edible Films Based on Modified Corn Starch for Food Applications

T. Arredondo-Ochoa, Y.M. Márquez-Hernández, B.E. García-Almendárez,  
and C. Regalado

## Abbreviations

ACLS	Acetylated cross-linked starch
$a_w$	Water activity
BW	Beeswax
DLS	Dynamic light scattering
EFs	Edible films
FS	Starch filmogenic suspension
LAE	Lauric arginate ester
MLC	Minimum lethal concentration
OS	Octenyl succinic anhydride
PDA	Potato dextrose agar
PDB	Potato dextrose broth agar
RBC	Rose bengal chloramphenicol
RH	Relative humidity
WCS	Waxy corn starch
WVP	Water vapor permeability

---

T. Arredondo-Ochoa • Y.M. Márquez-Hernández • B.E. García-Almendárez

C. Regalado (✉)

DIPA, PROPAC, Facultad de Química, Universidad Autónoma de Querétaro, C.U. Cerro de las Campanas s/n, Querétaro, 76010, Qro, México  
e-mail: [carlosr@uaq.mx](mailto:carlosr@uaq.mx)

## 1 Introduction

The lifestyle of consumers along with the desire to consume naturally healthy beneficial products has increased the demand for production of fresh produce. Minimally processed fruits and vegetables deteriorate over time, either by means of microbial activity or by physicochemical reactions with the food environment. Therefore, the food industry is investigating ways to protect the integrity and quality of their products by developing better packaging technologies that can maintain or improve the quality attributes of fresh produce, as well as extend their shelf life and ensure the microbiological stability (Rojas-Graü et al. 2007; Lin and Zhao 2007).

The development and characterization of edible films (EFs) is becoming an innovative field in the food preservation area due to the wide variety of delivery applications in the food and packaging industry, particularly the selective functionality given to fresh fruits and vegetables (Janjarasskul and Krochta 2010).

### 1.1 Functional Properties of Edible Films

The main function of EFs focuses on their ability to act as a complement to improve food quality and shelf life extension. Functional properties of EFs include the regulation of moisture transfer, reduction of gas transport ( $O_2$ ,  $CO_2$ ,  $C_2H_4$ ), retention of aroma and flavor components, improvement of mechanical properties, and support of foods' structural integrity. EFs may also serve as a vehicle for additives (flavors, colorants, antioxidants, antimicrobials in a food system), where in addition to being sensory acceptable, they can improve food quality, safety, and shelf life. However, each functional property of EFs depends on the type of material used, method of production and application. These attributes enable the success of storage and preservation techniques that will determine consumer preference (Tharanathan 2003).

### 1.2 Edible Films Composition

Materials used in the formulations of EFs are usually based on polysaccharides, proteins, and hydrophobic compounds such as lipids. They can be used alone or in combination, but selection will depend specifically on the type of intended application of the EF (Olivas and Barbosa-Cánovas 2009).

Another important component of EFs is plasticizers, the function of which is to impart extensibility and to improve flexibility of the films, thus reducing internal hydrogen bonds between chains of polymers that form the structural matrix and increase intermolecular space. Commonly used plasticizers are polyols such as

sorbitol, glycerol, and polyethylene glycol, followed by oils and waxes (McHugh and Krochta 1994). Beeswax (BW) used as a nanoemulsion may enhance hydrophobic properties of EFs, while some nanoparticles may provide useful properties to active EFs, such as oxygen scavenging, enzymes immobilization, antimicrobial effect, or indication of degradation of certain quality factors (de Azeredo 2009).

The addition of surfactants and emulsifiers reduces the rate of moisture loss, stabilizing the dispersed polymer phase in the suspension before casting to produce a dry film, or before coating food surfaces. Most emulsifiers are derivatives of glycerol and fatty acids such as polysorbate (Tween), which have the ability to improve adhesion at the interface between the food and the edible coating (Janjarasskul and Krochta 2010). Nanocomposites are promising materials due to their contribution to active EFs reinforcement at low concentrations, which produces enhanced mechanical, barrier, and thermal properties (de Azeredo 2009).

One of the most important functions arising from the application of EFs is their use as an antimicrobial support in order to ensure microbiological stability and longer shelf life of foods (Quetzada-Gallo 2009).

### 1.2.1 Edible Films Based on Starch

A variety of polysaccharides and their derivatives have been tested for potential use in EFs production due to their abundance, low cost, and ease of use. Commercially, the most important source is corn starch. Amylopectin is the major component of corn starch granules, typically accounting for up to 70–80 % (w/w), although waxy corn starch (WCS) can reach levels of 98–99 % (w/w). Some properties of WCS include high water solubility, ease of gelatinization, being less prone to retrogradation, as well as being inexpensive and generally available (Romero-Bastida et al. 2005). However, the main limitation on the use of native corn starch in EFs is its hydrophilic nature. Starch chemical modifications are a viable alternative to improve their properties, which are intended to change the characteristics of the starch granule to meet a desired function. Chemical modification is used to introduce functional groups to the starch molecule via esterification, cross-linking reactions, treatment with strong acids, enzymatic hydrolysis, or oxidation (Liu and Han 2005; Singh et al. 2007).

EFs based on modified corn starch are clear, flexible, and transparent and provide a good barrier against gases such as CO<sub>2</sub> and O<sub>2</sub>, despite exhibiting poor mechanical properties. Due to their hydrophilic nature, they offer little resistance to migration of water, leading to high water vapor permeability (WVP); values were compared with commercial packaging films (Kim et al. 2002; García et al. 2009).

## 1.3 Active Edible Films

The main cause of fresh produce deterioration is microbial growth on the surface of the food. Growth of fungi and bacteria during storage and distribution can drastically reduce the quality of food and compromise its safety. Reduction in water activity

( $a_w$ ) levels and protection with moisture-proof packaging are methods commonly used to prevent deterioration. However, reorganization of water inside the package due to temperature changes can lead to condensation of moisture on the food's surface, increasing the possibility of microbial growth (Quezada-Gallo 2009).

The incorporation of antimicrobials has been the main purpose for the new generation of active EFs due to their biodegradability, reduced moisture loss, and especially the prevention of microbial growth (Suppakul et al. 2003; Ozdemir and Floros 2003).

Antimicrobial compounds isolated from natural plant sources incorporated into EFs include spice extracts such as cinnamon, pepper, thyme, clove, rosemary, and oregano. In addition, other types of natural substances used against the action of fungi and bacteria are nisin, lauric arginate ester (LAE), and natamycin (Brody et al. 2001). Antimicrobial EFs could extend the shelf life of foods (fresh produce, meat, cheese slices, etc.) and improve food safety, where slow migration of antimicrobial agents to the product surface improves efficiency and helps maintain high concentration of these agents (Zhou et al. 2010).

The objective of this study was to design and characterize active edible films based on modified waxy corn starch, incorporating nano-emulsified beeswax as a hydrophobic agent.

## 2 Materials and Methods

Modified corn starch and non-crystallizable sorbitol (70 % w/v) was provided by CPIIngredientes (San Juan del Río, México). Tween 80 and BW were purchased from Sigma (St. Louis, MO, USA). Potato dextrose broth (PDB) and agar (PDA) were acquired from Bioxon (Cuautitlan, Mexico); rose bengal chloramphenicol (RBC) agar was provided by Difco; LAE was provided by Vedeqsa (Lamirsa Group, Valencia, Spain); natamycin was purchased from EcoBio (Columbus, OH, USA). All other chemicals used were of analytical grade or better.

### 2.1 Edible Films Formation

Starch filmogenic suspension (FS) was prepared by aqueous dispersion of modified corn starch (3 % w/v) and non-crystallizable sorbitol (2.4 % w/v) as plasticizer in distilled water under magnetic stirring at room temperature until complete dissolution. The FS was subsequently heated to 90 °C for 20 min to complete gelatinization of starch and cooled in an ice bath. BW nanoemulsion was prepared in accordance with Hagenmaier and Baker (1994), exposing the suspension to two pulses of 2,000 V for 1 min and a resting period of 1 min using an ultrasonic equipment fitted with a 3 mm tapered microtip (Vibra-Cell VCX 500, Newtown, CT, USA). The nano-emulsified BW (0.2, 0.6 and 1 % w/v) and Tween 80 (0.15 % w/v) were incorporated into the FS using a high speed mixer

(IKA-Ultra-Turrax T25, Wilmington, USA) fitted with a tapered S-25N-25F tip, at 21,500 rpm for 3 min. Films were obtained by pouring the FS into leveled glass plates and allowed to dry for 48 h, 50 % relative humidity (RH) at 25 °C. Particle size was analyzed using Dynamic Light Scattering (DLS) (Brookhaven, model BI200SM, NY, USA) equipped with a high speed digital correlator, and a He-Ne laser of 35 mW as the light source.

## 2.2 *Edible Films Properties*

A digital micrometer (Mitutoyo MDC-Lite, Naucalpan, Mexico) was used to measure EF thickness at five randomly selected points. Solubility was measured according to López et al. (2008). Film squares of  $3 \times 4$  cm were dried to constant weight at 60 °C and then placed in glass vials containing 80 mL distilled water for 1 h at room temperature and gentle agitation. The solution was filtered on a filter paper (Whatman #4) and undissolved film was dried again. Results were expressed as percentage of soluble matter (% SM). Opacity was determined using a UV-Vis spectrophotometer (Lambda 40, Perkin-Elmer, Waltham, MA) to calculate the area of an absorbance spectrum from 400 to 700 nm for each sample, and expressed as absorbance units  $\times$  nanometer (AU nm) (López et al. 2008; Hu et al. 2009). Water vapor permeability (WVP) of the films was determined according to a gravimetric method (ASTM E96-00 2000). Each test was performed in triplicate and the means were statistically analyzed using Tukey's test from JMP statistical software, version 5.0.1.

## 2.3 *In Vitro Minimum Lethal Concentration (MLC) of Natural Antimicrobials*

The MLC of two antimicrobials against *B. cinerea* ATCC 1481 were evaluated based on preliminary studies. LAE was tested at 100, 150, 200 and 250 ppm, while natamycin concentrations were 5, 10, 15, and 20 ppm. Antimicrobial effect was carried in test tubes containing PDB plus the antimicrobial concentration, and  $1 \times 10^6$  spores/mL. One hundred  $\mu$ l of each test tube contents were smeared on RBC agar, to selectively monitor spore germination. Fungal growth was monitored for 5 days, and the MLC found for each antimicrobial was used as a base for the antimicrobial incorporation into the EF formulation that presented the best characteristics. Antimicrobial activity may decrease due to interactions with FS, and thus concentrations tested when incorporated into EFs were  $\geq$  MLC. Active EFs were produced following the same procedure, incorporating the antimicrobials before high speed mixing. Dried EFs were cut into  $4 \times 4$  cm squares and placed in contact with PDA plates inoculated with  $1 \times 10^6$  spores/mL followed by incubation for 5–10 days at 28 °C.

## 2.4 Application of Active Edible Film in a Model Fruit

The best EF was used to coat fresh strawberries purchased from a local market. Following García et al. (1998), five strawberries showing uniform size, without mechanical damage or visible fungal infections were selected. The fruits were sanitized by immersion in a 250 ppm sodium hypochlorite solution for 1 min, and dried in a laminar flow cabinet for 30 min, then immersed for 1 min in the FS and dried for 2 h. A control was submerged with sterile distilled water. The samples were stored at 4 °C and 98 % RH and weight loss was recorded every day up to 9 days of storage. The experiment was performed in duplicate.

## 3 Results and Discussion

### 3.1 Characterization of Edible Films

Selected modified corn starches containing the nano-emulsified BW were capable of forming continuous and transparent EFs. Nano-emulsified BW showed a particle size of 300 nm, indicating good dispersion of BW particles. Physical properties and WVP of EFs based on acetylated cross-linked starch (ACLS) and octenyl succinic anhydride (OS) using different concentrations of nano-emulsified BW are shown in Table 1. In Statistical analysis showed that in relation to thickness of EFs there is an interaction between modified starch and %BW, where thickness increased with an increase in BW concentration. The highest value was  $64.47 \pm 0.95$  µm for OS and 1 % BW. Opacity increased with BW content for each type of modified starch, showing the highest values at 1 % BW of  $36.75 \pm 2.27$  AU nm for ACLS and  $41.15 \pm 2.35$  AU nm for OS. Similar values were reported by Pérez-Gallardo et al. (2012) for EFs based on ACLS and OS with 0.2 % (w/v) BW showing  $28.8 \pm 2.1$  and  $23.2 \pm 3.3$  AU nm, respectively. A significant interaction between

**Table 1** Effect of nano-emulsified beeswax on physical properties and WVP of active EFs

Formulation	Thickness µm ± SD	Opacity AU nm ± SD	Solubility % SM ± SD	WVP [(g mm)/( m <sup>2</sup> h kPa)] ± SD
ACLS-0.2 % BW	$52.67 \pm 0.50^d$	$23.48 \pm 0.90^c$	$97.38 \pm 0.15^a$	$0.77 \pm 0.01^a$
ACLS-0.6 % BW	$55.20 \pm 0.72^{bc}$	$29.98 \pm 0.84^c$	$96.65 \pm 0.07^{bc}$	$0.69 \pm 0.06^{bc}$
ACLS-1 % BW	$56.87 \pm 0.70^b$	$36.75 \pm 2.27^{ab}$	$96.03 \pm 0.12^d$	$0.57 \pm 0.04^d$
OS-0.2 % BW	$54.13 \pm 0.31^{cd}$	$26.56 \pm 1.29^c$	$97.01 \pm 0.13^b$	$0.74 \pm 0.02^b$
OS-0.6 % BW	$57.33 \pm 1.21^b$	$35.00 \pm 3.02^b$	$96.82 \pm 0.07^{bc}$	$0.63 \pm 0.04^{bc}$
OS-1 % BW	$64.47 \pm 0.95^a$	$41.15 \pm 2.35^a$	$96.51 \pm 0.20^c$	$0.56 \pm 0.05^c$

ACLS acetylated cross-linked starch; OS oxidized starch; BW beeswax. Values are the mean of three replicates ± SD. Means in columns not sharing the same letter are significantly different ( $p < 0.05$ )

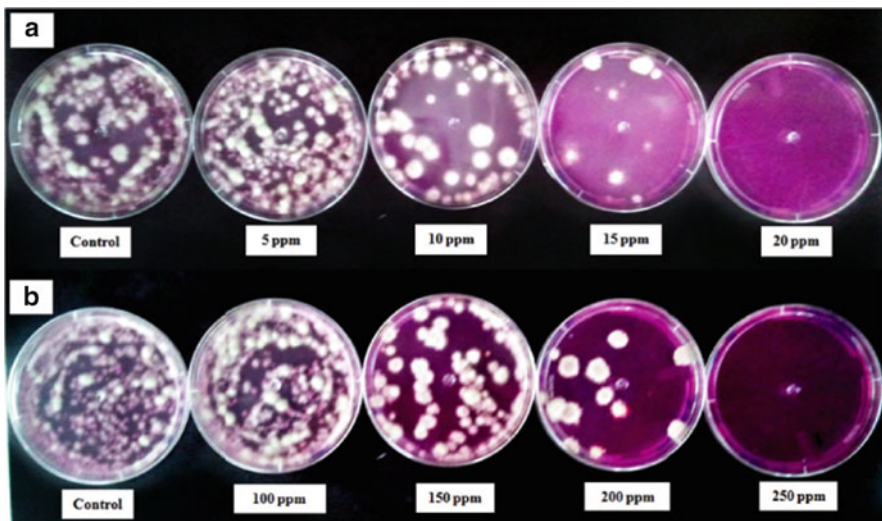


**Fig. 1** In vitro minimum lethal concentration (MLC) of natural antimicrobials in RBC agar. (a) LAE; (b) natamycin. Results are the average of three replicates

solubility and type of modified starch was observed at 0.6 % BW, where lower solubility was found at the highest BW concentration for both starches  $96.03 \pm 0.12\% \text{ SM}$  and  $96.51 \pm 0.20\% \text{ SM}$ .

### 3.2 Antimicrobial Effect

Complete inhibition of fungus was found when LAE was used at a concentration of 250 ppm, for initial fungal population of 5.5 log cfu/mL (Fig. 1a). A similar behavior for natamycin antimicrobial effect was found, where complete fungal inhibition was achieved at 20 ppm (Fig. 1b). The MLC is defined as the lowest concentration of antimicrobial that produces a 99.9 % reduction of tested microorganism (López-Malo et al. 2005). When the antimicrobials were incorporated into the active EFs, inhibition effects were observed at  $428 \mu\text{g cm}^{-2}$  for LAE and  $48 \mu\text{g cm}^{-2}$  for natamycin (Fig. 2).

### 3.3 Active Edible Coating in a Model Fruit

Strawberries were coated with the active EFs which gave a brilliant appearance. After 9 days of storage, the control treatment showed fungal growth and decay (Fig. 3). Weight loss of strawberries was reduced when using the active EF incorporated with  $428 \mu\text{g cm}^{-2}$  of LAE and 1 % BW (Fig. 3). Weight loss is a

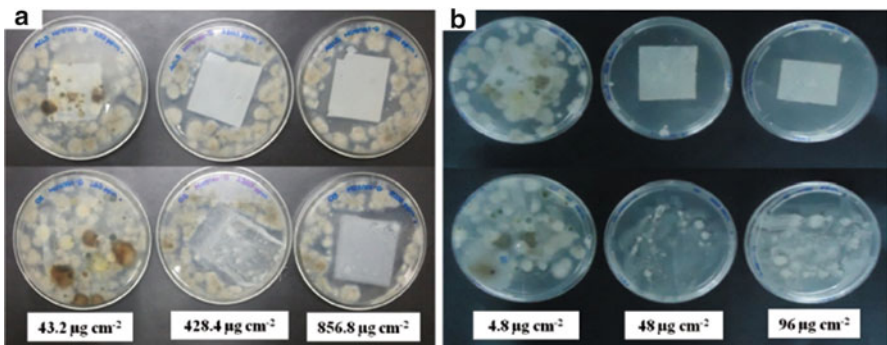


**Fig. 2** Inhibition effects of active EFs. (a) LAE; (b) natamycin

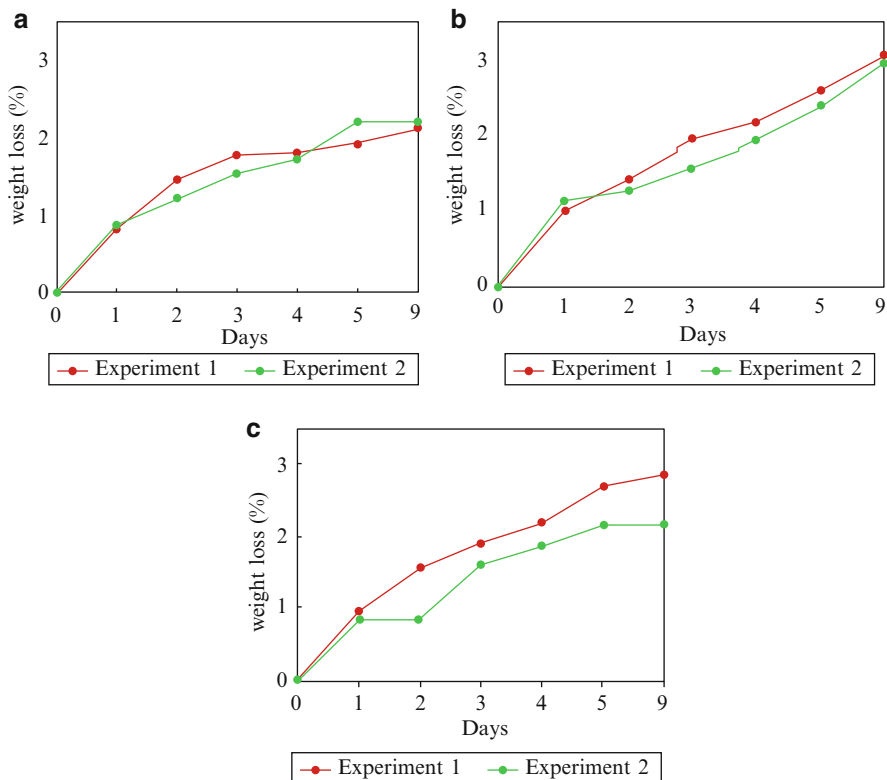


**Fig. 3** Percentage of strawberry weight loss. (a) ACLS and 1 % BW; (b) OS and 1 % BW; (c) Control

major cause of spoilage during storage of fresh fruits. The active EF provided a good moisture barrier and surface antimicrobial properties, which extended the shelf life of strawberries; therefore, the usefulness of this technology as applied to preservation of fresh produce is promising.

## 4 Conclusions

Modified corn starches ACLS and OS as major components of the structural matrix of FS are able to form EFs with good visual and mechanical properties, representing an excellent alternative for developing tailor-made films or coatings for specific food products. The use of BW nano-emulsion as a hydrophobic agent at 1 % (w/v) concentration showed lower WVP and provided good solubility properties to EFs, which is important to increase the shelf life of minimally processed fruits. Use of the natural antimicrobials LAE and natamycin incorporated into active EFs achieved complete inhibition of *B. cinerea*, the most common deteriorative fungus of strawberries. Strawberries coated with active EFs showed brighter appearance and lower weight loss than the control treatment.

## References

- ASTM (2000) Standard test method for water vapor transmission of materials. Standard Designation E96-00
- Brody AL, Strupinsky ER, Kline LR (2001) Active packaging for food applications. CRC Press, Boca Raton, pp 131–194
- De Azeredo HMC (2009) Nanocomposites for food packaging applications. *Food Res Int* 42:1240–1253
- García MA, Martino MN, Zaritzky NE (1998) Plasticized starch-based coatings to improve strawberry (*Fragaria ananassa*) quality and stability. *J Agric Food Chem* 46:3758–3764
- García MA, Pinotti A, Martino MN, Zaritzky NE (2009) Characterization of starch and composite edible films and coating. In: Embuscado ME, Huber KC (eds) *Edible films and coatings for food applications*. Springer, New York, pp 169–210
- Hagenmaier RD, Baker RA (1994) Wax microemulsions and emulsions as citrus coatings. *J Agric Food Chem* 42:899–902
- Hu G, Chen J, Gao J (2009) Preparation and characteristics of oxidized potato starch films. *Carbohydr Polym* 76:291–298
- Janjarasskul T, Krochta MJ (2010) Edible packaging materials. *Annu Rev Food Sci Technol* 1:415–448
- Kim KW, Ko CJ, Park HJ (2002) Mechanical properties, water vapor permeabilities and solubilities of highly carboxymethylated starch-based edible films. *J Food Sci* 67:218–222
- Lin D, Zhao Y (2007) Innovations in the development and application of edible coatings for fresh and minimally processed fruits and vegetables. *Compr Rev Food Sci F* 6:60–75
- Liu Z, Han JH (2005) Film-forming characteristics of starches. *J Food Sci* 70:31–34
- López OV, García MA, Zaritzky NE (2008) Film forming capacity of chemically modified corn starches. *Carbohydr Polym* 73:573–581

- López-Malo A, Palou E, Parish ME, Davidson M (2005) Methods for activity assay and evaluation of results. In: Davidson MP, Sofos JN, Branen AL (eds) *Antimicrobials in food*, 3rd edn. CRC Taylor & Francis, Boca Raton, pp 659–680
- McHugh TH, Krochta JM (1994) Edible coatings and films to improve food quality. CRC Press, Florida, pp 139–141
- Olivas GI, Barbosa-Cánovas G (2009) Edible films and coatings for fruit and vegetables. In: Embuscado ME, Huber KC (eds) *Edible films and coatings for food applications*. Springer, New York, pp 211–244
- Ozdemir M, Floros J (2003) Film composition effects on diffusion of potassium sorbate through whey protein films. *J Food Sci* 68:511–516
- Pérez-Gallardo A, Bello-Pérez LA, García-Almendárez B, Montejano-Gaitán G, Barbosa-Cánovas G, Regalado-González C (2012) Effect of structural characteristics of modified waxy corn starches on rheological properties, film-forming solutions, and on water vapor permeability, solubility, and opacity of films. *Starch-Starke* 64:27–36
- Quezada-Gallo JA (2009) Delivery of food additives and antimicrobials using edible films and coatings. In: Embuscado ME, Huber KC (eds) *Edible films and coatings for food applications*. Springer, New York, pp 315–334
- Rojas-Graü M, Raybaudi-Massilia RM, Soliva-Fortuny RC, Avena-Bustillos RJ, McHugh TH, Martín-Beloso O (2007) Apple puree-alginate edible coating as carrier of antimicrobial agents to prolong shelf-life of fresh-cut apples. *Postharvest Biol Technol* 45:254–264
- Romero-Bastida CA, Bello-Pérez LA, García MA, Martino MN, Solorza-Feria J, Zaritzky NE (2005) Physicochemical and microstructural characterization of films prepared by thermal and cold gelatinization from non-conventional sources of starches. *Carbohydr Polym* 60:235–244
- Singh J, Kaur L, McCarthy OJ (2007) Factors influencing the physicochemical, morphological, thermal and rheological properties of some chemically modified starches for food applications: a review. *Food Hydrocoll* 21:1–22
- Suppakul P, Miltz J, Sonneveld K, Bigger SW (2003) Active packaging technologies with an emphasis on antimicrobial packaging and its applications. *J Food Sci* 68:408–420
- Tharanathan RN (2003) Biodegradable films and composite coatings: past, present and future: a review. *Trends Food Sci Technol* 14:71–78
- Zhou GH, Xu XL, Liu Y (2010) Preservation technologies for fresh meat: a review. *Meat Sci* 86:119–128

# Influence of Moisture Content and Temperature on the Stability of a Dehydrated Probiotic Dairy Product Containing *Bifidobacterium infantis* or *Lactobacillus acidophilus*

G. Trujillo-de Santiago and C. Rojas-de Gante

## Abbreviations

$a_w$	Water activity
$a_w$ MS	Water activity of maximum stability
BET	Brunauer-Emmett-Teller monolayer
C	Constant
DLPB	<i>Bifidobacterium infantis</i>
DLPL	<i>Lactobacillus acidophilus</i>
GAB	Guggenheim-Anderson-de Boer monolayer
GSW	Goat's sweet whey
IDF	International Dairy Federation
K	Constant
$m_o$	Monolayer moisture
$M_w$	Equilibrium moisture content
RH	Relative humidity

## 1 Introduction

Since the beginning of the twentieth century, there has been growing interest in the health benefits provided by probiotic bacteria (Trebichavský and Šplíchal 2006). A variety of subjects of interest revolve around this theme, such as the mechanisms

---

G. Trujillo-de Santiago • C. Rojas-de Gante (✉)  
Instituto Tecnológico y de Estudios Superiores de Monterrey, Campus Monterrey, Ave.  
Eugenio Garza Sada 2501 Sur Col. Tecnológico C.P., 64849 Monterrey, Nuevo León, México  
e-mail: [crd@itesm.mx](mailto:crd@itesm.mx)

of action of probiotic bacteria in providing therapeutic effects, the research of probiotic microorganisms, and the development of new probiotic products.

The definition of the term “probiotic” has been polemic since the 1960s. Today, an accepted definition of probiotic is that it is a product or preparation which contains a sufficiently high concentration of well-defined viable microorganisms during its shelf life, which alters the microflora (by implantation or colonization) of certain compartments of the host (e.g., oral cavity, intestine, vagina, skin) and which improves overall health (Gill 2003; de Vrese and Schrezenmeir 2008). This concept includes the fundamental aspect of concentration of microorganisms. As a guide, the International Dairy Federation (IDF) suggests a minimum concentration of  $10^7$  cfu/g of probiotic organisms, retained until the date of the product expiration. The Japan Fermented Milk Association has established a minimum concentration of  $10^7$  bifidobacteria/g or ml (Farnworth 2008; Kailasapathy 2002). The minimum concentration of viable bacteria required to achieve therapeutic effects has been questioned several times for multiple commercial probiotic products (Kailasapathy 2002; Damin et al. 2008; Kailasapathy and Rybka 1997).

At the present time, probiotics are offered in essentially two presentations: food and pharmaceutical (e.g., sachet, tablets, or capsules). Fermented dairy probiotic products are still the most common and traditional presentations. These types of products are highly susceptible to spoilage because of their high water activity and nutrient contents. A proper cold chain is required, from the production plant to the consumer, in order to preserve product quality until the moment the product is consumed. Preservation of a cold chain is a process that requires substantial energy input and strict logistics, both of which have an impact on cost (Carrillo 2006). For this reason, dehydrated products, which are generally stable at room temperature, are very attractive in terms of cost, as they do not require a cold chain for transportation or storage.

Our research group has previously developed a dehydrated and laminated probiotic dairy product with *Bifidobacterium infantis* (DLPB) or *Lactobacillus acidophilus* (DLPL), inspired by the concept of a typical Mexican crispy wafer. During the process used for fabricating the product, probiotic strains were exposed to stress conditions (high temperature, aerobic and arid conditions). At the end of the process, the product had a probiotic concentration beyond that recommended, but a new concern emerged regarding the permanence of this characteristic. In addition to maintaining the probiotic concentration, water absorption by the food matrix was a concern, as this is a dehydrated product, and moisture content is a key determinant of the stability of the DLPB and DLPL.

The goal of the current research was therefore to study the stability of DLPB and DLPL based on three determinant factors: temperature, moisture content, and probiotic bacteria concentration.

## 2 Materials and Methods

### 2.1 Preparation of DLPB and DLPL

A process to obtain DLPB and DLPL was previously developed by our research group. The process consisted of five stages: (1) fermenting goat's sweet whey (GSW) with *B. infantis* or *L. acidophilus* until mid-log phase using 10 % inoculum concentrations and incubation conditions of  $38 \pm 2$  °C and vacuum equivalent of 22 mmHg; (2) formulating 58.33 % fermented GSW with 8.33 % of a 6 % p/v suspension of resistant starch (RS), 16.66 % of 15 % p/v solution of inulin, and 16.66 % of 10 % p/v solution of gelatin; (3) pouring the formulation onto a non-stick pan and letting it stand at 4 °C for 1 h; (4) drying in a convection oven at  $55 \pm 5$  °C for  $2.66 \pm 0.22$  h with an airflow of  $0.212 \pm 0.03$  m/min; and (5) dehydrating in a hermetic chamber at 22 °C and ~0 % relative humidity (RH), provided by CaCl<sub>2</sub>, for 22 h. At the final point of the process, the probiotic products of both strains were obtained with concentrations over  $10^9$  cfu/g of viable bacteria.

### 2.2 Sorption Isotherm

A sorption isotherm at  $22 \pm 1$  °C for the dehydrated and laminated dairy product, without probiotic microorganisms, was used as a tool to determine the monolayer moisture ( $m_o$ ) of the product that was considered as the maximum stability moisture. The sorption isotherm was conducted by a gravimetric static method. Eight vacuum desiccators were conditioned to a constant RH with saturated salt solutions in order to achieve the water activity ( $a_w$ ) range of 0.11–0.89 (Greenspan 1977). Triplicate samples of  $0.5 \pm 0.05$  g were previously dried in a desiccator containing pure phosphorus pentoxide. Brunauer-Emmett-Teller (BET) and Guggenheim-Anderson-de Boer (GAB) (Timmermann et al. 2001) monolayers were determined from the experimental sorption data according to Eqs. (1) and (2), respectively. The  $a_w$  of maximum stability ( $a_{w,MS}$ ) was determined by the interception of the  $x$  and  $y$  axes in the sorption isotherm, taking the value of the BET monolayer on the  $y$ -axis as a reference.

$$M_w = \frac{m_o C a_w}{(1 - a_w)[1 + (C - 1)a_w]} \quad (1)$$

where  $a_w$  represents water activity,  $M_w$  equilibrium moisture content,  $m_o$  monolayer moisture, and  $C$  constant.

$$M_W = \frac{m_o C K a_w}{(1 - K a_w)[1 + (C - 1)a_w]} \quad (2)$$

where  $a_w$  represents water activity,  $M_w$  equilibrium moisture content,  $m_o$  monolayer moisture,  $C$  constant, and  $K$  constant.

## 2.3 Stability of DLPB and DLPL

Two conditions of RH and temperature were chosen to study the stability of the DLPB and DLPL. A condition, designated “adequate,” consisted of the same temperature as the sorption isotherm ( $22 \pm 1$  °C) and an RH close to its analogue  $a_w$ MS. A second condition, designated “inadequate,” consisted of an RH that provided an  $a_w$  higher than  $a_w$ MS and a temperature above that of the sorption isotherm ( $37 \pm 2$  °C). This inadequate condition accelerated deteriorative reactions according to the Arrhenius Law (Taub and Singh 1998). DLPB and DLPL samples, without packaging, were exposed to each condition and triplicate specimens were analyzed weekly. Two parameters were evaluated: the product moisture content, by the gravimetric method, and the viable probiotic bacteria concentration, by the plate counting method. Plate counting was conducted in accordance with the Official Mexican Norm NOM-092-SSA1-1994, using conventional synthetic MRS agar (DIFCO, Laboratories). Agar plates were incubated in a vacuum incubator (Sheldon Manufacturing Inc., Cornelius, OR) at  $38 \pm 2$  °C and a vacuum of 20 mmHg.

## 3 Results and Discussion

### 3.1 Sorption Isotherm at $22 \pm 1$ °C

Figure 1 shows the experimental data fit to the BET and GAB models. A sigmoid type III isotherm was generated (Labuza and Bell 2000). An abrupt increase occurred after  $a_w = 0.5$ , which could reflect the dissolution of sugars (lactose) once equilibrium was achieved. The BET equation was only applied to  $a_w$  values below 0.5, whereas the whole  $a_w$  range was used for the GAB equation (Rangel-Marrón et al. 2010). Parameters are shown in Table 1. Considering the  $R^2$ , the experimental data fit better to GAB than to the BET model. The  $a_w$ MS was determined from the GAB monolayer; the interception used to obtain it is shown in Fig. 1. Since the  $a_w$ MS was very close to 0.33, this condition was employed as the “adequate” condition for the subsequent DLPs stability study.

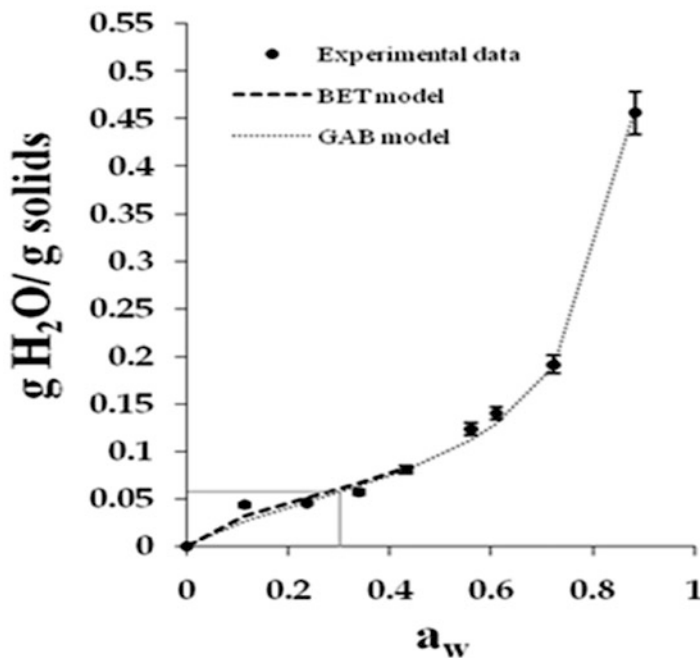


**Fig. 1** Sorption isotherm at  $22 \pm 1$  °C of a dehydrated and laminated dairy product using BET and GAB models. Determination of maximum stability  $a_w$  by interception of the y- and x-axis (the GAB monolayer in the y-axis is used as the reference data)

**Table 1** Estimated parameters of the BET model for the sorption isotherm at  $22 \pm 1$  °C for a dehydrated and laminated dairy product

Parameters	Model	
	BET	GAB
$m_o$ (g H <sub>2</sub> O/g solids)	0.045	0.057
$C$	18.51	5.6
$K$	NA	0.995
$R^2$	0.923	0.996
MRE	11.2	8.9

$m_o$  monolayer moisture,  $C$  constant,  $K$  constant, MRE mean relative error, NA not applicable

### 3.2 Stability of DLPB and DLPL

Based on the information derived from the sorption isotherm, the “adequate” and “inadequate” storage conditions were 33.9 % RH at 22 ± 1 °C and 53 % RH at 37 ± 2 °C, respectively. Figure 2 shows the evolution of moisture content during a month of storage in both storage conditions; moisture content did not exceed monolayer moisture in any case. DLPB and DLPL samples remained dry and crispy throughout the entire study. Figure 3 shows the probiotic bacteria concentrations for

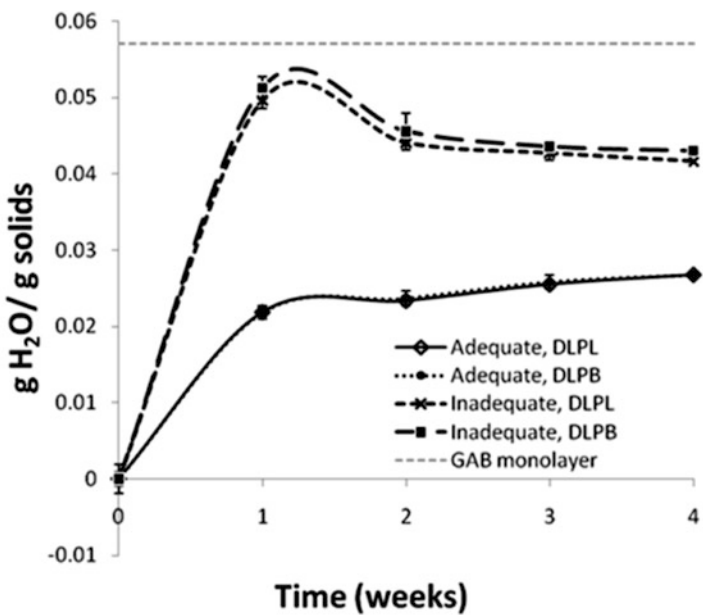


**Fig. 2** Kinetics of moisture content of dehydrated and laminated probiotic dairy product containing *Bifidobacterium infantis* (DLPB) and *Lactobacillus acidophilus* (DLPL), stored under two conditions for 4 weeks: “adequate” (33.9 % RH and  $22 \pm 1$  °C) and “inadequate” (53 % RH at  $37 \pm 2$  °C)

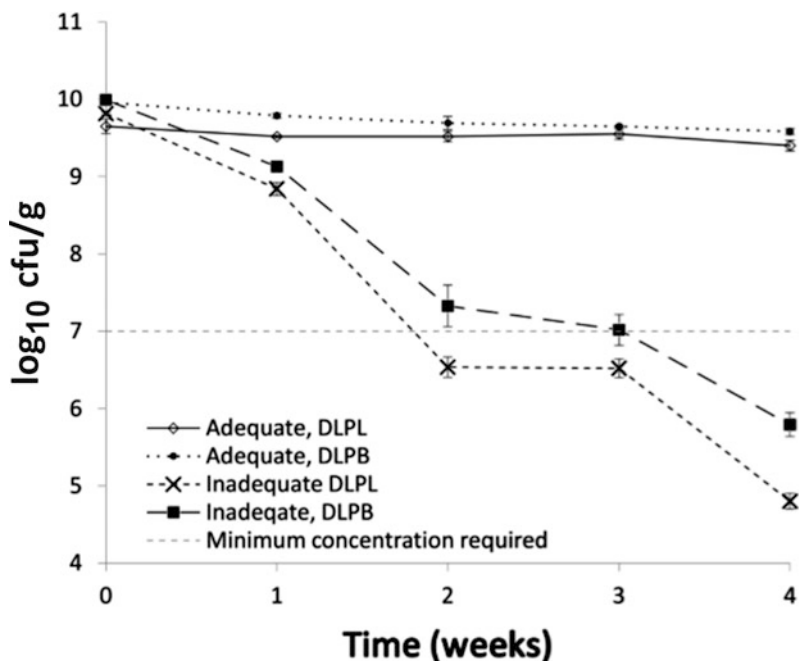


**Fig. 3** Kinetics of concentration of viable probiotic bacteria ( $\log_{10}$  cfu/g) of dehydrated and laminated probiotic dairy product with *Bifidobacterium infantis* (DLPB) and *Lactobacillus acidophilus* (DLPL), stored under two conditions for 4 weeks: “adequate” (33.9 % RH and  $22 \pm 1$  °C) and “inadequate” (53 % RH at  $37 \pm 2$  °C)

DLPB and DLPL at both conditions over the 4-week monitoring period. Both strains were stable under the adequate condition, maintaining concentrations above  $9 \log_{10} \text{cfu/g}$  over the 4 weeks. In contrast, bacterial viability decayed exponentially at the inadequate condition. DLPB and DLPL lost the minimal effective concentration at the fourth week and the third week, respectively.

Consistent with these results, the storage conditions studied did not significantly impact the DLPB and DLPL moisture content; in terms of moisture, both conditions were satisfactory. Nevertheless, the rate of cellular death was significantly accelerated at storage conditions of 53 % RH and  $37 \pm 2^\circ\text{C}$ . Cellular death rate could be considered as a deteriorative reaction that is potentiated at higher RH and temperature. Viability of *B. infantis* and *L. acidophilus* was a critical factor for DLPB and DLPL stabilities. When DLPB and DLPL were stored under proper conditions, they were as stable as the refrigerated set yogurt with microencapsulated bifidobacteria studied by Adhikari et al. (2000) and were more stable than yogurts with nonencapsulated cells, which usually do not maintain acceptable viable probiotic concentrations beyond 1 month of refrigerated storage.

## 4 Conclusions

DLPB and DLPL lasted more than a month when they were stored at 33.9 % RH and  $22 \pm 1^\circ\text{C}$ , and they retained their viable probiotic bacteria counts at over  $9 \log_{10} \text{cfu/g}$ . In contrast, cellular death rate was exponentially accelerated under conditions of 53 % RH and  $37 \pm 2^\circ\text{C}$ , and the probiotic concentration decreased to below the minimum required for a probiotic product ( $7 \log_{10} \text{cfu/g}$ ). As expected, increases in storage RH and temperature diminished the stability of the probiotic products studied, compromising their shelf life and their concentrations of viable bacteria that are highly associated with therapeutic effectiveness.

## References

- Adhikari K, Mustapha A, Grün IU, Fernando L (2000) Viability of microencapsulated bifidobacteria in set yogurt during refrigerated storage. *J Dairy Sci* 83(9):1946–1951
- Carrillo A (2006) Tratamiento y reutilización del suero de leche. *Mundo Lact Carn*:27–30
- Damin MR, Minowa E, Alcántara MR, Oliveira MN (2008) Effect of cold storage on culture viability and some rheological properties of fermented milk prepared with yogurt and probiotic bacteria. *J Texture Stud* 39(1):40–55
- de Vrese M, Schrezenmeir J (2008) Probiotics, prebiotics, and synbiotics. *Adv Biochem Eng Biotechnol* 111:1–66
- Farnworth ER (2008) The evidence to support health claims for probiotics. *J Nutr* 138(6):1250S–1254S
- Gill H (2003) Probiotics to enhance anti-infective defences in the gastrointestinal tract. *Best Pract Res Clin Gastroenterol* 17(5):755–773

- Greenspan L (1977) Humidity fixed points of binary saturated aqueous solutions. *J Res Nat Bur St Phys Chem* 81a(1):89–96
- Kailasapathy K (2002) Microencapsulation of probiotic bacteria: technology and potential applications. *Curr Issues Intest Microbiol* 3(2):39–48
- Kailasapathy K, Rybka S (1997) *L. acidophilus* and *Bifidobacterium* spp.: their therapeutic potential and survival in yogurt. *Aust J Dairy Technol* 52(1):28–35
- Labuza TP, Bell LN (2000) Moisture sorption: practical aspects of isotherm measurement and use, 2nd edn. American Association of Cereal Chemists, St. Paul, MN, USA, p 122
- Norma Oficial Mexicana NOM-092-SSA1-1994 (1994) Bienes y servicios. Método para la cuenta de bacterias aerobias en placa. <http://www.salud.gob.mx/unidades/cdi/nom/092ssa14.html>
- Rangel-Marrón M, Welti-Chanes J, Córdova-Quiroz AV, Cerón-Bretón JV, Anguebes-Franceschi F, Moreno-Martínez V (2010) Sorption isotherms of mango (*Mangifera indica* L.) pulp freeze-dried. In: Mladenov V et al (eds) Advances in control, chemical engineering, civil engineering and mechanical engineering. WSEAS Press, USA, pp 114–118
- Taub IA, Singh RP (1998) Food storage stability. CRC Press, Boca Ratón, USA, p 539
- Timmermann EO, Chirife J, Iglesias HA (2001) Water sorption isotherms of foods and foodstuffs: BET or GAB parameters. *J Food Eng* 48(1):19–31
- Trebichavský I, Šplíchal I (2006) Probiotics manipulate host cytokine response and induce antimicrobial peptides. *Folia Microbiol* 51(5):507–510

# **Effect of Relative Humidity on Shrinkage and Color Changes in Dehydrated Strawberry**

**L.M. Agudelo-Laverde, N. Acevedo, C. Schebor, and M.P. Buera**

## **Abbreviations**

CPMG	Carr-Purcell-Meiboom-Gill pulse sequence
CVS	Computer vision system
DSC	Differential scanning calorimetry
NMR	Nuclear magnetic resonance
RH	Relative humidity
$T_g$	Glass transition temperature

---

L.M. Agudelo-Laverde, C. Schebor, and M.P. Buera are CONICET members.

L.M. Agudelo-Laverde (✉) • N. Acevedo

Departamento de Industrias, Facultad de Ciencias Exactas y Naturales, Universidad de Buenos Aires, Buenos Aires, Argentina  
e-mail: [magudelo@di.fcen.uba.ar](mailto:magudelo@di.fcen.uba.ar)

C. Schebor

Departamento de Industrias, Facultad de Ciencias Exactas y Naturales, Universidad de Buenos Aires, Buenos Aires, Argentina

Ciudad Universitaria, Ciudad de Buenos Aires 1428, Argentina

M.P. Buera

Departamentos de Industrias y de Química Orgánica, Facultad de Ciencias Exactas y Naturales, University of Buenos Aires (FCEyN-UBA), National Council of Scientific and Technical Research (CONICET), Buenos Aires, Argentina

## 1 Introduction

Dehydrated fruits are prone to discoloration during storage. Many natural pigments are unstable in dried fruits, and brown pigments can be formed. The rate of physical and chemical changes in dried vegetables and food models is slow in the glassy state. At temperatures above the glass transition, in addition to decreasing viscosity and increasing rate, other changes such as crystallization and structural collapse affect the rate of discoloration (Karmas et al. 1992). Diffusion-controlled chemical reactions are particularly dependent on translational diffusivity of the reactants (or on the viscosity of the matrix material) and are thus susceptible to the physical state of the system (Slade et al. 1995). It has been shown that matrix collapse caused by storage above the glass transition temperature ( $T_g$ ) or by mechanical compression and porosity (Burin et al. 2004; White and Bell 1999) affected browning rates, indicating that besides water content, system structure plays a relevant role.

Color and size changes affect fruit appearance and organoleptic quality and may be an indication of decreased nutritional and functional properties of foods. Food discoloration can occur homogeneously, but most often, heterogeneous distribution of color is observed. Color meters typically claim to measure the average color of the food material's surface exposed to the measuring window of the instrument (Balaban 2008). However, many food products, such as strawberry slices, show heterogeneous color distribution. While averaging is acceptable for uniformly colored surfaces (Briones and Aguilera 2005; Mendoza et al. 2006; Venir et al. 2007; Acevedo et al. 2008a, b), when the colors change with location or are non-homogeneous, averaging may result in inaccurate color determination (Balaban 2008). The objective of this work was to assess the effect of relative humidity (RH) on color alterations and shrinkage in freeze-dried strawberry slices.

## 2 Material and Methods

### 2.1 Fruits

Fully ripe fresh strawberries were obtained from a local market and stored at 4 °C until the initiation of the experiment. The fruits were washed and then cut transversally into slices (2.0 cm diameter and 0.5 cm thickness). The cut material was immediately frozen with liquid nitrogen and stored at –20 °C.

### 2.2 Materials Preparation

Fruit slices were covered with liquid nitrogen before freeze-drying. A freeze-drier (ALPHA 1-4 LD2 Martin Christ Gefriertrocknungsanlagen GmbH, Germany) was used. The freeze-drier was operated at –55 °C, at a chamber pressure of 4 Pa, and

the process lasts 48 h. After freeze-drying, several pieces were distributed into vials for the determination of anthocyanin content. Samples used for all determinations were humidified in a range of 11–84 % RH for 14 days at 20 °C (Greenspan 1977). After humidification, the strawberry slices used to determine color changes were placed inside rubber O-rings and sandwiched between two glass plates and then hermetically sealed to avoid water loss, according to the method reported by Acevedo et al. (2008a, b). They were then placed in a forced air oven operated at  $45 \pm 1$  °C during 120 h. Two glass plates containing six strawberry slices for each relative humidity were removed from the oven after adequate time to acquire images and measured in their glass-covered containers.

### **2.3 Computer Vision System (CVS)**

Strawberry color changes were determined by image analysis. The CVS consisted of three elements: a lighting system, a digital camera, and a personal computer. The lighting system included a D65 lamp (corresponding to solar irradiation with a color temperature of 6,500 K, Lozano 1978) inside a gray chamber (N7 in the Munsell color space). Warm up of the lamps was 15 min before taking pictures. The angle between the camera axis and the sample plane was 90°, and the angle between the light source and the sample plane was 45°, in order to capture the diffuse reflection responsible for color produced at this angle (Yam and Papadakis 2004). A high-resolution (10.1 megapixel) digital camera EOS 40D (Canon Inc., Japan) was used, with an EF-S 60 mm f2.8 macro lens (Canon Inc., Japan). Samples were transferred from the forced air oven to the gray box, and images were acquired at different times during the entire storage period. The digital camera was operated in manual mode, with the lens aperture at f ¼ 6.3 and speed 1/8 s (no zoom, no flash) to achieve high uniformity and repeatability. The calibration of the camera and the parameters used for image capture are described in Briones and Aguilera (2005). Images have a resolution of  $3,888 \times 2,592$  pixels and were stored in JPEG format using Canon's Remote Capture program (EOS Utility, Canon Inc., USA). The images were taken using a white background.

### **2.4 Image Segmentation**

CVS permitted acquisition of information for the whole pieces directly inside the glass plates. Color images were obtained in lab values using Adobe Photoshop CS4 software (Adobe Systems Inc., San Jose, CA) and were then converted to standard CIELAB space using mathematical formulas described by Papadakis et al. (2000) from CIELAB coordinates ( $L^*$ ,  $a^*$ , and  $b^*$ ).

It is possible for the software to identify every pixel in an image that has color attributes ( $L$ ,  $a$ ,  $b$ ) lower than or higher than a given threshold or attributes between

2 threshold values. Once these pixels are identified and counted, then their percentage based on the total view area of an object can be calculated. In this way, images of the strawberry slices were segmented in two different zones, according to their  $a^*$  values. The selected intervals of  $a^*$  values were from 0.5 to 17 (representing the lighter sections) and from 17 to 28 (representing the reddish sections). The number of pixels of each zone of the strawberry slices was quantified, and their corresponding percentage was calculated. The color functions selected to follow browning changes in fruits were the  $L^*$ ,  $a^*$ , and  $b^*$ .

## 2.5 Collapse Determination

Collapse of the systems was determined by measuring the volume of the fruit discs from the pictures taken with the CVS (as previously described). Modeling program SolidWorks 2011 3D mechanical was used for analysis of collapse. Volume reduction was expressed as the diameter percentage with respect to a control disc without shrinkage. Six replicates of each sample were measured and the average and standard deviation determined.

## 2.6 Glass Transition Determination

Glass transition temperature ( $T_g$ ) was determined by differential scanning calorimetry (DSC; onset values) using a calorimeter model 822 (Mettler Toledo, Schwerzenbach, Switzerland). The instrument was calibrated with indium (156.6 °C), lead (327.5 °C), and zinc (419.6 °C). All measurements were performed at a heating rate of 10 °C/min. Approximately 10 mg of each sample was placed in 40 ml aluminum pans, which in turn were hermetically sealed. An empty pan served as a reference. Thermograms were evaluated using Stare software v. 6.1 (Mettler Thermal Analysis).

## 2.7 Water Mobility Determination

A pulsed nuclear magnetic resonance (NMR) instrument (Bruker mq 20 Minispec, with a 0.47 T magnetic field operating at resonance frequency of 20 MHz) was used for measurement. Humidified materials were removed from the desiccators, placed into 10 mm diameter glass tubes, and returned to the desiccators for an additional 24 h prior to analysis.

Proton transverse relaxation times  $T_2$  associated to slow relaxing protons (related to the populations of water molecules displaying less interaction with solids)

were measured using the Carr-Purcell-Meiboom-Gill pulse sequence (CPMG)  $90x-(\tau-180y \tau \text{ echo})n$ . All determinations were performed in duplicate, and the average and standard deviations are provided.

### 3 Results and Discussion

Figure 1 shows the global color changes observed for freeze-dried strawberries humidified at several RHs when stored at 45 °C as a function of time. At 11 % RH, the samples presented a lighter color, manifested by the higher L\* and lower b\* values, while at 43 % RH L\* and b\* values were relatively constant during storage time. Slight changes were observed in the L\* and b\* values at 52 % RH. In the rest of the samples, due to browning reactions, L\* and b\* values decreased, causing a change from the original light color to different brown degrees. However, the a\* component decreased drastically at all RH values, and the rate of these changes was more important with the increase in RH.

The rate of redness loss was approximated by the slope of the initial linear part of the curves shown in Fig. 1 (as pseudo-zero-order reaction rate), and shrinkage was determined as the % of volume reduction relative to the control sample. Both parameters were plotted in Fig. 2 as a function of  $(T-T_g)$ , the difference between storage temperature, and  $T_g$ , for the samples stored at 45 °C for 22.5 h.

As observed in Fig. 2, the volume reduction and redness loss increased at increasing  $(T-T_g)$  due to RH increase. The observed shrinkage was caused by storage at conditions well above the  $T_g$  ( $T-T_g > 40$  °C). The rate of initial redness loss showed a drastic increase at  $(T-T_g)$  values higher than 70 °C, when the sample shrinkage approximated 50 % (corresponding to 84 % RH). The  $^1\text{H}$  NMR signal decay of the transversal relaxation times,  $T_2$ , was obtained by the CPMG pulse sequence in order to relate the observed behavior of the change of the chromatic attributes with the molecular mobility in the samples. It is important to note that at these conditions, populations of water molecules with high mobility are present, as determined by pulsed  $^1\text{H}$  NMR, and frozen water is detected by DSC (Agudelo-Laverde et al. 2011).

Because strawberry slices presented heterogeneous color distribution, in addition to analyzing the global color changes, the image analysis of the slices was done by dividing the area into two different zones. The color changes were better represented by the a\* variable, showing a decrease along storage time because the heat treatment caused anthocyanin pigment destruction. Before storage at 45 °C, the a\* values could be distributed in different sections having different red degree, as expected for strawberry slices (Fig. 3). The pixel proportion of red areas in the pictures was greater at low RHs and short storage times. As RH and storage time increased, the areas with high a\* values decreased and the homogeneity of color distribution also increased.

**Fig. 1**  $L^*$ ,  $a^*$ , and  $b^*$  changes as a function of time at 45 °C for strawberry discs at several relative humidities

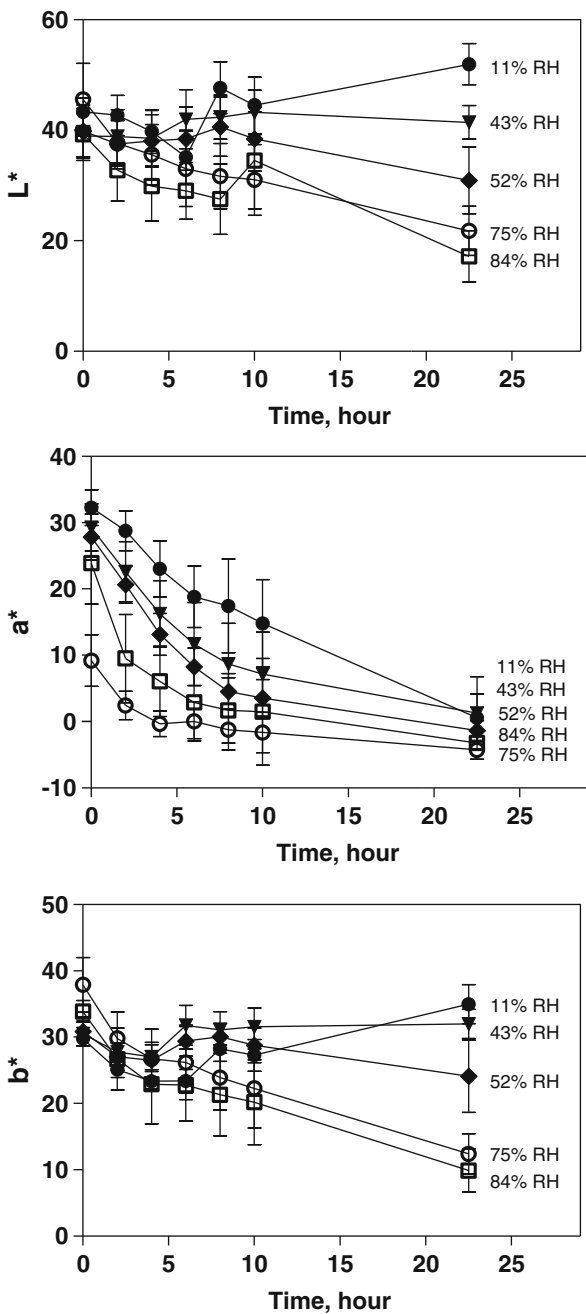


**Fig. 2** Shrinkage of strawberry slices (open circle) and rate of redness changes (asterisk) after 22.5 h of storage at 45 °C, as a function of  $(T-T_g)$

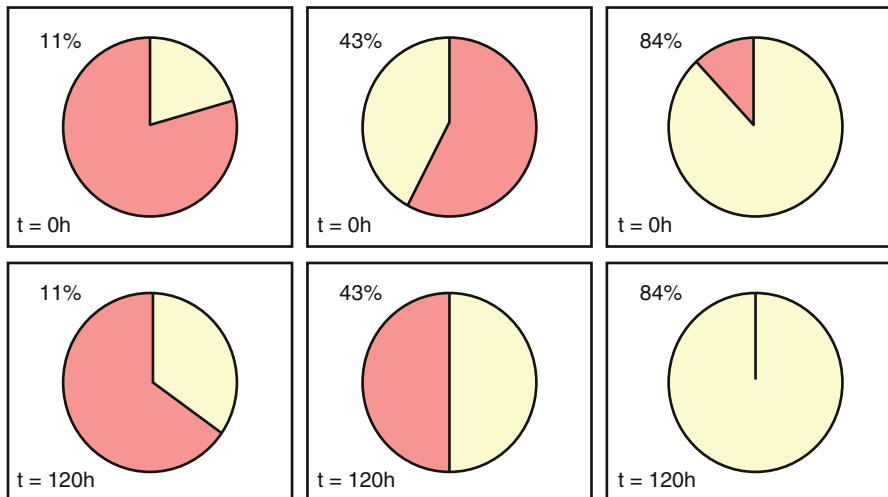
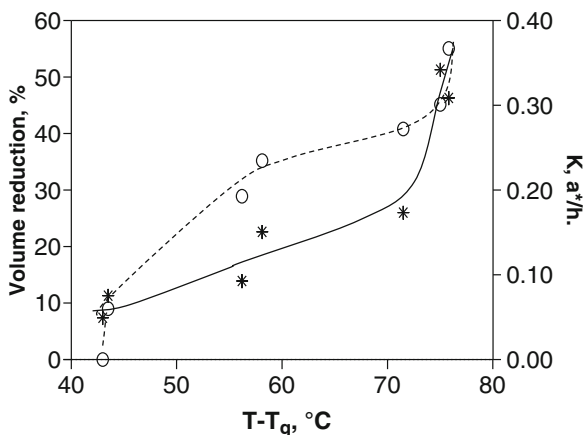


**Fig. 3** Proportion (%) of pixels corresponding to different sections of  $a^*$  values for 0 and 22.5 h of storage at 45 °C at 11, 43, and 84 % RH

#### 4 Conclusions

The final color of freeze-dried strawberries during storage was the result of loss of redness and browning development. Redness loss and browning could be related to the decrease of CIELAB coordinates  $a^*$  and  $L^*$ , respectively. During storage at 45 °C for 22.5 h,  $a^*$  constantly decreased with increasing RH, but  $L^*$  decrease was not significant below 43 % RH.

Sample shrinkage and redness loss were significantly affected by RH. Both shrinkage and color changes seem to be affected by RH and ( $T-T_g$ ) values at which water mobility is characterized by  $T_2$  relaxation times in the order of ms, and water is able to crystallize.

The segmented image analysis revealed that humidification level and storage time, besides influencing the kinetics of changes, were determinant factors in defining the degree of color heterogeneity in dehydrated strawberries.

## References

- Acevedo N, Briones V, Buera M, Aguilera J (2008a) Microstructure affects the rates of chemical, physical and color changes during storage of dried apple discs. *J Food Eng* 85(2):222–231
- Acevedo NC, Schebor C, Buera P (2008b) Non-enzymatic browning kinetics analyzed through water-solid interactions and water mobility in dehydrated potato. *Food Chem* 108(3):900–906
- Agudelo-Laverde LM, Acevedo N, Schebor C, Buera MP (2011) Integrated approach for interpreting browning rate dependence with relative humidity in dehydrated fruits. *LWT-Food Sci Technol* 44:963–968
- Balaban MO (2008) Quantifying nonhomogeneous colors in agricultural materials. Part I: method development. *J Food Sci* 73(9):431–437
- Briones V, Aguilera JM (2005) Image analysis of changes in surface color of chocolate. *Food Res Int* 38(1):87–94
- Burin L, Jouppila K, Roos Y, Kansikas J, Buera MP (2004) Retention of  $\beta$ -galactosidase activity as related to Maillard reaction, lactose crystallization, collapse and glass transition in low moisture whey systems. *Int Dairy J* 14(6):517–525
- Greenspan L (1977) Humidity fixed points of binary saturated aqueous solutions. *J Res Natl Bur Stand* 8:89–96
- Karmas R, Buera M, Karel M (1992) Effect of glass transition on rates of non-enzymatic browning in food systems. *J Agric Food Chem* 40(4):873–879
- Lozano R (1978) El color y su medición. Editorial América Lee, Buenos Aires
- Mendoza F, Dejmek P, Aguilera JM (2006) Calibrated color measurement of agricultural food using image analysis. *Postharvest Biol Technol* 41(3):285–295
- Papadakis S, Abdul-Malek S, Kandem R, Yam K (2000) A versatile and inexpensive technique for measuring colour of foods. *Food Technol* 54(12):48–51
- Slade L, Levine H, John EK, Taylor SL (1995) Glass transitions and water food structure interactions. *Adv Food Nutr Res* 38:103–269
- Venir E, Munari M, Tonizzo A, Maltini E (2007) Structure related changes during moistening of freeze dried apple tissue. *J Food Eng* 81(1):27–32
- White K, Bell L (1999) Glucose loss and Maillard reaction in solids as affected by porosity and collapse. *J Food Sci* 64:1010–1014
- Yam KL, Papadakis SE (2004) A simple digital imaging method for measuring and analysing color of food surfaces. *J Food Eng* 61(1):137

# **Effect of Blanching and/or Osmotic Dehydration on Texture and Rheological Properties of Apple Tissue**

**A.B. García Loredo, S. Guerrero, and S.M. Alzamora**

## **Abbreviations**

$A_1$	Area 1
Adh	Adhesiveness
ANOVA	Analysis of variance
B	Blanched apples
BOD	Blanched and osmotically dehydrated apples
C	Raw apples
Chew	Chewiness
Coh	Cohesiveness
$E_d$	Modulus of deformability
$F$	Fracturability
$G''$	Loss modulus
Gum	Gumminess
$G'$	Storage modulus
H	Hardness
$H_2$	Hardness 2
$J(t, \tau)$	Creep compliance
MANOVA	Multivariate analysis of variance
OD	Osmotically dehydrated apples
PCA	Principal component analysis

---

A.B. García Loredo, S. Guerrero and S.M. Alzamora are members of Consejo Nacional de Investigaciones Científicas y Técnicas de la República Argentina.

A.B. García Loredo (✉) • S. Guerrero • S.M. Alzamora  
Departamento de Industrias, Facultad de Ciencias Exactas y Naturales,  
Universidad de Buenos Aires, Ciudad Universitaria, Buenos Aires, Argentina  
e-mail: [analigloredo@yahoo.com.ar](mailto:analigloredo@yahoo.com.ar)

Sp	Springiness
T	Time
TPA	Texture profile analyses
$\gamma$	Strain
$\eta_i$	Coefficients of viscosity associated with the Kelvin-Voigt elements
$\eta_N$	Coefficient of viscosity associated with Newtonian flow
$\lambda$	Retardation times
$\tau$	Constant stress applied

## 1 Introduction

Texture is a key quality attribute that is critical in determining the acceptability of raw and processed fruits. Texture and rheological properties of biological tissues depend on the contribution of different levels of structure and their chemical and physical interactions. Heating process and mass transfer during osmotic dehydration of fruit tissues take place simultaneously, with complex physical and structure modifications that influence and produce specific rheological behaviors and sensory responses.

This study was aimed at analyzing and relating rheological properties (dynamic oscillatory shear test, creep/recovery test, and instrumental texture profile analysis), texture (sensory analysis), and microstructure (light microscopy) of apple parenchymatous tissue subjected to blanching, osmotic dehydration and blanching, as well as osmotic dehydration.

## 2 Materials and Methods

Apple slices (*Malus pumila*, Granny Smith cv) were cut parallel to the main axis (3 cm in diameter, 1 cm in thickness) and subjected to (1) osmotic dehydration at atmospheric pressure by immersion into a 22 % w/w aqueous glucose (®Cerelose, Refinerías de Maíz, Argentina) solution at 25 °C to reach  $a_w$  0.97 ( $\cong 6\frac{1}{2}$  h); (2) steam blanching by immersion in saturated steam for 90 s and cooling in water for 20 s at 5 °C; and (3) steam blanching followed by osmotic dehydration, as previously described. Rheological and texture characteristics and microstructure were analyzed in raw (C), blanched (B), osmotically dehydrated (OD), and blanched and osmotically dehydrated (BOD) apples.

Linear viscoelastic properties were characterized at 25 °C in a Paar Physica MCR 300 rheometer. Dynamic oscillatory tests were performed in a controlled strain mode (frequency range 0.1–100/s; strain amplitude 0.005 %; 10 replicates). Creep/recovery tests were conducted by applying a constant shear stress of 35 Pa until 100 s (recovery phase: 200 s; 15 replicates). Compliance data from creep

experiments were fitted by a mechanical model consisting of a spring connected in series with two Kelvin-Voigt elements (each Kelvin-Voigt element had a spring and a dashpot in parallel) and a dashpot element described by the following equation (Sherman 1970):

$$J(t, \tau) = (J_0) + \sum_{i=1}^2 (J_i) \left( 1 - e^{-t/\lambda_i} \right) + t/\eta_N \quad (1)$$

where  $J(t, \tau)$  is the creep compliance ( $= \gamma(t)/\tau$ ), with  $\gamma(t)$  being the strain at time  $t$  and  $\tau$  the constant stress applied.  $J_0$  is the instantaneous compliance at  $t=0$ ;  $J_i$  are the retarded compliances;  $\lambda_i$  ( $= \eta_i \times J_i$ ) are the retardation times and  $\eta_i$  are the coefficients of viscosity associated with the Kelvin-Voigt elements; and  $\eta_N$  is the coefficient of viscosity associated with Newtonian flow and its inverse, the steady-state fluidity of the material.

Instrumental texture profile analyses (TPA) were characterized at 25 °C (20 replicates, cross-head speed = 60 mm/min, two cycle compression, 70 % deformation, load range = 5,000 kgf) using an Instron Testing Machine model 3345. The test was set for calculating fracturability, hardness, hardness2, area1, adhesiveness to palate, cohesiveness, springiness, chewiness, gumminess, and modulus of deformability (Bourne 1978).

Sensory analysis was performed by nine assessors trained in the texture profile method following the procedure described by Civille and Szczesniak (1973) to recognize texture attributes of hardness, fracturability, juiciness, crispness, cohesiveness, and adhesiveness to palate.

Light microscopy observations of raw and treated fruit tissues were performed in a Carl Zeiss Axioskop 2 microscope according to conventional techniques (D'Ambrogio 1986).

Multivariate analysis of variance (MANOVA) and principal component analysis (PCA) were used to analyze rheological data. Analysis of variance (ANOVA) was used to analyze sensory data. Statistical analysis was conducted using Infostat v. 2009 software (Cordoba National University, Argentina).

### 3 Results and Discussion

All apple samples showed solid behavior with the storage modulus ( $G'$ ) exceeding the loss modulus ( $G''$ ) over the entire frequency range, but both dynamic moduli were reduced due to processing.  $G'$  and  $G''$  values for fresh and processed tissues showed a weak dependence on frequency (Fig. 1a, b, respectively). The storage modulus  $G'$  slightly increased with increasing angular frequency. The frequency dependence of  $G''$  was more complex. In general,  $\tan \delta$  was not sensitive for distinguishing physical differences between raw and treated apple tissues or between treatments. The pattern found for dynamic spectra was in agreement

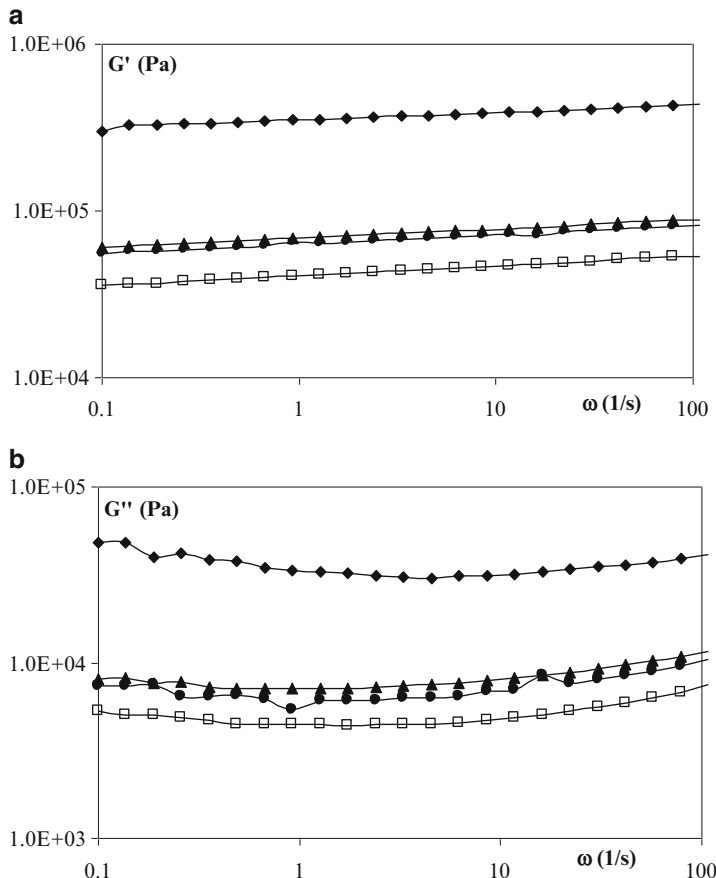


**Fig. 1** Variation of (a) storage modulus ( $G'$ ) and (b) loss modulus ( $G''$ ) with frequency for raw and treated apple tissue at a strain of 0.005 %. (Filled diamond) fresh, (open square) blanched, (filled triangle) osmotically dehydrated, (filled circle) blanched and osmotically dehydrated

with those previously reported for apple (Martínez et al. 2007), melon (Martínez et al. 2005), and Korla pear (Wu and Guo 2010).

Creep/recovery curves for fresh and treated samples are presented in Fig. 2. Creep curve parameters showed significant differences ( $p < 0.0001$ ) between fresh and treated samples and also between apples subjected to OD and heated samples (with or without OD) (Table 1). Instantaneous compliance ( $J_0$ ), retarded compliances ( $J_1, J_2$ ), and steady-state viscous compliance ( $1/\eta_N$ ) increased in different degrees for treated samples. Principal component analysis (PCA) showed the spatial relationships of creep parameters for each sample. The first two principal components described 86.8 % and 10.7 % of the variance, respectively. The first

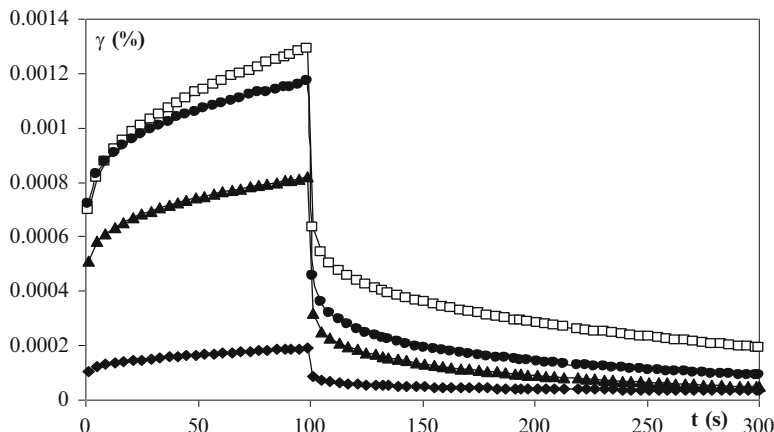


**Fig. 2** Experimental creep/recovery curves of apple tissue as affected by treatments. (Filled diamond) fresh, (open square) blanched, (filled triangle) osmotically dehydrated, (filled circle) blanched, and osmotically dehydrated

**Table 1** Viscoelastic parameters derived by fitting Eq. (1) to average compliance curves from the creep phase for fresh and treated apple tissue

Treatment	$J_0$ (1/Pa) ( $\times 10^5$ )	$J_1$ (1/Pa) ( $\times 10^5$ )	$J_2$ (1/Pa) ( $\times 10^5$ )	$\lambda_1$ (s)	$\lambda_2$ (s)	$\eta_N$ (Pa.s) ( $\times 10^{-7}$ )
C	0.34	0.11	0.083	25.45	2.16	11.2 <sup>a</sup>
B	2.1	0.73	0.42	23.81	2.7	1.38 <sup>b</sup>
OD	1.5	0.3	0.26	23.09	2.46	2.5 <sup>c</sup>
ODB	2.1	0.66	0.39	21.96	2.38	1.8 <sup>b</sup>

Treatments with same letter are not significantly different ( $p < 0.05$ )

axis was positively defined by  $J_0$ ,  $J_1$  and  $J_2$  and negatively by  $\eta_N$ , and the second axis was positively defined by retardation times ( $\lambda_1$  and  $\lambda_2$ ).

Figure 3 shows typical compression-time curves for fresh and treated apples. Significant differences ( $p < 0.0001$ ) were observed among all samples. The parameters for hardness (H), hardness 2 (H<sub>2</sub>), fracturability (F), area 1 (A<sub>1</sub>), cohesiveness (Coh), springiness (Sp), adhesiveness (Adh), gumminess (gum), chewiness (chew), and modulus of deformability ( $E_d$ ) decreased for heated samples (with or without OD) with respect to control. Hardness and fracturability slightly increased for osmotic dehydrated samples (Table 2). PCA indicated that the first two principal components explained 86.6 % and 9.8 % of the variance, respectively. The first axis was positively defined by hardness 2, area 1, springiness, cohesiveness, chewiness, and gumminess, and the second axis was positively presented by hardness and fracturability.

Sensory texture analysis (data not shown) showed significant differences in hardness ( $F_{3,12} = 5.52$ ,  $p = 0.0063$ ) between fresh and B tissues and between

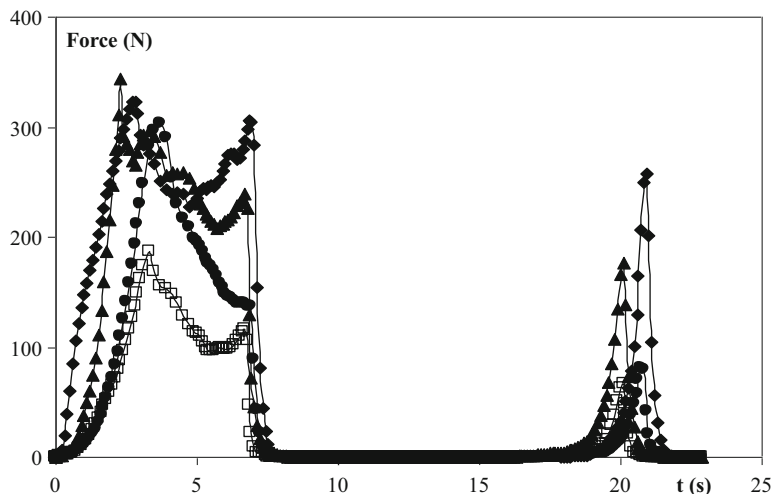


**Fig. 3** Force/time curves of raw and treated apple tissues. (Filled diamond) fresh, (open square) blanched, (filled triangle) osmotically dehydrated, (filled circle) blanched and osmotically dehydrated

**Table 2** TPA curve parameters for fresh and treated apple tissue

Treatment	F (N)	H (N)	H <sub>1</sub> (N)	A <sub>1</sub> (J)	Sp (-)	Coh (-)	Gum (N)	Chew (N)	E <sub>d</sub> (N/m <sup>2</sup> ) ( $\times 10^{-6}$ )
C	287.9	293.2	225	1.39	0.55	0.081	23.9	13.2	1.92 <sup>a</sup>
B	196.2	196.2	80.4	0.7	0.33	0.04	8	2.6	0.11 <sup>b</sup>
OD	337	337	187.4	1.31	0.53	0.064	21.3	11.4	0.17 <sup>c</sup>
ODB	0	288	92.6	0.93	0.41	0.045	12.8	5.3	0.09 <sup>d</sup>

Treatments with same letter are not significantly different ( $p < 0.05$ )

fresh and BOD tissues. Fracturability of treated samples significantly decreased ( $F_{3,24} = 52.3, p < 0.05$ ) with respect to the control. B and BOD samples slightly increased its cohesiveness during treatment, but the differences between samples were not significant ( $F_{3,15} = 1.97, p > 0.05$ ). Significant differences were observed in juiciness ( $F_{3,24} = 73.7, p < 0.05$ ) between control and treated samples, but there were no significant differences between juiciness of OD and B apples. Values for crispness significantly decreased ( $F_{3,12} = 10.9, p < 0.05$ ) in heated samples (with or without osmotic treatment). In all measurements, assessor factor was not significant, suggesting that panel performance was consistent. All assessors informed that the samples did not present adhesiveness to palate.

Optical microscopy studies were performed to evaluate structure changes produced at the cellular level by different treatments. In fresh apple, cells appeared turgid with parietal cytoplasm and darkly stained walls. In blanched tissues, disruption of membranes and slightly stained and swollen walls were observed.

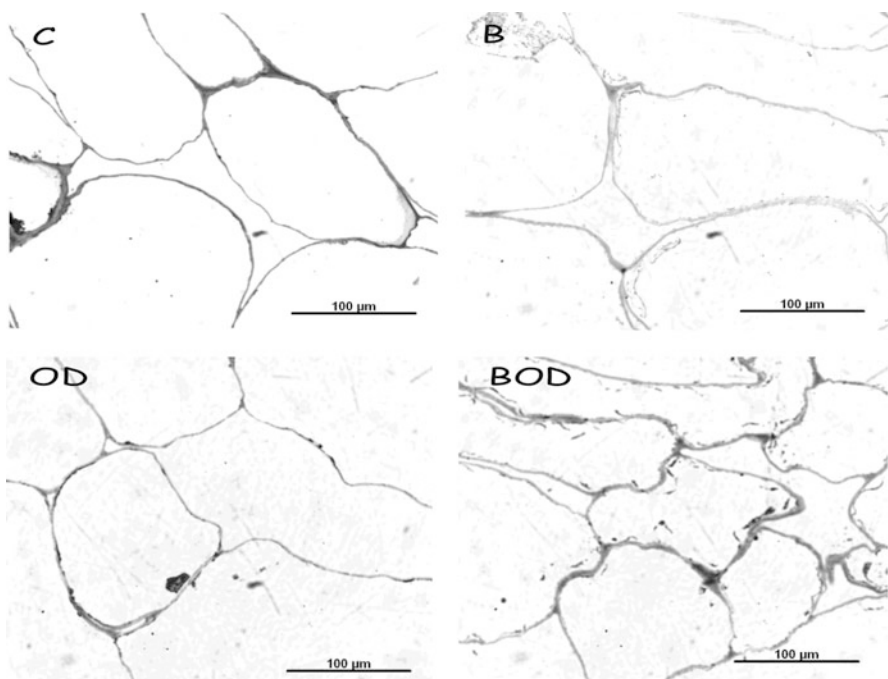


**Fig. 4** Light microscopy images from fresh and treated apple tissue. C: raw (control); B: blanched; OD: osmotically dehydrated; BOD: blanched and osmotically dehydrated

OD cell walls exhibited a slightly lower density of staining than did the control. BOD tissues showed disruption of membranes and severe folding of cell walls, probably due to the important loss of turgor. But walls appeared more stained than those of the only heated sample. Shrinkage of BOD tissue and reduction of intercellular spaces were notable (Fig. 4).

Considering structural changes, rheological properties behavior of treated tissues could be attributed to turgor loss (membrane breakage and/or plasmolysis), shrinkage of tissue or folding, and degradation of cell walls. The decrease in  $G'$  values, crispness, and instrumental and sensory fracturability of heated and/or osmosed apples could be attributed to the decrease in turgor pressure and the reduction of intercellular air spaces. In contrast, instantaneous compliance ( $J_0$ ) and retarded compliances ( $J_1$  and  $J_2$ ), instrumental and sensory hardness,  $G'$  and juiciness were most sensitive parameters to changes in cell wall structure. On the other hand, increase of  $G''$  and  $1/\eta_N$  and decrease of juiciness could be attributed in part to an increase of cell wall fluidity arising from solubilization and depolymerization of pectin and hemicelluloses as well as disruption of membranes and exosmosis.

## 4 Conclusions

Apple tissues (raw and treated) behaved predominantly as solids, but  $G'$  and  $G''$  moduli decreased because of processing. Texture parameters (hardness, fracturability, hardness 2, area 1, cohesiveness, springiness, gumminess, chewiness, and deformability modulus) decreased for heated tissues (with and without osmosis) and hardness and fracturability slightly increased in OD samples. Clear correlations could be suggested between some structural elements and sensory and rheological parameters, for instance: loss of turgor-crispness-fracturability (sensory and instrumental)- $G'$ ; cell wall degradation-hardness (sensory and instrumental)- $J_i$ ; and disruption of membranes- $G''$ -juiciness- $\eta_N$ . Blanching provoked a greater modification of structure and rheological properties than osmotic dehydration.

## References

- Bourne MC (1978) Texture profile analysis. *Food Technol* 32:62–66
- Civille GV, Szczesniak AS (1973) Guidelines to training a texture profile panel. *J Texture Stud* 4:204–223
- D'Ambrogio de Argüeso A (1986) Manual de Técnicas en Histología Vegetal. Hemisferio Sur, Buenos Aires
- Martínez VY, Nieto AB, Viollaz PE, Alzamora SM (2005) Viscoelastic behaviour of melon tissue as influenced by blanching and osmotic dehydration. *J Food Sci* 70:12–18
- Martínez VY, Nieto AB, Castro MA, Alzamora SM (2007) Viscoelastic characteristics of Granny Smith apple during glucose osmotic dehydration. *J Food Eng* 83:394–403
- Sherman P (1970) Industrial rheology. Academic, New York
- Wu J, Guo KG (2010) Dynamic viscoelastic behavior and microstructural changes of Korla pear (*Pyrus bretschneideri rehd*) under varying turgor levels. *Biosystem Eng* 106:485–492

# Water Activity Depression of Tejocote Fruit (*Crataegus pubescens*) Using Osmotic Solutions and Pressure Gradients

A. Valdez-Fragoso, J. Welti-Chanes, and H. Mújica-Paz

## Abbreviations

$a_w$	Water activity
IS	Isotonic solution
OS	Sucrose solution concentration
$p_v$	Vacuum pulse
$t$	Processing time
$t_v$	Vacuum pulse duration
$V_o$	Initial volume of the sample
$W_f$	Tejocote weight after impregnation
$W_o$	Tejocote weight before impregnation
$X$	Impregnated volume fraction
$\epsilon_r$	Real porosity
$\rho_a$	Apparent density of tejocote
$\rho_{IS}$	Density of the impregnation IS

## 1 Introduction

Tejocote (*Crataegus pubescens*) is a fruit that has been used in México since pre-Hispanic times (Núñez-Colín et al. 2008; Franco-Mora et al. 2010). It is commonly preserved by cooking in hypertonic sucrose solutions and then packing

---

A. Valdez-Fragoso • J. Welti-Chanes • H. Mújica-Paz (✉)  
Escuela de Ingeniería y Ciencias, Tecnológico de Monterrey, Av. Eugenio  
Garza Sada 2501 Sur, Col. Tecnológico, Monterrey, Nuevo León 64849, México  
e-mail: [a.valdez@itesm.mx](mailto:a.valdez@itesm.mx); [jwelti@itesm.mx](mailto:jwelti@itesm.mx); [h.mujica@itesm.mx](mailto:h.mujica@itesm.mx)

in hot sterilized jars. Thermal treatment also involves osmotic dehydration and solutes impregnation phenomena of the fruit. The overall effect of this mass transfer leads to  $a_w$  reduction of the product, which may contribute to its stability. In addition to inactivation of enzymes and deteriorative microorganisms, thermal treatment accelerates dehydration-impregnation of the product.

The mass transfer phenomena can also be accelerated by using a pressure gradient at ambient temperature, in addition to the concentration gradient (Tortoe 2010). Under these conditions, a minimally processed product can be obtained, while at the same time reducing undesirable quality changes of the product caused by high temperatures. The feasibility of pressure gradient application depends partially on the natural porous properties of the material and impregnation conditions (Zhao and Xie 2004). Two important porous properties are volume fraction of the sample occupied by the impregnating solution as a result of pressure changes ( $X$ ,  $\text{cm}^3 \text{ isotonic solution}/\text{cm}^3 \text{ sample}$ ) and real porosity ( $\varepsilon_r$ ), defined as the ratio of volume of voids in the sample to bulk volume of the material ( $\text{cm}^3 \text{ void}/\text{cm}^3 \text{ sample}$ ) (Gras et al. 2002; Zhao and Xie 2004).

Stabilization of tejocote by minimal processing has not been studied; therefore, the objectives of this work were to determine the best impregnation conditions of tejocote fruit using pressure gradients and to determine the effect of the osmotic solution and processing time on water activity ( $a_w$ ) of tejocote at ambient temperature, assisted by an initial pressure gradient.

## 2 Methodology

### 2.1 Raw Material and Sucrose Solutions

Fresh tejocotes (*Crataegus pubescens*) were supplied by producers of San Juan Tetla, Pue., México. Osmotic and isotonic solutions were prepared by dissolving sucrose food grade in distilled water.

### 2.2 Impregnation Treatment

Whole and peeled tejocotes were immersed in a sucrose isotonic solution (IS) ( $a_w = 0.982$ ) and subjected to pressure gradients by consecutive periods of vacuum and atmospheric pressure application (Table 1). Based on experimental data, the impregnated volume fraction ( $X$ ) and the real porosity ( $\varepsilon_r$ ) were calculated:

$$X = \frac{W_f - W_o}{\rho_{IS} V_o} \quad (1)$$

**Table 1** Variables and levels of the experimental design for impregnation of tejocote

Variables	Levels				
$t_v$ (min)	3	14	31	48	60
$t_r$ (min)	3	27	61	96	120
$p_v$ (cmHg)	15	22	32	43	50

**Table 2** Variables and levels of the experimental design for dehydration-impregnation of tejocote

Variables	Levels		
[Sucrose], (Brix)	30	40	50
$t_p$ (min)	0.5	2.75	5

$$\varepsilon_r = \frac{\rho_r - \rho_a}{\rho_a} \quad (2)$$

where  $W_o$  and  $W_f$  are tejocote weight before and after impregnation, respectively,  $V_o$  is the initial volume of the sample,  $\rho_{IS}$  is the density of the impregnation IS,  $\varepsilon_r$  is the real density of the tejocote puree, and  $\rho_a$  is the apparent density of tejocote (Mújica-Paz et al. 2003a,b; Zhao and Xie 2004).

### 2.3 Dehydration-Impregnation Treatments

Manually peeled tejocotes were immersed in sucrose solutions and subjected to dehydration-impregnation for 0.5–5 days (Table 1) in a tejocote/solution ratio of 1–5 (w:w). An initial pressure gradient was established by a short vacuum pulse ( $p_v = 50$  cmHg,  $t_v = 3$  min) after immersion of tejocotes.

Soluble solids, pH, and  $a_w$  of the treated samples were determined with a refractometer (Atago, Japan), a pH meter (Orion, USA), and a LabMaster- $a_w$  instrument (Novasina, Switzerland), respectively. Fresh fruit was characterized for acidity and moisture according to AOAC methods (1990).

### 2.4 Statistical Analysis

Experimental impregnation and impregnation-dehydration variables were studied using a central composite (Table 1) and a Box-Behnken design (Table 2), respectively (Montgomery 2001), and Design-Expert software v.7.1.5.

## 3 Results and Discussion

Table 3 shows the obtained physicochemical characteristics of fresh tejocote samples. The high value of  $a_w$  ( $0.982 \pm 0.002$ ) indicates that tejocote is very sensitive to deteriorative reactions (Leistner 1995).

**Table 3** Characteristics of fresh tejocote

Moisture (%)	78.26 ± 0.12
Titratable acidity (%)	2.30 ± 0.07
Soluble solids (°Brix)	9.20 ± 0.01
pH	3.63 ± 0.01
$a_w$	0.982 ± 0.002

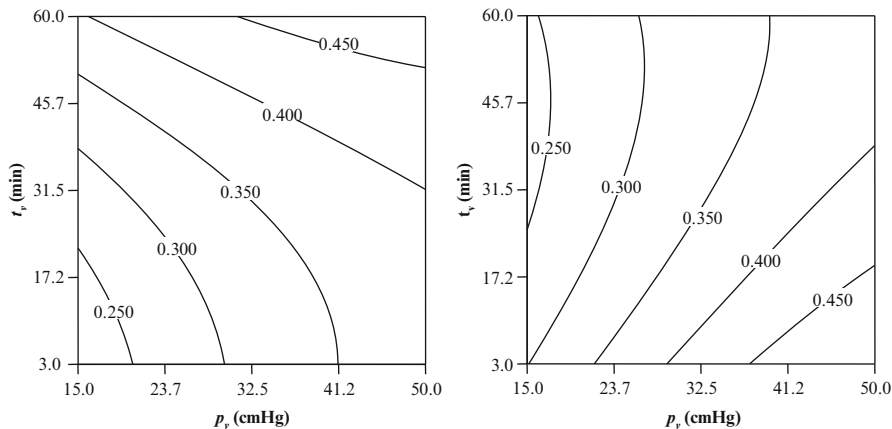


**Fig. 1** Effect of vacuum pressure and application time on the impregnated volume fraction of tejocote, at 3 and 120 min of relaxation

### 3.1 Impregnation Treatment

Real porosity of tejocote was 0.53; according to this fraction of total voids in tejocote, it is more porous than other whole products such as prickly pear (0.013), quince (0.142), red jalapeño pepper (0.120), and apple (0.273) (Valdez-Fragoso et al. 2007).

Significant polynomial ( $p < 0.05$ ) with  $R^2 = 0.805$  and no significant lack of fit was found to predict  $X$  in the experimental studied domain. The factors  $p_v$  and the interaction  $t_v-t_r$  showed significant effect on  $X$  levels. Nearly 45 % of the porous structure of tejocote can be occupied by external sucrose IS (Fig. 1), and due to the  $t_v-t_r$  interaction effect, this impregnation level can be attained at two combinations of independent factors:  $p_v = 50 \text{ cmHg}$ ,  $t_v = 60 \text{ min}$  y  $t_r = 3 \text{ min}$  or  $p_v = 50 \text{ cmHg}$ ,  $t_v = 3 \text{ min}$  y  $t_r = 120 \text{ min}$ .

Operating conditions  $p_v = 50 \text{ cmHg}$  and  $t_v = 3 \text{ min}$  were chosen to create a pressure gradient at the beginning of the impregnation-dehydration treatment of tejocote.

### 3.2 Dehydration-Impregnation Treatments

Experimental values of  $a_w$  obtained at different combinations of osmotic solution concentration and processing time are given in Table 4.

**Table 4** Water activity of tejocote treated by vacuum dehydration-impregnation in sucrose solutions

Treatment	[S] (%)	$t_r$ (days)	$a_w$
1	30	2.75	$0.952 \pm 0.005$
2	40	0.50	$0.949 \pm 0.004$
3	40	2.75	$0.938 \pm 0.003$
4	40	2.75	$0.945 \pm 0.004$
5	50	2.75	$0.933 \pm 0.001$
6	40	2.75	$0.940 \pm 0.003$
7	40	5.00	$0.944 \pm 0.002$
8	50	5.00	$0.936 \pm 0.004$
9	50	0.5	$0.936 \pm 0.002$
10	40	2.75	$0.945 \pm 0.004$
11	30	5.00	$0.955 \pm 0.003$
12	30	0.5	$0.961 \pm 0.001$
13	40	2.75	$0.945 \pm 0.004$

[S] sucrose concentration,  $t_r$  processing time; osmotic treatments with an initial vacuum pulse of 50 cmHg ( $p_v$ ) for 3 min ( $t_v$ )

Statistical analysis of  $a_w$  results allowed development of a significant model ( $p < 0.01$ ) with  $R^2 = 0.906$  and no significant lack of fit ( $F = 0.73$ ) to predict  $a_w$  of osmodehydrated tejocote as a function of the sucrose solution concentration [OS] (°Brix) and processing time  $t$  (h):

$$a_w = 0.986 - 1.044 \times 10^{-3}[S] - 1.481 \times 10^{-3}t - 7 \times 10^{-5}[S]t + 2.207 \\ \times 10^{-6}[S]^2 + 8.041 \times 10^{-4}t^2 \quad (3)$$

A quadratic effect of processing time ( $p < 0.1$ ) was obtained on  $a_w$  of osmodehydrated tejocote, while syrup concentration had a linear effect ( $p < 0.01$ ) (Eq. 3). The predicted  $a_w$  depression varied from 0.932 to 0.960. The former  $a_w$  value was achieved after nearly 3 days of processing in the OS of 50°Brix at ambient temperature (Fig. 2).

These results indicate that it is possible to obtain minimally processed tejocote by impregnation-dehydration treatment driven by concentration and pressure gradients. The  $a_w$  of peeled tejocote could be reduced to levels that might enhance its stability (Leistner 1995).

## 4 Conclusions

- Processing time and OS concentration significantly affected  $a_w$  of tejocote.
- Osmotic dehydration with a vacuum pulse, at ambient temperature, allowed the reduction of  $a_w$  of tejocote.
- Attained  $a_w$  levels of tejocote could enhance its stability.

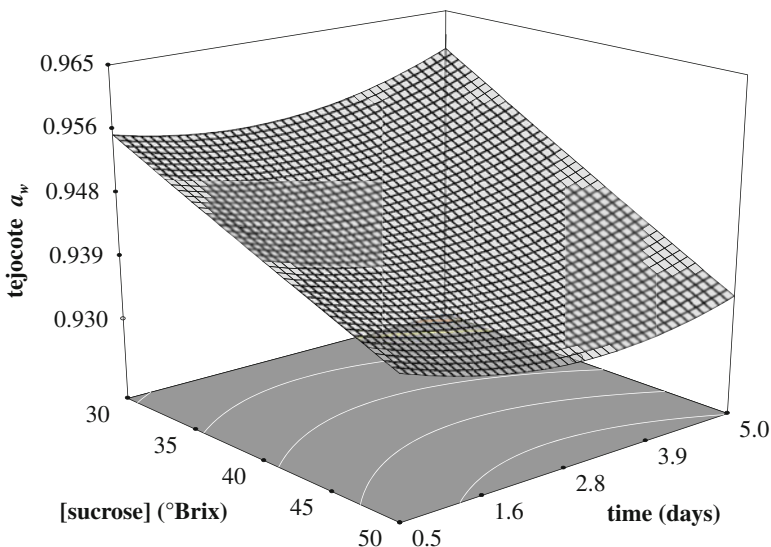


**Fig. 2** Effect of OS concentration and processing time on the  $a_w$  of tejocote

**Acknowledgments** The authors gratefully acknowledge support from Tecnológico de Monterrey (Research Chair Funds CAT-200) and tejocote producers of Sn Juan Tetla, Puebla, México.

## References

- AOAC (1990) Official methods of analysis of the Association of Official Analytical Chemists, 15th edn. AOAC International, Washington, DC
- Franco-Mora O, Aguirre-Ortega S, Morales-Rosales EJ, González-Huerta A, Gutiérrez-Rodríguez F (2010) Caracterización morfológica y bioquímica de frutos de tejocote (*Crataegus mexicana* DC), de Lerma y Ocoyoacac, Méx. Ciencia ergo Sum 17-1, 61-66. UAEM
- Gras M, Vidal-Brotóns D, Betoret N, Chiralt A, Fito P (2002) The response of some vegetables to vacuum impregnation. Innov Food Sci Emerg Technol 3:263–269
- Leistner L (1995) Use of hurdle technology in food processing: recent advances. In: Barbosa-Cánovas GV, Welti-Chanes J (eds) Food preservation by moisture control fundamentals and applications. Technomic Co., Lancaster, PA, USA, pp 377–392
- Montgomery DC (2001) Design and analysis of experiments, 5th edn. Wiley, New York, pp 170–210
- Mújica-Paz H, Valdez-Fragoso A, López-Malo A, Palou E, Welti-Chanes J (2003a) Impregnation and osmotic dehydration of some fruits: effect of the vacuum pressure and syrup concentration. J Food Eng 57:305–314
- Mújica-Paz H, Valdez-Fragoso A, López-Malo A, Palou E, Welti-Chanes J (2003b) Impregnation properties of some fruits at vacuum pressure. J Food Eng 56:307–314
- Núñez-Colín CA, Nieto-Ángel R, Barrientos-Priego AF, Sahagún-Castellanos J, Segura S, González-Andrés F (2008) Variability of three regional sources of germplasm of Tejocote (*Crataegus* spp.) from central and southern Mexico. Genet Resour Crop Evol 55:1159–1165
- Tortoe C (2010) A review of osmodehydration for food industry. Afr J Food Sci 4(6):303–324

- Valdez-Fragoso A, Soto-Caballero MC, Batista Ochoa MA, Loya-Gallardo AB, Welti-Chanes J, Mujica-Paz H (2007) Impregnation properties of prickly pear, quince and red jalapeño pepper. A response surface methodology study. In: Proceedings of the 3rd CIGR section VI international symposium on food and agricultural products: processing and innovations, Italy
- Zhao Y, Xie J (2004) Practical applications of vacuum impregnation in fruit and vegetable processing. Trends Food Sci Technol 15:431–451

# Prediction Approach to the Glass Transition Temperature of Amorphous Carbohydrate Polymer

K. Kawai, K. Fukami, P. Thanatukson, C. Viriyarattanasak,  
and K. Kajiwara

## Abbreviations

A	Constant (g/mol)
DP	Degree of polymerization
DSC	Differential scanning calorimetry
$k$	Constant reflecting the sensitivity to the water plasticizing effect
MW	Molecular weight
RH	Relative humidity
$T_g$	Glass transition temperature
$T_{g1}$	Glass transition of the anhydrous inulin
$T_{g2}$	Glass transition of water
$W_1$	Mass fraction of inulin
$W_2$	Mass fraction of water

---

K. Kawai (✉)

Department of Biofunctional Science and Technology, Graduate School of Biosphere Science, Hiroshima University, 1-4-4 Kagamiyama, Higashi-Hiroshima, Hiroshima 739-8528, Japan  
e-mail: [kawai@hiroshima-u.ac.jp](mailto:kawai@hiroshima-u.ac.jp)

K. Fukami

San-ei Sucrochemical Co., Ltd., 24-5 Kitahama-cho, Chita, Aichi 478-8503, Japan

P. Thanatukson • C. Viriyarattanasak • K. Kajiwara

School of Bioscience and Biotechnology, Tokyo University of Technology, 1404-1 Katakura, Hachioji, Tokyo 192-0982, Japan

## 1 Introduction

Most of carbohydrate polymers exist, at least partially, in an amorphous state, and thus, glass transition occurs during dehydration/rehydration and cooling/heating processing. Since various physical properties are changed drastically by the glass transition (Levine and Slade 1988; Roos 1995; Le Meste et al. 2002), it is important to understand the glass transition temperature ( $T_g$ ).

Inulin is a natural carbohydrate polymer that is linked by  $\beta(2\text{-}1)$  glycosidic bonds and contains either a terminal  $\beta\text{-D-fructose}$  or an  $\alpha\text{-D-glucose}$ . Chicory root, asparagus, and onions contain a large amount of inulin. The degree of polymerization (DP) of inulin is usually 2–60 units with an average DP = 12. Inulin has attracted much attention in the food and pharmaceutical industries for its multiple benefits, such as dietary fiber, prebiotic nature, and fat-mimetic material. Although there have been many efforts to understand the glass transition properties of amorphous inulin, the published data were limited for prediction of  $T_g$  (Hinrichs et al. 2001; Zimeri and Kokini 2002; Ronkart et al. 2009). In this study, the  $T_g$  of various types of amorphous inulin was investigated using differential scanning calorimetry (DSC), and an empirical  $T_g$  prediction of inulin was proposed.

## 2 Materials and Methods

### 2.1 Sample Preparation

Three types of inulin reagent, low molecular weight (low-MW), native, and high molecular weight (high-MW), were provided from San-ei Sucrochemical, Co., Ltd., Aichi, Japan. The average molecular weight of low-MW, native, and high-MW inulin samples was 1,197, 2,175, and 4,395 g/mol (DP = 7, 13, and 27), respectively. Since the high-MW reagent was preliminarily confirmed to be semi-crystal state by X-ray diffraction, amorphous reagent was prepared by thermal hydrolysis treatment (Zimeri and Kokini 2002; Ronkart et al. 2009). The fully dried reagents were held under various relative humidity (RH) conditions at 25 °C, and samples with varying of water content were prepared.

### 2.2 DSC

The  $T_g$  of the inulin samples was investigated using a DSC (DSC8230; Rigaku Co., Tokyo, Japan). The sample (2–10 mg) was placed in an aluminum pan and hermetically sealed. In order to evaluate anhydrous inulin  $T_g$ , inulin that had been vacuum-dried at 60 °C for 12 h was put into the pan and held at 105 °C for 2 h prior to sealing. DSC measurement was performed at 5 °C/min in the temperature range

of 0 and 180 °C. In order to cancel the effect of the thermal history on  $T_g$ , the samples were re-scanned after cooling, and  $T_g$  was evaluated from the onset point of an endothermic shift observed in the second scanning. All the tests were performed in duplicate and the results were averaged.

### 2.3 Water Content

Water content of the samples was investigated gravimetrically by drying at 105 °C for 18 h. All the tests were performed in triplicate and the results were averaged.

## 3 Results and Discussion

Typical DSC thermograms for the native inulin samples are shown in Fig. 1. The DSC thermograms showed an endothermic shift due to glass transition, and  $T_g$  value was evaluated from the onset point of the shift. It was noted that the  $T_g$  decreased with an increase in the RH of sample. Water content of the samples was evaluated gravimetrically, and the  $T_g$  was plotted against water content in Fig. 2. It was confirmed that the  $T_g$  decreased with an increase in water content because of water plasticizing. In order to understand the plasticizing effect, the data was fitted by the Gordon-Taylor equation (Eq. 1):

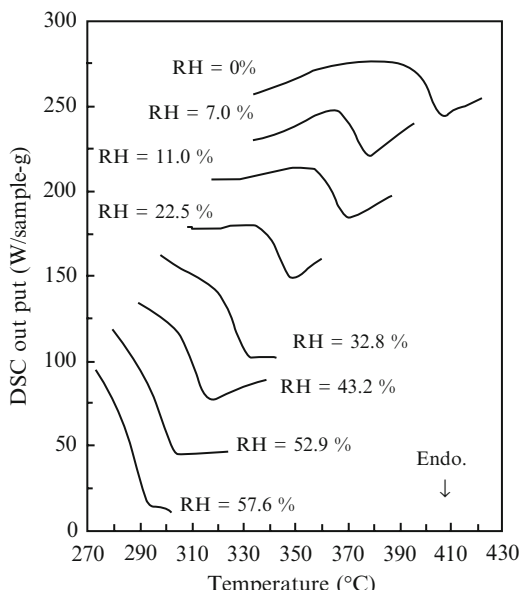
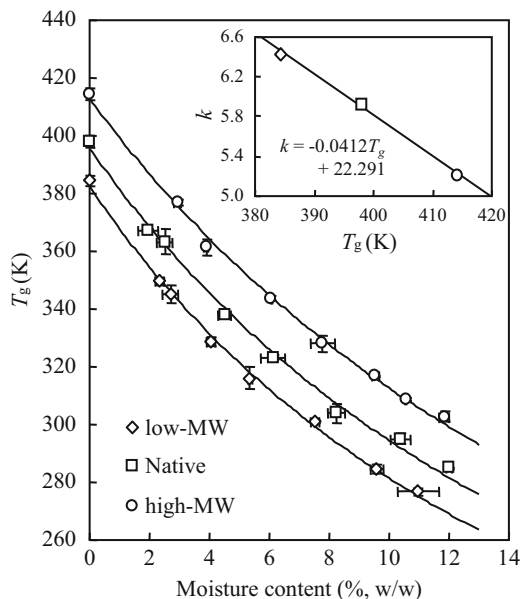


**Fig. 1** Typical DSC thermograms for the native inulin samples

**Fig. 2** Effect of moisture content on  $T_g$  of inulin sample. The solid lines were obtained by fitting Eq. (2) to the data. The inset figure shows a relationship between  $k$  and  $T_g$

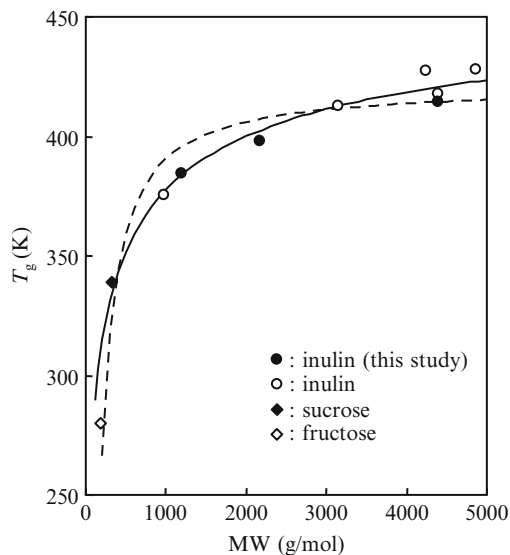


$$T_g = \frac{W_1 T_{g1} + kW_2 T_{g2}}{W_1 + kW_2} \quad (1)$$

where  $T_{g1}$  and  $T_{g2}$  are  $T_g$  of the anhydrous inulin and water,  $W_1$  and  $W_2$  are the mass fraction of inulin and water, and  $k$  is a constant reflecting the sensitivity to the water plasticizing effect. The  $T_{g2}$  was obtained as 136 K from a previous publication (Johari et al. 1987), and  $k$  was obtained as a fitted parameter. A relationship between the obtained  $k$  value and  $T_g$  of anhydrous inulin is shown in the inserted figure. In previous studies, it was reported that the  $k$  value of mono- and disaccharides increases linearly with an increase in  $T_g$  (Roos 1995; Crowe et al. 1996). However,  $k$  of three amorphous inulin samples decreased linearly with increases in  $T_g$  ( $R^2 = 0.9976$ ). Polysaccharides have generally a higher  $T_g$  and lower  $k$  than those of disaccharides, and thus the relationship between  $k$  and  $T_g$  will differ between mono- and disaccharides and oligo- and polysaccharides (Roos 1995). The empirical relationship shown in the inserted figure remains an outstanding theoretical problem but will be of practical use in the prediction of the effect of water content on amorphous inulin  $T_g$ .

The  $T_g$  increased with an increase in the MW of inulin. In order to understand the effect of MW on the  $T_g$ , the  $T_g$  of anhydrous amorphous inulin including previous results (Hinrichs et al. 2001; Ronkart et al. 2009) was plotted against MW (Fig. 3). For comparison, the  $T_g$  values of anhydrous fructose and sucrose (Levine and Slade 1988; Orford et al. 1989; Kawai et al. 2005) were also shown there. It is well known that the effect of MW on  $T_g$  of amorphous polymer can be described by Fox-Flory equation (Eq. 2):

**Fig. 3** Effect of MW on  $T_g$  of inulin. The *dotted* and *solid curves* were obtained by fitting Eqs. (2) and (3) to the data, respectively



$$T_g = T_{g\infty} - \frac{B}{\text{MW}} \quad (2)$$

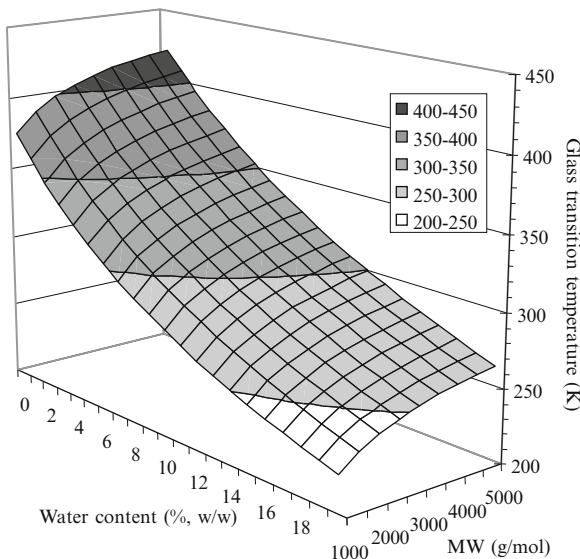
where  $T_{g\infty}$  and  $B$  are maximum anhydrous  $T_g$  and constant, respectively. From the fitting result,  $T_{g\infty}$  and  $B$  were determined to be 421.54 and 31,016, respectively. The obtained curve ( $R^2=0.93413$ ), however, did not appear to be reasonably consistent with the data. As the other approach, a stretched exponential function (Eq. 3) could be employed:

$$1 - \frac{T_g}{T_{g\infty}} = \exp\left(-\left(\frac{A}{\text{MW}}\right)^n\right) \quad (3)$$

where  $T_{g\infty}$  is a maximum anhydrous  $T_g$  (K),  $A$  (g/mol) is a constant, and  $n$  is a non-exponential parameter changing between 0 to 1. From the fitting result,  $T_{g\infty}$ ,  $A$ , and  $n$  were determined to be 455.99, 106.72, and 0.25278, respectively. In addition, the obtained curve ( $R^2=0.98829$ ) could describe the  $T_g$  data better than Eq. (2).

From these results, the effects of moisture content and MW on  $T_g$  of amorphous inulin could be described as shown in Fig. 4. The MW and moisture content of amorphous inulin will be affected by its growing and producing conditions, and thus, it is important practically to predict the  $T_g$ . The result shown in Fig. 4 will be useful in predicting the  $T_g$  of amorphous inulin.

**Fig. 4** The  $T_g$  value of amorphous inulin predicted by Eqs. (1) and (3)



**Acknowledgments** This work was supported by Japan Society for the Promotion of Science (grant-in-aid for young scientists (B); 21780126).

## References

- Crowe LM, Reid DS, Crowe JH (1996) Is trehalose special for preserving dry biomaterials? *Biophys J* 71:2087
- Hinrichs WLJ, Prinsen MG, Frijlink HW (2001) Inulin glasses for the stabilization of therapeutic proteins. *Int J Pharm* 215:163
- Johari GP, Hallbrucker A, Mayer E (1987) The glass–liquid transition of hyperquenched water. *Nature* 330:552
- Kawai K, Hagiwara T, Takai R, Suzuki T (2005) Comparative investigation by two analytical approaches of enthalpy relaxation for glassy glucose, sucrose, maltose, and trehalose. *Pharm Res* 22:490
- Le Meste M, Champion D, Roudaut G, Blond G, Simatos D (2002) Glass transition and food technology: a critical appraisal. *J Food Sci* 67:2444
- Levine H, Slade L (1988) Principles of “cryostabilization” technology from structure/property relationships of carbohydrate/water systems—a review. *Cryo-Letters* 9:21
- Orford PD, Parker R, Ring SG, Smith AC (1989) Effect of water as a diluent on the glass transition behaviour of malto-oligosaccharides, amylase and amylopectin. *Int J Biol Macromol* 11:91
- Ronkart SN, Paquot M, Fougnies C, Deroanne C, Blecker CS (2009) Effect of water uptake on amorphous inulin properties. *Food Hydrocoll* 23:922
- Roos YH (1995) Phase transitions in foods. Academic, London, pp 109–156
- Zimeri JE, Kokini JL (2002) The effect of moisture contention the crystallinity and glass transition temperature of inulin. *Carbohydr Polym* 48:299

# Effect of Sugars on the Release of Aroma Compounds in Model Systems

P. Pittia, P. Piccone, and M. Martuscelli

## Abbreviations

$A_{\text{H}_2\text{O}}$	Peak area of the volatile in water
$A_{\text{sol}}$	Peak area of the same volatile in the sugar solution
EA	Ethyl acetate
EB	Ethyl butyrate
EH	Ethyl hexanoate
FID	Flame ionization detector
GC analysis	Gas chromatographic analysis
HS-GC	Headspace gas chromatography
IA	Isopentyl acetate
$k$	Liquid–vapor partition coefficients
$R$	Retention index
$R_{\text{app}}^i$	Initial apparent rate of release

## 1 Introduction

Kinetic and thermodynamic mechanisms control the rate of release and the concentration of volatiles in the vapor phase in equilibrium with a food. Chemical nature of the aroma compounds, composition, and structure of foods are main characteristics that influence the transfer of aroma compounds within the foods and their release (Seuvre et al. 2006; Cayot et al. 2008). Besides the intrinsic

---

P. Pittia (✉) • P. Piccone • M. Martuscelli

Faculty of Bioscience and Technology for Food, Agriculture and Environment,  
University of Teramo, Via C.R. Lerici 1, Mosciano S. Angelo, 64023 Teramo, Italy  
e-mail: [ppittia@unite.it](mailto:ppittia@unite.it)

characteristics of aroma and food matrix and the environmental factors, interactions occurring between volatile and nonvolatile compounds (in particular those with food macromolecules like proteins, hydrocolloids, and carbohydrates) are major factors that limit the release of volatiles, and thus their perception, as demonstrated by many studies in this field.

In the case of carbohydrates, interactions with aroma compounds in general demonstrate weak energy, depending on various factors such as the nature and concentration of both aroma and carbohydrates that, in turn, affect both the kinetics and the concentration in the vapor phase in equilibrium above the matrix. While complex saccharides (e.g., starch) have been widely investigated for their role in affecting the release–retention of volatiles in food matrices, scarce attention has been given to mono- and disaccharides. In simple model systems, some studies (Roberts et al. 1996; Nahon et al. 2000) demonstrated that the latter solutes can induce an increase of release for some aroma compounds, especially those that are more polar, while an opposite effect was observed for those that are more nonpolar. In sucrose solutions at 65 % (w/v), Friel et al. (2000) found evidence of volatiles that showed a “salting out” effect (linalool) and others that showed a “salting in” effect (ethyl decanoate), while others remained not influenced by the solute (acetaldehyde).

Physical (e.g., viscosity) and physicochemical properties (e.g., water activity) of the matrix have been recognized as factors that could affect the liquid–vapor partition and the kinetics of the release of aroma compounds, but these factors have been studied only to a limited extent. This study was thus aimed to investigate the release of volatiles having different hydrophilicities (ethyl acetate, ethyl butyrate, isopentyl acetate, ethyl hexanoate) from solutions made of either saccharides (glucose, sucrose, trehalose) or sorbitol, at different solute concentrations as well as the related kinetics.

## 2 Materials and Methods

### 2.1 Model Systems

The release and release rate of four volatile esters (ethyl acetate (EA), ethyl butyrate (EB), isopentyl acetate (IA), and ethyl hexanoate (EH)) (Table 1) were investigated in aqueous binary (water–saccharide) solutions individually prepared with glucose, sucrose, trehalose, and sorbitol at solute concentration in the range 0–40 % w/v (glucose and sorbitol) or 45 % w/v (sucrose and trehalose). A mixture of volatiles was added in the sugar solution to make up a final concentration in the solution of 0.1 % v/v for EA, EB, and IA and of 0.05 % for EH.

**Table 1** Physicochemical characteristics of flavor compounds

Aroma compound	Saturated vapor pressure ( $P_s^*$ ) (MPa, 25 °C)	Water solubility (in H <sub>2</sub> O 25 °C, g/l)	$\log P$ (octanol/water)	$T_{\text{boil}}$ (°C)
Ethyl acetate (EA)	12.236	75	0.73	72
Ethyl butyrate (EB)	1.596	5.6	1.80	120
Ethyl hexanoate (EH)	0.585	2.0	2.13	108
Isopentyl acetate (IA)	0.133	0.52	2.80	142

## 2.2 Headspace Analysis

For analysis purposes, 2 mL of the aroma–sugar solution was immediately placed in 10 mL vials and immediately with a Teflon cap and a metallic ring.

For evaluation of the release of aroma under equilibrium conditions, gas chromatographic (GC) analyses of the headspace (HS-GC) were performed after equilibration of at least 3 h after closure; this equilibration time was defined by preliminary experiments (data not shown).

Release–retention of volatiles in the sugar solutions was evaluated by a retention index,  $R$  (%), computed according to the following equation:

$$R(\%) = \left[ \frac{(A_{\text{H}_2\text{O}} - A_{\text{sol}})}{A_{\text{H}_2\text{O}}} \right] \times 100 \quad (1)$$

where  $A_{\text{H}_2\text{O}}$  = peak area of the volatile in water and  $A_{\text{sol}}$  is the peak area of the same volatile in the sugar solution.

Kinetic curves of the release of volatiles from sucrose and trehalose solutions were obtained by analyzing the vapor phase of samples under static conditions at different times after closure (0.5, 1, 3, 5, 10, 20, 30, 60 min). Only one sample of the gas phase was obtained per vial, fitting the peak area of each aroma during time.

GC data were converted in partial pressure values according to Pittia et al. (2006). Initial apparent rate of release,  $R^{app}_i$  (min<sup>-1</sup>), of each aroma compound was computed in agreement with the experimental approach of Seuvre et al. (2007), taking into account the first two experimental data points corresponding to 0.5, and 1 min.  $R^{app}_i$  was computed for each volatile compound by using three repetitions for each sampling point.

### 2.3 Gas Chromatographic Analysis

Analyses were carried out using a PerkinElmer (mod. AutoSystem XL, Boston, MA, USA) gas chromatograph connected with a flame ionization detector (FID) detector and equipped with a capillary column Megawax (PerkinElmer, Boston, MA, USA; inner dia., 250 µm; length, 25 m; particle size, 0.1–0.15 µm). Operating conditions were as follows: gas carrier H<sub>2</sub> at a pressure of 14 bar; injection temperature, 200 °C; and FID temperature, 200 °C; temperature of the column was kept at 40 °C for 2 min, followed by an increase of 5 °C/min until a final temperature of 55 °C was reached. Identification of compounds was carried out by comparison with standards. Measurements were done in triplicate.

### 2.4 Water Activity

Water activity was measured at 25 °C using an AquaLab CX 2 dew point hygrometer (Aqualab Scientific Pty Ltd., Castle Hill, NSW).

### 2.5 Viscosity

Viscosity was measured at 25 °C using a Haake (Karlsruhe, Germany) thermo-type C falling ball viscometer; dynamic viscosity was computed as described in Neri et al. (2010).

## 3 Results and Discussion

At increasing sweetener concentration, a decrease of water activity and an increase in viscosity of solutions occurred. As expected, at similar concentration, glucose and sorbitol showed higher water binding ability than disaccharides, while a lower increase in viscosity was observed at increasing solute concentration (data not shown).

In Fig. 1, the R (%) of the four volatile compounds in the solutions prepared with different sugars at different concentrations as a function of correspondent  $a_w$  is reported. For the sake of clarity, a positive  $R$  value is an index of retention with respect to water; on the contrary, a negative  $R$  value is an index of water release.

It is clearly evident that, in general, at increasing sugar concentration (i.e.,  $a_w$  decrease), a progressively enhanced release of volatiles was noticed, depending on the sugar type, concentration, and polarity of the volatile compound. In solutions at similar  $a_w$  value, release of volatiles was thus affected mainly by polarity and

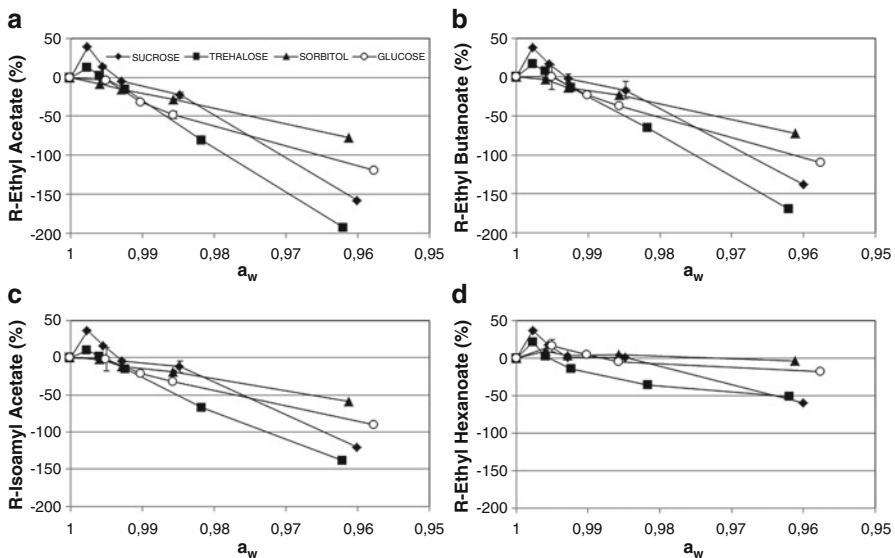


**Fig. 1** Retention index  $R$  (%) of the volatile compounds in sweetener solutions as a function of  $a_w$  values of sugar solutions (concentration 0–45 % p/v). (a) EA, (b) EB, (c) IA, (d) EH

volatility of volatile compounds being more marked for the more polar EA than for EH (Fig. 2). On the other hand, at the same  $a_w$  value, sorbitol resulted in solute with less effect on the release of all aroma compounds.

The effect of  $a_w$  on aroma release is in agreement with previous studies that indicate that a decrease of volume of nonassociated water at increasing solute concentration enhances partition in the vapor phase (Rabe et al. 2003). However, results obtained in these experiments provide evidence that the water state and the physicochemical parameter  $a_w$  cannot simply be considered as a good index to explain the so called “salting out” effect in flavor release due to an increase of a water binding solute.

To further investigate these results, liquid–vapor partition coefficients ( $k$ ) of the four volatile compounds in sucrose and trehalose solutions at increasing solute concentration were obtained, and an increase of  $k$  for EH and IA at increasing sugar concentration was observed; however, in solutions at sucrose concentration >45 % w/v, a significant decrease of  $k$  occurred for EH, suggesting that changes in physicochemical properties other than water–solute interactions in the solution occurred which also affected the release–retention of more hydrophobic volatiles.

Experimental conditions allowed the study of the release rate of aroma compounds from disaccharide solutions resulting from diffusion phenomena through the matrices and transfer of aroma compounds toward the vapor phase and diffusion in the vapor phase. The initial apparent rate of release  $R^{app}_i$  ( $\text{min}^{-1}$ ) of the four aroma compounds from water and sucrose and trehalose solutions at increasing concentrations was then computed.

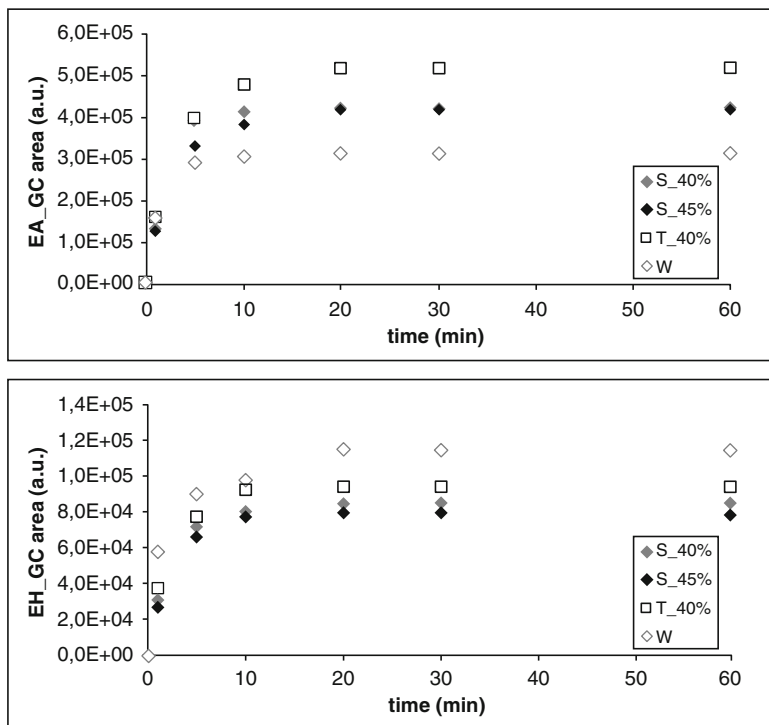


**Fig. 2** Release of ethyl acetate (**a**) and ethyl hexanoate (**b**) as a function of time in water and in sucrose (40 and 45 %) and trehalose (40 %) solution. *W* water, *S\_40%* sucrose 40 %, *S\_45%* sucrose 45 %, *T\_40%* trehalose 40 %, *T\_45%* trehalose 45 %

From water (Table 1), the quantity of released flavor compounds, based on partial pressures of the esters in the headspace, followed the volatility of the volatiles, with the exception of EH, which was added in the flavored solution in a lower concentration to avoid solubility constraints in the higher concentrated sugar solutions. The initial apparent rate of release  $R^{app}_i$  ( $\text{min}^{-1}$ ) of flavor compounds in water and solutions of sucrose and trehalose at different solute concentrations, as well as the ratio  $R^{app}_i$  in solution/ $R^{app}_i$  in water, is reported in Tables 2 and 3, respectively.

In water, it was observed that the rate of release of volatile esters was in ascending order as follows: EB < IA < EA < EH. The most hydrophobic ester (EH) showed a higher rate of release than the most hydrophilic (EA and EB) and the less volatile ester (IA). On the contrary, these last esters were more able to establish interactions with water molecules and have a lower tendency to partly to the vapor phase. When disaccharide solutions were taken into account, a general decrease of  $R^{app}_i$  was observed, with the exception of the trehalose solutions above 40 % w/v, where the initial apparent rate of release of all the aroma compounds showed a significant increase, likely related to major changes in the physicochemical properties of the solution approaching its solubility limit.

**Table 2** Initial apparent rate of release  $R^{app}_i$  ( $\text{min}^{-1}$ ) of flavor compounds in water and solutions of sucrose and trehalose at different solute concentrations

Aroma compound	Initial apparent rate of release $R^{app}_i$ ( $\text{min}^{-1}$ )			
	Ethyl acetate	Ethyl butyrate	Isopentyl acetate	Ethyl hexanoate
Water	0.486	0.411	0.414	0.502
Sucrose, 10 %	0.327	0.261	0.248	0.285
Sucrose, 40 %	0.309	0.259	0.256	0.371
Sucrose, 45 %	0.296	0.247	0.256	0.352
Trehalose, 10 %	0.431	0.359	0.334	0.403
Trehalose, 40 %	0.304	0.258	0.264	0.401
Trehalose, 45 %	0.604	0.536	0.527	0.629

**Table 3** Ratio of initial apparent rate of release  $R^{app}_i$  of flavor compounds in sugar solution to initial apparent rate of release  $R^{app}_i$  of flavor compounds in water

Aroma compound	$R^{app}_i$ in solution/ $R^{app}_i$ in water ratio			
	Ethyl acetate	Ethyl butyrate	Isopentyl acetate	Ethyl hexanoate
Water	1	1	1	1
Sucrose, 10 %	0.67	0.64	0.60	0.57
Sucrose, 40 %	0.64	0.63	0.62	0.74
Sucrose, 45 %	0.61	0.60	0.62	0.70
Trehalose, 10 %	0.89	0.86	0.81	0.80
Trehalose, 40 %	0.63	0.63	0.62	0.80
Trehalose, 45 %	1.24	1.30	1.27	1.25

In the case of sucrose solutions, in general, a steep and significant decrease with respect to water of the  $R^{app}$  of all the four aroma compounds was observed when 10 % w/v solutions were considered, while further increasing concentrations did not induce major effects on the initial rate of release, although a slight decrease was still observed for EA, EB, and EH. Furthermore, in the case of EH, a nonlinear decreasing trend in the  $R^{app}$  at increasing sucrose concentration was observed, although the initial rate of release was lower than that in water.

For trehalose, a decreasing trend of the  $R^{app}_i$  of the four aroma compounds at increasing solute concentration was also shown; however, with respect to sucrose, some differences were observed. In particular, the decrease in the initial apparent rate was of lower entity (Table 3) in the 10 % trehalose solutions than that determined in the sucrose solutions at similar concentration. On the contrary, at higher solute concentration (40 %) for the  $R^{app}$ , values were not significantly affected by sugar type, with the exception of EH, which did not change its initial rate of release due to an increased trehalose concentration.

Under these experimental conditions, results are attributed to the aroma molecules that vaporize as they become present at the vapor–water interface or could reach it in very short time (1 min). Thus, decrease in the initial apparent rate of release could be related in general to a reduction of the diffusion of the flavor

compounds within the disaccharide solutions due to the increased viscosity. However, at low concentration (10 %), the viscosity of sucrose and trehalose is quite similar, while a significantly different result occurred in the release rate of aroma compounds in the two sugar solutions. In contrast, at higher concentration (40 %), trehalose solutions are characterized by a higher viscosity than the correspondent sucrose solutions, while the relative decrease of the  $R^{app}$  of the compounds (Table 3) was similar.

It could be suggested that the chemical and physicochemical properties of the sucrose and trehalose aqueous solutions and their change in increasing concentration, other than viscosity, can affect aroma diffusion in the matrix and, thus, their release kinetics, which may imply effects on water–aroma, aroma–sugar, and sugar–water interactions, the nature of the aroma, and its specific affinity for the solute and, eventually, retention phenomena.

## 4 Conclusions

This study, carried out with simple sugar model systems at increasing concentration, evidenced that release in the vapor phase of volatile compounds is affected by the water state, but the nature of the solute, at the same water activity value, could differently favor or hinder partition. Regarding the kinetics of the release, viscosity of the matrix could be considered as a factor that limits the rate of release in the vapor phase of aroma compounds in sugar solutions at increasing concentration, although other physicochemical and physical properties must also be considered.

Based on these results, aroma compounds can be considered as showing reliable proof of physicochemical changes occurring in the liquid phase of saccharide solutions; thus, aroma release is an interesting tool for further investigation.

## References

- Cayot N, Dury-Brun C, Karbowiak T, Savary G, Voilley A (2008) Measurement of transport phenomena of volatile compounds: a review. *Food Res Int* 41:349–362
- Friel EN, Linforth RS, Taylor AJ (2000) An empirical model to predict the headspace concentration of volatile compounds above solutions containing sucrose. *Food Chem* 71:309–317
- Nahon D, Harrison M, Roozen J (2000) Modeling flavour release from aqueous sucrose solutions using mass transfer and partition coefficients. *J Agric Food Chem* 48:1278–1284
- Neri L, Pittia P, Bertolo G, Torreggiani D, Sacchetti G (2010) Influence of water activity and molecular mobility on peroxidase activity in salt and sorbitol–maltodextrin systems. *J Food Eng* 101:289–295
- Pittia P, Anese M, Manzocco L, Calligaris S, Mastrolcola D, Nicoli MC (2006) Liquid-vapour partition of ethanol in bakery products. *Flavor Frag J* 21:3–7
- Rabe S, Krings U, Berger RG (2003) Dynamic flavor release from sucrose solutions. *J Agric Food Chem* 51:5058–5066

- Roberts DD, Elmore JS, Langley KR, Bakker J (1996) Effects of sucrose, guar gum and carboxymethylcellulose on the release of volatile flavour compounds under dynamic conditions. *J Agric Food Chem* 44:1321–1326
- Seuvre AM, Philippe E, Rochard S, Voilley A (2006) Retention of aroma compounds in food matrices of similar rheological behaviour and different compositions. *Food Chem* 96:104–114
- Seuvre AM, Philippe E, Rochard S, Voilley A (2007) Kinetic study of the release of aroma compounds in different models systems. *Food Res Int* 40:480–492

# Wetting Behavior of Chitosan Solutions on Blueberry Epicarp With or Without Epicuticular Waxes

O. Skurty, P. Velásquez, and F. Osorio

## Abbreviations

CA	Contact angle
SFE	Surface free energy
vOCG	Theory of van Oss, Chaudhury, and Good
$Wa$	Work of adhesion of a liquid on a solid surface
$\gamma_{LV}$	Surface tension of the liquid
$\theta$	Contact angle
$\gamma_{LV}^{LW}$	Apolar component of liquid–vapor
$\gamma_{SV}^{LW}$	Apolar component of surface–vapor
$M_w$	Medium-molecular-weight chitosan
$W_c$	Cohesive energy
$S_{eq}$	Spreading coefficient
$S_{\text{with wax}}$	Spreading without chloroform wash
$S_{\text{without wax}}$	Spreading with chloroform wash
$S_{\text{diff}}$	Spreading difference
$G$	Glycerol

---

O. Skurty (✉)

Department of Mechanical Engineering, Universidad Técnica Federico Santa María, Santiago, Chile  
e-mail: [olivier.skurty@usach.cl](mailto:olivier.skurty@usach.cl)

P. Velásquez

Departamento de Ingeniería Química y Bioprocessos, Pontificia Universidad Católica de Chile (PUC), Avenida Vicuña Mackenna, 4860 Santiago, Chile

F. Osorio

Department of Food Science and Technology, Universidad de Santiago de Chile, Avenida Ecuador 3769 Santiago, Chile

## 1 Introduction

Edible coatings can prevent microbial spoilage and quality loss of blueberries due to mass transfer (e.g., moisture, gases, aroma compounds, etc.). The protection of blueberry (and in foods in general) by edible coatings depends on controlling the wetting of the coating solutions, which affects the adhesion and the thickness of the film (Park 2002). Indeed, the thickness of edible coatings is an important parameter since it directly affects the biological properties and the shelf-life of blueberries. The central parameter that characterizes the wetting of a blueberry epicarp is the equilibrium contact angle (CA) (Israelachvili 1992). By convention, the CA is the angle,  $\theta$ , at which a liquid–vapor interface meets the solid surface. Surface free energy (SFE) of blueberry epicarp can be obtained using different approaches. All of these methods are based on CA measurements of different sessile liquid drops with known surface tension deposited on the blueberry epicarp, but discrepancies have been shown in the obtained results (Etzler 2006). One of the main methods for the determination of SFE is the “acid–base” theory of van Oss, Chaudhury, and Good (vOCG) (van Oss et al. 1986, 1988).

Application of chitosan in the form of edible coatings on blueberries may be an effective and affordable treatment to extend shelf-life and enhance quality and safety of the produce (Park 2002). Chitosan shows antifungal and antibacterial properties, which are believed to originate from its polycationic nature (Tharanathan and Kittur 2003). Chitosan coatings, such as many polysaccharide-based films, tend to exhibit fat and oil resistance and selective permeability to gases, but lack resistance to water transmission (Bordenave et al. 2007). Dutta et al. (2009) reviewed the many applications of chitosan coatings. Plasticizers are generally required for polysaccharide-based edible films to improve elasticity and flexibility, reduce brittleness and toughness, and prevent cracking during handling and storage. The most common used plasticizers are polyols like propylene glycol, sorbitol, polyethylene glycol, and glycerol. Surfactants can be incorporated into the film formulation to reduce surface tension of the solution, improving the wettability and adhesion of the film (Goodwin 2004). Surfactants are usually organic compounds that are amphiphilic, meaning they contain both hydrophobic groups (apolar) and hydrophilic groups (polar). A typically used surfactant is Tween 20, which has been reported to decrease the water vapor permeability of coatings (Nieto 2009).

The aim of this study was to investigate the physical properties of blueberry epicarp in order to increase the effectiveness of chitosan-based coatings. SFE of blueberry epicarp with and without wax was calculated using the “acid–base” theory. Various chitosan-based coatings were applied to the blueberry epicarp. In particular, the effects of concentrations of a plasticizer (glycerol) and a surfactant (Tween 20) on the wetting of blueberry epicarp were studied. For that, the cohesive energy and the spreading coefficient were calculated for each solution. A mathematical relationship between concentrations and spreading coefficient was proposed. Finally, the optimum chitosan-based coating solutions were determined to promote the adhesion of the edible film.

## 2 Materials and Methods

### 2.1 Plant Material

Fresh highbush blueberries of the variety Duke (*Vaccinium corymbosum* L.) were supplied by Chilean producers in the province of Santiago (Hortifrut SA, Chile). Before measurements, blueberries were left at ambient temperature (~21 °C). The fruits were carefully selected to insure uniformity in maturity, size, color, and physical appearance according to visual analysis. They were almost spherical, between 11 and 15 mm in diameter, with a dark blue color. The blueberry cuticle consists of a polyester matrix or cutin layer (about 5 µm thick) and an epicuticular wax layer or waxy bloom. Epicuticular wax of undamaged fruits was removed by gentle rinses of the blueberries' surface with chloroform (Schreiber and Schönher 2009).

### 2.2 Wetting Measurements

SFE of each fruit epicarp was determined following wetting measurements using the contact angle technique coupled with a visualization technique. The core of the self-built instrument consists of an optic device and a light source mounted on a rigid support. The optics comprised a zoom video lens (Edmund Optics, NJ, USA) connected to a CCD camera (Pulnix, Inc., San Jose, CA, USA), which is piloted via software. The drops were manually deposited on fruit epicarps using a precision microliter pipette (Gilson Pipetman U2). The adequate drop volumes were chosen between 0.2 and 2 µl to avoid two experimental problems: first, the drop must be sufficiently smaller to be placed on a planar surface of the fruit epicarps; second, the drop volume was sufficiently small to assume the effect of gravity to be negligible on the drop shape. Five different liquids with known surface energy components (polar and nonpolar liquids) were used for the surface energy measurements: α-bromonaphthalene, ethylene glycol, formamide, glycerol, and distilled water. These liquids span the entire range of fluids, from dispersive to polar. CA were measured for each liquid on the two different surfaces: blueberry epicarp with and without wax. For statistical approaches, for each liquid at least 10 (mostly 15) right and left angles were measured. The root mean square of each set of measurements was smaller than 2.3°. All of the CA measurements were made at room temperature (~21 °C). In order to avoid liquid adsorption by the fruit, the typical CA equilibrium measurement was performed within 30–60 s after the drop placement on the surface. CA values were determined using ImageJ program with the plug-in drop shape analysis. The accuracy of the analysis is high since the plug-in used a method based on B-spline snakes (active contours) (Drop-analysis 2010).

## 2.3 Evaluation of the Surface Free Energy

### 2.3.1 Acid–Base Approach (vOCG)

SFE of a solid (or liquids) described by the vOCG approach is composed by  $\gamma = \gamma^{\text{LW}} + \gamma^{\text{AB}}$  where  $\gamma^{\text{LW}}$  and  $\gamma^{\text{AB}}$  are the Lifshitz–van der Waals (apolar) and Lewis acid–base (polar) components, respectively. According to the vOCG model, the Lewis acid–base component is modeled as follows:  $\gamma^{\text{AB}} = 2(\gamma^- \gamma^+)^{1/2}$  where  $\gamma^-$  and  $\gamma^+$  are the electron–donor (Lewis base) and the electron–acceptor (Lewis acid). The material is considered as a polar if both  $\gamma^-$  and  $\gamma^+$  are close to zero, monopolar if one of these components is negligible, and bipolar if the two components have appreciable values. The work of adhesion of a liquid on a solid surface is written  $Wa = \gamma_{\text{LV}}(1 + \cos\theta) = 2(\gamma_{\text{LV}}^{\text{LW}} \gamma_{\text{SV}}^{\text{LW}})^{1/2} + 2(\gamma_{\text{LV}}^- \gamma_{\text{SV}}^-)^{1/2} + 2(\gamma_{\text{LV}}^- \gamma_{\text{SV}}^+)^{1/2}$  where the surface tension ( $\gamma_{\text{LV}}$ ) of the liquid and the contact angle  $\theta$  between the solid surface and the liquid–vapor interface may be assessed experimentally. However, concerning  $\theta$ , the difficulty arises from the nonideal solid surfaces where measured static CA values may exhibit a large dispersion (CA hysteresis). In the last equation,  $\gamma_{\text{SV}}^{\text{LW}}$ ,  $\gamma_{\text{SV}}^-$ , and  $\gamma_{\text{SV}}^+$  are unknown. But if one assumes that the three dispersive and acid–base coefficients  $\gamma_{\text{LV},i}$  are known for each liquid ( $i = 1, 2, 3$ ), a linear set of three equations can be obtained in the form  $\gamma_{\text{LV},i}(1 + \cos\theta) = 2(\gamma_{\text{LV},i}^{\text{LW}} \gamma_{\text{SV}}^{\text{LW}})^{1/2} + 2(\gamma_{\text{LV},i}^- \gamma_{\text{SV}}^-)^{1/2} + 2(\gamma_{\text{LV},i}^- \gamma_{\text{SV}}^+)^{1/2}$ . This system of equations,  $Ax = B$ , is generally ill conditioned: small differences in experimental data or in the coefficients can induce strong variations in the results. One apolar ( $\text{C}_{10}\text{H}_7\text{Br}$ ) and two polar ( $\text{CH}_3\text{NO}$ ) and water liquids constitute a good set of the three fluids with a condition number equal to 7.13, as reported by Della-Volpe et al. (2004). Calculations were performed using the GNU free software Octave with the front-end user interface QtOctave.

## 2.4 Coating Preparations

Coating solutions were prepared from medium-molecular-weight chitosan ( $M_w \approx 200$  kDa, degree of deacetylation of  $80 \pm 5\%$ ), glycerol as plasticizer, and Tween 20 as surfactant. Chitosan was dissolved in 0.1 mol/L acetic acid aqueous solution (prepared from distilled water) to a concentration of 2 g/100 g during 24 h under continuous stirring at room temperature ( $\sim 21^\circ\text{C}$ ). The solution was then filtered. This stock solution was then dissolved to the desired concentrations with acetic acid aqueous solution. After dissolution, the pH was around 5. Glycerol/chitosan (or Tween 20/chitosan) coating solutions were prepared by vigorously mixing glycerol (or Tween 20) and chitosan during 20 min to reach complete interaction. The fraction of glycerol and Tween 20 varied across the entire range, between 1 and 20 g/100 g. The concentration of chitosan varied between 1 and 2 g/100 g.

## 2.5 Surface Tension Measurements of Coating Solutions

Interfacial tension measurements,  $\gamma_{LV}$ , were carried out by the pendant drop method. A small drop of liquid (about 10–20  $\mu\text{l}$ ) attached to the tip of a stainless-steel needle (inner diameter of  $1.651 \pm 0.005$  mm) was suspended into air under a constant temperature ( $\sim 21^\circ\text{C}$ ). The drop was formed by a controlled syringe pump. Images of the drop were taken as function of time with the optic device. The solution of the Laplace equation was obtained with the free software Octave 3.2.4. The accuracy of the measurements was  $\pm 0.3 \text{ mJ/m}^2$ .

## 3 Results and Discussion

### 3.1 Surface Free Energy Measurements

Blueberry with epicuticular wax had a SFE  $\gamma_{SV} = 29.1 \pm 4.1 \text{ mJ/m}^2$ . In both cases, blueberry surface is a low-energy surface. In comparison with other fruits (with wax), like Granny Smith apple ( $\gamma_{SV} = 43.5 \text{ mJ/m}^2$ ) or tomato ( $\gamma_{SV} = 36.9 \text{ mJ/m}^2$ ), blueberries (with wax) have a much lower surface energy, i.e., an epicarp more hydrophobic. However, this value was close to the SFE of strawberry, measured by the Owens–Wendt approach,  $28.94 \text{ mJ/m}^2$  (Ribeiro et al. 2007). After the wax removal, SFE increased significantly to  $38.3 \pm 2.8 \text{ mJ/m}^2$ . For a waterdrop (epicarp with and without wax), the contact angle was  $\theta = 124.9^\circ$  and  $100.9^\circ$  respectively. Therefore, epicarp with wax was more hydrophobic. Blueberry epicarps with or without wax have mainly an apolar (Lifshitz–van der Waals) character with a small polarity (Lewis acid–base). The apolar character is generally observed for the hydrocarbons, which dominantly have almost zero polar, but van der Waals attractive forces between molecules. Apolar surfaces are surfaces where hydrophobicity is observed; the interactions among the water molecules themselves exceed the water–surface interactions (Israelachvili 1992). Moreover, in both cases, the results indicate that the surfaces have low acidic and basic characters, implying that these epicarps are slightly bipolar. The acidic ( $\gamma_{SV}^+$ ) and basic ( $\gamma_{SV}^-$ ) are  $1$  (with wax)– $0.9 \text{ mJ/m}^2$  (without wax) and  $1.6$  (with wax)– $1.8 \text{ mJ/m}^2$  (without wax), respectively. The wetting of blueberry epicarps varies not only with chemical texture determined by the composition of the solid surface but also with the physical texture or the roughness. The roughness of the blueberry epicarp was enhanced by the three-dimensional wax structures and was measured at about  $42 \pm 10 \mu\text{m}$ . This value is in the range of measured values for three-dimensional epicuticular waxes on plant surfaces between  $0.5$  and  $100 \mu\text{m}$  (Jeffree 2006). Effect of surface roughness on the wetting is easily understood by the Wenzel equation. According to this equation, hydrophobicity is reinforced by roughness.

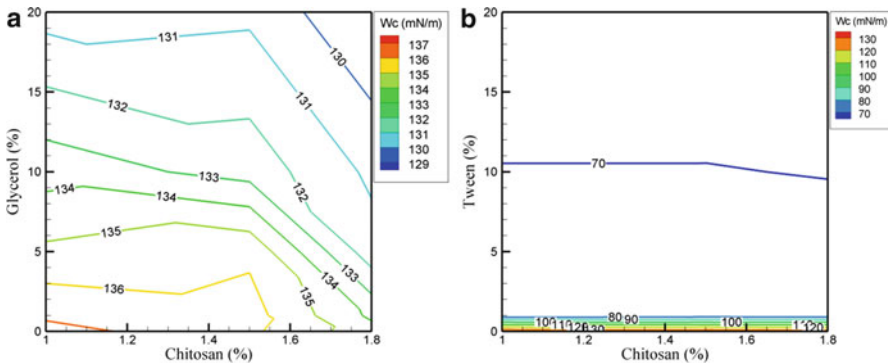


**Fig. 1** Cohesive energy  $W_c$  as a function of chitosan and (a) glycerol and (b) Tween 20 concentrations

### 3.2 Cohesive Energy

The cohesive energy,  $W_c = 2\gamma_{LV}$ , was calculated from surface tension measurements. In Fig. 1,  $W_c$  is plotted as function of chitosan, glycerol, and Tween 20 concentrations. It was observed that the  $W_c$  decreased as the concentration of glycerol [ $G$ ] or Tween 20 [ $T$ ] increased. The concentration of chitosan [ $C$ ] influenced the work cohesion values in solution with glycerol, while the influence of the latter was lower with Tween 20. From measurements, two-parameter equations describing the influence of glycerol/chitosan and chitosan/Tween 20 concentrations on the cohesive energy were determined using the free software Octave (Eqs. 1 and 2):

$$W_c^{\text{glyc/chit}} = 124.65 + 22.19[C] - 0.56[G] - 9.43[C]^2 + 0.09[C][G] \\ + 0.007[G]^2; (R^2 = 0.97) \quad (1)$$

$$W_c^{\text{glyc/chit}} = 130.15 - 4.30[C]\sqrt[3]{T} + 1.48\sqrt[3]{C} + 3.09[T]\sqrt[3]{C} - 42.01\sqrt[3]{T}; (R^2 = 0.92) \quad (2)$$

As strong adhesion and weak cohesion result in a high degree of wetting, the minimum of Eqs. 1 and 2 was calculated using the software Octave (2010).  $W_c^{\text{glyc/chit}} = -130 \text{ mJ/m}^2$  for the solution  $[C]=1 \%$  and  $[G]=20 \%$  and  $W_c^{\text{tween/chit}} = -68 \text{ mJ/m}^2$  for the solution  $[C]=1 \%$  and  $[T]=20 \%$ .

### 3.3 Wetting of Blueberry Epicarp by Coating Solutions

#### 3.3.1 Wetting of Blueberry Epicarp by Glycerol/Chitosan Coating Solutions

In Fig. 2, the spreading coefficient  $S_{eq} = W_a - W_c = \gamma_{sv} - \gamma_{SL} - \gamma_{LV} = \gamma_{LV} (\cos \theta_{eq} - 1)$  is plotted as a function of chitosan and glycerol concentrations. Partial wetting ( $S_{eq} < 0$ ) corresponds to drops, surrounded by a microscopically thin film adsorbed at the surface, and total wetting ( $S_{eq} = 0$ ) to a macroscopically thick layer. Good wetting (ideal  $S_{eq} = 0$ ) of the blueberry epicarp by the liquid coating solution is a necessary prerequisite to establish a good adhesion of the edible film. The difference in  $S$  between the unwashed and chloroform washed blueberry  $S_{eq} = S_{diff} = S_{with\ wax} - S_{without\ wax}$  is also presented. On the blueberry epicarp with epicuticular wax, the results show that the addition of glycerol to the chitosan solution diminished the wetting capacity of the blueberry by the solution (Fig. 2a). Indeed, at a fixed chitosan concentration,  $S$  decreased significantly, whereas at fixed glycerol concentration,  $S$  increased by about 105 to 90 mJ/m<sup>2</sup> when the concentration of chitosan increased between 1 % and 1.8 % (Fig. 2a). In general, the wax removal allows significant improvement of the wetting (Fig. 2b) since  $S_{diff}$  varied between 8 and 12 mJ/m<sup>2</sup> depending on glycerol/chitosan concentrations (Fig. 2c).

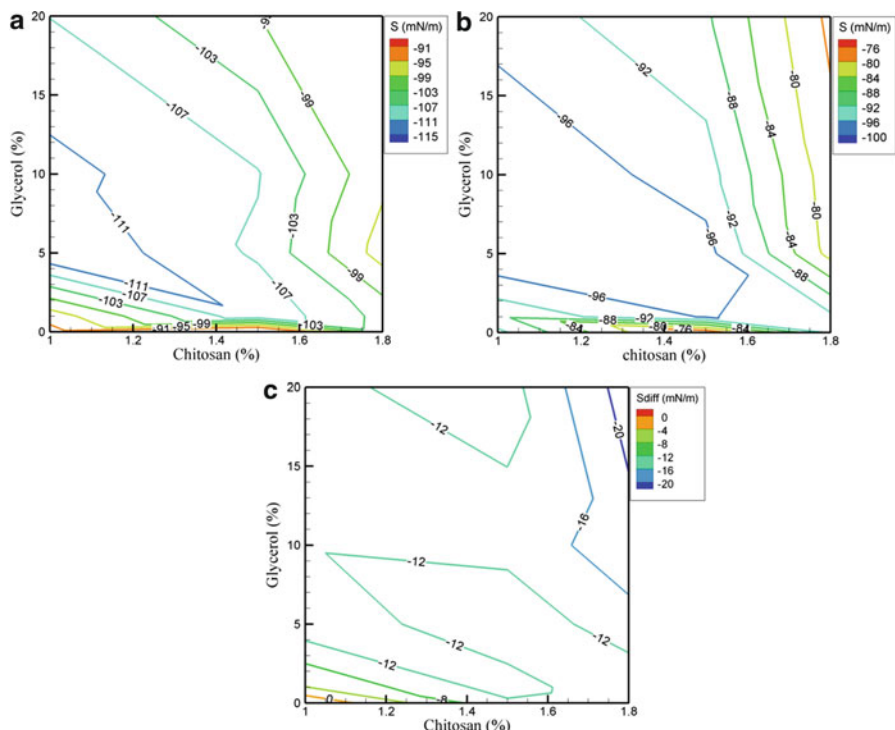


**Fig. 2** Spreading coefficient  $S$  as a function of chitosan and glycerol concentrations: (a) with wax, (b) without wax, (c) spreading coefficient difference  $S_{diff} = S_{with\ wax} - S_{without\ wax}$

The reason why  $S$  was smaller on the wax component of cuticle than on the cutin component of cuticle is that polar groups are capable of binding aqueous solutions through hydrogen bonds, while hydrocarbon chains of wax only attract aqueous solutions through the much weaker van der Waals forces (Israelachvili 1992). Thus, CA between aqueous chitosan solution and the epicuticular wax was slightly larger than those between water and the cutin component of cuticle. The influence of glycerol [ $G$ ] and chitosan [ $C$ ] concentrations on the spreading factor followed the equations:

$$S_{\text{with wax}}^{\text{glyc/chit}} = -37.87 + 11.86[C] \sqrt[3]{[T]} - 48.11 \sqrt[3]{[C]} + 0.83 \sqrt[3]{[C]} - 27.27 \sqrt[3]{[T]}; (R^2 = 0.64) \quad (3)$$

$$S_{\text{without wax}}^{\text{glyc/chit}} = -73.84 + 13.21[C] \sqrt[5]{[G]} - 11.58 \sqrt[5]{[C]} + 0.59[G] \sqrt[5]{[C]} - 25.70 \sqrt[5]{[G]}; (R^2 = 0.60) \quad (4)$$

Finally, for both cases, optimum values of chitosan/glycerol concentrations that generate a small  $S$  were obtained by maximizing the equation (Eqs. 3 and 4). With the epicuticular wax [ $C$ ]=1.1 % and [ $G$ ]=0.1 %, and without epicuticular wax [ $C$ ]=1.8 % and [ $G$ ]=20 %. On the other hand, the unfavorable values of  $S$  were obtained by minimizing the corresponding equations.

### 3.3.2 Wetting of Blueberry Epicarp by Tween 20/Chitosan Coating Solutions

In Fig. 3, the  $S$  is plotted as function of chitosan and Tween 20 concentrations. Surprisingly, the spreading coefficient is only slightly dependent on the chitosan concentrations. At a fixed chitosan concentration, the addition of Tween 20 allowed  $S$  to decrease significantly (Fig. 3a), i.e., the adhesion of the coating solution was enhanced. The removal of the epicuticular wax increased the wetting behavior of the Tween 20/chitosan solution slightly since  $S$  increased of 4–8 mJ/m<sup>2</sup>. Moreover, a comparison between the two coating solutions shows that Tween 20/chitosan solutions wet the blueberry epicarp more (with or without wax) than the glycerol/chitosan solution, since  $S$  was lower. The explanation of this phenomenon is the same described in the previous paragraph. The influence of Tween 20 and chitosan concentrations on  $S$  followed the equations:

$$S_{\text{with wax}}^{\text{tween/chit}} = -23.76 + 8.92[C] \sqrt[5]{[T]} - 62.42 \sqrt[5]{[C]} - 1.23[T] \sqrt[5]{[C]} + 33.47 \sqrt[5]{[T]}; (R^2 = 0.95) \quad (5)$$

$$S_{\text{without wax}}^{\text{tween/chit}} = -123.19 - 2.95[C] \sqrt[5]{[T]} + 35.73 \sqrt[5]{[C]} - 1.22[T] \sqrt[5]{[C]} + 50.70 \sqrt[5]{[T]}; (R^2 = 0.95) \quad (6)$$

Finally, it was possible to suggest an optimal concentration of Tween 20 and chitosan to optimize the spreading coefficient  $S$  by maximizing equations (Eqs. 5 and 6).

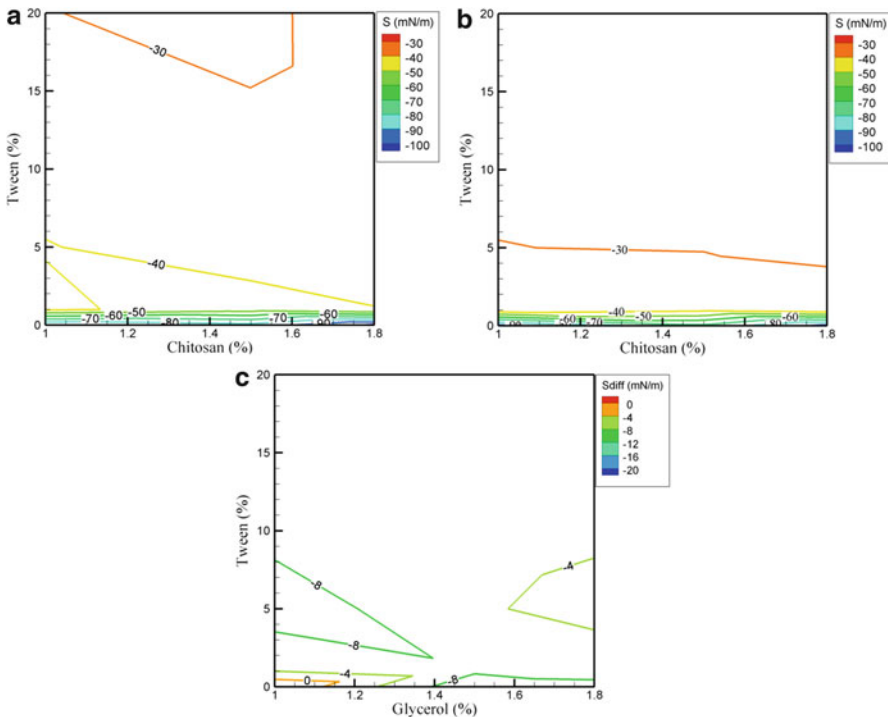


**Fig. 3** Spreading coefficient  $S$  as a function of chitosan and Tween 20 concentrations: (a) with wax, (b) without wax, (c) spreading coefficient difference  $S_{\text{diff}} = S_{\text{with wax}} - S_{\text{without wax}}$

With epicuticular wax  $[C]=1.4\%$  and  $[T]=20\%$ , and without epicuticular wax  $[C]=1\%$  and  $[T]=20\%$ . However, at this concentration, a phase separation during drying was observed, i.e., films obtained were of poor quality. This is due to the lack of strong interactions between the surfactant and the chitosan.

## 4 Conclusions

In this paper, the physical properties of fresh highbush blueberry epicarp were determined in order to increase the effectiveness of chitosan-based coatings. SFE of blueberry epicarp, with and without epicuticular wax, was a low-energy surface and presented an apolar character and a small polarity. Indeed, with wax  $\gamma_{SV}=29.1 \pm 4.1 \text{ mJ/m}^2$ , while after the wax removal,  $\gamma_{SV}$  was increased significantly to  $38.3 \pm 2.8 \text{ mJ/m}^2$ . Various chitosan-based coating solutions were applied to the blueberry epicarp with or without epicuticular wax. The effects of glycerol  $[G]$  and Tween 20  $[T]$  concentrations on the spreading coefficient  $S$  have been studied. For the glycerol/chitosan coating solutions, the results showed that the addition of glycerol to the chitosan solution diminished the wetting capacity of

the blueberry by the solution, whereas at fixed glycerol concentration an increase of the chitosan concentration wet more the blueberry epicarp. For the Tween 20/chitosan coating solutions,  $S$  was only slightly dependent on the chitosan concentrations, whereas at fixed chitosan concentration, the addition of Tween 20 allowed enhancement of the adhesion of the coating solution. More specifically, the results showed that wax removal of the epicarp improved the wetting capacity and that Tween 20/chitosan coating solutions wet the blueberry epicarp more (with or without wax) than glycerol/chitosan solutions, since  $S \sim 30$  and  $80 \text{ mJ/m}^2$ , respectively. Finally, solutions that better wet the blueberry with wax were  $[G] = 0.1 \text{ g/100 g}$   $[C] = 1.1 \%$  and  $[T] = 20 \%$   $[C] = 1.4 \%$  and without wax  $[G] = 20 \%$   $[C] = 1.8 \%$  and  $[T] = 20 \%$   $[C] = 1 \%$ .

**Acknowledgments** Support from projects CONICYT PBCT-PSD 62 (O.S.), Dicyt-USach 080771OL, and Innova Chile-CORFO CT11 PUT-20 is appreciated.

## References

- Bordenave N, Grelier S, Coma V (2007) Water and moisture susceptibility of chitosan and paper-based materials: structure-property relationships. *J Agric Food Chem* 55:9479–9488
- Della-Volpe D, Maniglio M, Brugnara S, Siboni MM (2004) The solid surface free energy calculation. I. In defense of the multicomponent approach. *J Colloid Sci* 271:434–453
- Drop-analysis (2010) [Http://bigwww.epfl.ch/demo/dropanalysis/soft](http://bigwww.epfl.ch/demo/dropanalysis/soft). Accessed March
- Dutta P, Tripathi S, Mehrotra G, Dutta J (2009) Perspectives for chitosan based antimicrobial films in food applications. *Food Chem* 114:1173–1182
- Etzler FM (2006) Contact angle, wettability and adhesion. Chapter surface free energy of solids: A comparison of models, edited by K- L. Mittal. Utrecht, The Netherlands, V.S.P. Intl Science, pp 215–236
- Goodwin J (2004) *Colloids and interfaces with surfactants and polymers: an introduction*. Wiley, West Sussex, England
- Israelachvili J (1992) *Intermolecular and surface forces*. Academic, New York
- Jeffree C (2006) Biology of the plant cuticle. The fine structure of the plant cuticle. Oxford, UK: Blackwell Publishing Ltd, pp 11–125
- Nieto M (2009) Edible films and coatings for food applications. Structure and function of polysaccharide gum-based edible films and coatings. Springer, Berlin, pp 57–112
- Octave (2010) [Http://www.gnu.org/software/octave/](http://www.gnu.org/software/octave/)
- Park HJ (2002) Fruit and vegetable processing: improving quality. *Edible coatings for fruits*. Edited by: W. Jongen Woodhead Publishing Limited, Cambridge, pp 331–355
- Ribeiro C, Vicente A, Teixeira J, Miranda C (2007) Optimization of edible coating composition to retard strawberry fruit senescence. *Postharvest Biol Technol* 44:63–70
- Schreiber L, Schönher J (2009) Water and solute permeability of plant cuticles. Springer Berlin Heidelberg
- Tharanathan RN, Kittur F (2003) Chitin—the undisputed biomolecule of great potential. *Crit Rev Food Sci Nutr* 43:61–87
- van Oss CJ, Chaudhury MK, Good RJ (1988) Interfacial Lifshitz-van der Waals and polar interactions in macroscopic systems. *Chem Rev* 88:927–941
- van Oss CJ, Good RJ, Chaudhury MK (1986) The role of van der Waals forces and hydrogen bonds in hydrophobic interactions between biopolymers and low energy surfaces. *J Colloid Interface Sci* 111:378–390

# Influence of Brine Concentration on Moisture and NaCl Transport During Meat Salting

C. Ozuna, J.A. Cárcel, J.V. García-Pérez, R. Peña, and A. Mulet

## Abbreviations

WHC	Water-holding capacity
MANOVA	Multifactor analysis of variance
LSD	Least significance difference
$C_w$	Moisture content
$D_w$	Average effective moisture diffusivity
$t$	Time
$x$	Characteristic coordinate in the infinite slab geometry
GRG	Generalized reduced gradient
% VAR	Explained variance
$S^2_w$	Variance of the sample
$S^2_{tw}$	Variance of the estimation

## 1 Introduction

Meat brining processes represent an alternative to dry-salting due to their ability to accelerate the mass transport process (Barat et al. 2006). These processes change the salt and moisture content of meat and affect not only the shelf life of the product but also its organoleptic characteristics. During meat brining, NaCl can modify the water-holding capacity (WHC) by affecting the myofibrillar proteins (Lambert

---

C. Ozuna • J.A. Cárcel (✉) • J.V. García-Pérez • R. Peña • A. Mulet

Grupo de Análisis y Simulación de Procesos Agroalimentarios, Departamento de Tecnología de Alimentos, Universitat Politècnica de València, Camino de Vera, s/n,  
E46022 Valencia, Spain  
e-mail: [jcarcel@tal.upv.es](mailto:jcarcel@tal.upv.es)

et al. 2001). Thus, brining with low NaCl content produces growth of the WHC linked to the protein solubilisation process, a phenomenon known as “salting in.” On the other hand, when high brine concentrations are used, a decrease in WHC is observed (“salting out”), probably due to the insolubilization of proteins (Graiver et al. 2009). Therefore, the solution concentration used can be expected to influence the mass transfer kinetics.

Mathematical modelling constitutes an interesting tool with which to quantify the influence of process variables, such as brine concentration, on transport phenomena. The transport of moisture and solutes in solid-liquid systems has been modelled using empirical models, such as the Peleg or Weibull models (García-Pascual et al. 2006) or theoretical models, such as the diffusion models based on Fick’s second law (Cárcel et al. 2007b). Diffusion models are more complex to solve but provide a more reliable tool for process simulation under different conditions.

In the literature, a great number of research can be found about meat brining processes using saturated or quasi-saturated brines (Fox 1980; Graiver et al. 2006, 2009; Cárcel et al. 2007a). Nevertheless, few studies exist on the effect of brine concentration on water and NaCl transport during brining, and these aspects are the main aim of this work.

## 2 Materials and Methods

### 2.1 Brining Experiments

Brining kinetics of pork meat samples (*Longissimus dorsi*) with slab geometry (length 50 × width 30 × thickness 10 mm) were carried out at different brine concentrations (50, 100, 150, 200, 240, and saturated at  $5 \pm 1$  °C 280 kg/m<sup>3</sup>), with each brining condition being tested in triplicate. In each experiment, samples were extracted at pre-set times (15, 30, 45, 60, 90, and 120 min), immersed in distilled water for 20 s to remove superficial brine, and then blotted. The moisture content of the brined and fresh meat samples was measured in triplicate following AOAC official method 950.46 (AOAC 1997). NaCl content was quantified by determining the ion Cl<sup>-</sup> concentration (Ciba Corning, mod. 926L; Halstead, Essex, UK) in a meat ( $1 \pm 0.1$  g) extract obtained with distilled water (100 mL) of the salted samples (Cárcel et al. 2007a). Each sample from a single experiment was analyzed in triplicate; thus, nine measurements were carried out to determine a point in the kinetics. The high number of replicates was used to obtain significant results by taking into account the variability of the raw material and experimental procedure. The results were reported as kg NaCl/kg initial dry matter. The multi-factor analysis of variance (MANOVA) and the estimation of least significance difference (LSD) intervals were chosen to evaluate the influence of brine concentration on moisture and NaCl experimental values. Statistical analysis was carried out using the Statgraphics Plus 5.1 software package.

## 2.2 Mass Transfer Modelling

Diffusion models based on Fick's second law were used to describe water and NaCl transport, respectively. Equation (1) shows the diffusion equation for water transport. An analogous equation was used for NaCl transport:

$$\frac{\partial C_w(x, t)}{\partial t} = D_w \left( \frac{\partial^2 C_w(x, t)}{\partial x^2} \right) \quad (1)$$

where  $C_w$  is the local moisture content (kg water/kg dry matter),  $D_w$  is the average effective moisture diffusivity ( $\text{m}^2/\text{s}$ ),  $t$  is the time (s), and  $x$  is the characteristic coordinate in the infinite slab geometry (m).

Equation (1) was solved by assuming the symmetry of the solid, a uniform initial moisture content and temperature, and that the effective moisture diffusivity and the sample volume remain constant during brining (Graiver et al. 2006). The effective diffusivity values of both moisture and NaCl were identified by using an optimization procedure, i.e., the generalized reduced gradient (GRG), available in Microsoft Excel™ spreadsheet from MS Office 2007. The explained variance (% VAR) was computed to determine the ability of the model to describe the experimental data (Cárcel et al. 2007b).

$$\% \text{ VAR} = \left[ 1 - \frac{S_{tw}^2}{S_w^2} \right] \times 100 \quad (2)$$

where  $S_w^2$  and  $S_{tw}^2$  are the variance of the sample and the estimation, respectively.

## 3 Results and Discussion

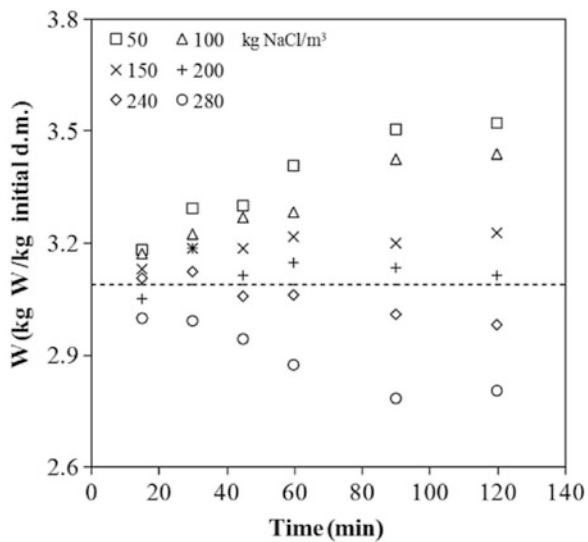
### 3.1 Experimental Results

#### 3.1.1 Water Transport

The evolution of sample moisture content during treatments was dependent on the concentration of brine used, as shown in Fig. 1. It must be emphasized that, in this figure, each point represents the average of nine measurements; three independently brined samples were analyzed in triplicate.

As can be observed in Fig. 1, below  $200 \text{ kg/m}^3$  brine concentration, samples showed an increase of moisture content, while those treated at brine concentrations above  $200 \text{ kg/m}^3$  showed a decrease. For samples brined at  $200 \text{ kg/m}^3$ , no net transport of moisture was identified. Similar results were reported by Graiver et al. (2009). From the ANOVA, it could be stated that both factors, time and brine concentration, were

**Fig. 1** Influence of brine concentration ( $\text{kg/m}^3$ ) on moisture kinetics of pork loin slices (thickness 10 mm)



significant ( $p < 0.05$ ), and from the estimation of the LSD intervals, three significantly different groups linked to treatments were identified. The samples showed a significant ( $p < 0.05$ ) water gain in the first group (brine concentrations of 50 and 100  $\text{kg/m}^3$ ), dehydration in saturated brine (280  $\text{kg/m}^3$ ), and moisture content which is not significantly different from that of fresh meat in the third group (intermediate brine concentrations: 150, 200, 240  $\text{kg/m}^3$ ).

### 3.1.2 NaCl Transport

From previous measurements, the NaCl content of fresh meat was considered negligible. The posttreatment NaCl content in meat samples was dependent on the brining time and the brine concentration (Fig. 2). As in the case of moisture content, each point shown in this figure represents the average of nine measurements; three independently brined samples were each analysed in triplicate.

The ANOVA showed brining time and brine concentration and their interaction to be significant ( $p < 0.05$ ). From the estimation of LSD intervals, the average NaCl content of samples from every brining concentration tested was found to be significantly ( $p < 0.05$ ) different, except for 200 and 240  $\text{kg/m}^3$ .

## 3.2 Mass Transfer Modelling

### 3.2.1 Water Transport

The results of fitting the diffusion model to the experimental moisture data are shown in Table 1. The low value of the percentage of explained variance

**Fig. 2** Influence of brine concentration ( $\text{kg/m}^3$ ) on NaCl kinetics of pork loin slices (thickness 10 mm)

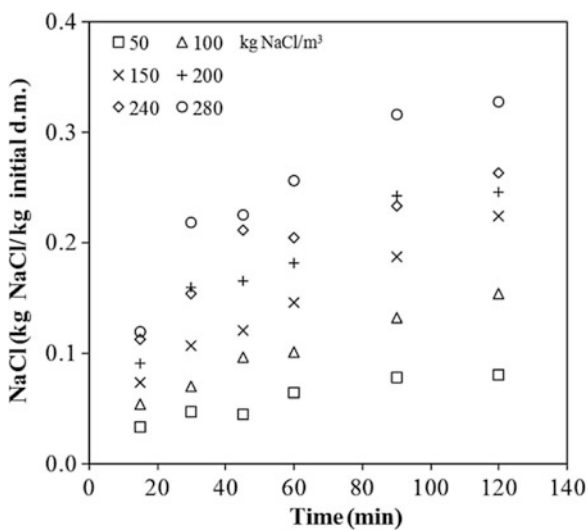


**Table 1** Effective diffusivity and percentage of explained variance for water and NaCl transport in pork meat brined in different brine concentrations ( $5 \pm 0.5^\circ\text{C}$ )

Brine concentration ( $\text{kg/m}^3$ )	Diffusivity ( $D_w$ ) ( $10^{-10} \text{ m}^2/\text{s}$ )	% VAR	Diffusivity ( $D_{\text{NaCl}}$ ) ( $10^{-10} \text{ m}^2/\text{s}$ )	% VAR
50	0.76	90.7	1.24	98.1
100	0.62	90.2	2.04	99.2
150	0.17	89.1	2.11	99.0
200	-	-	1.99	96.4
240	-1.04	81.1	1.73	96.1
280	-1.83	90.0	1.96	96.1

(81.1–90.7 %) can be linked to the great variability of the raw material. The similar trend between the experimental and calculated data (Fig. 3a) permitted the model to be considered as adequate. No fit was possible for treatments carried out at a brine concentration of  $200 \text{ kg/m}^3$  due to the fact that no net transport was identified.

The identified effective moisture diffusivity values decreased when brine concentration rose, from positive values ( $0.76 \times 10^{-10} \text{ m}^2/\text{s}$ ) at the lowest brine concentration,  $50 \text{ kg/m}^3$ , to negative ( $-1.83 \times 10^{-10} \text{ m}^2/\text{s}$ ) at the highest,  $280 \text{ kg/m}^3$ . The increase or decrease of the diffusion parameter shows the change in the direction of moisture transport. The hydration of meat samples, when treated at the lowest brine concentration tested ( $50 \text{ kg/m}^3$ ), could be attributed not only to osmotic pressure but also to the “salting in” phenomenon (Nguyen et al. 2010) produced by protein solubilization. On the other hand, dehydration of samples treated in saturated brine ( $280 \text{ kg/m}^3$ ) could also be explained by an increase in

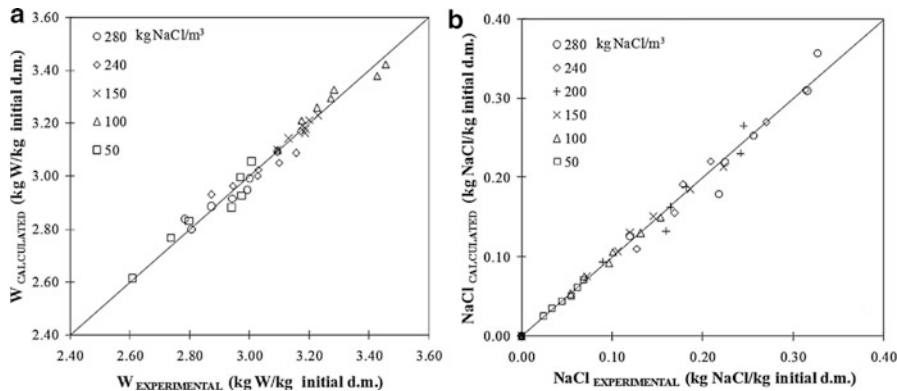


**Fig. 3** Experimental vs. calculated moisture (a) and NaCl (b) content of pork loin slices (thickness 10 mm)

the osmotic effect due to the “salting out” phenomenon (Nguyen et al. 2010) produced by the insolubilization of proteins. The variation in the effective diffusivity identified for samples treated in intermediate brine concentrations (150, 200 and 240 kg/m<sup>3</sup>) from positive to negative values could indicate the superposition of both phenomena. Thus, as brine concentration increased, the phenomenon of protein solubilization disappears and the phenomenon of protein insolubilization starts to be relevant. As this fact affected the structure of meat, the identified diffusivity was also affected.

### 3.2.2 NaCl Transport

The considered diffusion model was adequate to describe NaCl transport, as can be observed in the obtained values of the percentage of explained variance (Table 1). Moreover, the close agreement between experimental and calculated data can also be observed in Fig. 3b.

The identified effective diffusivity values were similar for all conditions tested, with an average value of  $(1.90 \pm 0.28) 10^{-10} \text{ m}^2/\text{s}$ . Because the diffusion model considers the difference of concentration to be the driving force for transport, and this variable is the only one that changes during experimentation, the identified diffusivity should be similar for every treatment (Table 1). Therefore, the identified constant value of diffusivity could indicate that although the NaCl brine concentration affected the water transport rate, NaCl diffusion was not affected by solubilization/precipitation of proteins. The values identified are similar to those reported by other authors (Wood 1966; Fox 1980; Siró et al. 2008).

## 4 Conclusions

Brine concentration had a significant effect ( $p < 0.05$ ) on water and NaCl transport during meat brining. Hydration or dehydration of samples could be achieved by using low or high brine concentrations, respectively. The more concentrated the brine, the greater the gain in NaCl. The effective diffusivity identified for moisture transport showed that the different direction of moisture transport depended on the brine concentration. The influence of NaCl concentration on the solubility of proteins and, therefore, on the water-holding capacity of meat could explain this behavior.

**Acknowledgments** This work is financed by CARNISENUSA (CSD2007-00016) included in the CONSOLIDER-INGENIO-2010.

## References

- AOAC (1997) Official method of analysis of the association of official analytical chemists international, 16th edn. AOAC, Washington, DC, 3rd revision
- Barat JM, Grau R, Ibáñez JB, Págán MJ, Flores M, Toldrá F, Fito P (2006) Accelerated processing of dry-cured ham. Part I. Viability of the use of brine thawing/salting operation. *Meat Sci* 72(4):757–765
- Cárcel JA, Benedito J, Bon J, Mulet A (2007a) High intensity ultrasound effects on meat brining. *Meat Sci* 76:611–619
- Cárcel JA, Benedito J, Rosselló C, Mulet A (2007b) Influence of ultrasound intensity on mass transfer in apple immersed in a sucrose solution. *J Food Eng* 78:472–479
- Fox JB (1980) Diffusion of chloride, nitrite and nitrate in beef and pork. *J Food Sci* 45:1740–1744
- García-Pascual P, Sanjuán N, Melis R, Mulet A (2006) *Morchella esculenta* (morel) rehydration process modelling. *J Food Eng* 72:346–353
- Graiver N, Pinotti A, Califano A, Zaritzky N (2006) Diffusion of sodium chloride in tissue. *J Food Eng* 77:910–918
- Graiver N, Pinotti A, Califano A, Zaritzky N (2009) Mathematical modeling of the uptake of curing salts in pork meat. *J Food Eng* 95:533–540
- Lambert IH, Nielsen JH, Andersen HJ, Ortenlund N (2001) Cellular model for induction of drip loss in meat. *J Agr Food Chem* 49:4876–4883
- Nguyen MV, Arason A, Thorarinsdottir KA, Thorkelsson G, Gudmundsdóttir A (2010) Influence of salt concentration on the salting kinetics of cod loin (*Gadus morhua*) during brine salting. *J Food Eng* 100:225–231
- Siró I, Vén C, Balla C, Jónás G, Zeke I, Friedrich L (2008) Application of an ultrasonic assisted curing technique for improving the diffusion of sodium chloride in porcine meat. *J Food Sci* 91:353–362
- Wood FW (1966) The diffusion of salt in pork muscle and fat tissue. *J Sci Food Agr* 17:138–140

# **Relationship Between Electrical Conductivity and Water Activity of Starch-Water Composites**

**E. Morales-Sánchez, M.L. Reyes-Vega, M. Gaytán-Martínez,  
J.D. Figueiroa-Cárdenas, and G. Velázquez**

## **Abbreviations**

$a_w$	Water activity
DSC	Differential scanning calorimeter
ANOVA	Analysis of variance
EC	Electrical conductivity

## **1 Introduction**

When electrical conductivity (EC) is studied in food hydrocolloids, such as starch, molecular structure is important because conductivity depends on the interaction of water with charged carboxyl group or hydroxyl groups (Marcotte et al. 1998). Several authors have found that EC of starch-water composites increases with temperature and decreases during starch gelatinization (Wang and Sastry 1997; Karapantsios et al. 2000; Fa-De Li et al. 2004). This behavior is explained considering granule

---

E. Morales-Sánchez (✉) • G. Velázquez  
CICATA-IPN Querétaro, Cerro Blanco 141, Querétaro ZP 76090, México  
e-mail: [emoraless@ipn.mx](mailto:emoraless@ipn.mx)

M.L. Reyes-Vega  
CICATA-IPN Querétaro, Cerro Blanco 141, Querétaro ZP 76090, México

UAC, Posgrado en Alimentos, Venustiano Carranza s/n, Saltillo ZP 25280, México

M. Gaytán-Martínez  
Universidad Autónoma de Querétaro, Cerro de las campanas s/n Querétaro ZP 76010, México

J.D. Figueiroa-Cárdenas  
CINVESTAV del IPN Unidad Querétaro, Querétaro ZP 76230, México

swelling, increase of viscosity, and reduction of the area for starch particle movement. Decreasing water content in the material decreases EC (Lewicki Piotr 2004).

All of these works have shown the important role of water on EC of foods and particularly on starchy foods. It is known that water is contained in composites as free water or as bound water, and one way to determine the state of water is to measure the water activity (Fennema 1985). In spite of abundant reported works about EC in food material, no studies relating water activity with EC were found in literature, with the exception of a brief report by Lewicki Piotr (2004).

The present work studies the relationship among electrical conductivity, water activity, and enthalpy of maize, potato, and rice starch-water composites heated at different temperatures.

## 2 Materials and Methods

Corn, rice, and potato starches (Sigma Chemical Co.) were used as study systems. The materials were suspended at different starch-water ratios (30:70, 50:50, and 70:30 w/w). Water activity ( $a_w$ ) was measured using an AquaLab® model C2 (Decagon Devices, Inc. Pullman, USA) at room temperature.

Electrical conductivity was measured using a self-designed resistive heating system (Morales-Sánchez et al. 2009) composed of a resistive heating cell, a type T thermocouple, a Watlow ramp-programmable temperature controller (Model 981, Watlow Electric Manufacturing Co., St. Louis, MO), an HP 34410A 6½ digital multimeter (Agilent Technologies), and a PC computer. Heating rate program was set at 5 °C/min, and the studied temperature range was from 30 to 90 °C to avoid boiling of water.

A differential scanning calorimeter (DSC Mettler® Toledo model 821e) equipped with a thermal analysis data station was used. The samples were heated in a 40 µL pan from 30 to 90 °C at a rate of 5 °C/min. Enthalpy was computed automatically in duplicated samples.

Data were analyzed using analysis of variance (ANOVA) procedures. Means were compared using Tukey's test ( $P = 0.05$ ). Statistical analyses were performed using SAS software. Pearson's correlation coefficient between EC,  $a_w$ , and enthalpy were determined.

## 3 Results and Discussion

Table 1 shows the electrical conductivity, water activity, and enthalpy of corn, potato, and rice starch-water composites at 50:50 w/w and 25 °C.

Rice starch showed higher electrical conductivity than cornstarch, and the latter was higher than that for potato starch; the same order was observed in water activity values. Cornstarch had the minimum water activity value, indicating that this type of starch establishes stronger interactions with water than the other two; it also has the minimum enthalpy value. Rice and potato starches had no significant ( $P > 0.05$ )

**Table 1** Electrical conductivity, water activity, and enthalpy of [starch-water] composites for corn, potato, and rice at 50:50 w/w and 25 °C

Starch	EC (S/m)	$a_w$	Enthalpy (J/g)
Corn	0.25178 <sup>c</sup>	0.965 <sup>b</sup>	2.04 <sup>b</sup>
Potato	0.29969 <sup>b</sup>	0.974 <sup>a</sup>	4.00 <sup>a</sup>
Rice	0.99639 <sup>a</sup>	0.973 <sup>a</sup>	2.38 <sup>b</sup>

Different letters in the same column indicate significant difference ( $P < 0.05$ )

EC electrical conductivity,  $a_w$  water activity

**Table 2** Effect of [starch-water] ratio on the electrical conductivity, water activity, and enthalpy of cornstarch at 25 °C

Starch-water	EC (S/m)	$a_w$	Enthalpy (J/g)
30:70	0.88861 <sup>a</sup>	0.976 <sup>a</sup>	2.99 <sup>b</sup>
50:50	0.65208 <sup>b</sup>	0.972 <sup>b</sup>	2.52 <sup>b</sup>
70:30	0.00717 <sup>c</sup>	0.964 <sup>c</sup>	2.14 <sup>a</sup>

Different letters in the same column indicate significant difference ( $P < 0.05$ )

differences in water activity and enthalpy values. However, electrical conductivity is significantly ( $P < 0.05$ ) different when the effect of the type of starch is considered, meaning that electrical conductivity has other influencing factors besides starch-water ratio, i.e., ions content. In the same way, water activity and enthalpy were influenced by the kind of starch, as shown in Table 1.

It must be taken into account that starches from different cereals have not the same structure, size, or behavior: with regard to the starch granule size, rice starch granules are the smallest and potato starch granules are the largest, while corn has both small and large starch granules; thus, electrical conductivity and water activity must be influenced by starch granule size and shape.

Table 2 shows the effect of starch-water ratio on the EC,  $a_w$ , and enthalpy of cornstarch at 25 °C. It can be observed that 70:30 maize starch-water composites had a higher electrical conductivity than 50:50 and 30:70 composites. Water activity was higher at high moisture content and decreased when water ratio decreased. Enthalpy is also related with water content. Data show that electrical conductivity had a direct relationship with water activity, and water content is the main factor.

Table 3 shows the electrical conductivity, water activity, and enthalpy of 30:70 w/w corn [starch-water] composites at different temperatures. EC and  $a_w$  increased linearly until gelatinization as a function of temperature. Wang and Sastry (1997) and Fa-De Li et al. (2004) attribute the change in electrical conductivity to the gelatinization phenomenon, which requires water. Electrical conductivity increases in a linear way with temperature, but when temperature reaches 70 °C (gelatinization temperature for cornstarch), the granule breaks down, collapsing its molecular alignment and generating other conduction mechanisms involving new hydrogen bonds that increase conductivity (Fa-De Li et al. 2004; Saiwarun Chaiwanichsiri et al. 2001). This phenomenon is associated with water activity, and data from this work show a linear relationship between electrical conductivity and water activity

**Table 3** Electrical conductivity, water activity, and enthalpy of 30:70 w/w corn [starch-water] composites at different temperatures

Temperature (°C)	EC (S/m)	$a_w$	Enthalpy (J/g)
55	0.424 <sup>d</sup>	0.972 <sup>ab</sup>	3.46 <sup>b</sup>
60	0.459 <sup>d</sup>	0.973 <sup>a</sup>	4.73 <sup>a</sup>
65	0.495 <sup>c</sup>	0.971 <sup>ab</sup>	3.36 <sup>b</sup>
70	0.541 <sup>b</sup>	0.973 <sup>a</sup>	2.32 <sup>c</sup>
75	0.575 <sup>ab</sup>	0.970 <sup>b</sup>	2.33 <sup>c</sup>
80	0.601 <sup>a</sup>	0.966 <sup>c</sup>	1.45 <sup>d</sup>

Different letters in the same column indicate significant difference ( $P < 0.05$ )

before gelatinization. However, gelatinization, electrical conductivity, and water activity have different mechanisms. After gelatinization, electrical conductivity has new hydrogen bonds available and the number of free water molecules decreases. Then, water activity decreases after gelatinization by water scarcity.

## 4 Conclusions

The importance of the role of water on electrical conductivity of starch-water composites has shown the positive relationship between electrical conductivity and water activity. The gelatinization process diminishes both electrical conductivity and water activity, due to the molecular rearrangement in the composite; this phenomenon was evident in enthalpy values calculated from DSC data, which had a positive relationship with water activity and a negative relationship with electrical conductivity. Starch source was also important because of differences in granule size; rice starch had a higher electrical conductivity than corn and potato starches and the smallest starch granules. It was also shown that the highest electrical conductivity was noted for starch-water ratio, as the highest electrical conductivity was registered for the highest starch-water ratio.

**Acknowledgements** The authors want to thank CONACyT and IPN for their financial support through project SIP-20090967 and SIP 20100209.

## References

- Fennema OR (1985) Food chemistry, 2nd edn. Marcel Dekker Inc., New York, pp 46–50
- Karapantsios TD, Sakonidou EP, Raphaelides SN (2000) Electrical conductance study of fluid motion and heat transport during starch gelatinization. J Food Sci 65(1):144–150
- Lewicki Piotr P (2004) Water as a determinant of food engineering properties. A review. J Food Eng 61:483–495
- Fa-De Li, Li-Te Li, Zaigui Li, Eizo Tatsumi (2004) Determination of starch gelatinization temperature by ohmic heating. J Food Eng 62:113–120

- Marcotte M, Piette JPG, Ramaswamy HS (1998) Electrical conductivities of hydrocolloid solutions. *J Food Eng* 21:503–520
- Morales-Sánchez E, Vazquez-Landaverde P, Gaytan-Martínez M, Huerta-Ruelas JA (2009) Electrical conductivity of heated corn starch water mixtures. *J Food Proc Eng* 32:817–827
- Saiwarun Chaiwanichsiri, Shigehiko Ohnishi, Toru Susuky, Rikuo Takai, and Osato Miyawaki (2001) Measurements of electrical conductivity, differential scanning calorimetry and viscosity of starch and flour suspensions during gelatinization process. *J Sci Food Agric* 81:1586–1591
- Wang W, Sastry SK (1997) Changes in electrical conductivity of selected vegetables during multiple thermal treatments. *J Food Proc Eng* 20:499–516

# **Water Content, $a_w$ , and Enzyme Activity (Xaa-Prolyl-Dipeptidyl Aminopeptidase) During the Germination Process of Cocoa Beans (*Theobroma cacao* L.)**

**M.L. Sánchez-Mundo, M.X. Quintanilla-Carvajal, C. Bautista-Muñoz,  
G.F. Gutiérrez-López, and M.E. Jaramillo-Flores**

## **Abbreviations**

Ala-Pro-pNA	Alanine-proline- <i>p</i> -nitroanilide
$a_w$	Water activity
CP	Carboxypeptidases
DCP	Dry cacao powder
PVPP	Polyvinylpolypyrrolidone
<i>U</i>	One unit of enzyme
<i>X</i>	Water content
Xaa-Pro-DAP	Xaa- <i>prolyl</i> -dipeptidyl-peptidase

## **1 Introduction**

### **1.1 Germination Process of Cacao Seeds**

Cacao seeds demonstrate epigeal (or epigeous) germination in which the hypocotyl elongates and forms a hook, pulling rather than pushing the cotyledons and apical meristem through the soil. Once it reaches the surface, it straightens and pulls the

---

M.L. Sánchez-Mundo • M.X. Quintanilla-Carvajal • G.F. Gutiérrez-López  
M.E. Jaramillo-Flores (✉)

Departamento de Graduados e Investigación en Alimentos, Escuela Nacional de Ciencias Biológicas-Instituto Politécnico Nacional, Carpio y Plan de Ayala s/n, Col. Santo Tomás, Miguel Hidalgo, C.P. 11340, México, D.F., Mexico  
e-mail: [jaramillo\\_flores@hotmail.com](mailto:jaramillo_flores@hotmail.com)

C. Bautista-Muñoz  
Laboratorio de Fisiología Vegetal y Biotecnología, Colegio de Posgraduados, Campus Tabasco, Periférico Carlos A. Molina s/n, C.P. 86500, Cárdenas, Mexico

cotyledons and shoot tip of the growing seedlings above the ground (Bewley 1997). After the cocoa seeds are removed from the fruit they germinate rapidly, 4–6 days after planting. The root and the hypocotyle emerge first, which causes the cotyledons to elevate above the substrate (10 or 15 days after planting). The cotyledons then open and expose the plumule, which begins to grow at the same time as the root, but it is much smaller. The first phase of growth is completed with the maturation of the first leaves (López-Andrade 2003). This means that germination commences with the uptake of water by dry seed imbibition and is completed when a part of the embryo, usually the radicle, extends to penetrate the structures that surround it (Bewley 1997).

## 1.2 *Stages of the Germination Process*

Water is the principal factor in germination stages. Uptake of water by a mature dry seed is developed in three phases, with a rapid initial uptake (imbibition) followed by a plateau phase (metabolic activation). A further increase in water uptake occurs only after germination is completed, as the embryonic axes elongate. Because dormant seeds do not complete germination, they cannot enter to the third phase (i.e., growth of the radicle).

*Phase I: Imbibition.* Important structural alterations are temporarily produced with the entrance of water into the seed, especially at the membrane level. In the dry seed, phospholipids of the membrane are presented as a gel, which lead to a rapid leakage of solutes and low-molecular-weight metabolites into the surrounding imbibition solution. Nevertheless, with re-hydration, the membranes return to crystalline hydrous status, a stable condition, at which time solute leakage is curtailed. The rehydration allows turnover or replacement of components occurring over several hours as full metabolic status is achieved (Bewley 1997).

*Phase II: Metabolic activation.* During this phase, the synthesis occurs. All of the components necessary for the resumption of protein synthesis upon imbibition are present. In the case of reserve proteins, these components are reduced to amino acids and peptides due to exopeptidases (carboxypeptidase) and endopeptidases. These enzymes break down the peptides to produce small polypeptides, which are degraded by a group of enzymes known as peptide hydrolases to produce amino acids (Herrera 2006).

*Phase III: Growth of the radicle.* Finally, radicle extension through the structures surrounding the embryo is the event that terminates germination and indicates the beginning of seedling growth (Bewley 1997).

### 1.3 Relations Between Moisture, Water Activity, and Enzymatic Activity

Seed germination depends on both internal and external conditions. The most important external factors include temperature, water, oxygen, and sometimes light or darkness. In the absence of any of these factors, most seeds remain in a quiescent state, even without a rest state. In the case of recalcitrant seeds, such as cocoa, there can be a rapid decline in seed longevity. The entry of water into the seed is due to a difference in water potential between the seed and the surrounding environment. Normally, the water potential is lower in dry seeds than in the external environment. Therefore, until the radicle emerges, water reaches the embryo through the cell walls of the seed coat. Although water is necessary for the rehydration of seeds, an excess of water can adversely affect germination, as well as hinder the delivery of oxygen to the embryo (Herrera 2006; Vashisth and Nagarajan 2010).

### 1.4 Xaa-Pro-DAP Activity in Cacao (*Theobroma cacao L.*)

*Theobroma cacao L.* has been described as a plant whose seed contains vicilin-class globulin, but not legumin, as vacuolar storage protein (Voigt et al. 1993). Proteolysis is initiated by an endopeptidase with high specificity for seed reserve proteins, which would be degraded partially as a consequence of the rupture of some specific peptide bonds. The resulting polypeptide chains from this action would then be apt for the action of endopeptidases that had remained inactive, and, eventually, for the action of carboxypeptidases (CP) (Abecia-Soria et al. 2005; Donaevsky et al. 1989). Among cacao proteins, proline content (0.72–1.97 g/100 g of cacao) stands out, and because of its specific conformation it possesses many restrictions on the structural aspects of peptides and proteins, and grants particular biological properties to a large range of physiologically important biomolecules (Kalvatchev et al. 1998; Kratzer et al. 2009). In contrast to the abundant reports regarding Xaa-prolyl-dipeptidyl-peptidase (Xaa-Pro-DAP) [EC 3.4.14.5] in lactic acid bacteria, there are few reports on this enzyme in plants (Besanova et al. 1987; Stano et al. 1994, 1997; Davy et al. 2000), and given the aforementioned proline content, this is one of the first works in regard to the Xaa-Pro-DAP activity in cacao.

## 2 Methods

### 2.1 Seed Material and Growth Conditions

Cacao (*Theobroma cacao* L.) seeds of the white almond criollo genotype, cultivated in the municipality of Cunduacan, state of Tabasco, Mexico, were used as study material. For analysis and preparation, only cotyledons were used. Mucilage was removed from seeds and these were placed in wet agrolite to germinate at 30 °C for 15 days (Sánchez-Mundo et al. 2010). Germinated seeds were collected every 24 h during all germinating processes. Water content ( $X$ ), enzymatic activity (Xaa-Pro-DAP), and water activity ( $a_w$ ) of germinating cocoa beans were monitored for 15 days.

### 2.2 Moisture content ( $X$ )

Seed water content ( $X$ ) was measured in triplicate by drying seeds at 100 °C for 2 h, according to international standards (International Seed Testing Association 1999) using a thermobalance (Brainweigh, model MB300, USA) until constant weight (Nollet 1996). Results are expressed on a dry-weight basis.

### 2.3 Water Activity ( $a_w$ )

The water activity of 2 g of seeds at different states was measured using an AquaLab 4TE water activity meter (Model 3TE, Decagon Devices, USA), which measures the dew point of the vapor phase in equilibrium with a bulk solution of known concentration in a sealed chamber according to AOAC Method 978.18 (2005), following the manufacturer's specifications (Vashisth and Nagarajan 2010).

### 2.4 Dry Cacao Powder

Dry cacao powder (DCP) was obtained according to the method described by Hansen et al. (1998).

## 2.5 Enzyme Extract

The enzyme extract was obtained from 15 mg of DCP and 30 mg of polyvinylpolypyrrolidone (PVPP) in 900  $\mu\text{l}$  of 0.1 M phosphate buffer (pH 7.0) containing 1 % Triton X-100. The mixture was stirred for 30 min at 37 °C and then centrifuged at 20,000  $\text{g}$  for 10 min at 4 °C.

## 2.6 Determination of Xaa-Pro-DAP Activity

The colorimetric *p*-nitroanilide substrate (Bachem, Bubendorf, Switzerland) alanine-proline-*p*-nitroanilide (Ala-Pro-*p*NA) at 10 mM was selected for analyzing Xaa-Pro-DAP activity during 15 days of germination process (Mercado-Flores et al. 2004; Sánchez-Mundo et al. 2010). One unit of enzyme (*U*) was defined as the amount of enzyme that liberates 1  $\mu\text{mol}$  of *p*-nitroaniline per minute at 37 °C.

## 3 Results and Discussion

### 3.1 Relation of Moisture, Water Activity, and Enzymatic Activity During Germination Cacao Process

During the study, three stages of germination with presence of peaks of water content and enzyme activity were observed (Fig. 1a, b): I. The first stage (1–7 days of germination), in which values of water contents (0.58  $\text{gH}_2\text{O/g ds}$ ) were detected: In this period, it was observed that starting from the third day of imbibition of the seed, the cotyledons emerged from substrate due to the growth of the hypocotyle. In addition, the white color disappeared from the seed, and clear green color was seen (Fig. 1a). These changes are attributed to the differentiation of the chloroplast in the cotyledons, transforming them in photosynthetic organs acting as leaves, corresponding to the epigeal germination type which presents the cacao (Herrera 2006). In day 7, at the end of stage I, the lowest levels in moisture (0.28  $\text{gH}_2\text{O/g ds}$ ) and water activity (0.9695) were identified; however, this amount was sufficient to continue the germination process. On the other hand, the enzymes also began to increase in activity (3.55 U). This phenomenon was more evident in the next few days.

II. In the second stage (II), during 8–10 days of germination, an increment of the enzymatic activity was detected, specifically on day 10 of the process, with 13 U of Xaa-Pro-DAP activity coinciding with the maximum value of water content and water activity, 1.32  $\text{gH}_2\text{O/g ds}$  and 0.98, respectively (Fig. 1b). These results indicate that, according to the germination conditions of this specific cacao criollo type, at day 10 exists a proteolytic activity stimulated by moisture and water content

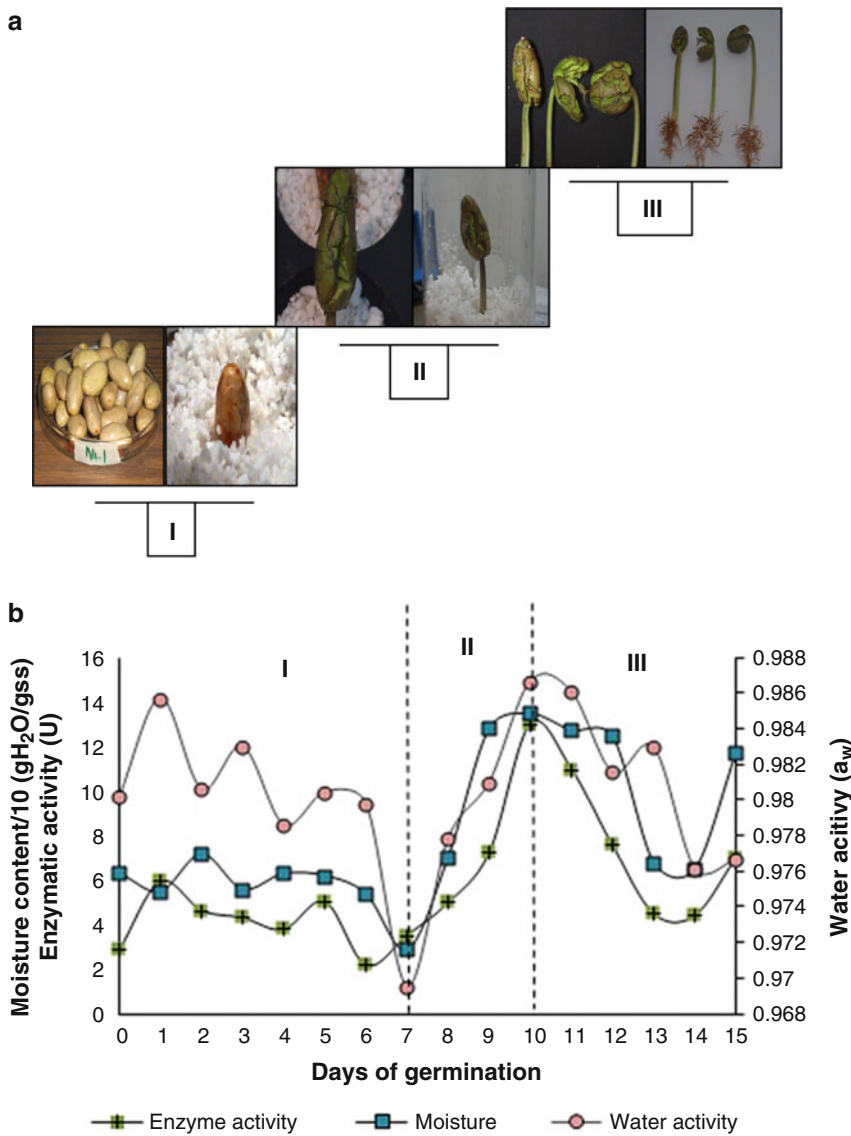


**Fig. 1** (a) Visible changes during germination process of cacao criollo seeds during 15 days. (b) Graphic representation of Xaa-Pro-DAP enzymatic activity profile, moisture content, and water activity

levels available for the reactions of the germinating process (Sánchez-Mundo et al. 2010). These results can be related to the reports by Biehl et al. (1982), in which the authors found by electron microscopy that drastic changes in protein vacuoles took place after 10–13 days of germination of cocoa seeds. During this period, protein vacuoles were inflated and fused to form one central vacuole, which appeared optically empty. Radicule penetrates the cotyledon and/or ruptures it, giving place to the growth of the epicotyl.

A third stage (III) was detected within days 11–15 of germination, in which a decrease in enzymatic activity (4.44 U) and water content (0.96 g H<sub>2</sub>O/g ds) was observed, and the development of the epicotyl is seen. Finally, on day 15, enzymatic activity and water content increased significantly, possibly due to the onset of the ensuing process of plantule development, which coincides with the appearance of the first leaves (Fig. 1a, b).

It is noteworthy that enzyme activity and water content concurrently showed maximum and minimum values during the entire germination process, which may indicate the existence of different levels of water-protein interactions (Bewley 1997). According to the results of this study, the fact that major levels of Xaa-Pro-DAP activity was observed during the last stage of germination suggests that enzymes with other peptidases play a possible role in the degradation of reserve proteins during the germination of cocoa beans taking part in the mobilization of necessary amino acids in embryo growth process; this phenomenon has also been attributed to other plants (Ramakrishna 2007). While this final stage corresponds to the initiation of morphologic visible changes, such as elongation of the embryonic axis and emergence of the radicule, the enzyme may be involved in the development of the plant and can be expressed in other organs.

## References

- Abecia-Soria p, Pezoa-García NH, Amaya-Farfan J (2005) Soluble albumin and biological value of protein in cocoa (*Theobroma cacao* L.) beans as a function of roasting time. *J Food Sci* 70 (4):294–298
- Anonymous (1999) International Seed Testing Association (ISTA). International rules for seed testing. *Seed Sci Technol* 27(Suppl): 27–32
- AOAC (2005) Official methods of analysis of AOAC international, 18th ed. Method No. 978.18
- Besanova M, Kovacs P, Psenak M, Barth A (1987) Dipeptidyl peptidase of poppy seedlings. *Biologia* 42:779–787
- Bewley DJ (1997) Seed germination and dormancy. *Plant Cell* 9:1055–1066
- Biehl B, Wewetzer C, Passern D (1982) Vacuolar (storage) proteins of cocoa seeds and their degradation during germination and fermentation. *J Sci Food Agric* 33:1291–1304
- Davy A, Thomsen KK, Juliano MA, Alves LC, Svendsen I, Simpson DJ (2000) Purification and characterization of barley dipeptidyl peptidase IV. *Plant Physiol* 122:425–431
- Donaevsky YE, Sarbakanova ST, Belozersky MA (1989) Wheat seed carboxypeptidase and joint action on gliadin of proteases from dry and germinating seeds. *J Exp Bot* 40:1323–1329
- Hansen CE, del Olmo M, Burri C (1998) Enzyme activities in cocoa beans during fermentation. *J Sci Food Agric* 77:273–281

- Herrera J (2006) Germinación y crecimiento de la planta. Editorial Universidad de Costa Rica, Costa Rica
- Kalvatchev Z, Garzaro D, Guerra F (1998) *Theobroma cacao L.*: Un nuevo enfoque para nutrición y salud. *Agroaliment* 4(6):23–25
- Kratzer U, Frank R, Kalbacher H, Biehl B, Wöstemeyer J, Voigt J (2009) Subunit structure of the vicilina-like globular storage protein of cocoa seeds and the origin of cocoa- and chocolate-specific aroma precursors. *Food Chem* 113:903–913
- López-Andrade P (2003) El cacao (*Theobroma cacao L.*) en Tabasco INIFAP-Huimanguillo, México 1–10
- Mercado-Flores Y, Noriega-Reyes Y, Ramírez-Zavala B, Hernández-Rodríguez C, Villa-Tanaca L (2004) Purification and characterization of aminopeptidase (pumAPE) from *Ustilago maydis*. *FEMS Microbiol Lett* 234:247–253
- Nollet LM (1996) Handbook of food analysis. Marcel Dekker Inc., New York
- Ramakrishna V (2007) Mobilization of albumins and globulins during germination of Indian bean (*Dolichos lablab L. var. lignosus*) seeds. *Acta Bot Croat* 66(2):135–142
- Sánchez-Mundo M, Bautista-Muñoz C, Jaramillo-Flores ME (2010) Characterization of the exopeptidase activity existing in *Theobroma cacao L.* *Process Biochem* 45(7):1156–1162
- Stano J, Kovács P, Nemec P, Neubert K (1994) Dipeptidyl peptidase IV in gherkin seedlings *Cucumis sativus L. cv. Pálava*. *Biol* 49:905–910
- Stano J, Kovács P, Psenak M, Gajdos J, Erdelsky K, Kákoniová D, Neubert K (1997) Distribution of dipeptidyl peptidase IV in organ tissue cultures of poppy plants *Papaver somniferum L.* *Pharmazie* 52:319–321
- Vashisth A, Nagarajan S (2010) Characterization of water distribution and activities of enzymes during germination in magnetically-exposed maize (*Zea mays L.*) seeds. *Indian J Biochem Biophys* 47:311–318
- Voigt J, Biel B, Wazir SKS (1993) The major seed proteins of *Theobroma cacao L.* *Food Chem* 47:145–151

# Water Fraction Effect in the Rheological Behavior of Jalapeño Pepper Pulp

F. Santoyo, J. Viganó, and J. Telis-Romero

## Abbreviations

$K$	Consistency index
$n$	Flow behavior index
$r^2$	Coefficient of determination
$\gamma$	Shear rate
$\eta_\infty$	High shear rate-limiting viscosity
$\sigma$	Shear stress
$\sigma_0$	Yield-stress parameter

## 1 Introduction

Chili (*Capsicum annuum*) is a spice-cum-vegetable of commercial importance. It is produced mainly in India, China, Mexico, and Southeast Asia, while the fruits are used in cuisines throughout the world (Ahmed et al. 2000) due to their color, flavor, and pungency. Hot peppers are widely produced and consumed in Mexico as raw, cooked, or processed products. Hot peppers are known to be good sources of different phytochemicals, including vitamins A and C, phenolic compounds, flavonoids, and carotenoids, among others (Topuz and Ozdemir 2007; Chuah

---

F. Santoyo

Departamento de Ciencias Exactas, Tecnologías y Metodologías, CUSur, Universidad de Guadalajara, Ciudad Guzmán, Guadalajara, Jalisco, Mexico

J. Viganó • J. Telis-Romero (✉)

Departamento de Engenharia e Tecnologia de Alimentos, Universidade Estadual Paulista, São José do Rio Preto, São Paulo, Brazil  
e-mail: [javier@ibilce.unesp.br](mailto:javier@ibilce.unesp.br)

et al. 2008). It has been estimated that hot peppers are the second most consumed vegetable by the Mexican population, after tomatoes. Approximately 75 % is consumed as fresh product for the preparation of different dishes. Other commonly consumed presentations of hot peppers include pickled, dried, and smoked, and in sauces. There are several varieties of hot peppers consumed in Mexico; two of the most popular varieties are jalapeño and serrano, in both fresh and processed forms (Álvarez-Parrilla et al. 2011).

Fresh spice vegetables, such as hot peppers, are mainly processed to obtain dehydrated products. The distinct aromatic odor, color, and pungency are seldom carried over to the processed products (Giridhar et al. 1996). The chemicals responsible for the delicate odors and attractive colors of spice vegetables are highly heat sensitive and are lost during dehydration (Pezzutti and Crapiste 1997). Spice-vegetable pulps, classified as minimally processed food (King and Bolin 1989), could serve the purpose by retaining the fresh spice odor in a form acceptable to consumers (Baranowski 1985).

During production, the vegetable pulps industry deals with a variety of concentrations of water and temperatures, with pulps being submitted to unit operations such as pumping, heat exchange, evaporation, and spray-drying, drum-drying, or freeze-drying. In order to allow adequate process design, operation, and control, knowledge of the rheological behavior of the vegetable pulps as affected by water fraction and temperature is of fundamental importance.

Several works are available concerning the influence of particle size and temperature on the rheology of green chili puree (Ahmed et al. 1999, 2000; Cepada and Gómez 2002). On the other hand, there is little information on the rheological parameters of pepper pulp under different conditions of water fraction. Under these considerations, the main purpose of this work was to determine rheological properties of jalapeño pepper pulp, as well as to develop simple correlations for predicting these properties under different conditions of water fraction.

## 2 Rheological Properties

The flow properties of pulp and puree are essential for the design and evaluation of food processing equipment. Rheological studies would provide information on how best to control the flow properties of the product. In addition, knowledge of the rheology of some suspensions also contributes to a better understanding of underlying mechanisms of momentum and heat transfer process.

In this chapter, results of investigations in rheology of jalapeño pepper pulp are presented. The pepper pulp was prepared at different water fractions, from 0.54 to 0.76. In order to obtain the experimental data of the jalapeño pepper pulp, rheological tests were carried out using a rheometer, AR-2000EX (TA Instruments, Delaware, USA), with concentric cylinder geometry under controlled shear rate and temperature. Flow curves were obtained in duplicate with shear rate ramps from 1 to 442 s<sup>-1</sup>, at a temperature of 30 °C.

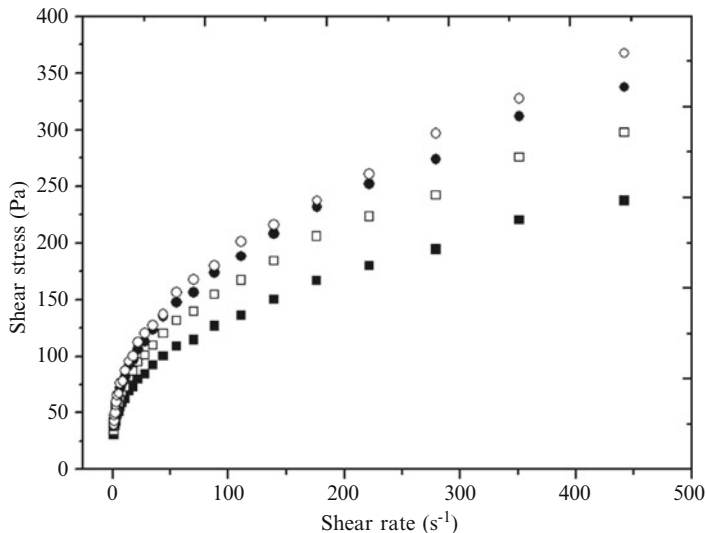


**Fig. 1** Flow curves of jalapeño pepper pulp at 30 °C and different water fraction (water fraction: filled square = 0.76; open square = 0.68; filled circle = 0.61; open circle = 0.54)

The flow curves of jalapeño pepper pulp at 30 °C and different water fraction are shown in Fig. 1. The points of each curve represent the average of the duplicates. The effect of the shear rate and water fraction in shear stress can be clearly observed. The shear stress increased with increasing shear rate and decreasing water fraction. In addition, we can see that the flow curves indicate a non-Newtonian fluid with pseudoplastic behavior.

## 2.1 Empirical Non-Newtonian Models

Flow curve modelling is interesting because simple equations are able to describe the shear stress behavior of a fluid when different strain rates are applied. To describe the shear stress ( $\sigma$ )–shear rate ( $\dot{\gamma}$ ) dependence of the jalapeño pepper pulps, a number of empirical rheological models were tested. The two-parameter power law, Casson and Bingham plastic, and the three-parameter Herschel-Bulkley and Sisko models were tested. These are given by the following equations:

Power law

$$\sigma = K \dot{\gamma}^n \quad (1)$$

Casson

$$\sqrt[2]{\sigma} = \sqrt[2]{\sigma_0} + K \sqrt[2]{\dot{\gamma}} \quad (2)$$

Bingham plastic

$$\sigma = \sigma_0 + K\dot{\gamma} \quad (3)$$

Herschel-Bulkley

$$\sigma = \sigma_0 + K\dot{\gamma}^n \quad (4)$$

Sisko

$$\sigma = \eta_\infty \dot{\gamma} + K\dot{\gamma}^n \quad (5)$$

In Eqs. (1)–(5)  $\sigma$  is the shear stress,  $\dot{\gamma}$  is the shear rate,  $K$  is the consistency index,  $n$  is the flow behavior index,  $\sigma_0$  is the yield-stress parameter, and  $\eta_\infty$  is the high shear rate-limiting viscosity.

This investigation provided important values for the process and facilitating the marketing of jalapeño pepper pulp for export and internal consumption. Fitted rheological models for the dependence of shear rate on shear stress and for the dependence of the obtained rheological parameters on water fraction were obtained by nonlinear estimation procedure from Statistica 8, minimizing the sum of squared errors. The suitability of the equations was evaluated by the coefficient of determination ( $r^2$ ).

Table 1 shows the obtained parameters and coefficients of determination of the fits. Based on the coefficient of determination, the better models to describe the flow curves of jalapeño pepper pulp, at 30 °C and in the range of studied water fraction, are power law, Herschel-Bulkley, and Sisko model ( $r^2 > 0.995$ ). However, among these three models, the Herschel-Bulkley and Sisko models are more appropriate, because they present coefficient of determination very close to unity ( $r^2 > 0.999$ ), and the Herschel-Bulkley model is widely used to describe fluid foods that present yield stress.

The presence of yield stress, which represents a finite stress required to achieve flow, is an important characteristic of the Herschel-Bulkley plastic material. Below the yield stress, a material exhibits solid-like characteristics; that is, it stores energy and does not level out under the influence of gravity to form a flat surface. This characteristic is very important in process design and quality assessment for materials (Steffe 1996) such as pepper pulp.

Results of some research have also shown that pepper purées presented pseudoplastic behavior. However, the power law model was fitted to experimental data only, which presented good coefficient of determination results. Cepada and Gómez (2002) fitted the power law model to experimental data of purée of three

**Table 1** Variation of the five model parameters with the water fraction for jalapeño pepper pulp

Water fraction	Model	Parameter <sup>a</sup>		$r^2$	Water fraction	Model	Parameter <sup>a</sup>		$r^2$	
0.76	Power law	$K$	26.557	0.997	0.61	Power law	$K$	32.717	0.997	
		$n$	0.356				$n$	0.379		
	Casson	$\sigma_0$	59.025	0.902		Casson	$\sigma_0$	76.958	0.910	
		$K$	0.697				$K$	0.840		
	Bingham plastic	$\sigma_0$	59.025	0.902		Bingham plastic	$\sigma_0$	76.958	0.910	
		$K$	0.486				$K$	0.705		
	Herschel-Bulkley	$\sigma_0$	15.566	0.999		Herschel-Bulkley	$\sigma_0$	19.243	0.999	
		$K$	16.906				$K$	21.466		
		$n$	0.422				$n$	0.442		
	Sisko	$\eta_\infty$	0.110	0.999		Sisko	$\eta_\infty$	0.162	0.999	
		$K$	29.983				$K$	37.289		
		$n$	0.304				$n$	0.325		
0.68	Power law	$K$	29.625	0.997	0.54	Power law	$K$	33.233	0.995	
		$n$	0.375				$n$	0.387		
	Casson	$\sigma_0$	68.975	0.907		Casson	$\sigma_0$	79.673	0.920	
		$K$	0.788				$K$	0.870		
	Bingham plastic	$\sigma_0$	76.958	0.910		Bingham plastic	$\sigma_0$	79.673	0.920	
		$K$	0.705				$K$	0.757		
	Herschel-Bulkley	$\sigma_0$	16.437	0.999		Herschel-Bulkley	$\sigma_0$	23.860	0.999	
		$K$	19.874				$K$	19.756		
		$n$	0.435				$n$	0.466		
	Sisko	$\eta_\infty$	0.134	0.999		Sisko	$\eta_\infty$	0.225	0.999	
		$K$	33.439				$K$	39.695		
		$n$	0.324				$n$	0.313		

<sup>a</sup>In this work,  $K$  is in Pa s<sup>n</sup>,  $\eta_\infty$  is in Pa s,  $\sigma_0$  is in Pa, and  $n$  is dimensionless

pepper varieties. The behavior index ( $n$ ) at 30 °C was very close to this research, from 0.30 to 0.37, while the consistency index ( $K$ ) was very diverged (4.42–13.9 Pa s<sup>n</sup>). Ahmed et al. (1999) also fitted the power law model to experimental data of pepper purée. Their  $n$  results at temperature of approximately 30 °C were lower than those of this work (0.228–0.300), while  $K$  values were similar (36.482–29.703 Pa s<sup>n</sup>). These differences are possibly due to differences in strain rate range used (0–100 s<sup>-1</sup>), differences of water fraction, or to particle size of the suspension.

The water fraction influence in the values of Herschel-Bulkley parameters was evaluated. Figures 2, 3, and 4 show the effect of the water fraction in the yield stress, consistency, and behavior index, respectively. The increase of yield stress values exponentially with decreasing water fraction can clearly be seen. The same effect was observed in the behavior index, while the consistency index increased linearly until water fraction of 0.61 and then decreased with decreasing water fraction.

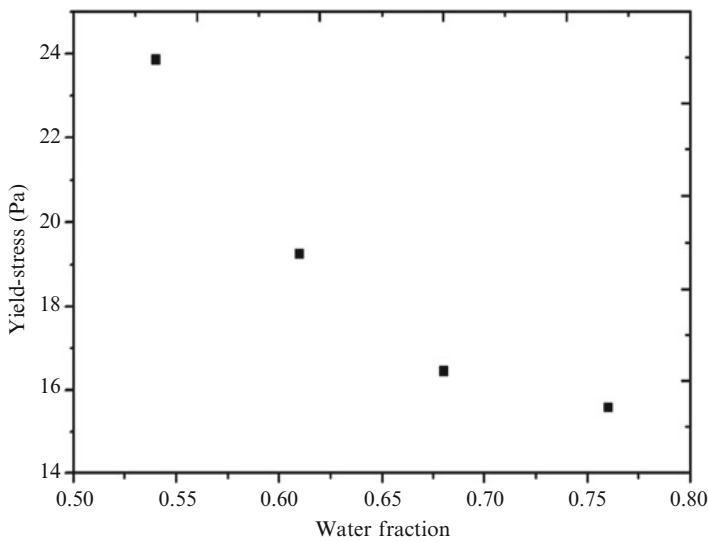


**Fig. 2** Water fraction effect in the yield stress

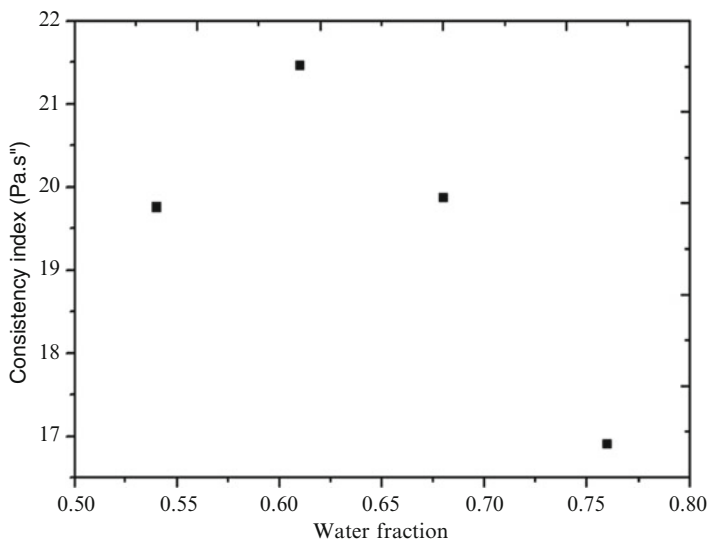


**Fig. 3** Water fraction effect in the consistency index

### 3 Conclusion

The shear stress increased with increasing shear rate and decreasing water fraction of jalapeño pepper pulp. Jalapeño pepper pulp behaved as a pseudoplastic fluid and the Herschel-Bulkley and Sisko models described well the shear stress–shear rate

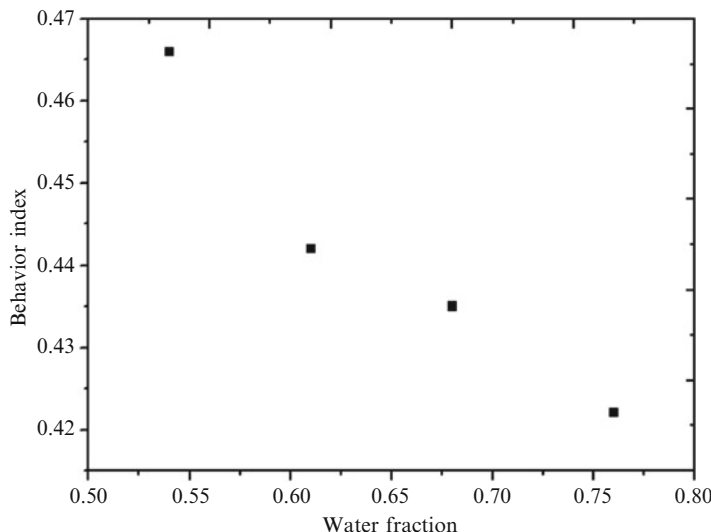


**Fig. 4** Water fraction effect in the behavior index

behavior, with coefficients of determination greater than 0.999. The parameters of Herschel-Bulkley model, yield stress, consistency index, and behavior index increased as the water fraction of the jalapeño pepper pulp decreased.

**Acknowledgements** The authors would like to acknowledge and thank FAPESP (Process Number 2009/11675-3) for their financial support.

## References

- Ahmed J, Gangopadhyay H, Shivhare US (1999) Effect of temperature on rheological characteristics of green chilli puree. *J Food Sci Technol* 36(4):352–354
- Ahmed J, Shivhare US, Raghavan GSV (2000) Rheological characteristics and kinetics of colour degradation of green chilli puree. *J Food Eng* 44:239–244
- Alvarez-Parrilla E, Rosa LA, Amarowicz R, Shahidi F (2011) Antioxidant activity of fresh and processed jalapeño and serrano peppers. *J Agric Food Chem* 59:163–173
- Baranowski JD (1985) Storage stability of a processed ginger paste. *J Food Sci* 50:932–933
- Cepeda E, Gómez R (2002) Rheological characteristics of pimento puree: theoretical interpretation. *Food Eng Phys Prop* 67(7):2734–2738
- Chuah AM, Lee YC, Yamaguchi T, Takamura H, Yin LJ, Matoba T (2008) Effect of cooking on the antioxidant properties of coloured peppers. *Food Chem* 111:20–28
- Giridhar N, Satyanarayana A, Joshi GJ (1996) Studies on preparation and storage of ginger-garlic paste. *Indian Food Pack* 50(3):13–21
- King AD, Bolin HR (1989) Physiological and microbiological storage stability of minimally processed fruits and vegetables. *Food Technol* 43:132–135
- Pezzutti A, Crapiste GH (1997) Sorptional equilibrium and drying characteristics of garlic. *J Food Eng* 31:113–123

- Steffe JF (1996) Rheological Methods in Food Process Engineering, 2nd edn. Freeman, East Lansing, p 418
- Topuz A, Ozdemir F (2007) Assessment of carotenoids, capsaicinoids and ascorbic acid composition of some select peppers cultivars (*Capsicum annuum* L.) grown in Turkey. *J Food Compos Anal* 20:596–602

# **Study of Water Quality Through Hydro-Chemical Signature in León, Guanajuato, Mexico**

**S.A. Cortés, G.A. Lozano, and J. Pérez**

## **Abbreviations**

CEAG	Guanajuato State Water Commission
MDWN	Mexican Drinking Water Norm
VL	Valle de León

## **1 Introduction**

The aquifer system of Valle de León (VL) is a free aquifer that consists mainly of sedimentary Tertiary rocks of lacustrine origin (Fig. 1). This valley presents different hydraulic conductivity stratifications that store water with various chemical and isotopic characteristics, so this water represents its different origins. According to the most recent census (Instituto Nacional de Estadística y Geografía, INEGI), VL has a population of 1,436,480 inhabitants, living in 11 population

---

S.A. Cortés

Instituto de Geofísica, Universidad Nacional Autónoma de México (UNAM), Circuito de la investigación científica s/n, Ciudad Universitaria, Delegación Coyoacán, C.P. 04510 México, D.F., Mexico

G.A. Lozano (✉)

Centro de Investigación en Ciencia Aplicada y Tecnología Avanzada (CICATA, Unidad Querétaro), Instituto Politécnico Nacional (IPN), Cerro Blanco No. 141, Col. Colinas del Cimatario, C.P. 76090 Santiago de Querétaro, Querétaro, Mexico  
e-mail: [alozano@ipn.mx](mailto:alozano@ipn.mx)

J. Pérez

Centro de Geociencias, Universidad Nacional Autónoma de México (UNAM), Campus Juriquilla, Querétaro, Mexico

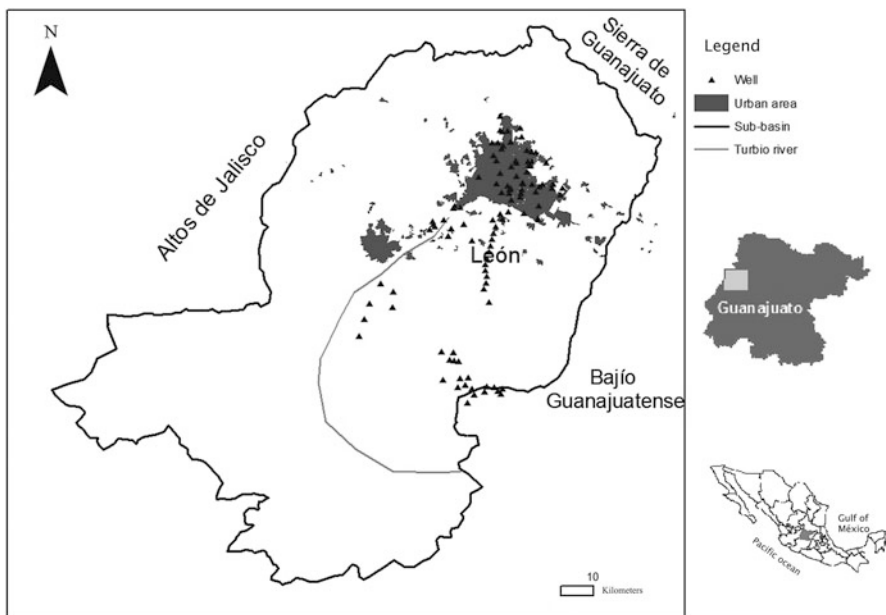


**Fig. 1** Location of the studied zone

centers; it is the region's most important industrial corridor and is included in one of Mexico's most productive agricultural zones. VL covers approximately  $687 \text{ km}^2$  surrounded by higher altitude topographic zones. The water supply of the population is mainly groundwater. This comes from deep wells, which are located mostly in irrigation zones but also in urban and rural zones of VL.

The Guanajuato State Water Commission (Comisión Estatal de Agua de Guanajuato, CEAG) reports that there are 1,154 active wells in VL, averaging 300–400 m depths. From this number of wells, 797 goes to irrigate 15,000 ha, 245 supply drinking water, 100 goes to cattle ranches, and 12 of them supply industry. The VL drainage system covers 2,672 km. Drainage comprising urban wastewater and pluvial water is 2,540 km long. Leon city (Fig. 1) itself generates 2,300 l/s of wastewater, generated by housing gray water and sewage released by urban industries.

## 2 Data Collected

Major and minor ions, heavy metals, and physicochemical parameters were collected from 1996 to 2007, resulting in 1,381 data sets (SAPAL 2007). From these sets, all incomplete sets were eliminated. The elimination criterion was a lack of information related with major ions, which are the ones used for ionic balance.

Only data sets with a load balancing less or equal to 16 % were taken into account. Based on this information, the behavior of the chloride, nitrate, and fluoride ions and the metals such as lead, chrome, cadmium, and arsenic was determined (Ramos-Leal et al. 2005). Analysis of these data showed concentration changes in time though their hydro-chemical signature showed that historical values tend to converge to those obtained for the 2007 sampling (Ramos-Leal et al. 2007).

### 3 Results

From all the studied wells, it was found that 92 % of them have water where bicarbonate ion is present. On the rest 8 %, chloride ion was predominant. The highest values of this ion were found in wells situated on zones irrigated with wastewater. It is noted that 10 % of this group are above the Mexican Drinking Water Norm (MDWN) (NOM-127-SSA1-1994). The anomalous situation appears in a group of wells located in the south of the study area and its origin is associated to the presence of faults and/or components of deep water. Nitrate high values are mainly in wells located on urban zones; quality is related to leaks in the sewer system. Results for heavy metals, in general, do not present inconsistencies, and most data are within the MDWN. Figure 2 shows piper diagram for the 2007 well sampling evenly distributed within VL. This diagram allows identifying four probable facies (water families). Facie I has the characteristic of having ion  $\text{Na}^+ > 80\%$  related to its relative abundance, and its principal anion is  $\text{HCO}_3^- > 80\%$ . Facie II is characterized by the relative abundance of  $\text{Na}^+ > \text{Ca}^{2+}$  cations. This facie can be described as  $\text{Na}^+ > \text{Ca}^{2+} - \text{HCO}_3^{3-} > \text{SO}_4^{4-}$ . Anion  $\text{HCO}_3^-$  is present in all wells related with facie III. For this facie, cations show high variability though in 15 wells predominant relation is  $\text{Ca} > \text{Na}$ . Facie IV presents  $\text{HCO}_3^- > \text{Cl}^-$  and predominant cations are  $\text{Ca} > \text{Mg}$ . Figure 3 shows the relation between field-measured water average temperature against milliequivalents per liter concentrations for  $\text{SO}_4^{2-}$ ,  $\text{Na}^+$ ,  $\text{Li}^-$ ,  $\text{F}^-$ , and boron ions for the previously described facies.

Figure 4 describes behavior of  $\text{N-NO}_3^{2-}$  ion for urban zone-located wells. Allowable value for this ion is 10 mg/l. From this figure, a gradual increment of this ion's value can be seen. This increment causes the allowable value for drinking water to be surpassed and, in extreme cases, the well to be closed. Within the Leon city might be illegal wells pumping out contaminated water without any control. So, this issue lives open the question on how exposed is the population to this kind of water.

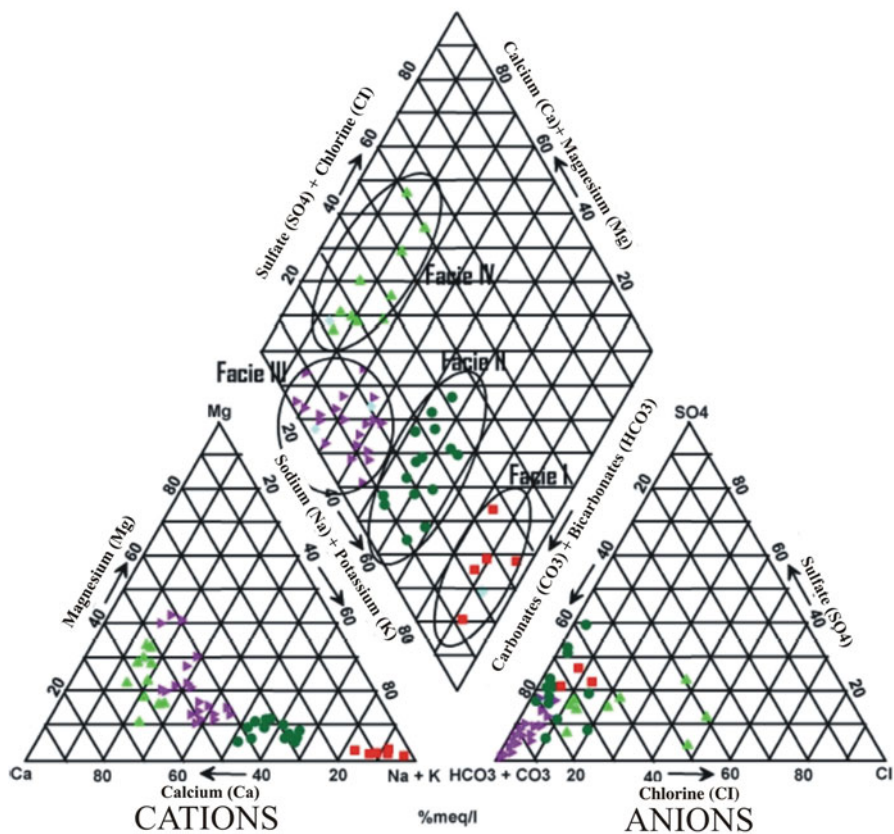


**Fig. 2** Piper diagram for some sampled wells

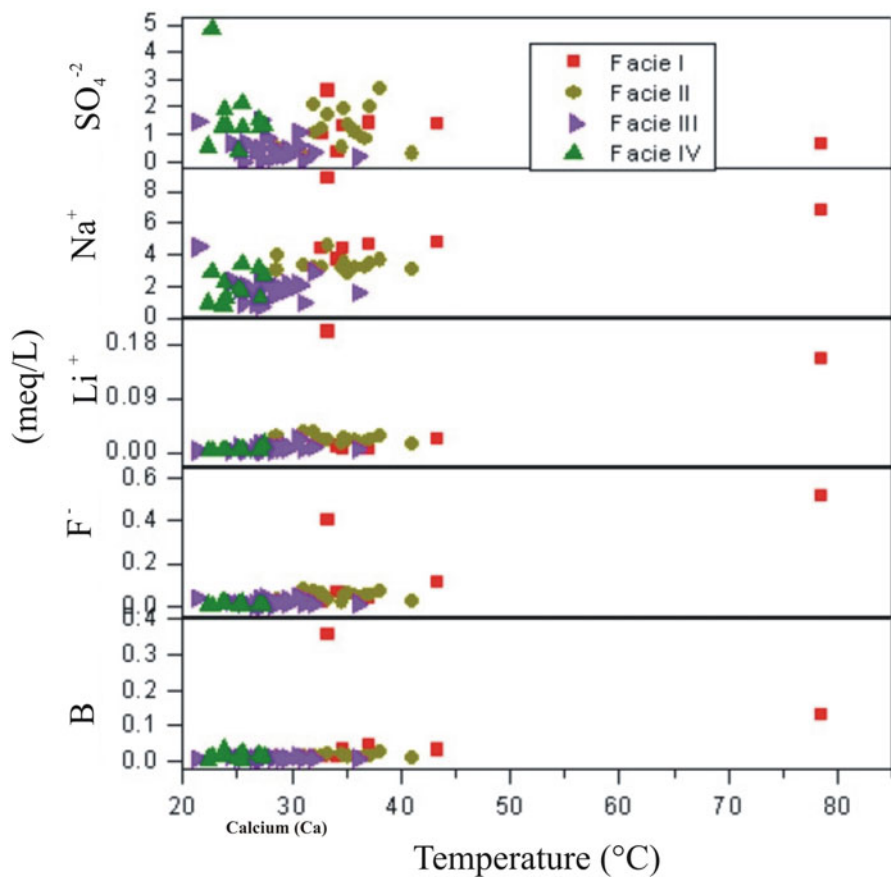


**Fig. 3** Water temperature versus milliequivalent per liter relation for facie identified at the studied zone

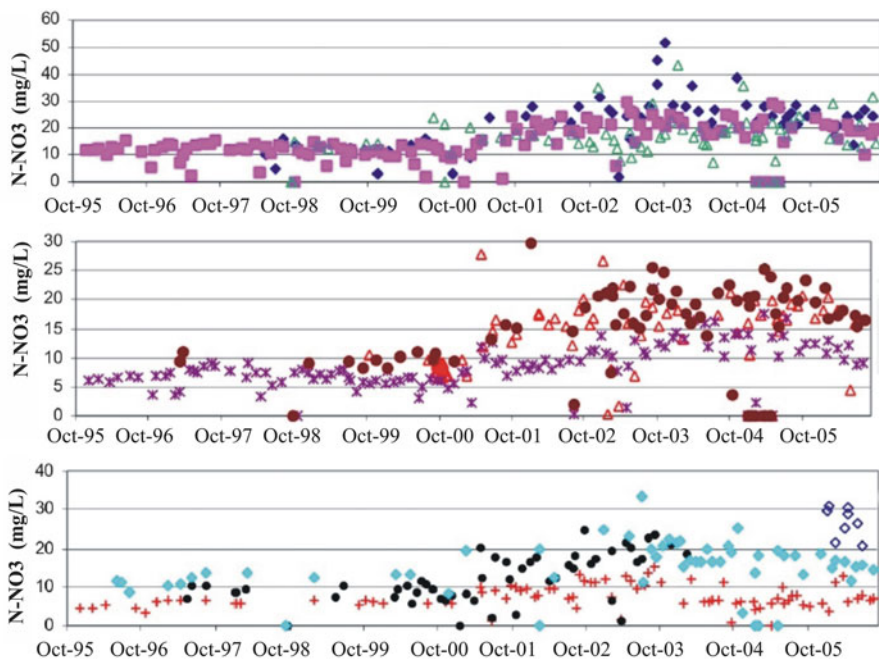


**Fig. 4**  $\text{N-NO}_3^{-2}$  ion behavior for urban zone-located wells

## 4 Conclusions

Results up to date show a significant variation, so time sampling and time of well operation seem to be of prime importance. Related to water quality, generally speaking, it can be said that its quality is acceptable and that drinking water is within the current standard. It has to be taken into account that sampling is carried out at the wells' output before chlorination takes place. So, sampled water is aquifer representative and different from that coming out from a house tap. It can be said that although there are pollution problems, both natural and anthropogenic, they can be kept controlled with a proper aquifer management.

## References

- INEGI, Instituto Nacional de Estadística Geografía e Informática (2011) <http://www.inegi.gob.mx>. Accessed 31 March 2011  
 Ramos-Leal JA, Durazo J, González-Moran T, Ramírez-Guzmán A, Johannesson KH, Cortés A (2005) Decay in chloride content of ground water due to excessive production of a web field near Leon, Mexico. *Geofísica Int* 44–4:385–390

- Ramos-Leal JA, Durazo J, González-Morán T, Juárez-Sánchez F, Cortés-Silva A, Johannesson K (2007) Evidencias hidrogeoquímicas de mezcla de flujos regionales en el acuífero de La Muralla, Guanajuato. Rev mexcien geol 24-3:293–305
- Secretaría de Economía, Norma Oficial Mexicana NOM-127-SSA1-1994, Salud Ambiental, Agua para uso y consumo humano. Límites permisibles de calidad y tratamientos a que debe someterse el agua para su potabilización (1994) <http://www.salud.gob.mx/unidades/cdi/nom/127ssa14.html>. Accessed 31 March 2011
- Sistema de Agua Potable y Alcantarillado de León, SAPAL (2007) [http://www.sapal.gob.mx/media/files/1393543102-sapal\\_21072011.pdf](http://www.sapal.gob.mx/media/files/1393543102-sapal_21072011.pdf). Accessed 30 March 2015

# **Calorimetric and Thermogravimetric Analysis of *Agave tequilana* Weber Fibers**

**C. De Dios-Naranjo, R. Mora-Escobedo, G.F. Gutiérrez-López,  
J. Solorza-Feria, A. Flores-Morales, H. Yee-Madeira,  
and L. Alamilla-Beltrán**

## **Abbreviations**

CI	Crystallinity index
DSC	Differential scanning calorimetry
FAAT	Fibers submitted to acid-alkaline hydrolysis at elevated temperature
FAATP	Fibers submitted to acid-alkaline hydrolysis with pressure and at elevated temperature
FAWT	Agave fibers without any treatment
FAWT	Fibers without treatment
FTIR	Spectroscopy Fourier transform infrared
TGA	Thermogravimetric analysis
XRD	X-ray diffraction

---

C. De Dios-Naranjo • R. Mora-Escobedo • G.F. Gutiérrez-López • L. Alamilla-Beltrán (✉)  
Departamento de Graduados e Investigación en Alimentos, Escuela Nacional de Ciencias  
Biológicas, Instituto Politécnico Nacional, Carpio y Plan de Ayala s/n, Col. Santo Tomás,  
Deleg. Miguel Hidalgo, C.P. 11340, México, D.F., Mexico  
e-mail: [lilianaalamilla@gmail.com](mailto:lilianaalamilla@gmail.com); [lalamill@ipn.mx](mailto:lalamill@ipn.mx)

J. Solorza-Feria  
Centro de Desarrollo de Productos Bióticos, Instituto Politécnico Nacional, Carretera  
Yautepéc-Joxtla, Km. 6, Col. San Isidro, C.P. 62731, Apartado Postal 24, Yautepéc,  
Morelos, Mexico

A. Flores-Morales  
Instituto Tecnológico del Altiplano de Tlaxcala, Km. 7.5 Carretera Federal San  
Martín – Tlaxcala, San Diego Xocoyucan, Tlax C.P. 90122, Mexico

H. Yee-Madeira  
Escuela Superior de Física y Matemáticas, I.P.N. Av. Instituto Politécnico Nacional S/N,  
San Pedro Zacatenco, C.P. 07738, México, D.F., Mexico

## 1 Introduction

*Agave tequilana* crop waste provides lignocellulosic material that can be exploited through the surface treatment of the fibers, such as by soaking in acid-alkali media, which allows for the separation of water-soluble components such as pectins, sugars, and fructooligosaccharides from insoluble components such as hemicellulose and lignin fibers. This treatment also improves the properties of the fibers in terms of their thermal stability and tensile strength, which is necessary for developing composites because it allows for the removal of impurities such as waxes, pectin, and minerals, increasing the fibers' surface area (Ben Sghaier et al. 2012; Rosli et al. 2013). The objective of this research was to characterize lignocellulose fibers from *A. tequilana* Weber by calorimetric and thermogravimetric techniques.

## 2 Materials and Methods

### 2.1 Materials

*Agave tequilana* Weber leaves aged approximately 8–10 years were collected from Morelos State, Mexico. The leaves were washed, weighed, had their cuticle excised, pressed, dried at 70 °C for 12 h, freeze-dried for 12 h, and finally milled into a powder with a mean particle size of 150 µm.

### 2.2 Agave Fiber Preparation

The leaf powder (FAWT) was subjected to two different treatments in an attempt to separate water-soluble components such as pectins, sugars, and fructooligosaccharides from fibrous components such as lignocellulosic materials. In treatment 1, a modified acid-alkaline hydrolysis process was used (Saucedo et al. 2010); the fibers obtained using this treatment was denoted as FAAT. Treatment 2 was conducted by applying the technique reported by Hernández-Salas et al. (2009). This treatment involved the application of elevated temperature and pressure (121 °C/1.1 kg/cm<sup>2</sup>) over a period of 4 h; the fibers obtained using this treatment were denoted as FAATP.

### 2.3 Chemical Composition

*Agave tequilana* fibers were submitted to chemical analysis to determine their ash content (AOAC—31 013, 1995) and content of total reducing sugars (Ting 1956).

The cellulose content was determined by differential cellulose-lignin analysis using the Klasson method and the ISO 13906:2008 method (Moller [2009](#)).

## **2.4 Thermogravimetric Analysis and Fourier Transform Infrared Spectroscopy**

Samples of agave fibers not submitted to any treatment (FAWT) and modified fibers (FAAT and FAATP) were analyzed by a thermogravimetry device (Equinox, Bruker, Finland) coupled to a thermoanalyzer (STA 409 PC Luxx, Netzsch, Germany). Thermograms were obtained at a heating rate of 10 °C/min and over a temperature range of 30–80 °C.

## **2.5 Differential Scanning Calorimetry**

The FAWT, FAAT, and FAATP samples were analyzed using a differential scanning calorimetry (DSC) 2010 calorimeter (TA-Instruments Inc., USA) over a temperature range of 30–620 °C in increments of 10 °C/min. Each scan was carried out separately under a nitrogen atmosphere at a flow rate of 20 cm<sup>3</sup>/min.

## **2.6 X-Ray Diffraction**

The FAWT, FAAT, and FAATP samples were analyzed using a diffractometer (D8 advance Vantec Bucker, Germany) with CuK $\alpha$  radiation source (1.5418 Å), a radioactive Ni filter, and a scintillation counter as a detector at 35 kV and 30 mA over a range of 2 $\theta$  angles of 3–37° via the technique reported by Singha and Rana ([2010](#)). The crystallinity index (CI) was determined using the diffraction signals obtained at 2 $\theta$  angles near 15 and 22°.

## **3 Results and Discussion**

The chemical compositions of the *Agave tequilana* leave powder (FAWT) and the fibers obtained by the modified acid-alkaline hydrolysis process without pressure (FAAT) and with pressure (FAATP) are shown in Table 1. These treatments induced the chemical breakdown of compounds due to reaction with acid and alkaline substances, allowing for the breaking of lignin and hemicellulose bonds

**Table 1** Chemical composition of lignocellulosic material of *Agave tequilana* (% dry base)

Sample	Lignin (%)	Cellulose (%)	Reducing sugars (%)	Ashes (%)	Others (%)	Total (%) <sup>1</sup>
FAWT	14.58 ± 2.48 <sup>b</sup>	68.37 ± 3.45 <sup>a</sup>	0.46 ± 0.02 <sup>a</sup>	7.25 ± 1.36 <sup>a</sup>	9.34 ± 1.5 <sup>a</sup>	100
FAAPT	19.85 ± 2.90 <sup>a</sup>	31.53 ± 0.91 <sup>a</sup>	0.02 ± 0.004 <sup>a</sup>	11.29 ± 1.19 <sup>a</sup>	37.31 ± 2.54 <sup>a</sup>	99.7
FAAT	13.52 ± 2.47 <sup>b</sup>	78.95 ± 2.62 <sup>a</sup>	0.15 ± 0.0 <sup>a</sup>	4.65 ± 0.11 <sup>a</sup>	2.73 ± 1.85 <sup>a</sup>	100

FAWT fibers without treatment, FAAPT fibers submitted to acid-alkaline hydrolysis with pressure and at elevated temperature, FAAT fibers submitted to acid-alkaline hydrolysis at elevated temperature

<sup>a</sup>Different lower case letters in the same column for each analysis indicate significant differences among treatments ( $P < 0.05$ )

<sup>b</sup>Different capital letters in the same column for each analysis indicate no difference among treatments ( $P > 0.05$ )

Total percentage of the sample. The values are the results for each component

(Rosli et al. 2013). Pressure also facilitated the hydrolysis of cellulose bonds, reducing the content of this component in FAATP.

Thermogravimetric analysis (TGA) revealed that the two extraction treatments affected the fibers in different ways; in fact, three main stages of weight loss of the fiber materials could be recognized at different temperatures. The FAWT showed a gradual release or loss of components as the temperature increased. During the first stage (between 25 and 104 °C), FAWT lost free water weakly linked to the structure and water-soluble solids such as simple sugars. Subsequently, in the second step (104–241 °C), the mass loss was attributed to the degradation of fructooligosaccharides, pectins, sugar monomers (maltose), and disaccharides such as sorbitol. In the third step (241–302.08 °C), the FAWT reached 60 % total weight loss. At this stage, the residual thermal degradation of hemicellulose occurred. With an increase in temperature, chemical changes in the hemicellulose components occurred due to cell wall rupture. This finding is consistent with previous studies indicating that hemicellulose degrades between 180 and 350 °C. Cellulose is more thermally stable due to its crystalline nature, which is composed of a network of hydrogen bonds that form microfibrils; it has been reported that the thermal degradation of cellulose is initiated at 350 °C (Yang et al. 2007). FAATP showed mass loss up to a temperature of 241 °C. These fibers were composed mainly of cellulose and lignin in lower proportion. The FAAT fibers exhibited a high loss of mass during the first stage, mainly due to the removal of large amounts of water, simple sugars, and water-soluble solids. The behavior observed in the second stage was similar to that observed for FAATP and FAWT. In the third stage, FAATP showed a higher percentage of mass loss (39 %) than that observed for the other fiber materials. The high thermal resistance of FAATP and FAAT is due to the materials' high lignin content; thus, these fibers were observed to thermally degrade between 200 and 700 °C at a mass loss rate much lower than the rates observed for cellulose and hemicellulose. This finding agrees with the lignin and cellulose contents observed for FAATP, FWAT, and FAAT, namely 19.85 and 31.53, 14.58 and 68.37, and 13.52 and 80.35, respectively (Fig. 1).

Differential scanning calorimetric analysis revealed two endotherms for FAWT (Fig. 2). The first one began at 94.91 °C with a plateau of 120.87 °C and  $\Delta H = 140.1 \text{ J/g}$ . The second endotherm occurred at 206.79 °C with a plateau of 220.33 °C and  $\Delta H = 23.09 \text{ J/g}$ . In addition, the FAAT cellulosic material showed two endotherms, one beginning at 105.79 °C with a plateau at 127.42 °C and  $\Delta H = 218.0 \text{ J/g}$  and the other beginning at 205.53 °C with a plateau at 225.05 and  $\Delta H = 17.78 \text{ J/g}$ . The first endotherm was likely due to the presence of D-fructose, whereas the second was likely due to hydrolyzed chains of fructans, based on the fact that agave fructans thermally decompose at temperatures near 200 °C (Espinosa-Andrews and Urias-Silvas 2012). Moreover, agave fructans show a decrease in their thermal decomposition rate at approximately 230 °C, which could be associated with the decomposition of branched chains of agave fructans. Chui et al. (2002) reported that the decomposition rate of cross-linked inulin is lower than that of native inulin.

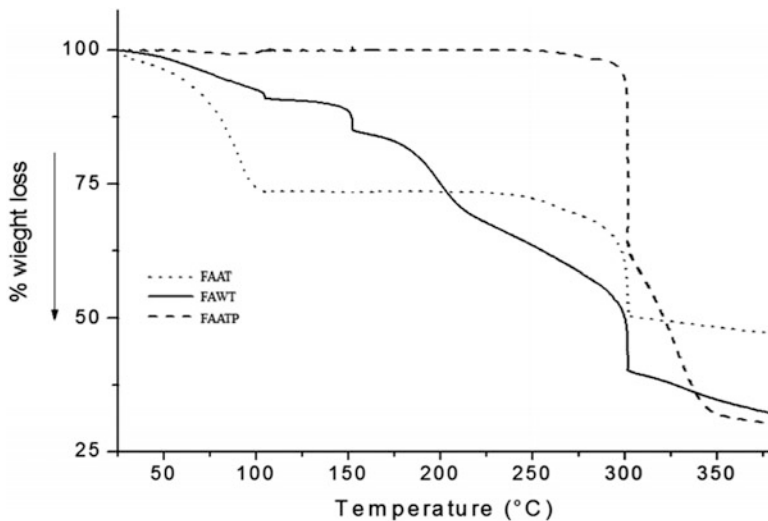


**Fig. 1** Thermogravimetric analysis of *Agave tequilana* Weber: sample of leaf powder (FAWT), fibers submitted to modified acid-alkaline hydrolysis without pressure (FAAT) and fibers submitted to modified acid-alkaline hydrolysis with pressure (FAATP)

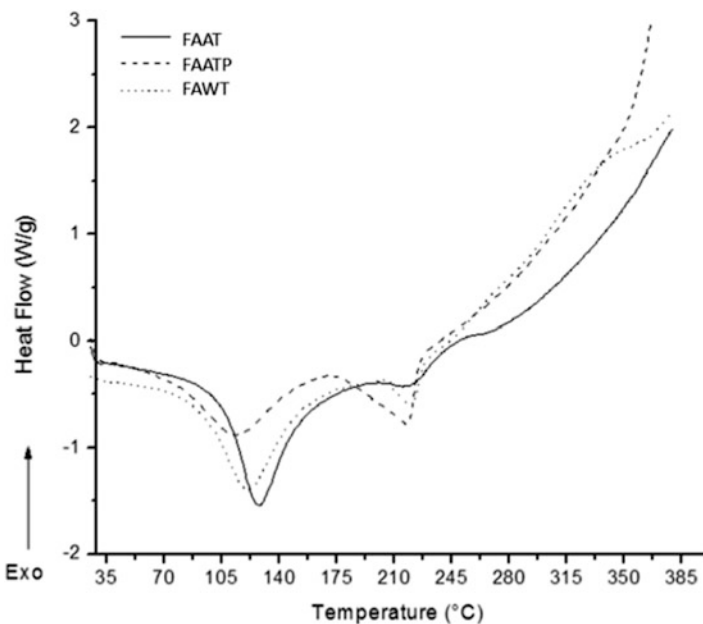


**Fig. 2** DSC results for different lignocellulosic materials of *Agave tequilana* Weber

FAATP showed two endotherms. The first began at 77.47 °C with a plateau of 113.68 °C and  $\Delta H = 139.1 \text{ J/g}$ . This behavior is likely due to sugar alcohols such as D-sorbitol due to the fructooligosaccharide decomposition that generates this monosaccharide (Roos 1995), whose onset occurs at 86 °C with a plateau at approximately 110–112 °C and  $\Delta H = 150 \text{ J/g}$ . The second endotherm occurred at 182.37 °C with a peak at 217.48 °C and  $\Delta H = 74.80 \text{ J/g}$ . This endotherm could be due to the decomposition of  $\alpha,\alpha$ -trehalose, whose onset occurs at 173 °C with a plateau at 214–216 °C and  $\Delta H = 118 \text{ J/g}$  (Roos 1995). The  $\Delta H$  reported may vary because sugars do not exhibit exact melting temperatures; thus, it is important to note that the fusion temperatures and  $\Delta H$  values may slightly differ between sugar monomers (Roos 1995). Waleckx et al. (2008) mention that *A. tequilana* Weber var. Azul and other Agave species contain a complex mixture of highly branched fructans and neo-fructans (referred to as agavins), with each type of linkage ( $\beta$ -(2–1) and  $\beta$ -(2–6)) between fructose moieties.

Changes in the structural arrangement of the lignocellulosic material determined by X-ray diffraction (XRD) are shown in Fig. 3. The chemical solutions of FAATP and FAAT showed changes in the crystallinity indexes (CIs). FAATP lignocellulose showed a CI of 41.49 %, 20.4 % greater than that of fibers without treatment. FAAT showed a similar CI, differing by 2.51 % compared to the CI of FAATP. It is possible that the diluted acid destroyed the amorphous regions of the fibers, whereas the alkali component helped increase the stiffness as well as remove impurities (Fengel and Wegener 1984; Mwaikambo and Ansell 2006).

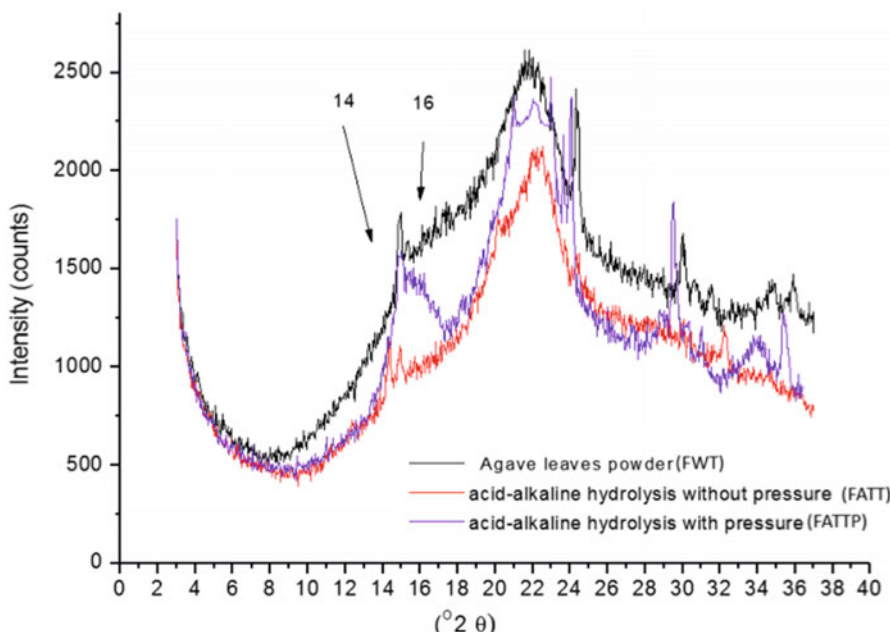


**Fig. 3** XRD results for different lignocellulosic materials of *Agave tequilana* Weber

## 4 Conclusions

Applying extraction processes that involve the use of acid-alkali solutions with or without pressure can enhance the removal of components within Agave fibers as well as the components of more open microfibrils within fiber complexes. At the beginning of the extraction process, important water-soluble components are removed; these include reducing sugars, chlorophylls, and pectins that are widely used in the food industry.

TGA coupled with Fourier transform infrared (FTIR) spectroscopy, DSC, and XRD is a useful tool for analyzing any changes that may occur during the dissolution of lignocellulosic materials contained in Agave fibers.

**Acknowledgments** The authors acknowledge the financial support of research projects SIP 20140253 and 20140100. The authors are fellows of EDI-IPN, COFAA-IPN, and SNI. Cuauhtémoc de Dios Naranjo was awarded a CONACyT grant.

## References

- AOAC (1995) Official method of analysis, 14th edn. Association of Official Analytical Chemists, Washington, pp 23–26
- Ben Sghaier AEO, Chaabouni Y, Msahli S, Sakli F (2012) Morphological and crystalline characterization of NaOH and NaOCl treated *Agave americana* L. fiber. *Ind Crops Prod* 36 (1):257–266
- Chui HC, Hsu YH, Lin PJ (2002) Synthesis of pH-sensitive inulin hydrogels and characterization of their swelling properties. *J Biomed Mater Res* 61(1):146–152
- Espinosa-Andrews H, Urias-Silvas JE (2012) Thermal properties of agave fructans (*Agave tequilana* Weber var. Azul). *J Carbohydr Polym* 87:2671–2676
- Fengel D, Wegener G (1984) Wood chemistry, ultrastructure, reactions. In: Chemical composition. Walter de Gruyter Press, Berlin, pp. 256–265
- Hernández-Salas JM, Villa-Ramírez MS, Veloz-Rendón JS, Rivera-Hernández KN, González-César CRA, Plascencia EMA, Trejo ESR (2009) Comparative hydrolysis and fermentation of sugarcane and agave bagasse. *Bioresour Technol* 100:1238–1245
- Moller J (2009) Gravimetric determination of acid detergent fiber and lignin in feed: interlaboratory study. *AOAC Int J* 92(1):74–90
- Mwaikambo LY, Ansell MP (2006) Mechanical properties of alkali treated plant fibres and their potential as reinforcement materials. I Hemp fibres. *J Mater Sci* 41:2483–2496
- Roos YH (1995) Phase transitions in foods. Food components and Polymers. Academic, USA, pp 113–115
- Rosli NA, Ahmad I, Abdulllah I (2013) Isolation and characterization of cellulose nanocrystals from *Agave angustifolia* fibre. *Bioresour Technol* 8(2):1893–1908
- Saucedo LJ, Castro MAJ, Rico JL (2010) Optimization of acid Hydrolysis if Bagasse from *Agave tequilana* Weber. *Rev Mex Ing Quím* 91(1):91–97
- Singha AS, Rana RK (2010) Graft copolimerization of methyl methacrylate (MMA) onto *Agave Americana* fibers and evaluation of their physicochemical properties. *Int J Polym Anal Charac* 15:27–42
- Ting SV (1956) Fruit juice assay, rapid colorimetric methods for simultaneous determination of total reducing sugars and fructose in citrus juices. *J Agric Food Chem* 4(3):263–266

- Waleckx E, Gschaedler A, Colonna-Ceccaldi B, Monsan P (2008) Hydrolysis of fructans from *Agave tequilana* Weber var. azul during the cooking step in a traditional tequila elaboration process. *J Food Chem* 108:40–48
- Yang H, Yan R, Chen H, Lee DH, Zheng C (2007) Characteristic of hemicellulose, cellulose and lignine pyrolysis. *Fuel* 86(12):1781–1788

# **Study of Allspice Fluidized Bed Drying (*Pimenta dioica* L. Merrill) by Biochemical and Structural Analysis**

**A.E. Carpinteyro-Díaz, I. Anaya-Sosa, M.T. Cruz y Victoria,  
and T. Santiago-Pineda**

## **Abbreviations**

$\bar{r}$	Logarithmic mean radius
$D_{\text{eff}}$	Effective diffusion coefficients
$D_L$	Diffusivity
$r_1$	Initial radius
$r_2$	Final radius
$r_{\text{eq}}$	Equivalent radius
SEM	Scanning electron microscopy
$X$	Free moisture content
$X^*$	Equilibrium moisture content
$X_{t1}$	Initial moisture content

## **1 Introduction**

Allspice (*Pimenta dioica* L. Merrill) is a spice native to Southern Mexico that can be used in different ways, from the pharmaceutical industry to the food industry, and it is well known for its flavoring properties from antiquity to today (Macía 1998). Allspice contains a number of antioxidants, which has caught the attention of researchers in this field.

---

A.E. Carpinteyro-Díaz • I. Anaya-Sosa (✉) • M.T. Cruz y Victoria • T. Santiago-Pineda  
Departamento de Graduados e Investigación en Alimentos, Escuela Nacional de Ciencias Biológicas (IPN), Prolongación de Carpio y Plan de Ayala s/n. CP 11340, México D.F., Mexico  
e-mail: [ianaya@encb.ipn.mx](mailto:ianaya@encb.ipn.mx)

The drying operation is a process which involves mass transfer between a gas and a solid product, where the moisture content of the solid is transferred by evaporation from the gas phase (Perry et al. 1997). The main purpose of drying is to extend the half-life of food and to reduce water activity in order to inhibit microbial growth and enzyme activity (Hui 1992; Rahman and Perera 1999).

Food dehydration presents problems related to the food's structural characteristics, which affects rehydration, retention of aroma and sensorial attributes, as well as mass and heat transport phenomena during the process (Aguilera 2003).

In a previous work Flores et al. (2009) it was found that during the drying of the allspice at 60, 70, and 80 °C, the product presents shrinking, but no deformation. This fact indicates that the operation is isotropic; this phenomenon is not common in foods. In addition, they evaluated the biochemical quality of this operation, and it was found that at 70 °C there was major retention of ascorbic acid, while at 80 °C lower retention of ascorbic acid was shown. Thus, the aim of this study is to evaluate the changes in the structure during drying with the help of scanning electron microscopy (SEM), as well as the determination of enzyme activity of peroxidase, polyphenol oxidase, catalase, glucose oxidase, and total phenols.

## 2 Materials and Methods

### 2.1 Drying Evaluation

The raw material was obtained from Cuetzalan, in the state of Puebla, having an initial moisture content of 0.627–0.617 db.

The equipment used was a fluidized bed dryer. Drying curves were carried out based on the measure of the broken record of loss weight by using the relation L/D = 0.5 (145 g of allspice). Air temperature was 70 and 80 °C, reaching a final moisture content of 0.11 db. Surface temperature was also evaluated during dehydration.

The effective diffusion coefficients ( $D_{\text{eff}}$ ) were determined using Fick's second law for a spherical geometry (Eq. 1). For the geometry calculation, the expression of logarithmic mean radius was used (Eq. 2):

$$\frac{X - X^*}{X_{t1} - X^*} = e^{-D_L t (\pi / r_{\text{eq}})^2} \quad (1)$$

where  $X$  = free moisture content;  $X^*$  = equilibrium moisture content;  $X_{t1}$  = initial moisture content;  $D_L$  = diffusivity; and  $r_{\text{eq}}$  = equivalent radius:

$$\bar{r} = \frac{r_2 - r_1}{\ln \frac{r_2}{r_1}} \quad (2)$$

and where  $\bar{r}$  = logarithmic mean radius;  $r_1$  = initial radius; and  $r_2$  = final radius.

## 2.2 Structural Evaluation

For the analysis of texture, relief, size, and material composition, the scanning electron microscope (SEM) of the Microscopy Center at Escuela Nacional de Ciencias Biológicas (IPN) was used. In order to take a sample of the allspice which contained cortex and seed, the allspice was cut in half and then a layer from the center was cut. The layer was fixed with 2 % glutaraldehyde and 1 % osmium tetroxide and sequentially dehydrated by using different ethanol solutions (10–100 %). Then was critical-point dried, cut, and assembled on slides which were covered with gold-palladium. In the case of green allspice, the samples were assembled on aluminum slides and coated with gold-palladium as well.

## 2.3 Biochemical Evaluation

Enzyme extract was prepared by weighing 20 g of allspice, previously ground, and added with 150 mL of 5 % NaCl. This mixture was left to sit for 48 h, and filtered after that. All measurements were made in triplicate.

The determination of catalase and peroxidase was made using the method reported by Mahely and Chance (1954), while the determination of polyphenol oxidase was made by the method of Kimberly and Lee (1981). The glucose oxidase enzyme was determined by the method of Voget et al. (1987). The amount of total phenol was determined by the method of Gutiérrez et al. (2008).

# 3 Results and Discussion

## 3.1 Drying Evaluation

Temperature of the allspice increased in the first 5 min, and reached the temperature of the dry bulb at 70 °C within 45 min of aeration, which indicates that drying occurs exclusively in the decreasing rate period. This behavior was also found at 80 °C.

Figure 1 shows the conventional drying curves, which can be observed with no significant difference because the standard deviation of the curves overlaps; this is

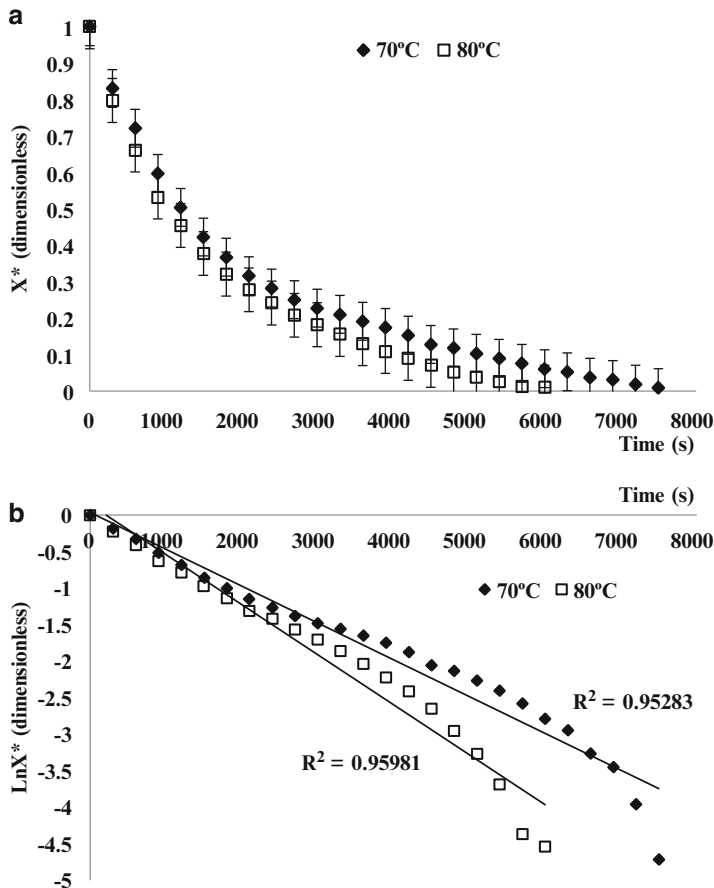


**Fig. 1** Conventional drying curves of allspice by fluidized bed drying (a) and curve of linearization carried out by the diffusion coefficient with the second Fick's law equation (b)

due to the way the allspice reaches the temperature of the bulb dry air; therefore, at 70 °C after 40 min, being a lower temperature, the drying extends 25 min more (Fig. 1a).

Figure 1b shows the corresponding line to the evaluation of the diffusion coefficient with the second Fick's law equation. The model used is consistent with the moisture loss of the allspice at 80 °C from 0 to 4,800 s, and at 70 °C the highest rate of water migration is at 6,300 s. In the linearization, it was found that, in these periods, the correlation coefficient is the highest; after these periods the slope decreases, extending the drying. This decreasing period is no longer a Fickian model. Table 1 shows values of logarithmic mean radius with no significant difference, as well as values of the effective diffusion. This last parameter is

**Table 1** Effective diffusion of the drying curves

Sample	Drying time (min)	Logarithmic mean radius (m)	$D_{\text{eff}}$ ( $\text{m}^2/\text{s}$ )
70 °C	120	0.00788	$3.172 \times 10^{-9}$
80 °C	100	0.00807	$4.523 \times 10^{-9}$
$P$	0.374	0.001	—

$P$  = significant difference if  $P \leq 0.05$ .  $D_{\text{eff}}$  = effective diffusion

affected by temperature, because at 80 °C the water migration velocity is higher. This behavior can be explained by the changes in the structure of the material.

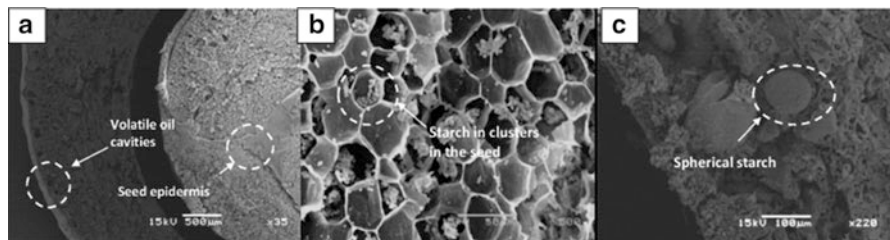
### 3.2 Structural Evaluation

Figure 2 shows the micrographs of green allspice, where the seeds and the cortex of the product can be observed. In Fig. 2a, some holes can be seen near the outer cell wall of the cortex. These holes are cavities of volatile oil; the epidermis can be seen as well (Winton and Barber-Winton 1939). The cell walls of the seed are reinforced with starch, which is found in clusters, and are composed of tiny spheres of this macromolecule (Fig. 2b). Also found in the cortex was the presence of starch having a spherical shape (Fig. 2c).

By comparing the allspice structure with the dehydrated products (Fig. 3), structure loss by cell compaction was found, which leads to fragility in the cortex that may cause fractures. When the cavities were compacted, the structure released volatile oils that give the characteristic smell of allspice (Fig. 3a). During drying, the structure of the starch begins to present a more elongated conformation that is probably caused by thermodegradation (Karlsson and Eliasson 2003) (Fig. 3b), while the appearance of calcium oxalate crystals in the vacuoles is the result of metabolic reactions of the product after dehydration (Nakata and McConn 2003) (Fig. 3c). When comparing the samples dried at 80 °C with the ones at 70 °C (Fig. 4), the latter show less cell compaction (Fig. 4a) because volatile oil cavities can be better seen. The presence of elongated starch (Fig. 4b) and the appearance of oxalate crystals can also be seen (Fig. 4c).

### 3.3 Biochemistry Evaluation

The enzymes evaluated in this study are from the group of oxidoreductases. Catalase, peroxidase, and polyphenol oxidase regulate the formation of free radicals like superoxide, hydrogen peroxide, and lipid peroxides. Figure 5 shows the results of enzyme activity in drying temperatures. It was found that peroxide and polyphenol oxidase are activated mostly at 80 °C because of the structural damage of the membrane and the release of enzymes present in the same, while catalase showed



**Fig. 2** Micrographs of green allspice obtained by SEM. Micrograph at  $\times 35$  (a),  $\times 500$  (b), and  $\times 220$  (c) of microscopic magnification

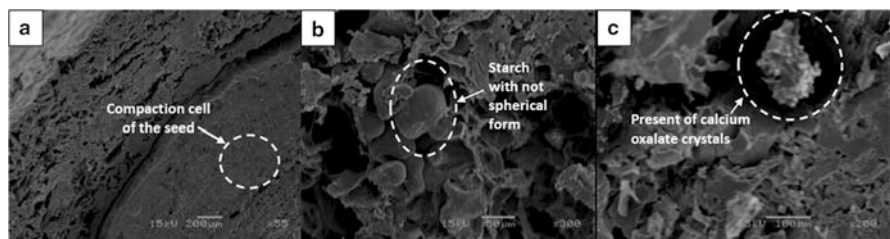


**Fig. 3** Micrographs of drying allspice at  $80^{\circ}\text{C}$

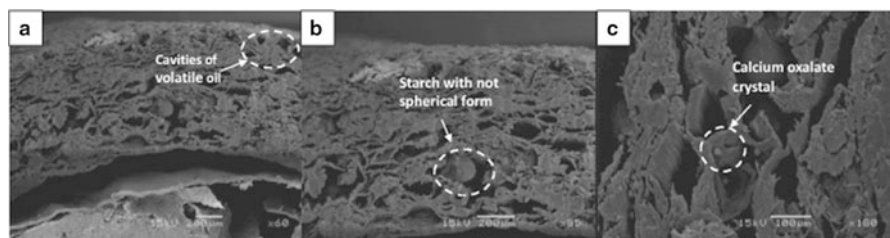


**Fig. 4** Micrographs of drying allspice at  $70^{\circ}\text{C}$

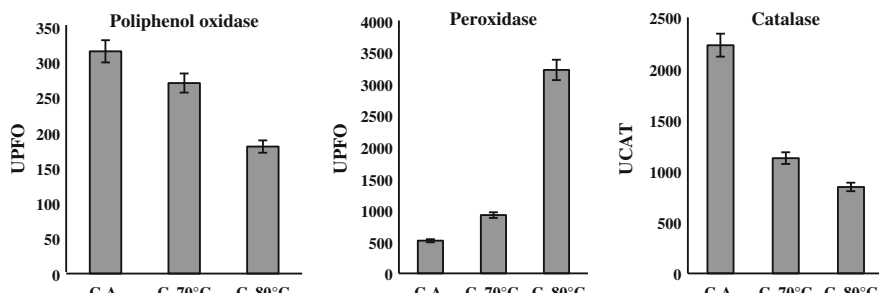


**Fig. 5** Peroxidase, polyphenol oxidase, and catalase in allspice. G.A. = green allspice, C. 70 °C = conventional at 70 °C, C. 80 °C = conventional at 80 °C

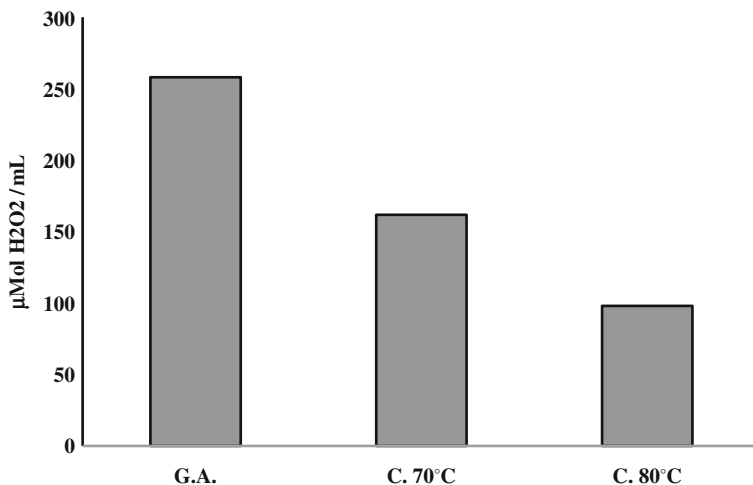


**Fig. 6** Glucose oxidase enzyme in the allspice. G.A. = green allspice, C. 70 °C = conventional at 70 °C, C. 80 °C = conventional at 80 °C

better results at 70 °C, because temperatures caused less damage to the structure (Whitaker 1994).

The same amount of total phenols was found in the samples dried at 70 and 80 °C (1.2386 mg of gallic acid/mL), so that the structure has the same damage because of dehydration. Hence, the decrease of the enzyme activity must be caused by the temperature used in the process. Glucose oxidase prevents nonenzymatic browning, so the presence of this enzyme indicates that the darkening of the allspice at 70 °C was lower than that at 80 °C (Fig. 6).

## References

- Aguilera JM (2003) Drying and dried products under the microscope. *Food Sci Technol Int* 9:137–143
- Flores NL, Cruz y Victoria MT, Anaya I (2009) Dehydration in fluid bed with tempering cycles, using residual enzymatic activity as a quality parameter. Paper presented at 3rd international congress on food science and food biotechnology in developing countries, Querétaro, México, 2009
- Gutiérrez DM, Ortiz CA, Mendoza A (2008) Medición de fenoles y actividad antioxidante en malezas usadas para alimentación animal. Paper presented at simposio de metrología, Querétaro, México
- Hui YH (1992) Encyclopedia of food science and technology. Wiley-Interscience, New York
- Karlsson ME, Eliasson AC (2003) Gelatinization and retrogradation of potato starch in situ as assessed by differential scanning calorimetry. *Lebens Wiss Technol* 36:735–741
- Kimberly WW, Lee CY (1981) Characterization of polyphenoloxidase. *J Food Sci* 46:506–514
- Macía MJ (1998) La pimienta de Jamaica (*Pimenta dioica* L., Merrill, Myrtaceae) en la Sierra Norte de Puebla (México). *An Jard Bot Madr* 56:337–349

- Mahely AC, Chance B (1954) The assay of catalases and peroxidases. In: Glick D (ed) Methods of biochemical analysis, vol I. Churchill, London, pp 408–424
- Nakata PA, McConn MM (2003) Calcium oxalate crystal formation is not essential for growth of *Medicago truncatula*. Plant Physiol Biochem 41:325–329
- Perry RH, Green DW, O'Mahoney JH (1997) Perry's chemical engineers' handbook, 7th edn. McGraw-Hill, New York
- Rahman MS, Perera CO (1999) Drying and food preservation. In: Rahman MS (ed) Handbook of food preservation. Marcel Dekker, Inc., New York, pp 173–216
- Voget CE, Maza LA, Balatti A (1987) Determinación colorimétrica de glucosa oxidasa en preparado enzimático y extractos celulares. Rev Latinoam Microbiol 30:47–52
- Whitaker JR (1994) Principles of enzymology for the food science, 2nd edn. Marcel Dekker Inc., New York, p 648
- Winton AL, Barber-Winton K (1939) The structure and composition of foods. Sugar, sirup, honey, tea, coffee, cocoa, spices, extracts, yeast, baking powder, vol IV. Wiley, New York, pp 408–413

# **Refined Hemisphaericin Stabilization by Microencapsulation with Arabic Gum and Spray Drying**

**L.A. Reyes, M.I. Cortés-Vázquez, M.C. Oliver-Salvador,  
J. Yáñez-Fernández, and R. Briones-Martínez**

## **Abbreviations**

AG	Arabic gum
CCD	Central composite design
PC	Protein concentration
RH	Refined hemisphaericin
RHME	Refined hemisphaericin microencapsulated
RS	Response surface
SEM	Scanning electron microscopy
T	Spray drying feed temperature
TU	Tyrosine unit
YIELD	Microencapsulation yield

---

L.A. Reyes • M.C. Oliver-Salvador

Laboratorio de Biotecnología Alimentaria, Unidad Profesional Interdisciplinaria de Biotecnología del IPN, Av. Acueducto S/N, Col. Barrio la Laguna Col. Ticoman, C.P. 07340, México D.F., Mexico

M.I. Cortés-Vázquez • R. Briones-Martínez (✉)

Laboratorio de Enzimas Vegetales, Centro de Desarrollo de Productos Bióticos del IPN, Carretera Yautepec-Joxtla Km 6, Calle CEPROBI 8, Col. San Isidro, 62731 Yautepec, Morelos, Mexico

e-mail: [rbrionessmartinez@gmail.com](mailto:rbrionessmartinez@gmail.com)

J. Yáñez-Fernández

Departamento de Bioingeniería de la Unidad Profesional Interdisciplinaria de Biotecnología, Instituto Politécnico Nacional. Av. Acueducto s/n, Barrio la Laguna Ticomán, Mexico City, DF CP 07340, Mexico

## 1 Introduction

Hemisphaericin, the protease from the fruits of *Bromelia hemisphaerica*, is found as a complex of nine multiple molecular forms, identified by isoelectric points distributed over a pH range from 3.5 to 9.0 (Garduño et al. 1974). Cortés-Vázquez et al. (2008) have reported the purification and characterization of hemisphaericin-C, a 24 kDa cationic protease with primary substrate specificity of dual type. On the other hand, several studies on industrial applications for hemisphaericin have been carried out successfully, including fish protein solubilization, beer chill proofing, malt adjunct hydrolysis, plant protein functional property improvement (Briones-Martínez et al. 1994), and antioxidative peptide production from whey proteins (Palma-Rodríguez 2008).

The incorporation of bioactive components in small capsules, like enzymes or derived products, allows the protection of these materials against the action of free radicals, humidity, and other unfavorable conditions that may alter their stability (Desai and Park 2005). Among the diverse techniques employed to form micro-capsules, spray drying has been widely used in food processing since the 1950s, due to its low cost and efficiency. One of the main advantages of microencapsulation by spray drying is the short time needed to perform the drying operation, especially for thermosensitive materials like enzyme preparations.

An ample range of wall materials is used in spray drying; the most common are modified starches, maltodextrins, arabic gum, and lipids or proteins. Arabic gum, a complex polysaccharide, with a highly branched chain structure formed by D-glucuronic acid, L-rhamnose, D-galactose, and L-arabinose, confers low viscosity, solubility, and excellent emulsifying properties to the formed particles (Dickinson 2003).

Isolated enzymes are more susceptible to loss of activity, since their instability as they remain in solution increases the liability of these biomolecules to the action of denaturing agents. Nowadays, the use of industrial enzymes is increasing, and it is necessary to produce stable preparations of proteases. Among industrial preparations, enzymes belong to a very delicate group, and manufacturers are looking for stability improvement, optimal shelf life, and protection against environmental factors (humidity, light, oxygen, and acidity). In previous work in our laboratory, Briones-Martínez et al. (1994) obtained refined hemisphaericin by spray drying at pilot plant scale, with hydrocolloid arabic gum as a protective agent; the preparations presented high levels of residual proteolytic activity. Later, Yáñez-Fernández et al. (2001) conducted preliminary studies on spray-dried hemisphaericin with maltodextrins 10DE and arabic gum; in this work they found that arabic gum (40 %) formulae provided the greatest protection to the proteolytic activity of hemisphaericin.

The objective of this study is the optimization of a set of microencapsulation conditions of hemisphaericin protease, with arabic gum and by spray drying, using response surface methodology (RSM), in order to improve the stability and shelf life of hemisphaericin.

## 2 Materials and Methods

### 2.1 Refined Hemisphaericin (RH) Preparation

RH was selected for the microencapsulation study. RH is a preparation obtained by the method of Briones-Martínez and Cortés-Vázquez (2000), which includes several operations: liquid-solid extraction, centrifugal clarification, ultrafiltration, and drying. After 30-kDa ultrafiltration, the enzyme activity of the preparation was specified as 444 tyrosine unit (TU) (assayed without cysteine) and 818 TU (assayed with cysteine).

### 2.2 Response Surface (RS) Experimental Design

RS design and analysis were carried out using Design Expert 5 software. A central composite design was used to investigate the variation of microencapsulation with respect to the factors arabic gum concentration and drying inlet temperature. The response variables were protein concentration, proteolytic activity, and microencapsulation efficiency, resulting in 13 experimental settings (runs) with five repetitions on the central point. The experimental conditions are listed in Table 1.

### 2.3 Microencapsulation of Refined Hemisphaericin

Microencapsulation was carried out by mixing 7–22 % AG with RH, followed by drying into a spray dryer (Mini Spray Dryer, B-290, Büchi). The range of assayed temperature at the inlet was between 105 and 135 °C, the feeding rate was 2.77 ml/min, and fixed airflow was at 100 %.

**Table 1** Central composite design (CCD) for microencapsulation of RH

Run no.	1	2	3	4	5	7	8	13	Central point
AG (%)	15	10	22.07	20	20	10	15	7.93	15
T (°C)	105.86	110	120	130	110	130	134.14	120	120

## 2.4 Refined Hemisphaericin Microencapsulated Yield (YIELD)

Yield was defined by

$$\text{Yield} = \frac{(\text{microencapsulated Refined hemisphaericin [g]} \times 100)}{(\text{AG concentration [g]} + \text{refined hemisphaericin protein concentration [g]})} \quad (1)$$

## 2.5 Scanning Electron Microscopy

The surface morphology of RH microcapsules was studied by SEM. Microcapsules were attached with a two-sided carbon tape, and then gold coated in a Desk II Denton Vacuum coater for 500 s. The coated microcapsules were examined in a JEOL SEM.

## 2.6 Protein Concentration Assay

The protein content in the refined hemisphaericin preparations and the microcapsules were determined by the Bradford method (1976) and using bovine serum albumin as a standard.

## 2.7 Proteolytic Activity Assay

Hemisphaericin activity was measured by the method of Ortega and del Castillo (1966), based on the hydrolysis of casein. A standard curve was generated with tyrosine. One unit of protease activity, tyrosine unit (TU), was defined as the amount of enzyme required to liberate 1 µg of tyrosine per minute per mg protein, under the used conditions.

# 3 Results and Discussion

The conditions for the microencapsulation of RH were analyzed by central composite design (CCD) of one block with five repetitions at the central point, with respect to the parameters for spray drying feed temperature ( $T$ ) and arabic gum concentration (AG). These parameters produced 13 experimental settings (Table 1)

at AG concentration from 7 to 22 % (w/v) and feed temperature ( $T$ ) from 105 to 135 °C in the spray drying operation.

No significant changes in protein concentration were observed in the RH micro-capsules obtained at AG concentrations from 7 to 22 % and T from 105 to 135 °C (data not shown). Statistical analysis of the results (variance analysis adjusted to a quadratic model with a significance level of  $p \leq 0.05$ ) generated the following equation:

$$\begin{aligned} \text{Protein concentration} = & -0.662 + 0.013X_1 + 0.027X_2 - 4.987 \times 10^5 X_1^2 \\ & - 7.295 \times 10^{-4} X_2^2 + 4 \times 10^5 X_1 X_2 \end{aligned} \quad (2)$$

where  $X_1$  is the temperature (°C), and  $X_2$  is the concentration of arabic gum [g].

Figure 1 shows response surface plots of refined hemisphaericin microencapsulated (RHME) variations as a function of AG concentration and feed temperature ( $T$ ): the effect on proteolytic activity assayed with cysteine (Fig. 1I) and the effect on proteolytic activity without cysteine (Fig. 1II). Also described in this figure are the observed changes in the microcapsules as a consequence of storage time at 5 °C: (A)  $t = 0$ , (B) 1 month, and (C) 2 months.

Higher proteolytic activity (816 TU), assayed in the presence of cysteine, was found for microcapsules obtained with AG concentration between 7 and 10 % dried at 120–130 °C. On the other hand, the response surface plot of proteolytic activity, without cysteine, exhibited the best value (117 TU) under the central point conditions: 120 °C and 15 % AG (Fig. 1I).

Surface response results showed that better conditions were located at 7–15 % AG and 120–130 °C of  $T$ , where greater activity levels (with and without cysteine) were achieved. Statistical analysis of the results generated the following equations:

$$\begin{aligned} \text{Proteolytic activity} = & 1,551.51 - 10.788 X_1 + 19.794 X_2 + 0.062 X_1^2 \\ & + 1.090 X_2^2 - 0.255 X_1 X_2 \end{aligned} \quad (3)$$

and without cysteine:

$$\begin{aligned} \text{Proteolytic activity} = & -5,464.44 + 83.256 X_1 + 70.836 X_2 - 0.322 X_1^2 \\ & - 1.084 X_2^2 - 0.323 X_1 X_2 \end{aligned} \quad (4)$$

After 1 month of storage, better proteolytic activity for RHME, without the reducing agent cysteine, was found in samples corresponding to experimental runs number 7 and 9 and in the central point, namely 10 % AG-130 °C, 15 % AG-135 °C, and 15 % AG-120 °C, respectively. Meanwhile, the better activity (almost 100 TU) of RH microcapsules stored for 2 months corresponded to capsules produced with 10 % GA-130 °C, the conditions in the experimental run 7 (Fig. 1IIC).

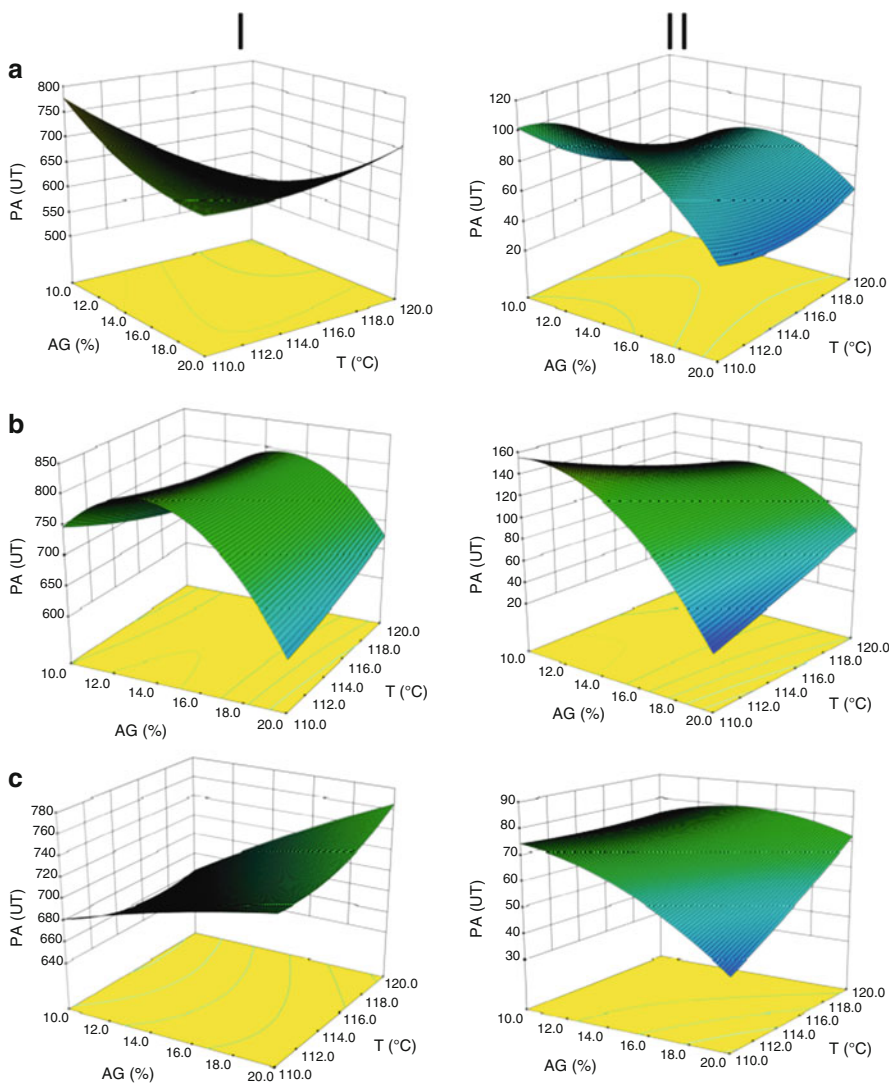


**Fig. 1** Response surface analysis showing the effect on proteolytic activity (PA) assayed with cysteine (I), and on proteolytic activity without cysteine (II), of arabic gum (AG) concentration and microencapsulation feed temperature (T). **(a)**  $t = 0$ ; **(b)** 1-month storage at  $5^{\circ}\text{C}$ ; **(c)** 2-month storage at  $5^{\circ}\text{C}$

The response surface graph for proteolytic activity of RHME with cysteine after 1 month of storage (Fig. 1IB) shows an increase for the experimental runs 4, 5, 7, 9, and 13, especially for the 7.93 % AG and 120 °C conditions of run 13. After the second month of storage, better activity (around 900 TU) was found for those conditions assayed in runs 7 and 13, that is, 10 % AG-130 °C and 7.9 % AG-120 °C,

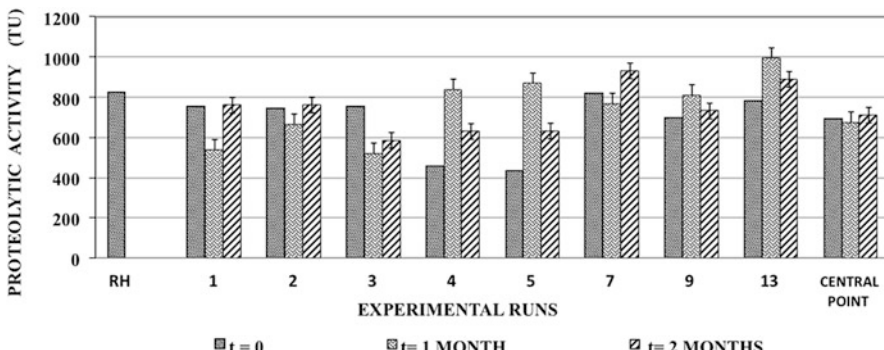


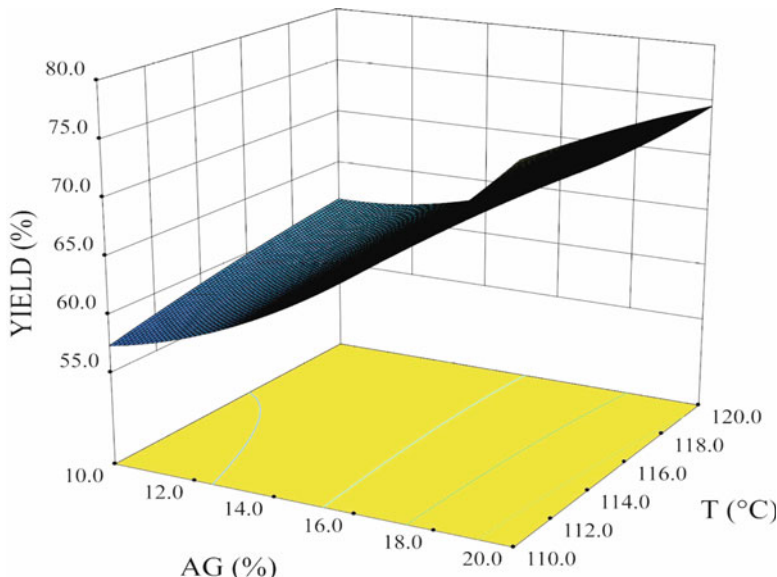
**Fig. 2** Proteolytic activity (cysteine activated) of microencapsulated refined hemisphaericin

respectively (Fig. 1IC). It is clear from surface response analysis of changes in proteolytic activity of RHME that after 2-month storage better conditions to achieve optimum microencapsulation would be 7–10 % AG and T between 120 and 130 °C.

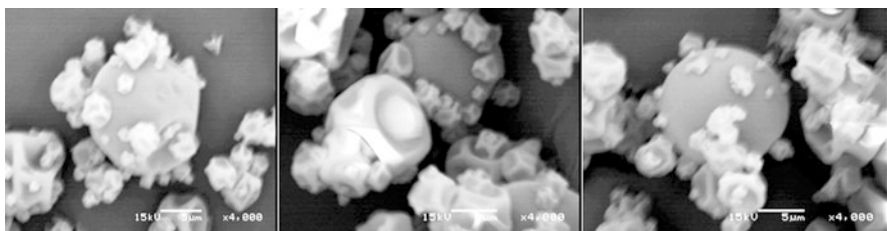
A decrease of almost 100 % in proteolytic activity without cysteine was observed in microcapsules after the drying process and after storage (data not shown), compared to initial activities (818 TU with cysteine and 444 TU no-cysteine). These results showed an oxidative effect on the enzyme, probably caused by the ingredient mixing operation and the spray drying process itself.

Figure 2 illustrates the effect of storage time on RHME proteolytic activity with cysteine. A decrease in activity was observed in samples of experimental runs 1, 2, and 3 and in the central point after the first month. Proteolytic activity rose above 100 %°C for the experimental runs 4, 5, 9, and 13. Later on, with these capsules and after 2 months, a drop in activity of 25 and 27 % was observed. The most active preparation was that obtained from run number 7, with a 21 % improvement over the original activity. In a period of 2 months, the conditions of runs 7 and 13 generated the least loss in activity (932 and 890 TU), 10 % AG-130 °C and 7.93 % AG-120 °C, respectively. The more stabilized preparation was the central point sample, obtained with 15 % AG-120 °C, in spite of the measured lower activity values (711 TU), compared to that from 7 and 13 preparations. A clear diminution in RH proteolytic activity was observed as a result of the high susceptibility of the enzyme to oxidation during the process of microencapsulation, due to its sulfhydryl nature as a thiol protease characterized by a cysteine residue at its active site, a situation that may be reverted when a reductive agent like cysteine is added.

The response surface for yield of microencapsulation of RH as a function of the parameters GA and T showed that an increase in the concentration of AG, at any temperature within the range tested (105–135 °C), results in a yield reduction of microencapsulation, while low concentrations of AG (10 %) and high drying temperatures (130 °C) provide higher yields (Fig. 3). The best conditions for microencapsulation of RH and the relationship between the response (%yield)



**Fig. 3** Response surface for yield of microencapsulation of RH as a function of the parameter arabic gum (AG) and feed temperature ( $T$ )



**Fig. 4** Scanning electronic microscopy of microencapsulated RH

and the variables were determined by an analysis of variance adjusted to a quadratic model, expressed by the following equation:

$$\text{YIELD (\%)} = 534.23 - 6.917X_1 - 3.591X_2 + 0.026X_1^2 - 0.042X_2^2 + 0.029X_1X_2 \quad (5)$$

The surface morphology and microcapsule size were observed by SEM of RHME preparations. The results are shown in Fig. 4. Particles were dispersed within sizes from 5 to 50  $\mu\text{m}$ ; greater diameters were observed for those dried under 135 °C and 22 % AG. The microcapsules were spherical and irregularly shaped, and small-sized particles were susceptible to agglomeration.

## 4 Conclusions

Better stability at the assayed time of storage was found for proteolytic preparations obtained with 7.9 % AG at 120 °C (experimental run 13), which improved the initial activity by 14.8 %; similarly, capsules prepared with 10 % AG at 130 °C (run 7) showed a 14.2 % greater activity than the initial sample (zero time). The sample with the most stability was that obtained at the central point, with 15 % AG and 120 °C; nevertheless, this sample presented lower activity (711 TU) than those obtained under the assayed conditions in runs 7 and 13 (932 and 890 TU).

**Acknowledgments** FOMIX-GOB CAMP-CONACYT 8996 and SIP-IPN 20090276 grants supported this work. The authors are SIBE-IPN and EDI-IPN grant holders.

## References

- Bradford MM (1976) A rapid and sensitive method for the quantitation of microgram quantities of protein utilizing the principle of dye binding. *Anal Biochem* 72:248–254
- Briones-Martínez R, Cortés-Vázquez MI (2000) Avances en los estudios científicos y tecnológicos de la hemisfericina: Una nueva proteinasa de interés industrial. In: Tapia M (ed) Contribuciones a la Investigación Regional en el Estado de Morelos. CRIM-UNAM, México, pp 425–467
- Briones-Martínez R, Oliver-Salvador MC, Cruz MT, Cortés MI (1994) Preparaciones enzimáticas de interés industrial con proteinasas de plantas mexicanas. *Inf Tecnol* 5–1:29–38
- Cortés-Vázquez MI, Muñoz-Sánchez JL, Briones-Martínez R (2008) Substrate specificity of a cationic peptidase from *Bromelia hemisphaerica* L. *Nat Prod Commun* 3(3):351–355
- Desai KGH, Park HJ (2005) Recent developments in microencapsulation of food ingredients. *Drying Technol* 23:1361–1394
- Dickinson E (2003) Hydrocolloids at interfaces and the influence on the properties of dispersed systems. *Food Hydrocolloids* 17:25–39
- Garduño R, Soriano M, Chávez E, Cruz VMT, Del Castillo LM, Castañeda-Agulló M (1974) Proteinases de plantas mexicanas II. Puntos isoeléctricos y caracterización de formas moleculares múltiples en enzimas de bromeliáceas. *Rev Lat Quím* 5:243–248
- Ortega ML, del Castillo LM (1966) Actividad de la mexicana en presencia de altas concentraciones de urea. *Ciencia Méx* 24(5/6):247–251
- Palma-Rodríguez HM (2008) Efecto de la hemisfericina refinada en la hidrólisis de proteína de suero lácteo. Master science thesis, CEPROBI-IPN, México
- Yáñez-Fernández J, Méndez-Montealvo G, Menéndez-Aguirre O, Cortés-Vázquez MI, Briones-Martínez R (2001) Spray drying of hemisphaericin from *Bromelia hemisphaerica*. In: Barbosa-Canovas GV et al (Eds). Proceedings of eight international congress of engineering and food, Technomic Publishing Co Inc, pp 1156–1160

# Salt Crystallization in Chitosan Films as Affected by Solvent pH and Moisture Content

M. Vargas, C. González-Martínez, and A. Chiralt

## Abbreviations

$\%E$	Percentage of elongation at break
$a_w$	Water activity
CH	Chitosan
DSC	Differential scanning calorimetry
EM	Elastic modulus
LSD	Least significant differences
Solvent I	Acetic acid-sodium acetate buffer solution (85.5 mM) at pH 3.8
Solvent II	Acetic acid-sodium acetate buffer solution (85.5 mM) at pH 5.2
TS	Tensile strength

## 1 Introduction

Chitosan (CH) is a cationic biopolymer used as a matrix to develop edible films and coatings for food applications. When developing chitosan-based film-forming dispersions and films, CH is usually dissolved in aqueous acetic acid solutions ( $\text{pH} = 3.8$ ); sodium hydroxide is often added to increase the pH of the solvent, thus preventing film solubilization at high relative humidity conditions, which can cause

---

M. Vargas (✉) • C. González-Martínez

Departamento de Tecnología de Alimentos-Instituto Universitario de Ingeniería de Alimentos para el Desarrollo, Universidad Politécnica de Valencia, Valencia, Spain

e-mail: [mavarco@tal.upv.es](mailto:mavarco@tal.upv.es)

A. Chiralt

Institute of Food Engineering for Development, Department of Food Technology,  
Universitat Politecnica de Valencia, Camino de Vera, s/n., 46022 Valencia, Spain  
e-mail: [dchiralt@tal.upv.es](mailto:dchiralt@tal.upv.es)

changes in the solvent properties (pH and ionic strength) affecting the structure and properties of the obtained films. This is particularly significant for chitosan, since its conformation in solution greatly depends not only on structural parameters like the degree of acetylation and chain length, but also on solution parameters such as ionic strength, solvent, temperature, and pH (Sorlier et al. 2002). During film drying, changes in solvent properties occur in line with water evaporation: increase in ionic strength, change in pH, and conformational modifications in the polymer chain. Moreover, when sodium hydroxide is added to chitosan-based film-forming dispersions, sodium-acetate tri-hydrate salts can crystallize, since these are oversaturated when the film reaches determined water content, depending on molecular mobility, which in turn is greatly affected by film moisture content.

The purpose of this work is to study the influence of solvent conditions in the film-forming dispersion (ionic strength and pH) on CH film properties such as water sorption behavior, and thermal (phase transitions), mechanical, and microstructural properties.

## 2 Materials and Methods

### 2.1 Preparation of Films

High-molecular-weight chitosan (1 g/100 g) was dispersed in acetic acid-sodium acetate buffer solution (85.5 mM) at pH 3.8 (solvent I) or 5.2 (solvent II). In each case, crystallization of acetate tri-hydrate-chitosan can occur in the dried film and the estimated ratios, by considering that the corresponding concentrations in the aqueous dispersion, are 0.245 g/g chitosan and 1.826 g/g chitosan, for solvent I and solvent II, respectively. All reagents were supplied by Sigma-Aldrich (Madrid, Spain). Chitosan (CH) solutions were poured into a framed and levelled polytetrafluorethylene plate and then dried at room temperature for 48 h. The surface density of polymer in the dry films was 56 g/m<sup>2</sup>. Film thickness was measured using a handheld digital micrometer (Palmer-Comecta, Spain, ±0.001 mm). The thickness of each film was measured in five random positions and the mean values were used to calculate the mechanical parameters.

### 2.2 Water Sorption Isotherms

For the adsorption experiments, dry film specimens, in triplicate, were placed at 20 °C in hermetic chambers containing oversaturated salt solutions with different water activity ( $a_w$ ): LiCl (0.11), MgCl<sub>2</sub> (0.34), K<sub>2</sub>CO<sub>3</sub> (0.43), Mg(NO<sub>3</sub>)<sub>2</sub> (0.54), KI (0.72), and KCl (0.85). Samples were weighed periodically until a constant value was reached, where the equilibrium was assumed to be achieved (Spiess and Wolf 1983). Finally, equilibrium moisture content was determined using a vacuum oven at 70 °C for 24 h.

### ***2.3 Differential Scanning Calorimetry***

Differential scanning calorimetry (DSC) was carried out using a DSC 220 CU-SSC5200 (Seiko Instruments, Tokyo, Japan). Small amounts (20–30 mg) of samples were placed onto aluminum pans and conditioned at various relative humidity conditions (saturated salt solutions, as mentioned above) in desiccators at 20 °C. When the equilibrium was reached, the samples were then hermetically sealed and heated between –50 and 150 °C in order to analyze phase transitions. Cooling scans were performed at 10 °C/min and heating scans at 5 °C/min. An empty aluminum pan was used as reference.

### ***2.4 Microstructure***

Dry films were stored in a desiccator with P<sub>2</sub>O<sub>5</sub> for at least 15 days to ensure that no water was present in the film. Microstructural analysis of cross sections of the films was carried out using SEM technique in a JEOL JSM-5410 (Japan) electron microscope. Pieces of 5 × 1 mm were cryo-fractured from films and mounted in copper stubs. Samples were gold coated and observed using an accelerating voltage of 10 kV.

### ***2.5 Mechanical Properties***

Dry films were preconditioned in desiccators at 20 °C and 58.5 % relative humidity for 2 weeks prior to testing ( $a_w = 0.54$ ). Mechanical properties were measured by using a Texture Analyzer TA-XT-plus (Stable Micro Systems, Surrey, UK), with a 500 N load cell equipped with tensile grips (A/TG model). Sample films were cut into 25.4 mm wide and 100 mm long strips, according to the ASTM D-882 standard (ASTM 2001). Grip separation was set at 50 mm, with a cross-head speed of 50 mm/min. Tensile strength (TS), percentage of elongation (%E) at break, and elastic modulus (EM) were evaluated in eight samples from each type of film.

### ***2.6 Statistical Analysis***

Results were analyzed by multifactor analysis of variance with 95 % significance level using Statgraphics<sup>®</sup>Plus 5.1. Multiple comparisons were performed through 95 % least significant difference (LSD) intervals.

### 3 Results and Discussion

Water sorption isotherms of films are shown in Fig. 1. Water sorption isotherms for CH film prepared with solvent I showed a typical sigmoid shape, increasing slowly in line with  $a_w$  up to 0.7, beyond which a steep rise in moisture content was observed, owing to the solubilization phenomenon. This sigmoid shape was also observed by other authors in pure CH films (Del Nobile et al. 2004; Vargas et al. 2009). Experimental adsorption data of films prepared with solvent I were fitted to the Guggenheim–Anderson–de Boer (GAB) model; the predicted sorption isotherm is shown in Fig. 1. Monolayer moisture content was 0.09 g water/g dry solids, which is in the range of the values reported in the literature (Fernández Cervera et al. 2004). For films prepared with solvent II, equilibrium moisture content values were higher and almost constant in films equilibrated at  $a_w$  values up to 0.7. The greater water sorption capacity of the films prepared with solvent II can be attributed to gain of crystallization water molecules of sodium acetate tri-hydrate, which supposed 0.256 g of crystallization water/g total dry solids if all of the present ions form crystals. At the lowest  $a_w$  values, no differences in equilibrium moisture contents were observed between films obtained with solvents I and II, but at  $a_w$  0.3 onwards, when molecular mobility in the film reaches a critical level, salt crystallization promotes the gain of water crystallization molecules. From  $a_w$  0.7 onwards, films prepared with solvent II also had greater water sorption capacity, showing more intense solvent effects, due to the presence of a higher amount of ions that can bond water molecules.

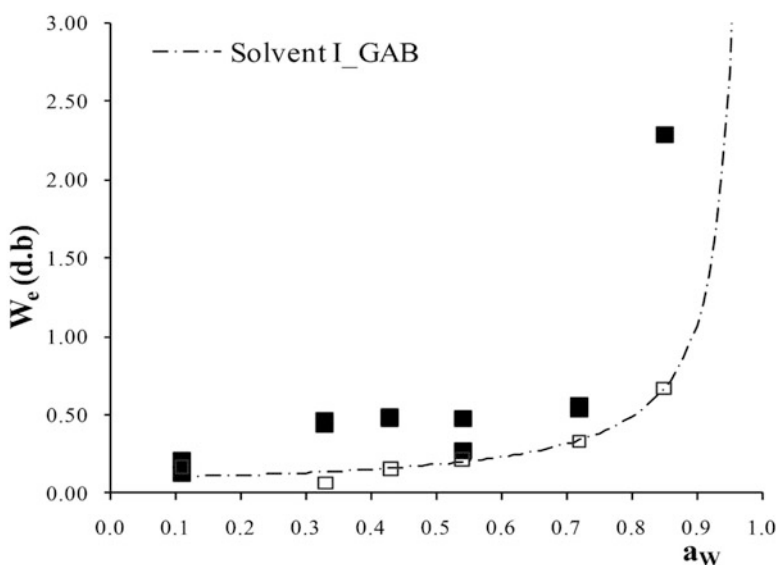


**Fig. 1** Water sorption isotherms (experimental values and GAB fitted model for solvent I) of CH films prepared with solvent I (empty symbols) or solvent II (filled symbols) at 20 °C

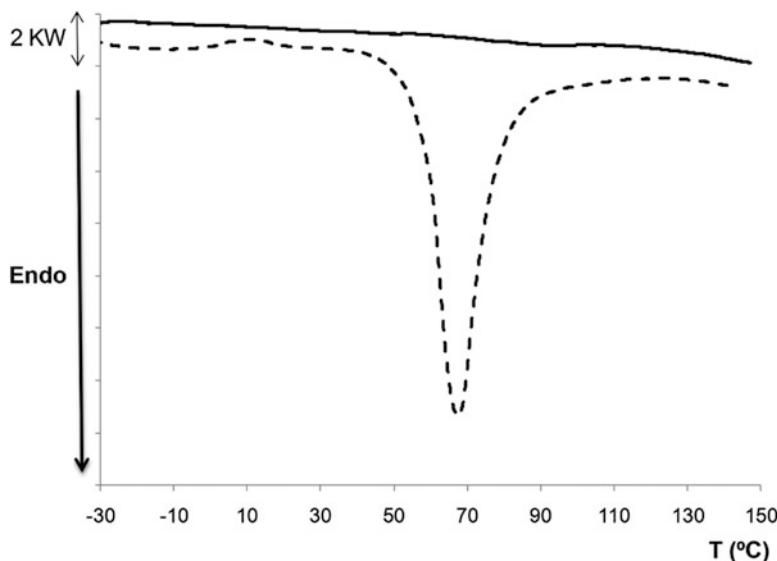


**Fig. 2** DSC thermograms of chitosan films prepared with solvent I (solid line) and solvent II (dashed line) equilibrated at  $a_w = 0.54$

**Table 1** Initial melting temperature and melting enthalpy ( $\Delta H$ ) of chitosan films prepared with solvent II and equilibrated at different water activity values

$a_w$	$T_m$	$\Delta H$ (J/g film)	$\Delta H$ (J/g sodium acetate tri-hydrate)
0.11	54 (1)	10 (3)	12 (1)
0.33	42 (3)	152 (2)	238 (1)
0.43	35 (3)	156 (8)	250 (12)
0.54	34 (1)	157 (7)	231 (16)
0.72	20 (5)	172 (26)	288 (47)

Mean values and standard deviation (in brackets)

DSC thermograms of chitosan films obtained with solvent I and II are shown in Fig. 2, where the characteristic melting endotherm of acetate tri-hydrate (melting temperature 55.6–56.5 °C, melting enthalpy 237–243 J/g, Cabeza et al. 2003) can be observed for films prepared with solvent II. This result corroborates salt crystallization in the film when ions are present at high concentration in the film-forming dispersion (solvent II), which notably does not occur at the lowest ionic strength (solvent I). Table 1 shows the values of initial melting temperature and the melting enthalpy of chitosan-based films prepared with solvent II as a function of their water activity. The initial melting temperature of sodium acetate tri-hydrate crystals decreases with increase in the sample water activity, whereas the melting enthalpy tends to increase. This result indicates that a different degree of salt crystallization occurs as a function of the film moisture content. When water uptake rises in the film and molecular mobility is promoted, crystallization occurs to a

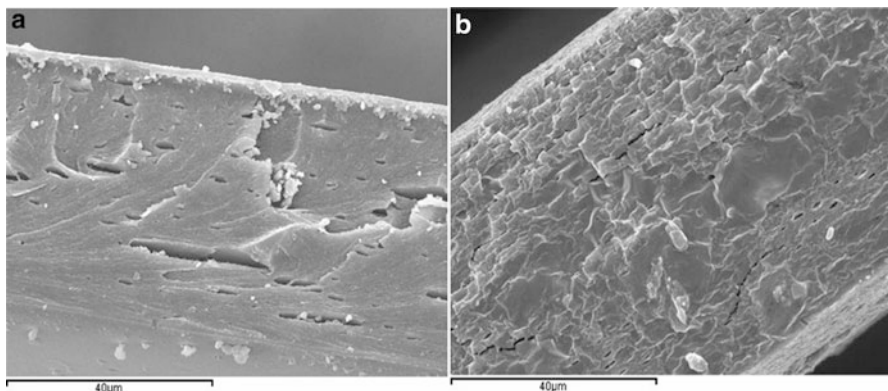


**Fig. 3** SEM micrographs of cross sections of chitosan films prepared with solvent I (a) or solvent II (b)

**Table 2** Mechanical properties of chitosan-based films ( $a_w = 0.54$ ) obtained with solvent I and II

Solvent	EM (MPa)	TS (MPa)	E (%)
I	1,383 (150) <sup>a</sup>	35 (3) <sup>a</sup>	12 (5)
II	392 (219) <sup>b</sup>	12 (7) <sup>b</sup>	15 (7)

Mean values and standard deviation (in brackets)

<sup>a,b</sup>Different letters indicate significant differences ( $p < 0.05$ )

greater extent and the area of the crystal melting endotherm increases. The values of enthalpy of melting were expressed per gram of salt, assuming that all of the present ions crystallized in accordance with the stoichiometric ratio. Enthalpy values were within the range reported for sodium acetate tri-hydrate pure salt when  $a_w$  in the film was 0.33 or higher; the latter indicates that the total amount of ions can crystallize when the threshold moisture content is reached, in accordance with the obtained equilibrium sorption data (Fig. 1).

Figure 3 shows SEM micrographs of chitosan films, where microcrystals of sodium acetate tri-hydrate can be clearly detected in films prepared with solvent II. These microcrystals interrupt the polymer matrix and hinder the regular and linear aggregation of the polymer chains, having a significant effect on the mechanical properties of the films (Table 2). Elastic modulus (EM), tensile strength (TS), and percentage of elongation at break (%E) values were lower than those reported in previous studies carried out with chitosan films prepared with acetic acid solutions ( $\text{pH} = 3.8$ ) without adjusting pH with NaOH (Sánchez-González et al. 2010). Moreover, all parameters drastically decreased in films prepared with solvent II, where crystallization of sodium acetate tri-hydrate led to softer and less stretchable films with less resistance to break. This finding is in agreement with both the occurrence of interruptions in polymer chain aggregation in the film matrix and the presence of more discontinuities in the polymer network (Fig. 3b).

## 4 Conclusion

Water sorption isotherms and mechanical properties of chitosan films prepared under different solvent conditions were significantly affected by ion concentration and pH. Increase in pH and ionic strength of the solvent led to an increase in the water sorption capacity of films, with a significant decrease in the resistance to break and the ability to stretch of chitosan films. The reported changes can be explained by the crystallization of sodium-acetate tri-hydrate in chitosan films prepared with solvent II ( $\text{pH} = 5.2$ ), which was revealed by the salt melting values obtained by DSC thermal analysis and film microstructure.

**Acknowledgements** The authors acknowledge the financial support provided by Universidad Politécnica de Valencia (Project 20091068) and Conselleria de Empresa, Universidad y Ciencia (GV/2010/082).

## References

- ASTM (2001) Standard test method for tensile properties of thin plastic sheeting Standard D882. In: ASTM (ed) Annual book of ASTM. ASTM, Philadelphia, pp 162–170
- Cabeza LF, Svensson G, Hiebler S, Mehling H (2003) Thermal performance of sodium acetate trihydrate thickened with different materials as phase change energy storage material. *Appl Therm Eng* 23:1697–1704
- Del Nobile MA, Buonocore GG, Conte A (2004) Oscillatory sorption tests for determining the water vapour transport properties of chitosan based edible films. *J Food Sci* 69:44–49
- Fernández Cervera M, Karjalainen M, Airakisan S, Rantanen J, Krogars K, Heinäimäki J, Iraizoz Colarte A, Yliruusi J (2004) Physical stability and moisture sorption of aqueous chitosan-amylose starch films plasticized with polyols. *Eur J Pharm Biopharm* 58:69–76
- Sánchez-González L, Cháfer M, Chiralt A, González-Martínez C (2010) Physical properties of chitosan films containing bergamot essential oil and their inhibitory action on *Penicillium italicum*. *Carbohydr Polym* 82:277–283
- Sorlier P, Viton C, Domard A (2002) Relation between solution properties and degree of acetylation of chitosan: role of aging. *Biomacromolecules* 3:1136–1342
- Spiess WEL, Wolf WR (1983) The results of the COST 90 project on water activity. In: Jowitt R et al (eds) *Physical properties of foods*. Applied Science Publishers, London, pp 65–91
- Vargas M, Albors A, Chiralt A, González-Martínez C (2009) Characterization of chitosan-oleic acid composite films. *Food Hydrocolloids* 23:536–547

# Water Antiplasticization Effect in Biscuits as Affected by Glucose and Sucrose Addition

P. Pittia, G. Di Teodoro, and G. Sacchetti

## Abbreviations

$a_w$	Water activity
B0	Short dough biscuit original formula
B12	Short dough biscuits with sucrose
Cg	Measure of the strength of binding of water to the primary binding sites
ERH	Equilibrium relative humidity
G12	Short dough biscuits with glucose
GAB	Guggenheim-Anderson-de Boer equation
Tg	Glass transition temperature
Tg <sub>dry</sub>	Matrix glass transition temperature
Xm	Amount of water capable of interacting with all of the available adsorption sites in a material

## 1 Introduction

Water is the most effective plasticizer in food matrices, decreasing glass transition temperature (Tg) and mechanical resistance and determining a softening effect with concentration increase.

An opposite effect (i.e., hardening, toughening), referred to as antiplasticization, was observed in some foods in a glassy state undergoing moisture uptake within a specific moisture or water activity ( $a_w$ ) range and below a specific moisture

---

P. Pittia (✉) • G. Di Teodoro • G. Sacchetti  
Department of Food Science, University of Teramo, Via C.R. Lerici 1,  
Mosciano S. Angelo, 64023 Teramo, Italy  
e-mail: [ppittia@unite.it](mailto:ppittia@unite.it)

threshold that must be exceeded before conventional plasticizing effects on physical properties can be manifested. Many hypotheses have been suggested for this phenomenon, but the causes are still unclear (Seow 2010; Pittia and Sacchetti 2008; Seow et al. 1999). This phenomenon, which occurs in food matrices of various compositional and structural properties, has been the subject of a limited number of investigations, and its complexity compels more research aimed at better understanding it.

Small solutes and polyols added in complex systems may hinder the antiplasticization upon moisture uptake by a so-called plasticizing mechanism (Peleg 1996). However, there is very scarce information about the effects of sugars on the changes of physical properties in glassy and amorphous starchy food products that are quite prone to exhibit toughening induced by moisture sorption (Katz and Labuza 1981; Suwonsichon and Peleg 1998; Marzec and Lewicki 2006).

An antiplasticization effect with increased stiffness due to the addition of mono- and disaccharides in both amorphous bakery products (Baltsavias et al. 1999a) and amylopectine-fructose systems (Kalichevsky and Blanshard 1993) has been evidenced, although sugar addition decreases the glass transition temperature range of the system which, in turn, may favor plasticization due to moisture sorption. Baltsavias et al. (1999a) studied the effect of sugar (sucrose and fructose) addition on the mechanical properties of starch biscuits without considering the consequences of an eventual increase of moisture content.

The aim of this study was to evaluate the effect of two small saccharides (glucose and sucrose) on the mechanical properties of short dough biscuits hydrated at different moisture content.

## 2 Materials and Methods

Short dough biscuits were made by using a laboratory mixing apparatus, according to a reference recipe that did not include added sugars, with the following composition (on weight basis): wheat flour (72 %), water (20 %), and margarine (8 %) (B0, in the text). In the modified recipe, sucrose (B12) and glucose (G12) were added in the formulation at a concentration of 12 % by reducing the same amount of flour, with a final concentration of 60 %. Manufacture of all types of biscuit was carried out according to a standardized procedure. The ingredients were weighed (on a 500 g batch basis), then mixed for an optimized time to make a dough that was sheeted, laminated, and cut to obtain specimens of 5.0 cm length, 2 cm width × 0.3 cm height; cooking was carried out at 160 °C for 20 min in a professional oven. After cooling, biscuits were packed in plastic bags and stored in a desiccator. One series of samples of each type of biscuits was analyzed 24 h after preparation, while the remaining samples were rehydrated upon water-glycerol solutions at different equilibrium relative humidity (ERH, 10–90 %) until a plateau state was reached in the weight increase due to moisture sorption.

$a_w$  was determined by an Aqualab (Decagon Devices, Pullman, WA) hygrometer; moisture content was evaluated by gravimetical analysis after drying at 75 °C for 12 h in a vacuum oven.

Mechanical tests were carried out at 20 °C by using a dynamometer INSTRON (mod. 5542, Instron Universal Testing Machine, UK) equipped with a 500 N-head. Shear test was carried out on single specimens by using a flat cutting probe of 1 mm thickness at a head speed of 100 mm min<sup>-1</sup>. These testing conditions and probe type were chosen to mimic the stress conditions applied to the product at the first bite with the incisors. Bending test analysis was carried out by using a “triple-beam” probe system at head speed of 2 mm min<sup>-1</sup>. In these tests, force, energy, modulus, and strain at fracture were determined. Data reported are the average of at least ten repetitions carried out on two series of biscuits prepared at different times.

Sensory analysis of the samples, hydrated at different moisture content, was performed by a panel composed of untrained judges who were frequent consumers of short dough biscuits. Panelists were asked to score descriptors related to textural properties including crispness, fracturability, toughness, adhesiveness, and overall acceptability on a range scale of 1–7.

Water-matrix interactions were determined by sorption isotherm and carried out as reported in Pittia et al. (2007); moisture- $a_w$  data were fitted by the Guggenheim-Anderson-de Boer (GAB) equation (Van den Berg and Bruin 1981).

### 3 Results and Discussion

Biscuits just after preparation showed moisture content and  $a_w$  values in the range of 1.73 and 1.86 % and <0.1, respectively, with no significant differences due to the presence of sucrose and glucose.

Shear test analysis evidenced a force *vs.* deformation graph typical of low-moisture, amorphous matrices characterized by a jagged trend and, after the first major brittle fracture event, a series of fractures at lower stresses occurred until fracture was completed. In the bending test, only one main peak related to the fracture of the specimen was evidenced (data not shown). The substitution of flour with sugars of different types, but at the same concentration (12 %), significantly affected the mechanical properties of the products at their lower moisture content and  $a_w$  value. In particular, a higher fracture force and modulus, as well as a lower fracture energy, was determined for B12 and G12 by both shear and bending tests (Table 1). Strain was not affected by the addition of sugars when shear stress was applied, while the application of a flexural force evidenced a significant ( $p < 0.05$ ) lower strain in both sucrose- and glucose-added products with respect to B0. The presence of sugar controls hydration in the dough and tends to disperse protein and starch granules, thereby impairing the formation of a continuous mass of the product and leading to a more fragile structure. Moreover, as biscuits cool after cooking, small saccharides also tend to crystallize, acting as hardening agents, leading to more crispy products (Bean and Setser 1992). Because of the different

**Table 1** Mechanical properties of differently formulated biscuits just after preparation ( $a_w \sim 0.1$ ) determined by shear and bending test

Sample	Sugar (12 % w/w)	Shear test			Bending test			
		Force (N)	Modulus (N/mm)	Energy (mJ)	Strain	Force (N)	Energy (mJ)	Modulus (N/mm)
B0 <sup>a</sup>	–	20.05 ± 4.60	16.95 ± 4.23	49.42 ± 14.00	0.44 ± 0.06	9.35 ± 1.82	3.27 ± 0.74	18.32 ± 5.31
B12	Sucrose	24.86 ± 2.72	19.42 ± 6.16	36.21 ± 7.26	0.44 ± 0.08	15.32 ± 4.06	2.90 ± 0.90	49.91 ± 7.97
G12	Glucose	29.91 ± 6.45	26.22 ± 5.27	36.91 ± 10.26	0.42 ± 0.04	19.10 ± 4.16	4.27 ± 0.71	57.17 ± 14.90

<sup>a</sup> Reference, no sugars added

**Table 2** Regression parameters of GAB equation applied to sorption isotherms of BO, B12, and G12 short dough biscuits

Sample	Xm (% dry basis)	Cg	K	R <sup>2</sup>
BO	3.553	50.22	0.916	0.997
B12	3.092	25.35	0.977	0.991
G12	3.254	28.71	0.972	0.985

physical properties of sucrose and glucose, as well as their tendency to crystallize, this could have contributed to the influence on overall mechanical properties of the G12 samples. The lower strain evidenced in the B12 and G12 samples by bending is an indication that inhomogeneities involved in the fracture are of different size than B0, and sugars have contributed to develop a finer structure, with lower resistance to deformation before fracture (Baltsavias et al. 1999a).

Sorption isotherms of the different biscuits were carried and, as shown by the values of the parameters obtained by GAB fitting of the sorption isotherms, presence of sugars modified the water-matrix interactions (Table 2). The partial substitution of flour consisting mainly of starch and proteins, with either sucrose or glucose, determines the decrease of the amount of water capable of interacting with all of the available adsorption sites in a material (Xm), as well as of the measure of the strength of binding of water to the primary binding sites (Cg). This result could be related to both a change of the microstructural and physical properties of the main protein-starchy biscuit three-dimensional matrix, due to the presence of sugars that become denser and with fewer binding sites, and the presence of sugars in a crystalline state. Such crystalline states are known to exert lower water binding capacity with respect to their amorphous state which, in turn, enhances the freedom of the adsorbed water.

The role of water has usually been viewed as that of a plasticizer, in that an increase in moisture content serves to soften the material (Levine and Slade 1988; Slade and Levine 1995). However, recent studies have provided evidence that in some foods, humidification from a dried state could lead to stiffer and/or harder and tougher matrices before becoming more flexible/ductile while exhibiting continuous decrease of the glass transition temperature (Seow et al. 1999; Pittia and Sacchetti 2008).

In all of the differently formulated short dough biscuits, both plasticization and antiplasticization occurred due to hydration, but of different extent and at different  $a_w$  value ranges, depending on the presence of sugar and its nature. Differences in the effects of water on mechanical properties of the products were also noticed due to the test used (shear vs. bending).

In Fig. 1, fracture force data, which could be considered an empirical measure of the strength of differently prepared biscuits obtained by shear (Fig. 1a) and bending test (Fig. 1b) as a function of the hydration degree, are reported. By shear reference, biscuits (B0) showed an increase of the fracture force at increasing  $a_w$  that was not significant due to the high standard error of the data, while a significant softening effect due to increased hydration was observed for  $a_w$  values  $>0.6$ . Similar behavior was noticed for the B12 product, but the plasticization effect was determined at a higher  $a_w$  value ( $>0.8$ ). In the case of the glucose-added product, a significant

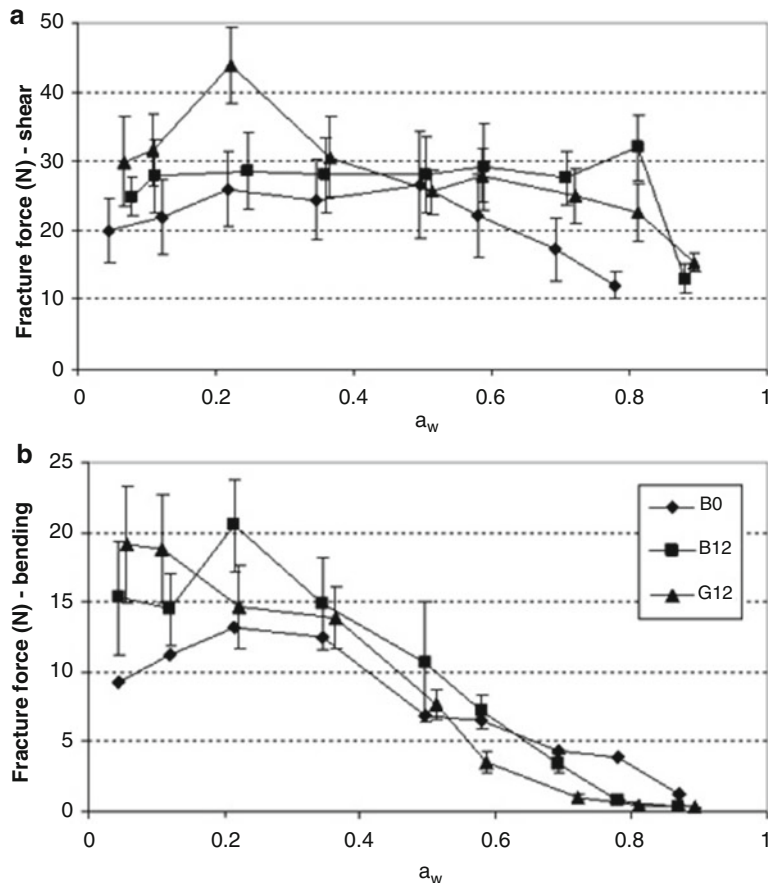


**Fig. 1** Fracture force of differently formulated biscuits hydrated at different  $a_w$  values evaluated by shear (a) and bending (b) test

increase of the fracture force occurred in the  $a_w$  range 0.1–0.4 before a significant decrease of strength occurred.

When flexural stress was applied, a lower fracture force was generally observed with respect to that obtained by shear (Fig. 1b). Different patterns of change in fracture force in response to moisture sorption were again observed in all biscuits types, but with other trends, and several are the factors that could have caused this result (Pittia and Sacchetti 2008).

Both B0 and B12 showed a softening and plasticizing effect of water at  $a_w$  values  $>0.5$ , as well as an increase of the strength for  $a_w$  values below 0.5, which is an index of antiplasticization. The role of water in biscuits added with glucose was, on the other hand, strictly that of a plasticizer with a progressive decrease of the fracture force at increasing  $a_w$ .

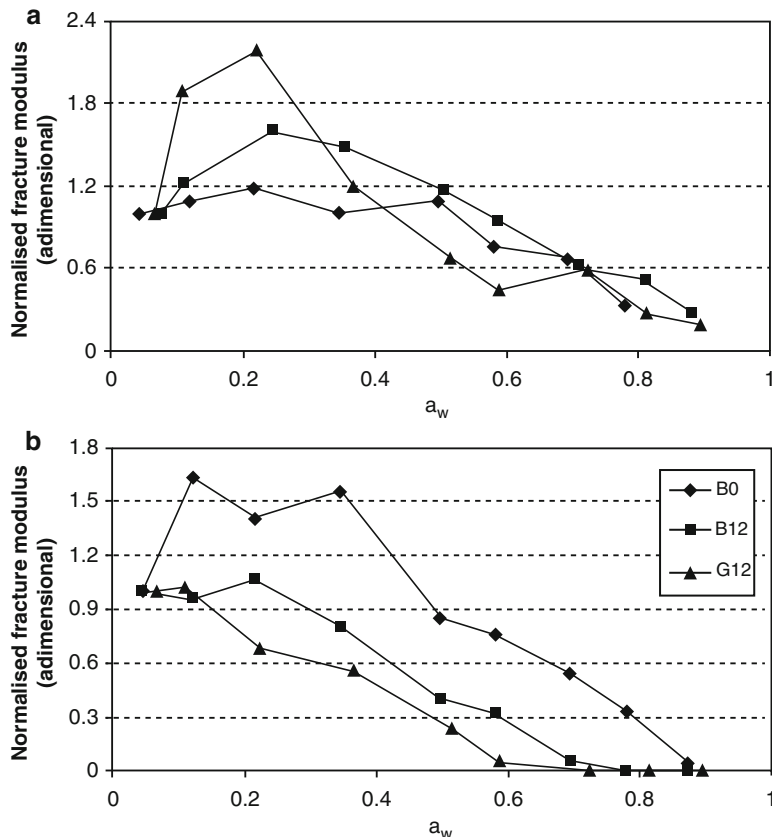


**Fig. 2** Normalized fracture modulus ( $m_{aw}/m_{aw=0}$ ) of differently formulated biscuits hydrated at different  $a_w$  values evaluated by shear (a) and bending (b) test

Data of the Young's modulus of both shear and bending tests were normalized with respect to the modulus of the dry product ( $a_w \approx 0.01$ ) to highlight the effects of sugars on the mechanical properties of matrices due to moisture uptake (Fig. 2). Young's modulus can be taken as a measure of the stiffness of a product, and is widely used to evaluate the effects of water on the textural properties of food matrices.

The reference sample evidenced only a decrease of the shear modulus at  $a_w > 0.5$ , while in the low  $a_w$  range an increased flexural modulus index of increased toughness was observed (Fig. 2b). The presence of sucrose in the product leads to an opposite trend, as increased shear modulus in the low  $a_w$  range occurred, while the normalized flexural modulus remained unchanged up to  $a_w$  values 0.3 above, showing a decrease due to moisture sorption. In the G12 product, a significant increase of stiffness in a short  $a_w$  range below 0.3 when shear was applied occurred, while upon flexure stress, only a plasticization effect was observed.

It is evident from these results that the presence of sugars in the short dough biscuit matrix had a significant, but not univocal, impact on textural properties due to moisture uptake. Variations in the response to textural testing may arise due to differences in sensitivity of different methods, which could influence the detection of certain changes in mechanical behavior (antiplasticization–plasticization) of food matrices at different  $a_w$  (Chang et al. 2000b) as the forces that act on a material when bending or shear/compressive stresses are applied are different. The same authors, however, suggested that opposite effects induced by water sorption as evaluated by similar textural tests could reflect the different macrostructural properties of the food matrices under study.

Several mechanisms have been identified to explain the moisture-induced hardening or toughening effect referred to as antiplasticization. Harris and Peleg (1996) hypothesized that partial plasticization by water would make the glassy state more cohesive and enable a higher deformation to be sustained, corresponding to higher stiffness. Chang et al. (2000a) proposed a “hole-filling” mechanism involving the filling of “holes” created under high stress-strain with water molecules effectively reducing free volume of the system.

The partial substitution of flour with either sucrose or glucose resulted in matrices with different structural and mechanical properties, as well as different abilities to interact with water which, in turn, modified the physical and mechanical properties of the matrix at increasing hydration degree. In the low moisture-glassy state, both sucrose and glucose became important components of the nonfat continuous phase (Baltsavias et al. 1999b), as shown by increased fracture force and modulus and lower strain at fracture upon bending.

Antiplasticization occurring in starch materials could also be due to change of density of the matrix, dependent on molecular packing and strength of the interaction between different species, with effects on mechanical properties. It is known that simple carbohydrate monomer-water mixtures have negative excess volumes of mixing, arising as a result of the strength of hydrogen-bonded interactions between water and carbohydrate. The same effect has been observed in a mixed system of oligomeric and small saccharides in the presence of water (Lourdin et al. 2003). Moisture uptake of biscuits could be associated with negative volume change with a correspondent increase in material stiffness and brittleness, although water depresses Tg. Sucrose and glucose could have further enhanced this phenomenon and favored the appearance of an antiplasticization effect due to moisture sorption; this may occur despite the decrease of matrix glass transition temperature ( $T_{g,dry}$ ) due to their addition (Peleg 1996). However, this addition may have affected the change from a glassy-to-rubber state of G12 and B12 biscuits by making them more prone to plasticization at increasing moisture uptake after toughening.

Levine and Slade (1993) suggested that the proportion of sucrose in the crystalline state and the size of sucrose crystals affect the rate and/or extent of dissolution in water in cookies. Further, the temperature–water loss profile during baking may influence the ratio of glassy to crystalline sucrose in the baked product. This, in turn, would affect the partitioning of water between other hydrophilic components because glassy sucrose has a higher affinity for water than the crystalline form. Even if water distribution remains unchanged, the ratio of glassy sucrose to water

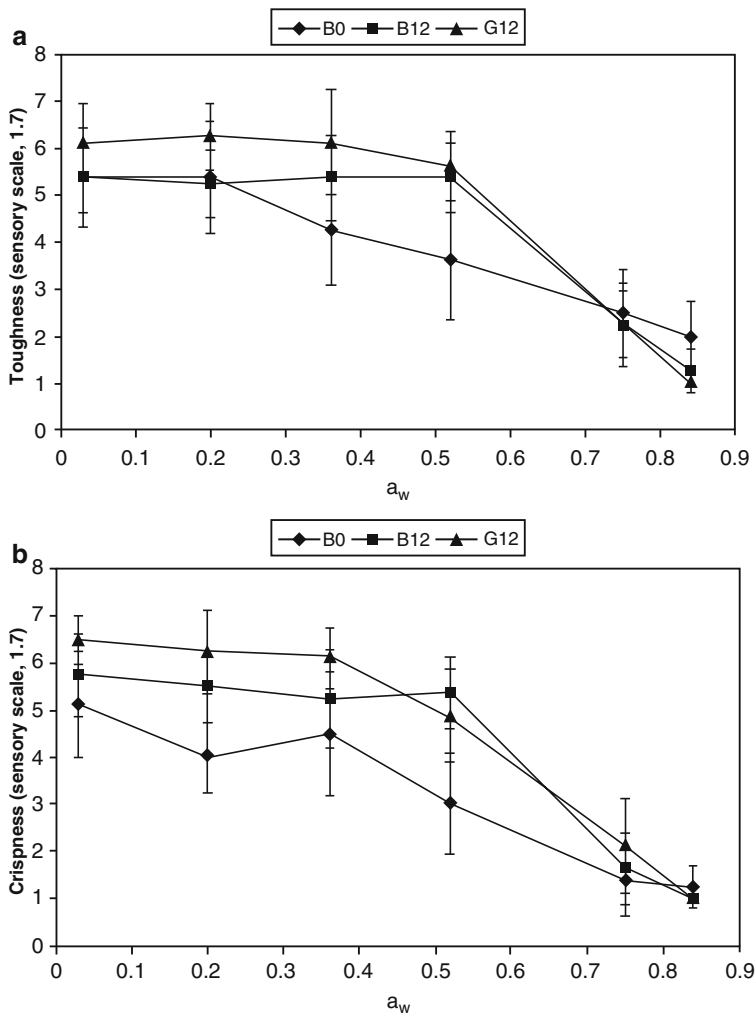


**Fig. 3** Score of hardness (a) and crispness (b) evaluated by sensory analysis of differently formulated biscuits just after preparation ( $a_w < 0.1$ ) and after hydration at increasing  $a_w$

may exert an influence on the mechanical properties of the product. Because they are similar, the process conditions applied to make the differently formulated products and the differences in the effects of water on the mechanical properties of the biscuits have to be referred only to the different affinity for water and physical properties of the small saccharides used in this study.

Differences in the textural properties of biscuits just after manufacturing and after rehydration at increasing  $a_w$  values were also evidenced by sensory analysis. A higher crispness and hardness of B12 and in particular of G12 with respect to B0 were observed, which is in agreement with the results of the mechanical evaluations (Fig. 3). When products at different hydration degrees were considered, contrary to

the mechanical results, only a decrease in toughness and crispness was perceived, with critical  $a_w$  values being different for the various biscuit types. B0 samples showed an early softening and loss of crispness due to water sorption, as determined at  $a_w$  values exceeding 0.2 and 0.4, respectively. The presence of glucose and, in particular, of sucrose was able to hinder the plasticizing effect of water by significantly increasing the  $a_w$  at which softening and loss of crispness occurred, in agreement with the study results of Valles Pamies et al. (2000) in extruded cereal products added with sucrose. Differences in initial microstructural and mechanical properties of products and different moisture sorption behavior due to the presence of sugars may have affected the perception of textural sensory changes of the biscuits, as well as hindered those related to antiplasticization.

## 4 Conclusions

Glucose and sucrose differently affected the mechanical properties of short dough biscuits by exerting both plasticizing and antiplasticizing agents at increasing hydration degree.

The different chemical and physical properties of two small saccharides, as well as their different affinity for water, seem to contemporaneously affect the response of the complex matrix to moisture increase with changes in mechanical properties in terms of strength and stiffness, as well as the sensory perception difficult to unravel. The use of two different mechanical tests seems to offer a good option to explain the effects of sugars in the matrix at low moisture, as well as at increasing hydration degrees, but these results warrant further investigation on both water state and mobility, as well as on the physical and structural properties of these complex food systems.

## References

- Baltsavias A, Jurgens A, van Vliet T (1999a) Fracture properties of short-dough biscuits: effect of composition. *J Cereal Sci* 29:235–244
- Baltsavias A, Jurgens A, van Vliet T (1999b) Properties of short-dough biscuits in relation to structure. *J Cereal Sci* 29:245–255
- Bean MM, Setser CS (1992) Polysaccharide, sugars and sweeteners. In: Bowers J (ed) *Food theory and applications*. Macmillan, New York, pp 69–198
- Chang YP, Cheah PB, Seow CC (2000a) Antiplasticisation-plasticisation effects of water on physical properties of tapioca starch films in the glassy state. *J Food Sci* 65:445–451
- Chang YP, Cheah PB, Seow CC (2000b) Variations in flexural and compressive fracture behaviour of a brittle cellular food (dried bread) in response to moisture sorption. *J Texture Stud* 31:525–540
- Harris M, Peleg M (1996) Patterns of textural changes in brittle cellular cereal foods caused by moisture sorption. *Cereal Chem* 73:225–231

- Kalichevsky MT, Blanshard JMV (1993) The effect of fructose and water on the glass transition of amylopectin. *Carbohydr Polym* 20:107–113
- Katz EE, Labuza TP (1981) Effect of water activity on the sensory crispness and mechanical deformation of snack food products. *J Food Sci* 46:403–409
- Levine H, Slade L (1988) Water as plasticiser: physico-chemical aspects of low moisture polymeric systems. In: Franks F (ed) *Water science reviews* 3. Cambridge University Press, Cambridge, pp 79–185
- Levine H, Slade L (1993) The glassy state in applications for the food industry, with an emphasis on cookie and cracker production. In: Blanshard JMV, Lillford PJ (eds) *The Glassy State in Foods*. Nottingham University Press, Loughborough, pp 333–373
- Lourdin D, Colonna P, Ring SG (2003) Volumetric behaviour of maltose/water, maltose/glycerol and starch/sorbitol/water systems mixtures in relation to structural relaxation. *Carbohydr Res* 338:2883–2887
- Marzec A, Lewicki PP (2006) Antiplasticization of cereal-based products by water. Part I. Extruded flat bread. *J Food Eng* 73(1):1–8
- Peleg M (1996) Mathematical characterisation of the plasticizing effect of fructose on amylopectin. *Cereal Chem* 73:712–715
- Pittia P, Nicoli MC, Sacchetti G (2007) Effect of moisture and water activity on textural properties of raw and roasted coffee beans. *J Texture Stud* 38:116–134
- Pittia P, Sacchetti G (2008) Antiplasticization effect of water in amorphous foods. A review. *Food Chem* 106:1417–1427
- Seow CC (2010) Antiplasticization of food polymer systems by low molecular mass diluents. In: Reid DS, Sajjaanantakul T, Lillford PJ, Charoenrein S (eds) *Water properties in food, health, pharmaceutical and biological systems: ISOPOW 10*. Wiley-Blackwell, Oxford, UK, pp 115–140
- Seow CC, Cheah PB, Chang YP (1999) Antiplasticisation by water in reduced moisture systems. *J Food Sci* 64:576–581
- Slade L, Levine H (1995) Water and the glass transition—dependence of the glass transition on composition and chemical structure: special implications for flour functionality in cookie baking. *J Food Eng* 24:431–509
- Suwonsichon T, Peleg M (1998) Instrumental and sensory detection of simultaneous brittleness loss and moisture toughening in three puffed cereals. *J Texture Stud* 29:255–274
- Valles Pamies B, Roudaut G, Dacremont C, Le Meste M, Mitchell JR (2000) Understanding the texture of low moisture cereal products: mechanical and sensory measurements of crispness. *J Sci Food Agric* 80:1679–1685
- Van Den Berg C, Bruin S (1981) Water activity and its estimation in food systems: theoretical aspects. In: Rockland LB, Stewart GF (eds) *Water activity: influence on food quality*. Academic, New York, pp 1–61

# **Physicochemical Characterization of Regional Breads Produced in the Northern Mountains of Puebla State, Mexico**

**N. Güemes-Vera, S. Soto-Simental, M.I. Reyes-Santamaría,  
and J.F. Hernández-Chávez**

## **Abbreviations**

$A_w$	Water activity
TPA	Texture profile analysis

## **1 Introduction**

Water exists in foods in free and bound forms; only unbound water is available for microbial growth and biochemical reactions (Prior 1979; Troller 1980). Measurement of unbound water is termed water activity ( $A_w$ ) and is defined as the ratio of partial vapor pressure of water in the air to the vapor pressure of water vapor in saturated air at the same temperature (Scott 1957). This measurement is numerically equal to the relative humidity at equilibrium expressed as a fraction. Techniques for measurement of  $A_w$  have been reviewed by Prior (1979) and Troller and Christian (1978). In addition, two collaborative studies have compared the various methods (Labuza et al. 1976; Stoloff 1978). Bread is one of the oldest food products consumed by humans. There is clear evidence of its use by different civilizations since prehistoric times. Bread has been a popular product because of its nutritive

---

N. Güemes-Vera (✉) • S. Soto-Simental • M.I. Reyes-Santamaría  
Instituto de Ciencias Agropecuarias, Universidad Autónoma del Estado de Hidalgo,  
Av. Universidad km 1, Ex-Hacienda Aquetzalpa, Rancho Universitario,  
CP 43600 Tulancingo, Hidalgo, Mexico  
e-mail: [njgv2002@yahoo.com.mx](mailto:njgv2002@yahoo.com.mx)

J.F. Hernández-Chávez  
Departamento de Ciencias Veterinarias y Agronómicas del, Instituto Tecnológico de Sonora,  
Ciudad Obregón, Sonora, Mexico

properties, and this product uses common ingredients as salt, sugar, and yeast (Serna 1996). Bread is a basic food made with cereals, usually in the form of flour, and liquid means, usually water. One of the greatest differences in bread production is the addition of leavening. Bread can be identified by very different names according to its form, weight, color, texture, etc., and the way in which it is presented in different countries as well as in different localities. In Mexico, baking product consumption is high, where approximately 750 varieties of sweet bread exist (CANAIMPA 2007).

## 2 Materials and Methods

### 2.1 Proximal Chemical Analysis

Proximate analyses of regional breads are conducted done with Kjeldahl method number 955.04 (Nx5.7), dietary fiber method 962.09, fat method 920.309, ashes method 923.03, moisture method 44-16, and following official methods (AOAC 1995).

### 2.2 Water Activity Determination

The equipment used for water activity measurement was an Aqualab/Sins electric hygrometer. The sample dish was modified by inserting a thermocouple through the wall of the sample holder in order to measure the temperature of the sample directly.

### 2.3 Texture Profile Analysis (TPA)

Using the same device, three samples for each region were placed in a steel tube and samples were compressed twice in the center to 20 % of sample height at a 1.7 mm/s rate with an acrylic probe for 15 min at a rate of 1.7 mm/s.

### 2.4 Color Measurement

Color was measured in each region, and rewritten as 250 µm, and was recorded using a Mini Scan Hunter Lab instrument (Minolta, 508d), following the method of Cortez Escobedo et al. (2010). Color difference for each sample was calculated

using the equation:  $\Delta E = (\Delta L_2 + \Delta a_2 + \Delta b_2)/2$ . Each assay was the average of 20 samples. The blank values were  $L = 92.26$ ,  $a = -0.81$ ,  $b = 0.62$ .

### 3 Results and Discussion

#### 3.1 Proximal Chemical Analysis

Table 1 shows the proximal chemical analysis of breads. In this table it is shown that the Concha Region 2 contained more protein in breads. Breads from Regions 1 and 3 did not contain protein, and fat content was increased in those regions. Breads from Region 2 showed a higher content compared to other regions. Biscuits from Region 1 showed more fat content. Conchas did not show significant differences for any of the regions.

#### 3.2 Water Activity

Table 2 shows the water activity of breads for Regions 1, 2 and 3. Region 1 showed more activity. The  $A_w$  was 0.8 in this region.

#### 3.3 Texture Profile Analysis

The wheat loaf bread of Region 1 showed more hardness, which affected elasticity and cohesiveness (Table 3). This result contrasts with the results of a study of bread dough in which addition of WPC decreased bread firmness (Güemes et al. 2009).

**Table 1** Chemical composition of regional (R1 = Tenango de Doria; R2 = Necaxa; R3 = Huachinango) breads produced in the northern mountains of Puebla state

Bread region	Moisture	Protein	Fat	Ashes	Fiber
Concha R1	11.61 <sup>a</sup>	7.41 <sup>a</sup>	6.72 <sup>a</sup>	0.5552 <sup>a</sup>	0.24 <sup>a</sup>
Concha R2	14.24 <sup>b</sup>	3.98 <sup>b</sup>	5.22 <sup>b</sup>	0.5538 <sup>a</sup>	0.16 <sup>b</sup>
Concha R3	10.89 <sup>a</sup>	6.26 <sup>c</sup>	4.73 <sup>c</sup>	0.5856 <sup>a</sup>	0.26 <sup>a</sup>
Bisquet R1	10.40 <sup>a</sup>	6.78 <sup>c</sup>	13.73 <sup>d</sup>	0.9100 <sup>b</sup>	0.21 <sup>a</sup>
Bisquet R2	10.79 <sup>a</sup>	4.30 <sup>b</sup>	11.72 <sup>d</sup>	0.6249 <sup>a</sup>	0.15 <sup>b</sup>
Bisquet R3	9.34 <sup>c</sup>	5.51 <sup>b</sup>	12.64 <sup>d</sup>	0.7520 <sup>c</sup>	0.21 <sup>a</sup>
Ojo de buey R1	13.25 <sup>d</sup>	6.33 <sup>c</sup>	8.77 <sup>e</sup>	0.8635 <sup>c</sup>	0.19 <sup>b</sup>
Ojo de buey R2	13.89 <sup>d</sup>	4.04 <sup>b</sup>	11.19 <sup>d</sup>	0.6397 <sup>a</sup>	0.15 <sup>b</sup>
Ojo de buey R3	11.78 <sup>b</sup>	6.2 <sup>c</sup>	8.58 <sup>e</sup>	0.7505 <sup>a</sup>	0.19 <sup>b</sup>

<sup>a, b</sup>Means with the same letter in the same row are not significantly different ( $P > 0.05$ )

<sup>a, b</sup>Means with the same letter in the same column are not significantly different ( $P > 0.05$ )

**Table 2**  $A_w$  of the breads produced in the northern mountains of Puebla state

	Tenango			Necaxa			Huauchinango		
	Concha	Bis	Ojo	Concha	Bis	Ojo	Concha	Bis	Ojo
Lithium chloride	Yes	No	Yes	Yes	Yes	Yes	Yes	Yes	Yes
Potassium carbonate	No	No	No	No	No	No	No	No	No
Sodium nitrite	No	No	No	No	Yes	No	Yes	Yes	
Sodium chloride	No	No	No	No	No	No	No	No	No
Potassium acetate	Yes	Yes	Yes	Yes	Yes	Yes	Yes	Yes	Yes
Magnesium nitrate	Yes	Yes	Yes	Yes	Yes	Yes	Yes	Yes	Yes

**Table 3** Texture profile analysis of the breads produced in the northern mountains of Puebla state (R1 = Tenango de Doria; R2 = Necaxa; R3 = Huauchinango)

Bread	Elasticity (cm)	Hardness (g)	Cohesivity
Concha R1	0.523 <sup>a</sup>	491.56 <sup>d</sup>	0.8683 <sup>a</sup>
Concha R2	0.436 <sup>c'b</sup>	725.40 <sup>b</sup>	0.8210 <sup>a</sup>
Concha R3	0.430 <sup>c'b</sup>	676.63 <sup>c</sup>	0.6817 <sup>ab</sup>
Bísquet R1	0.440 <sup>b</sup>	1,687.33 <sup>a</sup>	0.8037 <sup>a</sup>
Bísquet R2	0.406 <sup>c'b'd</sup>	818.72 <sup>c'b</sup>	0.7187 <sup>ab</sup>
Bísquet R3	0.377 <sup>c'd</sup>	870.91 <sup>b</sup>	0.8897 <sup>a</sup>
Ojo R1	0.450 <sup>b</sup>	515.11 <sup>d</sup>	0.8947 <sup>a</sup>
Ojo R2	0.386 <sup>c'd'e</sup>	830.23 <sup>c'b</sup>	0.4653 <sup>b</sup>
Ojo R3	0.342 <sup>e</sup>	356.66 <sup>d</sup>	0.7450 <sup>ab</sup>

<sup>a, b</sup>Means with the same letter in the same row are not significantly different ( $P > 0.05$ )

<sup>a, b</sup>Means with the same letter in the same column are not significantly different ( $P > 0.05$ )

**Table 4** Color of the breads produced in the northern mountains of Puebla state (R1 = Tenango de Doria; R2 = Necaxa; R3 = Huauchinango)

Bread	L	a	b	c	h
Concha R1	76.350 <sup>a</sup>	3.8647 <sup>a</sup>	24.239 <sup>a</sup>	24.507 <sup>a</sup>	81.122 <sup>a</sup>
Concha R2	76.227 <sup>a</sup>	4.4914 <sup>a</sup>	24.670 <sup>a</sup>	25.120 <sup>a</sup>	80.024 <sup>a</sup>
Concha R3	77.309 <sup>a</sup>	3.5950 <sup>a</sup>	22.968 <sup>a</sup>	23.257 <sup>a</sup>	81.200 <sup>a</sup>
Bísquet R1	48.610 <sup>a</sup>	20.7893 <sup>b</sup>	35.442 <sup>a</sup>	41.117 <sup>a</sup>	59.465 <sup>a</sup>
Bísquet R2	48.323 <sup>a</sup>	22.3212 <sup>a</sup>	37.597 <sup>a</sup>	43.745 <sup>a</sup>	59.259 <sup>a</sup>
Bísquet R3	33.226 <sup>b</sup>	15.1270 <sup>c</sup>	15.905 <sup>b</sup>	21.987 <sup>b</sup>	45.874 <sup>b</sup>

<sup>a, b</sup>Means with the same letter in the same row are not significantly different ( $P > 0.05$ )

<sup>a, b</sup>Means with the same letter in the same column are not significantly different ( $P > 0.05$ )

### 3.4 Color Measurement

Color is a vital trait in bread. Breads from Regions 1 and 2 showed more yellow coloration with respect to other regions (Table 4), due to the different ingredients used in bread formulation. The luminosity of breads was highest in conchas with respect to biscuits.

## 4 Conclusions

The best treatment was that used in Region 1; the conchas, the bisquets, and “ojos de buey” showed the best content of protein and texture. The bread of Region 3 showed the best content of  $A_w$ . The different ingredients used for these foods have influence in the physicochemical characteristics of regional breads.

## References

- AOAC (1995) Official methods of analyses, 15th edn. Association of Official Analytical Chemists, Washington, DC
- CANAIMPA (2007) [www.eleconomista.com.mx/articulos/200704-1634198](http://www.eleconomista.com.mx/articulos/200704-1634198). Accessed may 2008
- Güemes VN, Totosaus SA, Hernández Ch JF, Soto SS, Aquino Bolaños EN (2009) Propiedades de textura de masa y pan dulce tipo “concha” fortificados con proteínas de suero de leche. Ciencia Tecnología Alimentaria Campinas 29(1):70–75
- Cortez Escobedo L, Soto-Simental S, Reyes-Santamaría MI, Hernandez-Chavez JF, Guemes Vera N (2010) Physicochemical characterization of regional breads produced in the northern mounting of Puebla State Mexico. Paper presented at the annual meeting for the International of Food Technology, Chicago Illinois, July 18
- Labuza TP, Acott K, Tatini SR, Lee RY, Flink J, McCall W (1976) Water activity determination: a collaborative study of different methods. *J Food Sci* 41:910
- Prior BA (1979) Measurement of water activity in foods: a review. *J Food Protec* 42:668
- Scott WJ (1957) Water relations of food spoilage microorganisms. *Adv Food Res* 7:83
- Serna S (1996) Química almacenamiento e industrialización de los cereales. Primera edición AGT editor, SA, México
- Stoloff L (1978) Calibration of water activity measuring instruments and devices: collaborative study. *J Assoc Offic Anal Chem* 61:1166
- Troller JA (1980) Influence of water activity on microorganisms in foods. *Food Technol* 34(5):76
- Troller JA, Christian JHB (1978) Water activity and food. Academic, New York, NY

# Structural Relaxation of Salmon Gelatin Films in the Glassy State

J. Enrione, C. Sáez, D. López, O. Skurys, and C. Acevedo

## Abbreviations

Pro	Proline
Hyp	Hydroxyproline
$T_g$	Glass transition temperature
DSC	Differential scanning calorimeter
E	Elastic modulus
KWW	Kohlrausch–Williams–Watts model
$\Phi$	Decrease in the normalized stress
$\phi$	Relaxation function
$t$	Time
$\beta$	Width of the relaxation time distribution spectrum
$\tau_0$	Characteristic relaxation time
RH	Relative humidity
$\sigma$	Stress

---

J. Enrione (✉) • C. Sáez

Escuela de Nutrición y Dietética, Facultad de Medicina, Universidad de los Andes,  
Av. Monseñor Álvaro del Portillo 12.455, Las Condes, Santiago, Chile  
e-mail: [jenrione@uandes.cl](mailto:jenrione@uandes.cl)

D. López

Departamento de Ciencia y Tecnología de los Alimentos, Universidad de Santiago de Chile,  
Av. Libertador Bernardo O'Higgins 3363, Estación Central, Santiago, Chile

O. Skurys

Department of Mechanical Engineering, Universidad Técnica Federico Santa María, San  
Joaquín, Santiago, Chile

C. Acevedo

Centro de Biotecnología Dr. Daniel Alkalay Lowitt, Universidad Técnica Federico Santa  
María, Avenida España 1680, Valparaíso, Chile

$\gamma$	Engineering strain
$E$	Young's modulus
$T_a$	Storage temperature
$R^2$	Coefficient of determination
SE	Standard error
$\Delta H$	Enthalpy relaxation
$C_p$	Heat capacity
ANOVA	Analysis of variance
SD	Standard deviations
CV	Coefficient of variation

## 1 Introduction

The unique property of gelatin to form networks and induce plasticity and elasticity is considered beneficial in the preparation of biopolymer-based packaging materials. However, its use in food products has been limited by some religious groups (Gudmundsson 2002). Gelatins from marine sources have emerged as an alternative, although they are different from mammalian collagen in terms of their biochemical constituents and therefore in their functional properties. It has been shown that cold-water fish collagen can have a lower content of amino acids (~16–18 %) (Gilsenan and Ross-Murphy 2000). Joly-Duhamel et al. (2002) established a positive correlation of the concentration of amino acids, proline (Pro) and hydroxyproline (Hyp), with the melting temperature of native collagen (helix to coil) and gelatin molecular weight with renaturation temperature (coil to helix), suggesting an important effect of biochemical composition on the structure stability of the gel network. An aspect that has not been explored in detail for marine gelatin is the structural stability of these systems at temperatures below their glass transition temperature ( $T_g$ ). Early studies in glassy carbohydrates by Noel et al. (1999) described the ageing kinetics of maltose in the glassy state in terms of an overshoot in heat capacity on consecutive heating runs using a differential scanning calorimeter (DSC). Badii et al. (2005) evaluated the kinetics of enthalpic relaxation of bovine gelatin state as a function of the difference between ageing temperature and  $T_g$ . In their later work, the same authors quantified the enthalpic relaxation of the same model system by DSC, correlating enthalpic values with an increase in the elastic modulus ( $E$ ) obtained by mechanical spectroscopy. Work by Lourdin et al. (2002) described the mechanical relaxation of amorphous potato starch in the glassy state, obtaining characteristic relaxation parameters by the application of the Kohlrausch–Williams–Watts (KWW) model (Eq. 1). Anderssen et al. (2004) discussed the KWW equation in terms of a spectrum of relaxation times describing the ageing of a polymer. The KWW is an equation that can quantitatively describe the kinetics of the relaxation process toward an absolute relaxed state (Anderssen et al. 2004):

$$\phi(t) = \exp\left[-\left(\frac{t}{\tau_0}\right)^\beta\right] \quad (1)$$

where  $\phi$  is the relaxation function,  $t$  is time,  $\beta$  ( $0 < \beta \leq 1$ ) is the width of the relaxation time distribution spectrum, and  $\tau_0$  is the characteristic relaxation time, being dependent on temperature and material structure.

The lack of information on the structural relaxation kinetics of marine gelatin with known differences in mechanical properties from those from mammalian sources encouraged this work looking at the stability of gelatin extracted from salmon skin, an abundant by-product from the fish industry.

## 2 Materials and Methods

### 2.1 Preparation of Films

Salmon (*Salmo salar*) gelatin was extracted from skin by an acid–alkaline method giving a ~9 % w/v yield of dry gelatin. The gelatin was suspended at 7 % (w/v) in hot water (70 °C), which was then poured onto rectangular Teflon blocks (30 × 12 × 10 cm) and cold cast at 5 °C in an incubator for 5 days. The obtained films (~0.25 mm in thickness) were then cut (100 mm × ~10 mm) and stored over P<sub>2</sub>O<sub>5</sub> (~0 % relative humidity, RH) for 7 days at ambient temperature and later equilibrated under a ~54 % RH (saturated solution of Mg(NO<sub>3</sub>)<sub>2</sub>). The moisture content was determined gravimetrically in triplicates overnight at 105 °C giving ~18.4 % (db.).

### 2.2 Mechanical Characterization

The stress ( $\sigma$ ) versus engineering strain ( $\gamma$ ) curves were obtained by a texture analyzer (DO-FBO.5TS, Zwick, Ulm, Germany) using a uniaxial tension method. The application of tensile force was restricted to the linear zone of the stress–strain curve, giving Young's modulus ( $E$ ). Prior to the measurements, the thermal history of the films was eliminated at 15 °C above  $T_g$  in silicone (Dow Corning 200R) oil for 10 min, then hermetically packed and quickly cooled to the storage temperature ( $T_a$ ) (~29 °C), equivalent to 5 °C below  $T_g$ , and stored for 0, 4, 8, 16, and 40 h. The stress relaxation of the films was assessed at a constant strain of 1 %. The stress values were normalized and fitted using Eq. (1), obtaining the values  $\beta$  and  $\tau_0$  together with the coefficient of determination ( $R^2$ ), as well as the standard error (SE) of the fits. The moisture content and temperature of the films were kept constant throughout the measurements, using a silicone oil containing inner cylinder in a concentric cylinder chamber previously attached to the texture

analyzer. The outer cylinder was filled with circulating water tempered at the desired temperature ( $\pm 0.1$  °C). The rate of mechanical relaxation was predicted using the derivative of the function KWW with respect to measuring time ( $d\varphi/dt$ ) using the estimated  $\beta$  and  $\tau_0$  values. Four replicates were evaluated for each sample.

### 2.3 Determination of Enthalpy Relaxation

Tg and enthalpy relaxation ( $\Delta H$ ) were determined by DSC (Diamond DSC, Perkin Elmer), calibrated with indium  $T_m = 156.6$  °C and  $\Delta H = 28.4$  J/g. Ten milligram of each sample was placed in 30  $\mu$ L aluminum capsules and hermetically sealed.  $T_g$  was defined as the midpoint of the change in heat capacity ( $C_p$ ) on the second DSC scan giving a value of ~34 °C. The capsules were stored for the same time and temperature as the mechanical relaxation studies. The thermal history was erased by holding the sample at 10 °C above  $T_g$  for 15 min (Lourdin et al. 2002) and then cooled to the storage temperature (29 °C). The methodology used was the following: holding at -40 °C for 2 min, heating from -40 to 90 °C at 10 °C/min, holding for 2 min at 90 °C, cooling from 90 to -40 °C at 40 °C/min, and finally heating from -40 to 90 °C at 10 °C/min. The first DSC thermogram indicated denaturation and melting like endotherms at ~55 and ~70 °C, respectively (data not shown). The  $\Delta H$  was calculated from the area generated from subtracting the first and second DSC scans. Each sample was evaluated in triplicate.

The statistical significance of the experimental data was evaluated using the analysis of variance (ANOVA) with  $\alpha = 0.05$  using Data Analysis Suite in Excel (Office 2003. Microsoft Corp.). Standard deviations (SD) were calculated for replicates and plotted as error bars. Coefficients of variation (CV) were calculated and presented when necessary.

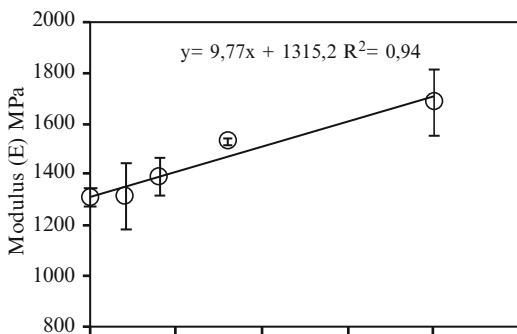
## 3 Results and Discussion

### 3.1 Mechanical Characterization

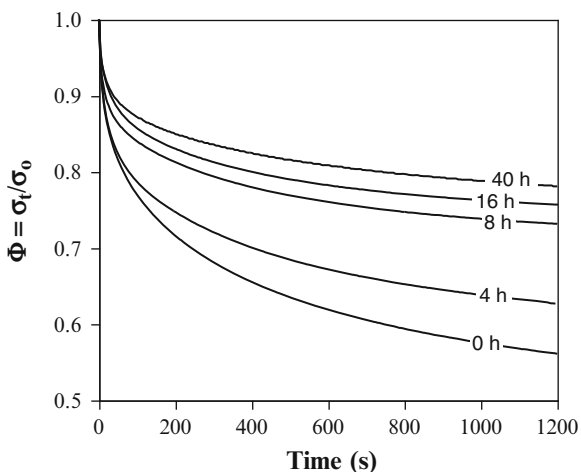
A significant increase in E ( $p < 0.05$ ) was detected after 40 h of storage, from ~1.2E+03 to ~1.6E+03 MPa (~33 %) (Fig. 1). The increase in stiffness was attributed to a decrease in specific volume of the amorphous polymeric structure by movement of the chains toward a lower energy state. The increase in modulus with time was linear-like, with a slight decrease in the slope at long ageing times. It was possible to fit the data with the equation:  $E = 9.8*t + 1315.2(R^2 = 0.94)$ .

Figure 2 shows a decrease in the normalized stress ( $\varphi$ ) at constant deformation. The reduction in  $\varphi$  follows an exponential behavior with a marked decrease during the first 200 s. A statistical analysis of the variances indicated significant

**Fig. 1** Modulus versus ageing time at 29 °C ( $T_g - T_a = 5$  °C). Vertical error bars represent  $\pm 1$  standard deviation (SD)



**Fig. 2** Stress relaxation,  $\varphi$  (normalized) for salmon gelatin films in glassy state aged at 29 °C ( $T_g - T_a = 5$  °C) for 0, 4, 8, 16, and 40 h. Significant differences ( $p < 0.05$ ) in  $\varphi$  at measurement time  $> 50$  s



**Table 1** Parameters  $\beta$  and  $\tau_0$ , percentage of mechanical relaxation ( $A$ ), and relaxation enthalpy  $\Delta H$ , for storage times 0–40 h

Ageing time (h)	$\tau_0$ (s)	SD $_{\tau_0}$	$\beta$	SD $_{\beta}$	SE	$A$ (%)	$\Delta H$ (J/g)	SD $_{\Delta H}$
0	6.1E+03	3.1E+02	0.32	0.03	6.4E-02	45.9	0	—
4	1.7E+04	1.9E+03	0.28	0.01	4.1E-02	40.4	1.1	0.40
8	1.3E+05	5.3E+03	0.24	0.03	6.4E-02	25.6	2.3	0.20
16	3.8E+05	1.9E+04	0.22	0.03	5.6E-03	24.5	2.3	0.25
40	9.0E+05	2.1E+04	0.21	0.01	3.0E-03	21.9	2.4	0.22

SE standard error from KWW equation fitting, SD standard deviation

differences ( $p < 0.05$ ) in stress between fresh aged films after 50 s of tensioning. Indeed, the amplitude of the decrease ( $A$ ) between  $\varphi$  at time 0 and 1200 s (Table 1) was ~46.0 % for the fresh sample and ~21.9 % for the film stored for 40 h. Such behavior was represented by the KWW model, whose parameters  $\beta$  and  $\tau_0$  were obtained individually (Table 1).  $\beta$  decreased from 0.30 to 0.21 ( $p < 0.05$ ) when the

ageing time increased to 40 h. According to the attachment theory proposed by Ngai (1998), this can be interpreted as strengthening of the coupling between the relaxing species and its close surroundings, which is related to an overall decrease in molecular mobility and to an increase in spread of the distribution of relaxation times (Lourdin et al. 2002). The decrease in  $\beta$  was attributable to the densification of the polymeric structure with increased storage time. As the intermolecular space is reduced, the mobility of the polymer chains becomes more restricted, decreasing the relaxation during tensioning.  $\tau_0$  increased significantly ( $p < 0.05$ ) from  $6.1E + 03$  to  $9.0E + 05$  s with ageing time.  $\beta$  versus ageing time ( $t_{\text{ageing}}$ ) was well fitted ( $\text{SE} < 0.01$ ) by the exponential,  $\beta = 0.32 - 0.037^* t_{\text{ageing}}^{0.32}$  ( $R^2 = 0.97$ ), whereas  $\tau_0$  followed the equation,  $\tau_0 = -3.2E + 04 + 2.4E + 04 \cdot t_{\text{ageing}}$  ( $R^2 = 0.99$ ) ( $\text{SE} < 0.01$ ) (figures not shown). Thus, the mechanical relaxation kinetics of the salmon gelatin could also be modeled by the KWW model with only one parameter, the ageing time,  $t_{\text{ageing}}$ .

Figure 3 shows the variation in the normalized relaxation rate,  $(d\varphi/dt)_t/(d\varphi/dt)_{t=0}$  generated from the derived Eq. (1) using the calculated  $\beta$  and  $\tau_0$  values. In all cases, a decrease in relaxation rate during the tension test was observed. The gelatin film stored for 40 h was the first to reach the minimum value of  $\sim 0.01$ , followed by the samples with 16, 8, 4, and 0 h storage.

It is interesting to note that the relaxation rate was slower for the aged samples at all times. It was also noted that approximately 90 % of the variation in relaxation rate occurred before 100 s, indicating that most of the structural changes in the matrix occurred at a small fraction of the overall relaxation time.

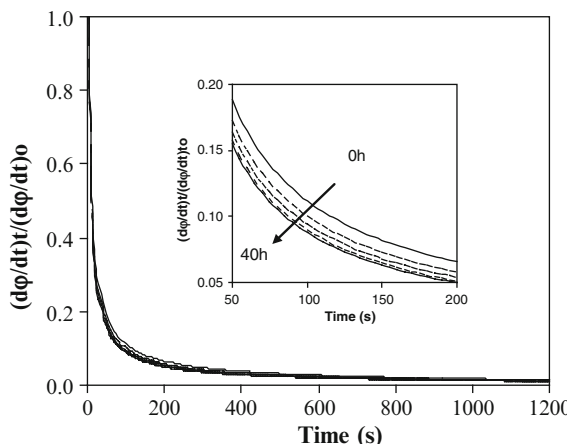


**Fig. 3** Normalized mechanical relaxation rate versus time for salmon gelatin films aged at 29 °C ( $T_g - T_a = 5$  °C) for 0, 4, 8, 16, and 40 h

### 3.2 Enthalpic Relaxation

Figure 4 shows the normalized values of heat capacity ( $C_p$ ) as a function of temperature for all gelatin films. An overshoot at  $T_g$  was observed for the aged samples, which was correlated to the increase in storage time. This behavior was similar to that observed in synthetic and natural polymers, where overshoots in heat flow at temperature close to  $T_g$  have been reported (Badii et al. 2006).

$\Delta H$  versus ageing time is shown in Fig. 5, where a two-stage behavior is observed, with a rapid increase in  $\Delta H$  from 0 J/g to  $\sim 2.3$  J/g (0–8 h) ( $p < 0.05$ ),

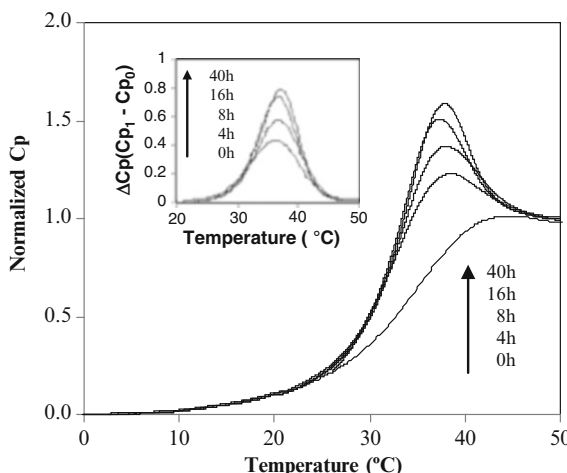
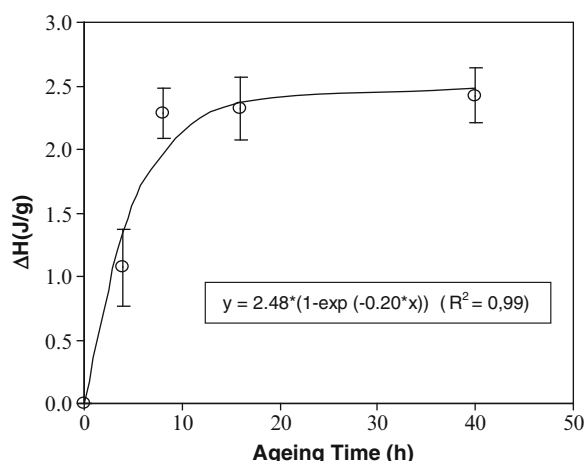


**Fig. 4** Normalized  $C_p$  versus temperature in salmon gelatin-based films aged at 29 °C ( $T_g - T = 5$  °C) for 0, 4, 8, 16, and 40 h. CV of  $C_p$  replicates <10 % of each ageing time

**Fig. 5** Enthalpy relaxation ( $\Delta H$ ) v/s ageing time for salmon gelatin films aged at  $T_g - T_a = 5$  °C for holding times of 0, 4, 8, 16, and 40 h. Error bars correspond to  $\pm 1$  SD



after which  $\Delta H$  leveled off ( $p > 0.05$ ). These results support the mechanical data in terms of a loss in the internal energy from the system by the spontaneous densification of a polymeric matrix approaching equilibrium. In terms of the structure stability, these data suggest that fish gelatin can undergo similar relaxation processes to those reported for biopolymers. In the future, comparative studies of structure relaxation in gelatin from different biological origins would help to understand the effect of biochemical composition on the kinetic of this phenomenon.

## 4 Conclusions

A spontaneous structural relaxation of salmon gelatin in the glassy state was observed by thermal and mechanical techniques. This behavior was related to a reduction in molecular mobility, as indicated by an increase in relaxation times ( $\tau_0$ ) and a decrease in relaxation rates estimated from the stress relaxation data. The reduction in  $\beta$  on ageing suggests a spreading of relaxation times occurring in the matrix. The excess in enthalpy in aged films was associated with lower-energy states as thermodynamic equilibrium was approached. This work shows that significant changes in structure can occur within a short time frame. This work will be continued using predictive models for the enthalpy data and will attempt to confirm or refute these findings. A direct comparison with gelatin from other sources, assessing the significance of biochemical structure on the kinetics associated with ageing, will also be carried out.

**Acknowledgments** We thank Professor John Mitchell for useful discussions. This work was funded by grants FONDECYT 11075053, PBCT PSD62, and Innova Chile-Corfo CT11 PUT-20.

## References

- Anderssen RS, Husain SA, Loy RJ (2004) The Kohlrausch function: properties and applications. *ANZIAM J* 45:C800–C816
- Badii F, MacNaughtan W, Farhat IA (2005) Enthalpy relaxation of gelatin in the glassy state. *Int J Biol Macromol* 36(4):263–269
- Badii F, Martinet C, Mitchell JR, Farhat IA (2006) Enthalpy and mechanical relaxation of glassy gelatin films. *Food Hydrocoll* 20(6):879–884
- Gilsenan P, Ross-Murphy S (2000) Rheological characterization of gelatins from mammalian and marine sources. *Food Hydrocoll* 14:191–195
- Gudmundsson M (2002) Rheological properties of fish gelatins. *J Food Sci* 67(6):2172–2176
- Joly-Duhamel C, Hellio D, Djabourov M (2002) All gelatin network. *Biodivers Phys Chem Langmuir* 18(19):7208–7217

- Lourdin D, Colonna P, Brownsey GJ, Noel TR, Ring SG (2002) Structural relaxation and physical ageing of starchy materials. *Carbohydr Res* 337(9):827–833
- Ngai KL (1998) Correlation between the secondary beta relaxation time at  $T_g$  with the Kohlrausch exponent of the primary alpha relaxation or the fragility of glass-forming materials. *Phys Rev E* 57(6):7346
- Noel TR, Parker R, Ring SM, Ring SG (1999) A calorimetric study of structural relaxation in a maltose glass. *Carbohydr Res* 319(1–4):166–171

# **Relationship Between Raw Material Characteristics and Dehydration Parameters of Vegetables Dried Using a New Kind of Solar Dryer**

**G. Bertolo, A. Maestrelli, and M. Della Campa**

## **Abbreviations**

F&V	Fruits and vegetables
C	Product slices conventional drying group
S	Product slices solar drying group
TQ	Before conventional drying
MC	Moisture content (g H <sub>2</sub> O/100 g solids)
E	Elastic module (g/mm)
<i>a<sub>w</sub></i>	Water activity

## **1 Introduction**

In the last few years, an increasing demand for innovative products in response to changing lifestyles has led to a strong increase in out-of-home food consumption. Consumers are also becoming more interested in consuming healthy, natural, and tasty foods because of their positive role in the treatment of a certain type of chronic degenerative diseases (Bazzano et al. 2002). Dried food products constitute an important sector of innovative snacks, in particular fruits and vegetables (F&V)-based products.

---

G. Bertolo  
ACU, Associazione Consumatori Utenti, Milan, Italy

A. Maestrelli • M. Della Campa (✉)  
Consiglio per la Ricerca e la Sperimentazione in Agricoltura, Unità di Ricerca per i Processi dell'Industria Agroalimentare C.R.A.-I.A.A., via G. Venezian 26, Milan, Italy  
e-mail: [marcello.dellacampa@unimi.it](mailto:marcello.dellacampa@unimi.it)

Dehydration represents an important option for processing a great number of products and an area of opportunity for the food industry including small producers. This process, historically considered a non-efficient system since, involves the removal of large quantities of water, which requires the usage of a great amount of expensive thermal energy.

Exploiting renewable energy sources seems to provide an appropriate alternative for a more sustainable production context. The use of thermal, photovoltaic energy has become particularly important, but for small producers their use is still difficult to implement for profitable purposes. On the other hand, small and local craft producers can profit from the usage of solar energy.

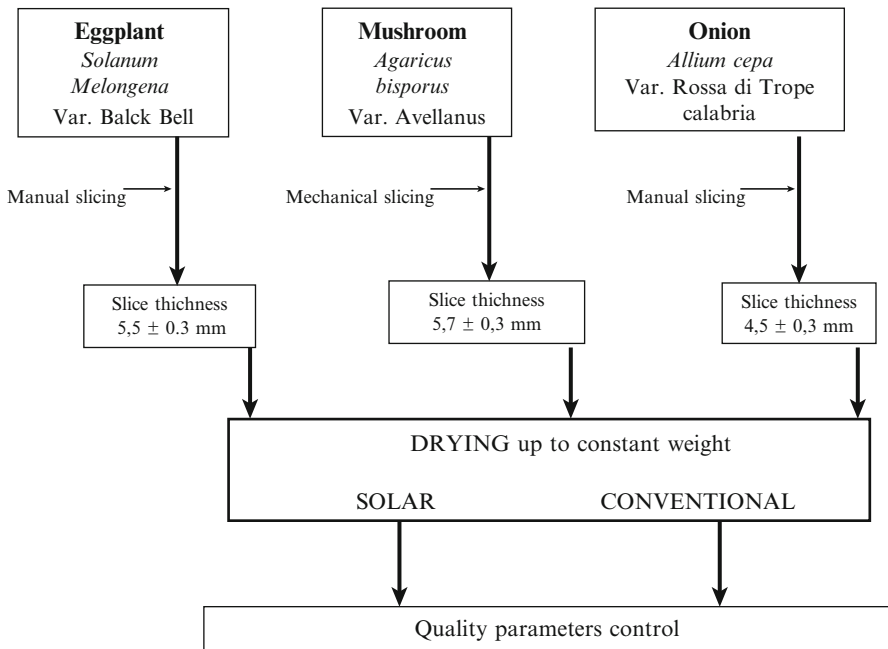
This research focuses on Mediterranean vegetables which, in their dried form, may be consumed directly (crispy snack products) or as ingredients in frozen or ready-to-use convenience foods.

## 2 Materials and Methods

Eggplant, *Solanum melongena* var. Black Bell; onions, *Allium cepa* var. Rossa di Tropea; and mushroom, *Agaricus bisporus* var. Avellanus, were purchased in the local market. All products were hand-washed before cutting and drying. Mushroom and onion were cut manually (slice thickness resulted  $5.7 \pm 0.3$  mm for mushroom and  $4.5 \pm 0.3$  mm for onion). Eggplant slices were cut manually into  $5.0 \pm 0.3$  mm-thick slices. The average weight of a slice resulted to be  $11.8 \pm 1.4$  g (eggplant),  $7.4 \pm 1.0$  g (onion), and  $3.9 \pm 0.6$  g (mushroom). The values of thickness were obtained according to Ertekin and Yaldiz (2004). Product slices were split into two groups, for conventional (C) and solar (S) drying, using the equipments and according to the conditions listed below. For all samples, end of drying was considered as completed when the product reached constant weight. The experimental scheme of the drying process is presented in Fig. 1.

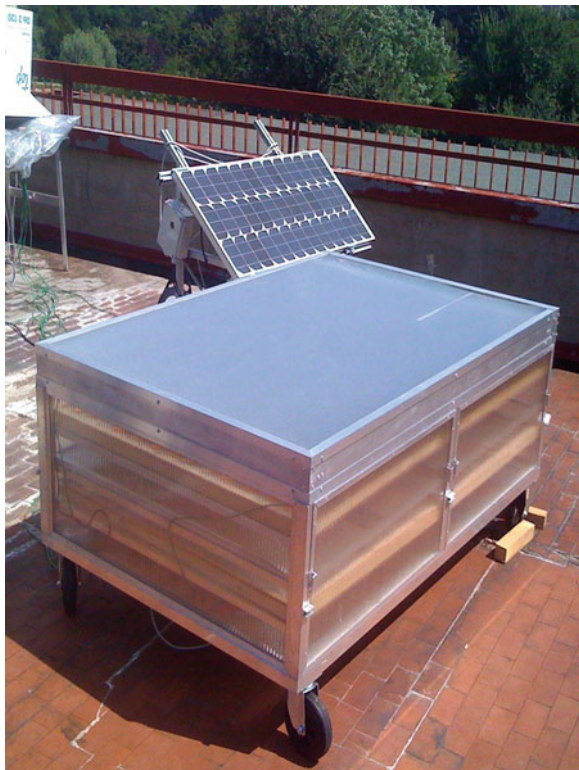
### 2.1 Solar Drying

Solar drying was performed using the prototype named “Eolo” (Figs. 2 and 3). This system consisted of a cabinet 54 cm high, 100 cm long, and 150 cm deep. All walls were made of alveolar polycarbonate transparent panels. Atmospheric air enters the heating chamber through slots on one of the cabinet’s sides, while the air outlet ducts are in the opposite side; airflow is induced by two fans placed on the bottom of the dryer, powered by a 12 V 50 A h battery, charged by a solar photovoltaic panel system, located at a side of the dryer. A 5 cm layer of steel wool located under the heating chamber roof receives the solar radiation and thus acts as an internal air heater. The heating layer also increases the heat transfer area and decreases airflow so increasing air temperature. The heated air enters the drying chamber, in which there are located four trays, with a total surface of  $2.4\text{ m}^2$  on which the fresh



**Fig. 1** Dried vegetable production diagram

**Fig. 2** The solar drying system “Eolo”



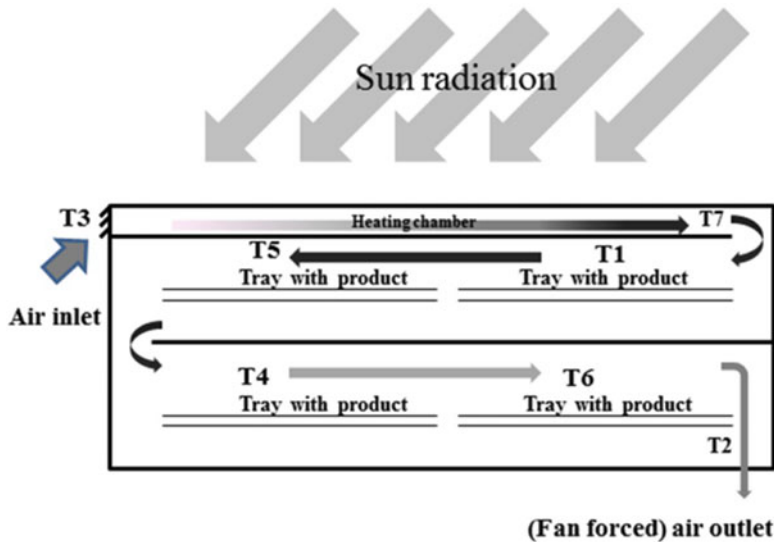


**Fig. 3** Scheme of the airflow inside the solar dryer and position of the thermal probes

material is distributed for drying. A metallic mesh is located at the air inlet to prevent the entrance of insects and particles. During the exposure to sun radiation, the temperature reached inside the system can be different if measured in indifferent positions inside the plant (see probe positions as shown in Fig. 3) and depends on the instant solar radiation intensity: an example of the dryer thermal performance during a sunny/cloudy summer day at the latitude of Milan, Italy, is shown in Fig. 4.

Although this solar dryer system is able to provide a forced hot airflow, it can operate completely independent from the electricity supply. Moreover, a thermal sensor stops the fans during the night, to prevent the entrance of moist air into the drying chamber. Structure of the cabinet also protects the product from the weather, dirt, and dust.

## 2.2 Conventional Drying

Conventional drying was performed at 70 °C until a constant weight was reached by using a pilot air dryer that is able to operate by alternating the airflow in upward–downward modes (Thermolab, Codogno, Italy) which handles an airflow of 1.5 m/s (Giri and Prasad 2007).

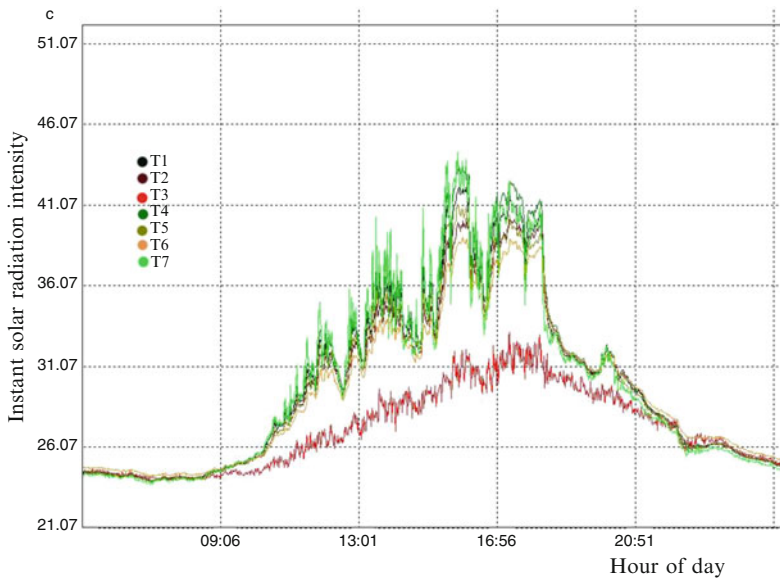


**Fig. 4** Example of solar dryer performance during a sunny/cloudy summer day at latitude of Milan, Italy

### 2.3 Dried Product Characteristics

Dried was considered complete, when the materials reached constant weight. Reported results are the mean of 3 measurements.

Water activity ( $a_w$ ) was evaluated by means of an electronic hygrometer (AquaLab CX-2—Decagon Devices, Pullman, USA). Reported results are the mean of 6 determinations.

Texture was determined by applying bending-snapping tests using a Stable Micro Systems TA XT II plus fitted with a 5 kg cell and a three-point bend rig. The elastic module, E, was determined as the slope of the stress-strain line before the first fracture (largest peak) and was calculated from the force-displacement curves and was considered as the crispness index (Konopacka et al. 2002). Dried eggplant slides were cut into strips 15 mm width and sliced lengthwise. No further cutting was necessary for mushroom and onion. Presented results are the mean value of 10 determinations.

Color was evaluated on fresh and dried samples by using a D65 illuminant/ $10^\circ$  observer refraction colorimeter (Minolta Chroma Meter CR 200—Minolta Camera Co. Ltd., Japan). Samples were placed on a white standard plate ( $L = 100$ ), and CIE La\*b\* coordinates were also evaluated. Presented results are the mean of 10 determinations.

### 3 Results and Discussion

Quality characteristics of the three dried vegetables depend on tissue (and cellular) structure and drying technique and rate. Solar drying gave place to products with higher moisture content and water activity than those obtained by conventional drying (Table 1) which were also softer than those obtained by hot air drying. As expected, both drying techniques caused a significant decrease of L and increase of  $a^*$  values (Fig. 5). No significant differences in L values were detected between solar and conventionally dried vegetables. Values for  $a^*$  corresponding to solar dried eggplant and onion slices were significantly higher than those for conventional vegetables, while no differences were observed for mushrooms.

During conventional drying, a power meter was used to evaluate the processing energy needs. Energy consumption for the conventional product was about 2 kW h for 514 g of eggplant, 1 kW h for 220 g of mushroom, 2 kW h for 580 g of red onion, and 0 W for the solar product.

**Table 1** Moisture content, water activity, and elastic module measured on dried strips of the different products

	Moisture content (MC) (g H <sub>2</sub> O/100 g product)			Water activity ( $a_w$ )		Elastic module (E) (g/mm)	
	TQ	C	S	C	S	C	S
Eggplant	92.18	4.77	13.90	26.05	53.53	260.88	245.89
Mushroom	90.91	2.13	5.52	18.40	36.37	425.60	353.85
Onion	91.71	6.73	15.92	25.25	51.5	189.81	114.45

Before (TQ) and after conventional (C) and solar (S) drying up to constant weight

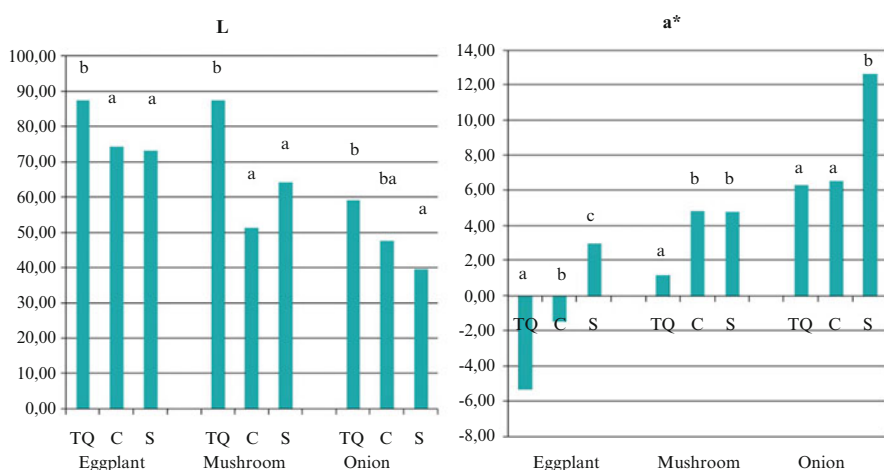


**Fig. 5** Comparison of initial color data L  $a^*$  of eggplant, mushroom, and onion slices before (TQ) and after conventional (C) and solar (S) drying up to constant weight. In each column, different letters stand for significant differences (Tukey's test,  $p < 0.05 \%$ )

## 4 Conclusions

Drying vegetables using solar drying systems (such as the prototype used in this work) can provide significant benefits to the quality of products as compared to those obtained by applying convection drying systems such as:

- Softer products although sticky in the mouth
- Improved product hygiene
- No additional energy to solar radiation required for drying

In addition, the low temperature reached during drying could preserve important thermo-labile/high-nutritional-value compounds; further investigation will be developed on this aspect.

## References

- Bazzano LA, He J, Ogden LG, Loria CM, Vupputuri S, Myers L, Whelton PK (2002) Fruit and vegetable intake and risk of cardiovascular disease in US adults: the first National Health Examination survey Epidemiologic Follow-up study. *Am J Clin Nutr* 76:93
- Ertekin C, Yaldiz O (2004) Drying of eggplant and selection of a suitable thin layer drying model. *J Food Eng* 63(3):349–359
- Konopacka D, Plocharski W, Beveridge T (2002) Water sorption and crispness of fat-free apple chips. *J Food Sci* 67(1):87–92
- Giri SK, Prasad S (2007) Drying kinetics and rehydration characteristics of microwave-vacuum and convective hot-air dried mushrooms. *J Food Eng* 78(2):512–521

# Caking Process and Microstructural Changes of Wall Materials Used in Spray-Drying Process

J. Porras-Saavedra, E. Palacios-González, J. Yáñez-Fernández,  
M.F. Mazzobre, M.P. Buera, and L. Alamilla-Beltrán

## Abbreviations

SPI	Soy protein isolate
MD	Maltodextrin
GA	Gum arabic
$T_g$	Glass transition temperature
$a_w$	Water activity
DSC	Differential scanning calorimetry
d. b.	Dry base
$D_{\text{bridge}}$	Bridge diameter
$D_{\text{particle}}$	Particle diameter
B	Bridging

---

J. Porras-Saavedra • L. Alamilla-Beltrán (✉)

Departamento de Graduados e Investigación en Alimentos, Escuela Nacional de Ciencias Biológicas, Instituto Politécnico Nacional, Carpio y Plan de Ayala s/n, CP 11340 Mexico City, DF, Mexico

e-mail: [liliana.alamilla@gmail.com](mailto:liliana.alamilla@gmail.com); [lalamill@ipn.mx](mailto:lalamill@ipn.mx)

E. Palacios-González

Laboratorio de Microscopía Electrónica de Ultra Alta Resolución (LAMEUAR), Instituto Mexicano del Petróleo, Eje Central Lázaro Cárdenas No 152, Edificio 33-11. Col. San Bartolo Atepehuacan, Mexico City, DF CP 07730, Mexico

J. Yáñez-Fernández

Departamento de Bioingeniería de la Unidad Profesional Interdisciplinaria de Biotecnología, Instituto Politécnico Nacional. Av. Acueducto s/n, Barrio la Laguna Ticomán, Mexico City, DF CP 07340, Mexico

M.F. Mazzobre • M.P. Buera

Departamentos de Industrias y de Química Orgánica, Facultad de Ciencias Exactas y Naturales, University of Buenos Aires (FCEyN-UBA), National Council of Scientific and Technical Research (CONICET), Buenos Aires, Argentina

A	Agglomeration
C	Compaction
L	Liquefaction
T	Storage temperature

## 1 Introduction

Microencapsulation process is applied to protect the core material or active agent against environmental factors. It helps to resist processing conditions of brittle materials, and improves flavor, aroma, stability, nutritional value, and appearance. Microencapsulation applications are found in agricultural, pharmaceutical, food, cosmetics, and fragrance industries (Madene et al. 2006). The retention of the active agent in this process is governed, among other factors, by type of wall material, so its selection is an important step. The most commonly used materials include carbohydrates such as maltodextrin (MD) and gum arabic (GA) and proteins such as whey and soy protein isolate (SPI) (Madene et al. 2006; Matalanis et al. 2011). During microencapsulation process, the final products are in the form of powder containing individual microparticles, agglomerates, or both. The food powders containing amorphous carbohydrates could experiment physical changes as stickiness and caking when the powder is exposed to temperature above the powder's glass transition temperature ( $T_g$ ). This temperature is a function of the moisture content and water activity ( $a_w$ ) of the powder (Foster et al. 2005; Schebor et al. 2010). At the  $T_g$ , the viscosity of amorphous materials decreases significantly, allowing greater molecular mobility, which has effect in sticky behavior (Foster et al. 2005). The caking of food powders is an unwanted and very common problem that occurs during processing, handling, and storage. The particles of amorphous powders may progressively be deformed until they stick to each other, and eventually form agglomerates (Saragoni et al. 2007). This phenomenon is affected by microstructure and hygroscopicity; however, other facts are reported as decisive like stress, humidity, and temperature for caking mechanism and caking kinetics (Hartmann and Palzer 2011). The caking phenomenon reduces the product quality and functionality, rehydration, dispersibility, and the shelf life and increases deterioration of organoleptic quality and the formation of lumps and agglomerates (Lipasek et al. 2012). Microscopy techniques have been applied to analyze powder microstructure, identifying useful factors to describe changes observed during processing and storage (Guadarrama-Lezama et al. 2014).

The aim of this work was to propose a correlation of caking with the glass transition temperature of different wall materials and the powder microstructure.

## 2 Materials and Methods

### 2.1 Materials

Soy protein isolate (SPI) (Cenit, México), maltodextrin 20 DE (MD) (Globe Corn Product International, Illinois, U.S.A.), and gum arabic (GA) (E number E414) (Morevo Quick Gum) were used as wall materials.

Suspensions of the wall materials SPI, MD, and GA were prepared according to Table 1, keeping constant a concentration of 20 % of total solids, using distilled water, and applying mechanical agitation during 12 h at room temperature (22 °C).

### 2.2 Methods

#### 2.2.1 Obtaining Powdered Wall Materials by Spray Drying

Dispersions were fed into a spray dryer (Mobile Minor™ 2000, GEA Niro, Denmark). The equipment was operated with cocurrent flow, pneumatic nozzle, 150 °C as inlet drying-air temperature, and 70 °C as outlet drying-air temperature. The powders were stored in polyethylene bags with a hermetic seal until later analysis.

#### 2.2.2 Water Activity and Moisture Content

Water activity ( $a_w$ ) of each powder was analyzed using an AquaLab (four TE model, Decagon Devices, USA). The moisture content was determinate gravimetrically following the official AOAC method (AOAC 2005).

**Table 1** Water content and  $a_w$  of wall materials obtained by spray dried

Sample	Composition (% total solids)			Moisture content (% d. b.)	Water activity ( $a_w$ )
	SPI	GA	MD		
SPI	20	0	0	3.32 ± 0.48 <sup>ab</sup>	0.1340 ± 0.007 <sup>a</sup>
GA	0	20	0	4.28 ± 0.23 <sup>bcef</sup>	0.1310 ± 0.004 <sup>a</sup>
MD	0	0	20	2.21 ± 0.45 <sup>d</sup>	0.1217 ± 0.003 <sup>c</sup>
SPI/GA	10	10	0	3.64 ± 0.11 <sup>a</sup>	0.1116 ± 0.003 <sup>c</sup>
MD/GA	0	10	10	2.88 ± 0.36 <sup>acd</sup>	0.0993 ± 0.003 <sup>d</sup>
SPI/MD	10	0	10	3.56 ± 0.11 <sup>abce</sup>	0.1386 ± 0.004 <sup>ab</sup>
13SPI/GA/MD	13.33	3.33	3.33	4.38 ± 0.37 <sup>bcef</sup>	0.1657 ± 0.001 <sup>f</sup>
SPI/GA/13MD	3.33	3.33	13.33	3.68 ± 0.18 <sup>ab</sup>	0.1487 ± 0.004 <sup>b</sup>

The samples that share the same letter mean no significant difference ( $p < 0.05$ )

### 2.2.3 Wetting of Wall Materials

One gram of powdered wall materials was placed in a sealed flask containing a saturated solution of NaCl (75 % relative humidity, RH); after a week, the sample was weighed and the difference of moisture gained was expressed as g of moisture/100 g dry solids (Tonon et al. 2008).

### 2.2.4 Microstructural Changes During Caking Process

Determination of caking stages developed in the wetted samples of wall material blends (individually, in binary, and ternary mixtures) was performed according to the steps proposed by Aguilera et al. (1995). Considering that, water vapor acts to increase union between individual microparticles of powders forming stable agglomeration. This process involves binding, agglomeration, and compaction. These stages are identified as bridging, contact points between particles; agglomeration, an irreversible union of bridges, resulting in a particle clumps with structural integrity; and compaction, loss of system integrity and reduction of interparticle spaces and deformation. In the final stage of caking, bridges disappear as a result of liquefaction. The development of stable aggregates (caking) after storage of microparticles of powdered wall materials was evaluated visually, comparing relation between bridge diameter ( $D_{\text{bridge}}$ ) and particle diameter ( $D_{\text{particle}}$ ); bridging, agglomeration, compaction, and liquefaction were observed in images acquired by scanning electron microscopy (SEM), adapting method proposed by Aguilera et al. 1995.

### 2.2.5 Glass Transition Temperature ( $T_g$ )

Differential scanning calorimetry (DSC, Perkin Elmer Diamond, USA) was used to measure wetted powder glass transition temperature range. Samples of powder (15 g) were prepared in a DSC aluminum pans (40  $\mu\text{L}$ ), and the pans were then hermetically sealed. All measurements were made at a scanning rate of 10  $^{\circ}\text{C}/\text{min}$ , from  $-20$  to  $-120$   $^{\circ}\text{C}$  (Acevedo et al. 2006).

## 3 Results and Discussion

All samples of powdered wall materials (spray dried) were constituted by individual microparticles of spherical geometry. The moisture content values varied between 2.21 and 4.38 (% dry base, d. b.) and  $a_w$  between 0.10 and 0.16 (Table 1). Cuq et al. (2010) indicate that food powders with low water activity values are

**Table 2** Properties of wetted powders at 75 % RH during 7 days

Sample	Water content (% d. b.)	Caking stages <sup>a</sup>				$T_g$ (°C)	$T - T_g$ (°C)
		B	A	C	L		
SPI	13.312 ± 0.38 <sup>a</sup>	—	—	—	—	58.28	-36.28
GA	20.167 ± 0.75 <sup>b</sup>	+	+	—	—	42.68	-20.68
MD	12.529 ± 0.75 <sup>ac</sup>	+	+	+	+	8.98	13.02
SPI/GA	13.796 ± 0.62 <sup>a</sup>	+	+	—	—	36.67	-14.67
MD/GA	15.678 ± 1.05 <sup>ad</sup>	+	+	+	—	34.49	-12.49
SPI/MD	14.820 ± 1.03 <sup>a</sup>	+	+	+	—	34.99	-12.99
13SPI/GA/MD	13.989 ± 1.08 <sup>a</sup>	+	+	—	—	38.05	-16.05
SPI/GA/13MD	14.098 ± 0.48 <sup>a</sup>	+	+	+	+	11.76	10.24

Storage temperature ( $T$ ) = 22 °C; glass transition temperature ( $T_g$ )

The samples that share the same letter mean no significant difference ( $p < 0.05$ )

B bridging, A agglomeration, C compaction, L liquefaction (Aguilera et al. 1995)

<sup>a</sup>(-) absent stage; (+) observed stage

stable and could have low biochemical reactivity; similar materials were obtained in this study.

The moisture sorption by the wall materials is an important physicochemical property that regulates processing conditions and storage stability. Values moisture content achieved by the samples (individually, in binary, and ternary mixtures) exposed at 75 % RH are observed in Table 2; in this case, GA was the material that absorbed the highest % of water (20.167 % d. b.); it means five times the initial moisture content. This could be related to the water-holding capacity of the GA, 5.7 g of water/g gum arabic, and its solubility 0.5 g GA/mL 1 mL of water (Robertson and Eastwood 1981).

Evident changes in the microstructure of storage powders 75 % RH were detected (Fig. 1). Bhandari and Howes (1999) reported similar results; in this context, Rao and Labuza (2012) indicated that changes in powders properties during storage affect its functionality and production. All samples suggested caking process, except SPI sample (Fig. 1). This one kept microstructural integrity due to its low water solubility, although this sample adsorbed fourfold initial moisture content. However, blends containing SPI (SPI/GA, 13SPI/GA/MD, and SPI/GA/13MD) may develop caking process, but its intensity depends on concentration of highly water-soluble components. In case of GA and its blends showed caking process with evident bridging, agglomeration, and stages of compaction. In blends of GA with high concentration of maltodextrin the liquefaction phenomenon was developed (Fig. 1b). Microstructure of samples containing high concentration of maltodextrin (MD, MD/GA, APS/MD, SPI/GA/13MD) suffered collapse. This phenomenon is a microstructural compaction that is associated with a pronounced loss of the integrity of the system, as result of the increase of diameter of bridges interparticles and reduction of interspaces. Microparticles prepared with the formulations MD and APS/GA/13MD achieved a structural collapse where the junctions between particles disappeared, due to solubilization of the low molecular weight fractions (Aguilera et al. 1995). Similar results were observed

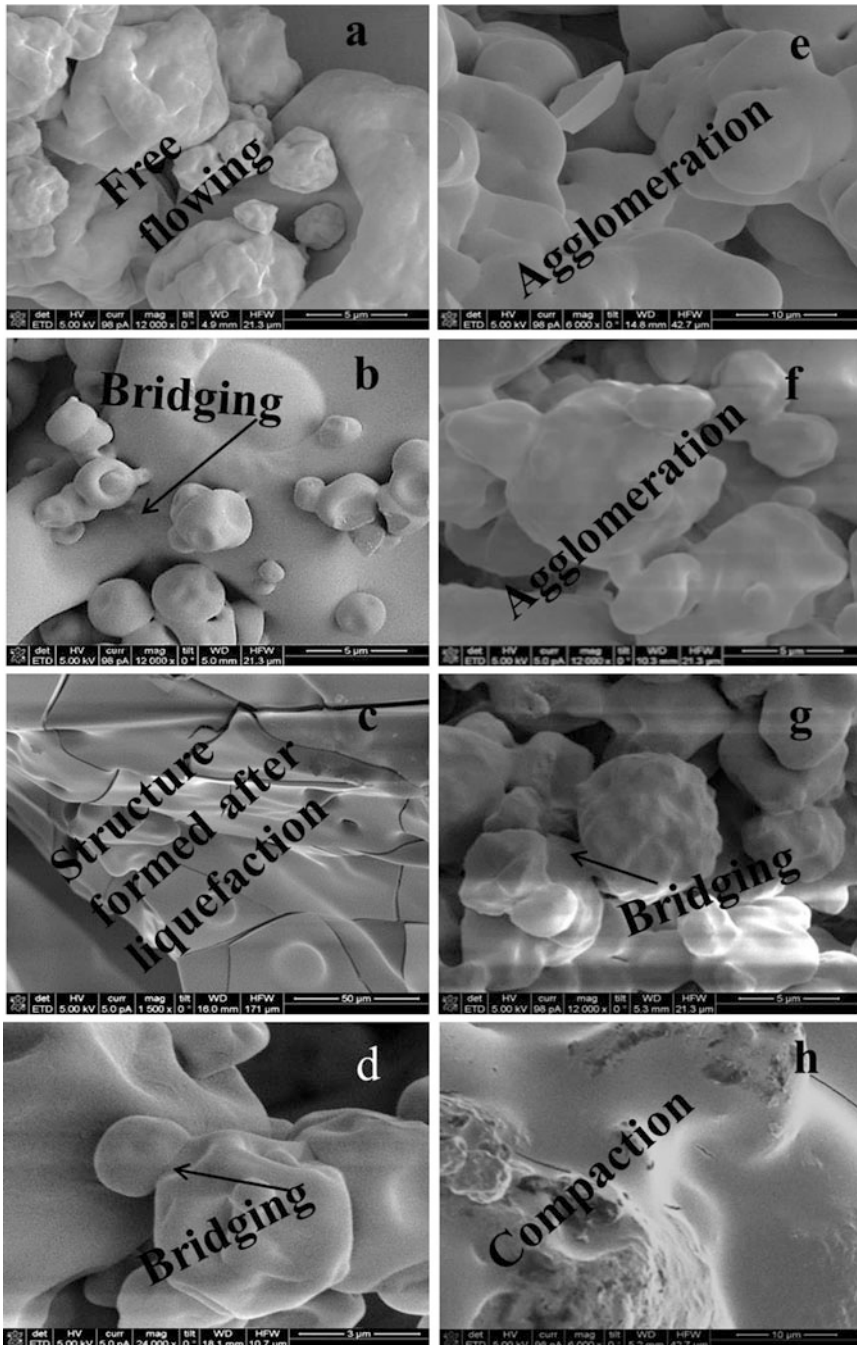


**Fig. 1** SEM images of powders stored at 75 % relative humidity, illustrating stages of caking process. (a) SPI, magnification 12000×, (b) GA, magnification 12000×, (c) MD, magnification 1500×, (d) SPI/GA, magnification 24000×, (e) MD/GA, magnification 6000×, (f) SPI/MD, magnification 12000×, (g) 13SPI/GA/MD, magnification 12000×, and (h) SPI/GA/13MD, magnification 6000×

by Hartmann and Palzer (2011), reporting that chemical composition is critical to the structural collapse of the particles. Also, these authors refer that systems with a higher amount of water-soluble compounds are more susceptible to collapse, as the case of maltodextrin; on the other hand, the addition of polymers with higher molecular weight (GA and SPI) could delay the physical changes.

In addition to the moisture content that increases and the microstructural modifications, reduction of glass transition temperature was observed. In this context, amorphous solids obtained by spray drying are prone glass transition related changes, as collapse and caking. In this work, water acts as an effective plasticizer for SPI, MD, and their blends, since a greater amount of water is needed to diminish the value of  $T_g$ , causing changes in its structure. Shrestha et al. (2007) indicated that proteins are large molecules that may affect the glass transition behavior of small molecules, as in the case of maltodextrin 20 DE.

In this regard, Foster et al. (2005) showed that changes in physical structure of amorphous sugar are linked to variable  $(T - T_g)$ , where  $T$  is the storage temperature and  $T_g$  is the glass transition temperature. For negative values of  $(T - T_g)$ , the analyzed system was in a highly viscous glassy state and was expected to be very stable; whereas values of  $(T - T_g)$  were positive, the system is set to supercooled, and its viscosity is less susceptible to change state. In case of blends of wall materials, the analyzed variable  $(T - T_g)$  at the same temperature and relative humidity (RH) (Table 2) gave negative and positive values. Correlating  $(T - T_g)$  with microstructural changes (Fig. 1) developed during caking was possible. Positive values of  $(T - T_g)$  were observed in blends containing highest concentration of maltodextrin (MD and SPI/GA/13MD); that means blends with  $(T - T_g)$  positive reveal compaction or liquefaction, with irreversible microstructural deformation. In samples of blends that exhibit  $(T - T_g)$  with negative values, the stages of caking were bridging and agglomeration. SPI kept its microstructural integrity with  $(T - T_g)$  highly negative.

## 4 Conclusions

At 75 % relative humidity and 22 °C, blends of powdered wall materials containing the highest concentration of maltodextrin, exhibit irreversible microstructural changes (bridging, agglomeration, compaction and liquefaction) identified using SEM technique. In contrast, the use of high concentration of SPI may reduce the caking process, keeping negative values of  $(T - T_g)$ .

**Acknowledgements** The authors wish to thank the Instituto Politécnico Nacional (National Polytechnic Institute) for the financial support provided through the SIP project: 20140253 and 20140554, BEIFI-IPN, COFAA-IPN, CONACyT, project 216044, and the scholarships for the PhD studies of Josefina Porras-Saavedra. The authors are grateful for experimental support of Universidad de Buenos Aires and Instituto Mexicano del Petróleo.

## References

- Acevedo N, Schebor C, Buera MP (2006) Water-solids interactions, matrix structural properties and the rate of non-enzymatic browning. *J Food Eng* 77:1108–1115
- Aguilera JM, del Valle JM, Karel M (1995) Caking phenomena in amorphous food powders. *Trends Food Sci Tech* 6:149–155
- AOAC (2005) Official methods of analysis of AOAC International (16th ed). Gaithersburg, USA
- Bhandari BR, Howes T (1999) Implications of glass transition for the drying and stability of dried foods. *J Food Eng* 40:71–79
- Cuq B, Rondet E, Abecassis J (2010) Food powders engineering, between knowhow and science: constraints, stakes and opportunities. *Powder Technol* 208:244–251
- Foster KD, Bronlund JE, (Tony) Paterson AH (2005) Glass transition related cohesion of amorphous sugar powders. *J Food Eng* 15:85–91
- Hartmann M, Palzer S (2011) Caking of amorphous-Material aspects, modelling and applications. *Powder Technol* 206:112–121
- Lipasek RA, Ortiz JC, Taylor LS, Mauer LJ (2012) Effects of anticaking agents and storage conditions on the moisture sorption, caking, and flowability of deliquescent ingredients. *Food Res Int* 45:369–380
- Guadarrama-Lezama AY, Jaramillo-Flores ME, Gutiérrez-López GF, Pérez-Alonso C, Dorantes-Álvarez L, Alamilla-Beltrán L (2014) Effects of storage temperature and water activity on the degradation of carotenoids contained in microencapsulated chili extract. *Drying Technol* 32 (12):1435–1447
- Madene A, Jacquot M, Scher J, Stéphane D (2006) Flavour encapsulation and controlled release: a review. *Int J Food Sci Technol* 41:1–21
- Matalanis A, Griffith JO, McClements DJ (2011) Structured biopolymer-based delivery systems for encapsulation, protection, and release of lipophilic compounds. *Food Hydrocoll* 25:1865–1880
- Rao Q, Labuza TP (2012) Effect of moisture content on selected physicochemical properties of two commercial hen egg white powders. *Food Chem* 132:373–384
- Robertson JA, Eastwood MA (1981) A method to measure the water-holding properties of dietary fibre using suction pressure. *Br J Nutr* 46:247–255
- Saragoni P, Aguilera JM, Bouchon P (2007) Changes in particles of coffee powder and extensions to caking. *Food Chem* 104:122–126
- Schebor C, Mazzobre MF, Buera MP (2010) Glass transition and time-dependent crystallization behavior of dehydration bioprotectant sugars. *Carbohydr Res* 345:303–308
- Shrestha AK, Howes T, Adhikari BP, Wood BJ, Bhandari BR (2007) Effect of protein concentration on the surface composition, water sorption and glass transition temperature of spray-dried skim milk powders. *Food Chem* 104:1436–1444
- Tonon RV, Bravet C, Hubinger MD (2008) Influence of process conditions on the physicochemical properties of acai (*Euterpe oleracea* Mart.) powder produced by spray drying. *J Food Eng* 88:411–418

# **Food Matrix Structure Quality Preservation: Water Removal Operation Conditions Control During Convective Drying**

**H. Necoechea-Mondragón, D.Y. Morales-Delgado, E. Parada-Arias,  
M. Cornejo-Mazón, and D.I. Téllez-Medina**

## **Abbreviations**

FPD	Food product development
A	Area
P	Perimeter
Fe	Feret diameter
FD	Fractal dimension
X	Instant moisture content (db)
X1	Initial moisture content (db)
m	Meter
s	Second

---

H. Necoechea-Mondragón (✉)

Dirección de Investigación, Secretaría de Investigación y Posgrado, Instituto Politécnico Nacional, Miguel Bernard Av. Luis Enrique Erro S/N, Unidad Profesional Adolfo López Mateos, Zacatenco, Delegación Gustavo A. Madero, México City, DF CP 07738, Mexico  
e-mail: [hugo.necoechea@gmail.com](mailto:hugo.necoechea@gmail.com)

D.Y. Morales-Delgado • E. Parada-Arias • D.I. Téllez-Medina

Departamento de Graduados e Investigación en Alimentos, Escuela Nacional de Ciencias Biológicas, Instituto Politécnico Nacional, Carpio y Plan de Ayala s/n, Mexico City, DF CP 11340, Mexico

M. Cornejo-Mazón

Departamento de Biofísica, Escuela Nacional de Ciencias Biológicas, Instituto Politécnico Nacional, Carpio y Plan de Ayala s/n, Mexico City, DF CP 11340, Mexico

## 1 Introduction: Food Product Development Challenges in a Globalized World

Food product development (FPD) is a systematic task with the objective of generating new products by either modifying any existing or producing a new and original one. Driven by consumers' expectations, new knowledge, globalization, and shorter product cycles, among others, companies must survive in a dynamic and often unpredictable markets characterized by high levels of competitiveness (De-Greef et al. 2014).

Development of new products has become more relevant to companies and, in the food industry, holds an important and strategic role, becoming a key aspect when trying to achieve higher levels of competitiveness. The development process of new products is fundamentally based on the ability for better identifying ways of meeting market needs and in the capacity of interpreting such information into products, which in fact offers a better solution for such needs in relation to its competition (Gonçalves-Moreira and De-Toledo 2005).

FPD is recognized as a core process that ensures the success of companies; improving process is a key factor for the success of a company. The importance of FPD continues to grow in response to increasingly rapid technological advances and to globalization, which has, worldwide, opened markets to free trade and giving place to high levels of competitiveness.

Product quality in the food sector is one of the priority criteria to analyze its performance in the consumer market and is a variable that directly affects the design and production process. Development time is an important factor, since it must follow changes in customer requirements, incorporate new technologies, and attend the increasing competitiveness of the market in the introduction of innovative products. Finally, productivity of the development process must be efficient, which means that new product development involves searching the best performance of material, financial, and human resources available on the company, and one of the main challenges of the food product development task is to manage the best combination of these three factors for an efficient process. Consequently, systematize appropriate models and tools will help to consolidate the process management (De-Greef et al. 2014).

In the literature there are several proposals to systematize the activities of FPD using models, according on the area of knowledge of the authors. A large number of FPD, best manufacturing practices, tools, methods, and systems have been developed throughout the years to help companies to improve their FPD schemes (Fig. 1).

Nonetheless, numerous companies have consistently failed in their attempts to develop their products on time, within budget, and with the expected features and quality (Rozenfeld et al. 2006). This is why the design of products based on market and consumer present and future demands is an important engineering issue in which food structuring tasks play an important role. Food matrixes are complex and active structures; water and other components interact during and after

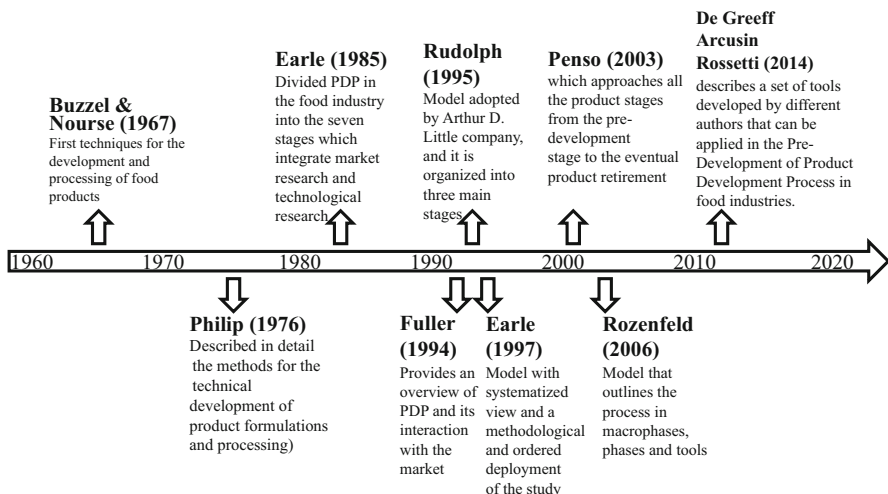


**Fig. 1** Evolution of food product development models

manufacturing, and preservation processes such as those related with water removal aim to slow the magnitude of these interactions to minimize rates of degradation. Knowledge and systematization of structure-function relationships are important towards development of products and processes.

## 2 The Water Functionality in Dried Food Product Development

The structured food systems (i.e., cellular tissues) are dissipative structures whose functionality mainly concerns their properties and characteristics (physical-chemical properties, chemical, and biochemical reactions), external interactions with surroundings (interactions with microorganisms, heat, and mass transport pathway), and especially, their interactions with consumers (nutritional value, quality, taste and flavor, texture, appearance: size, shape, color). Dehydration or rehydration processes involve heat and mass transport of water and solutes coupled with phase transitions as well as with nano-, micro-, and macrostructural changes, thus producing important effects on food functionality, and control of these phenomena is a major concern in FPD which must be applied not only to the changes in physical-chemical properties but also to those related with demands of consumers (Fito and Chiralt 2003).

Food matrix engineering is a branch of food engineering which aims to apply the knowledge of the food matrix composition, structure, and properties to promote and control changes which can improve some sensorial and/or functional properties in the food (Fito and Chiralt 2003). These changes are related to the phenomena of

heat and mass transfer such as vaporization-condensation, internal gas or liquid release, as well as to structure deformation-relaxation and phase transitions in matrix components and are usually coupled to processing conditions. The final product may be a new one with improved composition and sensorial properties and stability.

Food quality is essentially a multivariate concept, involving a number of properties, such as color, moisture content, texture, and others such as aroma and taste. Most fresh foods contain more than 70 % water, while fresh fruits and vegetables can contain up to 95 % water. Thus, water state in foods is deeply related to their quality.

Drying or dehydration improves the shelf life of foods by reducing the amount of water available for undesirable chemical reactions and microbial proliferation. In order to maximize consumer acceptability, it is generally accepted that the dry product should resemble the fresh one as much as possible. However, the removal of water during drying inevitably alters food structure and composition and can result in quality deterioration, the extent of which depends both on the drying method and processing conditions. Therefore, in order to optimize any drying method, it is necessary to quantify the extent of quality change that occurs during the drying process. Multiple parameters are typically measured to quantify these changes, such as color, texture, moisture content, and water activity (Gowen 2012).

The control of structure of the food for consumer acceptability and shelf life has become extremely important. In materials science foods can be treated as another material that has a dominance of water and polymers. As a recent development, food science has embraced the area of phase transition and nanotechnology. Researches in these two areas have contributed to a better understanding of the behavior of the food components and of the whole product as a composite mixture during processing and storage. These two emerging fields and the growing importance of food micro- and macrostructures have encouraged the shifting in the direction of research towards materials sciences (Bhandari and Roos 2012).

### 3 Digital Image Analysis Techniques for Systematize Food Product Development Process

It is accepted that relevant food properties are related to their structure and that key elements defining the architecture of same are not discernible by the eye (Ramírez et al. 2009). Thus, the use of several microscopy techniques and other imaging methods has become common in the study of food microstructures (Aguilera 2005). It follows that images (photomicrographs) are extensively used in the scientific literature as evidence of the structural features of food materials. These images are usually used as support for a qualitative description of the microstructure and complement data generated by rigorous protocols of sampling and preparation, chemical analyses, and determination of physical properties.

Several studies suggest relationships between bulk properties of foods (e.g., mechanical moduli, thermal properties, and so on) and their microstructural characteristics (based on images) (Gowen 2012). Also the evaluation of shrinking and deformation at different scales may be carried out by means of Digital Image Analysis, providing quantitative information on microstructural properties so as to differentiate between objects that have been subjected to different processes or treatments (Alvarado-González et al. 2012; Domínguez-Fernández et al. 2012; Chanona et al. 2003; Morales-Delgado et al. 2014; García-Armenta et al. 2014; Sánchez-Segura et al. 2015).

Parameters such as area (A), perimeter (P), and Feret diameter (Fe) are indicators of size of the analyzed objects, and one important parameter related to its irregularity that may also be calculated by Digital Image Analysis is the fractal dimension (FD). The word fractal comes from the Latin word *fractus* that means broken and its corresponding verb *frangere* meaning breaking. This term and concept was proposed by Mandelbrot (1982) to characterize nonlinear, temporal phenomena or to describe objects having a variable degree of irregularity. FD may be estimated by using various algorithms, among which the box counting method is widely used (Chanona et al. 2003).

Next, a revision of attempts to integrate food product development, comments on a recent works made by our research team on the dehydration operation, is presented within the frame of fractal and image analysis.

## 4 Convective Drying, Structure, and Diffusivity

Morales-Delgado et al. (2014) reported the effect of convective drying of strawberries (*Fragaria x ananassa Dutch*) on the cell morphological changes in the mesocarp by determining the variations in area (A), perimeter (P), Feret diameter, (Fe) and FD of parenchymal tissue cells, dried at 60, 70, 80, and 90 °C and 1 m/s airflow, and by using a hot-air experimental tunnel dryer. A decrease in values of A, P, Fe, and FD in cells of samples dehydrated at 60 °C was found, whereas no changes in A, P, and Fe were found in those dried at 70–90 °C in relation to those observed at 60 °C. The cell contour resulted smoother after high-temperature drying, as indicated by the decrease in FD (Morales-Delgado et al. 2014).

The four drying kinetics of sliced strawberries were obtained. Initial water content for all samples was  $92.2 \pm 0.4$  % wet basis which was similar to values reported for this fruit (Doymaz 2008). All samples reached equilibrium moisture content within 60–90 min. Higher temperatures resulted, as expected, in shorter drying times, and shape of drying curves and drying times are typical of operating conditions (Brennan 2011). Final moisture contents found were (dry basis) 2.8 % (drying air temperature, 60 °C), 1.42 % (drying air temperature, 70 °C), 1.63 % (drying air temperature, 80 °C), and 0.91 % (drying air temperature, 90 °C).

In Fig. 2, images in the final appearance of dried strawberry slices to different working temperatures are shown. All the products retained a good appearance, that

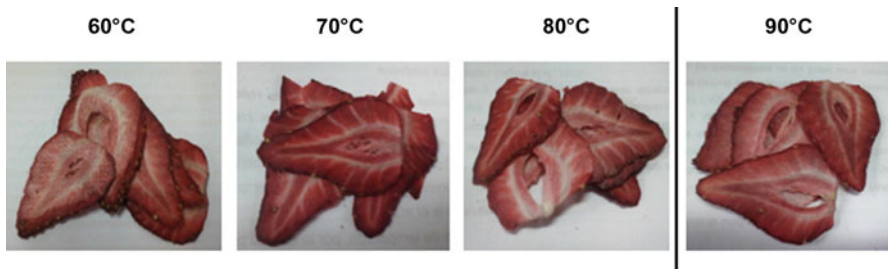


**Fig. 2** Images of strawberry dehydrated at four different temperatures: 60, 70, 80, and 90 °C

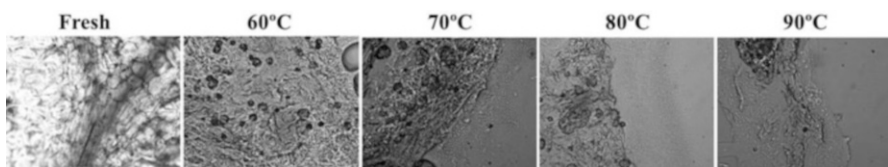


**Fig. 3** Images (*gray scale*) of strawberry tissues; fresh and after convective drying at indicated temperatures (20 $\times$ )

is, with increasing temperature of dehydration flakes of strawberry obtained with typical feature in color and shape (Contreras et al. 2008). At the microlevels (Fig. 3), cell contours of samples dried at higher temperatures were more disrupted than those observed at lower temperatures. This was due to higher tissue's internal pressures and to rapid formation of rigid structures at high drying temperatures which tend to be more fragile and break.

For all cases, a significant decrease ( $p < 0.05$ ) of morphometric parameters was observed between original and dehydrated samples. Reductions of 74.2, 49.8, 50.7, and 3.0 % were found for A, P, Fe, and FD, respectively, for samples dried at 60 °C (lowest drying temperature), which indicated a marked morphological damage for all dehydrated samples in relation to the initial one, except for irregularity of cell morphology (evaluated as FD) in which a slight decrement of this value was associated to a smoothening effect of dried tissue which resulted to be more intense in samples dehydrated at 90 °C, probably due to the pressure that the expansion of the water when changing to vapor phase exerted in the interior of the parenchymal tissue. Results indicated a higher level of shrinking when applying 70–90 °C drying air temperature, which may be due to the fact that no apparent crust formation was observed in all cases so that size decrement associated with crust and low shrinking did not seem to take place.

In Fig. 4, the lines  $\ln(X/X_1)$  against time for strawberry used to for calculating the effective diffusivity coefficient are presented. During drying, water loss on the surface of the material generates significant moisture gradients in the solid which will have important consequences towards the quality of the final product (Ramallo et al. 2001).

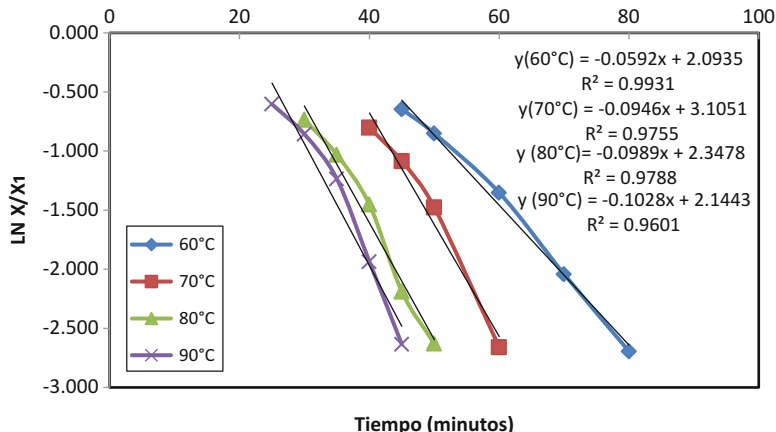


**Fig. 4** Representation of the solution to Fick's second law for the falling rate period of drying samples of strawberry at 60, 70, 80, and 90 °C, drying air speed of 1 m/s

**Table 1** Values of effective diffusivity coefficient for strawberry convective drying

Drying air temperature (°C)	Diffusivity coefficient Deff (m <sup>2</sup> /s)
60	2.25E-10
70	3.59E-10
80	3.76E-10
90	3.91E-10

Effective diffusivity values of strawberry samples that were evaluated during the drying process are shown in Table 1. It was observed that, when the temperature increases, the samples of strawberry shrink faster, and thus, water mobility increases.

Doymaz (2008) reported that the transport of water during drying of strawberry was well described by Fick's mechanisms and that the corresponding coefficients of effective diffusivity were between  $4.95 \times 10^{-10}$  and  $1.42 \times 10^{-10}$  m<sup>2</sup>/s (Doymaz 2008). The coefficients of effective diffusivity of the present study agreed with those reported by Doymaz 2008, concluding that the diffusion coefficients and drying rates increased with temperature.

## 5 Final Remarks

Since structure-property relationships in foods usually link information at the microlevel (microstructure) with lumped properties at the macrolevel (whole product), multi-scale approach must be considered by food product engineers, scientists, and companies in product development schemes. Digital Image Analysis

techniques and the numerical models that describe the relationships between the structure and properties could be used in different types of food designs for food matrix quality preservation as in water removal in drying processes, contributing to the systematization and integration of the food product development process in food companies. Water removal was studied at cellular levels during drying of strawberries; it was observed that at microlevels, the cell contours of samples dried at higher temperatures were more disrupted than those observed at lower temperatures.

## References

- Aguilera JM (2005) Why food microstructure? *J Food Eng* 67(1):3–11
- Alvarado-González JS, Chanona-Pérez JJ, Welti-Chanes JS, Calderón-Domínguez G, Pacheco-Alcalá SU (2012) Propiedades ópticas, microestructurales, funcionales y nanomecánicas de películas comestibles de gel de Aloe vera/goma gelano. *Revista Mexicana de Ingeniería Química* 11:193–210
- Bhandari B, Roos YH (2012) *Food materials science and engineering*. Blackwell Publishing Ltd., Oxford, UK
- Brennan JG (2011) Evaporation and dehydration. In: Brennan JG, Grandison AS (eds) *Food processing handbook*. Wiley-VCH Verlag GmbH & Co., Weinheim, Germany, pp 281–329
- Contreras C, Martín-Esparza ME, Chiralt A, Martínez-Navarrete NM (2008) Influence of microwave application of convective drying: effects on drying kinetics, and optical and mechanical properties of apple and strawberry. *J Food Eng* 88(1):55–64
- Chanona JJ, Alamilla L, Farrera RR, Quevedo R, Aguilera JM, Gutierrez GF (2003) Description of the convective air-drying of a food model by means of the fractal theory. *Food Sci Technol Int* 19:207–213
- De-Greef M, Arcusin L, Rossetti G (2014) Tools description for product development process management in food industries. *Int J Res Eng and Tech* 3(11):226–232
- Domínguez-Fernández RN, Arzate-Vázquez I, Chanona-Pérez JJ, Welti-Chanes JS, Alvarado-González JS, Calderón-Domínguez G (2012) El gel de Aloe vera: estructura, composición química, procesamiento, actividad biológica e importancia en la industria farmacéutica y alimentaria. *Revista Mexicana de Ingeniería Química* 11:23–43
- Doymaz I (2008) Convective drying kinetics of strawberry. *Chem Eng Process* 47(5):914–919
- Fito P, Chiralt A (2003) Food matrix engineering: the use of the water-structure-functionality ensemble in dried food product development. *Food Sci Technol Int* 9(3):151–156
- García-Armenta E, Téllez-Medina DI, Alamilla-Beltrán L, Arana-Errasquín R, Hernández-Sánchez H, Gutiérrez-López GF (2014) Multifractal breakage patterns of thick maltodextrin agglomerates. *Powder Technol* 266:440–446
- Gonçalves-Moreira LA, De-Toledo JC (2005) Food products development process and management in a cereal company: a case study. *Prod Manag Develop* 3(1):61–65
- Gowen AA (2012) Water and food quality. *Contemp Mat* 3(1):32–37
- Mandelbrot BB (1982) *The fractal geometry of nature*. W. H. Freeman, New York NY, 468
- Morales-Delgado DY, Téllez-Medina DI, Arellano-Cárdenas S, López-Cortez S, Hernández-Sánchez H (2014) Effect of convective drying on total anthocyanin content, Antioxidant activity and cell morphometric parameters of Strawberry parenchymal tissue (*fragaria x ananassa dutch*). *Revista Mexicana de Ingeniería Química* 13(1):179–187
- Ramallo LA, Pokolenko JJ, Balmaceda GZ, Schmalko ME (2001) Moisture diffusivity, Shrinkage, and apparent density variation during drying of leaves at high temperatures. *Int J Food Prop* 4 (1):163–170

- Ramírez C, Germain JC, Aguilera JM (2009) Image analysis of representative food structures: application of the bootstrap method. *J Food Sci* 74(6):65–72
- Rozenfeld H, Forcellini FA, Amaral DC, Toledo JC, Silva SL, Alliprandini DH (2006) Gestão de desenvolvimento de produtos: uma referência para a melhoria de processo. Ed. Saraiva, São Paulo
- Sánchez-Segura L, Téllez-Medina DI, Evangelista-Lozano S, García-Armenta E, Alamilla-Beltrán L, Hernández-Sánchez H (2015) Morpho-structural description of epidermal tissues related to pungency of Capsicum species. *J Food Eng* 152:95–104

## Editors' Biographies

**Gustavo F. Gutiérrez-López** received his Bachelor of Science in Biochemical Engineering and Master of Science in Food Science and Technology from the *Instituto Politécnico Nacional*, Mexico, and his Master of Science in Food Process Engineering and Ph.D. in Food Engineering from the University of Reading, UK. He is currently a Professor of Food Engineering and chair of the Ph.D. program in Food Science and Technology at the *Escuela Nacional de Ciencias Biológicas* of the *Instituto Politécnico Nacional*, México.

**Liliana Alamilla-Beltrán** received her Bachelor of Science in Biochemical Engineering from the *Instituto Tecnológico de la Paz*, México, and her Master of Science and Ph.D. in Food Science from the *Instituto Politécnico Nacional*, México. She is currently a Professor of Food at the *Escuela Nacional de Ciencias Biológicas* of the *Instituto Politécnico Nacional*, México.

**María del Pilar Buera** received her Bachelor of Science in Chemical Sciences from Facultad de Ciencias Exactas y Naturales, Universidad de Buenos Aires (FCEN-UBA); Master of Science in Food Science and Technology from Universidad Nacional de Mar del Plata, Argentina; and Ph.D. in Chemical Sciences from FCEN-UBA, where she is currently Titular Professor and develops activities as main researcher of CONICET, Argentina.

**Jorge Welti-Chanes** received his Bachelor of Science in Biochemical Engineering and Master of Science in Food Engineering from the *Tecnológico de Monterrey*, Mexico, and Ph.D. in Chemistry from the University of Valencia, Spain. He is currently Associate Dean at *Tecnológico de Monterrey (National School of Engineering and Sciences)*, México, and distinguished Visiting Professor at Texas Christian University and at the *Escuela Nacional de Ciencias Biológicas* of the *Instituto Politécnico Nacional*, México.

**Efrén Parada-Arias** received his Bachelor of Science in Biochemical Engineering and Master of Science in Food Science and Technology from the *Instituto*

*Politécnico Nacional*, Mexico, and his Ph.D. in Food Technology from the Polytechnic University of Valencia, Spain. He has been a Professor of Food Science and Food Engineering at the *Escuela Nacional de Ciencias Biológicas*, of the *Instituto Politécnico Nacional*, México, and Secretary General of this institute, Director General at *Instituto Mexicano del Petróleo*, and is currently Director General of *Centros de Formación para el Trabajo, Secretaría de Educación Pública*, México.

**Gustavo V. Barbosa-Cánovas**, a Fulbright Scholar, received his BS in Mechanical Engineering at University of Uruguay and MS and Ph.D. at University of Massachusetts. He also received a *Honoris Causa* Doctorate from Polytechnic University of Cartagena, Spain. He is a Professor of Food Engineering and Director of the Center for Nonthermal Processing of Food at Washington State University.

# Index

## A

- Acetylated cross-linked starch (ACLS), 456–458  
Acevedo, C., 611–618  
Acevedo, N., 469–476  
Adam, G., 19–21  
Adam–Gibbs theory, 122  
Adhikari, K., 467  
*Aesculus hippocastanum*, 235, 236  
AFM. *See* Atomic force microscopy (AFM)  
*Agave angustifolia* Haw, 346–350  
*Agave* powders  
    bulk and true densities, 349  
    dehydration, 346  
    fractal dimension, 346, 349–350  
    hot air transfers, 347  
    inlet and outlet temperature, 347, 349  
    moisture content, 347, 348  
    preparation, 346–347  
    properties, 350  
    restrictive drying, 347  
    SEM image, 347, 348  
    water activity, 347, 348  
    wettability and rehydration, 349, 350  
*Agave tequilana* leave powder  
    chemical composition, 558–561  
    DSC, 559, 561–562  
    Fourier transform infrared spectroscopy, 559  
    materials, 558  
    preparation, 558  
    thermogravimetric analysis, 559, 561–562  
    x-ray diffraction, 559  
*Agave tequilana* Weber fibers  
    FAAT and FAATP

- α,α-trehalose decomposition, 563  
chemical composition, 558–561  
DSC, 559, 561–562  
Fourier transform infrared  
    spectroscopy, 559  
fructooligosaccharide  
    decomposition, 563  
materials, 558  
preparation, 558  
thermogravimetric analysis, 559,  
    561–562  
    x-ray diffraction, 559  
FAWT  
    chemical composition, 558–561  
    DSC, 559, 561–562  
    Fourier transform infrared  
        spectroscopy, 559  
    materials, 558  
    preparation, 558  
    thermogravimetric analysis, 559,  
        561–562  
    x-ray diffraction, 559  
Agudelo-Laverde, L.M., 27–38, 469–476  
Aguilera, J.M., 21, 418, 471, 632  
Ahmed, H., 545  
Ajandouz, E.H., 59, 60  
Alamilla-Beltrán, L., 15–23, 319–326,  
    337–343, 345–350, 557–564,  
    629–635  
Alginate-chitosan beads  
    cooperative ionic bounds, 354  
    dehydration  
        freeze-drying, 355–357  
        vacuum-drying, 355–357

- Alginate-chitosan beads (*cont.*)
  - digital image analysis, 355
  - enzyme release, 355–358
  - gel bead preparation, 355
  - invertase activity, 356
  - transport mechanism, 358–359
- Allspice
  - biochemical analysis, 569, 571–573
  - fluidized bed drying analysis, 568–571
  - structural analysis, 569, 571–572
- Aloe vera* gel
  - GAB model, 321, 323–324
  - glass transition temperature
    - Gordon and Taylor model, 321–322, 325
    - $T_g$  and M, 321, 324–325
  - Mobile Minor 2000 spray dryer, 320–321
  - moisture content, 322–323
  - parallel and counter current flow, 320
  - powder analysis, 321
  - statistical analysis, 322
  - water activity, 322–323
- Alzamora, S.M., 245–259, 311–316, 375–382, 477–484
- Amorphous carbohydrates
  - anhydrous glucose
    - DSC, 164
    - enthalpy relaxation, 168–170
    - fragility of, 171–172
    - glass transition temperature vs. aging conditions, 166–167
    - vacuum oven method, 163
  - isothermal storage/aging, 162
  - KWW, 162–163
  - macroscopic properties, 162
  - maltose
    - DSC, 164
    - enthalpy relaxation, 168–170
    - fragility of, 171–172
    - glass transition temperature vs. aging conditions, 166–167
    - vacuum oven method, 163–164
  - maltotriose
    - DSC, 164
    - enthalpy relaxation, 168–170
    - fragility of, 171–172
    - glass transition temperature vs. aging conditions, 166–167
    - vacuum oven method, 163–164
  - structural relaxation, 162
- Amorphous sugar matrices
  - drying process, 300–301
  - glass transition temperature, 301–302
  - industrial process, 299–300
  - nonreducing sugars, 300
- phase transitions
  - carbohydrates, 304
  - enzyme concentration, 305
  - freeze-dried samples, 306–308
  - preservation agent, 306
  - sucrose, trehalose, and raffinose, 304
- thermal stability, 303
- Ampicillin trihydrate, 137
- Anaya-Sosa, I., 567–573
- Anderson, B.D., 1–12
- Anderssen, R.S., 611
- Angell, C.A., 68, 69, 163, 300
- Antiplasticization. *See* Short dough biscuits
- Antiplastizicing effect. *See* Cornflakes
- Apple discs drying
  - browning index, 313–314
  - causes, 316
  - CPMG sequence, 312–313, 315
  - FID method, 312, 315
  - $^1\text{H-NMR}$ , 314–315
  - MANOVA, 315
  - mechanical properties, 313
  - microscopic observations, 316, 317
  - RVP, 313–314
  - shrinkage, 313
  - structure changes, 313
  - thermal transitions, 313, 316
  - water mobility, 312
- Apples
  - blanched. (*see* Blanched (B) apples)
  - BOD. (*see* Blanched and osmotically dehydrated (BOD) apples)
  - compression curves, 378, 379
  - magnetization decay curves, 378, 381
  - mechanical behavior, 377
  - osmotic dehydration, 376
  - rheological behavior, 376
  - storage and loss modulus, 378, 379
  - transverse relaxation times, 377, 381
  - viscoelastic properties, 377, 378, 380
- Arabic gum (AG)
  - caking process, microstructural changes, 632–635
  - glass transition temperature, 632–633, 635
  - moisture content, 631–633
- RHME
  - CCD, 577–579
  - isolated enzymes, 576
  - preparation, 577
  - protein concentration assay, 578, 579
  - proteolytic activity assay, 578, 580
  - RS design, 577, 579–581
  - SEM, 578
  - yield, 578, 581–582

- wall materials, 631–633, 635  
water activity, 631–633
- Arenas-Ocampo, M.L., 345–350
- Aroma compounds  
GC analysis, 502  
headspace analysis, 501  
physicochemical characteristics, 500–501  
sugar concentration  
initial apparent rate of release, 503–505  
kinetics, 506  
liquid–vapor partition coefficients, 503  
release of volatiles, 502–503  
retention index, 502–503  
trehalose, 505  
vapor–water interface, 505–506  
water activity, 503  
viscosity, 502  
water activity, 502
- Arredondo-Ochoa, T., 451–459
- Arrhenius kinetics, 67
- Atomic force microscopy (AFM), 103
- Authelin, J.-R., 83
- Average standard error (ASE), 201, 333–335
- Avicennia marina*, 235, 236
- Azuara-Nieto, E., 15–23
- B**
- Backscattering (BS) profiles, 364, 365
- Badii, F., 611
- Baker, R.A., 454
- Baltsavias, A., 594
- Barbosa-Cánovas, G.V., 161–173, 347
- Bautista-Muñoz, C., 533–539
- Beeswax (BW) mixtures, 105
- Benzamide, 5–7
- Beristain-Guevara, C.I., 15–23
- Berjak, P., 235
- Bertolo, G., 289–297, 621–627
- β-cyclodextrin, 138
- β-lactoglobulin (BLG)  
alcohols and polyols  
aqueous solutions, 428–429  
folding/unfolding process, 428  
protein adsorption, 430–432  
thermal denaturation, 429–430  
viscosity, 432–433  
lactalbumin fraction, 441  
β-relaxation, 443–445
- Bhandari, B.R., 41–61, 437–448, 633
- Biehl, B., 539
- Bifidobacterium infantis* (DLPB)  
preparation, 463  
sorption isotherm, 463–465  
stability, 464–467
- Biliaderis, C.G., 105
- Biological materials  
dielectric relaxation times, 66, 68  
fluidness  
characteristics, 69–70  
food processing and storage. (*see* Food processing and storage)  
food materials, 65  
food solids properties, 66  
mechanical relaxation times, 67, 69  
time-dependent changes, 66
- Blanched and osmotically dehydrated (BOD) apples  
loss modulus, 479–480  
microstructure, 479, 482–483  
rheological properties  
creep/recovery tests, 478–481  
dynamic oscillatory tests, 478  
linear viscoelastic properties, 478  
statistical analysis, 479  
structural changes, 483  
storage modulus, 479–480  
texture properties  
sensory analysis, 479, 481–482  
TPA, 479, 481–482
- Blanched (B) apples  
loss modulus, 479–480  
microstructure, 479, 482–483  
rheological properties  
creep/recovery tests, 478–481  
dynamic oscillatory tests, 478  
linear viscoelastic properties, 478  
statistical analysis, 479  
structural changes, 483  
storage modulus, 479–480  
texture properties  
sensory analysis, 479, 481–482  
TPA, 479, 481–482
- Blanching. *See* Blanched (B) apples
- BLG. *See* β-Lactoglobulin (BLG)
- Blueberries  
Brigitte and Duke  
crystal water endotherms, 408, 409  
DSC, 406–407  
exothermic transitions, 408  
glass transition temperature, 406–408  
moisture content, 406  
normalized enthalpy values, 409–410  
thermal transitions, 407  
epicarp. (*see* Surface free energy (SFE))
- BOD. *See* Blanched and osmotically dehydrated (BOD) apples
- Boltzmann's constant, 20
- Bonner, F.T., 231

- Botrytis cinerea*, 455  
 Box-Behnken design, 487  
 Brain-heart infusion (BHI), 251  
 Bread. *See* Regional breads (Puebla State, Mexico)  
 Breeuwer, P., 251  
 Brewer, A., 249  
 Briones-Martínez, R., 575–583  
 Briones, V., 471  
 Brown, D., 9  
 Brunauer-Emmett-Teller (BET) equation, 17, 196, 202, 332, 463–465  
 Bruni, F., 232, 233  
 Buera, M.P., 17, 27–38, 125–133, 353–360, 469–476, 629–635
- C**  
 Califano, A.N., 367–373, 383–392  
 Cano-Higuera, D.M., 393–402  
*Capsicum annuum*, oily extract  
 antioxidant activity  
     ABTS<sup>+</sup> radical, 339  
     carotenoid consumption, 337–338  
     microencapsulation. (*see*  
         Microencapsulation process)  
     oil-in-water emulsion, 340  
     preparation, 339  
     wall materials, 338  
 Carabasa-Giribet, M., 45, 56  
 Carbohydrate polymers  
     degree of polymerization, 494  
     DSC, anhydrous inulin  $T_g$   
         endothermic shift, 495  
         evaluation, 494–495  
         moisture content, 495–498  
         molecular weight, 496–498  
         plasticizing effect, 495–496  
         polysaccharides, 496  
     sample preparation, 494  
 Carboxyfluorescein (CF), 221  
 Cárcel, J.A., 519–525  
 Carpintero-Díaz, A.E., 567–573  
 Carr-Purcell-Meiboom-Gill (CPMG)  
     sequence, 129–130, 312–313, 472–473  
 Carvajal, M.T., 175–184  
 Casim, S.M., 311–316  
 Central composite design (CCD), 577–579  
 Cepeda, E., 544  
 Cereal products  
     correlation coefficients, 36–37  
     ESEM and SEM, 35  
     flaked and toasted corn grits, 35  
     refractive index matching, 36  
 Chance, B., 569  
 Chang, H.D., 395  
 Chang, Y.P., 600  
 Chanona, J.J., 22  
 Charoenrein, S., 413–419  
 Chauvin, M.A., 128  
 Cheah, P.B., 46  
 Chen, P., 396  
 Chen, X.D., 396  
 Chiralt, A., 101–112, 585–591  
 Chirife, J., 17, 251  
 Chitosan (CH) films  
     DSC, 587, 589–590  
     mechanical properties, 587, 590  
     microstructural analysis, 587  
     preparation, 586  
     SEM micrographs, 590  
     statistical analysis, 587  
     water sorption isotherms, 586, 588  
 Choi, Y., 386  
 Christian, J.H.B., 17, 605  
 Chui, H.C., 561  
 Citral/sugar emulsions  
     equivalent volume-mean diameter, 363, 364  
     flow curves, 363, 364  
     <sup>1</sup>H NMR, 363–365  
     microencapsulation, 362  
     samples preparation, 362–363  
     stability, 364, 365  
     volume-surface mean diameter, 363, 364  
 Citrus seeds  
     DSC thermal transitions, 239–240  
     tolerance, 238  
     Unfrozen water content, 240–241  
     viability, 238, 239  
     water content, 238  
 Civille, G.V., 128, 479  
 Cocoa beans, germination, 533–534  
     DCP, 536  
     enzymatic activity, 535, 537–539  
     enzyme extract, 537  
     growth conditions, 536  
     imbibition, 534  
     metabolic activation, 534  
     moisture content, 535, 536  
     radicle growth, 534  
     seed material, 536  
     water activity, 535–539  
     Xaa-Pro-DAP activity, 535, 537

- Collins, G., 75–86  
Colloidal calcium phosphate (CCP), 439–440  
Computer vision system (CVS), 32, 471  
Convenience foods, 90  
Conventional drying, 624, 626  
Cornejo-Mazón, M., 637–644  
Cornflakes  
  gelatinization-flaking, 126  
  glass transition measurement, 127, 129  
  mechanical properties, 127–128, 130, 131  
  molecular mobility, 127  
  oral texture profile, 128–129, 131  
  RVP, 126  
  sensory properties of, 131–133  
  shelf life stability and textural properties, 126  
Corradini, M.G., 263–278  
Cortés, S.A., 549–554  
Cortés-Vázquez, M.I., 575–583  
Cortez Escobedo, L., 607  
Couchman-Karasz model, 43  
*Crataegus pubescens*. *See* Tejocote fruit  
Creep/recovery test, 377  
Cristina Pérez, 299–309  
Cross-linked dextran-water systems  
  Adam–Gibbs theory, 122  
  ESR, 116  
  Gordon–Taylor equation, 121  
  ice crystallization, 115–116  
  NMR, 116  
  Sephadex. (*see* Sephadex gel)  
  XRD, 116  
Crowe, L.M., 300  
Cruz y Victoria, M.T., 567–573  
Cryopreservation  
  cooling rates, 216–217  
  extracellular ice, 216  
  freezing process, 216  
  liposomes. (*see* Large unilamellar vesicles (LUV))  
  oyster oocytes  
    cryomicroscopy, 218  
    IIF, 221  
    post-thaw fertilization, 219, 220  
    TEM, 219, 221  
    viability, 217–218  
  protocols, 215  
  seeds  
    characteristics, 231  
    citrus. (*see* Citrus seeds)  
    definition, 230  
    desiccation tolerance, 235–237  
glass transition temperatures, 232, 233  
hydration levels, 230–231  
intermediate seeds, 234  
intracellular glasses, 231–232  
orthodox, 231, 232, 234  
plant genetic resources, 230  
recalcitrant seeds, 233–234  
reproduction, 230  
subzero storage temperatures, 237  
Cuq, B., 632
- D**
- Dairy powder  
  milk powder ageing effect  
    enthalpy relaxation, 443–445  
    lactose crystallization, 441–442  
    Maillard reaction, 442–443  
    protein conformational modification, 443  
    solubility and functional properties, 441  
    water–protein interactions, 446–448  
  protein stability, 438  
  structure and physicochemical properties  
    casein, 438–440  
    milk proteins, 438  
    whey proteins, 441  
Davis, M.E., 10, 11  
Dawson, K.J., 7  
*Debaryomyces hansenii*, 248, 249  
Deborah number, 150–151  
Decaglycerol palmitic acid ester (DG-Pam).  
  *See* Starch, gelatinization  
De Dios-Naranjo, C., 557–564  
Dehydrated probiotic dairy product  
  DLPB  
    preparation, 463  
    sorption isotherm, 463–465  
    stability, 464–467  
  DLPL  
    preparation, 463  
    sorption isotherm, 463–465  
    stability, 464–467  
Dehydrate system  
  crystalline hydrate, 139  
  desolvation, 139  
  DSC, 139  
  energetics of, 138  
  liquid-solid and solid-solid transformations., 139  
  solid-state transitions, 136

- Dehydration  
 alginate-chitosan beads  
   freeze-drying, 355–357  
   vacuum-drying, 355–357
- crystalline thymine  
   anhydrous form, 176, 177  
   DSC, 177, 178, 181  
   SEM, 177–179, 183  
   XRPD, 177–179
- cytosine  
   anhydrous form, 176, 177  
   DSC, 177, 178, 180  
   SEM, 177–179, 181  
   XRPD, 177–179
- FPD, 640
- hydrate, 176
- theophylline  
   anhydrous form, 176, 177  
   DSC, 177, 178, 181  
   SEM, 177–179, 182  
   TSPC experiment, 179, 182, 184  
   XRPD, 177–179
- Dehydration tolerance (DT), 254
- Del Castillo, L.M., 578
- Della Campa, M., 621–627
- Della-Volpe, P., 512
- de Moral, Y., 299–309
- Denaturation temperature ( $T_m$ ), 429–430
- Design-Expert software v.7.1.5, 487
- Díaz-Calderón, P., 405–410
- Differential scanning calorimetry (DSC), 76, 79, 632  
 amorphous inulin  
   endothermic shift, 495  
   evaluation, 494–495  
   moisture content, 495–498  
   molecular weight, 496–498  
   plasticizing effect, 495–496  
   polysaccharides, 496
- anhydrous glucose, 164
- cornflakes, 127
- cytosine, 178, 180
- dehydrate system, 139
- dough and cooked minced meat, 385, 386
- hydrates, 138
- longan, 415–417
- maltitol, sucrose and trehalose, 415, 416
- maltose, 164
- maltotriose, 164
- mango, 415–417
- phase transitions, 108
- rambutan, 415–417
- salmon gelatin films, 614, 617–618
- salt crystallization, CH films, 587, 589–590
- Sephadex gel, 117–120
- starch-water composites, 528
- TA Q1000 DSC, 177
- theophylline, 178, 181
- thymine, 178, 181
- Diffusion models  
 GRG, 521  
 NaCl transport, 522–524  
 water transport  
   brine concentration and samples, 521–522  
   explained variance, 522–523  
   LSD intervals, 522  
   salting in, protein insolubilization, 523–524  
   salting out, osmotic effect, 523–524
- Digital Image Analysis, 640–641
- 1,2-Dioleoyl-sn-glycero-3-phosphocholine (DOPC), 10, 11
- Dipalmitoylphosphocholine (DPPC)  
   cooling rates, 225  
   freezing temperatures, 224  
   holding temperatures, 225–226
- Di Teodoro, G., 593–602
- DLPB. *See Bifidobacterium infantis* (DLPB)
- Dorantes-Alvarez, L., 337–343
- Doruker, P., 9
- Dough and cooked minced meat  
   freezing times  
     Biot number, 392  
     finite element simulation, 390, 391  
     moisture contents, 390–391  
     time–temperature curves, 391–392
- thermo-physical properties  
   DSC measurements, 385, 386  
   numerical model, 388–390  
   thermal conductivity, 386–387
- Downton, G.E., 71, 72
- Doymaz, I., 643
- Dry cacao powder (DCP), 536
- Dubinin-Radushkevich model, 19
- Dussert, S., 238, 239
- Dutta, P., 510
- Dynamic dew point isotherm (DDI) method, 194–195
- Dynamic light scattering (DLS), 455
- Dynamic vapor sorption (DVS) method, 194

**E**

- Edible/biodegradable hydrocolloids  
  microstructure of, 102, 103  
  optical properties, 104  
  phase transitions, 108–111  
  plasticizers, 102  
  polar lipids, 103–104  
  protein-lipid ratio, 103  
WSC  
  film plasticizers, 104–105  
  hydrocolloid films, 105–108
- Edible films (EFs)  
  active EFs  
    antimicrobial compounds, 454  
    deterioration, 453–454  
    strawberry weight loss, 456–459  
  characterization, 457  
  functional properties, 452  
  lipids, 452  
  MLC, antimicrobial activity, 455, 457–458  
  modified corn starch, 453  
  plasticizers, 452–453  
  properties, 455  
  starch filmogenic suspension, 454–455  
  surfactants and emulsifiers, 453
- Egg yolk phosphatidylcholine (EPC)  
  cooling rates, 221, 222  
  freezing temperatures, 222–223  
  holding temperatures, 223
- Eichner, K., 42
- Electrical conductivity (EC), 528–530
- Electron microscope by environmental mode (ESEM), 35
- Electron spin resonance spectrometer (ESR), 116
- Emulsifier. *See* Starch, gelatinization
- Enrione, J., 405–410, 611–618
- Enterobacter sakazakii*, 249–251
- Enthalpy relaxation  
  amorphous carbohydrates  
    KWW, 162–163  
    MDSC, 164  
    molecular weight dependence, 167–171  
    milk powder, 443–445
- Equilibrium moisture content ( $M_w$ ), 463–464
- Equilibrium relative humidity (ERH), 446–447
- Ertekin, C., 622
- Esteban, M.A., 280
- Ewing, S., 75–86
- Extract of propolis (EEP), 108
- Eyring model, 303

**F**

- Fabela-Morón, M.F., 345–350
- Fabra, M.J., 101–110, 112
- Fa-De Li, 529
- Farroni, A.E., 27–38, 125–133
- Fermi equation, 128
- Fibers submitted to modified acid-alkaline hydrolysis without pressure (FAAT)  
   $\alpha,\alpha$ -trehalose decomposition, 563  
  chemical composition, 558–561  
  DSC, 559, 561–562  
  Fourier transform infrared spectroscopy, 559  
  fructooligosaccharide decomposition, 563  
  materials, 558  
  preparation, 558  
  thermogravimetric analysis, 559, 561–562  
  x-ray diffraction, 559, 563
- Fibers submitted to modified acid-alkaline hydrolysis with pressure (FAATP)  
   $\alpha,\alpha$ -trehalose decomposition, 563  
  chemical composition, 558–561  
  DSC, 559, 561–562  
  Fourier transform infrared spectroscopy, 559  
  fructooligosaccharide decomposition, 563  
  materials, 558  
  preparation, 558  
  thermogravimetric analysis, 559, 561–562  
  x-ray diffraction, 559, 563
- Fibers without treatment (FAWT). *See* Agave *tequilana* leave powder
- Fickian diffusion, 150
- Figueroa-Cárdenas, J.D., 527–530
- Film barrier properties, 108
- Fine, F., 253
- Finite element method (FEM), 384, 389
- Flame ionization detector (FID) method, 312
- Flores-Andrade, E., 15–23
- Flores-Morales, A., 557–564
- Flores, N.L., 568
- Flory-Huggins interaction parameter, 151, 153, 154
- Fluidized bed drying process, allspice, 568–571
- Fogliano, V., 48
- Food appearance  
  chromatic attributes, 32  
  cornflakes production, 31  
  Kubelka–Munk analysis, 32–33  
  opacity, 32  
  translucence changes  
    cereal products. (*see* Cereal products)  
    fruit products, 33–34
- transparency-opacity changes  
  dehydration or rehydration, 29–30  
  light scattering particles, 30–31

- Food morphology, 22  
 Food powders  
   advantages, 90  
   dissolution of carbohydrates  
     endo-or exothermic effect, 93  
     maltodextrin, 93–95  
     molecular weight (MW), 95  
     Setaram C80 Calvet-type  
       calorimeter, 93  
       SMP sample, 93, 94  
   dissolution of proteins  
     micellar casein, 96–98  
     Na-caseinate, 96–98  
   integrated approach, 91  
   reconstitution process, 90, 91  
 Food processing and storage  
   crystallization of amorphous sugars, 72–73  
   microstructure effect, 70  
   stickiness and caking properties, 71  
   structural relaxation times, 71–72  
 Food product development (FPD)  
   convective drying, 640–643  
   dehydration, 640  
   Digital Image Analysis, 640–641  
   effective diffusivity, 642–643  
   evolution, 638–639  
   food matrix, 639–640  
   food quality, 640  
   micro-and macrostructures, 639–642  
 Forny, L., 89–98  
 Foster, K.D., 324, 635  
 Fourier transform infrared (FTIR)  
   spectroscopy, 443  
 Fractal dimension (FD), 22, 641  
 Fractal dimension of contour (DFc), 350  
 Fractal dimension of texture (DFt), 350  
 Fragility index, 163  
 Freeze-dried strawberry  
   collapse determination, 472  
   CVS, 471  
   fruit slices, liquid nitrogen, 470  
   glass transition temperature, 472  
   image segmentation, 471–472  
   materials preparation, 470–471  
   relative humidity  
     pixel proportion, 473, 475  
     pseudo-zero-order reaction rate, 473–474  
     shrinkage and color changes, 473, 475  
     water mobility determination, 472–473  
 Freeze-drying process, 70  
 Freezing-point depression (FPD)  
   experimental results, 396  
   mathematical model, 397  
   product solids and water, 395  
   schematic diagram, 395, 396  
   Siebel's equations, 395  
 Friberg, S., 4  
 Friel, E.N., 500  
 Frozen physalis juice  
 FPD  
   experimental results, 396  
   mathematical model, 397  
   product solids and water, 395  
   schematic diagram, 395, 396  
   Siebel's equations, 395  
 thermal conductivity  
   coaxial dual-cylinder apparatus, 398  
   concentration and temperature, 399, 401  
   Fikiin equation, 401  
   frozen water fraction, 399, 400  
   non-steady-state method, 397  
   steady-state method, 397–398  
   unit operations, 394  
 Fukami, K., 493–498
- G**  
 Gaiani, C., 97  
 Galerkin method, 389  
 García-Almendárez, B.E., 451–459  
 García Loredo, A.B., 477–484  
 García-Luna, I.N., 319–326  
 García, M.A., 456  
 García-Pérez, J.V., 519–525  
 Gas chromatographic (GC) analysis, 502  
 Gaytán-Martínez, M., 527–530  
 Generalized reduced gradient (GRG), 521  
 Gervais, P., 253  
 Gianfrancesco, A., 89–98  
 Gibbs, J.H., 19–21  
 Giraldo, G.I., 427–434  
 Girlich, D., 76–78, 83  
 Glass transition temperature ( $T_g$ )  
   *Aloe vera* gel  
     Gordon and Taylor model, 321–322, 325  
      $T_g$  and M, 321, 324–325  
   amorphous carbohydrates, 162  
   amorphous sugar matrices, 301–302  
   blueberries, 406–408  
   cornflakes, 127, 129  
   cross-linked dextrans. (see Cross-linked dextrans-water systems)  
   cryopreservation, seeds, 232, 233

- DSC, amorphous inulin  
  endothermic shift, 495  
  evaluation, 494–495  
  moisture content, 495–498  
  molecular weight, 496–498  
  plasticizing effect, 495–496  
  polysaccharides, 496  
freeze-dried strawberry, 472  
fruit samples. (*see* Thai fruits)  
maltitol, sucrose and trehalose  
  DSC determination, 415, 416  
  HPLC sugar analysis, 418  
  non annealed and annealed  
    condition, 418  
nanostructuration, 17–18  
phase transitions, 108, 109  
sugar crystals, 31  
TSC method, 77
- Glucose oxidase–peroxidase method  
(GOPOD), 423
- Gluten-free pasta formulation. *See*  
  Response surface methodology  
  (RSM)
- Glycerol model system  
  color changes, 50  
  fructose-glycine, 50, 53, 58, 60  
  glucose-glycine, 56–58, 60  
  lactose-glycine, 50, 58  
  lysine and xylose, 49  
  moisture content, 49  
  pyrazine compounds, 47  
  sugar-glycine, 50, 52, 55, 59  
  water activity, 43  
  xylose/lysine, 42
- Goff, H.D., 416
- Gómez, R., 541–547
- González-Martínez, C., 585–591
- Gordon–Taylor equation, 110, 121
- Gould, G.W., 17, 251
- Graiver, N., 238, 241, 521
- GraphPad Prism v5 software, 356
- Gravimetric static method, 331, 463, 464
- Green, J.L., 300
- Gruzdev, N., 254
- Guadarrama-Lezama, A.Y., 337–343
- Guanajuato State Water Commission (CEAG)  
  reports, 550
- Güemes-Vera, N., 605–609
- Guerrero-Beltrán, J.A., 329–335
- Guerrero, S., 125–133, 477–484
- Guggenheim, Anderson, and De Boer (GAB)  
  equation, 196–197, 332, 334, 335,  
    463–465, 588
- Gutiérrez, D.M., 569
- Gutiérrez-López, G.F., 15–23, 319–326,  
    337–343, 533–539, 557–564
- H**
- Hagenmaier, R.D., 454
- Hahn spin echo sequence, 129
- Halophilic lactic acid bacteria  
  cheeses  
    chemical composition,  
      279–280  
  HALAB, 283  
  *L. acidipiscis*, 285  
  *L. lactis*, 283  
  logistic dose–response model,  
    284, 285  
  in Mexico, 284  
  roles of salt, 281  
  salt concentration, 280–281  
  water activity, 279  
  microorganisms, 281–283
- Halsey equation, 197–198
- Han, J., 176
- Hansen, C.E., 536
- Haque, E., 437–448
- Harnkarnsujarit, N., 413–419
- Harris, M., 128, 600
- Hartmann, M., 635
- Hatley, R.H.M., 172
- Headspace gas chromatography  
(HS-GC), 501
- Henderson equation, 198
- Henríquez, O., 405–410
- Hernández-Chávez, J.F., 605–609
- Hernández-Salas, J.M., 558
- Hernández-Sánchez, H., 279–286
- Herschel–Bulkley model  
  behavior index, 544–545  
  coefficient of determination, 544  
  parameters, 544–545  
  power law, 543–544  
  water fraction, 545–547  
  yield stress, 544
- Hofmann, T., 48
- Horowitz, J., 274
- Horseradish peroxidase (HRP) activity.  
  *See* Peroxidase
- Hor, Y.L., 241
- Hough, G., 128
- Howes, T., 633
- Hummer, G., 19
- Hussain, A., 75–86

**Hydrate system**

- ampicillin trihydrate, 137
- bioavailability standpoint, 137
- calteridol calcium, 138
- channel, 138
- critical RH value, 136
- crystal forms, drug, 144–146
- desolvation, 139
- DSC and TGA, 138
- formation of, 135, 136
- ion coordinated, 138
- isolated site type, 138, 139
- Le Chatelier's principle, 137
- nonequilibrium transformations, 144
- non-stoichiometric, 137, 138
- phase diagram, 143, 144
- solid-state transitions, 136
- stoichiometric, 137
- water sorption isotherms, 141
- water uptake isotherms, 141–143

X-ray powder diffraction, 140, 141

**Hydro-chemical signature.** *See* Valle de León (VL)

**Hydrogen bonding (HB) network**, 84

**Hydroxypropyl methylcellulose (HPMC)**, 108

**I**

Ibarz-Ribas, A., 45, 54, 56

Ijima, N., 115–123

**Indomethacin (IMC) glass**

- hydrogen bonding, 8
- MD simulation, 8
- probability distribution, 8
- water molecules distribution, 8
- water uptake profiles, 7

**InfoStat software**, 377

**Intracellular ice formation (IIF).**

*See* Cryopreservation

**Ion coordinated hydrates**, 138

Ishikawa, M., 283

**J**

**Jalapeño pepper pulp**

- experimental data, 542
- flow curves, 542–543
- non-Newtonian fluid. (*see* Herschel-Bulkley model)

Janello, C., 28

Jaramillo-Flores, M.E., 337–343, 533–539

Jha, A., 347

Jiménez-Aparicio, A., 345–350

Johari, G.P., 85

Joly-Duhamel, C., 611

Jones, S.J., 85

Judd, D.B., 33

Jumah, R.Y., 347

**K**

Kajiwara, K., 421–425, 493–498

Karel, M., 42, 71, 72

Kawai, K., 421–425, 493–498

Kimberly, W.W., 569

Kishi, A., 176

Kohlrausch–Williams–Watts (KWW) model, 162–163, 614–616

Kouassi, K., 292, 294

Koutsoumanis, K., 258

Kramers' theory, 290

Kristo, E., 105

Kubelka–Munk analysis

- cereal products, 36–37
- food materials, 32–33
- fruit products, 34
- paints and inks industry, 32

Kucukpinar, E., 9

Kühn equation, 198–199

Kurosaki, S., 20

**L**

Labuza, T.P., 43, 53, 289, 633

*Lactobacillus acidophilus* (DLPL)

- preparation, 463
- sorption isotherm, 463–465
- stability, 464–467

*Lactococcus lactis*, 283

**Large unilaminar vesicles (LUV)**

- carboxyfluorescein, 221
- DPPC
- cooling rates, 225
- freezing temperatures, 224
- holding temperatures, 225–226

EPC

- cooling rates, 221, 222
- freezing temperatures, 222–223
- holding temperatures, 223

Larrosa, V.J., 367–373

Lauric arginate ester (LAE), 454, 455, 457–458

**Least significance difference (LSD) intervals**, 520, 522

Lebedeva, T.L., 9

Le Chatelier's principle, 137

Lee, C.Y., 569

- Leibler, L., 152, 153  
León, M.F.M., 324  
Leopold, A.C., 232, 233  
Leprince, O., 232, 233  
Levine, H., 17, 69, 600  
Lewicki equation, 199–200  
Lewicki Piotr, P., 528  
Light microscopy, 479  
Lipid-based delivery system  
  molecular dynamics simulations, 3–4  
  monocaprin, 4, 6  
monoglycerides  
  distribution, 6  
  MD simulations, 6  
  molecular structures of, 4  
  water molecules distribution, 5–6  
self-emulsifying/self-microemulsifying  
  lipid dispersions, 2  
triglycerides  
  MD simulations, 6  
  molecular structures of, 4  
  water molecules distribution, 6  
  water uptake, 5
- Listeria monocytogenes*, 251
- Longan  
  annealing process, 416, 418  
  DSC determination, 415–417  
  HPLC, 415  
  statistical analysis, 416  
  sugar composition of, 418–419
- Long-term persistence (LPT), 254
- López, D., 611–618
- López-Malo, A., 245–259
- López, O.V., 455
- Lorentzian equation, 128
- Lorenzo, G., 367–373
- Lourdin, D., 611
- Low-density amorphous solid water (LDA), 84
- Lowithun, N., 413–419
- Lowithun, S., 415
- Lozano, G.A., 549–554
- Lüdemann, H.D., 76–78, 83
- Lumry model, 303
- M**
- Maestrelli, A., 621–627
- Mahely, A.C., 569
- Maillard pigment concentration, 30
- Maillard reaction  
  absorbance measurements, 44  
  ANOVA, 45  
  color development
- glycine-glycerol system, 46, 47  
moisture content effect, 49–50  
  sugar-glycerol system, 46, 47
- color parameters, 44, 50–55  
glycine and glycerol, 43, 44  
kinetic studies, 44–45  
nonenzymatic browning reaction, 42–43  
non-water semipolar model liquid  
  systems, 43  
nutritional values, 43  
Pyrex glass test tube, 43  
reaction rate and kinetic order, 54, 56–57  
reactivity reducing sugars, 57–60  
spectrum peak determination, 46–48  
water activity, 42–43
- Maltodextrin powders, 93–95
- Mandell, L., 4
- Mango  
  annealing process, 416, 418  
  DSC determination, 415–417  
  HPLC, 415  
  statistical analysis, 416  
  sugar composition of, 418–419
- Marabi, A., 89–98
- Marcos, A., 280
- Marinilactibacillus psychrotolerans*, 283
- Marque, G., 9
- Márquez-Hernández, Y.M., 451–459
- Martínez, L.M., 299–309
- Martínez-Velarde, R., 345–350
- Martuscelli, M., 499–506
- Matiacevich, S., 405–410
- Maximum stability ( $a_w$ MS), 463–465
- Mazzobre, M.F., 311–316, 353–360,  
  629–635
- McMahon, M.A.S., 257
- Meat brining processes  
  mass transport  
    effective diffusivity, 521  
    NaCl transport, 522–524  
    water transport, 521–524  
  slab geometry, 520  
  statistical analysis, 520
- Mederos, F., 299–309
- Meilgaard, M.C., 128
- Meinders, M.B.J., 149–158
- Melgar-Lalanne, G., 279–286
- Mexican Drinking Water Norm (MDWN)  
  N-NO<sub>3</sub><sup>-2</sup> ion, urban zone-located wells,  
    551, 554
- piper diagram, 551, 552
- water temperature vs. milliequivalent per  
liter relation, 551, 553

- Mexican plum  
advantage, 330  
ASE, 333  
BET model, 332–334  
freeze-drying, 331  
GAB model, 332, 334, 335  
moisture content vs. water activity, 330  
moisture sorption isotherms, 331–333  
Oswin model, 333–335  
physicochemical characteristics, 333  
pulper machine, 331  
transportation, 330
- Microencapsulation process  
encapsulated extract, 340  
moisture content, 341, 342  
nonencapsulated extract, 340  
RHME. (*see* Refined hemisphaericin  
microencapsulated (RHME))  
SEM, 341–343  
water activity, 341, 342
- Microorganism control. *See* Water  
activity ( $a_w$ )
- Miles, C.A., 387, 397, 399
- Milk protein concentrate (MPC) powder  
casein micelles, 440  
enthalpy relaxation, 443–445  
protein conformational modification, 443  
protein cross-linking, 443  
storage-induced loss, 441  
transverse relaxation time, 447
- Mimouni, A., 440
- Minimum lethal concentration (MLC), 455,  
457–458
- Modified corn starch, 453
- Modulated differential scanning calorimetry  
(MDSC), 151, 164
- Moisture sorption isotherms  
analysis, 201  
applications, 206–207  
chemical composition, 191  
dynamic methods  
DDI, 194–195  
DVS, 194  
microbial growth/physicochemical  
changes, 193–194  
enthalpy and entropy, 205–206  
hysteresis phenomenon, 189, 190  
isosteric heat, 206  
mathematical models  
BET equation, 196  
diverse food products, 203–204  
fruit products, 202  
GAB model, 196–197
- Halsey equation, 197–198  
Henderson equation, 198  
Kühn equation, 198–199  
Lewicki equation, 199–200  
Oswin equation, 199  
Peleg equation, 200  
Smith equation, 200  
vegetable products, 203
- Mexican plum, 331–332  
monolayer moisture content, 190–191  
properties, 188–189  
shelf life prediction, 208–209  
static methods, 192–193  
temperature effect, 191–192  
types, 189, 190
- Molecular dynamics (MD) simulations, 3–4  
amorphous indomethacin glass, 8  
DOPC, 10, 11  
monocaprylin, 6  
PVP, 9  
tricaprylin, 6
- Monedero, F.M., 101–112
- Monolayer moisture contents (MMC),  
190–191, 334
- Monroy-Villagrana, A., 15–23
- Monte Carlo method, 209
- Mora-Escobedo, R., 557–564
- Morales-Delgado, D.Y., 637–644
- Morales-Sánchez, E., 527–530
- Morales-Trejo, F., 279–286
- Mora, M., 299–309
- Mújica-Paz, H., 485–490
- Mulet, A., 519–525
- Multivariate analysis of variance (MANOVA),  
313, 315, 479, 520
- Murase, N., 115–123
- Mustapha, W.A.W., 42, 49
- Mystat v12.02 software, 284
- N**
- Nano-emulsified beeswax, 453–456
- Nanostructuration  
application of, 21–22  
cooperative rearrangement, 20  
food morphology, 22  
glass transition temperature, 17–18  
relative humidity, 16  
thermodynamic parameters, 18–20  
water activity, 17  
water confined, nanometric spaces, 18–19
- Natamycin, 454, 455, 457–458
- Nath, S., 303

- Necochea-Mondragón, H., 637–644  
Neri, L., 289–297, 502  
Newton's equations of motion, 3  
Neyertz, S., 9  
Ngai, K.L., 616  
Nieto, A., 375–382  
Noel, T.R., 611  
Nonequilibrium components. *See*  
    Biological materials  
Non-stoichiometric hydrates, 137  
Normand, M.D., 263–278  
Nuclear magnetic resonance (NMR)  
    cross-linked dextrans, 116  
    freeze-dried strawberry, 472–474  
    TSC method, 85
- O**  
Obanu, Z.A., 46  
Octenyl succinic anhydride (OS), 456–458  
Oil-in-water (O/W) emulsion, 340  
Oily extract of chile (OEC), 340, 341  
Okos, M.R., 386  
Oleic acid (OA), 105–107  
Oliver, C.M., 60  
Oliver, L., 149–158  
Oliver-Salvador, M.C., 575–583  
Optical density (OD), 422  
Ordinary differential equation (ODE), 271, 272  
Ortega, M.L., 578  
Osmotically dehydrated (OD) apples  
    loss modulus, 479–480  
    microstructure, 479, 482–483  
    rheological properties  
        creep/recovery tests, 478–481  
        dynamic oscillatory tests, 478  
        linear viscoelastic properties, 478  
        statistical analysis, 479  
        structural changes, 483  
    storage modulus, 479–480  
texture properties  
    sensory analysis, 479, 481–482  
    TPA, 479, 481–482  
Osmotic dehydration, 376, 487–490  
Osorio, F., 509–518  
Oswin model, 199, 333–335  
Otte, A.D., 135–147  
Ozuna, C., 519–525
- Palzer, S., 635  
Pamminger, N.W., 235  
Papadakis, S., 471  
Parada-Arias, E., 337–343, 637–644  
Pascual-Pineda, L.A., 15–23  
Peleg equation, 200  
Peleg, M., 128, 263–278, 600  
Peña, R., 519–525  
Peppas equation, 356–359  
Peppas, N.A., 359  
Pérez-Gallardo, A., 456  
Pérez, J., 549–554  
Pérez, O.E., 361–366  
PerkinElmer software, 415  
Peroxidase  
    enzymatic activity  
        ligand–polymer solutions, 291–294  
        system mobility, 291  
        ternary ligand–polymer solutions,  
            294–296  
        viscosity, 290  
        WLF equation, 290–291  
        water activity, 289  
Piccone, P., 499–506  
*Pimenta dioica* L. Merrill. *See* Allspice  
Pinal, R., 135–147  
Pittia, P., 289–297, 499–506, 593–602  
Polymer matrix. *See* Edible/biodegradable  
    hydrocolloids  
Polyvinylacetate (PVAc)  
    moisture uptake, 7  
    water concentrations, 9  
    water uptake, 7  
Polyvinylpyrrolidone (PVP)  
    amide carbonyl, 7  
    moisture uptake, 7  
    molecular dynamics simulations, 9  
    water uptake, 7  
Porras-Saavedra, J., 319–326, 345–350,  
    629–635  
Principal component analysis (PCA),  
    479–481  
Prior, B.A., 605  
Protein stability  
    alcohols and polyols  
        aqueous solutions, 428–429  
        folding/unfolding process, 428  
        protein adsorption, 430–432  
        thermal denaturation, 429–430  
        viscosity, 432–433  
    primary and secondary structures, 438  
Proton nuclear magnetic resonance ( $^1\text{H}$  NMR),  
    363–365

Prunier, V., 9  
 Pyne, A., 416  
 Pyrazine compounds, 47, 48

**Q**  
 Quintanilla-Carvajal, M.X., 533–539

**R**  
 Rambutan  
     annealing process, 416, 418  
     DSC determination, 415–417  
     HPLC, 415  
     statistical analysis, 416  
     sugar composition, 418–419  
 Ramos, J.J., 81  
 Rana, R.K., 559  
 Rao, Q., 633  
 Refined hemisphaericin microencapsulated (RHME)  
     arabic gum  
         CCD, 577–579  
         isolated enzymes, 576  
         preparation, 577  
         protein concentration assay, 578, 579  
         proteolytic activity assay, 578, 580  
         RS design, 577, 579–581  
         SEM, 578  
         yield, 578, 581–582  
     spray drying. (*see* Spray-drying process)  
 Regalado, C., 451–459  
 Regional breads (Puebla State, Mexico)  
     color measurement, 606–608  
     proximal chemical analysis, 606–607  
     TPA, 606–608  
     water activity, 606–608  
 Relative vapor pressures (RVP), 126  
 Rengsutthi, K., 413–419  
 Response surface (RS) design, 577, 579–581  
 Response surface methodology (RSM)  
     dough composition  
         starch gelatinization, 371–373  
         water mobility, 369–371  
     hydrocolloids and proteins, 368  
     structural functions, 368  
     surface response analysis, mixture designs, 368–369  
 Retention index, 502–503  
 Reyes, L.A., 575–583  
 Reyes-Santamaria, M.I., 605–609  
 Reyes-Vega, M.L., 527–530

Rivera-Espinoza, Y., 279–286  
 Roberts, C., 75–86  
 Rojas-de Gante, C., 461–467  
 Romero, C.M., 427–434  
 Roos, Y.H., 65–73, 83, 292, 294, 302, 414,  
     416, 419  
 Ruan, R., 20  
 Ruiz-Hernández, F., 329–335

**S**  
 Sablani, S.S., 161–173  
 Sacchetti, G., 289–297, 593–602  
 Sáez, C., 611–618  
 Sahagian, M.E., 416  
 Saleeb, F.Z., 21  
 Saleki-Gerhardt, A., 302  
 Salmon gelatin films  
     acid–alkaline method, 613  
     enthalpy relaxation, 614, 617–618  
     uniaxial tension method  
         constant strain, 613  
         KWW model, 614–616  
         modulus vs. ageing time, 614–615  
         moisture content and temperature,  
             613–614  
         normalized relaxation rate *vs.* time, 616  
         parameters, 615–616  
         stress relaxation, glass, 614–615  
         Young's modulus, 613  
 Salt crystallization  
     DSC, 587, 589–590  
     mechanical properties, 587, 590  
     microstructural analysis, 587  
     preparation, 586  
     SEM micrographs, 590  
     statistical analysis, 587  
     water sorption isotherms, 586, 588  
 Sánchez-Mundo, M.L., 533–539  
 Sandhu, K.S., 372  
 Santagapita, P.R., 353–360  
 Santiago-Pineda, T., 567–573  
 Santos, M.V., 383–392  
 Sastry, S.K., 529  
 Scanning electron microscopy (SEM), 35, 578  
     agave powders, 347, 348  
     allspice, 569  
     *Capsicum* extract, 340–343  
     cytosine, 179, 181  
     FEI Nova nanoSEM field emission,  
         177–178  
     theophylline, 179, 182  
     thymine, 179, 183

- Schebor, C., 361–366, 469–476  
Schmidt, S.J., 161–173  
Schwartzberg, H.G., 399  
Scott, W.J., 246  
Sekimoto, K., 152, 153  
Seow, C.C., 46  
Sephadex gel  
  density of, 116–117  
DSC  
  measurement, 117  
  rewarming traces, 117–120  
  sample preparation, 117  
Seuvre, A.M., 501  
SFE. *See* Surface free energy (SFE)  
Shalaev, E., 75–86  
Sheri, L.S., 302  
Sherwin, C.P., 43, 53  
Shifted logistic model, 266, 269  
Shinyashiki, N., 66  
Short dough biscuits  
  glucose  
    flexural modulus index, 599–600  
    fracture force data, 597–598  
    glass transition temperature, 597, 600  
    laboratory mixing apparatus, 594  
    sensory analysis, 595  
    shear and bending test, 595–597  
    sorption isotherms, 595, 597  
    structural and mechanical properties, 600  
    textural properties, 601–602  
    water activity, 595  
    Young's modulus, 599  
  sucrose  
    flexural modulus index, 599–600  
    glass transition temperature, 600  
    laboratory mixing apparatus, 594  
    shear test analysis, 595–597  
    sorption isotherms, 595, 597  
    structural and mechanical properties, 600  
    textural properties, 601–602  
    water distribution, 600–601  
Shrestha, A.K., 635  
Singh, P.C., 197  
Singh, R.K., 197  
Singha, A.S., 559  
Sisko model. *See* Herschel-Bulkley model  
Skim milk powder (SMP) samples, 93, 94  
Skurlys, O., 509–518, 611–618  
Slade, L., 17, 69, 600  
Smith equation, 200  
Solar drying, vegetables  
  atmospheric air, 622  
  color, 625  
conventional drying, 624, 626  
eggplant slices, 622  
elastic module, 625–626  
Eolo, 622–623  
heating layer, 622, 624  
moisture content, 626  
processes, 622–623  
sunny/cloudy summer day, Milan, 624–625  
thermal probes, 624  
water activity, 625–626  
Solorza-Feria, J., 557–564  
Soren fors, P., 387  
Sosa, N., 361–366  
Soto-Simental, S., 605–609  
Soy protein isolate (SPI), 104–107  
  caking process, microstructural changes, 632–635  
  glass transition temperature, 632–633, 635  
  moisture content, 631–633  
  wall materials, 631–633, 635  
  water activity, 631–633  
*Spondias purpurea* L. *See* Mexican plum  
Spray-drying process  
  agave powders. (*see* agave powders)  
  *Aloe vera* gel. (*see* *Aloe vera* gel)  
  antioxidant activity. (*see* *Capsicum annuum*, oily extract)  
citral/sugar emulsions  
  equivalent volume-mean diameter, 363, 364  
  flow curves, 363, 364  
  <sup>1</sup>H NMR, 363–365  
  microencapsulation, 362  
  samples preparation, 362–363  
  stability, 364, 365  
  volume-surface mean diameter, 363, 364  
gum arabic  
  caking process, microstructural changes, 632–635  
  glass transition temperature, 632–633, 635  
  moisture content, 631–633  
  wall materials, 631–633, 635  
  water activity, 631–633  
maltodextrin  
  caking process, microstructural changes, 632–635  
  glass transition temperature, 632–633, 635  
  moisture content, 631–633  
  wall materials, 631–633, 635  
  water activity, 631–633

- Spray-drying process (*cont.*)
- RHME
  - CCD, 577–579
  - isolated enzymes, 576
  - preparation, 577
  - protein concentration assay, 578, 579
  - proteolytic activity assay, 578, 580
  - RS design, 577, 579–581
  - SEM, 578
  - yield, 578, 581–582
- SPI
- caking process, microstructural changes, 632–635
  - glass transition temperature, 632–633, 635
  - moisture content, 631–633
  - wall materials, 631–633, 635
  - water activity, 631–633
- Standard Linear Solid (SLS), 154
- Starch
- analysis of variance, 528
  - DSC, 528
  - electrical conductivity, 528–530
  - enthalpy, 528–530
  - gelatinization, 529–530
    - amylopectin, 425
    - complex index, 422
    - dough composition, 371–373
    - endothermic peak, 423
    - hydrolyzed starch content, 424–425
    - melting temperature, 423
    - non-complexed Pam, 425
    - Pam samples, 423–425
    - sample preparation, 422
    - in vitro* digestibility, 423
  - heating rate program, 528
  - viscoelastic sorption behavior
    - boundary conditions, 152–154
    - Deborah number, 150–151
    - dynamical sorption, 156–158
    - Flory-Huggins interaction parameter, 151
    - isotherm, 152–156
    - MDSC, 151
    - multiscale thermodynamical theory, 151
    - non-Fickian features, 151
    - rheological model, 154
    - water transport equation, 152
    - water activity, 528–530
- State of water
- amorphous solids
  - molecular dynamics simulations, 3–4
  - self-emulsifying/self-microemulsifying lipid dispersions, 2
  - water uptake, 7–10
- lipid-based delivery. (*see* Lipid-based delivery system)
- Statgraphics Plus software, 377
- Stoichiometric hydrates, 137
- Stouch, T.R., 10, 11
- Structural relaxation times
- food processing and storage, 70
  - WLF. (*see* Williams-Landel-Ferry (WLF))
- Suarez, G., 60
- Sugar-amino acid-glycerol model systems, 45, 47
- Sugar-glycine-glycerol model systems, 46, 47, 49
- Sugar model system, 52, 54, 55
- Sun, W.Q., 232, 233
- Surface free energy (SFE)
- apolar surfaces, 513
  - chitosan and Tween 20 concentrations, 516–517
  - coating preparations, 512
  - cohesive energy, 514
  - contact angle, wetting measurements, 511
  - glycerol/chitosan concentrations, 515–516
  - interfacial tension measurements, 513
  - Lewis acid–base component, vOGC model, 512
  - polyester matrix/cutin layer, 511
- Suryanarayanan, R., 176
- Syamaladevi, R.M., 161–173
- Szczesniak, A.S., 128, 479
- T**
- Takato, S., 421–425
- Talens, P., 101–112
- Talja, R.A., 83
- Tao, L.C., 395
- Taylor, L.S., 9
- Tejocote fruit
- osmotic and isotonic solutions, 486
  - sucrose solutions, 486
  - water activity depression
  - dehydration-impregnation treatments, 487–490
  - impregnation treatment, 486–488
  - physicochemical characteristics, 487–488
  - statistical analysis, 487
- Tejwani, R.W., 10, 11
- Telis, V.R.N., 393–402

- Telis-Romero, J., 393–402, 541–547  
Téllez-Medina, D.I., 15–23, 637–644  
Texture profile analysis (TPA)  
    blanched (B) apples, 479, 481–482  
    bread, 606–608  
Thai fruits  
    longan. (*see* Longan)  
    mango. (*see* Mango)  
    maximal-freeze-concentration condition, 414  
    rambutan. (*see* Rambutan)  
Thanatukorn, P., 493–498  
*Theobroma cacao* L. *See* Cocoa beans, germination  
Thermal denaturation, 429–430  
Thermally stimulated current (TSC) method  
    calorimetric glass transition temperature, 77, 82, 83  
    dipole relaxation, 77, 84  
    DSC, 79, 81, 82  
    freeze-dried samples, 78  
    hexagonal ice, 85  
    hydrogen bonding network, 84  
    low-temperature molecular mobility, 77  
    NMR study, 85  
    sorbitol-water systems, 77–78  
    sucrose-water, 77, 83  
    TSC/RMA instrument, 78  
    TSdC, 78, 79, 82  
    TSpC, 78–82  
Thermally stimulated depolarization current (TSdC), 78, 79, 82  
Thermally stimulated polarization current (TSpC), 78–82, 179, 182, 184  
Thermograms, 472  
Thermogravimetric analysis (TGA), 138, 559, 561–562  
Thermogravimetric method, 347  
Tiganitas, A., 251  
Time-resolved proton nuclear magnetic resonance (H-TR-NMR), 127  
Torreggiani, D., 289–297  
Troller, J.A., 605  
Trujillo-de Santiago, G., 461–467
- U**  
Uniaxial tension  
    constant strain, 613  
    KWW model, 614–616  
    modulus *vs.* ageing time, 614–615  
    moisture content and temperature, 613–614  
    normalized relaxation rate *vs.* time, 616  
    parameters, 615–616
- V**  
Vacuum pulse, 487–490  
Valdez-Fragoso, A., 485–490  
Valle de León (VL)  
    CEAG reports, 550  
    data collection, 550–551  
MDWN  
    N-NO<sub>3</sub><sup>-2</sup> ion, urban zone-located wells, 551, 554  
    piper diagram, 551, 552  
    water temperature *vs.* milliequivalent per liter relation, 551, 553  
    sedimentary tertiary rocks, 549–550  
Valles Pamies, B., 602  
Vampa, V., 383–392  
van der Waals and electrostatic interactions., 3  
Vargas, M., 585–591  
Velásquez, P., 509–518  
Velázquez, G., 527–530  
Verdu, J., 9  
Vergara-Balderas, F., 319–326  
Vertucci, C.W., 230, 241  
Vicente, S., 375–382  
Videa, M., 299–309  
Viganó, J., 541–547  
Villa-Vélez, H.A., 393–402  
Viriyattananasak, C., 493–498  
Viscoelastic sorption behavior  
    gluten  
        boundary conditions, 152–154  
        Deborah number, 150–151  
        dynamical sorption, 156–158  
        Flory-Huggins interaction parameter, 151  
        isotherm, 152–156  
        MDSC, 151  
        multiscale thermodynamical theory, 151  
        non-Fickian features, 151  
        rheological model, 154  
        water transport equation, 152  
    starch. (*see* Starch)  
Viscosity, 432–433  
Voget, C.E., 569
- W**  
Waleckx, E., 563  
Walters-Vertucci, C., 232, 233  
Wang, W., 529

- Water activity ( $a_w$ )  
 agave powders, 347, 348  
*Aloe vera* gel, 322–323  
 arabic gum, 631–633  
*Capsicum* extract, 342  
 cocoa beans, germination, 535–539  
 dairy powder, 446–447  
 degradation, 264  
 food safety and stability, 258–259  
 influence of, 246  
 Maillard reaction, 42–43, 264  
 maltodextrin, 631–633  
 microbial growth  
   accelerated storage data, 269–270  
   asymptotic growth level, 266, 267, 269  
*D. hansenii*, 248, 249  
 ecological factors, 248  
*E. sakazakii*, 249–251  
 food-borne pathogens, 247, 248  
 Gompertz model, 265  
 Gompertz parameters, 249, 250  
 high-moisture foods, 252–253  
 inflection point location, 266, 268  
 intermediate-moisture foods, 251–252  
 intrinsic and extrinsic factors, 246–247  
*L. monocytogenes*, 251  
 maximum growth rate, 266, 268, 269  
 momentary growth rate, 270–271  
 ODE, 271  
 phases, 265  
 quasi-chemical model, 265–266  
*Salmonella*, 251  
 shifted logistic model, 266, 269  
 single rate parameter, 266, 267  
 slight reduction, 249  
 traditional approach, 271  
 types, 248  
 microbial inactivation  
   conventional method, 271  
   Weibullian model, 272, 273  
 microbial survival/inactivation  
   commercial and legal requirements, 253–254  
   DT and LPT, 254  
   fruit products, 254  
   low frequency ultrasound, 254–255  
   temperature effects, 253  
*Z. bailii*, 255, 256  
 nanostructuration, 17  
 osmotic stress  
   cell homeostasis, 256  
   cytoplasmatic solutes, 256–257  
   food preservation, 257  
   genomics technology, 258  
   heterogeneity, 257–258  
   homogeneity, 257  
   internal media stability, 255–256  
   NaCl growth, 258  
   peeled tejocote, 487–490  
   peroxidase, 289  
   probabilistic models  
     algebraic expression, 276  
     cell division and mortality, 274  
     momentary probability rates, 273–274  
     mortality curve, 275  
     resumed growth curve, 275–276  
     sigmoid growth curve, 275  
     sporadic and haphazard incidence, 273  
   vs. rate curve, 264  
 short dough biscuits, 595  
 solar drying, vegetables, 625–626  
 SPI, 631–633  
 spoilage products, 245–246  
 starch, 528–530  
 starch-water composites, 528–530  
 sugar concentration, 503  
 tejocote fruit, depression  
   dehydration-impregnation treatments, 487–490  
   impregnation treatment, 486–488  
   physicochemical characteristics, 487–488  
   statistical analysis, 487  
 Water-holding capacity (WHC), 523–524  
 Water interactions control. *See*  
   Nanostructuration  
 Water mobility, dough composition  
   DSC, 369–370  
   glass transition, 371, 372  
   peak melting temperature, 370–371  
   RSM, 370  
   unfrozen water content, 370, 371  
 Water plasticization, 68  
 Water sorption capacity (WSC)  
   film plasticizers, 104–105  
   lipids, 105–108  
 Water vapor permeability (WVP), 104, 455  
 Weibullian model, 272–273  
 Welti-Chanes, J., 319–326, 329–335, 485–490  
 White, P.J., 372  
 Wiechert model, 154  
 Wijayanti, H.B., 41–61  
 Wijewickreme, A.N., 46

- Williams-Landel-Ferry (WLF), 291  
  crystallization, 72  
  dielectric and mechanical relaxation times,  
    66–68  
  fluidness characteristics, 69–70  
  stickiness, 71
- Williams, M.C., 69
- Williams, R.J., 232, 233
- Wojtas, A., 409
- Wolkers, W.F., 302
- Wong, C.W., 41–61
- Wungtanagorn, R., 166
- Wyszecki, G., 33
- X**
- Xaa-*prolyl*-dipeptidyl-peptidase (Xaa-Pro-DAP)  
  activity, 535, 537
- Xiang T.-X., 9
- X-ray diffractometry (XRD), 116
- X-ray powder diffraction (XRPD)
- Bruker D5000 diffractometer, 177  
  crystalline thymine, 178, 179  
  cytosine, 178, 179  
  theophylline, 178, 179
- Y**
- Yaldiz, O., 622
- Yamauchi, M., 176
- Yáñez-Fernández, J., 575–583, 629–635
- Yee-Madeira, H., 557–564
- Z**
- Zaritzky, N.E., 229–241, 367–373, 383–392
- Zeller, B.L., 21
- Zero-order kinetic reaction, 56–57
- Zhang, Y., 175–184
- Zimmerman, J.R., 20
- Zografi, G., 302
- Zygosaccharomyces bailii, 255, 256